B. B. V. L. Deepak
M. V. A. Raju Bahubalendruni
D. R. K. Parhi
Bibhuti Bhusan Biswal *Editors*

Recent Trends in Product Design and Intelligent Manufacturing Systems

Select Proceedings of IPDIMS 2021

Springer

Lecture Notes in Mechanical Engineering

Lecture Notes in Mechanical Engineering (LNME) publishes the latest developments in Mechanical Engineering—quickly, informally and with high quality. Original research reported in proceedings and post-proceedings represents the core of LNME. Volumes published in LNME embrace all aspects, subfields and new challenges of mechanical engineering. Topics in the series include:

- Engineering Design
- Machinery and Machine Elements
- Mechanical Structures and Stress Analysis
- Automotive Engineering
- Engine Technology
- Aerospace Technology and Astronautics
- Nanotechnology and Microengineering
- Control, Robotics, Mechatronics
- MEMS
- Theoretical and Applied Mechanics
- Dynamical Systems, Control
- Fluid Mechanics
- Engineering Thermodynamics, Heat and Mass Transfer
- Manufacturing
- Precision Engineering, Instrumentation, Measurement
- Materials Engineering
- Tribology and Surface Technology

To submit a proposal or request further information, please contact the Springer Editor of your location:

China: Ms. Ella Zhang at ella.zhang@springer.com
India: Priya Vyas at priya.vyas@springer.com
Rest of Asia, Australia, New Zealand: Swati Meherishi
at swati.meherishi@springer.com
All other countries: Dr. Leontina Di Cecco at Leontina.dicecco@springer.com

To submit a proposal for a monograph, please check our Springer Tracts in Mechanical Engineering at https://link.springer.com/bookseries/11693 or contact Leontina.dicecco@springer.com

Indexed by SCOPUS. All books published in the series are submitted for consideration in Web of Science.

B. B. V. L. Deepak ·
M. V. A. Raju Bahubalendruni · D. R. K. Parhi ·
Bibhuti Bhusan Biswal

Editors

Recent Trends in Product Design and Intelligent Manufacturing Systems

Select Proceedings of IPDIMS 2021

Editors
B. B. V. L. Deepak
Department of Industrial Design
National Institute of Technology Rourkela
Rourkela, India

D. R. K. Parhi
Head Professor (HAG), Mechanical
Engineering
National Institute of Technology Rourkela
Rourkela, India

M. V. A. Raju Bahubalendruni
Department of Mechanical Engineering
National Institute of Technology
Puducherry, India

Bibhuti Bhusan Biswal
Mechanical Engineering
National Institute of Technology Meghalaya
Shillong, India

Preface

This book congregates selected research articles from the 3rd series of Innovative Product Design and Intelligent Manufacturing System (IPDIMS-2021), held at National Institute of Technology Rourkela, India. The book emphasises the recent technologies and advanced tools in the areas of product design and manufacturing technology. The main topics covered include ergonomics and human factors, UI/UX, design for 'X', Industry 4.0, smart manufacturing, advanced robotics and CAD/AM. The contents of this book are useful for academics as well as professionals working in the areas of industrial design, manufacturing, mechatronics, robotics and automation.

Reviewers

Contents

Product Design: Design for Cost, Reliability and Sustainability

Product Design: Materials Innovation in Product Design

Product Design: UI/UX

**Intelligent Manufacturing Systems: Advanced Manufacturing
Processes**

Intelligent Manufacturing Systems: Optimization of Process parameters

Intelligent Manufacturing Systems: Robotics and Automation

About the Editors

Dr. B. B. V. L. Deepak is currently working in the Department of Industrial Design at National Institute of Technology (NIT) Rourkela. He received his Master's and Ph.D. degrees from the NIT Rourkela in 2010 and 2015, respectively. He has 11 years of research and teaching experience in manufacturing and product design fields. He has produced 3 Ph.D. theses and is currently supervising 4 Ph.D. scholars. He has published over 100 papers in various peer-reviewed journals and conferences and holds one patent in his name. He is also currently handling two sponsored research projects in the field of robotics. He received several national and international awards such as Ganesh Mishra Memorial Award-2019, IEI Young Engineer Award-2018, Early Career Research Award-2017, etc.

Dr. M. V. A. Raju Bahubalendruni is currently working as Assistant Professor in the Department of Mechanical engineering at National Institute of Technology (NIT) Puducherry, India. He completed his masters in machine design at Andhra University College of Engineering, India. He has industry experience having worked on several aircraft programmes like c27J, Bombardier, Honda Jet, Bell -407. He completed his Ph.D. degree from NIT Rourkela. He is an active researcher in the manufacturing and automation domain (assembly, disassembly, industrial robotics, human-robot collaboration, additive manufacturing, topology optimization, advanced cellular structures, augmented reality/virtual reality). He has over 11 years of total academic, industrial and R&D experience. He has received multiple research grants from Science and Engineering Research Board (SERB), Department of Science and Technology (DST). He has published close to 80 articles in reputed national and international journals. He has been awarded with Gold Medal "BRUNDABANSAHU MEMORIAL AWARD" by Institute of Engineers India (IEI-Odisha) in 2016 for his research contribution, received National level (Indian) Young Engineer award 2017 in the mechanical stream by IEI.

Prof. D. R. K. Parhi is working at National Institute of Technology (NIT) Rourkela as a Professor. He is currently heading the Department of Mechanical Engineering. He received his Ph.D. in Mobile Robotics field from Cardiff School of Engineering, UK. He has 26 years of research and teaching experience in robotics and artificial intelligence fields. He has guided more than 20 Ph.D. theses and published more than 300 papers in various journals and conferences and holds 3 patents in his name. He has also completed and currently handling several sponsored research projects in the field of robotics.

Prof. Bibhuti Bhusan Biswal is currently acting as Director of National Institute of Technology (NIT) Meghalaya. He is also a Professor (HAG) in the Department of Industrial Design of NIT Rourkela. He has 33 years of research and teaching experience in FMS, CAD/CAM, and robotics. He has guided more than 15 Ph.D. theses and published more than 200 papers in various journals and conferences along with 3 patents/copyrights. He has international collaboration with Loughborough University and Slovak University of Technology in Bratislava. He has also completed and currently handling several sponsored research projects in his research field.

Product Design: Ergonomics and Human Factors

Analysis of Secondary Tasks Performed and Psychosocial Factors of Railway Loco Pilots

Suyash Krishna, Sangeeta Pandit, Rajat Kamble, and Jigyasa Hemant Patankar

1 Introduction

Indian Railway system occupies the first railway network system in Asia and is fourth largest in the world [1]. It is 167 years old and comprises 436 departments and 15.4 lakh employees working [1]. Indian Railway is the fourth largest Railway track network in the world [1]. It has a total of about 108,706 route-kms of track which covers 6853 stations [1]. Indian Railways runs 11,000 trains daily, consisting of passenger and goods trains [1]. This Indian transportation system handles 13 million passengers and 1.35 million tonnes of freight with a total of 11,000 trains on a daily basis [1]. Indian Railways is considered to be one of the safest and comfortable means of transportation for both man and material.

A study report on railway drivers found a higher incidence of stress compared to other jobs like assistant station masters, train examiners and office clerks [2]. Loco pilots get irregular sleeps and suffer stress-related diseases like hypertension, diabetes and frequent headaches [3]. The loco pilot of a high-speed train has to work for 400–500 km at a stretch without any food or toilet break. The driver of a high-speed train like Rajdhani has to observe a signal every 1 min 22 s on average, which means he has to be vigilant continuously [3]. The loco pilots operating at a long-distance route stay overnight in the running room away from the home station [3]. The night duty is only considered when the duty is between 10 pm and 6 am [3]. There is a high noise level in the cab which has adverse effects on the mind and ears of the drivers [3]. During hot summer days, the cab temperature goes as high as 54–56 °C [3]. Poor visibility due to foggy or rainy weather or sometimes because of not proper functioning of the wiper is often faced by the loco pilots. The workspace

S. Krishna · S. Pandit (✉) · R. Kamble · J. H. Patankar
Ergonomics Lab, Design Discipline, PDPM Indian Institute of Information Technology, Design and Manufacturing, Jabalpur, Madhya Pradesh 482005, India
e-mail: s.pandit@iiitdmj.ac.in

of a locomotive cab drivers is usually with seats without backrest and without toilet and pantry (Fig. 1). Presently, the work schedule of Loco Pilots is classified under 'continuous' roaster, which results in no fixed calendar off-day. In usual cases, the loco pilots must work for continuous 10 h duty and can take break after 12 h by giving notice to the controller [4]. Loco pilots do not have control on their work environment and often need to work with job schedules that disturb their personal life and social life, and planning leaves is also difficult [5].

Over the years, many research studies concerning the psychological effects, work-life balance, stress and fatigue, ergonomics and health effects of the loco pilots have been done [3, 5–8]. There is a need for analysis of the tasks they perform and psychosocial factors related to the duty of the loco pilots. The tasks taken here are secondary tasks performed by the Loco pilots for the smooth running of the train [6]. The secondary task is subdivided as blowing horn, operating vigilance switch—button to keep a check on alertness, use of walkie talky—verbal communication with the crew, signal exchange—to exchange speechless communication and leaning out—to check on the following train attached at the rear end visually [6]. Psychosocial factors are to understand the social conditions of the loco pilots, which affect mental health. The study aims to find out the tasks performed and psychosocial effects on the various designation levels of the Loco pilots.

2 Methodology

The study was conducted at Patna Junction. Patna Junction is one of the busiest railway stations in the country [9]. Patna Junction is operated by East Central Railways, and it lies on the busiest railway route, New Delhi to Kolkata.

There are some limitations in conducting this study due to the COVID situation resulting in a smaller number of respondents participating in the study. In this study, 38 respondents of different designations working in the Danapur division in Patna participated. All the respondents were randomly chosen and participated voluntarily. Among the total 38 respondents, all were male. The primary data source was collected through a self-administered questionnaire that was designed keeping in mind the objectives of the study. The self-administered questionnaire contained questions addressing the secondary tasks performed by the Loco pilots based on the study done by Subir Danda [6], and the questions related to psychosocial factors which they go through were based on the research findings [5, 7].

Total of 17 questions were generated based on the findings of the study [5–7]. Out of which, 5 questions addressed the physical factors of the Loco pilots and the rest 12 questions addressed psychosocial factors. The questionnaire was prepared for psychosocial factors like no job satisfaction, support from the co-pilots and supervisor, work health hazard anxiety, difficulty in relaxing, demand for hiding emotion, depression, responsibility of people, missing on quality family time, work overload, time pressure and no fixed working hours. Furthermore, the questionnaire was prepared for tasks like blowing horn, operating vigilance switch, using walkie talky, signal exchange and leaning out. The questions asked were as follows: 'How often in your work you Q1: are not satisfied with your job?; Q2: get support from Co-pilots?; Q3: get support from supervisors?; Q4: feel anxiety because of work related health hazard?; Q5: face difficulties to relax during relax hours?; Q6: have to hide your emotions?; Q7: feel like depression?; Q8: feel responsibility of people?; Q9: miss out quality time with family?; Q10: get overloaded with work?; Q11: get time pressure?; Q12: get uncertain working hours?; Q13: perform task of Blowing horn?; Q14: perform task of operating vigilance switch?; Q15: use walkie talky?; Q16: perform exchange of signals?; and Q17: lean out?'. The questions were to be answered in a 5-point scale. The 5-point scale used was as follows: 1 signifies rarely, 2 signifies rather rarely, 3 signifies sometimes, 4 signifies rather often, and 5 denotes often. Finally, the respondents were asked to rate each of the tasks and factors on the above scale. The answer ratings 1 and 2 were classified as 'No', and ratings 3, 4 and 5 were classified as 'Yes'.

For statistical analysis, basic statistics, including total mean and percentages, were calculated. The statistical differences between the various designation levels, psychosocial factors and tasks were found using the chi-square test. Here, $p < 0.001$ is being considered statistically highly significant, and $p < 0.05$ is being considered statistically significant throughout the study.

Table 1 Demographic data of survey participants

Gender	Male	38 (100%)
	Female	0
Designation	ALP	8 (21%)
	ALP goods	10 (26.3%)
	ALP passenger	6 (15.7%)
	LP goods	5 (13.1%)
	LP passenger	4 (10.5%)
	LP mail	5 (13.1%)
Marital status	Married	33 (66.7%)
	Unmarried	5 (33.3%)

3   Results

3.1   Demographic Profile

Among the total 38 respondents, all are men (Table 1). The respondents are from the 18–62 years of age groups and across all the designations of the Loco pilots. Asst Loco pilots (ALP) were 8, Asst Loco pilot goods (ALP goods) were 10, Asst Loco pilot passengers (ALP passengers) were 6, Loco pilot goods (LP goods) were 5, Loco pilot passengers (LP passengers) were 4, and Loco pilot mail (LP mail) was 5, respectively. Respondents were mostly the pilots of goods trains (23 out of 38), and the rest (15 out of 38) were of mail (passenger) trains. All the respondents belong to Patna Jn, which is under the Danapur division of Indian Railways.

3.2   Psychosocial Factors Affecting Loco Pilots

Table 2 shows the psychosocial factors which affect the Loco pilots across the levels of designation based in Patna Jn. The statistical differences among the different demographic groups were found to be insignificant for the psychosocial factors: support from co-pilots, support from supervisors, responsibility for people and missing family time. This suggested that all the above factors are prevalent across all levels of loco pilots. There was significant low job satisfaction among the Asst Loco pilots as compared to the Loco Pilots. In addition, there was a significant difference found in working health hazard anxiety ($p < 0.05$). Loco pilots with higher designations tend to have more anxiety of getting any health issues/hazards due to their duty. For the psychosocial factor: demand of hiding emotions and depression, there was a significant difference compared to higher and lower designation levels. Lower-level loco pilots tend to have high depression levels ($p < 0.05$), and they hide their emotions more ($p < 0.05$). Under no fixed working hours ($p < 0.001$), it was found that Loco

pilots with higher designation levels tend to have fixed working hours compared to lower designation levels.

3.3 Secondary Tasks Affecting Loco Pilots

Table 3 shows the tasks which affects the Loco pilots across the levels of designation based in Patna Jn. The statistical differences among the different demographic groups were found to be insignificant for the task: signal exchange. For the tasks: blowing horn and operating vigilance switch, there was a significant difference when compared to higher and lower designation levels. Higher-level loco pilots tend to blow horn ($p < 0.001$) and operate vigilance switch ($p < 0.001$) more as compared to lower designation levels. There was a significant difference found when it comes to use of walkie talky ($p < 0.05$). Loco pilots with lower designation levels tend to have more use of walkie talky. For leaning out tasks, there was a significant difference ($p < 0.001$) when compared across the levels of loco pilot. Loco pilots with lower designation levels tend to lean out more as compared to higher levels.

4 Discussion

In this study, we found that Loco Pilots with higher designation levels have more job satisfaction as compared to lower levels. Loco Pilots with higher designation levels experienced lower workload pressure as compared to others. The anxiety of health hazards related to work was found to have more with the Loco pilots as compared to Asst Loco pilots. It was also found that high designation Loco pilots feel uneasy about relaxing and sleeping during relaxing hours as compared to Asst Loco pilots. Quality family time is compromised across all levels of designation of Loco pilots. Similar studies have been done related to the work and life of the Loco pilots [5, 8]. Signs of depression were found to have with Asst Loco Pilots, and they also tend to hide their emotions during duty hours. Similar studies found in the research paper [5] suggested that the job demands lead to affect the mental health of the Loco pilots. It was found that there were no fixed hours of working for the Loco pilots. This was discussed in the previous research papers [10]. Loco pilots can be allotted any shift of duty, and number of working hours depends upon circumstances.

It was also found that tasks like use of walkie talky, signal exchange and leaning out were frequently seen among ALP, ALP goods and ALP passenger. And the tasks like blowing horn, operating vigilance switch and also signal exchange were most frequent among designations like LP goods, LP passenger and LP mail. These tasks are found to cause musculoskeletal disorders among the Loco pilots [6]. In the study done by Subir danda and Soumya Sarkar, the RULA score for the tasks like blowing horn, operating vigilance switch, use of walkie talky and leaning out was found to be 3–4 [6], which suggested that ergonomic intervention may be required

Table 2 Designation levels with respect to psychosocial factors of loco pilots

Designation	No job satisfaction		Support from co-pilots		Support from supervisors		Work health hazard anxiety		Difficulties to relax during relax hours		Demands for hiding emotions	
	N (%)	P value	N (%)	P value	N (%)	P value	N (%)	P value	N (%)	P value	N (%)	P value
ALP	7 (87.5)	0.006*	7 (87.5)	–	7 (87.5)	–	2 (25)	0.04*	3 (37.5)	0.015*	8 (100)	0.038*
ALP goods	10 (100)		9 (90)		9 (90)		5 (50)		7 (70)		10 (100)	
ALP passenger	5 (83.3)		6 (100)		6 (100)		3 (50)		6 (100)		6 (100)	
LP goods	3 (60)		4 (80)		5 (100)		4 (80)		5 (100)		4 (80)	
LP passenger	1 (25)		4 (100)		4 (100)		4 (100)		4 (100)		2 (50)	
LP mail	1 (20)		5 (100)		5 (100)		5 (100)		5 (100)		3 (60)	

Designation	Depression		Responsibility for people		Missing quality family time		Work overload		Time pressures		No fixed working hours	
	N (%)	P Value	N (%)	P Value	N (%)	P Value	N (%)	P value	N (%)	P value	N (%)	P value
ALP	6 (75)	0.02*	8 (100)	–	8 (100)	–	8 (100)	0.02*	8 (100)	0.015*	8 (100)	0.000**
ALP goods	8 (80)		7 (70)		10 (100)		9 (90)		10 (100)		10 (100)	
ALP passenger	3 (50)		6 (100)		6 (100)		6 (100)		6 (100)		4 (66.7)	
LP goods	1 (20)		2 (40)		5 (100)		5 (100)		1 (20)		5 (100)	
LP passenger	1 (25)		2 (50)		4 (100)		1 (25)		1 (25)		0 (0)	
LP mail	0 (0)		4 (80)		5 (100)		2 (40)		1 (20)		0 (0)	

* indicates $p < 0.05$, and ** indicates $p < 0.001$

Table 3 Designation levels with respect to secondary tasks of loco pilots

Designation	Blowing horn		Operating vigilance switch		Use of walkie talky		Signal exchange		Leaning out	
	N (%)	P Value	N (%)	P Value	N (%)	P Value	N (%)	P Value	N (%)	P Value
ALP	1 (12.5)	0.000**	0 (0)	0.000**	7 (87.5)	0.001*	8 (100)	–	8 (100)	0.000**
ALP goods	2 (20)		0 (0)		10 (100)		10 (100)		10 (100)	
ALP passenger	6 (100)		0 (0)		6 (100)		6 (100)		5 (83.3)	
LP goods	5 (100)		5 (100)		2 (40)		5 (100)		3 (60)	
LP passenger	4 (100)		4 (100)		1 (25)		3 (75)		0 (0)	
LP mail	5 (100)		5 (100)		1 (20)		4 (80)		0 (0)	

* indicates $p < 0.05$, and ** indicates $p < 0.001$

for these tasks. Furthermore, task like signal exchange which was the most frequent and repeating task across the designations such as ALP (100%), ALP goods (100%), ALP passenger (100%), LP goods (100%), LP passenger (75%) and LP mail (80%) had RULA score of 5 [6], which suggested ergonomic interventions should be done soon.

Limitations of this study are the smaller number of respondents considered for the study due to the pandemic situation. Therefore, larger data could help better understanding in this area of research.

5 Conclusion

Loco pilots are one of the important crew members responsible for the safety of the train by avoiding any accidents. It is important to understand the working conditions and their mindsets across all the levels of the designations of Loco pilot. The research shows that various psychosocial factors, like job satisfaction, work health hazard anxiety, no proper sleep, depression, work pressure, no fixed hours of duty, etc., are different across the higher and lower designation levels of the Loco pilots. To improve the conditions of Loco pilots, the above problems need to be analysed and dealt with at the hierarchy level of the Loco pilots. Some factors like lack of quality time with family, support from the crew members and feeling of responsibility are consistent across all the designation levels of the Loco pilots, which can also be dealt with to improve their working conditions. Higher designation level Loco pilots perform secondary tasks: blowing horn, signal exchange and operating the vigilance switch. This research can help to understand the tasks performed and task-related psychosocial issues of the Loco Pilots.

References

1. Indian Railways homepage: https://indianrailways.gov.in/, last accessed 18 Oct 2021
2. Kumar, D., Singh, J.V., Kharwar, P.S.: Study of occupational stress among railway engine pilots. Indian J. Occup. Environ. Med. **15**(1), 25 (2011)
3. Ranjan, R., Prasad, T.: Work-life of Indian railway's drivers (loco-pilots). IOSR J. Bus Manag. **9**(2), 39–48 (2013)
4. Kant, S.R.: Life of an Assistant Loco Pilot (ALP)/Assistant Driver. All India Loco Running (2008)
5. Ranjan, R., Prasad, T.: Job Demands And Its Effects On Health: A Study on Indian Loco-Pilots (Railway Drivers). IOSR JHSS (2017)
6. Danda, S., Sarkar, S., Bepari, B., Saha, K., Lahiri, B.N.: Ergonomic assessment of secondary task performed by Indian Railways Loco Pilots (2019)
7. Ranjan, R., Prasad, T.: Working-conditions, stress and their outcomes: a review study among loco-pilots (railway drivers) in India (2014)
8. Joy, M., Krishna, M. A. R.: Family environment, emotional regulation and job stress among loco pilots of Indian Railway (2020)

9. Patna Junction railway station: https://en.wikipedia.org/wiki/Patna_Junction_railway_station. Accessed 15 Oct 2021

10. Ranjan, R., Prasad, T.: Work-Life Balance of Loco Pilots. IOSR (2016)

Instructions for the Preparation Intervention of Shoulder Load Carrier for Porters Working in Vegetable Mandi of Jabalpur

Sangeeta Pandit [ID]**, Rajat Kamble** [ID]**, Avinash Sahu** [ID]**,
Bangaru Sai Prakash** [ID]**, and Vishal Patil**

1 Introduction

Manual material handling (MMH) is human act of lifting, lowering, pushing, pulling, carrying, holding, and releasing items. In India, due to the chief labor force, MMH is a major part of material handling activity in different transportation sectors [1, 2]. One such MMH activity is found by the porters in the fruits and vegetable wholesale markets commonly known as "sabji mandi". The porters of any wholesale markets are the backbone of transportation of goods between truck and shops of a mandi. MMH exposes workers to physical risk factors. If these tasks are performed repeatedly or for a longer period of time, it can cause injuries. Main risk factors associated with the development of injuries in MMH tasks include uncomfortable postures, repetitive actions, forceful exertions, loads. The present study was led in the main wholesale vegetable and fruit markets of Jabalpur from where the fruits and vegetables were supplied to different local markets. Around 300 tons of fresh vegetables and fruits are distributed daily throughout Jabalpur city. To keep the mandi running in the early morning peak business hours, around 150 porters were involved. The porters do not follow any standard ergonomic guidelines for lifting heavy weights, and the nature of work is highly repetitive in nature. In order to earn more, during the peak hours, they carry more weights without intervals. The nature of work is highly repetitive. In order to unload the trucks, the porters carry heavy load on their heads from trucks to the shops. This causes stress in the muscles, tendons, and ligaments. This high stress led to work-related injuries and health problems among the porters resulting early retirement and financial burden on the family and society. Manual load transportation is an occupation pursued by a good population of labor forces from economically

S. Pandit (✉) · R. Kamble · A. Sahu · B. S. Prakash · V. Patil
Design Discipline, PDPM Indian Institute of Information Technology, Design and Manufacturing, Jabalpur, Madhya Pradesh 482005, India
e-mail: s.pandit@iiitdmj.ac.in

poor family background but so far it has not received the attention it deserves. Porters do tasks like lifting, lowering, pushing, pulling, carrying, holding, and delivering tons of vegetables in awkward postures that may lead to musculoskeletal disorders (MSD). Musculoskeletal disorders (MSD) are injuries or disorders of the muscles, nerves, tendons, joints, cartilage, and spinal discs [3–6]. Environmental conditions such as extreme heat, cold, noise, and poor lighting may increase workers' chances of developing psychosocial risks [7].

A study among the porters working in markets of Calcutta, India found 95% of porters reporting MSDs in the last 12 months [8]. MSDs are considered to be work-related when the work environment and the performance of work contribute significantly to their development. The causes of MSDs in the workplace are high-task repetition, forceful exertions, repetitive, or sustained awkward postures. Porters do lift heavy loads repetitively and use force to lift the heavy weights while performing these tasks, they are working in the awkward positions which may lead to the work-related musculoskeletal disorders. Another study done in traditional markets of Indonesia showed that 72% of workers who carried loads on their backs suffered from low-back pain [9]. A study done at Tehran Grand Bazaar where the hand carts being pushed or pulled by porters to the destination, the corridors of the Bazaar were found to be narrow and difficult to manage the load on the handcart, here they found the prevalence of MSDs in at least one part of the body in last 7 days was 45.2% [10]. In a study done by Narayana [11], they found reduction in incidence of MSDs in upper and lower limb among the workers in medical device assembly plant by ergonomic improvements where the participatory approach was found beneficial.

This study aims to find MSDs and ergonomic risks among the porters working in Jabalpur market and reduce the same through an effective intervention through a participatory approach to eliminate the ergonomic risks and reduce MSDs among the porters.

2 Methodology

2.1 Field Study

The study was conducted in the early morning peak hours in the main vegetable wholesale market when trucks with vegetables were unloaded. A sample of 30 workers were randomly selected for the study.

2.2 Body Discomfort Study

Body discomfort was measured in different body regions among the workers in 5-point scale rating [12].

2.3 Potential Risk Factors

Through observation and task analysis, the different ergonomic risk factors associated with the manual material handling work were noted.

2.4 Design and Selection of Shoulder Load Carrier Concept from Participatory Approach

In this method, we involved the users and motivated them to participate give their views in development of different concepts. Their views and suggestions were also considered for further improvements in the concepts.

2.5 Development of the Final Concept

Anthropometric data were used to design the final concept of the carrier, and the concept was developed keeping in mind the ergonomic principles.

2.6 Evaluation of the Concept

Participatory approach was used for the selection and development of the final concept.

3 Result and Discussion

3.1 Body Discomfort Associated with Shoulder Loading in Conventional Method

Table 1 shows discomfort in most body parts, with highest percentage in back with 85%, followed by ankle (76%), foot (76%), knee (72%), shoulders (72%), wrist (71%), and lower arm (70%) from MMH involved in transporting of vegetable gunny bags from trucks to shops in vegetable mandis.

Table 1 Interview results for percentage of pain in different body parts

S. No.	Body part	Percentage (%)
1	Shoulder	72
2	Upper arm	69
3	Lower arm	70
4	Wrist	71
5	Thigh	64
6	Knee	72
7	Ankle	76
8	Foot	76
9	Neck	63
10	Back	85

3.2 Potential Risk Factors

The following risk factors were identified

- Awkward posture while transporting
- High-load stress on neck shoulder and wrists
- Slipping of gunny bags due to bad grip.

3.3 Design and Selection of Shoulder Load Manager

The following design needs were found

- Distribute the shoulder load over the body
- Improving the postures
- Eliminate the stress in arms and wrists.

Different concepts were generated in consideration with the view of the users, and the final concept was decided by using a participatory approach. Figure 1 shows generated concepts along with the final concept.

3.4 Development of Final Concept

Shoulder load carrier was divided and fabricated in three parts. Back frame to hold the load in position and support the shoulder, a curved shoulder frame was provided to distribute the load evenly on shoulder with better comfort. Chest area strap is provided to prevent the gunny bag from falling, as well as to dire tribute its load evenly and waist area strap is to support the lower limb.
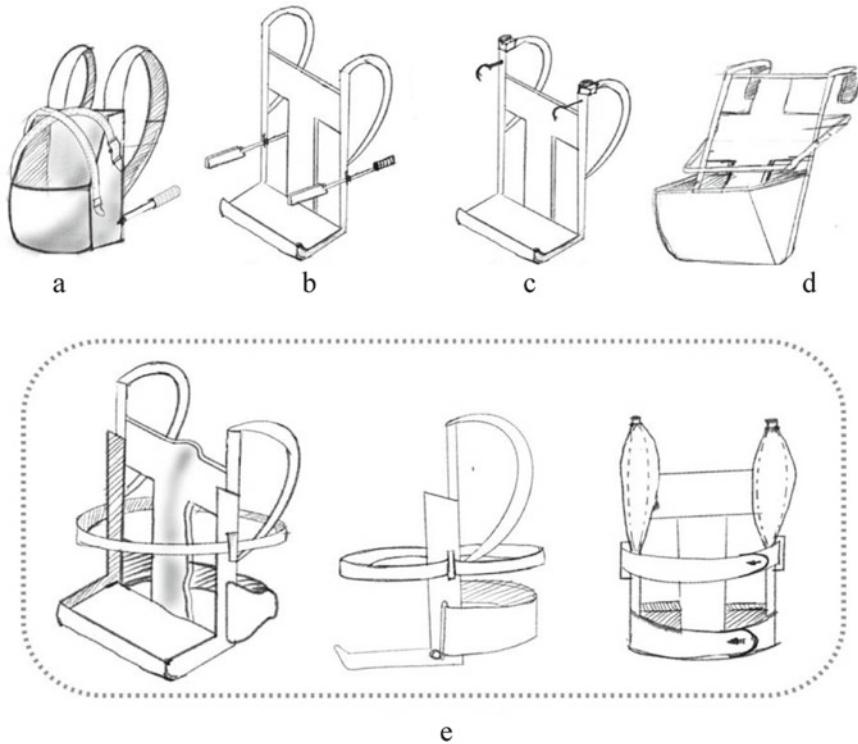
Fig. 1 Different concepts: **a** concept a, **b** concept b, **c** concept c, **d** concept d, **e** isometric view, side view, and front view of the final concept

Weight of the equipment and human anthropometric data were considered for the development and fabrication of the final concept. The dimensions of the concept and its features were considered as per anthropometric data for following body parameters: Bi-acromion, Bi-deltoid, waist, vertical trunk, and maximum body breadth. The decided dimension is shown in Table 2.

3.5 Concept Selection and Evaluation of Final Concept

Through Pugh's selection method, concept 5 was selected as shown in Table 3 and was further developed.

The selected concept of shoulder load manager was then fabricated as per dimensions were done through participatory approach by keeping in mind the ergonomic risk factors and the anthropometric data and the different features such as ease of off-loading of weight, weight distribution in shoulders, usability, and portability. The final concept is shown in Figs. 2 and 3.

Table 2 Features and dimension for shoulder load carrier

Features of the final concept	Dimensions mm	Functionality
Height of the frame from base to shoulder	410	Proper weight distribution in upper limbs
Width of the frame	300	Support for carrying weight
Width of the base	500	Holds the gunny bag in position
Length of the base	500	Holds the gunny bag in position
Shoulder curvature	60°	Proper and comfortable weight distribution over the shoulders
Strap1 (sturdy flexible material with hooks and loops ends)	500	Wraps around the gunny bag and fastens at the chest area with the help of hooks and loops
Strap2 (sturdy flexible material with hooks and loops ends)	250	Wraps around the waist area with the help of hooks and loops

Table 3 Pugh's concept selection method

Criterion	Concept 1	Concept 2	Concept 3	Concept 4	Concept 5
Usability	−	+	−	−	D
Ease of off-loading	−	−	+	+	A
Distribution of weight	+	−	−	−	T
Portability	0	0	−	−	U
Total "+"	1	1	1	1	M
Total "−"	2	2	3	3	
Total "0"	1	1	0	0	
Total	−1	−1	−2	−2	

(a) (b)
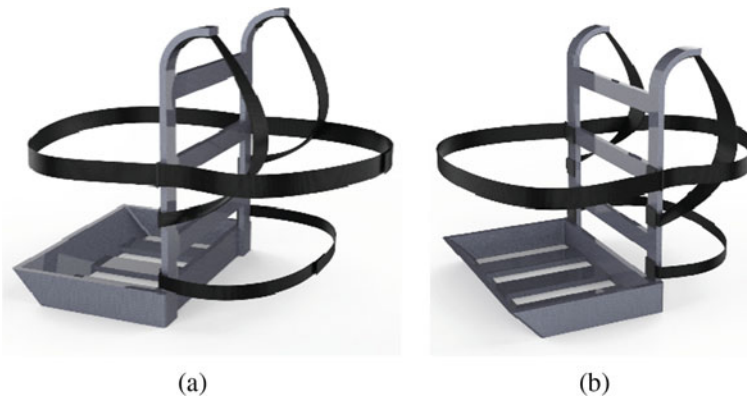
Fig. 2 a and **b** Isometric views of shoulder load carrier
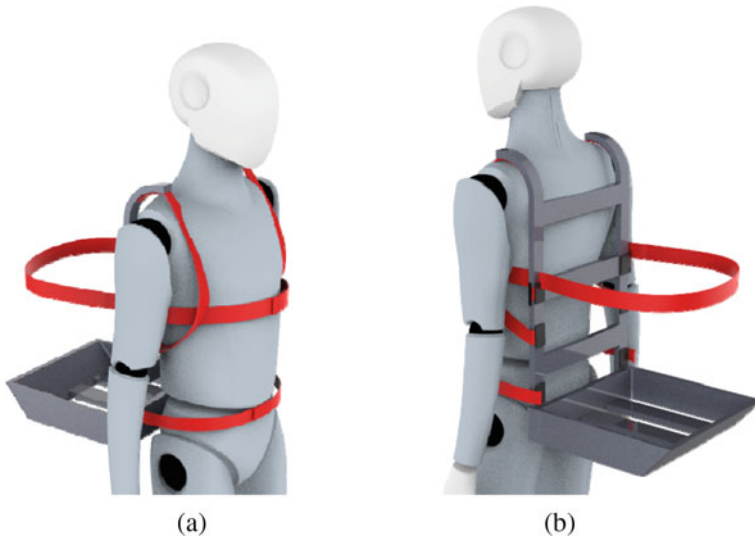
Fig. 3 **a** Front isometric view and **b** back isometric view of shoulder load carrier in use

Through participatory approach and evaluation of the proposed design as shown in Table 4, it was noted that the improved design of the shoulder load carrier would successfully reduce the risk factors such as awkward posture while transporting, high-load stress on neck shoulder and wrists and slipping of gunny bags due to bad grip, thus reducing pain in arms, shoulder, neck, and back.

Table 4 Evaluation of the proposed solution

Risk factors	Features implemented to solve the problems
Pain in arms and wrist	Proper weight distribution in upper limbs
Awkward back postures	Support for carrying weight
Slipping of loads	Holds the gunny bag in position
Pain in shoulders	Proper and comfortable weight distribution over the shoulders
Leaning of loads	Wraps around the gunny bag and fastens at the chest and waist area with the help of hooks and loops
Poor grip in holding	Belts and straps used for holding the load in position, keeping hands free of loads

4   Conclusion

From this study, it was concluded that the proposed design could successfully reduce the ergonomic risks involved in the MMH task, thus reducing the pain in the body parts such as wrist/hands, shoulders, neck, and back.

References

 1. McDermott, H., Haslam, C., Clemes, S., Shaw, K., Williams, C., Haslam, R.: Manual handling training: an investigation of current practice (2009)
 2. Amol, Pandit, S.: New hand-cart for old-Delhi whole sale market designed and engineered using generic product development process. Indian J. Pure. Appl. Phys. **58**, 698–705 (2020)
 3. Gangopadhyay, S., Das, T.: An ergonomic study on the onset of mental fatigue among the load handling workers of a central market area in Kolkata. Work **41**(Supplement 1), 2467–2471 (2012)
 4. Skovlund, S.V., Bláfoss, R., Sundstrup, E., Thomassen, K., Andersen, L.L.: Joint association of physical work demands and leg pain intensity for work limitations due to pain in senior workers: cross-sectional study. BMC Public Health **20**(1), 1–10 (2020)
 5. Rose, L.M., Eklund, J., Nilsson, L.N., Barman, L., Lind, C.M.: The RAMP package for MSD risk management in manual handling—a freely accessible tool, with website and training courses. Appl. Ergon. **86**, 103101 (2020)
 6. Kamble, R., Sahu, A., Pandit, S.: Occupational ergonomic assessment of hand pain symptoms among Bagh hand block print artisans of handicraft textile industry in Madhya Pradesh, India. Int. J. Occup. Saf. Ergon. 1–26 (2021)
 7. Sarkar, K., Dev, S., Das, T., et al.: Examination of postures and frequency of musculoskeletal disorders among manual workers in Calcutta, India. Int. J. Occup. Environ. Health **22**(2), 151–158 (2016)
 8. Muslim, K., Nussbaum, M.A.: Musculoskeletal symptoms associated with posterior load carriage: An assessment of manual material handling workers in Indonesia. Work **51**(2), 205–213 (2015)
 9. Chinichian, M., Mehrdad, R., Pouryaghoub, G.: Manual material handling in the Tehran Grand Bazaar, a type of traditional heavy work with musculoskeletal effects. Arch. Environ. Occup. Health **76**(1), 31–36 (2021)
10. Narayana, M., Rudoiph, L.: Ergonomic improvements in a medical device assembly plant: a field study. In: Proceedings of Human Factor and Ergonomic Society, pp. 812–816 (1993)
11. Deros, B.M., Daruis, D.D., Ismail, A.R., Sawal, N.A., Ghani, J.A.: Work-related musculoskeletal disorders among workers' performing manual material handling work in an automotive manufacturing company. Am. J. Appl. Sci. **7**(8), 1087 (2010)
12. Corlett, E.N., Bishop, R.P.: A technique for assessing postural discomfort. Ergonomics **19**, 175–182 (1976)

Design Intervention in the Manually Push Cart Used for Carrying the Vegetables in Hyderabad

Chelapareddi Anshuman Rao, Bangaru Sai Prakesh, and Sangeeta Pandit

1 Introduction

In India, so many street vendors live their lives by selling goods in pushcart [1]. These vendors provide a wide range of goods and commodities to the urban populations at reasonable prices and convenient locations. The type of goods they sell was daily needed like vegetables, fruits, fish, and snacks in occasional needs they sell goods like flowers and ready-made garments. The type of cart street vendors used for selling the good comes under non-motorized vehicles which were economical and environment friendly [2]. These pushcarts may be found everywhere in our country, from train stations to street foods to vegetable vendors. But, the cart which they were being used has the same features and mechanical principles developed by our ancestors.

Among the street vendors, the maximum percentage of people sells fruits and vegetables in pushcart [1], and the load carried on the vegetable pushcart was found to be approximately 200 kgs, and the distance covered usually varies between 5 and 10 km/day. The problem with a pushcart was the pushing action; the cart was designed in such a way that the vendor had to bend his or her upper body to push the cart which lead to work-related musculoskeletal disorders (WMSD), and there was no proper handle to the pushcart which could lead to carpal tunnel syndrome.

A street vendor comes under an unorganized sector (informal). It was discovered that the unorganized group of workers suffered from greater musculoskeletal disorders than the organized group of workers, particularly in manual material handling [3]. As vegetable vendors are from an unorganized sector, they face problems related to price fluctuation goods, street vendors' eviction. One of them is pushcart design which is not ergonomically designed and outdated.

C. A. Rao · B. S. Prakesh · S. Pandit (✉)

Department of Design, Indian Institute of Information Technology Design and Manufacturing Jabalpur, Jabalpur, Madhya Pradesh 482005, India

e-mail: 1914003@iiitdmj.ac.in; s.pandit@iiitdmj.ac.in

Studies have shown that people related to the pulling and pushing operation of heavy loads are countering with musculoskeletal disorders (MSDs) [4]. Vegetable vendor does a lot of manual material handling which lead to occupation fatigue. To reduce the MSDs in pushing the cart, there are many factors [5] like handle orientation (Height of the handle and inter-handle distance); it is one of the main factors [6, 7] as it only touchpoint (interaction) between vendor and cart; other factors are wheel diameter, braking, load weight, moving direction, motion phase, and floor type. Most of the studies were done related to the indoor environment (industries/factories) mainly for products like trolleys [6–8]. Research should be conducted on the vegetable cart, users (vendors), their working environments (effect of each season), and finally floor type (different road terrains).

- Using hierarchical task analysis and posture analysis, identify the tasks performed by the vegetable vendor and identify risk level in each task.
- Using questionnaires, interviews, and observation methods to understand the primary cause of the problem and other information about vendors.
- Finally, from an ergonomic standpoint, design the new cart.

2 Methodology

The data were collected using a few methods, namely hierarchical task analysis, postural analysis followed by questionnaires, interviews, and observation. Phase 1—hierarchical task analysis of various tasks was observed and recorded for study, with the help of mobile camera photographs, and videos were captured for postural analysis and anthropometry analysis. The posture analysis has been done with the help of a rapid entire body assessment method. Phase 2—the questionnaires were prepared for the vegetable vendors to get the basic information, and then, the interview was focused and conducted mainly with vegetable vendors and the manufactures. Finally, observation was done without disturbing any work, while the cart puller was performing to see how they perform the task of pushing the cart.

2.1 Hierarchical Task Analysis (HTA)

The first step in understanding the job done by a vendor was to know about the different tasks performed by him to achieve daily goals. Hierarchical task analysis is one of the best techniques for task analysis in a variety of domains and applications [9]. The process can be carried out by requesting the vendor to characterize their job in terms of sub-tasks or by personally witnessing the vendor do the task. This method help in finding task, sub-task done by the vegetable vendor clarity. Every sub-goal was given a unique integer number in order. Every task was photographed for future study purposes. The photos are captured using mobile (SAMSUNG M51).
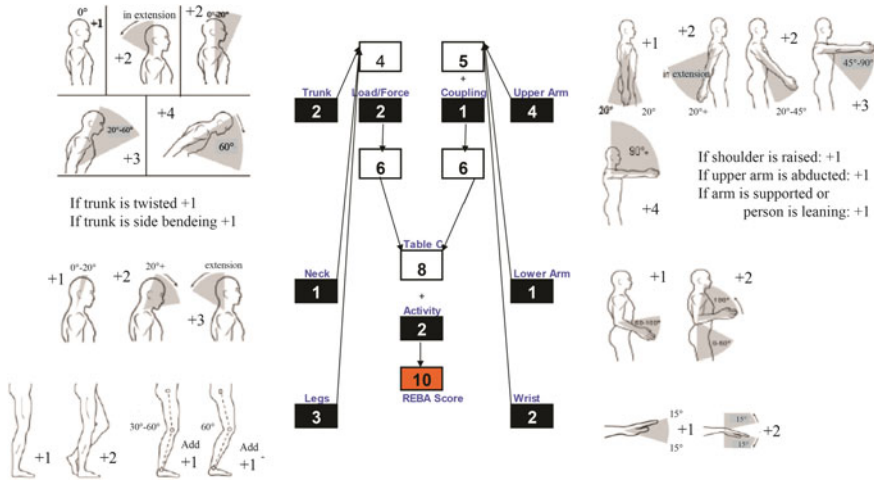
Fig. 1 REBA worksheet

2.2 Posture Analysis

Section 2 involves observation posture analysis using rapid entire body assessment (REBA). REBA was chosen because of its ability to analyze the complete body at the same time, addressing more characteristics (than Ovako Working Posture Analysis System or Rapid Upper Limb Assessment) [10] which is an important factor in this study. It is a tool used to assess the risk of musculoskeletal disorders (MSDs) associated with a specific task within a job, and results are obtained using a single sheet as shown in Fig. 1. The postures were been analyzed in kinovea® software which is an open-access software for postural analysis. This is a valid and reliable open-access software for postural analysis. Photography and video tape have been used in this process which is captured using a mobile phone (SAMSUNG M51). Finally, REBA scores generated give an indication of the level of risk and urgency with which action should be taken or not.

2.3 Questionnaire

The questionnaire has been asked to the vegetable cart vendors who use pushcart on daily basis. The questionnaire has been done face to face with structured questions related to usability and other aspects of the cart. The answers were being recorded using the mobile phone app (voice recorder); later, the answer has been analyzed and synthesized. The questionnaire is extensively used in surveys and to gather basic information from user which sometimes provides us with some deep insights about users [11].

2.4 Interview

The interviews were conducted on vegetable cart vendors. It has been done face to face the answers were being recorded using the mobile phone app (voice recorder). The type of questions used was open-end questions and contingency questions (cascade format) which elicits the user's perspective on a specific task. Each user has a different point of view over a particular problem. Interviews are very closely related to questionnaires as well as being linked with observation [12]. With help of an interview, one could identify the root cause of the problem.

2.5 Observation

Observation helps us to get insights that were neglected by the user. The vendors were observed without their knowledge and photos/videos were taken while doing different actives in their working environment. The observation was done on multiple users during their working hours. In the book of [13], observation allows the researcher to study users in their natural setting without their behavior being influenced by the presence of a researcher. The techniques used were direct and non-participation observation.

3 Results

For the completion of our study, the major group of people who participated were end-user, i.e., the vegetable vendors. They were our main test focus as they are the people who operate the cart. 10 vegetable male vendors helped us with our research, and they aged between 22–55 (all male). First, the hierarchical task analysis (HTA) had been done, which helped us to understand the task flow. The next logical step was to get their postural information while working which we used rapid entire body assessment (REBA), and the score's come out to be high-risk level, results also show that they are subjected to harsh pain and could lead to work-related musculoskeletal disorders (WMSDs). Then started research with questionnaires followed by interviews. This helped us gain the vendor's trust and we got vital information. Then, we used a direct observation technique to identify potential risks in vendors operations that may result in work-related musculoskeletal disorders (WMSDs).

Fig. 2 Hierarchical task analysis
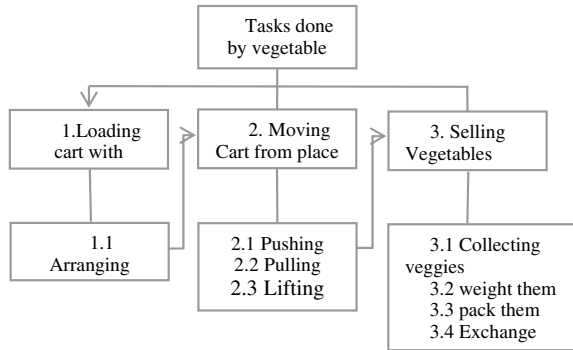
3.1 Hierarchical Task Analysis (HTA)

Vendors were required to describe their job in terms of sub-task operation and plans in this section. A total of eight significant tasks has been identified. HTA of vendors flowchart was as shown in Fig. 2. HTA has provided detailed task descriptions to clarify the task characteristics at each stage. Aside from providing clarity for better posture analysis, HTA has allowed us to distinguish the beginning and end of the movement performed by the vegetable vendor.

3.2 Posture Analysis

The working postures of the eight tasks were recorded using a mobile camera. Then, stick figures were extracted from photographs as shown in Fig. 3. With help the stick figures, tasks were analyzed using kinovea® software which is an open-access software for postural analysis. The scores are given in Table 1.

From Fig. 4, posture analysis of the 5 tasks named (1) Arranging vegetables in the cart, (2) pushing, (3) pulling, (4) lifting, (5) collecting vegetable in the basket were under the high severity zone. This could lead to musculoskeletal disorders (MSD).

The MSD among vegetable vendors could be reduced by developing a new cart from an ergonomic standpoint. Vendor's deeper insights, needs, and objectives must be known before creating a new cart. Questionnaires, interviews, and observation are excellent approaches to understanding end-users.

3.3 Questionnaire

The structured questionnaire was used to get the basic information about the cart pullers. The main reason to use a questionnaire is to ask the same questions with a
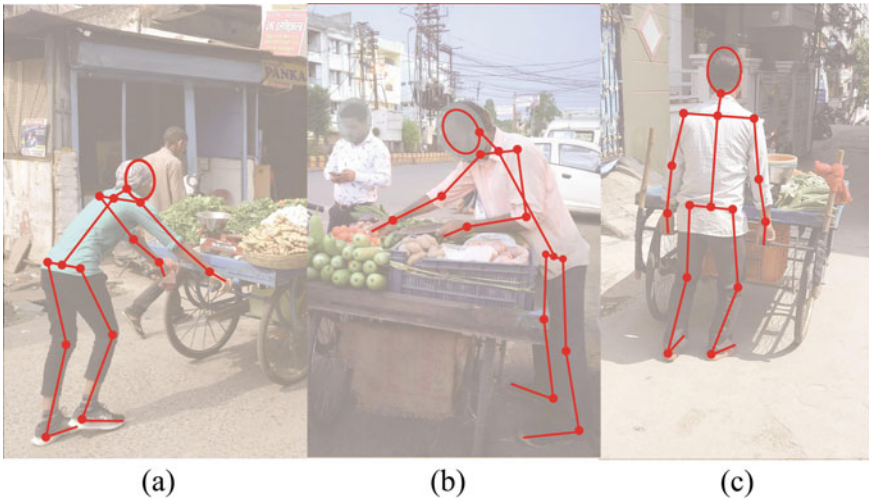
Fig. 3 Stick figures of different task postures: **a** pushing, **b** collecting vegetables, **c** lifting

Table 1 REBA scores of the vegetable vendor

Task no.	Description	Task type	Frequency	Duration	HTA code	REBA score
1	Arranging vegetables in cart	M	1/day	10–20	1.1	9
2	Pushing	M	Always	–	2.1	11
3	Pulling	M	Sometimes	–	2.2	9
4	Lifting	M	Always	5 s	2.3	10
5	Collecting vegetables in basket	M	As per order	2–5	3.1	8
6	Weight veggies	M	1/order	1–2	3.2	3
7	Pick them	M	1/order	< 1	3.3	3
8	Exchange money/veggies	M	1/order	1–2	3.4	5

M stands for manual, Duration is in minutes

bunch of people to get a different answer, and after getting the answer, we can gather the data. The questionnaire consisted of some simple questions, but the answer we got gave to quite a clear insight into the life of the end-user. There were 10 questions in the questionnaire, and the average answers are as follows in Table 2.
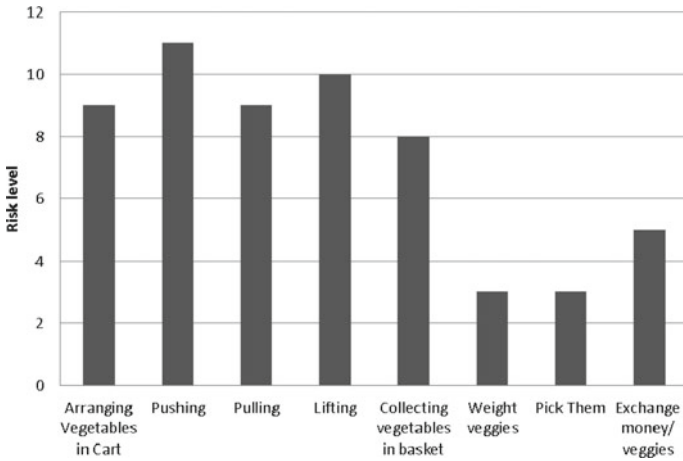
Fig. 4 Shows the risk level of each task

Table 2 Results of questionnaire

Sample size	10
Age	22–55
Cart pushing experience	2 months—10+ years
Distance travel daily	5–10 km
Good sells in cart	Vegetables and fruits
Max weight of goods they prefer	200 kgs
Working time	6–15 h
Income	150–300 per day
Body pain specifically	Hand, shoulders, back
Parking of the cart	Maximum people rent the cart due to parking problems They try to park in an area (roadside) where no one will complain
Maintenance of the cart	Filling air to tires Bearing lubrication

3.4 Interview

An interview is familiar to the user as a technique. Semi-structured combined with the face-to-face nature is likely to elicit more information. The information we got from interviews of the vendor gave us a common insight into the deep-rooted problems which they were being faced. The interview findings are as follows.

- A vegetable pushcart was designed for pushing (though one knows pulling is better than pushing).

- The vendor also wants to push instead of pull due to security issues, protecting vegetables from falling down, and also for easily controlling cart will turn.
- Pushing the cart on the crowded street was difficult due to vehicles and people crossing in front of the cart they have to stop the cart manually (no brake system in cart).
- Max weight vendor comfortable to push is 200 kg of goods + weight of the cart.
- The vendor finds it difficult for lifting the cart while turning.
- No problem related to vegetable storage (Cooling storage system) because they sell the vegetable within 1 or 2 days (max case within 1 day only).

3.5 Observation

Observation is the method of monitoring people's behavioral patterns without questioning or interacting with them. The technique used was direct and non-participation observation without interrupting any end-user doing their task. There were a lot of photographers and videos were taken so that they could be analyzed again and again to find the minutest details possible. The results are as follows:

- No handle to cart, vendors use two wooden sticks at the corner of the cart to push.
- They don't have a place to keep personal things (Lock system).
- They sometimes sit on the cart and sell.
- Lighting problem will be selling goods at night.
- The vendor uses plastic cover to cover vegetables to protect goods from rainfall and dust.
- They use wet gunny bags in summer to protect vegetables from heavy temperature.

Finally, ergonomics-related issues discovered through questionnaires, interviews, and observation are highlighted. (1) The cart was not designed with an appropriate handle, so the vendor had to bend his upper body to push the cart. (2) To change direction for turning the cart from one corner of the road to the other, the seller must stop the cart and lift the cart for one side, and due to barriers and road conditions, the vendor must frequently turn the cart on the road. (3) Collecting vegetables from corners requires him to bend frequently, resulting in back pain. Consider the following issues while constructing a new cart to help reduce risk leve/MSDs.

4 Design Methodology

4.1 Conceptual Design

With respect to the need and input of vegetable vendors through questionnaires, interviews, and observation, new model has been developed through, the conceptual design followed by 3D modeling, rough prototype, and fabrication process which is

Fig. 5 Conceptual design of proposed vehicle
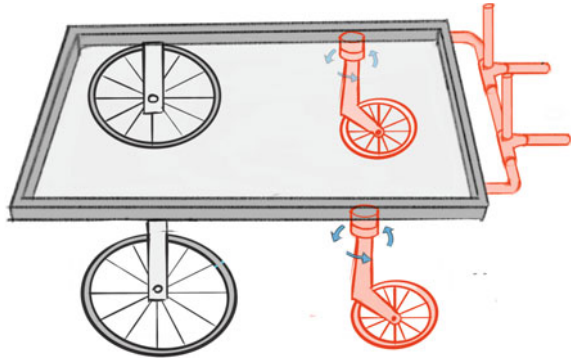
going on. All the components and design of the cart were explained in the drawing, so refer Fig. 5 of the vegetable cart and features of the project listed below.

A new pushcart design will be having.

- The adjustable handle.
- Stroller wheels for turning the cart.
- Increasing primary and secondary zone.
- Ergonomically designed using anthropometry dimensions.

4.2 Detail Design

The detail design was primarily concerned with anthropometric data of Indian males [14]. The new measurements are more suited to all people of various sizes as shown in Table 3.

Table 3 Anthropometric dimension cart body and handle

Part/area of measurement	Existing dimension	New dimension (mm)	Parameter—percentiles
Length of the cart	1500 mm	1549	Span—5th percentile
Width of the cart	1100 mm	954	Mid-position length—5th percentile
Height of the cart (ground level)	762 mm	779	Lower position height—50th percentile
Length of the handle	–	959	Span akimbo—95th percentile
Handle thickness	–	56	Grip inside diameter—95th percentile
Height of the handle (ground level)	–	945	Elbow—5th percentile

Fig. 6 3D render

4.3 Computer-Aided Design (CAD)

Developed 3D CAD Model as shown Fig. 6 software's used was Rhinoceros 3D (Rhino 6) and KeyShot 8.

4.4 Rough Prototype

Finally, the rough prototype was made on the scale of 1:12 ratio as shown in Fig. 7. The model was made using cart board, plaster of Paris, glue gun, acrylic colors, and two ball bearings.

Fig. 7 Scale model of prototype

5 Discussion

1. Results from posture analysis (REBA) show that tasks like pushing, stopping, and lifting the cart are under high-risk level.
2. In user research, we found there is a need for a handle, brakes, modular design (for parking).
3. Users are facing problem related to environmental conditions like rainfall, high temperature in the summer season, and also due to road conditions.
4. Studies have shown that a lot of research was going on designs related to installing a cooling system for preserving vegetables and fruits which is not required. Because a lot of time vendor buy goods which can be sold with 1 or 2 days, hence, it not their primary requirement.
5. As shown in Fig. 8, the new working postures are neutral in comparison (compare Fig. 8a, b, c, d, e and f), hence, the new design will aid in the reduction of work-related musculoskeletal disorders.
6. With minimal investment, an existing cart can be transformed into a new cart design.
7. The handle design is adjustable; it can be adjusted according to user body dimensions. Adjustable design is because maximum vendor rent the cart. So, it is impossible to rent the same cart every day.
8. A new handle design with a brake function can be introduced, which will be handy for the road uphill or slope as well as in traffic.
9. It is easy for vendors to turn the cart from one corner of the road to another road because of rear stroller wheels mechanism.
10. The cart's upkeep and production are straightforward and simple to put together.
11. Fabrication and testing with end-user are yet to be done.
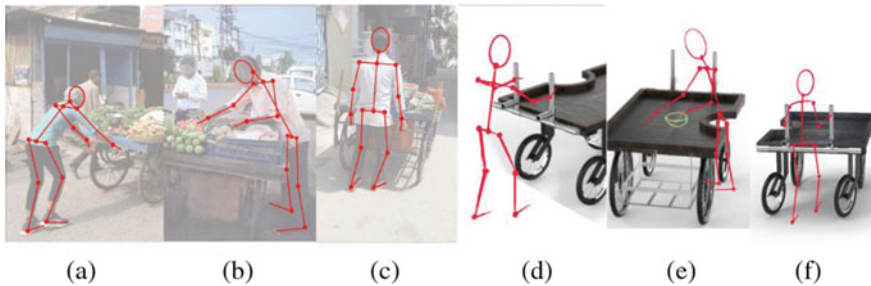
Fig. 8 Posture comparison between existing design with new design: **a** existing pushing posture, **b** existing collecting vegetable posture, **c** existing lifting posture, **d** new pushing posture, **e** new collecting vegetable posture, **f** new lifting posture

6 Conclusion

From the study it was observed that the vendors are facing musculoskeletal problems due to awkward posture while performing the task. The new cart design is more comfortable, with steering capabilities, a modular design handle, and a braking mechanism. All of these characteristics may lower the risk of work-related musculoskeletal (WMSD), which is an injury or disorder of the muscles, nerves, tendons, joints, cartilage, and spinal disks. Limitations are still fabrication, and test steps are going on. Finally, there are other problems that have to be solved like related materials of cart how could one reduce the weight of cart by replacing with other material, how to implant electric motor in cart with low cost-effective and protective cover which can protect vegetable and fruits from sun-rise, rainfall as well as dust.

References

1. Samarpitha, A.: Fruit and vegetable street vendors in urban informal sector in Hyderabad, India. Int. J. Curr. Microbiol. Appl. Sci. **8**(11), 967–973 (2019)
2. Amol, Pandit, S.: New hand-cart for old-Delhi whole sale market designed and engineered using generic product development process. Indian J. Pure Appl. Phys. **58**, 698–705 (2020)
3. Gangopadhyay, S., Das, S., Sarkar, I., Sarkar, K.: Pshychosocial factors in the development of musculosketal disorder among manual material handling workers of organized and unorganized sectors of West Bengal. J. Hum. Ergol. **46**, 1–8 (2017)
4. Lee, J., Nussbaum, M.A., Kyung, G.: Effects of work method during dynamic pushing and pulling. Int. J. Ind. Ergon. **44**, 647–653 (2014)
5. Jung, M.C., Haight, J.M., Freivalds, A.: Pushing and pulling carts and two-wheeled hand trucks. Int. J. Ind. Ergon. **35**, 79–89 (2005)
6. Renick, M.L., Chaffin, D.B.: An ergonomic evaluation of handle height and load in maximal and sub maximal cart pushing. Appl. Ergon. **26**(3), 173–176 (1995)
7. Ohnishi, A., Takanokura, M., Sugama, A.: Evaluation of interhandle distance during pushing and pulling of a four-caster cart for upper limb exertion. Saf. Health Work **7**, 237–243 (2016)
8. Tow, C.Y., Kuen, K.W.: Force evaluated and comparison for supply trolley in a hospital. Procedia Manuf. **3**, 1861–1864 (2015)
9. Stanton, N.A.: Hierarchical task analysis: development, applications, and extension. Appl. Ergon. **37**, 55–79 (2006)
10. McAtamney, L., Hignett, S.: Rapid entire body assessment. In: Handbook of Human Factors and Ergonomics Method, pp. 8–1 (2005)
11. Pushpanjali, K., Piddennavar, R., Mohan, M.: Art and science of questionnaire development. J. Indian Assoc. Public Health Dent. **2011**(18) (2011)
12. Young, M.S., Stanton, N.A.: Applying interviews to usability assessment. In: Handbook of Human Factors and Ergonomics Methods, pp. 29–1 (2005)
13. Baber, C., Stanton, N.: Observation as a technique for usability evaluation. In: Usability Evaluation in Industry, pp. 85–94 (1996)
14. Chartrabarti, D.: Indian Anthropometric Dimensions for Ergonomic Design Practice. National Institute of Design, India (1997)

Critical Posture Analysis During the Handling of Water Barrel with and Without Exoskeleton

R. Naveen Kumar, S. Shankar, R. Nithyaprakash, T. V. Srinivasan, R. Sunil Kumaur, and A. K. N. Venkatachalan

1 Introduction

The water barrel business is so competitive; it had been dominated in the water supply market for the past few years. The main marketing competition is over appealing packaging and labelling, which attracts a large customer base [1]. But in developing countries, a lack of drinkable water is still a major cause of illness [2]. The employees in various industries perform activities that involve awkward work posture [3–5]. Employees working in awkward work posture had complain of MSD [6]. MSD is one of the manual handling injuries that can have substantial consequences for both the company and the injured person [7].

On the other hand, the action of handling, lifting, moving and carrying items without the use of mechanical instruments is known as manual material handling (MMH) [6]. Apart from weight of the object, other factors like the frequency of lifting, posture during loading and unloading and holding the weight manually for prolonged period of time are also found to be correlated with occurrence of MSD [8, 9]. Instead of physically forcing the worker's physiology to adjust the work, ergonomics tries to build the workplace such that it is suited according to the demands and physical capacities of the workers [10]. The use of ergonomic values will aid in the improvement of worker performance and productivity, as well as support the operator in feeling safe and comfortable [11].

Through pilot study conducted among the water barrel delivery workers in Perundurai, Tamil Nadu, we found that operation of water barrel delivery system takes place as follows. Initially, water barrel company receives request from customer

R. N. Kumar (✉) · T. V. Srinivasan · R. S. Kumaur · A. K. N. Venkatachalan
Department of Mechanical Engineering, Kongu Engineering College, Erode, Tamil Nadu, India
e-mail: nawinerd@gmail.com

S. Shankar · R. Nithyaprakash
Department of Mechatronics Engineering, Kongu Engineering College, Erode, Tamil Nadu, India

from different location within the range of 5–10 km. The order ranges from 1–5 water barrels; once they received the order for minimum 20–30 barrels, they will begin their distribution to the individual customers. The frequency of delivery varies from 2–3 times per day based on the order received. During the delivery, delivery agent loads the barrel from the warehouse and transports to the customer location and unloads from the truck. The activity of loading, carrying and unloading water barrels on a flat surface or upstairs falls under the category of MMH. These activities involve awkward work postures to be carried out and result in MSD. From the literatures, it is found that there is no research conducted to improve manual handling of water barrels with the help of exoskeleton. The study's goal is to examine work postures and manual material handling in the water barrel handling process to prevent musculoskeletal problems caused by awkward work postures by using REBA and MAC Tool.

2   Methodology

The study of loading and unloading, carrying on a flat surface and carrying upstairs of the water barrel was carried out in the Kongu Engineering College campus, Erode, Tamil Nadu, India. Using the REBA method, the work postures were identified in the study, and with the MAC Tool method, the study was evaluated.

The various key indications considered in the MAC Tool method were duration of manual handling operation, force exertion's duration, type and frequency, movement and position of the hands and arms, force transfer, grip conditions, working conditions, body posture and work organization [12]. The variables considered in REBA were neck, trunk, legs, upper arms, wrist, lower arms, load and coupling [13].

The work postures during loading and unloading and carrying of a water barrel on a flat surface and climbing upstairs were assessed using REBA and were evaluated using MAC Tool. In REBA, if the activity score is more than 8, it is considered as a high-risk level and the action level is 3. In MAC, if the activity score is more than 12, the action is demanded shortly and the action level is 3. The work which falls under the category will be recommended for developments. By providing assistive device or redesigning the work station according to the work activity, the development in work posture of the workers considering the ergonomics is recommended.

2.1   Rapid Entire Body Assessment (REBA)

To evaluate manual handling of water barrels without exoskeleton, the work activity was photographed using Samsung isocell s5kg m2 sensor 48 mp and f/2.0 lens to collect the data. Then, by using the REBA the work was assessed. There are seven steps to be carried out for the REBA method to analyse the work posture [13]. The first step is to get the score in 'table A' according to the trunk, legs and neck angle of

Table 1 REBA work posture assessment

REBA final score	Risk level	Level	Action
1	Negligible	0	None required
2–3	Low	1	May be required
4–7	Medium	2	Required
8–10	High	3	Required soon
> 11	Very high	4	Required now

the worker's posture. The second step is the sum the score of 'table A' with the load score to arrive at 'score A'. The third step is to obtain 'table B' values by considering the lower arms, upper arms and wrist angle of the worker's posture. The fourth step is to sum the score of 'table B' with the coupling score to obtain 'score B'. The fifth step is to note the 'score A' and 'score B' in 'table C'. The sixth step is to sum the values in 'table C' to arrive at 'score C'. The seventh and last step is to consider 'score C' to assess the level of risk of the work postures. The same steps are carried out for manual handling of water barrel with exoskeleton by ergonomic work posture simulation using CATIA software [14]. Table 1 shows the REBA method work posture assessment classification [13].

2.2 Manual Handling Assessment Chart Tool (MAC Tool)

To identify the risk in manual handling, the MAC Tool was developed. By considering the team handling, the carrying process and lifting and lowering the common lift factors can be assessed by the researchers [12]. In this method, four colour codes are used to list the 11 risk factors in manual handling. The colour code Green:G stands for low risk, Amber:A stands for medium risk, Red:R stands for risk immediate action demanded, and Purple:P stands for high risk. To evaluate manual handling of water barrels without exoskeleton, the factors such as weight or frequency of the load, the waist and the arms distance, the position of the load being lifted, body's rotation or bending to the sides, grip type, body condition during the task, floor level regarding its flatness or pollution, other environmental factors, coordination of muscles in lifting, distance of load transfer and the barriers in the path are noted with the help of data taken for REBA analysis. Same factors are considered for manual handling of water barrels with exoskeleton by ergonomic work posture simulation using CATIA software [13]. Table 2 shows the MAC method score, reforming act and the act class [6].

Table 2 MAC method risk level determination and reformation steps

MAC score	Reforming act	Class
0–4	No act demanded	1
5–12	Act demanded in the near future	2
13–20	Act demanded shortly	3
21–31	Act demanded immediately	4

Fig. 1 Exoskeleton design
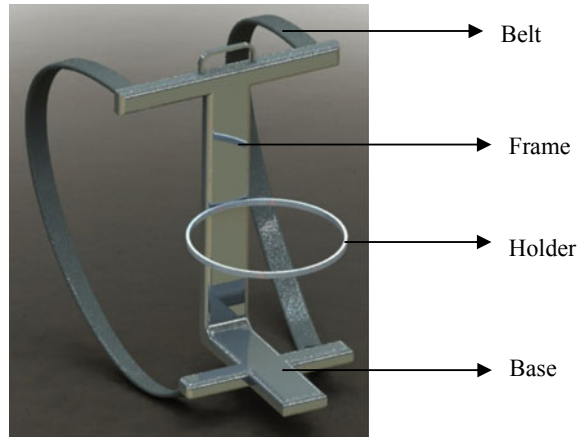
2.3 Design of Exoskeleton

To carry out the tasks of handling the water barrel, an exoskeleton is designed. Figure 1 shows the model of an exoskeleton. It has a J-shaped structure that acts as spinal support and T-like structure at the bottom to place the water barrel. The water barrel is supported by a ring-like structure and carried with the help of Sternum Strap. Instead of the L shape, the J shape is used to reduce the factor of failure. This exoskeleton is weightless and can withstand the weight of a water barrel. It will minimize the work of the person and reduce the consequence such as musculoskeletal disorder compared to manual material handling [5]. The exoskeleton is designed using SolidWorks design software.

3 Result and Discussion

3.1 Rapid Entire Body Assessment

For moving water barrel from one place to another, it involves three activities such as loading and unloading, carrying on a flat surface and carrying upstairs. Using

Table 3 Literal depiction of REBA assessment

Job	REBA final score	Risk level	Level	Action
Loading and unloading	12	Very high	4	Required now
Carry on a flat surface	10	High	3	Required soon
Carry upstairs	11	Very high	4	Required now

the REBA method, the activities were assessed. The Rapid Entire Body Assessment result is shown in Table 3.

Based on Table 3, two activities fall into action level 4 and one activity in action level 3. The action level 4 activities are at a very high-risk level, and the action level 3 activity is at a high-risk level. The activity of loading and unloading the water barrel is in action level 4 which is a very high-risk level, and development action is necessary now. The activity of carrying the water barrel is in action level 3 which is at a high-risk level, and development action is necessary soon. The activity of carrying the water barrel upstairs is in action level 4 which is a very high-risk level, and development action is necessary now.

3.2 Manual Handling Assessment Chart

The same activities which are assessed using REBA analysis are evaluated with MAC Tool method. Table 4 shows the assessment result of MAC Tool.

Based on Table 4, the three activities fall under action class 3. The process of loading and unloading the water barrel falls under action class 3, and the development action is demanded shortly. The process of carrying the water barrel on a flat surface is in action class 3, and the development action is demanded shortly. The process of carrying the water barrel upstairs is in action class 3, and the development action is demanded shortly.

Table 4 Literal depiction of MAC Tool assessment result

Work	MAC score	Act reform	Class
Loading and unloading	19	Act demanded shortly	3
Carry on a flat surface	17	Act demanded shortly	3
Carry upstairs	19	Act demanded shortly	3

3.3   The Development Recommendations

Based on the REBA and MAC Tool results, it is found that all three works are at a high level of risk. Musculoskeletal discomfort is the consequence experienced by the workers after carrying out the work. To avoid musculoskeletal discomfort, developments are necessary. The upcoming paragraphs convey the suggested developments. With the help of Human Activity Analysis in Ergonomics Design and Analysis available in CATIA V5 design software, the comparison between manual and exoskeleton handling of water barrel is carried out (Table 5).

The activity of loading and unloading the water barrel. The weight of the water barrel is 20 kg. This weight cannot be reduced as it is a constant weight [1]. According to the REBA and MAC Tool, the bending of the trunk, coupling and bending of the upper and lower arm should be avoided. Therefore, it is recommended to use an assistive device to carry out this activity. An exoskeleton is developed to reduce the bend in the trunk, upper and lower arm. It also improves grip and, therefore, decreases coupling. Figure 2 compares the work of lifting the water barrel manual and with the help of an exoskeleton.

The activity of carrying the water barrel on a flat surface. The weight of the water barrel is 20 kg. This weight cannot be reduced as it is a constant weight [1]. According

Table 5 Job suggested for developments

No.	Job	REBA score	MAC score
1	Loading and unloading	12	19
2	Carry on a flat surface	10	17
3	Carry upstairs	11	19

Fig. 2 Comparing of activities of lifting water barrel

BEFORE   AFTER

Fig. 3 Comparison of activities of carrying water barrel

BEFORE   AFTER

to the REBA and MAC Tool, coupling and bending of the upper and lower arm should be avoided. Therefore, it is recommended to use an assistive device to carry out this activity. An exoskeleton is developed to reduce the bending in the upper and lower arm. It also improves grip and, therefore, decreases coupling. Figure 3 compares the work of carrying a water barrel in manual and with the help of an exoskeleton.

The activity of carrying the water barrel upstairs. The weight of the water barrel is 20 kg. This weight cannot be reduced as it is a constant weight [1]. According to the REBA and MAC Tool, coupling and bending of trunk, upper and lower arm should be avoided. Therefore, it is recommended to use an assistive device to carry out this activity. An exoskeleton is developed to reduce the bend in the trunk, upper and lower arm. It also improves grip and, therefore, decreases coupling. Figure 4 compares the work of carrying the water barrel upstairs in manual and with the help of an exoskeleton.

3.4 The Development Results

By using REBA and MAC Tool, reassessment was conducted for the developments made. Tables 6 and 7 show the result of re-evaluation using REBA and MAC Tool.

Based on Table 6, there is a decrease in the risk level of all the work activities. The work activity of loading and unloading the water barrel before and after the development has a REBA score of 12 (level 4 with very high risk) and 5, respectively. The risk reduction is 58.3% compared to before the development assessment. The work activity of carrying the water barrel on a flat surface before the development

Fig. 4 Comparison of activities of carrying the water barrel upstairs

BEFORE   AFTER

Table 6 Before and after development REBA assessment results

Work	REBA final score		Reduction	
	Before development	After development	score	Percentage (%)
Loading and unloading	12	5	7	58.3
Carry on a flat surface	10	4	6	60
Carry upstairs	11	5	6	54.54

Table 7 Before and after development MAC assessment results

Work	MAC final score		Reduction	
	Before development	After development	score	Percentage (%)
Loading and unloading	19	9	10	52.63
Carry on a flat surface	17	7	10	58.82
Carry upstairs	19	7	12	63.15

REBA score is 10 (level 3 with high risk). The REBA score after development is 4, which is a 60% decrease in risk of doing the activity. The work activity of carrying the water barrel upstairs has REBA score before development as 11 (action level 4 with very high risk) and after development as 5, which is a 54.54% decrease in risk.

Table 7 shows the before and after development scores of the MAC Tool. The work activity of loading and unloading the water barrel before and after the development has a MAC score of 19 (action level 3) and 9, respectively. The risk reduction is 52.63% compared to before the development assessment. The work activity of

carrying the water barrel on a flat surface before the development had a MAC Tool score of 17 (the action level 3). The MAC score after development is 7, which is a 58.82% decrease in risk of doing the activity. The work activity of carrying the water barrel upstairs has MAC score before development as 19 (the action level 3) and after development as 7, which is a 63.15% decrease in risk.

4 Conclusion

The manual loading, carrying and unloading water barrel on a flat surface and upstairs are assessed using REBA. As a result, work of loading and carrying water barrels upstairs belonged to the action level 4 (very high risk) category and carrying water barrels on a flat surface belonged to the action level 3 (high-risk level) categories. By using a MAC chart, the same three work activities of handling the water barrel were analysed. In that, all three activities belonged to the action level 3 category in which the work needs an development shortly.

Based on the result of the REBA and MAC assessment, all three activities are considered for development as they had a high-risk consequence of the musculoskeletal disorder. An exoskeleton is designed to reduce the risk involved in the activities. The results of manual handling activity in REBA and MAC Tool are compared with working with an exoskeleton. REBA reveals that there is a 58.3%, 60% and 54.54% decrease in risk levels, and MAC Tool confirms that there is a 52.63%, 58.82% and 63.15% decrease in the risk involved in manual handling of water barrels.

References

1. Shafiee, M.N.: A study of consumer buying behaviour of package drinking water. **5**, 126–137 (2018)
2. Geere, J.L., Hunter, P.R., Jagals, P.: Domestic water carrying and its implications for health : a review and mixed methods pilot study in Limpopo Province, South Africa. 1–13 (2010)
3. Antwi-afari, M.F., Li, H., Edwards, D.J., Pärn, E.A., Seo, J., Wong, A.Y.L.: Automation in construction biomechanical analysis of risk factors for work-related musculoskeletal disorders during repetitive lifting task in construction workers. **83**, 41–47 (2017)
4. Mills, S., Qutubuddin, S.M., Hebbal, S.S., Kumar, A.C.S.: An ergonomic study of work related musculoskeletal disorder risks in Indian saw mills. (2014)
5. The W Academy.: Analysis of work posture and manual material handling in a flour production process. (n.d.)
6. Shokri, S., Varmazyar, S.: Manual material handling assessment and repetitive tasks with two methods MAC and ART in a subsidiary of a manufacturer of cleaning products. (2015)
7. Harold, C., Daniel, U.: Work-related musculoskeletal disorders among workers in brick making factory and building construction sites: an overview. **2**, 552–577 (2013)
8. Mohammadi, H., Motamedzade, M., Faghih, M.A.: Manual material handling assessment among workers of Iranian casting workshops. **3548** (2015)

9. Astuti, R.D., Susmartini, S., Kinanthi, A.P.: Improving the work position of worker based on manual material handling in rice mill industry. 020043 (2017)
10. Article, R.: Ergonomics : a bridge between fundamentals and applied research. **15** (2011)
11. Zaheer, A., Khalid, R.: Ergonomics : a work place realities in Pakistan ergonomics. (2018)
12. Klussmann, A., Liebers, F., Gebhardt, H., Rieger, M.A., Latza, U., Steinberg, U.: Risk assessment of manual handling operations at work with the key indicator method (KIM-MHO)—determination of criterion validity regarding the prevalence of musculoskeletal symptoms and clinical conditions within a cross-sectional study. 1–13 (2017)
13. Yahya, N.M., Zahid, M.N.O.: Evaluation of work posture and quantification of fatigue by rapid entire body assessment (REBA) evaluation of work posture and quantification of fatigue by rapid entire body assessment (REBA), (n.d.)
14. Yadi, Y.H., Kurniawidjaja, L.M., Susilowati, I.H.: Ergonomics intervention study of the RULA/REBA method in chemical industries for MSDs' risk assessment. 181–189 (2018)

A Graphical User Interface (GUI) System for a Stationary Trainer Used in Lower Limb Rehabilitation

Parvathi Sunilkumar, Santhakumar Mohan, and Larisa Rybak

1 Introduction

With the elderly society and deteriorating ecological sustainability, people's human lifestyle has degraded. The malfunction of the lower limb is one of the most common problems that the aged experience nowadays. Stroke is the most common cause of this, which can result in neurological damages or musculoskeletal problems [1]. Recent findings [2–6] have revealed that there are over 80 million stroke survivors worldwide. The majority of the consequent limb disabilities are treated using time-consuming therapeutic treatments that require the assistance of professional physiotherapists. As a result, a physiotherapist's task becomes laborious and tedious. Mechanical assistive devices can aid with this problem [7]. In this paper, we present a graphical user interface (GUI) interactive simulator for a stationary trainer for lower limb rehabilitation. Three parallel PRRR (prismatic-revolute-revolute-revolute) serial manipulators are coupled to the end-effector in the mechanical configuration of this stationary trainer. The GUI simulator development for the mechanism is based on a footplate operating system, where the footplate acts as the end-effector. A Cartesian parallel manipulator is used in the proposed stationary trainer. Parallel manipulators are formed of closed-loop mechanisms that use distinct serial chains to connect the fixed base to the end-effector which is moving [8]. Because of its inherent benefits of increased payload capacity and superior precision, a parallel manipulator

P. Sunilkumar · S. Mohan (✉)
Indian Institute of Technology (IIT) Palakkad, Palakkad 678623, India
e-mail: santhakumar@iitpkd.ac.in

P. Sunilkumar
e-mail: parvathi.s.edu@gmail.com

L. Rybak
Belgorod State Technological University (BSTU) Named After V.G. Shukhov, Belgorod 308012, Russia

is used here [9]. Parallel manipulators have less inertia than serial manipulators, resulting in faster working speeds [10]. The interactive simulator presented in this paper is predominantly designed for demonstrating the passive range of motion on the lower limb. The tasks executed thus focus on the hip and knee joints of the patient's leg. The stationary trainer concentrates on one leg at a time, for rehabilitation procedures. The application enables the user to choose from various therapeutic procedures such as hip abduction–adduction, hip flexion–extension, knee flexion–extension and gait training. The following sections detail the stationary trainer design and the features of the GUI interactive simulator developed as an application in MATLAB.

2 Modelling of the Simulator

In the authors' previous paper [7], the conceptual design of a new parallel manipulator-based stationary trainer is presented. Figure 1 is the solid model of the proposed Cartesian manipulator developed in SolidWorks. As can be seen, the parallel manipulator is linked to the footplate of the machine using three parallel kinematic chains of PRRR configuration. The manipulator is linked to a fixed frame that is stationary. Each of the manipulator arms has active linear (prismatic) joints that traverse along X, Y and Z guideways along the corresponding coordinate axes. An RRR serial kinematic chain is connected to each P joint. These three arms connect to the end-effector (footplate) on which the load will act. The kinematic configuration of the manipulator alone is represented in Fig. 2. A_i represents the prismatic joints and B_i, C_i and D_i represent the passive revolute joints in each kinematic leg where i = 1, 2, 3 is the kinematic leg.

As can be seen, r_1, r_2 and r_3 represent the linear joint variables which are active. The mathematical model of the manipulator gives the configuration space displacement vector in terms of the end-effector position P_x, P_y and P_z. The inverse (indirect) kinematics gives:

$$\zeta = \begin{bmatrix} r_1 \\ r_2 \\ r_3 \end{bmatrix} = \begin{bmatrix} P_x - d_x \\ P_y - d_x \\ P_z \end{bmatrix} \tag{1}$$

where, ζ is the configuration space displacement vector. d_x and d_y give the distance of the end-effector position from the adjacent R joints (D_1 and D_2) along X and Y axes respectively. The end-effector positions can be derived from the kinematic relations in terms of the lower limb angles namely the hip angle (angle in sagittal plane (Fig. 3)), frontal angle (angle in frontal plane (Fig. 3)) and knee angle. The kinematic relation gives:
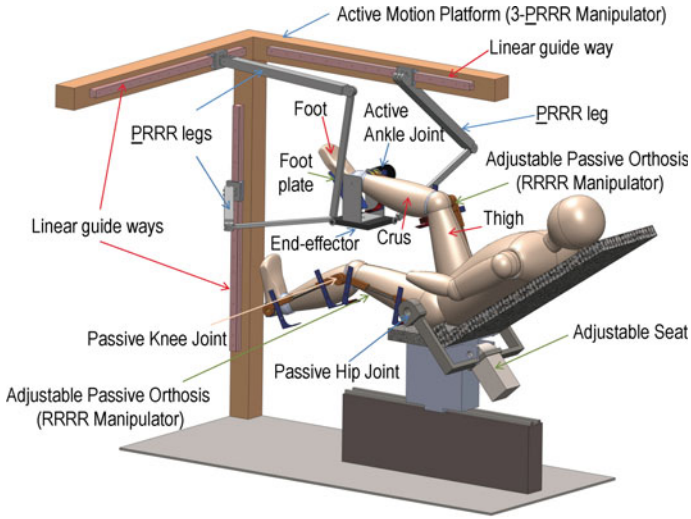
Fig. 1 Conceptual design of the parallel manipulator for lower limb rehabilitation
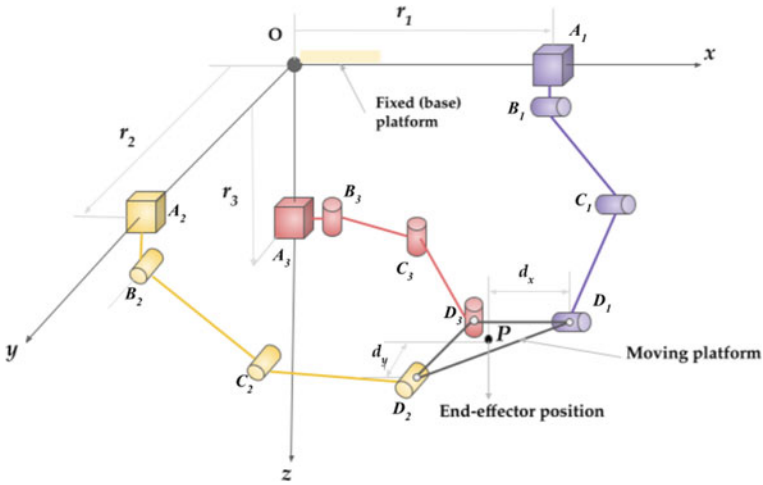
Fig. 2 Kinematic arrangement of the proposed stationary trainer

$$\eta = \begin{bmatrix} P_x \\ P_y \\ P_z \end{bmatrix} = \begin{bmatrix} x_0 - L_{\text{thigh}} \cos \alpha_{\text{hip}} \cos \alpha_{\text{frontal}} - L_{\text{crus}} \cos (\alpha_{\text{hip}} + \alpha_{\text{knee}}) \cos \alpha_{\text{frontal}} \\ y_0 - L_{\text{thigh}} \cos \alpha_{\text{hip}} \sin \alpha_{\text{frontal}} - L_{\text{crus}} \cos (\alpha_{\text{hip}} + \alpha_{\text{knee}}) \sin \alpha_{\text{frontal}} \\ z_0 - L_{\text{thigh}} \sin \alpha_{\text{hip}} - L_{\text{crus}} \sin(\alpha_{\text{hip}} + \alpha_{\text{knee}}) \end{bmatrix}$$

$$(2)$$

(a) Frontal Plane   (b) Sagittal Plane
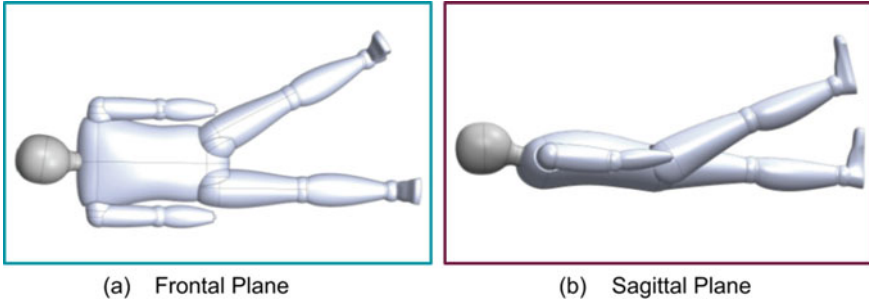
Fig. 3 Frontal and sagittal planes (developed in SolidWorks)

where x_0, y_0 and z_0 depict the initial position of the hip joint. α_{hip} and α_{knee} are the angles of hip and knee joints in the sagittal plane and α_{frontal} is the angle of hip joint in the frontal plane. L_{thigh} and L_{crus} are the thigh and crus lengths of the lower limb, which can be given as inputs to the simulator, by the user.

The dynamic model of the driving mechanism is required for designing the gait training trajectory tracking. This is developed using the Euler-Lagrangian formulation, obtaining the forces acting on each of the active joints as:

$$f_1 = \frac{d}{dt}\left(\frac{\partial L}{\partial \dot{r}_1}\right) - \frac{\partial L}{\partial r_1}, \;\; f_2 = \frac{d}{dt}\left(\frac{\partial L}{\partial \dot{r}_2}\right) - \frac{\partial L}{\partial r_2}, \;\; f_3 = \frac{d}{dt}\left(\frac{\partial L}{\partial \dot{r}_3}\right) - \frac{\partial L}{\partial r_3}. \quad (3)$$

where Lagrangian L is the difference between the total kinetic energy and total potential energy of the mechanism. f_1, f_2 and f_3 are the joint forces corresponding to r_1, r_2 and r_3.

3   GUI Interactive Simulator

A graphical user interface interactive simulator is developed as an application in MATLAB for the stationary trainer to execute lower limb rehabilitation therapy. This application demonstrates the passive range of motion (PROM) executable by the proposed stationary trainer. This interactive simulator can be used to view the possible motions for lower limb rehabilitation therapy of PROM. The mathematical model developed is used to design the application with variable inputs to be given by the user with the help of sliders provided. The design view of the application is shown in Fig. 4. The application has options of choosing the kind of therapeutic motions to be viewed. The box titled 'Therapy', as shown in Fig. 4, has different tabs, namely hip abduction–adduction, hip flexion–extension, knee flexion–extension and gait training. The following are the features of each tab:
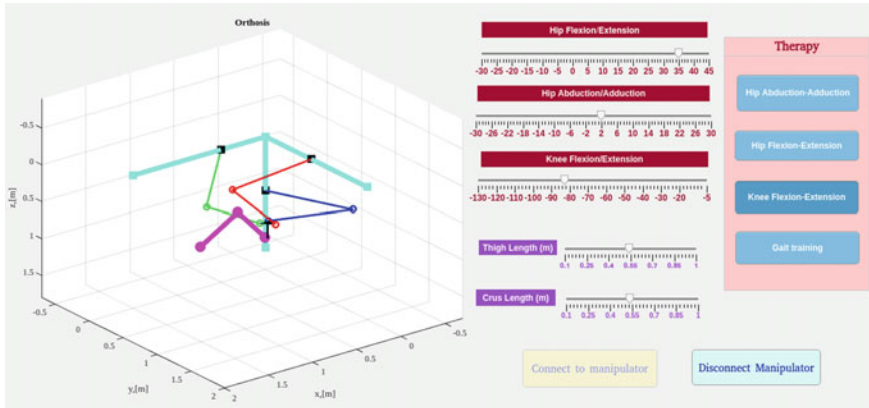
Fig. 4 Layout of the interactive simulator application

- Hip Abduction–Adduction: On clicking this tab, the sliders representing the Hip Abduction/Adduction and Knee Flexion/Extension will be active. On varying these two angles, the hip abduction and adduction motions of the lower limb can be viewed.
- Hip Flexion–Extension: On clicking this tab, the sliders representing the Hip Flexion/Extension and Knee Flexion/Extension will be active. On varying these two angles, the hip flexion and extension motions of the lower limb can be viewed.
- Knee Flexion–Extension: On clicking this tab, the sliders representing the Hip Abduction/Adduction, Hip Flexion/Extension and Knee Flexion/Extension will be active. On varying these three angles, the knee flexion and extension motions of the lower limb can be viewed.
- Gait training: On clicking this tab, all the sliders representing the lower limb angles will be active. On varying these angles, the trajectory motion in sagittal motion will be displayed.

In addition, the application enables the user to input the length of the subject's thigh and crus lengths with help of the respective sliders, as shown in Fig. 4. Once the appropriate angles for therapy are chosen, there are two options for displaying the mechanism as shown in Fig. 4. On clicking the button 'Connect to manipulator', the corresponding position of the limb connected to the manipulator, will be displayed. On the other hand, clicking the 'Disconnect manipulator' will display just the limb posture with respect to the angles, excluding the manipulator, as shown in Fig. 5.

4   Results and Discussion

In the application, the lower limb is designed such that the thigh length as well as the crus length (Fig. 6a) can be given as input by the user, with the help of sliders
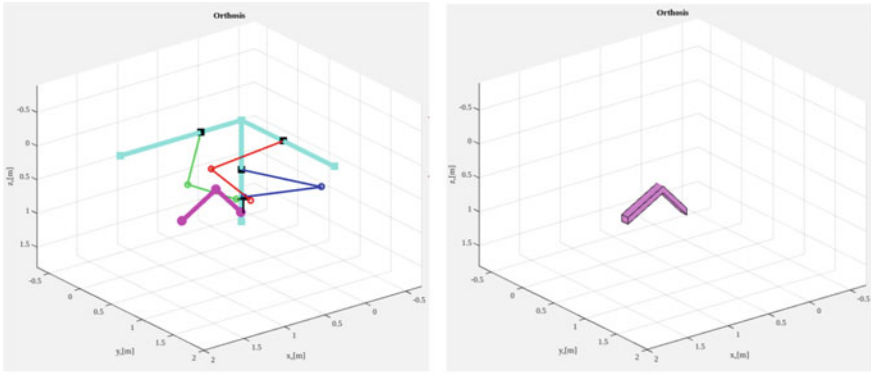
(a) View on clicking 'Connect to manipulator' button

(b) View on clicking 'Disconnect manipulator' button

Fig. 5 Display options in the simulator

provided. However the thigh height, thigh thickness, crus height and crus thickness are chosen as 0.2 m, 0.1 m, 0.1 m and 0.05 m respectively. The footplate dimensions along the X-axis and Y-axis are taken as an $x = 0.1$ m and a $y = 0.1$ m respectively. The range of angles have been chosen from the clinical data sets available from literature.

Hip abduction–adduction of the subject causes the lower limb to move away and towards the body in the frontal plane. For the therapeutic procedures in this plane, the angles to be varied are the frontal angle or the hip abduction/adduction angle and the knee angle or the knee flexion/extension angle. Thus on choosing this option in the interactive simulator, only these two angles will be active. The user can vary the
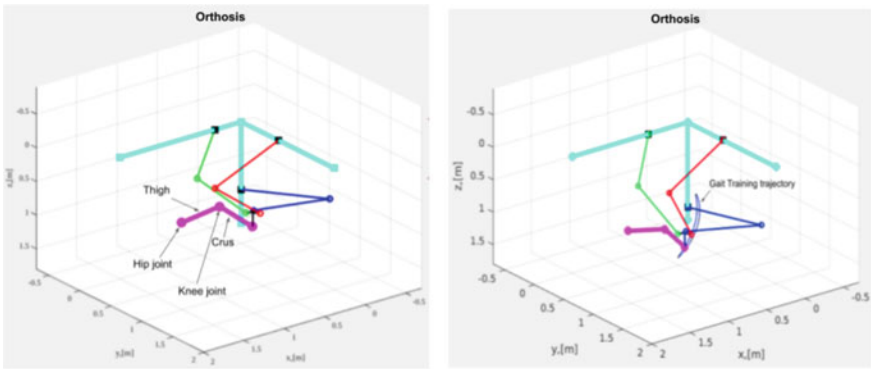
(a) Display on varying the limb angles

(b) Gait Training

Fig. 6 Display options in the simulator

angles and see the different postures of the lower limb for various angles and limb lengths.

Hip flexion–extension of the subject causes the lower limb to move away and towards the body in the sagittal plane. For the therapeutic procedures in this plane, the angles to be varied are the hip angle or the hip flexion/extension angle and the knee angle or the knee flexion/extension angle. Thus on choosing this option in the interactive simulator, only these two angles will be active. The user can vary these angles with the help of sliders and the different postures of the lower limb for various angles and limb lengths will be displayed.

Knee flexion–extension of the subject causes the knee of the lower limb to move away and towards the body in the sagittal plane. For the therapeutic procedures of the knee, the knee angle can be varied for different hip angle and frontal angle. Therefore, all three angles are active for this option and the user can view the lower limb posture by varying these angles with the help of sliders.

Gait Training option of the simulator displays the lower limb following a predefined trajectory. For this, the user can choose the hip angle and the knee angle with the help of sliders. A predefined trajectory corresponding to the angles chosen, as shown in the Fig. 6b, will be followed by the lower limb.

This interactive simulator designed is highly useful for the researchers in getting a better idea of the mathematically modelled design. It also makes it easier to convey the design and the working, pictorially with the help of this application. It helps in investigating the motion patterns of the manipulator without actually having to develop it physically, by viewing the different configurations of the limb and the manipulator for various limb angles. This application can be used to find the maximum angle achieved by the lower limb for different shapes of the footplate. By varying the thigh and crus length in the application, this application can be used to study the maximum range of motion possible for the manipulator.

5 Conclusions

Neurological problems have become more common as people's lives have changed. Stroke has been the predominant cause of this, leading to complete paralysis. The therapeutic operations for its rehabilitation can be carried out on a stationary trainer. This paper presents a graphical user interactive simulator as an application in MATLAB to study the motion mechanism of the proposed manipulator. The developed interactive system has been used to study the movements of the lower limb as well as the manipulator for various therapeutic procedures, namely, hip abduction–adduction, hip flexion–extension, knee flexion–extension and gait training. The obtained results give a vivid idea to the user on the different configurations of the limb while carrying out motions at different angles. This interactive simulator enables the researchers to study the model derived mathematically without having to build it in real time. This laborious and time-consuming task can be eliminated with the help of this application

and this user interactive interface can be further used to study the range of motion for various procedures.

References

1. Faizura, W.W., Luqman, M.Z.M., Hafiz, O.M., Naim, M.S., Armin, S.A., Irraivan, E.: Control techniques of multi-fingered hand for rehabilitation. J. Phys. Conf. Ser. **1532**, 012026 (2020)
2. Jiang, D., Shi, G., Pang, Z., Li, S., Tian, Y.: Control of a new cycling rehabilitation robot based on fuzzy PID. J. Phys. Conf. Ser. **1622**(1), 012119 (2020)
3. Kurmashev, S., Ospanov, S., Malik, A., Xydas, E., Mueller, A.: Flexibility in upper limb rehabilitation with the use of 1-DOF fourbar linkages. In: International Design Engineering Technical Conferences and Computers and Information in Engineering Conference, vol. 51807, p. V05AT07A058. American Society of Mechanical Engineers (2018)
4. Diaz-Caneja, D., Campa, F.J., Altuzarra, O., Diez, M., Lascurain-Aguirrebeña, I., Santisteban, L., Bengoetxea, A.: A compliant parallel manipulator for trunk rehabilitation after stroke. In: International Workshop on Medical and Service Robots, pp. 37–43 (2020)
5. Rabia, G.U.L., Sener, S., Hocaoglu, E.: A mobile parallel manipulator for the elbow rehabilitation of Parkinsonian patients. In: 2020 Medical Technologies Congress (TIPTEKNO), pp. 1–4. IEEE (2020)
6. Nurahmi, L., Kautsar, R., Jha, R.: Stiffness distribution of 3-RPS parallel manipulator based on the base-and-platform configuration. In: Mechanism and Machine Science, pp. 57–68. Springer, Singapore (2021)
7. Mohan, S., Sunilkumar, P., Rybak, L., Malyshev, D., Khalapyan, S., Nozdracheva, A.: Conceptual design and control of a sitting-type lower-limb rehabilitation system established on a spatial 3-PRRR parallel manipulator. In: International Conference on Robotics in Alpe-Adria Danube Region, pp. 345–355 (2020)
8. Sunilkumar, P., Choudhury, R., Mohan, S., Rybak, L.: Dynamics and motion control of a three degree of freedom 3-PRRR parallel manipulator. In: European Conference on Mechanism Science, pp. 103–111 (2020)
9. Briot, S., Arakelian, V., Guégan, S.: PAMINSA: A new family of partially decoupled parallel manipulators. Mech. Mach. Theory **44**(2), 425–444 (2009)
10. Briot, S., Bonev, I.A.: Are parallel robots more accurate than serial robots? Trans. Can. Soc. Mech. Eng. **31**(4), 445–455 (2007)

Identify and Understand the Physical Characteristics that Responsible for the Masculine Nature of a Car

Jitender Singh and Prabir Sarkar

1 Introduction

The capability to capture and describe customer liking is a main instrument for product designers. When developing a solution for new design, product designers require fruitful data related to particular or their target us customer so that they can better mold their designs. Consumers have always prefer to have things which are latest and expected to be future trending. Cars are one of the things which have become a most important part of human life. Humans used it not just to fulfill their daily transportation needs but also to maintain their life easy and status symbol as well. Therefore, car designers as well as manufacturers have to think about the need of consumers regarding what type of cars they actually want. Being a customer, if someone goes to buy a car then he/she will set his budget first then choose a car that has the best first impression on him [1]. Consumers always prefer to have such type of cars that have dashing look or scientifically we can say that looks aesthetically good to them. But a question arises that what type of car is aesthetically good looking. If some cars having the same power, seating capacity, color, similar price, etc. Then consumers will choose those one which having excellent aesthetic quality [4]. But, in case of some consumer they chose their vehicle based upon their ergonomics. According to Nagamachi [11], human being make their judgment based on their cognitive thinking, which were mainly influence through products visual as well as non-visual factors. Although in case of vehicle, all are most of them made out of steel, with somewhat same process and literal with another process. This understanding turn into more important when one recognizes that cognitive feelings are the uncooked

J. Singh (✉) · P. Sarkar

Department of Mechanical Engineering, Indian Institute of Technology Ropar, Rupnagar 140001, Punjab, India

e-mail: jitendernit1724@gmail.com; 2016mez0020@iitrpr.ac.in

51

statistics from where human beings try to predict that final conclusion about the product [10, 11].

Logically we can say aesthetics have a good impact on human interpretation about an object. Also talking about automotive industry trends, "Indian" automobile industries is moving very fast because of their population growth. Since, "India" is the second largest populated country in the world after China and, the demand of vehicles is also growing in exponential manner and it is one of the largest automobile hub of the world, 6th largest automobile manufacturer. It will impact 29 million population directly and indirectly [7]. Due to this the demand of the population quit versatile. Therefore, to meet the demand of this population designers, marketing peoples, and higher management have to work in very transformative way and try to leave the conventional path of manufacturing, designing, and advertisements. From last two decades, consumers start giving equal importance to the external shape/form of product as compare to their functionality. Therefore, the importance of product design and consumer psychology is come into the picture, in case of auto sector, packaging area, etc., [4]. With the passage of time consumers demands also changing and at the same time to gain the highest market share in this highly volatile environment, automobile industries have to in a very innovative way. Therefore, designers give importance to physical feature and put more and more efforts to the product aesthetics and subjective excellence of their products.

Other characteristics and metrics, such as functionality and usability often split the losers and winners [3, 7]. As if, aesthetic experiences are frequent in modern life. But they are unable to tell properly that what specific thing or which specific area is responsible for choosing the car as an aesthetically good looking car [8]. If we ask someone to compare among various cars and the reason for the liking of a specific car only, he will be unable to tell us because it is just a human perception, i.e., a hypothetical thing and no one till now able to predict human perception analytically [9]. Here the real problem arises, where manufacturers do not know the exactly about the specific design attribute which is mainly relied upon the likeness of the car. There is an evident lack of methodical, technical, and engineering approaches to support them make product design decisions and carry out aesthetic estimations [3].

In the case of SUVs, one of the main factors is more cargo space. In recent time, the demand for the current market is compact SUV's. Which provide better storage, when the boot space is required with good seating capacity. The important issue is; compact SUV's are not able to provide enough space as compare to Full-size SUV's, which provide great seating capacity, comfort, and large cargo space [6]. From last few years, space in the parking area and huge cities traffic is the main reason behind the need for compact SUV's [2]. Due to restrictions of variants models and space, companies must implement ground-breaking thoughts to meet the desires of the current market. They need not only adjust to the form of a car, but they also offer the finest storage space rearrangement, while not cooperating with their aesthetics [6]. Over the last twenty-five years, we saw the automotive industries achieved a significant reduction in aerodynamic drag. This has been achieved by the refinement of the inside space of the car and by the optimization of the upper shape of the car body. Even though this trend is to reduce in sedan segment cars over the last few

years, and now it is shifted toward the SUV's, MUV's, and 4 wheel drive cars. A constant reduction in the drag for these vehicles is necessary if they are to achieve the progressively strict GHGs goals that are being fixed by all developed countries and the fuel economy expectations of maximum consumers. This applies in particular for carbon footprint which is realized as the main part for global warming [5]. In this study, we try to reveal how some forms look more masculine in nature and express power as compare to others.

2 Aim and Methodology

When we are listening to the term masculine and powerful, the first think comes to our mind is the term reliability. When we see a big car in front of us we think it is more reliable and secure for example Sports utility vehicles (SUVs). In this study, we try to reveal find out which physical characteristics of a car change consumer perception and try to find out the impact at the time of purchase of new a car. When we see some car forms they look more masculine in nature and express power. But some consumer thinks opposite to it, they buy this type of vehicles just because they start relating their emotions, feeling with cars looks and even they also try to show their wealth by buying these type of vehicles. That's why nowadays car manufacturing companies start building or move toward sports utility vehicle and multi-utility vehicle segment also. In this study, our main focus is to find the physical characteristics of a car which make them masculine and powerful in term of their look at the time of purchase of a car. During this research work, we considered different images of SUV's as well as MUV's from different manufacturing companies. All the images were downloaded from google image. The resolution of the images should be 1024 * 720 or 800 * 600 because below this, the image looks so blur and it may affect the human cognitive perception. During the collection of the car image background of a car play a greater impact on the beauty of the car as well as it also impacts the cognitive appeal of consumers also. To avoid the influence of background on the perception of respondents, we downloaded the images with white background, i.e., black and also the background is white or transparent. Images with side views were downloaded/considered. Because side views provides a better view to candidates for their prediction about characteristics for representing the masculine, power, reliability, of a car. For getting satisfactory results, all side views of SUVs of about 150 different cars were downloaded. All of the cars are having a geographical location in India. As visual aspects (like color, shadow, background, etc.) were already considered in preliminary studies of the project, so here we have to be sure that background and color should not have any sort of impact on the feeling of likability of the specific car. Survey participants will prefer to look at sharp images.

Table 1 List of physical factor which we consider from SUV'

Front grill	Larger ground clearance	Larger wheelbase
Sitting position and windshield angle (70°–80°)	Position of the back spare wheel	More headroom
More engine cabin	Sharp edges	Metal parts
A larger distance between wheelbase and chassis	The color of the car	Name of the car

3 Data Collection

During this research work, first we collect the list of cars and their categories. From that list, we understand which car falls under which category. After that, a total of ten respondents from product design area were contacted through phone calls, LinkedIn, and e-mails. All respondents are from product design, creativity area and an experience of at least 3 year or more, and 7 out of the ten respondents agreed to be part of this study. Among seven-person one person is associate professor, and six are senior research scholar. First we conducted a brainstorming session with all the participants related to product design and car as well. During this session, we found different sets of factor related to product design and in case of automobile specially, we found out approximately twelve factors which characterize the masculine nature of a car and the list of characters is given in Table 1. A Fig. 1, as an example is shown Appendix 3.

4 Results and Discussion

To find the factors or the physical characteristics that were responsible for the masculine nature of the car. First, we paste the images of a car in a Google form as shown in Tables 3, 4, and 5. After pasting the images of car, we paste questionnaire after each images, and from each prospective buyer, we asked whether that particular car look masculine or not. If the prospective buyers reply is "Yes". Then, they move to next step, were they found the list of different features, which found from literature and during brainstorming session, and we asked them to provide their features or characteristics related to masculinity of the car. The sample survey form or questionnaire is provided in Appendix 1. To find the factors or the physical characteristics that are responsible for the masculine nature/look of the car. The agreement of car is shown in Tables 3, 4, and 5.

This closed-ended survey is sent through Gmail to thirty people. From which we get different sets of answer from different people for different cars. From the closed-ended question, we get responses in a various manner, Range rover sports, and Mahindra Thar will get the highest amount of response, i.e., twenty-seven

out of thirty, at the same time Jeep Wrangler and Isuzu MU 7 got a second-lowest place by considering twenty-six responses out-off thirty. Similarly, Jeep Grand Cherokee, Mercedes Benz G Class AMG were got third-lowest responses by considering twenty-five responses out-off thirty, Mahindra Bolero was got fourth-lowest responses by considering twenty-four responses out-off thirty, Toyota Land Cruiser, Volvo XC40, Isuzu MUX, Nissan Patrol was got fifth-lowest responses by considering twenty-three responses out-off thirty, Mahindra XUV got sixth-lowest responses by considering twenty-two responses out-off thirty, at the end SsangYong Rexton were got seven places by getting lowest response, i.e., twenty one out of thirty among all twelve SUV cars.

The combined results of all three Tables 3, 4, and 5 is provided in Table 2 as shown above. In Table 2, we saw some respondents say "yes" this car looks masculine in nature, few respondents say "no" this car is not looking masculine in nature and similarly some say "maybe or maybe not". During the closed-ended survey, if the respondent gives his or her consent as "no". Then, they do not need to go for further questionnaire. i.e., for him, that car does not look like masculine in nature.

On the other hand, if the respondent gives his or her consent as "yes". Then he or she needs to go with the questionnaire which is given in Tables 3, 4, and 5. There was thirteen factors and they have to think to recognize to express their feeling. At the time of analysis, we consider only the top three cars for each segment of the questionnaire. When we saw the Tables 3, 4, and 5, we analysis the front grills of "Jeep Wrangler", "Isuzu MUX", and "Mercedes Benz G Class AMG" impact more on consumer perception, i.e., out-off twenty-six respondents twenty-four (92.3%) respondents give their consent (Yes) for the feeling of masculine nature (Jeep Wrangler) and from twenty-four respondents 42.30% respondents think from the grill is the main factor which enhance the masculine nature of a car, at the same time out-off twenty-three respondents nineteen (82.6%) respondents give their consent (Yes) for the feeling of masculine nature car (Isuzu MUX) and from twenty-four respondents 43.50% respondents give more importance to front grills. Similarly, in the case of "Mercedes Benz G Class AMG" 42.30% from nineteen respondents which give their consent to the feeling of nature of a car out-off twenty-five respondents.

When we move toward the "Large ground clearance" we can also predict the masculine nature of the car. In case of "Jeep Wrangler" out-off twenty-six respondents twenty-four (92.3%) respondents give their consent (Yes) for the feeling of masculine nature and from twenty-four respondents 50.0% respondents think "Large ground clearance" is the main factor which enhances the masculine nature of a car, in case of "Range Rover Sport" out-off twenty-seven respondents twenty (74.10%) respondents give their consent (Yes) for the feeling of masculine nature a car and from twenty respondents 40.70% respondents give more importance to the "Large ground clearance". Similarly, in the case of "Isuzu MU 7", 50.00% from seventeen respondents give their consent for the feeling of masculine nature of a car out-off twenty-six respondents.

In Tables 3, 4, and 5, we saw that respondents give 61.50% to "Jeep Wrangler", following 52.20% to "Isuzu MUX" and 50.00% to "Mercedes Benz G Class AMG" by considering the "Large wheelbase". When they twenty-four out-off twenty-six,

Table 2 Results of views of participants about the masculine nature of different cars

Times	Mahindra Thar	Range Rover Sport	Jeep Grand Cherokee	Mercedes Benz G Class AMG	Jeep Wrangler	Isuzu MU 7	Mahindra Bolero	Toyota Land Cruiser	Isuzu MUX	Mahindra XUV	SsangYong Rexton	Nissan Patrol
Total response	27	27	25	25	26	26	24	23	23	22	21	23
Yes	19(70%)	20(74.1%)	20(76.9%)	19(73.1%)	24(92.3%)	17(65.4%)	18(75%)	18(78.3%)	19(82.6%)	11(50%)	15(71.4%)	17(73.9%)
No	6 (22.2%)	5(18.5%)	1(3.8%)	3(11.5%)	1(3.85)	3(11.5%)	4(16.7%)	4(17.4%)	2(8.7%)	8(36.4%)	3(14.3%)	5(21.7%)
May be	2(7.4%)	2 (7.4%)	4(15.4%)	3(11.5%)	1(3.85%)	6(23.1%)	2(8.3%)	1(4.3%)	2(8.7%)	3(13.4%)	3(14.3%)	1(4.3%)
List of factors which influence the masculine nature of a car												
Front grills (%)	22.20	25.90	38.50	42.30	42.30	38.50	25.00	17.40	43.50	13.60	19.00	26.10
Larger ground clearance (%)	29.60	40.70	30.80	38.50	50.00	50.00	37.50	30.40	34.80	13.60	42.90	30.40
Larger wheel base (%)	40.70	29.60	38.50	50.00	61.50	30.80	45.80	39.10	52.20	13.60	28.60	34.80
Sitting position and windshield angle (%)	18.50	14.80	30.80	30.80	26.90	19.20	16.70	39.10	21.70	13.60	19.00	17.40

(continued)

Table 2 (continued)

Times	Mahindra Thar	Range Rover Sport	Jeep Grand Cherokee	Mercedes Benz G Class AMG	Jeep Wrangler	Isuzu MU 7	Mahindra Bolero	Toyota Land Cruiser	Isuzu MUX	Mahindra XUV	SsangYong Rexton	Nissan Patrol
Position of back spare wheel (%)	7.40	7.40	26.90	15.40	19.20	11.50	20.80	13.00	30.40	13.60	14.30	8.70
More head room (%)	3.70	18.50	26.90	38.50	26.90	19.20	25.00	21.70	13.00	13.60	14.30	13.00
More engine cabin (%)	25.90	29.60	15.40	42.30	38.50	23.10	33.30	21.70	34.80	4.50	0.00	4.30
Sharp edges (%)	25.90	14.80	7.70	30.80	23.10	15.40	12.50	13.00	13.00	4.50	19.00	8.70
Metal part (%)	40.70	25.90	34.60	46.20	42.30	19.20	25.00	26.10	30.40	13.60	23.80	26.10
Name of car (%)	7.40	25.90	19.20	23.10	19.20	7.70	8.30	13.00	13.00	13.60	9.50	17.40
Color of car (%)	3.70	11.10	19.20	15.40	11.50	11.50	8.30	8.70	17.4	4.50	14.30	4.30
Large distance between wheelbase and chassis (%)	18.50	0.00	0.00		0.00	0.00	0.00	0.00	0.00	0.00	0.00	0.00
Other (%)	3.70	18.50	30.80	23.10	15.40	11.50	12.50	13.00	13.00	9.10	9.50	8.70

Table 3 List of car and the list features

Feeling of participants about masculine nature of car	Mahindra Thar	Range Rover Sport	Jeep Grand Cherokee	Mercedes Benz G Class AMG
Yes (%)	100	80	100	100
No (%)	0	20	0	0
May be (%)	0	0	0	0
Factors than influencing masculine nature of a car				
Front grill (%)	20	20	20	20
Large ground clearance (%)	40	60	60	40
Larger wheelbase (%)	60	40	80	80
Sitting position and windshield angle (%)	20	40	40	40
Position of back spare wheel (%)	0	20	20	20
More head room (%)	20	40	40	40
More engine cabin (%)	60	20	0	60
Sharp edges (%)	20	60	0	20
Metal parts (%)	60	20	60	60
Name of the car (%)	0	0	40	20
Color of the car (%)	0	20	20	0
Distance between wheelbase and chassis (%)	20	0	60	40

nineteen out-off twenty-three and nineteen out-off twenty-five give their consent in favor of feeling of masculine nature of a car. In these twelve factors, the respondents give the least importance to "Color of the car" and "Large distance between wheelbases". In the case of "Color of the car" "Mahindra Thar" get the lowest response, i.e., 3.70% compare to all the cars. On the other, "Mahindra Thar" is the only car which gets the highest response as compare to the car, i.e., 18.70% and respondent thinks "Large distance between wheelbases" of "Mahindra Thar" make them more masculine as compared to another car.

Table 4 List of car and the list features

Feeling of participants about masculine nature of car	Jeep Wrangler	Isuzu MU 7	Mahindra Bolero	Toyota Land Cruiser
Yes (%)	80	60	100	10
No (%)	0	0	0	0
May be (%)	20	40	0	0
Factors than influencing masculine nature of a car				
Front grill (%)	60	20	40	0
Large ground clearance (%)	80	60	60	60
Larger wheelbase (%)	60	40	80	80
Sitting position and windshield angle (%)	80	40	20	60
Position of back spare wheel (%)	40	0	40	40
More head room (%)	60	20	40	20
More engine cabin (%)	40	20	40	0
Sharp edges (%)	40	0	0	0
Metal parts (%)	60	20	40	40
Name of the car (%)	40	0	20	20
Color of the car (%)	20	0	0	0
Distance between wheelbase and chassis (%)	40	0	40	20

5 Conclusion

The automotive industry is very vast and now a day's it become an integral part of human lifestyle, and their importance is increasing gradually. There may be some factors that have a greater impact on consumers thinking when they purchase a new car. So, the industrial expert should understand and consider these factors when they are designing a new car. In this study, we consider SUVs and MUV's. From the online survey, we found out-off thirteen factors "Front grills", "Large ground clearance", "Larger wheelbase", "Sitting position and windshield angle" and "More engine cabin" make more masculine in nature. During analysis, we saw some respondents reject or not accept some car as masculine because of their look, i.e., in their viewpoint those are not in the category of SUV's or MUV's but actually those cars also fall in the categories of SUVs and MUV's. In future, industrial experts (car designers) with at least four year experience in designing of a car must be include into the brainstorming session. At the same time samples should be high in number.

Table 5 List of car and the list features

Feeling of participants about masculine nature of car	Isuzu MU X	Mahindra XUV	SsangYong Rexton	Nissan Patrol
Yes (%)	100	40	80	100
No (%)	0	40	0	0
May be (%)	0	20	20	0
Factors than influencing masculine nature of a car				
Front grill (%)	20	0	20	40
Large ground clearance (%)	60	0	60	60
Larger wheelbase (%)	80	20	40	60
Sitting position and windshield angle (%)	40	0	20	20
Position of back spare wheel (%)	40	20	20	20
More head room (%)	20	20	20	20
More engine cabin (%)	60	0	0	0
Sharp edges (%)	20	0	0	20
Metal parts (%)	40	20	40	20
Name of the car (%)	0	0	0	20
Color of the car (%)	0	0	20	0
Distance between wheelbase and chassis (%)	20	0	0	20

Appendix 1

During survey, we present car image in step wise manner and we requested each respondents to provide their response, whether that particular product look as a masculine in nature or not. If participant give their answer is "Yes". Then, we provide them the list of features which we find from literature search, and asked them to choose the feature which they think is appropriate in term of their cognitive thinking. The list of feature and questionnaire sample is given in Appendix 1.

Online open surveys were incorporated by using ten SUVs. Details are as follow; the surveys were performed on Google form. All side views were considered of some SUVs that were most masculine in nature as compare to all rest. For each question, one of the images of selected SUVs was taken and questions asked upon whether the car looks masculine or not if the participant says yes then following characteristics were asked based upon which he/she tick yes are:

 i. Front grill
 ii. Larger ground clearance

iii. Larger wheelbase
iv. Sitting position and windshield angle (nearly to 70°–80°)
v. Position of back spare wheel
vi. More head room
vii. More engine cabin
viii. Sharp edges
ix. Metal parts
x. Name of the car
xi. The color of the car
xii. A larger distance between wheelbase and chassis

Appendix 2

See Tables 3, 4 and 5.

Appendix 3

See Fig. 1
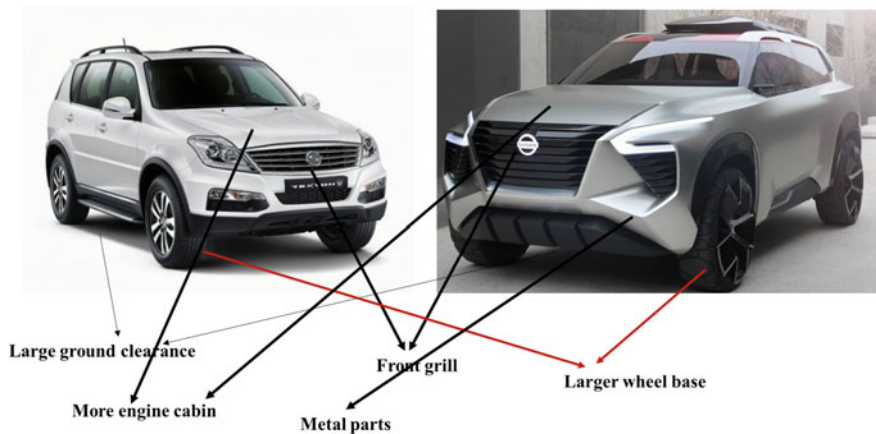
Fig. 1 With side view and some features

References

1. Anurit, J., Newman, K., Chansarkar, B.: Consumer behaviour of luxury automobiles: a comparative study between Thai and UK customers' perceptions (1998)
2. Bloch, P.H.: Product design and marketing: reflections after fifteen years: product design and marketing: reflections after fifteen years. J. Prod. Innov. Manag. **28**(3), 378–380 (2011)
3. Frens, J.W., Djajadiningrat, J.P., Overbeeke, C.J.: Form, interaction and function, an exploratorium for interactive products. In: Proceedings of the Asian Design Conference (2003)
4. Hekkert, P.: Design aesthetics: principles of pleasure in design. Psychol. Sci. **48**(2), 157 (2006)
5. Howell, J., Sherwin, C.: Aerodynamic drag of a compact SUV as measured on-road and in the wind tunnel (2002)
6. Kamp, I.: The influence of car-seat design on its character experience. Appl. Ergon. **43**(2), 329–335 (2012). https://doi.org/10.1016/j.apergo.2011.06.008
7. Karjalainen, T.-M.: It looks like a Toyota: educational approaches to designing for visual brand recognition. Int. J. Des. **1**(1) (2007)
8. Liu, Y.: Engineering aesthetics and aesthetic ergonomics: theoretical foundations and a dual-process research methodology. Ergonomics **46**(13–14), 1273–1292 (2003)
9. Martinez, A., Du, S.: A model of the perception of facial expressions of emotion by humans: research overview and perspectives. J. Mach. Learn. Res. **13**(May), 1589–1608 (2012)
10. Mei, Y., Lebin, J.: Study on Kansei engineering and its application to product design. In: 2009 Second International Symposium on Computational Intelligence and Design, pp. 525–528. IEEE (2009)
11. Nagamachi, M.: Kansei engineering: a new ergonomic consumer-oriented technology for product development. Int. J. Ind. Ergon. **15**(1), 3–11 (1995). https://doi.org/10.1016/0169-8141(94)00052-5

A Study on Musculoskeletal Disorders in Elderly Female Farmers in the Village Baruva, Srikakulam District of Andhra Pradesh

Sangeeta Pandit, Gaurav Pralhad Chindarkar, L. Dillieshwar Rao, Siddharth Das, Avinash Sahu, and Rajat Kamble

1 Introduction

Agricultural sector provides employment to almost one third of the worlds total working population, with approximately 60% of it working in developing nations, mainly in East and Southeast Asia [1]. Agriculture is one of the main contributors toward increasing Indian economy, accounting for over 17% of total GDP and almost one third of the rural households depend on it which provides work for more than 60% of the population [2]. In the past few decades, the Indian agriculture industry has recorded commendable growth [2]. The Indian Agriculture industry largely comes under the unorganized sector, where labor is the primary mode of manual work [3, 4]. Although a number of agricultural tasks are mechanized, a significant portion of farming related tasks are still done manually. Farmers owning small-scale agricultural lands totally rely on manual labor for cultivation. As a result of exposure to the manual tasks under challenging conditions like heat, wind, rains, etc. In the recent years, it was observed that the Indian youths are quitting farming and moving out to better places for job hunt. This has left the elder community to take up more responsibilities and tasks in the farming sector [5]. As working population is getting older, the percentage of older people in the workforce is predicted to rise from around 5% in 2020 to over 80% in 2040 [1].

Women in the agriculture sector play a crucial role and are often involved in the most exhausting tasks in agriculture. A study show that upper body strength is 40–75% less in females, while lower body strength is 5–30% less in females than in males [6]. In the current scenario, they account for a third of all agricultural production, and over half of them are self-employed farmers [7]. Already managing the burden

S. Pandit (✉) · G. P. Chindarkar · L. D. Rao · S. Das · A. Sahu · R. Kamble
Design Discipline, PDPM Indian Institute of Information Technology, Design and Manufacturing, Madhya Pradesh, Jabalpur 482005, India
e-mail: s.pandit@iiitdmj.ac.in

of the family, women tend to spend more time in field than men, especially those belonging to the poverty line [7]. The Indian agriculture industry is a challenging occupation where the farmers and workers are exposed to the health-related risks due to lifting loads repeatedly, frequently working with bend body posture and injuries from tools are the main causes of MSDs [8]. We observed in our survey that there are frequent injuries and pains in elderly women while working in agriculture field than other adults.

The objective of the study was to address and rectify the different physiological and musculoskeletal disorders due to poor ergonomic postures in elderly female farmers.

2   Methodology

2.1   Sample Selection

A study was done on agricultural workers of older age. The study was acted upon in the village Baruva, Srikakulam district in Andhra Pradesh. The sample size of 35 was collected out of which most of the participants belong to 15 units of older age group. Survey involves questions related to their working hours and their working experience in their respective activities. Videos and photos of the workers during activity were recorded.

2.2   Postural and Body Discomfort Analysis

Rapid Entire Body Assessment (REBA) represents the level of Musculoskeletal Disorders in entire body, Rapid Upper Limb Assessment (RULA) represents the level of Musculoskeletal Disorders in upper limbs of the body and Ovako Working Analysis System (OWAS) were used for postural analysis to know about the postural discomfort. Modified Nordic questions were also used to analyze the discomfort in different body parts. Pain was rated on a scale of 1–10 in various body regions, with 1 indicating "No Pain" and 10 indicating "Extreme Pain."

Table 1 Demographic data of elderly female farmers

Parameter	Min	Max	Standard deviation
Age (years)	48	70	61.17 (±6.5)
Height (cm)	140	155	147.47 ± (5.034)
Working experience (years)	15	60	32.428 (±12.025)
Working hours per day (h)	5	12	10.085 (±1.804)
Resting intervals (min)	20	90	51.911 (±21.140)

3 Results

3.1 Demographic Study

From demographic study in Table 1, out of 35 elder female participants having minimum age of 48 years and the average age of 61.17 (±6.5) years have an illiteracy rate of 77.14%. The results revealed that average working period is 10.085 (±1.804) h per day, where they spend maximum 12 h in farming. The average working experience is of 32.428 (±12.025) years and minimum of 15 years. Also workers take an average interval of 51.911 (±21.140) min.

3.2 Postural Data Analysis

From postural data analysis as shown in Table 2, it was found that RULA, REBA and OWAS score were high for the tasks such as weeding, field work and planting. Which suggest immediate change in the posture and tasks. High REBA scores above 11 were found for the tasks weeding, field work, planting and harvesting, with REBA scores as 11, 14, 12 and 11, respectively. High OWAS scores above 2 were found for the tasks weeding, field work, planting, with OWAS scores as 2, 3, 3, respectively.

3.3 Questionnaire Study

In Table 3, after analyzing the body discomfort through Modified Nordic Questionnaires the results show that neck pain in the upper body is being at high risk with a Nordic score of 66.28% followed by shoulder at 30.28% and wrist at 31.14%. In the lower body, Nordic score in the buttock's region is at 87.14%, lower body at 82% and thighs at 79.71% which shows that these parts have more discomfort.

Table 2 Body posture analysis

No. of activities involved	Body Posture	RULA score	Action category	REBA score	Action category	OWAS score	Action category
Weeding		6	Investigate further and change soon	11	Very high risk, implement change	2	Corrective measure in the near future
Field work		7	Investigate and change soon	14	Very high risk, implement change	3	Corrective measures as soon as possible
Planting		7	Investigate and change soon	12	Very high risk, implement change	3	Corrective measures as soon as possible
Carrying load		6	Investigate further and change soon	6	Medium risk, further investigation, change soon	1	No corrective measures
Harvesting		6	Investigate further and change soon	11	Very high risk, implement change	1	No corrective measures
Fertilization		6	Investigate further and change soon	6	Medium risk, further investigation, change soon	1	No corrective measures

Table 3 Nordic data for elderly female farmers discomfort

Disorders in body parts		Nordic score (%)
Upper body	Neck	66.28
	Shoulder	30.28
	Wrist	31.14
	Elbow	20.28
Lower body	Upper back	71.71
	Lower back	82
	Thighs	79.71
	Buttocks	87.14
	knees	70.57
	feet	52

Fig. 1 Discomfort while working barefoot
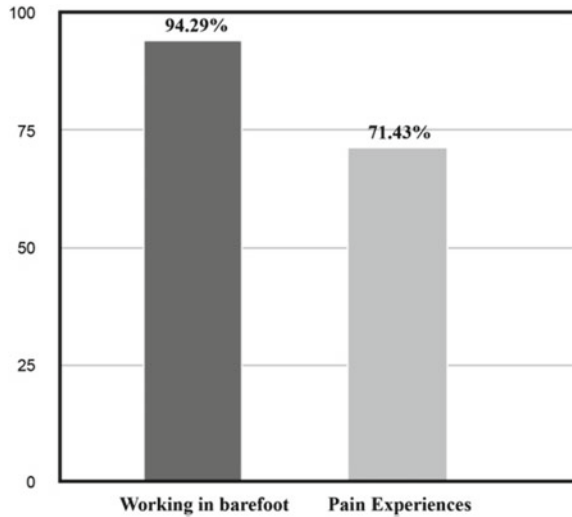
3.4 Work Condition and Injuries

From the Fig. 1 it is observed that 94.29% participants were working barefoot in the field from which 71.43% of the participant's experienced severe pain. During heavy field work they face several types of injuries like amputation and fracture. Sometimes using tools improperly may leads to cuts and other injuries due to which it get infected while staying for longer period in the flooded soil, (From Fig. 2) 25.71% of the workers got amputated due to same. Also 20% of the participants reported fracture got by the tools and heavy work.

4 Discussions

This study revealed that most of the female elderly farmers are prone to MSD due to awkward working posture. It has been observed that elderly female agricultural workers experience more pain in hip, lower back and knee, these findings are similar to the study conducted in Thailand with 481 older farmers among which 65% farmers experience extreme pain in lower extremities [1]. In this study from the postural analysis RULA and REBA score, it was found that the tasks such as weeding, field work, planting and harvesting, involved high risk postures indicating immediate change and intervention. The majority of the elderly workers in this study did physical material handling and walked on uneven paths or muddy fields. Work-related MSDs are more common in older workers than in younger workers, and the causes can be attributed to decreased muscle strength, endurance and functional capacity [9].

Fig. 2 Type of injuries
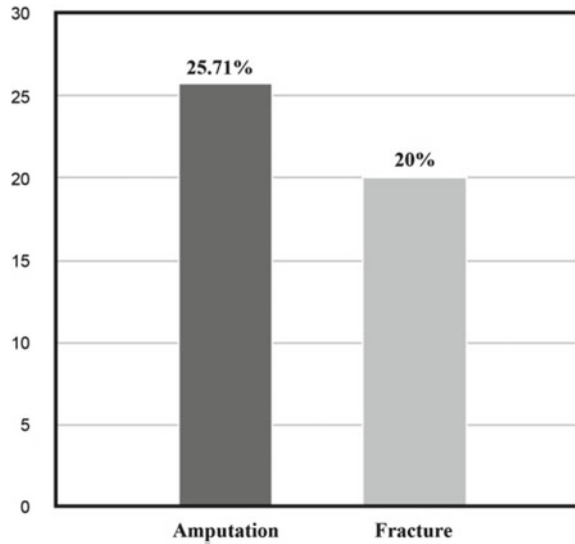
In this study, female elderly with an average age of 61.17 years is involved in hard physical work having an average work experience of 32.428 years. Agricultural activities such as weeding, planting and harvesting require repetitive bending and squatting, which causes severe pain in the lower extremities such as pain in buttocks reported by 87.14%, in lower back reported by 82%, and in thighs reported by 79.71%. Most of the farmers reported MSD symptoms in lower body regions followed by lower back and neck. Farmers working in Thailand [1] also stated that most of the time injuries occurred in their lower extremities. This study also found higher risk of development of neck pain among the farmers which has resulted from repetitive carrying of load on their head. From the study it is observed that 66.28% of the female elderly suffer from neck discomfort. This study also consistent with the study conducted in Iran with 377 farmers among which 59.9% of participants experienced discomfort [10].

Rice cultivation basically done in a clay soil which can retain water for longer period due to which farmers has to work in wetland. According to the study, 94.29% of farmers work in the field barefoot and avoid using boots or slippers owing to religious beliefs, and 71.43% of those farmers were injured. Activities such as fertilization and weeding are to be carried out in wetland due to which farmers faces difficulty in walking and using tools. Working in such an environment can result in serious injury from wounds and infections. Farmers were amputated in 25.71% of cases [11]. It was also observed that during the harvesting season, the foot impressions left by strolling in the wetland dry up and convert into solid tough and fertile ground. While harvesting and post harvesting, 20% of farmers reported fractures and other types of injuries [12].

A further study among the participants revealed injuries among the women from the usage of different tools. Similar finding was observed in research done Indian

agricultural industry where tool related injuries are found too be prevalent among the farmers [13]. It was found that many female farmers were feeling discomfort in their arms because of the heavier hand tools that were designed keeping in the anthropometry of male farmers [14]. The tool manufacturers consider 95th percentile while designing the tools [15].

During the survey, some female farmers said that they were gradually acquainted to the tools after a certain period of time. However, in the long term, they were suffering from some form of aches in the arm region. From the result, it observed that 31.14% of the participant had pain in the wrist region and 20.28% had pain in the elbow. Similar result were also found in research done among farm women [14]. During the study, the farmers also highlighted the possibility of incorporating lighter materials in the hand tools.

5   Conclusions

From the observations it was found that elderly farmers were highly affected by improper body postures and workload. Most of them complained about poor working conditions like awkward and improper work body postures, lack of breaks, improper or heavier tools, injuries followed by infection, amputation and other ailments. Twisting, bending and carrying loads repeatedly were the key factors responsible for the ergonomic discomfort in the elderly females in the agricultural sector. Lack of awareness was also a limiting factor for the elderly involved in farming.

References

1. Kaewdok, T., Sirisawasd, S., Taptagaporn, S.: Agricultural risk factors related musculoskeletal disorders among older farmers in Pathum Thani Province, Thailand. J. Agromedicine **26**(2), 185–192 (2021)
2. Arjun, K.M.: Indian agriculture-status, importance and role in Indian economy. Int. J. Agric. Food Sci. Technol. **4**(4), 343–346 (2013)
3. Kar, S., Dutta, M.: The unorganised sector and access to finance in rural India (2014)
4. Tiwari, R., Tiwari, S.: Women employment in unorganised sector in India: an empirical analysis. J. Rural Dev. **35**(4), 645–664 (2016)
5. Sharma, A., Bhaduri, A.: The "tipping point" in Indian agriculture: understanding the withdrawal of the Indian rural youth. Asian J. Agric. Dev. **6**(1362-2016-107622), 83–97 (2009)
6. Falkel, J.E., Sawka, M.N., Levine, L., Pimental, N.A., Pandolf, K.B.: Upper-body exercise performance: comparison between women and men. Ergonomics **29**(1), 145–154 (1986)
7. Pareek, K.: Analysis the factors effecting the farm women contribution in rural economy: a study of Bhilwara region
8. Jain, R., Meena, M.L., Dangayach, G.S., Bhardwaj, A.K.: Association of risk factors with musculoskeletal disorders in manual-working farmers. Arch. Environ. Occup. Health **73**(1), 19–28 (2018)
9. Okunribido, O.O., Wynn, T., Lewis, D.: Are older workers at greater risk of musculoskeletal disorders in the workplace than young workers?—a literature review. Occup. Ergon. **10**(1, 2), 53–68 (2011)

10. Dianat, I., Afshari, D., Sarmasti, N., Sangdeh, M.S., Azaddel, R.: Work posture, working conditions and musculoskeletal outcomes in agricultural workers. Int. J. Ind. Ergon. **77**, 102941 (2020)
11. Sachdev, P., Ravipati, A., Joshi, G.A.: Upper limb amputation in agricultural sector: centre based survey. In: Developments in Agricultural and Industrial Ergonomics: General Studies, vol. 1, no. 1, p. 361 (2009)
12. Nilsson, K.: Interventions to reduce injuries among older workers in agriculture: a review of evaluated intervention projects. Work **55**(2), 471–480 (2016)
13. Kumar, A., Singh, J.K., Mohan, D., Varghese, M.: Farm hand tools injuries: a case study from northern India. Saf. Sci. **46**(1), 54–65 (2008)
14. Singh, S., Arora, R.: Ergonomic intervention for preventing musculoskeletal disorders among farm women. J. Agric. Sci. **1**(2), 61–71 (2010)
15. Das, B.: Agricultural work related injuries among the farmers of West Bengal, India. Int. J. Inj. Control Saf. Promot. **21**(3), 205–215 (2014)

Ergonomic Risk Assessment Among the Welders Working in Darbhanga District of Bihar

Sangeeta Pandit, Shubham Kumar Thakur, Trushna Gopalrao Khalode, Aakriti, Avinash Sahu, and Rajat Kamble

1 Introduction

Welding jobs are widely exploited over the years as a result of rapid urbanization and industrialization providing jobs to many people. In India, almost 90% of general workers are associated with unorganized sector where 60% of them are independently employed and 30% belongs to other category [1, 2]. A huge part of the Indian economy relies on unorganized sector [3]. Developing countries such as India use welding as a vital occupation, but it is surrounded by health hazards [4]. Many companies and workplaces use welding as a standard procedure. Welders are one among the most ignored groups of labors, where workers were found to suffer from various occupational health issues and lack of safety standards among the workers [5, 6].

Previous studies in this area have found lack of awareness of safety precautions and occupational health issues such as injuries and accidents, discomfort in ears and eyes, skin-related issues, metallic fumes fever, respiratory problems, and musculoskeletal disorders among the welders [7]. Welders are prone to development of work-related musculoskeletal disorders (WMSDs), which has become a major concern [8]. Awkward postures, repetitive, forceful exertions, and movements were found to be the ergonomic risk factors causing work-related musculoskeletal disorders [8]. WMSDs were found to be affected by several individual risk factors such including age, gender, professional work, and addictions [4]. Welders' personal protective equipment is an important part of occupational health and safety standards, but most of these welding shops lack proper personal safety equipment's (PPE), and workers only wear a few types of PPE at work [7].

S. Pandit (✉) · S. K. Thakur · T. G. Khalode · Aakriti · A. Sahu · R. Kamble
Design Discipline, Design and Manufacturing, PDPM Indian Institute of Information Technology, Jabalpur, Madhya Pradesh 482005, India
e-mail: s.pandit@iiitdmj.ac.in

The purpose of this study is to investigate the welding process and to identify musculoskeletal disorders (MSDs) and different ergonomic risks involved among the welders working at different welding shops at Darbhanga district of Bihar, India.

2 Methodology

This study was conducted in the city of Bihar, Darbhanga, India, among the local welding workers. Direct observation techniques were used for this study through the help of photography, videography, and questioners. The sample was collected from 14 different workshops. The questions were prepared in such a way as to gather information about the problems related to general health-related issues, accidents, injuries, etc.

For postural analysis, rapid upper limb assessment (RULA) and rapid entire body assessment (REBA) were used. Modified Nordic questions were used to study the body part discomfort in welding activities. Five scale rating was used to measure the level of discomfort in welding activities, 1 denotes "less discomfort" and 5 denotes "extreme discomfort." For data analysis, descriptive statistics was used and tabulated.

3 Result

3.1 Data Study

In this study, 34 samples of welding workers had a minimum age of 22 years and a maximum of 55 years, with an average age of 35.14 ± 8.41 years. The workers had minimum work experience of 2 years and maximum of 32 years with average work experience of 15.73 ± 7.85 years, and the working hours ranged from minimum 1 h a day to maximum of 10 h a day with an average working time of 6.47 ± 2.60 working hours a day as shown in "Table 1."

Table 1 Demographic of welders

Parameters	Min	Max	Standard deviation
Age (years)	22	55	35.14 (±8.41)
Experience (years)	2	32	15.73 (±7.85)
Working hours (h)	1	10	6.47 (±2.60)
Working days per week	6	7	6.05 (±0.53)

Table 2 Welder's postures analysis

S. No.	Postures	RULA score	Action recommended	REBA score	Action recommended
1		4	Investigate further	8	Necessary soon
2		6	Further investigation and change needed	12	Necessary now
3		5	Further investigation and change needed	11	Necessary now
4		7	Investigation and immediate change needed	12	Necessary now
5		6	Further investigation and change needed	9	Necessary soon

3.2 Postural Analysis

From the postural analysis as shown in "Table 2," it was found that the RULA and REBA scores showed medium to high-risk level and action recommended for all the observed postures suggested "investigate and change immediately" and "necessary now," respectively.

3.3 Body Pain Discomfort

The data from the Nordic questioner were analyzed and tabulated as shown in "Table 3." In this study, it was found that the discomfort level was highest in arm's region with 42.35% reports of pain followed by discomfort in lower leg area with 41.76% reports of pain, and feet with 40.58% reports of pain among the welders.

3.4 Health Issues

Different health issues the welders faced were identified and tabulated as shown in "Table 4." In this study, it was found that high problems were reported for the general

Table 3 Modified Nordic score for discomfort in different body part

Discomfort in different body part	Nordic score (%)
Neck	37.64
Shoulder	37.05
Fore arm's	42.35
Wrist	36.47
Knee	37.64
Lower leg	41.76
Feet	40.58

Table 4 General health issues

Health symptoms	Reported symptoms (%)
Eye problem	85.29
Hearing problem	29.40
Headache problem	23.52
Respiratory problem	41.17
Sleep disorder	17.64
Heart problem	5.88

health-related issues and as per the study eye-related problems were high by 85.29% because of the intensive visible, ultraviolet, inferred radiation emitted by the welding arc and fumes and respiratory problems by 41.17% because of the fumes and harmful reaction gases.

3.5 Accident Reports

Data related to accidents were collected and tabulated as show in "Table 5." Here, it was founded that the occupational health also gets affected due to skin-related problems was reported by 67.64% and accidents and injury by 17.64% and 32.35%, respectively, and all these lead to absenteeism by 61.76%.

Table 5 Occupational health affected by different factors

Factor	Reported (%)
Accident	17.64
Injury	32.35
Skin problem	67.64
Use safety glasses (PPE)	35.29
Absenteeism	61.76

4 Discussion

Due to the current working condition of the welders and the increase in demand of welding activities, the welders are at high risk of development of MSDs, resulting in health issues, lower productivity, and thus live lower quality life. Thus there is an immediate need of ergonomic study in this unorganised sector. In our study, the most of the workers had experience less than 5 years which is similar to the results found among the welders from Banepa Municipality in Nepal [7]. The finding of this study revealed that the welding postures of welders scored high on both REBA and RULA postural analysis, indicating that the postures involved high risks, and suggested immediate change. Welders were found to be working in awkward and uncomfortable postures for a long duration of time as per the exposure time which was calculated for all shifts taking each posture into consideration. Similar findings have been found in another study which conducted on 60 welders of Jalandhar, India [4].

In our study, majority of respondents reported pain in their forearm, these results are in line in the research done among other informal sectors involving tasks with repeated hand motions [9]. The welders also reported pain in shoulder, similar results were observed in a study among the welders from Maharashtra, India [10] and also, among the workers in the German steel industry [11]. A study done among the welders working in Iranian steel industry reported pain in neck regions; [12] this study also supports similar results where the welders reported pain in neck regions.

This study also reports high accidents rates, with highest reports of eye injuries and respiratory issues. The study is consistent with the observation done in Accra, Ghana, [13] and in Jalandhar, India [4]. Welders also face skin-related problems which may increases the risk of developing skin cancer as observed in study of USA [14]. It was also observed that due to continuous exposure to the fumes over their hands they suffered from burns and itching, which is the result of not wearing protective gears. The existing PPE such as gloves were seen to cause hindrance in their work resulting in lesser productivity, and thus, the welders neglect the use of protective gears.

5 Conclusion

From this study, it is evident that the welder's health is negatively impacted by poor body postures and ergonomic risk factors involved in the work. Working for prolonged time in awkward postures and working with fumes have resulted in discomfort in shoulders and hand regions. In addition, neglecting the use of protective equipment's has resulted in discomfort in eyes, skin, and breathing. This study provides the base understating of the problems of welders working in welding shops of Darbhanga district of Bihar, India. This study suggests immediate interventions in the

area to improve the PPE and provide awareness of the same, thus encouraging the use of PPE and eliminating the discomfort among the workers.

References

1. Pingle, S.: Occupational safety and health in India: now and the future. Ind. Health **50**(3), 167–171 (2012)
2. Saha, R.K.: Occupational health in India. Ann. Glob. Health **84**(3), 330 (2018)
3. Dev, M., Bhardwaj, A.: Respiratory symptoms and spirometric abnormalities among welders in the welding workplace of the Indian unorganized sector. Work (Preprint), 1–10 (2021)
4. Dev, M., Bhardwaj, A., Singh, S.: Analysis of work-related musculoskeletal disorders and ergonomic posture assessment of welders in unorganized sector: a study in Jalandhar, India. Int. J. Hum. Factors Ergon. **5**(3), 240–255 (2018)
5. Tagurum, Y.O., Gwomson, M.D., Yakubu, P.M., Igbita, J.A., Chingle, M.P., Chirdan, O.O.: Awareness of occupational hazards and utilization of PPE amongst welders in Jos metropolis, Nigeria. Int. J. Res. Med. Sci. **6**(7):2227–2233 (2018). https://doi.org/10.18203/2320-6012.ijrms20182808
6. Beyene Gebrezgiabher, B., Tetemke, D., Yetum, T.: Awareness of occupational hazards and utilization of safety measures among welders in Aksum and Adwa towns, Tigray region, Ethiopia, 2013. J. Environ. Public Health (2019). https://doi.org/10.1155/2019/4174085
7. Joshi, M., Dhakal, G., Shrestha, S.: Occupational health problems, workplace environment and utilization of personal protective equipment among welders of Banepa municipality. Int. J. Occup. Saf. Health **10**(2), 100–107 (2020)
8. Nunes, I.L., Dias, N.: Analysis and risk assessment of work-related musculoskeletal disorders in a physical rehabilitation unit. Int. J. Hum. Factors Ergon. **1**(4), 318–332 (2012)
9. Nag, A., Vyas, H., Nag, P.: Occupational health scenario of Indian informal sector. Ind. Health 2015–0112 (2016)
10. Aswalekar, U.V., Tungikar, V.B.: Assessment of ergonomic environment and risk factors for musculoskeletal disorders among welders in micro small and medium sized enterprises. Ind. Eng. J. (2017)
11. Weyh, C., Pilat, C., Krüger, K.: Musculoskeletal disorders and level of physical activity in welders. Occup. Med. **70**(8), 586–592 (2020)
12. Shahriyari, M., Afshari, D., Latifi, S.M.: Physical workload and musculoskeletal disorders in back, shoulders and neck among welders. Int. J. Occup. Saf. Ergon. (2018)
13. Kwaku Tetteh, K.K., Owusu, R., Axame, W.K.: Prevalence and factors influencing eye injuries among welders in Accra, Ghana. Adv. Prev. Med. (2020)
14. Falcone, L.M., Zeidler-Erdely, P.C.: Skin cancer and welding. Clin. Exp. Dermatol. **44**(2), 130–134 (2019)

Identification of Postural Load on Sculptors of Sculpting Industry of India

Supriya Bawiskar, Avinash Sahu, Sangeeta Pandit, Bhakti Kirdat, Rajat Kamble, Saad Ahmed, Chetan Gohil, and Sanjuman Sinku

1 Introduction

Idol making or Murtikari is an important family tradition aiding in celebrations of various Hindu festivals. The artisans start their work 2–4 months before the festival and work on multiple idols, which the respective owners take home on the day of the festival. At times, along with the artisans, their family members are also involved in the idol-making process [1]. Chitar Oli (Etymology: Chitrane meaning sculpting/painting + Oli meaning lane) is one of the oldest neighborhoods in Nagpur known for its artistic heritage in idol making [2]. Similarly, Kumartuli is a street in the neighborhood of Kolkata. These streets are a repository of mud idols and home of artisans of all ages showcasing their talent [3]. Chitar Oli and Kumartuli are vital centers exporting the idols all over India and also abroad. However, during present times, this trade is seen to declining as very few people are willing to take forward their family tradition work, and also, the existing artisans are not able to contribute much in terms of hours spent due to age and ailment factors [2, 3].

Studies done in this sector have revealed that most of the work-related MSDs among the workers are due to cumulative disorders [4–6]. Researches have also found the evidences of pain in different body regions among the artisans working in different handicrafts sector [7, 8]. Solutions like redesign/retrofitting, optimization of tools and workspaces have found to reduce the musculoskeletal disorders among the artisans [9].

As this work is seasonal, the artisans are dependent on this work for their livelihood, and so have to take up more work during a short period of time, resulting in excessive repeated tasks with very little time for rest (Fig. 1). Thus, this paper aims to

S. Bawiskar · A. Sahu · S. Pandit (✉) · B. Kirdat · R. Kamble · S. Ahmed · C. Gohil · S. Sinku
Ergonomics Lab, Design Discipline, Indian Institute of Information Technology, Design and Manufacturing, Jabalpur, M.P. 482005, India
e-mail: s.pandit@iiitdmj.ac.in

Fig. 1 Existing ergonomic problems highlighted in the sculptors of Chitar Oli, Nagpur

identify occupational stresses of postural load on these artisans and the effects of age and experience on the discomforts and provides a base study for future interventions in the area.

Recently, the corporate houses have made their entry into different seasonal festivals and convert the idea of worship of idols to a creative exhibition which has imposed work stress among the sculptors. Commercialization and competition plays an important role in increasing to complete work in less time resulting more working hours and prolonged awkward postures.

2 Methodology

The study was divided into two phases. Phase-1 of the study was undertaken during the Ganeshotsav celebrations in Chitar Oli—Nagpur, Maharashtra. Phase-2 of the same was conducted during Durga Pooja Celebrations in Kumartuli, Kolkata. The

sample size consisted of the general inhabitant populace of both the places, respectively, where 120 artisans participated in the study from 30 families. The participants who had prevailing physiological disorders/post-operational conditions were excluded from the study. Understanding of the existing nature of work was done by the process of data collection. This involved observations (photography and videography), questionnaires, and process mapping. To identify ergonomic risks, the sculpting task was divided into 5 sub-tasks which are, preparing the soil with feet and hands, preparing the sculpture, drying the model, and coloring and finishing the sculptures. Rapid Upper Limb Assessment (RULA), Rapid Entire Limb Assessment (REBA) and Ovako Working posture Assessment System (OWAS) were used for the study of postural analysis. Modified Nordic questionnaire was used. The data were analyzed using simple descriptive statistics and tabulated.

3 Results

The workers were of age ranging from 30 to 60. The average age of the artisans was 45.73 ± 7.67. The average height and weight of the artisans was 172.88 ± 5.66 cms and 72.31 ± 5.73 kgs, respectively. The artisans had an average BMI of 24.18 ± 1.42. The average working hours daily was 9.6 ± 1.32, almost every day in a week. The artisans working there have an average work experience of 29.54 ± 8.87 years (Table 1.)

From the postural analysis, the RULA scores suggested investigation and implementing change (Table 2). Similarly, REBA scores also suggest investigation and implementing change. OWAS score suggested corrective measures in the near future. Sculpting has been a traditional activity of the artisans of Chitar Oli and is majorly unorganized resulting in high RULA (7), REBA (11), and OWAS (2) scores.

From the body part discomfort study (Table 3), most discomfort feeling was seen in following order of body parts in sculptors; palm, knee, neck, back, and shoulder area.

Table 1 Demographics of sculptors

Parameter	Min	Max	Standard deviation
Age (Years)	30	60	45.73 ($\pm$7.67)
Height (cm)	160	183	172.88 ($\pm$5.66)
Weight (kg)	58	85	72.31 ($\pm$5.73)
BMI (kg/m^2)	20.95	28.07	24.18 ($\pm$1.42)
Working experience (Years)	6	48	29.54 ($\pm$8.87)
Duration per day (h)	6	12	9.6 ($\pm$1.32)
Working days per week	6	7	6.66 ($\pm$0.47)

Table 2 Postural analysis on Chitaroli and Kumartuli artisans

Posture	Task	REBA score	Action category	RULA score	Action category	OWAS	Action category
	Preparing soil with feet	8	High risk, investigate and apply change	7	Investigate and apply change	1	No corrections required
	Preparing soil with hands	8	High risk, investigate and apply change	5	Further investigation, change soon	2	Corrections required soon
	Preparing Sculpture	11	Very high risk, apply change	7	Investigate and apply change	2	Corrections required soon
	Drying the model in the sun	5	Medium risk, further investigation	4	Further investigation, change may be needed	1	No corrections required
	Coloring the model	11	Very high risk, apply change	7	Investigate and apply change	2	Corrections required soon

Table 3 Discomfort feeling in different body parts among the sculptors

Different body parts	Discomfort	Non-discomfort
Palm	86	34
Shoulder	32	88
Neck	50	70
Knee	69	51
Back	48	72

The artisans were grouped into 3 categories (Table 4.) based on age (30–40; 41–50; 51–60). Modified Nordic questionnaire was used to assess body pain. Discomfort in the palm area was significantly high among the higher age group artisans. Discomfort rates were found to be highest among the age group 51–60 years in upper limb body regions such as palm (80%), neck (54.28%), shoulder (34.28%), and knee (80%). Whereas, discomfort in the back (56%) was high in the age group 30–40 year. Due to the use of traditional sculpting tools, more discomfort was seen in the upper limb.

Table 4 Resultant percentage pain area as per survey conducted following modified Nordic questionnaire

Age group	No. of participant	Palm (%)	Shoulder (%)	Neck (%)	Knee (%)	Back (%)
30–40	25	44	16	24	32	56
41–50	60	78.33	26.66	41.66	55	45
51–60	35	80	34.28	54.28	80	20

4 Discussion

The families of murti makers at Chitar Oli were seen to work day and night in devotion to the god ignoring the problems and body discomfort they face due to the work; thus, it is important to understand the health issues faced by the artisans working as murti makers. The majority of artisans belonged to the age group 40–60 years old as also found in other research done in the area [2]. These art form requires high skills and precisions which comes from many years of practice and thus getting exposed cumulative trauma from to different ergonomic risk factors such as repetitive work in awkward posture resulting in pain in different parts of the body. From postural analysis REBA, RULA and OWAS, high scores were found for the tasks such as preparing soil and sculpture and coloring the sculpture, suggesting immediate intervention in the area. A study involving similar tasks among saw mill workers found discomfort in the upper limb due to prolonged working in bad postures [4, 5] which is inline with the results of this study.

In our study, it was found that back discomfort was more in young age groups as compared to the older age groups. Similarly, more discomfort was seen in the knee in older age groups compared to young age groups. However, discomfort in the palm area was seen to be significantly high in every age group of sculptors; similar results were found among the stitching workers and which also involved integrate precision hand work [8, 10]; similar findings were also seen among the artisans working in hand block printing [11, 12]. Ergonomic risk involved among the Murti makers was found to be complex repetitive hand movement, extreme extensions of the body, prolonged sitting posture in crossed-legged, or on heels and prolonged slouching which resulted in discomfort in different body regions with highest percentage of reports in lower back and thigh region which. This ergonomic risk factors along with long working hours were seen to have developed humpback along with neck and knee flexion and also caused back pain among the artisans. Similar findings were seen among the potters where they found long working hours caused joint pain, fatigue, swelling, sprain of ligaments among the porters [7].

5   Conclusion

From this study, it is evident that the Murti makers at Chitar Oli and Kumartuli were in high risk of development of discomfort in lower back, neck, and palm region which is a result of tasks involving postures with high economic risks. Thus, there is a need for immediate intervention in the area to develop improved workstation and tools to eliminate the ergonomic risks involved and improve the health conditions of the artisans.

References

1. Guha-Thakurta, T.: Monuments, Objects, Histories. Columbia University Press (2004)
2. Pathe, S., Khare, S.: Establishing a Participatory Approach Among Communities and Citizens Towards the Urban Development Within the Chitar Oli District of Nagpur, Maharashtra, no. 4270. EasyChair (2020)
3. Chakrabarti, S., Iyer, V., Bhowal, R., Sengupta, S.: The 'God Makers' of Kolkata: can improved infrastructure mitigate the misery of artisans in Kumartuli? (2014)
4. Ali, A., Qutubuddin, S.M., Hebbal, S.S., Kumar, A.C.S.: An ergonomic study of work related musculoskeletal disorders among the workers working in typical Indian saw mills. Int. J. Eng. Res. Dev. **3**(9), 38–45 (2012)
5. Dev, M., Bhardwaj, A., Singh, S.: Analysis of work-related musculoskeletal disorders and ergonomic posture assessment of welders in unorganised sector: a study in Jalandhar, India. Int. J. Hum. Factors Ergon. **5**(3), 240–255 (2018)
6. Kumar, D., Rajeev, P. V., Tanty, G.: A literature review of ergonomics factors in handicraft sector. (2019)
7. Sahu, S., Moitra, S., Maity, S., Pandit, A.K., Roy, B.: A comparative ergonomics postural assessment of potters and sculptors in the unorganized sector in West Bengal, India. Int. J. Occup. Saf. Ergon. **19**(3), 455–462 (2013)
8. Sahu, A., Kamble, R., & Pandit, S.: Identification of ergonomic risk factors in dhokra bell metal handicraft industry of Chhattisgarh, India. In: International Conference of the Indian Society of Ergonomics, pp. 1327–1336. Springer, Cham (2022)
9. Mrunalini, A., Logeswari, S.: Musculoskeletal problems of artisans in informal sector—a review study. Int. J. Environ. Ecol. Fam. Urban Stud. **6**(1), 163–170 (2016)
10. Jadhav, G.S., Arunachalam, M., Salve, U.R.: Ergonomics design and evaluation of the stitching workstation for the hand-crafted Kolhapuri footwear using a digital human modeling approach. J. Ind. Prod. Eng. **36**(8), 563–575 (2019)
11. Kamble, R., Sahu, A., Pandit, S.: Occupational ergonomic assessment of hand pain symptoms among Bagh hand block print artisans of the handicraft textile industry in Madhya Pradesh, India. Int. J. Occup. Saf. Ergon. 1–9 (2021)
12. Kamble, R., Pandit, S., Sahu, A.: Occupational ergonomic assessment of MSDs among the artisans working in Bagh hand block printing industry in Madhya Pradesh, India. Int. J. Occup. Safety Ergonomics. 1–18. (2022)

Tribological Behavior of Co–Cr–Mo Alloy on Ultra High Molecular Polyethylene With and Without Third Body Particles Used in Hip Implant Application

G. B. Veeresh Kumar, H. S. Balasubramanya, T. Anil Kumar, R. Pramod, and S. M. Aradhya

1 Introduction

Biomaterial is natural or synthetic material used in the field of medical hip implantation, which is compatible with living tissues. Biomaterials are desired to have properties such as biocompatibility, bio inertness, conductivity, high wear resistance, and corrosion resistance [1]. Total hip joint replacement is unavoidable orthopedic application for the patient suffering from arthritis and for improving the quality life of patients [2]. A hip implant is an artificial substitute for replacement of damaged joints. Total hip replacement implants are made up of four individual components such as stem, cup, ball, and liner. Stem is the part inserted the femur bone, Cup is the part inserted into the pelvic bone, Ball is the part fitted onto the end of the stem and liner is the part inserted into the cup and becomes new cartilage [3]. Total hip replacement is considered to be landmark achievement of the twentieth century in the field of orthopedics. But the revision surgery that is performed due to wear is of

G. B. V. Kumar
Department of Mechanical Engineering, National Institute of Technology Andhra Pradesh, Tadepalligudem, Andhra Pradesh, India

H. S. Balasubramanya (✉) · T. A. Kumar
Department of Mechanical Engineering, Ramaiah Institute of Technology, Bengaluru, Karnataka, India
e-mail: baluhs.md@gmail.com

R. Pramod
Department of Mechanical Engineering, Amrita School of Engineering, Amrita Vishwa Vidyapeetham, Bengaluru, Karnataka, India

S. M. Aradhya
Department of Mechanical Engineering, Kalpataru Institute of Technology, Tiptur, Karnataka, India

implant is major concern [4]. Wear is the progressive loss of material from surfaces in contact, which occurs as a result of friction. The processes by which material experiences wear is known as wear mechanisms. The different types of wear mechanisms are abrasion, adhesion, third body, fatigue, and corrosion. As in [4] author has studied critical issues of wear of biomedical implants and tribological aspect and focuses on primary causes and concerns of the wear debris, various setups, and techniques by which wear of artificial joint materials are studied. The work also focuses on various implant materials. As in [5] author provides introduction, composition of bone cement, types of bone cement, and drawbacks of bone cement and concluded that particles from PMMA bone cement results in wear, loosening of implant, and complications in hip replacements. Wear caused by the third body particles on the hip joint replacement materials is an important factor affecting the service life of the hip-replaced joints [5, 6]. The wear debris from the material used for replacement causes adverse reactions with the tissue and third body particles cause the wear resulting in the implant failure. Wear caused by the third body particles on the hip joint replacement materials is an important factor affecting the service life of the hip-replaced joints [7]. The different sources of third body particles that results in wear and lead to failure of the implants are PMMA bone cement particles, hydroxyapatite coatings, metal debris from coatings, metal fragments from other fixation devices, and corrosion products from the metal tapers [5]. Out of which PMMA bone cement is the main cause for the third body particles. As in [6], author has compared mechanical property and biocompatibility of cobalt-based alloy to other metallic biomaterials for hip joint replacement. Result shows that a layer of cobalt-based alloy exhibit high corrosion resistance and good mechanical properties in chloride environment due to alloying additions and formation of chromium oxide (Cr_2O_3) passive layer.

Co–Cr–Mo alloys are used for hip implant application due to their excellent mechanical, wear, and corrosion resistance and are good choice of material for bearing surfaces. The Ni ions present in Co–Cr–Mo alloys is the reason for the allergic reactions, carcinogenicity [8] and the toxicity problem of cobalt nickel-based alloy and it can be avoided by decreasing Ni ions from Co–Cr–Mo alloy [9]. The wear resistance of Co-based alloy is higher than that of both Ti alloys and Stainless Steel alloys [10]. In artificial hip joints, the head of the joint is subjected to wear. Thus, hip joints have been fabricated from Co–Cr–Mo alloys, which exhibit high strength and ductility. Ultra high molecular weight polyethylene (UHMWPE) is a thermoplastic polymer is a biocompatible and nontoxic material. It is having good mechanical properties such as high corrosion resistance, high wear resistance, and low COF. As in [11], author has discussed processing technologies and principles. UHMWPE is derived from ethane monomers ($CH_2 = CH_2$) and is synthesized by polymerization process using Ziegler Natta catalyst at low-pressure conditions. The polymerization process results in a powder that can be molded or extruded into sheet rod or near net shape of the implant. In the present investigation, pin on plate wear test is carried out using ducom linear reciprocating tribometer, to evaluate average wear rate, COF, and frictional force between Co–Cr–Mo alloy and Ultra High Molecular Polyethylene with and without third body particles under load condition of 20 N,

Table 1 Chemical composition of ASTM Co, Cr and Mo alloy [12]

Element	Cr	Mo	Ni, Cu, Ti	Mn	Mo	Co	N	Si	Fe	C	O	P, S
Percent	28.1	5.3	0.01	0.69	5.36	64.86	0.2	0.67	0.04	0.039	0.02	0.001

Table 2 Mechanical specification of cobalt chromium molybdenum alloy

Parameter	Yield strength	Tensile strength	Elomgation	Hardness
Value	1082 MPa	1496 MPa	41%	410 HV

stroke of 6 mm, and frequency of 5 Hz. The test is carried out for one lakh cycles and sliding distance of 1200 m further the obtained results were discussed.

2 Material and Experimental Details

The tribological study is carried out for Co–Cr–Mo alloy on UHMPE using ducom liner reciprocating tribometer. The test standard followed is ASTM G133. The test is conducted with and without third body particles (5 g/l) PMMA bone cement in simulated body fluid. Ringers solution is used as simulating body fluid. The dimension of pin used is 6 mm in diameter and 15 mm in length. The dimension of plate used is 40 mm length × 40 mm width × 5 mm thickness. The parameters selected for experimentation are load: 20 N, frequency: 5 Hz, temperature: 37 °C (Human Body Temperature), test duration: 20,000 s, sliding distance: 1200 m, and no of cycles: 100,000 cycles.

The Co–Cr–Mo alloy used for the test is of ASTM F1537 standard. The chemical composition and mechanical characteristics of Co–Cr–Mo alloy is depicted in Table 1 and 2, respectively. The Co–Cr–Mo pin used for the current study is shown in Fig. 1.

The UHMPE plate is conditioned in distilled water before experimentation for 7 days. The UHMPE plate used for test is shown in Fig. 2. The Co–Cr–Mo pin on UHMPE plate tribological test setup is as shown in Fig. 3.

3 Results and Discussion

The results obtained after tribological study of Co–Cr–Mo pin on UHMPE plate specimen with and without third body particles (5 g/L PMMA bone cement) and comparison of the same is presented below. The wear rate of Co–Cr–Mo alloy pin

Fig. 1 Co–Cr–Mo alloy pin

Fig. 2 UHMPE plate

and UHMWPE plate specimen without third body particles (5 g/L PMMA bone cement) is depicted in Table 3.

The wear rate of Co–Cr–Mo and UHMWPE plate is 4.58×10^{-8} g/Nm and 3.33×10^{-8} g/Nm, respectively. The wear rate of pin specimen is greater than plate specimen. The average wear rate of pin and plate specimen is 3.95833×10^{-8} g/Nm.

The COF of Co–Cr–Mo alloy pin and UHMWPE plate specimen without third body particles (5 g/L PMMA bone cement) is depicted in Fig. 4. The COF of Co–Cr–Mo alloy pin on UHMWPE plate is initially high up to 0.119 due to the initial roughness of the material and it decreases as test duration increases. The COF at end of the test is 0.108.

The frictional force of Co–Cr–Mo alloy pin and UHMWPE plate specimen without third body particles (5 g/L PMMA bone cement) is depicted in Fig. 5. The frictional force of Co–Cr–Mo alloy pin on UHMWPE plate is initially high upto 2.38 N and it decreases with increase in test duration. The frictional force at end of the test is 2.161 N.

Fig. 3 Co–Cr–Mo pin on UHMPE plate
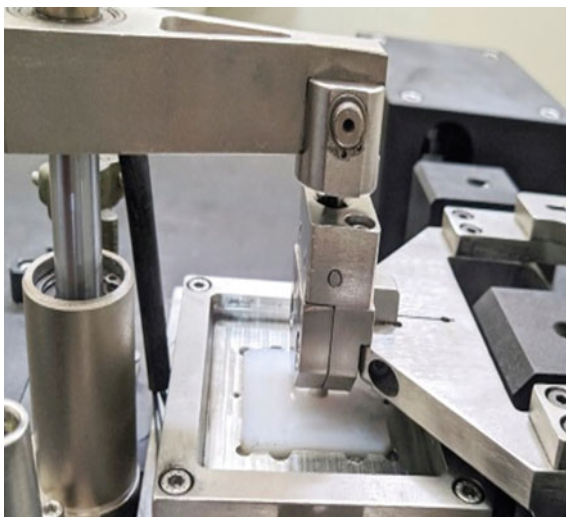
Table 3 Wear rate of Co–Cr–Mo alloy pin and UHMWPE plate specimen

Sample	Initial mass (gm)	Final mass (gm)	Wear rate g/Nm	Avg. wear g/Nm
Co–Cr–Mo pin	3.4666	3.4655	4.5833×10^{-8}	3.95833×10^{-8}
UHMWPE plate	7.9112	7.9104	3.3333×10^{-8}	
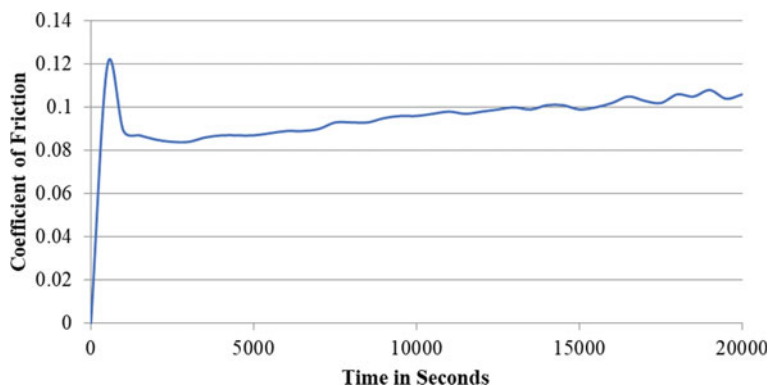
Fig. 4 COF plot of Co–Cr–Mo alloy pin on UHMWPE plate

The temperature plot of Co–Cr–Mo alloy pin and UHMWPE plate specimen without third body particles (5 g/L PMMA bone cement) as depicted in Fig. 6.

The tribological test of Co–Cr–Mo alloy pin on UHMWPE plate in simulating body fluid (ringer's solution) is conducted at $37 \pm 0.2\ °C$ for the duration of 20,000 s.
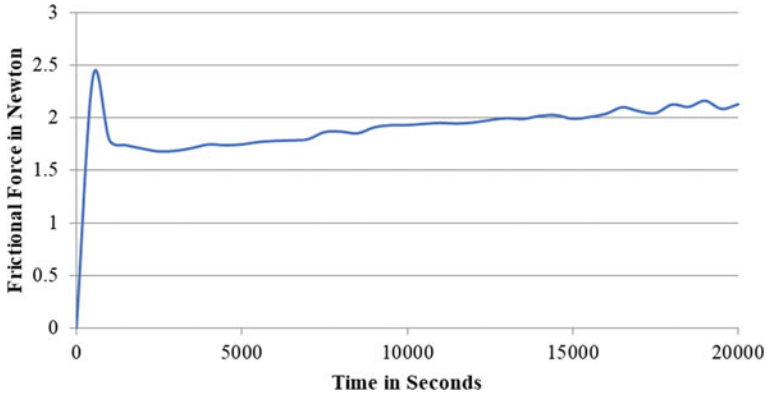
Fig. 5 Frictional force plot of Co–Cr–Mo alloy pin and UHMWPE plate
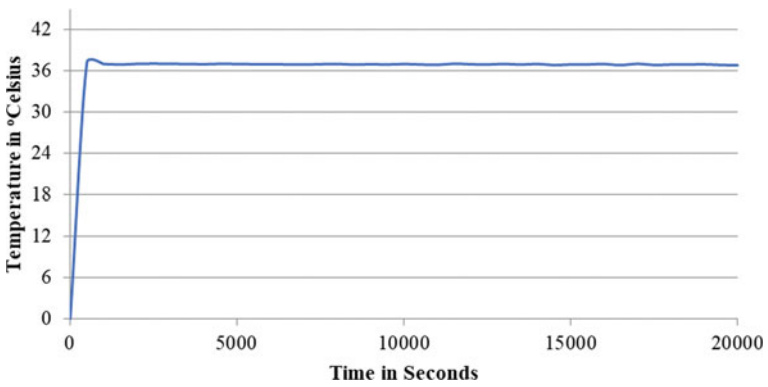
Fig. 6 Temperature plot of Co–Cr–Mo alloy pin and UHMWPE plate

The wear rate of Co–Cr–Mo alloy pin and UHMWPE plate specimen with third body particles (5 g/L PMMA bone cement) is depicted in Table 4.

The wear rate of Co–Cr–Mo alloy pin and UHMWPE plate with 5 g/L PMMA bone cement particles is 7.0833×10^{-8} g/Nm and 4.5833×10^{-8} g/Nm, respectively. The wear rate of pin specimen is greater than plate specimen. The average wear rate of pin and plate specimen is 5.8333×10^{-8} g/Nm. Wear scars are visible on the specimen.

Table 4 Wear rate of Co–Cr–Mo alloy pin and UHMWPE plate specimen with 5 g/L third body particles (PMMA bone Cement)

Sample	Initial mass (gm)	Final mass (gm)	Wear rate g/Nm	Avg. wear g/Nm
Co–Cr–Mo pin	3.4682	3.4665	7.0833×10^{-8}	5.8333×10^{-8}
UHMWPE plate	7.8077	7.8066	4.5833×10^{-8}	
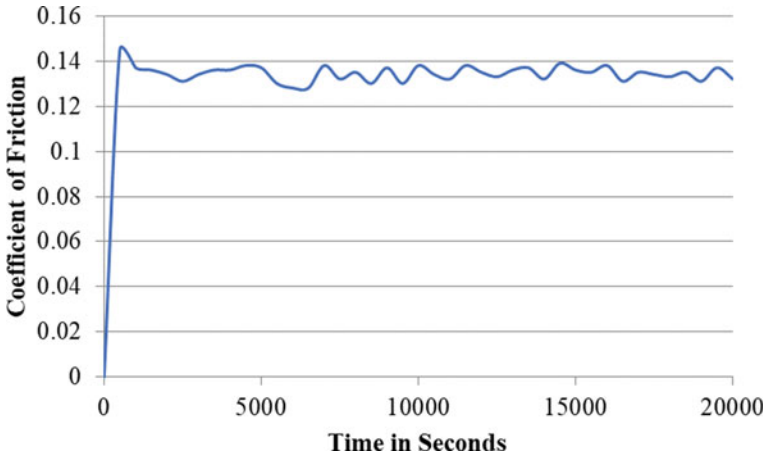
Fig. 7 COF plot of Co–Cr–Mo alloy pin and UHMWPE plate with 5 g/L third body particles (PMMA bone Cement)

The COF of Co–Cr–Mo alloy pin and UHMWPE plate specimen with third body particles (5 g/L PMMA bone cement) is depicted in Fig. 7.

The COF of Co–Cr–Mo alloy pin on UHMWPE plate with 5 g/L PMMA bone cement particles is initially high up to 0.145 due to the roughness of the material and it decreases as test duration increases. The COF at end of test is 0.137. The deviations in COF are due to interaction of PMMA particles between the surfaces.

The frictional force of Co–Cr–Mo alloy pin and UHMWPE plate specimen with third body particles (5 g/L PMMA bone cement) is depicted in Fig. 8. The frictional force of Co–Cr–Mo alloy pin on UHMWPE plate with 5 g/L PMMA bone cement particles is initially high up to 2.903 N and it decreases as test duration increases. The frictional force at end of test is 2.768 N. The deviations in frictional force are due to interaction of PMMA particles between the surfaces.

The temperature plot of Co–Cr–Mo alloy pin and UHMWPE plate specimen with third body particles (5 g/L PMMA bone cement) is depicted in Fig. 9. The tribological test of Co–Cr–Mo alloy pin on UHMWPE plate with 5 g/L PMMA bone cement particles in simulating body fluid (ringers' solution) are conducted at $37 \pm 0.2\ °C$ for the duration of 20,000 s.

The comparison of average wear rate of Co–Cr–Mo alloy pin on UHMWPE plate with and without third body particles (5 g/L PMMA bone cement) is shown in Fig. 10. The average wear rate of Co–Cr–Mo alloy pin on UHMWPE plate without third body particles is 3.96×10^{-8} g/Nm and with third body particles (5 g/L PMMA bone cement) is 5.83×10^{-8} g/Nm. The increase in average wear rate of trials with third body particles compared to without third body particles is due to interaction of third body particles between the surfaces of the specimen.

The comparison of COF of Co–Cr–Mo alloy pin on UHMWPE plate with and without Third Body Particles (TBP) (5 g/L PMMA bone cement) is shown in Fig. 11.
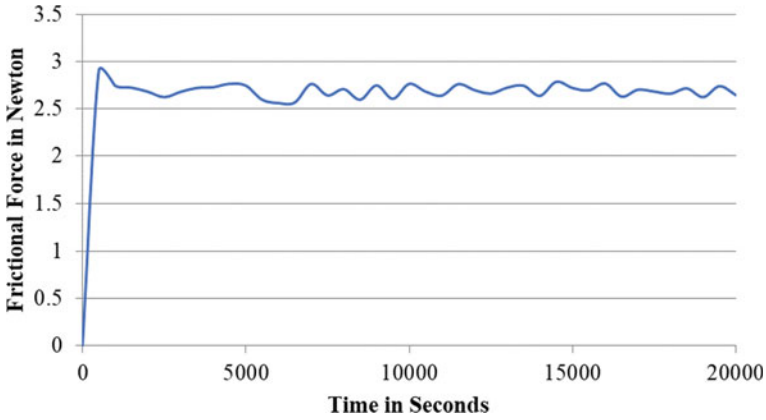
Fig. 8 Frictional force plot of Co–Cr–Mo alloy pin and UHMWPE plate with 5 g/L third body particles (PMMA bone Cement)
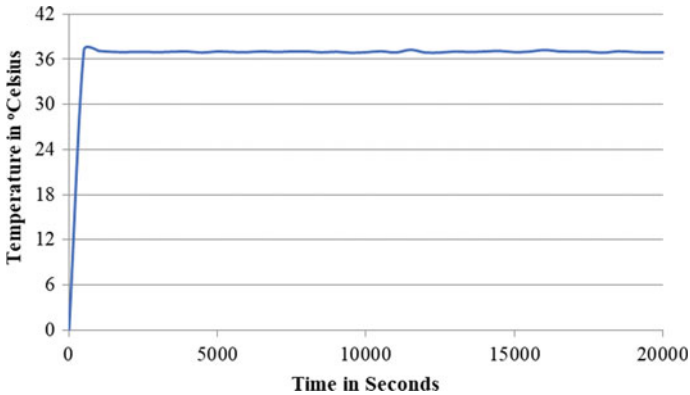
Fig. 9 Temperature plot of Co–Cr–Mo alloy pin and UHMWPE plate with 5 g/L third body particles (PMMA bone Cement)

The COF of Co–Cr–Mo alloy pin on UHMWPE plate without third body particles is 0.108 and with third body particles (5 g/L PMMA bone cement) is 0.137. The increase and deviations in COF in trials with third body particles compared to without third body particles is due to interaction of third body particles between the surfaces of the specimen.

The comparison of frictional force of Co–Cr–Mo alloy pin on UHMWPE plate with and without third body particles (5 g/L PMMA bone cement) is shown in Fig. 12.

The frictional force of Co–Cr–Mo alloy pin on UHMWPE plate without third body particles is 2.161 N and with third body particles (5 g/L PMMA bone cement) is 2.768 N. The increase and deviations in frictional force in trials with third body particles compared to without third body particles is due to interaction of third body
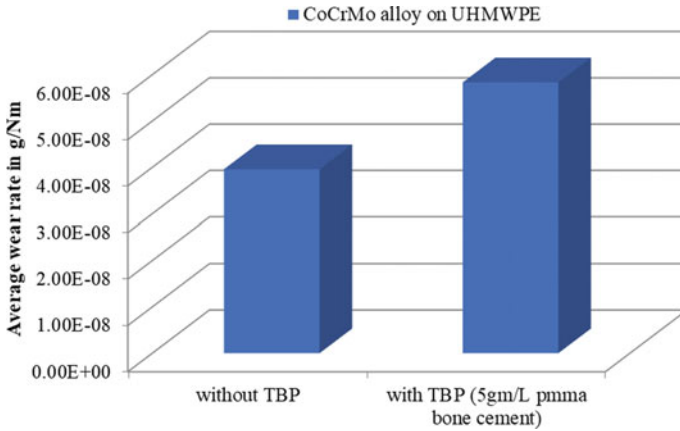
Fig. 10 Average wear rate plots of specimen with and without third body particles (5 g/L PMMA bone Cement)
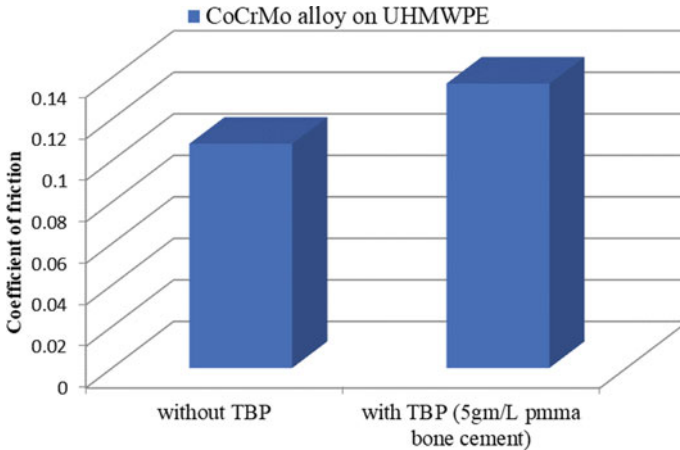
Fig. 11 COF plots of pin and plate specimen with and without third body particles (5 g/L PMMA bone Cement)

particles between the surfaces of the specimen. From the results, the proposed material is performing well and exhibits good wear properties when compared to the works done in calcia-doped zirconia [8].
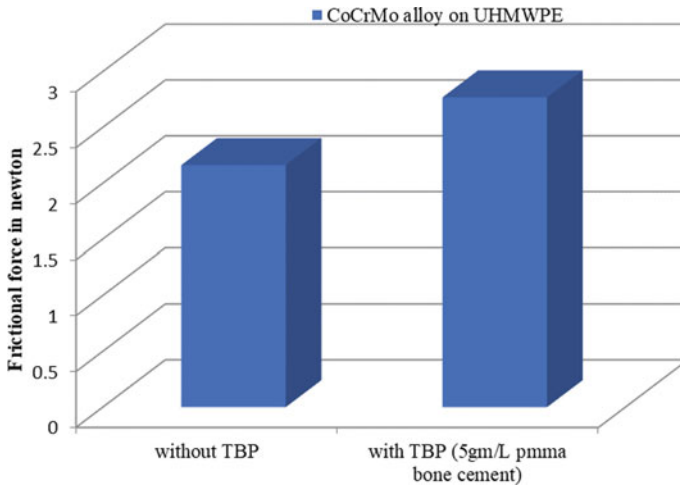
Fig. 12 Frictional force plots of pin and plate specimen with and without 5 g/L third body particles (PMMA bone Cement)

4 Conclusion

The tribological test was carried out on Co–Cr–Mo alloy pin on UHMWPE plate with load: 20 N, frequency: 5 Hz, temperature: 37 °C, test duration: 20,000 s, sliding distance: 1200 m, and no of cycles: 100,000 cycles. From the obtained results it is found that there is an increase in average wear rate, COF, and frictional force of Co–Cr–Mo alloy pin on UHMWPE plate with third body particles (5 g/L PMMA bone cement) compared to without third body (5 g/L PMMA bone cement) particles and it is due to interaction of third body particles between the surfaces of the specimen. The wear rate of pin specimen is greater than plate specimen. The test results suggest that there is effect of third body particles on wear rate of the specimens. The new class of Co–Cr–Mo alloy was investigated and proposed for the biomedical applications with few more studies.

5 Future Scope

With the further investigations on this new alloy of Co–Cr–Mo it is possible to replace traditional hip joint materials, which enhances the life of the joint.

References

1. Findik, F.: Wear properties of Ti based biomaterials. Curr. Trends Biomed. Eng. Biosci. **12**(3)
2. Ghalme, S.G., Mankar, A., Bhalerao, Y.: Biomaterials in hip joint replacement. Int. J. Mater. Sci. Eng. 113–125
3. Article on "what are hip and knee replacement implants made of?" American Association of Hip and knee Surgeons (2018)
4. Rama Sreekanth, P.S., Kanagaraj, S.: Wear of biomedical implants. In: Tribology for Scientists and Engineers
5. Ranjan, R.K., Kumar, M., Kumar, R., Ali, M.F.: Bone cement. Int. J. Orthop. Sci. 79–82 (2017)
6. Hongxi, L., Qian, X., Xiaowei, Z., Chuanqi, W., Baoyin, T.: Wear and corrosion behaviors of Ti6Al4V alloy biomedical materials by silver plasma immersion ion implantation process. Thin Solid Films **521**, 89–93 Oct (2012)
7. Ureña, J., Tabares, E., Tsipas, S., Jiménez-Morales, A., Gordo E.: Dry sliding wear behaviour of β-type Ti-Nb and Ti-Mo surfaces designed by diffusion treatments for biomedical applications. J. Mech. Behav. Biomed. Mater. **91**, 335–344 Mar (2019)
8. Nath, S., Sinha, N., Basu, B.: Microstructure, mechanical and tribological properties of microwave sintered calcia-doped zirconia for biomedical applications. Ceram. Int. **34**(6), 1509–1520 Aug (2008)
9. Hashemi, S.M., Parvin, N., Valefi, Z.: Effect of microstructure and mechanical properties on wear behavior of plasma-sprayed Cr_2O_3–YSZ–SiC coatings. Ceram. Int. **45**(5), 5284–5296 Apr (2019)
10. Aherwar, A., Singh, A.K., Patnaik, A.: Cobalt based alloy: a better choice biomaterial for hip implants. Trends Biomater. Artif. Organs **30**(1), 50–55 (2016)
11. Zhang, H., Liang, Y.: Extrusion processing of ultra-high molecular weight polyethylene (2018). https://doi.org/10.5772/intechopen.72212
12. Fleming, T.J., Kavanagh, A., Duggan, G.: The effect of melt temperature on the mechanical properties of cast ASTM F75 CoCrMo alloy as explained by nitrogen and oxygen content. J. Mater. Res. Technol. **9**(5), 9479–9486 Sep–Oct (2020). https://doi.org/10.1016/j.jmrt.2020.06.079

Product Design: Design for Cost, Reliability and Sustainability

Bio-inspired Design of Octafilar, Hexafilar and Quadrifilar Helical Springs

Prem Sangam Mishra, Eshaan Gupta, Amitabh Das, and Manasi A. Kanetkar

1 Introduction

Nature has given each species a speciality in its defence mechanism, locomotion and way of finding food to survive on the earth. Consider the chameleon for an example, which mostly feeds by shooting its tongue ballistically, in order to catch prey placed at a distance. Typically, it was assumed that its tongue is 1.5–2 times the length of the body without the tail. Duvernoy [1] proposed that the only accelerator muscle was mainly responsible for this ballistic tongue projection. Van Leeuwen [2] established the architecture of the chameleon's tongue through his mathematical model that anticipated precisely the orientation and the curved forms of the muscle fibres normally present in the accelerator muscle which was spiral in shape on the basis of his theoretical studies.

However, high-speed recordings of Snelderwaard et al. [3] indicated that the accelerator muscle alone was not sufficient to produce a large amount of power. Anderson [4] also estimated that the entire duration of the tongue protrusion of the chameleon's tongue is between 10 and 55 ms^{-1}. There have been reports of maximal accelerations from 500 to 2590 ms^{-2}, which require a peak power density between 3000 and 14,040 $W\,kg^{-1}$. Therefore, the power for this ballistic projection has mostly to be created in the tongue, and a system for energy storage and release must take place in order to achieve such action.

P. S. Mishra (✉) · E. Gupta · A. Das
School of Mechanical Engineering, Vellore Institute of Technology, Vellore, Tamil Nadu 632014, India
e-mail: premsangam.mishra2017@vitalum.ac.in

M. A. Kanetkar
Design and Innovation Center, Indian Institute of Technology Gandhinagar, Palaj, Gandhinagar, Gujarat 382355, India

Fig. 1 Chameleon captures a mantis with its tongue. *Picture credit* Scott Cromwell/Flickr

Further studies of De Groot and Van Leeuwen [5] falsified the hypothesis that the muscle accelerator is the primary direct tongue projection effector. They indicated that the maximum strengths required to create observed accelerations are at least five to ten times larger than accelerator muscle capacity. Their morphological and kinematic observations concluded that a cylinder-shaped connective tissue layer consisted of sheaths that have helically arranged collagen fibre forming clockwise and counter clockwise helices, which store elastic energy when the chameleon's tongue is at rest and is in the compressed state. When released, it provides most of the immediate power for the protrusion of the tongue (Fig. 1).

Moulton et al. [6] concluded that in the absence of intralingual sheaths, there is almost no resistance when the tongue is at rest. Because of the helically arranged collagen fibre, the intralingual sheaths are able to store high elastic power. They created a mathematical framework for the geometry of the chameleon tongue that consists of intralingual sheaths made up of collagen fibres organized in pairs of helices that are orientated oppositely resembling a tubular cylindrical structure and the accelerator muscle comprises fibres organized in logarithmic spirals. These shapes seem to be a good match and make good sense at a mathematical level. Hence, they tried to establish the fact that the level of resistance, the extent of extension and the energy stored rely heavily on the sheath angle.

This unique ballistic projection of the tongue and quick energy release mechanism has inspired several researchers to design manipulators who closely mimicked this action [7–9].

Narsaiah et al. [12] explain static analysis on springs; the paper explains how varying spring parameters like coil diameter, number of turns and material affect the spring performance in deformation, stress, etc. A similar approach was performed by Al-Sahlani et al. [13] which shows a comparative analysis on different materials used in springs, and after comparison on various performance parameters, carbon composite spring was proved as the best material. Banginwar et al. [11] explained various variables in the 3D modelling of springs and validated the design by various structural analysis on different materials to select the best. Also, the authors performed a modal analysis which is used to determine the natural frequency of various spring iterations having different materials, the higher the natural frequency the safer the design.

The suspension system is very crucial for any locomotive, as it aims to smoothen ride quality and maintain contact with the road surface, thus affecting the handling and braking performance of the vehicle by absorbing the shocks or impulses due to uneven surfaces. Springs can be tuned depending on the application; for example, a race car and a commercial vehicle have different spring rates. Spring rate, also known as spring constant, is defined as the constant amount of force it takes an extension or compression spring to travel one unit of distance [20]. Therefore, a higher spring rate would result in a stiff suspension setup and conversely for a low spring rate setup.

Despite all of this, a mechanical model of a spring-like structure resembling the geometrical arrangement of collagen fibre in the intralingual sheaths of a chameleon's ballistic tongue was missing. The aim of this work is to design such a bioinspired spring for implementing it in real-world uses. In this paper, we have redesigned the conventional spring and made various iterations consisting of the different number of helical coils and revolutions, and then, structural simulation like stress, strain, deformation, and modal analysis was also performed to collect data from each iteration so as to select the best spring for different applications.

2   Methodology

The biomechanical model of the tongue was studied, iteration (neglecting the counter clockwise helices) was made, and the quadrifilar, hexafilar and octafilar springs were designed as shown below which closely resemble the geometry of helically arranged collagen fibre in the intralingual sheaths and make sense in a mechanical level. The quadrifilar helical spring consists of four helical coils equally spaced circumferentially, each helical coil having 90° phase difference. Similarly, the hexafilar helical spring consists of six helical coils having 60° phase difference, and the octafilar helical spring consists of eight helical coils having 45° phase difference. All the springs were coupled with flat hollow discs in both ends that allowed even force distribution on the multiples of helical coils. This multiple helical coil arrangement is designed in such a way that it provides stability to the spring assembly, and the helical coils do not come in direct contact with each other when compressed thereby decreasing the possibility of wear and tear (Fig. 2).

Three different types of spring design were decided based on the number of helical coils, i.e. 8, 6 and 4, as shown above, each iteration has four different numbers of revolutions, i.e. 0.75, 1, 1.25 and 1.5 so a total of 12 different iterations were made, and the details are given below in Table 1. All the springs have a height of 337 mm, and the inner and outer diameter of the flat hollow discs are 186 mm and 212 mm, respectively. The wire diameter of the helical coils is decided in order to keep the volume of the springs as close as possible for a fair comparison.

Now, after the computer-aided design (CAD) models were developed using SOLIDWORKS 2018, simulations were performed using ANSYS 2020 R1 to collect data for stress, strain, total deformation and factor of safety, and the data collected was on three different materials, i.e. ASTM A 231, Inconel 718 and AISI 321.
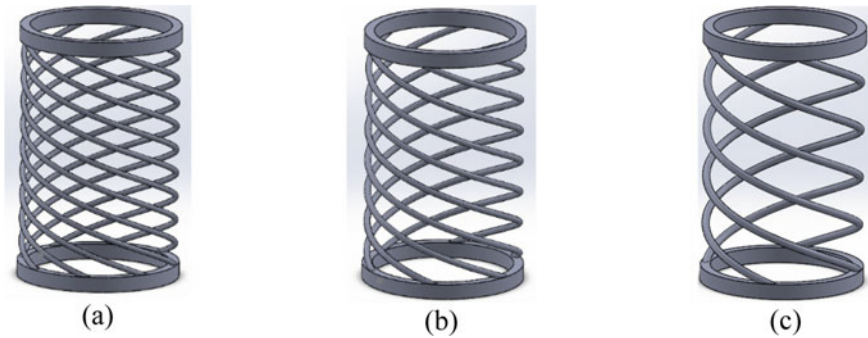
Fig. 2 Octafilar helical spring (**a**), Hexafilar helix spring (**b**), Quadrifilar helical spring (**c**)

Table 1 Spring data

No. of helical coils	Revolution	Pitch (in mm)	Wire diameter (in mm)	Mean diameter (in mm)	Outer diameter (in mm)	Volume (in mm^3 × 10^3)
8	0.75	420	8.10	200.00	204.05	545.48
8	1.00	315	7.26	200.42	204.05	545.07
8	1.25	252	6.62	200.74	204.05	545.53
8	1.50	210	6.10	201.00	204.05	545.21
6	0.75	420	9.36	199.37	204.05	545.33
6	1.00	315	8.40	199.85	204.05	545.41
6	1.25	252	7.66	200.22	204.05	545.96
6	1.50	210	7.06	200.52	204.05	545.77
4	0.75	420	11.48	198.31	204.05	545.15
4	1.00	315	10.30	198.90	204.05	545.07
4	1.25	252	9.38	199.36	204.05	545.12
4	1.50	210	8.66	199.72	204.05	545.70

2.1 Structural Analysis

For simulation, two plates were also attached to ends of the spring so as to simulate actual mounting, other boundary conditions included in the simulation were fixed support at one end and force at other, simulation results were calculated on three different forces, i.e. 800, 1000, 1200 N, and mesh settings were kept constant for each iteration. These settings are shown below. Mesh quality was also monitored to get reliable results. One of the mesh metrics to determine the quality of the mesh was the aspect ratio. The ideal aspect ratio is considered as 1, and for spring simulation as shown below the majority of the mesh elements have an aspect ratio of 1.16 which is considered as good quality. Once the mesh model was generated, simulations were

performed for total deformation, von Mises stress, strain and factor of safety as shown from Figs. 3, 4, 5 and 6.

The max total deformation achieved was along the Y-axis in which the spring compresses as shown in Fig. 3 the value was found to be 0.08401 m and factor of safety 1.7 in Fig. 6. The simulation results show even stress distribution among all the eight helical coils, which help to increase the durability of the spring. The structural simulations shown above were performed on all 12 iterations, and one of the iteration results of octafilar helical spring is shown above. The results are compiled in an excel table, and graphs are plotted for comparison as shown in Figs. 13 and 14.
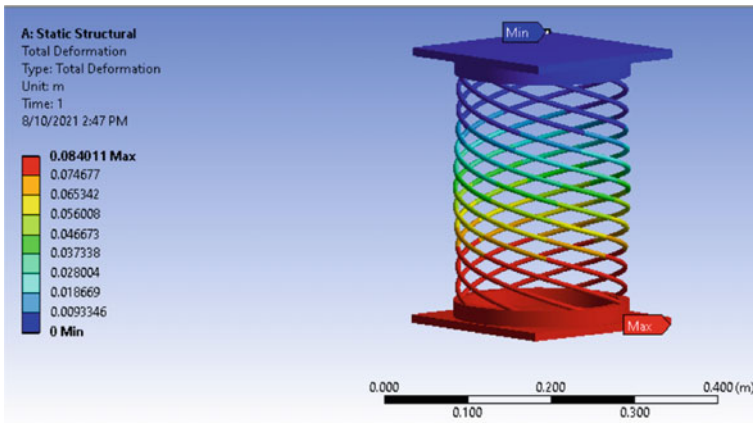
Fig. 3 Total deformation
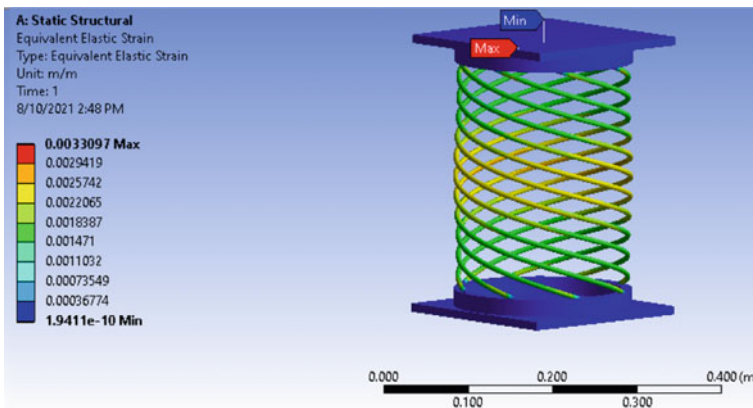
Fig. 4 Equivalent elastic strain
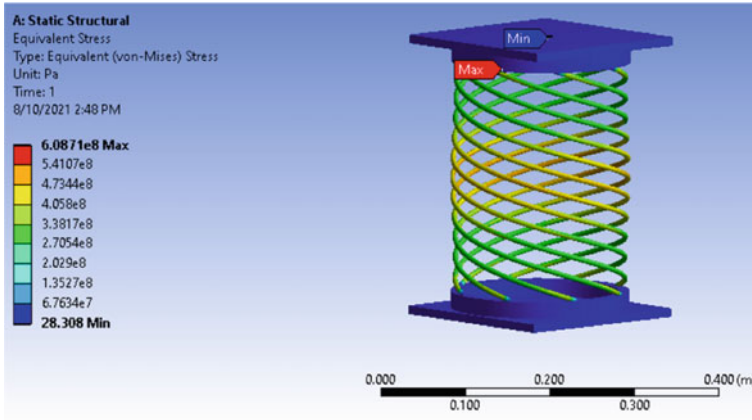
Fig. 5 Equivalent stress
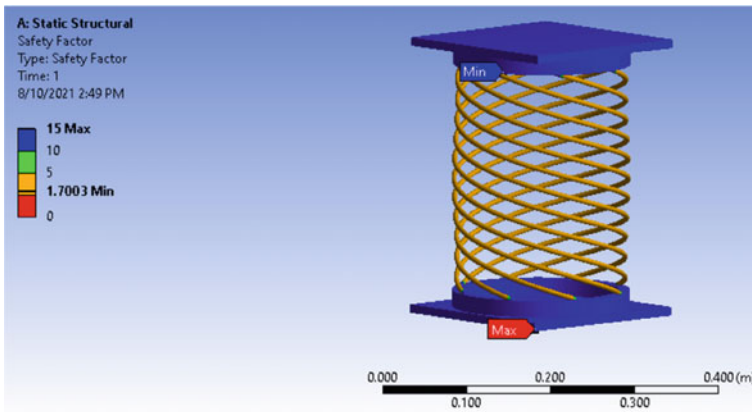
Fig. 6 Safety factor

2.2 Modal Analysis

After the structural analysis was completed, results were transferred for performing modal analysis on the twelve iterations. The main aim for modal analysis is to study different mode shapes and mode frequencies/natural frequencies. Understanding the natural frequency is important, as it is the frequency in which resonance occurs leading to increased amplitude and ultimately component failure. Hence, it is important to analyse all the modal frequencies. In modal analysis computing, the fundamental natural frequency (first mode frequency) is the most important as it is the frequency that is usually close to the working frequency of components; an approximation of this frequency can be made by using the below formula. Modal analysis

was performed on all the twelve iterations of spring; one of the iteration results of the hexafilar helical spring is shown below. For simulation, the spring was kept under the pre-stress condition of static structural analysis to get more realistic results, to visualize the different mode shapes, six different mode shapes and frequencies were simulated (as shown in Figs. 7, 8, 9, 10, 11 and 12), but for our design, the most important being the fundamental frequency was focused, and data for the iterations are shown in Table 2.
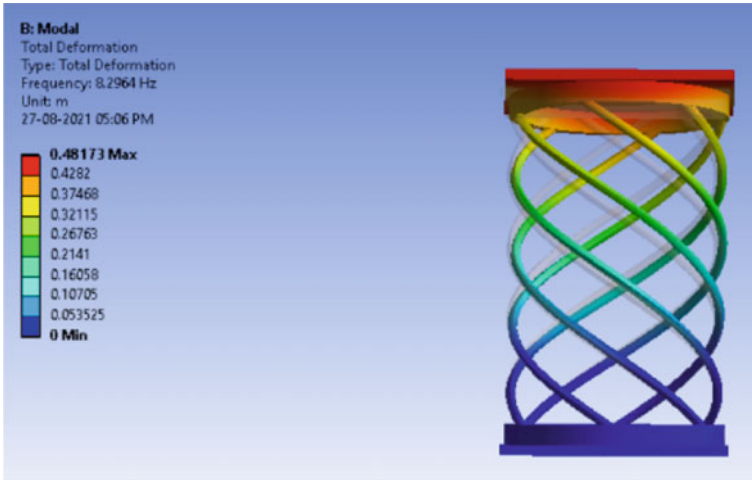
Fig. 7 First mode shape frequency—8.29 Hz
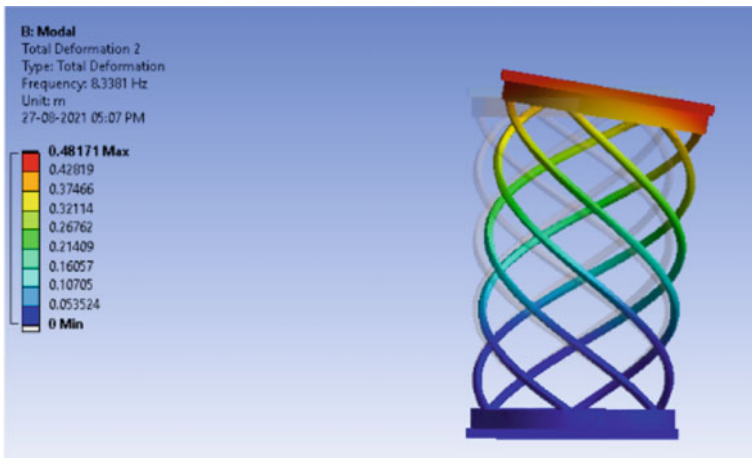
Fig. 8 Second mode shape frequency—8.33 Hz
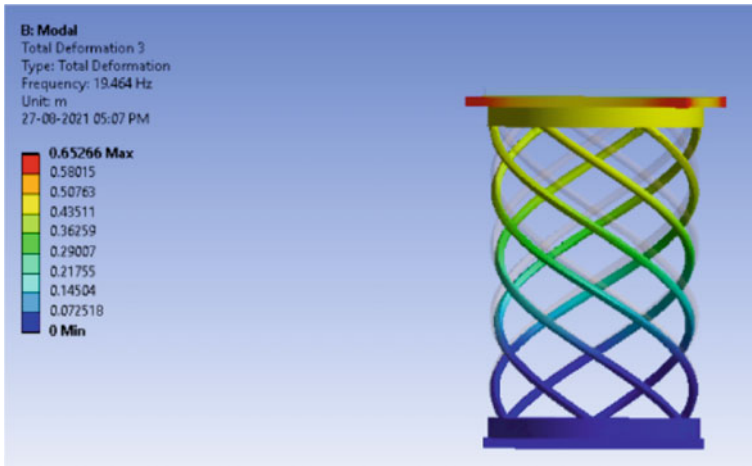
Fig. 9 Third mode shape frequency—19.46 Hz
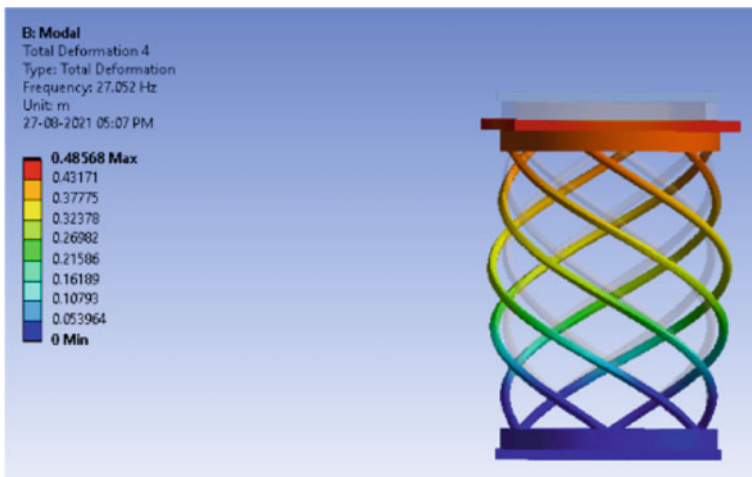
Fig. 10 Fourth mode shape frequency—27.05 Hz

According to DR Tuned Racing [10], the operating frequency of a passenger car or typical OEM spring is 0.5–1 Hz, whereas in the above modal analysis, the fundamental frequency was found to be 8.29 Hz which confirms that this design is safe for application. Results for all the twelve springs were computed, and among them, only a few springs had their fundamental frequency below 1 Hz.
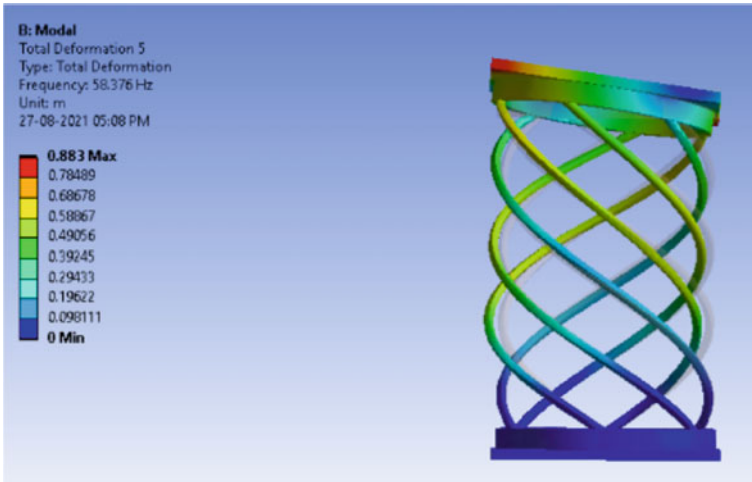
Fig. 11 Fifth mode shape frequency—58.37 Hz
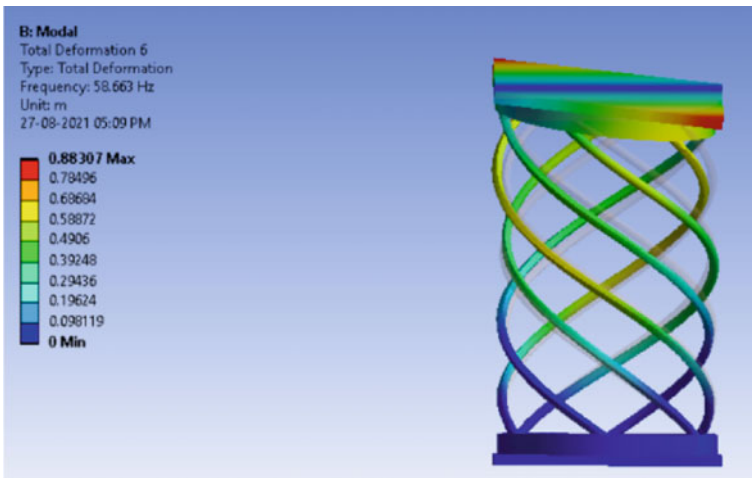
Fig. 12 Sixth mode shape frequency—58.66 Hz

Table 2 Fundamental frequency data

No. of helical coils	Revolution	Force (in N)	Fundamental frequencies (in Hz)		
			ASTM A 231	Inconel 718	AISI 321
8	1.5	800	0.15018	0.15842	0.15235
8	1.5	1000	0.0502	0.0575	0.0532
8	1.5	1200	0.0357	0.03912	0.0386
8	1.25	800	1.8104	1.8418	1.8292
8	1.25	1000	0.20758	0.22316	0.21796
8	1.25	1200	0.1882	0.1025	0.0916
8	1	800	4.0363	4.0674	4.0263
8	1	1000	3.6134	3.6751	3.6206
8	1	1200	3.1315	3.2334	3.1608
8	0.75	800	7.3499	7.3198	7.28
8	0.75	1000	7.138	7.1199	7.0747
8	0.75	1200	6.9191	6.914	6.8628
6	1.5	800	1.720159	1.7142	1.69235
6	1.5	1000	1.50998	1.5055	1.4932
6	1.5	1200	1.30973	1.30126	1.29868
6	1.25	800	2.9914	2.9828	2.9302
6	1.25	1000	2.3504	2.384	2.3054
6	1.25	1200	1.775	1.571	1.4209
6	1	800	5.2906	5.1964	5.1599
6	1	1000	4.970 3	4.8965	4.8511
6	1	1200	4.6261	4.5759	4.5201
6	0.75	800	8.6585	8.6112	8.5719
6	0.75	1000	8.4795	8.4422	8.3984
6	0.75	1200	8.2964	8.2695	8.2211
4	1.5	800	2.8511	2.8312	2.7744
4	1.5	1000	2.2223	2.1799	2.089
4	1.5	1200	1.75997	1.2076	0.99957
4	1.25	800	4.342	4.2704	4.2331
4	1.25	1000	3.925	3.883	3.8332
4	1.25	1200	3.5539	3.45	3.384
4	1	800	6.9784	6.9546	6.9233
4	1	1000	6.7448	6.7346	6.6974
4	1	1200	6.5021	6.5066	6.4631
4	0.75	800	10.92	10.855	10.81
4	0.75	1000	10.787	10.721	10.673
4	0.75	1200	10.644	10.586	10.534

3   Results and Discussion

After compiling the data for all the twelve iterations of our spring design, a certain trend was observed. As the number of revolutions increased the stress, deformation and strain increased, whereas the factor of safety decreased regardless of the number of the helical coils in spring. Then, if the force was increased from 800 N up to 1200 N, which is a normal load in a bike, the same trend was observed. This behaviour could help to categorize the spring into various stiffness categories such as soft, balanced and stiff setups. For example, a softer setup of spring is required in commercial road cars or bikes; a spring with a higher number of revolutions can be used, whereas for a race car where higher stiffness springs are required, a lower number of revolution springs can be used; this can also be explained by the deformation vs force graph as shown below. The factor of safety decreased as the number of helical coils increased. This was due to a decrease in the thickness of individual helical coils to keep the volume constant. The benefit of adding more helical coils was a better stress distribution that may result in higher fatigue life and adding more helical coils resulted in a softer spring setup. Spring comparison was done for all the iterations on two factors that are stiffness and safety (F.O.S and mode frequencies), graphs were made as shown in Figs. 13 and 14, and conclusions were drawn accordingly.
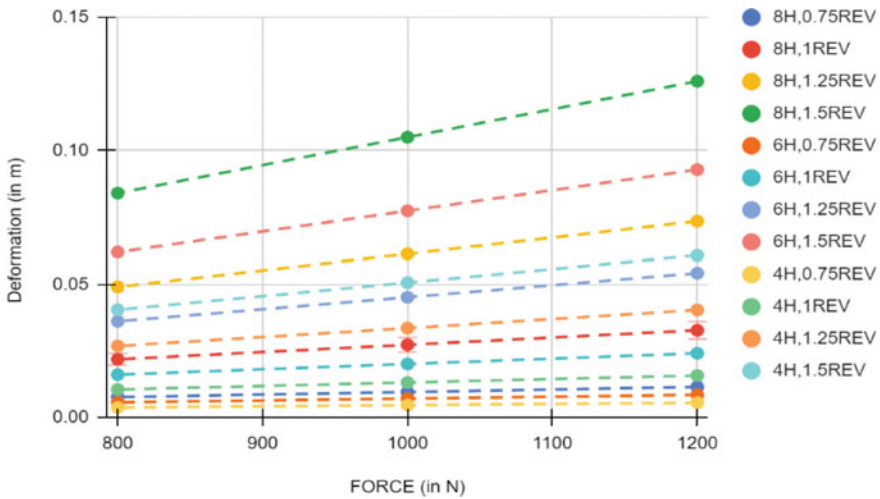
Fig. 13 Spring structure comparison graph (H = No. of helical coils, REV = revolution)

From the above graph, a good comparison of all the spring iterations can be made which can help to categorize them based on their application. To plot this graph, the material considered was Inconel 718 that was kept constant in order to compare the structural results. In the deformation vs. force graph (Fig. 13), the number of helical coils is compared. It is observed that with an increase in helical coils the stiffness reduces; this is because in order to keep the spring volume constant

the individual helix thickness had to be reduced which resulted in a decrease in stiffness. Now, if helical coils are kept constant, it is observed that on increasing the number of revolutions the stiffness decreases; this was due to the distribution of load between tensile and shear; as the revolutions increased, the shear component of force got greater which resulted in a higher deformation. From Fig. 13, springs can be categorized on the basis of deformation into three different setups, namely stiff, soft and balanced, the top three spring data lines can be grouped as stiff setup springs, the bottom four have less difference between them, so they can be categorized as soft spring setups, above them a gap occurs, and from there, the remaining springs can be grouped as balance setup springs. After analysing all the structures, it was decided to compare the three selected materials, from Fig. 14, all the three curves can be observed which represent the deformation results of the materials. On analysing them, it was concluded that ASTM A 231 is the best material, even though it had more deformation as compared to the other two materials the factor of safety and mode frequencies were in a safe range for all the twelve iterations, the higher variability offered a wide range of spring setup from stiff to soft without compromising the reliability, whereas in other materials, F.O.S fell below 1.2 with increasing deformation.

From modal analysis, various mode frequencies and shapes of the spring iterations were determined. It is important to ensure that the working frequency and the mode frequency are not the same or close to each other as this would give rise to resonance and ultimately structural failure of the component. For automotive applications, the operating frequency of suspension components is around 0.5–1 Hz [10], and the data compiled in Table 2 confirms that most of the iterations are safe as the majority have their fundamental frequencies above 1 Hz. Similar to structural analysis in the modal analysis, some trends were observed, among springs if helical coils are kept constant,
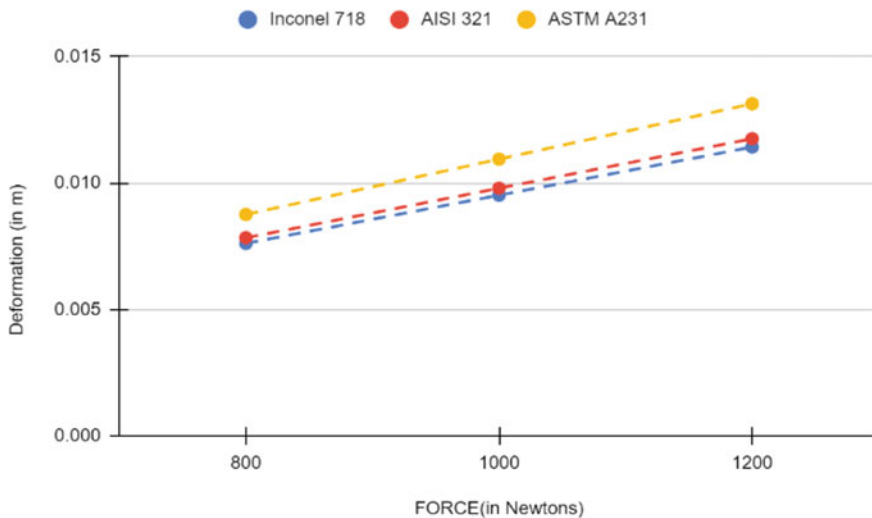
Fig. 14 Material comparison graph

the fundamental frequency decreases as the number of revolutions increases, as the number of helical coils increased, the fundamental frequency decreased in general, and the reason for this trend is thought to be the decreasing structural stiffness as the number of revolutions and helical coils increases. Overall, the paper confirms the functioning and safety of this novel spring design which can be implemented in real life. Many iterations had to be dropped as they showed poor F.O.S and had an unsafe fundamental frequency; these iterations are shown below with their respective materials.

Table 3 Rejected iterations

No. of helical coils	Revolution	Material
8	1.5	AISI 321, Inconel 718, ASTM A 231
8	1.25	AISI 321, Inconel 718, ASTM A 231
8	1	AISI 321
6	1.5	AISI 321, Inconel 718
6	1.25	AISI 321
6	1	AISI 321
4	1.25	AISI 321
4	1.5	AISI 321

4   Conclusion

The aim of the paper was to design and simulate quadrifilar, hexafilar and octafilar helical springs, a structure inspired by the geometry of helically arranged collagen fibre in the intralingual sheaths of a chameleon's ballistic tongue. The research work validates the concept and the functioning of this novel design as shown by the static structural analysis which was discussed in the above sections, a total of twelve iterations were designed based on different numbers of helical coil and revolution in all the designs volume was kept constant so as to have a fair comparison among these variables and how do they affect the spring performance. Three materials were also compared, namely Inconel 718, AISI 321 and ASTM A 231, and among the three materials ASTM A 231 showed the most reliable results even though it had more deformation compared to other materials (Fig. 14) for the loads 1200, 1000, and 800 N. Helical springs have higher load distribution characteristic leading to more stable and durable systems compared to conventional springs of the same volume. This adjustability in this design allows adding of more helical coils of different revolutions that can change the setup from soft to stiff or vice versa; the effect of change in stiffness with varying helical coils and revolutions was discussed in Fig. 13. The iterations whose modal frequencies coincided with the operating frequency were

rejected for applications as shown in Table 3. Overall, this confirms the functioning, benefits and safety of this novel design that is used for automotive applications.

References

1. Duvernoy, G.L.: Sur les movement de la langue du cameleon. Compt. Rend. Hebd. Seanc. Acad. Sci. Paris **2**, 349–351 (1836)
2. Leeuwen, J.L.: Why the chameleon has spiral-shaped muscle fibres in its tongue. Philos. Trans. R. Soc. Lond. B. Biol. Sci. **352**(1353), 573–589 (1997). https://doi.org/10.1098/rstb.1997.0039
3. Snelderwaard, P.C., Groot, J.H., Deban, S.M.: Digital video combined with conventional radiography creates an excellent high-speed X-ray video system. J. Biomech. **35**, 1007–1009 (2002)
4. Anderson, C.: Off like a shot: scaling of ballistic tongue projection reveals extremely high performance in small chameleons. Sci. Rep. **6**, 18625 (2016). https://doi.org/10.1038/srep18625
5. de Groot, J.H., van Leeuwen, J.L.: Evidence for an elastic projection mechanism in the chameleon tongue. Proc. Biol. Sci. **271**(1540), 761–770 (2004). https://doi.org/10.1098/rspb.2003.2637
6. Moulton, D.E., Lessinnes, T., O'Keeffe, S., Dorfmann, L., Goriely, A.: The elastic secrets of the chameleon tongue. Proc. Royal Soc. A.4722016003020160030 (2016) https://doi.org/10.1098/rspa.2016.0030
7. Debray, A.: Bioinspir. Biomim. **6**, 026002 (2011)
8. Debray, A.: Towards a manipulator mimicking the tongue of the chameleon. In: The Abstracts of the International Conference on Advanced Mechatronics: Toward Evolutionary Fusion of IT and Mechatronics (ICAM 2010), vol. 5, pp. 635–640 (2010). https://doi.org/10.1299/jsmeicam.2010.5.635
9. Hatakeyama, T., Mochiyama, H.: Shooting manipulation inspired by chameleon. IEEE/ASME Trans. Mechatron. **18**(2), 527–535 (2013). https://doi.org/10.1109/TMECH.2012.2225110
10. DR Tuned Racing, Spring Rates and Suspension Frequencies. Available: Spring Rates & Suspension Frequencies-Plus Calculator!—DR Tuned Racing
11. Banginwar, A.P., Bhusale, N.D., Totawar, K.V.: Design and analysis of shock absorber using FEA tool. Int. J. Eng. Res. Dev. **10**(2), 22–28 (2014)
12. Narsaiah S, S.R.V., Boorla, R., Manichandra, B.: Design and Static Analysis of a Suspension Helical Spring (2019). ISSN Print: 0976–6340 and ISSN Online: 0976–6359
13. Al Sahlani, A., Khashan, M.K., Khaleel, H.H.: Design and analysis of coil spring in vehicles using finite elements method. Int. J. Mech. Product. Eng. Res. Dev. **8**(4), 615–624 (2018)
14. Sun, W., Thompson, D.J., Zhou, J., Gong, D.: Analysis of dynamic stiffness effect of primary suspension helical springs on railway vehicle vibration. In: J. Phys: Conf. Ser. **744**(1), 012149 (2016). IOP Publishing
15. Kong, Y.S., Abdullah, S., Schramm, D., Omar, M.Z., Haris, S.M.: Vibration fatigue analysis of carbon steel coil spring under various road excitations. Metals **8**(8), 617 (2018)
16. Mohiyuddin, V.M.M.G., Patel, H.K., Patel, T.M.: Modeling, analysis and optimization of coil spring for suspension. Development **5**(04) (2018)
17. Win, D.H.H., Tun, D., Thang, Y.K.: Modal Analysis of Rear Coil Suspension System (2019)
18. Watanabe, K., Tamura, M., Yamaya, K., Kunoh, T.: Development of a new-type suspension spring for rally cars. J. Mater. Process. Technol. **111**(1–3), 132–134 (2001)
19. Pankaj, S., Rushikesh, A., Sanket, W., Viraj, J., Kaushal, P.: Design and analysis of helical compression spring used in suspension system by finite element analysis method. Int. Res. J. Eng. Technol. **4**(4), 2959–2969 (2017)
20. Performance Trends Inc. https://performancetrends.com/Definitions/Spring-Rate.html

Design and Development of Seed Drill Attachment to Tractor-Drawn Cultivator

K. Arun Kumar and **B. Rajeswari**

1   Introduction

Peanut, i.e. groundnut which is of global importance. Peanut is a row crop that requires agricultural machinery for effective cropping. It is grown in the tropics and subtropical regions. India is the second-largest producer of groundnut by producing 6.7 million tonnes of groundnut every year [1]. Groundnuts were majorly grown in Indian states like Tamil Nadu, Andhra Pradesh, Karnataka, Maharashtra, Gujarat and Orissa. In India, the groundnut is planted by manual sowing. But the disadvantages of manual sowing are the irregular distribution of seeds, seed wastage, arranging the plants manually after it has grown to a certain level and increased sowing time and manpower. These problems can be rectified by using a seed drill attachment to the tractor-drawn cultivator. Jethro Tull invented the seed drill in 1701. It helps the farmers to sow seeds in a better way. This attachment could overcome the disadvantages of manual sowing. This seed drill attachment is a separate attachment to the cultivator, which is the secondary tillage equipment used regularly for tillage of soils in the field during plantation. This attachment is cost-effective can be easily assembled and dismantled to the cultivator whenever necessary. This attachment is specially made for groundnut, which is a seasonal crop that has very little usage in the whole year. Hence, the disc with the cup is not permanently joined therefore it can be changed for different types of seeds.

K. Arun Kumar (✉)
Department of Mechanical Engineering, Sri Shakthi Institute of Engineering and Technology, Coimbatore 641062, India
e-mail: acwarun@gmail.com

B. Rajeswari
Department of Mechanical Engineering, Government College of Technology, Coimbatore 641013, India

1.1 Problems Identified

As stated by Dhawan et al. [2] to cultivate and drill row crops requires an animal or tractor-drawn cultivator or seed drill with a specific mechanism. There are many types of seed drill mechanisms and attachments to the tractor but the main disadvantage of the seed drill attachment is that it cannot be used for all the seeds.

It can only be used for a particular seed type and variety due to variation in size of the seed, planting length, width and height varies for various seeds. The seed of different types has to be sown at different distances and has to be placed at different heights depending on the seed for the optimum growth of the plant and reduce wastage of seeds. The distance of seed has to be maintained to get improved crop yield and the crop can grow without disturbing the adjacent crop. Also, the seed drill mechanism should be such that it should not damage the seeds while sowing. Here, the seed is chosen for drilling is groundnut which is a cash crop of Tamil Nadu. The appropriate mechanism which does not damage groundnut seed is the cup feed type. The other disadvantages of the seed drill are eliminated by using the detachable disc with cups in the seed drill. The disc can be made detachable so that the cup size can be varied to accommodate various seeds. The length of the seed can be varied by changing the number of cups. Thus the entire seed drill does not need to be varied for various seeds; only the disc with cups can be varied for various seeds which are affordable by the farmers. This project reduces the cost of using multiple units.

1.2 Objective of the Project

The main objective of undertaking this project is to design and fabricate a seed drill attachment to a tractor-drawn cultivator for drilling groundnut seed without damaging the seed. To reduce the cost of the equipment the seed drill attachment is designed to be attached to the cultivator so that the farmers can afford to buy it easily at a low cost. The other objective of the project is to conduct trials on the manufactured seed drill at various operating speeds of the tractor evaluate the readings and give the optimum speed of operation of the tractor for seed drilling. It reduces the wastage of seed which occurs normally by manual sowing. Since it is detachable from the cultivator it can be dismantled while using the cultivator alone. The seeds drilled are in a regular pattern and which increases the crop yield. The labour cost of the manual sowing can be reduced as this equipment is a one-time investment.

2 Seed Drill

Shweta et al. [3] state that a row crop is a type of crop that is planted in a series of rows and columns in an organized manner. These types of crops are cannot be
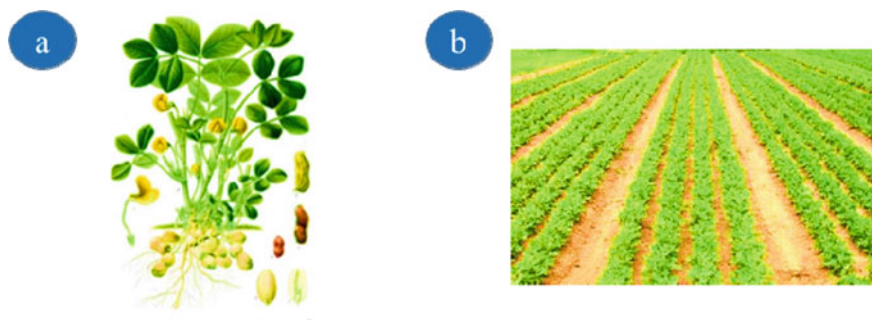
Fig. 1 **a** Groundnut plant. *Source* https://www.mtpr.org/post/legume-conquered-world-food-guys-talk-peanuts, **b** row planting. *Source* https://agritech.tnau.ac.in/ta/Agriculture/images-new/oilseeds

planted using broadcasting techniques. Rather, they have been sown by drilling. This uses agricultural machinery which can till the soil and make it ready for sowing. The crop rotation strategies were meant to protect the quality of the soil. This helps in maximizing the soil's annual productivity.

2.1 Peanut

Peanut is widely grown in the tropics and temperate regions. It is being important crop to large commercial producers and also small landholders. It is over about 46 million tonnes per year of world annual production. These peanuts can fix nitrogen and improve soil fertility. This helps in crop rotations and reduces infertility. The simple picture of the peanut plant is shown in Fig. 1a.

The peanut production with the countries ranked India in the second position with 6.7 million tonnes of production. Hence, this seed drill attachment will be very much useful for the farmers in India.

A garden with row planting shown in Fig. 1b is more visually appealing. Crops and plants grow better in rows because roots that need space to crawl freely. Row planting is beneficial to farmers because it gives more effective utilization of the land. These plant crops need agricultural machinery and tools for better planting in the equispaced manner which is tedious process while doing manually.

2.2 Hand Sowing

Hand sowing is the process of scattering seeds over prepared ground. Usually, a plough is used to make a furrow to incorporate the seed into the soil. Though, it is labour-intensive work in many instances small landholders use this method. Highly skilled labours or proper practice are required to sow evenly the seed at the proper
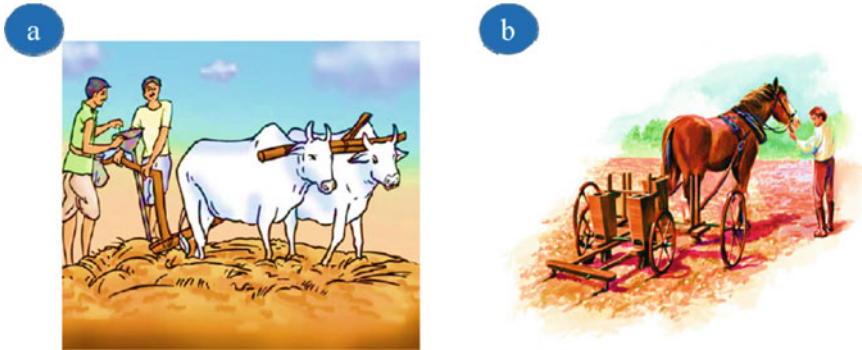
Fig. 2 **a** Hand sowing of seeds. *Source* https://www.learncbse.in/crop-production-and-manage ment-class-8-notes, **b** Horse-drawn seed drill. *Source* https://historyoflangarforyoungpeople.jim dofree.com/a-little-history/thegeorgians

distance at the desired rate without the overcrowding of crops. Hand sowing makes the production and productivity reduce in overcrowding of crops or improper spacing which reduces necessary nutrients for the crops. The hand sowing using bull is shown in Fig. 2a.

2.3 Seed Drill Usage in India

Kepner et al. [4] stated that the performance of the seed drill is based on the seed metering mechanism. Also, the soil and field condition, preparation of seedbed, speed of operation and power source affect the performance. Ojha et al. [5] stated that the crop yield is affected by various parameters like plant population, row spacing, plant-to-plant spacing, type and variety of seed.

The fluted roller feed type is suitable for grain crops is popular in India. Moreover, Goel et al. [6] said that in this device where seed damage exceeds 3%. Another one used was of cell feed type where controlling the seed rate was difficult. Sahoo et al. [7] said that cups having semi-circular types were introduced but due to vibration and shock, were modified to cylindrical at the top and conical at the bottom for better retention of seeds.

Garg et al. [8] claimed that the seed drills having a cup feed metering mechanism can be utilized for various crops only by changing the cups and with minor modifications. Needham et al. [9] said that single-tube and multi-tube iron seed drills have been given an efficient food production system that allowed it to support its large population for millennia. Jethro Tull studied new farming techniques invented the machine that greatly helped to increase yield by planting seeds in straight lines. He also developed a horse-drawn mechanical seed drill shown in Fig. 2b.

3 Materials and Methods

The project components were manufactured using mild steel because it is easily available, easy to machine and weld, easy to operate, cheap in cost, can be recycled easily. There are various components used in the seed drill assembly and their design consideration are discussed.

3.1 Design Considerations

As stated by Quasim et al. [10] the no of tynes and disc is selected based on the power of energy available from the tractor [11–14]. As stated by Devnani et al. [15] the box capacity is selected and is designed such that the seed will have a continuous flow. It is also designed to house the disc, funnel and seeds. It drops seeds at the desired seed distance. As stated by Qasim et al. [10], Noor et al. [16] for clay soil drilling the cultivator shovel selected is the shoe type into which pipe from the funnel to be attached. As stated by Vershney et al. [17] the power is transmitted by chain and sprocket from wheel to disc to have better performance. The rugged wheel is designed based on various considerations such as seed-to-seed distance, positive power transmission. Sahu et al. [18] have made a performance evaluation of seed drill in terms of seed rate which is calculated by the experimental setup. Sarker et al. [19] made a drum type low-cost multi-seed drill as it is hand-operated which is less effective than the tractor-drawn type. Verma et al. [20] which is has a seed metering mechanism of fixed type but this seed drill can be added as an attachment to the cultivator. Sedara et al. [21] developed a hand-operated seed drill that is used specifically for sowing amaranth seeds also has a low seed caring capacity and is manually operated. Vagadia et al. [22] had developed a new seed metering mechanism with screw conveyer type to increase productivity but it has limitations with the seed type.

3.2 Design of Components

The box is designed based on the angle of repose of seeds so that the seeds will have a continuous flow. The upper half of the box is for storing the seeds and the lower half is provided to house the nine discs with cups and funnels. The disc with cups is the main mechanism is shown in Fig. 3. The number of cups in the disc is selected based on the seed, seed distance and transmission ratio between the rugged wheels to the disc. The funnel is placed inside the box to collect the seeds from the cups in the disc and then transfer them to the pipe to drop the seeds in the ground.

It is a box-shaped funnel with a gradual taper to have a continuous unobstructed flow of seeds and collect seeds from the disc. It transfers to pipe which drops into
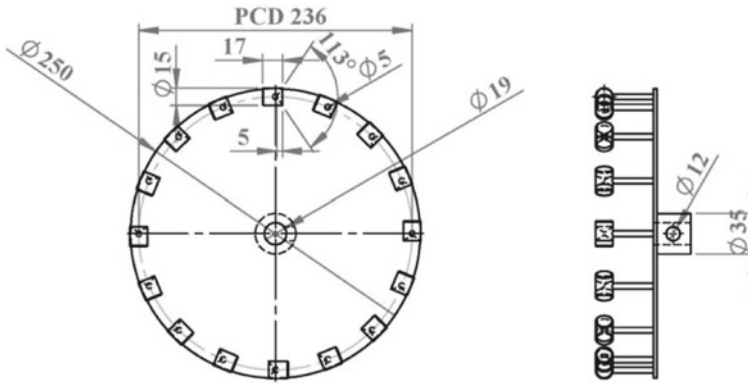
Fig. 3 Disc design with the seed picking cups welded to it

the furrows in soil. It has sprocket to transmit the motion between the wheel and the discs. It also holds the clutch and the spring. Spring is used to have better contact of the wheel with the soil. It is also used to reduce the damage of the wheel from obstacles or unwanted loads. The sprocket is used to transmit power between the wheel and the shaft with discs. It is designed to provide an appropriate gear ratio and also provides positive transmission of the wheel power without any slip. The base frame holds the various components of the seed drill such as boxes, discs with cups, wheel assembly, transmission assembly, clutch assembly, funnels and pipes used to attach the seed drill attachment to the cultivator to be used along with the tractor.

3.3   Conceptual Design of the Seed Drill

The designed cad model is shown in Fig. 4a. The detailed and overall dimensions of the designed seed drill are shown in Fig. 4b.

4   Experimental Calculations and Observations

The experimental setup is used for conducting trials so, the motor speed for various speeds of the disc is calculated. The various speed of the tractor and disc for which the experiment was carried out is shown in Table 1.
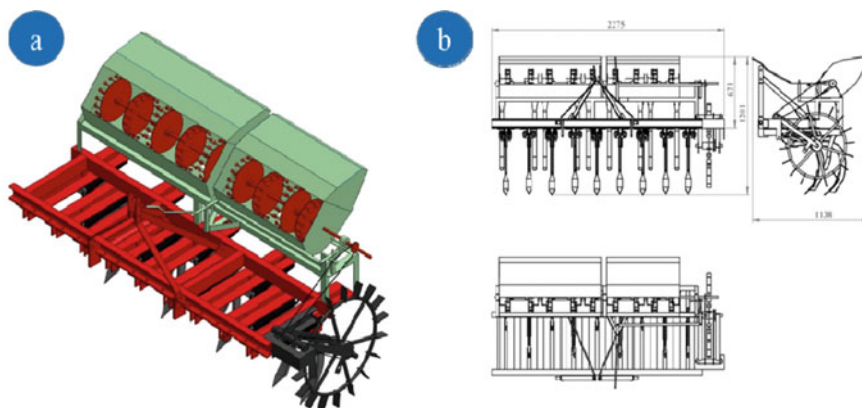
Fig. 4 **a** Conceptual design of the seed drill, **b** detailed design of the seed drill assembly

Table 1 Various speeds of the tractor, disc and motor for experiment

Speed of tractor (km/hr)	Disc speed (rpm)	Motor speed (rpm)
4	30	60
5	37	74
6	44	88
7	53	106
9	68	136

4.1 Calculation of Area Covered by Seed Drill for 100 Revolutions

Circumference of wheel	=	$2 \times \pi \times 358$
	=	2314.097 mm
For 1 rev. Distance covered	=	2.314 m
For 100 rev. Distance covered	=	231.4097 m
Width of land covered by cultivator	=	225×9
	=	2.025 m
Area covered for 100 revs. of disc	=	$231.4097 \times 2.025 \text{ m}^2$
Area covered for 100 revs. of disc	=	0.04686 ha

Table 2 Observed readings

Speed (km/h)	Disc speed (rpm)	Weight of seeds dropped by three discs per 100 rev. (kg)	Time for 100 revs. (min)	Weight of seeds dropped by nine discs per 100 rev. (kg)	Weight of 1000 seed	Area of land covered in 100 revs. (ha)	Seed rate (kg/ha)	Average seed rate (kg/ha)
4	30	1.321	3.369	3.962	280	0.0469	84.55	86.813
		1.337	3.345	4.011			85.61	
		1.411	3.374	4.231			90.29	
5	37	1.344	2.687	4.032	280	0.0469	86.04	86.213
		1.281	2.658	3.841			81.95	
		1.416	2.712	4.248			90.65	
6	44	1.331	2.263	3.992	280	0.0469	85.19	84.751
		1.325	2.246	3.974			84.81	
		1.316	2.209	3.948			84.25	
7	53	1.016	1.919	3.048	280	0.0469	65.04	67.777
		1.096	1.941	3.288			70.17	
		1.064	1.925	3.192			68.12	
9	68	0.648	1.508	1.944	280	0.0469	41.49	42.087
		0.576	1.525	1.728			36.88	
		0.748	1.529	2.244			47.89	

After conducting experiments on the manufactured equipment the various readings recorded are tabulated as shown in Table 2.

Based on the observed readings, inference graphs have been drawn to have a clear and quick understanding of the equipment.

The average rate of seed and the speed of the tractor is shown in Fig. 5a. It is clear that the seed rate is constant when the speed of the tractor is in the range of 4–6 km/h. If the speed is increased beyond a limit seed rate decreases due to the spilling of seed due to excess centrifugal force on seeds. The average seed drops into the furrows is reduced because the seed thrown out of the box. The graph between the time for 100 revolutions of the disc and the speed is shown in Fig. 5b. It is clear that the speed of the tractor increases the time for sowing decreases. The graph has a negative linear relationship hence speed and time is inversely proportional from this graph.

The graph between the area covered by the seed drill and the speed of the tractor is given in Fig. 6a. It is found that if the speed of the tractor is increased the weight of seeds dropped for 100 revolutions of the disc is decreased. If the speed of the tractor is increased beyond 6 km/h the seed rate decreases due to the spilling of seeds. This results in the wastage of seeds. Also, the area covered for 100 revolutions of the disc is constant for all speeds but the time varies for different speeds. The graph between the time and the average seed rate is given in Fig. 6b. From the graph, it is found that
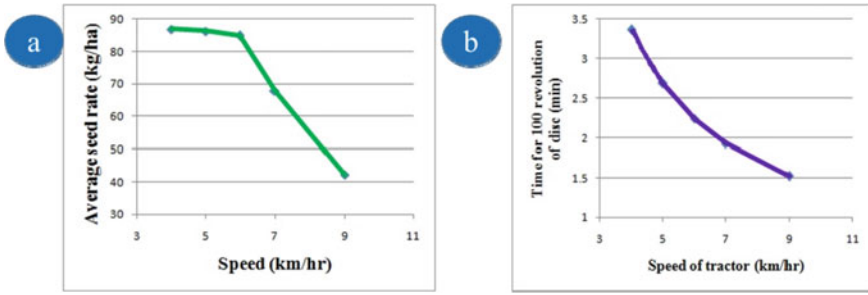
Fig. 5 a Speed versus average seed rate, **b** speed versus time for 100 revolutions of the disc
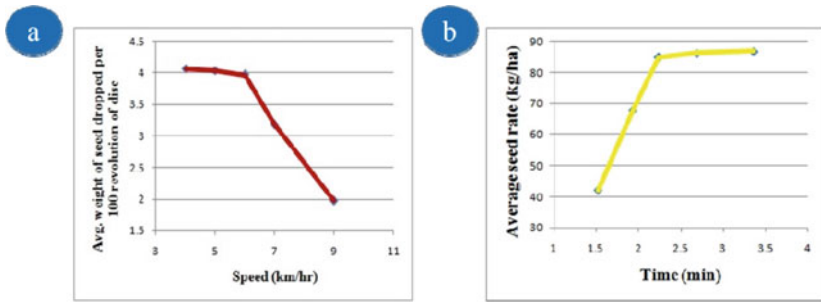
Fig. 6 a Speed versus avg. weight of seeds dropped per 100 revolutions, **b** time versus average weight of seed

the weight of seed dropped is optimum at only a certain time range. This is because at other times, the speed will be more hence the seed will be spilled at the high speed, i.e. at low time.

4.2 Fabricated Seed Drill Attachment

The fabricated seed drill attachment as per the designed model is shown in Fig. 7.

4.3 Discussion

First, the experiments were conducted for the tractor speed of 5, 7 and 9 km/h. After getting the readings it is found out that at the speed of 9 km/h more amounts of seed are thrown outside without falling into the funnel. Also at the speed of 7 km/h, some amount of seeds were thrown out and seed rate is 68 kg/ha which is less than 5 km/h (86 kg/ha). So, to find the optimum speed of operation of the seed drill trials were

Fig. 7 Seed drill attachment with cultivator

conducted at other speeds of 4 and 6 km/h. From the readings, it is found that the seed rate is nearly the same for the speeds 4, 5 and 6 km/h. The seed rates for the speeds 4, 5 and 6 km/h are, respectively 87, 86 and 85 kg/ha. Thus from the trials, it is concluded that the optimum speed of operation of seed drill is 4, 5 and 6 km/h. Also from Figs. 5a, b and 6a, b it is clear that the seed rate is optimum at 4, 5 and 6 km/h speeds. Thus if the seed drill is operated at 4 km/h and for constant 100 revolutions of the disc the time taken is 3.36 min with a good seed rate of 87 kg/ha. If the seed drill is operated at 6 km/h and for constant 100 revolutions of the disc the time taken is 2.24 min with a good seed rate of 85 kg/ha. The seed drill attachment is the comparatively best method for sowing the seed instead of the manual method.

The various advantages of seed drill are as follows:

- Seed drills can be used to drill seeds accurately in a row and in a correct pattern.
- It increases the crop yield by providing the appropriate sunlight, minerals and water for the plant.
- Various kinds of seeds can be sown by modifying the cups.
- The equipment can be easily attached and dismantled from the cultivator whenever required.
- It reduces the human work, cost of labour and time for sowing the given area of land.

5   Conclusion

Finally, the seed drill to the tractor-drawn cultivator is designed and manufactured. Also, an experimental setup is made to evaluate or test it. Various experiments were

conducted at various speeds of operation and results and graphs are obtained. It is found and suggested that the optimum speed of the tractor is 4–6 km/h as at this speed a good seed rate of 86 kg/ha is obtained. Also, it can be used along with a cultivator to sow seeds in a regular pattern without damaging them. This equipment increases the crop yield and also provides optimum sunlight, minerals and water to every plant which is not possible by manual sowing due to overcrowding of crops. Seed drill increases crop yield and reduces labour cost and time for sowing.

References

1. https://pjtsau.edu.in/files/AgriMkt/2020/may/KPSF_Groundnut_May_2020.pdf
2. Dhawan, K.C., Mittal, J.P.: Role of fertilizer in increasing yields of various crops in India. Econ. Aff. Calcutta **39**(2), 92–99 (1981)
3. Shweta, G.: Eaton's Markets Agriculture and Forestry Row Crop Farming. Eaton Corporation (2014). Retrieved 2 Feb 2014
4. Kepner, R.A., Bainer, R., Barger, E.L.: Principles of Farm Machinery. CBS Publishers and Distributors, New Delhi (2000)
5. Ojha, T.P., Michale, A.M.: Principles of Agriculture Engineering, vol. 1. Jain Brothers, New Delhi (2000)
6. Goel, A.C., Verma, K.S.: Comparative study of direct seeding and transplanted rice. Indian J. Agric. **34**(3), 194–196 (2000)
7. Sahoo, P.K., Srivastava, A.P.: Development and performance evaluation of okra planter. J. Agric. Eng. **37**(2), 15–25 (2000)
8. Garg, I.K., Dixit, A.: Development and evaluation of manually operated garlic planter. Agric. Mech. Asia Africa Latin Am. **34**(2), 19–22 (2003)
9. Needham, J., Lu, G.D., Wang, L.: Science and Civilization in China, pp. 48–50. Cambridge University Press (1987)
10. Quasim, M., Verma, V.P.: Indira Seed Drill for Rainfed Upland Paddy Cultivation. Central Rice Research Institute, ICAR, Orrisa, India (1982)
11. Mishra, T.N., Singh, B., Singh, K.N., Seth, G.S., Ghosh, A.: Effect of machinery management on energy requirement and yield of wheat after paddy harvesting. Indian J. Agric. Eng. **26**(1), 24–29 (1989)
12. Adil, S.A., Ashfaq, M., Yaqoob, M.: Energy output relationship: a case study of cotton and wheat. J. Rural Dev. Adm. **24**(4), 133–138 (1992)
13. Prasanna Kumar, P.S., Hugar, L.B.: Economic analysis of energy use in paddy cultivation under irrigated situations. Karnataka J. Agric. Sci. **24**(4), 467-470
14. Yadav, S.N., Chandra, R., Khura, T.K. Chauhan, N.S.: Energy input-output analysis and mechanization status for cultivation of rice and maize crops in Sikkim. Agric. Eng. Int. CIGR **15**(3), 108–116 (2013)
15. Devnani, R.S.: Agricultural Machinery Design and data Hand Book. RNAM ESCAP (1991)
16. Noor, R.S., Hussain, F., Farooq, M.U., Noor, R., Waqas, M.M.: Evaluating performance of water seed drill for wheat production: a sustainable technique under rainfed agricultural system. In: Big Data In Agriculture. Zibeline International Publishing (2021). ISSN: 2682-7786
17. Vershney, A.C., Bohara, C.P. Narang, S.: Design, development and evaluation of power drawn seed cum fertilizer drill. A.M.A. **22**(1), 39–41 (1991)
18. Sahu, V., Naik, R.K.: Performance evaluation of tractor drawn FYM applicator cum seed drill for mung bean crop. Pharm. Innov. J. SP. **10**(8), 712–716 (2021)
19. Sarker, T.R., Alam, M., Ali, M.R., Saha, C.K., Haque, M.A.: Design and development of a multi-crop manual seed drill. CIGR J. **21**(3), 51 (2019). Open access at http://www.cigrjournal.org

20. Verma, A., Shrivastava, A.: Design and development of shovel type-spring steel furrow opener for cultivator mounted seed metering mechanism. BIBECHANA, Multi. J. Sci. Technol. Math. 79–84 (2018). ISSN 2091-0762 (RCOST, p. 79)
21. Sedara, A., Ibrahim, Y., Manuwa, S., Sedara, O.: Development of a low-cost seed drill for sowing amaranth seed. World Acad. J. Eng. Sci. **7**(3), 39–45 (2020). E-ISSN: 2348-635X
22. Vagadia, R., Kadegiya, H., Desai, P., Gautam, A., Chaudhary, H., Rao, N.R.N.V.G.: Development of a mechanism for seed cum fertilizer drill. Mater. Today Proc. (2021)

Product Design Intervention in Household Water Consumption Through Circular Economy

Sangeeta Pandit and Sachin R. Gupta

1 Introduction

In 2015, United Nation Member States, as a general source of inspiration, called on the action plan to end poverty, protect the planet, and ensure that all the people should enjoy peace and harmony by 2030. On this action, they decided 17 different sustainable development goal (SDG) and recognized that action in one area would affect outcomes in another and this outcome must balance social, economic, and environmental sustainability [1]. Of the 17 SDG, goals 11 and 12 focus on the sustainability of the cities and community and the responsible consumption and production of the resources. Every country on the planet is needed to reach these ambitious targets by 2030. Considering the behavioural pattern of the Homo sapiens, humans are more reactive to things than being proactive; a classic example is consumption of household water and its disposal and wastage.

1.1 Type of Household Wastewater

Household wastewater originates from houses, residential buildings, and different institutions. Based on the contamination and composition, it can be classified as follows:

(1) Greywater—the water used in household activities such as bathroom shower, kitchen sinks, dishwasher, washing machine, hand washing sink, that have not come in contact with human faecal.

S. Pandit (✉) · S. R. Gupta
Department of Design, Indian Institute of Information Technology Design and Manufacturing Jabalpur, Jabalpur, Madhya Pradesh 482005, India
e-mail: s.pandit@iiitdmj.ac.in

(2) Black water—the water that comes out from toilet outlet, this type of water contains bacteria, virus, protozoa, and other pathogen that can infect humans when contact with skin or by ingesting.

Greywater has been taken into interest based on the feature that can be taken as a feasible alternative intake of water for non-potable use over the last few decades after a specific treatment process.

1.2 Household Water Consumption and Usage Habit

According to the Bureau of Indian Standard (BIS), IS: 1172-1993, a supply of 200 Lpcd is recommended for cities for domestic consumption and 135 Lpcd for the lower-income community. Researchers have found that water consumption in Indian major metropolitan cities is much lower than the BIS norms [2]. People have limited their aspiration and adapted to the available limited water supply [2]. Consumption of water per individual in India is less when compared internationally, but India's population density is very high, which increases the daily requirement of water supply based on per day consumption. India also struggles with the disposal and reuse of household wastewater. In India, approximately 80% of the water that reaches households is drained out as waste flow through sewage, polluting other water bodies such as rivers and land [3]. Taking the case of rural India, people in rural India are reducing household water consumption to meet the shortage of water during the summer season. The increase in water consumption by the privileged class people is also putting pressure on rural India [4]. More water is consumed by residential building than the standalone house for household activities [5]. An increase in water using habits for personal hygiene and increased living standards have increased water demand which will strain the existing wastewater treatment infrastructure, which will reduce the main water supply by per capita [5]. People prefer manual dishwashing to the automatic dishwasher, though the device consumes less water than manual operation. Considering dishwashing habit, people wash the utensil 2–3 times a day regularly. The survey showed that people prefer to wash utensils daily, accounting for 30 per cent population washed once a day, 40% population twice a day, and 30 per cent population thrice a day of the total population [5]. It may be hard to change the habit of people, and people resist sudden change. In an experiment conducted, participants were taught effective method for manual dishwashing, but 2 out of 3 participants denied adopting the method regularly [6]. With the growing awareness for health and hygiene, the tendency to move towards sustainable products in dishwashing and laundry will become a global trend [7]. According to a study, achieving the SDG target for 2030 is impossible without appropriate integrated policies. Despite the government's campaign, there is still a very low awareness of sustainable knowledge [8]. This indicates a need for further intervention to create a constraint on how people consume commodity and product in urban areas.

1.3 The Role of Design in Circularity

Design helps in the upliftment of the human lifestyle. A designer designs according to human needs, with the context of time. Any product starts affecting the human from a conscious being to an unconscious character. The new circular approach to any design should be such that it considers the inside and outside approach to design with reducing, reusing, and keeping resource always in the continuous usage cycle by increasing the product's life cycle [9].

2 Methodology

A design research-based pilot study was conducted involving existing field data with secondary data. For secondary data, search was done on Google Scholar with the keyword combinations (i.e. greywater, household water consumption, behaviour, filtration technology, circular economy, and water).This review contributed that how different aspects such as behaviour, water, and circular economy are interrelated. Further a direct observation study, questionnaire, and interview were conducted with the participants to get into an in-depth knowledge of user behaviour, their thinking process about the problem, and their solution and goal in term of water-saving habit. The study was conducted at Vapi, a city of Gujarat state in India. It is one of the rapidly developing industrial cities in the southern part of Gujarat, attracting people from neighbourhood villages for job opportunities. Due to population explosion and rapid infrastructure development activity, the Vapi city has started facing an acute water crisis in the recent year, and still, the demand for water is increasing. Direct observation was carried out on the domestic help 3 number of maid and 5 number of homemaker. Their physical and behavioural aspects were observed and recorded. The study was conducted at residential apartments where water is available 24/7. The household activity such as manual cloth washing, sweeping is carried out with the help of a bucket, so the amount of water consumed in litre/day is calculated based on the number of buckets of water used. The water consumption in litre was calculated using the capacity of the water bucket used in washing clothes at each home. In addition to direct observation, 12 face-to-face interviews of homemakers took place for 45–60 min in February 2021. Of the 12 participants in the interview and questionnaire round, five participants (homemaker) involved in the direct-observation study have also participated in the questionnaire round. Table 1 shows the demographics of the interview of the participants. For data collection, participants are asked a set of formal and informal questions. A semi-structured interview was carried out using an updated questionnaire [10].

Question related to the circular economy, recycling, and greywater was intentionally avoided to make the whole process of research more frugal in nature. The total focus in research was towards the routine and behaviour of the participants, to know the micro-behavioural aspect and action of the user in household activities

Table 1 Participant demographics of interview

Sample size	12	
Gender	Female	
Age group	30–45	
Level of education	12th	7
	Graduate	4
	Post-graduate	1
Occupation	Type	No of participant
	Home-maker	8
	Professionals	4

such as manual cloth washing, sweeping, and the product used in these activities in Indian scenario, to understand the scope where wastewater reuse can be applied. Two opportunities were mapped for these purposes, first opportunity in the direction of reusing wastewater from manual cloth washing, and second opportunity was reusing water from the RO water purifier. After considering the behaviour and discussing the idea with the participant, as a design case study, the design and development of a virtual concept design using computer-aided design software Rhino 6.0 and rendering software Keyshot 9.0 were used for designing the concept.

3 Result

This section provides the result in the structure manner of articulated data.

3.1 Direct Observation

The daily water consumption in the cloth washing process is shown in Table 2. It was observed that if two buckets of water are consumed in washing, overall a quantity remained in the bucket and when collected at end indicate that minimum of 1 bucket of greywater generated, so it is taken into consideration that the greywater produced in washing clothes is equivalent to half of the water consumed in manual cloth washing. After washing clothes, the remaining water was directly poured into the drainage. The min and max water usage in the eight residences was found to be 24 L and 45 L, respectively, for manual clothes washing, so min and max greywater generation for the same would be 12 L and 22.5 L. While sweeping the floor, only 1 bucket of water was used at every residence.

Table 2 Water consumption in manual cloth washing

Residential building apartments	Family size	Bucket volume (litre/day)	No. of bucket used	Total consumption of water (litre)	Greywater production (litre/day)
1	4	15	2	30	15
2	5	15	3	45	22.5
3	4	19	2	38	19
4	3	15	2	30	15
5	4	20	2	40	20
6	4	24	1	24	12
7	4	19	2	38	19
8	5	20	2	40	20

3.2 Interview and Questionnaire

The goal and problem were mentioned by the participant and the action taken in that direction. The major goal is to save on electricity bill and water saving. The interviewed participant mentioned the past and ongoing problem related to water in the city and their cause and solution. The working professional participant had hired domestic help for the household work. The majority of participants had no previous knowledge or experience of greywater, but they were conscious of rainwater harvesting. During summer, the water supply is timely managed in the residential building twice a day during morning and evening for 3–4 h. Washing of clothes was carried out manually in summer, even though some resident had access to washing machine, due to shortage of water for machine requirement and for electricity bill saving. Those who once resided in a locality where there was a water availability problem had adopted sustainable habits when there was a water shortage, but their behaviour changed when they moved to a complex with 24-h water facilities. In the same neighbourhood, a residential building with 24/7 water supply was discovered, but many residential communities were found struggling to meet their daily water requirements due to a lack of groundwater. Participant highlighted the area's progress, as well as the concern about population growth and its impact. They also mentioned that they were concerned about their children's future in terms of what kind of environment they would have to live in and the problems they would have to face in the future. Discussion with peers happens frequently within the circle on water problems. Wastewater from RO filter was drain out in 9 out of 12 residences, other use the water for planting purpose and water for air-cooler. On discussion of using grey water, Interest on the idea of using grey water was shown by only 7 participants, that is also subjective in nature depend on the quality of the water and its safety, but participant agreed on idea of using the treated and filter grey water from the cloth washing in the current context, also agreed that this should be the future where

every product and commodity should be such that as nature function, everything is recyclable in nature.

4   Discussion

In India, major household work was taken care of by the homemaker or the family hired domestic help, so they were the primary consumer, creating demand for any product. When there is limited water availability, the domestic help and homemakers washed their clothes in limited water and compromise due to the water shortage. Floor sweeping was a daily activity; the domestic help or maids and the homemaker had a habit of taking a calculated quantity of water based on her experience with the activity and the surface area to be cleaned. For generating sustainable behaviour, there had been a possibility of product design intervention by reusing greywater from manual cloth washing for sweeping purpose. People had been shifting from a colony with a limited water supply to a residential building (low-income living to high-income living) with economic growth. This residential building had facilities such as 24/7 water supply, so the fear of water scarcity and commitment to water-saving habit was diminished from the mind and the behaviour of the users. The same situation was found in Jaipur, where a hike in living standards has increased water consumption [5]. Moreover, sustainable behaviours are subjective, and consumer behaviour plays a significant role in sustainability to a higher and lower degree [11]. People knew the importance of saving, but any major behavioural change in their daily lives had not been implemented, so it becomes necessary to make the people feel the need of saving water and reuse greywater. Campaign in the direction of environmental benefits of using greywater and pollution control by using greywater should be carried out by government [11]. The future trend of product design is moving towards a sustainable lifestyle by consuming eco-product [12]. The focus was more towards product design intervention where wastewater from manual cloth washing can be reused after treatment. So, a mop unit was conceptualized where wastewater can be treated for reuse. This product will have two benefits for society; first, it would stop detergent mixed water from directly contaminating water bodies, and the second greywater will be reused. It takes on average 4 glass of water to be purifier to get 1 glass of purified water. People are not dedicated to saving water, so water that is lost in the RO water purifier is directly disposed of in the sewage. Water waste from water purifiers is a major problem that the general public ignores. It is also the manufacturer's ignorance to a case like this, Recent ban of Ro-water purifier in India pushes the manufacturer to innovate and develop a new design which give 2 glass of drinkable water from 4 glass of intake water, remaining 2 glasses is shifted to over head tank for reuse purpose [13], still we are just shifting the water and not directly using it, there is opportunity to design water purifier as a multifunctional device.

4.1 Design Case Study of Mop

The present mop unit available in the Indian market does not have any provision for reusing the wastewater. Adding a feature such as a filter that can strain greywater can increase the viability of the product. The mop unit—the product (Fig. 2) is a mop system where greywater from manual cloth washing can be filtered and used for the sweeping floor. The bucket has an estimated capacity to filter detergent water in the range of 8–10 L and reused. Recyclable polymer such as ABS is recommended for mop component through injection moulding manufacturing process [14]. The mop unit has an activated charcoal filter used to retreat detergent water from manual cloth washing which will take a minute to filter the detergent water as it passes through the filter. Activated carbon is a form of carbon that has been processed to have a massive surface area. Olive stones, natural asphaltites; peach stones base activated charcoal had enough close value to high adsorption capacities towards the surfactant in the detergents was found in a study [15]. The greater advantage of the filter is that it can be recycled and reused by the thermal activation process, which facilities a circular design for reuse [16]. The exploded view (Fig. 1) of the product demonstrates different component of the concept and its supporting function. For using the mop, the wastewater obtained from the manual cloth washing at the end is poured in the mop bucket through channel where the wastewater pass through the activated charcoal filter and post filter, so that the micro-particle and surfactant get trap and adsorb in the filter, and filter water is collected in the bucket for non-potable use for sweeping.
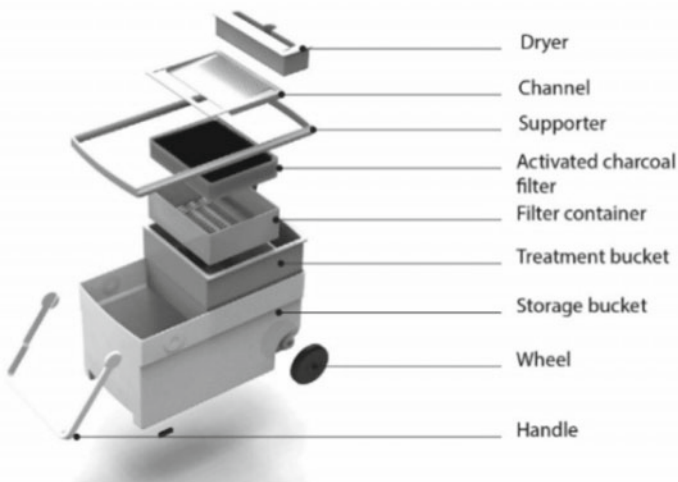
Fig. 1 Exploded view of mop unit with greywater filter unit

Fig. 2 Representation of mop unit design with greywater filter unit

4.2 Design Case Study of Multifunctional Product

Around 4 glass of ground water is used to RO-based water purifier to get 1 glass of
potable water, Where 3 glass of water is got waste. One of the design opportunities

Fig. 3 Multifunctional product (water purifier cum cooler)

is to collect the water and use in air cooler. The multifunctional product—the multifunctional product (Fig. 3) is a water purifier cum air cooler where the wastewater from the purifier is used in air cooler for cooling the space such as kitchen.

Schematic and working of the product

The product combined system which consists of Component of the RO-Water purification system which consist of RO-based purifier, pre-filter unit, Water storage unit along with piping system and an air-cooling unit consist of cooling pad, submersible pump, fan, motor and controlling unit (Fig. 4). The water pass through pre-filter and through RO-based filter, where the potable water is then pumped to water storage unit, and the by-product water is collected into the cooler section where it is pumped through a submersible pump to the cooling pad. The water gets evaporated by the hot air, and in return, the hot air gets heat dissipated and turns to cold and moist air, which is blown to the environment through fan.

4.3 Concept Evaluation

Based on the concept evaluation (Table 3), The multi-functional product water purifier cum cooler is selected, as it confront majority of the requirement of the user, and considering various factor based on circular design, eliminating water waste and ruse in other application along with safety consideration of the user.

The product can save 75% of water loss in the previous RO water purifier, which was getting lost in the current stage in the eco-system. On average in the family of four per house, maximum of 48 L of water per day can be saved and reused.
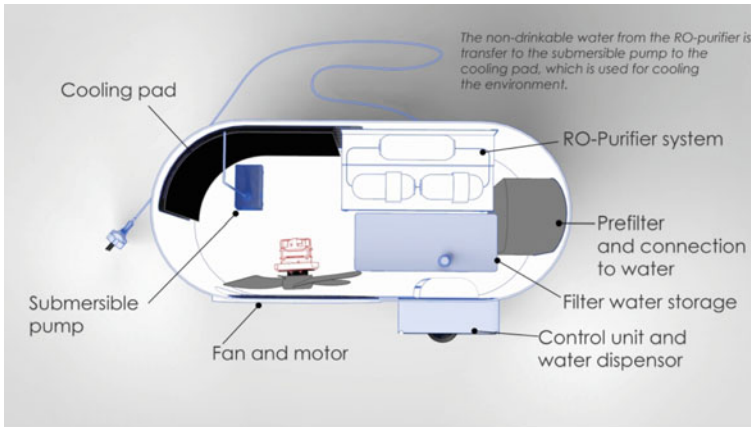
Fig. 4 General schematic and internal component of the product (top view)

Table 3 Concept evaluation based on user requirement

	User requirement	Greywater-based filter mop	Multifunctional product
1	No disturbance in regular activity in life	The product has to be used when required, other than this the product required further cleaning operation on regular basis by the user	No disturbance in daily life
2	Safe to use	There is risk of bacteria and virus infection	There is no risk involved
3	Water saving and reuse	The min and max value of greywater generation in manual cloth washing is 12–22.5 L/day So approximately after filtration 10 L to 20 L water can be saved and reused	An average human consumes 4 L of water /day, so a family of 4 will consume 16 L of potable water To get 16 L potable water from RO water purifier, we have to waste 48 L of water in the system So, in this product, 48 L water can be reused

5 Conclusion

Circular economy, behaviour study, and greywater filtration have been a significant subject of numerous researchers in different fields. However, the research majorly gets limited to policymaking, governance input, and theoretical design framework. There was a lack of design input to translate the behavioural result into an idea and then to a concept which can be implemented in the real condition to reach the sustainable development goal of responsible consumption and production. The paper

have further taken help of circular philosophy and design research method to study user behaviour and given case study that how to make changes in product design with view of circular design can make a change in the user habit and environment. The case study enables other researchers and designers to develop more conceptual product as a circular design reference with reducing and reuse by observing the user in a controller environment. Consumer behaviour and habit can be controlled by imposing constraint through design. Setting constraint in design becomes necessary, as people self-motivation to make an extra effort apart from their regular life does not last long. It changes with time and external situation.

References

1. The Global Goals. https://www.globalgoals.org/. Last accessed 20 May 2021
2. Shaban, A., Sharma, R.: Water consumption patterns in domestic house-holds in major cities. Econ. Polit. Wkly. **42**(23), 2190–2197 (2007)
3. Why India does not have enough water to drink. India Today. https://www.indiatoday.in/india/story/why-india-does-not-have-enough-water-to-drink-1557669-2019-06-28. Last accessed 21 June 2021
4. Singh, O., Turkiya, S.: A survey of house-hold domestic water consumption patterns in rural Semi-Arid Village India. GeoJournal **78**(5), 777–790 (2012)
5. Sadr, S., Memon, F., Jain, A., Gulati, S., Duncan, A., Hussein, W., Savić, D., Butler, D.: An analysis of domestic water consumption in Jaipur, India. British J. Environ. Clim. Change **6**(2), 97–115 (2016)
6. Porras, G., Keoleian, G., Lewis, G., Seeba, N.: Corrigendum: a guide to house-hold manual and machine dishwashing through a life cycle perspective. Environ. Res. Commun. **2**(4), 049501(2020)
7. Geetha, D., Tyagi, R.: Consumer behavior and fascinating challenges on house-hold laundry and dishwashing. Tenside Surfactants Deterg. **53**(6), 568–575 (2016)
8. Shittu, O.: Emerging sustainability concerns and policy implications of urban house-hold consumption: a systematic literature review. J. Clean. Prod. **246**, 119034 (2020)
9. Paper, W.: Water and circular economy https://www.ellenmacarthurfoundation.org/assets/downloads/ce100/Water-and-Circular-Economy-White-paper-WIP-2018-04-13.pdf. Last accessed 20 June 2021
10. Ramsey, E., Berglund, E., Goyal, R.: The impact of demographic factors, beliefs, and social influences on residential water consumption and implications for non-price policies in Urban India. Water (Basel) **9**(11), 844(2017)
11. Lubowiecki-Vikuk, A., Dąbrowska, A., Machnik, A.: Responsible consumer and lifestyle: sustainability insights. Sustain. Prod. Consumption **25**, 91–101 (2021)
12. Oteng-Peprah, M., de Vries, N., Acheampong, M.A.: House-holds' willingness to adopt greywater treatment technologies in a developing country—exploring a modified theory of planned behaviour (TPB) model including personal norm. J. Environ. Manage. **254**, 109807 (2020)
13. Saraswathy, M.: Money-control Homepage (2019). Kent RO launches 'zero water-wastage' purifier. https://www.moneycontrol.com/news/business/companies/kent-ro-launches-zero-water-wastage-purifier-4743771.html. Last accessed 21 June 2021
14. García, M.D., Schlatter, M., Cabrera, F.M., Manzanares, J.T., Hanafi, I.: Recycling of acrylonitrile–butadiene–styrene using injection moulding machine. Procedia Technol. **22**, 399–406 (2013)

15. Tsyntsarski, B., Petrova, B., Budinova, T., Petrov, N., Teodosiev, D.K., Sarbu, A., Sandu, T., FerhatYardim, M., Sirkecioglu, A.: Removal of detergents from water by adsorption on activated carbons obtained from various precursors. Desalin. Water Treat. **52**(16–18), 3445–3452 (2013)
16. Bhagawan, D., Poodari, S., Ravi kumar, G., Golla, S., Anand, C., Banda, K.S., Himabindu, V., Vidyavathi, S.: Reactivation and recycling of spent carbon using solvent desorption followed by thermal treatment (TR). J. Mater. Cycles Waste Manage. **17**(1), 185–193 (2015)

Numerical Analysis for Roof Rack Crossbar Wind Noise Prediction and Minimization

Anand Amrit, Simar Sodhi, and Suhant Ranga

1 Introduction

The wind noise around a bluff body is a fundamental problem of fluid dynamics and is important in many engineering applications. Few examples include automotive external parts, aircraft landing gears, antennae of submarines, and many more architectural design concepts. It is important for engineers to develop a clear understanding of aerodynamic noise generation using computationally efficient models for quiet technology development in a timely manner.

The sources of wind noise from crossbars can be divided into three types: (1) monopole (fluctuation in mass flow), (2) dipole (surface pressure fluctuation), and (3) quadrupole (turbulent wakes). For a typical bluff body like crossbars in a roof rack, dipole (Aeolian noise) and quadrupole (broadband noise) are major sources of noise that gets propagated to the vehicle interior. An Aeolian tone is a typical aero-acoustic phenomenon of dipole nature which is caused by periodic shedding of Karman vortices down the flow [1]. Vortex can be induced through many ways, i.e., (1) airflow detaches from the crossbar surface and the flow reverses, (2) airflow passes over the crossbar surface and loses its energy, and (3) the horseshoe effect, where airflow with high pressure moves to the low-pressure flow region. The shed vortices manifest in two ways: (1) fluctuating lift forces on crossbars and (2) generation of acoustic waves from the crossbar surface. The radiation of sound pressure and the structural vibrations are more correlated to fluctuating reaction forces on crossbars [2]. The annoying Aeolian tone due to the unstable flow is concentrated around a certain frequency and the level of dipole noise increases with the 6th power of velocity.

A. Amrit (✉) · S. Sodhi · S. Ranga
Rivian Automotive, LLC, Irvine, CA, USA
e-mail: amrit38@gmail.com

Reduction of overall vehicle noise has become a high priority for automakers with the automotive industry moving toward electrification. Hence, it is important to optimize [3–5] the shape of the crossbar to reduce the wind noise at high vehicle speed. There have been several attempts to investigate and minimize the broadband and narrowband wind noise from a circular cylinder [6–8]. Further, numerical analysis on flow over various bluff bodies has been analyzed to investigate the Aeolian tones associated with each of them [9]. An extensive study of wind noise generated by vehicle roof racks has already been performed using computational fluid dynamics models [10].

The focus of the paper is to develop numerical models to predict and minimize the tonal noise from the crossbar exposed to turbulent airflow using a faster and accurate computational fluid dynamics (CFD) methodology. Karbon et al. [10] worked on minimizing the wind noise by analyzing various orientations of the crossbar with respect to the wind flow. Lee et al. [2] utilized asymmetric cross-section geometry for Aeolian noise reduction. Wang et al. [11] optimized the mounting location of the crossbar on the vehicle roof to minimize wind noise. This paper investigates innovative configurations on the crossbar surface to mitigate the wind noise issue without significant alteration to cross-sectional geometry, orientation, or location.

2 Methodology

This section describes the governing equations utilized to solve the unsteady aerodynamic problem. Further, it describes the technique to obtain the dipole wind noise in terms of sound pressure level.

2.1 *Governing Equations for Fluid Flow Simulations*

The unsteady fluid flow problem is solved using commercial computational fluid dynamics (CFD) software, FloEFD. It solves the Navier–Stokes equations, which are formulations of mass, momentum, and energy conservation laws for fluid flows. The equations are supplemented by empirical dependencies of fluid density, viscosity, and by fluid state equations defining the nature of the fluid. A Reynolds number defines the type of flow which can be either laminar or turbulent or both. The flow is said to be turbulent when the Reynolds number exceeds a certain critical value. Favre-averaged Navier–Stokes equations are used to predict the turbulent flows, where time-averaged effects of the flow turbulence on the flow parameters are considered, whereas the large-scale, time-dependent phenomena are considered directly. Additional information is needed to solve the extra terms known as the Reynolds stresses. The transport equations for the turbulent kinetic energy and its dissipation rate are solved using the $k - \varepsilon$ model.

2.2 Governing Equations for Noise Prediction Simulations

Using Proudman's [12] work, Lilley [13] re-derived the formula for acoustic power by accounting for the retarded time difference which was neglected in Proudman's original derivation. The acoustic power due to the unit volume of isotropic turbulence (W/m^3) can be given by

$$P_\alpha = \alpha \rho_0 \left(\frac{u^3}{l} \right) \frac{u^5}{\alpha_0^5}, \tag{1}$$

where u and l are the turbulence viscosity and length scales, respectively. Also, α_0 is the speed of sound and α is a model constant. Equation (1) can be also be written in terms of k and ε (epsilon)

$$P_\alpha = \alpha_\varepsilon \rho_0 \varepsilon M_t^5, \tag{2}$$

where

$$M_t = \frac{\sqrt{2k}}{\alpha_0}, \tag{3}$$

The rescaled constant of α_ε is considered as 0.1 [14]. The acoustic power is computed from

$$L_p = 10 \log \left(\frac{P_\alpha}{P_{\text{ref}}} 10 \right), \tag{4}$$

where $P_{\text{ref}} = 10^{-12}$W/m^3.

A point is selected in the fluid domain situated far away from the body under investigation and the pressure fluctuations history in the time domain is captured. The time domain measurements are necessary to obtain spectral information about the frequency domain. The discrete time domain information is converted into its counterpart frequency domain using discrete Fourier transform (DFT) as shown here:

$$y(f_n) = \sum_k y(t_k) e^{-i \frac{2\pi n}{N} k}, \tag{5}$$

where N is the number of sample points in time domain, n is the frequency index, $f_n = \frac{n}{N \Delta t}$ is the frequency, $\Delta t = \frac{T}{N}$ is the time step, and T is the sample period. DFT can be computed efficiently using a fast Fourier transform (FFT) algorithm. Power spectral density, which is the distribution of signal power in the frequency domain, is obtained using FFT as:

$$E(f_0) = \left[\frac{|y(f_0)|}{N}\right]^2, E(f_0) = 2\left[\frac{|y(f_n)|}{N}\right]^2, n = 1, 2, \ldots N/2. \tag{6}$$

Further, the sound pressure level (dB) obtained using FFT is given by:

$$L_{sp}(f_n) = 10\log\left(\frac{E(f_n)}{P_{ref}^2}\right), n = 0, 1, 2, \ldots N/2. \tag{7}$$

where $P_{\text{ref}} = 2 \times 10^{-5}$ Pa.

2.3 Numerical Solution Technique to Resolve Boundary Layer

It is always a best practice to perform a grid convergence study before carrying out any CFD simulations. It means the grid/mesh on which the Navier–Stokes equations are calculated needs to be refined until the results are close to the physical experiments. However, FloEFD utilizes two unique approaches known as the "Two-Scales Wall Functions (2SWF) model" to couple the boundary layer calculations with main flow properties. They are:

Thick Boundary Layer Approach: This approach is applicable where the number of cells across the boundary layer is 6 or more. It utilizes Navier–Stokes equations to calculate the laminar boundary layer parameters and the well-known wall function approach model [15] to solve the turbulent boundary layer.

Thin Boundary Layer Approach: A mesh model with 4 or fewer cells across a boundary layer utilizes this approach to perform the boundary layer calculations. The Prandtl boundary layer equations are integrated along the normal to the wall to the dynamic boundary layer thickness (δ) and are solved along a fluid streamline covering the walls. Successive approximations based on the Shvetz trial functions technology [16] are used to solve a laminar boundary layer. A turbulent or transitional boundary layer is solved employing the Van Driest hypothesis [15]

A compilation of the above two approaches is used to solve intermediate cases (laminar and turbulent flows). The latter approach is very useful as it helps to obtain almost accurate results in a short time. The solution accuracy may fall off as the number of computational mesh elements is increased which can be seen in the grid convergence study discussed in Sect. 3.1. The main reason behind this is that the mesh might be too refined for the thin boundary layer approach, but insufficiently fine for the thick boundary layer approach. The accuracy improves gradually on further refinement of the computational mesh.

3 Numerical Results

This section validates the numerical results with experimental data using an aerodynamic problem involving a right circular cylinder. Further, wind noise prediction from crossbar and minimization of the same is discussed.

3.1 Validation Case: Three-Dimensional Circular Cylinder

The aerodynamic problem consists of a circular cylinder with a diameter of 10 mm and a free-stream wind velocity of 72 m/s corresponding to Re $\approx$ 48,300 [7, 8]. Figure 1a depicts the dimensions of the fluid domain utilized to perform the computational fluid analysis. A spatial mesh resolution of wall y-plus value approximately equal to 1 (distance of the first layer from the wall is equal to 1e-5 mm) is employed on the cylinder wall to resolve the near-wall flow as shown in Fig. 1b. Based on the type of flow, the mesh region near the cylinder wall is refined (boundary layer thickness, $\delta = 3$ mm) to properly resolve the boundary layer flow. Point A which is 1850 mm right above the circular cylinder is selected to capture the pressure fluctuations due to flow over the cylinder. A grid convergence study is performed to obtain the mesh size needed to capture the near-field pressure fluctuations as given in Table 1. The lift coefficient (C_l), drag coefficient (C_d) (see Fig. 2a), and the maximum sound pressure level (SPL) in the frequency domain of the cylinder are evaluated and compared against experimental results [7, 8]. Table 1 indicates Mesh 5 is in good agreement with the experimental data. The CFD model is also able to capture the Aeolian tone accurately as shown in Fig. 2b. Thus, the capability of the CFD software and the models involved are validated.
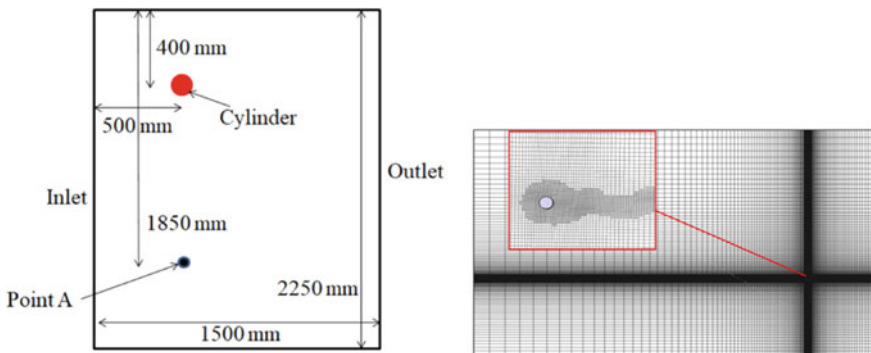
Fig. 1 **a** Fluid domain and **b** Mesh architecture of the fluid domain

Table 1 Grid convergence study

	Number of fluid mesh elements	Number of fluid surface mesh elements	Max C_d	Max C_l	Max sound pressure level (dB)
Mesh 1	483,727	6768	0.9	0.9	93
Mesh 2	498,950	6768	0.78	0.7	84
Mesh 3	551,168	26,496	0.9	0.9	86
Mesh 4	839,516	11,808	0.85	0.85	84
Mesh 5	1,165,632	184,128	0.9	0.9	84
	Experiment value [7, 8]:		1.01	0.9	84
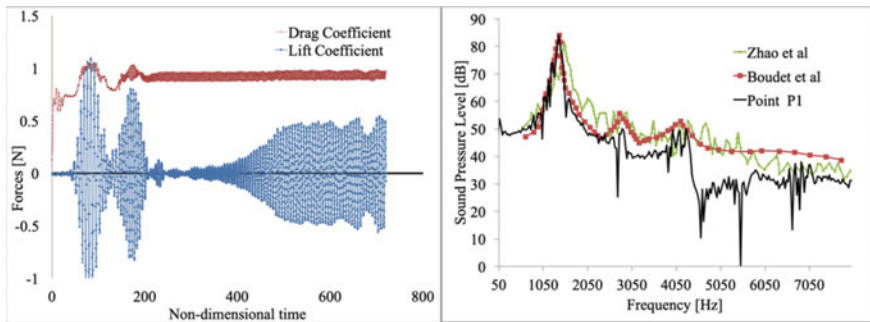
Fig. 2 **a** Aerodynamic forces on the cylinder and **b** verification of computational results

3.2 Single Crossbar

The three-dimensional computational model consists of a single crossbar inside a cuboidal domain, as shown in Fig. 3a. The cross-section (see Fig. 3b) is like that of an airfoil with a thickness to cord ratio (t/c) of 43% and chord length (c) of 70 mm. The length of the crossbar is approximately 1000 mm which demanded a large computational domain. Since such a large computational domain can be significantly time-consuming, only 50 mm length of crossbar is utilized for CFD analysis with periodicity boundary condition as shown in Fig. 3a. Points A and B are selected within the computational domain (as shown in Fig. 3c) to capture the fluctuations in static pressure from the time-averaged CFD solution. They are further postprocessed to obtain the sound pressure level (dB) in the frequency domain as described in Sect. 2.2.

The objective of the analysis is to predict the wind noise from the horizontal crossbars of roof rack system. To capture a perfect von Karman vortex shedding, the crossbar is rotated to 20° with respect to the wind flow direction which replicates the vehicle mounting configuration. The wind speed maintained at 40 m/s with a Reynolds number of 7×10^4 is expected to produce von Karman vortex shedding
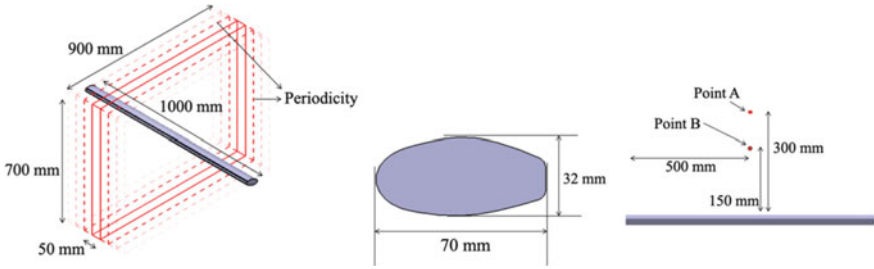
Fig. 3 **a** Fluid domain, **b** cross-section of the crossbar, and **c** noise measurement point

corresponding to $St = 0.2$ [17]. The following equation gives us a first-order estimate of the frequency of the expected tones

$$f = \frac{St\,V}{d} \sim 300 \text{ Hz,} \tag{8}$$

where St is the Strouhal number and V is the wind speed. Further, d is the characteristic vortex shedding dimension which is also the height of the wake behind the crossbar and can be determined by the following equation

$$d = c \sin(\text{AoA}) \sim 24 \text{ mm,} \tag{9}$$

where AoA is the angle of attack of the wind flow with respect to the crossbar.

The CFD parameter settings used to run the simulation are given in Table 2. The transient flow analysis is run for 0.4 physical seconds, and the pressure fluctuations at Point A and B are recorded for 0.3 to 0.4 s only. The pressure data is processed using Fast Fourier Transformation as explained in Sect. 2.2, and the Aeolian tones are obtained at a frequency of 300 Hz as expected (see Fig. 4a). The Karman vortex street behind the crossbar is clearly captured in Fig. 4b where the vortices are shed from alternating sides (top and bottom). These shed vortices interact with each other and significantly contributes toward a high Aeolian tone of 102 dB at Point A and 91 dB at Point B. Figure 5 indicates a fluctuating lift force on the crossbar due to pressure fluctuations and an average drag force of 0.63 N. The aerodynamic forces indicated in this paper are calculated only on 50 mm length of the crossbar.

Table 2 List of parameters utilized in the numerical analysis

Parameters	Values
Platform	20 processors
Density	1.225 kg/m^3
Dynamic viscosity	1.85e-05 N-s/m^2
Velocity	40 m/s
Reynolds number	7×10^4
Boundary layer thickness	3 mm
Turbulence intensity	4%
Turbulence length	17 mm
Wall spacing	1e-5 m
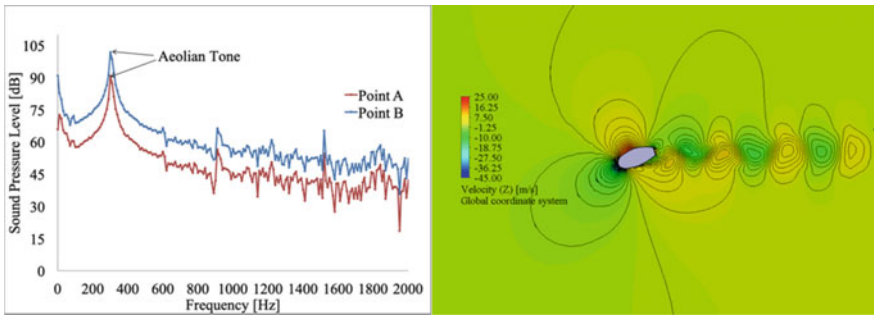
Fig. 4 **a** Comparison of Aeolian tones and **b** wind velocity contour
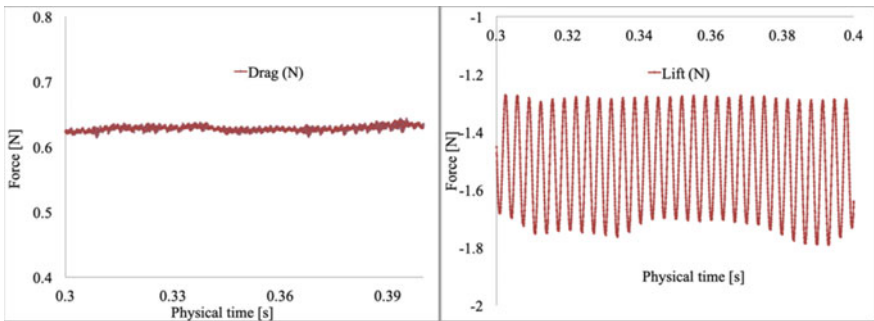
Fig. 5 **a** Drag force on the crossbar and **b** lift force on the crossbar

3.3   Wind Noise Minimization

Several crossbar configurations are investigated to understand their effect on the overall wind noise and aerodynamic forces (as given in Table 3). Following modifications are added on the entire length of the top surface to obtain three different crossbar designs (as shown in Fig. 6):

(1)   Circular holes
(2)   Oval holes
(3)   Spiral ribs.

CFD analysis (similar to that in Sect. 3.2) is performed on each of the three configurations and compared to a plain crossbar as given in Table 3. Clearly, there is a rise in drag and negative lift forces with hole configurations. However, the drag was reduced and lift remained almost the same with spiral ribs configuration. Further, all three configurations (b, c, and d) generate an Aeolian tone that is significantly less than that by the plain crossbar. Figure 7a indicates the circular hole configuration has two peaky

Table 3   Comparison of aerodynamic forces and wind noise

	Crossbar configuration	Geometry details (mm)	Spacing (mm)	Average drag (N)	Average lift (N)	Max. SPL at Point B (dB)
(a)	Plain	–		0.63	−1.52	101.89
(b)	Circular hole	Diameter = 16 Hole depth = 3	50	0.80	−2.38	77.8
(c)	Oval hole	Major axis = 35, Minor axis = 15 Hole depth = 4	60	0.94	−2.76	61.26
(d)	Spiral ribs	Max. rib height = 1.5 Max. rib length = 17	50	0.64	−1.66	56.44
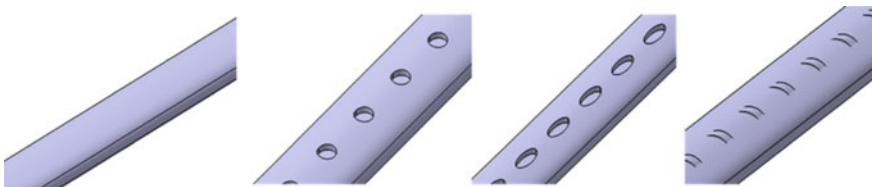
Fig. 6   a Plain crossbar, **b** circular holes, **c** oval holes, and **d** spiral ribs
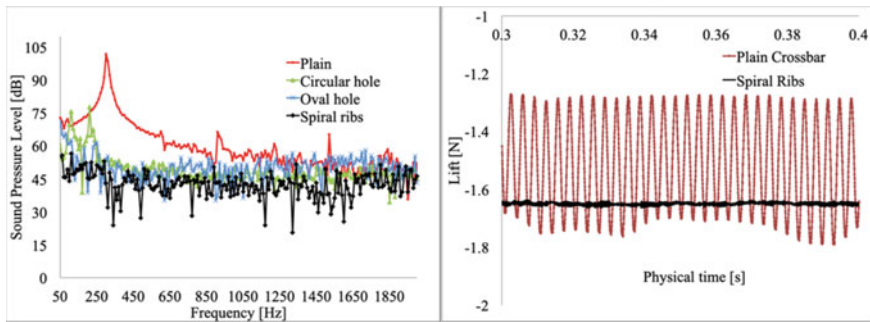
Fig. 7 Comparison of **a** Wind noise and **b** lift forces

noises within 0–300 Hz but its intensity is still less than that produced by the plain crossbar. Oval-shaped hole configuration and spiral ribs configuration have almost equivalent noise reduction effects within 0–300 Hz with the latter hardly generating any Aeolian tone. Among the three configurations (b, c, and d), the crossbar with oval holes generates relatively higher broadband noise similar to that by the plain crossbar in the high-frequency range (>1000 Hz). The crossbar with spiral ribs is the best design as it has the least aerodynamic forces and wind noise in both narrow and broadband. Further, Fig. 7b indicates the intensity of vibration is significantly less than that of plain crossbar which makes spiral ribs the best choice.

The velocity component field perpendicular to the direction of wind flow shows periodic vortex shedding from the alternate directions, as shown in Fig. 8a. However, as we move from (a) to (d), the flow stabilizes and changes its distribution from the time-dependent behavior with vortex shedding to the steady-state symmetric shape. Since there is no periodic vortex shedding in crossbar with spiral ribs, the intensity of the fluctuating lift force is reduced significantly (see Fig. 7b). Thus, no Aeolian tones are generated.

4 Conclusion

Numerical analysis and design modifications are performed to predict and minimize the wind noise generated by the crossbars of a roof rack system on a vehicle. A commercial CFD software is utilized to solve the aerodynamic problem. The pressure fluctuations data is collected from a point in the fluid domain that is some distance above the crossbar. Further, the same data is processed using Fast Fourier Transformation (FFT) to obtain the narrowband (Aeolian tones) and broadband noise in terms of sound pressure level. Next, several crossbar configurations involving modification to its surface are analyzed to investigate their effect on the wind noise. It is concluded that crossbars with spiral ribs will lead to a remarkable reduction in both narrowband and broadband noise.
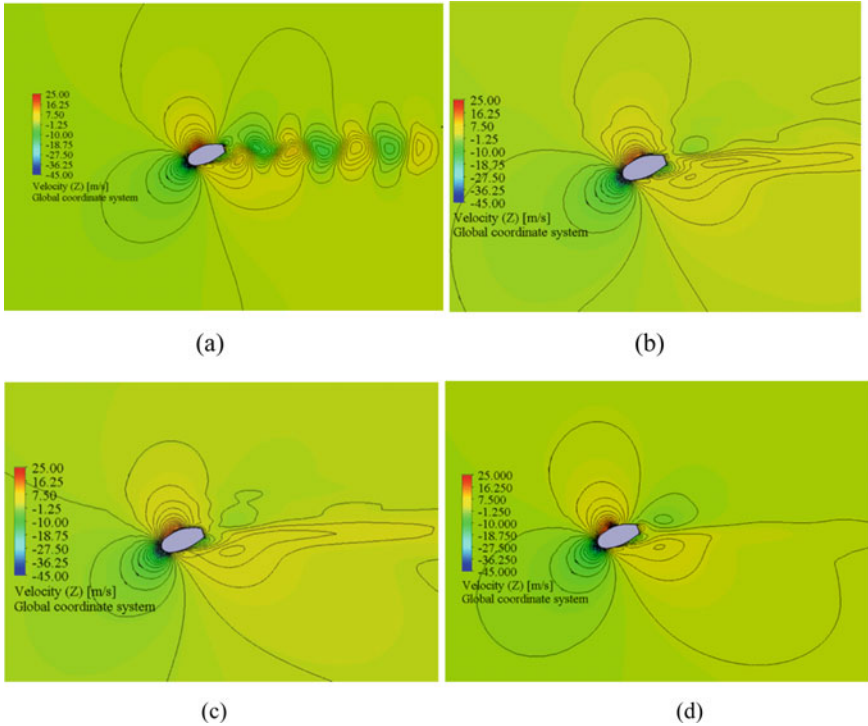
Fig. 8 Wind velocity component perpendicular to upstream flow: **a** plain crossbar, **b** crossbar with circular holes, **c** crossbar with oval holes, and **d** crossbar with spiral ribs

References

1. Senthooran, S., Duncan, B., Freed, D., Hendriana, D. et al.: Design of roof-rack crossbars for production automobiles to reduce howl noise using a lattice boltzmann scheme. SAE Technical Paper 2007-01-2398 (2007). https://doi.org/10.4271/2007-01-2398
2. Lee, M., Lee, J., Kim, D.: Reduction of aeolian noise from roof rack crossbars using asymmetric cross-section geometry. SAE Technical Paper 2002-01-1275 (2002). https://doi.org/10.4271/2002-01-1275
3. Amrit, A., Leifsson, L., Koziel, S.: Design strategies for multi-objective optimization of aerodynamic surfaces. Eng. Comput. **34**(5), 1724–1753 (2017). https://doi.org/10.1108/EC-07-2016-0239
4. Amrit, A., Leifsson, L., Koziel, S.: Multi-Fidelity aerodynamic design trade-off exploration using point-by-point pareto set identification. Aerosp. Sci. Technol. **79**, 399–412 (2018)
5. Amrit, A., Leifsson, L., Koziel, S.: Aerodynamic design exploration through point-by-point pareto set identification using local surrogate models. In: AIAA/ASCE/AHS/ASC Structures, Structural Dynamics, and Materials Conference. Kissimmee, Florida (2018)
6. Railway, Mitsuru, L.K.: Study of the aerodynamic noise characteristics of bluff bodies as a pantograph member (2002)
7. Zhao, Q.: Sound source localization of flow around circular cylinder by a virtual microphone array technique. AIP Adv. **8**, 055130 (2018). https://doi.org/10.1063/1.5023457

8. Boudet, J., Casalino, D., Jacob, M.C., Ferrand, P.: Prediction of sound radiated by a rod using large eddy simulation. In: AIAA, pp. 2003–3217 (2003)
9. Ali, M.S.M., Shaikh Salim, S.A.Z.B., Ismail, M.H., Muhamad, S., Mahzan, M.I.: Aeolian tones radiated from flow over bluff bodies. Open Mech. Eng. J. **7**, 48–57 (2013)
10. Karbon, K.J., Dietschi, U.D.: Computational analysis and design to minimize vehicle roof rack wind noise. SAE Trans. **114**, 649–56 (2005). http://www.jstor.org/stable/44725097
11. Wang, X., Watkins, S.: Reduction of roof rack noise and vibration. Int. J. Veh. Noise Vib. **6**, 105–117 (2010). https://doi.org/10.1504/IJVNV.2010.036680
12. Proudman, I.: The generation of noise by isotropic turbulence. Proc. Roy. Soc. **A214**, 119 (1952)
13. Lilley, G.M.: The radiated noise from isotropic turbulence revisited. NASA Contract Report 93–75, NASA Langley Research Center, Hampton, VA (1993)
14. Sarkar, S., Hussaini, M.Y.: Computation of the sound generated by isotropic turbulence. NASA Contract Report 93–74, NASA Langley Research Center, Hampton, VA (1993)
15. Van Driest, E.R.: On turbulent flow near a wall. J. Aeronaut. Sci. **23**(10), 1007 (1956)
16. Ginzburg, I.P.: Theory of Drag and Heat Transfer. LGU, Leningrad (1970).(in Russian)
17. Norton, M.P.: Flow-induced vibration. In: R.D. Blevins, Van Nostrand Reinhold, New York, 1990, 451 (1991)

Development of Close Celled Cenosphere Based Polymer Syntactic Foams

Ch. Sri Chaitanya, P. Gopinadh Chowdary, G. Chitti Babu, and R. Narasimha Rao

1 Introduction

Transportation is a major cause of the release of greenhouse gases. The vehicles manufactured utilizing materials with higher densities require large amounts of energy to transport them. The research to prepare composite materials that can be used as auto-motive structures is required to reduce the energy demand in the transportation sector and thereby reduce emissions. The density of the composite material can be reduced by adding porosity to it [1]. The porosity in the syntactic foams is achieved by adding hollow micro balloons to the matrix. These balloons can be a ceramic, polymer or fly ash based [2].

The porosity reduces the weight of the composite material but it is expected to lose its strength with the additional porosity. Hence, most of the initial research concerning the development of the syntactic foams was focused on the compression deformation of the foams. The micro balloons that are present in the foam compact during its compression. This compaction of the hollow particles creates a wide densification region in the stress-strain curve of syntactic foams. The wider the densification strain zone of the syntactic foam, the higher is the area under the stress-strain curve [3]. The compression properties were studied in the low-velocity impact [4], quasi-static compression [5–7] and dynamic compression [7–9] conditions.

The study of wear properties was conducted once the mechanical properties of the syntactic foams appear to be good. The wear debris collected in the pores created

Ch. Sri Chaitanya (✉) · P. Gopinadh Chowdary
Department of Mechanical Engineering, VR Siddhartha Engineering College, Vijayawada 520007, India
e-mail: srichaitanya@vrsiddhartha.ac.in

G. Chitti Babu · R. Narasimha Rao
Department of Mechanical Engineering, National Institute of Technology Warangal, Warangal 506004, India

by the broken cenospheres acted as the protective layer and reduced the wear rate. Based on the tribological parameters, the shells from the micro balloons are either crushed to powder or remain as hard shells. These influence the wear rate and the coefficient of friction. The powdered shells of micro balloons or the wear debris help in reducing the coefficient of friction and wear rate. If the shells remain coarse, the debris will stick in between the sample and counter surface. These will damage the surface of the sample and increase the wear rate [6, 10, 11]. Cenospheres, which are the by-products of thermal power plants, can be used as hollow micro balloons if the size of the balloons is graded to get an even distribution of size [2, 10].

In the present study, the development of epoxy-based syntactic foams was reported. The manufacturing of the foams and compression strength of the foams, when manufactured by using mechanical mixing of the cenospheres, was reported.

2   Materials and Methods

Polymer matrix-based syntactic foams were manufactured for the current study. The matrix was made of bisphenol-based epoxy resin (LY551) and hardener (HY951). The epoxy resin and the hardener are used in the ratio of 10:1 by weight as a matrix. The mixing was done until a visibly uniform distribution of the cenospheres was achieved in the epoxy resin. The mixture was then allowed to settle for a minute. One part of the hardener was taken for ten parts of epoxy resin and added to the epoxy–cenosphere mixture. The stirring process was continued to mix the hardener to the epoxy–ceno- sphere mixture. The mixture was then poured into dies as shown in Fig. 1. The dies, if placed in the open air, may affect the strength of the foam and the cenospheres move to the surface due to the density variations. The dies were sealed with polythene sheets to reduce the effect of the atmosphere on syntactic composites while curing. After the curing time, the samples were checked whether they were cured and removed from the dies.

Fig. 1 PVC pipe dies are used during the manufacturing of syntactic composites

   The samples obtained were checked for the external defects on the surfaces of the samples. The defective samples were discarded. Accumulation of cenospheres reduces the bond strength between the cenospheres and matrix due to the lack of sufficient matrix. To check the uniformity in distribution of the cenospheres in the matrix, some samples were randomly selected and the surfaces were observed under a scanning electron microscope. The samples were then machined to the dimensions of the samples required for the experiments. These samples were cleaned with acetone and tested for density.

   The density of the syntactic foams was studied in this work. Density can be obtained theoretically using the rule of mixtures or experimentally using Archimedes' principle. From the rule of mixtures, the density of a sample was obtained as the combination of the densities of the constituents and their volume fractions. The equation to calculate the density of syntactic foam using the rule of mixtures is

$$\rho_{\text{foam}} = \rho_c v_c + \rho_e v_e + \rho_h v_h \tag{1}$$

   The volume fraction of each material is given by v. The weight of the sample was measured in air and then when immersed in water. The specific gravity of the sample was obtained by dividing the weight of the sample in air with the weight loss in water. The weight loss in water is the weight of the sample subtracted from the weight of the sample in air. Equation 2 shows the calculation of density using Archimedes' principle.

$$S.G. = \frac{(W_{\text{foam}})_{\text{air}}}{(W_{\text{foam}})_{\text{air}} - (W_{\text{foam}})^{\text{water}}} \tag{2}$$

   In the present study, both the theoretical and experimental methods were used to calculate the density and compared with each other.

   The compression testing was done using a universal testing machine (UTM). The UTM machine used for the study can impart a maximum load of 100 kN. The speed range of compression or tension of the machine is 0.0005 mm/min to 500 mm/min. The testing space for sample placement is of 600 mm × 600 mm with the scope to measure the deformation of the sample from 10 to 800 mm. The test follows ASTM D638 standard for tensile properties of plastics and ASTM D695 for the compressive properties.

   It can be used to test the behaviour of a material in tension, compression, bending, shearing and torque. Axial strain is a dominant strain during the compression tests. The axial strain measures the deformation of the sample due to the force along the axis of the sample. Strain gauges are used to measure the strain. Control parameters and the sample dimensions are given to the computer. The displacement rate of the moving arm of the universal testing machine was given in mm/min. The specimen dimensions like the diameter of the sample and the length to diameter ratio were given to the machine which calculates the strain and stress from the displacement data and the load system. The data from the strain gauge was obtained from the machine and converted to digital. The data was used to calculate the strain rate and

the stress with the software that is connected to the machine. The software outputs the time, load, compression, stress and strain. This data was used to plot the stress vs strain curves and the area under the stress vs strain curves was calculated from the data using Eq. 3.

$$\text{Energy} = \int \sigma \, d\varepsilon \tag{3}$$

The stress-strain curves obtained above will have a linear deformation zone at the initial stages of compression. The slope of this linear deformation zone is called the effective modulus of the syntactic foam. The effective modulus of syntactic foams is calculated from the obtained stress-strain data and compared with the effective modulus of syntactic foams obtained from finite element studies of the same.

3   Results and Discussion

The density of the syntactic foams is measured using theoretical techniques and experimental techniques. The density is obtained theoretically by using the rule of mixtures principle. The densities of each of the constituent materials and their concentration in the sample are used to calculate the density of the syntactic foam. The densities of the syntactic foams obtained experimentally and theoretically are shown in Fig. 2. The densities of samples obtained from both methods should be near to each other. Differentiation between the results is attributed to the defects induced into the samples during manufacturing, some human errors during the experimentation, machine zero errors in weighing balances and rounding of the density values of the constituent materials.

Among the above-mentioned reasons, the difference between the densities due to defects induced into the samples during manufacturing is significant. The samples with defects will reduce the strength of the material and interfere with the experiments. Avoiding these samples reduces the discrepancies in the experimental results. Hence, the samples with the experimental density outside the range of 5% around the

Fig. 2 Comparison of theoretical and experimental density of Syntactic foams with the variation of the cenosphere volume fraction
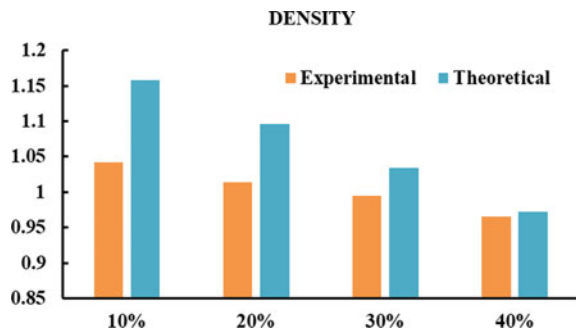
theoretical density are discarded from usage for experimentation. From the experiments, it is observed that the density of the 40% syntactic foam was reduced by 7.8% when compared to the 10% syntactic foam.

The scanning electron microscope is employed to observe the surfaces of the syntactic foam samples manufactured for the study. The samples were sealed and kept in an air-tight container to avoid atmospheric interaction with the material. The non-uniform distribution of cenospheres leads to a strong variation in syntactic foam. The non-wettability of cenospheres leads to the lack of superior quality bonding between the matrix and cenosphere surface. The distribution of the cenospheres in the matrix of syntactic foams is shown in Fig. 3. Syntactic foam samples are randomly chosen, at least three per variety of foam and observed under a scanning electron microscope at different locations on a surface and on different surfaces along the axis. The lack of cracks or gaps at the interface of the cenosphere and matrix indicates that the syntactic foam samples are suitable for experimentation. There are no damages to the surface of the syntactic foams. Minor damages may have been caused during the transportation and preparation of samples for the study. These are minute in number and smaller in size and can be neglected.

The samples used for the compression test are cylindrical in shape with a diameter of 2.5 cm and length to diameter ratio of 1.5, i.e. 3.75 cm. The epoxy matrix and cenosphere mixture were poured into dies of 1.25-inch (3.175 cm) diameter and
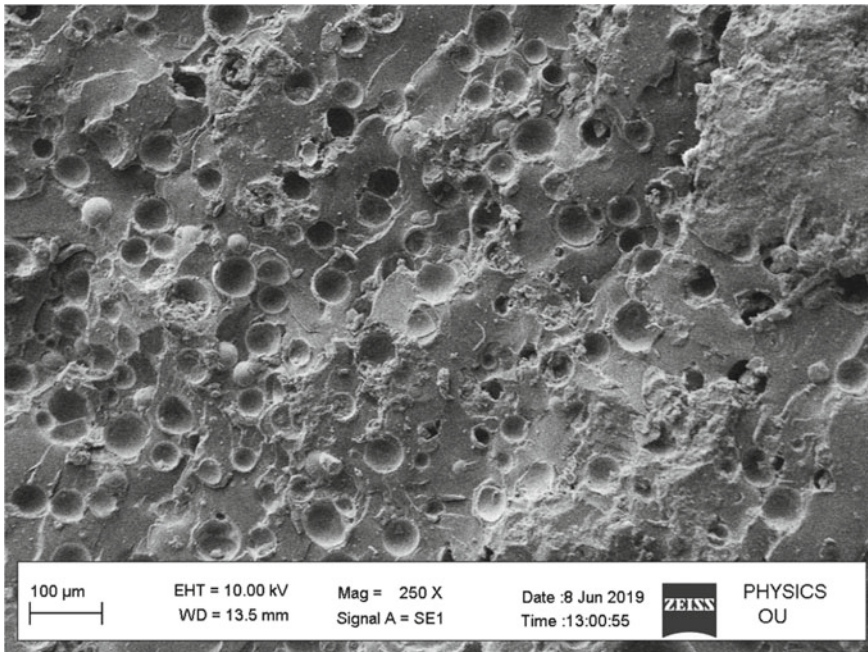
Fig. 3 The scanning electron micrograph of a syntactic foam sample shows the cenosphere distribution in the epoxy matrix

Fig. 4 The schematic of the syntactic foam samples prepared for the compression test
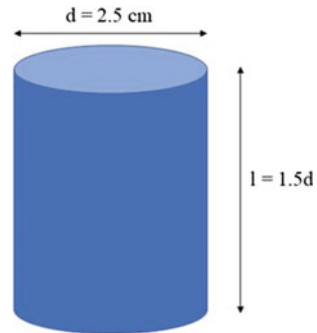
sealed. Syntactic foams with three different volume fractions of 20%, 30% and 40% were chosen for the study. The lower volume fraction of 10% of porosity was not included in the study because the trends of the compression behaviour do not vary significantly at lower volume fractions of the porosity. Adding experiments and their repetitions for the 10% volume fraction foams increase the experimental cost without significant addition of insights to the study. The schematic of the sample was shown in Fig. 4. After curing, the samples were taken out of the dies by cutting the dies. Obtained samples will have some protrusions and waviness on the surface along with some surface damage. These damages can be removed by machining.

The peak strength of the syntactic foams manufactured with the lowest size grade cenospheres (0–75 µm) and three-volume fractions was shown in Fig. 5. The experiments that are presented in Fig. 5, are conducted at a strain rate of $0.0004~\text{s}^{-1}$. The syntactic foams with lower porosity fractured earlier compared to the foams with higher porosity. This may be due to the compaction of the cenospheres being more in higher porous materials. The stress-strain curves follow a linear pattern until the peak strength is reached and then a wide densification region is observed. The variation in the peak strength with the variation of porosity of the syntactic foams is negligible. The variation of the peak strength of the syntactic foams with cenosphere volume fraction is within the range of 2%. Hence, it can be concluded that the effect of the volume fraction on the peak strength.

The syntactic foams with higher porosity absorbed more energy than the foams with lower porosity. The energy absorption capability of the syntactic foams more than doubled when the cenosphere volume fraction increased from 30% volume fraction to 40% volume fraction. The wider densification region increases the area under the stress-strain curve thereby the total energy absorption capability of the syntactic foam. The total energy absorbed per unit volume of the syntactic foams made using different volume fractions of cenospheres is shown in Fig. 6. Total energy absorbed by 40% cenosphere syntactic foam is three times higher than the syntactic foam with a 20% cenosphere volume fraction in this case.

The stress increases linearly in the initial phase until the plastic deformation starts. The slope of the linear portion of the curve is the modulus of syntactic foam. The modulus of the syntactic foams remains the same for all the cenosphere volume
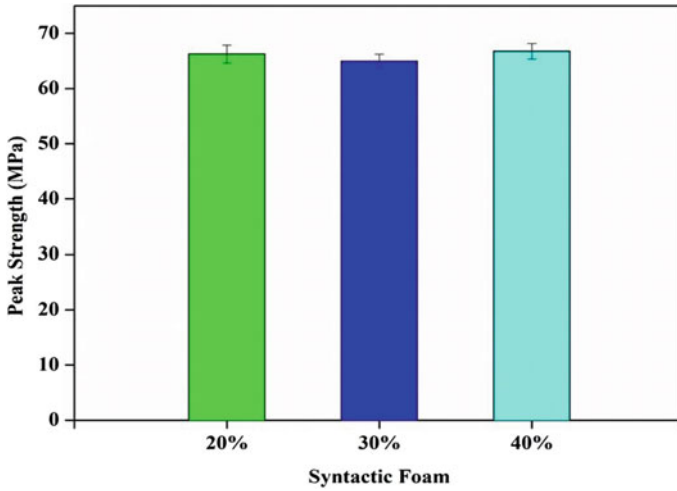
Fig. 5 The peak compression strength of the syntactic foams with 20%, 30% and 40% volume fraction cenosphere when compressed at a strain rate of 0.0004/s
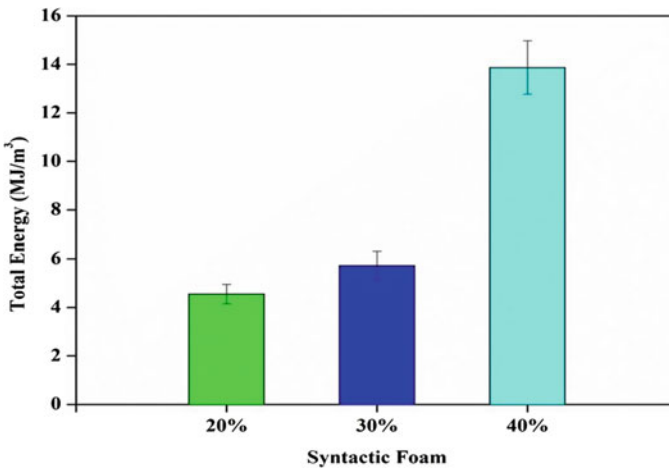
Fig. 6 The energy absorbed by the 20%, 30% and 40% vol. cenosphere syntactic foams when compressed at a strain rate of 0.0004/s

fractions. The compressive strengths of the cenospheres used in manufacturing the cenospheres vary from the compressive strength of the matrix. This variation of the strength has little effect on the peak strength of the syntactic foams. This shows that the cracks initiated in the matrix and are propagated to the cenosphere shells. The cenosphere shells are made up of alumina and silica, which are brittle in nature and the epoxy resin matrix is brittle. The syntactic foams made from the combination of these two materials exhibit similar properties, i.e. brittle nature. The compaction

of the pores formed from the cenospheres is lower compared to the syntactic foams manufactured using the matrix with elastic properties. As the syntactic foams are compressed, the shearing and the crushing of the cenospheres suddenly change the stress abruptly. This abrupt change in stresses causes the stress-strain curve to fluctuate in the densification region. The failure occurs by shearing and crushing the cenosphere shells. The more compression in the foam indicates the larger energy absorption as the peak stress is the same for all three types of foam. As mentioned earlier the cracks may have started in the matrix and propagated through it to the failure. The probability of the crack to avoid the cenosphere shell during propagation is higher for lower volume fraction cenosphere syntactic foams when compared to higher volume fraction cenosphere syntactic foams. When the cracks reach the cenosphere shell, they can propagate either by cracking the cenosphere shell or by debonding the bond between the cenosphere shell and the matrix. Both cracking the cenosphere shell and debonding the cenosphere shell from the matrix require more energy than the crack propagating through the matrix. More porosity also increases the densification strain.

4 Conclusions

The epoxy-based syntactic foams were manufactured using a mechanical mixing pro- cess. To study the effectiveness of the manufacturing procedure, the densities of the samples were noted and observed using SEM. The conclusions of the study are presented here.

- The samples with higher cenosphere volume fractions showed densities closer to the theoretical densities. This can be attributed to the easier mixing and ability to get uniform distribution is good for higher concentrations
- The Scanning Electron Micrographs showed negligible damage to the cenospheres during the manufacturing process. Acceptable distribution and bonding were achieved.
- The volume fraction of the cenospheres does not have a considerable effect on the peak compressive strength of the syntactic foams.
- The energy absorption capability of the syntactic foams increases with the increase in the cenosphere concentration.

References

1. Taherishargh, M., Belova, I. v., Murch, G.E., Fiedler, T.: Pumice/aluminium syntactic foam. Mater. Sci. Eng. A. **635**, 102–108 (2015)
2. Ranjbar, N., Kuenzel, C.: Cenospheres: a review, (2017)
3. Sri Chaitanya, Ch., Rao, R.N.: Energy absorption capabilities of cenosphere reinforced epoxy syntactic foams. Mater. Res. Express. **6** (2019)

4. Castro, G., Nutt, S.R., Wenchen, X.: Compression and low-velocity impact behavior of aluminum syntactic foam. Mater. Sci. Eng. A **578**, 222–229 (2013)
5. Szlancsik, A., Katona, B., Bobor, K., Májlinger, K., Orbulov, I.N.: Compressive behaviour of aluminium matrix syntactic foams reinforced by iron hollow spheres. Mater. Des. **83**, 230–237 (2015)
6. Manakari, V., Parande, G., Doddamani, M., Gaitonde, V.N., Siddhalingeshwar, I.G., Kishore, Shunmugasamy, V.C., Gupta, N.: Dry sliding wear of epoxy/ce- nosphere syntactic foams. Tribol. Int. **92**, 425–438 (2015)
7. Wu, G.H., Dou, Z.Y., Sun, D.L., Jiang, L.T., Ding, B.S., He, B.F.: Compression behaviors of cenosphere-pure aluminum syntactic foams. Scripta Mater. **56**, 221–224 (2007)
8. Goel, M.D., Peroni, M., Solomos, G., Mondal, D.P., Matsagar, V.A., Gupta, A.K., Larcher, M., Marburg, S.: Dynamic compression behavior of cenosphere aluminum alloy syntactic foam. Mater. Des. **42**, 418–423 (2012)
9. Zou, L.C., Zhang, Q., Pang, B.J., Wu, G.H., Jiang, L.T., Su, H.: Dynamic compressive behavior of aluminum matrix syntactic foam and its multilayer structure. Mater. Des. **45**, 555–560 (2013)
10. Sri Chaitanya, C., Narasimha Rao, R.: Tribological behavior of cenosphere- filled epoxy syntactic foams in dry sliding conditions. J. Tribol. **142** (2020)
11. Mondal, D.P., Das, S., Jha, N.: Dry sliding wear behaviour of aluminum syntactic foam. Mater. Des. **30**, 2563–2568 (2009)

Design of Snake Robot with 28015 PING Ultrasonic Distance Sensor and Arduino

Nikita Venkatesh Mishra, Amiya Dash, and Shuvabrata Bandopadhaya

1 Introduction

The snake robots can be provided with tools for making them self-sufficient. We can use these snake robots to move through small underground pipe networks. They can travel in any direction, making them useful for assessing small spaces. They may also be utilized for search and rescue missions at disaster sites [1]. The need something that can move in any possible direction and can move through small holes, can climb hills or trees, and even can dig the earth. This gave the idea of the robot that completely resembles the real snake [2] and can use its motion for reaching the places where human intervention is not possible. The serpent: Snakes are biological creatures that can move in every possible direction. They can move forward, backward, and even sideways. The snakes are non-vertebrate reptiles that are commonly known for their way of motion. The most common motion of the snake is the lateral undulation [2].

For these expectations to be fulfilled, the SnakeBot has a modular design with, here, seven segments. This replicates the spinal muscles of the snakes which are responsible for its motion. The body of the robot is designed using 3D printing, and then, seven servo motors are connected to Arduino Uno serially. The Arduino receives signals from the sensor, which in turn controls the servo motors. For having certain amount of control with the operator, a Bluetooth module can be connected to the Arduino. This would help the operator to guide the Arduino using an app connected through using the Bluetooth module. And to further detect the presence of human, a thermal sensor can also be connected in the head. When facing an obstacle,

N. V. Mishra · S. Bandopadhaya
Banasthali Vidyapith, Tonk, Rajasthan, India

A. Dash (✉)
BML Munjal Univarsity, Gurugram, Haryana, India
e-mail: dash.amiya@gmail.com

157

it can record the temperature and instruct whether it resembles the heat transmitted through humans [3].

Based on this theoretical study, designing a real-life prototype of the SnakeBot, to verify the usability, will be costly and time-consuming. Instead, using Tinkercad with the help of a Web browser, an online program for modeling and simulating 3D designs will be efficient [8].

In this paper, a snake robot with an ultrasonic sensor, to have an autonomous motion, using Arduino has been proposed. The stimulated prototype of this SnakeBot consists of a head segment followed by seven segments that induce the lateral undulation motion. In the head, Arduino Uno acts as centralized controlling unit and is connected to an ultrasonic distance sensor. This paper follows a structure for understanding the various aspects of the proposed design. We will discuss the design methodology proposed in Sect. 2, discuss the communication flow in Sect. 3, and conclude the paper in Sect. 4.

2 Design Methodology

This section describes how to design a robot snake. This mainly can be discussed by dividing into two phases. The physical design will be covered in the first phase of designing the robot, whereas the second phase will involve the control panel design. The methodology for designing the snake robot consisting of distance sensor and Arduino is discussed here. Figure 1 shows the components involved in the proposed design of the snake robot.

Physical design of robot: A snake robot is hyper-redundant and resembles a biological snake. Designing of these snake robots is done in such a way so that the motion of the snake can be exactly copied. This can be achieved by transferring the muscle

Fig. 1 Components in proposed snake robot
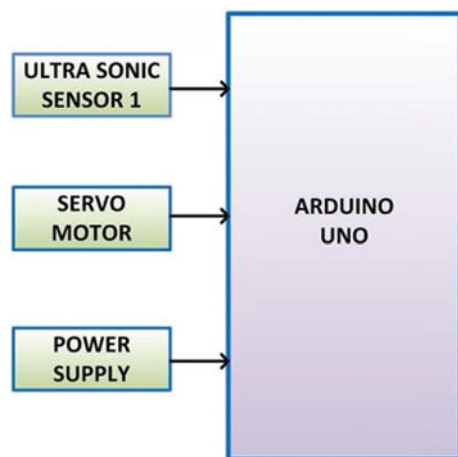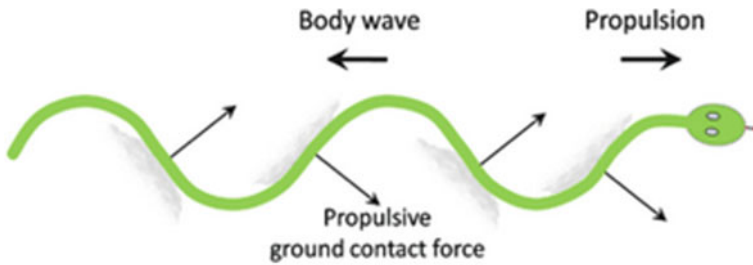
Fig. 2 Forces acting on segments of the SnakeBot

movement of a real snake into the robot. The movement of the snake is because of the contraction of the muscles around the joints which are present in the spine.

Lateral undulation is the most common motions of all the serpents. It is also referred as serpentine crawling. The muscle in the spine helps them to perform the wavelike motion which can also propagate backward direction along with the body. The sides of the body push against the irregularities which are present on the ground and exert force perpendicular to the existing position [4]. This is shown in Fig. 2 [7]. This is replicated in the robot with its modular structure of the model. The frictional forces act at different points on the robotic segments of our snake. Consider points at the end and the front of a segment. When the endpoint pushes against ground, a force is generated, at the point which is center of mass of the segment, which pushes the front end forward [5].

Designing of the robot is the resultant of the global demands and is extended to include specific requirement for the design and as well as necessities [7]:

1. The robot must be autonomous, which means that it can perform tasks without any external interference.
2. The friction between the robot and the ground must be anisotropic for the lateral undulation to be proper.
3. The energy source must deliver enough energy to drive the angular actuators.
4. Microcontroller must be able to handle the control algorithm and communicate with the hardware.
5. The structure and material of the robot should be stable as well as strong to hold the stress that will occur during the movement of the robot.

Considering the above requirements, the design proposed here consists of a distance sensor to make the robot autonomous, segmented body to get proper friction between the ground and the robot, an energy source of 9 V to sufficiently provide power to each segment in the body, Arduino Uno with ATmega328P microcontroller to give commands to the snake robot [9].

A robot's physical model can generally be divided into two parts: the snake's head and its entire body. The front part of the snake robot forms its head. The electronic control device required for movement and the required sensor are connected to the head. A microcontroller board is also added here (we can also add a Bluetooth module

if operator control is required). In order to design the robot to have autonomous movements, it must be responsive to the surroundings it is in. This can be achieved through multiple choices of visual inputs, such as global positioning systems and integrated sensors. In this proposed design, the robot uses range-detecting ultrasonic sensors. In an ultrasonic distance sensor, ultrasonic waves are emitted which collide with any item at the front, if any. After collision, the waves get reflected back to the sensor, where they are converted to electrical signals which can be read to find out the distance of the item at front [10]. The sensor used here is 28015 PING REVC ultrasonic distance sensor, which is at the forefront to measure and analyze the space in front of the snake robot. Ultrasonic distance sensor's SIG is connected to Arduino's A0, 5 V to 5 V power supply pin, and Arduino's Gnd is connected to ground pin (GND) [11].

To handle the movement and the sensor input, an Arduino Uno microcontroller is used. The Arduino card is equipped with an Atmega328 processor running on 16 MHz clock frequency. It has 6 analog inputs, 14 pins for digital input and output (among these six allow pulse-width-modulated signals as output). One of the analog inputs are used for monitoring the sensor. The board can communicate at a speed which works well with the chosen servo motors. The microcontroller, here, utilizes Arduino Uno, with ATmega328P microcontroller. This Arduino Uno helps with the commands needed to operate the robot's mobility [12]. A common energy source for the Arduino and ultrasonic distance sensors has been used. Both the microcontrollers and sensors need 5 V to function. The Arduino has an on-board voltage regulator that provides 5 V output when supplied with a 7–12 V input. It is used for driving both the microcontrollers and the sensors.

The body of the robot is made up of seven segments connected serially, which follow the head. Each segment comprises of a micro servo motor that help in the serpentine motion. The servo motors' axes form an angle of 90° between them (perpendicular to each other), allowing them to have motion in all the axes at the same time (movement in three axes). The servos operate at a voltage of 9–12 V. A 9 V power supply is used to supply power to the motors. Every micro servo motor's power and ground pins are linked to the positive and negative terminals of the battery, respectively. The servos' signal pins are linked with the digital pins, namely D3, D4, D5, D6, D7, D8, and D9 on the Arduino board [13]. The connections in the circuit are depicted schematically using Fig. 3.

3   Communication Flow

The communication flow in the robot is shown in Fig. 4. The space in front of the robot is analyzed whether to have an obstacle by the 28015 PING sensor [14]. PWM (pulse-width modulation) signals delivered from the Arduino to the servo's signal line drive the motor. The pulses' width is used to control the positioning of the servo's output shaft, which can then be utilized to adjust the snake robot's direction. The servo will shift to the neutral position (90°) when a signal with a pulse width of
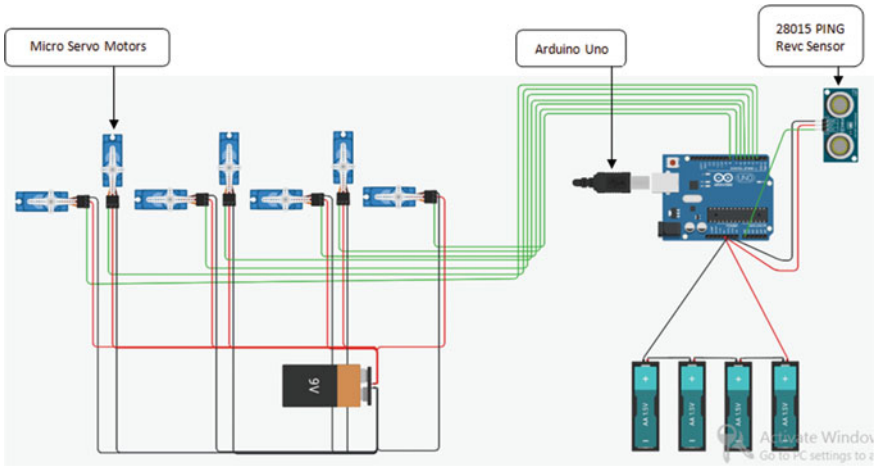
Fig. 3 Schematic of circuit connection

1.5 ms (ms) is sent, i.e., it will face forward to resume the serpentine motion in the same path. The pulse widths for the min (0°) and max (180°) positions are commonly 1 and 2 ms, respectively. These will tell the servos to shift their directions to the left or right, respectively [6].

Here, the distance to the obstacle is checked whether it is less than the tolerable distance (an already assigned value of distance in the code). If the distance is more than the tolerable distance, the sensor sends the signal to Arduino, and as per the commands given to the servo motors by the Arduino, the robot continues its motion in the same direction. If the distance is less than the tolerable distance, the sensor sends the signal to Arduino, and as per the commands given to the servo motors, the Arduino stops the motion of snake robot, and it also commands the head to turn in right and left directions. The sensor again measures the distance of the obstacles in these directions and sends signal to the Arduino. The Arduino accordingly in turn gives the commands to servo motors to continue the motion in the desired direction.

Fig. 4 Communication flow
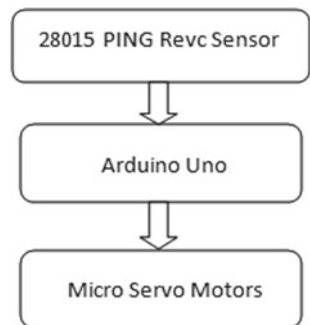
4 Conclusions

The design of a snake robot using the 28015 PING REVC ultrasonic distance sensor and Arduino is proposed in this paper. The distance sensor inspects the space in front of the snake robot and signals the centralized control unit, which in turn accordingly controls the locomotion of SnakeBot. These snake robots will be effective and have a wide range of application. Because of their snake like structure, they can move through tight place such as narrow pipes, tunnels, can dig the ground, and even they can climb hill and trees. Because of their structural advantages, they can even swim under water. With additional technical integrations like GPS systems, cameras, and thermal sensors, the versatility of these robots can be increased. The scope of integrating artificial intelligence in SnakeBot is being researched at NASA. These prospects will help the snake robots become an integral part of the search and rescue team.

References

1. Chirikjian, G.: Theory and applications of hyper-redundant robotic manipulators. Calif. Inst. Technol. (1992)
2. Giralt, G., Gerhard Hirzinger, G.: Robotics Research. The Seventh International Symposium. Springer, London (2012)
3. Katic, D., Vukobratovic, M.: Intelligent Control of Robotic Systems. Springer, Netherlands (2013)
4. Hu, D., Nirody, J., Scott, T., Shelley, M.: The mechanics of slithering locomotion. In: Proceedings of National Academy of Sciences, USA, vol. 106, pp. 10081–10085. (2009)
5. Mariappan, M., R. Arshad, M., Akmeliawati, R.: Control engineering in robotics and industrial automation. In: Malaysian Society for Automatic Control Engineers (MACE) Technical Series 2018, (2021)
6. Matsuoka, Y., Durrant-Whyte, H., Neira, J.: Robotics. MIT Press, Science and Systems VI (2011)
7. Liljebäck, P., Y. Pettersen, K., Stavdahl, Ø., T. Gravdahl, J.: Snake Robot Modelling, Mechatronics and Control. Springer London, (2013)
8. https://www.instructables.com/Snake-Robot-1/Accessed. (2021)
9. https://www.youtube.com/watch?v=LrOM2GABK1g. Accessed (2021)
10. https://www.fierceelectronics.com/sensors/what-ultrasonic-sensor
11. https://www.parallax.com/product/ping-ultrasonic-distance-sensor
12. https://robu.in/what-is-arduino-uno/
13. https://howtomechatronics.com/how-it-works/how-servo-motors-work-how-to-control-servos-using-arduino/
14. Chauhan, R., et al.: Design of Robotic Snake with ESP 32 CAM and Arduino. In: 2021 19th OITS International Conference on Information Technology (OCIT), pp. 6–9. (2021). https://doi.org/10.1109/OCIT53463.2021.00013

Arduino-Based Unmanned Vehicle to Provide Assistance Under Emergency Conditions

V. Pavan Kumar, B. Venkateswara Rao, G. Jagadeesh Harsha, M. D. John Saida, and A. B. V. Mohana Rao

1 Introduction

"Catastrophe", whether it's artificial or inborn, for instance earth tremors, inundation, tornados, multi-storied collapse present a never-ending challenge for the aid team services [1]. So as to tackle with alike disaster effects and damages in a rapid and steady coordinated manner, the accurate information at its best is the much-needed requirement and would be an asset for aiding teams [2]. Considering an incident that occurred in the Vishakhapatnam gas spill around 5 villages are affected because of the lack of appropriate information in time, near the village of Venkata Puram [3]. The UAV gain more popularity, with their flexibility and movability and reasonable price, unmanned aerial vehicle (UAV), well known as drones, remarkably came in to spot light by being use of diverse applications over the past few decades. The development of these UAV regarding various aspects are due to the increase in the number of the users and innovative thoughts due to the necessity and requirements of the modern age scholars, currently biggies like universities, tech companies are researching on UAV according to their requirements.

In 1960s a monocopter was built which is not effective control has excluded from the practical applications. So, dynamics of monocopter not demonstrated deeply [4, 5]. Emphasizing on the thermodynamics properties, monocopter was the first flying machine to be developed [6]. The quadcopter alone is unable to monitor long distances beyond the field of vision. By deploying an artificial eye known as the camera integrated into the drone, it can be monitored for long distances [7]. To establish an emergency communication system for contingencies an end-to-end communication is necessary for the rescue operations, as we are living in the era of

V. Pavan Kumar · B. Venkateswara Rao (✉) · G. Jagadeesh Harsha · M. D. John Saida · A. B. V. Mohana Rao
Department of EEE, V R Siddhartha Engineering College, Kanuru, Andhra Pradesh, India
e-mail: bvrao.eee@gmail.com

rapid development of speed of network, however, previous life savers in the communication sector like the walkie-talkie system and RF communication system are still maestros in scenarios where a remote with reasonable price in short distance communication manner is required [8].

Basically, the communication with victim and controller (Quadcopter operator) of UAV is started with radio frequency & satellite technology, due to the advancements of communication systems, the cellular technology came into the existence for communication [9]. The cellular technology is having wide range of features, but there is some drawbacks like reliability and cyber-threatening issues [10, 11]. There are other communication systems such as Bluetooth, WiFi and ZigBee [12]. In order to make the best approach to rescue services, one of the above technologies called radio frequency with the help of Arduino makes the communication system reliable and more secure. In terms of security, military operations need this type of communication system, which is strong enough to sustain cyber threats because the information is confidential. Nowadays, the communication used by the military is walkie-talkie, which works with frequency converted to voltage signal & vice-versa.

- No requirement of a separate base station for controlling the drone and receiving the information from it as any mobile device can be used to communicate with it.
- It has an altitude range of 1500 m while the voice communication medium has a range of 1 km
- Two-way communication can be established between the victim and the rescue team.
- Very few persons are required to control and monitor the drone, even a single person equipped with a mobile device can act as surveillance unit for the rescue team.
- Relatively cost efficient compared to other drones in the working in which have a similar function.

Research Motivation

The driving force behind this paper development, one of the reasons is COVID-19 pandemic. In the pandemic, everything is closed, in the area most affected by COVID, municipal workers roam around to announce in contagious areas. There was a high potential for an effect among municipal workers. As a result, we need vehicles with no human presence. So, deploying the Unmanned Aerial Vehicle equipped with a microphone and speaker will help the municipal workers to help the victims and protect themselves from being affected. Here, Unmanned Aerial Vehicle equipped with a microphone and speaker will help the operating person to cover a large distance within the time and can know the victim's condition and to make them an appropriate solution.

Table 1 Hardware components used for design of proto type

Hardware	Range	Rating	Quantity
Propellers	–	10 * 4	4
Brushless motor	–	1400 kV	4
Electronic speed controllers	–	30A, 11.7 kV	4
Flight controller	–	–	1
Transmitter and receiver	1500 m	–	1
Battery	10 km	3300 MAH	1
Camera	10 m	–	1
Mic-Speaker	30–50 m (indoor) 800–900 m (outdoor)		1

2 Literature Review

Authors in [4] proposed using a fixed wing UAV that can quickly survey the disaster area. Once people or vehicles have been detected, 7 quadcopters can be sent to these critical spots to gather the real-time information. Authors in [6] highlights the setting up the communication network between victims, survivors and designated rescue team using camera survey in real-time. In addition to the papers mentioned above in this paper a two-way communication using nRF module with Arduino UNO is used for real-time communication between victims and ranger teams, along with that it's also equipped with high definition camera.

3 Hardware Description

The flight controller is brain of the Quadcopter. Flight controller is embedded with receiver, ESCs, Gyroscope, Accelerometer and Communication system. The software is programmed in C language. Hardware components used for design of proto type is presented in Table 1.

4 UAV Aided Communication

The Mechanism of Aerial Vehicle is shown in Fig. 1 [13]. The Fig. 2 demonstration of NRF24L01 is an RF communication module used for long-range communication through interfacing with Arduino. The flight of UAVs will operate under remote control by a human operator, as it can go into each zone and transmit the information with the help of the speaker and the microphone which is able to obtain the status of the victim. The incorporated sensors are able to sense the human's presence in
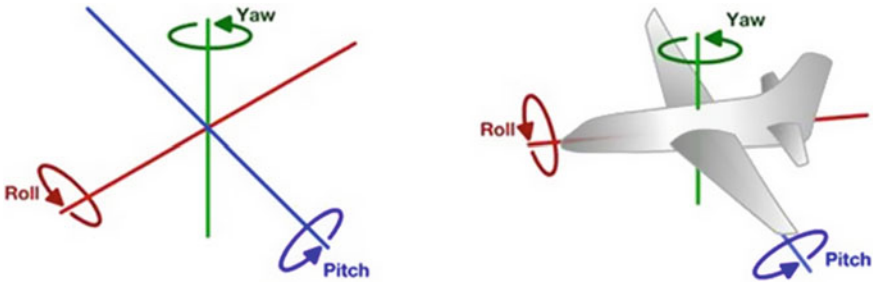
Fig. 1 Mechanism of aerial vehicle
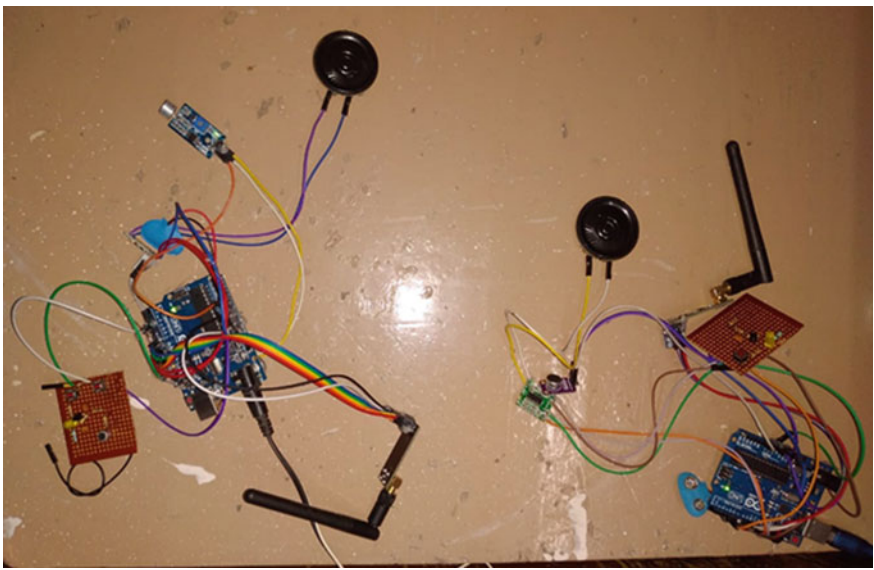
Fig. 2 Walkie-Talkie using nRF module with Arduino

the incident area and it will give the notification to the remote operator about the situation of the incident area with real-time monitoring [14].

5 Methodology

From the Fig. 3, it can be observe that the person's side there consists of a remote set, the throttle which we give in remote sends a signal to the receiver through the transmitter and then it to flight controller. Then based on input the flight controller sends a signal to ESC and based on PWM to motors is sent and speed and direction
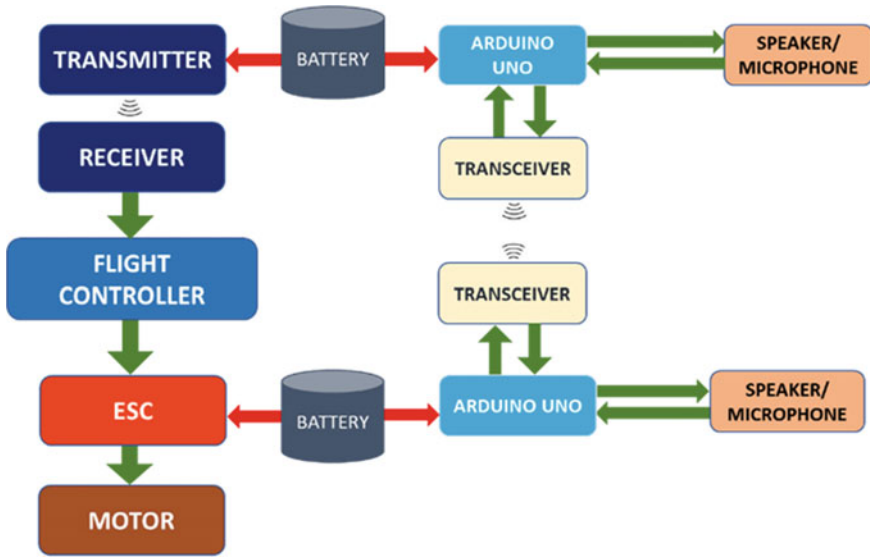
Fig. 3 Block diagram of UAV

controlled accordingly. To maintain altitude and drone to be stable the gyroscope and GPS both combined act as a closed-loop system. On both the drone side and person side there basically consists of a transceiver set for the mic-speaker set. Communication between the victim and the rescue team is maintained through an Arduino based microphone and speaker called as walkie-talkie. The walkie-talkie module is placed in a separate box which is at drone side is operated by a dc motor which is an added advantage of avoiding the noise obtained by propellers. The GPS along with image sensors can be able to sense indoor locations [15].

6 Results and Discussion

The objective of the paper is to identify and communicate with the victim; here the RF based communication using Arduino results in lowering the cost of the equipment. The pipe channels are created for NRF24Lo1 in which one set of equipment is equipped with the drone and another set is with the rescue team operator. As the two Nrf24l01 modules are communicated, the output of sound sensor is observed from one module and Complete Quadcopter under its development phase is shown in Fig. 4. The low-cost RF based communication is established using unmanned aerial vehicle, regarding this project there is also future scope to extend the features of it by proper implementation of GPS hold and Advanced image processing using AI technology and by means of GPS technology there is also a scope to stream the data

Fig. 4 Complete Quadcopter under its development phase

of the particular area all over the world and have an analysis regarding particular area where most probability of disasters are going to happen in a certain period of time.

7 Conclusion

The Arduino board is used here with great flexibility. The GPS module is used here to overcome the problem of hovering. Here GPS is used along with a gyroscope, the GPS equipped in the drone studies the longitude and latitude at that every particular moment to overcome the hovering problem & tries to stay constant while controlling. The camera, microphone & speaker modules assist to communicate. Using the above elements, the UAV is highly useful in rescue operations. Understanding the present calamities Unmanned Aerial Vehicle is assisted in rescue operations.

References

1. Demir, K.A., Cicibaş, H., Arica, N.: Unmanned aerial vehicle domain: areas of research. Defence Sci. J. **65**(4), 319–329 (2015). https://doi.org/10.14429/dsj.65.8631
2. Meissner, A., Luckenbach, T., Risse, T., Kirste, T.: Design challenges for an integrated disaster management communication and information system. 1–2 (2002)
3. Siva, G.: 11 killed in pre- dawn disaster as gas leaks at vizag plant. Article from https://timeso findia.com (2020)

4. Safaee, A., Moussavi, S.Z., Mehrabani, M.S., Menhaj, M.B.: Construction and control of monocopter using MEMS AHRS. In: 2014 11th IEEE International Conference on Control & Automation (ICCA), pp. 219–224. (2014)
5. Das, M.K., Kumar, P.M., Anitha, A.: ORBOT—an efficient & intelligent mono copter. In: ICCS, pp. 168–171. (2017)
6. Khajure, S., Vaibhav Surwade, Vivek Badak Quadcopter design and fabrication. IARJSET **3**(2), 33 (2016)
7. Harveya, M.C., Rowlanda, J.V., Luketinab, K.M.: Drone with thermal infrared camera provides high resolution georeferenced imagery of the Waikite geothermal area, New Zealand. J. Volcanol. Geoth. Res. **325**, 61–69 (2016)
8. Sharma, A., Vanjani, P., Paliwal, N., Basnayaka, C.M.W., Jayakody, D.N.K., Wang, H.-H., Muthuchidambaranathan, P.: Communication and networking technologies for UAVs: a survey. J. Netw. Comput. Appl. **168** (2020)
9. Tunaa, G., Nefzib, B. Contec, G: Unmanned aerial vehicle-aided communications system for disaster recovery. **41**, 27–36 (2014)
10. Javaid, A.Y., Sun, W., Devabhaktuni, V.K., Alam, M.: Cyber security threat analysis and modeling of an unmanned aerial vehicle system. In: IEEE (2012). https://doi.org/10.1109/THS.2012.6459914
11. Wzorek, M., David, L., Doherty, P.: GSM technology as a communication media for an autonomous unmanned aerial vehicle. In: 21th Bristol UAV Systems Conference, pp. 1–15. (2006)
12. Shet, K., Shilamkar, N., Kamble, P., Choudhary, H., Vengurlekar, P.: Network security enabled Arduino devices for military communication. **13**(3), 103–109 (2020)
13. F13: Quadcopter—embedded systems learning academy
14. Manoj, C.H., SaiTeja, N., Kumar, R.A., Pemeena Priyadarsini, M.J., Murugesan, K., Inabathini, S.R.: Unmanned aerial vehicle based bomb detection. 2385–2389 (2016)
15. Murphy, S.O., Sreenan, C., Brown, K.N.: Autonomous unmanned aerial vehicle for search and rescue using software defined radio. IEEE (2019)

Lifecycle Assessment of Handicrafts Products: The Case Study of Bamboo and Aluminium Lamps

Trisha Bordoloi and Dipanka Boruah

1 Introduction

The life cycle assessment is a systematic method of evaluating the environmental aspects of a product's life cycle, from raw material extraction to disposal or recycling [1]. It is also known as 'cradle to grave' cycle. It helps in accounting and supporting environmental decision-making and helps in managing environmental risks. The assessment cycle includes five different stages—material extraction, manufacturing, packaging, transportation, use and end of life (EoL) [2]. Therefore, LCA is used to understand a product and how environmentally friendly it is and evaluate the environmental burdens. An LCA comprises four components, i.e. (a) goal and scope definition, (b) generation of life cycle inventory, (c) inventory analysis and (d) interpretation [3]. This study focusses on the life cycle assessment of daily used home products such as aluminium- and bamboo-made lamps and evaluates the sustainability from the material extraction to end of life. The study's boundaries are inclusion of raw material extraction, processing, manufacturing, assembling, transportation, usage phase and end of life based on the life cycle. The study intends to assess two different lifestyle products which are made of bamboo and aluminium. Three key questions are investigated in the study, i.e. (a) how does the environmental impact contributes from the different life cycle phases of lamps? (b) What can be learned from comparing and contrasting the issue on environmental impacts between aluminium and bamboo lamps? (c) How to identify the impact distribution of the different stages and end of life?

T. Bordoloi (✉)
Department of Design, Indian Institute of Technology, Guwahati, Assam 781039, India
e-mail: t.bordoloi@iitg.ac.in

D. Boruah
Sustainable Materials Lab, National Institute of Design, Jorhat, Assam 785014, India
e-mail: dipanka@nidj.ac.in

1.1   Need of LCA in Handicrafts Sector

The handicraft products are widely used nowadays but the impact on the environment is a growing concern. It is an important contributor to the Indian economy because the handicraft sector is one of the largest environment providers and accounts for a significant percent of economy [4]. The LCA identifies environmental hotspots in handicraft products and materials. It is important to know the benefits of a sustainable product and renewable natural resources involved in the daily use products at home. Bamboo and aluminium lamps have been used in this study of LCA because these products are trending in the market and people are using or choosing them without knowing their impact on the environment or how much it is environment friendly. This LCA study will give the users a rough idea of the steps involved in the daily used products and help them to choose the products wisely without harming the environment. LCA also evaluates the environmental impact of a handicraft product over the course of its entire life cycle. It offers a standard against which improvements can be measured. However, LCA plays an important role when a handicraft product's environmental footprint is essential to its commercialisation in future with defining cost structure.

1.2   Environmental Sustainability and LCA

For several decades, the environmental awareness of India has quickly been increasing. A new phrase has emerged as a result of a shift in attitude towards the environment [5]. Author Zbicinski defined in his book "Product design and life cycle assessment" that LCA is a method for assessing the technical systems, analysing and determining the environmental elements and potential impact of a product.

2   Methodology

The study intends to use LCA software to assess the sustainability of two different wall-mounted home appliances, such as aluminium- and bamboo-made lamps, that are manufactured, used, disposed and recycled in different states of India. Figures 1 and 2. show the life cycle system boundaries of the two lamps studied in this study. The study's limits are primarily divided into six phases based on the life cycle thinking: (a) raw material extraction, (b) raw material processing, (c) manufacturing of other lamp parts, (d) assembly, (e) usage phase and (f) end of life. In Figs. 1 and 2, transports are represented by arrows. The raw material extraction and processing stages only apply to the lamp's exterior covering or the frame; the rest of the lamp's components, such as the hanging hook, glass panel, nuts and bolts are divided into 'other elements

of the lamp'. Bamboo cultivation harvest and treatment are part of the raw material extraction process for bamboo-made lamp frames.

Functional Unit (FU)

FU = to measure the environmental impact based on lamp per year of usage. Assumption of life span (average): bamboo—5 years; aluminium—15 years.
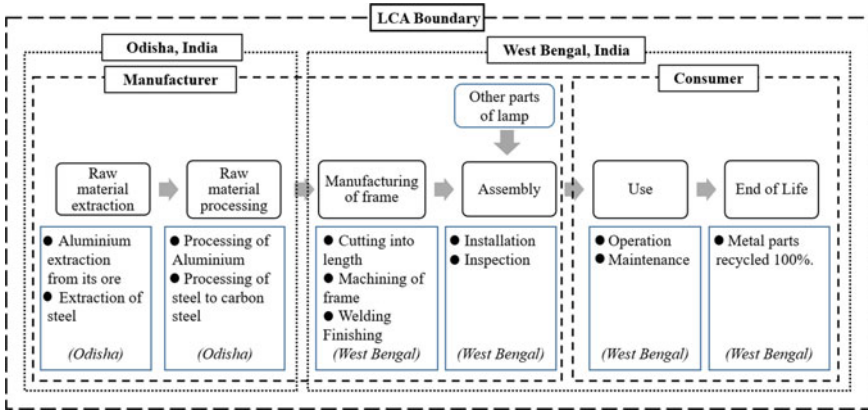
Fig. 1 System boundaries of the aluminium-made decorative lamp [2]
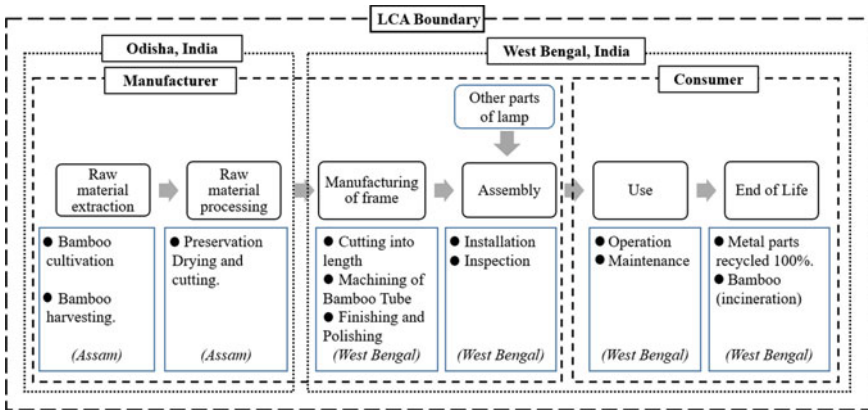
Fig. 2 System boundaries of the bamboo-made decorative lamp [2]

3 Aluminium Decorative Lamp

This lamp is made of aluminium metal. Aluminium is the third most abundant metallic element in the earth's crust, accounting for 8% of the planet's soil and rocks (oxygen and silicon account for 47% and 28%, respectively) [6]. Aluminium is only found in chemical compounds with other elements like sulphur, silicon and oxygen in nature. Only aluminium oxide ore can be cheaply manufactured as pure, metallic aluminium. The raw material for the aluminium-made decorative lamp has been extracted from Odisha as it is one of the highest producers of Bauxite in India. Bauxite is an important ore which is used for making of aluminium metal.

Part (A): Full frame. The whole frame of the aluminium-made decorative lamp is moulded and structured according to the design specification as shown in Fig. 3. The weight of the frame is between 1 and 1.3 kg. (approx.). Colour is customised and upgraded accordingly. Metallic aluminium has a number of qualities that make it helpful in a variety of situations. It is nontoxic, lightweight, robust and nonmagnetic. It reflects heat and light and conducts heat and electricity. It is tough but malleable, and it retains its toughness properties under extreme cold without turning brittle.

Surface of aluminium forms an impenetrable corrosion barrier due to its quick oxidisations. Furthermore, aluminium can be recycled simply and cost-effectively into new items.

Part (B): Hanging Hook. The part is called hanging hook which is made of carbon steel. Because of its versatility and low manufacturing costs, this metal has become one of the most preferred metals for a variety of common occupations and uses, ranging from agriculture to the heavy machinery industry. Low-carbon uses can be found in everyday life all across the world. Hook is manufactured and given desired shape needed. Usually, it is of the shape of S. The durability and ability to withstand

Fig. 3 Example of aluminium-made decorative lamp for life cycle assessment [7]

weight are effectively achieved by a carbon steel hook. Approximate weight of the hook would be 20–30 g. Colour and shape can be customised accordingly.

Part (C): Nut and Bolt. It is made of steel. Steel is generally made in one of the two ways: in a Blast Furnace or in an electric Arc Furnace. The Blast Furnace is the initial step in turning iron oxides into steel. Pig iron is made in a Blast Furnace with coke, iron ore and limestone. Coal is an important component in the production of coke. Approximate weight of the 25 mm nut and bolt would be 4–5 g. It is available in many sizes according to use. Here, aluminium is extracted through various techniques from its ore and sent to workshop for various work. At last, the frame is manufactured and polished with minute details and sent for further work. Here, all part is aluminium, and thus, it can be used for a long time without any difference and thus can be recycled even after. The various extraction of aluminium from its Bauxite ore happens in Odisha, Kerala, West Bengal and different parts of India. So, the raw material is extracted from Odisha and the assembling and final product use are done in West Bengal.

Part (D): Glass Panel. The glass panel is made of glass/tiffany glass/paper/plastic/parchment/fabric. Tiffany glass can be made in a number of ways. Streaky or striated glass can be formed by mixing two or more colours of molten glass together. Confetti glass is formed by scattering coloured glass into heated glass or pouring molten glass on top of coloured glass pieces. Parchment is manufactured by soaking an animal skin in lime generally from goat, sheep or calf, stretching it on a frame, scraping away extra tissue and allowing it to fry under strain. The skin's collagen is reorganised, but not chemically altered, during this procedure.

Approximate weight of the glass panel would be 300–400 g. Size and dimensions can be customised according to shape and requirement. Different parts of this lamp are made of aluminium and thus can be recycled after many years of use. The hanging hook (part B) is used for holding the structure, and it is made from carbon steel and therefore used for withstanding the weight of the cage where the bulb stays. Carbon steel hook is also recyclable. The glass panel (part D) is made from silicon, etc., and thus, it can be recycled after years of use. The 'thread-rolling' method is utilised to make the vast majority of screws, and it is also used in the mass-production phase. The first step is 'cold-heading' which involved feeding a wire through a pre-straightening equipment. The glass panel are manufactured and transported from different places and vendors of India. These nuts and bolts (part B) are also recycling items.

4 Bamboo Decorative Lamp

Bamboo has been considered to be transported from Jorhat, Assam. Varieties of bamboo are found in this north-eastern place of Assam for which the treatment process becomes easier. Moreover, handcrafted items made from bamboo are sold and exported from Jorhat, Assam. The following processes are involved in making
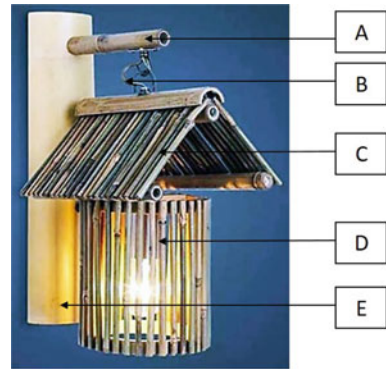
bamboo-handcrafted lamp, i.e. (a) cutting bamboo, (b) separating bamboo parts, (c) skin removal, (d) collection and relocation to transportation sites, (e) transportation of bamboo materials to West Bengal, (f) splitting bamboo and (g) polishing, drying, finishing, etc. [8]. This lamp is preferable for home and restaurants. Description of various parts is shown in Fig. 4. All bamboo parts are chemically treated with borax, boric and water solutions f($NA_2B_4O_2.10H_2O$), as it is the most popular preservation method, especially for indoor use. It protects the bamboo from fungi, bacteria and other insects and the process is called vacuum pressure impregnation treatment for bamboo [9]. There are various sizes of bamboo used in the wall-mounted lamp. Bamboo hollow sticks (pole) (part A) are used in the top where whole lamp structure is mounted. A node was kept on the bamboo pole for the strengthening of bamboo pole which holds the lamp structure. The electricity wire connection is gone through the part A and part B.

Part A: Full Frame. 35-mm-diameter bamboo hollow pole is fixed in the top of the lamp, and it is approximately 100–150 g.

Part B: Hanging Hook. Existing metal plate and metal hook are fixed on the top of the bamboo pole. The existing metal hook looks like a spring, and it is approximately 4–5 g. Metal hook and metal suspended spring procured from existing ceiling lamp. Varnishing (maintenance) is required every 2 years. The raw materials and the processing (treatment) have been extracted from Assam, and the assembling and final products are used in West Bengal.

Part C: Panel. Bamboo small poles (locally called as Lekechi in Assamese) are placed as inclined as bamboo house pitch roofing, and it is approximately 10–20 g. About 200-mm length small bamboo hollow pole is arranged along with circular-shaped bamboo strips as vertical fins and fixed with small bamboo hollow sticks with glue for low weight of the pendent bamboo frame, and the weight of cage looking is approximately 100–120 g (part D).

Part E: Nut and Bolts. The nuts and bolts used is 250 mm long and are made from Balcooa Bamboo (Bhaluka bamboo in Assamese), where the whole lamp structure is

fixed along with pendent parts of the lamp, and the weight is approximately 300–350 g.

5 Life Cycle Assessment Results

The analysis in the IdematLightLCA app includes six phases: raw material extraction, raw materials processing, manufacturing of other parts of the lamp, assembly, use phase and end of life. Table 1 shows the material comparison of both the materials. It is necessary to compare the material of the products before the assessment process in the IdematLightLCA application. Similarly, Table 2 includes the different manufacturing composition of both aluminium- and bamboo-made lamps. Table 3 and Table 4 describe the various factors of material uses, energy input and transportation for both decorative lamps in the whole assessment process. The transportation includes the distance of raw material extraction, processing, production, assembly, use phase and end of life.

Table 1 Material comparison of both lamps (aluminium and bamboo)

Item	Bamboo lamp	Aluminium lamp
Full frame	Different types of bamboo	Aluminium
Hanging hook	Steel/carbon steel/brass	Carbon steel
Panel	Bamboo panel	Glass/tiffany/plastic Panel/parchment fabric, etc
Nut and bolt	Steel	Steel

Table 2 Manufacturing composition of both lamps (aluminium and bamboo)

Item	Bamboo lamp	Aluminium lamp
Full frame	Naturally grown bamboo is crafted using traditional technique	Parts of frame are casted, welded and painted
Hanging hook	Casted from steel and shaped	Casted through carbon steel and shaped
Panel	Traditional bamboo is crafted	Panel is crafted through melting, refining, etc
	Cold forging, threading, heat treatment, surface treatment, etc	Cold forging, threading, heat treatment, surface treatment, etc.
Nut and bolt	Naturally grown bamboo is crafted using traditional technique	Parts of frame are casted, welded and painted

Table 3 Materials and energy input of both decorative lamps (aluminium and bamboo)

Item	Aluminium lamp	Bamboo decorative lamp	Unit
Full frame	1.2	0.65	Kg
Hanging hook	20	5	Grams
Panel	300	120	Grams
Nuts	25	25	Grams
Bolts	4	4	Grams
Varnishing	–	0.5	Litre

Table 4 Transportation of two decorative lamps

Transportation step	Site	Transportation type	Distance (kms.)
Raw material extraction/processing for the aluminium frame lamp			
Export alumina	Odisha	28-ton truck (one way)	30
For primary and secondary aluminium production	Odisha–West Bengal		463.6
Raw material extraction/processing for the bamboo frame lamp			
Send bamboo stems from plantation area to processing plants	Jorhat–Guwahati, Assam	5-ton truck (empty truck load for return)	300
Export the stems	Guwahati, Assam–West Bengal	28-ton truck (one way)	942.1
Frame production and assembly			
Bamboo frame/aluminium frame for production/assembly	West Bengal region	7.5-ton truck (one way)	20
Use phase			
Send decorative lamps to retailers	West Bengal region	7.5-ton truck (one way)	30
End of life			
Incineration and metal collection	West Bengal region	7.5-ton truck (one way)	15

6 Limitations in Calculating LCA Data from IdematLightLCA

- The raw materials for bamboo lamp are being taken from Jorhat and Assam and being used in West Bengal; however, in the IdematLightLCA app analysis, we have considered the bamboo to be imported from China as it has the closest resemblance to the bamboo available in Jorhat.

- The raw material used for aluminium lamp is supposed to be extracted and then used for making the frame but for the IdematLightLCA app. analysis, the data for recycled aluminium has been used as it has the closest resemblance to the material.
- Similar type of fluorescent bulb is used with both lamps.
- The bamboo lamp undergoes certain sawing and grinding.

7   Discussion

LCA is a method of assessing the environmental implications of a product or process over its entire life cycle. Material extraction, processing, production, distribution, usage, disposal and recycling are all parts of the life cycle. It aids in the selection and comparison of two environmentally friendly items [11]. The study aims to assess the life cycle of an aluminium- and bamboo-made decorative lamp. To examine the life cycle assessment, the raw materials for the aluminium lamp are considered to be extracted from Odisha. In addition, the manufacturing, assembling, distribution, and use of the aluminium lamp are considered and assumed to be in West Bengal, India. The raw materials of bamboo-made lamp have been procured from Jorhat those used in West Bengal. In this study, IdematLightLCA intended in assessing the life cycle of both products, i.e. aluminium- and bamboo-made decorative lamps. The cost analysis has not been carried out in this study as the application has not updated all the places of bamboo availability. Only China has been shown in the IdematLightweight LCA. The places cannot be edited in the application, and if we consider China for the bamboo extraction analysis instead of Jorhat, it will show a false cost analysis. The carbon footprint (kg CO_2e) for the aluminium lamp in landfills resulted in 19.21 kg while the bamboo-madess lamp is 31.09 kg. It identifies that bamboo-made lamp has more impact on the environment than aluminium lamp. However, due to the limitations in the IdematLightLCA application in the raw material extraction, the result cannot be considered accurate. In this regard, we cannot conclude that the lowest environmental impact product is aluminium decorative lamp.

8   Conclusion

In this practical case study of an aluminium-made decorative lamp and a bamboo-made decorative lamp, LCA is one of the best tools for assessing the sustainability in manufacturing process. Except for ionizing and acidification, the results of the life cycle evaluation show that aluminium lamps have more environmental impacts as compared to bamboo lamps. Framed structure of bamboo-made lamp was manufactured by using of process for treatment and preservation of raw materials. Every analysis is done on the basis of landfill LCA assessment. In view of this, from the transportation side, the distance covered by the raw materials to process and then

assembling have the biggest factor. Carbon footprint for aluminium lamp came as 19.21 kg., while for bamboo lamp 31.09 kg. in landfill. Therefore, bamboo-made lamp has more impact to environment when compared to aluminium lamp. Life of bamboo-made lamp is usually 5–6 years (approx.). Life of an aluminium lamp is usually 15–17 years (approx.). Certain polishing and varnishing between intervals highlight their look but not much affect their life.

References

1. Khasreen, M.-M., Banfill, P.F.G., Menzies, G.F.: Life-cycle assessment and the environmental impact of buildings: a review. Sustainability **1**(3), 674–770 (2009). https://doi.org/10.3390/su1030674
2. Chang, Y.-J., Schau, E., Finkbeiner, M.: Application of life cycle sustainability assessment to the bamboo and aluminum bicycle in surveying social risks of developing countries. 953 (2019). https://doi.org/10.3390/wsf2-00953
3. Phuong, T.V., Xuan, N.V.: INBAR working paper technical paper life cycle assessment for key bamboo products in Viet Nam. (2020)
4. IBEF: Indian Handicrafts: Handicrafts Exports, Industry & Manufacturer in India. (2021). https://www.ibef.org/exports/handicrafts-industry-india.aspx. Accessed 29 Nov 2021
5. Ireneusz, Z.: Product design and life cycle assessment. Baltic Univ, Press (2006)
6. MadeHow. How aluminum is made—material, manufacture, making, used, processing, aluminium, composition, product. (2021). http://www.madehow.com/Volume-5/Aluminum.html. Accessed 29 Nov 2021
7. Myntra, Buy Homesake bronze toned textured classic country wall lamp—wall lamps for Unisex 13762312- Myntra, (2021). https://www.myntra.com/wall-lamps/homesake/homesake-bronze-toned-textured-classic-country-wall-lamp/13762312/buy. Accessed 29 Nov 2021
8. Lught, V.P., Vogtlander, J.G.: International network for Bamboo and Rattan INBAR, the International Network for Bamboo and. (2015)
9. Boruah, D.: A Human Centered Approach to Redesign Prefab and Modular Bamboo Houses. In: (HWWE 2021)—19th International Conference on Humanizing Work and Work Environment. IIT Guwahati, Spinger (2021)
10. Exporters India: available in many colors Bamboo Lamps, 5285670 2020. (2021)
11. FibreNet: life cycle assessment: benefits and limitations, (2018). http://fibrenet.eu/index.php?id=blog-post-eleven. Accessed 29 Nov 2021
12. Inbar. Bamboo & Rattan for inclusive and green development—INBAR 2021. https://www.inbar.int/. Accessed 29 Nov 29 2021

Concept Design of Amphibious Military Patrolling Vehicle

Debashis Majumder, Rohit Kumar, and Kushagra Dhall

1 Introduction

The brief of the project is to introduce an Amphibious Military Patrolling Vehicle (AMPV). The advancement in the defense sector of our nation is a high priority and our government always takes some solid steps to strengthen our force. Some major border areas of INDIA are partially over water. The military has the means which allow them to patrol in water but the means are now very old as compared to the advancement in the sector. This AMPV will fill in the need gap between the new entries in the defense sector. The major thinking behind this vehicle is to make it run efficiently over water and for that a whole new technology is needed. This new vehicle is not simply a boat with wheels. It is designed by taking care of the surroundings and the consumer of the vehicle. For patrolling on water, the troops get on to a vehicle that takes them to the shore and then they split and move toward the base station with the help of a boat that does not has any protection or supplies system. The AMPV will allow the troops to travel over land and water in a single go with a protective shelter and some supplies, also allowing them to go on longer patrolling.

1.1 Scenario Research

India has a perennial problem of border infiltration. India is surrounded by Bangladesh, Myanmar, Pakistan, Nepal, China, and Bhutan. Being the 7th largest

D. Majumder (✉) · R. Kumar · K. Dhall
School of Design (SoD), University of Petroleum and Energy Studies (UPES), Bidholi, Dehradun, Uttarakhand 248007, India
e-mail: mejda1166@gmail.com

country in area and 2nd most populous country and democratic country it has its reason to be strict on infiltration. The infiltration not only happens through the land border by from the seaside also. India is surrounded by sea on all three sides. In the south, there are vulnerabilities from Srilanka and Maldives also. The border where water is there is difficult to protect. A border over a riverine or sea or even lake is called a fragile border. India has a very high rate of unauthorized infiltration from Bangladesh and Pakistan. There are 4095 km of border with Bangladesh surrounded by five Indian states namely West Bengal, Assam, Meghalaya, Mizoram, and Tripura. India's defense and financial stability is very important to stop unauthorized infiltration in India [1, 2].

1.1.1 India-Pakistan Border

This is the second-largest border in India with a neighboring state. This border is 3323 km long, starting at Gujarat and going up to Jammu & Kashmir. This is one of the most dangerous borders in the world [3]. The Line of Control which demarcates India and Pakistan occupied Kashmir is also falling on this border. The infiltration of militants and Jihadis from Pakistan is also possible due to this fragile border.

There are different Integrated Check posts on this border like:

- Attari and Wagah, are the most famous and prominent border crossings.
- Munabao, a village in Barmer District, Rajasthan.
- Hussainiwala Border, Punjab.
- Fazilka Border, Okara District.

In spite of all efforts, the unauthorized infiltration is maximum through this border and is responsible for all miscreants in India.

The India-Pakistan border also has some water bodies which run along the border. Jhelum River is one of them and forms the major part of the border. The river has a minimum of 10 entry and exit points between both nations. Most part of the river border is between hills but requires a high watch. There are other rivers also and two lakes that are also on the border area on the border like Ravi, Chenab, Sutlej, Tawi, Kunhar, and Indus. Apart from the river there, one is Shakoor Lake, and the other is Rann of Kutch Lake, both are in Gujarat, India. These water bodies either enter the border or make a major part of the border. The rivers which enter Pakistan from the North are mostly running in valleys. The major role is played by the Jhelum River and Ravi River, as both were the part of the Punjab part that got into Pakistan after the partition [3] (Fig. 1).

Fig. 1 Border rivers (taken from Google Earth)

Fig. 2 Border river (taken from Google Earth)

1.1.2 India-Bangladesh Border

It is an international border that demarcates the division between the Indian and Bangladeshi Provinces. Being the fifth-longest land border of the world, it passes through Assam, Tripura, Mizoram, Meghalaya, and West Bengal. The total length of the border is 4156 km the maximum part lies in West Bengal, India. The major threat on this commute is animal trafficking, drugs, weapons dealing, and border trespassing. This international border also has some water bodies which run all along the borderline. Gomati River, Tripura is one of the rivers which flows near the border. The Ganga River enters Bangladesh as the Padma River. Teesta River which forms the border of Sikkim and West Bengal and the Brahmaputra River enters Bangladesh from Assam, India. The major role is played by the Ichhamati River which touches the borderline from near Hasnabad, West Bengal, and keeps on flowing all along the border till the tip of Sundarban Forest and finally finishes off in the Bay of Bengal. 40% parts of the river are on the Indian side and the remaining 60% is on the Bangladesh side. The transport between both the countries is done by boats and big ships [4].

The longer part flows from the Mathabhanga River, a tributary of the Padma, Bangladesh and after flowing for 208 km it joins the Kalindi River near Hasnabad in North 24 Parganas and Debhata in Satkhira District, West Bengal, India. The Indians and the Bangladeshi people use this river as their source of water for irrigation, commute, and also for Goddess Durga immersion. On the contrary, some folks use the flow of river for domestic animal trafficking. They used to tie the cows around a bamboo hold and then leave them in the river to reach the other point at night time. The images are the screen snips, taken from the Google Earth Studio, showing the Ichhamati River Scenario, on and around the India-Bangladesh Border [4] (Fig. 2).

1.1.3 Border Security

The above-mentioned borders are guarded by the Border Security Force (BSF) of India. Both the International Borders are on high security and the troops are always active and ready to take crucial steps at the time of any miss happening. The water part of the international border is taken care with the help of Border Outposts, also known as BOP in short. Apart from the BOP, the troops use speedboats for patrolling in the water. They use the speedboat for patrolling inside the Sundarbans forests and for the security checks of the boats or big ships coming in and out of the nation.

1.1.4   Border Outpost (BOP)

It is a kind of floating control station. It looks like it's a normal building but keeps on floating at low speed. The hull of the BOP is very flat as compared to a regular ship or boat which does not allow it to move very fast in water. The normal speed of a BOP is 14 km/hr. It has the capacity of holding a complete troop of 40 crew members and also has shelter for them. It's equipped with kitchen; AC rooms to keep the moisture level balance and surprisingly has the capacity of holding 15 tonnes of fuel which is used for all the purposes of the BOP. It stays almost at a distance of 50 km from the shore of the river and goes for re-fueling near Hasnabad, West Bengal, India. After every 15 days, the troops get (Figs. 3 and 4).

Fig. 3 Border outpost (BOP)

Fig. 4 Speedboat

2 Changes in the Technology of Amphibious Vehicles

When the early concepts were not there, boat was used to be a boat and a car was simply a car. Both having different applications and different surroundings. But the early inventions and concepts of amphibious vehicles were just a mere attachment of wheel to the hull of a boat. Not really efficient but it was an invention and after those new ideas came up which had different working technologies. After many ideas, an idea of putting a track in place of wheels to a boat from New Jersey came and it showed some new features like that vehicle did not require a flat solid ground to start propelling in water. There was no extra equipment added to it for water propulsion. The whole vehicle was propelled by the use of tracks only both in water and on land. This technology, later on, was used in making amphibious defense vehicles, especially the battle tanks. Their solid ballistic proof bottom was made in a shape of a flat hull and the tracks helped it to float and move in water. But being such heavy steel installed machinery, it was not able to make the movement very fast on water, but still solving the purpose.

Nowadays, there is a huge change in the propulsion of amphibious vehicles. Today it is achieved by making lightweight and more efficiently designed hulls and jet propulsion systems in order to achieve a higher number on the speedometer while moving on water. These technologies are not only limited to sports or personal use vehicles only. The amphibious defense vehicles which were made in the mid-1950s were also using the jet propulsion systems attached to a heavy-duty engine. In fact today also the amphibious defense vehicles use the track system to move in water or the jet propulsion system coupled with a heavy-duty turbocharged engine but the issue is speed. They are still not very agile and active on the water. Reasons being, the materials used in the making of defense vehicle is the same as that of the past, ballistic steel. There have been advancements in engines, and jet propulsions but the material used is extremely heavy for any vehicle to move fast on the water.

3 Amphibious Military Patrolling Vehicle

Patrolling vehicles are used by the Indian military as a part of their daily patrol or delivery of supplies from one place to other. Currently military uses the vehicles which are manufactured by some Indian manufacturers like Maruti Gypsi, Tata Safari, Mahindra Scorpio for common land, and some heavy-duty like Renault Sherpa, Mahindra Mine Protected Vehicle, Tata Mine Protected Vehicle, Mahindra Marksman for some heavy operation or anti-terrorist operations. All have an armor range from light to heavy-duty depending on the use. Many of the vehicles are made for an amphibious purpose, like Tata Kestrel, it is a medium armored patrolling amphibious vehicle, which can accommodate up to 12 personnel and is equipped with small shooting windows and a machine gun at the top of the vehicle. It uses a twin jet

propulsion system to move over water and can travel at a speed of 10 km/h which is not at all a great speed but still appreciable because of its weight of 26 tones [5].

4 Design Constraints of Defense Vehicles

The major principle of a defense vehicle is to be of maximum functionality. If there is no function then there is no use of that vehicle on defense land. From the very starting, the defense vehicles have a very boxy kind of appeal and construction with hardened edges and flat surfaces welded at an angle. The materials used are also extremely heavy and not that easy to bend so that curved surfaces can be achieved. Also, if a defense vehicle will have a curved surface just to make it beautiful then it is of zero use in real and will burden the manufacturer to bend that heavy steel to that curve surface. The hinges, bolts, and window frames are all exposed because of the added protection [6].

There are visually appealing armored vehicles that are being used by the nation's high command authorities but having them on the defense land or on the battlefield is not at all valid. The defense vehicle, especially patrolling one, have to carry supplies, and personnel from one point to another. It should be armored but also purpose-solving. An armored Cadillac or an armored Mercedes will not solve the purpose. Moreover, their powerful engines can be used to provide power to the defense vehicles but not their beautiful designs. Alone or in a joint venture, each and every company has some part of it in the defense sector, providing the necessary equipment and raw materials. A regular car with some initial level of armoring can be used for a military purpose. It can be used as a normal city patrol vehicle but if it has to go on the battlefield or on border patrol then it should have some necessary armoring in order to handle the at- tacks from the other side and to tackle the unusual terrain situations, keeping the armed force safe and secure [7].

5 Advancements in Design of Defense Vehicles

The defense vehicle market is ever emerging and the need for advancements will never stop in the future. Today, if we compare the visuals of defense vehicles from the past then it is clear that there are changes in the treatment of surfaces, they are flat but the way they interact with other surfaces is different. The turrets of the tanks are now more edgy and stylized in a minimal fashion. The body structure is the same rugged but the technology and the engines are also updated now. More power means more output on the battlefield. The design of the vehicle is restricted because of the application and the material used in making the vehicles [8].

The advancements can be introduced in the design of a defense vehicle, whether an assault vehicle or patrolling by using minimal curved surfaces, and that can be achieved by the use of new materials which are lightweight and strong than regular

steel. For example, The metal foam which is developed by the researchers of Rice University and has the capability of shattering the armor-piercing bullets on impact. Polycarbonate is a really strong plastic and at a certain thickness is impervious to bullets. So, if the thick ballistic steel is completely or partially replaced by these advanced lightweight materials, the curved surface can be achieved. This doesn't mean making the whole vehicle visually impressive because a curved surface also eats volume and makes the accessible area less as compared to the straight ones [9].

The newly designed vehicles can be modular, which means if it gets damaged from one part then there should be the modes of replacing that part on our own. The working technology for an amphibious vehicle is updating over time but it is using the same old method of propelling. Also, the interior of a defense vehicle should be easily accessible to the troop in every condition, so that when a situation comes the troop can take the support of the vehicle for rescue operation or as a safe place. The inner comfort also needs to be good in order for troops to relax and comfortable travel while on longer patrol and on unusual terrains [10].

6 Design Concept—Amphibious Military Patrolling Vehicle

6.1 Brief

To introduce a new kind of amphibious patrolling vehicle that will be used for border patrol where there is a water body on or near the international border of the nation. The vehicle will have new and advanced armor capabilities, a new working technique that will help to run the vehicle on both land as well as water and will also tackle the situation of the muddy, swampy, and other unusual terrains.

6.2 Scenario

The international land borders of India which are connected to Pakistan and Bangladesh have a major part of water near or along or on the borderline between the two nations. Currently, the border patrol on both ends is done by speedboats which can accommodate only 4–6 soldiers and does not have any protection and are unable to take the troop on longer patrols.

6.3 Features

- Concept vehicle can run on different types of land terrain and water if required.

- The vehicle can be used by Indian military for border protection where border is on watery area.
- Can accommodate four personnel and one person for operating with ample space for supplies to go on long patrolling.

6.4 Design Concept

The design concept is generated from a mood board which is made to give a particular attribute to visual aesthetics. Initially, the function and environment are analyzed and a visual metaphor from 'tortoise' is taken as it is amphibian in nature and it has a protective shell for self-protection as shown in Figs. 5 and 6.

Here the interior is worked out for four soldiers and the luggage space for belongings [11]. The side of the vehicle is converted to V shape as it is a requirement for the bullet protection. The grid structure and the firing ports are arranged in such a

Fig. 5 Mood board
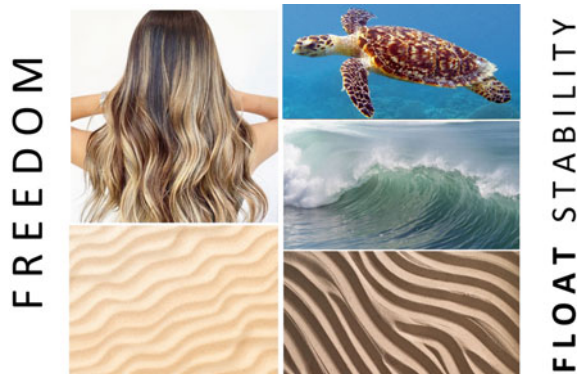
Fig. 6 Initial concept sketch from tortoise
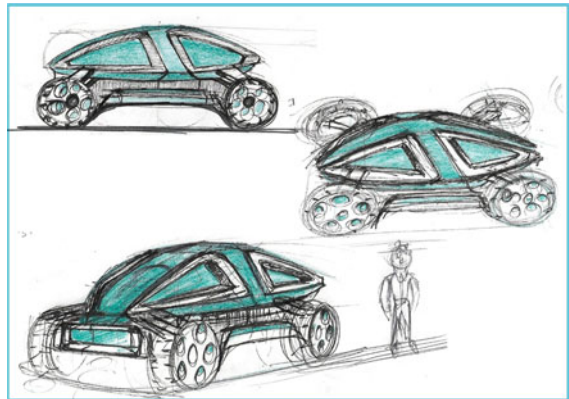
Fig. 7 AMPV concept with functionality

Fig. 8 Rear door concept
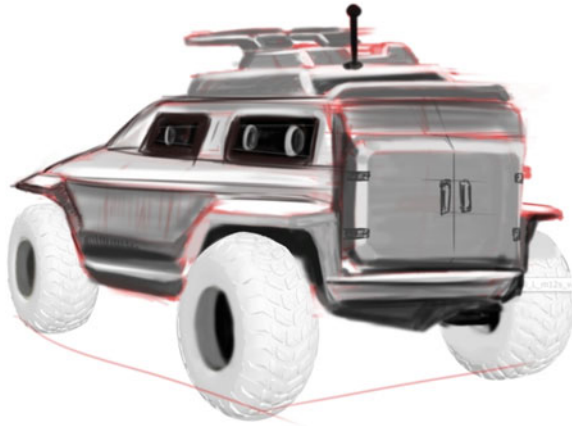
way to enhance the vehicle's aesthetics and styling. The more refined sketches are worked out from the concept sketch as shown in Figs. 6, 7 and 8.

In this figure there are two seats in the operator's cabin, the first one is of the operator and the other three are for the other soldiers. These two seats are placed here because if the operator is busy in tackling the vehicle through any situation, then there should be someone to give cover to him/her. The rear passenger cabin seating layout is in such a way that seats can be folded and top roof can be opened for firing at standing position. The soldiers can egress from rear door also. This kind of layout makes the interior of the vehicle more modular and easily accessible [12].

7 Exterior Development

The exterior development is done using CAD software. Here the focus is to design the exterior in such a way that it is a mix of form and function. The initial form

Fig. 9 Final view of AMPV

Fig. 10 Side view of AMPV

blends well with the required function. The material and finish are to give it a special purpose vehicle that has got to do with military operation and to give an amphibious character.

The digital cad model is made to show the finish and aesthetics involved in this concept as shown in Figs. 9 and 10.

8 Interior Development

The interior is also designed using a theme and mood board. The interior is designed with a theme of order and rugged features with maximum utilization of space. The interior is also designed using a CAD software. The interior aesthetics are shown in Figs. 11 and 12.

It is designed in a clean and simple fashion, making sure to achieve the best possible output from the vehicle and the troop in an unusual situations also. The seating is based on the packaging providing ample space for ingression and egressing the vehicle and storing some supplies on board [13, 14].

Fig. 11 Interior design of AMPV
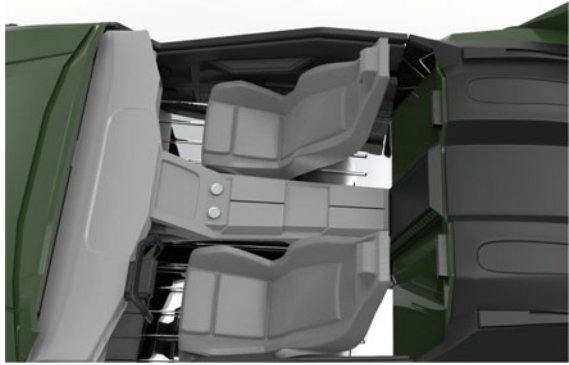
Fig. 12 Seats for the military application

9 Conclusion and Future Scope

From the overall journey of this project, starting from the concept till the final design and details, this can be concluded that the defense vehicles can be advanced on the basis of their design and looks and can be made stronger by investing proper theme in visual design [15].

As compared to the current patrolling vehicles, the outcome of the concept is more advanced on the basis of amphibious mechanism, controlling, and design of the overall concept. The whole purpose of making the amphibious patrolling vehicle is more advanced in terms of operation and application for a surrounding and AMPV design will solve border protection in a much better way.

References

1. Sur, M.: Time at its margins: cattle smuggling across the India-Bangladesh border. Cult. Anthropol. **35**(4), 546–574 (2020)
2. Zeb, R.: Cross border terrorism issues plaguing Pakistan-Afghanistan relations. China Eurasia Forum Q. **4**(2), 69–74 (2006)
3. Omrani, B.: The Durand line: history and problems of the Afghan-Pakistan border. Asian Aff. **40**(2), 177–195 (2009)
4. Khalid, I.: Bangladesh water concern. South Asian Stud. **25**(1), (2020)
5. Helvacioglu, S., Helvacioglu, I.H., Tuncer, B.: Improving the river crossing capability of an amphibious vehicle. Ocean Eng. **38**(17–18), 2201–2207 (2011)
6. Kim, M.-C., Chun, H.-H., Kim, H.Y., Park, W.K., Jung, U.H.: Comparison of waterjet performance in tracked vehicles by impeller diameter. Ocean Eng. **36**(17–18), 1438–1445 (2009)
7. Jing, F.J., Liu, Y.J., Liu, G.K.: An overview on dynamic research of amphibious vehicles. Appl. Mech. Mater. **635**, 112–116 (2014). Trans Tech Publications Ltd.
8. GUO, W.-F., Pan, Y.T.: Research on calculation method of static stability performance of wheeled amphibious vehicle. J. North Univ. China (Nat. Sci. Edn.) 01 (2013)
9. Routson, M.: Advanced amphibious assault vehicle (AAAV). General Dynamics Amphibious Systems Woodbridge VA, (1999)
10. Baldovino, R.G., Garcia, G.R.: Amphibious electric tricycle: mechanical design, simulation and dynamic analysis. Adv. Sci. Lett. **22**(9), 2141–2144 (2016)
11. Sun, C., Xu, X., Wang, L., Tang, Y., Yang, Y., Huang, Z.: Research on hydrodynamic performance of a blended wheel-track amphibious truck using experimental and simulation approaches. Ocean Eng. **228**, 108969 (2021)
12. Frejek, M., Nokleby, S.: Design of a small-scale autonomous amphibious vehicle. In: 2008 Canadian Conference on Electrical and Computer Engineering, pp. 000781–000786. IEEE, (2008)
13. Russell, A. L.: Amphibious Vehicles. Proc. Inst. Mech. Eng. Automobile Div. **183**(1), 99–111 (1968)
14. Simon, M.A., Toups, L.: Innovation in deep space habitat interior design: lessons learned from small space design in terrestrial architecture. In: AIAA Space 2014 Conference and Exposition, p. 4474. (2014)
15. Ongiri, A.A.: Seize the time!: military aesthetics, symbolic revolution and the black panther party

Planned Obsolescence: A Bibliometric Analysis

Vishwajit Kumar, Yogesh Mishra, and M. L. Meena

1 Introduction

The world is big enough to satisfy everyone's needs but will always be too small to meet individual greed. Planned obsolescence results from this greed which has significant relevance in achieving 17 World Sustainable Goals by 2030 [1]. The design of a product is of great importance due to raised concerns about sustainable development's social, economic, and environmental factors [2]. The planned obsolescence aims to force the buyer to replace their product with a newer one before really essential [3]. Industries design their product to become obsolete by shortening their natural end. The concept was first used formally during the great depression of the USA, which lowered down the purchasing power of consumers. This resulted in the accumulation of products in the industry due to low demand. To counter this problem, experts suggested this concept which companies later misused to gain various profits. It gave rise to multiple physical and technological obsolescence mechanisms to foster a short replacement time [4–6]. This area of study has such an impact that in June 2017 European Parliament called on European Commission and the Member States to take necessary action against planned obsolescence [7–9]. France became the first country to pass a law to combat this concept legally [10]. There are two sides to every coin, and so this topic has. On one side of this topic, the author perceives positive outcomes of this concept. Byggeth et al. [11] notify planned obsolescence as a tool to recover market share and achieve technological progress. The country's economy and progress mainly depend on the research and development integrated with the new product development process. The faster product development process boosts the rate of innovation, which directly affects the country's growth rate [12, 13]. Many researchers claim that durable goods can lead to economic stagnation due to slow

V. Kumar (✉) · Y. Mishra · M. L. Meena
Malaviya National Institute of Technology, Jaipur, Rajasthan, India
e-mail: iamvishwajit90@gmail.com

innovation, so they perceive planned obsolescence as a tool for economic growth [14].

In contrast, Çetiner and Gündoğan [15] accuse planned obsolescence of promoting product discard in short intervals fostering waste in the environment. The faster manufacturing strategies require resources at an increased rate resulting in the depletion of natural resources [16]. Due to new upgrades in the product within a short period, consumers tend to buy the product for fun, worsening their debt level [17]. The faster replacement cycle can foster poor product quality, resulting in reduced consumer satisfaction [18, 19].

To any researcher, advancement in the research field plays a key role. Analyzing literature motivates researchers to identify feasible areas and a comprehensive methodology [20]. Since the focus on planned obsolescence has increased significantly, there is a need for a study that provides a broad image representing field development across different parameters. There is a lack of study that present the detailed bibliometric analysis on planned obsolescence considering data from the two most widely used databases, i.e., Web of Science and Scopus. Hence, the present study aims to fill this gap along with the representation of concern studies on a single platform. The significant contributions of this paper are as follows:

- We conducted a detailed bibliometric analysis of "planned obsolescence", extracting data from the widely used Web of Science and Scopus database.
- The development of research in this stream has been documented annually.
- We have examined variables such as annual citations, leading productive authors, leading highly cited authors, leading journals, leading countries publishing on this topic.
- We visualized and presented the most used keywords on both the indexing platforms.
- In the end, we have discussed the core conclusion and further research directions.

2 Methodology

In this study, we have compared the results of Scopus and Web of Science databases on the most commonly used different parameters in the bibliometric analysis. We collected the bibliometric data by performing a Boolean search on planned obsolescence using keywords: TS = ("Planned Obsolescence" OR ("Product" AND "Planned Obsolescence")) on Web of Science while TITLE-ABS-KEY ("Planned Obsolescence") OR TITLE-ABS-KEY ("Product" AND "Planned Obsolescence") on Scopus. We extracted different labels such as author, abstract, title, country, author affiliation, and citation record from these databases for further analysis. Keyword search from the Web of Science retrieved 136 documents in total, consisting of 82.35% (112) articles, 5.88% (8) review articles, 4.41% (6) book reviews, 2.94% editorials, 0.74% (1) early access papers, 2.20% (3) proceedings papers, 0.74% (1) film reviews, 0.74% (1) poetry whereas Scopus retrieved 191 documents consisting of 64.92% (124) articles, 8.371% (16) review articles, 9.94% (19) book chapters,

Table 1 Document type in web of science and Scopus

Web of science			Scopus		
Document type	Total numbers	Contribution (%)	Document type	Total numbers	Contribution (%)
Articles	112	82.35	Article	124	64.92
Review articles	8	5.88	Review articles	16	8.37
Book reviews	6	4.41	Book chapter	19	9.94
Editorials	4	2.94	Book	1	0.52
Early access articles	1	0.74	Conference paper	24	12.56
Proceeding papers	3	2.20	Conference review	2	1.04
Film reviews	1	0.74	Editorial	2	1.04
Poetry	1	0.74	Letter/note	3	1.57

0.5% (1) book, 12.5% (24) conference papers, 1.04% (2) conference reviews, 1.04% (2) editorials, 1.57% (3) letter/note.

Table 1 shows the document types on Web of Science and Scopus related to planned obsolescence. For bibliometric analysis in this paper, we have obtained various performance parameters such as citation per paper (CPP), total citation (TC), and total papers (TP). TP indicates the total publications count extracted from the database, TC denotes the total citations count acknowledged by the journal, and CPP is the ratio of overall citations to the overall publications.

2.1 Bibliometric Analysis

Bibliometric analysis, also termed scientometric analysis in the research field, helps analyze the current trend providing guidelines and motivation for future work. It supports extracting standard procedures and the overall framework of the research topic from various databases. In this section of the paper, we have shown the results of bibliometric analysis aligned same as by Muhuri et al. [21] computed on multiple factors such as annual research growth, leading productive authors, leading highly cited authors, leading journals, leading countries publishing on this topic, and most used keyword.

2.2 Annual Growth of Research in Planned Obsolescence

A significant increase in research related to planned obsolescence can be noticed from 2015 when all 193 United Nations member countries pledged to achieve 17 world sustainable development goals by 2030. The plan 2030 emphasizes economic, social, and environmental spheres with some mutually dependent goals [22]. Figure 1 shows year-wise total publication in the Web of Science and Scopus databases. In the Web of Science, first publication was in the year 2002 with three papers, whereas in Scopus, it was in 1971 with one paper. The maximum publication was recorded in 2016 with 16 documents in both databases, indicating researchers' involvement in the topic just after agenda 2030.

Figure 2 shows the year-wise record of total citations in the Web of Science and Scopus. Total citation count plays a vital role in measuring the influence of an article, author, or publication. It indicates the number of times one work has been referred to in the work of another. In the papers related to planned obsolescence, the Web of Science and Scopus recorded their maximum citation count of 438 and 468, respectively, in 2008. Total citations later decreased in 2021 to 13 and 5 in the Web of Science and Scopus, respectively, as these are the latest publications and are expected to be referred to more in future.

Fig. 1 Research growth in Web of science and Scopus
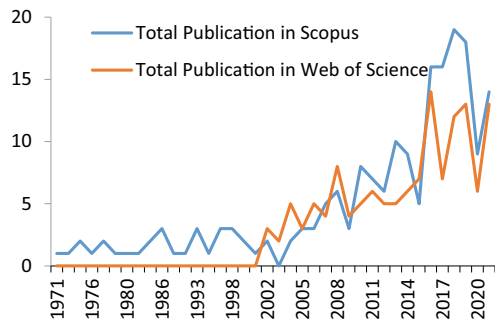
Fig. 2 Total citations in Web of science and Scopus
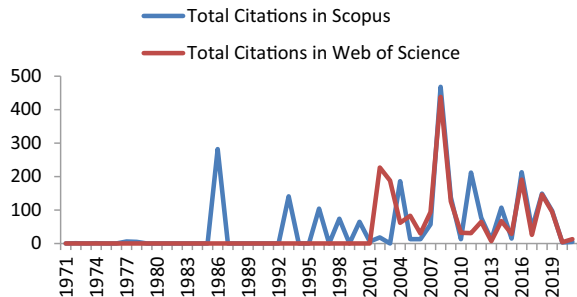
Table 2 Leading productive authors

	Web of science				Scopus			
Rank	Authors	TP	TC	CPP	Authors	TP	TC	CPP
1	Waldman M	7	461	65.86	Goering GE	5	56	11.2
2	Utaka A	6	31	5.17	Dalhammar C	3	63	21
3	Johnson JP	4	63	15.75	Na Na	3	2	0.67
4	Dalhammar C	3	62	20.67	Cooper T	2	176	88
5	Miao CH	3	33	11	Miao CH	2	25	12.5
6	Hahn JH	3	19	6.33	Utaka A	2	16	8
7	Carlton DW	2	221	110.5	Pickren G	2	13	6.5
8	Bhaskaran SR	2	84	42	Mcdonald R	2	5	2.5
9	Gilbert SM	2	84	42	Lee SH	2	2	1
10	Goering GE	2	36	18	Hahn JH	2	0	0

2.3   Leading Productive Authors

On the basis of TP, we extracted the details of the ten leading productive authors from the concern databases, as shown in Table 2. In the case of tie-in TP, we used TC to rank them.

Waldman M is the most productive author in Web of Science with 7 papers, followed by Utaka A and Johnson JP with 6 and 4 papers. There are 3 authors from rank 4 to 6 whose TP is 3 and 4 authors from rank 7 to 10 whose TP is 2. Authors ranked from 4 to 6 are Dalhammar C, Miao CH, Hahn JH, and those ranked from 7 to 10 are Carlton DW, Bhaskaran SR, Gilbert SM, Goering GE.

In Scopus, Georing GE tops the list with 5 publications, smaller than the most productive author in the Web of Science list. Dalhammar C and NaNa have a TP of 3, whereas Cooper T, Miao CH, Utaka A, Pickren G, Mcdonald R, Lee SH, and Hahn JH have a TP of 2. Interestingly, five authors are similar in both the databases in terms of ten leading productive authors with different rankings except Miao CH, placed at fifth spot in both the databases. Georing GE, which tops in the list from Scopus, stands at tenth rank in the Web of Science database.

2.4   Leading Highly Cited Authors

We created the list of leading highly cited authors based on the TC count in all papers shown in Table 3. The leading productive author with 7 articles, Waldman M is also highly cited in the Web of Science with 461 citations. Carlton DW stands in the second spot with 221 citations and 2 papers. There are two authors Bhaskaran and Gilbert SM, with TC of 84. Johnson JP, who was at spot 3 in the leading productive author list of the Web of Science, stands at spot 5 with 63 total citations and 4

Table 3 Leading highly cited authors

	Web of science				Scopus			
Rank	Author	TP	TC	CPP	Author	TP	TC	CPP
1	Waldman M	7	461	65.86	Waldman M	2	229	114.5
2	Carlton DW	2	221	110.5	Cooper T	2	176	88
3	Bhaskaran SW	2	84	42	Dalhammar C	3	63	21
4	Gilbert SM	2	84	42	Goering GE	5	56	11.2
5	Johnson JP	4	63	15.75	Albert M	1	25	25
6	Dalhammar C	3	62	20.67	Miao CH	2	25	12.5
7	Goering GE	2	36	18	Agrawal VV	1	19	19
8	Miao CH	3	33	11	Adolphson DI	1	16	16
9	Utaka A	6	31	5.17	Utaka A	2	16	8
10	Morita H	2	22	11	Pickren G	2	13	6.5

papers. Authors ranked from 6 to 10 in the Web of Science are Dalhammar C with 62 citations, Georing GE with 36 citations, Miao CH with 33 citations, Utaka A with 31 citations, Morita H with 22 citations.

On the other hand, Waldman M, with only 2 publications, leads with a TC of 229 in the Scopus. Goering GE having the highest TP is ranked 4 in the highly cited authors list from Scopus with a TC of 56.

2.5   Leading Journals

A research journal is a scholarly publication published periodically containing articles written by researchers or other experts in a particular field of study. We retrieved the leading publishing journals in the field of planned obsolescence. Table 4 shows the top 10 journals with TP and TC count from the Web of Science and Scopus. The list is ranked based on the total publication count.

Journal of Cleaner Production, Rand Journal of Economics, Japanese Economic Review, and Design Journal are common in both databases. Journal of Cleaner Production has the highest TP with 7 articles in the Web of Science and 5 articles in Scopus. Rand Journal of Economics is at spot 2 with 6 TP and the highest TC of 329 in the Web of Science. In contrast, it has 4 TP with 179 TC in Scopus. Japanese Economic Review is at spot 3 with 5 TP in the Web of Science. It stands last in Scopus with 2 TP. Design Journal is at spot 9 in the Web of Science but spot 7 in Scopus with the same TP of 2.

In the Web of Science, Journal of Economics and Management Strategy is at position 4 followed by European Journal Operational Research, Information Economics and Policy, Technology In society, New Media and Society with 3 TP. Economic Inquiry is at last position with 2 TP in the Web of Science category.

Table 4 Leading journals

| Rank | Web of science | | | Scopus | | |
	Sources	TP	TC	Sources	TP	TC
1	Journal of cleaner production	7	83	Journal of cleaner production	5	78
2	Rand journal of economics	6	329	Journal of consumer policy	4	181
3	Japanese economic review	5	6	Rand journal of economics	4	179
4	Journal of economics and management strategy	3	54	communications in computer and information science	3	1
5	European journal of Operational research	3	44	IFIP advances in information and communication technology	2	21
6	information economics and policy	3	20	International journal of industrial organization	2	11
7	Technology in society	3	19	Design journal	2	7
8	New media and society	3	4	Environmental and resource economics	2	3
9	Design journal	2	4	Applied mechanics and materials	2	2
10	Economic inquiry	2	3	Japanese economic review	2	2

In Scopus, with 4 TP and 181 TC Journal of Consumer Policy is at position 2, communications in computer and information science with 3 TP are at position 4 followed by IFIP Advances in Information and Communication Technology, International Journal of industrial organization with 2 TP. Further with 2 publications, Environmental and Resource Economics and Applied Mechanics and Material stand at 8 and 9 spots.

2.6 Leading Countries

Country-wise scientific production indicates the awareness of the people of that country in the concerned area. Table 5 represents the details of leading countries (top 10) out of 33 countries listed in Web of Science and 40 countries listed in Scopus.

In listing by Web of Science, USA is at the top with 72 TP and maximum TC of 908 followed by UK, Japan, China, Canada with 19, 18, 15, 10 publications. Five

Table 5 Leading countries

Rank	Web of science				Scopus			
	Region	TP	TC	CPP	Region	TP	TC	CPP
1	USA	72	908	12.61	USA	86	336	3.91
2	UK	19	388	20.42	UK	22	658	29.91
3	Japan	18	49	2.72	China	14	5	0.36
4	China	15	62	4.13	Brazil	12	54	4.5
5	Canada	10	94	9.4	Sweden	9	78	8.67
6	Australia	7	38	5.43	Japan	9	38	4.22
7	Sweden	7	20	2.86	Germany	8	90	11.25
8	Germany	6	104	17.33	France	8	35	4.38
9	Spain	6	46	7.67	Australia	8	20	2.5
10	Brazil	5	52	10.4	Italy	8	11	1.38

countries have published papers less than 10. These are Australia, Sweden, Germany, Spain, Brazil. With 5 TP and TC, Brazil is at 10th position.

In Scopus, the USA again tops the list with 86 TP. The UK is at spot 2 with 22 TP and the highest citation count of 658. Interestingly, China at third position with 14 TP has the least citation count of 5. Brazil, at tenth spot in Web of Science, is at 4th in Scopus with 12 TP. Sweden, Japan, Germany, France, Australia, and Italy have a TP of less than 10.

2.7 Most Used Keywords

In this portion of bibliometric analysis, we used VOS viewer to obtain the list of most used keywords in the research field of planned obsolescence. VOS Viewer is the most extensively used software to visualize various informations in research [10]. Occurrences of keyword help to identify research gaps and trends of research. To extract the top keywords in Web of Science and Scopus, we used a co-occurrence type of analysis based on all keywords. The minimum number of occurrences of a keyword was five in both databases. In the Web of Science, out of 583 keywords, 29 met the threshold forming 4 clusters. Figure 3 exhibits the network diagram of the most frequently used keywords Web of Science. The size of the circular node depicts the intensity of the keyword occurrence. Planned obsolescence is the most used keyword in cluster 1 with the other seven items. Monopoly, innovation, durability, technology, and quality are the other keywords placed in different clusters.

In Scopus, out of 1150 keywords, 26 met the threshold forming 3 clusters. Representation of the frequently used keywords in the Scopus database is shown in Fig. 4. Obsolescence is the most used keyword surrounded by sustainability, environmental impact, planned obsolescence, consumer behavior, etc., in different clusters. It is
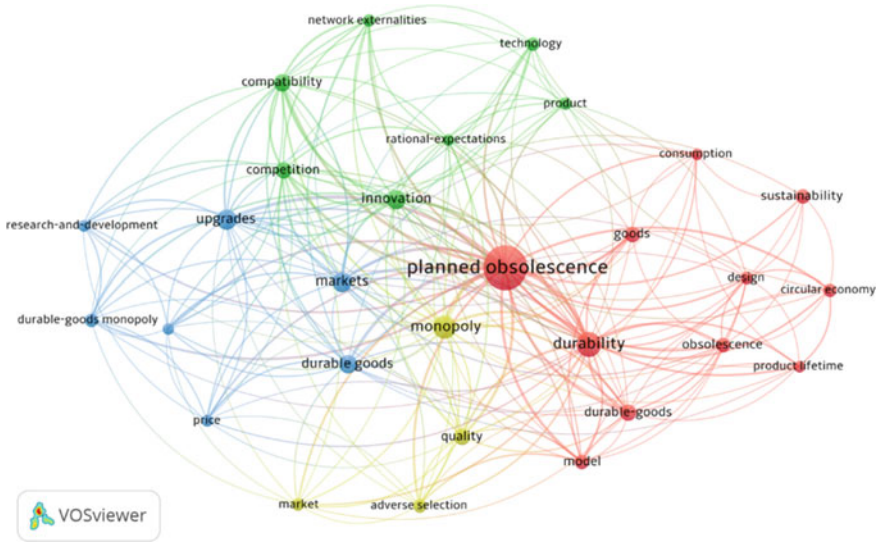
Fig. 3 Most popular keywords in Web of science

observed that most keywords used in both the databases are the same indicating commonality of thoughts across databases.
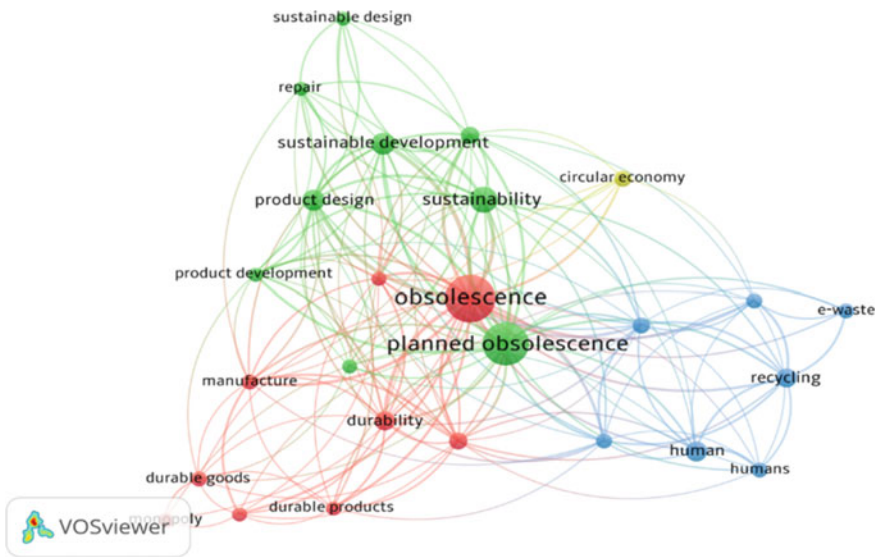
Fig. 4 Most popular keywords in Scopus

3 Conclusions

The main contribution of this paper is the bibliometric analysis based on data extracted from the two most widely used databases, i.e., Web of Science and Scopus. We assessed the result of concern databases utilizing factors like annual research growth, leading productive authors, leading highly cited authors, leading journals, leading countries publishing on this topic, and frequently used keywords. In these two databases, 136 papers are indexed in Web of Science, and Scopus mentioned 191 papers. Waldman M is the highly cited author in concerned databases. Waldman is also the leading productive author in Web of Science, even as Georing Ge is the leading productive author in the Scopus database. Journal of cleaner production is the leading journal, and the USA is the top country publishing in planned obsolescence in both databases. In visualizing the most important keywords, we found planned obsolescence sustainability, environmental impact, monopoly, innovation is frequently used in this field.

In our bibliometric analysis, though we utilized Web of Science and Scopus databases, but there is still a provision of few other sources which can be used for further analysis, and that can be considered as future scope of this study. Further, this study only focuses on quantitative analysis of publications, not quality. So, in future, authors can focus on qualitative analysis of the concerned topic focusing on its various consequences.

References

1. Aladeojebi, T.K.: Planned obsolescence. Int. J. Sci. Eng. Res. **4**(6), 1504–1508 (2013)
2. Satyro, W.C., Sacomano, J.B., Contador, J.C., Telles, R.: Planned obsolescence or planned resource depletion? A sustainable approach. J. Cleaner Prod. **195**, 744–752 (2018)
3. Guiltinan, J.: Creative destruction and destructive creations: environmental ethics and planned obsolescence. J. Bus. Ethics **89**(1), 19–28 (2009)
4. Waldman, M.: A new perspective on planned obsolescence. Q. J. Econ. **108**(1), 273–283 (1993)
5. Morita, H., Waldman, M.: Durable goods, monopoly maintenance, and time inconsistency. J. Econ. Manage. Strategy **13**(2), 273–302 (2004)
6. Carlton, D.W., Waldman, M.: The strategic use of trying to preserve and create market power in evolving industries. (1998)
7. Maggiolino, M.: Planned obsolescence: a strategy in search of legal rules. 405–407 (2019)
8. Maitre-Ekern, E., Dalhammar, C.: Regulating planned obsolescence: a review of legal approaches to increase product durability and reparability in Europe. Rev. Eur. Comp. Int. Environ. Law **25** (3), 378–394 (2016)
9. Svensson-Hoglund, S., Richter, J.L., Maitre-Ekern, E., Russell, J.D., Pihlajarinne, T., Dalhammar, C.: Barriers, enablers and market governance: a review of the policy landscape for repair of consumer electronics in the EU and the US. J. Cleaner Prod. **288**, 125488 (2021)

10. Gecit, B.B.: Planned obsolescence: a keyword analysis. J. Manage. Mark. Logistics **7**(4), 227–233 (2020)
11. Byggeth, S., Broman, G., Robèrt, K.-H.: A method for sustainable product development based on a modular system of guiding questions. J. Cleaner Prod. **15**(1), 1–11 (2007)
12. Fishman, A., Rob, R.: Product innovation by a durable-good monopoly. Rand J. Econ. 237–252 (2000)
13. McMaster, M.T., Fisher, S.J.: Placental development. 213–219 (2003)
14. Godfrey, P.C., Hatch, N.W.: Researching corporate social responsibility: an agenda for the 21st century. J. Bus. Ethics **70**(1), 87–98 (2007)
15. Çetiner, B.G., Gündoğan, M.: Defying planned obsolescence: paradigm change for macro level sustainability of supply chain management systems. In: CIE 2014–44th International Conference on Computers and Industrial Engineering and IMSS 2014–9th International Symposium on Intelligent Manufacturing and Service Systems, Joint International Symposium on "The Social Impacts of Developments in Information, Manufacturing and Service Systems", Istanbul, Turkey—Proceedings, pp. 809–814. (2014)
16. Woidasky, J., Cetinkaya, E.: Use pattern relevance for laptop repair and product lifetime. J. Clean. Prod. **288**, 125425 (2021)
17. Echegaray, F.: Consumers' reactions to product obsolescence in emerging markets: the case of Brazil. J. Cleaner Prod. **134**, 191–203 (2016)
18. Rodrigues, T.V., Gonçalves, A.L., Maciel, P.S.P., de Paiva, P.A.R.: Ethical education of an engineer with responsibility for a sustainable world. In: 2014 IEEE International Symposium on Ethics in Science, Technology and Engineering, pp. 1–7. IEEE (2014)
19. Sverdrup, H.U., Ragnarsdottir, K.V., Koca, D.: An assessment of metal supply sustainability as an input to policy: security of supply extraction rates, stocks-in-use, recycling, and risk of scarcity. J. Cleaner Prod. 140, 359–372 (2017)
20. Shukla, A.K., Muhuri, P.K., Abraham, A.: A bibliometric analysis and cutting-edge overview on fuzzy techniques in big data. Eng. Appl. Artif. Intell. **92**, 103625 (2020)
21. Muhuri, P.K., Shukla, A.K., Abraham, A.: Industry 4.0: a bibliometric analysis and detailed overview. Eng. Appl. Artif. Intell. **78**, 218–235 (2019)
22. Pradhan, P., Costa, L., Rybski, D., Lucht, W., Kropp, J.P.: A systematic study of sustainable development goal (SDG) interactions. Earth's Future **5**(11), 1169–1179 (2017)

A Sustainable Approach Toward Tangible Interactive Setup for Improving the Learning Experience of Primary School's Children in Rural India

Krishna Kant Gupta, Shubhangi Agarwal, Anmol Srivastava, and Rakesh Sah

1 Introduction

Rural primary education in India is discussed as a challenging subject in terms of insufficient infrastructure, teaching staff or the quality of teaching, [1] shares that even the number of student enrollment is increasing but more than half of the fifth-grade students are finding it difficult to read second grade English textbook and mathematical problem efficiently. Another published article [2] finds lack of infrastructural resources as a common underlying problem for an unsatisfactory level of rural education. Literacy is the first factor contributing directly to human resource development, social equity and shaping the good quality of life [3]. Historically, children are observed as most curious and collaborative in their behavior. A study [4] discusses how young children are attached to physical objects which instills curiosity in their mind and help them in collaborative learning. Thus, tangible interactive learning setup (TILs) can act as a powerful tool in facilitating such activity [5].

The study focuses on Uttarakhand, where still social equity and infrastructure support and socio-economic backgrounds are in a challenging situation [6].

Due to these hurdles, the affordability and feasibility of required technology seem to be a major challenge, and this paper shared the development based on channeling the learner's attention during the teaching–learning process through TILs with a reusability and sustainable approach to make the technology and interactive learning setups equitable to all.

K. K. Gupta (✉) · S. Agarwal · A. Srivastava · R. Sah
School of Design, University of Petroleum and Energy Studies, P.O. Bidholi Via-Prem Nagar, Dehradun, Uttarakhand 248007, India
e-mail: krishnakantgupta797@gmail.com

A. Srivastava
e-mail: asrivastava@ddn.upes.ac.in

2   Literature Review

2.1   *Literature on Rural School Education*

Rawat et al. as cited in Mondal et al. [7] emphasize that if physical accessibility like the accessibility of location of the school, children's place of living and commuting vehicles gets improved then it would be a great way to increase the enrollments in rural primary schools. The education of private schools is given more attention and their teachers' availability is high in comparison with public schools [8]. A published study carried out by Harma [9], on 'School choice for the poor?' notes down that the financial income of the parents affects the school choice of their children. ASER the latest reports put light on how 75% of students in a class of 505 faces difficulty in reading and solving arithmetic problems [10].

2.2   *Literature on Tangible Interactions for Children*

Horn et al. [11] on tangible interaction and learning talk about a different interactive medium for learning which would enhance the whole classroom learning patterns and activities. Children would learn much faster if they use their knowledge along with physical actions (e.g., gestures) in their responses. A toolkit was given to teachers to use while teaching which proved to be very beneficial in the whole curriculum of rural education [12]. A comparative study by Antle et al. [13] over the digital and tangible input methods reveals that using tangible input methods would be better for enhancement of the mental ability of the students as they give users the chance to physically place the puzzle pieces and solve it. Miller et al. [14] say that computer games help in improving the cognitive skills of the student.

2.3   *Literature on Outdoor Learning Experiences*

This paper discusses how outdoor activities could also be involved along with classroom setup in a learning environment. Outdoor activities improve the physical and mental ability of preschool children and enhance their motor skills while also increasing the collaboration among children [15].

Another study shows that how parents and teachers support outdoor activities like gardening and playing with tangible materials because it helps children in exploring their environment, socializing and also increasing their physical activity [16].

2.4 Social Perspective of Technology in Education

According to Pal et al. [17] study, parent–teacher interaction is the key to improving the concept of collaborative and fun learning as parents want their children to achieve what they could not do in their lives.

Kam et al. [18] in their study, put emphasis on the fact that video games could be a good way for adaption of new technology for rural students and could be introduced along with different levels so that the students who are slow at learning can learn at their own pace. Halloluwa et al. [19] in this study says that if a collaborative approach to learning and a safe environment is given to a child, he would not be afraid to ask any kind of questions to his teachers and classmates.

Malik [20] discuss in his study that the lack of proper resources in the rural schools like weak infrastructure and the low socio-economic backgrounds of the parents is the reason due to which technological affordability and feasibility are the biggest challenges in rural primary education.

2.5 Sustainable Technology and Accessibility

The above literature suggests that there is a considerable gap between the Govt. Schemes and its effect on enhancing rural education. This paper focuses on how the technological advancements in education happening due to pandemic is not helping the unprivileged students of Rural India. In order to encourage underprivileged families to accept new technological services, the services should meet family needs and prove to be beneficial [20]. Equality in terms of provision of services but equity in terms of cost of the services is important for the families which cannot afford it [21]. The literature also foreseen the opportunity of a sustainable approach toward technology which could help every corner of India. Circular economy states that what has been taken from earth has to be given back sometime. According to Ellen MacArthur Foundation, circular economy is the way for sustainable future and technological advancements [22].

Another study by Yeboah et al. [23] on the reusability of waste material and its value associated with primary education describes the use of waste materials in their educational courses will help them to understand the process and importance of reusability, and also at the same time, they understood that instead of disposing of waste, it can be reused for different purpose.

2.6 Literature Review Conclusion

So, hereby, it is concluded from the literature review that the addition of new mode of learning in the form of tangible interactive medium in the curriculum of rural primary

education would help in its enhancement and increase the student enrollments. Also, using the circular economy system to refurbish the used or discarded phones for the classroom activities and fun learning approach would give a feeling of equity to the rural students and would help them to have an experience of the technology just like students of private schools has.

3 Methodology

The methodology utilizes design thinking to identify the underlying problems and current scenario. Design thinking approach, which is known as design thinking, brings together what is desirable from a human point of view with what is technologically feasible and economically viable [24].

By using contextual design guidelines by Holtzblatt et al. for the field study, ethnographic research and contextual inquiry were conducted to get in-depth knowledge and understanding of the context of the rural primary education and current adaptions of learning in their curriculum [25].

3.1 Data Collection

Ethnographic research was done in Dehradun city. The pictures of different Dehradun schools and a field study map are shared in Fig. 1. The contextual inquiry [25] was captured, while the teachers were teaching in the class and also by observing the students after giving them classroom activities. Interviews were also taken of both the teachers and students in $N = 11$ schools including the city, outskirts and remote schools of Dehradun.

The research study also covers the Education Block offices such as Vikasnagar, Sahaspur and Kalsi Block offices of Dehradun as the administration plays a vital role in running of the rural schools in India. NGOs which are also working same

Fig. 1 Govt. P.S. Schools with students, teacher and classroom of rural primary school

Table 1 List of schools

Block name	Area	School name	Student (I–V)		Teacher	
			Total	Present	Total	Present
Sahaspur	Doonga	Govt. P. S. Bidholi	32	28	2	3 (Locals)
	Doonga	Govt. P. S. Bishanpur	37	32	2	1
	Doonga	Govt. P. S. Kandoli Upper	35	18	2	1
Vikasnagar	Harbartpur	Govt P. S. Vikasnagar	115	51	6	4
	Barotiwala	Govt P. S. Goodrich	41	34	3	3
	Barotiwala	Govt P. S. Chhotuwala	43	40	2	2
Kalsi	Kalsi Gate	Govt. P. S. Haripur	44	44	7	7
	Kalsi Gate	Govt. P. S. Kalsi Bazar (Boys)	40	3	2	0
Chakrata	Kwanu	Govt. P. S. Kwanu-II (Manjhgoan)	40	3	2	0
	Kwanu	Govt P. S. Sainj Aasoie	45	10	2	0
	Tyuni	Govt P. S. Hataal	80	84	3	1

Source District Project Office SSA, Sahastradhara, Dehradun, Uttarakhand | 2019

initiatives using interactive medium were also approached during the study to get their experience with the rural student (Table 1).

4   Insights and Inferences

4.1   Students

The study reveals that lack of confidence in the classroom is one of the main reasons because of which student is not able to clarify his doubts from the teachers or fellow students. The methods which instill curiosity in their minds, and the fun approach of teaching helps to channel the focus of students toward the learning.

4.2   Teachers

It has been observed that the rural primary teachers have a lot of responsibility over their shoulders as they have to take the classes together. They are not able to focus on each student individually.

Lack of proper facilities in the school to support the education and learning methods also led teachers to resign from their jobs or take transfers specially in remote areas.

4.3 Block Offices and NGOs

The study revealed that the block offices have less staff support to monitor and supervise the conditions of rural schools and also they do not have enough time and options for reaching all the schools and villages.

Some NGOs have started working efficiently toward the initiative of fun learning but due to lack of resources and government support, and they are not able to reach all the schools and villages.

4.4 Inference

Insights and in-depth study infer that the traditional teaching methods are not being much successful in the rural primary schools as the curriculum has fixed methods and weak infrastructure affecting both the teacher and the student's mindset. State Government is also playing its role as implicating many schemes but it is not very effective for rural primary education.

Considering resources and to solve the problem from its roots of this issue, there is study proposes, a need of an independent mode of medium, which can be effectively implemented by enhancing the authentic teaching–learning, where students can have their own setup in which they can explore and learn with the help of teacher's guidance. A process into a collaborative fun and interactive tangible medium could be provided to them in order to enhance the classroom learning approach using tangible interactive mediums which is sustainable and to get the good academic results. Technologically affordable as well as feasible in low socio-economic scenarios.

5 Ideation

5.1 Design Principle

This study utilizes the framework that incorporates the Stanford five-stage design thinking model, key sustainability indicator (i.e., social, environmental and economic), and digital fabrication components (i.e., material and process) aimed at evaluating sustainable prototyping processes and outcomes [26] (Table 2; Fig. 2).

6 Final Concept and Prototype

The final concept was based on printable fiducial markers and a camera-based marker tracking computational resources, i.e., reacTIVision. It utilizes the basic available

Table 2 Ideation phases and exploration showing the different solution and modification

Phase	Idea name	Pros	Cons
1st ideation phase	Spin and learn: Simple tangible board game based on board game	Cardboard and pins as material, low cost, sturdy and easy to rebuild	No interactive feedback, lack of guidance, less engaging
2nd ideation phase	Tile tutor: Interactive tangible game based on capacitance sensing	Food metal foil, sun-board and IOT device (Arduino board), affordable cost, audio feedback	Capacitance sensing was overlapping, poor performance
3rd ideation phase	Place and play: RFID card-tag tangible game based on RFID sensing	Sun-board, RFID tags and sensors as material, accurate feedback, cognitive psychology of shapes, immersive experience	Expensive materials, hard to repair because of so many technical parts and connections
4th ideation phase	Place and Play 2: Fiducial marker cards tangible game based on reacTIVision technology	Cardboard box, photo frame and glass, discarded usable mobile device and computer as material, immersive audio-visual feedback with right/wrong assistance, affordable technology for bulk, easy to repair and assemble	Need a scheme to help in procuring the raw materials at bulk

resources which is easily procurable, and also at the same time, using the waste and discarded materials into a novel use of education [27] (Fig. 3).

6.1 Prototype

The prototype was fabricated by using the below mentioned items:

- Cardboard box
- Discarded photo frame
- Photo frame glass
- Tracing paper
- Used/ discarded old working mobile phones with camera
- Computer (for display purpose) (Fig. 4).
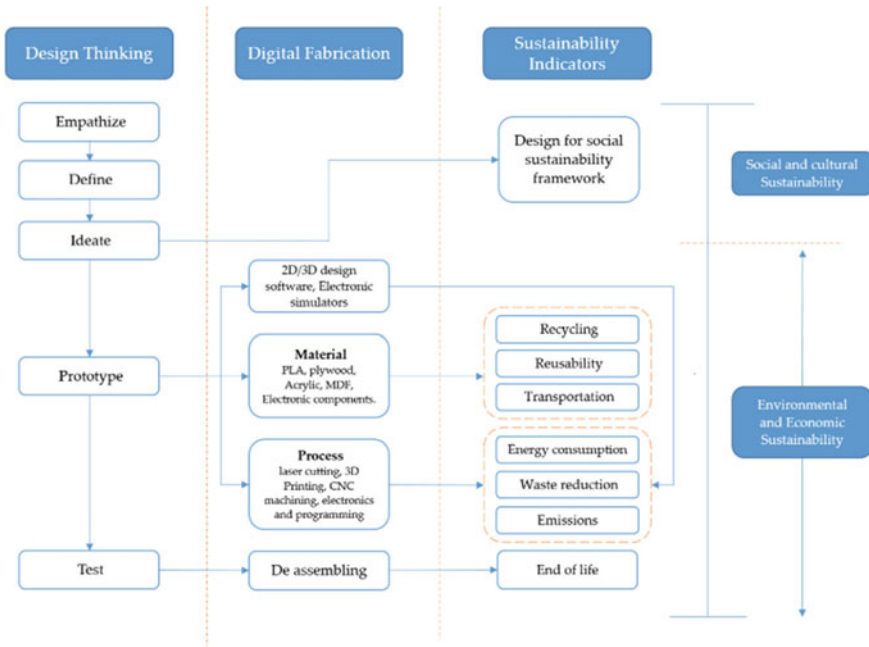
Fig. 2 Framework for digital fabrication based sustainable design and prototyping. *Source* Sustainable Design and Prototyping Using Digital Fabrication Tools for Education Sohail Ahmed Soomro et al. [26]
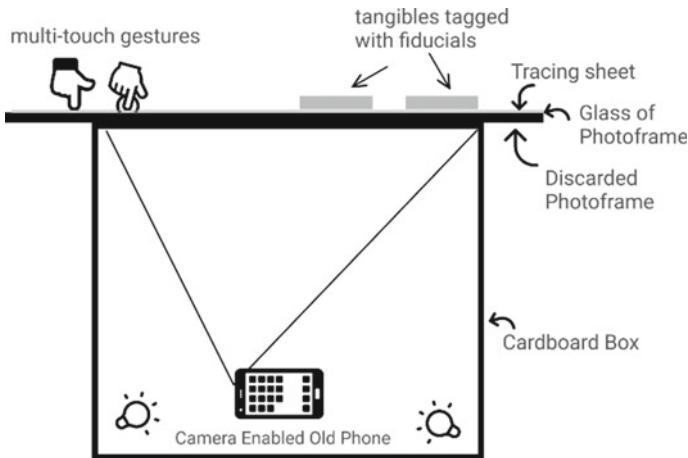
Fig. 3 Framework representing the working principle and scheme behind reacTIVision Technology used for the final concept [27]

Fig. 4 Showing the game interface with the answer cards (far left), the setup with the box, photo frame, etc., (middle top and middle bottom right) printed cards with fiducial marker at back (middle bottom left), used phones as camera (far right)

7 Conclusion

This study demonstrates that how tangible interactive learning approach could be of a great help for primary school children. During prototype testing, we observed how fun the tangible learning was for the children and how fast they were learning and grasping new things. Introduction of games and fun learning methods really helped them in creating a sense of competitiveness and collaboration among children.

Also, these tangible interactive solutions in remote and hilly areas would help students to learn on their own if the teacher is unavailable. The use of sustainable materials out of used or discarded things would further help to make technology reach every corner of the country.

8 Future Scope

This study is working in progress toward finding a solution that is a way to introduce tangible interactive setups to these rural primary schools that is capable of reaching every corner of the country. Due to COVID-19 pandemic, this study was not able to test the prototype into the field and its concepts around it, and it seeks to test the concept of reusability in the 4th phase of ideation to enhance the teaching–learning process with a new dimension of flexibility to change the tangible interactive games around different subjects to make it more relevant to the curriculum by keeping the underlying working principle same.

The available material from the surroundings like the stones or stickers/ photographs of some famous politicians could be used as cards which would serve as an effective learning material, and the facilitator will be able to reconstruct the question around the cues to make a whole new game out of the same working principle. In this way, the study scopes the future to make the solution more sustainably viable to the mass and economically feasible.

References

1. Asercentre.org. http://img.asercentre.org/docs/Publications/ASER%20Reports/ASER%202014/fullaser2014mainreport_1.pdf. Accessed 21 Dec 2021
2. Kaur, R.: Rural education in India (2013)
3. Kremer, M., Chaudhury, N., Rogers, F.H., Muralidharan, K., Hammer, J.: Teacher absence in India: a snapshot. J. Eur. Econ. Assoc. **3**(2–3), 658–667 (2005)
4. Somerville, R.M., Montessori, M., George, A.E.: The Montessori method. J. Marriage Fam. **27**(4), 547 (1965)
5. Shaer, O.: Tangible user interfaces: past, present, and future directions. Found. Trends® Hum. Comput. Interact. **3**(1–2), 1–137 (2009)
6. Schemes, Gov.in. https://mhrd.gov.in/schemes-school. Accessed 21 Dec 2021
7. Mondal, S., Gupta, S.: Accessibility to rural primary schools: a case study of the district north 24 Parganas, West Bengal, India. Indian J. Econ. Dev. **7**(6), 1–7 (2019)
8. Muralidharan, K., Kremer, M.: Public-private schools in rural India. In: School Choice International, pp. 90–109. The MIT Press (2008)
9. Harma, J.: School Choice for the Poor? The Limits of Marketisation of Primary Education in Rural India (2010)
10. Das, S., Biswas, A.K.: Quality and determinants of primary education in rural India. SSRN Electron. J. (2019)
11. Horn, M.S., Crouser, R.J., Bers, M.U.: Tangible interaction and learning: the case for a hybrid approach. Pers. Ubiquitous Comput. **16**(4), 379–389 (2012)
12. Rowe, R.C.: Microindentation-a method for measuring the elastic properties and hardness of films on conventionally coated tablets. J. Pharm. Pharmacol. **28**(4), 310–311 (1976)
13. Antle, A.N., Droumeva, M., Ha, D.: Hands on what?: Comparing children's mouse-based and tangible-based interaction. In: Proceedings of the 8th International Conference on Interaction Design and Children—IDC '09 (2009)
14. Miller, D.J., Robertson, D.P.: Educational benefits of using game consoles in a primary classroom: a randomised controlled trial. Br. J. Edu. Technol. **42**(5), 850–864 (2011)
15. Yıldırım, G., Akamca, G.Ö.: The effect of outdoor learning activities on the development of preschool children. S. Afr. J. Educ. **37**(2), 1–10 (2017)
16. Khan, M., Bell, S., McGeown, S., Silveirinha de Oliveira, E.: Designing an outdoor learning environment for and with a primary school community: a case study in Bangladesh. Landsc. Res. **45**(1), 95 110 (2020)
17. Pal, J., Lakshmanan, M., Toyama, K.: My child will be respected: parental perspectives on computers and education in Rural India. Inf. Syst. Front. **11**(2), 129–144 (2009)
18. Kam, M., Kumar, A., Jain, S., Mathur, A., Canny, J.: Improving literacy in rural India: cell-phone games in an after-school program. In International Conference on Information and Communication Technologies and Development (ICTD), pp. 139–149 (2009)

19. Halloluwa, T., Vyas, D., Usoof, H., Hewagamage, K.P.: Gamification for development: a case of collaborative learning in Sri Lankan primary schools. Pers. Ubiquit. Comput. **22**(2), 391–407 (2018)
20. Malik, R.S.: Educational challenges in 21st century and sustainable development. J. Sustain. Dev. Edu. Res. **2**(1), 9 (2018)
21. Santana, J.C.C., et al.: Refurbishing and recycling of cell phones as a sustainable process of reverse logistics: a case study in Brazil. J. Clean. Prod. (2021)
22. Circular economy diagram: Ellenmacarthurfoundation.org. https://ellenmacarthurfoundation.org/circular-economy-diagram. Accessed 21 Dec 2021
23. Yeboah, R., Asante, E.A., Opoku-Asare, N.A.: Teaching interactive art lessons with recycled waste materials as instructional resources. J. Educ. Pract. **7**(14), 38–59 (2016)
24. IDEO: IDEO design thinking. https://designthinking.ideo.com/. Accessed 21 Dec 2021
25. Holtzblatt, K., Beyer, H.: Contextual Design: Defining Customer-Centered Systems. Elsevier (1997)
26. Soomro, S.A, Casakin, H, Georgi, G.V.: Sustainable Design and Prototyping Using Digital Fabrication Tools for Education, vol. 1
27. Kaltenbrunner, M., Bencina, R.: reacTIVision: a computer-vision framework for table-based tangible interaction. In: Proceedings of the 1st international conference on Tangible and embedded interaction—TEI '07 (2007)

A Solution Toward Providing a Faster Means of Ambulance Service Through Multimedia Design Approach

Hari Brat Saikia and **Bhaskar Saha**

1   Introduction

Indian population strength holds second rank in the world. It has very exciting road dynamics [1]. The traffic is a blend of high-speed supercars, overloaded trucks, a wide range of passengers' buses, bumper-to-bumper private vehicles, and home to the largest number of motorized two-wheelers in the world [2]. Adding to the dynamism, bullock carts, horse carts, and various estranged animals and creatures are also seen on the roads. All these factors lead up to heavy traffic mounting up the congestion on the road [3]. It often becomes difficult for emergency medical services (EMS) to work along the same road condition to maintain an optimum ambulance response time (ART) as the ambulance and other vehicles use the same road [4]. With fatalities and emergencies rising due to road accidents across India, it is adding to the burden for EMS [5]. As per the National Institute of Emergency Medicine, almost 20% of patients requiring urgent medical attention lost lives solely because of traffic delays [6]. According to the Times of India, approximately 146,133 persons were killed because of street level accidents in India during 2016. It is important to note that, out of the total fatalities about 30% lost their lives solely due to delay in medical response time. Many Governments and private ambulance or emergency vehicles are running across the country but are fragmented in terms of service, not easily accessible to the public, and lack modern infrastructure and coordination. Lack of proper emergency medical service (EMS) service is a hindrance to better healthcare [7]. Along the way of providing emergency medical services, an important factor that goes rather unnoticed is the fact that several times an ambulance carrying a patient meets with an accident. Such accidents are potentially hazardous and catastrophic

H. B. Saikia · B. Saha (✉)
Department of Multimedia Communication and Design, Central Institute of Technology Kokrajhar, Kokrajhar, India
e-mail: b.saha@cit.ac.in

Table 1 Table showing the rising trend of ambulance accidents across India

Year	Cases	Incident
June 19, 2018	3 dead	A pregnant woman and two others were killed after the ambulance carrying them was hit by a bus [8]
October 9, 2018	3 dead	A patient and two others on board were killed after the ambulance was hit by a tractor [9]
January 4, 2019	2 dead	Ambulance staff and patient die as their ambulance hits a tree along the road [10]
June 9, 2019	8 dead, 4 injured	Ambulance collided with a mini truck [11]
November 4, 2020	2 dead	Another vehicle rammed in to the ambulance [12]
November 17, 2020	3 dead	Ambulance had a head on collision with a passenger car [13]
November 20, 2020	3 dead,3 injured	Ambulance hits another vehicle [14]
January 28, 2021	2 dead	Ambulance rushed into a scooter killing 2 people after violating traffic rules [15]
January 26, 2021	5 dead	Ambulance carrying 5 people hit a stationary truck due to low visibility caused by fog [16]
February 20, 2021	3 dead, 3 injured	Ambulance hit a truck [17]

in nature because ambulances consist of many lifesaving equipment and chemical substances. After many mishaps, if those substances accidentally mix with oxygen cylinders, it can turn out to be seriously fatal in case of fire and another chemical spillage. Incidents of such nature fail the basic purpose of lifesaving and providing medical assistance.

Ambulance accidents happen primarily during emergencies to reach the intensive care unit (ICU) or hospital in the shortest time, sometimes ignoring the safety concerns and traffic norms. A summary of such incidents and data collected across India are presented in Table 1.

Looking at the above table which summarizes the number of accidents occurred in the country over a span of 4 years, the trendline suggests that, incidents of ambulance meeting with an accident are quite dominant across the country. In all of the cases, there are serious fatalities and injuries. It is the nature of ambulances to move with high velocity so as to reach a hospital or tertiary health center as fast as possible. In the process, most often traffic norms are violated, such as crossing speed limit, unmarked turns, and overtaking, this leads to misjudgments of other fellow drivers and mishaps happen. Not to mention there are also various inevitable circumstances such as fog, rain, wind, and other vehicles hitting from behind. Over the years, the data suggest that such cases are on rise, and the situation needs attention.

A lot of study and research has been done over the years to help mitigate the issue of better ambulance response time. The Internet of things (IoT) way has been used extensively to come about finding solutions to the issues with various smart ambulance systems. A smart calling feature of an ambulance during an emergency was proposed using microcontroller components, GPS modules, GSM modules, and

several crash sensors. The whole setup was meant to reach the accident spot in the shortest possible time and inform the emergency contacts [18]. Another study used a similar approach of a fully automated system reaching accident sites by detecting accidents and thus reducing the delay in treatment. The system relied on GPS modules, GSM modules, and several sensors [19]. In a fresh study, a system named automatic ambulance rescue system (AARS) was introduced. The idea was to offer a steady route for ambulance to reach a medical care center within a short time. It controlled main flow of traffic for optimization and smooth movement for ambulance services without delay [20]. In another attempt to provide a faster response by providing the shortest route to the accident spot was devised. It relied on centrally switching the traffic lights according to the ambulance movement near the vicinity of the accident scene, thus saving time from being stuck in traffic jams [21]. Research conducted by Ethan Erkut studied the scenario and proposed a theory to minimize the response time for medical attention. It proposes a new location layout for medical service stations. The stations are strategically set up to coordinate with existing models and help with better survival chances by providing faster emergency assistance [22]. Cloud-based solutions were also devised for better ambulance services. An intelligent bot does all the calculations in conjunction with artificial intelligence and machine learning to detect ambulances and immediate dispatch to accident spots [23]. The Govt. of India has been pushing states to come up with their emergency medical services (EMS) models across the country. Various states have been implementing such models under their capacity and infrastructure such as "EMRI 108" Services, "Janani Express Scheme", and "Bihar Model 102 and 1911". Most of them are covered under National Rural Health Mission (NRHM). It primarily focused on providing fast transportation to emergency cases [24]. It is worth mentioning that all the research and analysis done to improve the medical response time uses the same road area to provide its services whether to reach the accident spot or in case of transporting patients to the hospital. Thus, the possibility of ambulance accidents meeting with other road vehicles is still in place.

The present system of providing Emergency Services does not have a well-defined operational workflow and is not efficient in terms of ambulance response time. There lacks a systematic structure by which an individual calls for an ambulance to a residence or an accident spot. To overcome the issues, there is a need of smart ambulance calling system easily accessible to general public and a distinct travel route which should be free of road traffic at any point of time so that it can maintain a definite and faster ambulance response time. This paper explores the ways to overcome the issues.

The aim of the study is to visualize a mechanism which will provide a low cost and a faster means of ambulance service along the existing road structure in urban environments using multimedia approach. The objectives are as follows:

- To provide an efficient route or track for the emergency vehicles to work which is independent of road traffic.
- To make a smart and eco-friendly vehicle which will run on electricity, thus, cost of travel will be cheaper.

- To infuse a multimedia design approach to demonstrate the possibility of its operation.

2 Design Process and Method

To understand the problems in detail, an area of study, Guwahati, was considered. It is the capital city of Assam, India. Guwahati is considered as the gateway to the North-East region of the country. As per the census 2011, the city population is 957352 [25] out of which 62,000 people have commercial and private vehicles during 2011–12 [26]. Vehicle registration data put an approximate of 92,000 vehicles including buses, trucks, vans, cars, etc., utilizing the road for various tasks such as office work, utility vehicles, and good transports [27]. This staggering number of road traffic creates a major congestion in the city roads and thus causes a major delay in movement of private vehicles and emergency vehicles. The Government. of Assam has introduced several ambulance services catering the emergency medical transportation needs. "102" service was introduced in September, 2013 to shift any patients from a lower medical center to a better medical facility. Similarly in November, 2008, "108 Mritunjoy" service was introduced to reduce the gap of ambulance response time in coordination with local police and fire authorities. 108 service also has an integral boat ambulance service which accounts to a total of 5 such ambulances across the state. They serve as mobile medical units. The Government sponsored ambulances available are of two types, namely basic life support (BLS) and advanced life support (ALS) [28]. A number of private ambulances also provide services in the city. As there are no common registration platforms, the exact data were not available. Even after the given capacity of pre-hospital care and ambulances, the city has witnessed an average of 1000 accidents per year between 2010 and 2014. The average number of people involved in those accidents are approximately close to 1300 each year. The point of interest is that out of 1300 cases of accidents each year, approximately 220 cases are fatal in nature [29]. A similar study by Raktim Tamuli showed that in the majority of cases, the accident victim succumbs to death within the hour as patients are unable to reach any tertiary healthcare center in time [30].

2.1 Pragmatic Approach

The process followed to understand the primary concern is categorized into various steps. Firstly, the general idea was framed and was expanded to a broader scenario to test the existence of any similar problems. Upon finding that issue existed on a national level, it was required to verify the same with inputs from local medical professionals and the public associated with the medical system, they were categorized under focused groups. The data were again validated among an open group, a

wider section of people using quantitative methods. Lastly, both the problems established were discussed to frame a conclusion. The entire process is depicted in the Fig. 1.

The study started with general observation as to how the recent increase in population affects valuable resources, time, and sometimes costs life. Ambulance using the same road stuck in jams is the worst affected of all shown Fig. 2a. The problem is not just limited to a part of a region but can be seen as a matter of grave concern for the entire country. Looking at the images given below, we can have a brief idea as to how the ambulance stands helpless in beating the traffic to reach a medical center/hospital in time.

Experiment-I: Interaction with Local Health Center People

To further understand the issue in detail, it was necessary to make a focused group, which consists of people who are associated with ambulance services and also to get inputs from doctors who are always dealing with such scenarios. After
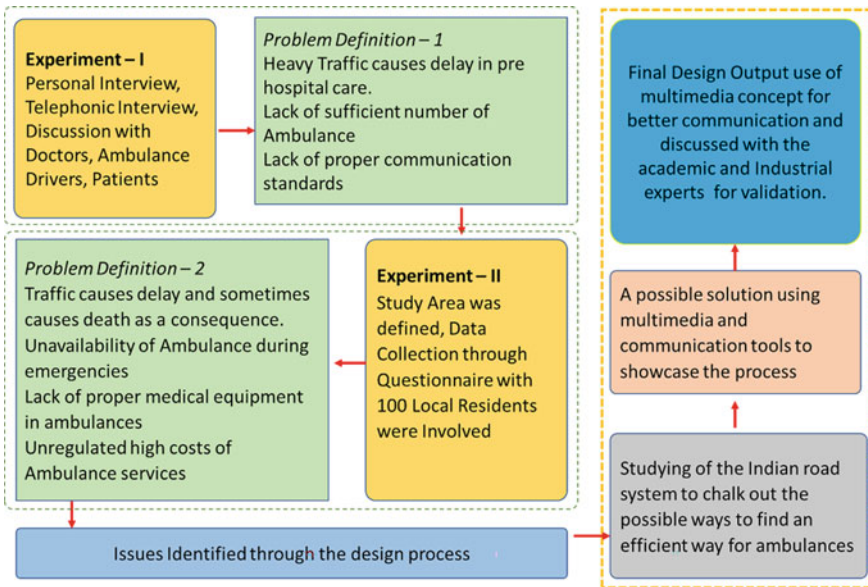
Fig. 1 Flowchart of the process undertaken during the research

Fig. 2 **a** Showing ambulances face issues in traffic (retrieved from www.google.com) **b** Survey or discussion with the doctors, ambulance drivers, etc.

an interaction with Dr. Achinta Sundar Sarma shows in Fig. 2b, Superintendent, Rupnath Brahma (RNB) Civil Hospital, Kokrajhar, BTC, Assam, India, underlined the shortage of ambulance services at any given time. "Public faces issues in the process of acquiring an ambulance and reaching the hospital in time. There is no dedicated helpline. The situation worsens during night wherein reaching out to an ambulance becomes rather difficult and is located in different places. Thus, it takes time for one to reach the location of the patient and take them to a hospital". Ambulance drivers were also crucial during this study as they possess first-hand information and are always involved in the process of movement of ambulances, dealing with patients and complexities of issues that exist during the whole process of transit. Mr. Ratul Narzary, Driver, Mrityunjoy — 108, Ambulance Service, he mentioned, ambulances more often are given the right of way, still it is insufficient to make it in time to the hospital. Another fact that remains unnoticed is that not everyone avails services of an ambulance to reach hospital but uses private vehicles. Due to heavy traffic, most of those in emergency too cannot make it in time. He also mentioned the importance of opting for an ambulance instead of private vehicles as it helps the patient with the first aid and necessary care required during critical hours.

Experiment-II: Interaction with Local People for Data Collection

After gathering information from the focused group, it was clear to summarize that ambulance services were really facing problems due to heavy traffic in the urban areas. Now, the problem in discussion needs to be tested in an open environment. To understand the concern of the public domain, input from a large community of users was a must to understand the issues in detail. This was categorized under open groups. Since target users will be the public, it would make sense to gather information from the users. There were multiple factors to consider before going for the survey such as not all people dwell in similar surroundings. Some reside in remote locations and some in urban compounds. The configurations are different so are the needs and nature. To reach out to a greater range of public views, an online survey was conducted using google forms. The questionnaire was segmented into two categories: multiple choice questions (MCQ) and explanatory questions. The sampling was of 100 participants which included different age groups, gender, and professions. The age group participated consisted of 60% in the age group of 18–25, 38% of 26–45 and 2% in the age group of 45 and more. In gender classification, male participants accounted for 42% while females responses recorded were 58%. The background of participants included 68% students, 3% are from the business sector, Government sector constituted for 12 and 18% belonged from various professions. The questions were framed to understand the gaps in the whole process, right from calling for an ambulance, getting the proper medication inside an ambulance, and reaching a medical care center in the shortest possible time through users perspective. The multiple choice-based questions were to the point, intended to understand the basic facts associated with the system. The questions were devised to frame a picture about the common issues which can be seen on a regular basis, and no solution has been framed. To understand the public opinion, questions of the following nature were devised. The focus was to understand whether there is a need for an ambulance service rather than a private vehicle to go to the hospital if someone is sick. To understand

whether there is a need for a safe, comfortable, and fast ambulance service. If the hospital is far from the user's location? To understand how traffic congestion affects ambulances while reaching a hospital. What are the impacts of high-speed movement of the ambulance? Whether an innovative approach of mobility for an ambulance and other emergency vehicles can be thought of.

On other hand, explanatory questions framed were to understand in depth the practical issues that were faced by the public, which are usually overlooked in general. Instead of generalizing that traffic delay causes problems, users were asked to share any real-life experiences that happened during such adverse conditions. It was to analyze whether there exist any other complications which arise during delay, and any possible measures to solve it. Whether the fact that, fast moving ambulance during an emergency can cause accidents. The users were also asked about various flaws and whether there is a need for a new framework to improvise the existing system of emergency medical services. Gathering the results of the survey conducted through online questionnaires are displayed below in Fig. 3 as a graphical representation. The graph is formed out of the seven primary questions that were asked to the public. The responses were collected in terms of agree, strongly agree, disagree, and strongly disagree.

While answering to the question, whether preference should be given to ambulances rather than private vehicles to shift any patient to hospital — 62% of the users agreed and 38% of the users agreed strongly to it. Next question was to understand the experience inside an ambulance during transit. So users were asked whether there was a need for more comfortable, safe, and faster means of service, to which 49% of the public agreed to it and 50% of users strongly agreed to it. The next question was to understand whether road traffic congestion was indeed the reason causing delay in ambulance response times? 61% of the public agreed to the question and 37% agreed strongly to it. To understand whether a patient suffers the most while stuck in traffic, 59% of the public agreed to verify the question along with 37% agreed strongly to it. To confirm while stuck in traffic, most often patients die? — to which
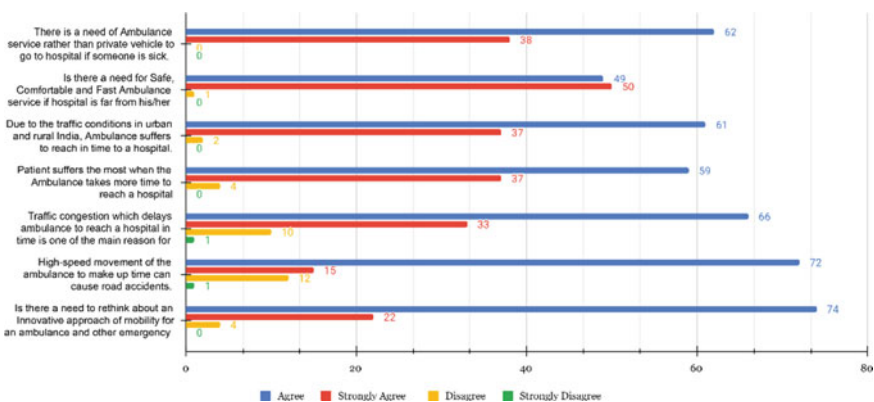
Fig. 3 Survey results

66% of the public agreed to it and 33% agreed strongly whereas 10% disagreed. In order to confirm another important factor about ambulance meeting with accidents, a question was asked whether high-speed movements cause accidents? In reply, 72% of the public agreed to the fact, 15% agreed strongly, 12% disagreed, and 1% disagreed completely. To have a broader view about the existing infrastructure and system, the users were asked whether there was a need for better mobility solutions or a better design for betterment of the public. In reply, 74% agreed to accept that the system needs a better workaround and think about new innovative ideas. Exploring the explanatory questions, it was understood that the users were indeed having issues about the medical transportation framework present in Indian road conditions. At any given point in time, it is always difficult to call for an ambulance for the general public, thus an average user always resorts to using a private vehicle either personal or rented one to reach a healthcare center. In doing so, certain acute cases or emergency cases miss out on first aid.

3 Outcome of the Study: Ambulance Design and Development

As the issues pertaining to delay in existing ambulance service have been established, a new solution to overcome the issue needs to be defined. This section deliberated about the step-by-step process toward creating a new and innovative way to provide a faster way out for the ambulance service.

3.1 Necessary Road Modifications

After surveying the road dynamics of defined area of study, it was learnt that, the median area of the road can be used in a more efficient way. If modified in a certain way, it can be used as a dedicated route for emergency vehicle like ambulance to run along the existing road network. The advantage of using the same road route will be that very less amount of road modifications will be required. Taking inspirations for the tram rail line which are used in conjunction with road lines, similar rail tracks can be laid along the center of the road, and foot barriers can be laid along the width. Similarly, the traffic signal structures present in the middle of the road can be shifted to the side of the road along the foot barriers. Figure 4a shows the existing road system, and the modifications required are presented in Fig. 4b.

Fig. 4 **a** Existing road system of Guwahati city, **b** the proposed modifications

3.2 Concept Art and 3D Renders

Initial 2D sketches were drawn to understand the proportion, layout, and basic functionalities of the model. After analyzing further and taking inspirations from existing ambulance vehicles, the final 3D model is created. Figure 5a shows the concept drawings, and Fig. 5b shows the final 3D output of the model.
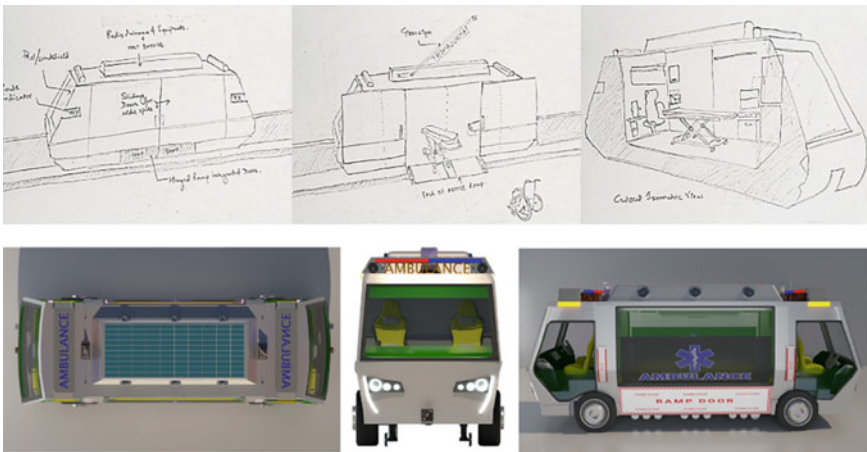
Fig. 5 **a** 2D concept sketches of the ambulance model, **b** 3D renders of the final 3D model

Retractable steel wheels to run on track

Regular wheel for door to door for picking and dropping patient from resident to hospital
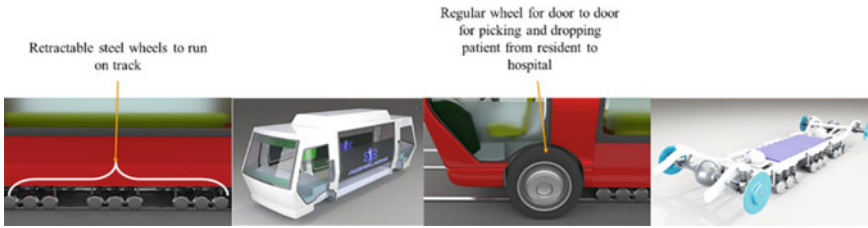
Fig. 6 Shows the body frame, chassis, and the final placement in the vehicle

3.3 Frame Construction and Working of Dual Mode of Operation

The ambulance is designed to run along the rails with help of steel wheels as well as regular wheels which are attached to the same chassis frame and axle. Figure 6 shows the body frame and the chassis in which steel wheels and tire wheels are attached.

The ambulance is primarily designed to run on electricity. The electrified tracks will the main source of power to run the motors which in turn will power the vehicle. The chassis has a built-in battery bed as shown in Fig. 6 as an auxiliary power. The battery will power the vehicle when running only on wheels. Solar panels too are installed on the roof as a secondary power source. Modern technologies such as regenerative breaking, advanced driver assistance system (ADAS), lane assist and departure, infrared track alignment, and safety components are integrated. As the ambulance will be required to pick up patients from residence to hospital, the vehicle will need to change its direction away from the track. Figure 7 shows the mechanism how during a turn (say while entering to a hospital), the steel wheels will disengage, and the vehicle will run only using the tires. Again, while returning to the track, same mechanism will be activated.

The whole system has an inbuilt smart summoning technology wherein any user can call for the ambulance using a dedicated mobile app or standard emergency number like 101 or 100. After receiving the call, the inbuilt global positioning system (GPS) mechanism or using callers input the ambulance reaches the spot and attends the patient. The ambulance is designed as a type C: basic life support ambulance

Fig. 7 Track departure and rejoin mechanism
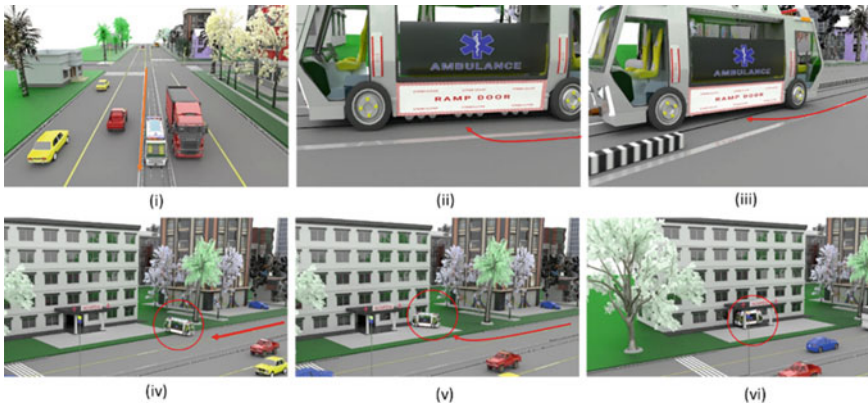
Fig. 8 Story board of the ambulance leaving track route to reach a hospital

which will have the basic medical aid and support conforming to the guidelines prescribed by National Ambulance Code (NAC). After receiving a user's call and picking up the patient, the following set of images as shown in Fig. 8. depicts a brief storyboard sequence (i) to (vi) as how the ambulance initially runs on track and while nearing a hospital/medical care facility changes its track where steel wheels disengage and turn toward the hospital. After leaving the track, it runs solely on regular wheels to reach hospital. After patient boarding or deboarding, it returns to the main track and continues to next call.

While attending to a nationwide issue of delay in pre-medical care, a solution is presented using multimedia tools and approach. The advantage of using multimedia tools is to visualize and understand the feasibility of the working mechanism without actually have to build such a system and test it. It would incur lot of cost and cannot be error free. There have been many studies toward finding a possible solution to provide a faster ambulance service to patients or any accidents spot but have not been able to turn into reality. This idea presented in this paper has been shared for feedback with various academic and industry experts. Table 2 presented below summaries the feedback of various experts.

4 Conclusion

An analysis of ambulance service in India in conjunction with road traffic condition was discussed. The focus was to identify and think of a comprehensive solution that would address the major areas of interest such as reducing accidents related to an ambulance and other vehicles, creating a way for the fastest ambulance response time with minimal cost of travel, a safe, and comfortable experience and eco-friendly means of transport.

Table 2 Summaries the feedback of various experts

Subject matter is very impressive, and idea is productive. The concept is futuristic but needs to work on road structure in civil engineering viewpoint
Design concept is necessary, and approach is good
Building of such vehicular structure is possible given it falls under governing laws
It is a need of hour solution to the rising issues of road accidents and for providing pre-medical care within the golden hour
The concept can be only applied to specified area owing to the road width in existing urban road environments and suggested to work on better functionality of the vehicle
Good design approach for futuristic project. To develop on certain areas of visual aspects. Ergonomics should be enhanced properly

References

1. Worldometer. https://www.worldometers.info/world-population/india-population/. Accessed 26 Dec 2021
2. Times of India Bikes Page. https://timesofindia.indiatimes.com/auto/bikes/india-is-now-worlds-biggest-2-wheeler-market/articleshow/58555735.cms. Accessed 26 Dec 2021
3. Zahoor, T., Singh, B.K.: Traffic situation in India: a review. Int. J. Technol. Res. Eng. **4**(7) (2017)
4. Lam, S.S.W., Nguyen, F.N.H.L., Ng, Y.Y., Lee, V.P.X, Wong, T.H., Fook-Chong, S.M.C., Ong, M.E.H: Factors affecting the ambulance response times of trauma incidents in Singapore. Accid. Anal. Prev. (2015)
5. Singh, S.K.: Road Traffic Accidents in India: Issues and Challenges, WCTR July 2016, Transp. Res. 25, 4708–4719 (2017)
6. Ajitha: Emergency Vehicle and Health Monitoring System. https://innovate.mygov.in/innovation/emergency-vehicle-and-health-monitoring-system/. Accessed 02 Mar 2021
7. Sharma, M., Brandler, E.: Emergency medical services in india: the present and future. Prehospital and disaster medicine: the official journal of the national association of ems physicians and the world association for emergency and disaster medicine in association with the acute care foundation (2014)
8. NDTV. https://www.ndtv.com/cities/pregnant-woman-among-three-killed-as-bus-hits-ambulance-1869909. Accessed 22 Aug 2021
9. NDTV. https://www.ndtv.com/india-news/patient-two-others-killed-as-ambulance-hits-tractor-trolley-in-madhya-pradesh-1929273. Accessed 22 Aug 2021
10. Orissapost. https://www.orissapost.com/patient-and-ambulance-staff-die-as-108-ambulance-runs-into-a-roadside-tree/. Accessed 22 Aug 2021
11. NDTV. https://www.ndtv.com/kerala-news/8-killed-4-injured-after-ambulance-collides-with-mini-truck-in-kerala-2050591. Accessed 22 Aug 2021
12. Times of India. https://timesofindia.indiatimes.com/city/vijayawada/two-die-as-unidentified-vehicle-rams-into-ambulance-on-nh-16/articleshow/79027543.cms. Accessed 22 Aug 2021
13. Times of India. https://timesofindia.indiatimes.com/city/hyderabad/3-die-in-ambulance-accident/articleshow/79253186.cms. Accessed 22 Aug 2021
14. Times of India. https://timesofindia.indiatimes.com/city/jaipur/ambulance-overturns-after-hit-by-a-vehicle-3-die/articleshow/79216205.cms. Accessed 22 Aug 2021
15. Times of India. https://timesofindia.indiatimes.com/city/kolkata/ambulance-kills-dad-daughter-critical/articleshow/80498297.cms. Accessed 22 Aug 2021
16. Indiatvnews. https://www.indiatvnews.com/news/india/uttar-pradesh-bhadohi-ambulance-hit-truck-road-accident-dense-fog-680517. Accessed 22 Aug 2021

17. Orissatv. https://odishatv.in/odisha-news/odisha-patient-among-3-dead-as-ambulance-rams-into-container-truck-near-tangi-519666. Accessed 22 Aug 2021
18. Karthikeyan, S., Srinivasan, S.R., J. Syed Ali, J., Veeraraghavan, A.K.: Smart Summoning Of Ambulance during a Vehicle Accident. In: 2018 2nd International Conference on Green Computing and Internet of Things (ICGCIoT) pp 418–423. (2018)
19. Dagade, P: Accident detection and ambulance rescue system using wireless technology. Int. Res. J. Eng. Technol. (IRJET) **4**(5) (2017)
20. Athavan, K., Balasubramanian, G., Jagadeeshwaran, S., Dinesh, N.: Automatic Ambulance Rescue System. 2nd International Conference on Advanced Computing and Communication Technologies **2012**, 190–195 (2012)
21. George, A.A., Krishna, A., Dias, T., Vargheese, A.S., Divya, R.S.: Golden aid an emergency ambulance system. International Conference on Networks and Advances in Computational Technologies (NetACT) **2017**, 473–476 (2017)
22. Erkut, E.: Ambulance Location for Maximum Survival. Wiley InterScience (2007)
23. Mohapatra, P.: Ambulance Hub: Cloud Based Solution for Ambulance Services. In: 2nd IEEE International Conference on Computational Systems and Information Technology for Sustainable Solutions (2017)
24. National Health Systems Resource Centre, Emergency Medical Service (EMS) in India: A concept paper. Ministry of Health and Family Welfare, Government of India
25. Ministry of Urban Development, Government of India
26. Economic Times. https://auto.economictimes.indiatimes.com/news/passenger-vehicle/cars/vehicle-registrations-in-guwahati-show-declining-trend/29210394. Accessed 26 Dec 2021
27. Govt. of Assam. https://comtransport.assam.gov.in/frontimpotentdata/motor-vehicle-statistics. Accessed 26 Dec 2021
28. https://hfw.assam.gov.in/information-services/108-mrityunjoy
29. Chakraborty, R., Bhattacharyya, S., Roy, M., Paul, P.: Accident analysis and the suggestion of an accident prediction model for Guwahati city. Int. J. Innov Res. Sci. Eng. Technol. **4**(11) (2015)
30. Tamuli, R.P., Das, N.K., Sarmah, S., Sharma, R.K.: A study of 200 skull fracture cases following vehicular accidents in the city of Guwahati: the Gateway to North–East India (2018)

Droplet Distribution Effected by Multi-Rotor Flight Parameters

Umamaheswara Rao Mogili, B. B. V. L. Deepak, D. R. Parhi, and Aezeden Mohamed

1 Introduction

Agriculture is one of the most economic sources that affect the Indian economy. If the growth of agricultural products increases the economy is in a reasonable state, otherwise it could be a disaster for developing countries like India. Till now, the agriculture fields are cultivated using manual techniques. In these techniques, pesticide spraying is the most hazardous process, and it also affects the farmer's health. But dramatically development in the technology, the cultivation in the agriculture fields takes a new role. The introduction of multi-rotor vehicles is also called remotely piloted aircraft (RPA) or an unmanned aerial vehicle (UAV), which can be piloted remotely or perform a flight autonomously along a planned route. Unmanned aerial vehicles are divided into rotors (multi-rotor) and fixed-wing aircraft constructions. Rotors can quickly change flight direction, zero-distance takeoff, and landing, precise "hovering" over the scene of the event and can operate in very narrow spaces [1].

The presence of UAV type chopper changes the paradigm of drone and technology the application, including in INDIA. Various activities currently, it is common to use drones such as entertainment, agriculture monitoring, precision agriculture, and disaster mapping [2, 3]. Multi-rotor-based aerial photography applications are one of the high-level applications in agriculture applications, especially monitoring and

U. R. Mogili (✉)
Department of Computer Science and Engineering, Sri Satya Sai University of Technology and Medical Sciences, Sehore, India
e-mail: umajrfnit@gmail.com

B. B. V. L. Deepak · D. R. Parhi
Industrial Design Department, National Institute of Technology, Rourkela, India

A. Mohamed
Mechanical Engineering Department, PNG University of Technology, Lae, Papua New Guinea
e-mail: aezeden.mohamed@pnguot.ac.pg

dimensional measurements [4]. The ability to produce detailed images with the help of coupled GPS system which could help getting accurate result [5]. The ground station communicates with a multi-rotor system using MAV link protocol to transmit the field locations and operations which can be performed while spraying the pesticides [6]. The use of agrochemicals and water the diversity of the physical and biological environment optimize production cost and improve the efficiency of crop fields to reduce the environmental impacts [7].

Another major application of the multi-rotors is pesticide spraying. The first pesticide UAV vehicles Rotomotion SR200 and SR20 were developed by Yamaha Company. These are the low-volume spray system for pesticide spraying with a lightweight video digital camera for real-time applications [8, 9]. A simpler study was done using a WPH642 single-rotor electric vehicle which affects the scattering parameters on the distribution of droplets over rice plants [10]. Using unmanned helicopters, the spray droplet deposition concentration, uniformity, and flight height, the relationship between speed and interaction between the two other factors were studied [11, 12]. The influence of spray parameters was studied using a UAV on the droplet deposition and distribution over the corn canopy [13]. Different methods are used to explore the low-volume and high-concentration multi-rotor application operations of two conventional agents on rice quality [14].

The optimal path planning of the multi-rotor vehicles or unmanned robots is developed using a hybrid algorithm in an assorted environment like agriculture fields [15]. Also, the path planning of the agriculture environments is different compare with the other environments. The droplet collectors such as water-sensitive papers, polyester, and mylar cards are used to collect the droplets while spraying the pesticides over the agriculture fields [16–18]. The droplets can be sampled in various types of artificial surfaces and later it to be measured using different techniques. The surfaces considered as default for droplet sampling with a method of volume mean diameter showed a constant relationship between the diameter and density.

In this paper, a multi-rotor was developed to perform pesticide spraying operations in the agriculture fields. The multi-rotor sprays pesticide over the agriculture fields with different flight parameters such as speed and height. These two parameters decide the droplet densities and spray uniformity of the droplets that reside in the droplet collectors. The standard deviation and coverage rate of the droplet densities and spray uniformity were calculated for different layers. The rest of the paper is organized as follows: The introduction part introduces the development of multi-rotor vehicles and spraying systems of different eras. Materials and methods section deals with the implementation of a multi-rotor spraying system and its flying parameters. The results and discussion section deals with droplet densities and spray uniformity of the droplets collected from the droplet collectors. The last section deals with the conclusion and future scope of the paper.

Fig. 1 Ready to fly the multi-rotor vehicle

2 Materials and Methods

2.1 Multi-Rotor Parameters

The development of multi-rotor unmanned aerial vehicle spray equipment was carried out in the labs of the industrial design department of the National Institute of Technology, Rourkela, India. For developing the multi-rotor, a custom F450 platform with the following components was used as F450 frame with integrated PCB wiring, four 30A E300 electronic speed controllers (ESCs), four 2212 920 kV E300 brushless direct current motors (BLDC), four carbon fiber propellers of self-tightening, one 14.8 V 4000mah 30C Li-Po battery. The propellers and motors are chosen based on a study of takeoff constraints for building a pesticide spraying multi-rotor system shown in Fig. 1 [19].

Spraying was done with a multi-rotor equipped pesticide tank, with twin-jet nozzles, with a constant flow of the pesticide in the steady air pressure. The experiment consisted of concomitant spraying over the water-sensitive paper cards to collect the samples. The tank is equipped to the downside of the multi-rotor. The capacity of the tank is 0.75–1 L; the spray width is 1.5 m, and the speed of the multi-rotor is 2 and 4 m/s. Duration experiment, the nozzle was positioned at approximately 20 cm in height above the samples.

2.2 Experimental Method

The experiment was conducted in the fields of the National Institute of Technology, Rourkela, India. An experiment was conducted in the field of Iresine plants. The experiment consisted of concomitant spraying of water-sensitive paper cards with the size of 7.5 cm × 2.5 cm, used as a droplet collector. The water-sensitive paper lays on the plant in three different places. The places are the top, middle, and bottom layers of the plant. The height of the plant is approximately 140 cm, and the layers

are placed at 120 cm (top layer), 80 cm (middle layer), and 40 cm (bottom layer). The placement of the droplet collectors is shown in Fig. 2. During the application, the twin-jet nozzles are positioned at approximately 20 cm in height about the droplet samplers. Water is used in the place of pesticides to reduce pollution in experimental areas. The droplet collectors were set up on each layer of the plant so that they remained one to the top to bottom and positioned parallel to the direction of the leaf. Spraying was done with a multi-rotor spraying system, developed at the National Institute of Technology, Rourkela, with cone pattern twin-jet nozzles angled at 50°, with constant flow rate and air pressure.

During the experiment, the multi-rotor initiated at its initial position with the normal speed and started spraying at the desired location. The spraying starts with a speed of 4, 6 m/s at different heights shown in Fig. 3. Initial multi-rotor speed is 4 m/s at the height of 2, 3, and 4 m. Next iteration, the speed increased for 6 m/s at the same heights described earlier. After completing alliteration of the spraying, the multi-rotor returns its home location using return to launch (RTL) mode.

After completing the six test flights for spraying, the droplet collectors were collected from the different layers of the Iresine plant and stored in the zip lock cover to further process. Further, the droplet collectors collected from each layer at different speeds were scanned using a DropLeaf public domain application for analysis. The analysis of different heights and speeds is shown in Fig. 4a, b. The

Fig. 2 Positing of water-sensitive papers
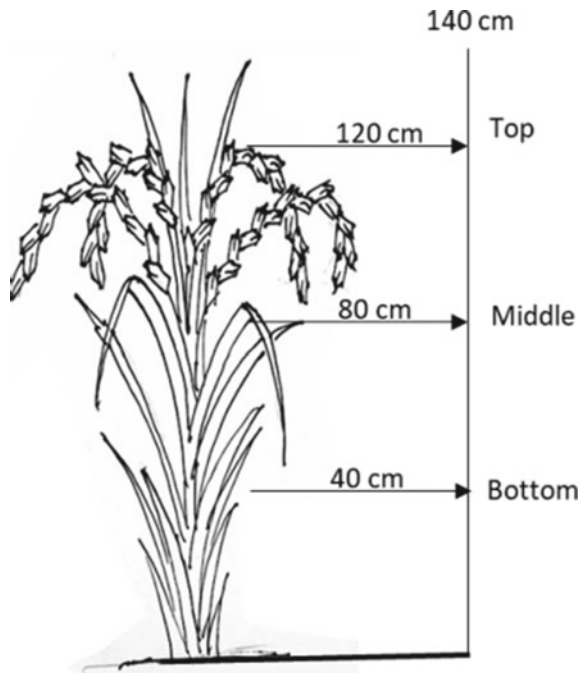
Fig. 3 Pesticide spraying over the Iresine plants

dimensions of the water-sensitive paper in the DropLeaf application are chosen as height (cm) of 7.5, width (cm) as 2.5, and minimum droplet size (pixel) is taken 1.

3 Results and Discussion

3.1 Droplet Deposition

The droplet deposition density was tested at different flying heights and speeds of the multi-rotor. The droplet collectors collected from the field were analyzed using the DropLeaf application, and the results are shown in Table 1. In the tested method, the use of droplet collectors that presents the different values in the progression of droplet density allows that drops of a sample to be distributed and improved the performance of the analysis in terms of height and speed. Droplet density and uniformity were calculated using different techniques that should give an absolute result. In this case, it would be enough to accurately measure droplet density and uniformity by the drops that hit the target. However, the accuracy of the technique tends to decrease when drops of varied collectors are collected in the sampling surfaces or when to perform manually measuring, sorting, and counting of the prints of the drops.

The droplet size in the droplet collectors is calculated using the mean diameter (μm). The values of mean diameter Dv 0.1 (μm), Dv 0.5 (μm), and Dv 0.9 (μm) are shown in Table 2. In general, the mean diameter values that can interface with accuracy are human error in measuring the impressions caused by the drops, so
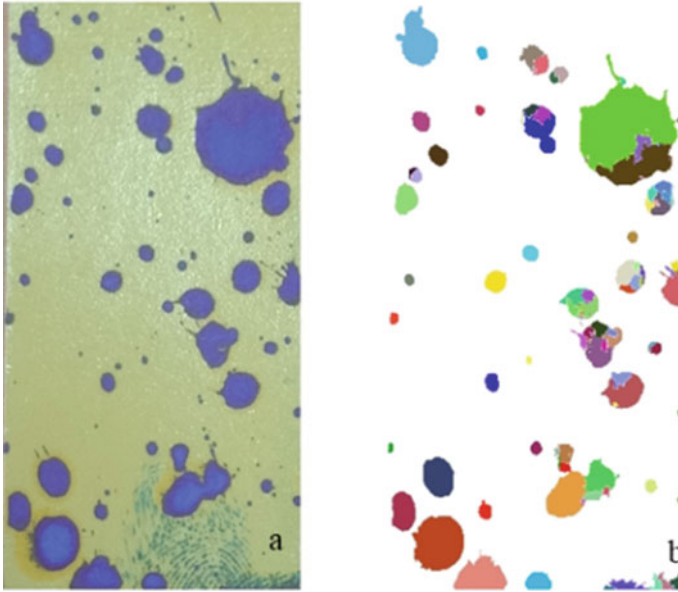
Fig. 4 **a** Original collected WSP, **b** Analyzed WSP

Table 1 Samples collected from Iresine plants

Multi-rotor height (m)	Multi-rotor speed (m/s)	Number of drops	Coverage area (%)	Droplet density (drop/cm^2)		
				Top layer	Middle layer	Bottom layer
2	4	64	2.72	3.41	2.01	1.25
	6	124	5.13	6.61	4.25	2.31
3	4	104	7.65	5.55	3.86	2.56
	6	243	12.82	12.96	9.63	7.52
4	4	243	12.01	12.26	8.96	6.75
	6	294	18.02	15.68	11.54	7.52

much for the difficulty of judgment in the diameter values classification manually. In addition to these problems, the manual drop classification process is extremely tiring.

The coverage area was taken to sort the drops from each sample. The calculated droplet densities shown in Table 2 were having the lowest values at multi-rotor flying height 2 m and speed 4 m/s with the values of 3.41 (Top layer), 2.01 (Middle layer), 1.25 (Bottom layer) droplets per cm^2. At the same time, the droplet densities value is high at the multi-rotor flying height of 4 m and speed of 6 m/s with the values of 15.68 (top layer), 11.54 (middle layer), 7.52 (bottom layer) droplets per cm^2.

Table 2 Analyzed results from DropLeaf

Multi-rotor height (m)	Multi-rotor speed (m/s)	Mean diameter (μm)	Dv 0.1 (μm)	Dv 0.5 (μm)	Dv 0.9 (μm)
2	4	963.38	583.35	909.44	1460.97
	6	898.08	543.01	748.63	1755.99
3	4	1063.13	379.56	880.56	2110.29
	6	937.41	323.36	727.75	1828.57
4	4	892.69	328.87	657.76	1884.78
	6	939.17	249.89	669.33	2017.92

While comparing all six tests, the flying speed with 4 m/s and height 2 m has the lowest values, and flying height 6 m/s and height 4 m have the highest values. However, the average droplet density for the six tests of the top layer is 7.36%; the middle layer is 6.70%, and the bottom layer is 4.65%. The droplet coverage area of test 1 is the lowest with a value of 2.72% and the highest value with a value of 18.02%. The average coverage area of all six tests is 9.73%. According to the speed and height of the multi-rotor system, the experiment was conducted in six experimental tests for the top, middle, and bottom layers. Figure 5 represents the droplet densities that occurred in the above side three layers. In Fig. 5, the x-axis presents multi-rotor height in m; the y-axis presents multi-rotor speed in m/s, and the z-axis presents droplet densities per cm^2 of the three layers.
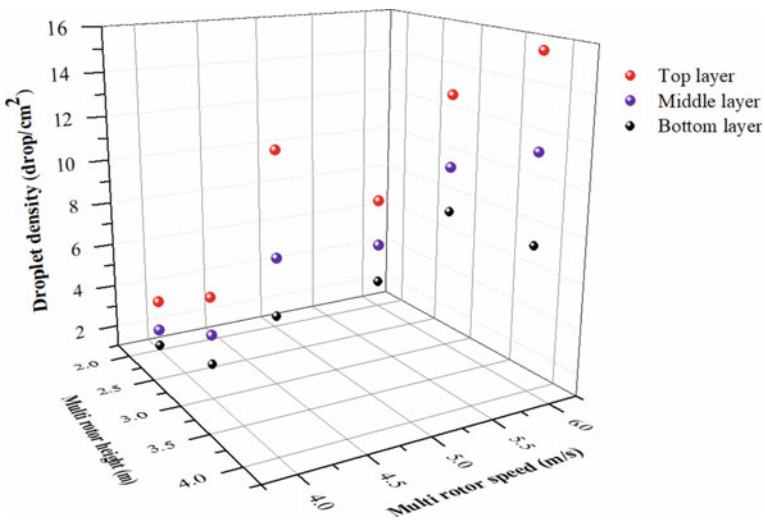
Fig. 5 Droplet densities over the three layers of each test

3.2 Statistic Analysis

The spray uniformity is calculated using a coefficient of variation over the droplet densities of three layers. The coefficient of variation (CV) is derived based on the standard deviation of the discrete variable. The discrete variables are defined as values obtained from the six tests conducted in the field. The coefficient of variation is calculated by using the following formula.

$$CV(\%) = \frac{S}{\overline{V}} * 100 \tag{1}$$

S indicates standard deviation, and $\overline{V}$ indicates several droplets occupied per unit area over the water-sensitive paper.

$$S = \sqrt{\frac{\sum_{i=1}^{n}(V_i - \overline{V})^2}{(n-1)}} \tag{2}$$

V_i indicates the number of droplets occupied on the water-sensitive paper of each test unit, and n indicates the total number of tests. The standard deviation and coefficient variation values are shown in Table 3. The incidents of the fields were most suitable for water-sensitive paper, as it increased droplet densities and the observations of small spots. In the case of top and bottom layers, the values are shown as highest and lowest as per the table referenced.

Table 3 shows the results of the determination of the deposits, by the multi-rotor system, for water-sensitive paper targets. This was probably due to the difference in droplet spray between speed and height at the end of the application. However, it is recommended to do statistical planning based on results of pre-tests, to establish the number of samples necessary to obtain a result reliable, even with the disposal of a certain percentage of samples not suitable for analysis.

The coefficient of variation is small; then, the spray uniformity of the droplet deposition is the lowest value, and the coefficient of variation is high; then, the spray uniformity of the droplet density is high. The CV value is low 27.32% at flight height

Table 3 Spraying uniformity of droplet densities

Multi-rotor height (m)	Multi-rotor speed (m/s)	Droplet density (drop/cm^2)			Std	CV (%)
		Top layer	Middle layer	Bottom layer		
2	4	3.41	2.01	1.25	1.10	49.13
	6	6.61	4.25	2.31	2.15	49.05
3	4	5.55	3.86	2.56	1.50	37.57
	6	12.96	9.63	7.52	2.74	27.32
4	4	12.26	8.96	6.75	2.77	29.72
	6	15.68	11.54	7.52	4.08	35.23

at 3 m, and speed of flight is 6 m/s, and the highest value is 49.13% at a flight height of 2 m and speed of 4 m/s.

4 Conclusion

In this paper, a multi-rotor pesticide spraying system was used to perform the pesticide spraying in the experimental field. Overall six tests were conducted in the field, and results are collected. The collected results are analyzed using statistic analysis techniques standard deviation and coefficient of variation. Also, it is possible to estimate the amount of pesticide which is deposited in a given area through droplet analysis using droplet densities. The results describe the flying height 2 m and speed 4 m/s with the values of 3.41, 2.01, 1.25 droplets per cm^2. At the same time, the droplet densities value are high at the multi-rotor flying height of 4 m and speed of 6 m/s with the values of 15.68, 11.54, 7.52 droplets per cm^2. The coefficient of variation is smaller than the spray uniformity of the droplet deposition is the lowest value, and the coefficient of variation is high; then, the spray uniformity of the droplet density is high. The flight parameter's speed and height affect the droplet distribution over the crop fields. As a result, the top layer with 3 m height with 6 m/s speed defines the highest droplet deposition in the agriculture fields.

References

1. Zhang, C., Kovacs, J.M.: The application of small unmanned aerial systems for precision agriculture: a review. Precis. Agric. Springer **13**(6), 693–712 (2012)
2. Hunt, E.R., Jr., Daughtry, C.S.: What good are unmanned aircraft systems for agricultural remote sensing and precision agriculture? Int. J. Remote Sens. **39**(15–16), 5345–5376 (2018)
3. Mogili, U.R., Deepak, B.B.V.L.: Review on application of drone systems in precision agriculture. Procedia Comput. Sci. **133**, 502–509 (2018)
4. Niethammer, U., James, M.R., Rothmund, S., Travelleti, J., dan Joswig M.: UAV-based remote sensing of the Super-Sauzed landslide: evaluation and result. Eng. Geol. **128**, 2–11 (2012)
5. Keller, R.J., Lange A.F.: GPS guidance system for use with circular cultivated agricultural fields. U.S. Patent 6,087,984, issued July 11 (2000)
6. Mogili, U.R., Deepak, B.B.V.L.: An intelligent drone for agriculture applications with the aid of the MAVlink protocol. In: Innovative Product Design and Intelligent Manufacturing Systems, pp. 195–205. Springer, Singapore (2020)
7. Bachmann, R.J., Boria, F.J., Vaidyanathan, R., Ifju, P.G., Quinn, R.D.: A biologically inspired micro-vehicle capable of aerial and terrestrial locomotion. Mech. Mach. Theory **44**, 513–526 (2009)
8. Huang, Y., Hoffmann, W.C., Lan, Y., Wu, W., Fritz, B.K.: Development of a spray system for an unmanned aerial vehicle platform. Appl. Eng. Agric. **25**(6), 803–809 (2009)

9. Huang, Y., Hoffman, W.C., Lan, Y., Fritz, B.K., Thomson, S.J.: Development of a low-volume sprayer for an unmanned helicopter. J. Agric. Sci. **7**(1), 148 (2014)
10. Zhang, J., He, X., Song, J., et al.: Influence ofspraying parameters of unmanned aircraft on droplets deposition[J]. Trans. Chin. Soc. Agric. Mach. **43**(12), 94–96 (2012)
11. Baijing, Q., Liwei, W., Donglin, C., et al.: Effect of flight altitude and speed of unmanned helicopter on spray deposition uniform [J]. Trans. Chin. Soc. Agric. Eng. **29**(24), 25–32 (2013)
12. Mogili, U.R., Deepak, B.B.V.L.: Influence of drone rotors over droplet distribution in precision agriculture. In: Innovative Product Design and Intelligent Manufacturing Systems. Springer, Singapore (2021)
13. Weicai, Q., Xinyu, X., Lixin, Z., et al.: Effects of spraying parameters of unmanned aerial vehicle on droplets deposition distribution of maize canopies. Trans. Chin. Soc. Agric. Eng. **30**(5), 50–56 (2014)
14. Xue, X., Tu, K., Lan, Y., et al.: Effects of pesticides aerial applications on rice quality. Trans. Chin. Soc. Agric. Mach. **44**(12), 94–98 (2013)
15. Gunji, B., Deepak, B.B.V.L., Saraswathi, M.B.L., Mogili, U.R.: Optimal path planning of mobile robot using the hybrid cuckoo–bat algorithm in the assorted environment. Int. J. Intell. Unmanned Syst. (2019)
16. Qin, W., Xue, X., Zhang, S., Gu, W., Wang, B.: Droplet deposition and efficiency of fungicides sprayed with small UAV against wheat powdery mildew. Int. J. Agric. Biol. Eng. **11**(2), 27–32 (2018)
17. Tang, Y., Hou, C.J., Luo, S.M., Lin, J.T., Yang, Z., Huang, W.F.: Effects of operation height and tree shape on droplet deposition in citrus trees using an unmanned aerial vehicle. Comput. Electron. Agric. **148**, 1–7 (2018)
18. Zhou, Q., Xue, X., Qin, W., Chen, C., Cai, C.: Analysis of pesticide use efficiency of a UAV sprayer at different growth stages of rice. Int. J. Precis. Agric. Aviat. **3**(1) (2020)
19. Mogili, U.R., Deepak, B.B.V.L.: Study of takeoff constraints for lifting an agriculture pesticide sprinkling multi-rotor system. In: Advances in Materials and Manufacturing Engineering, pp. 203–210. Springer, Singapore (2020)

Performance Analysis of Electro-pneumatic Hybrid Vehicle with ANSYS

S. Palani, R. Lokesh, S. Hariharan, R. Vivek Ramachandran, M. Bharathraj, K. Manikandan, R. Paul Linga Prakash, and M. Selvam

1 Introduction

Based on pneumatic and electric vehicles, numerous researches have been conducted previously, and some of them are studied and presented as literature surveys. Rynbrandt [1] proposed the better system for transportation with electrical energy through the automotive vehicles which are powered by electrical energy. Tajima [2] made some modifications in the permanent magnets and auxiliary magnets to make an electric car of low vibration and noiseless to avoid the expanses of fuel through the loss of iron in permanent magnet with respect of magnetic flux during the brake apply while running. Zhang [3] proposed a system with battery charging by utilizing grids with AC power which transmits required energy for the vehicle contain with control module and other devices. Thipse [4] used a system with novel for controlling the movement of four-stage piston with a single crank shaft in second generation. Hasebe [5] depicted that for an electric car, the drive mechanism can be small sized and to increase the traveling time and torque by minimize vehicle weight. Engine size and weight are also reduced, and it provides high efficiency, accuracy, and rigidity. Barth [6] used the expansion chamber in all cylinders in pneumatic-based motor system which has piston plate separated by slide plate, and the power is extracted by the pneumatic engine at the end of the cycle.

Kawamoto [7] improved the cooling capacity in the electric car drive and also minimizes the diameter of the motor. They arranged the axial alignment for mounting all motors with the mechanism of reduction gear coaxially. Jose [8] constructed a pneumatic vehicle that started with the help of combustion engine in the front end which is coupled to the air compressor. The air will pass through the air tank having

S. Palani (✉) · R. Lokesh · S. Hariharan · R. Vivek Ramachandran · M. Bharathraj ·
K. Manikandan · R. Paul Linga Prakash · M. Selvam
Department of Mechanical Engineering, Vel Tech Multitech, Avadi, Chennai, Tamilnadu 600 062, India
e-mail: palaniraji.s@gmail.com

a thermal device at the outlet and then leads to an air motor. The motor is operatively connected to the rear axle which is located the vehicle rear end. Viteri [9] proposed an engine collects air from surroundings and removes at least a portion of nitrogen using liquefaction. The remaining, primarily oxygen, is compressed in a gas generator which has an igniter which uses oxygen and a high-pressure hydrogen containing fuel leaving water and carbon dioxide as by-products. The water is then partially reverted back into the gas generator to regulate the temperature. Brown [10] fabricated a compressed air engine is coupled with an electric motor. The motor is used to increase the pressure of the air, and upon reaching, it initiates the auxiliary compressor. Then, it is engaged with the crank shaft to continue build up to a maximum predetermined air pressure, and it is maintained for the operation of the engine.

Figenbaum [11] and Song et al. [12] stated that the main objective in hybrid vehicle minimizes the size of the engine for reducing consumption of the fuel with applies carbon-free sources. Mourad and Mahmoud [13] found that the reason of minimum of I.C. engine overall efficiency reduces the harmful emissions, so they find as one successful result is the employ of hybrid vehicles. Wang et al. [14] stated that for crossing the driving cycle standard, it needed about 770 ml fuel at the end of drive cycle. Fang et al. [15] found that the option of connecting the system through the system of air supercharging for increasing performance of volumetric along with enhance engine efficiency.

From the above literature, the electro-pneumatic car is the combination of both electrical and pneumatic setup providing 100% eco-friendly vehicles, and it clearly shows that it is necessary to modify the cam shaft by 2-stroke for better operation.

The novelty of our research work is modifying the camshaft of 4-stroke into 2-stroke with respect of valve operation. We make modification of cam lobe from V-shaped to I shape with oval provision for obtaining better torque.

2 Methodology

The project initially started with collection of required data through Internet and various books. Various research papers regarding electrical and pneumatic vehicles have been studied to understand the basic principles of both the electric and pneumatic engines by means of literature survey. Then, the materials required for the fabrication of the vehicle have obtained, and the design of the vehicle frame, cam, and chassis was drawn with the help of Solidworks. Then, as by the process, the fabrication of the various components, procurement of the different components required assembling an electrical drive, and the conversion of the internal combustion engine are done simultaneously. Then, both pneumatic and electrical part of the vehicle has assembled, and the vehicle is developed and tested at its peak performance. By measuring the different dimensions and values, the required calculations have been made, and the results are discussed and documented.

3 Construction (Key Components) of the Vehicle

3.1 Modified IC Engine

A conventional internal combustion engine primarily uses fossil fuels to extract power and generally comprises of 4 strokes. The piston moves back and forth inside the cylinder and compresses the air fuel mixture, and it is ignited to perform a controlled combustion. Modifications have been made in the traditional IC engine by altering the cam and by sealing the passages where the compressed air can possibly escape. Since no volatile fuel is used, the temperature of the engine also didn't exceed limits, and thus, the atmospheric surrounding is enough to keep the engine at operational temperature without utilizing any specific coolants. The proposed pneumatic engine is shown in Fig. 1.

Fig. 1 Pneumatic engine

3.2 Modified CAM

The conventional cam used in the IC engine was modified in order to convert the 4-stroke engine into a 2-stroke engine. An external lobe is added in the other end of the cam, and the traditional "V" shape of the cam is altered into an "I" shape, and the ends of the lobes are grinded into an oval shape to ensure the engine smooth operation. The valve timing is also modified, and the displacement diagram with the cam profile diagram is also traced for the modified cam in order to make the cam operational at its full functional level. Thus, the cam is made to actuate the inlet and exhaust valves twice as much as the normal IC engine in one complete cycle, and the valve timing ratio is also increased. The modified cam is shown in Fig. 2.

3.3   Motor with Electric Power

Motor with electric power converts the energy of electric into mechanical rotation. Generally, the electrical motor is working with the principle of interaction between fields of magnetic and the electric current in wire winding for generating force with respect of applied torque on the shaft. The power supply is given to the motor through the sources of direct correct by batteries or rectifiers and the sources of alternating current by power grid, inverters, or electrical generators. The vehicle comprises of a 48 V brushless DC motor for propulsion, and it has the power of 750 W and current range of 15.6 amps. The brushless electric DC motor is shown in Fig. 3.

Fig. 3 Brushless DC motor

3.4   Battery

For getting power for the devices of electrical, a battery which is consist one or more electro chemical cells through external connections. It includes both positive as well as negative terminal to discharge power. The vehicle is powered by a lithium-ion battery with the range of 48 V and current over a range of 100 amps which transmits power to the electric motor to withstand longer duration and at peak energy density.

It is a simple rechargeable battery with low self-discharge which is ideal for a go-kart vehicle. The proposed lithium-ion battery is shown in Fig. 4.

Fig. 4 Battery

3.5 Controller of Motor

The controller of motor is a device which can be used to co-ordinate the electric motor performance. It comprises either manual or automatic means to initiate the motor, halting the speed, choosing forward or reverse rotation, and to regulate the speed, torque. It also aids in the protection of the motor in the circumstances of overloads and electrical faults. The motor is coupled with the controller by a set of wires, and the controller is directly connected with the vehicle accelerator in order to regulate the vehicle motion. The proposed motor controller device is shown in Fig. 5.

Fig.5 Motor controller device

4   Working Principle of the Vehicle

This hybrid vehicle comprises of two modes of operation, and it can be powered by means of compressed air and electric power. The actual vehicle photo-graphical view is presented in Fig. 6.

Fig. 6 Actual vehicle photo-graphical view
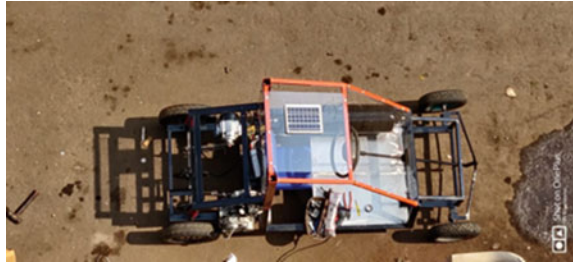
The system includes an air tank of 30 L capacity, 750 mm length, and 210 mm diameter that can hold compressed air up to the pressure of 10 bars. Initially, compressed air should be filled in the air tank with maximum pressure, and the backflow of the compressed air is halted with a single-way valve. Then, the engine is initially started with a help of a kicker to provide the necessary initial torque to the vehicle. Then, the compressed air is supplied into the engine through a tube. The engine is an air-tight chamber with sealed openings. When high-pressure air enters the cylinder, it actuates the piston, and thereby, power and torque are produced from the pneumatic engine. Torque is altered with the help of in-built gear mechanism of the engine. The engine is coupled with the rear axle by using a chain drive, and it helps vehicle to provide the required motion. Whereas in electrical setup, a 48 V battery made up of Li-ion is used as a source of power along with it transmits power to the motor. The motor controller is linked with a motor to control the speed. Motor is coupled with the rear axle through a chain drive. Ackerman steering mechanism is used to navigate the vehicle in the desired direction since it is a simple and efficient mechanism for the vehicle operation. A disk brake is implied on the vehicle to control/stop the motion of the vehicle. Spring coil suspensions are installed on the rear end of the vehicle since 2/3 of the vehicle load acts on the rear frame of the vehicle.

5 Design Calculation and Analysis

Vehicle load distribution in front and rear end of the vehicle.

R_f and R_r

$$R_f = \frac{l}{b + \mu h} w = 616.03 \tag{1}$$

$$R_r = \frac{lb + \mu h}{b + \mu h} w = 938.5 \tag{2}$$

$R_f < R_r$. Hence, the assumption is correct.

F and F_r

$$F = ma = 44.19 \text{ N/m}^2 \tag{3}$$

$$R = F_r \times w \tag{4}$$

$$R = R_f + R_r$$

$F_r = 6.216$

W_f and W_r

$$W_f = \frac{L2}{L} w - \frac{h}{L} \left[Ra \pm w \sin\theta + \frac{w}{g} a \right] \tag{5}$$

$W_f = 17.89 \text{ kg}$

$$W_r = \frac{L1}{L} w - \frac{h}{L} \left[Ra \pm w \sin\theta + \frac{w}{g} a \right] \tag{6}$$

$W_r = 232.03 \text{ kg}$

$(F_{\max})_t$ and $(F_{\max})_r$

$$(F_{\max})_t = \mu W_f \tag{7}$$

$$(F_{\max})_t = 2.68 \times 10^3 \text{ N/m}^2$$

$$(F_{\max})_r = \mu W_r \tag{8}$$

$(F_{\max})_r = 34.8 \times 10^3 \text{ N/m}^2$
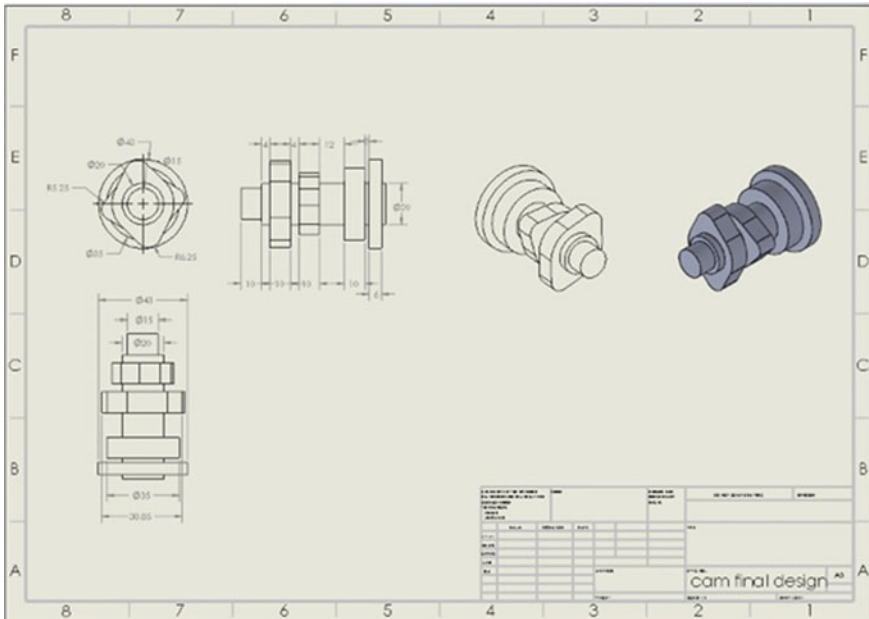
Fig. 7 Designing and modeling of the cam using modeling software (Solidworks)

$F_{\max}$

$$F_{\max} = \frac{\mu w \left(L2 + \frac{\text{Frh}}{L}\right)}{1 + \frac{\mu w}{L}} \tag{9}$$

$F_{\max} = 3.64 \text{ N/m}^2$

Cam is a mechanical device that actuates the inlet and exhaust valves of the engine. Figures 7 and 8 represent the designing and modeling of the cam using modeling software (Solidworks).

6   Results and Discussion

The frame of the vehicle is made of the mild steel-steamed square pipe. The frame is the main component of the vehicle since it experiences all the forces (both compressive and tensile) under varying conditions. It is estimated that the dimensions of the vehicle using modeling software (Solidworks) and welded the mild steel rods to give a rigid structure for the frame. The front and background clearance of the frame was 150 mm and 250 mm, respectively. Figure 9 shows the 3D frame of the vehicle is made of the mild steel-steamed square pipe.
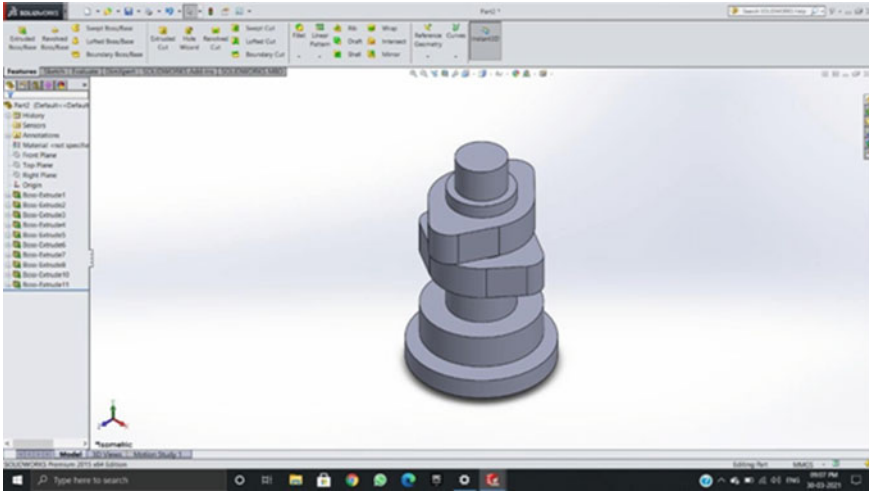
Fig. 8 3D design of cam using ANSYS

Fig. 9 3D frame of the vehicle is made of the mild steel-steamed square pipe
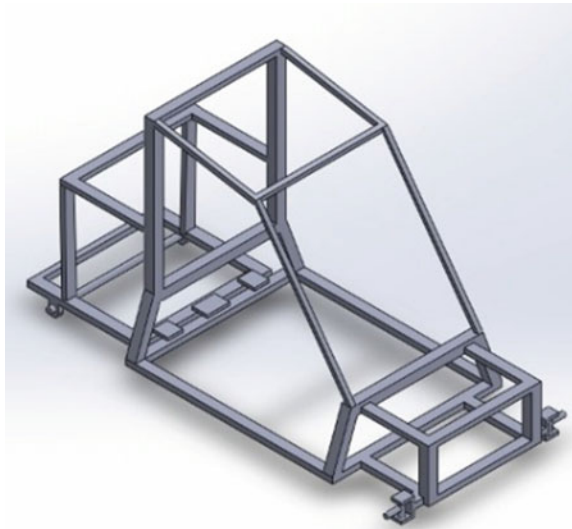
Figure 10 represents the state of the vehicle frame when the load is acted at the center of the vehicle.

Figure 11 represents the state of the vehicle frame when the vehicle components are loaded in the center of the vehicle using ANSYS software.

Figure 12 represents the state of the vehicle frame when the vehicle components are loaded in the rear end of the vehicle using ANSYS software. At different pressure of the air, the corresponding velocities are recorded. Different pressures were
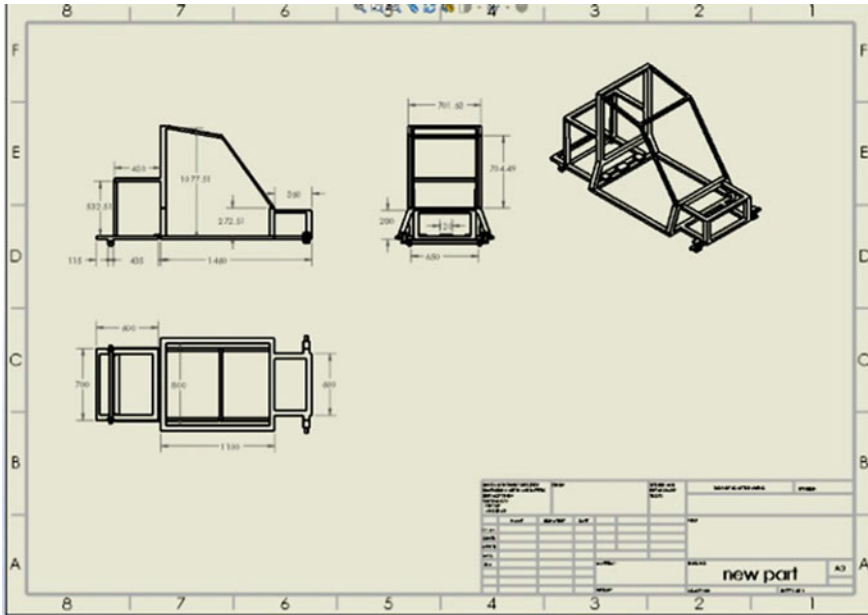
Fig. 10 2D vehicle frame when the load is acted at the center
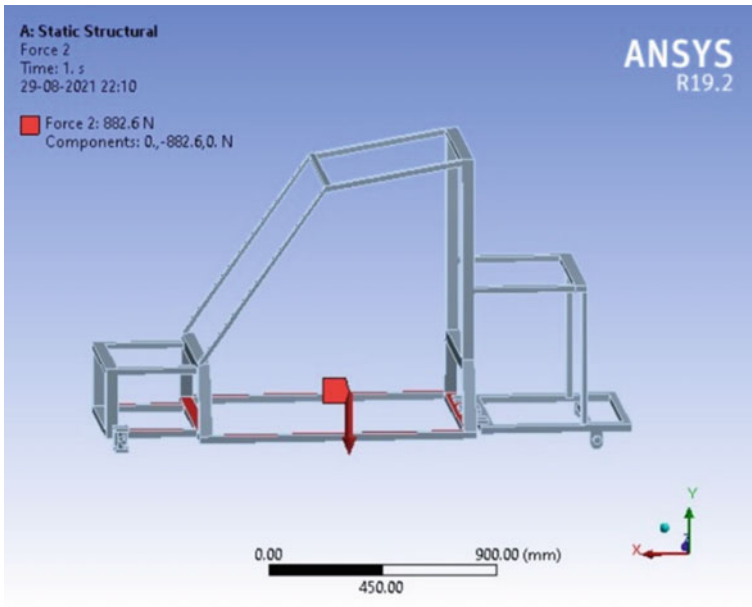
Fig.11 ANSYS analysis of the vehicle components are loaded at center

applied with the help of pressure gauge and pressure regulator, and velocities were measured using a digital speedometer. The following results were obtained when the vehicle was tested with varying pressure and velocities. The results obtained from the compressed air engine in the test run are shown in Table 1.

From the table, it is evident that the pressure applied from the cylinder is directly proportional to the velocity of the vehicle, and Fig. 13 is plotted.
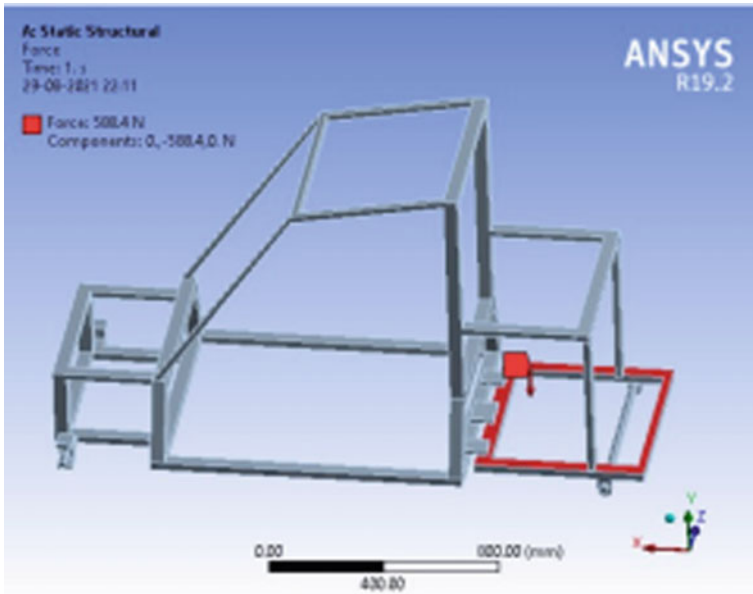
Fig. 12 ANSYS analysis of the vehicle components are loaded at rear

	S. No	Pressure (Bar)	Velocity (km/h)
Table 1 Results obtained from the compressed air engine in the test run	1	5.5	0
	2	6	2
	3	6.5	8
	4	7	9.6
	5	7.5	13
	6	8	17

Fig. 13 Cylinder pressure versus vehicle velocity proportionality
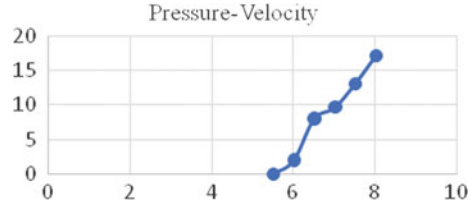
The electrical-driven part powered by the battery has a power backup of 8 h and top speed of about 50 km/h and a load pulling capacity of 350 kgs. Battery has a three-way charging system consisting of a power port and solar-powered charging when remained intact, and a dynamo is used to charge when the vehicle is in motion.

7 Conclusion

In the project of design and fabrication of electro-pneumatic hybrid vehicle, tests and analysis were performed, and the concurrent data have been depicted. The design and analysis of the vehicle frame and cam were performed with the help of Solidworks and ANSYS.

- The initial design of the frame failed when the main components such as engine and motor were assembled at the rear end of the vehicle.
- Post-work design was then commenced after the correction of frame for the establishment of vehicle load distribution.
- The pressure tank can't be refilled while the vehicle is in motion due to unavailability of necessary equipment.
- By using a high pressure and increased volume cylinder, the run time and velocity can be improved.
- By establishing battery-charging ports in various locations can help the vehicle charge in both pneumatic and electrical part.

References

1. Rynbrandt, J.D.: Electrical car and roadway system, patent number-4476947 (1984)
2. Tajima, F.: Permanent rotating electric machine and electric car, patent number-5419406 (1995)
3. Zhang, J.: Electric car charging systems, patent number-7768229 B2 (2010)
4. Thipse, S.S.: Compressed air car, tech monitor (2008)
5. Hasebe, M.: Drive mechanism for electric car, patent number-5396968 (1995)
6. Barth, W.: Method of and means for driving a pneumatic engine, patent number-537541766
7. Kawamoto, M.: Drive system for electric car, patent number-5419406
8. Jose, R.B.: Compressed air driven vehicle, patent number-1932698 (1933)
9. Viteri, F.: Clean air engines for transportation and other power applications, patent number-6247316 B1 (2001)

10. Brown, R.R.: Compressed air engine, patent number-3765180 (1973)
11. Figenbaum, E.: Perspectives on Norway's supercharged electric vehicle policy. Environ. Innov. Societal Transitions **25**, 14–34 (2017)
12. Song, K., Wang, X., Li, F., Sorrentino, M., Zheng, B.: Pontryagin's minimum principle-based real-time energy management strategy for fuel cell hybrid electric vehicle considering both fuel economy and power source durability. Energy **205**, 118064 (2020)
13. Mourad, M., Mahmoud, K.R.M.: Performance investigation of passenger vehicle fueled by propanol/gasoline blend according to a city driving cycle. Energy **149**, 741–749 (2018)
14. Wang, Z., Zhang, J., Liu, P., Qu, C., Li, X.: Driving cycle construction for electric vehicles based on Markov chain and Monte Carlo method: a case study in Beijing. Energy Procedia **158**, 2494–2499 (2019)
15. Fang, Y., Lu, Y., Roskilly, A.P., Yu, X.: A review of compressed air energy systems in vehicle transport. Energy Strategy Rev. **33**, 100583 (2021)

Generic Classification and Automatic Extraction of Mechanical Interlocking Features from CAD Model

Shantanu Kumar Das

1 Introduction

Mechanical interlocking feature has wide application in aircraft, defense, construction, furniture, and automotive industry [1–3]. Mechanical interlocking features (MIFs) are now receiving increased attention for its advantages like, low cost, easily disassemble, and ability to join dissimilar material with no change in its microstructure and generation of lightweight product as compared to other joining processes like welding and adhesive bonding process [3]. Different forms like liaison [4], connection interface [5], and joint design type [6] are used in different literatures to study assembly features in disassembly sequence generation [7], assembly planning [8], collaborative product design [6], etc. The features associated with the welding, riveting, and gluing processes are mostly addressed in the literature [4, 6, 9]. Therefore, there is a need to extract the MIFs for various assembly design and its process planning application [10].

Over the last few decades, several assembly features have been studied [4, 6, 9]. In most literatures, the relation between components is taken for the representation of assembly features to solve design problems [11]. Van Holland and Bronsvoort [8] addressed few elementary and compound MIFs in very abstract level without any proper representation to capture the MIFs. Popescu and Iacobs [5] used the connection features for disassembly planning which includes some MIFs like rib-slot, T-shape, rectangular, and pin-hole connection. The joint information of these MIFs are used as input data for determination of valid escape directions. In most of the literature, the MIFs are explicitly represented where connection type is already known to the designer. Several methods have been used to extract MIFs from CAD model [4, 12–14]. The tongue and groove elementary MIFs are extracted by using

S. K. Das (✉)
Ajeenkya DY Patil University, Pune, Maharashtra, India
e-mail: shantanuds0206@gmail.com
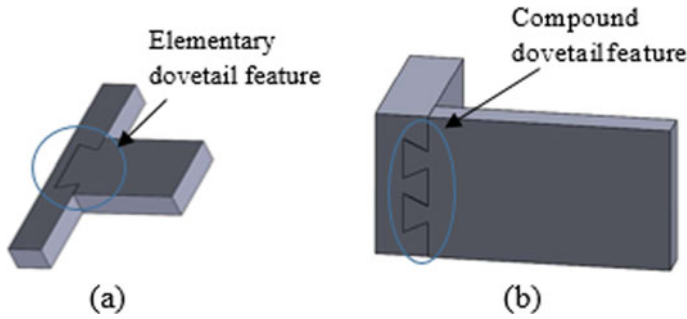
Fig. 1 **a** Elementary MIF **b** Compound MIF

graph-based algorithm by matching the features with a user-defined feature library [13, 14]. Das et al. [9] developed algorithms to extract adhesively bonded assembly features from CAD model which can be extended with addition of some algorithms to extract MIFs. As a result, a new modified algorithm is developed to automatically retrieve MIFs from the CAD template. The MIFs are classified into three types (i) Rigid (ii) Elastic (iii) Plastic. In this paper, the static complete rigid MIFs are addressed. The static complete rigid MIFs are classified as below:

i. Elementary MIF: The commonly used mechanical interlocking features generated due to involvement between two form features (e.g., plain dovetail) exist on the components' surface called elementary MIF as shown in Fig. 1a.
ii. Compound MIF: The combination of more than one elementary MIF [8, 14] as shown in the Fig. 1b is called compound MIF. The extraction of compound mechanical interlocking features is rarely studied in the literature.

MIFs systematic classification and automatic retrieval contribute to better integration of design information with the planning of the assembly process. The main aim of the paper is the automatic extraction of mechanical interlocking features as this information is neither explicitly available in the part model nor in the assembly model. This paper's contributions to this goal include the following (i) Definition of elementary and compound MIFs as a typical arrangement of joint surface (ii) Generic classification of MIFs (iii) Automatic identification of both elementary and compound MIFs by developing several algorithms.

The remainder of the paper is set out as follows. The various studies pertained to proposed work are reviewed in Sect. 2. A data structure is created for representation and classification mechanical interlocking features in Sect. 3 using various attributes. The automatic identification of mechanical interlocking features with detail descriptions is defined in Sect. 4. In Sect. 5, the results of implementation along with its discussions are explained. The paper ends by discussing the proposed work and its various future applications in Sect. 6.

2   Literature Review

Extraction of mechanical interlocking feature (MIF) is rarely addressed in literature. There are many ways of representation of assembly feature have been defined in the literature, but very few researchers have tried to automatically identify some of the MIFs from the CAD model [4, 9]. The literature related to MIFs representation and its extraction is studied in this section.

2.1   Representation of MIFs

In literature, the region of parts of assembly components and the associated geometric and non-geometric information which has significance in an assembly activity is defined as an assembly feature. In most of the literature, assembly features are represented using different forms like liaison [4] and connection interface [5]. Also, these assembly features are represented for different joining processes like riveting, welding, and gluing [4, 9]. But, the representation of mechanical interlocking features is very rare. Popescu and Iacob [5] proposed unit ball mobility operator concept and used the connection interface for disassembly sequences generation which includes some MIFs like rib-slot, T-shape, rectangular, and pin-hole connection. The valid escape directions are determined from the interface information of these MIFs. Van Holland and Bronsvoort [8] developed a product model using connection features includes some MIFs like dovetail, compound tongue, and groove feature. The connection feature class in this product model stores and retrieves information for a particular joint where the joint design type is already known. Shyamsundar and Gadh [15] used the assembly feature relational graph for the representation of assembly features and relation between the assembly features. The assembly features are categorized into form and relational assembly features. The form assembly features define the common shape features between the two form features of components which include some MIFs like peg and hole and lack the details information about the interface. Further, this representation is used to perform real-time modification of product components during collaborative product design. However, these connection types are not explicitly existing in the CAD model.

Hamidullah et al. [16] classified the assembly features into fit, against; single, multiple; soft, hard, composite and functioning, interlocking type using the concept of assembly intents like mating relations, assembly operation, position, and orientation of feature or degree of freedom. Chan et al. [17] developed a method to automatically generate the assembly feature by splitting of a single solid model and also classified these assembly features into elementary, compound type and positioning, interlocking type based on the complexity, and degree of freedom of connecting feature, respectively. The literatures provide very few information about MIFs, and in most of the cases, the MIFs are explicitly defined.

2.2   Extraction of MIFs

Graph-based method has recently evolved for the extraction of MIFs in the literature. Vemulapalli et al. [14] developed a framework for identifying certain MIFs, such as tab and slots, from the user-defined feature library using multi-graph matching algorithm from a STEP file. Xiao et al. [13] used the improved subgraph isomorphism algorithm for the identification of MIFs like tongue and groove and dovetail. However, the major disadvantage of these graph matching techniques of feature recognition is high computational complexity in case of complex assembly and not applicable to features that only differ geometrically. Swain et al. [4] automatically extracted different basic liaison like lap, butt, corner, t-joint, and edge joint from the CAD assembly model useful for riveting, welding, and gluing purpose. Das et al. [9] extracted various adhesively bonded assembly features from CAD model where algorithms are developed to extract the joint feature. But, algorithms for capturing the interlocking joint features are not addressed in this paper.

Most of the assembly features available in the literature are applicable to riveting, welding, and adhesive bonding purpose. It is concluded from the extensive literature survey that various representations exist are not directly capable to capture MIFs required for different product design applications.

3   Mechanical Interlocking Features

The mechanical interlocking features are categorized and represented in terms of number of joint surfaces exist in particular joint feature and the adjacency relationships exist between joint surfaces. The definitions and classification of these MIFs attributes are defined below.

3.1   Terminology

In order to capture the MIFs, various attributes like contact faces (shown in Fig. 2a), joint surface [number and its types (shape and topology)], joint feature (shown in Fig. 2c), and Euler angle are required. The definitions of some of these attributes are defined already by Das et al. [9], and its diagrammatic representations are shown in Fig. 2 to capture MIFs.

Joint surface: Common surface generated due to overlapping between two contact faces is called joint surface as shown in Fig. 2b.

Euler angle: Maximum value of angle between the unit normal of the all joint surfaces of a joint feature is called as Euler angle of a respective joint feature as shown in Fig. 2d.
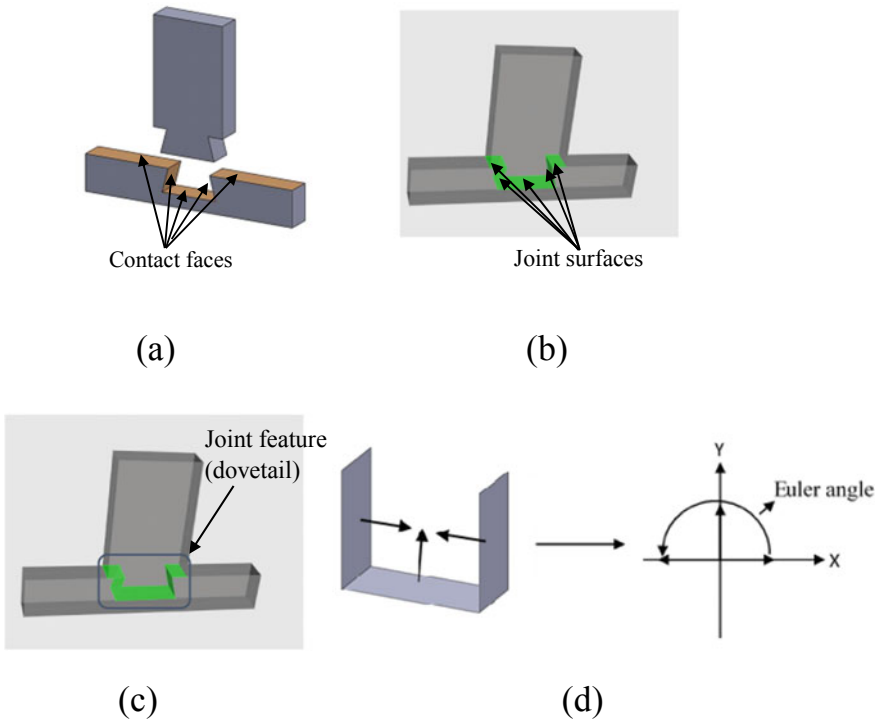
Fig. 2 Pictorial representation of MIFs attributes

3.2 Classification of Joint Surfaces

The joint surfaces in each part that creates the MIF are categorized based on two concepts like topology and shape. The joint surfaces are classified based on their shape into several types (i) Planar surface (PS) (ii) Cylindrical surfaces (CSs) (iii) Conical (CC) and (iv) Spherical (SC) surfaces. In this paper, the topology representing a cylinder or cone or sphere is taken as two half-cylindrical or conical or spherical faces. The classification of joint surfaces based on their topology is defined as follows:

(i) Common base surface (CBS) and (ii) Wall surfaces (WSs): The joint surface, the edges of which are at least connected to the edges of two joint surfaces, is referred to as CBS, and the adjacent joint surfaces connected to the CBS are considered as WS.

(iii) Distant joint surfaces (DJSs): Distant joint surfaces are the joint surfaces which don't share a common edge. Further, these non-adjacent joint surfaces are classified onto two sub types: Directional blocking joint surfaces (DBJSs) and directional-free joint surfaces (DFJSs).

The surface of the non-contiguous joint is swept into space in a specified direction with other surfaces, and its collision is verified. If there is collision, both are called

directional blocked joint surfaces (DBJSs). If there is no collision, then both are called directional-free joint surfaces (DFJSs). If it collides with more than one non-coplanar surface along the normal, then the surface of the joint is referred to as repeated directional blocked joint surfaces (RDBJSs), otherwise it is called as single-directional blocked joint surfaces (SDBFSs). Again, the above each DBJS and each DFJS are classified as two types depending upon the angle between them. If the DBJS is parallel, then they are called parallel directional blocking joint surfaces (PDBJSs), otherwise they are inclined directional blocking joint surfaces (IDBJS). Similarly, the DFJS surfaces are classified into PDFJS and IDFJS types.

3.3 Interlocking Feature

A joint feature is said to be an interlocking feature based on the classification of joint surfaces and various attributes defined above. The following condition should be satisfied for capturing the interlocking feature:

(i)   The root gap between the contact faces of two opposite part should be zero.
(ii)   Check if all the surfaces of a joint feature are planar or not.
(iii)   If planar and number of joint surface greater than equal to three, then check whether both DBJS and CBS exist in a joint feature.
(iv)   If both exist, then the joint feature is an interlocking feature.
(v)   Else if one or more joint surfaces are cylindrical or conical or spherical, then the degree of freedom is one (either in *x* or *y* or *z* direction), so the joint feature is an interlocking feature.
(vi)   If number of joint surfaces is equal to two and type of surface is planar, then find the Euler angle of the joint feature.
(vii)   If Euler angle is greater than 180°, then the joint feature is an interlocking feature.
(viii) If one or more joint surfaces are cylindrical or conical or spherical and number of joint surface is less then equal to two, then find the Euler angle of the joint feature.
(ix)   If Euler angle is equal to 0° or 90°, then the joint feature is an interlocking feature.
(x)   Before classification of MIFs, the joint feature needs to check whether the feature is an interlocking type or not. Then, the MIFs classified using the attributes described in Sect. 3.2 and its detail taxonomy is defined below.

3.4 Classification of MIFs

MIFs generic taxonomies are defined with basic parameters such as Euler angle, number, and types of joint surfaces and its different characteristics after checking

Table 1 Classification of elementary MIFs (open)

Interlocking feature	Illustrative example	Euler angle (E)	Joint surface(JS)	Characteristics
Plain tongue and groove		180°	3 < JS < 5	OPWS, PDBJS = 1, SDBJS
Tapered tongue and groove		<180°	3 < JS < 5	OPWS, IDBJS = 1, SDBJS
Dovetail		>180°	3 < JS < 5	OPWS, IDBJS = 1, SDBJS
Cylindrical tongue and groove		180°	3 < JS < 5	OPWS,CS, PDBJS = 1, SDBJS
U tongue and groove		0°	3	OPWS, CS, PDBJS = 0
T-slot		180°	7	OPWS, PDBJS = 4, SDBJS
Dovetailed step		>180°	2	OPWS
			3 ≤ JS ≤ 4	OPWS, IDBJS = 0

if the joint feature is an interlocking feature or not. This generic MIFs are further classified into elementary and compound MIFs as described below.

3.4.1 Classification of Elementary MIFs

3.4.2 Classification of Compound MIFs

The compound joint features are evolved due to the combination of more than one elementary feature. The compound features which are in a pattern are called sequential compound MIFs, and those are having feature with in a feature are called mixed

Table 2 Classification of elementary MIFs (closed)

Interlocking feature	Illustrative example	Euler angle (E)	Joint surface(JS)	Characteristics
Plain tongue and groove		180°	5 ≤ JS ≤ 9	CWS, PDBJS = 2, IDBJS = 0, SDBJS
Tapered tongue and groove		180°	5 ≤ JS ≤ 9	CWS, IDBJS ≤ 2, PDBJS ≤ 1
Dovetailed step		180°	3 ≤ JS ≤ 8	CWS, IDBJS ≤ 2, PDBJS ≤ 1
Cylindrical tongue and groove		180°	3	CWS, CS
			4	CWS, CS, PDFJS = 1

compound MIFs. The MIFs attributes like Euler angle of joint feature, joint surface types, and its characteristics help in classification of compound joint features. Both sequential and mixed compound MIFs are further categorized into open or closed type, and classification of mixed compound MIFs (closed) is given in Table 3 with some illustrative example.

The elementary and compound MIFs are classified based on the MIFs attributes defined above, and its extraction procedure is defined in the below section.

4   Extraction of MIFs

The extraction of MIFs is shown in Fig. 3 as a flowchart, and the detail procedures are defined in the below steps:

Step 1:   The STEP file of the assembly CAD model is used in the visual studio platform along with open-cascade geometric library [18] to get the various geometric information. The root parts are determined by calculating the distance between the components between which the MIF exist using the extracted geometric information which is always zero.

Table 3 Classification of mixed compound MIFs (closed)

Interlocking feature	Illustrative example	Euler angle (E)	Joint surface(JS)	Characteristics
Compound plain tongue and groove		180°	≥9	CWS, PDBJS > 2, IDBJS = 0, SDBJS
Compound cylindrical tongue and groove		180°	≥5	CWS, CS, PDFJS = 1, PDBJS = 0, SDBJS
Mixed cylindrical tongue and groove		180°	≥7	CWS, CS, PDBJS ≥ 2, IDBJS = 0, SDBJS
Compound tapered tongue and groove		180°	≥8	CWS, IDBJS ≥ 2, PDBJS = 1, SDBJS
Mixed planar tongue and groove		180°	≥8	CWS, IDBJS = 1, PDBJS = 2, SDBJS
Stepped tongue and groove		180°	≥8	CWS, IDBJS = 0, PDBJS = 2, SDBJS

Step 2: In this step, the contact faces and joint surfaces involved at the joint location are determined as shown in Fig. 3, and detailed procedure for extraction is adopted by Das et al. [9].

Step 3: A joint feature is said to be an interlocking feature if it obeys the various conditions as defined in the Sect. 3.2. After getting the interlocking feature, its various classifications are done based on the various characteristics of joint surfaces like joint surface types and Euler angle of a joint feature to capture both elementary and compound MIFs. The distant joint surfaces types like PDBJS, IDBJS, PDFJS, IDFJS, SDBJS, and RDBJS are identified by displacing the joint surface along the normal, and the collision with the other surfaces is verified as described in Sect. 3.2.

Step 4: The Euler angle is retrieved using the pseudo-code specified in algorithm 1. The number of joint surface, its different types, and Euler angle help in extracting the both elementary and compound MIFs.
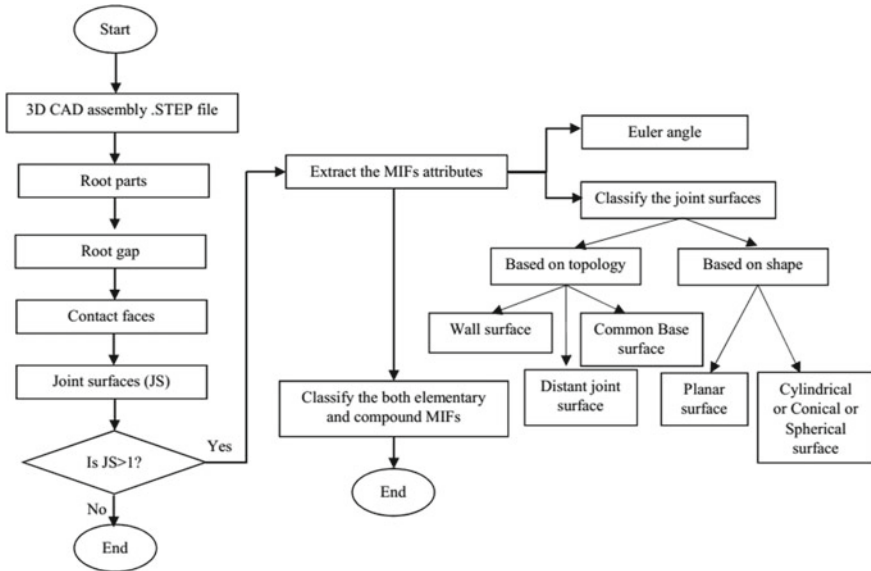
Fig. 3 Flowchart for the extraction of MIF

5   Results of Implementation and its Details

A hornet of an unmanned aerial vehicle is used as an industrial CAD assembly model to validate the proposed work. Using the Microsoft Visual Studio platform, the mechanical interlocking features are extracted using an open-cascade 3D geometric kernel.

Figure 4 shows a hornet of an unmanned aerial vehicle which carry nine parts. In Figs. 4 and 5, the extracted various MIFs types and their relevant attributes are shown, and the accompanying text window gives details about the various assembly features information required for extracting the MIFs by the program.

5.1   Discussions

MIFs are used frequently in various lightweight product due to its low cost as compared to riveting, welding and adhesive bonding, and also helpful for disassembly. In literature, various joining features have been extracted which are especially useful for adhesive bonding, riveting, and welding process [4, 9]. Although few studies about MIF are available [8, 9, 12, 14], however, they are limited to few elementary MIFs having one joint surfaces. Also, compound MIFs [8, 9] are rarely addressed. In most of the cases, the MIFs are explicitly represented having little assembly feature information. The proposed method is able to identify mechanical
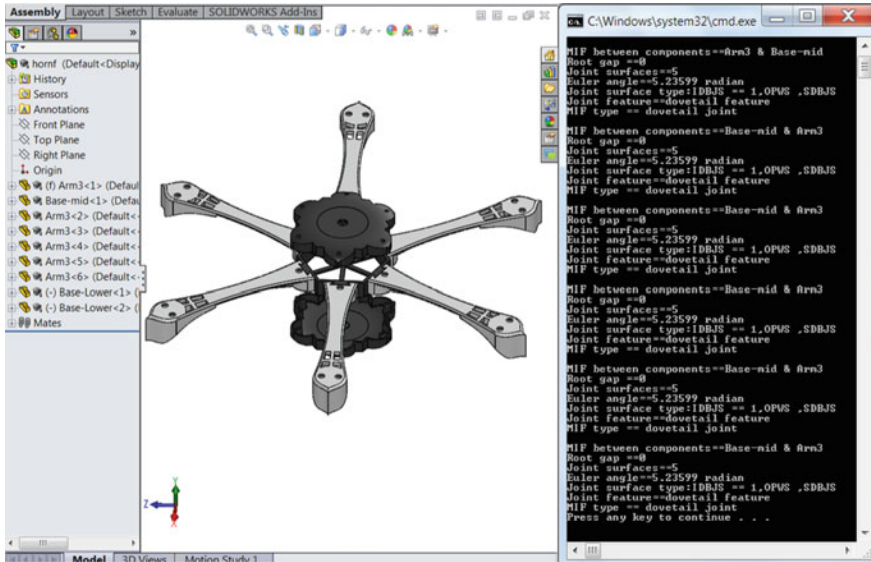
Fig. 4 Extraction of MIFs from hornet of an unmanned aerial vehicle (UAV)
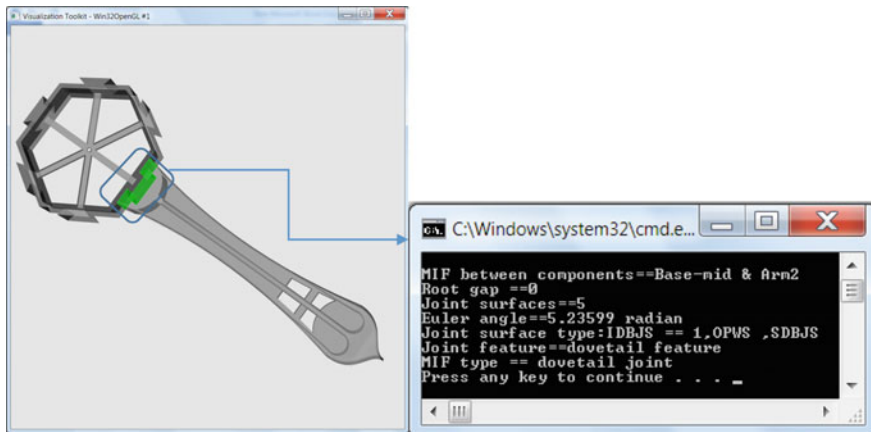
Fig. 5 MIF between base-mid and arm2

interlocking features as characteristics composition of joint surfaces, the Euler angle by checking the existence of interlocking feature as shown in the result. Earlier in the literature, graph-based technique [13, 14] is used for the extraction of few elementary MIFs.

Algorithm 1 Determination of Euler angle

Input: Parts Pi, Pj
Output: Euler angle (E)

---

1. *J ← Jointsurface(Pi,Pj)*
1. *For each surface J ∈ (Pi,Pj)*
2. *Surface-list(SL)=surfaces ← J ∈ (Pi,Pj)*
3. *End for*
4. *For each surface S_i ∈ SL*
5.   *For each surface S_{i+1} ∈ SL*
6.   *Ang=FaceNormal(S_i).Angle (FaceNormal(S_{i+1})*
7.   *Angle-list(AL)=angles ← Ang(S_i, S_{i+1})*
8. *End for*
9. *End for*
10. *If (AL.Size( )!=0)*
11. *E ← AL[0]*
12.   *For each angle Ang ∈ AL*
13.   *If (Ang > E)*
14.   *E= Ang*
15.   *End if*
16.   *End for*
17. *Return E*
18. *End if*

This technique needs too much user input which increases the level of difficulty in complex assembly. Therefore, an extended algorithm is developed to extract the MIFs. The extracted MIFs convey various information associated to mechanical interlocking joints. These interlocking feature information are helpful for deciding the process planner to select whether further any joining process is required or not depending upon the strength of the joint. So, this extraction of MIFs also helpful in assembly process planning of variant product design [19] where there are variations in the liaison information due to change in the joint design [20].

6   Conclusions and Future Work

An extended data structure for capturing the mechanical interlocking features (MIFs) from CAD has been developed in this research. The proposed algorithms are capable to capture both elementary and compound MIFs. These algorithms rely on geometrical and topological information extracted from the root parts. A new classification of MIF is developed by capturing the existence of interlocking feature, Euler angle, and various joint surface types. In order to validate the proposed algorithm, industrial CAD assembly model is used for implementation. The proposed work can be extended to capture the MIFs involved between free-form features.

References

1. Fischbach, C.W., Zaeh, M.F., Hottner, S.C., Hornung, J., Voit, M.: Development, analysis, and validation of an economically efficient process chain for a rigid CFRP plate assembly using finger joints. Proc. CIRP **66**, 227–232 (2017)
2. Fu, C.W., Song, P., Yan, X., Yang, L.W., Jayaraman, P.K., Cohen-Or, D.: Computational interlocking furniture assembly. ACM Trans. Graphics (TOG) **34**(4), 91 (2015)
3. Messler, R.W.: Integral Mechanical Attachment: A Resurgence of the Oldest Method of Joining. Butterworth-Heinemann (2011)
4. Swain, A.K., Sen, D., Gurumoorthy, B.: Extended liaison as an interface between product and process model in assembly. Robot. Comput.-Integr. Manuf. **30**(5), 527–545 (2014)
5. Popescu, D., Iacob, R.: Disassembly method based on connection interface and mobility operator concepts. Int. J. Adv. Manuf. Technol. **69**(5–8), 1511–1525 (2013)
6. Kim, K.Y., Yang, H., Kim, D.W.: Mereotopological assembly joint information representation for collaborative product design. Robot. Comput.-Integr. Manuf. **24**(6), 744–754 (2008)
7. Mandolini, M., Favi, C., Germani, M., Marconi, M.: Time-based disassembly method: how to assess the best disassembly sequence and time of target components in complex products. Int. J. Adv. Manuf. Technol. 1–22 (2017)
8. Van Holland, W., Bronsvoort, W.F.: Assembly features in modeling and planning. Robot. Comput.-Integr. Manuf. **16**(4), 277–294 (2000)
9. Das, S.K., Swain, A.K.: Classification, representation and automatic extraction of adhesively bonded assembly features. Assem. Autom. **39**(4), 607–623 (2019)
10. Das, S.K., Swain, A.K.: An ontology based framework for decision support in assembly variant design. J. Comput. Inform. Sci. Eng. ASME Trans. **21**(2) (2020)
11. Deneux, D.: Introduction to assembly features: an illustrated synthesis methodology. J. Intell. Manuf. **10**(1), 29–39 (1999)
12. Song, P., Fu, C.W., Jin, Y., Xu, H., Liu, L., Heng, P.A., Cohen-Or, D.: Reconfigurable interlocking furniture. ACM Trans. Graph. (TOG) **36**(6), 174 (2017)
13. Xiao, H., Li, Y., Yu, J.F., Cheng, H.: Dynamic assembly simplification for virtual assembly process of complex product. Assem. Autom. **34**(1), 1–15 (2014)
14. Vemulapalli, P., Mohan, P., Shah, J.J., Davidson, J.K.: User defined assembly features and pattern recognition from step AP203. In: ASME 2014 International Design Engineering Technical Conferences and Computers and Information in Engineering Conference (pp. V01AT02A067-V01AT02A067). American Society of Mechanical Engineers (2014)
15. Shyamsundar, N., Gadh, R.: Internet-based collaborative product design with assembly features and virtual design spaces. Comput. Aided Des. **33**(9), 637–651 (2001)
16. Hamidullah, E.B., Irfan, M.A.: Assembly features: definition, classification, and instantiation. In: International Conference on Emerging Technologies, 2006. ICET'06, pp. 617–623. IEEE (2006)
17. Chan, C.K., Tan, S.T.: Generating assembly features onto split solid models. Comput. Aided Des. **35**(14), 1315–1336 (2003)
18. Open CASCADE Technology. http://www.opencascade.org
19. Das, S.K., Swain, A.K.: Knowledge-based application of liaison for variant design. In: IFIP International Conference on Product Lifecycle Management, pp. 365–374. Springer, Cham (2016)
20. Woo, T.C., Dutta, D.: Automatic disassembly and total ordering in three dimensions. J. Eng. Ind. **113**(2), 207–213 (1991)

Design and Fabrication of Vehicle Rollover Prevention by Counter Steering Mechanism

S. Deepankumar, C. Jegadheesan, S. Sathiskumar, N. Boopalan, N. Praveenkumar, and S. Arulkumar

1 Introduction

An account of rollovers, factors used during this challenge, and their varieties, the variable alternatives of the climate unit are referred to beneath. Any greater structural strengthening inside the roll cage might sooner or later boom the weight of the overall automobile [1]. The automobile rollovers unit is divided right into an aggregate of categories: tripped and untripped. Tripped rollovers unit due to forces from an accomplice outside item, the form of a curb, or a collision with every other automobile [2]. Untripped crashes unit the results of guidance input, speed, and friction with the bottom. Untripped rollovers arise as soon as cornering acting forces destabilized the automobile sector. As an automobile rounds an area, three acting forces act on it

---

S. Deepankumar (✉)
Department of Automobile Engineering, Bannari Amman Institute of Technology, Sathyamangalam 638401, India
e-mail: deepankumar@bitsathy.ac.in

C. Jegadheesan · S. Sathiskumar · N. Boopalan
Department of Automobile Engineering, Kongu Engineering College, Perundurai 638060, India
e-mail: cjegadheesan.auto@kongu.edu

S. Sathiskumar
e-mail: sathiskumar.auto@kongu.edu

N. Boopalan
e-mail: boopalan.auto@kongu.ac.in

N. Praveenkumar · S. Arulkumar
Department of Automobile Engineering, Dr. Mahalingam College of Engineering and Technology, Pollachi 638401, India
e-mail: praveen5speed@gmail.com

S. Arulkumar
e-mail: arulkumar@mcet.in

269

and tire forces, herbal phenomenon effects (the centrifugal pressure), and gravity [3]. The required forces from the tire push the automobile toward the center of the curve. This pressure acts at floor level, beneath the center of mass [4]. The pressure of inertia acts horizontally through the middle of the automobile of mass off from the center of the flip. This aggregate of forces builds the automobile to roll toward the surface of the curve. The pressure of the weight of the automobile acts downward through the center, the most, not unusual place reasonably tripped amendment occurs as soon as an automobile is slippery sideways, and at the same time the tires strike a curb, penetrate the tender floor, or a steady occasion occurs that finishes up at some point of an upward thrust in lateral pressure [5]. The physics sq. measures almost like cornering rollovers. Another reasonably tripped amendment occurs as a consequence of a collision with every other automobile or item. These arise as soon as the collision reasons the automobile to grow to be unstable, like as soon as a narrow item reasons one issue of the automobile to boost up upwards, but now no longer the choice [6].

Turned-down railing end sections are proven to try and strive for this. An issue effect will boost up an automobile sideways. The tires face up to the amendment, and at the same time, the coupled forces rotate the automobile [7]. Crash assessments confirmed that lightweight vehicles had been vulnerable to rolling over as soon as colliding with certain early varieties of the manual rail. Factors vessel than 30 third (one vertical unit upward thrust or fall in line with three horizontal units) unit declared as "critical slopes" because of which may also motive maximum automobiles to various and might place alongside arise as an automobile crosses a ditch or slope [8]. Slopes overturn. An automobile may also roll over for numerous reasons, like as soon as touching an accomplice's outsize impediment with one in every one of its wheels or as soon as maneuvering over an accomplice's choppy tract. All automobiles unit is vulnerable to rollovers to several extents. Generally, amendment tendency will boom with the height of the center of mass, the narrowness of the shaft track, guidance sensitivity, and enlarged speed. The amendment threshold for non-public automobiles is over one g of lateral acceleration [8]. The Tesla Model S contains an unusually low amendment risk of 5.7% as a consequence of its low middle of mass. Lightweight vehicles can roll over at lateral accelerations of 1.2 g. commercial enterprise quarter vehicles can roll at lateral accelerations as little as 0.2 g. Trucks unit any probably to roll over than non-public automobiles because they on occasion have taller bodies and higher floor clearance [9–11]. This increases the center of mass. SUVs units are significantly vulnerable to amendment, significantly the ones geared up with long-journey cross suspensions. The enlarged suspension peak for enlarged clearance cross increases the center of mass. Amendment crashes unit appreciably lethal for the participants of an automobile as compared to frontal, facet, or rear crashes because, in historic character automobiles, the roof might be attending to crumble in toward the occupants and motive severe head injuries. The employment of roll cages in automobiles might construct them extravagantly safer, but, in maximum character automobiles, their use might cut product and character region maximum that their use isn't sensible [12]. The automobile that is temporary, narrow, and designed for use at the choppy track, is uncommon at some point of this it comes with a roll bar as historic instrumentation. The decline in high-satisfactory

of convertibles inside the U.S. become an element due to difficulty bearing on to loss of safety in amendment accidents, as a result, maximum convertibles don't have any safety at the maximum facet of the display frame [13, 14]. Some convertibles provide amendment safety exploitation an aggregate of sticking bowed bars at the back of the head rests. Some Mercedes-Benz convertibles have a retractile roll bar that deploys simply definitely in case of an accomplice accident. Race automobiles almost continuously have roll cages, because the game is extraordinarily probably to influence an amendment. To boot, the roll cages chassis-stiffening effect is normally visible as an income to the motorcar [15].

1.1 Arduino UNO

The Arduino could be an easy microcontroller used for academics and has an open offer digital platform for hardware and coding device shown in Fig. 1. The board is supplied with units of virtual and analog input/output (I/O) pins which can be interfaced to numerous increased forums (shields) and extraordinary circuits. The board has fourteen digital pins, analog pins, and is programmable with the Arduino IDE (Integrated Development Environment) through USB cable. It is going to be powered with the aid of using the USB cable or with the aid of using AN outside 9-V battery, even though it accepts voltages among seven and twenty volts [16].

A worldwide network of designers, artists, college students, programmers, hobbyists, and specialists has gotten this open delivery stage, their donations have extra as much as an outstanding number of sizable records which may be of large facilitation to novices and experts alike. It is composed of every microcontroller and a district of the code or Integrated Development setting (IDE) that runs for your PC, want to write & switch code to the bodily board. The platform of AN Arduino has grown to be extraordinarily wonderful with designers or college students starting with physics, and for a fabulous motive, indifference to the maximum in advance programmable circuit forums, the Arduino wouldn't really like a separate place of hardware accordingly on software a substitute code onto the board you'll use a USB cable. As well, the Arduino IDE makes use of a primary model of C++, growing it less complex to discover the software. At last, the Arduino board gives a typical type of problem that breaks out the features of the microcontroller into an extra provided bundle. The

Fig. 1 Arduino UNO

Arduino board has been used for growing fully extraordinary engineering comes and extraordinary applications. The Arduino code is highly easy to apply for novices, but flexible sufficient for superior customers. It runs Windows, is a working device bundle, and is waterproof. The lecturers and college students inside the faculties put it to use to style low-fee clinical gadgets to affirm the concepts of physics and chemistry. Their unit's numerous extraordinary microcontroller structures are available in the marketplace for bodily computing. The Arduino collectively makes the operative approach of a microcontroller, but it offers a few advantages over absolutely extraordinary structures for lecturers, college students, and novices. Arduino is AN yank normal code for records Interchange file physics area supported for hardware and code. You can inform your board what to try and to adapt and deal with causing a group of commands to microcontroller. For long time the Arduino board is used from normal gadgets to superior clinical gadgets. The Arduino board began out dynamically to conform to new requirements and differentiate it from easy 8-bit forums to final products for Internet of Thinking (IOT) applications, embedded environments, and 3-D printing [17].

Servo motors as shown among Fig. 2 unit nice devices which can communicate a nearby position. Normally, they are having servo arm that can flip 180°, victimization of the Arduino, It tends to be ready to tell information to a servo to travel a nearby position and it will reach there. Initially, the servo motor is used in the remote areas and their applications were transferred to RC cars to control the steering [18].

Figure 3 shows the Interfacing of servo motor and Arduino. The 1st motor that was connected to the Arduino, seven years ago, was a servo motor, unhappy moment over, back to work as a result of servo motors mistreatment feedback to work out the position of the shaft, you'll manage that position exactly. As a result, the servo motors unit is accustomed to management the position of objects, rotate objects, move legs, arms, or hands of robots, move sensors, and so forth with high preciseness. Servo motors unit size, and since they have inherent equipment to manage their movement [19].

Fig. 2 Servo motor
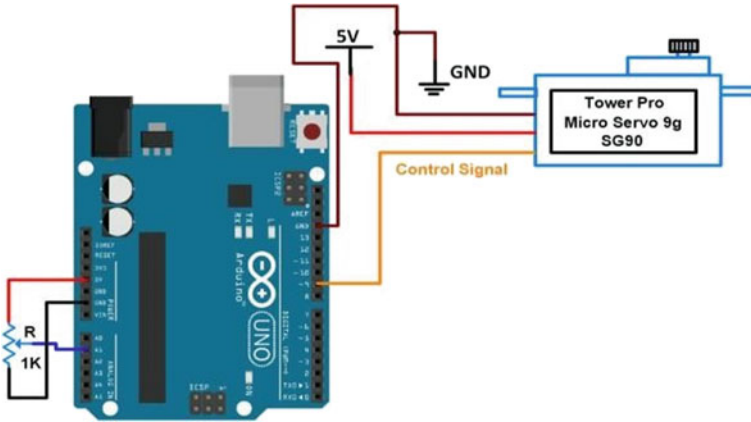
Fig. 3 Interfacing of Servo with Arduino UNO

2 Design and Fabrication

2.1 Design Process

The process sequence is described with the use of design layout shown in Fig. 4.

The steps which were followed for the execution of the project is given below as methodology. Collection and study of literature/patent of similar projects and identification of problem is done after which the mathematical modeling for rollover to occur and steering torque calculation is derived, then the development of working model layout and selection of microcontroller and sensor as per the requirement is completed. The study of patents gives a broad view of the concepts related to the
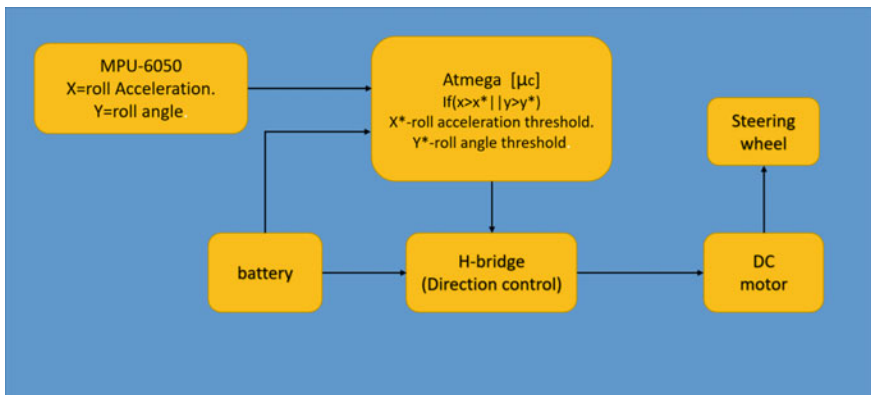
Fig. 4 Design layout

rollover prevention system and the similar methodologies adapted in order to prevent the rollover of the vehicles. From the patent study, a clear view on the problem is obtained which results in identification of single specific problem, after which the procedures need to be followed is sorted out. Mathematical modeling is done assuming the vehicle is in beginning of its rollover and taking moments and reaction forces with one wheel lifted off gives the clear condition for the rollover, the arrived equations are the threshold lateral acceleration and threshold roll angle. Coding is done using Arduino IDE software in which the deciding equations are coded and burned to the microcontroller in order to actuate the servomotor in a particular direction in accordance with the direction of the occurring rollover. Selection of servo motor is done based on the steering torque calculation. Prototype is made of sheet metal and toy car wheels and the components are assembled on board. Finally, generation of the program and the prototype testing is done [20].

2.2 Fabrication Process

A prototype is made with sheet metal and toy car wheels. The servomotor, sensor, and the Arduino are fixed onboard of the prototype shown in Fig. 5.

The connections are given to interface the sensor, LCD display, and the servomotor to the Arduino by using jumper wires and components are fixed on board to the
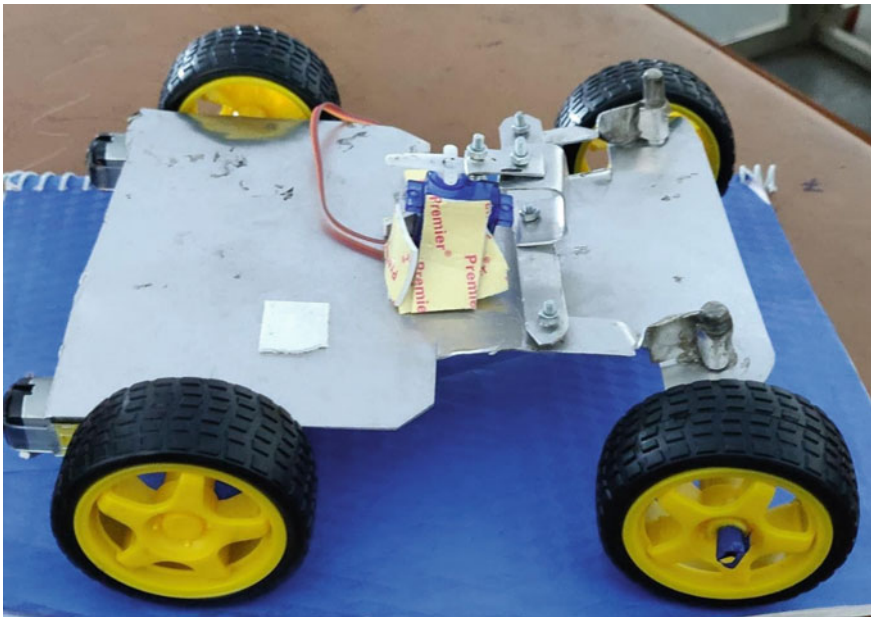
Fig. 5 Prototype model

prototype. The steering system is made with simple four-bar linkage made out of sheet metal and steel rods. The linkage is then connected to the servomotor [21].

3 Result and Discussion

The double lane modification maneuver at 80 kph was performed victimization the instrumented vehicle. For simulation, the steering angle input as shown in Fig. 6 was taken from the handwheel detector.

The double lane change maneuver at 80 kph was performed using the instrumented vehicle. For simulation, the steering angle input as shown in Fig. 7 was taken from the steering wheel sensor [22].

The roll angle result of the body and center of gravity in vehicle for the 1800 step steer take a glance at speed of 50 km per hour for passive system, Proportional, Integral, and Derivative control (PID) rejection loop without the roll moment and Proportional, Integral and Derivative control (PID) rejection loop with the roll moment is given in Fig. 7. As shown within Fig. 7, Proportional, Integral, and Derivative control (PID) roll moment without rejection loop reduces the body moving motion whereas Proportional, Integral, and Derivative control (PID) with the roll moment rejection loop drastically reduces the roll angle of the vehicle body. Reduced body leans throughout cornering decreases the tendency for amendment. The event of the roll
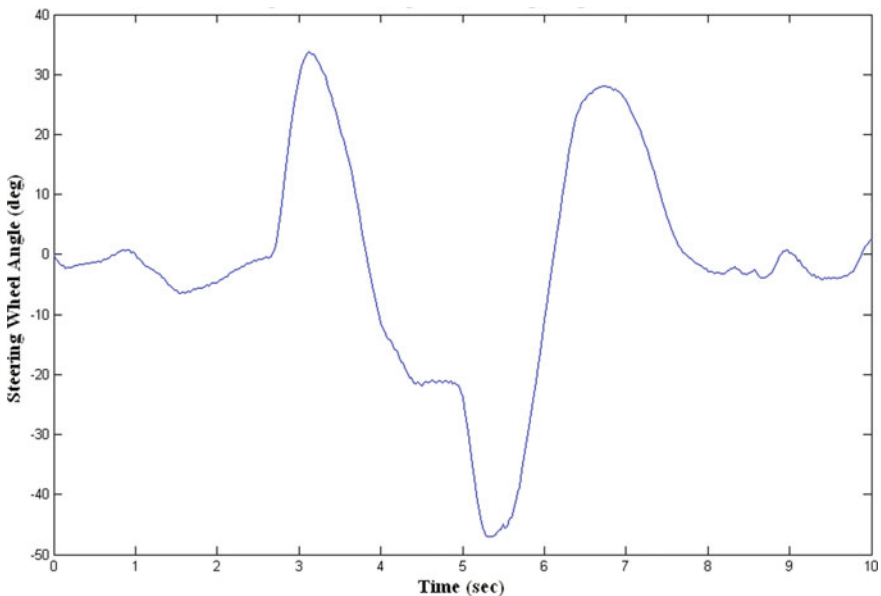
Fig. 6 Graph of steering wheel angle against time
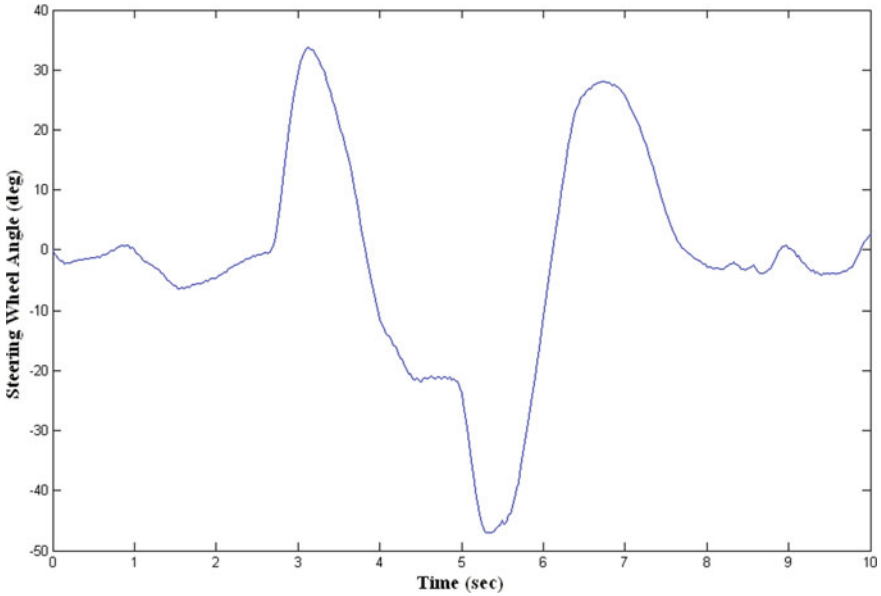
Fig. 7 Graph of steering wheel angle against time

motion additionally reduces the load transfer from the inner wheels to outer wheels and thus will increase the road holding throughout cornering [23].

For double lane modification maneuver, the handwheel angle input was taken from CarSimEd software at vehicle speed of 80 km/h. Figure 7 shows the roll rate result at the body and center of gravity in vehicle for the double lane modification check at a speed of 80 km/h for passive system, Proportional, Integral, and Derivative control (PID) roll moment without the rejection loop and Proportional, Integral and Derivative control (PID) with roll moment rejection loop. A double lane modification is usually utilized in avoiding obstacles in an emergency. As shown among Fig. 8, the inflammatory PID control without roll moment rejection loop shows slight improvement in roll rate response and PID control with roll moment rejection loop shows important improvement in reducing the roll rate response compared to passive system [24].

The impact of the active roll management in rising the roll rate and roll angle for step steer and double lane modification maneuvers were studied. For each 180° step steer check at 50 km/h and double lane modification check at 80 km/h, PID control with roll moment rejection loop shows terribly important improvement in terms of roll angle and roll rate responses and followed by PID control without roll moment rejection loop that shows slight improvement compared to passive vehicle. It is verified that the active roll management has the ability in reducing the roll motion of the vehicle and thence reduces the tendency to alter as shown the Fig. 9. ARC additionally reduces the load transfer throughout cornering thus improves the road holding to a lower place through steering input [25].
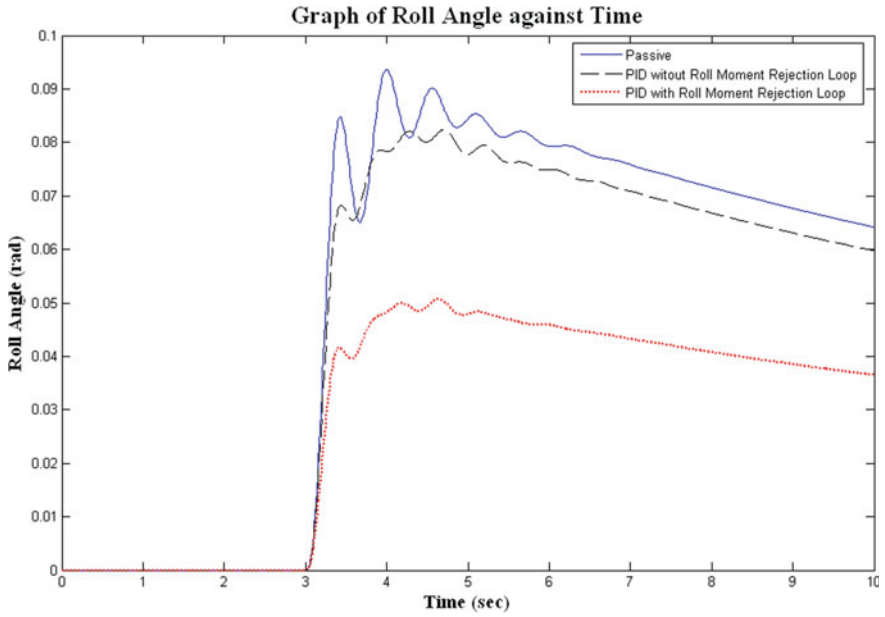
Fig. 8 Roll angle response for ARC performance during 1800 step steer test at 50 kph
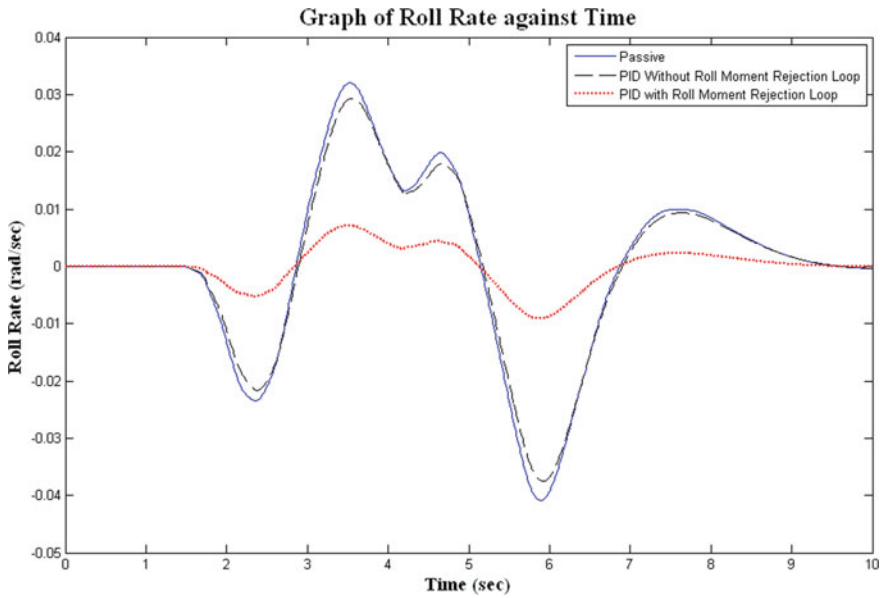
Fig. 9 Roll rate response for ARC performance during double lane change test at 80 kph

4 Conclusion

A prototype for a rollover prevention system using a counter steering mechanism was developed. The system successfully detects the roll angle when the vehicle is maneuvered aggressively during cornering or during a collision with an obstacle on the road and actuates the steering electronically when the roll angle reaches the threshold value and avoids the eventual rollover of the vehicle. Thus, the prototype was tested successfully and the following objectives are accomplished.

1. The roll angle was monitored by the 3-axis accelerometer.
2. The angle was read and processed successfully by the controller.
3. The roll angle was displayed by the LCD display.
4. The signal for stepper motor was sent corresponding to the direction of eventual rollover.
5. The stepper motor was actuated to steer the vehicle in the direction of rollover.

References

1. Ataei, M., Khajepour, A., Jeon, S.: Model predictive rollover prevention for steer-by- wire vehicles with a new rollover index (2018)
2. Zhao, W., Ji, L., Wang, C.: Control of integrated rollover prevention system based on improved lateral load transfer rate (2018)
3. Ghazali, M., Durali, M., Salarieh, H.: Vehicle trajectory challenge in predictive active steering rollover prevention (2017)
4. Chu, D., Lu, X.Y., Wu, C., Hu, Z., Zhong, M.: Smooth sliding mode control for vehicle rollover prevention using active antiroll suspension (2015)
5. Aripina, M.K., Samb, Y.M., Kumeresanb, A.D., Ismailc, M.F., Kemaodapril, P.: A review on integrated active steering and braking control for vehicle yaw stability system. Jurnal Teknologi **71**(2), 105–111 (2014)
6. De Novellis, L., et al.: Direct yaw moment control actuated through electric drivetrains and friction brakes (2014)
7. Lemmen, M., Eidam, D.U., Vliem, E., Wey, T., Jacobson, B.J.H., Hulten, J.: Roll stability control and rollover mitigation by steering (2013)
8. Naqvi, S.G.H.: the rollover prediction and prevention of bullet proof vehicles for improved stability. Life Sci. J. **10**(4s), 209–214 (2013)
9. Lee, M.., et al.: Modelling and control of an anti-lock brake and steering system for cooperativecontrol on split-mu surface. Int. J. Automot. Technol. (2012)
10. Yoon, J., Cho, W., Yi, K., Koo, B.: Unified chassis control for vehicle rollover prevention (2011)
11. Palkovics, L., Semsey, Á., Gerum, E.: Roll-over prevention system for commercial vehicles— additional sensorless function of the electronic brake system (2010)
12. Yoon, J.: Unified chassis control for vehicle rollover prevention. In: Proceedings of the 17th World Congress the International Federation of Automatic Control Seoul, Korea (2008)
13. Goodarzi, A., et al.: Automatic path control based on integrated steering and external yaw moment control. **222**(2), 189–200 (2008) (Article first published online: 30 June 2008; Issue published: 1 June 2008)
14. Elhefnawy, A.M., Sharaf, H.M., Ragheb, H.M., Hegazy, S.M.: Integrated vehicle chassis control based on direct yaw moment and active front steering (2005)

15. Rao, N.V.: An approach to rollover stability in vehicles using suspension relative position sensors and lateral acceleration sensors (2005)
16. Carlson, C.R., Gerdes, J.C.: Optimal rollover prevention with steer by wire and differential braking. In: Proceedings of ASME International Mechanical Engineering Congress and Exposition, Washington D.C. (2003)
17. Odenthal, D., Bun¨te, T., Ackermann, J.: Nonlinear steering and braking control for vehicle rollover avoidance. IEEE (2003). Print ISBN: 978-3-9524173-5-5
18. Deepankumar, S., Saravanan, B., Balaji, J., Gobinath, R.: Experimental investigation of performance and emission characteristics of diesel-bio diesel (CSOME)-ethanol-diethyl ether blends in CI engine. J. Therm. Energy Sys. **2**(3), 148–155
19. Rajamurugan, G., Deepankumar, S., Ramakrishnan, A., Krishnasamy, P., Dhanabalan, D.: Corrosion characteristics on friction stir welding of dissimilar AA2014/AA6061 alloy for automobile application, 2019-28-0063
20. Deepankumar, S., Boopathi, M., Balaji, J., Balachandran, S., Gobinath, R.: Experimental analysis of performance and emission characteristics of single cylinder direct injection diesel engine using algae as a biodiesel and barium oxide as a nano-fuel. Int. J. Mech. Prod. Eng. Res. Develop. (IJMPERD) **9**(1), 35–42
21. Deepankumar, S., Raja, T., Tamilselvan, A., Gobinath, R.: Enhancing the four stroke ci engine performance and reducing emission by preheating and oxidation process using biodiesel. Int. J. Mech. Prod. Eng. Res. Develop. (IJMPERD) **8**(7), 230–240
22. Deepankumar, S., Jegadheeswaran, S., Thangavel, R.: Experimental investigation on emission analysis of multi-cylinder direct injection diesel engine using manifold injection of ethanol. Int. J. Mech. Prod. Eng. Res. Develop. (IJMPERD) **8**(7), 704–710
23. Deepankumar, S., Gobinath, R, Balachandran, S., Boopathi, M.: Experimental investigation of performance and emission characteristics of diesel-bio diesel (CSOME) with nano additive blends in CI engine. Adv. Automob. Eng. **7**(176), 2
24. Deepankumar, S., Gobinath, R, Balachandran, S.: Experimental investigation of performance and emission characteristics of diesel-bio diesel (CSOME)-ethanol-diethyl ether blends in CI engine. J. Therm. Energy Sys. **2**(3), 148–155
25. Saravanan, B., Deepankumar, S., Praveen, S.M., Kumar, V.S., Vignesh, M.: Experimental exploration of a reflex leveler prototype using gyro sensor. Mater. Today Proc. **45**(2), 1280–1284 (2021). https://doi.org/10.1016/j.matpr.2020.05.018

Experimental Investigation Towards Enhancement of Catalytic Converter by Modifying the Elements of Honeycomb Section

B. Saravanan [ORCID]**, N. Natarajan, S. Deepankumar, S. Dhayaneethi, K. Vinithkumar, and S. B. Kumaragurubaran**

1 Introduction

The air pollution posed a serious threat to the health. Poor air quality raises the risk of diseases such as asthma and bronchitis, as well as the chance of cancer. Every year, 30,000 people die as a result of air pollution [1]. Private vehicles have become a major source of pollution. Nitrogen oxides (NO—a harmful gas), carbon monoxide (CO—a source for acid rain and smog), and hydrocarbons are the main contaminants (HC—a cause of smog). Recent vehicles are fortified with a component known as a catalytic converter to minimize air pollution.

A chemical component that minimizes depleted emissions by catalyzing an oxidation reaction that converts toxic particulate emissions to less hazardous pollutants is called catalytic converter.

Although it is a pollution control device, it has been used in the exhaust systems of vehicles and lean-burn engines, electronic power systems, naphtha heaters, manufacturing stoves, and heavy machinery [2]. Its use is directly dependent on specific government responses to environmental, or health and safety laws. Carbon monoxide (CO), oxygen (O_2), and other hydrocarbons (HC) are mixed in these converters producing water (H_2O) vapors and carbon dioxide (CO_2). Catalytic converters also reduce the oxides of nitrogen (NO_x).

B. Saravanan (✉) · S. Deepankumar · S. Dhayaneethi · K. Vinithkumar
Department of Automobile Engineering, Bannari Amman Institute of Technology, Sathyamangalam, Erode, India
e-mail: bsaravana2010@gmail.com

N. Natarajan
Department of Mechanical Engineering, Excel Engineering College, Komarapalayam, Namakkal, India

S. B. Kumaragurubaran
International Centre for Automotive Technology, Chennai, India

There are two types of catalytic converters.

- Two-way catalytic converter
- Three-way catalytic converter.

1.1 Advantages of Catalytic Converter

The approximate decrease in HC emission by 87% and NO_x emission by 62% for an entire span of an average vehicle is executed by the catalytic converter.

The aim of this project is to investigate alternative catalysts in order to improve catalytic converter emission conversion at the lowest cost. In catalytic converters, cerium (Ce), iron (Fe), manganese (Mn), and nickel (Ni) are also used. Modifications in the material of the catalyst used in a catalytic converter would be utilized to test emissions of different pollutants from a CI engine in this study. By undertaking these experiments, we will enhance engine performance by lowering pollutants like NO_x, CO, and HC, resulting in reduced air pollution than the current catalytic converter model.

The materials that replacing the noble are listed below

- Titanium dioxide (TiO_2).
- Cupric oxide (CuO).
- Calcium oxide (CaO).

The goal of this study was to eliminate NO_x, CO, and HC out of a diesel engine's exhaust gas. This was achieved by enabling exhaust gas to pass through a coated catalytic chamber with aluminum meshes layered in stacks coated with titanium dioxide, cupric oxide, and calcium oxide. The primary goal was to figure out how the catalytic converter performed, while the secondary goal was to see how the experiment's outcome and development comparison to earlier results. When compared to conventional catalytic converters, MCC is low cost, wide substrate area, and domestic availability that claims it be more competent in oxidizing/reducing pollutants.

2 Review of Literatures

The literature review has been done on the papers which is regarding to the exhaust gas emission using catalytic converter with different types of noble catalyst in accordance with their performance compared to the existing model of catalytic converter. So, the idea for the project work has been obtained by referring the different papers.

Warju et al. [3] analyzed the impact of a TiO_2-based metallic catalytic converter (MCC) in a four-stroke motorbike engine. When the TiO_2-based MCC is compared to traditional MCC Ph&Rh exhaust, it results in higher vehicle power and less fuel usage.

Shah et al. [1] implemented Cu_2O has been used in catalytic converters alongside noble metals like rhodium, palladium, and platinum, which resulted in a significant reduction in CO and HC emissions compared to the conventional system.

Reji et al. [4] evaluated the reduction of HC, CO, and NO_x pollution by means of exhaust gas recirculation (EGR) and catalytic converter; EGR has drastically reduced NO_x pollutants while the catalytic converter has reduced the level of HC and CO emissions.

Dey et al. [2] explored the reduction of carbon monoxide (CO) using a catalytic converter that uses the non-noble metal copper to substitute noble elements. CO oxidation is strongly controlled by the crystal size of catalysts and reduces as the crystallite size of the catalyst decreases. Increasing the temperature of the catalyzed reaction improves CO conversion rates unless the catalyst sinters.

Manojkumar et al. [5] have substituted the noble catalysts and tested the VCR engine under various loads. In comparison with the conventional catalytic converters, the catalytic converter having copper oxide characterizes both reduction and oxidation operations utilizing copper oxide only. Its major benefit over traditional catalytic converters is that the abundant obtainability of copper oxide and its cost-effectiveness, which eliminates the need for rare earth materials.

Hossain et al. [6] studied about reducing the amount of carbon oxides utilizing copper metal braced on titanium oxide nanotubes (TNT) catalysts was studied. In order to examine the activity of their proposed materials for ideal copper loading and ERC, the tests were made in home-made H-cell for the catalysts produced using 0.5 M Na-HCO_3 aqueous solution. Their improved oxidation stability, higher CO_2 adsorption capability, and stabilization of the reaction intermediate, layered titanates, are all factors.

Gadlegaonkar et al. [7] investigated the characteristics of the catalytic exchanger and engine efficiency after replacing noble catalysts with copper and modifying the catalytic converter architecture to lower backpressure in the engine without compromising engine efficiency. When alterations are made to the design, it allows the honeycomb to spread evenly and decreases backpressure while maintaining a consistent profile and enhancing the absorptive capacity of the honeycomb.

Atzl et al. [8] studied photocatalytic oxidizing, which includes using TiO_2 and UV light to convert NO_x to nitrates. The rates fluctuate immediately and are influenced by humidity levels, with a comparatively higher humidity indicating a improved adaptation. There was a notable change in irradiance likewise; when the brightness was raised, the conversion rate decreased.

Venkatesan et al. [9] developed a program that utilizes chemical reactions to reduce the intensity of harmful exhaust fumes to a more acceptable level. The noble catalyst is replaced by copper oxide in this system, which is installed in the engine exhaust. As an outcome, at 100% load, the highest reductions for HC, NO_x, and CO are 32%, 61%, and 21%, respectively.

Davis et al. [10] were studying the exhaust gas for the engine, investigated the effect of TiO_2 in lowering dangerous and poisonous gases and their effect on the environment. By studying the exhaust gas for the engine, they investigated the effect of TiO_2 in lowering dangerous and poisonous gases and their environmental impact.

Royer et al. [11] analyzed the catalytic reduction of carbon monoxide on metallic nanoparticles was investigated. It is necessary to catalyze CO oxidation in order to eliminate CO. The most active materials appear to be those comprising elements with very active single oxides (e.g., Cu and Co).

Kalam et al. [12] studied a novel catalytic converter for hydrocarbon engines that is built on catalyst materials that include metal-ions like cobalt oxide (CoO) and TiO_2 with a substrate of wire mesh. In comparison with the OEM catalytic converters, an estimation of decrease in CO and NO_x and increase in HC emissions was found in TiO_2/CoO-based catalytic converter.

Lanje et al. [13] copper oxide nanoparticles were synthesized and studied. CuO nanoparticles are made using copper acetate and NaOH in a fluid precipitation process. The rectangular morphology of CuO nanoparticles as synthesized was revealed by scanning electron microscopy (SEM). CuO nanoparticles as synthesized were 5–6 nm in size, according to electron microscopy (TEM).

Jang et al. [14] have studied the influence of size of particles, and elemental composition of TiO_2 nanoparticles on the characteristics of photocatalysts was investigated. The photocatalysts characteristics of TiO_2 nanoparticles, such as breakdown of methylene blue and bacteria and dissolution of ammonia gas, were studied in terms of anatase mass fraction and particle size.

Neeft et al. [15] have studied impact of interaction among catalyst and soot, as in the reactivity with a gas (oxygen) of a solid (soot) over another (the catalyst). The goal of their research was to test candidate catalysts for their activity in the oxidizing of soot in a systematic manner. CaO can also be converted to an assorted calcium oxide or calcium hydroxide or calcium carbonate, while PbO can be converted to a mixed oxide/carbonate. According to TGA mass loss, $CaCO_3$ is generated first by the reaction of CaO with soot deposits that decays at higher temperatures to CO or CO_2 and CaO.

3 Objective

The main objectives of our project are to understand the concept and working of catalytic converter and overcome the negative aspects. To determine pressure and velocity analysis of catalytic converter. To minimize the backpressure effect on the engine. To examine the value of the exhaust gases after changing the materials.

Fig. 1 Cut section of catalytic converter
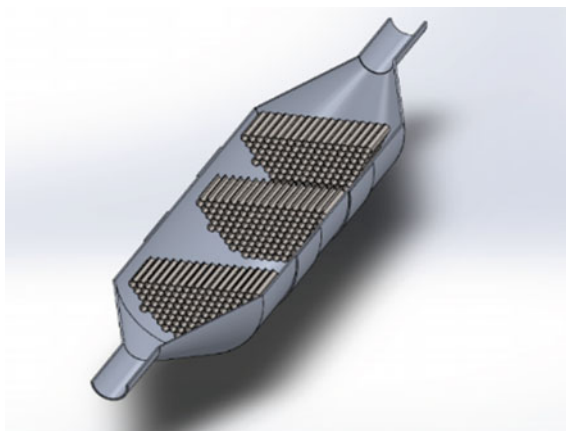
4 Experimental Setup

4.1 Designing of Catalytic Converter

The designing of catalytic converter for changing noble catalysts with nanocatalysts and reducing the backpressure has been made using SOLIDWORKS is shown in Fig. 1. The honeycomb section was replaced by using the aluminum meshes. For that, the aluminum baffle plates are cut into circular pieces in 4 in. diameter. The thirty set of coated aluminum baffle plates which are coated with TiO_2, CuO, and CaO, respectively, in the distance of 3 in.

4.2 Material Selection

The materials selected for the study of enhancement of catalytic converter are listed in Table 1.

Table 1 Materials selection

Materials selected	Purpose
Nanocatalysts	Titanium dioxide (TiO_2) Cupric oxide (CuO) Calcium oxide (CaO)
Insulator	Glass wool
Serpentine chamber/converter chamber	Aluminum wire mesh/baffle plate
Housing	PVC pipe

Fig. 2 Aluminum wire
mesh—substrate

4.3   Material Selection

4.3.1   Catalyst

Many standard solutions with diversified weight ratios and aqueous molar ratios were
made use in our work. CuO, TiO$_2$, and CaO were implemented as a catalyst of metal
oxide. The reducing agent was identified as CuO, while the oxidizing agents were
identified to be CaO and TiO$_2$. The inertness to form sulfate and properties of surface
that makes it favored transporter in chosen catalytic reduction reaction of CO, NO$_x$,
and from the still sources of pollution.

4.3.2   Substrate

Aluminum is the chosen material for substrate and is shown in Fig. 2. It is most widely
implemented in vehicle exhaust, because it has more advantages comparing other
metals and it also low-cost metal. The substrate to be used for the catalytic converter
must have high-physical properties and high-melting point. Aluminum is selected
for its betterment in its physical and chemical properties which has the melting point
of about 600 °C.

4.4   Substrate of Wire Mesh—Treatment

To remove all the impurities from the substrates of wire mesh, they were dipped for
half-an-hour into a dilute solution of 10% hydrochloric acid (HCl). Before drying at
100 °C in an oven, the substrates were rinsed in distilled water. It takes almost one
hour for the drying process before it is coated with the catalyst.

5 Nanocatalysts

Nanocatalysts aid in the scientific problem of catalysis in the field of nanotechnology. Exploration of efficient catalytic processes, particularly nanocatalysis, is one of the main areas for reaching this goal. Alternative activation methodologies, such as mechanochemical mixing, microwave and ultrasonic irradiation, and the use of nanocatalysts with magnetic cores, could all be part of the desired approach; environmentally friendly applications in catalysis could be best addressed via magnetically recoverable and recyclable nanocatalysts for oxidation reduction and condensation reaction.

In this study, a catalytic converter based on $TiO_2/CuO/CaO$ materials was created to oxidize, decrease, and absorb NO_x, HC, and CO emissions. As oxidizing catalysts, pure TiO_2 and CuO are employed, whereas CaO is used as a reducing catalyst.

5.1 Titanium Dioxide, Calcium Oxide, Copper Oxide

TiO_2, as a bulk substance, is a food additive. Small sized main particle may benefit TiO_2, and the percentage of TiO_2 produced in or near the nanorange is predicted to rise significantly. CaO nanoparticles are easier to work with than homogenous base catalysts. In this cyclization reaction, CaO nanoparticles are the most effective catalyst. The larger surface area of nanomaterials accounts for the improved catalytic activity of CaO nanoparticles over commercially accessible bulk CaO. Because of their surface characteristics, CaO nanoparticles have a highly effective catalytic activity. The nanoparticles of CuO are seen as product of high interest because of their efficacy in heat transfer applications a nanofluids. Recent reports have been made regarding the nano-chemical approach, one-step solid-state reaction method at ambient temperature, technique of sol–gel, pre-cursors thermal deposition, and co-implementation of oxygen ions and metal among others.

5.2 SEM Test of TiO_2, CaO, CuO

In the presence of UV light, a sample of the TiO_2 mixed paint coated tile was collected in a sample vial and sealed. The particles are rectangular in shape and range in size from 25 to 75 nm. In the sample bottle, a sample of the CaO coating mixture was collected and sealed. The particles in this sample are spherical in shape and have a size of 30–40 nm, according to the analysis. In the sample bottle, a sample of CuO coating mixture was collected and sealed. The SEM image of the materials used in metallic catalytic converter as shown in Fig. 3 demonstrates that the particles in this sample are rectangular in shape and have a size of 5–6 nm, according to the analysis.

(a) (b) (c)
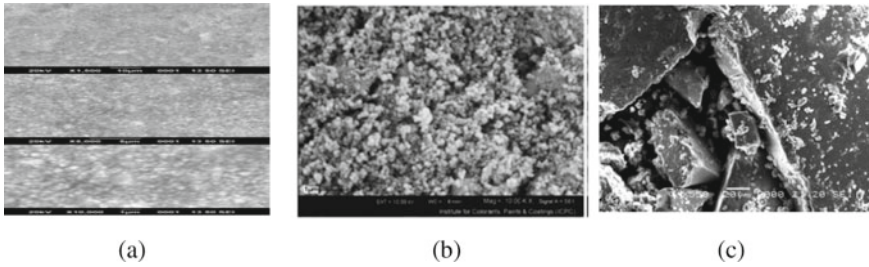
Fig. 3 SEM image of **a** TiO$_2$, **b** CaO, **c** CuO

Table 2 Properties of materials for metallic catalytic converter (TiO$_2$, CaO, and CuO)

Properties	TiO$_2$	CaO	CuO
Purity (%)	98.5	96.5	96
Particle size (nm)	25–75	30–40	5–6
Color	White	White	Brownish black
Thermal conductivity (W/m K)	4–11	2.5	33
Density (g/cm^3)	4.23	3.3	6.31

The properties of TiO$_2$, CaO, CuO used in this process have been shown in Table 2.

6 Result and Discussion

6.1 NDIR Analyzer and Exhaust Gas Analyzer

An NDIR analyzer and an exhaust gas analyzer were used to examine the catalytic converter. The non-dispersive infrared (NDIR) analyzer is a gas detecting sensor that measures gas concentrations in the surrounding atmosphere and examines CO and CO$_2$ emissions from engine exhaust, whereas the exhaust gas analyzer tests NO$_x$ and HC emissions. The production of the emissions studied is quantified in parts per million (ppm).

The emission characteristics of a CI engine are investigated at different speeds with constant loads, and hence, the following efforts have been reported.

1. For various loads, the engine was run without a catalytic converter.
2. For various loads, the engine is equipped with a conventional and metallic catalytic converter.
3. For various speeds, the engine is equipped with a conventional and metallic catalytic converter.
4. Different speeds were achieved without the use of a catalytic converter.
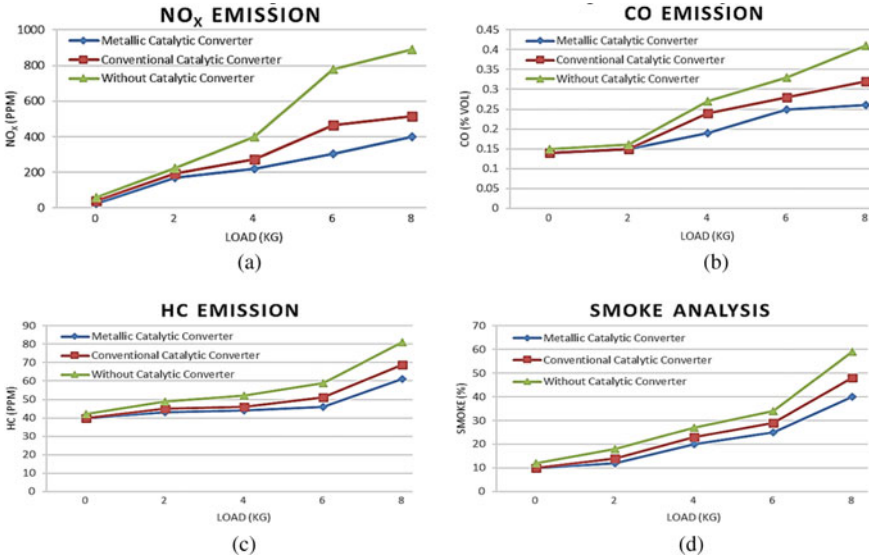
Fig. 4 Emission results. **a** NO_x, **b** CO, **c** HC, **d** smoke analysis

6.2 Study of NO_x, CO, and HC Emission

The concept is based on the response of a water–gas shift-fuse and the responses of steam transforming. Figure 4a shows that the usage of a CuO-based catalytic converter results in a 61% reduction in NO_x. NO_x is broken down into nitrogen (N_2) and carbon dioxide (CO_2). With the use of a catalytic converter, CO is reduced by around 21% which is illustrated in Fig. 4b. CO_2 is formed when CO is oxidized. When the nanocatalysts in the catalytic converter react with CO, they reduce it to carbon-di-oxide and cause Cu and Cl to be deposited due to CO's reduction property. The reduction of hydrocarbons by a conventional catalytic converter is because of the fact, a small amount of fuel in a big volume of air results in lower CO and HC emissions. H_2O and CO_2 are produced when HC is oxidized as represented in Fig. 4c.

6.3 Smoke Analysis

The reduction of smoke emissions utilizing a catalytic convertor is seen in Fig. 4d. Soot or smoke consisting of μm in diameter particles. Particulate matter has a variety of severe health impacts, including respiratory disorders and cancer. Smoke has a density of about 38 kg/m^3. The use of a catalytic converter with nanocatalysts reduces smoke by roughly 32%.

6.4 Speed Analysis

For each attempt, engine metrics like as HC, NO_x, and CO, and the efficiency of the conversion are plotted for various speeds. Figure 5a depicts the variance in NO_x emissions as a function of engine speed. It is clear that reduced NO_x emissions are achieved only slightly with the help of a catalytic converter. With the application of a catalytic converter, the NO_x level does not change significantly. This is because the CO and HC emissions are oxidized by a copper-coated catalyst. The emissions of HC and CO from an engine without a catalytic converter are significantly higher. Due to the decreased bed temperature of the catalytic converter, CO emissions are first reduced only somewhat. The CO level drops by roughly 2.5% by volume after 30 km/h as shown in Fig. 5b. This is owing to the significant influence of higher bed temperature, which is caused by the metal-supported catalyst converter's ability to achieve the temperature of the light faster. The catalytic converter bed's temperature rises as a result of the converter's resistance to the chemical activity in the bed and the flow of exhaust gases. When compared to a regular engine, the catalytic converter reduces HC levels uniformly, resulting in a reduction of around 100 ppm when the engine speed is maximum as represented in Fig. 5c.

A reduction in NO_x, HC, and CO is achieved as a result of the appreciable reduction in NO_x emissions as summarized as a decreased value of about 300 ppm at the maximum engine speed.
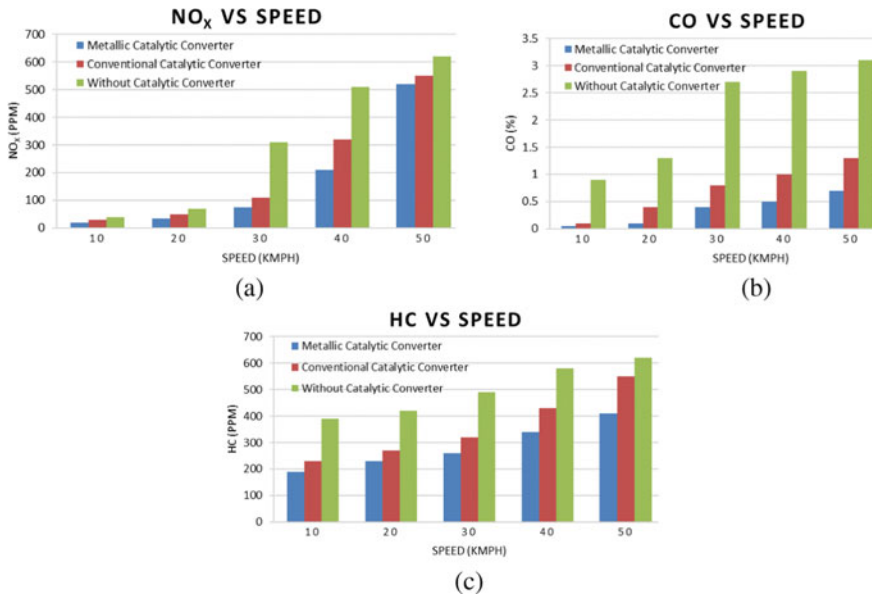
Fig. 5 Emissions versus speed. **a** NO_x, **b** CO, **c** HC

7   Conclusion

The most important findings of the experimental study are summarized here. The following observations were made as a result of the aforesaid analysis. When a catalytic converter is installed on an engine, CO and HC emissions are dramatically reduced. In comparison with an engine without a conventional catalytic converter (CCC), the volume CO, 300 ppm NO_x, and 100 ppm HC are reduced by 2.5%. When the engine is permitted to operate with a metallic catalytic converter (MCC) at complete loads, NO_x levels are dramatically decreased. When the emissions are compared without a catalytic converter and conventional catalytic converter (CCC), the result reveals an extreme reduction of 61% in NO_x emissions in maximum operating condition of 8 kg load.

When the emissions are compared of a metallic catalytic converter (MCC) with nanocatalysts to that of a catalytic converter without nanocatalysts at all loads, that is clear that hydrocarbon emission is reduced. At full load, the highest reduction in HC is recorded to be 32%. A significant reduction in smoke and CO emissions where achieved when analyzed with those engines without a conventional catalytic converter (CCC) and nanocatalyst-based catalytic converters demonstrates. At full load, the highest drop in smoke and carbon mono oxide (CO) is measured to be 32% and 21%, respectively.

As a result, we may conclude that the catalytic converter with nanocatalysts outperforms current OEM catalytic converters. In comparison with the OEM catalytic converter, the catalytic converter with nanocatalysts emits less, is less expensive, and has lower backpressure. As a result, a catalytic converter including titanium oxide, cupric oxide, and calcium oxide as catalysts will reduce NO_x, HC, and CO emissions to an acceptable level.

References

1. Shah, S.: Changing the material of a diesel engine catalytic converter to reduce exhaust emissions. Easy Chair Preprint (2021)
2. Dey, S., Dhal, G.C.: Controlling carbon monoxide emissions from automobile vehicle exhaust using copper oxide catalysts in a catalytic converter. Mater. Today Chem. **17**, 100282 (2020). https://doi.org/10.1016/j.mtchem.2020.100282
3. Warju, W., Drastiawati, N.S., Ariyanto, S.R., Nurtanto, M.: The effect of Titanium Dioxide (TiO_2) based metallic catalytic converter on the four-stroke motorcycle engine performance. J. Phys. Conf. Ser. **1747**(1) (2021). http://doi.org/10.1088/1742-6596/1747/1/012031
4. Reji, A., Nair, P.A., Saurav, A.K., Ismail, I., Babu, N.: Emission reduction in four-stroke S.I. engine using EGR and catalytic converter, pp. 109–116 (2021). http://doi.org/10.1007/978-981-15-6267-9_13
5. Manojkumar, R., Haranethra, S., Muralidharan, M., Ramaprabhu, A.: I.C. engine emission reduction using catalytic converter by replacing the noble catalyst and using copper oxide as the catalyst. Mater. Today Proc. (2020). http://doi.org/10.1016/j.matpr.2020.02.804

6. Hossain, S.K.S., Saleem, J., Rahman, S., Mohammed, S., Zaidi, J.: Synthesis and evaluation of copper-supported titanium oxide nanotubes as electrocatalyst for the electrochemical reduction of carbon oxide to organics, pp. 1–19. http://doi.org/10.3390/catal9030298

7. Gadlegaonkar, N., Patil, V., Pardeshi, V., Bajgude, T.: Design and analysis of catalytic converter of automobile engine (2019)

8. Atzl, B.A., Pupp, M., Rupprich, M.: The use of photocatalysis and titanium dioxide on diesel exhaust fumes for NO_x reduction. Sustainability **10**(11), 1–13 (2018). https://doi.org/10.3390/su10114031

9. Venkatesan, S.P., Uday, D.S., Hemant, B.K., Kushwanth Goud, K.R., Kumar, G.L., Kumar, K.P.: I.C. engine emission reduction by copper oxide catalytic converter. IOP Conf. Ser. Mater. Sci. Eng. **197**(1) (2017). http://doi.org/10.1088/1757-899X/197/1/012026

10. Davis, D., Divya, C.: Reduction of air pollution from vehicles using titanium dioxide. Int. Res. J. Eng. Technol. **2**(5), 1308–1314 (2015)

11. Royer, S., Duprez, D.: Catalytic oxidation of carbon monoxide over transition metal oxides, pp. 24–65 (2011). http://doi.org/10.1002/cctc.201000378

12. Mahlia, T.M.I.: Development and test of a new catalytic converter for natural gas fueled engine (2009). http://doi.org/10.1007/s12046-009-0022-0

13. Lanje, A.S., Sharma, S.J., Pode, R.B., Ningthoujam, R.S.: Synthesis and optical characterization of copper oxide nanoparticles, vol. 1, no. 2, pp. 36–40 (2010)

14. Jang, H.D., Kim, S., Kim, S.: Effect of particle size and phase composition of titanium dioxide nanoparticles on the photocatalytic properties, pp. 141–147 (2001)

15. Neeft, J.P.A., Makkee, M., Moulijn, J.A.: Catalysts for the oxidation of soot from diesel exhaust gases. I. An exploratory study, vol. 8, no. 95, pp. 57–78 (1996)

Analyzing Wear Resistance Characteristics of Al 5052/Al₂O₃/Gr Stir Cast Hybrid Composite

Balakrishnan Rajeswari, Chinnachamy Manikandan, and Koduvayur Sankaranarayanan Amirthagadewaran

1 Introduction

Aluminum metal matrix composites (AMMCs) have been enroll main role in the usage of agricultural, marine, military, automotive, and aircraft applications. Generally, it is having the following mechanical properties: higher corrosion resistance, hardness, tensile strength, and compression strength. The AMMC's recorded benefits over than unreinforced aluminum materials like good fatigue strength, wear resistance damping property, electrical and friction coefficient, and good wear resistance [1, 2].

Hybrid composites include more than one reinforcement or one matrix. Hybrid metal matrix composites, the new development of materials, discover various applications in several industrial fields and perform as substitute for various materials [1, 3].

In the composite fabrication technology, the aluminum preferred as matrix material majority, whereas boron carbide (B_4C), silicon carbide (SiC), alumina (Al_2O_3), cubic boron nitrate (CBN), and graphite (Gr) are considered as reinforcement because of its physical and mechanical characteristics [4, 5].

Powder metallurgy, deposition techniques, and diffusion bonding are all used to prepare the aluminum composites, but liquid metallurgy exemption is the most popular because it is a commercial one that allows for uniform reinforcement distribution in the liquid metal, bulk fabrication of components with less time [6].

B. Rajeswari (✉) · K. S. Amirthagadewaran
Government College of Technology, Coimbatore, Tamilnadu 641013, India
e-mail: rajeswari_b@gct.ac.in

C. Manikandan
C.M.S. College of Engineering and Technology, Coimbatore, Tamilnadu 641032, India

K. S. Amirthagadewaran
United Institute of Technology, Coimbatore, India

In stir casting method, composition elements and melt temperature and stirrer speed, pouring temperature, number of blades and die material and die preheating temperature were taken into account as input process variables. To assign these input process parameters to fabricate composites, Taguchi method has been followed effectively. It reduces the experimental designing duration as well as provides better combinations on assigned input parameters [7].

In the present study, hybrid composites fabricated in stir casting route with the composition of Al5052 (matrix), Al_2O_3, and graphite (Reinforcements) at different percentages of composition to enhance mechanical properties. The optimal process parameters for improving the wear resistance of composites have been investigated by Taguchi optimization and compared with base matrix.

2 Material Selection

The composites elements are selected based on applications requirements and cost and bonding characteristics during fabrication. The aluminum alloy Al5051 has chosen as matrix material owing to its better mechanical characteristics and economical status. The alloys composition of Al5051 is given in Table 1.

The aluminum oxide and graphite are used as reinforcement in hybrid composites fabrication through stir casting method. The Al_2O_3 having the properties of better wettability with aluminum and thermal stability, it improves the fabrication stability with the evident bonding with aluminum. Graphite having a solid lubricant can improve the machinability the composites. Furthermore, the conducting capabilities of aluminum composites were improved by graphite because of its excellent thermal and electrical conductivity [8, 9].

3 Experimental Work

3.1 Composite Composition

The mechanical properties of hybrid composites with ceramic and graphite increase up to 2.5% and then reduced. The adding of graphite powder lowers the hardness value due to the raise in porosity [10]. So, the reinforcement elements Al_2O_3 (2%, 3%, and 4%) and graphite (2%) are added with metal matrix Al5052 aluminum alloy. The reinforcements were preheated about 300 °C and matrix melted at the temperature of 800 °C. The different compositions of the hybrid composites are shown in Table 2.

Table 1 Al 5052 chemical composition

Element	Mg	Cr	Cu	Fe	Mn	Si	Zn	Others	Al
%	2.20–2.80	0.14–0.36	0.05–0.10	0.01–0.40	0.05–0.10	0.1–0.25	0.05–0.1	0.06 max	Balance

Table 2 Composite composition

Sample No.	Matrix composite Al 5052 (%)	Reinforcement (%)	
		Al_2O_3	Graphite
1	96	2	2
2	95	3	2
3	94	4	2

3.2 Hybrid Composites Fabrication in Stir Casting

The stir casting machine to fabricate hybrid composite of Al5052-Al_2O_3-graphite is shown in Fig. 1. It has electric furnace with the capacity of 2 kg and a mechanical stirrer which has the speed variation of 100–1000 rpm.

The furnace hearth temperature and stirring speed are monitored through digital display and controlled by the switched availed in the panel board.

The ingots of Al5052 were sectioned as small pieces and loaded into the furnace crucible for melting. About 1–2 h, the aluminum alloy heated to attain the semi-liquidus state (600 °C). Further, the reinforcement of Al_2O_3 was preheated in the muffle furnace about 300 °C to make their surface oxidized. Figure 2 shows the muffle furnace used for the reinforcement preheating. The EN8 steel die is preheated about 200 °C to retain fluidity of the liquid metal. Again the aluminum alloy heated at 800 °C, the reinforcements were added at the pre-determined proportions. The composition at the highest temperature mixed with the stirrer mechanism at a speed

Fig. 1 Stir casting setup

Fig. 2 Reinforcement
preheater

Fig. 3 Casted samples

of 600 rpm about 3 min. To eliminate the soluble gases present in the molten, the Ar gas was into the melt.

The elements of the hybrid composite attain the liquid state at 850 °C and transferred as composite with the better wettability. The liquid state of the composite poured into the metal mold to cast the specimens as shown in Fig. 3. The metal die replicates cast specimens with its dimension 30 mm diameter and 250 mm length. The fabrication procedure was preceded for three specimens as per the experimental design.

3.3 Wear Test Machine and Specimens

From the stir-casted samples, the wear test specimens were preferred as per the ASTM G99 standard of dimension Ø10 mm and 30 mm length as shown in Fig. 4. The wear resistance is important one for the dynamic components of the machineries. To pertain wear resisting nature of the hybrid composites, the Ducom POD TR 20 wear tester machine is used to conduct the wear tests (Figs. 5 and 6).

Fig. 4 Wear test specimens, diameter: 10 mm, length: 30 mm

Fig. 5 Ducom pin-on-disk wear tester

Fig. 6 Digital controllers

The responses of the wear test such as frictional force and wear rate were recorded as digital and graphical modes. The rotating disk made of EN32 steel disk with hardness 65 HRC is used for the rubbing action of the wear tests.

Table 3 Wear test experimental results

S. No.	(%) of reinforcement	Load (N)	Sliding speed (RPM)	Wear rate (μm)	Friction force (N)
1	2	10	500	116	4.9
2	2	20	600	107	9.4
3	2	30	700	1372	9.8
4	3	10	600	132	6.2
5	3	20	700	617	13.2
6	3	30	500	146	11.7
7	4	10	700	377	6.4
8	4	20	500	451	7.7
9	4	30	600	939	20.6

3.4 Wear Test

Taguchi method orthogonal array of L$_9$ design matrix was followed to design wear test experiment trials [11]. The percentage of reinforcement rate in the hybrid composites, applying load, and sliding speed were considered as input variables for the wear test experimentation. The percentage of reinforcement in the range of 2, 3, and 4, the applying load (10–30 N), and sliding speed of 500 rpm, 600 rpm, and 700 rpm were used in the wear test experiments [12, 13]. The sliding distance 100 m was taken as constant factor. Experimental design matrix based on L9 trials are shown in Table 3. The wear test specimen is held vertically against the rotating disc to perform the wear test. At the constant sliding distance with the variation of wear test input variables, the wear rate and the frictional force extracted are accounted and tabulated in Table 3.

4 Results and Discussion

4.1 Microstructure

The dispersion of ceramic particles in the matrix alloy is analyzed by means of inverted microscope. Specimens were prepared creating flat surfaces by facing, well-polished by fine-grade ceramic particle pasted paper and then cleaned with etching solution as per test reference.

Figure 7 shows the microstructure of the hybrid composite samples. The micrograph evidently relates that the dendritic pattern is neutral in all the samples under study.

In the microstructure analysis, the structure indicates the alumina and graphite particles are dispersed evenly in the composite material. The structure denotes fine

| Sample:1(100X) | Sample2:(100X) | Sample 3:(100X) |
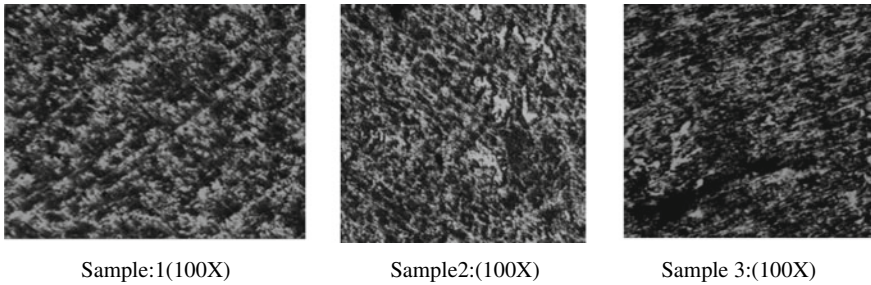
Fig. 7 Microstructure of composite materials

attachment between the reinforced powders and the base alloy where the porosity occurred in lowest level, and it is not noted by the microstructure, and also, clustering can be viewed at some of the spaces in the matrix alloy.

4.2 ANOVA for Wear Rate and Frictional Force

The wear rate and friction force values at the different input variables are found and analyzed to obtain optimal functional parameters for the sliding composite elements. The MiniTAB-16 was used to analyze the wear test investigational results such that the analysis of variance (ANOVA) and signal-to-noise ratio (*S/N* ratio) defines the significant contribution of individual input variables on output responses and percentage of accuracy of the test results, respectively.

From the result, smaller is better in the wear rate that the reinforcement 3%, load 10 N, and sliding speed 500 rpm are the optimal process parameter settings found in Taguchi optimization as shown in Fig. 8.

From the result, smaller is better in the frictional force that the reinforcement percentage 2%, load 10 N, and sliding speed 500 rpm are the optimal process parameter settings found in Taguchi optimization as shown in Fig. 9. The wear resistance and sliding force are minimized through the addition of moderate reinforcement and minimum sliding speed and applied load.

Figure 10 shows a screen shot wear rate for the operating parameters of 20 N load, 700 rpm speed of the disk, and 3% composition. The optimal parameters setting produce less wear rate comparing to other process factors settings.

5 Conclusion

The aluminum alloy hybrid composite (Al 5052/alumina/graphite) was casted in stir casting process with varying percentage of alumina and 2% graphite. The stir casting route enhanced the uniform distribution of reinforcement particles with the matrix
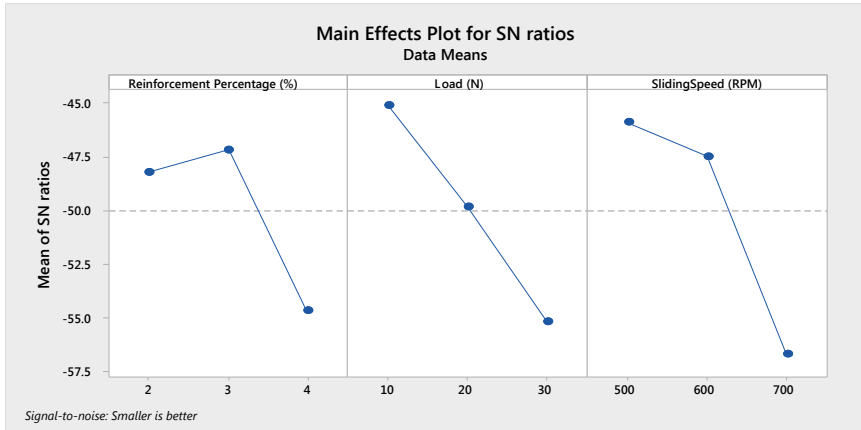
Fig. 8 *S/N* ratio-wear rate
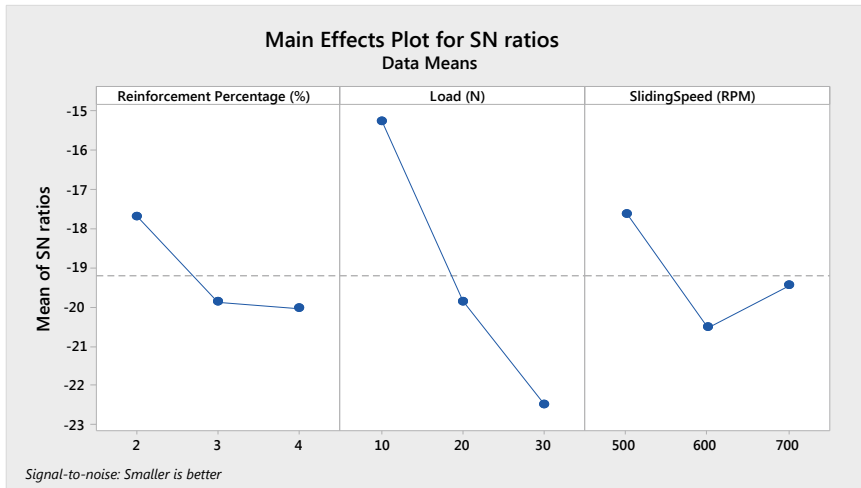
Fig. 9 *SN* ratio-frictional force

element. The examination of wear test reveals that the composite of 3% Al$_2$O$_3$ and 2% Gr and 95% Al alloy combination with load of 10 N and 500 rpm sliding speed is having superior wear resistance compared to other combinations. The addition of percentage of graphite contributes significant effect on wear resistance and frictional load of the composites. The higher wear resistance components can be fabricated with this hybrid composite.
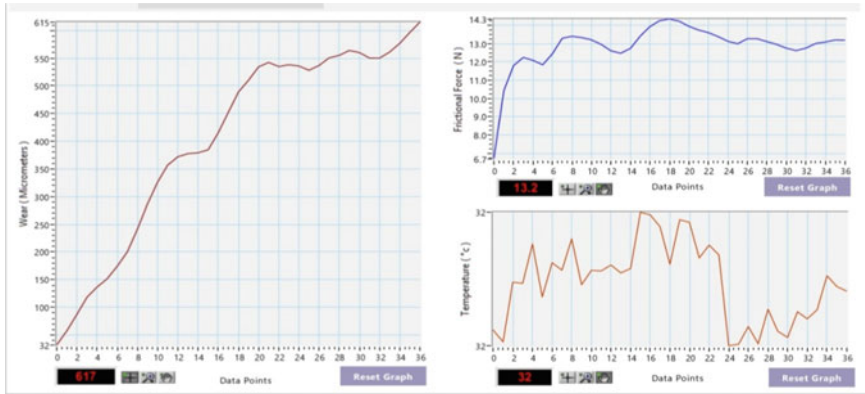
Fig. 10 Load 20 N, sliding speed 700 rpm, and 3% composition

References

1. Singh, J., Chauhan, A.: Characterization of hybrid aluminum matrix composites for advanced applications—a review. J. Mater. Res. Technol. **5**, 159–169 (2015)
2. Anthony Xavior, M., Ajith Kumar, J.P.: Machinability of hybrid metal matrix composite—a review. Procedia Eng. **174**, 1110–1118 (2017)
3. Kumar, R., Dhiman, S.: A study of sliding wear behaviors of Al-7075 alloy and Al-7075 hybrid composite by response surface methodology analysis. Mater. Des. **50**, 351–359 (2013)
4. Singh, K.K., Singh, S., Shrivastava, A.K.: Comparison and wear behaviour of aluminium matrix alloy (Al7075) and silicon carbide based aluminium metal matrix composite under dry condition at different sliding distance. Mater. Today Proc. **4**, 8960–8970 (2017)
5. Sharma, P., Paliwal, K., Garg, R.K., Sharma, S.: A study on wear behavior of Al/6061/graphite composites. J. Asian Ceram. Soc. **4**, 858–187 (2017)
6. Prabu, B., Karunamoorthy, L., Kathiresan, S., Mohan, B.: Influence of stirring speed and stirring time on distribution of particles in cast metal matrix composite. J. Mater. Process. Technol. **171**, 268–273 (2006)
7. Rajeswari, B., Amirthagadeswaran, K.S.: Investigation on mechanical properties of aluminium 7075-silicon carbide-alumina hybrid composite using Taguchi method. Aust. J. Mech. Eng. **13**, 127–135 (2015)
8. Ravindranath, V.M., Shiva Shankar, G.S., Basavarajappa, S., Siddesh Kumar, N.G.: Dry sliding wear behavior of hybrid metal matrix composites reinforced with boron carbide and graphite particles. Mater. Today Proc. **4**, 11163–11167 (2017)
9. Sharma, P., Khanduja, D., Sharma, S.: Dry sliding wear investigation of Al 6082/Gr metal matrix composites by response surface methodology. J. Mater. Res. Technol. **5**, 29–36 (2016)
10. Suresha, S., Sridhara, B.K.: Friction characteristics of aluminium silicon carbide graphite hybrid composites. Mater. Des. **34**, 576–583 (2012)
11. Hemanth Kumar, T.R., Swamy, R.P., Chandrashekar, T.K.: Taguchi technique for the simultaneous optimization of tribological parameters in metal matrix composite. J. Miner. Mater. Charact. Eng. **10**, 1179–1188 (2011)
12. Allwyn Kingsly Gladston, I., Dinaharan, N., Mohammed Sheriff, J., Selvam, D.R.: Dry sliding wear behavior of AA6061 aluminium alloy composites reinforced rice husk ash particulates produced using compo casting. J. Asian Ceram. Soc. **3**, 1645–1653 (2017)
13. Anitha, P., Shrinivas Balraj, U.: Dry sliding wear performance of Al/7075/Al$_2$O$_3$/graphite hybrid metal matrix composites. Mater. Today Proc. **4**, 3033–3042 (2017)

Analytical Hierarchy Process Strategy for Assessment of Overall Equipment Effectiveness

Dillip Kumar Biswal, Kamalakanta Muduli, and Jitendra Narayana Biswal

1 Introduction

Customers in the present day have high expectations from procedures to produce excellence products on time and a reasonable price. This necessitates the use of extremely reliable production machines and processes. In today's industrial and production environment, increasing demands to cut costs, achieve a zero-tolerance policy, and optimize resource allocation needs a progressive producer to continuously look up and raise productivity and quality, as well as to measure what hinders them from doing so on a daily basis. OEE is a measure used in Total Productive Maintenance (TPM) to accurately predict and decrease/eliminate the six major losses that take place in a production practice for continual equipment improvement.

The notion of Total Productive Maintenance provides a standardized framework for measuring manufacturing productivity termed Overall Equipment Effectiveness. The Overall Equipment Effectiveness is determined by calculating the equipment's availability, performance efficiency when it is in action, and the rate of quality items manufactured [1–3]. With the use of analytic hierarchy methodology, A. N. Madu proposes a constrained regression meta models [4]. The OEE is implemented as a metric of TPM's objective of maximizing equipment effectiveness [5]. Production losses, as well as numerous other indirect and hidden expenses, account for the majority of overall production costs [6]. As a corollary, Nakajima summarized OEE as "a measure that aims to identify these hidden costs" [1].

D. K. Biswal (✉) · K. Muduli
Department of Mechanical Engineering, C. V. Raman Global University, Bhubaneswar, Odisha 752054, India
e-mail: dillipkumarbiswal@gmail.com

J. N. Biswal
Department of Mechanical Engineering, Einstein Academy of Technology and Management, Bhubaneswar, Odisha 752060, India

303

Richard Oechsner et al. demonstrates modeling methodologies, for estimating and monitoring OEE in a semiconductor production plant [7]. The relationship between Value Stream Mapping (VSM) and OEE, as well as a method for determining the benefits of VSM and their impact on the OEE measure was investigate [8]. A program that incorporates a simulation tool and OEE measurements to make it easier to evaluate a manufacturing system was created [9]. Raouf in 1994 introduced a novel approach for determining OEE that used different weights for different parameters, concluding that elements impacting OEE are not all equally essential in all circumstances and that alternative weights should be assigned [10].

Fuzzy AHP was used to determine the best maintenance plan for the best selection of equipment [11]. In cases where there are numerous choices with various and inconsistent criteria accessible, Multi Criteria Decision Making may be employed to make a decision [12, 13]. The AHP can be used for effective priority ranking of potential failure causes [14]. For the criticality analysis of a paper mill's forming unit, AHP methodology was employed [15]. Fuzzy AHP was used to identify essential components in the distribution of power networks [16]. AHP was used to rate power plant equipment based on a set of multiple criteria [17]. Combination of goal programming and fuzzy-AHP was employed to find the best mix of maintenance procedures [18]. A modified two-step decision making process was proposed by employing AHP to identify important equipments [19].

All of the multiplication essentials are given equal weightages in the traditional OEE computation, as explained and promulgated by Nakajima [1]. This is a rare instance when a one percentage reduction in downtime seems to have the similar commercial or beneficial economic influence as a one percentage reduction in effectiveness or a one percentage reduction in quality. In reality, giving equal weight to all of the OEE aspects may not be appropriate. According to the nature of their job, the weighting factor is likely to differ from one organization to the next. Analytic Hierarchy Process (AHP) can be used to determine these weightages for the OEE performance factors. Saaty [20, 21] proposed AHP, a mathematical strategy for multi-criteria judgments. When both qualitative and quantitative components of a proposal must be addressed, AHP is a strong and adaptable decision making technique that reduces complex problems to a series of one-to-one matched comparisons to help individuals define personal preferences and choose the optimal option. AHP not only assists decision makers in arriving at the best option, but also gives them a strong sensation that it is the best option.

2   The Purpose of This Study

Because the Kneader Buss Mixer is such an important piece of equipment in the aluminum manufacturing sector, it is important to understand the aspects that influence its production and how to acquire the best return. The goal of this investigation is to determine the OEE of a Kneader Buss Mixer that is used to make paste for aluminum pots anodes. The study also provides an Analytic Hierarchy Process (AHP)

technique for assigning varying weightages to distinct OEE elements, resulting in a normalized OEE that is mainly useful to the interest group.

3 Overall Equipment Effectiveness

"Overall Equipment Effectiveness (OEE)" is the key TPM metric for identifying and quantifying important process-related losses, as well as a performance indicator for measuring the effectiveness of the equipment, by acquiring data on equipment availability, performance, and quality. "It is a metric used in TPM to measure how well a company's production process or individual piece of equipment performs against its full capacity," according to the definition of OEE [8]. It is a percentage calculated by multiplying the equipment's availability, the performance rate while in use, and the quality rate at which a product is manufactured over a period. The link between OEE and performance factors is depicted in Fig. 1.
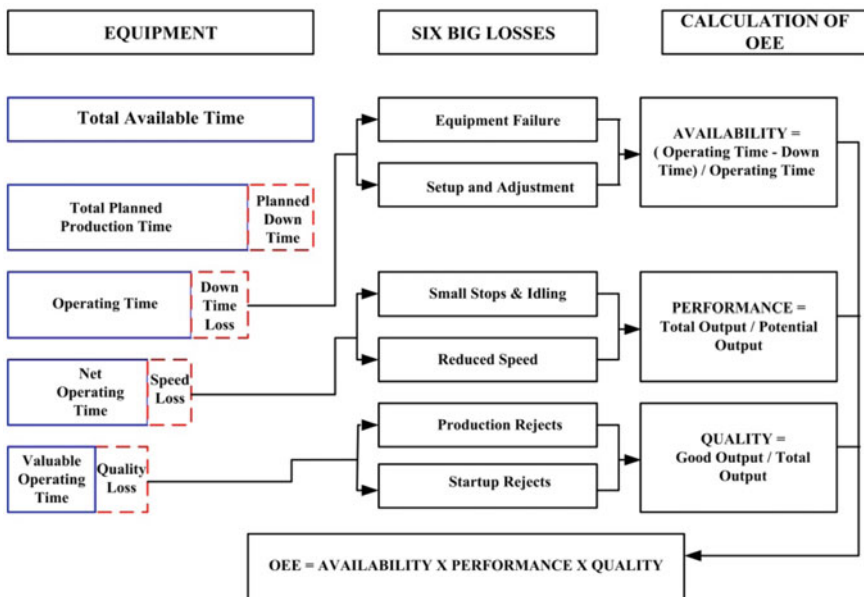
Fig. 1 Link between overall equipment effectiveness and performance factors

4 Assessing OEE When Performance Metrics Contain Different Weights

The computed rating of OEE is not totally correct. It is presumptively assumed that the fundamental elements of availability, efficiency and quality losses are all equally important. It is an uncommon occurrence when a 1% loss of productivity or quality seems to have the commercial or beneficial economic influence as a 1% efficiency or quality loss.

4.1 Estimating Relative Weights Using AHP Methodology

The AHP methodology can be used to assign weightages to performance indicators. The following is the AHP methodology for determining weightages.

The decision problem's structure: Implementing Analytical Hierarchy Process to develop multi-criteria decision making involves four basic phases [22].

Model Specification: The specification of feasible alternatives comes first, followed by the creation of criteria for evaluating alternatives.

Comparison of categories and criteria in pairs: Pairwise comparisons employing a square matrix structure are used to determine the relative importance of criteria within each category and within each category within the group of categories. The important values are based on Saaty's 1–9 scale [20].

Rating of decision alternatives: Each chosen alternative is assessed to every criterion in the assessment method.

Rankings for making decisions: Finally, the alternative ratings are added to the criteria ratings to get an overall rating for each investment option.

4.2 Pairwise Comparison Matrix

The scales of comparison used to create the various pairwise comparison matrices. A matrix, consisting of three rows and three columns, is developed to determine the priorities for the three performance factor in terms of performance, quality, and availability as shown in Table 1.

Table 1 Pairwise comparison matrix

	Performance	Quality	Availability
Performance			
Quality			
Availability			

4.3 Formulation

Following the development of the matrix, the relative importance for each of the performance elements is estimated using the procedures below.

Step 1: Add the values in each pairwise comparison matrix column.
Step 2: Divide each column's element by the matching column totals. The normalized pairwise comparison matrix is the output of this process.
Step 3: In the normalized matrix, compute the average of the entries in each row. These averages provide an assessment of each performance element's relative priority in relation to the criterion.

4.4 Weighted OEE Calculation Algorithm

Raouf's Methodology: Raouf [10] outline a methodology for calculating OEE that involved different weights. He came to the conclusion that not all factors impacting OEE are highly relevant in all circumstances, and they should be given varied weights.

If Availability (P_1) has a weight of w_1, Performance (P_2) has a weight of w_2, and Quality (P_3) has a weight of w_3, where $0 \leq w_i \leq 1$ and $\sum w_i = 1$, OEE can be computed as follows:

$$\text{OEE} = \left(P_1^{w_1}\right) \times \left(P_2^{w_2}\right) \times \left(P_3^{w_3}\right) \tag{1}$$

All of the performance elements, i.e., P_1, P_2, and P_3, are assigned identical weights ($w_i = 1$) in the traditional OEE calculation presented by Nakajima, and the sum of the weightages is equal to three. We can deduce the following using a common-sense approach:

- If all performance elements are given equal weighting, the adjusted OEE value should not differ from the conventional OEE number.
- If the performance element with the highest value is given more weight and/or the performance element with the lowest value is given less weight, the normalized OEE value should increase when compared to the conventional OEE value.
- If the performance element with the lowest value is given more weight and/or the performance element with the highest value is given less weight, the modified OEE value should be lower than the conventional OEE value.

However, when Raouf's method (Eq. 1) is examined, it is discovered that the value of modified OEE increases in every situation when compared to conventional OEE. When compared with the traditional OEE value, it is clear that OEE has becoming more. Similarly, it can be seen that the OEE value is increasing in each of the three scenarios listed above.

In this research, a method is proposed for using the Analytic Hierarchy Process (AHP) to assign different weights to distinct OEE performance criteria and then determining a modified OEE that meets the aforementioned three conditions.

Proposed Methodology:

$$\mathrm{WF} = \begin{bmatrix} P_1 & P_2 & P_3 \end{bmatrix} \begin{bmatrix} w_{P1} \\ w_{P2} \\ w_{P3} \end{bmatrix}$$

$$= (P_1 \times w_{P1}) \times (P_2 \times w_{P2}) + (P_3 \times w_{P3}) \tag{2}$$

$$\Rightarrow N_{wf} = \frac{\mathrm{WF} \times n}{(P_1 + P_2 + P_3)} \tag{3}$$

$$\mathrm{OEE}_{\mathrm{modified}} = N_{wf} \times \mathrm{OEE}_{\mathrm{conventional}} \tag{4}$$

where the observed values of specific performance elements are P_1, P_2, and P_3. The weightage of the respective performance elements is represented by w_{P1}, w_{P2}, and w_{P3}, where $\sum w_i = 1$ and WF is the weighting factor. N_{wf} stands for the Normalized Weightage Factor (NWF). The number of performance elements is denoted by the letter n.

5   Collection of Data

In order to achieve accurate results that are useful to plant management, overall equipment effectiveness analysis normally requires the collection of trustworthy and sufficient data on down time, total production, rejection, and so on. The data gathered in the field is regarded to be the most accurate. Field data, on the other hand, is costly and longer period to obtain. Information must be gathered over a length of time in order to provide a satisfactory depiction of the machine's genuine operational characteristics.

Over the course of 28 weeks, the newly installed Buss Mixer in the carbon plant was monitored. The operation is divided into two shifts of eight hours each, six days a week. Each shift had one hour of planned downtime for task like inspecting the machinery and its associated equipment, cleaning of the machine, and completing paperwork, among other things. During the twenty-eight-week observation period, the machine was either left idle or operated under a different set of parameters to produce paste for sale to outside organizations for thirty days. As a result, the OEE computation excludes the data from the previous two weeks.

Table 2 Rating for the factors of performance

	Performance	Quality	Availability
Performance		8	
Quality			
Availability	7	4	

5.1 Rating of Performance Factors Through Questionnaire

A questionnaire was created to gather feedback and rate performance factors using the Saaty's scale. The following is the completed questionnaire.

How do you think you will rank availability in terms of quality and performance?

- Availability to Quality [ ]
- Availability to Performance [ ]

How will you rank the performance in terms of quality?

- Performance to Quality [ ]

Table 2 contains the numerical rating (Saaty's scale) details rated by Hindalco managements.

6 Analysis of Data Collected

By recording machinery statistical information, a cause-and-effect graphic is created to illustrate the key failures for organized enhancement. The success of organized enhancement efforts and countermeasures put in place to reduce severe losses or problems can then be measured and communicated using OEE data.

6.1 Estimating the Overall Equipment Effectiveness

The six major losses that prohibit effective operation have an impact on the equipment's capability. Faulty operation, equipment failure, and support equipment failure are the main causes of these losses. These losses must be discovered and corrective action done to enhance the equipment's performance. Figure 2 depicts the losses that occur regularly in a Buss Mixer.

Calculation of OEE

From the data collected from the Kneader Buss mixture, total production and rejection was calculated for different months as shown in Table 3.

By using the formulas shown in Fig. 1, availability, performance efficiency and quality rates are calculated as shown in Fig. 3.
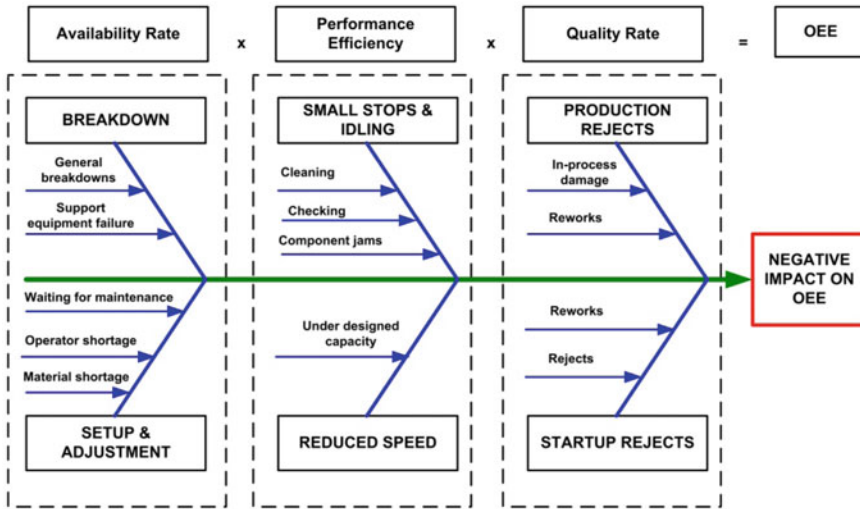
Fig. 2 Cause-and-effect diagram for a buss mixer

Table 3 Total production and Rejection for different months

	Planned production time (min)	Actual down time (min)	Operating time (min)	Total production (kg)	Rejection (kg)	Good production (kg)	Potential output at rated speed
January	8040	2154	5886	896,725	11,600	885,125	980,960.76
February	19,920	2621	17,299	2,840,940	13,700	2,827,240	2,883,051.34
March	18,120	1315	16,805	2,781,405	11,800	2,769,605	2,800,721.3
April	17,760	2980	14,780	2,428,300	17,600	2,410,700	2,463,234.8
May	17,220	468	16,752	2,740,085	17,800	2,722,285	2,791,888.32
June	17,220	673	16,547	2,756,750	19,500	2,737,250	2,757,723.02
July	16,800	750	16,050	2,694,720	23,300	2,671,420	2,674,893

$$\text{OEE} = \text{Availability} \times \text{Performance Efficiency} \times \text{Quality Rate}$$
$$= 0.90475 \times 0.98769 \times 0.99327$$
$$= 0.887607 \, \text{i.e.} \, 88.76\%$$

To assess the relative significance of the criteria in relation to one another

Using the AHP technique, the weightages of each of the three performance components can be computed by using the different steps as discussed in Sect. 4.4, i.e., weighted OEE calculation algorithm. Table 4 displays the weightages (w_i) for the
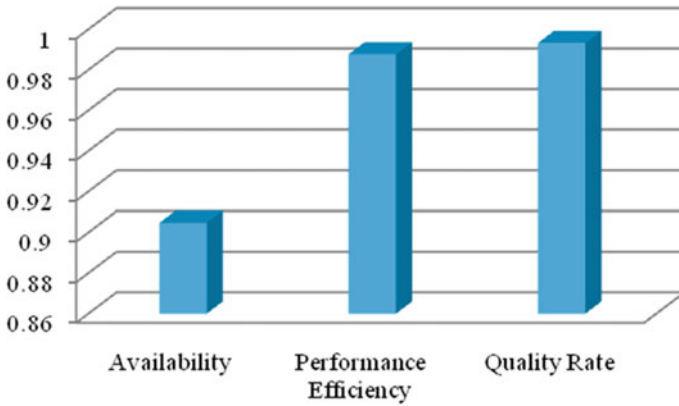
Fig. 3 Calculated availability, performance efficiency, and quality rate

Table 4 Weightages of the performance elements

Criteria	Weightage	Value
Performance (P_2)	w_{P2}	0.28
Quality (P_3)	w_{P3}	0.09
Availability (P_1)	w_{P1}	0.629

availability, performance, and quality performance criteria, which were determined using the AHP method on data from interviews and a pairwise comparison matrix.

Determination of Overall Equipment Effectiveness employing Raouf's Methodology

Using Eq. (1) and by employing equal weightages to all the OEE elements,

$$OEE_{Raouf's} = 0.9597 = 95.97\%$$

Determination of OEE using Proposed Methodology

Using Eqs. (2, 3, 4) and employing different weightages to all the OEE elements

$$OEE_m = 0.9719 \times 0.8876 = 0.8626 = 86.26\%$$

Testing of the Developed Framework

- As previously noted, the OEE value should fluctuate rationally based on the weighting applied to performance elements.
- If this proposed model is given equal weight, the updated OEE value should remain constant.

By giving the performance factors equal weight, i.e., $w_{P1} = w_{P2} = w_{P3} = 0.333333$

$$OEE_m = 0.9999 \times 0.8876 = 0.8875 = 88.76\%$$

When we provide equal weightages to the performance elements, we observe that the modified OEE value remains unchanged, whereas it increases in Raouf's model.

7 Conclusion

In general, when calculating OEE, all elements are given equal weightage, but this is a rare circumstance in which a one percentage reduction in downtime seems to have the similar commercial or financial influence as a one percentage reduction in effectiveness or quality. In practice, giving equal weight to all of the OEE aspects may not be appropriate. According to the nature of their job, the weighting factor is likely to differ from one organization to the next. Analytic Hierarchy Process can be used to determine these weightages for the OEE performance factors (AHP). In this research, a modified AHP methodology is utilized to calculate the weighted OEE by measuring and allocating relative priority weightings to each performance parameter. When different weightages can be given to the performance factors, the suggested model can be used to determine updated OEE.

References

1. Nakajima, S.: Introduction to Total Productive Maintenance, 11th edn. Productivity Press, Cambridge (1988)
2. Dal, B., Tugwell, P., Greatbanks, R.: Overall equipment effectiveness as a measure for operational improvement. Int. J. Oper. Prod. Manag. **20**(12), 1488–1502 (2000)
3. Ljungberg, O.: Measurement of overall equipment effectiveness as a basis for TPM activities. Int. J. Oper. Prod. Manag. **18**(5), 495–507 (1988)
4. Madu, A.N.: On the total productivity management of maintenance float system through AHP applications. Int. J. Prod. Econ. **34**(2), 201–207 (1994)
5. Waeyenbergh, G., Pintelon, L.: A framework for maintenance concept development. Int. J. Prod. Econ. **77**(3), 299–313 (2002)
6. Ericsson, J.: Disruption analysis—an impact tool in lean production. Ph.D. thesis, Department of Production and Materials Engineering, Lund University, Lund (1997)
7. Oechsner, R., Pfefter, M., Pfitzner, L., Binder, H., Muller, E., Vonderstrass, T.: From overall equipment efficiency (OEE) to overall fab effectiveness (OFE). Mater. Sci. Semicond. Process. **5**, 333–339 (2003)
8. Dadashnejad, A.A., Valmohammadi, C.: Investigating the effect of value stream mapping on overall equipment effectiveness: a case study. Total Qual. Manag. Bus. Excell. **30**(3), 466–482 (2019)
9. Mahadevan, S.: Automated simulation analysis of overall equipment effectiveness metrics. M.S. thesis, University of Cincinnati (2004)
10. Raouf, A.: Improving capital productivity through maintenance. Int. J. Oper. Prod. Manag. **14**(7), 44–52 (1994)
11. Ghosh, D., Roy, S.: A DM framework for process plant maintenance. Eur. J. Ind. Eng. **4**(1), 78–98 (2009)
12. Fântână, G.I., Oae, S.A., Gurau, A.M.: Decision making using the AHP. In: International Conference on MEQAPS, vol. 13, pp. 119–124 (2013)

13. Gonçalves, C.D.F., Dias, J.A.M., Machado, V.A.C.: MCDM for selecting maintenance key performance indicators. Int. J. Manag. Sci. Eng. Manag. **10**(3), 215–223 (2015)
14. Braglia, M.: MAFMA: multi-attribute failure mode analysis. Int. J. Qual. Reliab. Manag. **17**(9), 1017–1033 (2000)
15. Sachdeva, A., Kumar, D., Kumar, P.: A methodology to determine maintenance criticality using AHP. Int. J. Prod. Qual. Manag. **3**(4), 396–412 (2008)
16. Dehghanian, P., Fotuhi-Firuzabad, M., Bagheri- Shouraki, S., Kazemi, A.A.R.: Critical component identification in reliability centered asset management of power distribution systems via fuzzy AHP. IEEE Syst. J. **6**(4), 593–602 (2012)
17. Singh, R.K., Kulkarni, M.S.: Criticality analysis of power-plant equipments using the AHP. Int. J. Ind. Eng. Technol. **3**(4), 1–13 (2013)
18. Meddaoui, A., Bouami, D.: Decision making in maintenance using AHP and time-driven activity based costing. Int. J. Prod. Qual. Manag. **13**(4), 450–470 (2014)
19. Khaira, A., Dwivdy, R.: A two step decision making approach for identification of critical equipment using analytical hierarchy process and preference ranking organization method for enrichment evaluations with improved normalization. Eng. Rev. **39**(2), 174–185 (2019)
20. Saaty, T.L.: The Analytic Hierarchy Process. McGraw-Hill, New York (1980)
21. Saaty, T.L.: Multicriteria Decision Making: The Analytic Hierarchy Process. RWS Publications (1990)
22. Oeltjenbruns, H., Kolarik, W.J.: Strategic planning in manufacturing systems—AHP application to an equipment replacement decision. Int. J. Prod. Econ. **38**, 189–197 (1995)

Plant Layout Improvement Using CRAFT: A Case of Food Packaging Unit

Dillip Kumar Biswal, Kamalakanta Muduli, and Jitendra Narayan Biswal

1 Introduction

Due to recent technological advancements, all types of sectors have seen significant growth in the previous several decades throughout the globe, and Papua New Guinea is no exception. In particular, Ramu-Agri Enterprise Limited (RAIL) is an agriculturally based industry in Papua New Guinea that produces sugar and distributes it to the country's strong demand for the commodity. In addition to the various expenses associated with the industry, certain costs are incurred as a result of a layout design fault in the RAIL sugar packing section layout, which may be reduced. Layout design engineers are required to develop industries such as RAIL in Papua New Guinea in order for them to be successful in their endeavours. The fact that industries invest in their operations implies that the government receives a considerable amount of tax revenue from them to operate the nation. It is thus necessary to enhance the packaging part of RAIL by using CRAFT.

When it comes to manufacturing, plant layout is the arrangement of facilities in a systematic framework that ensures long-term efficiency of operation. Determine and arrange a detailed floor plan for designing equipment and machinery of a plant, whether it is already operational or is under consideration, in the best location to allow for the best and most efficient material flow at the lowest possible cost while requiring the least amount of ability to handle the product from raw material receipt to finished product shipment. It is a time-consuming and expensive process. Layout,

D. K. Biswal · K. Muduli (✉)
Department of Mechanical Engineering, C. V. Raman Global University, Bhubaneswar, Odisha 752054, India
e-mail: kamalakantam@gmail.com

J. N. Biswal
Department of Mechanical Engineering, Einstein Academy of Technology and Management, Bhubaneswar, Odisha 752060, India

according to Deshpande [1], is the science of determining the most efficient way of organising facilities in manufacturing industries, which has an impact on the efficiency of operation and the minimization of material handling costs, primarily through the optimization of plant layout using ALDEP and CRAFT approaches, among other things. In 1963, Armour and Buffa [2] developed a technique of using CRAFT, which was not officially recognised until then. When Prasad et al. [3] used the CRAFT algorithm to build their manufacturing plant layout design, they came up with what has come to be recognised as a "typical manufacturing plant layout design using the CRAFT approach." Gia Elizabeth Abraham was the first person to employ the CRAFT algorithm for plant layout design and development [4] in the United States. In accordance with the CRAFT approach, Hombal and Shobha [5] developed an improvement plan for the metro coach manufacturing process and factory architecture. Singh and Singh [6] employed CRAFT to perform a literature review on assembly line balancing and plant facility design, and they found it to be quite useful. According to Naik and Kallurkar [7], they conducted a literature survey on plant layout design, in which they found that an efficient plant layout design allowed for a well-ordered physical arrangement of various facilities in a manufacturing industry such as departments, workstations, machines, equipment, storage areas, and common areas. With the help of AHP, Pinto and Shayan [8] conducted experiments on a variety of heuristic strategies in order to apply them to a real-world facility problem at a furniture manufacturing business, where the types of models are contrasted [9]. In a research conducted by Okpala and Chukwu-muanya, the authors looked at plant layout designs that enhance labour utilisation efficiency, ease of production, and simplicity of maintenance. Patil and Sagare [10] conducted a case study on selecting the most effective method of organising plant physical facilities that allows for greater efficiency in an industry's operation, using an improvement algorithm for plant layout design that was based on the CRAFT algorithm, and presented their findings in a paper. It has been demonstrated that the systematic placement of various types of facilities in the industry, such as machinery, production facilities, and people, results in the most efficient use of plant facilities and increases output rates, thereby increasing the overall efficiency of the industry's operation.

For the purpose of this study, CRAFT will be used to re-allocate the placements of the departments (machines) inside RAIL's packaging division in order to reduce overall expenses associated with its current arrangement. This is done to save money on material handling and enhance the layout.

2   Methodology

The method employed here to achieve the objective of this paper is the implementation of CRAFT algorithm to improve the initial layout of the sugar packing section.

2.1 Selection of an Industry and Data Collection

In order to achieve the objective of this paper, we first have selected an existing industry in the country that is Ramu-Agri Industry Limited (RAIL) in Madang Province. The selection of the industry was based on the fact that CRAFT algorithm is best recommended to be applicable to a manufacturing industry. Automated Layout Design Program (ALDEP), Computerized Relationship Layout Planning (CORELAP) and Plant Layout Networking (PLANET) are also used to solve the plant layout-related problem in construction. However, these techniques give better performance while developing initial layout. In contrast CRAFT gives better result while employed to improve existing layout. Further, CRAFT algorithm is a widely known technique used in manufacturing industry because of its advantage in minimising the material handling costs [10]. The industry has seven major departments. They are pre-milling, milling, process, boiler, distillery, packing and stores departments. The survey was conducted primarily on packing department taking into consideration the packing machines, workstations, feed tables, workers and so forth of the packing section facilities layout. There were ten machines in the packing section. Eight of them are vertical packing machine (VPM), a controlled packing machine (CPM) and a new packing machine. The flow data of each machine that the sugar travels from one machine to another was obtained. The cost of the initial layout was on unit cost per ton basis.

2.2 Types of Layout Identified

The type of plant layout of the packing section was identified based on the way the machines and the workers are arranged. The VPMs and the CPM were arranged in a straight line, and the workers are also in a line manner arrangement that makes the flow of the sugar material easy. Thus, it is seen that the layout of the packing section is a product layout.

2.3 CRAFT Algorithm Implementation

CRAFT typically begins with the basic arrangement and then enhances it by swapping around the paired departments in order to reduce the transportation costs as much as possible. The operation continues until there is no more pairwise exchange feasible to be performed. The answer provided by CRAFT is not the optimal solution, but it is quite near to the optimal solution.

Procedures for CRAFT implementation: There are a total of 12 phases involved in implementing CRAFT in order to enhance the current layout. Each stage is detailed in further detail below:

Step 1: Input parameters

The following are the prerequisites for CRAFT: initial layout, flow data and test data. Cost per unit of miles travelled. The total number of departments is shown as the number and placement of established departments, as well as the area occupied by the departments.

Step 2: Computation of centroids of the departments

Centroids of all departments are computed and plotted on the *X* and *Y* axes in the following manner:

Step 3: Formation of distance matrix using the centroids

Distance between two departments is represented by the rectilinear distance between the centroids of their respective departments. The distance matrix may be calculated with the help of the following formula:

$$D_{ij} = (X_i - X_j) + (Y_i - Y_j) \tag{1}$$

where

D_{ij} is the distance matrix from department *i* to department *j*.
(X_i, Y_i) is the centroid of the department *i*.
(X_j, Y_j) is the centroid of the department *j*.

Step 4: Calculation of total handling costs

Assuming that information on the flow of goods, the distance between goods and the cost of goods is available, the total handling cost may be calculated using the following formula:

$$\text{Total cost} = \sum_{n=1}^{1} (F_{ij} \times D_{ij} \times C_{ij}) \tag{2}$$

where F_{ij}, D_{ij} and C_{ij} represent flow, distance and cost per unit distance from department *i* to *j*.

Step 5: Pairwise interchanges of departments

The departments are examined for pairwise exchange based on two criteria that they share, namely a shared boundary and an equal area, and an estimated cost is calculated based on these considerations.

Step 6: Determining the pairwise interchange that gives minimum handling costs

It is possible to identify the pairwise exchange department that has the lowest handling expenses possible.

Step 7: Comparing the cost of present layout with that of the previous

If the former layout's cost is less than the new layout's cost, go to step 8. If the new layout's cost is less than the prior layout's cost, proceed to step 11.

Step 8: Interchange of selected pairs of departments

Interchange selected pairwise departments, and take this as the new layout. Calculate the distance matrix, the centroids and the total costs of the new layout.

Step 9: Evaluate the new layout in terms of cost with the initial layout.

Evaluating and comparing the costs of the new layout with the costs of the original arrangement is essential. If the cost of the new layout is larger than the cost of the original configuration, then go to step 10 of the process. It is necessary to go to step 11 if it is less than the original arrangement.

Step 10: Evaluate the costs of the new layout and initial layout again

When you have evaluated and verified that the centroids, distance matrix and cost of the revised plan are the same as those of the original configuration, return to step 5 and continue. If it is less than the original layout, the new layout is referred to as the PRESENT LAYOUT, and the process continues to step 11.

Step 11: Final layout

The industry's final layout should be printed in this form.

Step 12: STOP.

3   Calculation and Results

From the case study conducted on Ramu-Agri Industry Limited (RAIL) in Madang Province, we have found that the industry is made up of seven departments, and these are Crop Service, Harvesting and Transportation (HNT), Research and Development (RND), Sustainability, Central Workshop, Human Resource (HR) and Factory Departments.

3.1   Data Analysis

We have selected the packing section of the department and focused our survey on its layout. We have collected the following types of data available at the industry that could help us to implement CRAFT algorithm to improve the layout. According to the sugar packing section layout, the manufactured sugar packets travel from one department (VPM) to another in three separate lines in the way they were arranged in a typical product layout.

- Sugar packets travel from VPM 1 to 2 and then to 3, and sugar packets from VPM 2 also travel to 3 in a straight line. VPM 3 is the end of the flow of sugar packets in that line of departments (VPMs) and the sugars are piled in pallets and picked up by forklifts to the warehouse.
- Next the sugar packets travel from VPM 4 to 5 and then to 6, and sugar packets from VPM 5 also travel to 6 in a straight line. VPM 6 is the end of the flow of sugar packets in that line of departments (VPMs) and the sugars are piled in pallets and picked up by forklifts to the warehouse.
- The sugar packets from VPM 7 travel to CPM 8 and then to VPM 9, and the sugar from CPM 8 also travel to VPM 9. VPM 9 is the end of the flow of sugar packets

in that line of departments and the sugars are piled in pallets and picked up by forklifts to the warehouse.

The new packing machine is a complete system of its own that it is automated that the raw materials enter at one end of the machine and give out the product at the other end. Therefore, we consider it a fixed machine because it is separated from the 9 machines, and it has neither equal area to one of the departments nor sharing common border with them. The CPM 8 is also considered a fixed department though it is included in the layout where the sugar from VPM 7 travels to it or sugar from it travels to VPM 9 because it has neither equal area to the VPMs nor sharing common borders with them. Therefore, the careful analysis of data was made on the 8 VPM machines based on the fact that they all have equal areas.

3.2 Calculation of Existing Layout

The initial layout of the sugar packing section is given here with the vertical packing machines, VPM numbered from 1 to 9 being referred to as departments as shown in Fig. 1.

Compute the centroids of the departments of the initial layout

Determine the centroids

The X and Y coordinates are the coordinates of the centroid of each department from the reference point (0, 0). Table 1 shows the initial packing layout departments X and Y values of their centroids.

Determine the rectilinear distances

The distance from one department to another is measured in a rectilinear distance from one centroid to the other by using formula (1)
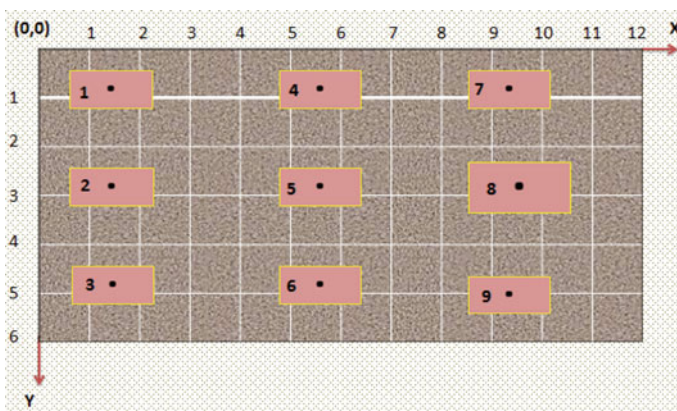
Fig. 1 RAIL initial packing layout departments being plotted on grids determining their centroids

Table 1 RAIL initial packing layout departments x and y values of their centroids

Departments	X	Y
1	1.3	0.9
2	1.3	2.9
3	1.3	4.9
4	5.6	0.9
5	5.6	2.9
6	5.6	4.9
7	9.3	0.9
8	9.5	3.0
9	9.3	5.0

The rectilinear distance for flow of sugar from department 1 to 2 as denoted in from-to matrix is calculated using the centroids:

$$D_{ij} = \left(X_i - X_j\right) + \left(Y_i - Y_j\right) = (1.3 - 1.3) + (2.9 - 0.9) = 2m \qquad (3)$$

The rectilinear distance for flow of sugar from department 1 to 3 as denoted in from-to matrix is calculated using the centroids:

$$D_{ij} = \left(X_i - X_j\right) + \left(Y_i - Y_j\right) = (1.3 - 1.3) + (4.9 - 0.9) = 4m \qquad (4)$$

Determine the cost matrix

The cost matrix comes from the cost that the initial layout consumes in relation to the layout. That is the unit cost of the material handling in the sugar packing section as shown in Fig. 2.

The total cost (TC) of the original layout is calculated as follows:

For the calculation of the TC, we use the formula (2) that has been provided.
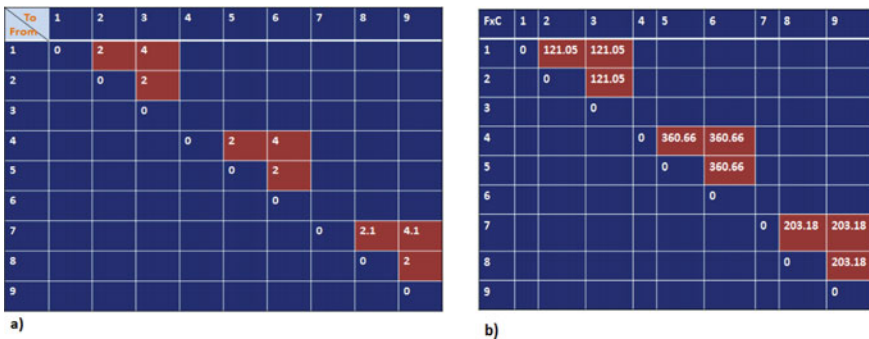
Fig. 2 **a** From–to matrix, **b** reward matrix (cost matrix) of initial packing layout

$$\text{Total cost} = (2 \times 121.05) + (4 \times 121.05) + (2 \times 121.05) + (2 \times 360.66)$$
$$+ (4 \times 360.66) + (2 \times 360.66) + (2 \times 203.18) + (4.1 \times 203.18)$$
$$+ (2 \times 203.18) = \text{K5, 519.80} \tag{5}$$

The cost that we have considered for the above calculation is the unit cost per ton for unit flow of sugar from one department to another.

To determine the total cost for the target production of packing section per day, we used the production rate of the machines. Though the production rate may alter due to the fluctuation in demand, we consider this calculation base on constant demand and constant production target to meet that demand per day.

250 g *sugar production details per day*

There are 3 machines, VPM 4, 5 and 6 with sugar packaging rate at 38 packets/min.

Minutes per day = 24 h $\times$ 60 min = 1440 min.

Target number of sugar packets per day = 38 pcts/min $\times$ 1440 min = 54,720 packets.

Target number of bales per day = 54,720 packets/40 packets/bale = 1368 bales.

Target numbers of pallets per day = 1368 bales/126 bales/pallets = 10.8 pallets.

Target tonnes of sugar per day = 54,720 packets $\times$ 250 g = 13,680,000 g = **13.68 tons**.

Target tons of 250 g sugar packets for 3 VPM = 13.68 tons $\times$ 3 = **41.04 tons**.

3.3   Calculation to Propose a New Layout

Determine the possible pairwise exchanges. There are four possible pairwise exchanges.

- 1 and 6: These two departments can be exchanged for they have equal areas as shown in Fig. 4.
- 3 and 5: These two departments can be exchanged for they have equal areas.
- 2 and 7: These two departments can also be exchanged for they have equal areas.
- 4 and 9: These two departments can be exchanged for they have equal areas.

The department 8 cannot be exchanged with one of the other departments because it does not have equal area or sharing common border with them as shown in Fig. 3 (Fig. 4).

(i) *Departments 1 and 6 pairwise exchange*

Determine the centroids of the new pairwise exchanged layout (Table 2).
Determine the rectilinear distances
The distance calculated will be same as discussed in Sect. 3.2.
Determine the cost matrix
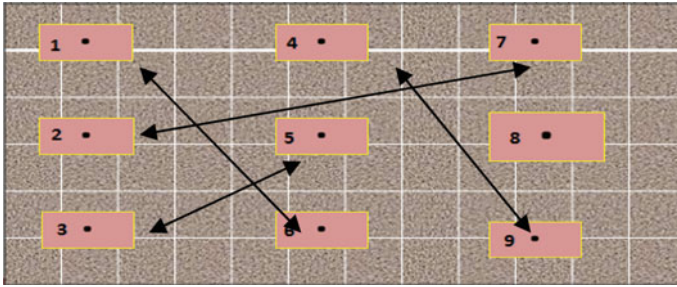
Fig. 3 RAIL initial packing layout showing possible pairwise departments exchanges
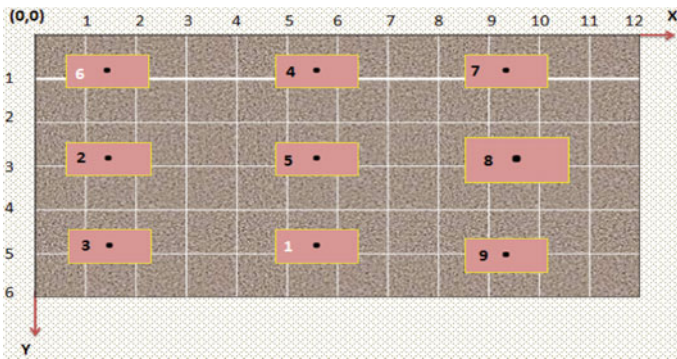
Fig. 4 Layout showing departments 1 and 6 exchanged being plotted on grids indicating their centroids

Table 2 Layout showing departments centroids X and Y values after departments 1 and 6 exchanged

Departments	X	Y
6	1.3	0.9
2	1.3	2.9
3	1.3	4.9
4	5.6	0.9
5	5.6	2.9
1	5.6	4.9
7	9.3	0.9
8	9.5	3.0
9	9.3	5.0

The cost matrix comes from the cost that the initial layout consumes in relation to the layout. That is the unit cost of the material handling in the sugar packing section as shown in Fig. 5.

Calculate the total cost of new layout from switching departments 1 and 6.

a)

To / From	6	2	3	4	5	1	7	8	9
6	0	2	4						
2		0	2						
3			0						
4				0	2	4			
5					0	2			
1						0			
7							0	2.1	4.1
8								0	2
9									0

b)

FxC	6	2	3	4	5	1	7	8	9
6	0	360.66	360.66						
2		0	121.05						
3			0						
4				0	360.66	360.66			
5					0	360.66			
1						0			
7							0	203.18	203.18
8								0	203.18
9									0
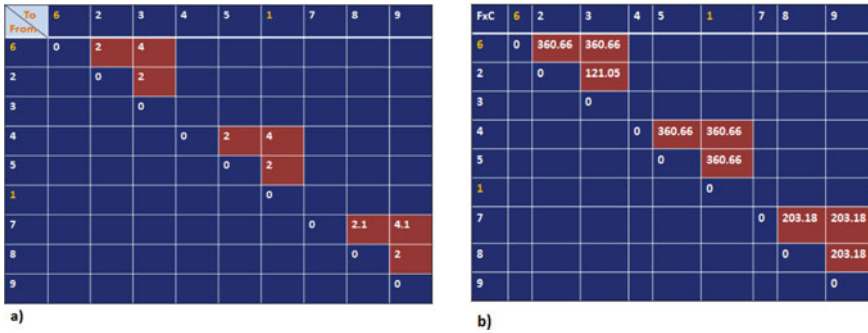
Fig. 5 **a** From–to matrix, **b** reward matrix (cost matrix) of new packing layout

We use the given formula (2) for computation of the TC for the initial layout.

$$
\begin{aligned}
\text{Total cost} = {} & (2 \times 360.66) + (4 \times 360.66) + (2 \times 121.05) + (2 \times 360.66) \\
& + (4 \times 360.66) + (2 \times 360.66) + (2.1 \times 203.18) + (4 \times 203.18) \\
& + (2 \times 203.18) = \text{K}6957.40
\end{aligned} \tag{6}
$$

This pairwise exchange is not feasible because the cost is greater than the initial cost.

In the similar way, all the pairwise exchange matrix was calculated.

(ii)　*Departments 3 and 5 pairwise exchange*

$$
\begin{aligned}
\% \text{ Savings} &= \frac{\text{Initial total cost} - \text{New total cost}}{\text{Initial total cost}} \\
&= \frac{5519.80 - 5204.80}{5519.80} = 5.7\%
\end{aligned} \tag{7}
$$

(iii)　*Departments 2 and 7 pairwise exchange*

$$
\begin{aligned}
\% \text{ Savings} &= \frac{\text{Initial total cost} - \text{New total cost}}{\text{Initial total cost}} \\
&= \frac{5519.80 - 5174.80}{5519.80} = 6.25\%
\end{aligned} \tag{8}
$$

(iv)　*Departments 4 and 9 pairwise exchange*

$$
\begin{aligned}
\% \text{ Savings} &= \frac{\text{Initial total cost} - \text{New total cost}}{\text{Initial total cost}} \\
&= \frac{5519.80 - 4052.10}{5519.80} = 26\%
\end{aligned} \tag{9}
$$

In terms of the target production of 301.68 tons per day for the 3 shifts in the operation of the packing section, the company can save 26% of total cost, K1,665,213.30 of the initial layout which is calculated as:

$$\%Savings = 26\% \text{ of } K1,665,213.30 = K432,955.50 \qquad (10)$$

The four different total costs calculated from the three different pairwise exchanges can be used to propose the new layout of the sugar packing section based on its feasibility that it can help the company save much. This means that the new layout total cost of the new layout from a pairwise exchange must be less than the other pairwise exchanges attempted and the total costs of the initial layout for it to be the feasible proposed layout.

- The initial cost of the layout as was calculated is K5519.80
- The first pairwise exchange of departments 1 and 6 cost is K6957.40. This is not feasible because it is more than the initial cost.
- The cost of the second pairwise exchange of departments 3 and 5 is K5204.80. This saves about 5.7% which is equivalent to K315.00.
- The cost of the third pairwise exchange of departments 2 and 7 is K5174.80, and this saves about 6.25% which is equivalent to K345.00.
- The cost of the fourth pairwise exchange of departments 4 and 9 is K5174.80, and this saves about 26% which is equivalent to K1437.70.

Comparing these results, we have selected the new layout for the sugar packing section to be one that the departments 4 and 9 have been pairwise exchanged because it saves 26% of the initial cost.

4   Conclusion

The importance of CRAFT is that it uses the data of the initial layout and allows pairwise exchanges to improve the initial layout. The space utilisation by the initial layout was unchanged. The total distance travelled by the sugar packets was constant because the interchanges between departments were based on the fact that they have equal area and not sharing common borders so their centroids remain the same. Once they were exchanged, they also exchanged the centroids and distance matrix so it did not affect the total distances the sugar travels in the new layout. Everything remained the same except that the flow of one type of sugar from one department to another was regulated with their varying unit costs in the new improved layout.

The sugar packing section of RAIL was improved by 26% savings from the initial total cost of K5519.80 on unit-based calculation. The other pairwise exchanges that gave the saving of 5.7% and 6.25% were less than 26%, so they were not recommended for the new layout because the reduction of the cost of the initial layout is less so we have to select the layout that when pairwise exchanged gives the most savings. When we consider the target production of 301.68 tons sugar packets

per day by RAIL, the total cost for this was calculated to be K1,665,213.30. The 26% of this total cost that can be saved by the industry with the new layout is K432,955.50. Such savings by the industry can help it extend the business and build the lucrative nature of the company.

References

1. Deshpande, V., Patil, N.D., Baviskar, V., Gandhi, J.: Plant layout optimization using CRAFT and ALDEP methodology. Prod. J. Nat. Prod. Counc. **57**(1), 32–42 (2016)
2. Armour, G.C., Buffa, E.S.: A heuristic algorithm and simulation approach to relative location of facilities. Manage. Sci. **9**(2), 294–309 (1963)
3. Prasad, N.H., Rajyalakshmi, G., Reddy, A.S.: A typical manufacturing plant layout design using CRAFT algorithm. Proc. Eng. **97**, 1808–1814 (2014)
4. Gia Elizabeth, A., Sasikumar, R.: Layout planning for sustainable development. Int. J. Innov. Res. Sci. Eng. Technol. **2**(1), 655–665 (2013)
5. Hombal, R.R., Shobha, R.: Improvement of process and product layout for metro. Int. Res. J. Eng. Technol. **4**(7), 470–473 (2017)
6. Singh, P., Singh, M.: Optimization of assembly line and plant layout in a mass production industry—a literature survey. Int. J. Eng. Sci. Invention **4**(4), 1–4 (2015)
7. Naik, S.B., Kallurkar, S.: A literature review on efficient plant layout design. Int. J. Ind. Eng. Res. Dev. **7**(2), 43–51 (2016)
8. Pinto, W.J., Shayan, F.: Layout design of a furniture production line using formal methods. J. Ind. Syst. Eng. **1**(1), 81–96 (2007)
9. Okpala, C.C., Chukwumuanya, O.: Plant layouts' analysis and design. Int. J. Adv. Eng. Tech. **7**(3), 201–206 (2016)
10. Patil, V.M., Sagare, P.M.: Case study of improvement algorithm of layout design using craft algorithm. Int. J. Eng. Technol. Sci. Res. (IJETSR) 38–43 (2017)

Finite Element Analysis of Gas Turbine Blade

R. Rudrabhi Ramu, K. Leela Kumar, B. Gangadhar, and P. H. J. Venkatesh

1 Introduction

Gas turbine plant is one of the power generation unit works on Brayton cycle. It consists a rotary compressor which is connected to a turbine, as well as a combustion chamber or region, known as a combustor, in the middle [1]. The basic operation of a gas turbine is similar to that of a steam power plant, but instead of water, air is employed [2]. Fresh ambient air passes through a compressor, which increases its pressure [3]. The energy is then added by spraying fuel into the air and lighting it, resulting in a high-temperature flow from the combustion [4]. This high-temperature and high-pressure gas rush into a turbine and expand to exhaust pressure, by generating shaft work through this process [5]. The compressor, electric generator, and other auxiliary devices that are linked to the turbine shaft are driven by the work produced by turbine shaft [6, 7]. The surplus energy that is not participated for shaft work is released through the exhaust gases, which are either very hot or very fast [8]. The design of a gas turbine is determined by its objective, which is to maximize the most desirable energy form. Aircraft, trains, ships, electricity generators, and tanks all employ gas turbines for propulsion [9]. The present study is carried out by considering various blade geometry and material properties. By make use of ANSYS, a profile is generated with necessary assumptions, and it is meshed and analyzed by a tetra mesh 16,150 nodes and 80,300 elements with a growth rate of 1.2 and an average aspect ratio 1.89 [1]. Under all working conditions, two different materials stainless steel and chromium have been tested, and the best results were noticed after completion of successful trials [10] (Fig. 1).

R. Rudrabhi Ramu (✉) · K. Leela Kumar · B. Gangadhar · P. H. J. Venkatesh
Department of Mechanical Engineering, Vignan's Institute of Information Technology (A), Visakhapatnam, Andhra Pradesh, India
e-mail: ramumittuusha@gmail.com

1-2 Isentropic compression (in a compressor)
2-3 Constant-**pressure** heat addition
3-4 Isentropic expansion (in a turbine)
4-1 Constant-**pressure** heat rejection
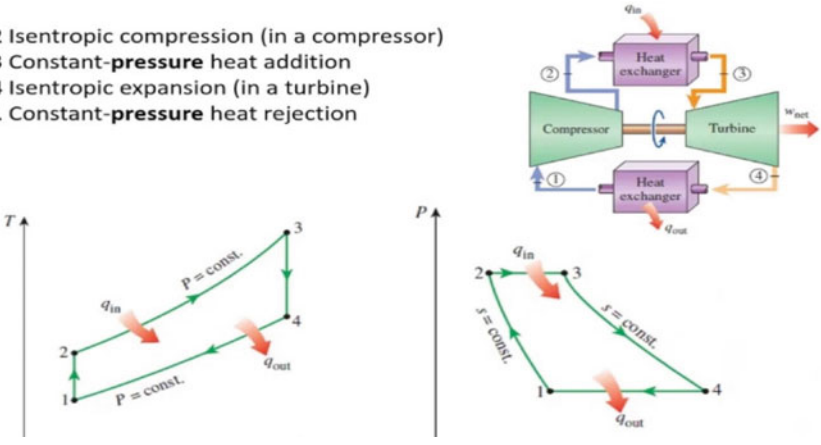
Fig. 1 Brayton cycle P-V and T-S diagram

1.1 Gas Turbine Blade

The major component of gas turbine unit is its turbine section which is made by series of blades based upon the power requirements. Each blade plays an important role to transmit power. The blades are arranged in such a manner that the charge of extracting energy from the combustor's gas is being absorbed spontaneously to produce power. In both steam and gas turbines, blade fatigue is a primary cause of failure. The stress created by vibration and resonance caused during its operation results fatigue [11]. Friction dampers are utilized to protect blades from these high-dynamic loads. Wind turbine and water turbine blades are designed to function in various environments, with lower rotating speeds and temperatures (Fig. 2).

Fig. 2 Gas turbine blade

2 Methodology

Modeling, meshing, and simulation analysis:

In this paper, a standard gas turbine blade profile is designed using ANSYS software, and the geometry is imported and meshed using CFX preprocessor. The deformations subjected to standard boundary conditions against different materials are shown below (Figs. 3, 4, 5, 6, 7, 8, 9, 10 and 11).

Similar way, all other values are determined using ANSYS and tabulated for the comparison.
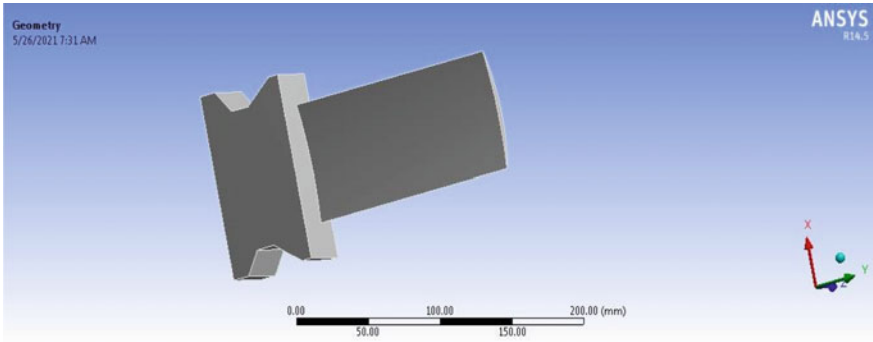
Fig. 3 Gas turbine blade designed in ANSYS
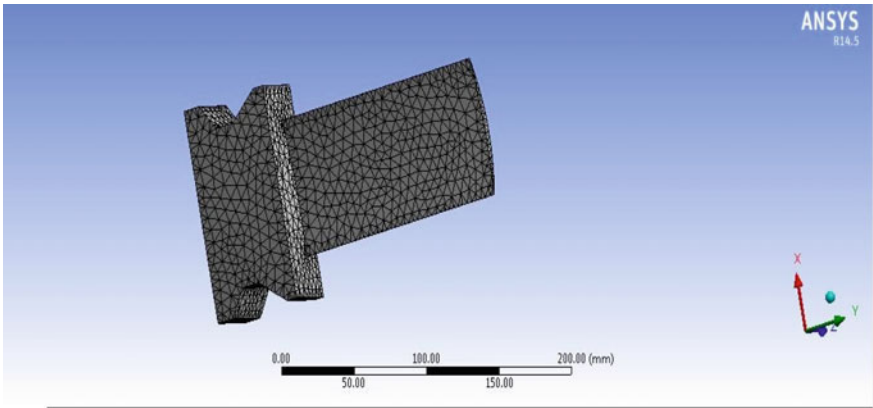
Fig. 4 Gas turbine blade meshing
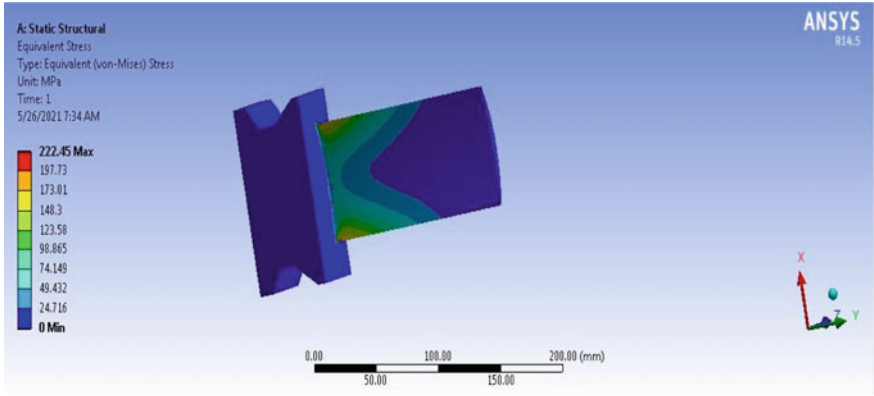
Fig. 5 Deformation of stainless steel 316L
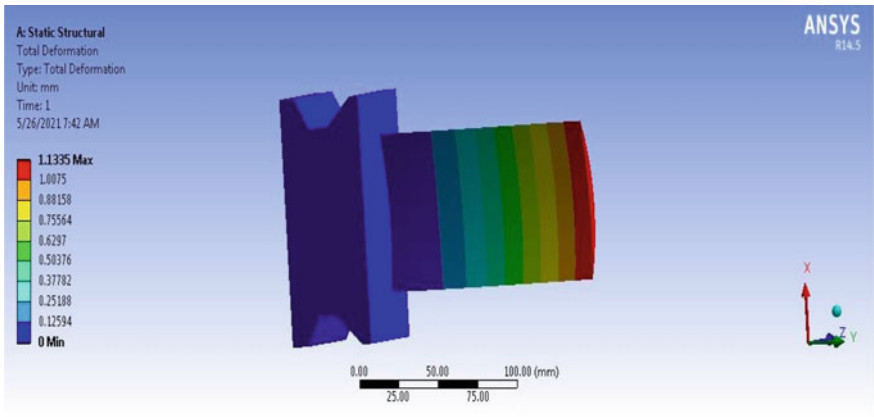
Fig. 6 Stress value of stainless steel 316L
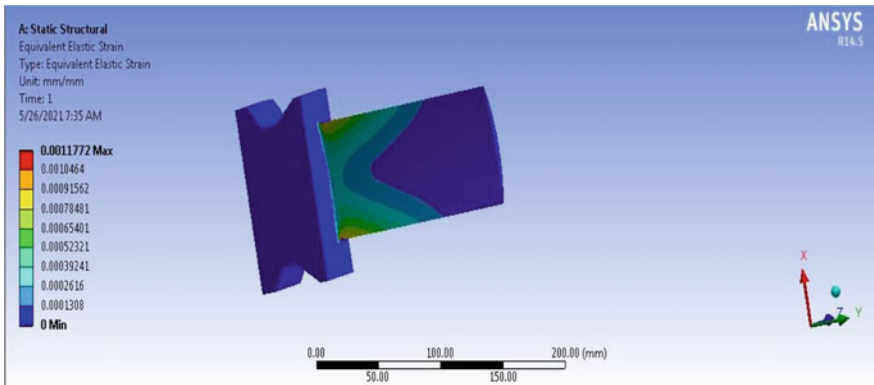
Fig. 7 Strain value of stainless steel 316L
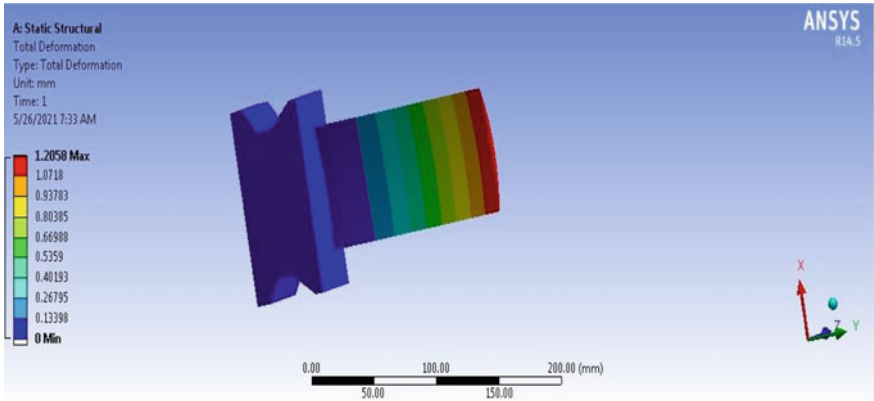
Fig. 8 Deformation of chromium stress
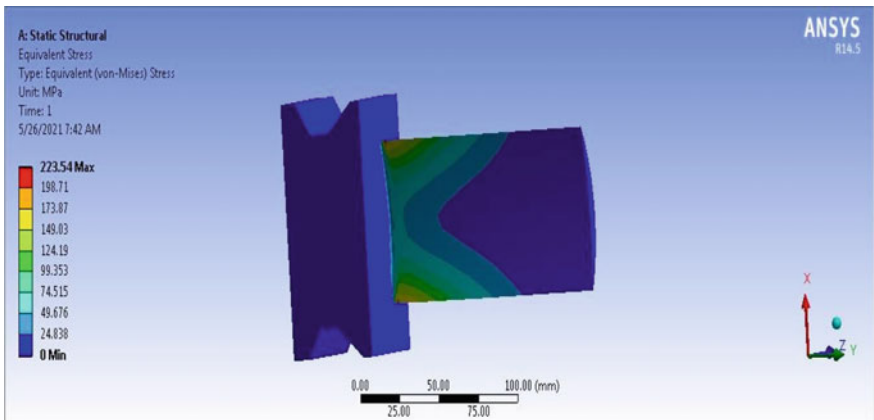
Fig. 9 Stress value of chromium steel

3 Results

See Tables 1 and 2.

4 Conclusions

In this project, the analysis is made by considering several models such as turbine blades with and without holes, internal cooling, exterior cooling, and internal–external cooling. In this project, a turbine blade is numerically simulated using two distinct materials. It is concluded that stainless steel 316L with an internal–external
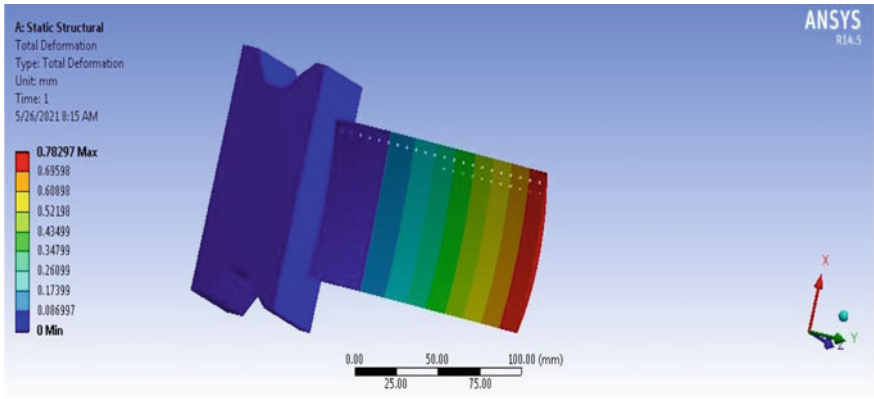
Fig. 10 Strain value of chromium steel
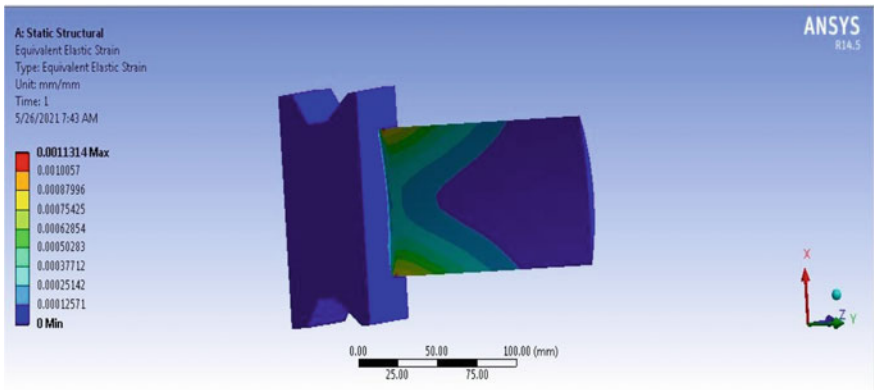
Fig. 11 Internal and external cooling

Table 1 Static analysis values

Cases	Material	Deformation (mm)	Stress (N/mm^2)	Strain
Without holes	Chromium steel	1.1897	227.16	0.0011601
	Stainless steel 316L	1.2058	225.45	0.001772
Internal cooling	Chromium steel	1.1335	223.54	0.0011314
	Stainless steel 316L	1.1485	220.42	0.001159
External cooling	Chromium steel	0.85002	218.22	0.0011088
	Stainless steel 316L	0.87911	217.56	0.0011452
Internal and external cooling	Chromium steel	0.78297	204.26	0.0010376
	Stainless steel 316L	0.80993	203.55	00.0010713

Table 2 Thermal analysis values

Cases	Material	Temperature (°C)	Heat flux (W/mm^2)
Without cooling	Chromium steel	650.26	15.05
	Stainless steel 316L	650.25	19.056
Internal cooling	Chromium steel	651.12	16.002
	Stainless steel 316L	651.04	20.685
External cooling	Chromium steel	651.66	17.583
	Stainless steel 316L	651.56	22.722
Internal and external cooling	Chromium steel	650.45	19.805
	Stainless steel 316L	650.42	25.594

cooling system produces positive outcomes in all areas. Thermal flux is higher for stainless steel 316L and chromium steel, according to the thermal data. As a result, stainless steel 316L is preferable over chromium steel. The major advantage which possesses is its weight. The same procedure may be carried out with modal analysis which gives the better results and mechanical properties.

5 Future Scope

With reference to the above results, same profile can be tested under different operating conditions with different alloying elements. Nowadays, so many smart materials and advanced materials with latest technology have been introduced, the same thesis can be extended to test the same, and there is a lot of scope to improve the results further with optimum parameters.

References

1. Mohamad, B.A., Abdelhussien, A.: Failure analysis of gas turbine blade using finite element analysis. Int. J. Mech. Eng. Technol. (IJMET) **7**(3), 299–305 (2016)
2. Htwe, W.L., Win, H.H., San, N.A.: Design and thermal analysis of gas turbine blade. Int. J. Mech. Prod. Eng. **3**(7), 62–66 (2015)
3. Jabbar, A.A., Rai, A.K., Ravinder Reedy, P., Dakhil, M.H.: Design and analysis of gas turbine rotor blade using finite element method. Int. J. Mech. Prod. Eng. Res. Dev. **4**(1), 73–94 (2014)
4. Sulaiman, K.S., Ramesh Kumar, G.R.: Vibration diagnosis approach for industrial gas turbine and failure analysis. Br. J. Appl. Sci. Technol. **14**(2), 1–9 (2016)
5. Ikpe, A.E., Owunna, I., Ebunilo, P.O., Ikpe, E.: Material selection for high pressure (HP) turbine blade of conventional turbojet engines. Am. J. Mech. Ind. Eng. **1**(1), 1–9 (2016)

6. Kalapala, P., Prasad, B.A., Anandarao, M.: Material optimization and dynamic approach for performance criteria in application to gas turbine blade to overcome resonance. Int. J. Sci. Eng. Res. **8**(6), 189–196 (2017)
7. Jabbar, A.A., Rai, A.K., Ravinder Reedy, P., Dakhil, M.H.: Design and analysis of gas turbine rotor blade using finite element method. Int. J. Mech. Prod. Eng. Res. Dev. (IJMPERD) **4**(1), 73–94 (2014)
8. Vijaya Kumar, V., Lalitha Narayana, R., Srinivas, C.: Design and analysis of gas turbine blade by potential flow approach. Int. J. Eng. Res. Appl. **4**(1), 187–192 (2014)
9. Umamaheswararao, L., Mallikarjunarao, K.: Design and analysis of a gas turbine blade by using FEM. Int. J. Latest Trends Eng. Technol. (IJLTET) **4**(4) (2014)
10. Nithin Kumar, K.C., Tandon, T., Silori, P., Shaikh, A.: Structural design and analysis of gas turbine blade using CAE tools. Int. J. Eng. Res. Technol. **3**(10), 469–474 (2014)
11. Prasad, R.D.V., Narasa Raju, G., Srinivasa Rao, M.S.S., Vasudeva Rao, N.: Study state thermal and structural analysis of gas turbine blade cooling system. Int. J. Eng. Res. Technol. (IJERT) **2**(1), 1–6 (2013)

Static and Fluid Analysis of a Marine Propeller

Gill Santosh Kumar and Boddapalli Mahesh

1 Introduction

A large boat travels deep around bodies of water carrying passengers or goods for colorful purposes such as defense, exploration, and fishing [1]. Various ships include high-speed vessels, tugs, planters, dry-weight vessels, liquid weights, passenger ships, ocean liners, luxury cruise yachts, and warships. However, no matter how light marine propellers become, conventional marine propellers will continue to be the standard propulsion medium for face boats and aquatic vehicles for the foreseeable future [2, 3]. Variations of introductory propeller shape into water spurt propulsions and alternate style thrusters on aquatic vehicles haven't significantly changed [4], how we determine and dissect propeller performance [5]. We still need propellers to induce acceptable thrust to propel a vessel at some design speed with some care taken in icing some "reasonable" propulsive effectiveness [6]. Nowadays the composite materials are gaining much interest among researchers as it show enhanced properties with lightweight structures [7]. The main advantages are strength to weight ratios is high when compared to other conventional materials [8]. The objective of the work is to analyze to compare the three-blade and four-blade propellers for static structural and CFD analysis using NX and Ansys software tools.

G. Santosh Kumar (✉) · B. Mahesh
Department of Mechanical Engineering, Vignan's Institute of Information Technology (A),
Visakhapatnam, Andhra Pradesh, India
e-mail: gillsantoshkumar@gmail.com

1.1 Geometry Definitions

Geometry definitions apply to the overall propeller geometry and area function of radius. Pitch: The pivotal distance went by the segment whenever turned on insurgency insect interpreted along the part nose-tail line (bend) Mid chord line: line delivered from the mid harmonies (for example Midpoint of segment nose-tail line) of each segment along a propeller sharp edge [9]. Rake: Axial separation from the mid harmony point at the center segment and the segment of interest [10]. Slant or Skew Angle: Tangential part of the point framed on the propeller between an outspread line going through the center segment mid harmony point and a spiral [11].

2 Methodology

2.1 Theoretical Calculations

Geometric specifications of the Propeller and model is INSEAN E779A

> Diameter of the Propeller = 227.2 mm
> Number of blades = 4
> Type of propeller = Controllable pitch propeller
> Materials considered = Aluminum and CFRP

Calculate Pitch, Total area of the circle, Total blade area

> Given ratio of Pitch/Diameter = 1.1
> Total Area of the circle = πr^2
> Total blade area = total area of the circle × disk area ratio
> Where Disc area ratio = 0.51

Calculate Boat Speed, Mass flow rate,

$$\text{speed} = \frac{\text{RPM}}{\text{RATIO}} \times \left[\frac{\text{Pitch}}{c} \right] \times \left[1 - \frac{S}{100} \right] \qquad (1)$$

[Assume Ratio = 1/2; gear ratio (c) = 1; slip (s) = 0]
Mass flow rate per hour (m) = total blade area × speed of the boat

Calculate Advance Velocity, Thrust, the thrust (T) is equal to the mass flow rate (m) times the difference in the velocity

$$T = m \times [V_b - V_a] \qquad (2)$$

where Advance Velocity $V_a = V_b \times (1 - w)$ [w = wake fraction]

Determine variation of Pitch and Thickness along the radius:

Pitch at 25%, 50%, 60%, 70%, 80%, and 90% of radius, represented by P0.25, P0.5, P0.6, P0.7, P0.8, P0.9, was computed using the method shown below to estimate the pitch along the radius of the propeller blade [12] (Table 1)

$$p(x) = (x) \times (\text{Radius of the propeller blades} \times \text{pitch/diameter}) \qquad (3)$$

Similarly, using the blade thickness fraction $= 0.05 = (t_0/D)$, the thickness of the blade is determined for the radius, which means

$$t_0 = D \times 0.05 \qquad (4)$$

Hence, along the radius of the propeller, the thickness is estimated from Eq. 5 (Tables 2, 3 and 4),

$$t_0 = 0.05 \times (R \text{ in percentage}) 12 \qquad (5)$$

Table 1 Variation of pitch along the radius

S. No.	Pitch %	Radius of propeller	Variation of pitch
1	P0.25	113.6	31.24
2	P0.5	113.6	62.48
3	P0.6	113.6	74.98
4	P0.7	113.6	84.47
5	P0.8	113.6	99.97
6	P0.9	113.6	112.48
7	P1.0	113.6	124.96

Table 2 Variation of thickness along the radius

S. No.	Thickness %	Radius of the propeller	Variation of the thickness
1	T0.1	113.6	0.568
2	T0.2	113.6	1.136
3	T0.3	113.6	1.704
4	T0.4	113.6	2.272
5	T0.5	113.6	2.84
6	T0.6	113.6	3.408
7	T0.7	113.6	3.976
8	T0.8	113.6	4.544
9	T0.9	113.6	5.112
10	T1.0	113.6	5.68

Table 3 Properties of aluminum 5052 [4]

Parameters	Values
Young's modulus	69.3 GPa
Poisson ratio	0.33
Mass density	2.68 g/cc
Damping coefficient	0.03

Table 4 Properties of CFRP [4]

Parameters	Values
Young's modulus	116.04 GPa
Poisson ratio	0.28
Mass density	1.6 g/cc
Damping coefficient	0.018

3 Results

Results based on Stress and Strain: The graphs of Stress versus Strain have been drawn by taking into account the results obtained in that particular propeller's Static Analysis. All propellers of both the materials are seen to follow Hooke's Law and while the blade won't immediately fail; it gradually might crack due to fatigue when it crosses the value of Yield Stress (Figs. 1, 2 and 3).

From the CFD analysis, the following behavioral patterns were observed for the three-blade and four-blade propellers (Figs. 4, 5, 6, 7, 8 and 9).

4 Conclusions

As per the values of stress, strain, and deformation, the boundary conditions were taken correctly. The behavior of the propeller was assumed to be like that of a cantilever beam, and hence, the deformations were maximum at the tip of the blade and zeroed at the blade-hub intersection. The edge was supposed to be a cantilever beam fixed at the hub end. The stress created in the four-bladed aluminum propellers was roughly 0.34% more than that originated in the CFRP propeller, according to static structural analysis. The strains and deformations were seen though they were 0.60% less in the CFRP propeller when compared to the aluminum propeller. The Stress versus Strain plots proved that the curves were linear and that both the materials obeyed Hooke's Law until they eventually failed due to fatigue. The aluminum propeller was seen to be heavier than the CFRP propeller by 40.3%. For boats or ships where higher pressures and speeds are the requirements, the four-bladed propellers perform better than the 3 blade propeller. If lesser deformation and strain are the requirement, then the four-bladed propellers of CFRP material act better than the aluminum propeller. Hence, CFRP is seen to outperform aluminum on both counts.
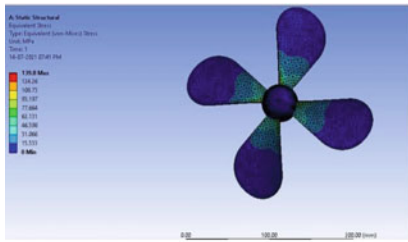
i. Equivalent (von-misses) stress
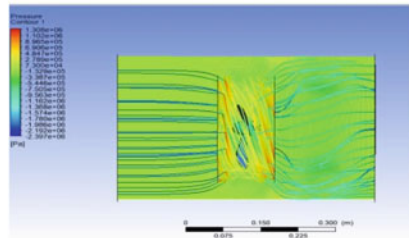
ii. Velocity   Contour of 4 blade aluminum propeller
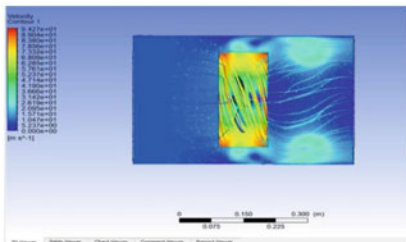
iii. Pressure Contour of 4 blade aluminum propeller
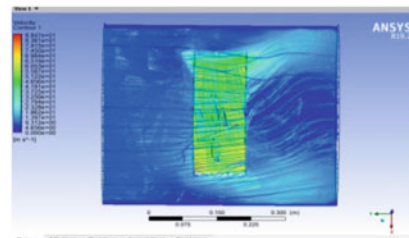
iv. Velocity contour of 3 blade propeller
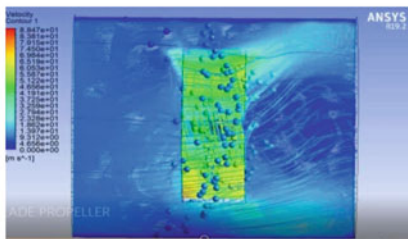
v. Pressure contour of 3 blade propeller
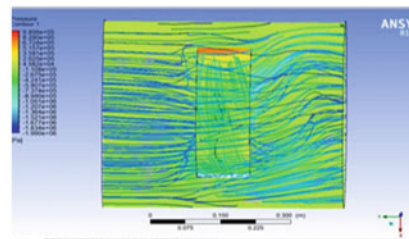
vi. Streamline velocity of 3 blade propeller

Fig. 1 Velocity and pressure contours of three-blade and four-blade propellers

Future Scope of Work

Only Static Structural analysis and CFD analysis are used in this project. It can also be used for Modal analysis, with different materials such as aluminum and CFRP being used to minimize noise and even capitalization. Different materials like GFRP, Epoxy Resin reinforced with different kinds of reinforcements can also be tested.

Fig. 2 Stress versus strain of aluminum propeller

Fig. 3 Stress versus strain graph of CFRP propeller
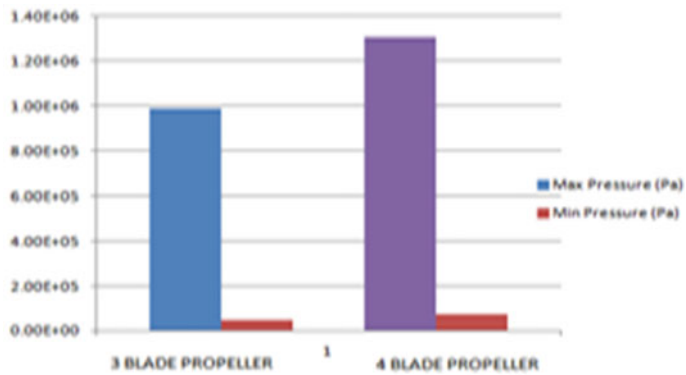
Fig. 4 Comparison of pressures created
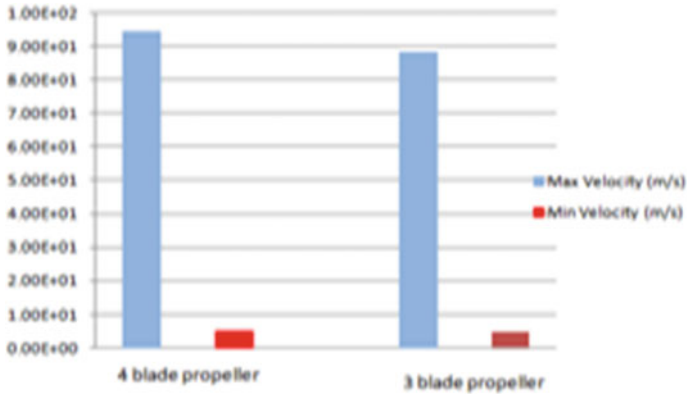
Fig. 5 Comparison of velocity created
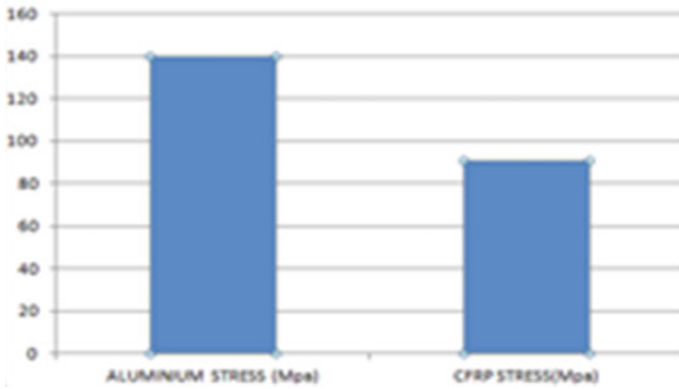
Fig. 6 Comparison of stresses developed (MPa)
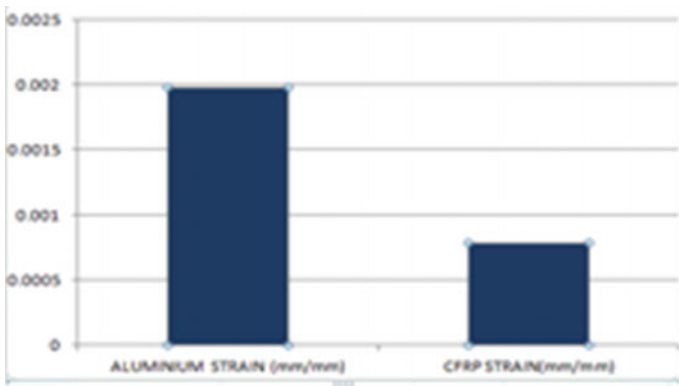
Fig. 7 Comparison of strains developed
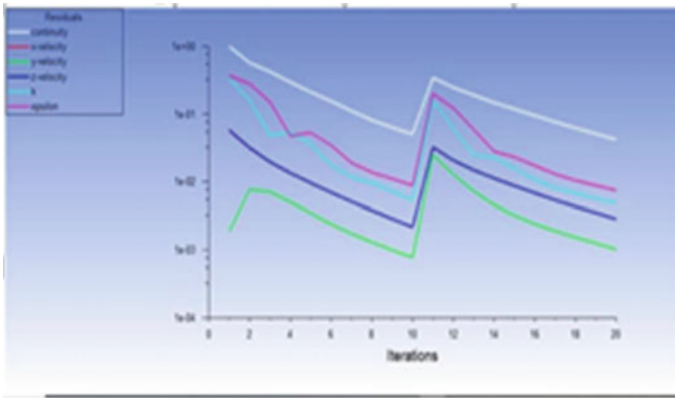
Fig. 8 *x*-velocity, *y*-velocity, k-epsilon, and time/iteration of four-blade propeller
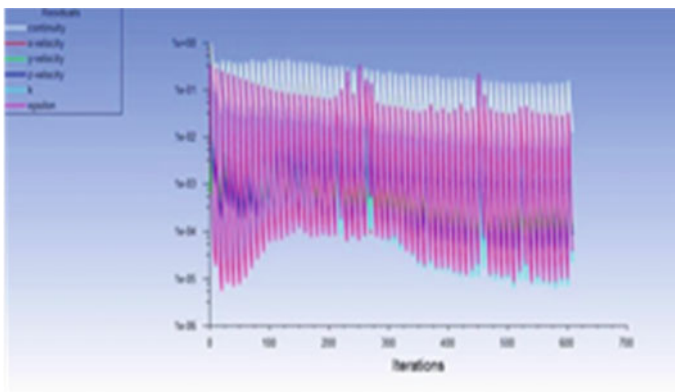
Fig. 9 *x*-velocity, *y*-velocity, k-epsilon, and time/iteration of three-blade propeller

References

1. Bammidi, R., Spandana Veronika, K.: Dynamic analysis of composite propeller of ship using FEA. Int. J. Comput. Aided Eng. Technol. **10**, 650–672 (2018). http://doi.org/10.1504/IJCAET.2018.095201
2. Prasad, P., Babu, L.B.: Design and analysis of the propeller blade. Int. J. Adv. Mech. Civ. Eng. **4**, 14–19 (2017)
3. Rao, Y.S., Rao, K.M., Reddy, B.S.: Stress analysis of composite propeller by using finite element analysis. Int. J. Eng. Sci. Technol. **4**, 3866–3875 (2012)
4. Ganesh, V., Pradeep, K., Srinivasulu, K.: Modeling and analysis of a shaft blade for its strength. Int. J. Sci. Res. **5**, 1412–1415 (2016). http://doi.org/10.21275/v5i2.nov161351
5. Krasilnikov, V., Zhang, Z., Hong, F.: Analysis of unsteady propeller blade forces by RANS. In: First international symposium on marine propulsors, pp. 1–11 (2009)
6. Durganeeharika, P., Babu, P.S.: Design and analysis of ship propeller using Fea. In: Proceedings of international conference on recent trends in mechanical engineering, pp. 74–77 (2015)

7. Dhanunjayarao, B.N., Sanivada, U.K., Naidu, N.V.S., Fangueiro, R.: Effect of graphite particulate on mechanical characterization of hybrid polymer composites. J. Ind. Text. 1–9 (2021). https://doi.org/10.1177/15280837211010670

8. Dhanunjayarao, B.N., Naidu, N.V.S., Kumar, R.S., Phaneendra, Y., Sateesh, B., Olajide, J.L., Sadiku, E.R.: 3D printing of fiber reinforced polymer nanocomposites: additive manufacturing. In: Handbook of Nanomaterials and Nanocomposites for Energy and Environmental Applications (2020). https://doi.org/10.1007/978-3-030-11155-7_166-1

9. Søntvedt, T.: Propeller blade stresses, application of finite element methods. Comput. Struct. **4**, 193–204 (1974). http://doi.org/10.1016/0045-7949(74)90082-0

10. Senthil, J., Ramesh, S.: Static and dynamic analysis of composite propeller. J. Chem. Pharm. Sci. **9**, 1724–1726 (2016)

11. Kishore, M.L.P., Behera, R.K.: Replacement of nab propeller blade with composite for strength criteria, pp. 42–46 (2010)

12. Pawar, A.B., Petkar, T.S., Pitale, P.S., Salagare, S.S.: Design and simulation of marine propeller with different blade geometry. Int. J. Innov. Sci. Res. Technol. **4**, 109–117 (2019)

Analytical Estimation of Power for a Fabricated Power Generating Train Using Rack and Pinion Mechanism

L. Daloji, M. Venkatesh, Narasinga Rao, and M. Venu

1 Introduction

The extensive usage of the energy resulted in energy crunch, due to that there is a need in developing new techniques of energy generation. New method of energy generation is not only solving the crunch but also saving the environment [1]. The increase in population and decrease in conventional methods for electricity generation shows the importance of nonconventional energy resources. In order to reduce the shortage of energy crunch, the need of implementing the methods of optimal utilization of conventional sources for conservation of energy. Also, identify the new source for producing renewable energy [2]. The focus is toward renewable sources of energy because fossil fuels are polluting the environment and nuclear energy needs careful controlling of raw material. Nonconventional technologies have been discovered to improve various energy generation methods and also to ensure they are more sustainable.

Non-conventional energy sources generated by wind, tides, solar, geothermal heat, and biomass including farm and animal waste are natural, renewable, or inexhaustible and do not cause environmental pollution and are eco-friendly [3]. The energy produced from railway tracks is an unconventional energy. Whatever the energy generated, will be stored into the battery and used to station appliances [4].

Chahande et al. [5], explained about a new design mechanism which carries load and generates power using hydraulic press and chain drive. This is another way to

L. Daloji (✉) · N. Rao · M. Venu
Faculty of Mechanical Engineering, Vishnu Institute of Technology, Bhimavaram, Andhra Pradesh 534202, India
e-mail: daloji.iiitbasar@gmail.com

M. Venkatesh
Mechanical Engineering, Vishnu Institute of Technology, Bhimavaram, Andhra Pradesh 534202, India

store the energy which is produced using trains when passing over the railway tracks. Raj et al. [6] investigated the generation of power by using crank mechanism method. When a train goes over the railway track, by application of load, the spring interconnected with the track gets compressed. Therefore, motion starts in rack and pinion setup including chain drive. This motion, when it passes through the flywheel, rectifier, and DC motor, will lead to the generation of electricity. Kaur et al. [7] proposed a new technique to generate electricity from railway tracks using simple gear drive mechanisms. The generated power can be used in trackside infrastructure and has a range of 8–10 W power. Agenjos et al. [8] explained diesel-electric traction by using non-regenerative braking. This system reduces consumption of diesel and CO_2 emissions which are economically feasible. Abramovich et al. [1] developed an apparatus for energy harvesting by using piezoelectric generators where the setup comprises multiple numbers of piezoelectric sensors and fixed in the system to generate the power. Jiang et al. [9] explained about the generation of energy from railway cars by applying a regenerative braking system. Dong [10] proposed a fully automatic control system for high-speed railway applications. The objective of this work is modeling and analysis of train operated systems for generating power. De Pasquale et al. [11] studied the design procedure for energy harvesters. From the coupled study, output power of the system is calculated and compared both experimental and simulation tests.

The proposed method will save a lot of electricity which is produced from power plants. It is having various advantages like maximum utilization of energy, pollution free power generation, uninterrupted power generation during day and night, easy construction, emerging technology, and low maintenance.

2 Methodology

2.1 Design of the Model

The present work aims to show how energy can be used for a common system. Design of each component in the assembly has been carried out using standard procedure. The proposed model was fabricated and showed the power generation, which can be used to run the signal light, lights and fans in the train. Whatever the power generated is stored in the batteries and can be used when the train is in off condition.

The frame structure shown in Figs. 1 and 2 for the total assembly is made of mild steel.

Both rack and pinion are fabricated using Duracon M90 material, where the rack is joined to the railway track arrangement and the pinion has thirty-six teeth is fitted on the shaft at the starting and then fastened. Pinion tooth was exactly designed to mate with the teeth of the rack. The pinion wheels are welded to the shafts.

The principle of this research work is the "Conversion of mechanical energy into electrical energy." In the proposed method, the train carriage and railway track are

Fig. 1 Pinion
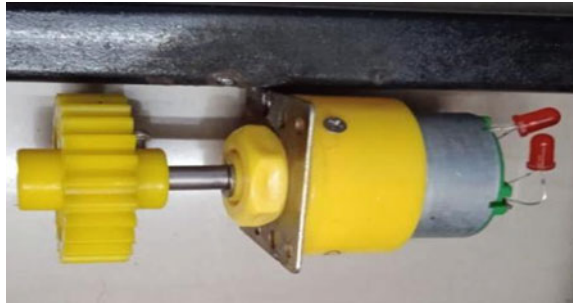
Fig. 2 Rack

fixed with rack and pinion arrangement. Whenever the train starts moving on the railway track, the pinion on the carriage meshes with the rack on the railway track, and then, the pinion gets rotated. In the similar way, when the rack on the carriage comes in contact with the pinion on the railway track, the pinion gets rotated because of the impact load that was created between the two gears because of meshing. Both the pinions which are connected to the carriage and the railway track are equipped with 12 V DC dynamo. When the pinion gets rotated, the power is generated by means of DC dynamo as shown in Fig. 3. The energy generated is stored in the battery and can be used for running the lights and fans when the train is in stationary condition.

Block Diagram:
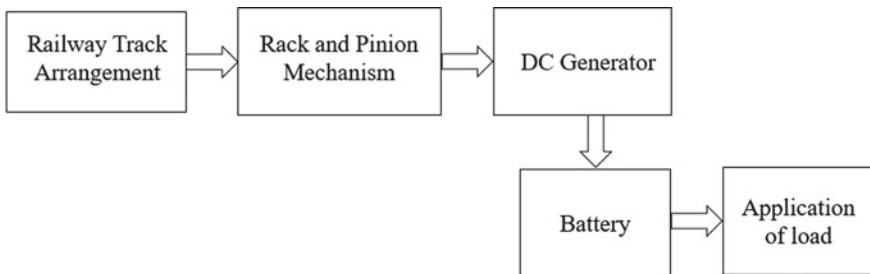
Fig. 3 Block diagram of power generation

2.2   Assembly Process

The main components of this method are as follows: railway track, carriage, rack and pinion arrangement, DC generator, battery, medium-density fiberboard.

In the first step, required dimensions of the square inch pipes are welded using oxyacetylene gas welding to make the original railway track. Cut the square inch pipes according to the dimensions and weld them by using oxyacetylene gas welding; therefore, original railway track is obtained. The pinion is connected to a 12 V DC dynamo such that it acts like a DC generator with which the LED bulbs will glow. And also, rack is connected to the railway track with the help of high-tension strings. In the second step, medium-density fiberboards are taken according to the dimensions and then fixed on a standard rack to that board such that it contacts the pinion which is connected to the railway track, and therefore, this arrangement gets rotated, and power is generated.

After assembling all the components, input power supply is provided to the geared motor so that the train moves on the railway track. Therefore, two-way power generating trains by using rack and pinion mechanisms are achieved. The modified railway track and assembly of the prototype is shown in Figs. 4 and 5, respectively.

Fig. 4 Modified railway track

Fig. 5 Assembly of prototype

3   Experimental Results and Discussions

Fabrication of a two-way power generating system is done by assembling all the components, where production of electricity was done from both railway track and carriage. The generated power is used for lightening the LED bulbs which is shown in Fig. 7.

Figure 6 represents the pinion which is connected to the railway track and gets rotated by means of a rack that is fixed to the carriage. The contact of rack and pinion results in the rotation of pinion. The rotational energy of a pinion is converted into electrical energy by connecting a DC dynamo to the pinion. Figure 7 represent the pinion which is connected to the carriage gets rotated by means of a rack that is fixed to the railway track. The contact of rack and pinion would result in the rotation of pinion. This method produced a very high amount of energy when compared to the other where the pinion is connected to the railway track.

Angular speed is measured by a tachometer for power calculation. The power generated is directly proportional to speed and torque. In this proposed method, the power produced at different speeds and torque is calculated and shown in Table 1. In the real-world applications, a very high amount of power can be produced as torque, and speeds are very high. There is a loss of energy due to friction, drag n thrust force, and impact of this phenomenon is very less. Drag thrust force is negligible, whereas loss of energy due to friction is calculated (Fig. 8 and Table 2).

Fig. 6 Generation of power when contact with pinion
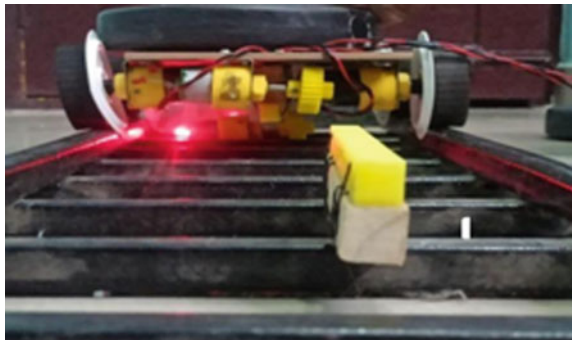
Fig. 7 Generation of power when contact with rack
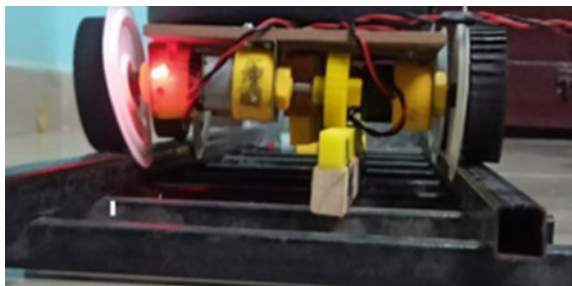
Table 1 Calculation of power at different speeds

S. No.	Speed in RPM	Angular velocity in rad/sec	Torque in N m	Power in W
1	70	7.33	1.22	8.9426
2	90	9.43	1.22	11.5046
3	130	13.61	1.22	16.6042
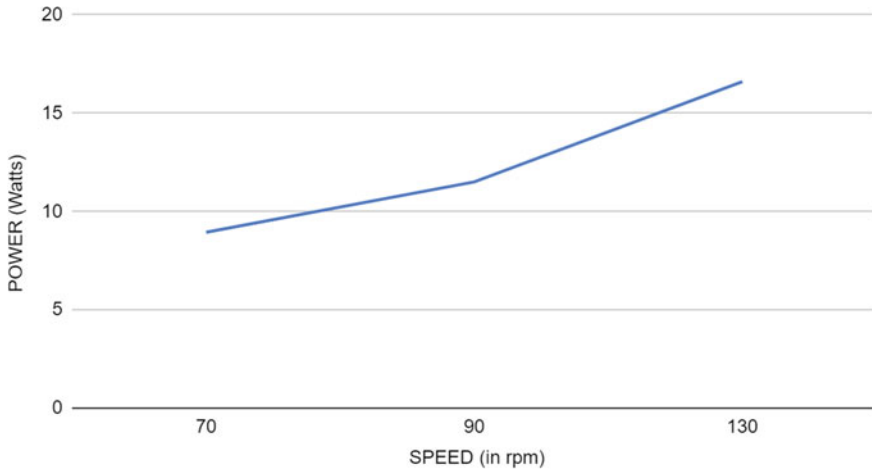
Fig. 8 Graph between speed and power

Table 2 Energy generated after neglecting losses

S. No.	Power in W	Time to cover 1 km in s	Loss of energy in J	E_g in J	E_f in J
1	8.9426	5456.7	8422.2	48,794	40,372
2	11.504	4244.6	8422.2	46,829	38,407
3	16.604	2939.2	8422.2	49,967	41,545

Enormous amount of energy is produced from simple rack and pinion arrangement by installing the rack gear throughout the track and also by installing the pinion gear to each and every carriage. Power calculated for spur gear arrangement at 70, 90, and 130 rpm is 40,372, 38,407, and 41,545 J; this is done by analytical calculations. Very high amount of energy is obtained when train is running at medium speeds. While calculating generation of energy, there is a loss of energy due to friction and drag and thrust force. Drag and thrust force is negligible, whereas loss of energy due to friction is calculated (Fig. 9).

The energy losses are of two types called major and minor loss, where major loss is the energy lost in friction when our railway carriage is moving on railway track. Minor loss is neglected in the system. Initially, calculated the energy generated and energy lost in friction for 1 km travel of train, and in the next stage, calculated the
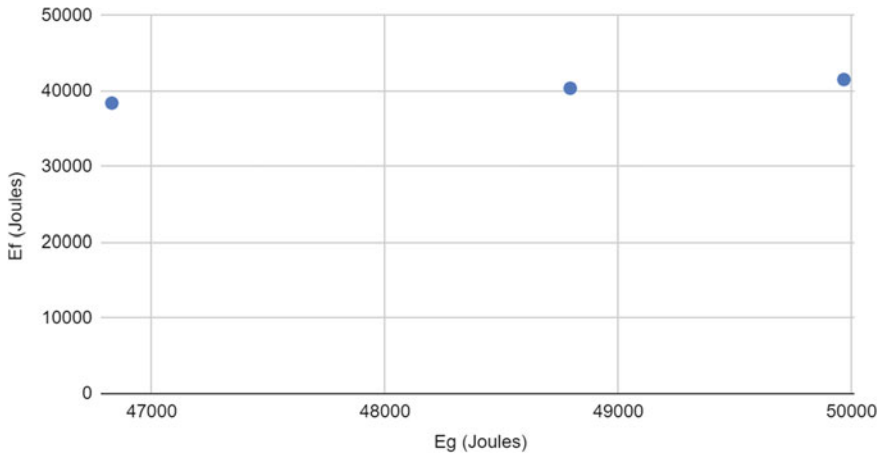
Fig. 9 Graph between E_g and E_f

effective energy developed (for 1 km travel of train) by subtracting losses from the energy that has been actually generated. Analysis can be done at any speed; sample speeds were taken to calculate energy. The increase speed results in producing more power.

4 Conclusion

The present work deals with generation of electricity from railway tracks and trains, where this system used is reliable and this finding will help to conserve our natural resources. In the proposed method, the rack and pinion are directly connected to railway carriage and track which enables production of more energy from the system, which is not possible by existing methods. It impacts the economy of the country in a positive way. The generated power supplied for railway station appliances like lights, fans, and signal lights.

References

1. Abramovich, H., Harash, E., Milgrom, C., Amit, U., Azulay, L.E.: Power harvesting from railway; apparatus, system and method, pp. 365–395 (2010)
2. Hwang, H.-S.: Control strategy for optimal compromise between trip time and energy consumption in a high- speed railway. IEEE Trans. Syst. Man Cybern. Part A Syst. Hum. **28**(6) (1998)
3. Knothe, K.L., Grassie, S.L.: Modeling of railway track and vehicle/track interaction at high frequencies (2007)

4. Gokul, K., Gowtham, R., Jothibalaji, S., Kathiresan, P.: Power generation by using railway track. Int. J. Sci. Eng. **1**(1) (2016). In: Recent Advancements in Mechanical Engineering—RAME'18. ISSN: 2454-2016

5. Chahande, J., Shirke, B.S., Goswami, V.B., Malnas, A.A., Zakane, G.R.: Electricity generation using railway tracks. Glob. Res. Dev. J. Eng. **2**(5) (2017). ISSN: 2455-5703

6. Raj, A., Verma, A., Joshi, H., Gupta, M., Mustafa, J.: Generation of electricity by crank mechanism method in railway track. In: International Conference on Computational and Experimental Methods in Mechanical Engineering (2017). ISBN:978-93-86171-85-6

7. Kaur, L., Kumar, A., Lakde, A., Sharma, A., Rai, A., Sharma, M.: Railway tracks based energy generation using racks and pinion and its application. Int. J. Adv. Res. Electr. Electron. Instrum. Eng. **7**(4) (2018). ISSN (Online): 2278–8875

8. Agenjos, E., Gabaldon, A.: Energy efficiency in railways: energy storage and electric generation in diesel electric locomotives (Electricity distribution—Part 1), pp. 122–172 (2009)

9. Jiang, Y., Liu, J., Tian, W., Shahidehpour, M., Krishnamurthy, M.: Energy harvesting for the electrification of railway stations: getting a charge from the regenerative braking of trains, pp. 881–891 (2014)

10. Dong, H.: Automatic train control system development and simulation for high-speed railways (2010)

11. De Pasquale, G., Somà, A., Zampieri, N.: Design, simulation, and testing of energy harvesters with magnetic suspensions for the generation of electricity from freight train vibrations (2012)

OEE in Sustainable Can-Making Manufacturing

Aezeden Mohamed, Kieren Piso, Umamaheswararao Mogili, and Kamalakanta Muduli

1 Introduction

Advanced smart manufacturing with innovative strategies is now a global motivation that pushes toward wining in the competitive market that it is today. Such innovation is basically with the core values to achieve sustainable development and efficiency in all aspects of business, production, and manufacturing [1–4]. While innovations in a competitive market move a IFC company one step ahead of its competitors, efficiency measures (i.e., OEE) can be regarded as the power behind the benefits and success in the development of the product through each challenge and variant [5]. Manufacturing industries around the world established OEE, nevertheless, some use it as the key measure toward their performance has been widely used by various manufacturing industries. Factors used under OEE are of three and are measured with time; they are availability ensure the availability of equipment meaning are available to be used for its intended purpose when needed, performance is the production speed, and it assures that the productions run at the average speed or faster depending on the availability, and the last factor is quality that covers all from raw materials to finished products [5, 6].

This paper's objective is to study the can-manufacturing data and procedure of the can-making department [7–10].

Data management and organization on a can production basis motivates an effective production line performance in the can-making department in the International Food Corporation IFC. The production line to achieve the transformation tin cans to finished profitable food packaging goods, and this is as a benefit of time management,

A. Mohamed (✉) · K. Piso · K. Muduli
Mechanical Engineering Department, PNG University of Technology, Lae, Papua New Guinea
e-mail: aezeden.mohamed@pnguot.ac.pg

U. Mogili
Industrial Design Department, National Institute of Technology Rourkela, Rourkela, India

precise positioning function of the can-producing equipment or machines from line to line toward the entire production line. The production line of the can-manufacturing production line at CMD-IFC includes employers' poor maintenance strategies that would facilitate for higher break downtime which more or less adds to higher production time (overtime included), less available time that will all contribute toward higher production cost. However, the tracking of time by incorporating smart data entering technique toward the production line identifies losses encountered, and energy usage and wastage can also be monitored and controlled under the surveillance of data so to achieve sustainable manufacturing [11–14]. Each equipment performance can optimize which will subsequently enable adjusting each machine to achieve better productivity.

2 Literature Review

IFC-CMD presently witnesses so much pressure to increase the production line efficiency to uphold the needs of its customer demand or in whole the market. This cannot be sustained unless the production line performance improvement is impeccable; therefore, it should and must be improved to bring the utmost performance; this is achieved by checking and eliminating faults on each system on the line that may have an impact on the production line directly or indirectly. Hence, to succeed in developing and improving the efficiency of line productions, it is important to have data that give a crystal perspective of the performance [1–3].

In doing so, to achieve quality products, each piece of equipment and the behavior of each system of the production line are kept in surveillance to collect data and observe [15]. By the authors, to improve the equipment and production line, data must be analyzed properly since it is essential to identify faults and setbacks toward the efficiency of performance.

Out of the many methods used in analyzing the performance of production lines, one of the methods used is the analytical method that is established with mathematical modeling that can be done either experimentally by stopwatch, pen, and paper or with computer aid. Analytic methods can be hybrid of the mentioned two methods as well; nevertheless, in any of the three ways, the interpretations can be put into a mathematical model of real production line systems that would result in approximations or exacts. As elaborated by Jarrhai, mathematical modeling can be programed linearly that can have broken down into individual workstations to measure the time cycle of production, yet each station has a probability to fail [15–19]. On the other hand, Kosters stated that a continuous process flow production line can also be established within a multi-staging model that would explain why some machines are more unreliable and why there are buffers repeatedly to achieve better efficiency. In addition, Conway carried out an experimental investigation of the buffered machines in the line and concluded with a discovery of synchronizing the buffers along the line [20].

2.1 Key Indicators of OEE

The key indicator of OEE is time; the study and understanding of time play a vital role in the performance rate of a production line such as in CMD-IFC. Decision basics can be made to conclude whether the performance needs improvement is time dependent within the 8 h shift. A time behavior tracking of individual equipment can be identified with a time study along the process, and to do this, breaking the entire production line into parts helps the evaluation to easier approach. Henceforth, each performance can also be identified by measuring the actual individual performance and then later added onto one another to achieve the overall entire production line performance. Such conduct helps in reducing unnecessary production stops and time waste due to bottlenecks along the production line or process [14].

According to Fredrick W. Taylor, the application of a stopwatch with the use of a paper and a pen can give an actual performance readout for a simple small production line [13] but cannot be effective enough for a more complex line; therefore, monitoring software's and program are required for detailed analysis. In addition, the author describes that errors and faults are more likely to occur when in production, which is why it is more important to check the individual performance of machines in the production line to identify failure and minor delays.

First, the production line should be familiarized, and then set beginning and endpoints which would allow breaking the production line into parts. These parts from end to end with all the machines and equipment involved are identified with brief descriptions which would allow easy understanding of time parameters for both complex production line or simple production line when time study is carried out. The second step would be to pay attention to identifying each failure, bottlenecks, minor frequent line stops, and errors while collecting data from one point to the other successively. In all, the final step is analyzing the data from one point to the other and from the most important to the least important with the intended purpose of comparing actual recorded time to the standard operating time. The following steps pursued will help optimize and improve the individual system and in all the production lines for better performance as well as quality [14].

2.2 Overall Equipment Effectiveness

In manufacturing industries such as the Industry 4.0, application of OEE is firm and carried out entirely for its intended purposes that helps in less rejections and higher productivity [7]. The current trend today in sustainable manufacturing toward being competitiveness reliability and OEE is the fundamentals of increasing performance of equipment in turn favoring profitability [3]. On the other hand, OEE can also be defined as a method used for evaluating performance [11]. Further defining OEE, it is the ratio of the time of operation to the loading time and as elaborated by Iannone, operation time, the time where actual quality product is being produced,

and loading time is the time required of an equipment to run [12]. In the evaluation of the production line in a manufacturing system, several parameters are considered to improve productivity [17]. Each of the parameters is known for their input toward performance, and they are for instance as inventory, quality, profitability, or flexibility. However, OEE is one of the parameters that gives the percentage of the time of productivity, and there are three aspects considered in such, and they are quality, performance, and availability.

Thus, in relation to time studying, OEE eliminates any form of time that can be considered as waste from present to none as fast as it can; true production time with OEE nearly 100% is promised to be of world-class with a more productive production line [4].

Furthermore, OEE is not only limited to time studying or studying time to get the best output of performance; it also is providing a well-integrated sophisticated process that identify losses so that necessary plans and steps can be taken toward eliminating losses identified as well as increasing the life of equipment [1]. The main objectives that drive OEE in all aspects such as performance, availability, quality, and identifying losses are to increase profit of a company, reduce unnecessary costs, and establish a relationship of ownership toward each machine in a production. The relationship of calculating the percentage of OEE with their aspects as with availability, performance, and quality is mathematically modeled as in Eq. (1) [5].

$$OEE = Availibility \times Performance \times Quality \qquad (1)$$

The availability can be defined as the ratio of time, i.e., the run time is to the planned time of the entire production line taking into consideration all the downtime (the loss of availability), which is the time when the machines and the production are down during the production time or the time the line should be running. Also, in addition, several unplanned minor stoppages can be encountered during production due to small faults and failures, and they can also be identified as availability loss or down time. On the other hand, the run time can be defined as the when the machine or the line is up and running after the downtime, unplanned and planned stops [17]. The mathematical modeled Eq. (2) of availability and if that equals to 100%, then it simply means there was no stop or down time encountered during the production time.

$$Availability = \frac{Runtime}{Planned\ Production\ Time} \qquad (2)$$

Performance is the second parameter of OEE which also is a ratio of time, i.e., the net runtime is to the run time; here is the parameter that pays attention to the speed of the production line while taking into consideration that may cause the performance loss that in sense would mean minor stoppages and slow line cycles. The mathematical model of identifying performance is as Eq. (3), where the total count is the total count produced

$$\text{Performance} = \frac{\text{Ideal Cycle Time} \times \text{Total Count}}{\text{Run Time}} \tag{3}$$

The first two parameters of OEE consider time, but the final parameter is quite different; the final parameter takes into consideration quality products manufactured in a particular production while taking into consideration every aspect of quality loss. Quality loss can mean the final product not meeting quality requirements and standards, or in other words, the final product that has defects present and needs rework. The mathematical model of quality is as describe in Eq. (4) where good count describes the number of quality products produced.

$$\text{Quality} = \frac{\text{Good Count}}{\text{Total Count}} \tag{4}$$

2.3 Improving Sustainable Manufacturing

Sustainable manufacturing in accordance with the organization of economic and department is a reorganized formal an id not legalized in some countries for business that challenges individuals toward new exciting implementation that can be valuable toward manufacturing. One of the key forces behind achieving green manufacturing processes and of finished products that were of higher concern in the past is manufacturing sustainably, hence praised for the achievement for an exciting new way of doing business and creating value [8–12]. To further simplify in more simplified sense, the initiation of practice of sustainable manufacturing is all about uniting all business strategies by giving them one purpose that minimizes all possible disastrous practices, initiating challenges for new innovations of improvement toward products and process. Table 1 [18] is the seven sustainable manufacturing requirements setup steps, and with the organization of economic and department, the eight highlighted factors in Fig. 1 are considered when considering sustainable manufacturing.

So far, the discussion carried out has narrowed the attention that OEE of an equipment or if for the whole production line begins as time as the key factor toward sustainability. So far, to fully assess and achieve sustainability only, time cannot cut it in terms of energy; hence, Lai-ling suggested that efficiency of energy cannot only be achieved with only the perspective of time [21]. Moreover, energy performance is indicated by the consumption of energy in a period such as KWh/week and KWh/equipment. Hence, a relationship between the consumption of energy and time is possible to achieve [21].

The author proposed that, putting time and energy in to a specific period that can be discrete or continues with the state of energy in watts, then a relationship can be achieved by studying the studying the cause and effect of the input and the output taken. Both energies consumed with the time spent which enable reduction of both factors to achieve efficiency.

Table 1 Seven sustainable manufacturing requirements setup steps and with the organization of economic and department [9]

Factors	Steps	Description
Preparation	Identifying and mapping the impacts and setting priorities at hand	All the environmental impacts of manufacturing industries, small or big, are all interviewed, assessed and revised, while setting priorities and sustainable manufacturing objective are defined as well
	Choose promising useful key productive indicators	Purposely for continues improvement, indicators are placed in order to increase performance for collection of data
Measurement	Measure the input scales of the line	The measure of how raw material is turned into useful products, measure of all the input that adds to environmental influence
	Asses the manufacturing faculties	The intensity of efficiency and environmental impacts in manufacturing industries should be identified in all faculties; some parameters may include emission, energy usage intensity, and green effects
Improvement	Product evaluation	Identifying faults at where that is addressed with sustainable manufacturing is required in manufacturing industry with regards to energy consumptions reduction and recycling of hazardous products
	Establish a relationship by understanding the results from measurement	Paying attention to the indicators in order to understand the trends of performance
	Actions suggestion toward performance improvement	Taking necessary action steps toward implementing plans to establish opportunities to improve the production line performance production line should be executed

The German University of Technology has carried out this experiment toward analyzing performance with time with a significant method of handling equipment in a supply of auto-part. Notes taken from such a method, it can be defined as a manufacturing of a smaller scale system in functionality of limited period [22]. Hence, it is in a small-scale educational background, implementation of this method, and collecting data should be from a short-length period so that to prevent any further damages, and then moving on, the period can be expanded slowly.

For the implementation of such practices described, the challenges faced are highlighted in detail when evaluating the practices. In this study, a detailed methodology for small production line is targeted together with it. The describe case study is an example of a small production line with a simple manufacturing practice. The data
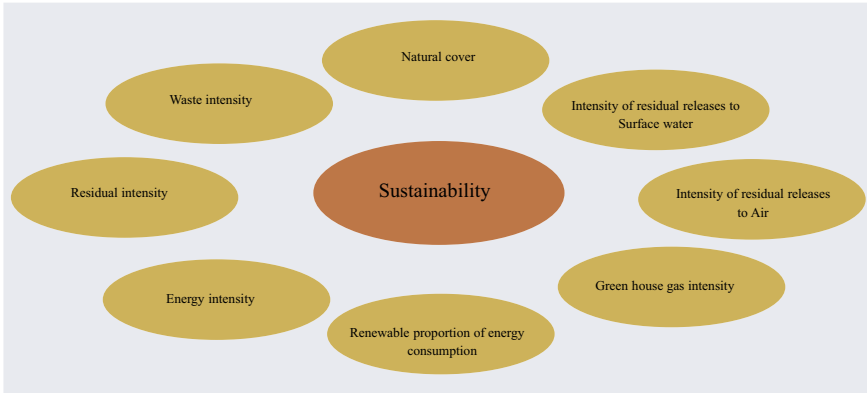
Fig. 1 Eight factors when considering sustainable manufacturing

used were collected and implement a smooth and efficient sustainable can manu-
facturing. For such achievement to be possible, all OEE standards and practices are
evaluated and proposed, the data used here in order to aim, achieve, and maintain
sustainability, with the utilization of time as the key performance indicator measure-
ment. Moreover after, the energy consumption with the effect and their relationship
time can also be investigated.

3 Can-Making System Description

3.1 Droplet Deposition

In terms of quality and marketing, the tin is designed with its own decoration for
advertisement purposes and for their own unique color that differentiate them from
all other same products. Nevertheless, for quality, the tin cans are given a clean weld
and are coated both inside and outside to protect from rust. The production line is
mainly continuing, and any disturbance in the line could cause a disturbance along
the entire line.

The production line can be defined as a simple manufacturing production line,
and it is not a complex production line as describe in Fig. 2. The production line
starts from tin sheets placed into the Soucan machine. The Soucan machine is a
highly integrated advanced welding machine; it is easy to use with a control panel
attached to it, and it is well engineered, with high performance welding capabilities.
The Soucan capabilities as a result of well-engineered highly integrated circuits that
do most of the work in the production, its efficient, fast, and easy to use that od which
has high productivity having maximum efficiency. It also equipped with automatic
rejects, a cooling system, and a control system that is capable to read any stoppages
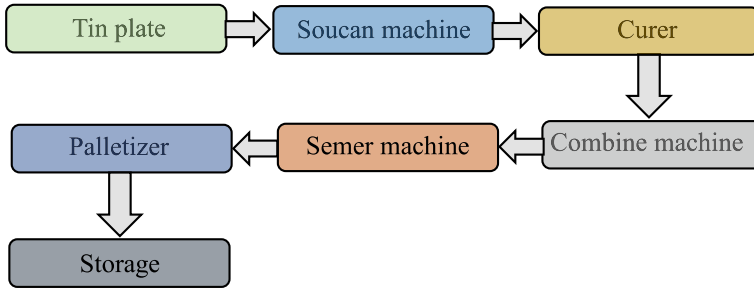
Fig. 2 Process involved in Soucan machine

or failure in the entire line. The Soucan machine uses copper for the welding, and it also has a powder compacting system for that coats the internal welded area, liquor system that coats external area for the can and all another system as entire production line of CMD-IFC as shown in Fig. 2.

The tin can is cleaned and wiped before they are fed into the Soucan machine, while compressed cleaned soft yet clean air enters the machine through the valves and are blown across the plates to make them separable from one another which makes them easier to flow through the welding machine one after other. The machine automatically transfers plates to welding and to coating. The coating is simply described as the barrier against oxidation and rust of the can that may cause food poisoning for most cases. The last part of the Soucan machine is the rejection; every can is identified and scanned, any faults found such as, no powder, less liquor applied, and welding faulty are all identified and rejected at this point before the cans are conveyed to the curer. Table 2 identifies some of the properties of the can making in terms of energy and performance or speed of the machine.

After tins plates are welded into round tin cans in the Soucan machine, this same goes through a process of heat treatment in a curer. The welded three-piece cans are conveyed into blazing fire that use propane gas that keeps the fire burning in the burners. The burners are initially ignited by an external spark and are kept in a

Table 2 Some parameters of Soucan machine

Model	Soucan 650
Production max	300 cpm
Sheet specifications	Electrolytic alloy tinned sheets
Copper wire specification	⌀1.24, 1.38 or 150 mm
Welding speed un tool	9–70 m/min
Welding speed standard tool	9–60 m/min
Welding current	2.1–6.0 kA
Connected load	18.1 P(kW)
Welding frequency	100–760 Hz
Cooling requirement	21 kW

standard required heat by manual adjustments before the productions. The conveyer belts are made of magnetic metals with higher melting point than those of the burning flame; the conveyers because of their magnetic property do hold the cans steadily through the process with a perfect alignment. Throughout the entire process of curing, the pressure of process is disturbed evenly to the burner at a pressure of 360 mmH$_2$O. For a clearer visual, the heat treatment is by far done in order to melt the powder around the welded area to coat the welded area which prevents bacteria, corrosion, food poisoning as well as giving the weld strength.

From the curer, the can bodies headed to the combine, and along the production line, the cans are cooled down by ambient.

A short description of the combine machine is that it consists of the flinger, nicker, and the beaded, all three are designed in such a way to work vertically for acquiring the tins in a best way possible required standard as possible as it can. All the cans also have eight heads that per revolutions, for the first mechanism in the combine machine is the nicker, the nicker is defined by its principal and work in accordance with it; it gives the necks of the tin making; after the necks are made the flinger comes into play, the flinger bends the neck given to the tin cans by the nicker so that it can be made easier for the seamer to attach lids into the tin cans; the nicker and the flinger give the shape both at the bottom and at the top of the tin cans. After they are done, the beaded makes the tin cans a little harder to bend by giving it a ring-like shaper. This ring-like shape gives the tin cans their strength.

After the tin passes through combine machine, the tin cans go through the seamer machine with six heads that in one revolution. The seamer machine works as a synchronizing device. The device synchronizes the lid with the tin can body, with an automated interlocking system. The seamer machine is designed perform closing cylindrical can bodies, by centering the lid and mounting it onto the can body as one. The seeming is done to withstand pressure from both within and outside. The process is also known as double see process because of the two-seaming roll in use. The final and last transfer in the can-making department is from the seamer machine to the palletizer where it stores the tin cans in pallets where the layers of each pallets are separated by sheets of boxes. The mechanisms of the palletizer start with the finish tin cans are placed in hopper of 3–4 m high that rests slightly above two, one on the left and the other on the right chains that give a lift mechanism. Layers are achieved through mechanism; the stack is raised by the lift mechanism, while the second bottom pallet is held by the holding mechanism from the pallets stack.

4 Methodology

Can-manufacturing process is set to a time study that will evaluate each part of the machine in order to estimate and evaluate individual equipment or machine in the production line. The objective toward the time study is to analyze the time utilized by resources; then, a compression is made between the records done at can-manufacturing data provided as a cross-check to give a functionality of the record.

The results obtained would light to each machine performance as well as the overall performance as well as identifying limitations, faults, and production layout limits that can be addressed to achieve efficiency in performance.

To carry out the investigation utensils used were a pen, stop watch, and paper was used to investigate the time taken for a can production one tin plate placed into the Soucan machine toward the end of the line where it is packed in the palletizer in order to get a clear picture of the production performance of each machine with time. Hence, as already mentioned, the production line was divided into 4 points in the production line, time calculated mentioned the above methodology from the individual point which gives the performance for of the machine in each line and the production line as one. Several readings were taken, and results were recorded down and put in range from the lowest probable time and the highest probable time for each machine (Table 3).

The observed data from time study are generated in each conveyers, machine, and motors individually. This data collected from each between each point are later combine to give a time study compressive for the whole system or line. In addition, from Table 3, the activities done in the time constrains can also be identified and

Table 3 Shows the data and results obtained in the line

Production lines	Machine and conveyers	Motor type	RPM	Production, s/tin
Point 1	Soucan machine motor	3-phase induction motor, AEVF	1370 1430	2.5–4 2–2.5
Point 2	Curer motor (2x)	3-phase induction motor, AEVF	1350 1370	39–40 3.9–4.27
	Momentum	NA	NA	4.26–4.46
	Motor (2x)	3-phase induction motor AEAP	1420–1720	44.74–46
Point 3	Combine machine	Mitsugi 3 phase	1400	2.75–2.85
	Motor	3-phase induction motor, AEVF	1370	2–2.5
	Momentum	NA	NA	2.13–2.23
	Motor 1 Motor 2	3-phase induction motor AEAP	1420–1720 1420–1720	30.37–31 10.20–11
Point 4	Seamer machine	3-phase breaker motor, BBFO	1440	5.95–6
	Motor	3-phase induction motor, AEVF	1370	2–2.5
	Momentum	NA	NA	1.9–2.2
	Motor	3-phase induction motor AEAP	1420–1720	30.37–31
Overall can line	NA	NA	NA	187.71–195.01

describes, such as it takes about 3.5 s average for the Soucan machine to weld; it takes the combine machine 2.8 s and 5.975 for seamer machine to complete each task describe in the process or system description above. Even though the values of time may vary, they are approximately close in their value, which would tell that there are minor problems such as sensor delay or small setbacks in the performance that can be addressed.

In all the time measured, one factor that cannot be changed is the idle time, and they can be treated as constant for which is for 300 cans/min is for the Soucan machine, but in cases where the idle time is reset, it would be important to adjust and optimize speeds of each point of conveyer as well. Some conveyers are belts, and some are of magnetic metals alloys such as the conveyer in the heat treatment has magnetic and heat resistance properties.

From the data collected, it can be noticed that for overall performance the conveyer lines from curer to the combine machine, point 2 has the highest passing time that is which is reasonable because the cans are heated in the curer and passed through the line and cools down using the ambient air temperature of the room but of how much heat needs to be cooled and of how much time is a question. Followed by point 4, the conveyer from the seamer machine to the palletizer, which is unreasonable but however if necessary the plant layout can be questioned and if possible addressed to get the ultimate performance of the production. In all to get an efficient better overall performance, the time contribution that add no value to the production line can all be reduced by doing, so increasing an overall reliable performance time can be achieved (Fig. 3).
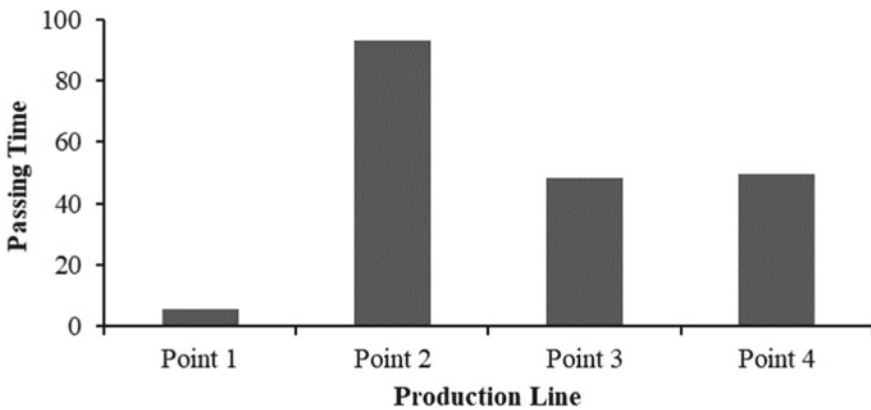
Fig. 3 Representation of time study in each point along the production line

5 Data Analysis and Findings

From the data analyzed with compression to the data provided from is CMD, we will analyze and establish better ways in terms improvement and efficiency. Below is Table 4, showing the products produced in a day for the month of February 2021. From the data shown in Table 4, CMD data analysis in plain and unclear, the production time study is confused; however, a corrective and analytic approach is assured toward estimating the OEE for CMD plant. The total shift is 8 h from Monday to Friday and 4 h every Saturday that is about 44 h of production time in a week. Hence, below is the time analysis for CMD, leading to OEE.

The main downtime in CMD is generally due to the lack of planning, inadequate data analysis, and poor maintenance strategies. Break down is the most likely and occurs more frequently; in other words, break down is defined as the unplanned down time in a production. This unplanned downtime or down time in CMD daily 4 h but from the results provided is 6.58 h. Another time factor that contributes to the loss of production time in CMD is the setup time; the setup time is about 30 min every day. The available time or manned time per day is, followed by the operating or run time,

$$\text{Manned Time} = \text{Total Time} - \text{Unused Time}$$
$$= (8 \times 60) - 30 \text{ min} = 450 \text{ min} \tag{5}$$

$$\text{Operating Time} = \text{Actual Production Time} - \text{Breakdown Time}$$
$$= 450 - 394.8 = 55.2 \text{ min} \tag{6}$$

There are other time factors that need to be considered for a most sustainable efficient production but are never considered can be time such as the operating working time; this categorized under aspects of down time that are unplanned and can be regarded as loss such as, power outage, meetings, refuel, operators unavailable, etc. Also, in terms of the measurement of performance in the production line, small minor stoppages other recordings along the line are not clear because of poor documentation and data analysis but with from observation powder recycling readjusted in 5 min every other 30 min, and new tin plate insertion takes up to 30 min every day maximum one exchange every day; small can stuck in Soucan machine consumes 15 min for new calibration every other hour. However, they are not recorded properly.

From the experiment of time study conducted, the can produced in the line is recorded as 3.2 min/can. Taking that into consideration, if there are 300 cans produced per minute, then the cans produced at the end of the production line, i.e., a constant can be used to determine the relationship between can produced ideal time of the Soucan machine and the overall production ideal time.

$$K = \frac{300}{3} = -100 \text{ can}^2/\text{min}^2 \tag{7}$$

There for if Soucan machine produces 500 cans, then if the production line is running smoothly, one would tell that if the ideal time is changed to 500 cans/min, or it is turned down to 200 can per minute than one should tell that the finish product approaching the palletizer is at the rate of; $500/100 = 5$ min/can or the entire production line is producing at $200/100 = 2$ min/can. This relationship can also be used to understand the ideal time of Soucan machine if the end product at the production time is also predicted.

Moreover, the OEE would be calculated as; from Eqs. 1–7.

$$\text{Availability} = \frac{\text{Runtime}}{\text{Planned Production Time}} = \frac{55.2}{450} = 0.1227 \qquad (8)$$

From sufficient information given from data, the performance of the line cannot be clearly investigated by the provided data; however, using the raw data calculated in Table 3, we can achieve a glimpse of the performance. The target daily collected as shown in Table 4 gives 28,175 cans, and it also shows that the target was met but how? If the operating time was 55.2 min that is less than an hour, either the breakdown time report is incorrect or the target met is incorrect. However, there is one possible explanation and that is overtime expenses, unless there was overtime; then, the target was met, but it comes with a cost of the company. Since OEE measure does not extend toward overtime, performance will be based upon data in Table 3. Therefore, the total time a single can is produced from the Soucan to the palletizer 187.71–195.01 s that is an average of 191.36 s (3.2 min). Hence, if the run time is 55.2 min, that means;

$$\text{Performance} = \frac{\text{Ideal Cycle Time} \times \text{Total Count}}{\text{Run Time}}$$
$$= \frac{\frac{300\,\text{can}}{\text{min}} \times 55.2}{28,205} = 0.587 \qquad (9)$$

Now, let's calculate the quality;

$$\text{Quality} = (\text{Good Count})/(\text{Total Count})$$
$$= 28,175/28,205 = 0.998 \qquad (10)$$

Therefore, the OEE $= 0.1227 \times 0.587 \times 0.99 = 0.066$.

The above information is illustrated as shown in Fig. 4.

The OEE has studied from the given result shows how poorly OEE is achieved in CMD; however, it makes it easier to identify and eliminate faults and issues arising in the production line. The availability should be checked, availability of resources, spare parts, and machine should be paramount importance in order achieve an effective OEE which would have a positive impact on the overtime and the resources/equipment downtime as well as idle and production time. The performance on the other hand if based on Table 3, time study, a precise performance target would
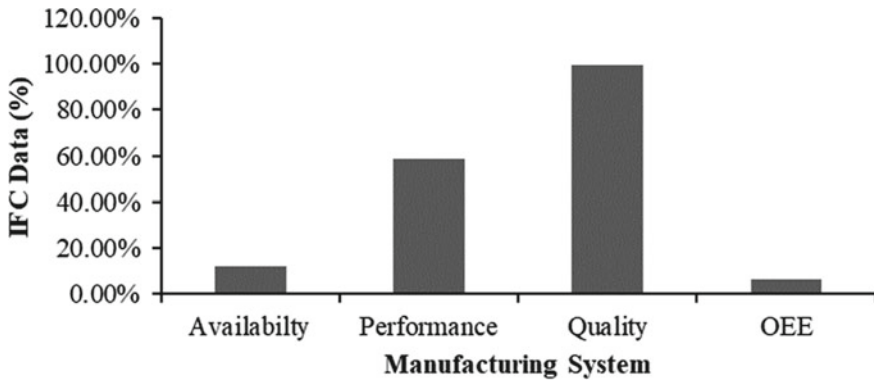
Fig. 4 Showing OEE for the IFC data

be achieved which would also have an impact on the planning of maintenance as well as overtime and resource available, idle time, and quality resource control.

The relationship of performance also shows that because the idle time has less idle time and more run time leading to imbalance and producing as slow as possible which should be matched in terms of production target, production time, customer satisfactory, and resource availability. At CMD, the performance is mostly dependent idle time of Soucan machine, the run rime, and the total number of product count.

6 Achieving Sustainability

As mentioned and actioned, a time study has been achieved and in terms have perused OEE; hence, the sustainability of can production will be investigated, and to achieve sustainability, different step by step aspects will be identified. Figure 5 shows a visual explanation on what will be mentioned accordingly.
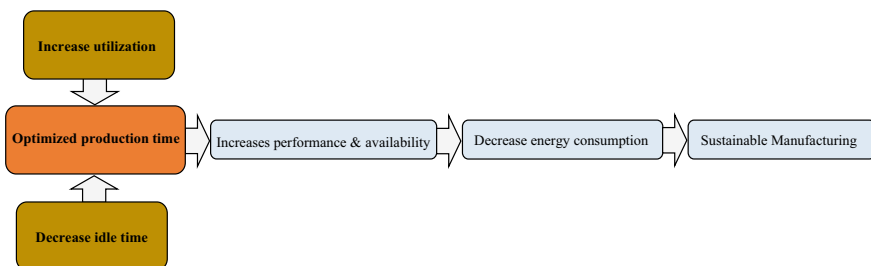
Fig. 5 Showing OECD, measuring sustainability with OEE

The outmost impact on the environment results in relation to manufacturing is the consumption of energy that in terms could be the only highest priority in consideration. Reason being can be connected to in proportional to the type of equipment and machine used in the particular production line. In terms when the energy source of electricity is not categorized in the common electricity, then the only impact with no other is energy intensity.

The next step after would be to select a most effective indicator, with the current work objective being time as a performance indicator; the other necessary indicators are ignored in the manufacturing system. In this paper, the sustainable manufacturing aspect to be investigated to pursue the influence of material components toward manufacturing and environmental impacts.

Time having an impact in OEE with the methodology used in the research, the possible relationship with time and energy collaboration is analyzed and investigated. The efficiency of the production line as proven with the time study is dependent on time meaning any enhancement done to the production line will directly have an impact on the time aspects of manufacturing. However, with individual machine utilization time, may it be idle time or other also have a direct impact energy consumption. The OEE analysis has proven that if an increase in run time while decrease in is revived and engaged in the production line then, there is also increase in both the availably and performance would be expected consequently. The concept understood is the idle time is somehow proportional to energy consumption; further, elaborating the concept is that if runtime is kept under constant and the idle time decreased, then the energy consumption decreases in proportion to the idle time.

The organization for economic corporation and development (OECD) ruled that time is the utmost effective factor for analyzing performance in a manufacturing system. Therefore, electricity being the only aspect of energy intensity that potentially has an impact sustainable manufacturing is to be tamed and to do so is to increase run time and decrease idle time.

7 Conclusions

A well-integrated intelligent approach in terms of analytic skills in CMD for the differentiation of product and object has been designed and established. The developed is proposed to CMD but also can be regarded for other simple production line for obtaining efficiency and effectiveness. A purposeful identification has been observed to control the production line, and it is reassured techniques that can be used it identify faults and eliminate for a better manufacturing system. If the approach proposed is taken seriously and is implemented, then CMD would reduce cost through a sustainable effective and efficient CMD for the evaluation purposely covers all aspects of CMD with time being the effective key factor.

OEE is selected for the production to be a standard measure that exposes the influence time has in manufacturing productivity through time being able two aspects of OEE being availability and performance as well as OEE itself in percentage with

a time study being properly executed. The results from analyzing OEE together with the time study carried out have brought forward some faults, limitation, and errors with in CMD.

The obtained results in the analysis of OEE and time study can be used in means of optimizing and improving CMD productivity. To simply put it, overtime cost and expenses can be reduced, and higher capital investing can be adjourned, down time being reduced as well as idle time and machine operator's performance are more likely to be polished with the establishment of OEE. In terms with OECD, sustainable manufacturing can be achieved in term of OEE with selecting time and electricity, respectively, as the main effective factors.

All in all, to sum it all up this research study, the study tried providing a solution for CMD to achieve a smooth sustainable can manufacturing by trying to meet one aspect of sustainability. The case study in this paper can be put as a simple production. Hence, in regards to complex production lines, the methodology and results cannot be entertaining or results as expected than it would in a simple production line such as of CMD.

The simple study deals with a small number of machine equipment and lines, and so is limited to a shorter length period. Therefore, considering a more complex production line with longer period of time study with more equipment to work with can be proposed for future work in reference to this paper.

References

1. Esmaeel, R.I., Zakuan, N., Jamal, N.M.: The mediating role of overall equipment effectiveness on the relationship between fit manufacturing and business performance. Int. J. Eng. Technol. **7**, 1089–1093 (2018)
2. Azizi, A.: Introducing a novel hybrid artificial intelligence algorithm to optimize network of industrial applications in modern manufacturing. Complexity **2017**, 1–18 (2017)
3. Yasin, M.F., Das, G.S.: A new approach based on OEE to improve equipment effectiveness in SMEs: an application in a wood processing facility. J. Fac. Eng. Archit. Gaz. **32**, 22–30 (2017)
4. Singh, M., Narwal, M.: Measurement of Overall Equipment Effectiveness (OEE) of a manufacturing industry: an effective lean tool. Int. J. Recent Trends Eng. Res. **8**, 246–256 (2017)
5. Ramesh, C., Manickam, C., Prasanna, S.: Lean six sigma approach to improve overall equipment effectiveness performance: a case study in the Indian small manufacturing firm. Asian J. Res. Soc. Sci. Hum. **2**, 122–128 (2016)
6. Jarrahi, F., Abdul-Kader, W.: Performance evaluation of a multi-product production line: an approximation method. Appl. Math. Model. **1**, 3619–3636 (2015)
7. Benjamin, S.J., Marathamuthu, M.S., Murugaiah, U.: The use of 5-WHYs technique to eliminate OEE's speed loss in a manufacturing firm. J. Qual. Maintenance Eng. **21**, 419–435 (2015)
8. Roni, M., Jabar, J., Mohamad, M., Yusof, M.: Conceptual study on sustainable manufacturing practices and firm performance. In: Proceedings of the International Symposium on Research in Innovation and Sustainability (ISoRIS), Melaka, Malaysia, 15–16 Oct 2014
9. Prakash, N., Prasad, C.: Lean practices in small and medium manufacturing enterprises—a structured literature review. J. Basic Appl. Eng. Res. **1**, 419–435 (2014)

10. Palanimally, Y.R.: The growth of small and medium enterprises in Malaysia: a study on private limited companies in Perak Malaysia. IOSR J. Econ. Financ. **7**, 55–60 (2016). Organization for Economic Co-operation and Development: Seven Steps to Environmental Excellence. OECD, Paris, France (2014)
11. Lannone, R., Nenni, M.E.: Managing OEE to optimize factory performance. In: Operations Management. In Tech, London, UK (2013)
12. Kumar, J., Soni, V., Agnihotri, G.: Maintenance performance metrics for manufacturing industry. Int. J. Res. Eng. Technol. **2**, 136–142 (2013)
13. Verbano, C., Venturini, K.: Managing risks in SMEs: a literature review and research agenda. J. Technol. Manag. Innov. **8**(3) (2013)
14. Huang, S.H., Dismukes, J.P., Shi, J., Su, Q., Razzak, M.A., Bodhale, R., Robinson, D.E.: Manufacturing productivity improvement using effectiveness metrics and simulation analysis. Int. J. Prod. Res. **41**, 513–527 (2012)
15. Koster, R.D., Wijngaard, J.: Local and integral control of workload. Int. J. Prod. Res. **27**, 43–52 (2000)
16. Babu, V.R.: Industrial Engineering in Apparel Production. Woodhead Publishing Limited, Cambridge, UK (2012)
17. Radam, A., Abu, M.L., Abdullah, A.M.: Technical Efficiency of small and medium enterprise in Malaysia: a stochastic frontier production model. Int. J. Econ. Manag. **2**, 395–408 (2008)
18. Stevenson, W.J., Hojati, M.: Operations Management. McGraw-Hill/Irwin, Boston, MA, USA (2007)
19. Caldeira, M.M., Ward, J.M.: Using resource-based theory to interpret the successful adoption and use of information systems and technology in manufacturing small and medium-sized enterprises. Eur. J. Inf. Syst. **12**, 1159–1169 (2003)
20. Jonsson, P., Lesshammar, M.: Evaluation and improvement of manufacturing performance measurement systems—the role of OEE. Int. J. Oper. Prod. Manag. **19**, 55–78 (1999)
21. Lai-Ling Lam, M.: Challenges of sustainable environmental programs of foreign multinational enterprises in China. Manag. Res. Rev. **34**, 1153–1168 (2011)
22. Azizi, A., Ghafoorpoor Yazdi, P., Humairi, A.: Design and fabrication of intelligent material handling system in modern manufacturing with industry 4.0 approaches. Int. Robot. **4**, 186–195

Product Design: Materials Innovation in Product Design

Preparation and Characterization of Eggshell Particulate Pellet: As a Future Prospect for Wastewater Treatment

Manoj Panchal, G. Raghavendra, M. Omprakash, and S. Ojha

1 Introduction

Eggshells and eggshell membrane are often used in the removal of impurities; they used as catalysts for biodiesel production, as reinforcing materials in composites, and use of eggshells is also common in the medical field due to the high percentage of calcium carbonate for the synthesis of hydroxyapatite and as a calcium supplement [1].

In earlier days, calcium carbonate was the usual choice for water purification. It is generally observed the water flowing through capillary cracks in the rock is filtered water; these rocks generally contain calcium carbonate. Calcium carbonate is a major constituent of eggshells beside calcium carbonate; it contains small amounts of organic protein and other chemical compounds (calcium phosphate, magnesium carbonate) [1, 2]. Eggshell generation is huge every year [3], therefore, the environmental aspects should be taken into consideration in order to add value to eggshell and avoid their dumping in an open atmosphere [3]. Moreover, the use of eggshells as a substitute for calcium carbonate may reduce the burden on nonrenewable natural sources of calcium carbonate. There are a few examples found in the literature where research work has been carried using eggshells for water treatment.

For instance, Vijayaraghavan et al. [4] used eggshells for the elimination of copper from wastewater. Tsai et al. [5] had tested adsorption of dyes (blue 9 and orange 51)

M. Panchal (✉)
Department of Mechanical Engineering, RGMCET, Nandyal, Andhra Pradesh 518501, India
e-mail: er.manojpanchal@gmail.com; manojpanchal@rgmcet.edu.in

G. Raghavendra
Department of Mechanical Engineering, NIT Warangal, Warangal, Telangana 506004, India
e-mail: raghavendra.gujjala@nitw.ac.in

M. Omprakash · S. Ojha
Department of Mechanical Engineering, KITS Warangal, Warangal, Telangana 506015, India

from wastewater using eggshells. Köse and Kıvanç [6] used eggshells for adsorption of phosphate. Eggshells have also been used for the elimination of heavy metals from contaminated water [7–9]. Use of eggshells for the removal of pharmaceuticals wastes also found in literature [10, 11]. Based on the literature, it may be concluded that the eggshells could be a potential material for water filtration application. This investigation is an effort to discover the prospects of eggshell particles as a filtering agent for wastewater. In this study, the capability of eggshells as filtering agent for wastewater is examined.

2 Materials and Method

2.1 Raw Materials

The following are materials used for preparation of eggshell nanoparticles and its pellet.

1. Eggshell flakes.
2. Polyvinyl alcohol.

2.2 Eggshell Nanoparticle Synthesis

The eggshell was collected from native market. The collected eggshell was thoroughly rinsed with water and subsequently with ethanol to get rid of foreign contamination and bacterial or viral impurities. Then, the flakes were sundried for a period 48 h. Then, dried flakes converted into power form in mechanical grinder. The powdered eggshell was further milled in a Retsch-PM100 planetary ball mill to synthesize the nanoparticles.

The parameters used for milling are following a ball to weight ratio-20:1, rotational speed of stainless steel jars containing 100 balls: 400 rpm, and milling time: 8 h [12]. The morphology of eggshell particles was observed through high-resolution transmission electron microscope (JOEL 3010). The surface characteristics and size of can be noticed from TEM image as illustrated in Fig. 1.

It is noticed from TEM image that the particles fall within range of 1–20 nm. The surface analysis proposes that particles are irregularly shaped.

2.3 Preparations of Eggshell Pellet

Eggshell nanoparticulate pellet was prepared using compression molding. Polyvinyl alcohol (PVA) was used as a binding material. Polyvinyl alcohol solution prepared
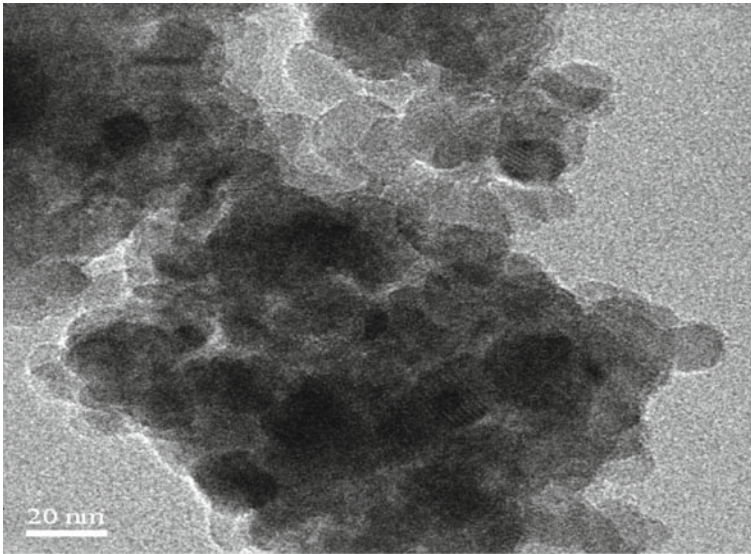
Fig. 1 TEM image of eggshell nanoparticle

from 4 g of PVA in 100 g of water. Eggshell nanoparticles were mixed with PVA solution and then compression molded using 40 kN load at a strain rate of 1 mm/min. the dwell period was 5 min. The green sample was further sintered carbolite tube in inert atmosphere. The sample was sintered at 150 °C at a heating rate of 10 °C/min for a period of 1 h. The hardened pellet sample is then taken out of furnace and stored for further testing. Figure 2 shows the process of fabrication of eggshell nanoparticulate pellet.

2.4 Characterization of Pellet

The microstructural assessment of the eggshell nanoparticulate pellet was performed on Vega 3 Tescan SEM at Center of advanced instrumentation facility, NIT Warangal. For dye adsorption test, eggshell nanoparticulate pellet was put in to 500 ml of dye solution of methylene blue, prepared with various initial dilutions ranging from 50 to 500 mg/L of methylene blue. The dye adsorption experimentation was conducted on Beckman UV–vis spectrophotometer. The sample was put into a 500 ml solution into a beaker and stirred 300 rpm for a period of 4 h to reach the equilibrium.

Adsorption ability of pellet was calculated using Eq. (1) [3], and Eq. (2) was used for kinetic analysis to quantitatively assess the rate of adsorption of dye.

$$q_e = \frac{(C_i - C_e) \times v}{m} \tag{1}$$
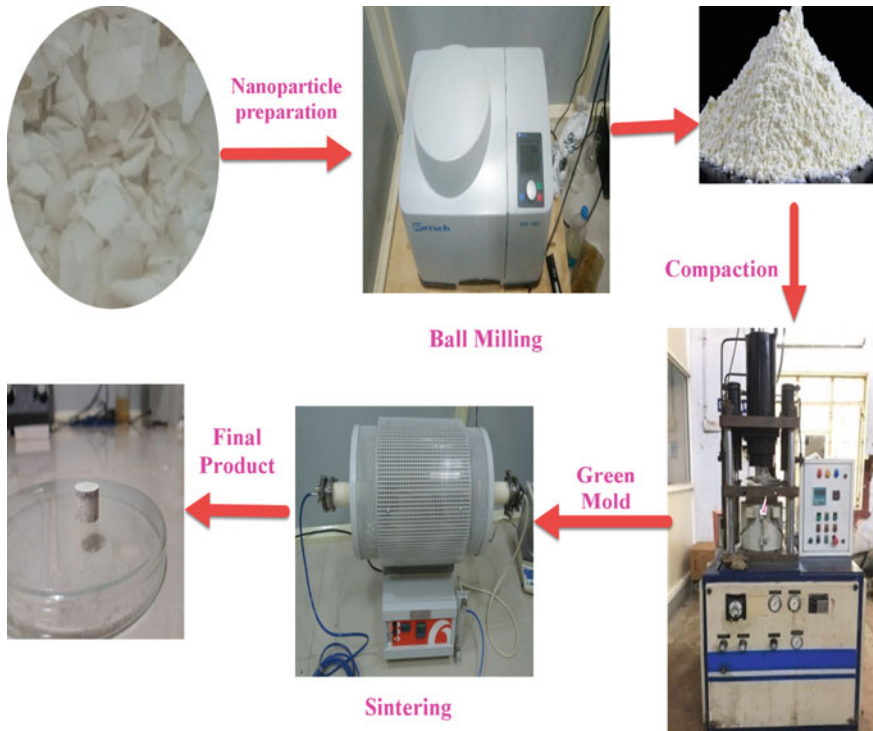
Fig. 2 Preparation process of eggshell nanoparticulate pellet

Adsorption rate of dye at time t, q_t (mg/g) was quantified using Eq. (2) [3].

$$q_t = \frac{(C_i - C_t) \times v}{m} \tag{2}$$

Further, the total dissolved solid (TDS) value of wastewater was evaluated prior to the filtration and after the filtration through the pellet. A portable TDS meter was utilized for the evaluation of TDS value. The pH value of water was also assessed before and after the experimentation. A portable pH meter was used to assess the pH value.
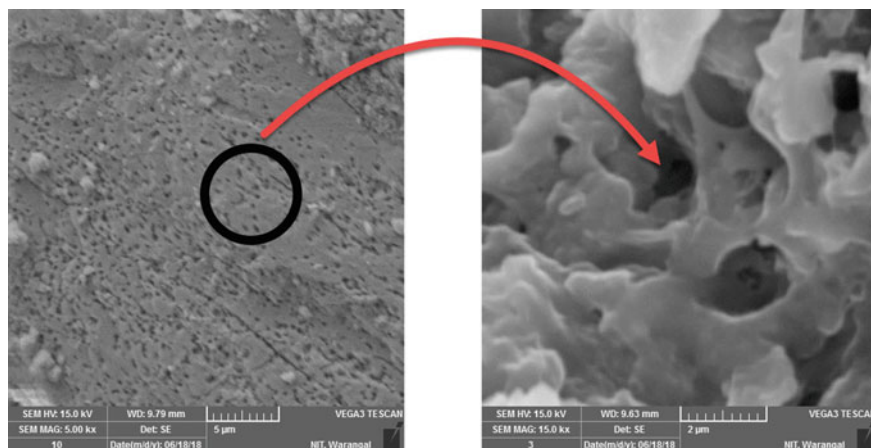
Fig. 3 Morphology of the eggshell nanoparticulate pellet

3 Results and Discussion

3.1 Microstructural Assessment of Eggshell Nanoparticulate Pellet

Figure 3 shows SEM image of prepared eggshell nanoparticulate pellet. The image shown in 3 distinctly shows development of pores on the surface of the sample. The enlarged image shown in Fig. 1 shows that the pores are clear and strong. The pores also deep into thickness of pellet as shown in enlarge image in Fig. 1. The pore size ranges from micrometer to nanometer. The formation of pores could be attributed to burning of binder during the sintering of pellet. The pores visible on surface make the way filtration of impurity.

3.2 Adsorption Test

Influence of interaction time: Fig. 4 highlights the influence of interaction time on adsorption capability of eggshell nanoparticulate pellet for various initial concentrations of methylene blue ranging from 50 to 500 mg/L of dye in dye solution. It is gathered from Figure 4 that there upward trend in dye adsorption with rise in interaction time. The equilibrium was achieved after 4 h of interaction time. The graph illustrates the quick adsorption rate the beginning due to numerous easily accessible open pores results high rate of diffusion, however, as the time increases, the pores are inhabited with ions of methylene blue. Once pores are occupied, the equilibrium is
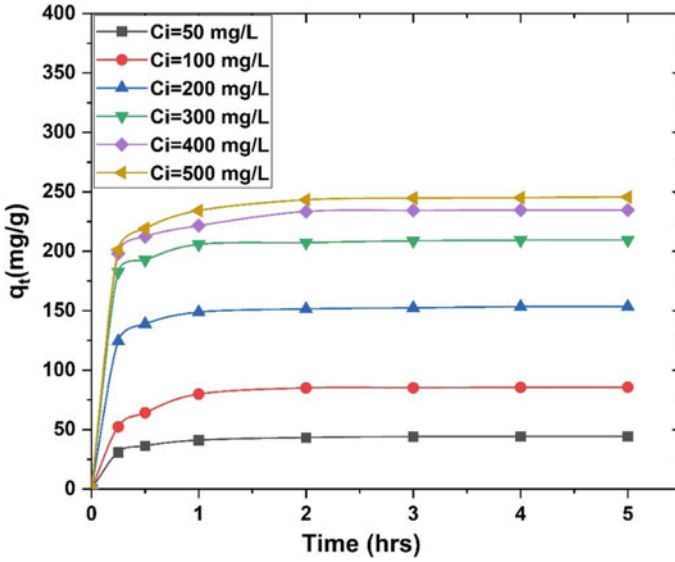
Fig. 4 Influence of interaction time on adsorption ability for various initial dilutions

reached, and there no further adsorption of ions. Figure 4 also portrays that adsorption increases with increase in initial concentration of dye. This may be due high amount of initial concentration of dye behaves as propelling force to overcome the barriers between solid mass and aqueous phase, which further results in upsurge in dye adsorption.

Adsorption studies. Langmuir isotherms [13] and Freundlich isotherms [14] were obtained by fitting experimental values by Eqs. (3) and (4).

$$q_e = \frac{q_m \times K_L \times C_e}{1 + K_L \times C_e} \tag{3}$$

$$q_e = K_F C_e^{1/n} \tag{4}$$

Langmuir constant K_L is correlated to R_L by Eq. (5) [15].

$$R_L = 1/(1 + K_L C_i) \tag{5}$$

It is perceived from Fig. 5 that the Langmuir isotherms provide best fit for experimental values of dye adsorption with R^2 value of 0.9967. The Langmuir isotherms suggest the monolayer adsorption of methylene blue dye ions by eggshell nanoparticulate pellet. The Langmuir and Freundlich parameters are shown in Table 1. R_L was calculated from Eq. (1) was turn out to be 0.0602 ($0 < R_L < 1$, favorable), which
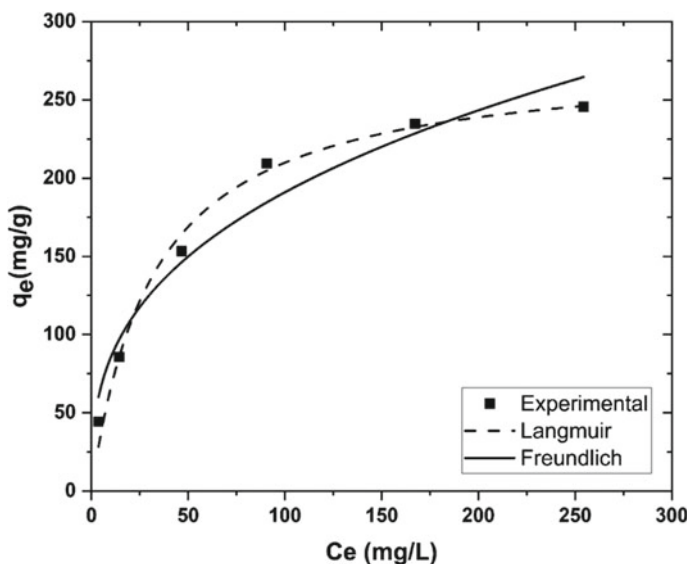
Fig. 5 Adsorption isotherms

Table 1 Isotherms parameters

q_m	R_L	R^2	K_L	K_F	n	R^2
277.084	0.0602	0.988	0.03121	38.19	2.86	0.957

propose fact that the pellet is suitable for dye adsorption. The results of dye adsorption were compared with earlier research. It was found this method of fabrication better result compare to earlier ones [5, 16–18].

3.3 TDS Concentration and pH

TDS test results revealed that the contaminated, which was having TDS value of 800 ppm, the ppm value, was reduced to 467 ppm. This significant reduction in TDS may be attributed to adsorption of impurities and filtration though the large number of pores available on the pellet. Further, the test results of pH value indicate that the pH number was improved from 6.5 to eight. The increase in pH was clearly noticed, the pellet makes the water alkaline, and this may be attributed to presence of $CaCO_3$ eggshell nanoparticles.

4 Conclusion

The experimentation leads to following concluding remarks.

1. It can be concluded from TEM analysis suggest that eggshell nanoparticles were in nanorange ranging from 1 to 20 nm.
2. The pellet of eggshell nanoparticulate was successfully prepared, and it was observed from SEM analysis that there were plenty of pores in the surface of pellet. The deep, strong, and transparent pores were observed.
3. The highest dye adsorption was noticed for 500 mg/L of initial dilution of methylene blue dye. The highest adsorption was turn out to be 277.084 mg/g. significant adsorption though pellet makes it a potential option for treatment of textile run-off. The TDS value was also observed to be significantly reduced with an improvement in pH, making this pellet a suitable candidate for wastewater treatment.
4. This research can be further extended to include few water quality checks such as hardness, total suspended solid, bacterial analysis of water sample, turbidity test to further verify the ability of pellet for water treatment.
5. Pellet could be combined with activated carbon pellet to further enhance the filtration capacity

References

1. Toro, P., Quijada, R., Yazdani-Pedram, M., Arias, J.L.: Eggshell, a new bio-filler for polypropylene composites. Mater. Lett. **61**(22), 4347–4350 (2007)
2. Panchal, M., Raghavendra, G., Prakash, M.O., Ojha, S., Bose, P.S.C.: Moisture absorption behavior of treated and untreated eggshell particulate epoxy composites. Silicon, 1–9 (2018)
3. Panchal, M., Raghavendra, G., Omprakash, M., Ojha, S.: Fabrication and characterization of silica based ceramic composite for filtration applications. Silicon **13**, 1951–1960 (2021). https://doi.org/10.1007/s12633-020-00595-y
4. Vijayaraghavan, K., Jegan, J., Palanivelu, K., Velan, M.: Removal and recovery of copper from aqueous solution by eggshell in a packed column. Miner. Eng. **18**, 545–547 (2005)
5. Tsai, W.-T., Hsien, K.-J., Hsu, H.-C., Lin, C.-M., Lin, K.-Y., Chiu, C.-H.: Utilization of ground eggshell waste as an adsorbent for the removal of dyes from aqueous solution. Biores. Technol. **99**, 1623–1629 (2008)
6. Köse, T.E., Kıvanç, B.: Adsorption of phosphate from aqueous solutions using calcined waste eggshell. Chem. Eng. J. **178**, 34–39 (2011)
7. Baláž, M., Bujňáková, Z., Baláž, P., Zorkovská, A., Danková, Z., Briančin, J.: Adsorption of cadmium(II) on waste biomaterial. J. Colloid Interface Sci. **454**, 121–133 (2015)
8. Asgari, G., Dayari, A.: Experimental dataset on acid treated eggshell for removing cyanide ions from synthetic and industrial wastewaters. Data Brief **16**, 442–452 (2018)
9. De Angelis, G., Medeghini, L., Conte, A.M., Mignardi, S.: Recycling of eggshell waste into low-cost adsorbent for Ni removal from wastewater. J. Clean. Prod. **164**, 1497–1506 (2017)
10. Mittal, A., Teotia, M., Soni, R.K., Mittal, J.: Applications of egg shell and egg shell membrane as adsorbents: a review. J. Mol. Liq. **223**, 376–387 (2016)

11. Mutavdžić Pavlović, D., Ćurković, L., Macan, J., Žižek, K.: Eggshell as a new biosorbent for the removal of pharmaceuticals from aqueous solutions. Clean Soil Air Water **45**, 1700082 (2017)
12. Panchal, M., Raghavendra, G., Reddy, A.R., Omprakash, M., Ojha, S.: Experimental investigation of mechanical and erosion behavior of eggshell nanoparticulate epoxy biocomposite. Polym. Polym. Compos. **29**(7), 897–908 (2021). https://doi.org/10.1177/0967391120943454
13. Langmuir, I.: The adsorption of gases on plane surfaces of glass, mica and platinum. J. Am. Chem. Soc. **40**, 1361–1403 (1918). https://doi.org/10.1021/ja02242a004
14. Freundlich, H.M.F.: Over the adsorption in solution. J. Phys. Chem. **57**, 385–471 (1906)
15. Hall, K.R., Eagleton, L.C., Acrivos, A., Vermeulen, T.: Pore- and solid-diffusion kinetics in fixed-bed adsorption under constant pattern conditions. Ind. Eng. Chem. Fundam. **5**, 212–223 (1966). https://doi.org/10.1021/i160018a011
16. Liang, Z., Zhao, Z., Sun, T., Shi, W., Cui, F.: Enhanced adsorption of the cationic dyes in the spherical CuO/meso-silica nano composite and impact of solution chemistry. J. Colloid Interface Sci. **485**, 192–200 (2017). https://doi.org/10.1016/j.jcis.2016.09.028
17. Liu, S,, Wei, J., Chen, X., Ai, W., Wei, C.: Low-cost route for preparing carbon-silica composite Mesoporous material from coal gasification slag: synthesis, characterization and application in purifying dye wastewater. Arab. J. Sci. Eng. **45**, 4647–4657 (2020). https://doi.org/10.1007/s13369-020-04383-z
18. Ye, J., Nyobe, D., Tang, B., Bin, L., Li, P., Huang, S., Fu, F., Cai, Y., Guan, G., Hao, X.: Facilely synthesized recyclable mesoporous magnetic silica composite for highly efficient and fast adsorption of methylene blue from wastewater: thermodynamic mechanism and kinetics study. J. Mol. Liq. **303**, 112656 (2020). https://doi.org/10.1016/j.molliq.2020.112656

Performance of Automobile Engine Radiator by Using Nanofluids on Variable Compression Diesel Engine

K. Leela Kumar, R. Rudrabhi Ramu, and P. H. J. Venkatesh

1 Introduction

Nanofluids are yet another type of liquid by scattering nano-meter-sized materials (nanoparticles, nano-fibers, nanotubes, nano-wires, nanorods, nano-sheet or beads) in base liquids. As such, nano-liquids are nanoscale colloidal suspensions containing consolidated nano-materials. They are two-stage frameworks with one stage (strong stage) in another (fluid stage). Nanofluids have been found to have upgraded thermophysical properties like warm conductivity, warm diffusivity, consistency, and convective hotness move coefficients contrasted with those of base liquids like oil or water. It has shown incredible expected applications in many fields history about composites [1]. These nano-molecule liquid suspensions are named nanofluids, acquired by scattering nano-meter-estimated particles in a traditional base liquid like water, oil, thylene glycol regular liquids like glycols, refrigerants, polymeric courses of action, bio-fluids, oils, and other ordinary liquids. Overall, the size of these nanoparticles varies from 1 to 100 nm. Nanoparticles of materials like metallic oxides (Al_2O_3, CuO), nitride ceramics (AlN, SiN), carbide stoneware (SiC, TiC), metals (Cu, Ag, Au), semi-conductors (TiO_2, SiC), single, twofold, or multi-walled carbon nanotubes (SWCNT, DWCNT, MWCNT), and alloyed nanoparticles ($Al_{70}Cu_{30}$) have been used for the preparation of nanofluids. These nanofluids have been found to have an overhauled warm conductivity similarly as additional created hotness move execution at low groupings of nanoparticles [2]. The nanofluid is most certainly

K. Leela Kumar · R. Rudrabhi Ramu · P. H. J. Venkatesh (✉)
Department of Mechanical Engineering, Vignan's Institute of Information Technology (A),
Visakhapatnam, Andhra Pradesh, India
e-mail: venky61788@gmail.com

K. Leela Kumar
e-mail: leelamech36@gmail.com

not a direct liquid solid blend [3]. The primary premise while cultivating the nano-liquid [4] is a sans agglomerate long stretch stable suspension. Robustness of the nano-liquid is huge for its conceivable application as a hotness move fluid.

2 Methodology

Figure 1 shows schematic chart for trial setup which comprises of shut circle circuit. The exploratory test rig incorporates repository and warming component, lowered siphon, radiator fan (speed control DC engine), and automobile radiator. Attractive-drive siphon gives the streams 16–18 LPM; the stream speed of the test region is constrained by two globe valves which is fitting versatile to the reuse line as shown in diagram [5]. The functioning fluid fills 30% of the limit tank whose total volume is 35 L. The outright volume of the surrounding liquid is reliable in all of the tests. The circuit consolidates 0.30 m distance across pipeline which is made of the steel pipe.

This engine has a volume of 1761 cc. The four-chamber engine has a strain extent of 9.25:1 and produces a power of 97 drives at 6000 RPM and a biggest power of 148 N/m at 3500 RPM. It has 8 valves and has a standard Euro II release limit regard. Stimulus PGM20 is used to confine exhaust tainting. The volume of oil gobbled up is 4.4 L (4.75 L if a channel is used). The volume of water and coolant is 6.6 L [6]. The particular information for this engine is cooling game plan of XU7 engine. In this assessment study, the cooling structure of the XU7 engine is mulled over. The cooling course of action of this engine is a closed circuit with an electric fan that is shown in Fig. 1. The nuances of the cooling system are introduced. The radiator has been made of aluminum. It is of a level kind, so the working fluid streams inside the even radiator from the right to the left [4].

Fig. 1 Four-cylinder engine

3   Results

To look at better hotness retaining limits of various cooling substances like water, water + ethylene glycol, 0.02% volume part of SiC, 0.05% vol. part of SiC, 0.08% vol. part of SiC from motor cooling coat at various stacking conditions, and at various pressure proportions, variable pressure diesel motors are utilized

(a)   Heat carried by cooling water,

$$Q_c = m_c * c_p * (T_{out} - T_{in}) \qquad (1)$$

$m_c =$ mass flow rate of cooling water

$C_p =$ specific heat of water

$\quad = 4180\,kj/kg\text{-}k$

$T_{out} =$ outlet temperature of cooling substance

$T_{in} =$ inlet temperature of cooling substance
(b)   Mass of fuel consumed per minute, m_f:

$$m_f = (\text{pipette} * \rho_d * 60)/(t * 1000) \qquad (2)$$

$\rho_d =$ density of diesel
(c)   Total fuel consumption (TFC):

$$\text{TFC} = m_f * 60, \ \ kg/h$$

where m_f is in kg/min
(d)   Heat carried away by exhaust gases:

$$Q_{eg} = m_{eg} * c_{pg} * \left(T_g - T_{air}\right) \qquad (3)$$

$C_{pg} = 1.05\,kj/kg\text{-}k$

$m_{eg} = m_f + m_a$
(e)   Heat equivalent to break power:

$$\text{BP} = (2\Pi NT)/60{,}000, \ \ KW \qquad (4)$$

where $N =$ speed of the engine, rpm

$T =$ Torque applied on drum
(f)   Heat input:

$$HI = (TFC/3600) * C_v, \text{ kw} \tag{5}$$

C_v = calorific value of diesel

(g) Mass flow rate of air

$$m_a = \rho_a * A * V_a \tag{6}$$

ρ_a = density of air

$V_a = [2 * 9.81 * h_m * ((\rho_w/\rho_a) - 1)]^{1/2}$

(h) Un-account losses = $\left[HI - \left(Q_c + Q_{eg} + BP\right)\right]$ \hfill (7)

(see Tables 1, 2, 3 and 4).

3.1 Air Fuel Ratio Graphs

See Figs. 2, 3 and 4.

3.2 BSFC Versus BP at Different Compression Ratios

See Figs. 5, 6, 7, 8 and 9.

4 Conclusion

From the above outcomes, it is inferred that at 15:1 pressure proportion EG + distilled water + 0.05% volume part SiC blend nanofluid exhibits greatest air fuel proportion at 1/3 and 2/3 burdens, and at 17:1 pressure proportion, EG + distilled water + 0.08% volume division SiC combination nanofluid shows most extreme air fuel proportion at 1/3, 2/3, and full loads. Greatest air fuel proportion prompts admit maximum air into the burning chamber during pull stroke and complete ignition of hydro carbons is happened. Eventually, the exhaust gas emissions are diminished. The outcomes it is inferred that at 15:1 pressure proportion EG + distilled water + 0.05% volume part SiC blend nanofluid exhibits greatest air fuel proportion at 1/3 and 2/3 burdens, and at 17:1 pressure proportion, EG + distilled water + 0.08% volume division SiC combination nanofluid shows most extreme air fuel proportion at 1/3, 2/3 and full loads. Greatest air fuel proportion prompts admit maximum air into the burning chamber during pull stroke, and complete ignition of hydro carbons is happened.

Table 1 Observation table for water

Mixture	CR	N (RPM)	Load (kg)	Fuel time consumption (s)	Air flow (mm)		Air inlet (T_o)	Engine CW		Wall temp (T_w)	Exhaust temp (T_g)
					h_1	h_2		T_{in}	T_o		
Water	15:01	1530	0	82	16	92	26	33	36	33	153
		1530	2.5	55	15	90	26	40	42	35	216
		1520	5	43	12	89	25	45	47	35	286
		1500	7.5	37	9	85	26	48	51	37	340
	16:01	1560	0	79	16	91	27	42	45	37	190
		1540	2.5	57	15	89	28	40	43	37	235
		1520	5	46	13	87	28	40	42	38	280
		1500	7.5	38	9	85	26	39	41	38	340
	17:01	1615	0	91	22	97	29	41	44	39	170
		1530	2.5	60	14	89	29	40	43	39	240
		1525	5	49	11	88	29	40	43	39	275
		1500	7.5	37	9	85	27	39	42	39	337

Table 2 Observation table for water + ethylene glycol

Mixture	CR	N (RPM)	Fuel time consumption (s)	Air flow (mm)		Air inlet (T_o)	Engine CW		Exhaust temp (T_g)	Wall temp (T_w)
				h_1	h_2		T_{in}	T_o		
Water + EG	15.1	1620	73	22	98	25	34	43	166	36
		1570	54	19	95	23	31	41	173	36
		1530	44	14	89	23	35	39	175	36
		1510	38	12	86	22	36	41	180	36
	16.1	1550	89	15	91	24	42.5	44	154	36
		1550	62	13	89	22	40	46	160	37
		1520	50	13	89	22	35	39	160	36
		1510	38	11	86	22	36	40	160	35
	17.1	1650	91	21	97	26	39	44	167	36
		1530	60	14	90	26	37	46	200	37
		1520	45	12	92	24	35	38	200	38
		1500	37	10	85	24	36.5	40	200	37

Table 3 Observation table for water + ethylene glycol + 0.02% volume fraction SiC

Mixture	CR	N (RPM)	Load (kg)	Fuel time consumption (s)	Air flow (mm)		Air inlet (T_o)	Engine CW		Exhaust temp (T_g)	Wall temp (T_w)
					h_1	h_2		T_{in}	T_o		
Water + EG + 0.02%	15.1	1560	0	84	15	91	37	48	51	180	35
		1540	2.5	60	14	90	37	47.5	51	230	36
		1520	5	45	13	87	37	47.5	51.5	280	36
		1500	7.5	36	10	85	37.5	48	53	340	36
	16.1	1580	0	86	17	93	36	45	48	175	34
		1530	2.5	60	15	89	37	46	50	230	34
		1520	5	46	14	86	37	46	51	290	34
		1500	7.5	37	10	84	37	47	52	350	34
	17.1	1540	0	78	18	93	36	31	35	160	32
		1530	2.5	58	15	91	35	38	41	220	35
		1520	5	45	14	89	35	41	44	280	36
		1500	7.5	37	12	86	36	43	48	342	36

Table 4 Observation table for water + ethylene glycol + 0.05% volume fraction SiC

Mixture	CR	N (RPM)	Load (kg)	Fuel time consumption (s)	Air flow (mm)		Air inlet (T_o)	Engine CW		Wall temp (T_w)	Exhaust temp (T_g)
					h_1	h_2		T_{in}	T_o		
Water + EG + 0.05%	15.1	1550	0	81	16	90	33	42.6	45.3	36	180
		1535	2.5	61	15	89	33	42.5	45.2	37	225
		1520	5	45	13	87	33	43.4	47	37.5	292
		1485	7.5	36	10	83	33	46.4	50	38	360
	16.1	1560	0	82	18	91	32.5	44	47	37	188
		1540	2.5	58	15	89	32.5	46	49.5	36	263
		1520	5	45	14	87	32	46.4	50.5	37	315
		1500	7.5	36	10	84	32	45.3	50.4	37	372
	17.1	1540	0	82	17	92	31	37	39	35	160
		1530	2.5	50	15	90	30.5	37.4	39.6	35	218
		1520	5	43	14	89	30.5	39.5	42.4	35	278
		1500	7.5	36	12	87	31	41.8	46	37	353
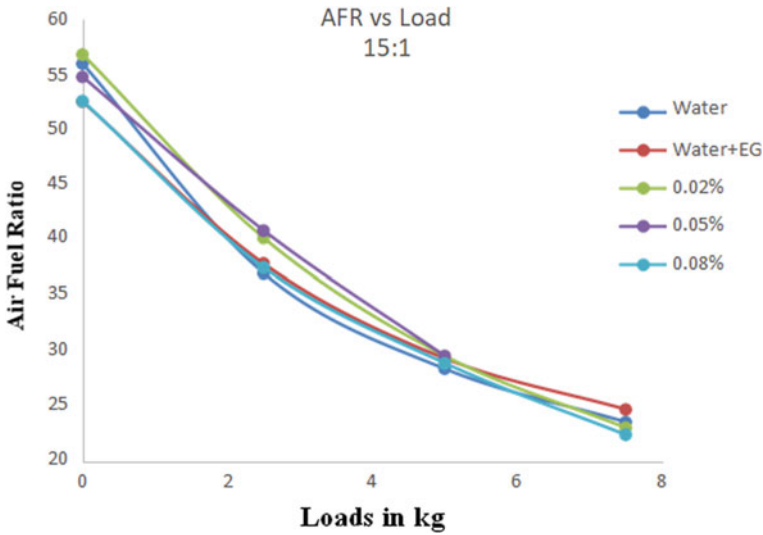
Fig. 2 AFR versus load at 15:01 compression ratio
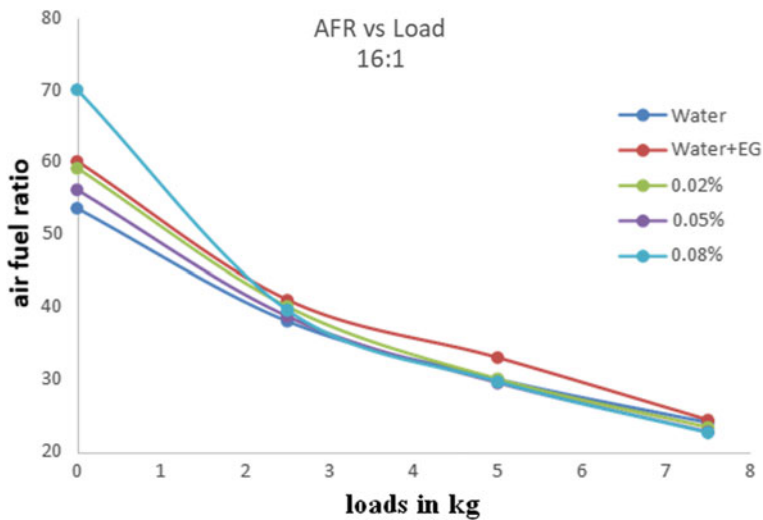
Fig. 3 AFR versus load at 16:01 compression ratio

Eventually, the exhaust gas emissions are diminished. The 17:1 compression ratio EG + distilled water + 0.08% volume fraction of SiC nanofluid is having break-specific fuel consumption is very less compared to other volume fractions of SiC. Performance of radiator is tested with various coolant mixtures ranging of different nanofluids concentrations. Heat enhancement of coolant fluid is reported in terms
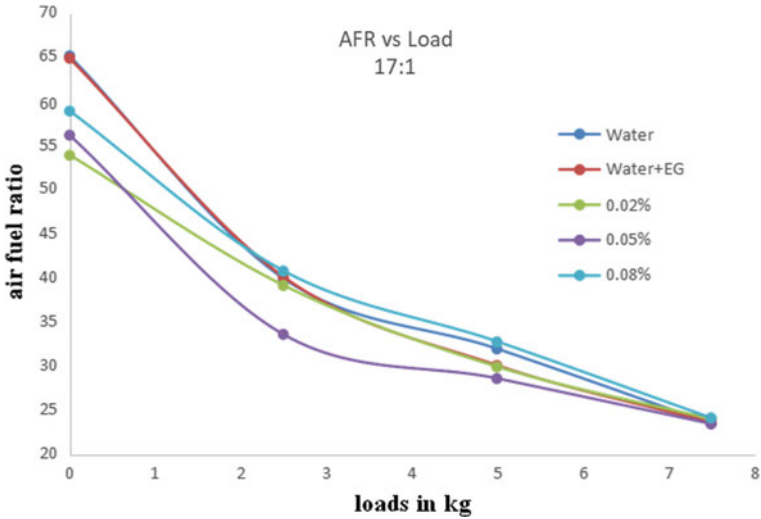
Fig. 4 AFR versus load at 17:01 compression ratio
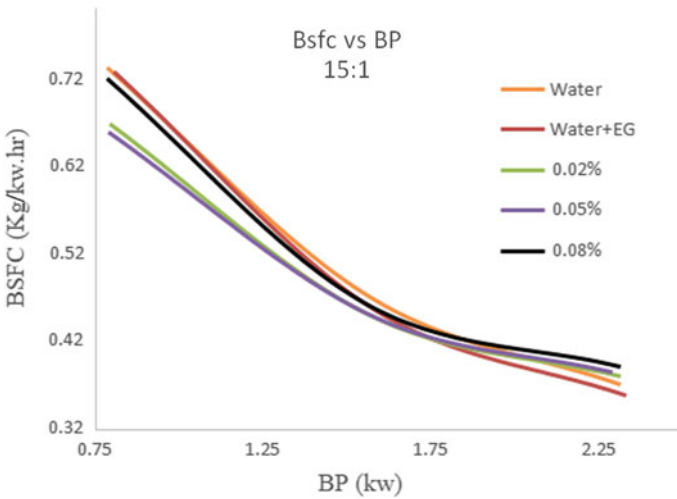
Fig. 5 BSFC versus BPat 15:01 compression ratio

of dimensionless Nusselt number. Heat transfer coefficient of fluids improved at lowest compression ratio with increase in volume concentration of nanofluids. At intermediate load, a steep increase in heat enhancement is observed.

Air Fuel Ratio
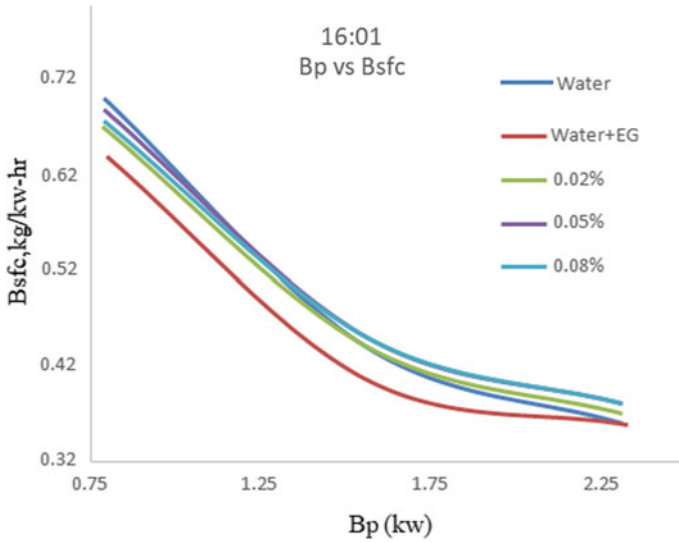
Fig. 6 BSFC versus BPat 16:01 compression ratio
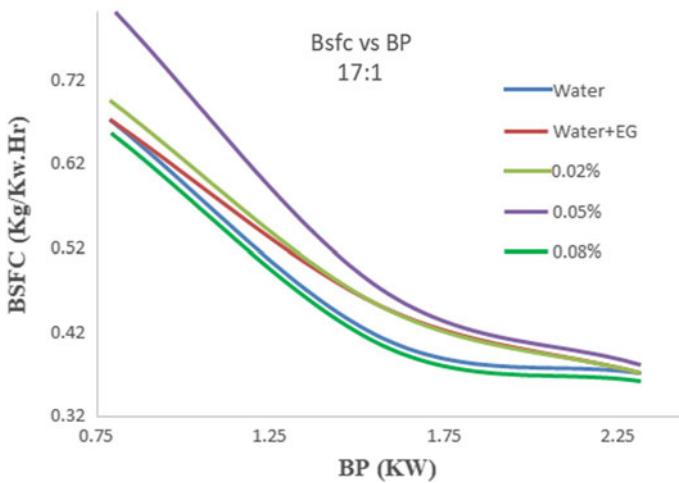
Fig. 7 BSFC versus BPat 17:01 compression ratio

1. At 15:1 compression ratio as SiC volume fraction increases, the air fuel ratio mixture is increasing up to 0.05% volume fraction of SiC.
2. At 17:1 compression ratio as SiC volume fraction increases, air fuel ratio mixture decreases up to 0.05% volume fraction but suddenly increases at 0.08 volume fraction of sic.
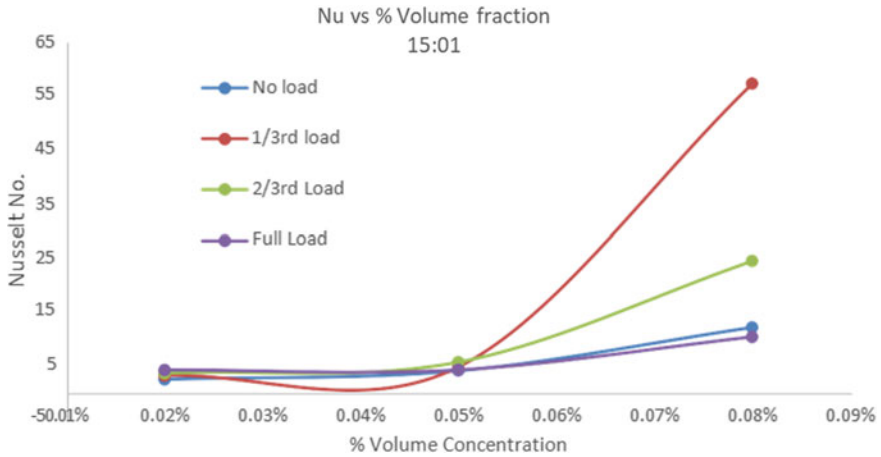
Fig. 8 Nusselt no. versus % vol. concentration at 15:01 compression ratio
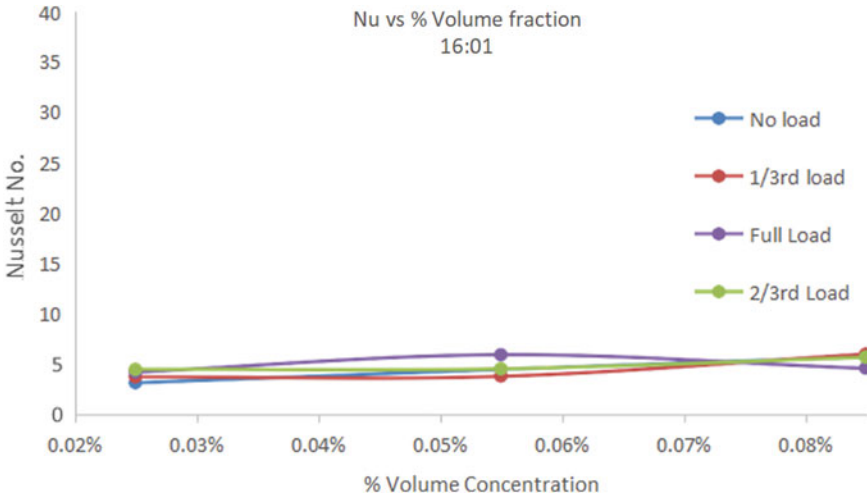
Fig. 9 Nusselt no. versus % vol. concentration at 16:01 compression ratio

3. A maximum air fuel ratio result in maximum air is admitted into the combustion chamber during suction stroke, and complete combustion of hydro carbons is occurred. So finally minimizing the exhaust gas emissions.

Break Thermal Efficiency

1. At 17:1 compression ratio, EG + distilled water + 0.08% volume fraction of SiC nanofluid is having maximum break thermal efficiency at 1/3, 2/3, and full load.

2. At 15:1 compression ratio, BTE increases as SiC volume fraction increases up to 0.05% at 1/3 and 2/3 loads.

Unaccounted Losses

1. At 17:1 compression ratio, percentage of losses increases up to 0.05% volume fraction of nanofluid and suddenly deceases at 0.08% volume fraction of SiC nanofluid, and at the same time, break power at 0.08% volume fraction of SiC nanofluid increases at every load.
2. Hence, the utilization of input power is more at 0.08% volume fraction of SiC nanofluid.

Break-Specific Fuel Consumption

1. At 17:1 compression ratio, EG + distilled water + 0.08% volume fraction of SiC nanofluid is having break-specific fuel consumption is very less compared to other volume fractions of SiC.

Effects of Particle Concentration on Nusselt Number

1. Heat transfer coefficient of fluids improved at lowest compression ratio with increase in volume concentration of nanofluids. At intermediate load, a steep increase in heat enhancement is observed.
2. Overall better heat enhancement is observed through convective heat transfer of nanofluid of 0.08% concentration.
3. At higher volume concentration, tube has attained near values of coolant bulk mean temperature. Thus, nanofluids can be recommended as coolants in radiator at optimum compression ratio at intermediate loads.

5   Future Scope of Work

The splendid future for nano-liquids as a class of incredible material needed for different applications in automobiles. But, a great deal of exploration work is expected to investigate its other potential spaces of uses in this specific field of designing, so the future creating vehicles will be more efficient, smaller, and eco-friendly. The potential warm conductivity ought to be accordingly taken advantage of in the cutting edge heat transfer fluid. Changing petroleum products with elective energizes for controlling outflows and expanding the exhibition of motor.

References

1. Chaurasia, P., Kuma, A., Yadav, A., et al.: Heat transfer augmentation in automobile radiator using Al_2O_3 water based nanofluids. SN Appl. Sci. **1**, 257 (2019).https://doi.org/10.1007/s42 452-019-0260-7
2. Seraj, M., Yahya, S.M., Badruddin, I.A., Anqi, A.E., Asjad, M., et al.: Multi-response optimization of nanofluid-based I. C. engine cooling system using fuzzy PIV method. Processes **8**(1), 30 (2020). https://doi.org/10.3390/pr8010030
3. Elbadawy, I., Elsebay, M., Shedid, M., Fatouh, M.: Reliability of nanofluid concentration on the heat transfer augmentation in engine radiator. Int. J. Automot. Technol. **19**, 233–243 (2018)
4. Li, X., Zou, C., Zhou, L., Qi, A.: Experimental study on the thermo-physical properties of diathermic oil based SiC nanofluids for high temperature applications. Int. J. Heat Mass Transf. **97** (2016)
5. Nogueira, É.: Thermohydraulic performance in the flow of copper oxide (CuO) or aluminum oxide (Al_2O_3) water borne nanofluids in a finned flat tube heat exchanger (automotive radiator). IOSR J. Mech. Civ. Eng. (IOSR-JMCE) **16**(5 Ser. IV), 01–12 (2019)
6. Godson, L., Raja, B., Mohan Lal, D., Wongwises, S.: Enhancement of heat transfer using nanofluids—an overview. Renew. Sustain. Energy Rev. **14**(2), 629–641 (2010)
7. Zou, C.: Thermo-physical properties of water and ethylene glycol mixture based SiC nanofluids: an experimental investigation. Int. J. Heat Mass Transf. **101**, 412–417 (2016)
8. Uddin, M.J., Kalbani, K.S., Rahman, M.M., Alam, M.S., Al-Salti, N., Eltayeb, L.A.: Fundamentals of nanofluids: evolution, applications, and new theory. Biomath. Syst. Biol. Off. J. Bio Math. Soc. India **2**(1) (2016)
9. Selvam, C., Mohan Lal, D., Harish, S.: Thermophysical properties of ethylene glycol-water mixture containing silver particles. J. Mech. Sci. Technol. **30**(3), 1271–1279 (2016)
10. Du, X., Zhang, W., Yang, L., Yang, Y.P.: Thermal and hydraulic performance of water/glycol mixture and the application on power electronics cooling. Environ. Ear. Sci. Res. J. (EESRJ) **3**(1), 1–6 (2016)
11. Kulkarni, D.P., Vajjha, R.S., Das, D.K., Oliva, D.: Application of aluminum oxide nanofluids in diesel electric generator as jacket water coolant. Appl. Therm. Eng. **28**, 1774–1781 (2009)
12. Parikh, H.B., Prajapati, V.M., Thakkar, K.H.: Performance evaluation and emission analysis of 4-s, IC engine using ethanol biodiesel blended with diesel fuel. ISSN: 2319-1163 (2013)
13. Srinivasa Rao, P., Srinivas, K.: Experimental analysis of single cylinder diesel engine fuelled with methyl ester of palm kernel oil blending with eucalyptus oil. Int. J. Eng. Res. Appl. (IJERA). ISSN: 2248-9622 (2012)
14. Sharma, G., Dandotiya, D., Agrawal, S.K.: Experimental investigation of performance parameters of single cylinder IC engine using mustard oil. Int. J. Mod. Eng. Res. (IJMER). ISSN: 2249-6645 (2013)
15. Peyghambarzadeh, S.M., Hashemabadi, S.H., Seifi Jamnani, M., Hoseini, S.M.: Improving the cooling performance of automobile radiator with Al_2O_3/water nano fluid. Appl. Therm. Eng. **31**, 1833–1838 (2011)
16. Ramadhas, A.S., Muraleedharan, C., Jayaraj, S.: Performance and emission evaluation of a diesel engine fueled with methyl esters of rubber seed oil. Renew. Energy **30**, 1789–1800 (2005)
17. Wu, Y.Y., Kao, M.-J.: Using TiO_2 nano fluid additive for engine lubrication oil. Ind. Lubr. Tribol. 63(6), 440–445 (2011)
18. Bozorgan, N., Krishnakumar, K., Bozorgan, N.: Numerical study on application of CuO water nanofluid in automotive diesel engine radiator. Mod. Mech. Eng. **2**, 130–136 (2012)
19. Senthilraja, S., Karthikeyan, M., Gangadevi, R.: Nanofluid applications in future automobiles: comprehensive review of existing data. Nano-Micro Lett., 306–310 (2010)

Comparative Performance Analysis of R134a/CuO and R134a/SiO$_2$ Nanorefrigerant-Based Refrigeration System

Rajneesh Kaushik and Rajeev Kamal Sharma

1 Introduction

With the advancement of technology, there is continuous work going on to find energy-efficient systems. So, conventional systems are being replaced with more power-saving alternate systems. One such alternate field is the use of nanoparticles in the existing conventional systems. From the start of the twenty-first century, uses of nanomaterial in different technical fields have gained lots of traction, and it has been prevalent in many research areas [1–3]. So the focus has been to identify the use of nanoparticles in various applications and what challenges it brings to introduce them in larger fields by removing the obstacles [4]. Subsequently, different kinds of fluids can be used which have better thermophysical properties and that can replace conventional fluids [5, 6]. Nanoparticles are very small particles of the size ranging between 1 and 100 nm, and nanofluids are the emulsions of nanoparticles and primary (base) fluid. Generally, the base fluids are refrigerants, lubricants, biofluids, organic fluids, and fluid such as water whereas nanoparticles are metal, oxides/carbides/nitrides of metal. The mixing of the nanoparticles in the previous researches has shown moderate to significant improvement in the fluids heat transfer characteristics which also enhances fluids thermophysical properties [7, 8]. It has been found in the previous research studies that the increment of the weight % of the nanoparticles in the base fluid improves the heat transfer properties up to a certain value and after that, it may not change or negatively affects these properties [9]. Nanorefrigerants still hold lots of curiosity because many of their aspects still need to be explored such as the complexity observed during the phase change of

R. Kaushik (✉) · R. K. Sharma
Chitkara College of Applied Engineering, Chitkara University, Rajpura, Punjab, India
e-mail: rajneesh.kaushik@chitkara.edu.in

R. K. Sharma
e-mail: rajeev.sharama@chitkara.edu.in

the nanorefrigerants, nanofluids, and nano-lubricants. It has been also observed that with the increase of the nanoparticles concentration, the stability of nano-lubricant decreases substantially whereas this had a positive impact on evaporator temperature gradient [10]. There is a considerable amount of energy saving by using nanofluids in a refrigeration system. It has been an important factor that impacts energy efficiency in a significant way because of the phase change heat transfer properties of nanorefrigerants in the evaporator. So it is important to understand the heat transfer characteristics of nanorefrigerants flow during the boiling to find out its true effect on the performance of the evaporators of refrigeration systems using nanorefrigerants [11]. From the past experimental research, it has been found that carbon nanotubes are among the ones that have very high-heat transfer capabilities because of their typical geometry and their thermophysical properties [12]. Because of this behavior, multi-walled carbon nanotubes, which tremendously enhance heat transfer characteristics, have been largely used by researchers [13]. Nanoparticles also help to reduce the frictional coefficient of the nano-lubricants which results in a considerable reduction in viscosity and helps to reduce the power consumption of the compressor [14]. It has been noted that nanorefrigerants improve the pool boiling heat transfer compared to the pure refrigerant which improves overall evaporation and condensation characteristics of any vapor compression-based refrigeration system [15]. It has been found that even hybrid nanoparticles have been used in the fluid, and there have been mild to moderate improvement in overall heat-carrying characteristics by changing the concentration of the nanoparticles. The improvement in heat transfer characteristics is because of the presence of Brownian motion between base fluid and nanoparticles which acts as a heat carrier through convection between nanoparticles and base fluid [16]. These improved heat transfer properties help to reduce power consumption significantly in the heating, ventilation, and air conditioning field. There has been a constant challenge of the suspension of nanoparticles in base fluid for all the time, and it was achieved to a certain extent by the addition of a compound of sodium $(C_{18}H_{29}NaO_3S)$ [17] which leads to a remarkable improvement in coefficient of performance [18]. The research carried till now brings us to a logical conclusion that nanoparticles may be applied to different combinations of refrigerant and lubricant which enhances the efficiency substantially of a cooling system. This infers that there is a remarkable improvement in the performance measuring parameters such as an increase in refrigeration effect, better heat rejection in the condenser, and enhancement in subcooling. Hence, it has been observed that colloidal fluids can enhance various thermophysical properties which help to work refrigeration systems more efficiently. However, some points require further detailed investigation to bring the research in a forward direction. First, the procedure of charging nanorefrigerant is not streamlined, which may influence the thermophysical properties of the nanofluids in a big way. Second, the suspension of nanoparticles in refrigerants for long durations should be evaluated. In the vapor compression cycle, refrigerant works in two phases while nanoparticles do not change their phase. So it may improve individual component performance and that should be explored. Hence, the present study is carried out by dispersing two types of nanoparticles (CuO and SiO_2 individually) nanoparticles into the refrigerant R134a, and their comparative analysis has been also done. Due

to the very good thermophysical properties of the R134a and a popular refrigerant in refrigeration makes it a suitable choice to check the effect of nanoparticles on its properties. On other hand, because CuO has very good thermal conductivity and silica has comparatively low-thermal conductivity, so these nanoparticles give us a broad range of data to see its effect on the performance of the refrigerant.

2 Experimental Setup

To carry out an investigation, a vapor compression cycle-based refrigeration system is designed and fabricated in the refrigeration lab as given in Fig. 1. The current system is of capacity 170 L along with components like the hermetic reciprocating compressor, naturally convection condenser, manual expansion valve, and water dip evaporator. To control the heat input, a heating element (2000 W) is used in a water dip evaporator insulated with foam and digital temperature control. An energy meter (600 revs/KWh, 0–20 A) is incorporated into the system to measure heat load and compressor power consumption. To run the system at a constant mass flow rate, a rotameter (4 LPH–35 LPH) along with two manual refrigerant control valves is used. Data of pressure are recorded by pressure gages at compressor suction and discharge end, and temperature is noted with the help of a mercury glass thermometer at the suction of all basic four components. In addition to this, a voltmeter (0–310 V) and an ammeter (0–20 A) are used to measure the overall voltage and current of the refrigeration system. The detailed parts of the experiment setup along with their specifications have been given in Table 1.

2.1 Nanoparticles Structural Analysis

Nanorefrigerants can be made by mixing the nanoparticles in the refrigerant which should be chemically compatible and does not show any anomaly in the behavior of the mixture. The fundamentals of the cooling process in any vapor compression-based refrigeration cycle are the heat extraction from the product by phase change, and so, the nanorefrigerants should not deviate in the basics of the heat transfer process. So the structural compatibility and chemical stability have been of the utmost importance in its study and how miscibility and dispersion of the nanoparticles change its performance in the system. The general properties of the copper oxide nanoparticles and silica nanoparticles have been depicted in Tables 2 and 3, and refrigerant (R134a) properties have been shown in Table 4. To check nanorefrigerants compatibility structurally, nanorefrigerant is put into the refrigeration system with nanoparticles in proper proportions of copper oxide (CuO) nanoparticles and another case with silica nanoparticles (SiO$_2$). The typical size of nanoparticles which have been used in the current research is 0–40 nm. The CuO nanoparticles of size 0–40 nm having a density of 6.3 g/cm^3 and SiO$_2$ nanoparticles of size 0–40 nm having a density of 2.63 g/cm^3

Fig. 1 Experimental testing unit

Table 1 Components list used in VCC refrigeration system

S. No.	Component	Qty	Description
1	Hermetic reciprocating compressor	One	4.56 cc
2	Condenser	One	$0.2632\ m^2$
3	Throttling valve	One	Manual
4	Evaporator	One	$0.145\ m^2$
5	Heating element	One	230 W
6	Condenser side—pressure meter	Two	$0–290\ lb/in.^2$
7	Evaporator side—pressure meter	Two	$-25\ to\ 145\ lb/in.^2$
8	Flowmeter	One	0–35 L/h
9	Mercury-based temperature sensor	Four	$-15\ to\ 95\ °C$
10	Digitally controlled temperature meter	One	$-35\ to\ 55\ °C$
11	Power recorder	Two	600 revs/KWh
12	Ampere meter	One	0–20 A
13	Voltmeter	One	0–310 V

Table 2 Properties of CuO nanoparticles

Primary particle size (nm)	Thermal conductivity (w/m k)	Molecular weight (g mol^{-1})	Density (g cm^{-3})	Purity (%)	Crystal phase	Appearance	Melting point (K)	Boiling point (K)
0–40	33	78.9245 g/mol	6.31	98	Quartz	Black powder	1474	2273

Table 3 Properties of SiO₂ nanoparticles

Primary particle size (nm)	Thermal conductivity (w/m k)	Molecular weight (g mol^{-1})	Density (g cm^{-3})	Purity (%)	Crystal phase	Appearance	Melting point (K)	Boiling point (K)
0–40	1.2–1.4	60.0843	2.634	98	Quartz	White powder	1986	2503

Table 4 Properties of R134a refrigerant

Chemical formula	Molecular mass (g mol^{-1})	Normal boiling point	Critical temperature	Critical pressure	Density (kg m^{-3})	Thermal conductivity (w/m k)	Dynamic viscosity
CH_2FCH_3	102.03	−26.1	101.1	4.06	1199.7	0.09208	0.1905

are procured from an America-based company (Sigma-Aldrich Chemicals) and are used for analysis in the present experimental study.

2.2 Structural Characterization

To analyze characteristics of CuO nanoparticles, XRD technique is being used to check the peaks of intensity at 2 points, and no further other characteristic peaks are observed in the samples while the size and shape of the nanoparticles are observed with the TEM technique as shown in Fig. 2a. Similarly, silica nanoparticles peaks are checked with the help of the XRD technique as depicted in Fig. 2b.

3 Result and Discussion

The experimental analysis of the vapor compression refrigeration system was done with eight types of nanorefrigerants. (i) Pure refrigerant R134a, (ii) 5 types of nanorefrigerant with a weight percentage of CuO nanoparticles (0.1, 0.2, 0.3, 0.4, 0.5 g) in 100 g of R134a, and (iii) 5 types of nanorefrigerant with a weight percentage of
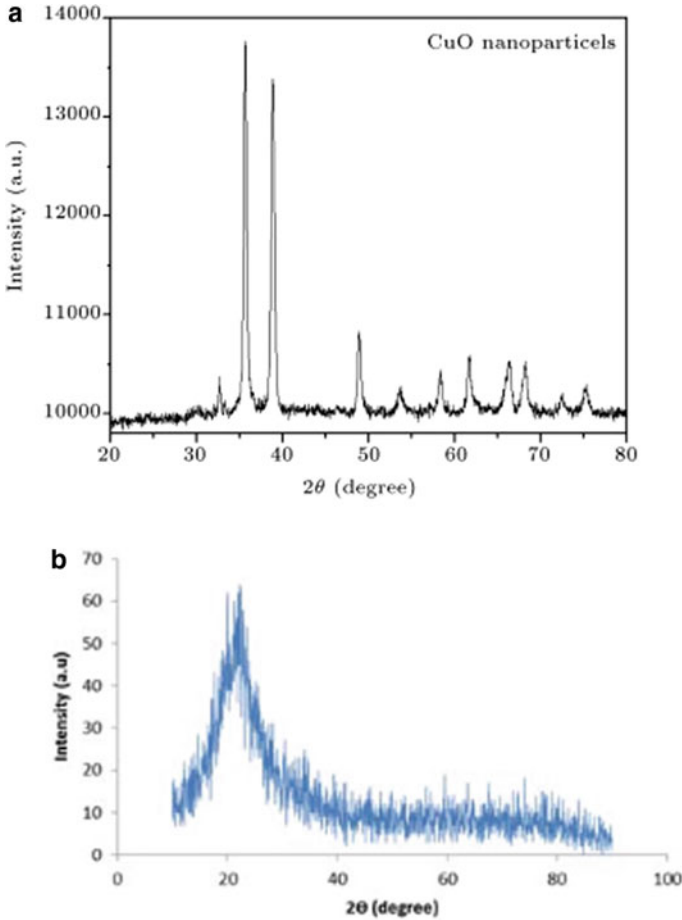
Fig. 2 a XRD of nanoparticles (CuO). **b** XRD of nanoparticles (SiO_2)

SiO_2 nanoparticles (0.1, 0.2, 0.3, 0.4, 0.5 g) in 100 g of R134a and to find out the effect on performance. This parameter in the cooling system can be evaluated by calculating COP which is the ratio of the desired effect to the total work input as shown in Eq. (1).

$$COP = \frac{\text{Desired refrigerant effect}}{\text{Compressor work}} \tag{1}$$

It has been found that COP of the system improves significantly with the addition of CuO nanoparticles in R134a, whereas with SiO_2 nanoparticles, COP of the system improves marginally.
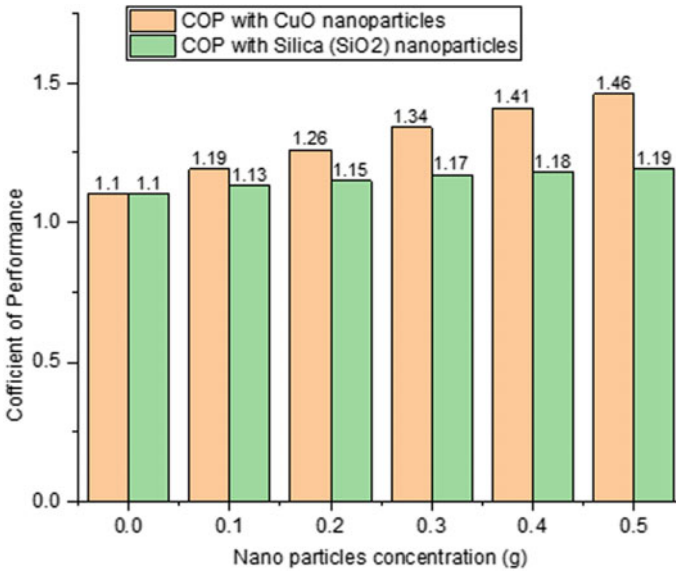
Fig. 3 Coefficient of performance with nanoparticles (CuO/SiO$_2$)

3.1 Coefficient of Performance

COP is the performance parameter of any refrigeration system which helps to check its efficiency to cool the product. Understandably, a higher COP depicts the better performance of the system, and emphasis is always to work on achieving the higher COP for the refrigeration system. It can be improved by either changing the working conditions or parameters of COP. COP is the ratio of the cooling effect produced to the consumed power by the compressor. To find out the COP, the refrigeration effect has been measured by the heating load given to the evaporator, and power consumption is measured by the energy meter to bring the desired temperature to the evaporator. The COP is found for varying concentrations at constant load which is depicted in Fig. 3. It has been found that COP of the refrigeration system is consistently increasing with the addition of CuO nanoparticles, while this trend is there with SiO$_2$ nanoparticles but it has less impact on the performance of the system.

3.2 Power Consumption

Energy consumption is total power consumed by the refrigeration system in a single day. It has been calculated once the system achieves the steady-state conditions. Energy consumption of the cooling is lowest if it works with maximum efficiency, and that is the best condition to work a system. From the present study, it has

Fig. 4 Power consumption
with nanoparticles
(CuO/SiO_2)
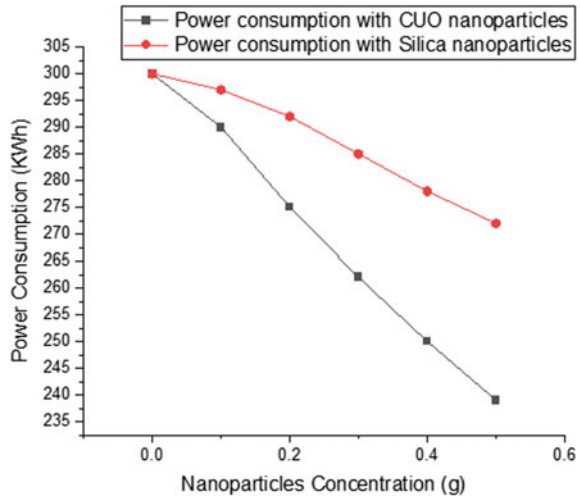
been observed that nanorefrigerants have been reasonably effective to reduce energy consumption compared to the pure refrigerant, and it consumes the lowest energy if the CuO nanoparticles concentration is 0.5 g in the base refrigerant R134a as shown in Fig. 4. The same kind of trend has been observed with SiO_2 nanoparticles, but overall; the power consumed is lowered in all concentrations, but it is relatively higher compared to CuO nanoparticles.

3.3 Cooling Speed

Cooling speed is defined as the rate of temperature drop at a particular time. Faster is the drop, and better cooling speed of the system is considered. It has been an important parameter to check the cooling rate of the refrigeration system. Less cooling time is considered as a desirable characteristic, and in the present experimental work; cooling speed has been measured by noting the time taken to bring down the evaporator temperature from 40 to 25 °C with testing outer conditions of 30 ± 2 °C. It has been found that cooling speed increases directly with the addition of nanoparticles in base refrigerant till 0.5 g of CuO nanoparticles concentration as depicted in Fig. 5. While pure refrigerant took 60 min to bring the cooling from 40 to 25 °C, whereas CuO nanoparticles-based nanorefrigerants took the same temperature drop in 41 min, and SiO_2-based nanorefrigerants have taken 57.5 min to observe the same temperature drop. So to achieve the same temperature, CuO is considered a better nanoparticle than silica nanoparticles due to better thermal conductivity.

Cooling speed chart of Pure refrigerant & Nano refrigerants (R134a + CuO/Silica nanoparticles)
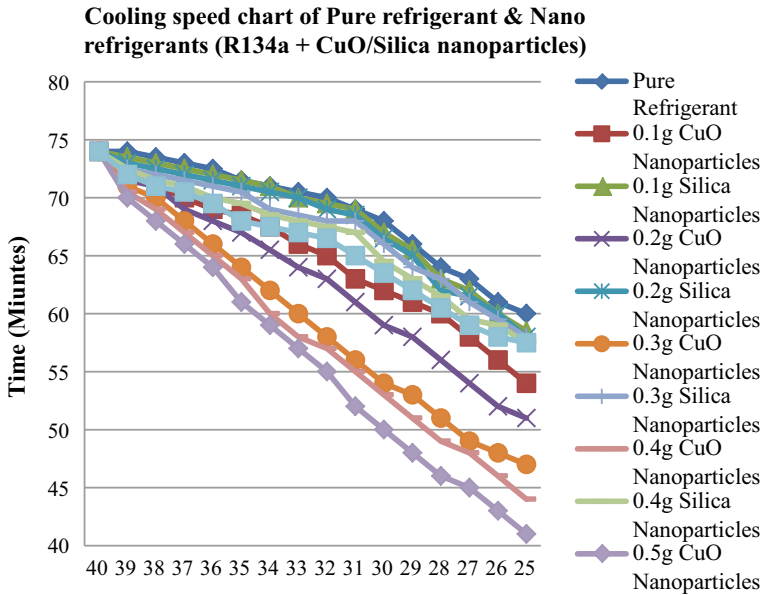
Fig. 5 Cooling speed of pure refrigerant (R134a) and nanorefrigerants (CuO/SiO$_2$ nanoparticles) between time and temperature

4 Conclusions

The present experimental work titled "comparative performance analysis of R134a/CuO and R134a/SiO$_2$ nanorefrigerant-based vapor compression system" was done, to use check the effect of copper oxide nanoparticles and silica nanoparticles with R134a refrigerant. The CuO/SiO$_2$ nanoparticles of 0–40 nm size have been used. To analyze the performance, different combinations of nanoparticles by varying concentrations were mixed with R134a refrigerant.

(i) Overall, a maximum of 15% of cooling speed has improved with R134a + Silica at 0.5 g, while almost 32% of improvement in cooling speed has been found with R134a + CuO at 0.5 g.

(ii) Overall, a maximum of 8% of COP enhancement has been observed with R134a + Silica at 0.5 g, while almost 32% of improvement has been found with R134a + CuO at 0.5 g.

(iii) There is around 9.3% of power consumption has been saved with R134a + Silica at 0.5 g, while almost 20.3% of power consumption reduction has been found with R134a + CuO at 0.5 g.

References

1. Akhavan-Behabadi, M.A., Sadoughi, M.K., Darzi, M., et al.: Experimental study on heat transfer characteristics of R600a/POE/CuO nano-refrigerant flow condensation. Exp. Therm. Fluid Sci. **66**, 46–52 (2015)
2. Alawi, O.A., Sidik, N.A.C.: The effect of temperature and particles concentration on the determination of thermo and physical properties of SWCNT-nano-refrigerant. Int. Commun. Heat Mass Transf. **67**, 8–13 (2015)
3. Alawi, O.A., Sidik, N.A.C.: Influence of particle concentration and temperature on the thermophysical properties of CuO/R134a nano-refrigerant. Int. Commun. Heat Mass Transf. **58**, 79–84 (2014)
4. Zawawi, N.N.M., Sharif, M.Z., et al.: Thermo-physical properties of Al_2O_3–SiO_2/PAG composite nanolubricant for refrigeration system. Int. J. Refrig. **80**, 1–10 (2017)
5. Pinto, R.V., Fiorelli, F.A.S.: Review of the mechanisms responsible for heat transfer enhancement using nanofluids. Appl. Therm. Eng. **108**, 720–739 (2016)
6. Azmi, W.H., Sharif, M.Z., et al.: Potential of nanorefrigerant and nanolubricant on energy saving in refrigeration system—a review. Renew. Sustain. Energy Rev. **69**, 415–428 (2017)
7. Yang, L., Jiang, W., et al.: Dynamic characteristics of an environment-friendly refrigerant: ammonia-water based TiO_2 nanofluids. Int. J. Refrig. **82**, 366–380 (2017)
8. Manoj Babu, A., Nallusamy, S., Rajan, K.: Experimental analysis on vapour compression refrigeration system using nanolubricant with HFC-134a refrigerant. Nano Hybrids **9**, 2234–9871 (2015)
9. Javadi, F.S., Saidur, R.: Thermodynamic and energy efficiency analysis of a domestic refrigerator using Al_2O_3 nano-refrigerant. Sustainability **13**, 5659 (2021)
10. Redhwan, A.A.M., Azmi, W.H., Sharif, M.Z., Mamat, R., Zawawi, N.N.M.: Comparative study of thermo-physical properties of SiO_2 and Al_2O_3 nanoparticles dispersed in PAG lubricant. Appl. Therm. Eng. **116**, 823–832 (2017)
11. Kundan, L., Singh, K.: Improved performance of a nanorefrigerant-based vapor compression refrigeration system: a new alternative. Proc. Inst. Mech. Eng. Part A J. Power Energy **0**(0), 1–18 (2020)
12. Kedzierski, M.A., Kaul, M P.: Horizontal nucleate flow boiling heat transfer coefficient measurements and visual observations for R12, R134a, and R134a/ester lubricant mixtures. In: Proceedings of the 6th International Symposium on Transport Phenomena in Thermal Engineering, vol. 1, pp. 111–116 (1993)
13. Peng, H., Ding, G., Jiang, W., Hu Hand Gao, Y.: Heat transfer characteristics of refrigerant-based nanofluid flow boiling inside a horizontal smooth tube. Int. J. Refri. **32**, 1259–1270 (2009)
14. Bi, S.S., Shi Land Zhang, L.L.: Application of nanoparticles in domestic refrigerators. Appl. Therm. Eng. **28**, 1834–1843 (2008)
15. Yang, L., Du, K.: An optimizing method for preparing natural refrigerant: ammonia-water nano fluids. Int. J. **147**(1), 24–33 (2013)
16. Xing, M., Wang, R., Yu, J.: Application of fullerene C_{60} nano-oil for performance enhancement of domestic refrigerator compressors. Int. J. Refrig. **40**, 398–403 (2014)
17. Huminic, A., Huminic, G., Fleece, C., Dumitrache, F., Morjan, I.: Thermal conductivity, viscosity, and surface tension of nanofluids based on FeC nanoparticles. Powder Technol. **284**, 78–84 (2015)
18. Sendil Kumar, D., Elansezhian, R.: Experimental study on Al_2O_3-R134a nano refrigerant in the refrigeration system. Int. J. Mod. Eng. Res. **2**(5), 3927–3929 (2012)

An Experimental Study on Plaster of Paris Composite Reinforced with Multi-form Rice Husk for Thermal Insulation

Gurdyal Singh (ORCID)**, Prabhjot Singh, Anoop Aggarwal, Sunil Kumar, and Gaurav Jain**

1 Introduction

Thermal insulation is ability of any material or medium to prevent the passage of heat energy through it. It may be required to contain the heat within a particular system to prevent its escape or to act as a barrier from surrounding environment to create a comfort zone. Thermal insulation is measured in form of thermal conductivity, which denotes the ease with which, heat energy can flow through a material or system by conduction principle. Hence, the determination of thermal conductivity will help in analyzing insulation effectiveness of any part or material and its further use as an insulator.

Conventionally, inorganic materials such as asbestos-sheet, fiber-glass, rock-wool, mineral-wool, are used as an insulating material in various applications. The production route of these materials is generally associated with excessive energy consumption and the subsequent disposal can cause the environmental pollution [1]. Additionally, their use has shown undesirable effect on human health too [2]. The minute size fiber-glass and glass-wool particles are skin-irritant and can cause respiratory problems upon direct exposure [3]. Most inorganic materials contain formaldehyde resin that can cause asthma [4]. Cellulose insulators have boric-acid to inculcate fire-retarding properties, but on the other hand, it has shown toxicity effect on human health [3]. Since the currently used insulation materials have shown adverse effects on human health along with expenditure occurred on their production until their after-life disposal, the quest to explore eco-friendly materials with better insulating properties is today's demand. An ideal insulation material must have low thermal conductivity, fire resistance, low moisture absorbance and ease in production in

G. Singh · P. Singh (✉) · A. Aggarwal · S. Kumar · G. Jain
Chitkara University Institute of Engineering and Technology, Chitkara University, Rajpura, Punjab, India
e-mail: prabhjotsinghbawa23@gmail.com

407

addition to being harmless for human as well as environment. Hence, the alternative materials with comparable or superior properties need to be investigated to offer viable replacement.

A lot of attention has been given by the researchers for the development of green composites by using different agro-based wastes along with conventional matrix and reinforcement materials. Agro wastes such as rice husk, corn-cob, rice-straw, wheat-straw sugarcane-stalks, coconut-husk, palm-shell, palm-leaves and straw from cereal crops are rich in fibrous content due to lingo-celluloses and can be suitably used as reinforcements in manufacturing of composite materials for insulation [5]. These bio-composites consumes comparatively less energy for their production, de-grade naturally upon disposal and can be termed as green materials [6]. For the agriculture based country like India, abundant source of agro-wastes is available directly from fields or agro-processing units at cheap price. This will not only help in generating revenues for farmers, but also help in tackling safe disposal of agro by-product, which otherwise is considered as burden and burnt in the fields, causing pollution.

This paper reports the potential of RH (agro-waste) as insulating material. It is produced as a by-product from rice processing and is available in abundance in rice producing regions in India. Conventionally, RH has been used by rice mills as energy source in boilers as well as in some cases in making concrete blocks, bricks for construction work [7, 8]. Despite it, the quantity of RH production is in excess then its economic utilization at local level and thus creating dumping problems. Researchers have been exploring various ways to utilize RH, which will not only beneficial from economic point of view, but also will provide a safe and environment-friendly way for its disposal. Muthuraj et al. [5] fabricated bio-composites comprising RH, textile waste fibers, wheat husk and wood fibers. The evaluation of thermal and mechanical properties of it displayed promising results. Among these, Sutas et al. [7] explored use of RH as fiber and as an ash form for making bricks and found reduction in density as well as in compressive strength of specimens due to porosity after RH inclusion. The inclusion of RH ash reinforced with different volume proportions (10, 20, 30, 40, 50%) in POP matrix were investigated by Ochang et al. [9] and found reduction in thermal conductivity, diffusivity and density with increase in ash content, whereas specific heat capacity and thermal resistance increased with ash content. Alaneme et al. [10] used RH ash as a reinforcing element along with alumina in making Al–Mg–Si hybrid composites and reported increase in friction as well as wear-rate of the composites with the increase of RH ash proportions. Kishore et al. [11] mixed the RH ash with cement and investigated the mechanical properties of resultant concrete mixture. Masoud et al. [12] employed RH for treatment of drain water and found excellent results in removing iron and manganese. These studies established that the use of RH in various forms has great potential. Its use as an insulating material will not only reduce the insulation cost, but also assists in converting discarded item into a beneficial product, leading toward a healthier environment. The novelty of presented work is in terms of testing of different particle forms of RH as insulating material as well as eco-friendly solution to its disposal problem. The authors have not found any related work in open literature regarding inclusion of RH as fiber, powder and fly ash form into POP matrix and their effects on the insulation capability of

resultant composite. Hence, present paper will help in exploring the beneficial use of Rice Husk as bio-degradable reinforcement in promoting manufacturing of green composites.

2 Experimental Details

2.1 Materials

The materials consist of RH as reinforcement and POP as matrix material to fabricate composite specimens. RH was incorporated in three different form as Rice Husk Fiber (RH-F), Rice Husk Grinded (RH-G) and Rice Husk Ash (RH-A). RH as raw material mainly comprises 75–90% organic matter in form of cellulose, lignin, etc. with silica, alkalis and other trace elements as mineral components [13]. The raw RH fiber was grinded and then sieved with 300 µm sieve to obtain RH-G. The RH-A with mesh size under 50 µm was prepared from complete burning of the RH, followed with thermal processing and sieving as per the procedure mentioned in the references [14, 15]. POP, chemically known as calcium sulfate hemihydrate ($CaSO_4 \cdot 2H_2O$) and is generally available in form of while powder with fine particle size. POP is prepared by heating gypsum or calcium sulfate dehydrate in temperature range of 120–180 °C. and possessed 0.1185 W/mK of thermal conductivity and 8.4388 mK/W of thermal resistivity [16].

2.2 Sample Preparations

Samples were prepared in form of board or slabs by manual mixing the reinforcement with POP powder followed with hand lay-up technique.

The size of each sample board was 400 mm × 400 mm × 10 mm and final weight was controlled as 2000 g. Figure 1 shows the sample preparation and finally prepared specimen boards. The RH was mixed into POP matrix in three different forms with varying proportions. The samples nomenclature along with mixing proportions have been listed in Table 1.

2.3 Experimental Set-Up

An experimental set-up was prepared to measure the thermal conductivity by measuring the temperature across the sample board. The schematic and actual experimental set-up is shown in Fig. 2a, b, respectively. The set-up consists of two boxes to confine the heat within enclosed space and to avoid the heat energy loss to the
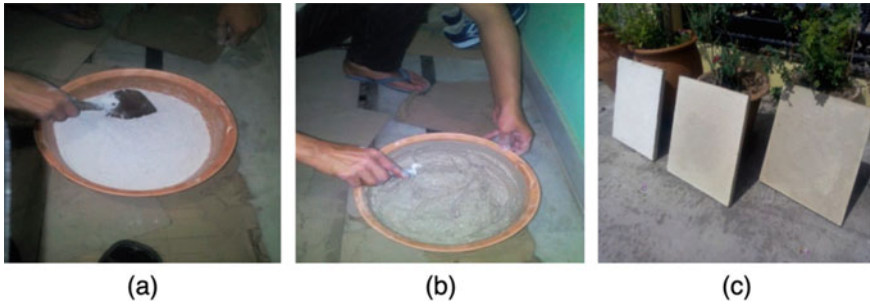
Fig. 1 **a** POP powder, **b** RH mixing and **c** prepared samples

Table 1 Sample designation as reinforcement type and percentage

Reinforcement type	Sample designation	RH concentration (wt%)	RH weight (g)	POP weight (g)
Pure-POP	POP-0	0	0	2000
Rice husk fiber (RH-F)	RH-F1	1	20	1980
	RH-F3	3	60	1940
	RH-F5	5	100	1900
Rice husk grinded (RH-G)	RH-G1	1	20	1980
	RH-G3	3	60	1940
	RH-G5	5	100	1900
Rice husk ash (RH-A)	RH-A1	1	20	1980
	RH-A3	3	60	1940
	RH-A5	5	100	1900

surroundings. The sample boards were placed in between the open-end of two boxes to expose them to heating. A heating coil with a capacity of 1000 W was placed in one of the boxes. Two thermocouples (*K*-type) were placed in each box, at a distance of 10 mm from the sample board to measure the temperature T_1 on heat source side and T_2 on other side of sample. The thermocouples were connected to the control panel with digital temperature display. Both the temperatures were recorded at start of experiment ($t_1 = 0$ min) and after set duration ($t_2 = 45$ min) for each of the sample. This difference of temperature over the given duration was further used to measure thermal conductivity.

2.4 Thermal Conductivity Evaluation

Fourier's Law of heat conduction was used to measure the thermal conductivity of the fabricated specimens. It states that the rate of heat transfer through a material
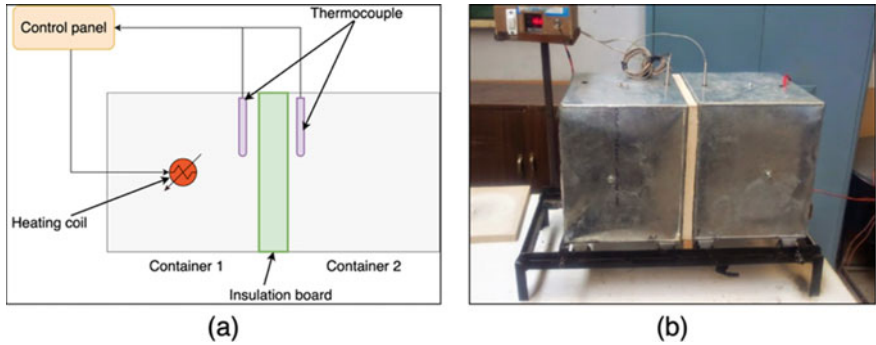
Fig. 2 **a** Schematic of experimentation. **b** Experimental set-up

is proportional to the section area at right angles to the heat flow direction, and to the temperature-gradient across heat flow path. The relationship for one-dimensional heat conduction in steady-flow is given in Eq. (1):

$$Q = -kA\frac{dT}{dx} \tag{1}$$

where Q is heat transfer rate in watts, A is the area of heat transfer surface in m^2, k is the thermal conductivity of material in Watt/meter Kelvin, dT is the temperature differences in between two boxes in Kelvins and dx is the thickness of insulating boards in meter.

2.5 Strength Evaluation

The strength to the prepared samples to withstand the loads was carried out by subjecting the samples to static transverse weights. The applied weights were started with load of 20 kg and were increased gradually in step of 1 kg until visible cracks appear on the surface of the samples.

3 Results and Discussion

The recorded value of temperatures by thermocouples on both sides of samples at over the set time duration is listed in Table 2 along with the calculated values of thermal conductivity. The graphical interpretation of calculated thermal conductivity is presented in Fig. 3.

As we are aware that lower the thermal conductivity of the material, better is its thermal insulation capability. It is evident from the results listed in Table 2 and also

Table 2 Experiment readings for temperature and calculated thermal conductivity for samples

Reinforcement type	Sample designation	Reading time = 0 min (initial)		Reading time = 45 min (final)		Thermal conductivity, k (W/mK)
		T_1 (°C)	T_2 (°C)	T_1 (°C)	T_2 (°C)	
Pure-POP	POP-0	35	35	426	97	0.103652
RH-F	RH-F1	35	35	426	97	0.103794
	RH-F3	38	38	443	85	0.099025
	RH-F5	38	38	432	95	0.102433
RH-G	RH-G1	35	35	425	86	0.097324
	RH-G3	38	38	442	74	**0.091023**
	RH-G5	38	38	432	79	0.096692
RH-A	RH-A1	37	37	426	97	0.102892
	RH-A3	37	37	443	85	0.101987
	RH-A5	36	36	432	95	0.099553
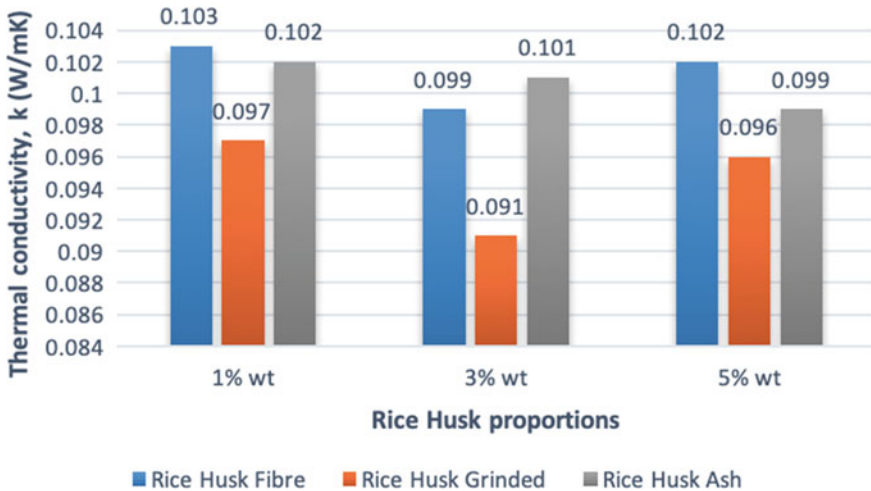
Fig. 3 Comparison of thermal conductivity for different Rice Husk types

depicted from Fig. 3 that incorporation of RH in different forms have different effect on thermal conductivity of the samples. Among the proportions, addition of 1 wt% of RH in fiber and ash form (RH-F and RH-A samples respectively) barely had any influence on thermal conductivity in comparison with the control sample (POP-0), whereas grinded form had shown some effect in terms of reduction in thermal conductivity. As concentration of RH content was increased to 3 wt%, better insulation was observed with grinded form sample (RH-G3) shown least thermal conductivity of 0.091023 W/mK followed with ash form (RH-A3) and fiber form (RH-F3). The use of 5 wt% proportions had shown further increase in thermal conductivity or reduction

in insulation for all the three forms. Among the different forms of reinforcement, grinded form (RH-G) has provided maximum potential as heat insulating reinforcement, followed with ash form (RH-A). The order of effectiveness in terms of thermal insulation as shown in Fig. 3 can be listed as RH-G > RH-A > RH-F. The superior insulation exhibited by RH-G samples may be due to reason that rice husk in grinded form consist of fine particles, that blend well with POP matrix, resulted into compact and denser structure, which provided resistance to heat conduction. Inclusion of RH as fiber form (RH-F) caused the porosity in structure with pores acted as micro-channels for heat flow, leads to poor thermal insulation. The insulation ability of RH in ash form (RH-A) lied in between of two reinforcements forms. Thus, RH-G3 with 3 wt% proportions proved to be optimal concentration in terms of thermal insulation capabilities. Further, it was observed from the results that the thermal conductivity value of all RH reinforced samples are comparable to the corresponding values of commercially available inorganic insulating materials [13]. But contrary to the side-effects associated with inorganic insulators, the use of these green composites may result in reduced insulation costs as well as cleaner environment.

The strength evaluation results for different samples are shown in Table 3. It is evident from the results that the RH in fiber form (RH-F) has least strength for different proportions due to porous structure caused by bigger size fiber particles. The strength provided by RH grinded form samples (RH-G) was better than fiber form (RH-F) samples, but lower than ash form (RH-A) samples. The reinforcement of RH in ash form (RH-A) has shown superior strength in terms of better load carrying capacity before rupture, with RH-A3 having 3 wt% of ash content showed the ability to sustain 44 kg before visible cracks appeared on surface. It may be due to better dispersion and filler-effect between ash and POP molecules [17].

Table 3 Strength evaluation samples in terms weight sustained

Reinforcement type	Sample designation	Weight sustained (kg)
Pure-POP	POP-0	35
RH-F	RH-F1	34
	RH-F3	32
	RH-F5	30
RH-G	RH-G1	37
	RH-G3	40
	RH-G5	41
RH-A	RH-A1	38
	RH-A3	**44**
	RH-A5	42

4 Conclusions

The potential of RH as an insulating material was explored by combining it as fiber, grinded and ash form into POP matrix. Their effect on thermal conductivity as well as strength was analyzed and compared. The experimental results showed that all the three forms of RH offered good insulation by restricting the heat conduction through composite material, wherein RH in grinded form (RH-G) offered least thermal conductivity or better thermal insulation, followed with RH in ash form (RH-A) and then RH fiber (RH-F). Among the three tested proportions of wt% inclusion, RH-G3 with 3 wt% proved to be optimal content which offered least thermal conductivity of 0.091023 W/mK. The strength evaluation of reinforced samples against transverse loading revealed that inclusion of ash form (RH-G) formulated better bonding with POP matrix resulting into increased strength as compared grinded form (RH-G) or fiber form (RH-F). These findings established the capability of RH to provide the insulation and strength comparable with existing inorganic industrial insulators. It will further support their utilization in manufacturing of sustainable green composites to offer a viable replacement for interior thermal insulation.

References

1. Panyakaew, S., Fotios, S.: Agricultural waste materials as thermal insulation for dwellings in Thailand: preliminary results. In: PLEA 2008—Towards Zero Energy Building: 25th PLEA International Conference on Passive and Low Energy Architecture, Conference Proceedings. Dublin, pp. 1–6 (2008)
2. Liang, H.H., Ho, M.C.: Toxicity characteristics of commercially manufactured insulation materials for building applications in Taiwan. Constr. Build. Mater. **21**(6), 1254–1261 (2007)
3. Synthetic Mineral Fibers, Occupational Safety and Health Administration (OSHA). https://www.osha.gov/synthetic-mineral-fibers/health-effects. Last accessed 15 Nov 2021
4. Myers, G.E., Nagaoka, M.: Environmental Protection Agency. EPA Hazard Summary: Formaldehyde. https://www.epa.gov/sites/production/files/2016-09/documents/formaldehyde.pdf. Last accessed 15 Nov 2021
5. Muthuraj, R., Lacoste, C., Lacroix, P., et al.: Sustainable thermal insulation biocomposites from rice husk, wheat husk, wood fibers and textile waste fibers: elaboration and performances evaluation. Ind. Crops Prod. **135**(4), 238–245 (2019)
6. Manohar, K.: Renewable building thermal insulation-oil palm fibre. Eng. Technol. **2**(3), 475–479 (2012)
7. Sutas, J., Mana, A., Pitak, L.: Effect of rice husk and rice husk ash to properties of bricks. Proc. Eng. **32**, 1061–1067 (2012)
8. Ahiduzzaman, M., Islam, A.K.M.S.: Development of biomass stove for heating up die barrel of rice husk briquette machine. Proc. Eng. **56**, 777–781 (2013)
9. Ochang, M.B., Jubu, P.R., Amah, A.N., Oche, J.L.: Investigation of thermal properties of fabricated plaster of Paris-rice husk ash composite with varying matrix-filler volume fractions for thermal insulation applications. Am. J. Eng. Res. **7**, 215–222 (2018)
10. Kanayo Alaneme, K., Apata Olubambi, P.: Corrosion and wear behaviour of rice husk ash-Alumina reinforced Al–Mg–Si alloy matrix hybrid composites. J. Market. Res. **2**(2), 188–194 (2013)
11. Kishore, R., Bhikshma, V., Jeevana Prakash, P.: Study on strength characteristics of high strength rice husk ash concrete. Proc. Eng. **14**, 2666–2672 (2011)

12. Masoud, M.S., El-Saraf, W.M., Abdel-Halim, A.M., et al.: Rice husk and activated carbon for waste water treatment of El-Mex Bay. Alexandria Coast, Egypt. Arab. J. Chem. **9**, S1590–1596 (2016)
13. Jindal, H., Singh, P., Bansal, H.: Evaluation of thermal conductivity of insulations prepared from mixture of rice husk and plaster of Paris. J. Basic Appl. Eng. Res. **2**(16), 1381–1384 (2015)
14. Alaneme, K.K., Adewale, T.M., Olubambi, P.A.: Corrosion and wear behaviour of Al–Mg–Si alloy matrix hybrid composites reinforced with rice husk ash and silicon carbide. J. Market. Res. **3**(1), 9–16 (2014)
15. Alaneme, K.K., Akintunde, I.B., Olubambi, P.A., et al.: Fabrication characteristics and mechanical behaviour of rice husk ash—alumina reinforced Al–Mg–Si alloy matrix hybrid composites. J. Market. Res. **2**(1), 60–67 (2013)
16. Newton, F., Roy, A.A., Solomon, I.: Investigation of the thermal insulation properties of selected ceiling materials used in Makurdi Metropolis (Benue State-Nigeria). Am. J. Eng. Res. (AJER) **03**(11), 245–250 (2014)
17. Rukzon, S., Chindaprasirt, P., Mahachai, R.: Effect of grinding on chemical and physical properties of rice husk ash. Int. J. Miner. Metall. Mater. **16**(2), 242–247 (2009)

An Analysis of the Behavior of Peepal Fiber Reinforced Polyester Composites for Tensile, Flexural and Impact Strengths

Obulasu Tapela, G. Dilli Babu, and Ginka Ranga Janardhana

1 Introduction

In recent years the polymer composite material has been playing a dominant role in many engineering applications like Aerospace, Automobiles, Food Packing, electronic cabinets, etc. Therefore, lot of interest is being taken by manufacturing industries, scientists, and researchers in the development of natural-based materials to meet the requirements of disposal, clean environment, green engineering, and various other aspects of sustainability [1, 2]. Usually, synthetic polymer products produce adverse effects during the end of its life [3, 4]. There are so many polymers-based products available in our daily life as utilities. Disposal of these polymer-based products is a severe concern toward our environment.

On the other hand, fiber reinforced polymer composites have some specific characteristics like low density, higher stiffness-weight ratio, etc. Polyester is a polymer-based material widely being used as fibers, composites, plastics, and in coating applications, etc. [5]. Researchers have tried to improve the properties of Polyester with different reinforcements. Some of those reinforcements are, polyester and sisal and glass fiber [6], polyester and Alfa fiber [7], polyester and coconut shell and Palm fruit particles [8], polyester and Nano-based graphene oxide and graphite [9].

In recent decades most research works have been carried out on natural fiber and polymer-based composites due to the low cost of production as compared with synthetic fibers [10]. But, in recent year's researchers are showing more interest

O. Tapela
J N T U University Kakinada, Kakinada, Andhra Pradesh 533003, India

G. Dilli Babu (✉)
Department of Mechanical Engineering, VRSEC, Vijayawada, Andhra Pradesh 520007, India
e-mail: gdillibabu@gmail.com

G. Ranga Janardhana
J N T U University Anantapur, Anantapur, Andhra Pradesh 515002, India

in natural-based fiber combination for the polyester reinforcement [11–13], due to the green engineering requirements. Moreover, nature has abundant raw source of natural fibers like coir, bamboo, banana, sisal, etc.

Peepal is a natural material [14] that has been used in different applications such as, biomedical, pharmacy, [15]. Furthermore, few researchers have made an attempt to enforce the material with peepal fibers [16]. Unfortunately, Knowledge related to peepal fiber reinforcement to a polyester matrix remains blank in the literature. The current study is to understand the behavior of peepal fiber reinforcement to a polyester matrix in terms of mechanical properties such as tensile, flexural, and impact strengths. In this regard, peepal fiber reinforced polyester composite samples have been prepared with different fiber fractions. Then, the samples are tested for tensile, flexural, and impact strengths. The subsequent part of this article discussed the procedure of the sample preparation, the materials used and the testing methods applied in detail.

In recent decades most of the researchers, industrialists, and scientists are striving to accommodate the polymer products in terms of thermoplastic and thermoset polymer for most of the engineering applications due to the strength to weight requirements, thermal insulation, cost concern, etc. Numerous research works have been carried out to improve the mechanical performance of the polymer products. The literature reveals that different materials such as synthetic fibers, natural fibers, nano materials are used as a reinforcing element to the polymers to enhance the mechanical, thermal, and tribological properties. Daniel et al. [17] have discussed the more information related to syntactic polymers and composites in his book regarding; Phases of composite, the significance of thermoset and thermoplastic, macro mechanics, micromechanics, and mechanical characterization. Since the present research work is on natural fiber reinforcement to a polyester matrix, the discussion will be focused on different natural fiber's reinforcement to the polyester matrix in terms of the mechanical properties. Durowaye et al. [8] have fabricated the composite samples of natural coconut shell reinforced polyester and Palm fruit particles reinforced polyester matrix. The polyester strength is improving with the palm fruit particles reinforcement in terms of tensile and impact up to the 20% fiber fraction. Also, found some improvement of the polyester matrix on the addition of coconut shell particles for lower fiber fractions. Brahim and Cheikh [7] have evaluated the tensile properties of Alfa fiber reinforced polyester composites based on the fiber fraction. The experiment results concluded that the Alfa fibers play a major role in the polyester matrix to improve the tensile strength, and also the stiffness of the composite. Prasad and Rao [18] worked on rice straw reinforced polyester composites. The samples are investigated for the tensile, impact properties. The polyester strength is improving with the rice straw reinforcement in terms of tensile and impact for the fiber fraction of more than 20% volume fraction. Prasad et al. [19] have presented the mechanical performance of banana empty fruit bunch fiber reinforced polyester composites. The experiment results reviled that the tensile and impact properties were increased for higher fiber fractions, which are greater than 20% of the volume fraction. Also, concluded

that the low-density banana (EFB) fiber can be used, is tough and lightweight engineering applications. Ahlawat et al. [20] have investigated the mechanical performance and tribological properties of walnut shell powder doped polyester composites and found higher wear resistance and coefficient of friction for all doped polyester composites compared to a pure polyester. Concluded this by saying that all favorable factors gained by the walnut shell powder can be a potential filler, where the frictional properties are greatest desirable. Example, the research article presented by Marian et al. [21] have investigated the influence of Graphene Oxide and Graphite filled Polyester composites based on varying weight proportions of nanofillers. The experimental results concluded that the both additives are value added in, improved glass transition temperature and decreased coefficient of linear thermal expansion, but greatest influence was obtained with the graphene Oxide polyester composite compared to graphite polyester composite.

It was found in the literature that the usage of natural fiber is of two kinds; one is as direct substitution and another one as chemically modified. The literature reveals that usage of chemically treated or modified fibers gives better strengths compared to the untreated fibers. The present paper focus is on alkali-treated fibers, i.e., chemically modified fibers with a NaOH solution. Because the NaOH solution is used for alkali treatment in many research articles. For example, Benyahia et al. [22] have compared the sodium hydroxide (1, 3, 5 and, 7 wt%) alkali-treated Alfa reinforced polyester composites with untreated Alfa fibers to analyze the properties in terms of tensile, flexural strengths, and concluded the increased performance in terms of the mechanical properties after the treatment. Negawo et al. [23] have compared the NaOH treated Ensete stem fibers for various fiber fractions (2.5, 5.0, and 7.5% by weight) and found the improved properties in terms of mechanical, morphologica, l and dynamic-mechanical analysis. Akhtar et al. [24] have used the NaOH at 6 wt% concentration for the kenaf (Hibiscus cannabinus) fibers reinforced polypropylene composites with 10, 20, 30, 40, 50 wt% fiber fraction to suite for different applications such as automotive, sports equipments, and other engineering purpose in terms of physical and mechanical properties. After performing the tests, it was concluded that 40 wt% treated fiber into polypropylene composites exhibited higher mechanical performance. Researchers proved that the alkali treatment is also a function of time. For example, Rokbi et al. [25] have reported the effect sodium hydroxide treated Alfa fiber reinforced in a polyester matrix at varying weight percentages (1, 5, 10 wt% of NaOH) over different timings (0, 24, and 48 h) changes the flexural strength.

Apart from the NaOH solution, usage of some other chemical treatment methods also improves the quality of the fiber surface modification for better interaction with the polymer matrix and this has been demonstrated by some research articles. For example, Sreekumar et al. [26] have presented the various chemical solutions (mercerization, permanganate treatment, benzoylation, and silanization) to treat the sisal fibers to reinforce in a polyester matrix to enhance mechanical properties, water absorption capacity, and improve fiber-matrix interfacial bonding.

Chaudhary et al. [27] have characterized the natural (Jute, Hemp, and Flax) fiber reinforced epoxy composites respectively and their hybridization followed by Hand Lay-up method for the tensile, flexural, impact, and hardness properties as well as an

interfacial bond adhesion. Srinivas and Dilli Babu [28] have presented the fabrication of calotropis gigantean fruit fiber reinforced polyester composites followed by Hand Lay-up method to evaluate the mechanical and machining properties. The scientific name of the peepal is Ficus Religiosa [14]. Its bark looks as light gray, Moreover, can be peeled off easily. Prasad et al. [29] have made a new composite by peepal, banyan and Copper foil fiber reinforced epoxy matrix composite followed by Hand lay-up method on basis of 0°, 45°, and 90° orientation to evaluate hardness and flexural properties and found some improvement in the mechanical properties.

The overall conclusions on the hand literature are that peepal fiber reinforced polyester composites is a unique combination, there is a possibility of improving the polyester properties through peepal fiber reinforcement. Since peepal is a natural fiber and commonly available, the peepal fiber reinforcement to polyester can meet the requirements of green engineering and sustainability. The objective of present work is to fabricate the peepal fiber reinforced polyester composites by using Hand lay-up method and to evaluate the mechanical performance in terms of tensile, flexural, and impact strength.

2 Experimental Procedure

2.1 Materials

Materials used to make the peepal fiber reinforced polyester composite are; Peepal fibers and Polyester resin as the base material along with the MEKP Accelerator and cobalt naphthenate catalyst, NaOH and distilled water for fiber treatment and Rubber sole material for molding purpose.

The peepal tree and its nativity, characteristic and fiber extraction have been discussed in the literature review. Polyester is a synthetic polymer, belongs to the thermoset group. Here, Methyl ethyl ketone peroxide (MEKP) has been used as a curing agent, which is a catalyst as well cobalt naphthenate is used as an accelerator [28]. Moreover, Sodium hydroxide (NaOH) and distilled water have been used for the treatment and washing of fibers, respectively.

2.2 Methodology

The test sample of peepal fiber reinforced polyester composite has been prepared by using Hand lay-up method discussed by Srinivas and Dilli Babu [28]. The sample preparation or fabrication part is divided into two parts—one is fiber treatment (i.e., Alkali treatment) and other is composite molding (i.e., fabrication part). Fibers can be purchased from some potential suppliers. These purchased fibers are cleaned and chemically treated with a NaOH solution during the fiber treatment. Initially, the

Fig. 1 Soaking of Peepal fibers in NaOH solution and Verifying the PH value

purchased peepal fibers must be combed and rubbed gently to remove dust particles. Then the fibers were placed in sunlight for a few hours. When fibers get dried, they must be treated with a NaOH solution. 5% by weight of the NaOH was added to the water to make the NaOH solution. After stirring, the NaOH particles get dissolved into the water properly. The dried fibers are dipped into NaOH solution for three hours (i.e., soaking Fig. 1) then washing was done with distilled water to eliminate impurities. To this concern, the fibers were cleaned to such level that pH value was maintained to 7 (Fig. 1). Then the cleaned fibers were dried in the sunlight on a hot summer day.

2.3 Fabrication of Specimens

The composite sample preparation (i.e., fabrication part) is carried out by using the Hand lay-up technique. Here, peepal fiber is reinforcement in the polyester matrix. The accelerator and the catalyst are used as reactive agents for good adhesive bonding between the peepal fiber and polyester matrix. The Hand lay-up technique is one of the simplest methods compared with the other manufacturing methods, in terms of tooling and cost. Molds are prepared according to the sample sizes. The sample sizes are taken according to the ASTM D 638M for tensile, ASTM D790M-86 for flexural, and ASTM D256-97 for impact samples.

Petroleum jelly is applied on the mold surface to avoid the sticking of the polymer matrix to the edge surface. One milliliter of each accelerator and catalyst is thoroughly mixed into the polyester resin before it is poured into the mold cavity (Fig. 2). Before filling the polyester resin into the mold, the weight fraction of fiber must be calculated based on the mold cavity size. After pouring the polyester resin into the mold cavity, the hand roller was used to spread uniformly into the mold cavity. The process was repeated for each layer of fiber until the required thickness is attained. 0.5 KN load is applied on the tile plate and kept for 24 h for curing at the room temperature. After the curing time, the mold is opened and composite samples are taken out. Finally, the grinding process is done to ensure the standard dimensions. Grinding of specimens and a set of finished samples were shown in Fig. 2.

Fig. 2 Pouring of polyester solution into the mold cavity, grinding of samples and final test samples of the composites

3 Results and Discussion

The molded samples are tested for tensile, flexural, and impact strengths. Figure 3 is showing the image of a set of broken samples during the tensile, flexural, and impact test, respectively.

Table 1 represents the results of the experiment for tensile, flexural and impact strengths of the samples based on the fiber fraction. The properties of pure polyester have been referred from the articles [18, 29]. Figures 4 and 5 shows the behavior of peepal fiber reinforced polymer matrix composite samples for tensile strength and tensile modulus respectively. Figure 3 is evident that the peepal fiber reinforced polymer matrix composite exhibits better tensile strength as a function of fiber fraction loading. This happens, only because the polyester matrix has a better ability to transfer the load stress to the peepal fibers. Thus, the composite samples sustain the maximum external load before failure.

Fig. 3 Fractured test sample specimens

Table 1 Experimental results of tensile, flexural, and impact strengths

Fiber weight fraction	Density (g/cc)	Tensile strength (MPa)	Tensile modulus (GPa)	Specific tensile strength	Flexural strength (MPa)	Flexural modulus (GPa)	Impact strength (KJ/m^2)
0	1.20	31.5	0.63	26.23	55.08	1.71	6.30
10	1.21	67.94	1.96	56.57	–	–	22.05
15	1.26	60.54	1.80	50.41	187.60	6.77	33.07
20	1.24	107.11	1.89	89.18	229.13	11.01	36.22
25	1.30	75.30	2.51	62.70	238.00	8.61	37.80
30	–	116.26	2.19	–	270.20	9.92	62.99
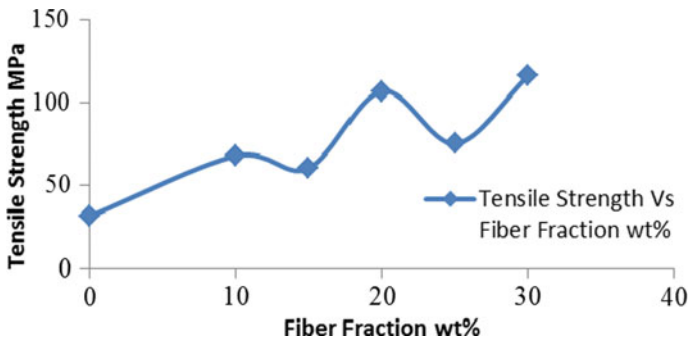
Fig. 4 Tensile strength versus fiber fraction
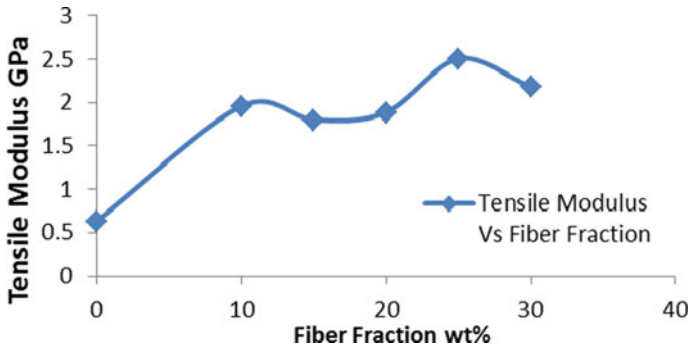
Fig. 5 Tensile modulus versus fiber fraction

In Fig. 4, it is observed that the 30 wt% peepal fiber fraction reinforced polyester composite exhibited the maximum tensile strength (σu) of 116.26 MPa, which is higher, compared to those of the other weight fractions. And, it is also noticed that there is an increment of tensile strength about 72.90% compared with the pure polyester material.

Similarly, the tensile modulus (E) of peepal fiber reinforced polyester composite for 10, 15, 20, 25, and 30% of fiber fraction has been shown in Fig. 5. The results in the figure represent an increasing trend of tensile modulus with respect to the fiber fraction up to 25 wt%, but, there is some slight decline of tensile modulus at the fiber fraction at 30 wt%. The maximum tensile modulus is found as 2.51 GPa at 25 wt% of fiber, which is 74.9% higher as compared to pure polyester matrix. It was observed that there is no fiber pullout during the testing. It is considered a good sign for a good composite, as there is a good interfacial bonding between the fiber and matrix.

Figure 6 shows that the outcome of a specific tensile strength of peepal fiber reinforced polyester composite with respect to the fiber fraction. The experimental results stated that the specific tensile strength of polyester is increased with the peepal fiber fraction loading. Here, at 20 wt% of fiber fraction, the specific tensile strength has attained a maximum of 89.18 MPa/(g/cc). Which is 70.58% higher than pure polyester.

Figures 7 and 8 show the variation of peepal fiber reinforced polyester matrix composite's flexural strength and flexural modulus, respectively. The flexural strength (σ_f) and flexural modulus (E_f) are calculated based on the Eqs. (1) and (2), respectively [29].

$$\text{Flexural strength } \sigma_f = \frac{3PL}{2bt^2} \tag{1}$$

$$\text{Flexural Modulus } E_f = \frac{L^3 m}{4bt^2} \tag{2}$$

where 'P' is maximum applied load, L is the length of the span, 'b' means breadth, 't' is the thickness of the beam and 'm' represents the slope of the load versus deflection curve. Figure 7 gives evidence that there is an effective increment of flexural strength of the peepal fiber reinforced polyester composite for the percentages of 10, 15, 20, 25, and 30 of fiber loading. Moreover, a positive linear trend is seen. The maximum
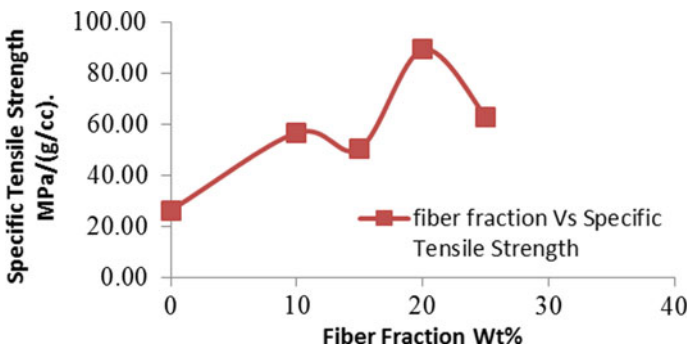
Fig. 6 Fiber fraction versus specific tensile strength
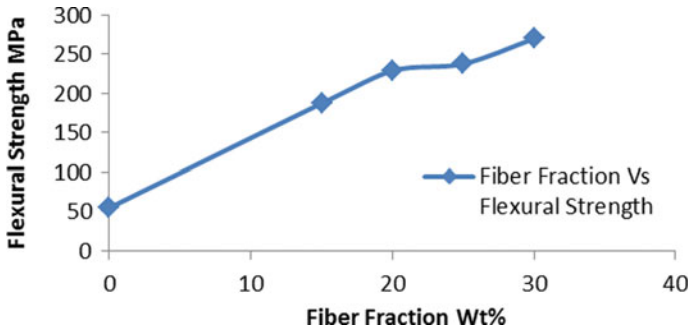
Fig. 7 Flexural strength versus fiber fraction
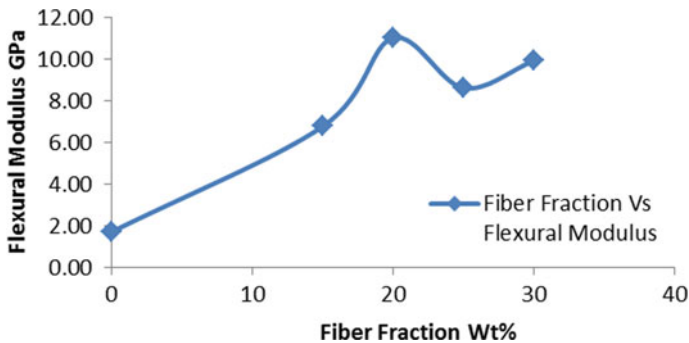
Fig. 8 Flexural modulus versus fiber fraction

flexural strength is found as 270.20 MPa, which is obtained at 30% of fiber loading. In overall, there is 79.61% of increment of flexural strength as compared to a pure polyester's flexural strength. Similarly, the flexural modulus of peepal fiber reinforced polyester composite at the percentages of 15, 20, 25, and 30 fiber weight fraction is shown in Fig. 8. According to the experiment results, the flexural modulus is noticed as incremental behavior. The maximum flexural modulus of 11.01 GPa is attained at 20% of fiber loading. This flexural modulus is 84.46% higher compared to pure polyester.

Figure 9 shows that the variation of impact strength of peepal fiber reinforced polyester matrix composite with respect to the fiber loading at the percentages of 10, 15, 20, 25, and 30. Figure 9 shows that the impact strength of peepal fiber reinforced polyester matrix composite with respect to the fiber fraction. The behavior of impact strength is increasing w.r.t. fiber fraction. The maximum impact strength of 62.99 kJ/m^2 is obtained at 30% weight of peepal fiber fraction polyester matrix composite. This impact strength is 89.99% higher compared to a pure polyester matrix.

Since the experiments are done with the Hand lay-up method, there are some chances of manual defects such as fiber straightness along the sample length and
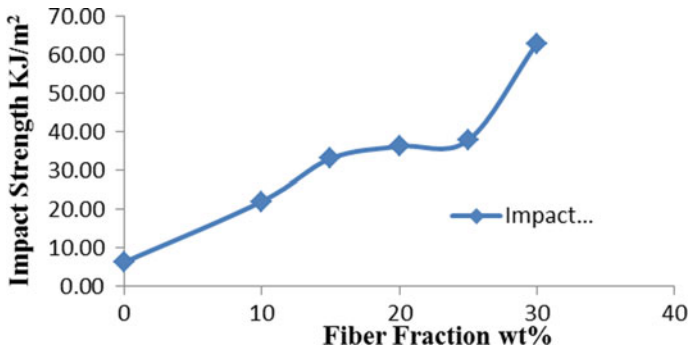
Fig. 9 Impact strength versus fiber fraction

fibers distribution across the sample cross-section and some variation in measuring instruments. The results are presented based on the best efforts and skills of the experimenter. For better results in terms of accuracy, advanced machine tools and DOE techniques (ANOVA) must be implemented. The research work to investigate the behavior of the polyester with the peepal fiber reinforcement and feasibility of peepal fiber addition to a polyester material has attained its objective and the experiment is successful.

4 Conclusions

The present study depicts the effect of alkali-treated peepal fiber reinforced polyester composite in terms of mechanical performance have been studied.

The mechanical properties of peepal fiber reinforced polyester matrix composite in terms of tensile, flexural, and impact are tested. The mechanical strengths increased with respect to the fiber fraction. Fiber fraction loading polyester composites exhibited higher mechanical properties in terms of tensile, flexural, and impact strengths than the pure polyester behavior. Among the all treated peepal fiber weight fractions, the 30 wt% peepal fiber weight fraction loading polyester composite has better performance in tensile, flexural, and impact aspects. The impact strength also observed continuous improvement with increased fiber fraction. It is a good sign that the peepal fiber reinforced polyester composite has the potential capacity to take the sudden higher applied loads. The results with the aid of alkali treatment and fiber fraction are more authentic key factors in improving mechanical performance. By observing the overall results one can understand that the specific strengths in terms of tensile have increased. So that, the peepal fiber is value added potential reinforcement with the thermoset polyester matrix composite.

Finally, all these considerable factors are summarized to tell that the peepal fiber is also a promising material to reinforce the polyester matrix. The addition of 30% of peepal fibers will improve the mechanical properties of the polymer and also

improves the sustainable character. Even though the results are satisfactory in terms of mechanical and environmental aspects, still, there is a need to explore more on peepal fiber reinforcement in the polyester application for a variety of engineering products/ applications individually.

References

1. Liu, L., et al.: Poly(vinyl alcohol)/Chitosan composites: physically transient materials for sustainable and transient bioelectronics. J. Clean. Prod. **195**, 786–795 (2018). https://doi.org/10.1016/j.jclepro.2018.05.216
2. Ramesh, M., Palanikumar, K., Reddy, K.H.: Plant fibre based bio-composites: sustainable and renewable green materials. Renew. Sustain. Energy Rev. **79**, 558–584 (2017). https://doi.org/10.1016/j.rser.2017.05.094
3. Haider, T.P., Völker, C., Kramm, J., Landfester, K., Wurm, F.R.: Plastics of the future? the impact of biodegradable polymers on the environment and on society. Angew. Chem. Int. Ed. **58**(1), 50–62 (2019). https://doi.org/10.1002/anie.201805766
4. Meier, M.: Sustainable polymers: reduced environmental impact, renewable raw materials and catalysis. Green Chem. **16**(4), 1672 (2014). https://doi.org/10.1039/c4gc90006e
5. Polyesters/Vol. 1, Saturated Polymers/I. Goodman and J. A. Rhys. (Book, 1965) [WorldCat.org]. https://www.worldcat.org/title/polyesters-vol-1-saturated-polymers-i-goodman-and-ja-rhys/oclc/769333808. Accessed 08 Mar 2021
6. Mishra, S., et al.: Studies on mechanical performance of biofibre/glass reinforced polyester hybrid composites. Compos. Sci. Technol. **63**(10), 1377–1385 (2003). https://doi.org/10.1016/S0266-3538(03)00084-8
7. Ben Brahim, S., Ben Cheikh, R.: Influence of fibre orientation and volume fraction on the tensile properties of unidirectional Alfa-polyester composite. Compos. Sci. Technol. **67**(1), 140–147 (2007). https://doi.org/10.1016/j.compscitech.2005.10.006
8. Durowaye, S.: Mechanical properties of particulate coconut shell and palm fruit polyester composites. Int. J. Mater. Eng. **4**(4), 141–147 (2014). https://doi.org/10.5923/j.ijme.20140404.04
9. Bastiurea, M., Rodeanu, M., Dima, D., Murarescu, M., Andrei, G.: Thermal and mechanical properties of polyester composites with graphene oxide and graphite. Dig. J. Nanomater. Biostruct. **10**(2), 521–533 (2015). https://www.chalcogen.ro/521_Bastiurea.pdf
10. Naveen, J., Jawaid, M., Amuthakkannan, P., Chandrasekar, M.: Mechanical and physical properties of sisal and hybrid sisal fiber-reinforced polymer composites. In: Mechanical and Physical Testing of Biocomposites, Fibre-Reinforced Composites and Hybrid Composites, pp. 427–440. Elsevier (2018)
11. El-Tayeb, N.S.M.: A study on the potential of sugarcane fibers/polyester composite for tribological applications. Wear **265**(1–2), 223–235 (2008). https://doi.org/10.1016/j.wear.2007.10.006
12. Senthilkumar, K., et al.: Evaluation of mechanical and free vibration properties of the pineapple leaf fibre reinforced polyester composites. Constr. Build. Mater. **195**, 423–431 (2019). https://doi.org/10.1016/j.conbuildmat.2018.11.081
13. Zuccarello, B., Marannano, G., Mancino, A.: Optimal manufacturing and mechanical characterization of high performance biocomposites reinforced by sisal fibers. Compos. Struct. **194**, 575–583 (2018). https://doi.org/10.1016/j.compstruct.2018.04.007
14. Reddy, D.: Properties of ligno-cellulose ficus religiosa leaf fibers. Ser. Publ. 29–35 (2010)
15. Charde, R.M., Dhongade, H.J., Charde, M.S., Building, E.Z.: Evaluation of antioxidant, wound healing and anti-inflammatory activity of ethanolic extract of leaves of Ficus religiosa. IJPSR **1**(2), 32–40 (2010)

16. Sankar, R., Maheswari, R., Karthik, S., Shivashangari, K.S., Ravikumar, V.: Anticancer activity of Ficus religiosa engineered copper oxide nanoparticles. Mater. Sci. Eng. C **44**, 234–239 (2014). https://doi.org/10.1016/j.msec.2014.08.030

17. Daniel, I., Ishai, O., Daniel, I., Daniel, I.: Engineering Mechanics of Composite Materials. Oxford University Press (2006). ISBN 978-0-19-515097-1

18. Prasad, R., Murali, K., Rao, M., Gupta, A.V.S.S.K.S.: Tensile and Impact Behaviour of Rice Straw-Polyester Composites (2007). Accessed 08 Mar 2021 [Online]. Available: http://nopr.niscair.res.in/handle/123456789/323

19. Prasad, R., Rao, M., Nagasrinivasulu, G.: Mechanical Properties of Banana Empty Fruit Bunch Fibre Reinforced Polyester Composites (2009). Accessed 08 Mar 2021 [Online]. Available: http://nopr.niscair.res.in/handle/123456789/4387

20. Ahlawat, V., Kajal, S., Parinam, A.: Experimental analysis of tensile, flexural, and tribological properties of walnut shell powder/polyester composites. Euro Mediterr. J. Environ. Integr. **4**(1) (2019). https://doi.org/10.1007/s41207-018-0085-6

21. Marian, B., Magdalena Silvia, B., Dumitru, D., Murarescu, M., Gabriel, A.: Thermal Properties of Polyester/Graphene Oxide and Polyester/Graphite Determined by TMA (2015). Accessed 08 Mar 2021 [Online]. Available: http://avestia.com/NewTech2015_Proceedings/files/papers/ICNFA306.pdf

22. Benyahia, A., Merrouche, A., Rokbi, M., Kouadri, Z., Ce, D.: Laboratoire des Matériaux Non Métalliques. Algerie (1900)

23. Negawo, T.A., Polat, Y., Buyuknalcaci, F.N., Kilic, A., Saba, N., Jawaid, M.: Mechanical, morphological, structural and dynamic mechanical properties of alkali treated Ensete stem fibers reinforced unsaturated polyester composites. Compos. Struct. **207**, 589–597 (2019). https://doi.org/10.1016/j.compstruct.2018.09.043

24. Akhtar, M.N., et al.: Influence of alkaline treatment and fiber loading on the physical and mechanical properties of kenaf/polypropylene composites for variety of applications. Prog. Nat. Sci. Mater. Int. **26**(6), 657–664 (2016). https://doi.org/10.1016/j.pnsc.2016.12.004

25. Rokbi, M., Osmani, H., Imad, A., Benseddiq, N.: Effect of Chemical Treatment on Flexure Properties of Natural Fiber-Reinforced Polyester Composite (2011) https://doi.org/10.1016/j.proeng.2011.04.346

26. Sreekumar, P.A., Thomas, S.P., Marc Saiter, J., Joseph, K., Unnikrishnan, G., Thomas, S.: Effect of fiber surface modification on the mechanical and water absorption characteristics of sisal/polyester composites fabricated by resin transfer molding. Compos. Part A Appl. Sci. Manuf. **40**(11), 1777–1784 (2009). https://doi.org/10.1016/j.compositesa.2009.08.013

27. Chaudhary, V., Bajpai, P.K., Maheshwari, S.: Studies on mechanical and morphological characterization of developed jute/hemp/flax reinforced hybrid composites for structural applications. J. Nat. Fibers **15**(1), 80–97 (2018). https://doi.org/10.1080/15440478.2017.1320260

28. Srinivas, C.A., Dilli Babu, G.: Mechanical and machining characteristics of calotropis gigentea fruit fiber reinforced plastics [Online]. Available: www.ijert.org

29. Prasad, R., Murali, K., Rao, M., Kumar, A.: Flexural properties of rice straw reinforced polyester composites. Indian J. Fiber Text. Res. **172**, 335–338 (2006). http://nopr.niscair.res.in/handle/123456789/24525

Preparation of Cellulose Nanofibers (CNFs) from *Cajanus cajan* (Pigeon Pea) and *Acacia arabica* (Babul Plant)

R. Mrudhula, P. Dinesh Sankar Reddy, and G. B. Veeresh Kumar

1 Introduction

The cellulose biopolymer is the abundant resource in the world. With increased awareness about environment, natural polymers are gaining maximum importance in day-to-day life. Of all this, cellulose is the most abundant biopolymer, which is present in almost all plants, animals, bacteria, etc., which has attracted many researchers to work on various aspects of this biopolymer. Cellulose biopolymer structure is established by fibrils, which is surrounded by lignin and hemicellulose. Cellulose is composed of 1-β, 4D-linked glucose chains with glucose units grouped in 6-membered rings (pyranoses) and linked by a single atom of oxygen (acetal linkages) between the C-4 of the next ring and the C-1 of one pyranose ring [1]. Due to their unique features and applications in various industries, the cellulose nanofibers (CNFs) development has significant attention in recent decades. For commercial applications, isolating cellulose nanofibers from the cellulose matrix necessitates a lot of energy. Their usage has been limited in the previous decades. After the discovery of a strong impact of pretreatment methods aimed at facilitating mechanical disintegration, such as 2,2,6,6-tetramethylpiperidine-*N*-oxyl (TEMPO)-mediated oxidation [2] or enzymatic hydrolysis [3–5], CNFs are more interesting in commercial applications.

R. Mrudhula
Department of Chemical Engineering, JNTUA Anantapur, Anantapur 515002, India

P. Dinesh Sankar Reddy (✉)
Department of Chemical Engineering, National Institute of Technology—Andhra Pradesh, Tadepalligudem, Andhra Pradesh, India
e-mail: pdsreddy@nitandhra.ac.in

G. B. Veeresh Kumar
Mechanical Engineering Department, National Institute of Technology—Andhra Pradesh, Tadepalligudem, Andhra Pradesh, India

Charreau et al. patent studies [6], book chapters from Chauve and Bras [7], Bardet and Bras [8] and Lindstrom et al. [9], studies focusing on industrialization and market issues, show that it is widely available as a commercial product and that interest in industrial applications is growing [10].

Nanocellulose fibers from different agricultural products have been extracted such as banana [11], mulberry [12], cotton [13], wheat straw [14], bamboo [15, 16], pea hulls [17], hemp [18], coconut husk fibers [19], bacterial cellulose and kenaf core [20], palm [21], pinecone biomass [22]. The extraction techniques consist of mechanical treatments, like cryocrushing [23, 24], high-pressure homogenization [25, 26], acid hydrolysis [27] enzyme-assisted hydrolysis [5, 28, 29], electro spinning methods [3], and ultrasonication [30, 31]. Depending on the cellulose, all these processes produce distinct types of nanofibrillar materials.

Acacia arabica species are frequently known in India as "Babool" and have got long been utilized ethnomedicinally for skin treatment, stomach, genital, and dental disorders. In India, *Cajanus cajan* (pigeon pea) branches are utilized as a natural fence, and *Cajanus cajan* (pigeon pea) branches are classified agricultural waste and were used to extract nanocellulose fibers. In the current study, alkali treatment was used to extract cellulose fibers from the branches of these two plants, which were then hydrolyzed by sulfuric acid to yield cellulose nanofibers. Using sulfuric acid and an ultrasonic technique, nanofibers from *Acacia arabica* and *Cajanus cajan* were isolated. Scanning electron microscope (SEM), X-ray diffraction (XRD), and thermogravimetric analysis were used to examine the morphology, crystallinity, and thermal properties of the isolated nanofibers (TGA).

2 The Materials of Fiber and Methods Followed

2.1 Materials

Cajanus cajan (received from Kadiri, Andhra Pradesh), *Acacia arabica* (collected from Anantapur, Andhra Pradesh), sodium chlorite, sodium hydroxide, sulfuric, and acetic acid. All analytical grade chemicals were used without any purification.

2.2 Extraction of Cellulose Fibers

The branches are cut into a length of 3 cm and washed using distilled water to remove dust on the surface and ground. The test samples were 1st dewaxed in a Soxhlet device with 2:1 (v/v) mixture of benzene and ethanol for 6 h. The test samples were later treated with 2 wt% NaOH solution at 90 °C for 2 h and next samples treated with sodium chlorite 0.3 g and 0.1 ml acetic acid per gram of dry test sample, and the reaction temperature was maintained at 75 °C for 1 h [32]. Subsequently, the chemical

treatment of the test samples was filtered and washed using distilled water till the samples were neutral.

2.3 Acid Hydrolysis

Acid hydrolysis of nanocellulose fibers for 2 h at 55 °C in 64 wt% sulfuric acid with continuous stirring resulted in an aqueous suspension of nanocellulose fibers. The flask was chilled in ice-cold water once the hydrolysis was completed. The aqueous solution of fibers was diluted and centrifuged many times before being neutralized with 1.0 wt% aqueous NaOH. After 30 min of sonication treatment, drop of chloroform is added and stored in refrigerator at 4 °C.

2.4 Chemical Composition Estimation

Chemical analysis of stalk samples at different stages was carried out in accordance with the standard methods of TAPP1, 2002, New York.

2.5 Scanning Electron Microscopic Analysis

A Zeiss DSM 960 microscope was used to study the morphology of each fiber. With an accelerating voltage of 10 kV, a drop of aqueous dispersion suspension of each fiber was dried and inspected without any sputter coating.

2.6 Crystallinity Measurement

XRD examination was done utilizing a Bruker D8 Advance, Germany with Kα Cu radiation ($\lambda = 1.54$ Å) at scan speed 0.04 s^{-1} for crystallinity measurement. XRD patterns of cellulose test samples were recorded over a 2θ range of 10–35°.

2.7 Thermogravimetric Analysis

Thermogravimetric analysis (TG) were used to inspect the cellulose fibers' properties of degradation at each step up from the two sources. A thermogravimetric analyzer (Perkin Elmer, Diamond) was used to investigate the thermal steadiness of each sample over a range of temperature from 25 to 700 °C with 10 °C/min heating rate.

Table 1 Plant materials chemical composition at different stages

Raw material	Cellulose (%)	Hemicellulose (%)	Lignin (%)
Cajanus cajan	47.31	32.5	18.6
Acacia arabica	36.2	22.3	25.7
Bleached CC fibers	85.2	8.26	1.7
Bleached AA fibers	83.4	13.6	4.2

3 Results and Discussion

3.1 Chemical Composition Estimation

The chemical composition of two samples at different extraction stages was as shown in Table 1. The initial *Cajanus cajan* bark contains of cellulose—47.31%, lignin—18.6%, and hemicellulose—32.5%, and *Acacia arabica* consists of 37.2% cellulose, 22.3% lignin, and 25.7% hemicellulose. Due to the elimination of lignin and hemicellulose following chemical treatments, the percentages of cellulose in the two samples have increased. The cementing elements in plant materials, hemicellulose, and lignin form a matrix around the cellulose fibers. Lignin and hemicellulose must be removed to isolate cellulose efficiently.

3.2 Scanning Electron Microscopic Analysis

The SEM micrographs in Figs. 1 and 2 show that sulfuric acid hydrolyzed fibers of *Cajanus cajan* (pigeon pea), *Acacia arabica* (Babul plant) which triggered breakdown of fibers into rod-like structures. The crystalline sections were unharmed, whereas the amorphous parts were selectively hydrolyzed. Individual cellulose fibers were measured to have an approximately average diameter of 20 and 40 nm length, respectively. SEM revealed no significant differences in length or diameter among the nanofibers. The hydroxyl esterification groups by sulfate ions happens when sulfuric acid treated cellulose. When sulfate groups are introduced along the surface of crystallites, the surface takes on a negative charge. The anionic stabilization of the crystallite colloidal suspensions is most likely owing to the attraction/repulsion forces of the electrical double layers at the crystallites [33]. The crystalline particles, on the other hand, were rod-like and clumped together after drying to some extent. The micro-sized cellulose fibers did, in fact, include strong hydrogen bonding nanofibers [34]. After ultrasonic treatment, separate or individual nanofibers were obtained.

Fig. 1 *Cajanus cajan* nanocellulose fibers SEM images
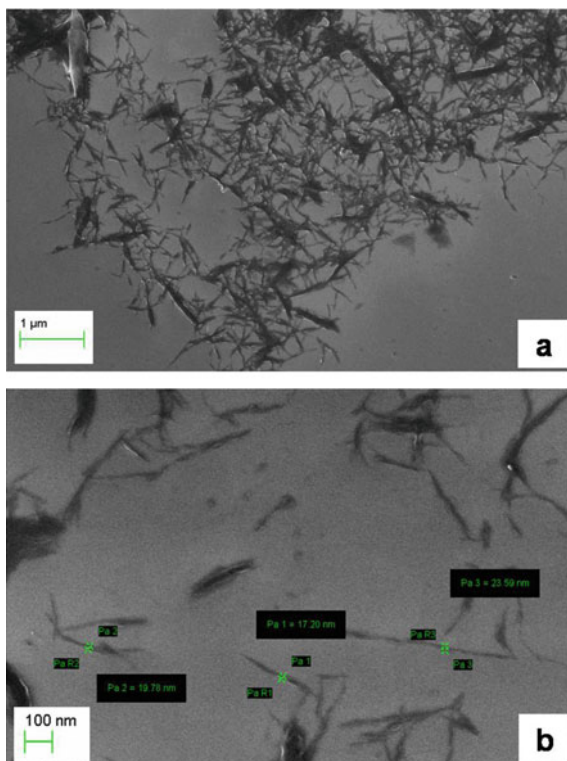
3.3 Crystallinity Measurement

Studies of XRD treated, untreated cellulose fibers, and their respective fibers of nanocellulose were conducted to investigate the fibers crystalline behavior. Table 2 and Fig. 3 presented with the XRD diffraction patterns and crystallinity percentage. In Fig. 3a, all the peeks are observed at $2\theta = 22.7°$ and in Fig. 3b, $2\theta = 22.4°$ which characterize the representative cellulose I structure [35]. The crystallinity percentage was showed in table, where it is observed that crystallinity of original *Cajanus cajan* and *Acacia arabica* was 53.8% and 47.6%, respectively, and their nanofibers are 73.6% and 62.5% which is undoubtedly due to the removal of hemicellulose and lignin during chemical treatments.

Fig. 2 SEM images of *Acacia arabica* nanocellulose fibers
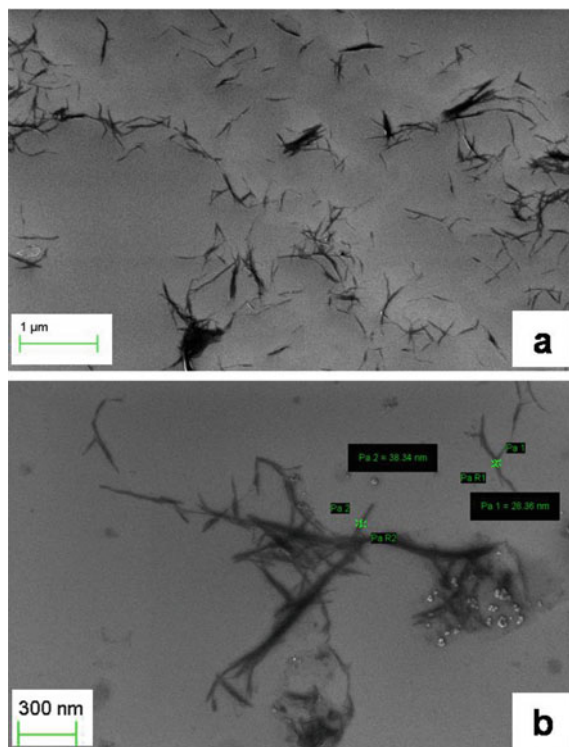
Table 2 Crystallinity of *Cajanus cajan* and *Acacia arabica* at different stages

Material	Crystallinity (%)
Cajanus cajan	53.8
Acacia arabica	47.6
Bleached CC fibers	65.2
Bleached AA fibers	53.8
Nano-CC fibers	73.6
Nano-AA fibers	62.5

3.4 Thermogravimetric Analysis

Cajanus cajan and *Acacia arabica* raw, bleached, and nanocellulose fibers are subjected to thermogravimetric analysis to compare their degradation characteristics. Figure 4 shows the TGA curves of both. In these curves, initial drop was started from around 50°–150 °C which corresponds to moisture present in the sample. Due to the presence of different components in the untreated plant materials, degradation starts from 220 °C, but in bleached and nanocellulose fibers, degradation starts at the temperature above 300 °C. And in the figures, the broad peek from 200 to 500 °C
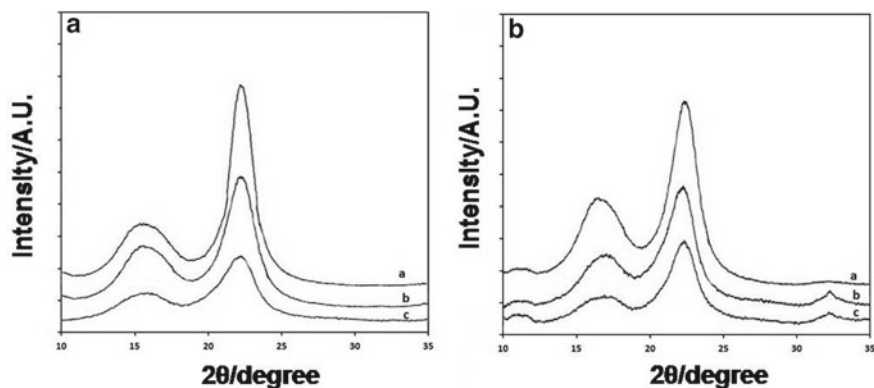
Fig. 3 X-ray diffraction patterns of **a** *Cajanus cajan* and **b** *Acacia arabica* (a) nanocellulose fibers, (b) bleached cellulose fibers, (c) original cellulose fibers

represents the degradation of lignin, but the degradation temperature in the nanocellulose fibers of *Cajanus cajan* and *Acacia arabica* is increased to 356 and 337 °C due to the fact that lignin and hemicellulose are removed by different chemical treatments [36], even though the enhanced weight residue of the cellulose whisker was for the reason that the sulfate groups acting as flame retardants [37].

From the observations, the fibers of *Cajanus cajan* and *Acacia arabica* are extracted with best quality, and the method followed in this fabrication process is very effective in producing quality nanofiber when compared with works on plant cellulose fibers [14], pea starch, and cellulose nanowhiskers [17].
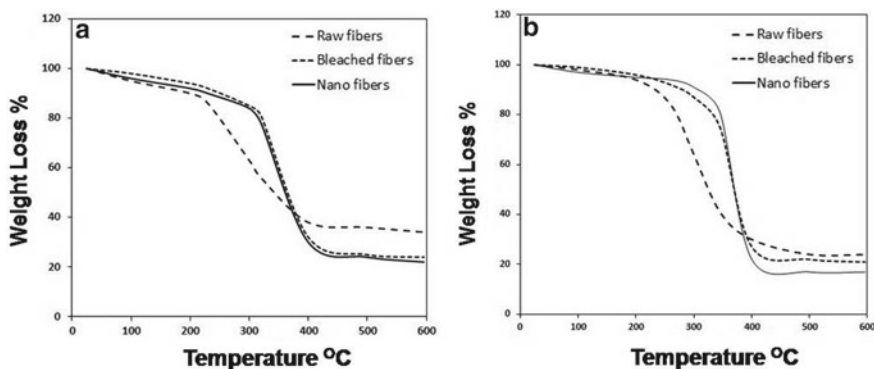
Fig. 4 TGA curves of **a** *Cajanus cajan* and **b** *Acacia arabica*

4   Conclusions

Nanocellulose fibers were extracted from *Cajanus cajan* and *Acacia arabica* fibers using chemical treatments followed by ultrasonication. Chemical analysis of the fibers revealed that hemicelluloses and lignin were removed in part during the chemical procedure. These threads were successfully split into nanofibers with sizes ranging from 20 to 40 nm. *Cajanus cajan* crystallinity was greater than 73 percent, while *Acacia arabica* crystallinity was 62.5%. The thermal properties of the nanofibers were also improved, with high-thermal degradation temperatures exceeding by 330 °C, compared to 210 °C for their untreated counterparts. These findings suggest that the nanofibers produced have better thermal properties, making them ideal for use as reinforcing components in the manufacture of bio-renewable composite materials.

References

1. Siró, I., Plackett, D.: Microfibrillated cellulose and new nanocomposite materials: a review. Cellulose **17**(3), 459–494 (2010)
2. Isogai, A., Saito, T., Fukuzumi, H.: TEMPO Oxidised Cellulose nanofibres. Nanoscale **3**(1), 71–85 (2011)
3. Frenot, A., Henriksson, M.W., Walkenström, P.: Electrospinning of cellulose-based nanofibers. J. Appl. Polym. Sci. **103**(3), 1473–1482 (2007)
4. Janardhnan, S., Sain, M.M.: Targeted disruption of hydroxyl chemistry and crystallinity in natural fibres for the isolation of cellulose nano-fibres via enzymatic treatment, BioResources **6**(2), 1242–1250 (2011)
5. Pääkkö, M., Ankerfors, M., Kosonen, H., Nykänen, A., Ahola, S., Österberg, M., Ruoko-lainen, J., Laine, J., Larsson, P.T., Ikkala, O., Lindström, T.: Enzymatichydrolysis combined with mechanical shearing and high-pressurehomogenization for nanoscale cellulose fibrils and strong gels. Biomacromolecules **8**, 1934–1941 (2007)
6. Charreau, H., Foresti, M.L., Vazquez, A.: Nanocellulose patents trends: a comprehensive review on patents on cellulose nanocrystals, microfibrillated and bacterial cellulose. Recent Pat. Nanotechnol. **7**(1), 56–80 (2013)
7. Chauve, G., Bras, J.: Industrial point of view of nanocellulose materials andtheir possible applications. In: Handbook of Green Materials, pp. 233–252. World Scientific (2014)
8. Bardet, R., Bras, J.: Cellulose nanofibers and their use in paper industry. In: Handbook of Green Materials, pp. 207–232. World Scientific (2014)
9. Lindström, T., Aulin, C., Naderi, A., Ankerfors, M.: Microfibrillated cellulose. In: Encyclopedia of Polymer Science and Technology. Wiley (2014)
10. Lindström, T., Aulin, C.: Market and technical challenges and opportunities in the area of innovative new materials and composites based on nanocellulosics. Scand. J. For. Res. **29**, 345–351 (2014)
11. Deepa, B., Abrahama, E., Cherian, B.M., Bismarck, A., Blaker, J.J., Pothan, L.A., Leao, A.L., Souza, S.F., Kottaisamy, M.: Structure, morphology and thermal characteristics of banana nano fibers obtained by steam explosion. Bioresour. Technol. **102**, 1988–1997 (2011)
12. Li, R., Fei, J., Cai, Y., Li, Y., Feng, J.Q., Yao, J.: Cellulose whiskers extracted from mulberry: a novel biomass production. Carbohydr. Polym. **76**, 94–99 (2009)
13. de Morais, T.E., Corre, A., Manzoli, A., de Lima, L.F., de Oliveira, C., Mattoso, L.: Cellulose nanofibers from white and naturally colored cotton fibers. Cellulose **17**(3), 595–606 (2010)

14. Chen, W., Yu, H., Liu, Y., Hai, Y., Zhang, M., Chen, P.: Isolation and characterization of cellulose nanofibers from four plant cellulose fibers using a chemical-ultrasonic process. Cellulose **18**, 433–442 (2011)

15. Abe, K., Yano, H.: Comparison of the characteristics of cellulose microfibril aggregates isolated from fiber and Parenchyma cells of Moso bamboo (*Phyllostachys pubescens*). Cellulose **17**(2), 271–277 (2010)

16. Qian, Y., Qin, Z., Vu, N.-M., Tong, G., Chin, Y.C.F.: Comparison of nanocrystals from tempo oxidation of bamboo, softwood and cotton linter fibres with ultrasonic-assisted process. Bioresources **7**(4), 4952–4964 (2012)

17. Chen, Y., Liu, C., Chang, P.R., Cao, X., Anderson, D.P.: Bionanocomposites based on pea starch and cellulose nanowhiskers hydrolyzed from pea hull fibre: effect of hydrolysis time. Carbohyd. Polym. **76**, 607–615 (2009)

18. Wang, B., Sain, M., Oksman, K.: Study of structural morphology of hemp fiber from the micro to the nano scale. Appl. Compos. Mater. **14**(2), 89–103 (2007)

19. Rosa, M.F., Medeiros, E.S., Malmonge, J.A., Gregorski, K.S., Wood, D.F., Mattoso, L.H.C., Glenn, G., Orts, W.J., Imam, S.H.: Cellulose nanowhiskers from coconuthusk fibers: effect of preparation conditions on their thermal and morphological behavior. Carbohydr Polym **81**(1), 83–92 (2010)

20. Jonoobi, M., Harun, J., Tahir, P.M., Zaini, L.H., Azry, S.S., Makinejad, M.D.: Characteristics of nanofibers extracted from Kenaf Core. BioResources **5**(4), 2556–2566 (2010)

21. Mohamad Haafiz, M.K., Hassan, A., Abdul Khalil, H.P.S., Nurul Fazita, M.R., Islam, M.S., Inuwa, I.M., Marliana, M.M., Hazwan Hussin, M.: Exploring the effect of cellulose nanowhiskers isolated from oil palmbiomass on polylactic acid properties. Int. J. Biolog. Macromol. **85**, 370–378 (2016)

22. Rambabu, N., Panthapulakkal, S., Sain, M., Dalai, A.K.: Production of nanocellulose fibers from pinecone biomass: evaluation and optimization of chemical and mechanical treatment conditions on mechanical properties of nanocellulose films. Ind. Crops Prod. **83**(2016), 746–754 (2016)

23. Alemdar, A., Sain, M.: Biocomposites from wheat straw nanofibers:morphology, thermal and mechanical properties. Compos. Sci. Technol. **68**, 557–565 (2008)

24. Abe, K., Iwamoto, S., Yano, H.: Obtaining cellulose nano fibers with a uniform width of 15 nm from wood. Biomacromolecules **8**(10), 3276–3278 (2007)

25. Herrick, F.W., Casebier, R.L., Hamilton, J.K.: Microfibrillated cellulose: morphology and accessibility. J. Appl. Polym. Sci. Appl. Polym. Symp. **37**, 797–813 (1983)

26. Kaushik, A., Singh, M.: Isolation and characterization of cellulose nanofibrilsfrom wheat straw using steam explosion coupled with high shearhomogenization. Carbohydr. Res. **346**, 76–85 (2011)

27. Araki, J., Wada, M., Kuga, S., Okano, T.: Birefringent glassy phase of a cellulose microcrystal suspension. Langmuir **16**(6), 2413–2415 (2000)

28. Hayashi, N., Kondo, T., Ishihara, M.: Enzymatically produced nano-ordered short elements containing cellulose I$_\beta$ crystalline domains. Carbohydr Polym **61**(2), 191–197 (2005)

29. Morais, J.P.S., de Freitasrosa, M., de sa Moreirade Souza Filho, M., Nascimento, L.D., Nascimento, D.M., Cassales, A.R.: Extraction and characterization of nanocellulose structures from raw cotton linter. Carbohydr. Polym. **91**(1), 229–235 (2013)

30. Tischer, P.C.S.F., Sierakowski, M.R., Westfahl, H., Tischer, C.A.: Nanostructural reorganization of bacterial cellulose by ultrasonic treatment. Biomacromolecules **11**(5), 1217–1224 (2010)

31. Lu, Q., Tang, L., Lin, F., Wang, S., Chen, Y., Chen, X., Huang, B.: Preparation and characterization of cellulose nanocrystals via ultrasonication-assisted FeCl$_3$-catalyzed hydrolysis. Cellulose **21**(5), 3497–3506 (2014)

32. Kerr, A.J.: Ash, silica, and lignin in New Zealand beech, no. 952. New Zealand J. For. Sci. **6**(1), 108–13 (1976)

33. Marchessault, R.H.: Steam explosion: are fining process for lignocellulosics. In: Focher, B., Marzetti, V., Crescenci, V. (eds.) Steam Explosion Techniques: Fundamentals and Industrial Applications, pp. 1–19. Gordon and Breach Science Publishers, Philadelphia (1991)

34. Abe, K., Yano, H.: Comparison of the characteristics of cellulose micro fibril aggregates of wood, rice straw and Potato tuber. Cellulose **16**(6), 1017–1023 (2009)
35. Klemm, D., Heublein, B., Fink, H.P., Bohn, A.: Cellulose: fascinating biopolymer and sustainable rawmaterial. Angew. Chem. Int. Edit. **44**(22), 3358–3393 (2005)
36. Nguyen, T., Zavarin, E., Barrall, E.M.: Thermal-analysis of lignocellulosic materials. Part 1: unmodified materials. J. Macromol. Sci. Part C Polym. Rev. **20**, 1–65 (1981)
37. Maren, R., William, T.W.: Effect of sulfate groups from sulfuric acid hydrolysis on the thermal degradation behavior of bacterial cellulose. Biomacromolecules **5**, 1671–1677 (2004)

Investigation and Assessment of Mechanical Properties of Al-Fly Ash

K. Chinna Maddaiah and G. B. Veeresh Kumar

1 Introduction

The blend of two or more materials known as composite material exhibits improved properties than the individual constituents when used alone. Individual materials in metallic alloys, on the other hand, retain their unique physical, chemical, and mechanical properties. Reinforcement and matrix, on the other hand, are two distinct elements of MMCs. Composites have stronger strength, stiffness, and low density than bulk materials, allowing for weight reduction in finished parts. Researchers have extensively investigated composites' unrivalled the performances [1–3]. The wear-resistant particulate-filled MMCs are used in applications such as vehicle segments such as piston blocks, cylinders, cylinder rings, calipers, impellers, space structures, contactors, and vibrator segments [4]. Al-based composites shown exceptional mechanical characteristics among MMCs [5, 6]. The wear resistance of Al6061 and Al6061-TiO_2 MMCs is influenced by sliding distance, weight % of reinforcement, and normal load [7, 8]. Prakash Rao [9] experimental results presented that the increasing content of fly ash as reinforcement content in the composites reduces cutting tool failure by reducing built up edge formation. Ankush Sachdeva [10] checked possibility by means of using different reinforcement materials fly ash, silicon carbide (SiC), and the graphite (Gr) to empower properties of A15020 alloy. Different test specimens were fabricated using Al with different reinforcements and studied mechanical properties such as strength and hardness. Udaya Prakash [11] fabricated the hybrid composites using Al as matrix material, boron carbide (B_4C)

K. Chinna Maddaiah (✉) · G. B. Veeresh Kumar
Department of Mechanical Engineering, National Institute of Technology—Andhra Pradesh,
Tadepalligudem, Andhra Pradesh, India
e-mail: chinnasiri0424@gmail.com

K. Chinna Maddaiah
Department of Mechanical Engineering, CMR Engineering College, Hyderabad, Telangana, India

and fly ash as the reinforcement materials. They have investigated the effects rein-
forcements like surface roughness, gap voltage, and pulse on and off time, by means
of wire electro-discharge machining process. Ramachandra et al. [12] fabricated the
MMCs using liquid metallurgy route with Al–Si 12 wt% alloy as matrix material
and 15 wt% fly ash fine particulates-reinforced composite. Results exhibited that the
resistance to wear of the composite reinforced with fly ash material increases with
increasing fly ash content but declines with the increasing applied sliding velocity
and normal load. Manoj Singla et al. [13] fabricated MMCs using Al as base metal
and reinforcement with varying weight fractions of SiC from 5 to 30% in the steps of
5%. The results showed that as the weight percent of SiC increases, so does the hard-
ness and impact strength. At 25 wt% SiC, the extraordinary results (maximum impact
power of 36 nm and maximum hardness of 45.5 BHN) were achieved. Yigezu et al.
[14] used a full factorial design plan to evaluate abrasive wear of in-situ produced Al–
12% Si/TiC MMCs. The percentage of TiC in the coating and the sliding distance had
a bigger impact on coefficient of friction (COF), according to findings. Considering
the aforementioned, the current research effort intends to develop and test AA1050-
fly ash-reinforced MMCs. In this study, fly ash particles were used to strengthen
the Al-1050 matrix material at varied weight percent. The mechanical and tribolog-
ical characteristics of Al-fly ash composites that have been manufactured have been
characterized and investigated.

2 Materials and Fabrication

2.1 Material

The material being Al-1050 ingots from was supplied by Fenfe Metallurgical,
Bangalore, India.

Al alloy AA1050 because of its low density, limited capacity to be strengthened via
precipitation, strong thermal and electrical conduction, superior corrosion resistance,
and good damping capacity, was chosen as the metal matrix in this investigation.
The chemical compositions of AA1050 alloy are shown in Table 1. The properties of
AA1050 and the reinforcing fly ash are shown in Table 2. Reliance Industries Limited
provided injection grade HDPE (M60075), and NTPC of West Bengal, India provided
fly ash. Fly ash was selected as a reinforcement alloy because it is a byproduct of
coal combustion and is inexpensive, as well as having high electrical resistivity, poor
thermal conductivity, and low density. In the current work, three different proportions
of fly ash (1, 2, 4%) are taken. For 1%, 500 gm of Al and 5 gm of fly ash are taken.
For 2%, 500 of Al and 10.5 gm of fly ash are taken, and finally, for 4%, 500 gm of
Al and 21 gm of fly ash are taken.

Table 1 Chemical composition of AA1050 [15]

Element	Cu	Mg	Si	Fe	Mn	Zn	Ti	Al
Percentage	0.001	0.003	0.123	0.259	0.004	0.008	0.01	Balance

Table 2 Physical and mechanical characteristics of the base alloy AA1050 [15] and reinforcement fly ash

Materials	Hardness (HB500)	Density (g/cc)	Tensile strength (MPa)
AA1050	34	2.71	78
Fly ash	500	2.17	450

2.2 Fabrication and Testing

The fabrication of Al-fly ash MMCs via stir casting procedure was selected; crucible is heated up to 720 °C, and then, Al is placed in crucible; the temperature was maintained till the Al is melted. The fine powder particles of fly ash were selected as the reinforcement material and were added in molten Al after effective degassing with hexachloroethane degassing tabled, and it will be mixed continuously by stirring continuously at 400 rpm for about 10 min simultaneously about 5 g of Mg chips were added to molten mixture to improve the wettability of reinforcement in the matrix material. In the meanwhile, the molds were cleaned and preheated up to 300 °C. After effective stirring of the molten mixture of AA1050 and fly ash MMCs can be poured into the preheated circular-shaped permanent mold box made of cast-iron. After solidification, specimen should remove from the molds, and the excess material from the specimen will be removed by using filling and by using emery papers. Using a CNC lathe machine, the cast MMCs obtained from stir casting were machined to the requisite specifications in accordance with ASTM standards. Mechanical qualities are tested, such as tensile strength, hardness, and wear resistance. The UTM model TUE-C-600 was used according to ASTM standard E8M-04, at JNTU Hyderabad. Hardness test machine model VH-1, SR. No: 27497 was used specimens were prepared according to ASTM standard E384-11. Hardness test is made by using Vickers micro-hardness tester. ASTM-G99 standards were used in this wear experiment. The sliding speed is maintained at 3.14 ms^{-1}. The pin-on-disk device is used to perform the wear test. The pin-on-disk tribometer is used to simulate friction as well as investigate and investigate wear mechanisms under sliding circumstances. The speed was selected from 0 to 500 rpm, temperature control, normal force, wear rate, number of turns, frictional coefficient, speed, and other parameters are registered and then displayed. The weight of the specimen will be carried out by using digital microscope weighing machine. Then, the pin will be rotated on the disk at given speed for 5 min. Wear test is carried out at four different loads (9.81, 19.62, 29.43, 39.24 N). After conducting the test, obtained values are tabulated as below (Figs. 1, 2 and 3).
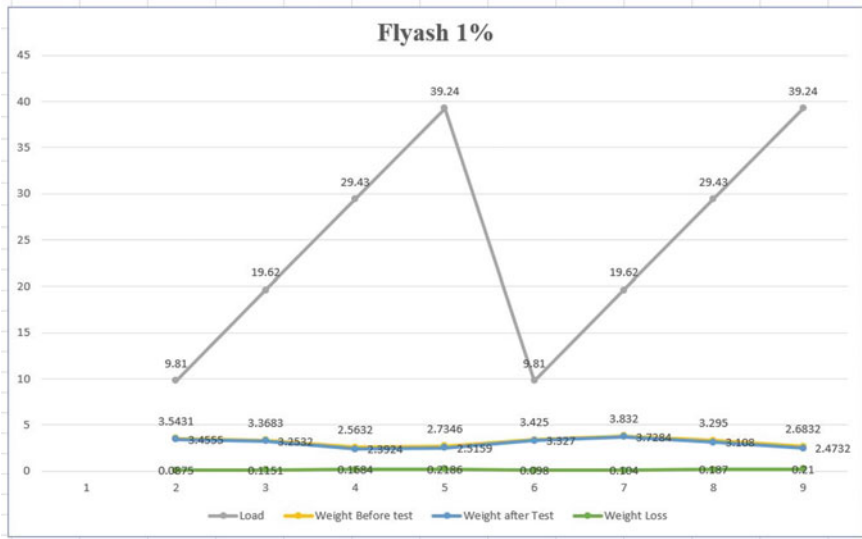
Fig. 1 Wear characteristics of Al-flyash 1 wt% composite
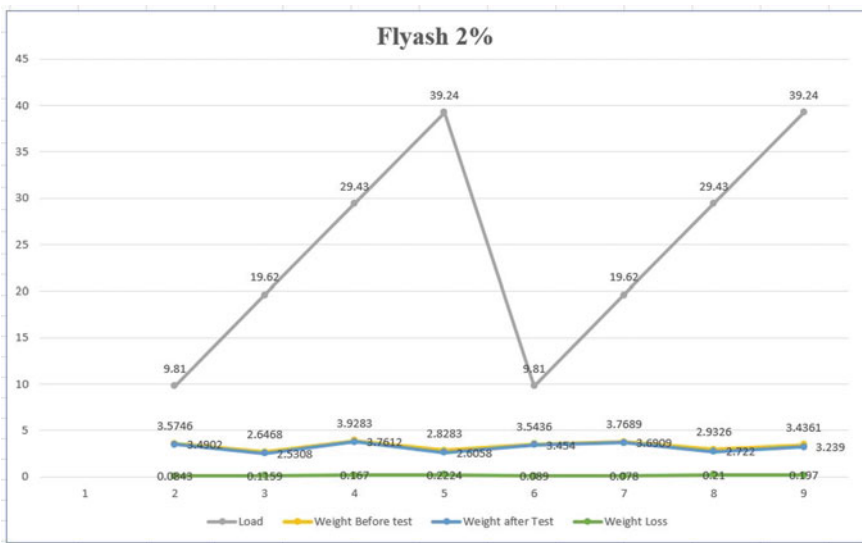
Fig. 2 Wear characteristics of Al-flyash 2 wt% composite
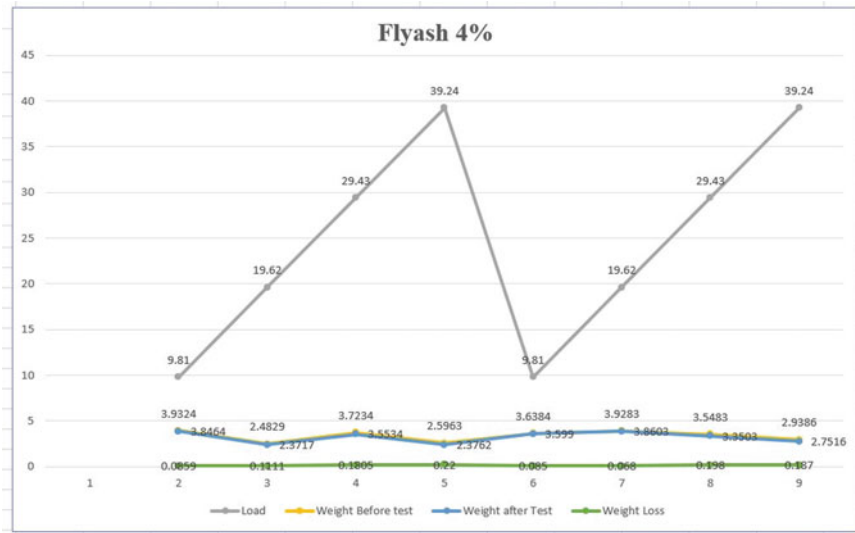
Fig. 3 Wear characteristics of Al-flyash 4 wt% composite

2.3 Factorial Design Methodology

In this case, a 2^2 factorial design was employed to investigate four components. Compression, hardness, bulk density, and permeability were the four parameters chosen. Investigational work based on two levels and two factors was evaluated and carried out to assess the influence of factors studied on Al castings. The weight loss has an impact on the wear rate, as shown by the ANOVA technique. Table 3 shows the corresponding design parameters. The 2^2 designs for weight loss are shown in Table 4 (Figs. 4 and 5).

Factors	: 2	Base designs	: 2, 4
Runs	: 4	Replicates	: 1

Table 3 For design parameters

S. No.	Factors	Low (−)	High (+)
1	(Al-fly ash%)	2	4
2	Load	9.81	39.24

Table 4 For 2^2 design for weight loss

A	B	Replicates		Total	Avg.	Labels
		I	II			
−	−	0.0843	0.0890	0.1733	0.466	(1)
+	−	0.0859	0.0850	0.1709	0.0854	A
−	+	0.2224	0.1970	0.4194	0.2097	B
+	+	0.2200	0.1870	0.4070	0.2035	AB
Total				1.9293	0.9646	
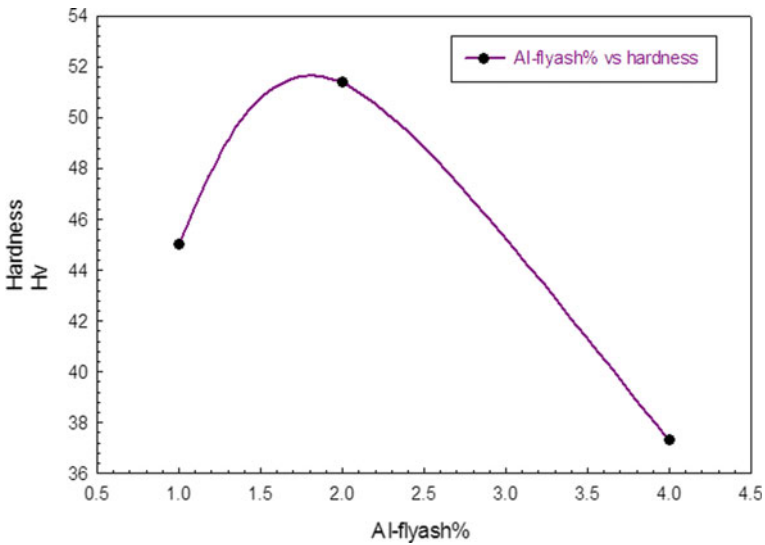
Fig. 4 Variation of hardness for Al-fly ash%

3 Results and Discussion

3.1 Tensile Strength Test

The AA1050 and fly ash MMCs were subjected to evaluate tensile, yield strength, and percentage elongation shown in Table 5. The reduction in mechanical properties of the MMCs is attributed to the decrease in solid solution strengthening.
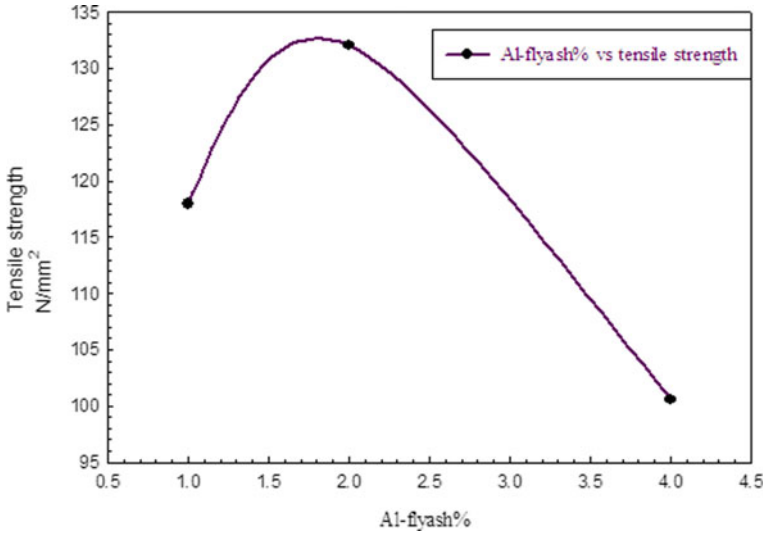
Fig. 5 Variation of tensile strength for Al-fly ash%

Table 5 Tensile test results

S. No.	Al-fly ash% (%)	Tensile strength (MPa)	Yield strength (MPa)
1	0	100	–
2	1	117.955	93.357
3	2	132.090	108.731
4	4	100.599	79.346

3.2 Hardness Test

Hardness test has done for 3 different proportions of Al-fly ash%. From those, different values are obtained for hardness values as mentioned in Table 6.

Table 6 Shows the results for hardness test

S. No.	Al-fly ash% (%)	Hardness values HV
1	0	30HV
1	1	45.0HV0.5
2	2	51.4HV0.5
3	4	37.3HV0.5
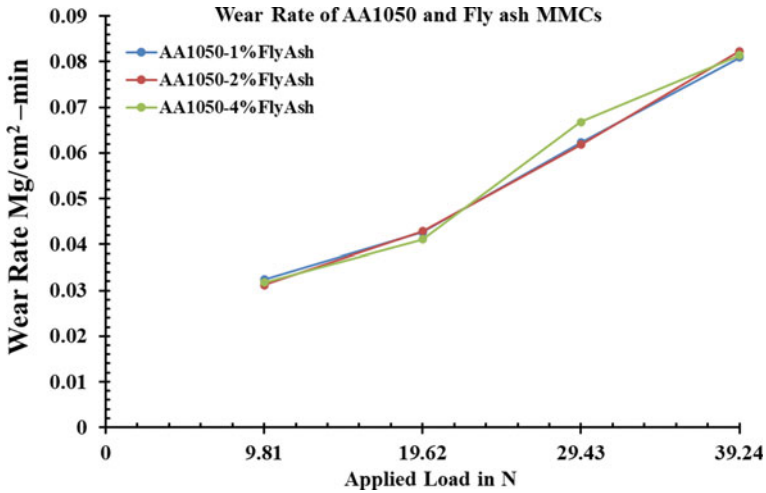
Fig. 6 AA1050-flyash results for wear rate

3.3 Wear Test

Pin-on-disk wear tests were performed for three different amounts of Al-fly ash percent. The results of the testing for wear rate are given in Fig. 6.

3.4 Factorial Design

The estimated effect and coefficient of weight loss will be R-sq. $= 98.31\%$ and R-sq. (pred) $= 88.00\%$. The estimated and coefficient of the design matrix were shown in Table 7

The predicted values of pipe volumes are determined from the formula given below.

Weight loss $(Y1) = 0.14575 - 0.002775A + 0.0659B + 0.000125AB$ (Table 8).

Table 7 Shows the estimated and coefficient of design matrix

Term	Effect	Coefficient	SE coefficient	T	P
Constant		0.146325	0.004591	31.87	0.0000
Block		0.006825	0.004591	1.49	0.234
A	−0.003700	−0.001850	0.004591	−0.40	0.714
B	0.120550	0.0620275	0.004591	13.13	0.001
A * B	−0.002500	−0.001250	0.004591	−0.27	0.803

Table 8 Shows ANOVA of variance

Source	DF	Seq SS	Adj. SS	Adj. MS	F	P
Blocks	1	0.0003726	0.0003726	0.0003726	2.21	0.234
Main effects	2	0.0290290	0.290290	0.0145460	86.26	0.002
A	1	0.0000274	0.0000274	0.0000274	0.16	0.714
B	1	0.0290646	0.0290646	0.0290646	172.36	0.001
2-way interactions	1	0.0000125	0.0000125	0.0000125	0.07	0.803
Residual error	3	0.0005059	0.0005059	0.0001686		
Total	7	0.0299830				

3.5 Main Effect Plots and Interaction Plots

3.5.1 Main Effect Plot

The principal effect is a plot of the means at each level of a component. When the mean response changes across values of a factor, the main effect plot is used to analyze the relative strength of the effects across the components. When the line is horizontal (parallel to the x-axis) in this graph, there is no major effect; nevertheless, there is a main effect when the line is not horizontal. Al-fly ash% (A) climbs from low to high levels in the principal impact graph, whereas loads (B) decrease. The load has the biggest influence on lowering the wear rate of all the factors (Fig. 7).
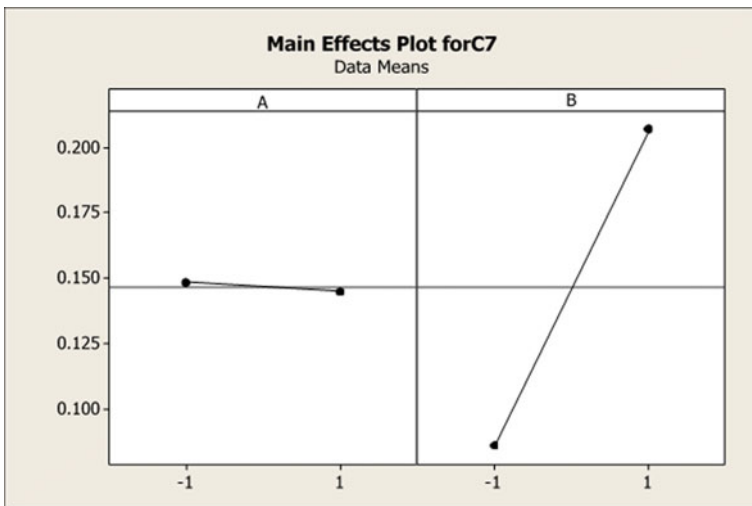
Fig. 7 Main effect plot
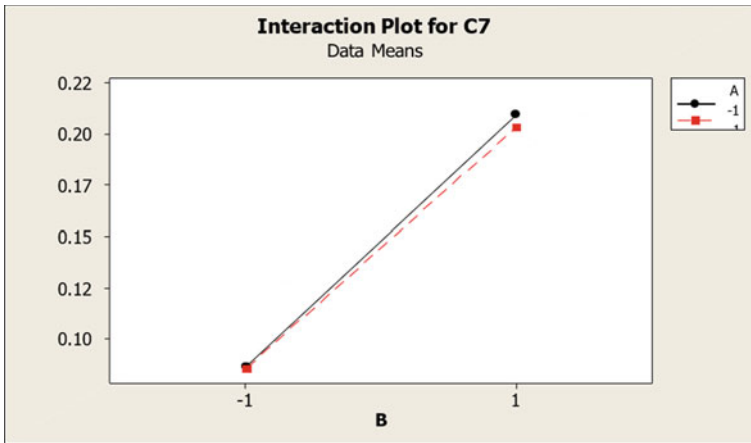
Fig. 8 Interaction plot

3.5.2 Interaction Plot

For two variables, it creates a single interaction map. Interaction plots can be used to determine whether there is interaction; if the interaction plot has a parallel line, there is no interaction (Fig. 8).

3.5.3 Residuals Plots

In regression and ANOVA, residual plot is used to measure the degree of goodness of model. The probability plot, histogram, versus fits, and versus order are all available in Minitab (Fig. 9).

3.5.4 Residuals Versus Fitted Value

This graphic should show a random distribution of residuals on both sides of 0. An outlier is a point that deviates significantly from most other points. In the residual plot, there should be no noticeable patterns.

3.5.5 Histogram of the Residual

General residual attributes such as typical values, distribution, and shape are displayed with this exploration tool. A skewed distribution could be indicated by long tail on one side. Outliers are points that stand out from the rest of the bars in some way.
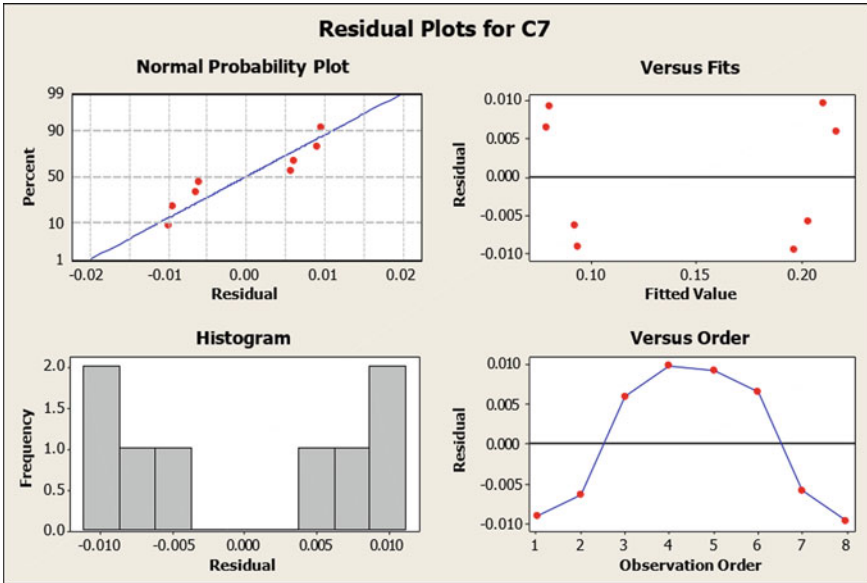
Fig. 9 Residuals plots

3.5.6 Residual Versus Order of Data

This is a plot of all residuals in the order in which they were collected, and it may be used to identify non-random errors, particularly time-related effects. This graph serves in the verification of the uncorrelated residuals assumption.

3.6 Discussion

The results of this study indicate how reinforcing affects the mechanical characteristics of stir-cast Al alloy composites. The results of mechanical parameters like as hardness and ultimate tensile strength are provided in Table 9.

Table 9 Shows the results

S. No.	Al-fly ash%	Tensile strength (N/mm^2)	Hardness HV	Wear rate (mg/cm^2-m)
Al (AA1050)		100	30	9.81
1	1	117.955	45.0	0.2186
2	2	132.090	51.4	0.2224
3	4	100.599	37.3	0.2200

Hence, from the above table, we can clearly say that there is a higher value at 2% reinforcement.

4   Conclusions

In this work, Al-MMCs test samples were prepared using fly ash as reinforcement in various weight percentages 1, 2, and 4 into the AA1050 base metal and performed various tests. From the tests carried out, it may be concluded that the tensile strength can be increased with adding fly ash in aluminum metal matrix. The hardness of MMCs of Al-fly ash increased by adding the fly ash. Wear rate decreased by adding fly ash in the wear melt. Up to 20% of weight, fly ash can be used in stir casting to produce composite. It may be concluded that fly ash may be used to produce Al-MMCs which can be used to turn industrial waste to wealth.

References

1. Pramod, R., Veeresh Kumar, G.B.: Influence of WC particulate reinforcement on the mechanical properties and sliding wear of Al6061 alloys. Appl. Mech. Mater. **813/814**, 67–73 (2015)
2. Oghenevweta, J.E., Aigbodion, V.S.: Mechanical properties and microstructural analysis of Al–Si–Mg/carbonized maize stalk waste particulate composites. J. Eng. Sci. (2014)
3. Sujan, D., Oo, Z., Rahman, M.E., Maleque, M.A.: Physio-mechanical properties of aluminium metal matrix composites reinforced with Al_2O_3 and SiC. World Acad. Sci. Eng. Technol. **6** (2012)
4. Veeresh Kumar, G.B., Rao, C.S.P., Selvaraj, N.: Mechanical and tribological behavior of particulate reinforced aluminum metal matrix composites—a review. J. Miner. Mater. Charact. Eng. (USA) **10**(1), 59–91 (2010)
5. Sidesh Kumar, N.G., et al.: Mechanical and wear behavior of Aluminium and hybrid composites. In: International Conference on Advances in Manufacturing and Material Technology, vol. 5, pp. 908–917 (2014)
6. Koli, D.K., Agnihotri, G., et al.: Properties and characterization of Al–Al_2O_3 composites processed by casting and powder metallurgy routes. J. Latest Trends Eng. Technol. **2** (2013)
7. Elango, G., Raghunath, B.K.: Tribology behaviour of hybrid (LM25A1 + SiC + TiO_2) metal matrix composites. In: International Conference on Design and Manufacturing, vol. 64, pp. 671–680 (2013)
8. Veeresh Kumar, G.B., Rao, C.S.P., Selvaraj, N., Bhagyashekar, M.S.: Studies on Al6061-SiC and Al7075-Al_2O_3 metal matrix composites. J. Miner. Mater. Charact. Eng. (JMMCE) (USA) **9**(1), 47–59 (2009)
9. Prakash Rao, C.R., Bhagyasekhar, M.: Machining behavior of A160061-flyash composites. In: International Conference on Advances in Manufacturing and Material Technology, vol. 5, pp. 1593–1602 (2014)
10. Sachdeva, A., Narayan, R.: Evaluation and comparision of mechanical properties of aluminium alloy 5052 reinforced with siliconcarbide, graphite and fly ash hybrid metal matrix composites. Int. J. Eng. Sci. Tech, **5**, 0975–5462 (2013)
11. Udhay Prakash, J., et al.: Experimental investigtion on machinability of aluminium alloy (A413)/flyash/B4 C hybrid composites using wire EDM. In: International Conference on Design and Manufacturing, vol. 5, pp. 1344–1353 (2013)

12. Ramachandra, M., Radhakrishna, K.: Effect of reinforcement of flyash on sliding wear, slurry erosive wear and corrosive behavior of aluminium matrix composite. J. Wear **262**, 1450–1462 (2007)
13. Singla, M.: Development of aluminium based silicon carbide particulate metal matrix composite. J. Miner. Mater. Charact. Eng. Technol. **8**, 455–467 (2009)
14. Yigezu, B.S., et al.: On modeling the abrasive wear characteristics of in situ Al–12%Si/TiC composites. J. Mater. Des. **50**, 277–284 (2013)
15. Avcu, Y.Y., Gönül, B., Yetik, O., Sönmez, F., et al.: Modification of surface and subsurface properties of AA1050 alloy by shot peening. Materials **14**(21), 6575 (2021). https://doi.org/10.3390/ma14216575

Investigation on Wear Characteristics of a PLA-14% Bronze Composite Filament

P. Sneha and K. Balamurugan

1 Introduction

PLA material plays a significant role in the 3D printed samples, and the effect of printing orientation and infill density depends upon the layer thickness and layer height. It increases the strength of the mechanical properties, and percentage depends on the infill density which implies the ductility property [1]. The effects of the wear behaviour have been evaluated using pin-on-disc apparatus where the load and speed can be varied and performed on coefficient of friction. The speed performs the capability of the friction in all static loads, and the rate of change of load plays a major significant [2].

PLA reinforced material is obtained for 3D printed specimens where biocarbon material can be used for mechanical applications and improved the performance of the structured material. The particle distribution of the material are in homogenous and while extrusion through nozzle was highly imparted in 3D printing. The surface of the PLA material has many advantages and increases the volume of the printed biocarbon material [3]. The formation of the phase composition of a wear characteristics has a fragment structure, layers depend upon the pressure of the nozzle friction and speed intensity of the flow material, and the printing conditions of a specimen are observed. Using the low-carbon and copper materials in the printing, the wear samples have observed the friction and magnitude of the printed sample and explain the surface nature [4]. Polymer materials such as PLA produce the prototyping of the samples using Fused Deposition Method (FDM) technology and depend upon the infill density. The samples are printed by varying the infill density and American Society for Testing and Materials (ASTM) standard; the mechanical properties

P. Sneha · K. Balamurugan (✉)
Department of Mechanical Engineering, VFSTR (Deemed to be University), Guntur, Andhra Pradesh 522213, India
e-mail: kbalan2000@gmail.com

were evaluated and improve the printing condition [5, 6]. The orientation of the 3D printed samples can be manufactured with mechanical behaviour and layer thickness to investigate the layer thickness and layer orientation [7, 8]. The possibilities of reinforcement material imply in various engineering fields. By varying the parameters such as load, track diameter and speed with a sliding distance in an apparatus, the wear rate and friction rate were investigated. It indicates the reinforcement material has a significant improves the behaviour of the wear in a polymer composite and analyse the wear mechanism for different composite [9].

The matrix nature of the 3D printed samples is reinforced with polyester material. By varying the load and distance, the wear characteristics were performed [10–15]. Orientation of the sample is predominated and compared by varying the load, speed and distance.

This study explains the extrusion process in 3D printing using FDM conditions, PLA-14% Bz material characterized the performance of load, track diameter and speed getting the wear behaviour, and the properties of the material are studied and documented.

2 Materials and Methods

2.1 Wear Set-Up Description

To analyse the friction and wear behaviour, a pin-on-disc tribometer T-201was employed, and the printed parameters on PLA-14% Bz composite filament were used. The schematic apparatus is shown in Fig. 1a, and detailed observation is shown in Fig. 1b.

The disc is made up of EN31 hardened steel to 60 Hardness Rockwell C scale (HRC), and surface roughness is 1.6 Ra of maximum wear length of 80 mm with a thickness of 8 mm. The specimen was placed in the specimen holder and a stationary pin clammed with a rotating disc. The load, track diameter and speed were varied and concluded the coefficient of friction and wear.

Fig. 1 **a** Pin-on-disc tribometer set-up. **b** Specimen set-up

2.2 Experimental Procedure

As per the ASTM G99-95 standard was considered to perform the wear characterization. The requirement of the wear specimen is rectangular shape, of size 30×8 mm^2. They were cut and performed the printed composite specimen. As shown in Fig. 2, the PLA-14% Bz specimen is clammed with counter face sliding motion. Before performing the wear, first the specimen is checked with the required dimension and the surface of the specimen was cleaned with the emery papers of different sizes such as P220 as coarse grain and 2/0 as fine grain to check the surface and to maintain the constant roughness of the specimen. The rotating disc is cleaned with acetone and dried before starting the experiments, and the specimen is clammed to check the contact surface of the rotating disc in counter face direction.

As the observation starts between the rotating disc and specimen, the sliding friction occurs tangentially to the specimen where the track diameter, speed and the load are varied. The values of frictional force and wear were plotted in the graph to evaluate the coefficient of friction as stated below:

Coefficient of friction:

$$\mu = \frac{F_f}{F_n}$$

where

F_f = "frictional force" (N) and
F_n = "normal force" (N).

While measuring the initial and final values of the required specimens, changing the track diameter is in mm (40, 50, 60), speed is in rpm (400, 500, 600), and load is in N (20, 30, 40); the material removal rate is calculated. By calculating the material
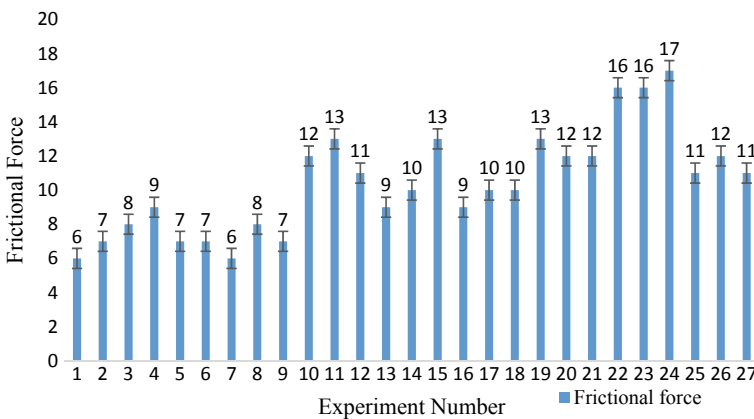
Fig. 2 Frictional force

Table 1 Printing conditions of a FDM parameters

S. No.	Factors	Levels		
		1	2	3
1	Load (N)	20	30	40
2	Track diameter (mm)	40	50	60
3	Speed (rpm)	400	500	600

removal rate (MRR), the rate of wear and frictional force was obtained. For each and every observation, the disc is cleaned with acetone and dried. The surface of the specimen was machined fully, so as to complete contact with the disc; the specimen was stable to the apparatus perpendicular to the disc. By an electronic balance with the least count of ±0.01 mm, weight of the specimen was calculated before and after the working condition where the load, track diameter and speed can be varied by the conditions. Table.1 shows the printing conditions of a FDM for a wear.

The frictional force of a PLA-Bz filament was printed at various conditions to optimize the values by considering the three different levels and to determine the orthogonal network (L27) to get the output response as stated in Fig. 2. The overall performance of the frictional force results that the values are particularly sizeable and decrease the friction. The impact of the frictional force is depending on the surface contact of the specimen and sliding distance. By increasing the number of levels, the friction force is reduced with respect to speed. At different experiment conditions, the maximum friction force is occurred, in between 22 and 24 where the material property was highly influenced with the effect of sliding speed.

The wear rate of the PLA-Bz matrix material was performed as shown in the Fig. 2; the rate of wear is consequently changed by varying the track diameter and speed. The maximum wear rate can be occurred at 27 levels, and the condition of the specimen progressively changes by sliding the surface and depends upon the load applied on the disc. To optimize the conditions, L27 network is considered by varying the variables and number of levels. The formation of the matrix can be analysed by considering the track diameter and speed.

3 Result and Discussion

3.1 Grey Relational Analysis (GRA)

The GRA technique is obtained for analysing the complexity and the multi-input response. The correlation between the factors, level of geometry which is known as a grey relation degree and the correlation degree between the (S/N) signal to noise ratio and normalization. This results, quality of a response and describes the behaviour of the material and the inter-correlation between the wear and friction factors and

to optimize the characteristics and ranking the grey relation coefficient. The steps involved for the estimation of the grey correlation degree are given below.

3.1.1 Normalization and S/N Ratio

Smaller the better:

$$\frac{S}{\text{NSB}} = -10 \log 10 \left[\frac{1}{n} \left(\sum_{i=1}^{n} y_{ij}^2 \right) \right] \tag{1}$$

where y_{ij} is the ith value analysed of the jth test, and 'n' is the overall value.

The process of grey relation analysis is associated with data recorded and the 'n' value is among '0' and '1' to normalize; the wide variety of number of objects are eliminated, and the observation values are minimized. Consistency explains the better results.

Smaller the best

$$X_{ij} = \frac{\left[\max_j y_{ij} - X_{ij} \right]}{\left[\max_j y_{ij} - \min_j y_{ij} \right]}$$

The calculation of the S/N ratio and normalization is shown in Table 2.

3.1.2 Grey Relation Coefficient and Grade

The grey relation coefficient explains the experiment's actual levels, and the results show that the objective feature is emphasized.

$$\delta_{ij} = \frac{\min_i \min_j \left| X_i^0 - X_{ij} \right| + \zeta \max_i \max_j \left| X_i^0 - X_{ij} \right|}{\left| X_i^0 - X_{ij} \right| + \zeta \max_i \max_j \left| X_i^o - X_{ij} \right|} \tag{3}$$

For output performance, the grey relational coefficient is calculated from the relation given below:

$$Y_j = \frac{1}{m} \sum \zeta_{ij} \tag{4}$$

The grey relation coefficient is calculated from Eq. (4) and tabulated in Table 3; accordingly, the grey grade and rank are tabulated.

Table 2 Normalization and S/N ratio

Exp. No.	S/N ratio		Normalization	
	Wear (mm)	μ (N)	Wear (mm)	μ (N)
1	−17.942039	−1.249387	0.091157	−0.71591
2	−18.355731	−2.588323	0.111158	−0.65118
3	−18.750613	−3.748162	0.13025	−0.5951
4	−17.507654	−4.771213	0.070155	−0.54564
5	−17.050397	−2.588323	0.048047	−0.65118
6	−16.056641	−2.588323	0	−0.65118
7	−18.355731	−1.249387	0.111158	−0.71591
8	−18.555416	−3.748162	0.120812	−0.5951
9	−18.355731	−2.588323	0.111158	−0.65118
10	−25.510884	−7.269987	0.4571	−0.42482
11	−25.421797	−7.965229	0.452793	−0.39121
12	−25.510884	−6.514216	0.4571	−0.46136
13	−31.442397	−4.771213	0.743881	−0.54564
14	−31.487055	−5.686362	0.74604	−0.50139
15	−31.575687	−7.965229	0.750325	−0.39121
16	−19.311187	−4.771213	0.157353	−0.54564
17	−19.490284	−5.686362	0.166012	−0.50139
18	−19.12832	−5.686362	0.148512	−0.50139
19	−22.833012	−7.965229	0.327629	−0.39121
20	−23.070997	−7.269987	0.339135	−0.42482
21	−23.187588	−7.269987	0.344772	−0.42482
22	−29.876663	−9.768762	0.66818	−0.30401
23	−29.930114	−9.768762	0.670764	−0.30401
24	−30.036041	−10.295341	0.675886	−0.27855
25	−36.690929	−6.514216	0.997641	−0.46136
26	−36.666428	−7.269987	0.996456	−0.42482
27	−36.739727	−6.514216	1	−0.46136

3.1.3 Analysis of Grade Relationship

Grade relation grade (GRG) settings are used to determine the orthogonal network. GRG with a greater value is thought to be more efficient. The multiple responses lead to provide the network of the second experimental state. The values are plotted in the Table 4.

The input parameters for machining conditions for load at level '3', the track diameter at level '3' and speed at level '1' based on GRG are displayed in Fig. 3. All observations have the necessary values to calculate the final responses. The maximum

Table 3 GRA and ranking

Exp. No.	Grey relation coefficient		Grey relational grade (GRG)	Rank
	Wear (mm)	μ (N)		
1	0.523877	0.368201	0.446039	25
2	0.529425	0.377191	0.453308	22
3	0.534831	0.385342	0.460086	19
4	0.518176	0.392829	0.455503	21
5	0.512307	0.377191	0.444749	26
6	0.5	0.377191	0.438596	27
7	0.529425	0.368201	0.448813	24
8	0.532145	0.385342	0.458743	20
9	0.529425	0.377191	0.453308	22
10	0.64813	0.412401	0.530266	11
11	0.646326	0.418198	0.532262	10
12	0.64813	0.406279	0.527205	12
13	0.796103	0.392829	0.594466	7
14	0.797474	0.399778	0.598626	5
15	0.800208	0.418198	0.609203	4
16	0.542698	0.392829	0.467763	18
17	0.54526	0.399778	0.472519	16
18	0.540106	0.399778	0.469942	17
19	0.597953	0.418198	0.508076	14
20	0.602096	0.412401	0.507249	15
21	0.604146	0.412401	0.508274	13
22	0.750852	0.434026	0.592439	9
23	0.752312	0.434026	0.593169	8
24	0.755222	0.438875	0.597049	6
25	0.997646	0.406279	0.701963	3
26	0.996469	0.412401	0.704435	1
27	1	0.406279	0.703139	2

Table 4 GRG response table

Annotations	Printing parameters	Response Table			Delta
		L1	L2	L3	
A	Load (N)	0.4510	0.4970	**0.5058**	0.0548
B	Track diameter (mm)	0.5336	0.5471	**0.5598**	0.0262
C	Speed (rpm)	**0.6018**	0.5423	0.5208	0.081
Error		0.1507	0.0501	0.0540	0.0967

Higher the level value shows significant effect. Here the bold letters means, at level 3 of load and track diameter; level 1 of speed is the optimum machining conditions
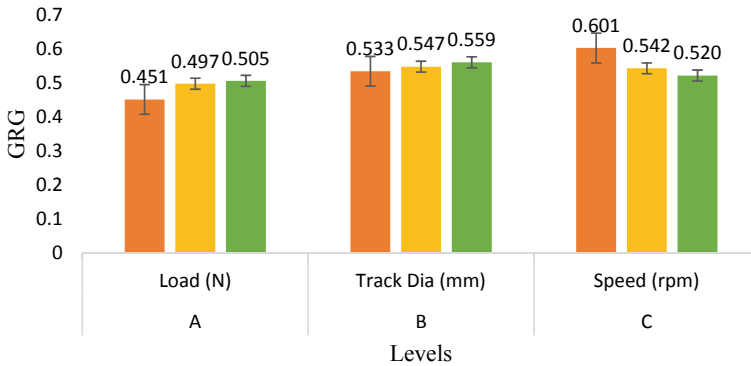
Fig. 3 Grey relations grade versus levels

load is significantly higher than the remaining loads which have greatly influenced on the printing condition of the specimen.

Coefficient of friction is highly influenced on the wear rate of the required machining conditions [13], and the GRG approach is considered for the optimizing levels in the response table as shown in the Table 4.

4 Conclusion

The wear behaviour of the PLA/bronze composite is printed using FDM technique. The maximum load imparts the high efficiency of the track diameter with respect to speed. The sliding distance can be varied and plays a key role, for finding the composite properties of a material, and layer height and layer thickness depend upon the printing condition and the structure of a specimens. The significance of the material is improved by the strength of the layer thickness and temperature resistant. It improves the properties of a composite material, and structure is more effective.

Future Scope of Work

1. Study the wear characteristics by varying the different percentages of bronze with the combination of PLA.
2. Prepare the material by changing the manufacturing techniques to check the suitable method.
3. Adopting different optimizing techniques to get a better wear rate with good accuracy.

References

1. Almajid, A.A.: Mechanical, physical and wear properties of 3D printed polylactic acid materials. Key Eng. Mater., 118–125 (2020)
2. Betancourt-Dougherty, I.C., Smith, R.W.: Effects of load and sliding speed on the wear behaviour of plasma sprayed TiC-NiCrBSi coatings. Wear 147–154 (1998)
3. Ertane, E.G., Reisel, A.D., Baran, O., Welzel, T., Matner, V., Svoboda, S.: Processing and wear behavoir of 3D printed PLA reinforced with biogenic carbon. Adv. Tribol. **11** (2018)
4. Garbar, I.I.: The effect of load on the structure and wear of friction pair materials (example of low-carbon steel and copper). Wear 240–245 (1997)
5. Gunasekaran, K.N., Aravinth, V., Muthu Kumaran, C.B., Madhankumar, K., Pradeep Kumar, S.: Investigation of mechanical properties of PLA printed materials under varying infill density. Mater. Today Proc. (2020)
6. Hemalata, J., Arun Kumar, P., Mihir Kumar, P.: Study of slod particle erosion wear behaviour of bamboo fiber reinforced polymer composite with cenosphere filler. Adv. Polym. Technol., 21718–21226 (2015)
7. Hervan, H.Z., Altnkayanak, A., Parlar, A.: Hardness, friction and wear characteristics of 3D-printed PLA polymer. J. Eng. Tribol., 1–9 (2020)
8. Narendiranath Babu, T., Chauhan, M., Alam, M.I., Shah, J.: Improving wear properties of musti kusa grass fiber reinforced with aluminium oxide and silicon carbide. Mater. Today Proc., 13003–13009 (2017)
9. Pramendra Kumar, B., Inderdeep, S., Jitendra, M.: Tribological behavior of natural fiber reinforced PLA composites. Wear, 829–840 (2013)
10. Singh, R., Kumar, S., Bedi, P., Hashmi, M.S.J.: On wear of 3D printed Al_2O_3 reinforced Nylon6 matrix based functional prototypes. Mater. Today Proc. 2214–7853 (2019)
11. Singh, R.K., Telang, A., Das, S.: The influence of abrasive size and applied load on abrasive wear of Al-SiCp composite. Arbian J. Sci. Eng. (2021)
12. Srinivasan, R., Aravind Kumar, N., Aravind Krishna, S., Aadhishwaran, S., John, G.: Influence of fused deposition modelling process parameters on wear strength of carbon fibre PLA. Mater. Today Proc. (2020)
13. Siva Surya, M., Gugulothu, S.K.: Fabrication, Mechanical and Wear Characteristics of Silicon Carbide Reinforced Aluminium 7075 Metal Matrix Composite (2021)
14. Thomsorn, S., Mathurosemontri, S., Nagai, S., Hamada, H.: Investigation of friction and wear behavior of polyoxymethylene/poly (lactic acid) blends. Key Eng. Mater., 229–234 (2017)
15. El-Tayeb, N.S.M., Yousif, B.F., Yap, T.C.: An investigation on worn surfaces of chopped glass fibre reinforced polyester through SEM observations. Tribol. Int., 331–340 (2008)

Tribological Properties of Metal Particulate Reinforced Polymeric Functionally Graded Materials

Vasavi Boggarapu, Raghavendra Gujjala, Shakuntala Ojha, Rakesh Kanakam, Somaiah Chowdary Mallampati, and Praveen Kumar Jatothu

1 Introduction

Polymer composites play a significant role in various engineering applications owing to their superior mechanical and tribological characteristics [1–3]. Metallic components such as gears, bearings and seals are now being replaced by reinforced composites due to their self-lubricating property [4, 5]. However, composites have a delamination failure where the fibers detach from matrix at elevated temperatures. To overcome this, researchers have introduced advanced composites which are referred as functionally graded materials (FGMs). The composition or microstructure of constituents varies gradually in specific directions to achieve unique material properties as opposed to homogeneous composites [6]. Variation in properties enables FGMs to withstand coarse environmental conditions with reduced failures during service. Hence, it is essential to study the tribological characteristics. Materials having poor tribology properties generate wear during operating conditions which reduce the performance of machinery components. In a tribosystem, friction and wear are the responses and with coefficient of friction (COF) represent the state of contact between the bodies. Different types of wear such as adhesive, corrosive, abrasive, fatigue and erosion were reported in the materials. Among them, abrasive wear is responsible for 63% of total wear cost. Therefore, it is necessary to evaluate abrasive wear properties [7]. This wear can be classified as two-body and three-body abrasive wear depending on contact medium. When a harder body removes material from the

V. Boggarapu · R. Gujjala (✉) · R. Kanakam · S. C. Mallampati · P. K. Jatothu
Department of Mechanical Engineering, National Institute of Technology, Warangal,
Warangal 506004, India
e-mail: raghavendra.gujjala@nitw.ac.in

S. Ojha
Department of Mechanical Engineering, Kakatiya Institute of Technology and Science,
Warangal 506015, India

surface of softer body, then two-body abrasive occurs. The removed material in the form of wear debris acts as an abrasive between contacting surfaces in three-body abrasive wear. This wear is identified by grooves and scars on the worn-out surfaces, and wear mechanism was characterized as micro-plowing, cracking and cutting.

Researchers have developed polymer FGMs with various filler particles like TiO_2, Al_2O_3, CNT's, fly ash, SiC, etc. [8–12]. On the other hand, polymers in combination of electro-conducting fillers like aluminum, silver, nickel and copper were being practically used in several applications [13]. Among the thermoset polymers, epoxy resin is most popularly used polymeric matrix in advanced composites due to its high stiffness, adhesion strength, chemical resistive and least shrinkage. Mechanical characteristics of epoxy components depend on curing time and temperature [14]. Inclusion of different reinforcements enhances the strength and wear resistance of pure epoxy. Processes like centrifugal casting, compression molding, stir casting, hand lay-up and hot isostatic pressing were adopted in manufacturing of polymer FGMs [15]. Owing to low cost and fabrication ease, hand lay-up is extensively used. However, to obtain layer homogeneity and good interfacial bonding between the layers, curing temperature must be provided.

Concerning this, the aim of present research is to fabricate epoxy-based FGMs reinforced with aluminum (Al) and copper (Cu) particles using hand lay-up technique for tribological applications. The study was carried out at dry sliding and coarse environment to evaluate wear rate and coefficient of friction (COF) of two different FGMs. Dominant wear mechanisms on worn-out surface of samples were observed using Scanning Electron Microscopy (SEM).

2 Experimentation

2.1 Raw Materials

Metallic fillers like copper and aluminum of 99% purity having 44 μm particle size each, purchased from SRL Chemicals Pvt. Ltd., India, were used as reinforcement. Morphology of filler particles was observed using SEM. Al shows spherical shaped, while Cu particles have dendritic structures as represented in Fig. 1. Epoxy resin (LY 556) was used as polymeric matrix and Aradur (HY 951) as a hardener. To obtain gradation along thickness direction of PFGMs, four different layers with varying filler content from 5 to 20% were chosen in the study. Thickness of each layer was maintained constant to achieve layered homogeneity. Table 1 presents the composition of elements and thickness of each layer. For the ease of understanding, two types of FGMs samples were represented as FG-Al and FG-Cu.
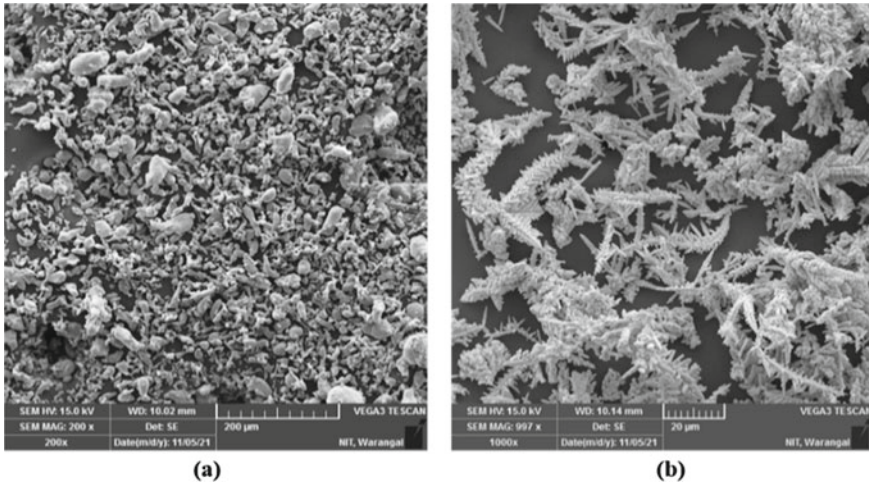
Fig. 1 Morphology of **a** aluminum particles **b** copper particles

Table 1 Composition of PFGMs at individual layers

No. of layer	FG-Al	FG-Cu	Thickness of layer (mm)
	Vol % of Al/epoxy (%)	Vol % of Cu/epoxy (%)	
4 (top)	20/80	20/80	7.5
3 (middle)	15/85	15/85	7.5
2 (middle)	10/90	10/90	7.5
1 (bottom)	05/95	05/95	7.5

2.2 Fabrication of Samples

Using hand lay-up methodology, the PFGM samples were fabricated in a cylindrical molds made up of polypropylene. The weight of constituents for each layer was measured and mixed in individual containers using mechanical stirrer to achieve uniform distribution. Initially, bottom layer having 5% filler was poured in the mold and thermally cured in autoclave at 60°. Similarly, the subsequent layers were impregnated into a mold and cured successively. The cured samples were removed from the molds to obtain final specimens as shown in Fig. 2b.

2.3 Tribological Testing

Following ASTM G99-17 standards [15, 16], abrasive wear testing was performed on pin-on-disk test rig as depicted in Fig. 2a. The test apparatus consists of stationary
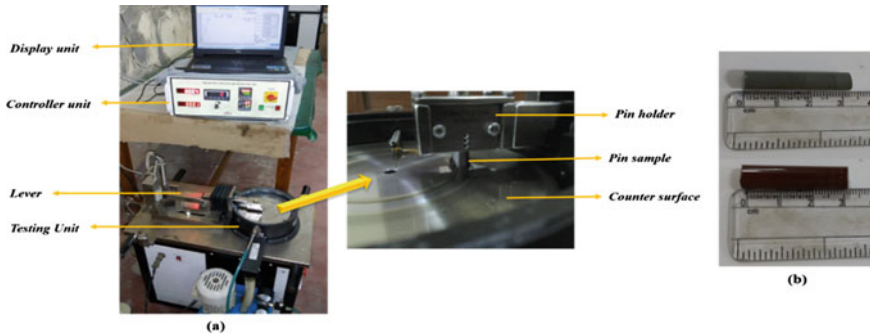
Fig. 2 **a** Pin-on-disk test apparatus. **b** Fabricated samples

pin on which normal load is applied with the help of lever and is pressed against rotating disk (counter surface). The pin sample is having diameter of 10 mm and height of 30 mm. Here, disk was made of EN 31 steel material with diameter and thickness of 165 mm and 8 mm, respectively. The apparatus mainly comprises testing unit, controller and display unit. Testing unit includes lever, pin holder and Linear Variable Differential Transformer (LVDT) sensors to measure wear and frictional force. Controller unit helps to control the motor speed, and display unit presents the readings of friction coefficient, wear and frictional force through a computer. Experiment was carried out in room temperature to minimize environmental effects.

To study the abrasive wear behavior of PFGMs on coarse surface, samples were tested against P320 grit silicon carbide paper pasted onto the rotating disk. Samples were rotated at fixed speed of 300 rpm and constant sliding distance of 500 m by adjusting the corresponding test duration. Experiments were conducted at 5 and 10 N loading conditions. After every test, acetone was used to clean sample in order to wipe out wear debris from the surface. A well-calibrated analytical balance having least count of ± 0.0001 gm was used to measure the weight loss. Each experiment is repeated on five identical samples, and their average values were recorded. Wear rate was estimated as $\Delta w / \rho L$, where Δw represents the weight loss of sample (in gm), ρ is density (gm/cm^3), and L denotes sliding distance (m). As the samples were graded along the direction of thickness, the test was conducted at top (layer 4) and bottom (layer 1) layers only, rather than at layers 2 and 3 to evaluate tribological characteristics.

3 Results and Discussion

Figure 3 shows the wear rate of FG-Al and FG-Cu at layers 1 and 4 subjected to constant sliding distance of 500 m and different loading conditions. Due to variation in filler content, samples exhibit different wear rate at individual layers. Irrespective of loading conditions, the wear rate of FG-Cu was higher than FG-Al samples. This
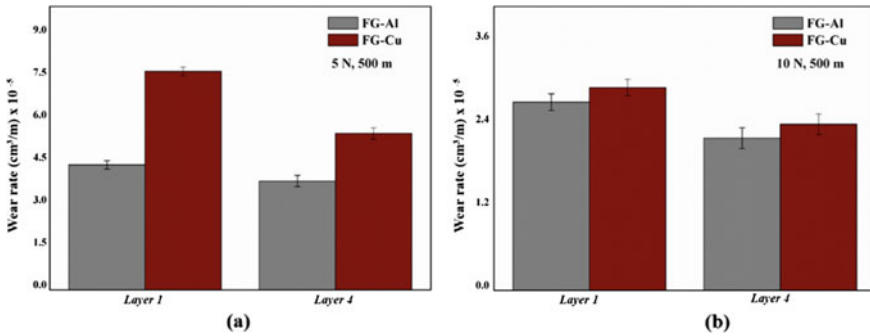
Fig. 3 a–b Wear rate of FG-Al and FG-Cu at layers 1 and 4 for 5 N and 10 N loading conditions, respectively

may be due to the hardness of copper which is greater than aluminum. Besides, the test was performed on 320 grit abrasive paper which comprises coarse particles. Sliding of harder particles on coarse paper resulted in greater wear loss. Moreover, presence of coarse abrasive grit leads to inadequate contact with the Cu particles by developing high stresses which resulted in greater wear. Wear rate of FG-Cu was 40% higher than FG-Al at first layer in 5 N loading condition. Effect of load on abrasive wear of FGMs samples was shown in Fig. 3a, b.

It was observed that wear loss tends to decrease with an increase in load from 5 to 10 N. As the filler particles are ductile in nature, they undergo large plastic deformation with increase in applied pressure during test. Thus, wear rate decreases with an increment in applied load. Furthermore, wear rate at layer 4 was lower than layer 1 for all the test samples. At high filler content, particles form clustering within the matrix, and during loading, these particles detach from the surface and get accumulated on counter surface. These wear debris may act as lubricating layer, thereby decreasing the wear loss. Wear rate of FG-Al at layer 4 was 12.5% and 8.69% lesser as compared to layer 1 for 5 N and 10 N loading, respectively, whereas abrasive wear of FG-Cu at layer 4 was reduced by 33.3% and 17.39% than layer 1 at 5 N and 10 N load, respectively. Variation in the abrasive wear rate at different layers of individual test samples confirms the filler gradation. The obtained results followed a similar trend as reported by Srivastava et al. [17] and Suresha et al. [18].

The opposing frictional force between pin sample and counter surface was also measured during experimentation. Coefficient of friction between sliding surfaces was obtained by dividing frictional force with the applied load on sample. COF of FG-Al and FG-Cu samples at different loading conditions was shown in Fig. 4a, b. At high filler loading (layer 4), COF was observed to be lower as compared to low filler content (layer 1). This may be due to the formation of softer wear debris which act as lubricant at contact surfaces resulting in less COF. There exists only little variation in COF among different layers indicating no inclusions or defects at the surfaces. Furthermore, frictional coefficient gets increases with an increase in applied pressure. At higher loading condition, filler particles were pressed against
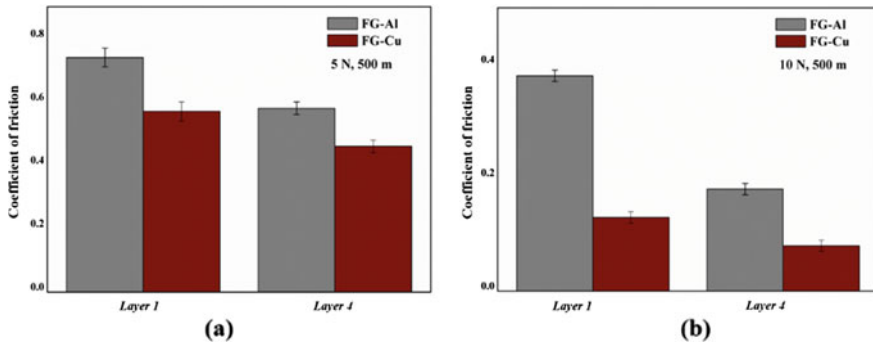
Fig. 4 a–b COF of FG-Al and FG-Cu at layers 1 and 4 for 5 N and 10 N loading conditions, respectively

the coarse grit which may result in heat generation and thereby increase COF. The average COF for FG-Cu was reported to be lower than FG-Al samples. Thus, Cu particles were more efficient in reducing friction than Al.

Figure 5a, b represents the worn-out surfaces on P320 grit abrasive paper at 5% filler loading of FG-Cu samples. Formation of deep grooves was observed on the surface which signify the greater material loss. When the samples slide against abrasive surface, the coarser particles get penetrated into the pin samples causing plowing as seen from Fig. 5c. Due to cutting action, abrasive lines were clearly visible on the surfaces. At 20% filler loading, narrow grooves were seen on surface of FG-Cu samples (see Fig. 5d). The broken filler particles detach from the matrix and stick to the abrasive paper acting as a lubricant which reduces the wear rate.
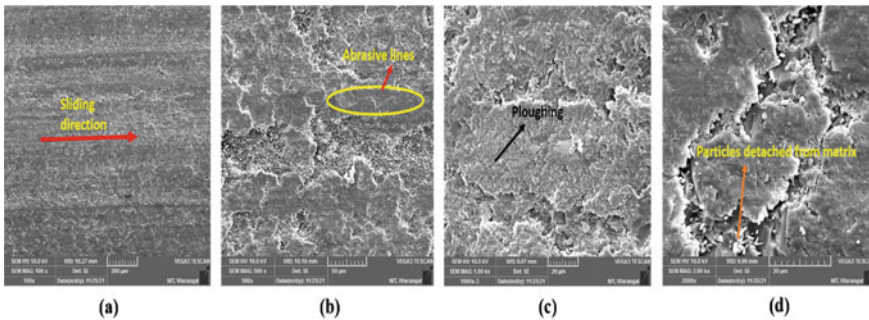
Fig. 5 SEM micrographs depicting the failure mechanisms of FGMs samples

4   Conclusions

In the present research, polymeric functionally graded materials were fabricated using epoxy matrix and aluminum and copper as filler particles (FG-Al and FG-Cu). Gradation along thickness direction was achieved in conventional hand lay-up methodology by providing the curing temperature of 60°. Tribological characteristics such as wear rate and coefficient of friction at different layers were evaluated, and comparison is made among the test samples. From the experimental results, following conclusions were drawn.

- Wear rate of FG-Cu samples was higher than FG-Al due to hardness of copper particles. Furthermore, the COF of FG-Cu was lower than FG-Al indicating the capability of Cu in reducing friction as compared to Al.
- Irrespective of loading conditions, wear rate at layer 4 was lower than layer 1 due to the presence of high filler loading, which acts as a lubricant between sliding surfaces.
- Worn-out surface examination revealed the abrasive wear mechanism caused by coarser counter surface on the PFGM samples.

References

1. Mangalgiri, P.D.: Composite materials for aerospace applications. Bull. Mater. Sci. **22**, 657–664 (1999)
2. Dixit, S., Goel, R., Dubey, A., Shivhare, P.R., Bhalavi, T.: Natural fibre reinforced polymer composite materials-a review. Polym. Renew. Resour. **8**, 71–78 (2017)
3. Chowdary, M.S., Raghavendra, G., Kumar, M.N., Ojha, S., Boggarapu, V.: Influence of nano-silica on enhancing the mechanical properties of Sisal/Kevlar fiber reinforced polyester hybrid composites. Silicon, 1–8 (2020)
4. Singh, A.K.: A novel technique for in-situ manufacturing of functionally graded materials based polymer composite spur gears. Polym. Compos. **40**, 523–535 (2019)
5. Singh, A.K.: Siddhartha, Development and investigation on transmission efficiency of functionally graded material-based polybutylene terephthalate spur gears. Proc. Inst. Mech. Eng. Part J J. Eng. **234**, 473–489 (2020)
6. Boggarapu, V., Gujjala, R., Ojha, S., Acharya, S., Chowdary, S., Gara, D.K.: State of the art in functionally graded materials. Compos. Struct., 113596 (2021)
7. Babu, P.V., Ismail, S., Ben, B.S.: Experimental and numerical studies of positive texture effect on friction reduction of sliding contact under mixed lubrication. Proc. Inst. Mech. Eng. Part J J. Eng. **235**, 360–375 (2021)
8. Mishra, S.K., Shukla, D.K., Patel, R.K.: Effect of particle morphology on flexural properties of functionally graded epoxy-alumina polymer nanocomposite. Mater. Res. Expr. **6**, 1250i9 (2020)
9. Patnaik, A., Bhatt, A.D.: Mechanical and dry sliding wear characterization of epoxy–TiO_2 particulate filled functionally graded composites materials using Taguchi design of experiment. Mater. Des. **32**, 615–627 (2011)
10. Kurd, S.M., Hassanifard, S., Hartmann, S.: Fracture toughness of epoxy-based stepped functionally graded materials reinforced with carbon nanotubes. Iran Polym. J. **26**, 253–260 (2017)

11. Doddamani, M., Shunmugasamy, V.C., Gupta, N., Vijayakumar, H.B.: Compressive and flexural properties of functionally graded fly ash cenosphere–epoxy resin syntactic foams. Polym. Compos. **36**, 685–693 (2015)
12. Krumova, M., Klingshirn, C., Haupert, F., Friedrich, K.: Microhardness studies on functionally graded polymer composites. Compos. Sci. Technol. **61**, 557–563 (2001)
13. Xu, Y., Chung, D.D.L., Mroz, C.: Thermally conducting aluminum nitride polymer matrix composites. Compos. Part A Appl. Sci. Manuf. **32**, 1749–1757 (2001)
14. Fu, S.Y., Feng, X.Q., Lauke, B., Mai, Y.W.: Effects of particle size, particle/matrix interface adhesion and particle loading on mechanical properties of particulate-polymer composites. Compos. Part B Eng. **39**, 933–961 (2008)
15. Stabik, J., Dybowska, A.: Methods of preparing polymeric gradient composites. J. Achiev. Mater. Manuf. **25**, 67–70 (2007)
16. Syed, I., Beera, S.B.: Influence of positive texturing on friction and wear properties of piston ring-cylinder liner tribo pair under lubricated conditions. Ind. Lubr. Tribol. **71**, 515–524 (2019)
17. Srivastava, V.K., Verma, A.: Mechanical behaviour of copper and aluminium particles reinforced epoxy resin composites. Am. J. Mater. Sci. **5**, 84–89 (2015)
18. Suresha, B., Ravi Kumar, B.N.: Two-body abrasive wear behavior of particulate filled polyamide66/polypropylene nanocomposites. J. Appl. Polym. Sci. **119**, 2292–2301 (2011)

Comparative Study on Microhardness of the Electroless ZnO and SiC Reinforced Ni–P Coatings

Vinod Babu Chintada, Sudhakar Uppada, and M. Vykunta Rao

1 Introduction

Surface coating is the process in which surface of the material is coated partially or fully for the functional and decorative purposes. In this, the surface is coated with film-forming materials along with additives, pigments, and solvents to fulfill the preferred mechanical properties. Electroless nickel coatings (EN) are extensively used in various fields of engineering because of their excellent tribological and mechanical properties, since it is introduced by Brenner and Riddell in 1946. In this, without the electric current nickel alloy is coated on the substrate by using an aqueous solution. Electroless nickel coating is an auto-catalytic process, Ni^{2+} gets oxidized and reduced, and nickel ions are coated on the substrate. Among the several surface deposition techniques, electroless Ni–P coatings gain more interest due to low cost and uniform thickness generated over complex geometries. Hypophosphite reducing agent reduces the Ni ions from the metal source to produce the Ni–P coatings. Reports confirm that Ni–P coatings enhance corrosion resistance and hardness of steels [1, 2]. The heat treatment method significantly alters the mechanical properties of electroless nickel coatings. Hard crystalline Ni_3P phase developed up to 400 °C temperature, which enhances the properties of the deposit. Above 400 °C, the growth of coarse structure impedes the coating's characteristics. To create Ni–P composite coatings, a soft and hard secondary particle is impinged into the Ni matrix [3, 4]. The tribological and mechanical characteristics of Ni–P coats are improved by introducing secondary phase particles of macro-, micro-, and nanosizes to the Ni–P lattice. The wear, resistance to corrosion, and hardness of coatings are enhanced by the co-deposition of diverse ceramic hard second-phase particles. The reduction in

V. B. Chintada (✉) · S. Uppada · M. Vykunta Rao
Department of Mechanical Engineering, GMRIT, Rajam, A.P. 532127, India
e-mail: vinodbabu.chintada@gmail.com

surface tension and increase in the wettability of the particles with increasing surfactant increase the deposition rate of the secondary particles [5, 6]. The dispersion rate of the PTFE particles is maximum in the presence of polyoxyethylene nonyl phenyl type non-ionic surfactant. PTFE particle deposition rate increases with an increase in the surfactant (fluorinated alkyl quaternary ammonium iodides) concentration up to 200 μmole/L [7, 8].

Ni–P-coated mild steel microhardness is increased by 13% by incorporating nano-Al_2O_3 particles into the nickel lattice [9]. Intermetallic products such as Al_3Ni_2, Al_3Ni, nickel silicide, and crystalline Ni_3P are formed at 400 °C/h, which improves the hardness, wear, and adhesion of Ni–P/Al_2O_3/SiC coatings [10, 11]. The hardness of Ni-W-P-Al_2O_3 (6 g/L) coatings is slightly equivalent to Ni-P-W coatings in as-plated circumstances, according to Balaraju et al. [12]. Up to 400 °C, annealing temperature improvement in microhardness is noticed in Ni-P-W coatings, whereas hardness is enhanced in Ni-W-P-Al_2O_3 coatings up to 500 °C annealing temperature. The addition of copper to a Ni-W-P deposit increases the size of the grains from 2.5 to 8.8 nm, lowering the coating hardness. Copper co-deposition reduces the Ni-W-P coating's microhardness by 7% [13]. The optimal number of reinforcing particles to generate a homogeneous Ni-P-SiO_2-MoS_2 coating was determined to be 7 g/L. The wear resistance of the annealed sample has been increased by combining hard Ni_3P and SiO_2 phases, where activating the sliding mechanism by MoS_2 phase reduces the friction coefficient of the non-heat-treated sample [14]. The wear loss in Ni-P-SiC-Gr coatings increases as Gr concentration increases. The Ni-P-SiC-Gr coating has a maximum wear loss of 25.69×10^{-6} g/m at a Gr concentration of 12 g/L [15]. After CNT [16] inclusion to the coating matrix, the Ni-P-Cu coating microhardness was enhanced by 140%. The formation of Ni_3P and Cu_3P phases at 400 °C improves the coating microhardness even further. Most of the researchers focus on the influences of various oxide and carbide particles reinforcement on the characteristics of the EN coatings. Only a few studies have been done on ZnO and SiC reinforced Ni–P coatings. Literature is very limited on comparative analysis among the carbide and oxide particle reinforced EN coatings. Present investigation EN coatings are formed by reinforcing one oxide (ZnO) and carbide (SiC) particles into the alloy matrix individually. This research aimed to compare the microhardness of SiC and ZnO reinforced Ni–P coatings prior to and after annealing. Comparative analysis is conducted between the coatings to know the good hardness resistive particles to achieve better Ni–P composite coating with superior microhardness.

2 Experimental Procedure

Mild steel plate with surface area 15×15 mm^2 was considered a substrate material for the fabrication of electroless coatings. To achieve a mirror polished surface, substrate material was abraded using 100, 220, 320, and 420 grades of SiC grained sheets. To remove unwanted oil and dust particles, substrate surface was rinsed with acetone and deionized water. Pretreated substrate was activated in diluted HCl solution for 60 s

Table 1 Electroless solution elemental composition

Coating bath elements	Concentration (g/L)
Nickel chloride (NiCl$_2$)	40.0
Sodium hypophosphite (NaPO$_2$H$_2$)	20.0
Ammonia chloride (NH$_4$Cl)	50.0
Trisodium citrate (Na$_3$C$_6$H$_5$O$_7$)	25.0
SDS	0.60
Zinc oxide/silicon carbide (ZnO/SiC)	1.0–3.0
Temperature	88 ± 2
pH	4.50–5.50

before immersion into the electroless solution to achieve better adhesion. Suitable chemical bath, as shown in Table 1, was selected from past literature to develop Ni–P composite coating [17, 18].

Pretreated substrate is immersed into the EN solution alone for 60 min to create Ni–P film, which enhances the adhesion strength of Ni-P-SiC/ZnO coating. The Ni–P-coated surface is then submerged in a solution containing ZnO/SiC nanoparticles for 120 min to generate a Ni-P-SiC/ZnO film. The coating solution was heated using a constant temperature oil bath apparatus. Throughout the deposition process, solution volume was upheld at a fixed value of 150 ml. Pen-type pH meter is used to monitor the solution pH value at regular intervals. To know the result of annealing process on microhardness of the developed deposit, thermal process is carried out at 400 °C temperature. The deposit microhardness was determined before and after heat treatment by means of a Vickers microhardness tester at a 100 g load and dwell duration of 10 s. An average of 5 readings are carried out at various locations on the coating to quote the microhardness value. Schematic representation of experimental setup is shown in Fig. 1.

3 Results and Discussions

Individual incorporation of ZnO and SiC particles to the Ni lattice enhances the hardness of the deposit. The microhardness of Ni-P-ZnO/SiC coatings made at various ZnO and SiC particle concentrations is represented in Fig. 2.

Reinforcement of nano-SiC particles into Ni–P coatings has a considerable impact on microhardness when compared to ZnO nanoparticles. In comparison with ZnO nanoparticles, silicon carbide particle reinforcement into the Ni–P lattice is minimal at 1 g/L concentration. As a soft metal oxide, ZnO nanoparticles cause the Ni-P-ZnO coating to flex more plastically under load [19, 20]. As a result, even at lesser concentrations of SiC particles (1 g/L), microhardness of coating Ni-P-SiC is approximately equivalent to the Ni-P-ZnO coating. Microhardness of Ni-P-ZnO/SiC
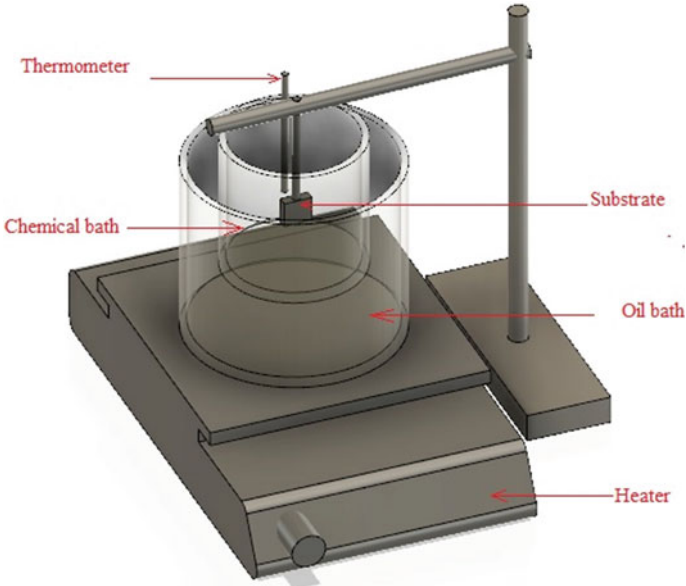
Fig. 1 Schematic representation of experimental setup
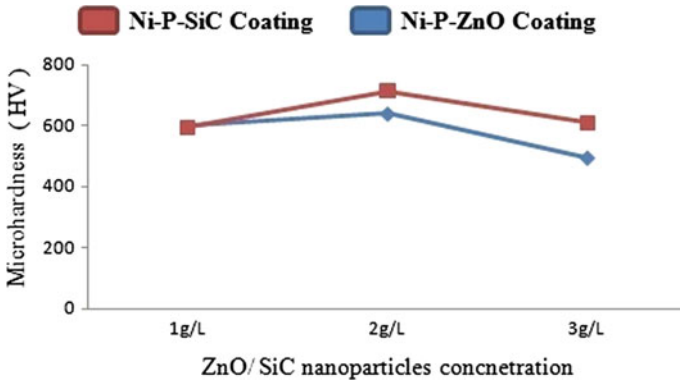
Fig. 2 Microhardness of the composite coating (Ni-P-ZnO and Ni-P-SiC)

coatings increases with the increase of particle concentration. The maximum micro-hardness value was found in both the deposits generated at a nanoparticle concentration of 2 g/L. The hardness of the Ni-P-SiC coating created at the amount of 2 g/L SiC is 713 HV. This value is 12% larger than the Ni-P-ZnO coating created at the similar level. Because SiC nanoparticles are more resistant to load transfer than ZnO nanoparticles, the Ni–P matrix has the highest resistance to plastic deformation and the Ni-P-SiC coating has the highest microhardness [21, 22]. At 3 g/L concentration, ZnO nanoparticle deposition in the Ni alloy matrix is greater than SiC nanoparticles.
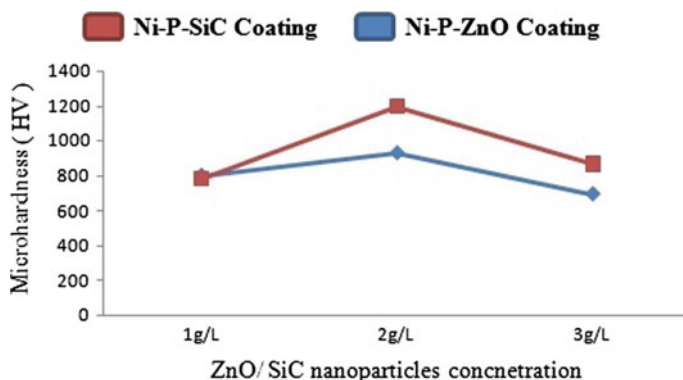
Fig. 3 Microhardness of the coatings after the annealing process

Because of the softening property of ZnO particles, the Ni-P-ZnO coating becomes softer at higher concentrations [23]. As compared to Ni-P-SiC coating, the Ni-P-ZnO coating has a 24% lower microhardness.

Many studies show that heat treatment at temperatures ranging from 350 to 450 °C has a noteworthy impact on the characteristics of EN coatings [24, 25]. Therefore, the thermal process, which is conducted at a temperature of 400 °C, increases the microhardness of both coatings. After the thermal process, the microhardness of both coatings produced at various amounts of ZnO and SiC particles is greater than the as deposited conditions. The heat treatment approach converts the amorphous nickel phosphide coating phase to crystalline nickel phosphide [26, 27]. The phase shift of the material after heat treatment coatings formed at 1 g/L SiC and ZnO particle concentration is the same, resulting in similar microhardness of both coatings. At 2 g/L nanoparticle concentration, the microhardness of the Ni-P-SiC coating after heat treatment is 29% greater than that of the Ni-P-ZnO coating. Annealed Ni-P-SiC coatings generated with 3 g/L SiC nanoparticle concentration have microhardness value of 25% greater than Ni-P-ZnO coatings. Figure 3 depicts the hardness of both the coatings after the heat treatment process.

4 Conclusions

At all nanoparticle proportions, microhardness of Ni-P-SiC coating is superior to the Ni-P-ZnO coating. SiC and ZnO particles of nanosize are spread more uniformly in the coatings generated after electroless immersion containing 2 g/L SiC and ZnO nanoparticles compared to the 1 and 3 g/L concentrations. Ni-P-SiC coating with homogeneously dispersed hard SiC particles generated at a particle concentration of 2 g/L in the coating bath provides the strongest resistance to plastic deformation. As a result, the Ni-P-SiC coatings as deposited had a maximum microhardness value of 713 HV. During the heat treatment procedure, hard nickel phosphates are formed,

which improve the microhardness of all coatings. The hardness of the Ni-P-SiC film produced at 2 g/L SiC nanoparticles increases up to 68% after annealing. Post-heated Ni-P-SiC (2 g/L) coating microhardness is 28% more than thermal processed Ni-P-ZnO coating made using 2 g/L zinc oxide nanoparticles.

References

1. Hari, K.K., et al.: An overall aspect of electroless Ni-P depositions—a review article. Metall. Mater. Trans. A **37**(6), 1917–1926 (2006)
2. Chintada, V.B., Koona, R., Raju Bahubalendruni, M.V.A.: State of art review on nickel-based electroless coatings and materials. J. Bio- Tribo-Corros. **7**(4), 1–14 (2021)
3. Afroukhteh, S., Dehghanian, C., Emamy, M.: Preparation of electroless Ni–P composite coatings containing nano-scattered alumina in presence of polymeric surfactant. Prog. Nat. Sci.: Mater. Int. **22**(4), 318–325 (2012)
4. Chintada, V.B., Koona, R.: Preparation and properties of composite electroless Ni-P-ZnO coatings. Mater. Res. Innov. **24**, 67–74 (2019)
5. Zielińska, K., Stankiewicz, A., Szczygieł, I.: Electroless deposition of Ni–P–nano-ZrO$_2$ composite coatings in the presence of various types of surfactants. J. Colloid Interface Sci. **377**(1), 362–367 (2012)
6. Tamilarasan, T.R., et al.: Effect of surfactants on the coating properties and corrosion behaviour of Ni–P–nano-TiO$_2$ coatings. Surf. Coat. Technol. **276**, 320–326 (2015)
7. Ger, M.-D., Hwang, B.J.: Effect of surfactants on codeposition of PTFE particles with electroless Ni–P coating. Mater. Chem. Phys. **76**(1), 38–45 (2002)
8. Matsuda, H., et al.: Effect of surfactants addition on the suspension of PTFE particles in electroless plating solutions. Trans. IMF **73**(1), 16–18 (1995)
9. Karthikeyan, K., Vijayaraghavan, L.: Effect of co-deposition of Al$_2$O$_3$ particle on the properties of electroless Ni–P coating. Int. J. Eng. Res. Technol. (IJERT). NCRAIME-2015, Bangalore, conference proceedings
10. Novák, M., Vojtěch, D., Vítů, T.: Influence of heat treatment on microstructure and adhesion of Al$_2$O$_3$ fiber-reinforced electroless Ni–P coating on Al–Si casting alloy. Mater. Charact. **61**(6), 668–673 (2010)
11. Chintada, V.B., Koona, R.: Influence of SiC nano particles on microhardness and corrosion resistance of electroless Ni–P coatings. J. Bio- Tribo-Corros. **4**(4), 1–8 (2018)
12. Balaraju, J.N., Rajam, K.S.: Electroless ternary Ni–W–P alloys containing micron size Al$_2$O$_3$ particles. Surf. Coat. Technol. **205**(2), 575–581 (2010)
13. Balaraju, J.N., et al.: Studies on electroless Ni–W–P and Ni–W–Cu–P alloy coatings using chloride-based bath. Surf. Coat. Technol. **200**(16–17), 4885–4890 (2006)
14. Rezaee, B., et al.: Nanoparticle concentration and heat treatment effects on microstructure and tribological behavior of the Ni-P nanocomposite coating. Adv. J. Sci. Eng. **2**(2), 71–78 (2021)
15. He, M.-F., et al.: Effect of wear conditions on tribological properties of electrolessly-deposited Ni-P-Gr-SiC hybrid composite coating. Trans. Nonferrous Met. Soc. China **22**(10), 2586–2592 (2012)
16. Yucheng, W., et al.: Preparation and characterization of Ni–Cu–P/CNTs quaternary electroless composite coating. Mater. Res. Bull. **43**(12), 3425–3432 (2008)
17. Chintada, V.B., Koona, R., Gurugubelli, T.R.: Investigation on microhardness and corrosion resistance of ZnO reinforced Ni-P composite coatings at various annealing temperatures. Adv. Mater. Process. Technol. 1–14 (2020)
18. Balaraju, J.N., Ezhil Selvi, V., Rajam, K.S.: Electrochemical behavior of low phosphorus electroless Ni–P–Si$_3$N$_4$ composite coatings. Mater. Chem. Phys. **120**(2–3), 546–551 (2010)
19. Chintada, V.B., Koona, R.: Influence of surfactant on the properties of Ni-P-nano ZnO composite coating. Mater. Res. Express **6**(2), 025030 (2018)

20. Chintada, V.B., Uppada, S., Sharma, R.C.: Properties of the multi layer electroless Ni-P-ZnO/Ni-P-SiC coatings. J. Crit. Rev. **7**(19), 268–271 (2020)
21. Wu, Y.C., Li, G.H., Zhang, L.: Wear resistance of electroless deposited Ni–P and Ni–P/SiC composite coatings on low alloy cast iron. Surf. Eng. **16**(6), 506–510 (2000)
22. Chen, X.H., et al.: Dry friction and wear characteristics of nickel/carbon nanotube electroless composite deposits. Tribol. Int. **39**(1), 22–28 (2006)
23. Sharma, S., et al.: Co-deposition of synthesized ZnO nanoparticles into Ni–P matrix using electroless technique and their corrosion study. J. Mater. Eng. Perform. **25**(10), 4383–4393 (2016)
24. Zhao, G., et al.: Effect Of low-temperature annealing on the properties of Ni–P amorphous alloys deposited via electroless plating. Arch. Metall. Mater. **60** (2015)
25. Goettems, F.S., Ferreira, J.Z.: Wear behaviour of electroless heat treated Ni–P coatings as alternative to electroplated hard chromium deposits. Mater. Res. **20**, 1300–1308 (2017)
26. Farzaneh, A., et al.: Electrochemical and structural properties of electroless Ni-P-SiC nanocomposite coatings. Appl. Surf. Sci. **276**, 697–704 (2013)
27. Alishahi, M., et al.: The effect of carbon nanotubes on the corrosion and tribological behavior of electroless Ni–P–CNT composite coating. Appl. Surf. Sci. **258**(7), 2439–2446 (2012)

Application of Process Capability and Design of Experiments to Improve Quality Parameters

Deepak Kumar, B. N. Vinay Kumar, M. C. Vinay, H. M. Yogesh, and Ashmitha Prabhu

1 Introduction

The granular form of the needed material is filled into the container during the injection moulding process, from which it will be transferred to the high-temperature zone. The granules will be converted into a semi-fluid form at the high-temperature zone and the semi-fluid will then be injected into the casting and filled in. The mould component holds together for the stipulated time after the semi-fluid is filled in the cast. The mould is then chilled, with the cooling period defined. This results in the desired outcome.

In 1939, Shewhart [10] the first sophisticated statistical process control (SPC) to measure exceptional and variability at a manufacturing system's point of origin. Every procedure, according to this system, is subject to two types of variation: version from a regular motive that is clearly present in any natural system is innate in the process and it is expected to be present; variation from special reasons is the version that arises from the fact that an incredible event has occurred. Stages of the SPC regime are used. Phase I aims for a deeper understanding of the approach and an assessment of method stability. The goal of Phase 2 is to find an assignable motivation of variation to keep the system under control [4]. Capability studies commonly observe the so-called 'strong processes', i.e. techniques showing uniformity of behaviour. Variability measures the uniformity of the function feature of the outgoing product and it could be of sorts: herbal variability, relating to a particular moment (additionally on the spot variability) and variability in preference to time [7]. As previously anticipated, it's miles now greater evident that Process Capability assessment is vital for any software aiming at improving nice [2]. In this paper, the theoretical assessment has been evolved with Normal information; that is to say,

D. Kumar · B. N. Vinay Kumar (✉) · M. C. Vinay · H. M. Yogesh · A. Prabhu
Department of Industrial Engineering and Management, MSRIT, Bangalore, India
e-mail: deepak.kr246@gmail.com

the Normality hypothesis for the distribution of the method output, because, while carried out to non-normal information, statistical indices may want to turn out to be unreliable [3]. By the usage of Capability Indices, Process Capability Analysis compares the output of a robust technique to the specification limits and it's miles a length with respect to inherent precision of a production procedure. Process Capability may be calculated via several Process Capability ratios and indices. Therefore, it identifies possibilities to decorate excellent and operational performance [8]. Process Capability Index (PCI) shows the quantity to which the way can produce the output that conforms to high-quality requirements. It is decided through the usage of evaluating the natural variability of a way to the purchaser or engineering specs [5]. Cp, additionally called precision index is the primary Process Capability Index acting in literature and it is described because the ratio of specification width (US–LSL) over the technique spread (6σ), with US and LSL, stand for Upper and Lower Specification Limits. The specification width represents client and/or product requirements [4]. The primary gain of SPC is that it detects a faulty process, which is corrected, prevents the producing of defective merchandise. This is in assessment to standard first-rate manipulating workout that identifies faulty merchandise after they have been produced. The conventional strategies of perfect control outcomes in a luxurious manufacturing process [9].

The objective of the work is to

1. To lessen the variety of rejections.
2. To lessen the quantity of components that calls for transform through decreasing the flash defects.
3. To discover most fulfilling values for procedure parameters to obtain the suitable component weight the use of DOE.
4. Use the DMAIC approach to outline and resolve the trouble, in addition, to make certain the adjustments make certain sustained fine improvement.
5. To enhance the cost of procedure functionality index, i.e. to lessen the range of the procedure.

1.1 Methodology Adopted

.

1.2 Define

The first step of solving a problem according to DMAIC method is to define it. This phase is aimed at defining the scope and goals of this project.

1.3   Measure

This is the second step of the DMAIC procedure which focuses on measuring the initial state of the system or the process. This can be done using control charts. To plot the control charts, each process parameter was measured using the real-time HMI monitor present on the Engel 220t machine, following a pre-determined schedule. The schedule was as follows, following a pre-determined sampling plan. The sampling plan was as follows:

1.   All parameters measured once after every five shots of the machine.
2.   5 measurements taken every hour.
3.   Measurements taken for 15 subgroups of 5.

1.4   Analyze

With all the main process parameters identified in the 'Measure' phase, factors that are easier to control are chosen to conduct the Design of Experiments method to determine their optimal values as well as the magnitude of effect they have on the output or yield of the process. Thus, the experiments were designed to determine optimal settings for the process, i.e. determining optimal values for the process parameters will be designed taking Injection Pressure, Nozzle Temperature and Injection Speed as the factors. For designing the test, Taguchi Technique with the use of orthogonal arrays is used to reduce the quantity of experiments in a normal factorial design (27) to just nine. An L9 orthogonal array was used that can accommodate four factors at three levels each. Since only three factors were considered, the orthogonal array was modified by leaving out the last column. The modified orthogonal array is given in Table 1. The resulting experimental design with the values of the levels is given in Table 2.

Table 1   Modified L9 orthogonal array

L9 (3^3)	1	2	3	4	5	6	7	8	9
1	1	1	1	2	2	2	3	3	3
2	1	2	3	1	2	3	1	2	3
3	1	2	3	2	3	1	3	1	2

Table 2   Experimental design

Factors	L9 (3^3)	1	2	3	4	5	6	7	8	9
Injection pressure	1	119	119	119	122	122	122	125	125	125
Nozzle temperature	2	228	230	232	228	230	232	228	230	232
Injection speed	3	75	80	85	80	85	75	85	75	80

Table 3 Experimental design with response column

S. No.	Injection pressure	Temperature	Injection speed	Part weight
1	119	228	75	54.6
2	119	230	80	55.2
3	119	232	85	55.2
4	122	228	80	55.0
5	122	230	85	54.8
6	122	232	75	55.2
7	125	228	85	54.4
8	125	230	75	54.8
9	125	232	80	56.0

Each of the nine treatment combinations for Injection Pressure, Nozzle Temperature and Injection Speed was run on the machine and the weights of the resulting parts were recorded against every treatment. The part weight data was introduced as the response column of the Taguchi design, as in Table 3 and then the 'Analyze Taguchi Design' option was used to analyze and get results of analysis.

Results of analysis of a Taguchi design include response Table for means, plots of main effect of the factors, ANOVA Table and regression analysis and the residual plots for means.

The effects of analysis are mentioned in the following segment. The main effect plot (Fig. 1) shows that the factors Injection Pressure and Nozzle Temperature have a positive correlation to the response, i.e. an increase in the value of the factor will cause an increase in the value of the response for the range of levels considered. The factor Injection Speed has a positive correlation to part weight from the first level to the second and a negative correlation to part weight from the second level to the third.

The Response Table for Means (Table 4) gives estimates of the effects of the factors and Minitab assigns them ranks in descending order of their effect on the response. The ranks of Injection Pressure, Nozzle Temperature and Injection speed are 3, 1 and 2, respectively, suggesting that the Nozzle Temperature is the factor that has the largest impact on the part weight followed by Injection Speed.

1.5 ANOVA

Null Hypothesis—H_0

All factors and their interactions are not significant. Alternative Hypothesis—H_1: Factors and their interactions are significant. The ANOVA for Means, Table 5, lists an F-value for each term. The F-value is the test statistic used to determine whether the term is associated with the response. A sufficiently large F-value indicates that
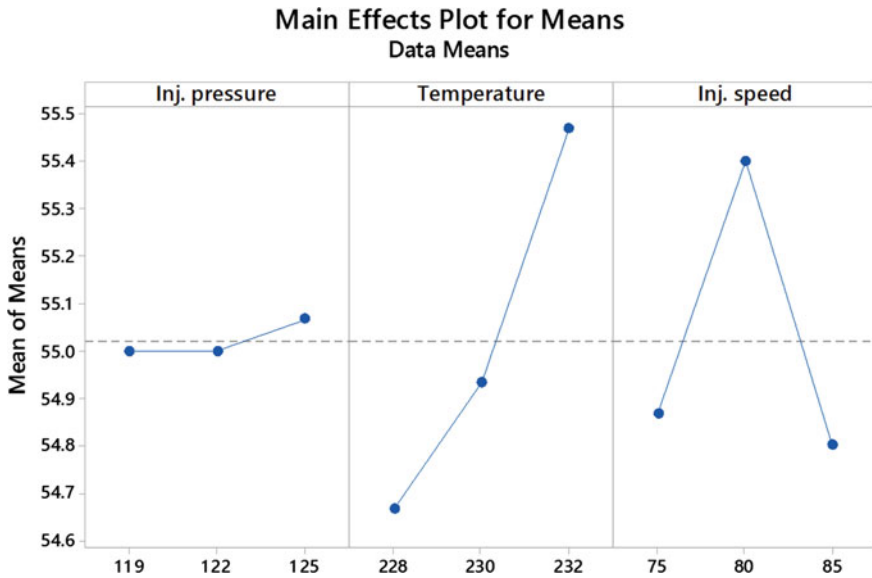
Fig. 1 Main effects plot

Table 4 Response table for means

Level	Injection pressure	Temperature	Injection speed
1	55.00	54.67	54.87
2	55.00	54.93	55.40
3	55.07	55.47	54.80
Delta	0.07	0.80	0.60
Rank	3	1	2

the term or model is significant. To decide whether or not to reject the null hypothesis, the F-value is in comparison to the critical value. The critical value can be determined using F-distribution Table under the selected confidence level. The confidence level is selected to be 0.10 at which the critical value $\alpha = 9.00$. Thus, the factors having F-value above 9.00 are significant terms to the model.

Thus, the factors Nozzle Temperature (F-value 16.00) and Injection Speed (F-value 10.43) are significant with Nozzle Temperature being the most significant. Since the factors are significant, we reject the Null Hypothesis H_0. The four-in-one plot (Fig. 2) of residuals shows that the residuals are randomly distributed.

Taguchi Results Prediction

Given a model of a process through Taguchi Design, Minitab offers a module to predict the mean value for a chosen level of each factor. This function was used to find the optimum settings of the factors to produce parts with a mean equal to the target part weight. By trial and error, the levels of 122 bar for Injection Pressure,

Table 5 Analysis of variance of means

Source	DF	Seq SS	Adj SS	Adj MS	F	P	Predicted values Prediction
Inj. pressure	2	0.00889	0.008889	0.004444	0.14	0.875	Mean = 55.0222
Temperature	2	0.99556	0.995556	0.497778	16.00	0.059	Settings
Inj. speed	2	0.64889	0.648889	0.324444	10.43	0.087	Inj. pressure: 122
Residual error	2	0.06222	0.062222	0.031111			Temperature: 228
Total	8	1.71556					Inj. speed: 80
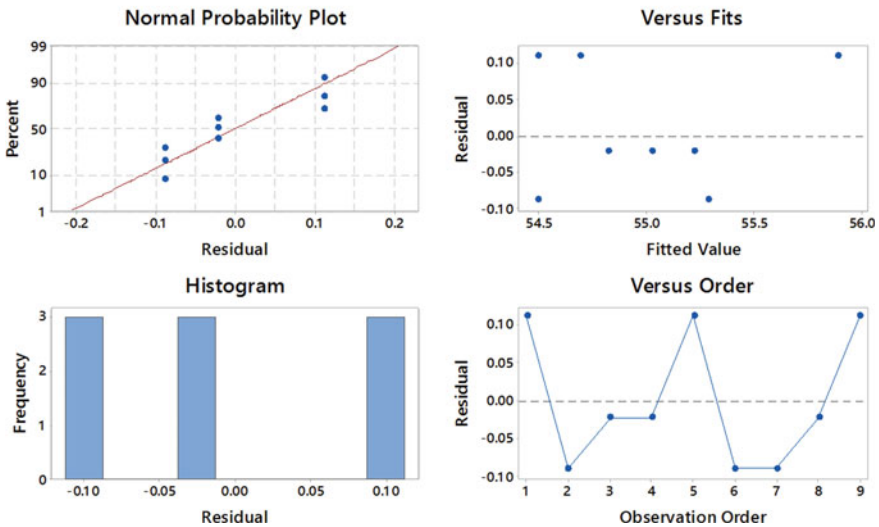
Fig. 2 Residual plots for means

228 °C for Nozzle Temperature and 80 mm/s for Injection Speed were found to result in a mean of 55.02 g for part weight. Thus, optimum settings of factors for the process to produce acceptable parts were found.

1.6 Improve

With the optimum levels of each of the considered factors determined and the extent and nature of their effects known, 'Improve' phase of this project was implemented.

Table 6 Data collected of injection pressure

Subgroup No.	1	2	3	4	5	6	7	8
X1	118.8	121.5	118.7	119.7	121	118.2	119.5	118.5
X2	120.4	118	121.9	118.5	118.5	119.8	119.1	119.8
X3	121.2	119.5	121.5	118.9	122	118	121.7	120.1
X4	120.6	118.6	118.5	118.3	119.9	118	118.1	119.7
X5	121	119.3	118.9	121.5	120.4	118.3	121.4	119.9
Subgroup No.	9	10	11	12	13	14	15	
X1	119.3	120.1	119.9	120.8	119.6	119.7	121.6	
X2	119.8	120.4	119.9	121.1	118.2	118.6	118.2	
X3	119.4	118.2	119.9	119.1	121.8	120.5	121.3	
X4	118.8	119	118.2	119.1	118.9	120.1	119.6	
X5	121.1	121.1	120.2	118.5	118.9	119	121.9	

1.7 Control

The aim of the 'Control' phase is to provide means and methods to hold the gains reported in the 'Improve' phase.

2 Data Collection

2.1 Injection Pressure (in bar)

The nominal value set for injection pressure on the machine was 120 bar. The data and control chart plotted are given in Table 6 and Fig. 3.

As observed in the control chart, no data point plotted has fallen above the upper control limit or below the lower control limit which indicates the process is in statistical process control. The eight control chart tests performed by Minitab on the data find no presence of special or identifiable causes.

2.2 Nozzle Temperature (in °C)

The nominal value set for nozzle temperature on the machine was 230 °C. The data and control chart plotted are given in Table 7 and Fig. 4.

As observed in the control chart, no statistical point plotted has fallen above the UCL or below the LCL which indicates the system is in statistical manner. The eight
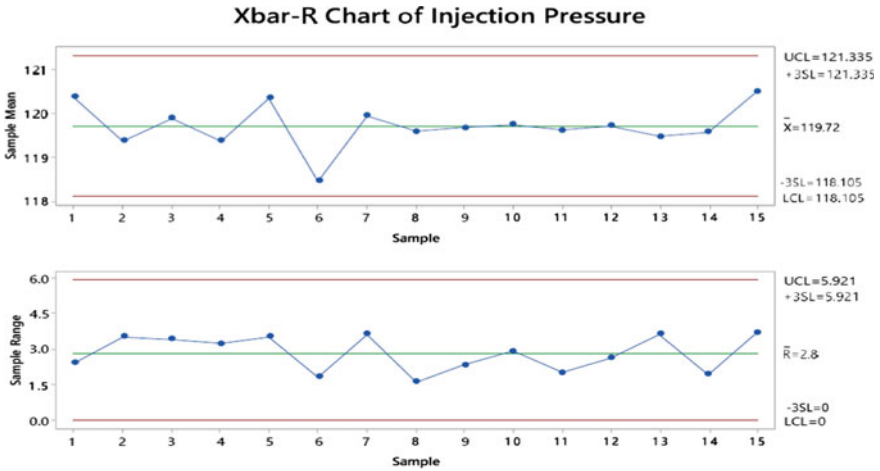
Fig. 3 Xbar-R chart of injection pressure

Table 7 Data collected of nozzle temperature

Subgroup No.	1	2	3	4	5	6	7	8
X1	229.7	228.5	230.5	229.6	231	229.1	229.9	229.3
X2	229.7	230.6	228.8	230.7	228.6	228	228.2	229.1
X3	231.6	228.9	228.7	228.1	228.8	230.8	231.5	230.3
X4	228.1	229	228.3	230.3	232	231	229.9	228.7
X5	228.3	231	231	228.4	231.4	229.7	228.1	230.6
Subgroup No.	9	10	11	12	13	14	15	
X1	229.5	229.3	229.7	231.2	228.2	230	228.9	
X2	228.4	229.8	230.3	228.6	231	228.4	230.3	
X3	229.2	231.5	228	228	229.5	229.9	228.8	
X4	229.1	230.7	231.6	229.8	231.3	231.2	229.1	
X5	231	229.2	230.5	230.9	230	231.8	228	

control chart tests performed by Minitab on the data find no presence of special or identifiable causes.

2.3 Injection Speed (in mm/s)

The nominal value set for nozzle temperature on the machine was 75 mm/s. The data and control chart plotted are given in Table 8 and Fig. 5.
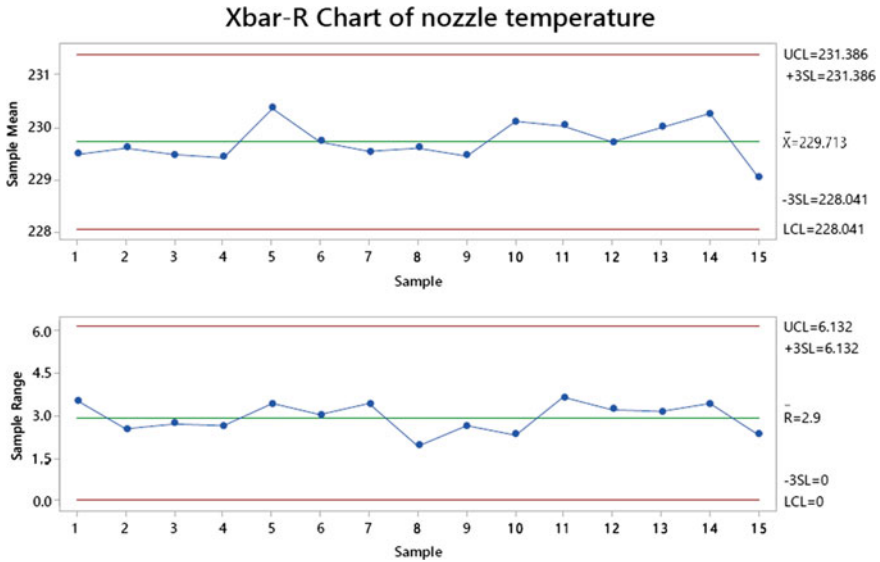
Fig. 4 Xbar-R chart of nozzle temperature

Table 8 Data collected of injection speed

Subgroup No.	1	2	3	4	5	6	7	8
X1	73.6	73.4	76.3	76.2	75	75.1	73.8	73.9
X2	77	77	76.2	75.9	76.4	74.6	75.6	76.1
X3	76.6	75.8	73.2	76.7	74.1	76.6	76.2	75.3
X4	75.7	76.6	74.3	73.5	73.5	73.6	74.3	73.7
X5	73.4	73	73.5	73.9	75.7	75.4	73.4	73.9
Subgroup No.	9	10	11	12	13	14	15	
X1	76.3	75.4	75.5	76.6	74.1	73.3	76.2	
X2	74.7	75.6	76.7	75.6	75.4	73	75.8	
X3	75.2	73.5	76.8	74.2	76.2	75.7	74.2	
X4	76.5	76.5	74.3	76	76.7	76.5	76.2	
X5	76.2	74.4	74.1	73	76.7	74	74.7	

As observed in the control chart, no statistical point plotted has fallen above the UCL or below the LCL which indicates the system is in statistical manner. The eight control chart tests performed by Minitab on the data find no presence of special or identifiable causes.
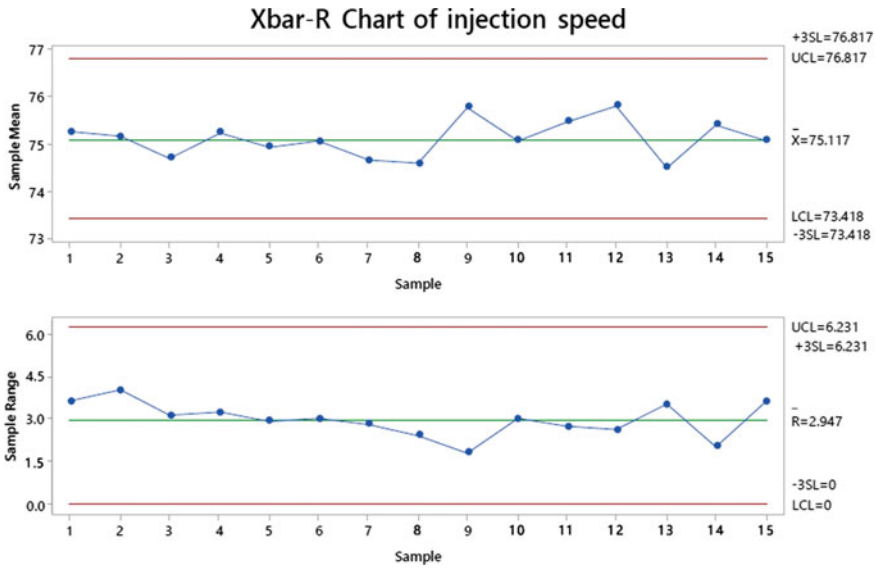
Fig. 5 Xbar-R chart of injection speed

2.4 Cooling Time (in Seconds)

The nominal value set for cooling time on the machine was 25 s. The data and control chart plotted are given in Table 9 and Fig. 6.

Table 9 Data collected of cooling time

Subgroup No.	1	2	3	4	5	6	7	8
X1	28	28	25	21	29	24	22	21
X2	27	28	29	25	25	24	21	24
X3	28	23	25	25	22	25	22	28
X4	23	25	23	25	21	21	26	25
X5	29	26	25	24	30	25	22	23
Subgroup No.	9	10	11	12	13	14	15	
X1	29	25	20	28	23	28	22	
X2	20	22	20	28	30	30	28	
X3	23	29	30	20	29	24	22	
X4	24	27	28	20	30	28	24	
X5	27	23	24	28	22	25	26	
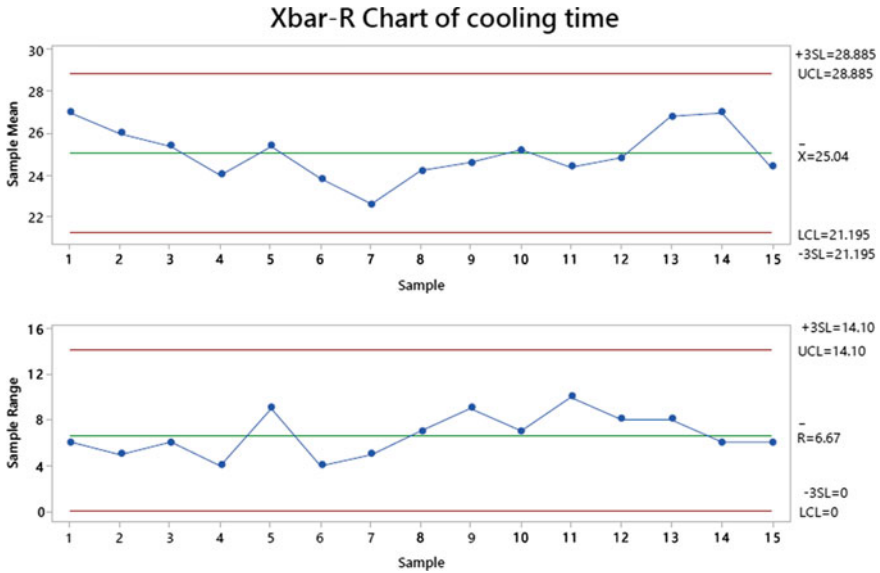
Fig. 6 Xbar-R chart of cooling time

2.5 Holding Pressure (in bar)

The nominal value set for holding pressure on the machine was 50 bar. The data and control chart plotted are given in Table 10 and Fig. 7.

As observed in the control chart, no statistical point plotted has fallen above the UCL or below the LCL which indicates the system is in statistical manner. The eight

Table 10 Data collected of holding pressure

Subgroup No.	1	2	3	4	5	6	7	8
X1	52	48	47	48	51	53	47	53
X2	47	52	52	48	47	47	51	48
X3	53	53	52	53	49	50	51	47
X4	50	52	48	49	53	51	51	53
X5	49	49	49	53	52	52	49	47
Subgroup No.	9	10	11	12	13	14	15	
X1	52	51	51	50	47	51	53	
X2	47	48	50	50	48	51	50	
X3	47	53	49	50	50	49	50	
X4	48	47	49	49	48	51	48	
X5	48	52	51	53	49	53	51	
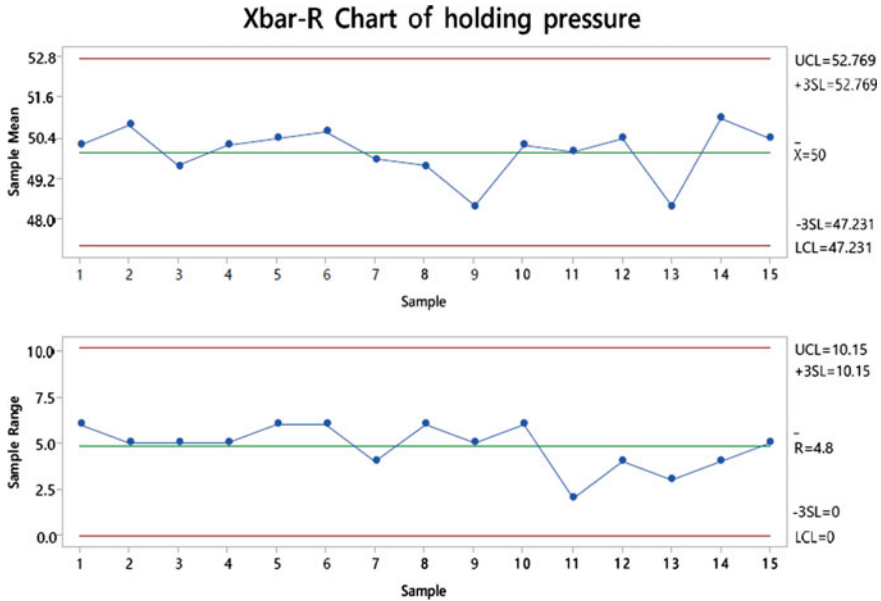
Fig. 7 Xbar-R chart of holding pressure

control chart tests performed by Minitab on the data find no presence of special or identifiable causes.

Recording number of rejections and reworks

The wide variety of parts that had been rejected and the number of components that needed rework was recorded in line with the sampling plan. The data was then used to create a pie chart to visually represent the fractions of parts produced that were accepted, rejected or needed rework. The data as in Table 11.

After plotting control charts, an initial process capability study was conducted on weight of the parts produced during the same period in order to determine the

Table 11 Rejection-rework data of part

Subgroup	1	2	3	4	5	6	7	8	9
Number of defectives	1	0	0	1	0	2	0	0	0
Rejection/rework	Rew	Nil	Nil	Rew	Nil	Rew-rew	Nil	Nil	Nil
Subgroup	10	11	12	13	14	15		Rework	6
Number of defectives	2	1	1	0	0	0		Rejection	2
Rejection/rework	Rej-rew	Rew	Rej	nil	nil	nil		Accepted	67
								Total	75

initial value of the process capability index, Cpk. For this, the process capability tool of Minitab was used where the part weight data was fed along with the target value (55 g) and tolerances (±2 g). Minitab estimates the various process capability indices as well as plots a histogram for the data.

It also plots an Xbar-R control chart. The data collected of weight of pats is shown in Table 12. The results from the initial process capability study are as follows.

The Xbar-R chart of part weight (1) is shown in Fig. 8. From the process capability report, Fig. 9, the process capability index Cpk is found to be 1.56 which translates to approximately two parts per million produced falling outside specification limits. The histogram accompanying the report has a single mode at 55.8 g which indicates that the most frequently occurring value for part weight in the given data is 55.8 g. To prove this hypothesis, the optimal values of the process parameters must be determined theoretically and then must be proven physically. This can be achieved by setting the optimal values on the machine and a process capability study similar to the initial one conducted to ascertain the improvement due to the optimal settings of the process parameters.

The process capability (Table 13) was collected, Xbar-R chart of part weight (2) is shown in Fig. 10 and Minitab was used to generate the Process Capability Report (Fig. 10).

The data for the number of parts rejected and needing rework are given in Table 14. Also, a comparison of the initial and final number of rejections and reworks is made in Fig. 11 (Fig. 12).

3 Result and Discussion

1. The optimal levels of injection pressure, nozzle temperature and injection speed were found to be 125 MPa, 230 °C and 80 mm/s, respectively.
2. The Cpk of the process improved from 1.56 to 1.76 as a result of implementation of the optimal levels for the factors found using DOE.
3. Number of accepted parts increased from 89 to 95%.
4. Number of parts rejected reduced by 50%.
5. Number of parts needing rework reduced by 50%.
6. The Cpk improvement can be stated in terms of defects per million as 4 ppm initially to less than 0.5 ppm finally.

4 Conclusion

Key parameters for injection moulding were identified and their behaviour was studied. DMAIC approach for problem-solving was successfully applied to produce quantitative results. Design of experiments and Taguchi technique were used successfully to determine the optimal levels of the process parameters to result in ideal

Table 12 Data collected of weight of parts

Sub group	1	2	3	4	5	6	7	8	9	10	11	12	13	14	15
X1	55.8	55.8	55.8	55.8	55.1	55.8	55.2	55.8	56.1	55.8	55.8	55.8	55.3	55.2	55.6
X2	55.6	55.4	55.6	56.1	55.8	55.8	55.6	55	55.3	55.3	55.4	55.9	55.5	56.1	55.3
X3	55.8	55.8	56.1	55.8	55.8	54.9	55.4	55.3	55.8	55.8	55.8	55.6	55.6	55.8	55.8
X4	55	55.3	55.8	55.4	54.9	55.3	55.8	55	55.9	55.4	54.9	55.8	56.1	55.7	55.8
X5	55.2	55.1	55.5	55.6	55.2	55.4	55.7	55.9	55.8	55.6	55.3	55.3	55.8	55.5	55.6
Sum, à X	277.40	277.40	278.80	278.70	276.80	277.20	277.70	277.00	278.90	277.90	277.20	278.40	278.30	278.30	278.10
Avg, X	55.48	55.48	55.76	55.74	55.36	55.44	55.54	55.40	55.78	55.58	55.44	55.68	55.66	55.66	55.62
Range, R	0.80	0.70	0.60	0.70	0.90	0.90	0.60	0.90	0.80	0.50	0.90	0.60	0.80	0.90	0.50

Xbar-R Chart of part weight (1)

Fig. 8 Xbar-R chart of part weight
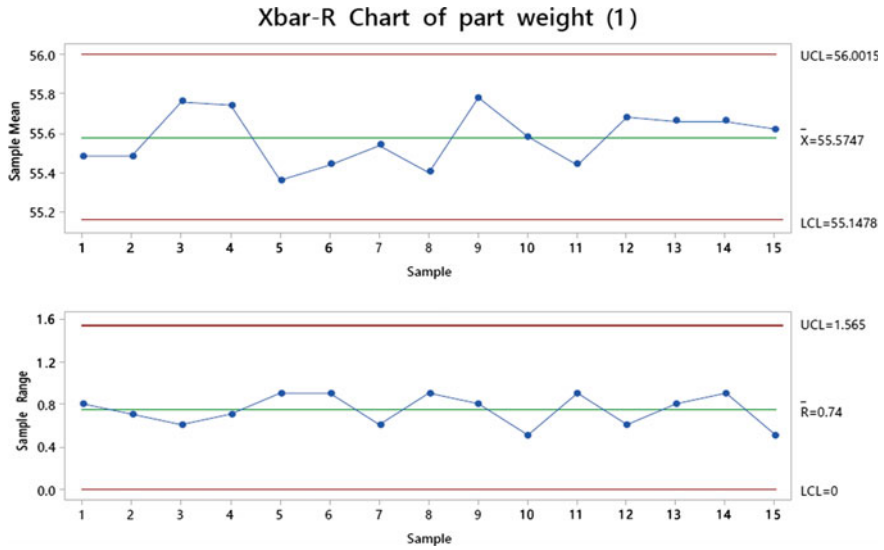
Process Capability Report-1
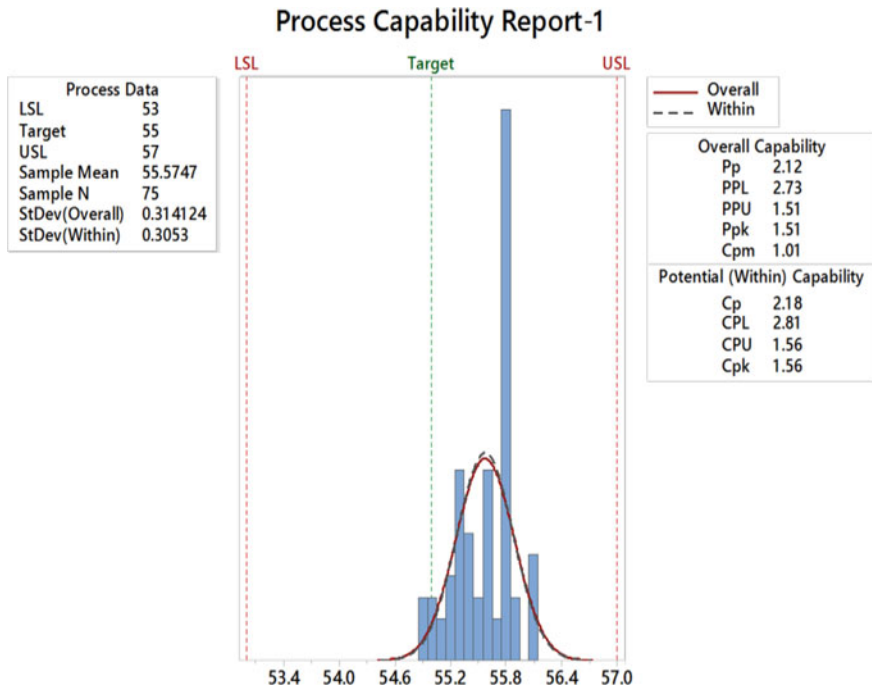
Fig. 9 Process capability report-1

Table 13 Process capability data

Sub group	1	2	3	4	5	6	7	8	9	10	11	12	13	14	15
Date	04.06.21						04.06.21 and 5.06.21							05.06.21	
Time	10AM	11AM	12PM	1PM	2PM	3PM	10AM	11AM	12PM	1PM	2PM	3PM	4PM	10AM	11AM
X1	55	55.7	55	55.3	55.1	55	55.2	55.5	54.8	55	55.1	55	54.2	55.3	54.2
X2	55.2	55.1	55.4	55	55	55	55.4	54.8	55.2	54.9	54.2	54.9	55	54.6	55.3
X3	55.3	55	55.1	54.6	55	54.6	55.1	55.1	55	54.5	54.9	54.4	55	55	55.5
X4	54.7	55.3	55	55	54.5	54.7	54.6	54.5	55.1	55.4	54.9	55.2	55.6	54.7	55
X5	55.1	55	54.6	54.7	54.3	55.1	54.8	54.6	54.6	54.9	55.3	55.2	55.2	55.6	54.9
Sum, å X	275.30	276.10	275.10	274.60	273.90	274.40	275.10	274.50	274.70	274.70	274.40	274.70	275.00	275.20	274.90
Avg, X	55.06	55.22	55.02	54.92	54.78	54.88	55.02	54.90	54.94	54.94	54.88	54.94	55.00	55.04	54.98
Range, R	0.60	0.70	0.80	0.70	0.80	0.50	0.80	1.00	0.60	0.90	1.10	0.80	1.40	1.00	1.30
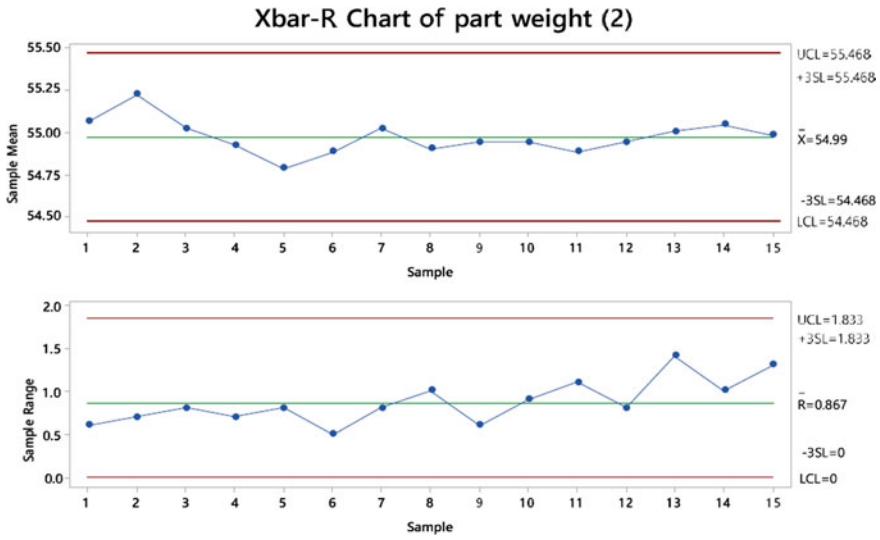
Fig. 10 Xbar-R chart of part weight

Table 14 Rework-rejection-accepted part data

Subgroup	1	2	3	4	5	6	7	8	9
Number of defectives	0	1	1	0	0	0	0	0	1
Rejection/rework	Nil	Rej	Rew	Nil	Nil	Nil	Nil	Nil	Rew
Subgroup	10	11	12	13	14	15		Rework	3
Number of defectives	0	0	0	0	0	1		Rejection	1
Rejection/rework	Nil	Nil	Nil	Nil	Nil	Rew		Accepted	71

part weight. The factors injection pressure and injection speed were found to have the largest impact on the mean of the part weight. Process capability studies were successfully conducted to determine Cpk of the process both before and after the implementation of the solution to act as a direct indicator of quality improvement.

Process Capability Report-2

Process Data	
LSL	53
Target	55
USL	57
Sample Mean	54.968
Sample N	75
StDev(Overall)	0.332135
StDev(Within)	0.3726

Overall Capability
Pp   2.01
PPL   1.98
PPU   2.04
Ppk   1.98
Cpm   2.00

Potential (Within) Capability
Cp   1.79
CPL   1.76
CPU   1.82
Cpk   1.76
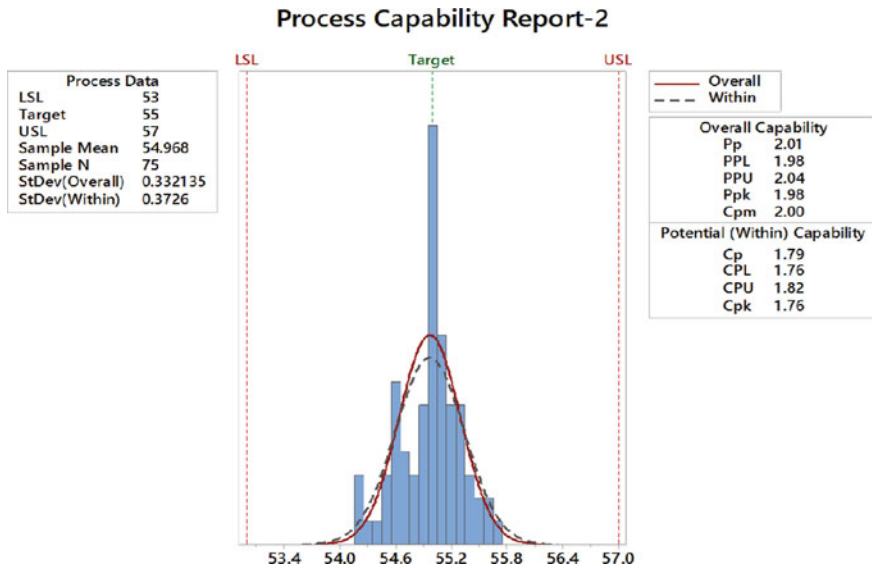
Fig. 11 Process capability report
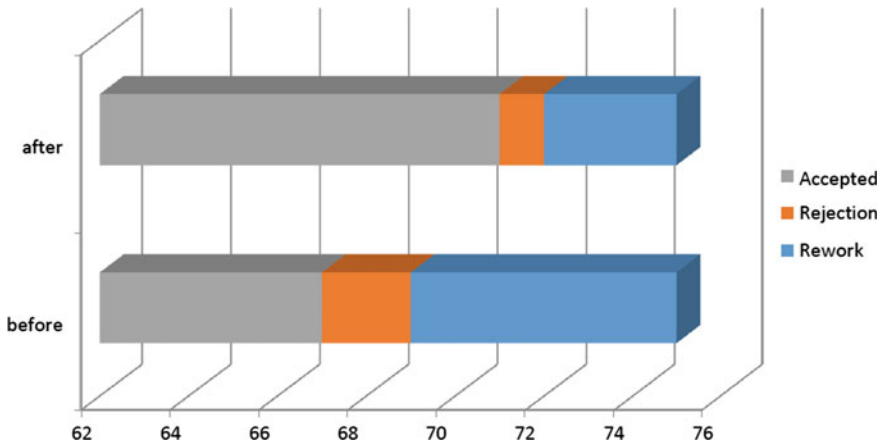
Fig. 12 Comparison of defects of before and after

References

1. Arcidiacono, G., Costantino, N., Yang, K.: The AMSE lean six sigma governance model. Int. J. Lean Six Sigma **7**(3), 233–266 (2016)
2. Bissell, A.F.: How reliable is your capability index? Appl. Stat. **39**(3), 331–340 (1990)
3. Chakraborti, S., Human, S.W., Graham, M.A.: Phase I statistical process control charts: an overview and some results. Qual. Eng. **21**(1), 52–62 (2008)

4. Chao, M., Lin, D.K.J.: Another look at the process capability index. Qual. Reliab. Eng. Int. **22**(2), 153–163 (2006)
5. Hoffman, L.: A general approach for testing the process capability index. Qual. Reliab. Eng. Int. **9**(5), 445–449 (1993)
6. Liu, P.H., Chen, F.L.: Process capability analysis of non-normal process data using the burr XII distribution. Int. J. Adv. Manuf. Technol. **27**(9–10), 975–984 (2005)
7. Montgomery, D.C.: Introduction to Statistical Quality Control, 7th edn. Wiley, Hoboken (2013)
8. Nagesh, P., Wooluru, Y., Swamy D.R.: Process capability indices for non- normal distribution—a review. Paper presented at the International Conference on Operations Management and Research (ICOMAR 2016)—"Towards Operational Excellence", 21–22 Jan 2016, Mysuru, India (2016)
9. Kanu, R.C.: A Study of Process Variability of the Injection Molding of Plastics Parts Using Statistical Process Control (SPC), American Society for Engineering Education, pp. 23.110.1–23.110.9 (2013)
10. Shewhart, W.A.: Statistical Method from the Viewpoint of Quality Control. The Graduate School, the Department of Agriculture. Washington, DC (1939)
11. Sreedharan, J., et al. Optimization of plastics injection molding process using response surface methodology. Int. J. Eng. Technol. (IJET) **10**(1) (2018). ISSN (Print): 2319-8613, ISSN (Online): 0975-4024
12. Sharma, V., et al.: Quality improvement of plastic injection molded product using DoE and Taguchi techniques. Int. J. Recent Adv. Mech. Eng. (IJMECH) **4**(2), 201 (2015)
13. Wold, S., Josefson, M.: Multivariate calibration of analytical data. In: Meyers, R.A. (ed.) Encyclopedia of Analytical Chemistry, pp. 9710–9736. Wiley, Chichester, UK (2000)

Numerical and Experimental Investigation of the Finite Life of Low-Carbon Steel Cylindrical Notched Specimens

K. Durga Hemanth Kumar, L. Daloji, J. Chandra Sekhar, and I. Ramu

1 Introduction

Methods which increase the surface strength (e.g., surface hardening) and those which introduce compressive residual stresses improve the fatigue strength significantly. It is common practice to shot peen steam-turbine blades for this reason. The effects of environment on fatigue strength are complex, although in most cases, fatigue strength is reduced by aggressive environments. In certain circumstances, the filling up of the crack with corrosion products can decrease crack growth rates. The basis of the stress-life method is S–N curve, where alternating stress, S, versus cycles to failure, N.

Marines-Garcia [1] fatigue test conducted on HSLA steel, at load ratio, $R = 0.1$ and -1, under 20 kHz and 35 Hz, it was noticed that the test frequency does not have impact on fatigue data. Fatigue endurance is decreasing with increasing number of cycles for $R = -1$, whereas fatigue failure was not happened at $R = 0.1$. Liu and Mahadevan [2] proposed a general methodology for fatigue life prediction under variable amplitude loading condition. This methodology is combination of nonlinear fatigue damage accumulation principle and a stochastic S–N curve representation. Subramanyan [3] developed a simple method for estimating the fatigue limit, based on the convergence of damage lines at the knee point of an S-log N diagram. By conducting a high-low (two levels) step test, the fatigue limit is estimated. The experimental data obtained on unnotched C35 steel specimens and other reported data on

K. Durga Hemanth Kumar (✉)
Department of Mechanical Engineering, Vishnu Institute of Technology, Bhimavaram, Andhra Pradesh 534202, India
e-mail: kondreddi.hemanthkumar@gmail.com

L. Daloji · J. Chandra Sekhar · I. Ramu
Department of Mechanical Engineering, Vishnu Institute of Technology-Bhimavaram, Bhimavaram, Andhra Pradesh 534202, India

steel in rotary bending confirm the validity and reliability of the method proposed. Zhang et al. [4] summarized various methods available for characterization of fatigue properties of thin metal films.

Kokavec et al. [5] estimated that the fatigue behavior of a specimen is mainly dependent on the material and their surface condition. This work describes the influence of the surface roughness on the fatigue behavior of nodular cast iron. Identified fracture surfaces were to determine the micro-mechanisms associated to the various fatigue lives.

1.1 Novelty of the Work

The present work is related now a day's work is notched steel specimens find finite life of materials in low-costing methods. So many experiments on this way find the finite life in experimental and analytical way.

2 Experimental Study

The present work is to find fatigue life by using stress-life method for low-carbon steel specimens, which are with and without burnishing. To verify the proposed stress fatigue life relation, tension-impact fatigue tests are conducted on drop hammer type equipment fabricated in the laboratory. The intensity of impact stress was altered by changing the weight of the falling mass. Tensile-impact stresses are developed in the specimen due to sudden application of the attached load which is made to fall from a controlled height. The drop height was kept constant, and the attached weight is varied for changing the stress level. By reciprocating the process of impact a number of times, the specimen is made to fail under fatigue. All the tests are conducted on carbon steel specimens. The experimental studies include the design and fabrication of tension-impact fatigue testing machine with necessary relay circuit arrangement to feed the required electric power to the electromagnet, selection of material and properties of the test specimen, development of a simple and inexpensive burnishing tool.

2.1 Fabrication of Tension-Impact Fatigue Testing Machine Comprises of the Following Steps

The four columns are welded over a base in such a way that enough space is provided between the stop shoes so that the weight attached to the specimen could move freely through this space and columns are parallel to each other. A sliding block is made
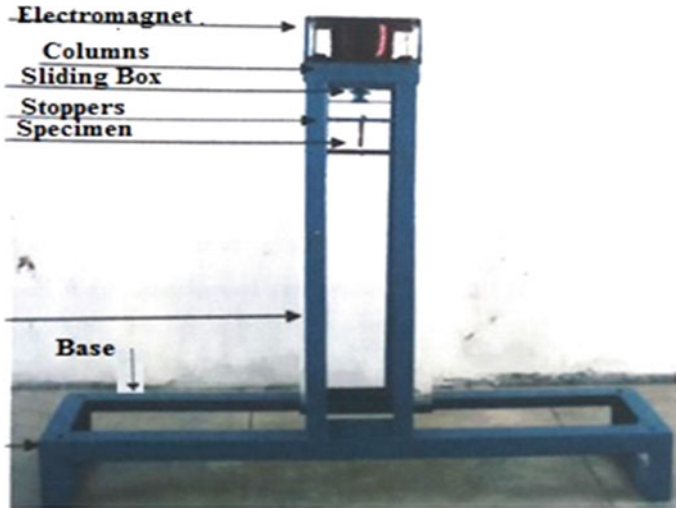
Fig. 1 Fabricated diagram of a tension-impact fatigue testing machine

to which a vertical galvanized iron pipe is welded for the up and down movement through the slots provided in the columns. The upper end of the sliding block consists of a cylindrical rod is lifted with the help of an electromagnet which is placed over a platen and is controlled by a relay circuit. A check ring was provided for controlling the minimum height of the sliding block above the stop shoes. As soon as the current was cut off, the iron core falls freely under gravity and the sliding block struck back over the stop shoes. Since the specimen suddenly came to rest, it gave rise to an impact leading situation. The attached weight acted as if at it was being applied with certain velocity and a fatigue stress developed moment all over a cross section at plane portion of the specimen. Due to reputation of impact, after each one second interval, the specimen underwent a process of impact fatigue. Fabricated machine is as shown in Fig. 1.

2.2 Selection of Material and Properties of the Test Specimen

All the test specimens were made of low-carbon steels. The engineering properties of this steel were determined from tension test conducted on universal testing machine of 40 ton capacity. Hardness value was determined on Rockwell hardness testing machine. The chemical composition and engineering properties of this specimen material are given in Table 1.

Figure 3 shows test specimens are made of 100 mm long and 8 mm in diameter. A 4 mm radius circular notch is provided at the middle span of the specimen with a minimum diameter of 4 mm at the notch root as shown in Fig. 2 line diagram with

Table 1 Chemical composition (% wt) and engineering properties of low-carbon steel

Material	C	S	P	Si	Yield strength (MPa)	Ultimate tensile strength (MPa)	Rockwell hardness
Low-carbon steel	0.77	0.16	0.26	1.49	391	710	66
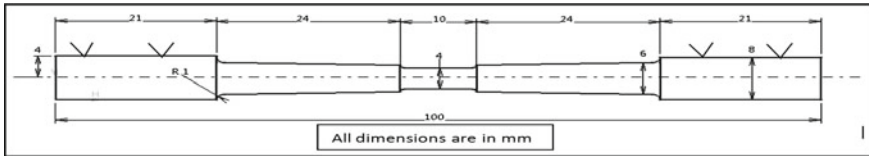
Fig. 2 Line diagram of the specimen with dimensions

Fig. 3 Test specimen

dimensions. Notch is provided mainly to make sure that the failure always occurs at the middle of the specimen.

Before conducting the experiment, the weight of the attached mass and the weight of the specimens are determined on an electronic balance. A high ratio between these two weights is maintained to minimize the effect of stress waves. Five weights of 100, 200, 300, 400, and 500 g are selected for varying the peak stress levels. The number of impacts for specimen failure is obtained by keeping the height of drop fixed at a level of 60 mm. The fatigue life is obtained for five different weights.

2.3 Development of Burnishing Tool

A simple and inexpensive ball burnishing tool was fabricated due to the flexible design of the tool holder; the ball can rotate freely with the work piece rotation. The ball has the following composition: High-chromium carbon steel of 1% carbon, 1.4% chromium, and 0.2% vanadium with surface roughness varies between 0.05 and 0.09 µm. In each case of the experiments, a fresh ball was used for burnishing operation [6]. To ensure that the surfaces are free from stress concentration, both plane and notched portions are sufficiently polished to eliminate the scratches leftover due to machining.

The experimental work was conducted on a turn master lathe. A specifically designed burnishing tool is the main element in the burnishing process. It accommodates a bearing steel ball of various diameters. The ball is located in position by means of rod and screw. The tool was held stationary and rigidly on the tool post of the lathe machine.

The values of the burnishing parameters used in the present investigation based on the availability are ball diameter 16.5 mm, speed 22.62 m/min, feed 0.085 m/rev, burnishing force 25 kgf.

3   Results and Discussion

The tension-impact fatigue test is conducted on drop hammer type equipment fabricated. Five different weights 100, 200, 300, 400, and 500 g are taken, respectively, for varying the peak stress levels. Before carrying the experiment, the weights of the attached mass and weight of the specimens were determined using electronic balance.

The numbers of impacts for specimen failure were obtained by keeping the weight of drop fixed at 60 mm of pre-adjusted level. The fatigue life was obtained for five different weights (five stress levels). The fatigue lives of unburnished and burnished specimens for different weights are as shown in Fig. 4 and Table 2.

The values of impact stresses were calculated on the basis of strain energy distribution using FEM applied to the notched specimen. In this approach, a complete shape of stress has been considered in the notched portion of the specimen, and complete energy balance has been satisfied.

An expression of specific deformation work can be written as

$$U = U_{\text{SD}} = \text{constant}$$

$$N^k U = U_{\text{SD}}$$

where

Table 2   Fatigue life of burnished, unburnished specimens at different weights

S. No.	Weight (gmf)	Fatigue life, N (cycles)		% improvement of fatigue life
		Unburnished	Burnished	
1	100	19,384	23,618	21.80
2	200	18,612	23,014	23.65
3	300	18,336	22,592	23.21
4	400	17,798	21,998	23.59
5	500	17,387	21,519	23.76
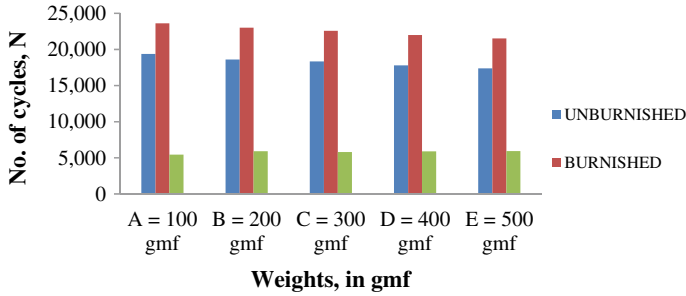
Fig. 4 Fatigue life of burnishing, unburnished specimens at different weights

N = number of impacts,
U = deformation work in single impact,
U_{SD} = specific deformation work.
Also $U = \frac{Wh}{V}$.
Therefore,

$$N = \left[U_{SD} \times \frac{V}{Wh} \right]^{\frac{1}{k}}$$

where k = constant, which depends on the loading conditions and material of specimen.

It has been shown using the wave propagation approach, that the maximum stress is related to the axial impact load (W) by the relation

$$\sigma = \sigma_0 \left[\sqrt{\frac{W}{V\rho g}} + 1 \right]$$

where $\sigma_0 = u_0 \sqrt{E \times \rho}$.

Hence,

$$\sigma = \sqrt{\left(\frac{2E}{V} \right)(Wh)} \left[1 + \sqrt{\frac{W}{w}} \right]$$

where
W = weight on the specimen, gmf,
w = weight of the specimen, gmf,
$u_0 = \sqrt{2gh}$, velocity of impact, m/s,
E = modulus of elasticity, N/m^2,
ρ = density of the material, kg/m^3.

3.1 Computational Analysis of the Specimen

In order to find the stress, the computational analysis is carried out in ANSYS software. The boundary conditions are taken in such a way that one end of the specimen is fixed, and force is taken at the other end (as shown in Fig. 5) for different weights 100, 200, 300, 400, and 500 gmf, respectively. The force applied on the specimen in ANSYS is shown in Table 3, and stresses obtained are as shown in Figs. 7, 8, 9, 10 and 11 (Fig. 6).

The values of impact stresses for different weights are shown in Table 4.

Figure 13 shows the relation between the impact stresses and the corresponding experimentally observed fatigue lives plotted on log scale. It can be observed that all the experimental points almost lie on a straight line. Therefore, impact stress fatigue life relation can be of polynomial form similar to Basquin's equation (Fig. 12; Table 5).

Using least square approximation, an equation of straight line in Fig. 13 is obtained as (Table 6)
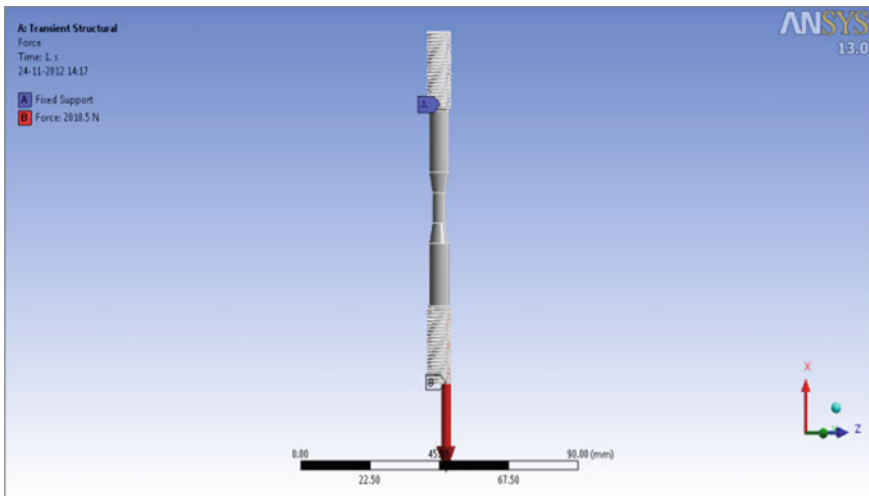
Fig. 5 Boundary conditions on the specimen in ANSYS

Table 3 Different forces applied on the specimen in ANSYS

Weight (g)	Force applied (N)
100	1591.14
200	1687.77
300	1777.88
400	1862.82
500	1943.37
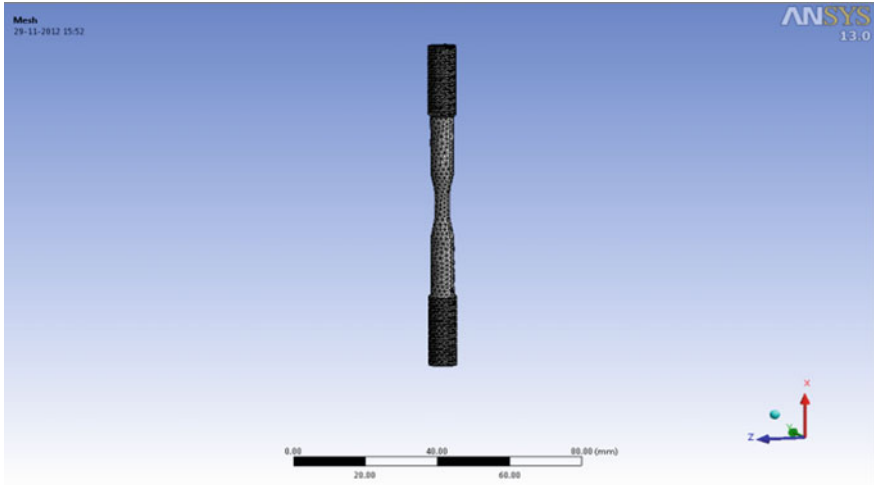
Fig. 6 Mesh on the specimen in ANSYS
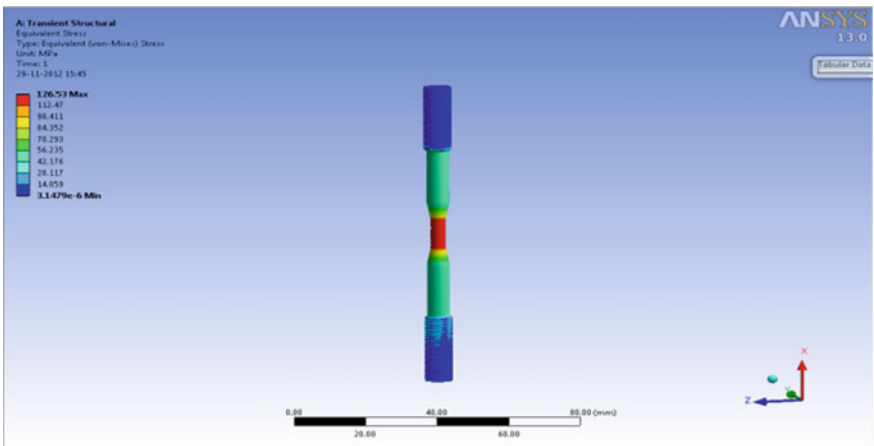
Fig. 7 Stress for 100 g weight on the specimen

$$N\sigma^{\mathrm{a}} = C \ \text{(required curve to be fitted)}$$

$$\Sigma Y = A\Sigma X + nB \tag{1}$$

$$\Sigma XY = A\Sigma X^2 + B\Sigma X \tag{2}$$

Substituting the values of ΣX, ΣY, ΣX^2, ΣXY in Eqs. (1) and (2), we get equations in A, B solving, then we get values of A and B (Table 7)
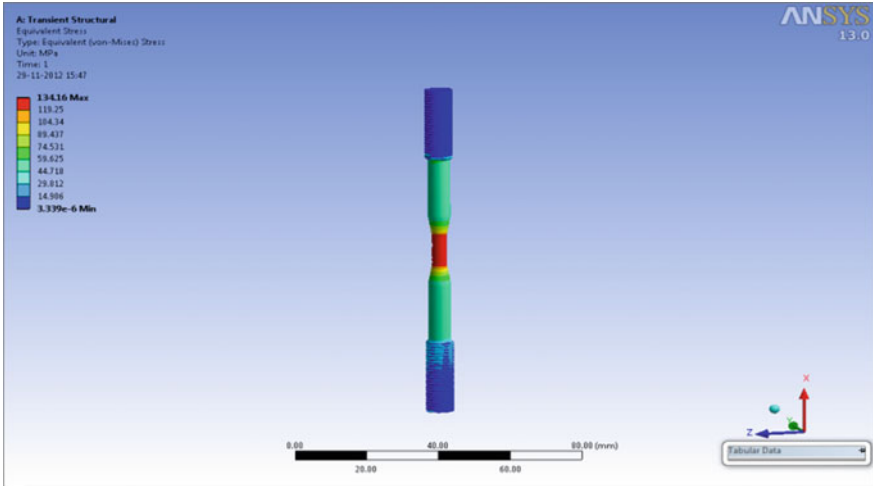
Fig. 8 Stress for 200 g weight on the specimen
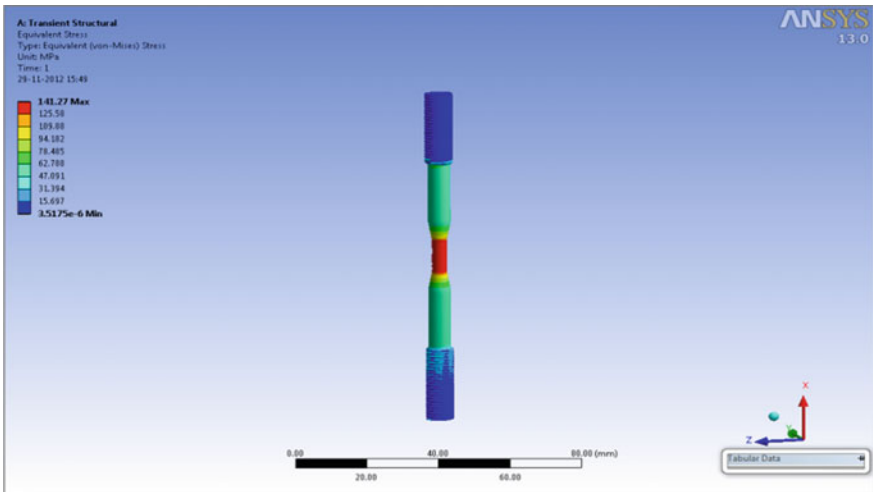
Fig. 9 Stress for 300 g weight on the specimen

$$10.7382 = 21.3109A + 5B \tag{3}$$

$$45.7654 = 90.8319A + 21.3109B \tag{4}$$

This provides a Basquin's type relation between the stress σ and fatigue life N. Hence, the experimental results support the peak stress and fatigue life relation under the impact loading situation.
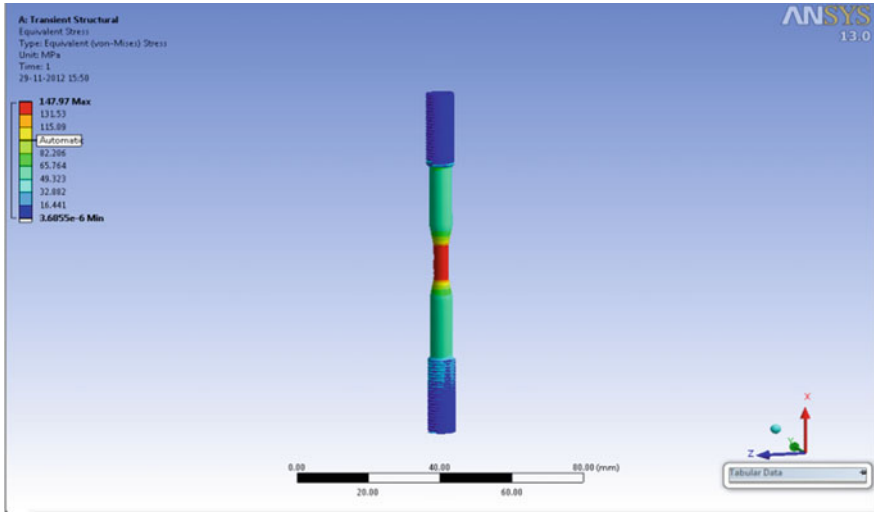
Fig. 10 Stress for 400 g weight on the specimen
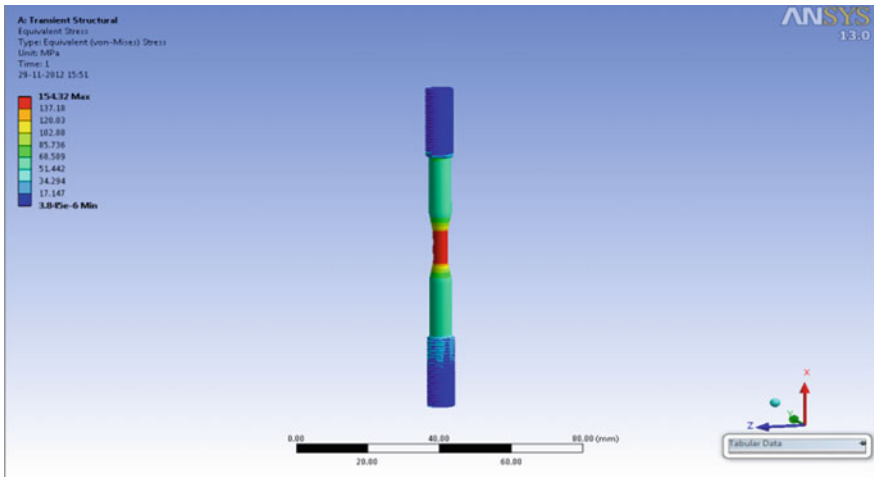
Fig. 11 Stress for 500 g weight on the specimen

Table 4 Impact stress variation according to the weight

Weights (gmf)	Impact stress, σ (MPa)
100	126.53
200	134.16
300	141.27
400	147.97
500	154.32

Fig. 12 Stress versus no. of cycles curve
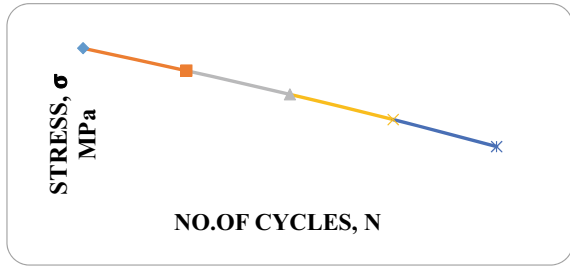
Fig. 13 Impact stress-fatigue life relation
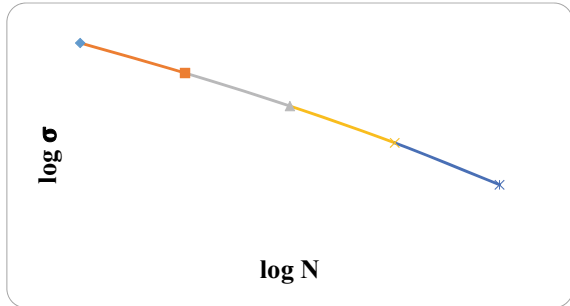
Table 5 Logarithmic values of stress and no. of cycles

Stress, σ (MPa)	Log σ	No. of cycles, N	Log N
126.53	2.1021	19,384	4.2874
134.16	2.1276	18,612	4.2697
141.27	2.1500	18,336	4.2633
147.97	2.1701	17,798	4.2503
154.32	2.1884	17,387	4.2402

Table 6 The constant values found by least square approximation method

S. No.	No. of cycles, N	Stress 'σ' (MPa)	X Log$_{10}$ N	Y Log$_{10}$ σ	X^2	Y^2	XY
1	19,384	126.53	4.2874	2.1021	18.3817	4.4188	9.0125
2	18,612	134.16	4.2697	2.1276	18.2303	4.5266	9.0842
3	18,336	141.27	4.2633	2.1500	18.1757	4.6225	9.1660
4	17,798	147.97	4.2503	2.1701	18.0650	4.7093	9.2235
5	17,387	154.32	4.2402	2.1884	17.9792	4.7890	9.2792
			$\sum X =$ 21.3109	$\sum Y =$ 10.7382	90.8319	23.0662	45.7654

Table 7 The values of A and B

1	$A = -2.6862$
2	$B = 13.5967$
3	Therefore, the values $A = -2.6862$, $B = 13.5967$ $a = -1/A$ $a = 0.3722$ $C = (a\,B)^{10}$ $C = 11,015,903.21$

4 Conclusions

The present work deals with experimental investigation on notched low-carbon steel specimens emphasize that the relation between fatigue life and impact stress which obeys Basquin's law. It is observed that burnishing as a beneficial cold working process in order to improve the fatigue life during normal and overstress working conditions. Relation between impact stress and fatigue life has been derived which comes out in the form of Basquin's law. Impact-tension fatigue equipment was fabricated, and experiments were conducted for low-carbon steel specimens. The impact stresses obtained from finite element method have been plotted and compared with experimentally observed fatigue lives, drawn a relation between two methods. The fatigue performance of steel specimens is greatly improved by 23% by ball burnishing process. The beneficial effects like induced macroscopic compressive residual stress, work hardening, and increased hardness serve to retard or inhibit the surface crack initiation and propagation and result in fatigue performance enhancement.

References

1. Marines-Garcia, I., Galván-Montiel, D., Bathias, C.: Fatigue life assessment of high-strength, low-alloy steel at high frequency. Arab. J. Sci. Eng. **33**, 237–248 (2008)
2. Liu, Y., Mahadevan, S.: Fatigue limit prediction of notched components using short crack growth theory and an asymptotic interpolation method. Eng. Fract. Mech. **76**(15), 2317–2331 (2009)
3. Subramanyan, S.: Estimation of fatigue limit through high-low step tests. J. Inst. Eng. **58**, 118–122 (1978)
4. Zhang, G.P., Volkert, C.A., Schwaiger, R., Monig, R., Kraft, O.: Fatigue and thermal fatigue damage analysis of thin metal films. Microelectron. Reliab. **47**, 2007–2013 (2007)
5. Kokavec, M., Konečná, R., Nicoletto, G.: Influence of surface quality on fatigue behavior of nodular cast iron. Acta Metall. Slovaca **17**(2), 99–105 (2011)
6. Srinivasa Rao, D.: Surface hardening of high-strength low alloy steels (HSLA) dual-phase steels by ball burnishing using factorial design. Mater. Manuf. Process. **22**, 1–5 (2007)
7. Sikora, J., Klopocki, J., Majewski, W.: Research of fatigue resistance of metal hydrodynamic journal bearings. J. KONES. Intern. Combust. Eng. **7**(1–2), 458–462 (2000)
8. Shul'ginov, B.S., Degtyarev, V.A.: Installation for fatigue testing of materials and their welded joints under high-cycle impact loading. Strength Mater. **30**(3), 350–354 (1998)
9. Kraft, O., Schwaiger, R., Wellner, P.: Fatigue in thin films: lifetime and damage formation. Mater. Sci. Eng. A **319–321**, 919–923 (2001)

10. Kim, J.-Y., Jacobs, L.J., Qu, J., Littles, J.W.: Experimental characterization of fatigue damage in a nickel-base superalloy using nonlinear ultrasonic waves. Acoust. Soc. Am. **120**, 1266–1273 (2006)
11. Troshchenko, V.T., Khamaza, L.A.: Fatigue limits of steels and stress gradient. Strength Mater. **43**(4), 417–425 (2011)
12. Jabur, K.S.: Surface roughness effect on fatigue life predictions under cumulative damage. Eng. Technol. J. **29**(6) (2011)
13. Bader, Q., Njim, E.K.: Effect of V notch shape on fatigue life in steel beam made of mild steel AISI 1020. Int. J. Mech. Prod. Eng. Res. Dev. (IJMPERD) **4**(4) (2014). ISSN(P): 2249-6890; ISSN(E): 2249-8001

Mechanical and Tribological Study of Bioactive Borosilicate Glass Fabricated Partially from Natural Waste

Satish Jain, Raghavendra Gujjala, Sushil Patel, Raj Kumar Samudrala, P. Abdul Azeem, and Shakuntala Ojha

1 Introduction

The deterioration of human body parts is inevitable. It can occur as a result of natural occurrences like aging or any unnatural trauma. As a consequence of these events, demand for synthetic organs, prosthetics, and other biological materials has continued to rise. The first generation of biomaterials emerged in the early 1970s with the objective to achieve physical compatibility and biological inertness [1]. Later, in the decade, Prof. L. L. Hench introduced revolutionary bioactive glasses that set the tone for second-generation biomaterials. A bioactive material is one that elicits a distinct physiological response at implant tissue interface resulting in bond between them [2]. Some of the examples of bioactive materials are hydroxyapatite, dense calcium phosphate ceramics, bioglass, etc.

A vast amount of research has already been conducted out on bioactive glasses and glass ceramics for applications in therapeutic, orthopedic, and dental fields due to their unique properties of quick bone bonding, tunable degradation, and triggered proliferation [3, 4]. The most popular of these glasses is 45S5 or bioglass which consists of 45% SiO_2, 24.5% Na_2O, 24.5% CaO, and 6% P_2O_5 all in wt.%. It is in vivo study revealed incredible bonding strength between bioglass and host. It was nearly impossible to separate them without breaking the bone [5]. However, their

S. Jain · R. Gujjala (✉)
Department of Mechanical Engineering, National Institute of Technology, Warangal, Telangana 506004, India
e-mail: raghavendra.gujjala@nitw.ac.in

S. Patel · R. K. Samudrala · P. Abdul Azeem
Department of Physics, National Institute of Technology, Warangal, Warangal 506004, India

S. Ojha
Department of Mechanical Engineering, Kakatiya Institute of Technology and Science, Warangal, Telangana 506004, India

slow rate of degradation and weak mechanical properties limit their applications in load bearing applications [6].

Silica-free borate glass has been fabricated which showed relatively higher rate of degradation and quicker formation of HCA layer in SBF fluid [7]. Hence, borosilicate glass was synthesized with the goal to optimize the degradation rate in order to match tissue formation rate in vivo. Also, study of mechanical and tribological properties and optimizing the same with tailored compositions is important for expanding its application domain.

In a study conducted by Samudrala et al. [8], a borosilicate glass was proposed with base composition synthesized by pure chemicals. In vitro bioactivity and cell culture studies were conducted on glass with SBF and MG-63 cells, respectively. The results suggested formation of HCA layer after 5 days of immersion in SBF and its cytocompatible nature. Even though there has been a lot of biological studies conducted, there is insufficient data about their mechanical and tribological behavior. Hence, the current study investigates the mechanical and tribological properties of Borosilicate glass synthesized partially from natural waste.

2 Materials and Methods

2.1 Materials

Boric anhydride (B_2O_3, 99.5%, Himedia), sodium carbonate (Na_2CO_3, 99.9%, Merck) along with silica (SiO_2) and calcium oxide (CaO) are used to fabricate glass. Silica and calcium oxide have been extracted from natural waste, i.e., rice husk and egg shell, respectively.

2.2 Extraction of Calcium Oxide from Egg Shells

Eggshell counts as one of the highest waste products in the food processing industry. Some of the researchers have also remarked about its hazardous nature in our environment. The eggshell weighs approximately 11% of the total weigh of the egg, and it consists of calcium carbonate ($CaCO_3$). The extraction of CaO from eggshells has been done by Palakurthy et al. [9], and it is pictorially represented in Fig. 1. Eggshells were collected from NIT Warangal canteen and washed thoroughly to get rid of dust and dirt. It was boiled later for 20 min to remove egg's inner membrane and then washed again with distilled water to separate both. The eggshells were then kept in oven overnight at 60 °C to eliminate all its moisture content. The dried eggshells were then transferred to pestle and mortar and hand ground into fine particles. The ground particles were then kept in furnace, and heating was conducted in 2 stages. First stage heating included heating up to 450 °C at rapid heating rate (5 °C/min)
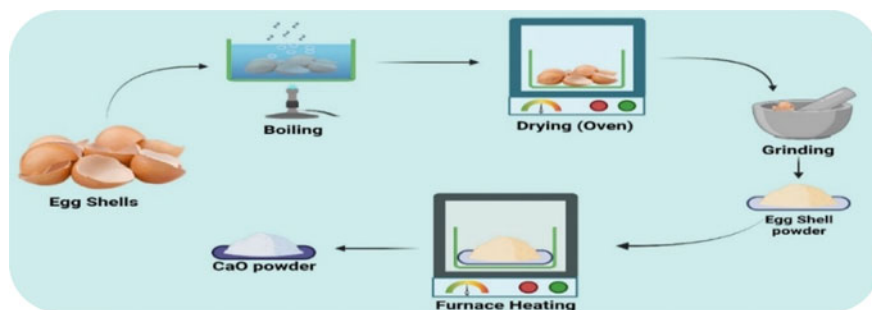
Fig. 1 Pictorial representation of calcium oxide extraction from eggshell

with holding time of 2 h to get rid of organic residuals, and second stage heating included heating up to 900 °C at slow rate (0.5 °C/min) and holding for another two hours to eliminate carbon dioxide from calcium carbonate and leave pure calcium oxide.

2.3 Extraction of Silica from Rice Husk

ice husk is the outer most protection layer of rice and weighs almost 23% of the rice production in agriculture. It is biodegradable substance but acts as an air pollutant when burnt. It consists of more than 85% silica (SiO_2). The extraction of silica from rice husk has been done by Srinath et al. [10] and is pictorially represented in Fig. 2. The rice husk was procured from a rice mill in Warangal. It was washed rigorously with normal water to separate dirt and dust. It was then HCL treated under continuous stirring for 2 h. The rice husk was then filtered, washed, and rinsed in DI water to let go of all the acid. It was then dried in an oven at 100 °C and left overnight. The dried rice husk was then heated in furnace at 600 °C with holding time of 4 h followed by furnace cooling. The color change of rice husk to white color confirmed its transformation to silica (SiO_2).

2.4 Fabrication of Borosilicate Glass

Borosilicate glass has been fabricated successfully with 31% B_2O_3, 20% SiO_2, 24.5% CaO, and 24.5% Na_2O all in wt.% using melt-quench technique. Respective compositions were taken and hand ground using pestle and mortar to reduce the particle size and get rid of any trapped air within particles. The ground powder was then transferred to platinum crucible and kept in furnace at 1200 °C. The holding time was 30 min, and it was stirred in between to get proper uniformity. The melted powder was then poured in preheated mold and quickly transferred to another furnace at
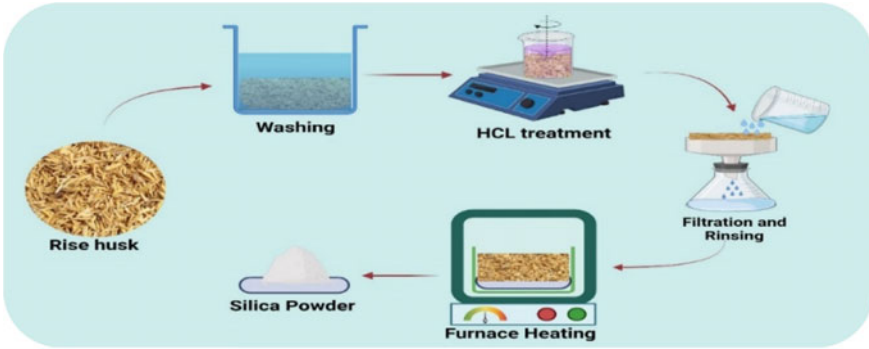
Fig. 2 Pictorial representation of silica extraction from rice husk
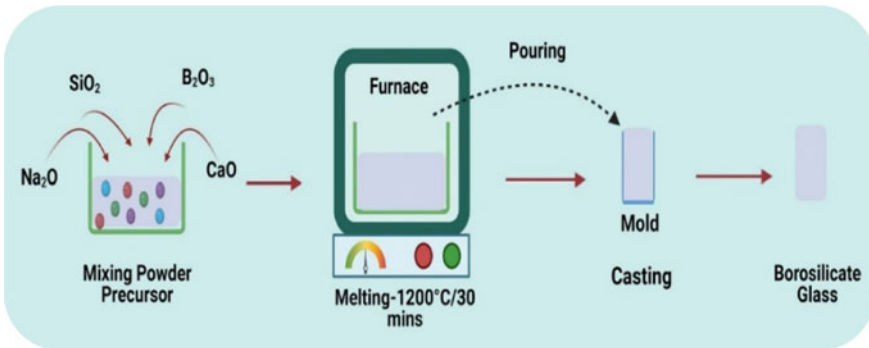
Fig. 3 Schematic representation of borosilicate glass through melt-quenching technique

300 °C for 2 h. The glass was then furnace cooled to relieve its internal stresses. A schematic of glass fabrication technique is shown in Fig. 3.

2.5 Mechanical Studies

The theoretical density (ρ_t) of borosilicate glass had been calculated using the formula:

$$\rho_t = \sum_i x_i \rho_i \tag{1}$$

where x_i and ρ_i are the mole fraction and densities of individual oxides present in glass, respectively.

The actual density of glass (ρ_a) was measured using Archimedes principle. Distilled water was used as the buoyant medium. The void fraction of glass was calculated from the equation given below:

$$\text{Void Fraction (\%)} = \left(1 - \frac{\rho_a}{\rho_t}\right) \times 100 \tag{2}$$

Hardness test of glass specimen was performed by Vickers microhardness tester (S MATSUZAWA). A load of 200 g was applied with holding time of 15 s.

Compression test of glass specimen was performed on universal testing machine (UTM) having maximum working load of 3000 kg (Advance equipment). The sample was cylindrical in nature with 11 mm bore diameter and 15 mm height. Samples were tested at a speed of 2 mm/min.

2.6 Tribological Studies

The wear behavior analysis of borosilicate glass was performed on pin-on-disk tribometer (Magnum Make) as per ASTM G99-05. The samples were cylindrical in shape with bore diameter of 11 mm and height of 35 mm. An emery paper with grit size of 180 was used as counter surface. All the tests were carried out at room temperature and humidity. Tests were carried out taking speed and load as variable, while distance covered by each sample was kept constant.

The specific wear rate of each sample was calculated using formula written below:

$$W_s = \frac{\Delta W}{\rho \cdot d \cdot F}. \tag{3}$$

where ΔW, ρ, d, and F represent wear (loss in weight) after performing test (kg), density of the sample (kg/m^3), sliding distance (m), and load (N), respectively.

The debris particle of the most worn out sample was collected and analyzed using field electron scanning electron microscopy (FESEM) (Model–Quanta 200FEG, FEI).

3 Results and Discussions

3.1 Mechanical Studies

The theoretical and actual density of borosilicate glass synthesized using natural wastes were found to be 2.667 and 2.56, respectively. The lesser actual density is due to presence of voids which may have been caused due to air entrapment or glass

Fig. 4 Typical indentation imprint on borosilicate glass during hardness test
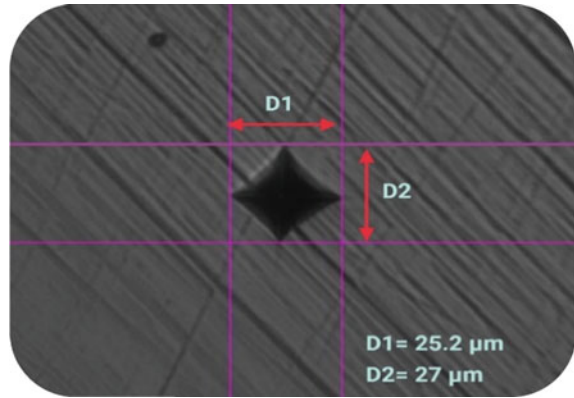
shrinkage during cooling. The void content in the sample was found to be around ~4%. The presence of voids may interfere in mechanical and tribological properties of glass.

The hardness value of prepared glass specimen was found to be 534 ± 10 HV which came in line with study conducted by Samudrala et al. [11] who synthesized the glass using pure chemicals. An indentation imprint under Vickers microhardness tester is shown in Fig. 4.

The load–displacement graph for borosilicate glass is shown in Fig. 5. The glass being brittle in nature ruptured at peak load of 8237.59 N. The sudden failure of glass specimen took place by rapid crack formation and its propagation. The compression strength and modulus of elasticity of the glass specimen was found to be 86.72 and 891.53 MPa, respectively. The strength of borosilicate glass has been found in between the strength values of pure silicate glass and borate glass as indicated by a study conducted by Deliormanlı et al. [12]. The variation in compressive strength value is a result of difference in strength of Si–O and B–O bonds.

3.2   Tribological Studies

The cylindrical specimens of borosilicate glass were polished using a grinder and emery paper to get a mirror-like finish. The samples were then operated on emery paper with 180 grit size. Testing was done taking 3 different loads (5, 10, 15 kg) and three different speeds (200, 300, 400 rpm). Figure 6a shows the variation in wear as a function of time at 3 different loads keeping speed of 200 rpm. It is clear that wear is directly dependent on load (at constant speed). After 180 s, maximum wear was observed at 15 N (670 µg), and minimum wear was observed at 5 N load (590 µg). This may be due to higher frictional force generated as result of higher normal load applied at 200 rpm. The value of wear rate at 10 N was found between 5 and 15 N. The variation is similar in case of other speeds (300 and 400 rpm) too.
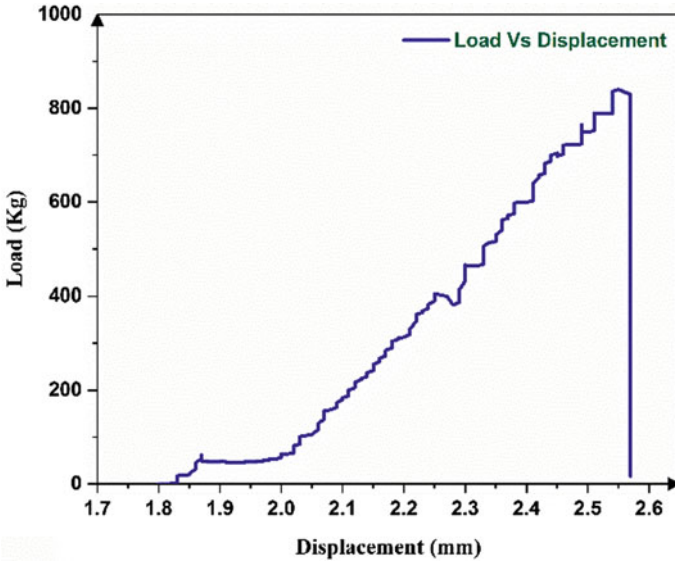
Fig. 5 Load versus displacement graph of borosilicate glass conducted via UTM
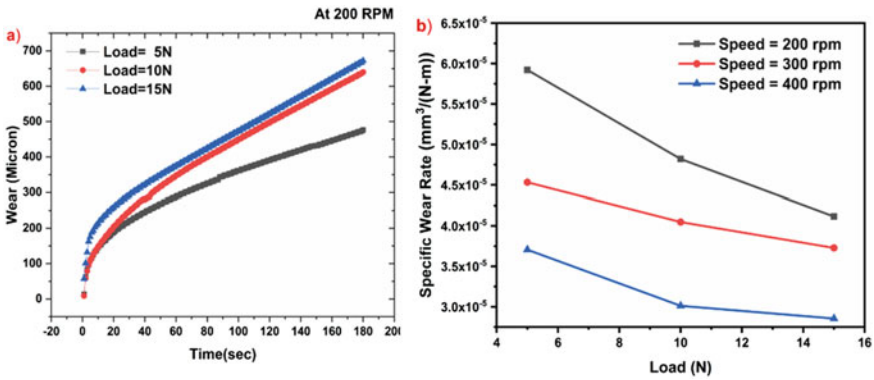
Fig. 6 a Variation of wear rate at 200 rpm **b** specific wear rate vs load at different rpms for borosilicate glass

Figure 6b shows a plot of specific wear rate vs load at different rpms for borosilicate glass. The specific wear rate is decreasing with increasing load and speed, respectively. Maximum specific wear rate was observed at 5 N load and 200 rpm (5.921×10^{-5} mm^3/N m), while minimum value was observed for 15 N load and 400 rpm speed (2.854×10^{-5} mm^3/N m). The specific wear rate graph showed similar trends at all 3 speeds. The debris of specimen with maximum specific wear rate was collected and observed under scanning electron microscope under different resolutions to study its nature.
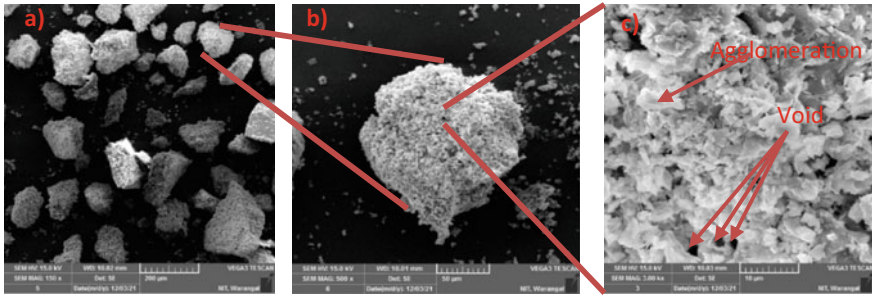
Fig. 7 Debris particle of specimen with maximum specific wear rate at different resolutions of **a** 200 μm **b** 50 μm and **c** 10 μm

The agglomeration of different particles and voids after abrasive wear can been in Fig. 7. The agglomeration may have happened due to bonding between particles as a result of heat produced during sliding.

4 Conclusions

From various studies conducted on Borosilicate glass, following conclusions have been drawn:

1. Borosilicate glass have been successfully synthesized using natural wastes like egg shell and rice husk.
2. The theoretical and actual density of Borosilicate glass synthesized using natural wastes were found to be 2.667 and 2.56 respectively.
3. The hardness value of prepared glass specimen (534 ± 10 HV) was in range with the similar glass fabricated by pure chemicals.
4. The compression strength and modulus of elasticity of the glass specimen was found to be 86.72 and 891.53 MPa respectively. The inclusion of Boron weakened the glass structure and hence the strength.
5. Maximum specific wear rate was observed at 5 N load and 200 rpm (5.921×10^{-5} mm^3/N m) while minimum value was observed for 15 N load and 400 rpm speed (2.854×10^{-5} mm^3/N m).

References

1. Hench, L.: Biomaterials. Science **208**, 826–831 (1980)
2. Hench, L.L., Ethridge, E.C.: Biomaterials: An Interfacial Approach, p. 385. Academic (1972)
3. Ll, H., Jm, P.: Third-generation biomedical materials. Science **295**, 1014–1017 (2002)
4. L.L. Hench, Bioceramics: from concept to clinic. J. Am. Ceram. Soc. **72**, 93–98 (1993); J. Am. Ceram. Soc. **74**, 1487–1510 (1991)

5. Hench, L.L., Splinter, R.J., Allen, W.C., Greenlee, T.K.: Bonding mechanisms at the interface of ceramic prosthetic materials. J. Biomed. Mater. Res. **5**, 117–141 (1971)
6. Huang, W., Day, D.E., Kittiratanapiboon, K., Rahaman, M.N.: Kinetics and mechanisms of the conversion of silicate (45S5), borate, and borosilicate glasses to hydroxyapatite in dilute phosphate solutions. J. Mater. Sci. Mater. Med. **17**, 583–596 (2006)
7. Day, D.E., White, J.E., Brown, R.F., McMenamin, K.D.: Transformation of borate glasses into biologically useful materials. Glas. Technol. **44**, 75–81 (2003)
8. Samudrala, R., Reddy, G.V.N., Manavathi, B., Azeem, P.A.: Synthesis, characterization and cytocompatibility of ZrO_2 doped borosilicate bioglasses. J. Non Cryst. Solids **447**, 150–155 (2016)
9. Palakurthy, S., Reddy, K.V., Patel, S., Azeem, P.A.: A cost effective SiO_2–CaO–Na_2O bio-glass derived from bio-waste resources for biomedical applications. Prog. Biomater. **9**, 239–248 (2020)
10. Palakurthy, S., Venu Gopal Reddy, K., Samudrala, R.K., Abdul Azeem, P.: In vitro bioactivity and degradation behaviour of β-wollastonite derived from natural waste. Mater. Sci. Eng. C **98**, 109–117 (2019)
11. Samudrala, R., Abdul Azeem, P., Penugurti, V., Manavathi, B.: Cytocompatibility studies of titania-doped calcium borosilicate bioactive glasses in-vitro. Mater. Sci. Eng. C **77**, 772–779 (2017)
12. Deliormanlı, A.M.: Synthesis and characterization of cerium- and gallium-containing borate bioactive glass scaffolds for bone tissue engineering. J. Mater. Sci. Mater. Med. **26**, 1–13 (2015)

Computer Aided Analysis of Involute Gear Tooth for Minimization of Bending Stress

Rapeta Sundara Ramam

1 Introduction

The most efficient way of delivering power from the source to the driven part is through gear drives. They are very effective in transmitting torque when the centre distance between the driver and the driven members is very close. The designs of these gears for various industrial applications are over a century old. Many researchers have contributed to the development of materials, modified geometry, analyzed the gears for various applications, and have proposed developments over those of the existing ones in the past.

Cavdar et al. [1] devised a method for estimating the bending stress minimization of an involute spur gear. A computer programme was used to analyze the variation of bending stress and contact ratio dependent on the pressure angle on the driving side. Kapelevich [2] presented a method for boosting load capacity while lowering weight, vibration, and size, and his research shows that asymmetric tooth geometry allows for increased load capacity while reducing dimensions and weight for specific gear types. Litvin et al. [3] developed a redesigned geometry to allow them to more easily localize and stabilize the bearing contact while obtaining a more advantageous form of transmission errors. Shekhtman and Kapelevich [4] discussed how to reduce bending stress by adjusting the fillet radius. By optimizing the fillet profile, the maximum bending stress in the gear tooth root area is lowered by 10–30%. Direct gear design, introduced by Kapelevich and Kleiss [5], allows for the assessment of a wide range of parameters for all feasible gear combinations to discover the optimal solution for a given application. Direct gear design with an asymmetric tooth profile opens up new sources for development in gear drives with unidirectional load cycles,

R. Sundara Ramam (✉)
Department of Mechanical Engineering, Vignan's Institute of Information Technology, Visakhapatnam, Andhra Pradesh 530049, India
e-mail: sundar.ramam@gmail.com

523

such as those present in many mechanical gearboxes. According to McNamara and Kapelevich [6], when compared to traditionally made gears, direct gear design leads to a 15–30% reduction in stress. This translates to greater load capacity (15–30%), smaller and lighter size and weight (10–20%), longer life, lower costs, increased dependability, lower noise and vibration, higher gear efficiency, and lower maintenance costs. Karpat et al. [7] presented innovative gear designs that are required due to rising performance demands such as long life, high endurance, high load capacity, quick speed, and low cost. Deng et al. [8] discussed the newly developed and modified gear models that could be used for mating analysis. According to the findings, the involute modification of the produced gear helped improve transmission performance. Senthil Kumar et al. [9] investigate the use of an asymmetric tooth edge that can be used to improve the bending capacity of symmetric involute gears constructed using a standard technique since the tipping development limits the load-bearing capacity at higher pressure angles. Masuyama and Miyazaki [10] presented the asymmetric tooth profile gear strength when the load-sharing ratio is taken into account and the performance of the gear is compared to the torque transmission capacity. The researchers looked at tooth pressure angles ranging from 20° to 45°. Vaghela and Prajapati [11] addressed how to lessen the bending stress of asymmetric involute spur gear teeth by optimizing the root shape. The Von Mises stress of the optimized root profile is investigated and compared to the regular asymmetric gear fillet profile. The root profile is optimized, and the Von Mises stress is lowered by 16.68%. The stress concentration of the improved asymmetric spur gear has been considerably reduced. According to Olguner and Filiz [12], asymmetric gears with a bigger pressure angle on the driving side contribute significantly to boosting load-bearing capacity and flow rate, as well as lowering flow rate volatility, which is detrimental to the gear pumps' dynamic behaviour. Mallesh et al. [13] examined bending stresses and how they decreased with the increasing number of teeth and pressure angle on the drive side. When all gear teeth are subjected to the same load, the one with the most teeth will be stressed less. According to research, bending stress reduces when the pressure angle on the drive side increases. Prabhu Sekar [14] proposes that asymmetric teeth can be used to enhance gear efficiency by increasing contact force and load carrying capacity, as well as improving wear resistance. He analyzed the load shared by a tooth pair, frictional power losses, wear resistance, fillet and contact stresses, and respective mechanical efficiencies to conduct comparative performance research of symmetric and asymmetric spur gears.

An asymmetric gear tooth profile and modifying the root fillet radius are considered in this work to reduce bending stresses. The advantages of reducing the bending stress are increased life, a reduction in cost, and increased efficiency.

2 Materials and Methods

The material used to make gears is determined by its strength and service conditions such as wear, noise, and so on. Metal or non-metallic materials can be used to make

the gears. Commercially available metallic gears with cut teeth are made of cast iron, steel, and bronze. Non-metallic materials including wood, rawhide, compressed paper, and synthetic polymers like nylon are used in gears to reduce noise.

Because of its outstanding wear qualities, excellent machinability, and ease of manufacturing intricate geometries using the casting method, cast iron is commonly used in the production of gears. Where a smooth motion is not required, cast iron gears with chopped teeth might be used. Plain carbon steel or alloy steel may be utilized for high-strength gears. To achieve a good balance of toughness and tooth hardness, steel gears are frequently heat-treated. Worm gears are commonly made of phosphorus bronze to decrease wear, which would be extreme with steel or cast iron.

2.1 Geometric Modelling and Analysis of Gear Tooth

The bending stresses of the gear tooth have been reduced in this study by either utilizing an asymmetric tooth or modifying the root fillet radius of the tooth. The next two sections go over these two options in detail.

2.1.1 To Minimize the Bending Stress in the Gear Tooth, the Asymmetric Gear Tooth is Considered as the First Alternative Design

The following are the specifications for a single reduction spur gear.

Gear ratio = 10:1,
Centre to centre distance = 660 mm,
No. of teeth on gear = 150,
Module (m) = 8 mm,
Pitch circle diameter = 1200 mm,
Addendum = Module (m),
Dedendum = 1.25 m,
Tooth thickness = 1.5708 m,
Minimum clearance = 0.25 m,
Fillet radius = 0.4 m.

The values of the theoretical bending stresses and percentage reduction in bending stresses are calculated for various angles of pressure on the drive side and are given in Table 1.

Input parameters for analysis of gear tooth using in a software package

Thickness of gear = 40 mm, Force applied (W) = 50 N.
Properties of material: E = 3e6, μ = 0.24.

Table 1 Percentage reduction in bending stress

S. No.	Pressure angle (Ø) in degrees	Stress (σ) in kgf/mm^2	% reduction in σ_b (%)
1	20–20	1.091	–
2	20–25	0.975	10.5
3	20–30	0.874	20.18
4	20–35	0.814	25.32
5	20–40	0.756	31.19
6	20–45	0.629	42.29

Figure 1 shows the involute profile of the gear tooth for the selected pressure angles of 20–20°, 20–25°, 20–30°, 20–35°, 20–40° and 20–45° respectively.

For comparison, the bending stresses obtained from ANSYS software along with theoretical values are given in Table 2.

Figure 2 shows the distribution of bending stresses in the gear tooth with respective numerical values for the pressure angles of 20–20°, 20–25°, 20–30°, 20–35°, 20–40° and 20–45° respectively.

The bending stresses are found to be decreasing from 1.091 to 0.629 kgf/mm^2 as the pressure angle on the drive side increased from 20° to 45°. Further, to investigate the bending stresses in the tooth, a modified root fillet radius is also considered. This is discussed in the following section in detail.

2.1.2 Minimization of Bending Stress in the Gear Tooth by Modifying the Root Fillet

It is proposed to study the effects of the bending stresses concerning modified fillet radii. Keeping all parameters of alternative 1 except the fillet radii, an attempt is made to explore the possibility of obtaining better bending stresses by a suitable curve fitting method. (Best curve fit method).

The concept is given below:

Bending stress minimization is achieved by designing a fillet profile that has a low bending stress concentration and meets specific requirements (e.g., manufacturability). This problem can be solved in a variety of ways. They are based on a curve-fitting technique in which the trochoid fillet profile, which is common in rack or mating gear generating methods, is substituted by an ellipse, parabola, chain line, or other curves to decrease bending stress.

The trace of the mated gear tooth is the initial fillet profile. This profile is the top-level boundary that limits the optimization search area to avoid interfering with the mating gear. The start and last fillet positions on the form diameter circle cannot be changed throughout the optimization process. In the random search approach, the fillet nodes (save the first and last) are relocated along the beams that pass between the fillet centre and the initial fillet profile nodes. The fillet's centre corresponds to the centre of the best-fitting circular. For each new fillet point combination, the bending
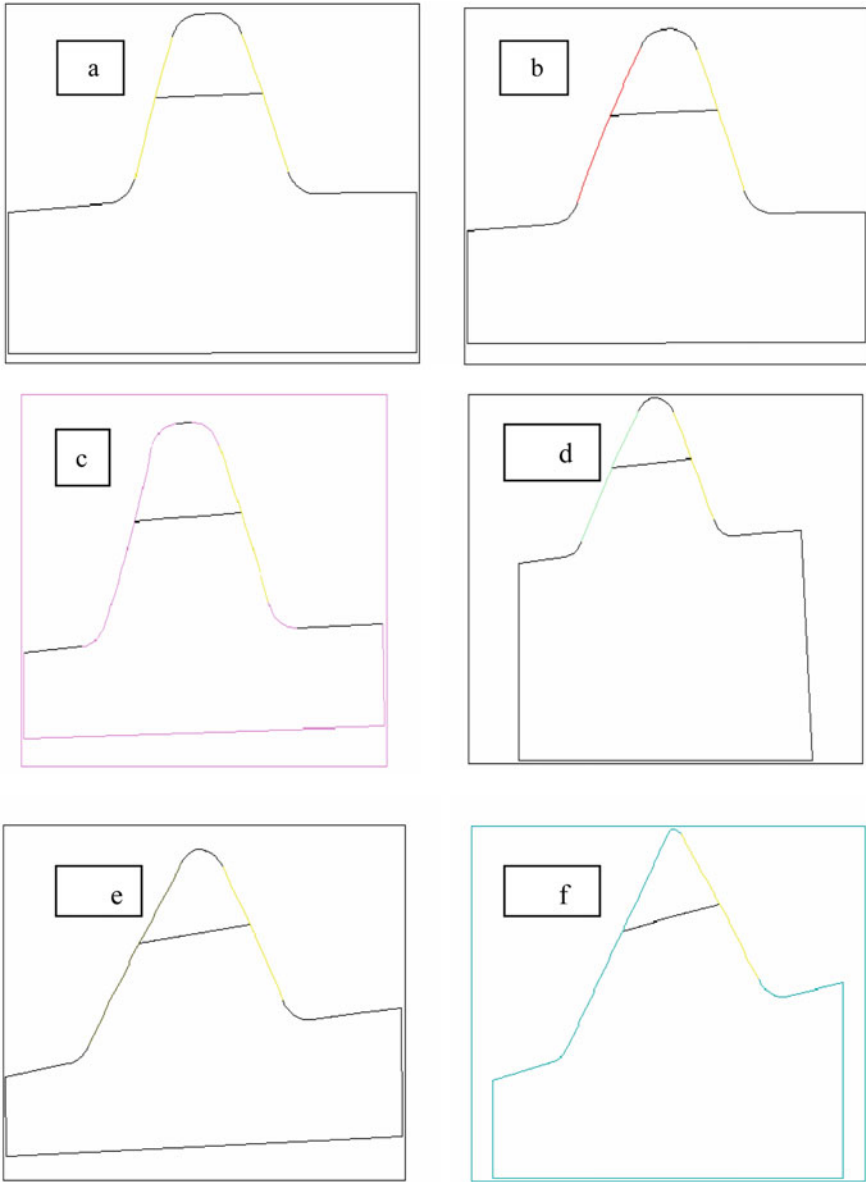
Fig. 1 Involute profile of gear teeth when pressure angles on coast side and drive side are **a** 20–20° **b** 20–25° **c** 20–30° **d** 20–35° **e** 20–40° **f** 20–45° respectively

Table 2 Comparison of theoretical and ANSYS software calculated stresses

S. No.	Pressure angle (Ø) in degrees	Theoretical stress, $\sigma_{Bending}$ (kgf/mm^2)	Stress has shown by ANSYS (kgf/mm^2)
1	20–20	1.290	1.090
2	20–25	1.117	0.975
3	20–30	1.027	0.875
4	20–35	0.904	0.814
5	20–40	0.762	0.756
6	20–45	0.638	0.629

stresses are calculated, and the figures and results for each of the adjusted fillet radii are as follows:

Table 3 shows the bending stresses at different root fillet shapes of 20° involute symmetric teeth.

Figures 3, 4, 5 and 6 show the involute profile of the gear tooth for the designed fillet, circular root fillet, and elliptical root fillets, respectively.

Figures 7, 8, 9 and 10 show the distribution of bending stresses in the gear tooth for different root fillet shapes.

The best-fit curves at root are tried to study the trend of the bending stresses right from the designed fillet radius to an elliptical[2] shape. The obtained stresses and the percentage reduction in bending stresses are given in Table 3.

3   Results and Discussions

The goal of this study was to reduce the bending stresses in the gear wheel teeth by considering the asymmetric tooth and modifying the root fillet radius. The values for the above two cases are given in detail in the above section. The discussions about these results are given in the following sections.

While considering the asymmetric teeth to explore the possibility of reducing the bending stresses, the theoretical values of 20° pressure angle symmetric teeth are compared with asymmetric teeth of different pressure angles on the drive side, and the percentage reduction in bending stresses is also given in Table 1.

From the above table, it is found that as the pressure angle varied from 20–20° to 20–45°, the reduction in bending stresses was found to be 42.29%.

Table 2 shows the comparison of theoretical and ANSYS software calculated values. The decreasing trend of the theoretical values of bending stresses due to the use of asymmetric teeth is further confirmed by using ANSYS software.

While considering the modification of the root fillet radius according to the best-fit curve technique, the resulting bending stresses for various alternative best-fit curves are given in Table 3. From the table, it is found that as the root fillet profile is modified

Fig. 2 Analysis of Involute profile of gear teeth when pressure angles on coast side and drive side **a** 20–20° **b** 20–25° **c** 20–30° **d** 20–35° **e** 20–40° **f** 20–45° respectively

from the design fillet to an elliptical shape, the reduction in bending stresses is found to be 48.51%.

Table 3 Bending stresses at different root fillet shapes of 20° involute symmetric teeth

S. No.	Root fillet shape	Obtained stress in kgf/mm^2	% reduction in bending stress
1	Designed fillet	1.091	– -
2	Circular root	0.7287	33.20
3	Elliptical[1]	0.6728	38.33
4	Elliptical[2]	0.5617	48.51

Fig. 3 Involute profile of symmetric gear tooth with designed fillet
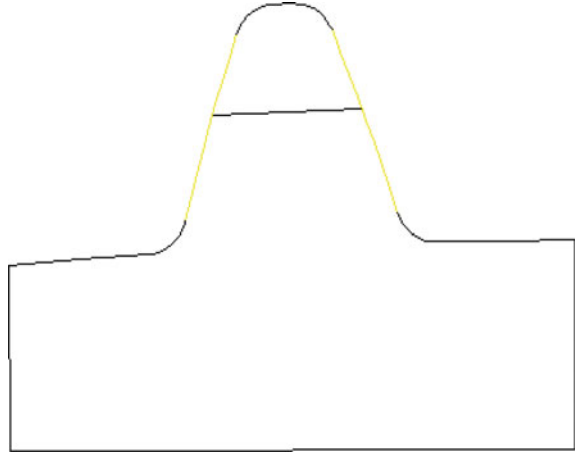
Fig. 4 Involute profile of symmetric gear tooth with circular fillet
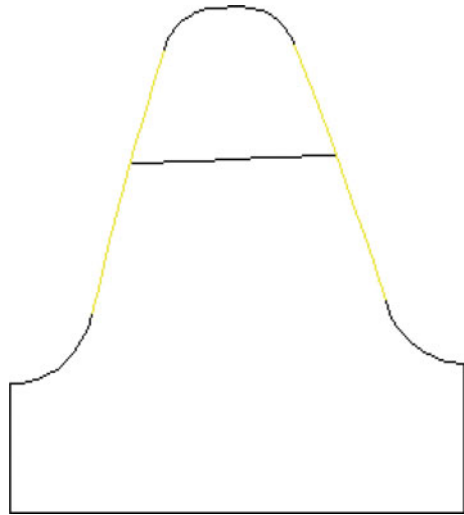
Fig. 5 Involute profile of symmetric gear tooth with elliptical[1] root fillet
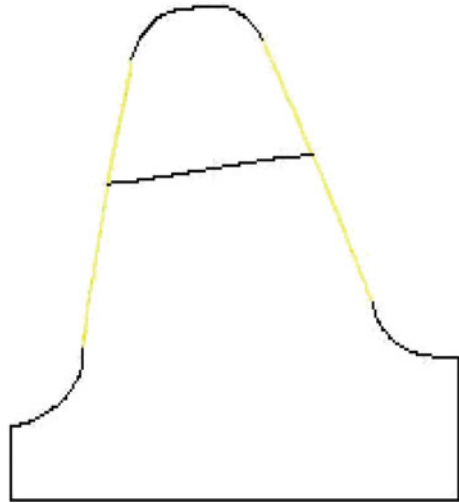
Fig. 6 Involute profile of symmetric gear tooth with elliptical[2] root fillet
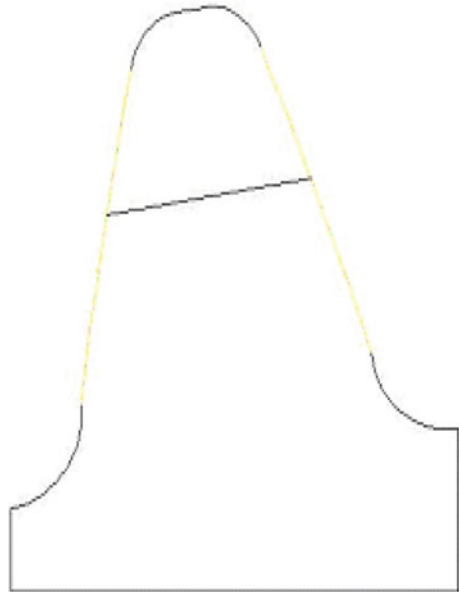
4 Conclusions

In the first suggested consideration, in which the asymmetric teeth are considered with an increased pressure angle on the drive side from 20–20° to 20–45°, it is noted that the bending stresses in the gear teeth are going to be reduced to a maximum value of 42.29%. As the pressure angle on the drive side is further increased beyond
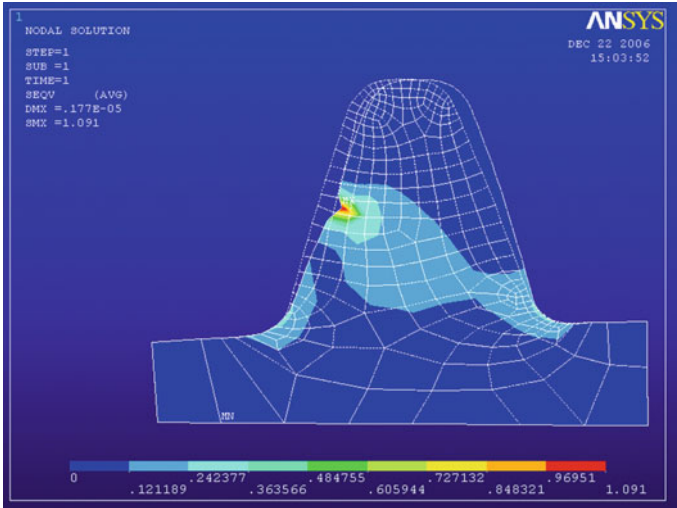
Fig. 7 Analysis of Involute profile of symmetric gear tooth with designed fillet
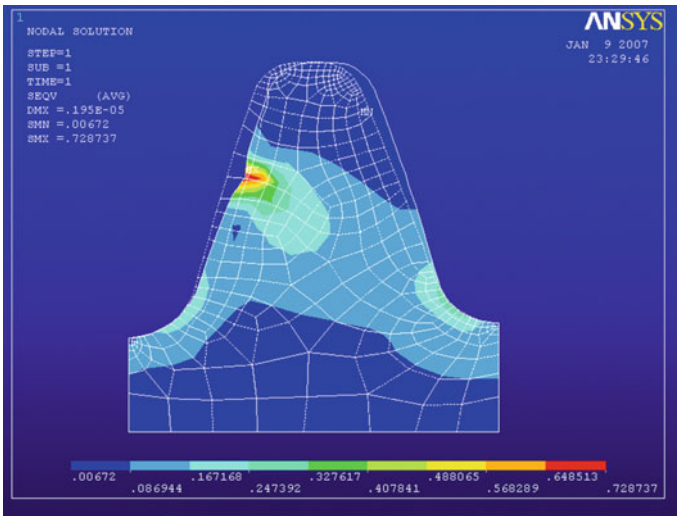
Fig. 8 Analysis of Involute profile of symmetric gear tooth with circular fillet

45°, the top land of the tooth is going to narrow and finally result in a single line because of the intersection of the two involute profiles on either side of the tooth.

In the second consideration, it is observed that the bending stresses are reduced by up to 48.51% for the modified fillet radius employing an elliptical profile.

From the above two, it is found that modifying the root fillet radius is the better option to employ in the manufacture of gears for reduced bending stresses. Longer
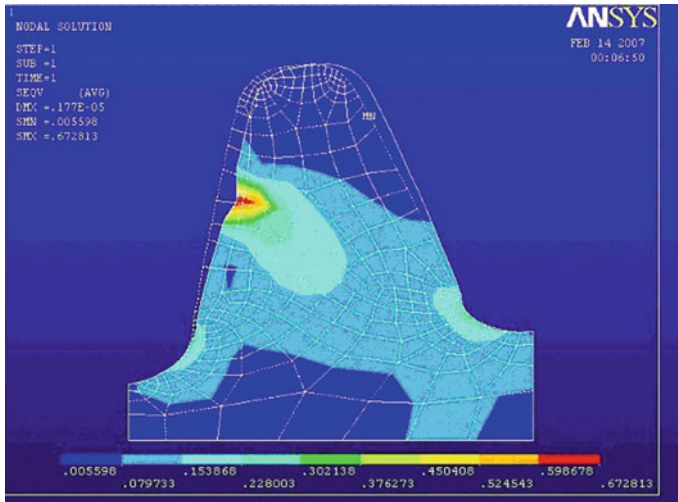
Fig. 9 Analysis of Involute profile of symmetric gear tooth with elliptical[1] root fillet
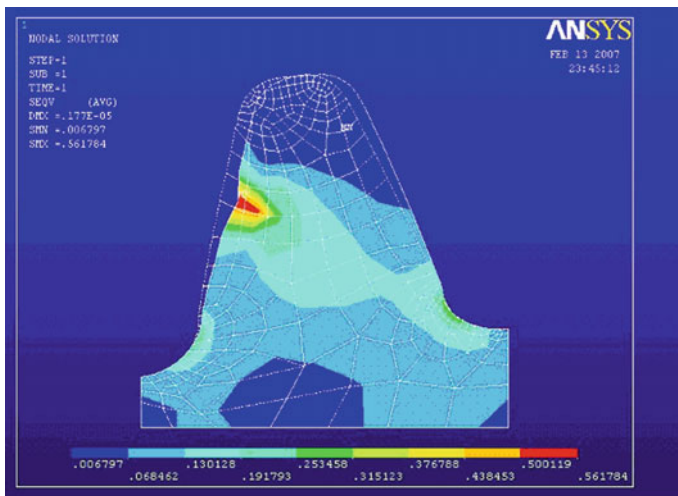
Fig. 10 Analysis of Involute profile of symmetric gear tooth with elliptical[2] root fillet

life, reduction in size and weight, application with a higher load, reduction of noise and vibration, cost reduction, and increased efficiency are all benefits of bending stress reduction.

References

1. Cavdar, K., Karpat, F., Babalik, F.C.: Computer aided analysis of bending strength of involute spur gears with asymmetric profile. J. Mech. Des. **127**, 477–484 (2005)
2. Kapelevich, A.L.: Geometry and design of involute spur gears with asymmetric teeth Mech. Mach. Theory **35**, 117–130 (2000)
3. Litvin, F.L., Lian, Q., Kapelevich, A.L.: Asymmetric modified spur gear drives: reduction of noise, localization of contact, simulation of meshing and stress analysis. Comput. Methods Appl. Mech. Eng. **188**, 363–390 (2000)
4. Kapelevich, A.L., Shekhtman, Y.V.: Direct gear design: bending stress minimization. Gear Technol. 44–48 (2003)
5. Kapelevich, A.L., Kleiss, R.E.: Direct gear design for spur and Helical Involute gears. Gear Technol. 29–36 (2002)
6. Kapelevich, A.L., McNamara, T.M.: Direct gear design for automotive applications. 2005 SAE International Paper 05P-14
7. Karpat, F., Ekwaro-Osire, S., Cavdar, K., Babalik, F.C.: Dynamic analysis of involute spur gears with asymmetric teeth. Int. J. Mech. Sci. **50**, 1598–1610 (2008)
8. Deng, X., Hua, L., Han, X.: Research on the design and modification of asymmetric spur gear. Math. Probl. Eng. **2015**, 1–13 (2015)
9. Senthil Kumar, V., Muni, D.V., Muthuveerappan, G.: Optimization of asymmetric spur gear drives to improve the bending load capacity. Mech. Mach. Theory **43**, 829–858 (2008)
10. Tomoya Masuyama and Naoki MiyazakI, "Evaluation of load capacity of gears with an asymmetric tooth profile", International Journal of Mechanical and Materials Engineering (2016) 11:11, Pg.No's-1–9.
11. Vaghela, P., Prajapati, J.: Optimization of tooth root profile using Bezier curve with G2 continuity to reduce bending stress of asymmetric spur gear tooth. In: MATEC Web of Conferences, vol. 237, D2ME, 2018, p. 03010 (2018)
12. Olguner, S., Filiz, İ.H.: A study on the design of asymmetric spur gears in gear pump applications. In: International Gear Conference 2014: 26–28 Aug 2014, Lyon, pp. 406–417
13. Mallesh, G., Math, V.B., Venkatesh, Shankarmurthy, H.J., Shiva Prasad, P., Aravinda, K.: Parametric analysis of asymmetric spur gear tooth. In: 4th National Conference on Machines and Mechanisms (NaCoMM09), NIT, Durgapur, India, 17–18 Dec 2009, NaCoMM-2009-MMRAIAG16
14. Prabhu Sekar, R.: Performance enhancement of spur gear formed through asymmetric tooth. J. Eng. Tribol. 1–18 (2019)

A Review on Fabrication, Mechanical and Tribological Behaviour of Polymer Functional Graded Material

**K. Prudhvidhar, K. Vamshi, B. Rohith Kumar, Y. M. Manjunath,
Shakuntala Ojha, K. Raja Narendar Reddy, and Raghavendra Gujjala**

1   Introduction

Human quest for finding a novel material which can sustain under specific environmental condition is never ending. In the history of the novel materials, composite materials are one of the most significant materials which offer excellent properties which are homogenous over entire surface. Still, composite materials cannot be used to achieve required gradient in the various applications such as aerospace, automotive and power generation [1].

The overall thought of functionally graded materials (FGMs) were formerly anticipated in 1972 keeping composites and polymer-related materials in perspective [2].

In 1984 during the design of space craft research project, this functionally graded materials (FGMs) were first applied by Japanese to fulfil these requirements [3]. The foremost purpose to develop FGMs that can withstand in high-surface temperature of 2000 K and a temperature gradient of 1000 K across a 10 mm section [4]. The novel concept was applied to produce such type of material which have varying composition from one end to another, and also one side of the material can withstand in high-temperature environment, similarly other side of the material can have better thermal conductivity. Anyway, the notion of FGMs is available in nature as the human bone and cellulose. Human bone developed with the combination of collagen and

K. Prudhvidhar · K. Vamshi · B. Rohith Kumar · Y. M. Manjunath · S. Ojha (✉) ·
K. Raja Narendar Reddy
Department of Mechanical Engineering, Kakatiya Institute of Technology & Science,
Warangal 506015, India
e-mail: so.me@kitsw.ac.in

R. Gujjala
Department of Mechanical Engineering, National Institute of Technology, Warangal 506004, India

hydroxyapatite. Collagen is acting as a ductile protein polymer, and hydroxyapatite is a brittle calcium phosphate ceramic plying an important role inside human bone.

FGMs offered incredible potential in various applications, subjected to high wear and friction because FGMs minimize interfacial stresses between the different materials which is occur due to temperature variation and also it acts as a better adherence of a protective layer against corrosion.

Initially, many researchers classified FGMs depending upon the used of constituents to produce FGMs. Beforehand, combination of metal and ceramic materials mainly used to develop FGMs which is utilized either in structural or transport field. Recently, FGMs concept has been applied in the area of polymer composite.

2 The Concept of Functionally Graded Composite Materials

Figure 1 shows the clear difference between the conventional composite and FGMs.
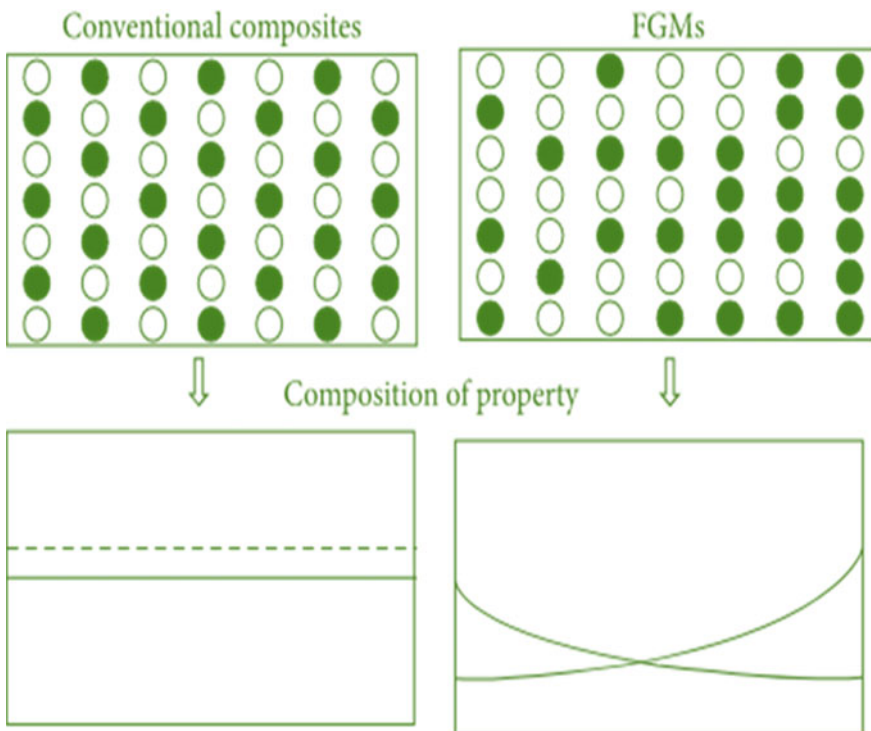
Fig. 1 Difference between the conventional composite and FGMs
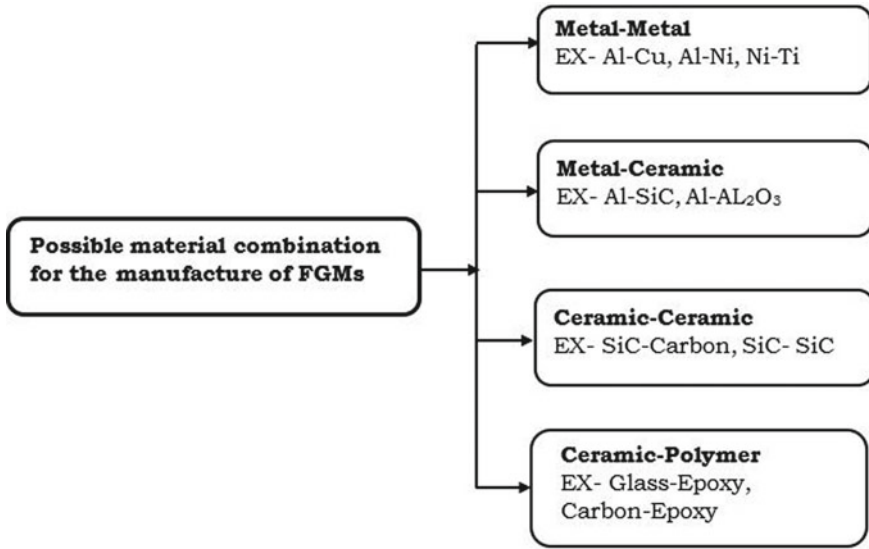
Fig. 2 Example of possible material combination used in FGMs

The concept of functionally graded hybrid polymer composite (FGHPC) or dual filler used in functionally graded polymer composite became one of the most innovative perceptions introduced into the FGMs era. The most common combinations of material than can be used to develop FGMs are shown in Fig. 2.

In various literature, many researchers focus on the details portrayal about the various production methods of FGMs and their advantages, limitations and their future applications in various industry [5, 6].

3   Fabrication Techniques of Polymer-Based FGMs

There are several no. of well-known fabrication techniques such as physical, chemical and combination of both physical and chemical which are applying for the manufacture of functionally graded polymer composite or dual filler functionally graded polymer composite.

Naebe et al. [7] present an overview on development of manufacturing process and characterization of functionally graded materials with their future prospects in various scientific and technological fields. Functional graded materials are fabricated using various manufacturing methods. Presently, researchers are using enormously vapour deposition methods, powder metallurgy methods and centrifugal casting methods for manufacturing of functional graded materials.

According to fundamental principle, FGMs manufacturing method can be summarized as physical combination method, chemical combination method and physical

and chemical synthesis method are shown in Fig. 3a–c. From 2000 to 2021, various manufacturing techniques are used in the production of functional graded materials is shown in Fig. 4.

Even if the beginning of FGMs in the mid of 1980s, but the real launch was in the early 1990s. Subsequently in the past 20 years, the number of publications has been increasing in this area. Figure 5 portrays the number of publications annually published based on FGMs during the year of 2000–2021.
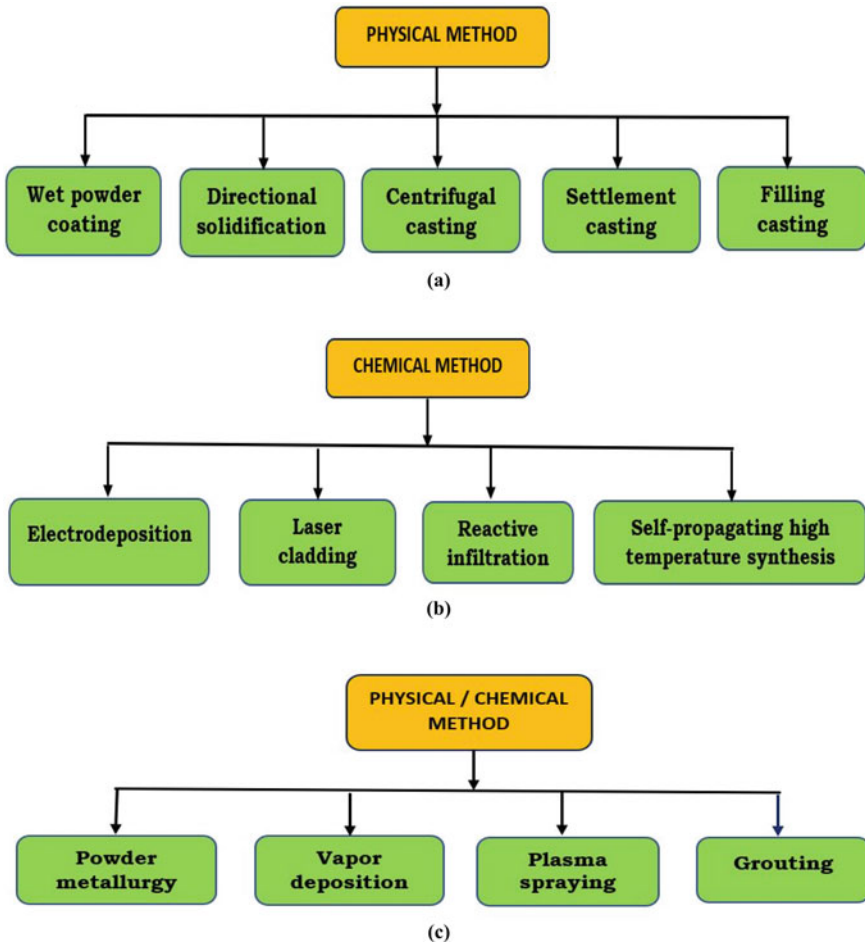
Fig. 3 a–c Various fabrication methods of FGMs
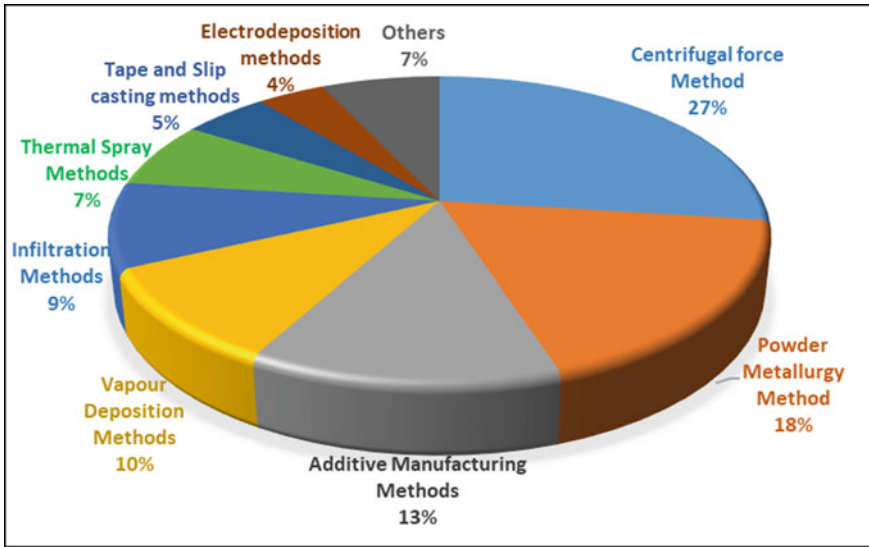
Fig. 4 Presents the various fabrication techniques in the production of FGMs in the duration of 2000–2021
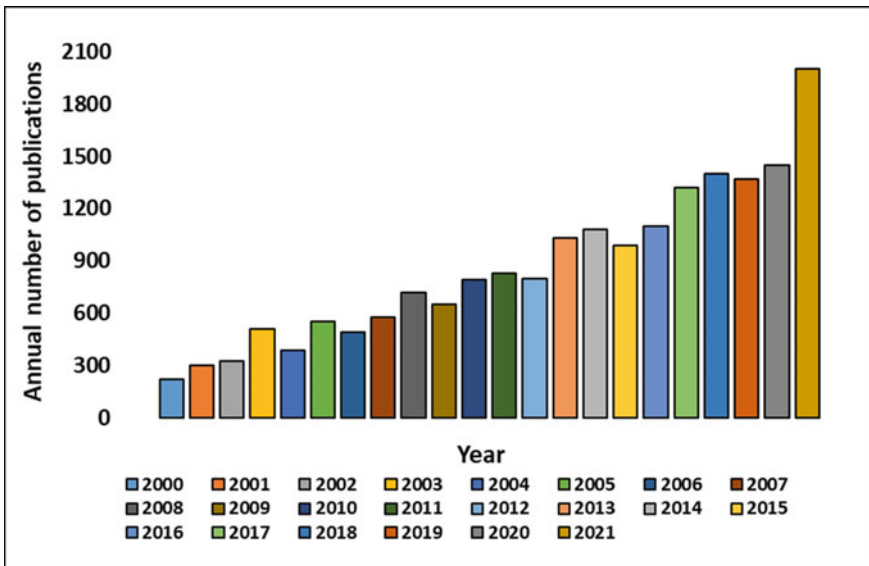
Fig. 5 Number of publications published annually based on (FGMs)

4 Mechanical and Tribological Behaviour

In most recent literature, it is clearly viewed that most researchers focussed on the mechanical, tribological and thermal characterization of FGMs materials. It is also revealing from the literature survey that various natural or synthetic reinforcements drastically improve the mechanical, tribological, physical and thermal properties of the engineered composite.

A comparative study was drawn by Radhika et al. [8] evaluated mechanical and tribological properties between functionally graded A359/10 wt% B4C and homogenous A359/6 wt% B4C composite. It was observed from the stud, as weight percentage increases the wear rate, and coefficient of friction decreases. Mishra et al. [9] fabricated functionally graded epoxy-based alumina nanocomposite and compare the mechanical properties with non-filled epoxy composites. The flexural strength and modulus are 11% and 22% higher in comparison with non-epoxy composition, respectively. Tables 1 and 2 provide overview of recent works performed on mechanical and tribological behaviour of FGMs composite.

Table 1 Different filler percentages and its effects on the mechanical properties of FGMs polymer composites

Filler/fibre and polymer used	Results	Conclusion	References
Wollastonite and epoxy with different filler percentage	Filler of 0 wt%, the fracture toughness is 200 MPa, whereas the 6 wt% of filler percentage increase the fracture toughness of 250 MPa. Filler weight of 0 wt% has flexural modulus of 3000 MPa, whereas the 4 wt% have the flexural modulus of 2000 MPa. The different (0, 2, 4, 6, 8 wt%) filler is used to fabricate the FGM	Fracture toughness of the graded polymer-reinforced composite is higher than that of nongraded and unreinforced epoxy Flexural modulus found to be lower in reinforced composite than that of the nongraded composite	[10]
Glass fibre along with epoxy resin	30% of filler has flexural stress of 758.96 MPa, whereas 50% have the flexural stress of 969.28 MPa	Flexural stress increases with increase in weight percentage of filler	[11]

Table 1 (continued)

Filler/fibre and polymer used	Results	Conclusion	References
Alumina-epoxy graded composites	The flexural strength and modulus are 11% and 22% higher in comparison with non-epoxy composition, respectively	Flexural strength increases with increase in filler percentage, and flexural modulus also increases with alumina filler percentage	[12]
Hydroxyapatite-reinforced poly (vinyl alcohol) gel	(0/3/6) wt.% in each layer and 20% of PVA shows 2.73 MPa of compressive strength, whereas the filler percentage of (3/6/9) wt.% in each layer, 20% PVA has 3.25 MPa of compressive strength	Compressive strength increases with increase of HA content, but decreases with increase of interlaminar gradient composite	[13]
Glass and silica as fibre and unsaturated polyester resin	As the filler content increases (0/3/6/9 wt%), the glass filled composite withstand high load than the silica filled composite	Glass filled PFGM has more variation in properties than the silica filled FGM	[14]

Table 2 Coefficient of friction and wear rate of the different filler/fibre % of FGMs polymer composites

Reinforcement	Results	Conclusion	References
SV94 graphite and PV 60/95 with epoxy resin	Coefficient of friction for PV60/95 is 0.2 for 4 min of time lap, whereas the coefficient of friction for SV94 is 0.25 for the same time	Coefficient of friction for SV94 is higher than PV 60/95	[15]
Marble dust, short glass fibre and vinyl ester resin	As the filler content increases from (0, 2, 4, 6 wt%), the wear rate decreases from (3.91E−06 to 1.56E−06)	Increase with the filler percentage of marble dust increases the tribological property	[16]

Table 2 (continued)

Reinforcement	Results	Conclusion	References
Kevlar fibre, carbon fibre, silica along with epoxy polymer	Pure epoxy resin shows coefficient of friction 0.7, whereas centrifuged sample shows coefficient of friction 0.5	Addition of Kevlar fibre, carbon fibre and silica decreases the coefficient of friction	[12]
Graphite/glass microspheres, polytetrafluoroethylene and polymer include phenol novalac epoxy resin (NPPN-638) and triglycidyl phosphate	As graphite weight% increases from (0 to 30%), the wear rate decreases uniformly from (0.7 to 0.2).If (NPPN-638 and TGP) were added, the sudden decrease of wear rate takes place	High concentration of graphite on top layer provides less friction and wear resistance. The bottom layer due to vary in density and viscosity provides heat protective coating due to triglycidyl phosphate	[17]

5 Conclusions

Functional graded materials (FGM'S) were essential in order to enhance the characteristics of a respective material or component and to yield the respective functional properties of it. FGMs are considered as effective and efficient amongst other modern materials with respective to their enormous range of applications in today's world. The applications of functional graded composite materials (FGCM) include in aerospace, automobiles and are also developed as resistant materials in a particular parameter (ex: temperature) and other engineering applications. Polymeric FGMs are recently developed grade of materials having unique and progressive variety in practical properties and use certain techniques to develop polymer graded composite materials.

References

1. El-Galy, I.M., Saleh, B.I., Ahmed, M.H.: Functionally graded materials classifications and development trends from industrial point of view. SN Appl. Sci. **1**, 1–23 (2019)
2. Bohidar, S.K., Sharma, R., Mishra, P.R.: Functionally graded materials: a critical review. Int. J. Res. **1**, 289–301 (2014)
3. Ruys, A., Sun, D.: Functionally graded materials (FGM) and their production methods (2002)
4. Mahamood, R.M., Akinlabi, E.T.: Types of functionally graded materials and their areas of application. Functionally Graded Materials, pp. 9–21. Springer (2017)
5. Tan, C., Wang, C., Wang, S., Wang, G., Ji, L., Tong, Y., Duan, X.-M.: Investigation on 316L/316L-50W/W plate functionally graded materials fabricated by spark plasma sintering. Fusion Eng. Des. **125**, 171–177 (2017)
6. Gasik, M.M.: Functionally graded materials: bulk processing techniques. Int. J. Mater. Prod. Technol. **39**, 20–29 (2010)
7. Naebe, M., Shirvanimoghaddam, K.: Functionally graded materials: a review of fabrication and properties. Appl. Mater. Today. **5**, 223–245 (2016)

8. Radhika, N., Sasikumar, J., Sylesh, J.L., Kishore, R.: Dry reciprocating wear and frictional behaviour of B4C reinforced functionally graded and homogenous aluminium matrix composites. J. Mater. Res. Technol. **9**, 1578–1592 (2020)
9. Mishra, S.K., Shukla, D.K., Patel, R.K.: Flexural properties of functionally graded epoxy-alumina polymer nanocomposite. Mater. Today Proc. **5**, 8431–8435 (2018)
10. Muslim, N.B., Hamzah, A.F., Al-kawaz, A.E.: Study of mechanical properties of wollastonite filled epoxy functionally graded composite. Int. J. Mech. Eng. Technol. **9**, 669–677 (2018)
11. Atta, M., Abu-Sinna, A., Mousa, S., Sallam, H.E.M., Abd-Elhady, A.A.: Flexural behavior of functionally graded polymeric composite beams. J. Ind. Text. (2021)
12. Singh, S., Dwivedi, U.K., Shukla, S.C.: Recent advances in polymer based functionally graded composites. Mater. Today Proc. (2021)
13. Pan, Y., Shen, Q., Pan, C., Wang, J.: Compressive mechanical characteristics of multi-layered gradient hydroxyapatite reinforced poly (vinyl alcohol) gel biomaterial. J. Mater. Sci. Technol. **29**, 551–556 (2013)
14. Lucignano, C., Quadrini, F.: Indentation of functionally graded polyester composites. Measurement **42**, 894–902 (2009)
15. Stabik, J., Dybowska, A.: Electrical and tribological properties of gradient epoxy-graphite composites. J. Achiev. Mater. Manuf. Eng. **27**, 39–42 (2008)
16. Gangil, B., Kukshal, V., Sharma, A., Patnaik, A., Kumar, S.: Development of hybrid fiber reinforced functionally graded polymer composites for mechanical and wear analysis. In: AIP Conference Proceedings, p. 20059. AIP Publishing LLC (2019)
17. Amirova, L.M., Andrianova, K.A., Amirova, L.R.: Processing method, properties and application of functionally graded polymer materials based on the mixtures of poorly compatible epoxy resins, Polym. Polym. Compos. (2021)

Analysis of an Emission and Performance Characteristics of Single Cylinder 4 Stroke VCR Engine by Using Palm Biodiesel Blends and Comparison at the Compression Ratio 18:1

Savadana Venkataramana and N. Ramanaiah

1 Introduction

The deficit of fossil fuels, abnormal increase in demand from transport and subsequent severe detrimental effects in pollution. Modern trend in lifestyle paves the way to deploy transport to the largest extent, which necessitates retention of fuel supply. Biodiesel is found to be best option to get rid of bottlenecks of fuel stock. Prominent researchers worked out works with biodiesel for its suitability with current model of diesel engine in the absence of engine alterations. M. Suresh, P. Jawahar, Arun Richard et al. analyzed a synthesis of biofuels from different available sources of fried oil, palm oil, cooking oil, jatropha biofuel and Engine performance along with emissions in case of variable compression ratio engine. It is also studied with the combination of blends. The work supported the option of variable compression ratio engine with better outcome of fuel efficiency, reduction in the fuel consumption and emission control comparatively with diesel engines [1]. Ambarish Datta, Bijan Kumarmandal et al. presented synthesis, performance and emission trends with immense discussion of comparison from the different alternative fuels. It also illustrated different case studies in the form of graphical representation. It was emphasized about deterioration of engine with biofuels compared to diesel, but with better environmental effects [2]. Pali Rosha and Saroj Kumar Mohapatra studied the role of compression ratio in the emission and performance analysis for the palm biodiesel blend with 20%. It shows that the ignition delay was decreased at the peak pressure along with thermal efficiency when the compression ratio is increased from 16 to 18. It is also shown that there was average reduction in the HC, CO by 47.8% and

S. Venkataramana (✉)
Mechanical Engineering Department, Vignan's IIT, Visakhapatnam, India
e-mail: savyasvr@gmail.com

N. Ramanaiah
Mechanical Engineering Department, Andhra University, Visakhapatnam, India

41.0%, respectively, while NO_x is found 41.1% increase. Therefore it was concluded that the 20% biodiesel shows better performance at the maximum compression ratio [3]. Supriya B. Chavan, Rajendra Rayappa Kumbhar et al. carried out the emission analysis for the variable compression ratio engine by fuelling with chosen blends dealing with synthesis of Jatropha biofuel. It is considered the blend with 10, 20 and 30% along with pure diesel and Jatropha at 40 °C. NO_x, CO and HC were compared with diesel with the results CO is reduced by 43%, HC is by 50% while NO_x is increased by 20% and 30% biodiesel is found optimum at the lowest compression ratio of 15:1 [4]. Obed M. Ali, Rizalman Mamat et al. performed experimentation to characterize properties for the blends with different ratios to analyze engine performance. It is also identified optimum blend based on the test result, which is up to 30% biofuel. It is concluded that there is reduction of energy by 1.4% for every 10% increase and found that no significant reduction in brake thermal efficiency for tested blended [5]. Hariram, N. Balakarthikeyan et al. worked on the palm stearin wax which was extracted as a residue which is further processed for the extraction of the Palm biofuel transesterification with the blending of sodium hydroxide and methanol along with PSBD. In this engine performance and emission analysis was also carried out under the change in the compression ratios for the stipulated biodiesel blends. An experiment was conducted with 17, 17 and 18 compression ratios. Among all the fuel blends 20% is found to be optimum [6]. K. Srinivas, Balu Naik et al. analyzed dual fuel blends of Palm and Eucalyptus oils in the variable proportions of 15 and 10% of Eucalyptus oil. It is studied. In the performance analysis, Exhaust Temperature, Brake Thermal and Mechanical Efficiency were analyzed and found to increase. Whereas emission analysis dealt with NO_x, CO_2 and HC with exhaust gas analyzer and were found mitigated with an increase in compression ratio and also with amount of blend [7]. Savadana Venkataramana and N. Ramanaiah carried out experimentation in order to assess the brake specific fuel consumption (BSFC) and also Brake Thermal Efficiency (BTE). In case of Exhaust Emission, it was analyzed HC, CO, CO_2 and NO_x for the 4 Stroke Single cylinder Variable Compression Ratio Engine by using diesel and palm biofuel at the compression ratio of 18. At a maximum load, thermal efficiency of an engine with palm biofuel is 29.01% and brake-specific fuel consumption (BSFC) is 0.292 kg/kWh which are nearby values as correlated with diesel fuel. Referring to emission analysis, NO_x from the biofuel is 415 ppm indicated 50%less and others like CO_2% and CO% were recorded as 2.6 and 0.024, respectively, at the peak load condition in case of palm biofuel. Results display that, Brake thermal efficiency is increased with the increase in the load [8]. A. Sajith et al. carried out the emission and performance analysis for the set of biofuels from their respective stocks. It is carried out to evaluate performance and emission analysis. Analysis considered BSFC, BTE for the engine performance, while HC, CO, CO_2 and NO_x in case of emission analysis. Outcome depicts variation of parameters for different types of biofuels. There are supporting pragmatic conditions for the biodiesel and it is concluded that the diesel can be deployed in place of diesel. Therefore there is a need to go for optimization as future scope [9]. Ganesh S. Warkhade et al. evaluated engine performance by considering the effect of supercharging and compression ratio for a single cylinder direct injection CI engine. The compression ratios 14, 16,

Table 1 Properties of diesel and palm biofuel

Parameters of the process	Units	Palm biodiesel	Diesel
Percentage of ash	%	0.00178	0.09
Carbon residue	%	0.516	0.1
Pour point	°C	4	−1
Flash point	°C	187	68
Kinematic viscosity at 40 °C	CST	8.41	2.76
Sedimentation	%	0.08	0.05
Density (at 15 °C)	Gram/cc	0.85	0.82
Sulphur content	%	0.69	0.1
Content of water	%	0.0139	0.051
Calorific value (gross)	kcal/kg	10,100	10,000

17.5 and 18 were considered while centrifugal blower type supercharger. Results thus obtained are compared with standard condition at 17.5:1 and observed that the BTE and BSFC higher at minimum load and maximum compression ratio. It is also shown that BSFC and BTE were increased by 25% and 15%, respectively [10].

Motivation of the present study

From the foregoing research work done on the palm biofuel and other biofuels reveals that the performance of IC engines with these fuels is comparatively closer to the diesel fuel. In this context, it is important to consider the trends of BSFC and NO_x with respect to brake power. Economy and availability are also play role in the usage of palm biodiesel as they are available abundantly. Most of the properties of palm biodiesel are closed to the conventional fuel and also confined to standard testing methods. Hence current work deploying palm biodiesel in the test engine to study characteristics of performance and emission. Palm biodiesel was prepared with the transesterification method. Experiment was conducted on the test engine with specifications shown in Table 2 and results reveal that the test engine operated with palm oil performed closed to the conventional fuel performance representing reliable efficiency and emission characteristics. Therefore it is immensely important to consider palm biodiesel as alternative fuel even though there were several studies existing so far.

2 Materials and Methods

2.1 Methodology

Figure 1 shows the extraction of palm biodiesel as the palm biodiesel is transformed into biodiesel from stock by the process of transesterification. It has undergone

Table 2 VCR engine specifications

Make	Kirloskar Oil Engines (Ltd)
Model	Single cylinder four stroke water cooled and naturally aspirated
Dia of bore	87.5 mm
Length of stroke	111 mm
Cylinder volume	661 cm^3
Compression ratios waked out	12:1–18:1
Injection timing	25° before botton dead centre
Injection pressure	0.2 MPa
Max. power	5.2 kW at 1500 rpm
Nozzle	1 Hole

sequence of operations sterilization, stripping, etc. Followed by secondary operations to pressers for biofuel. Finally, purification is applied by dryers for the further followed by the process of refining [08].
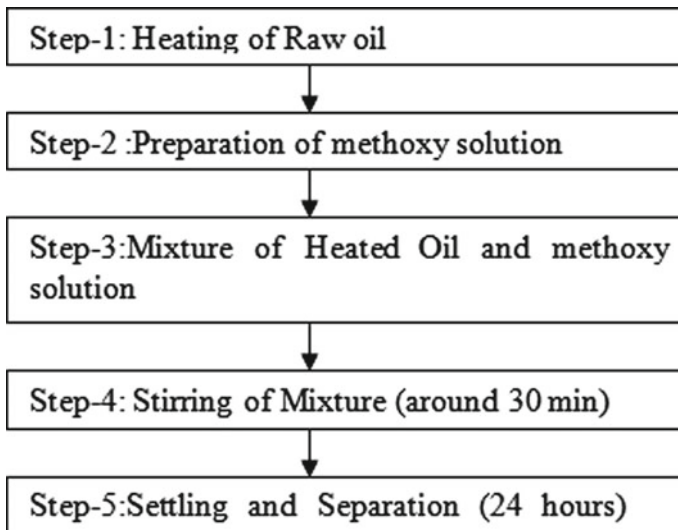
Fig. 1 Transesterification process

2.2 Experimental Setup

It is a single cylinder four-stroke water-cooled direct injection engine. It consists of block for the compression ratio adjustment. Engine is connected with eddy current dynamometer for the load application provided with water cooling effect. The erection has a provision to support fuel tanks for diesel and biofuel, manometers and controls. Manometer is used for the measurement of air into the engine, and fuel consumption with the sensor.

2.3 Pollutant Metering System

It is to study the composition of emissions by adopting the principle of Non-Dispersive Infra-Red where infra-red is applied to the gas, then based on the amount of absorption, NDIR principle is used to measure CO, HC and CO_2, while Electro-Chemical (EC) sensors are meant for O_2, NO_x, SO_x (Table 3).

3 Analysis of Experimental Outcomes

The totality of experimentation depicts extent of utility in an engine and conversion of chemical energy into brake power along with characteristics of combustion. It generates intuitive perception of influence on environment. As a whole influence of a brake power on the functional fitness and properties of exhaust gas is depicted as below.

Table 3 Specifications of the exhaust gas analyser

Measured exhaust gases	CO_2%, CO% and NO_x in ppm
Operating mechanism	Infrared sensors for CO, CO_2
	Electrochemical sensors for NO_x
Set of readings	Table 1: properties of biodiesel
Start uptime	<2 min
Re set time	24 min with auto intake of air supply
Gas discharge	500–l000 ml/min
Handling system	S. S. Probe, P-U detachable tubing connectors, water filter, particulate fine filter
Boundary conditions	Temperature: 5–45 °C
	Pressure: 13–1060 mbar
	Humidity: 0–90%
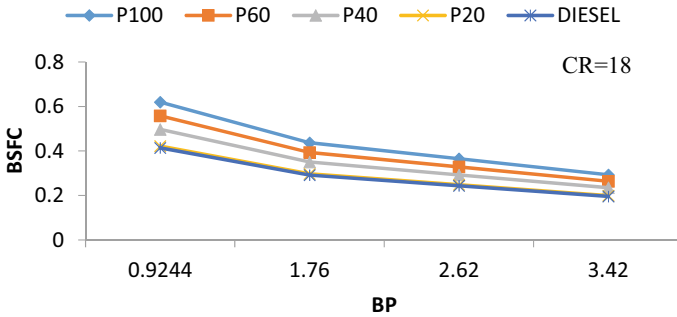
Fig. 2 BP versus BSFC at compression ratio 18

3.1 Discussion of Results Pertaining to Engine Operation

3.1.1 Brake Specific Fuel Consumption (BSFC)

The BSFC is the rated consumption of the fuel to generate 1 kW power which can be treated as the engine performance index to measure the fuel supply for the rated power output. Figure 2 reveals effect of brake power on the brake-specific fuel consumption at the different blends at the ratios 18:1. The BSFC was kept minimum for diesel, which was increased when the amount of blend is increased for the blends P20, P40 and P60 at the various operating loads due to the lower heating value of the biofuels and poor combustion process. At the maximum load, brake specific fuel consumption of P100 is 0.293 kg/kWh at 18:1 compression ratio. At the maximum load P60, P40 and P20 were recorded as 0.26, 0.230 and 0.20 kg per kWh, respectively. It is also observed that BSFC was closed to diesel at the lower blends and is increased at higher loads.

3.1.2 Brake Thermal Efficiency (BTE)

The BTE is the ratio between the amount of chemical energy and energy generated at the crankshaft. Figure 3 shows that the change in BTE with the BP for the various palm biofuels blends at the 18:1 compression ratio. Brake thermal efficiency (BTE) rises as the brake power increases at the given compression ratio. Reduction in the power lost at increased loads. It also presented effectiveness of conversion system from fuel energy into mechanical power [08, 09], which represents tally of brake thermal efficiency of engine with diesel and palm biodiesel and found higher value with palm biodiesel preset loading at this compression ratio 18:1. At the maximum load, performance of an engine with palm biodiesel is 29.01%, whereas diesel is of 39.15%. BTE is decreased as the percentage of blend increases due to viscosity and calorific values.
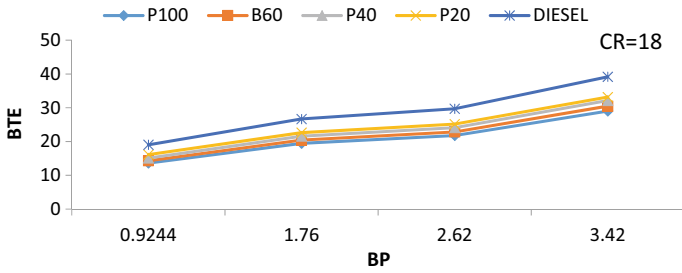
Fig. 3 Effect of brake power (BP) on BTE for the Diesel fuel and biodiesel fuel at compression ratio of 18

3.2 Emission Characteristics

3.2.1 CO Emission

Figure 4 shows effect of brake power on CO% for diesel fuel and biodiesel fuel at compression ratio of 18:1. At given compression ratio palm biodiesel emits comparatively less CO pollutant at the maximum load by 0.006% less than that of diesel due to incomplete combustion heterogeneous mixture with diesel [08]. It also exhibits decreasing trend of percentage CO on par with increasing trend of brake power at opted loads due to complete combustion and increase in the prevailing pressure and temperature which is valid for the diesel, blends and biodiesel also. It is found that 0.006% by volume CO% emission for diesel and 0.010% by volume that of palm biodiesel at the maximum load. The condition of prevailing elevated temperature is found to be much more favourable for oxidation and hence further reduces emissions of CO [08].
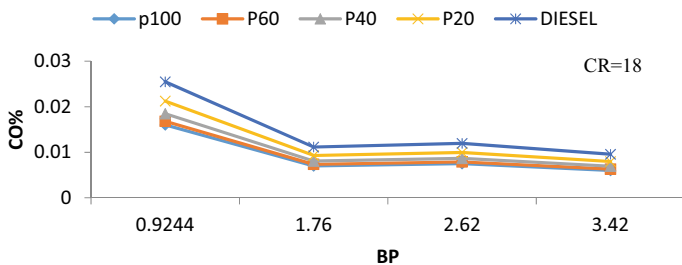
Fig. 4 Effect of brake power on CO% for diesel fuel and biodiesel fuel at compression ratio of 18
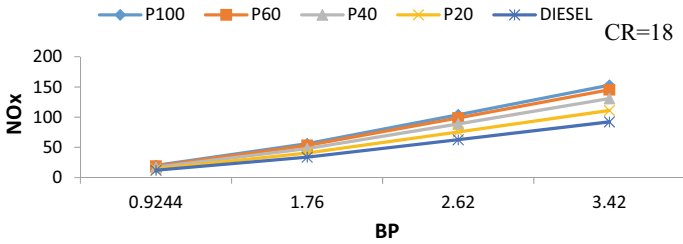
Fig. 5 Effect of brake power on NO_x for diesel fuel and biodiesel fuel at compression ratio of 18

3.2.2 NO_x Emission

Figure 5 reveals the influence of load on the NO_x when the test diesel engine is operated by using diesel fuel and palm biofuel at the compression ratio of 18:1. Palm biodiesel releases fewer NO_x comparatively at the opted loads. As the load increases NO_x was increased due to increase in prevailing pressure and temperature. As the percentage of blends increases NO_x increases due to viscosity and calorific value. As the prevailing temperature is maximum in the chamber makes a reasonable condition for NO_x outflow. NO_x discharge at maximum load is observed as 92 for diesel and 153 ppm for biodiesel at pressure ratio of 18:1 [5, 8]. Rate of increase of NO_x is less comparatively at the lower loads than the higher load.

3.2.3 CO_2 Emission

Figure 6 influence of brake power on CO_2 emission in VCR Engine with diesel, palm biodiesel and different blends. First of all, at each load increase in percentage blend increases CO_2 emission as palm biodiesel is oxygenated one comparatively. It is valid for all the opted loads as shown. It is also observed that CO_2 increases as the load increases due to increase in prevailing temperature in turn complete combustion [5, 8]. Apart from above said effect it is evident numerically that there is only 2.09% of CO_2 at maximum load for the biodiesel at compression ratio of 18:1.

4 Conclusions

Palm Biodiesel sample was tested for the assessment of properties to judge the suitability for the test engine. From the test fuel, properties mentioned in Table 1 were closer to standard fuel. The experiment was done on the 1 cylinder-4 stroke water-cooled, naturally aspirated VCR Engine using palm biofuel and conventional fuel by varying compression ratios. At the peak load, the BSFC of palm biofuel is more than that of standard diesel by 31.7% due to viscous nature of the palm biofuel and
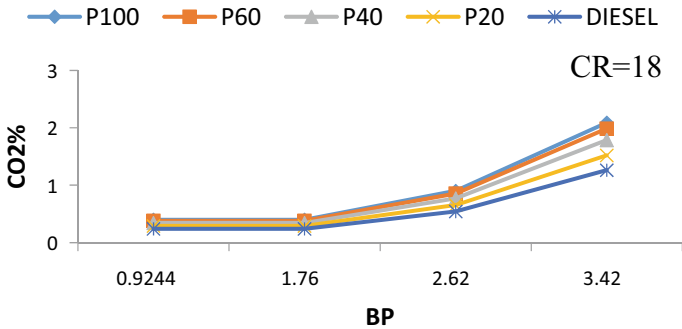
Fig. 6 Effect of brake power on CO_2 for diesel fuel, biodiesel and different blends at the compression ratio of 18:1

calorific value. Higher viscosity makes the combustion incomplete due to improper blending of air–fuel mixture and weak atomization causing an increasing BSFC. At full load, BTE for the palm biofuel was 26% due to the complete combustion of palm biodiesel. Palm biofuel releases less CO% pollutants as the palm biodiesel is the oxygenated fuel comparatively by 40%. Palm biofuel releases fewer NO_x compared to a standard diesel engine. At each load increase in percentage, blend increases CO_2 emission as palm biodiesel is oxygenated one comparatively by 48%. Emission of NO_x is 40% less at the maximum load with the palm biofuel [08]. By considering the experimental evidence from the research carried out, the palm biodiesel is required to be considered as alternative fuel in the diesel-operated engine without any modification in the engine. The resultant combinations possess good oxidation stability, better properties which increase engine performance while engine run with palm biofuel as it leads to complete combustion of the fuel. In future works, alternative measures are to be applied to refine fuel so as to produce better properties. And also EGR to control the emission characteristics.

References

1. Suresh, M., Jawahar, P., Richard, A., et al.: A review on biodiesel production, combustion, performance, and emission characteristics of non-edible oils in variable compression ratio diesel engine using biodiesel and its blends. Renew. Sustain. Energy Rev. **92**, 38–49 (2018). https://doi.org/10.1016/j.rser.2018.04.048
2. Datta, A., Mandal, B.K.: A comprehensive review of biodiesel as an alternative fuel for compression ignition engine. Renew. Sustain. Energy Rev. **57**, 799–821 (2016). https://doi.org/10.1016/j.rser.2015.12.170
3. Rosha, P., Mohapatra, S.K., Mahla, S.K., Cho, H., Chauhan, B.S., Dhir, A.: Effect of compression ratio on combustion, performance, and emission characteristics of compression ignition engine fueled with palm (B20) biodiesel blend. Energy **178**, 676–684 (2019). https://doi.org/10.1016/j.energy.2019.04.185
4. Chavan, S.B., Kumbhar, R.R., Kumar, A., Sharma, Y.C.: Study of biodiesel blends on emission

and performance characterization of a variable compression ratio engine. Energy Fuels **29**(7), 4393–4398 (2015). https://doi.org/10.1021/acs.energyfuels.5b00742

5. Ali, O.M., Mamat, R., et al.: Analysis of blended fuel properties and engine performance with palm biodiesel–diesel blended fuel. Renew. Energy **86**, 59–67 (2016). https://doi.org/10.1016/j.renene.2015.07.103

6. Hariram, V., Balakarthikeyan, N., et al.: Effect of variable compression ratios on performance and emission phenomena of DI CI engine fuelled with palm stearin biodiesel-diesel blends. Nat. Environ. Pollut. Technol. **19**(4), 1517–1526 (2020). https://doi.org/10.46488/nept.2020.v19i04.018

7. Srinivas, K., Naik, B.B., et al.: Impact of fuel injection pressure and compression ratio on performance and emission characteristics of VCR CI engine fueled with palm kernel oil-Eucalyptus oil blends. Mater. Today: Proc. **4**(2), 2222–2230 (2017). https://doi.org/10.1016/j.matpr.2017.02.069

8. Venkataramana, S., Ramanaiah, N.: Experimental analysis of performance and emission characteristics of four stroke single cylinder VCR diesel engine using palm biodiesel and diesel along with comparison. https://doi.org/10.1007/978-981-15-9853-1_21

9. Sajith, A., et al.: Production of palm and jatropha based biodiesel and investigation of palm-jatropha combined blend properties, performance, exhaust emission and noise in an unmodified diesel engine. J. Clean. Prod. https://doi.org/10.1016/j.rser.2015.06.031

10. Warkhade, G.S., Babu, A.V.: Impact of supercharging and compression ratio on performance characteristics in a single cylinder DICI engine. Int. J. Heat Technol. https://doi.org/10.18280/ijht.360323

Product Design: UI/UX

Designing an Experience for Conducting Online Exams, Evaluation, and Feedback

Jaison K. Thomas, M. Vishnu, Sarvesh Tripathi, and Tripti Singh

1 Introduction

Online education has always been debated for quite a long time. Research on the growth of online education and the factors leading to its full-scale adoption had shown that wild-cards like natural calamities and man-made disasters could largely accelerate the full-scale adoption of online education [1]. The studies proved right, as the relevance of online education increased hugely during the Covid-19 pandemic [2]. The United Nations Education, Scientific, and Cultural Organization (UNESCO) has officially declared that the Covid-19 has affected the education of about 87% of the students globally. The organization also acknowledges the need for innovative technologies that aid the improvement in online education and help make it accessible to all [3]. Across the country, 15 lakh schools were closed down, affecting the education of about 28.6 crore students [4]. The only alternative for the halt in education was about going completely online. This push led to a digital revolution in the educational sector [5]. Although there are a number of platforms to conduct online classes, the lack of a specialized platform for conducting exams is adding to the difficulty in online education. Our work focuses on this unexplored area, where the teachers can effectively conduct online examinations and provide feedback to students. The solution also helps tackle the issues like low network connectivity, need for multiple devices, and management of documents.

J. K. Thomas (✉) · M. Vishnu · S. Tripathi · T. Singh
Indian Institute of Information Technology, Design and Manufacturing, Jabalpur, Madhya Pradesh 482005, India
e-mail: 20mds009@iiitdmj.ac.in

557

2   Literature Review

The major reasons for transition to online education included increasing the accessibility, improving skills, making education more cost-effective, increasing the capacity, and adding a universal element to the educational system [6]. However, there are quite a lot of challenges during this transition to online education.

A study conducted during the pandemic, identifies the difficulties faced by the stakeholders during online education [7]. In this, 87% of students was not comfortable with the current online exams, due to multiple issues. The difficulties included non-familiarity, complicated processes, and connectivity issues. Current online exams also have huge usability issues [8]. Apart from usability issues, the factors such as need for support, options for feedback, options for scheduling, and need for reliability were the major issues that were acting as barriers for wider adoption. Research on the impact of Covid-19 on the education system in developing countries, showed that during online exams, teachers find huge difficulties in conducting examinations, and evaluating the answer sheets in mobile devices [2]. Limited access to computers and low network connectivity was the other issues faced by them. Students too face several issues such as need for devices, poor network, and the need to stay connected during examinations. A study conducted on the effect of Covid-19 on students in Afghanistan showed that students faced issues like limitations in resources required for online learning [9]. Many students lacked access to devices, and those with devices faced issues with Internet connectivity. The research paper also suggests the government to come up with an online educational platform that can work with limited Internet connectivity.

Research on the issues during the transition from offline to online, found out that a majority of students are concerned about learning without exams [10]. Exams play a crucial part in the learning process, and challenges regarding the conduct of examinations have to be addressed. While the effects of the pandemic on higher education, and the ways to its securitization were analyzed, suggestions included that the transition to e-learning should be seen as a new normal which can be implemented post-pandemic along with the offline classes, rather than defining it as an emergency response [11].

3   Methodology

The problem was approached using the design thinking methodology. The steps involve empathize, define, ideate, prototype, and test. The 'empathize' phase consisted of both quantitative and qualitative research. Quantitative research was conducted using surveys, while interviews and contextual inquiries were conducted for getting qualitative data. The 'define' phase consisted of developing user persona on the basis of data from the previous step. The problem statement was defined, which led to the 'ideation' phase. Various concepts were ideated, and a final list of

concepts was prepared for the 'prototype' phase. Once low-fidelity prototypes were built, they were tested among users, and the final prototype was built.

3.1 Empathize

Understanding Situation

The pandemic created new needs in the educational sector. As people realized that the halt in education cannot be further continued, education started going online, without even considering the needs and issues faced by teachers and students [2]. But, several teachers not even having a smartphone had no option, other than to adapt to the situation.

There were several platforms to conduct online classes; however, platforms to conduct examinations were limited and did not meet the needs of a major section of people who had just entered the tech space. Tools like Zoom, Google Meet, WhatsApp, Google Classroom, and Google Forms were the major options available for educational needs [12]. In most schools, WhatsApp groups were created by teachers, and students were added, which then served as an official platform for discussions [13]. WhatsApp was the most popular platform, followed by Google Classroom and Google Forms, to conduct online examinations, and both teachers and students faced many issues which are being discussed in detail in the further sections. Several parents also faced difficulties such as providing facilities for all their children when exams happen for all of them simultaneously [14]. Working parents, as well as parents with low IT skills, also faced bigger problems of time management and less skills for helping out their children.

Understanding Users through Quantitative Research

User Survey. The survey was conducted using Google Forms, among teachers. A total of 24 teachers participated in the survey. A pilot survey was run among 2 teachers, and then, questions were refined so that teachers understood it more properly. After this, the survey form was circulated.

Among the participants, 62.50% conducted exams in mobile devices, mostly due to not having a computer. This shows the importance of mobile friendly platforms for conducting examinations. Among the applications used, WhatsApp was the most popular, with 46.70% users conducting exams in WhatsApp, mostly due to its ease of use. Though there were a lot of difficulties faced, the difficulty in giving feedback to students was the most negative aspect in the current examination system.

Understanding Users through Qualitative Research

User Interviews. Ten user interviews (3 students, 4 teachers, and 3 parents) were conducted online. All the teachers were high school teachers, who had started conducting online examinations during the pandemic and were adapting to the new situation, but had a lot of difficulties in the process. Among students, 2 were class 7
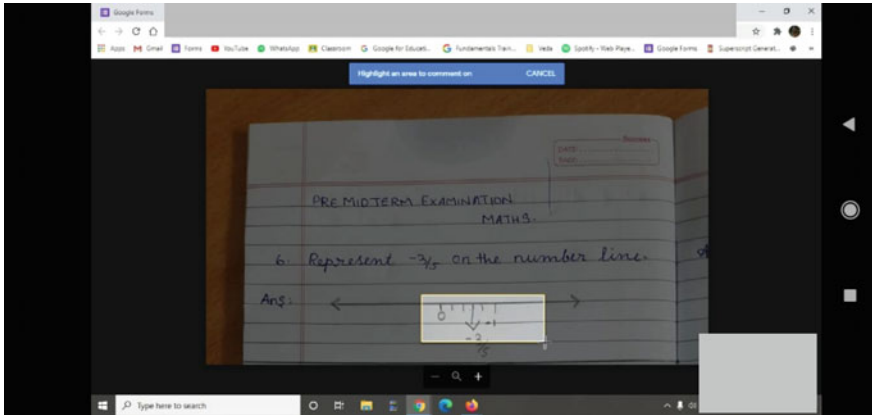
Fig. 1 Evaluation of a class 9 answer sheet using Google Classroom

students (twins), and one was a class 10 student. Among parents, 2 were the parents of the above-mentioned students, and 1 was the mother of a class 3 kid.

Contextual Inquiry. Contextual inquiry was performed during the evaluation of an answer sheet (Class 9) using Google Classroom (Fig. 1).

The evaluation was done by a high school teacher (37, Female) for Class 9 Mathematics. She conveyed her comfort with using Google Classroom on a computer. However, she mentioned about the difficult learning curve and the reluctance of her peers in using Google Classroom in mobile devices. Students had to upload images of each answer in a subjective test. Teachers have the option to highlight the areas, and she mentioned about not using the type feature for giving feedback since she faced difficulty in typing.

3.2 Define

The insights gained in the empathize phase were used to pinpoint specific issues and goals that the users have. Teachers and students both faced difficulties during online examinations.

Among teachers, the most prevalent problems were as follows:

- Difficulty in giving feedback to students
- Difficulty in typing
- Poor network connectivity
- Managing documents
- Fear of technology in extreme users.

The most prevalent problems among students were as follows:

- Poor network connectivity
- Limited number of devices in a family
- Not getting enough feedback from teachers.

3.3 Ideate and Prototype

On the basis of the problems defined, various concepts were ideated, and three among them were selected for prototyping.

Concept 1—The Exam Model

We tried to closely relate this concept with the real exam halls in schools. The rooms created would only be valid during exams, and the data may be stored for a short time period. Exams would be created, and students would be added. After the final export of the marksheet, exams get deleted. Although students can see the file icons of other students, these would be password protected. Password protection could be disabled for teachers (Fig. 2).

Concept 2—The Class Model

In this concept, classes would be created, and students would be added to each class. Different exams could be created inside a class. Student portals would be present, where documents of students remain stored, and could be analyzed. Although students would see the file icons of other students, they will not be able to access those files since they are password protected (Fig. 3).

Password protection can be disabled for teachers. Data may be stored for a longer time period.
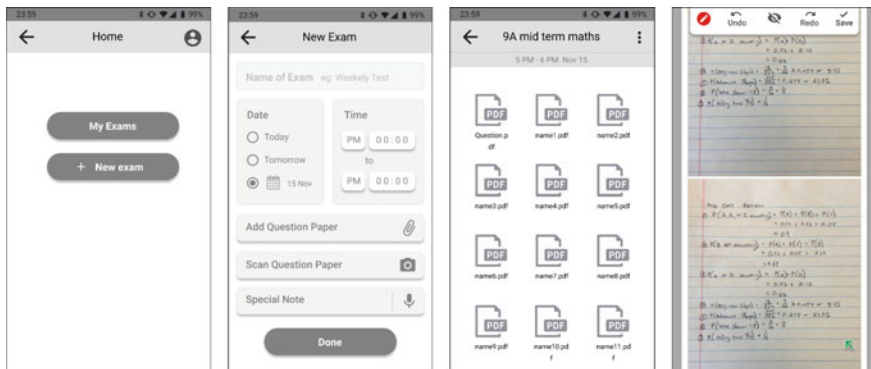
Fig. 2 Mid-fidelity wireframes of concept 1: teachers can create exams, wherein they can share the question paper to students. Students can upload their answer sheets, and teachers can use the tools provided for evaluation and feedback
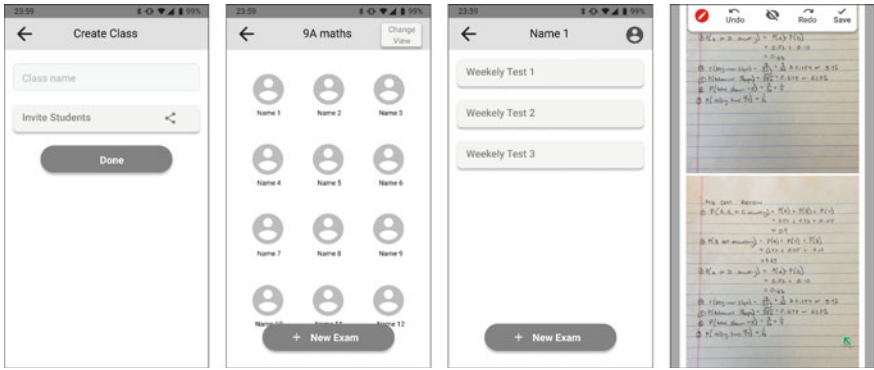
Fig. 3 Mid-fidelity wireframes of concept 2: teachers create classes where students are added. Exams are created inside the classes; students can upload their answer sheets, and teachers can use the tools provided for evaluation and feedback

Concept 3—The Evaluation Model

This concept would only be meant for evaluation, where teachers can upload answer sheets, evaluate them, and then download these documents. No option would be provided to share answer sheets. Sharing has to be done through other external platforms (Fig. 4).
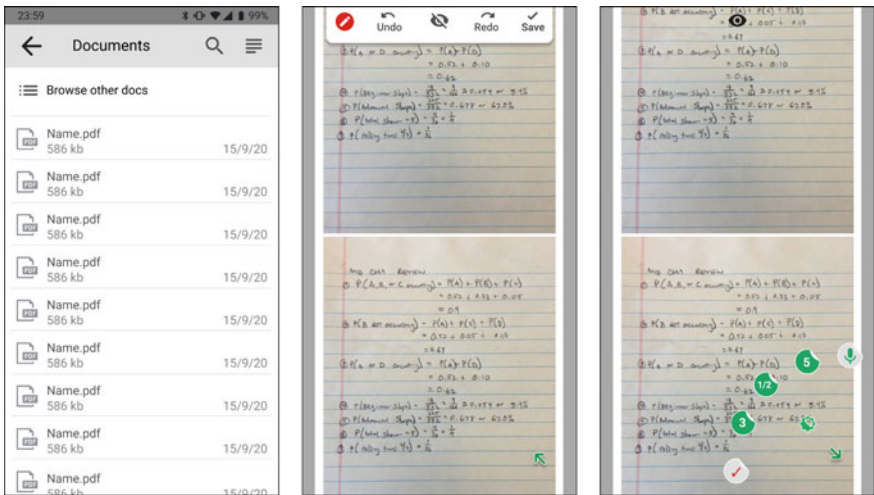
Fig. 4 Mid-fidelity wireframes of concept 3: teachers can only perform evaluation and feedback using the tools provided

3.4 Testing

The initial prototypes were tested among 12 users. Zoom meetings were set up individually. Links for the prototypes were shared, and participants were asked to try on their own to conduct an exam. The prototype was screenshared during testing.

Prototype 1 was found the easiest. Prototype 2 was preferred by eight teachers. Although the rest four teachers found Prototype 1 as the easiest, they preferred the Prototype 2 since it had more features. None of the participants opted for Prototype 3 having the minimum features. Considering the insights from user feedback, the final prototype was designed as the solution.

3.5 High-Fidelity Prototyping

See Figs. 5, 6 and 7.
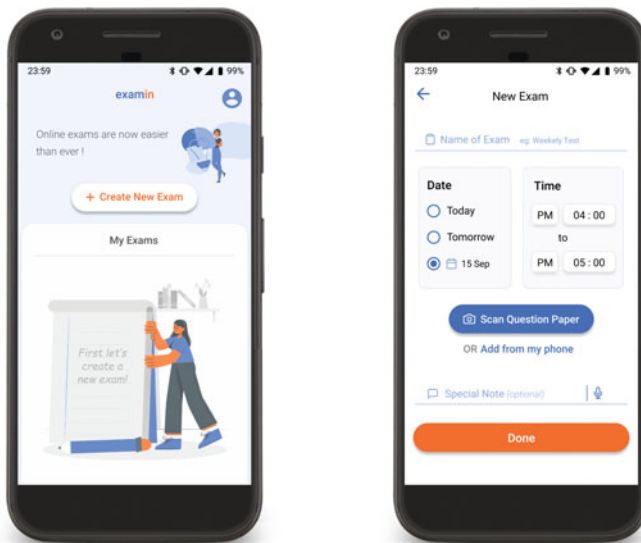
Fig. 5 Teacher schedules a new exam and shares question papers by either uploading from phone storage or by taking photos using the scanning tool. After this, students are invited to the exam using the link generated in the app. The link may be shared over other mediums such as WhatsApp or Email
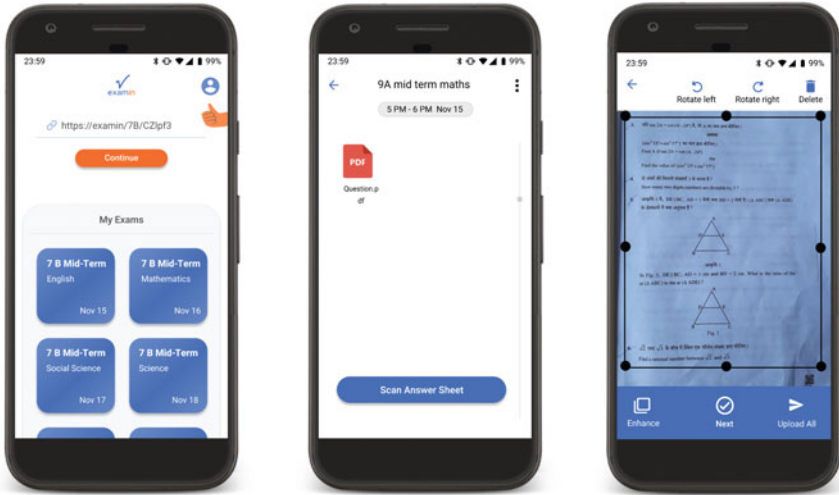
Fig. 6 Students enter the link and get access to the question paper, only at the scheduled time. After writing the answers in the answer sheet, students take photos of the answer sheets and upload them
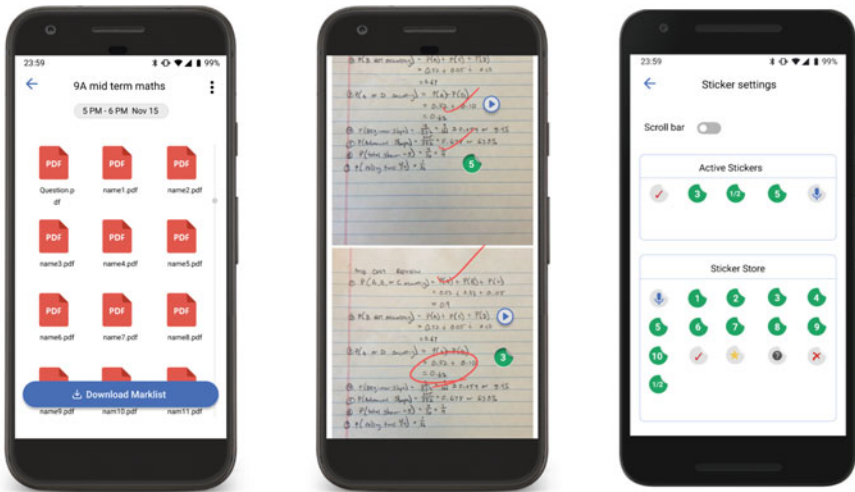
Fig. 7 Teacher sees the answer sheets uploaded and evaluates using the tools provided. Pen tool allows the teachers to mark their feedback. Customizable sticker packs help teachers to allot scores for answers and in automatically calculating the overall score. The voice sticker feature enables the teachers to give voice feedback to the students

4 Conclusion

The final high-fidelity prototype was tested among three teachers (secondary school level) for subjects English, Science, and Mathematics. All of them found the product to be significantly easier and comfortable than a conventional online exam through the competitors. The option to give feedback was appreciated the most, and the interface was found to be having a less learning curve. The positive feedback from the teachers indicated a demand for the product and pointed toward desirability of the solution.

5 Discussion

On further development, the product could also have features that help the teachers to handle classes as well, as it would make it convenient for the teachers and students to have a single app for all of their educational needs.

References

1. Sener, J.: Why online education will attain full scale. J. Asynchronous Learn. Netw. **14**(4), 3–16 (2010)
2. Tadesse, S., Muluye, W.: The impact of COVID-19 pandemic on the education system in developing countries: a review. Open J. Soc. Sci. **8**(10), 159–170 (2020)
3. https://en.unesco.org/news/unesco-rallies-international-organizations-civil-society-and-private-sector-partners-broad/. Accessed 8 Dec 2021
4. https://www.unicef.org/india/media/6121/file/Report%20on%20rapid%20assessment%20of%20learning%20during%20school%20closures%20in%20context%20of%20COVID-19.pdf/. Accessed 8 Dec 2021
5. Strielkowski, W.: COVID-19 pandemic and the digital revolution in academia and higher education (2020)
6. Sun, A., Chen, X.: Online education and its effective practice: a research review. J. Inf. Technol. Educ. **15** (2016)
7. Selvaraj, A., Radhin, V., Nithin, K.A., Benson, N., Mathew, A.J.: Effect of pandemic based online education on teaching and learning systems. Int. J. Educ. Dev. **85**, 102444 (2021)
8. Kuikka, M., Kitola, M., Laakso, M.J.: Challenges when introducing electronic exams. Res. Learn. Technol. **22** (2014)
9. Noori, A.Q.: The impact of COVID-19 pandemic on students' learning in higher education in Afghanistan. Heliyon **7**(10), e08113 (2021)
10. Twesige, D., Gasheja, F.: Challenges and opportunities of moving to online learning in the higher learning institutions in Rwanda: lessons learnt during Covid-19 pandemic (2020)
11. Murphy, M.P.: COVID-19 and emergency eLearning: consequences of the securitization of higher education for post-pandemic pedagogy. Contemp. Secur Policy **41**(3), 492–505 (2020)
12. Kapasia, N., Paul, P., Roy, A., Saha, J., Zaveri, A., Mallick, R., Chouhan, P.: Impact of lockdown on learning status of undergraduate and postgraduate students during COVID-19 pandemic in West Bengal, India. Child. Youth Serv. Rev. **116**, 105194 (2020)

13. https://theprint.in/india/education/how-whatsapp-has-become-the-new-classroom-for-school-students/235443/. Accessed 8 Dec 2021
14. https://www.unicef.org/northmacedonia/stories/learning-online-problems-and-solutions/. Accessed 8 Dec 2021

Clubhouse—A UX/UI Case Study on the Audio Social App

M. Vishnu, Jaison K Thomas, Sarvesh Tripathi, and Tripti Singh

1 Introduction

Founded during the time of the COVID19 pandemic in March 2020, Clubhouse is a social media app that makes use of the human voice as the basic key for information sharing [1]. The popularity of the app among tech giants like Mark Zuckerberg, Elon Musk, etc., and the ability to involve in discussions in the rooms through audio, without switching on the cameras gave the app quick popularity. Initially, the app was released only on the iPhone Operating System (iOS) platform, which also gave it a larger-than-life image in the beginning unlike other social media apps [1]. It was the first social media app that would allow users to interact with each other through audio only, without a need to show their faces, which added on to the privacy factor for the users, which in turn became another major reason for the exponential growth of the app in a very short span of time, the primary reason being the pandemic related shutdowns [2]. In a span of 8 months after its release, the app was having almost 10 million downloads across the world, and its valuation increased from $100 million to $1 billion, making the app to be nicknamed the 'Silicon Valley's hottest start-up'. Clubhouse bridges the social gap that people lacked due to the isolation caused by

M. Vishnu (✉) · J. K. Thomas · S. Tripathi · T. Singh
Design Discipline, Indian Institute of Information Technology, Design & Manufacturing, Jabalpur, Madhya Pradesh 482005, India
e-mail: 20mds022@iiitdmj.ac.in

J. K. Thomas
e-mail: 20mds009@iiitdmj.ac.in

S. Tripathi
e-mail: 20pdso02@iiitdmj.ac.in

T. Singh
e-mail: ts@iiitdmj.ac.in

the COVID19 pandemic. It allowed users to express themselves and interact only through voices rather than focusing on their appearance [1].

Through this research paper, the issues related to the User Experience of the platform which would affect user retention are being analyzed and discussed.

2 Literature Review

The Clubhouse is a social audio app founded by Paul Davison and Rohan Seth, both having solid previous experience in running a tech company. Paul Davison was the Chief Executive Officer (CEO) of Highlight (now under the ownership of Pinterest) and Rohan Seth was the CEO of Lydian Accelerator and Memory Labs (currently owned by Open Door). With the release of Clubhouse, it became one of the first social networking apps to incorporate a setting where users could listen and speak in discussions without switching on their cameras, which was a matter of privacy to a large population of users [3]. Furthermore, Clubhouse is an app that does not have any recorded sessions. Whatever the app hosts are live, just like a group discussion. Initially, when the app was launched, it was an invitation-only app that worked only in iPhones which were having iOS platforms. But later on, due to the sudden surge in popularity, the Android versions of the app were developed. The working model of the Clubhouse resembled a lecture session and surfing through Clubhouse reminded a group therapy session that is often used in psychology for treating mental disorders and chronic pain [4]. They also introduced the 'rotating app icon' that features photographs of its community members with an interesting story behind it, which also increased the curiosity factor among the new users, which pushed them to try it out [5] (Fig. 1).

The clubhouse was launched during a time when the world was having a tough time dealing with the pandemic. It emerged as a new medium where people were able to express themselves through their voices, and still maintain their privacy intact up to a great extent. These features lead to the sudden growth of the app, making it a billion-dollar evaluation startup in around 8 months [2] (Fig. 2).

But, statistics show that the user engagement capacity of Clubhouse is slowly decreasing (Fig. 3). The pandemic situation and the salient features made the app attain an initial attraction across demographic boundaries in a very short span of time [2]. But as per the reports by Google, the Clubhouse app is slowly losing its initial popularity. Even after launching the android version and allowing uninvited user entries, the graph is going down [2]. The scarcity of content and the inability of the app to provide insights on active room discussions, finished discussions etc. make the user reluctant to use the app again, adversely affecting user retention [7]. In this research, Strength-Weaknesses-Opportunity-Threats (SWOT) Analysis is being carried out to deeply understand Clubhouse (Table 1).
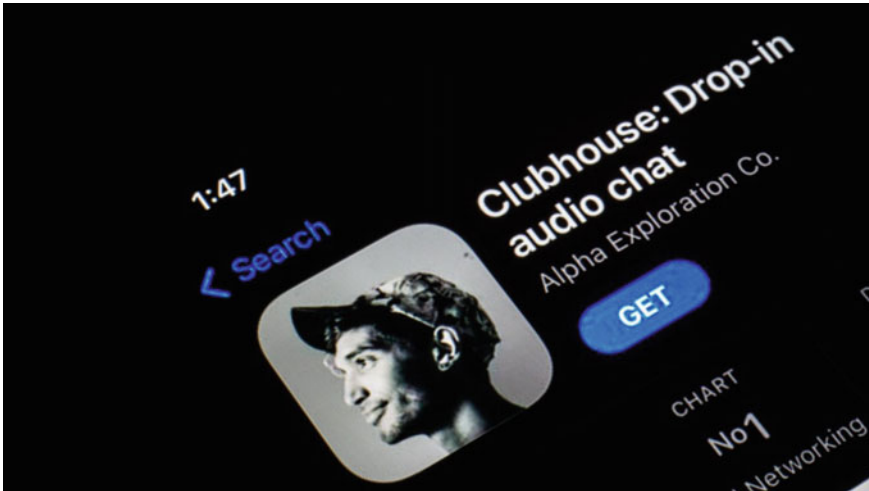
Fig. 1 Clubhouse app page in the app store
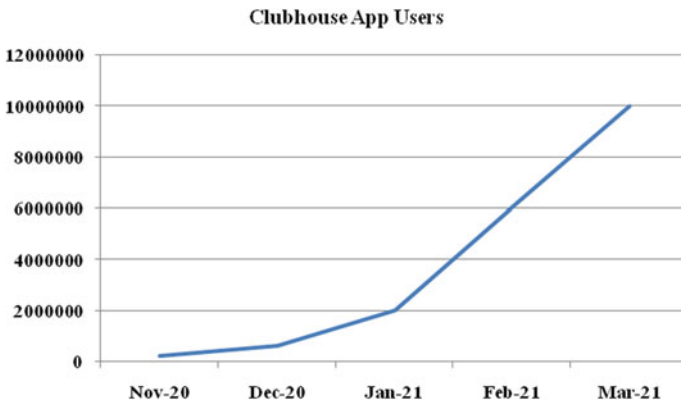
Fig. 2 Months on the *x-axis* and user count on the *y-axis*. Clubhouse app users from November 2020 to March 2021 [6]

3 Research Question

The research also aims to find out what are the issues which might have hindered the exponential growth of the app in terms of User Interface/User Experience (UI/UX) and will be suggesting some solutions to overcome these UI/UX issues which could assist the platform in having a better User Retention.
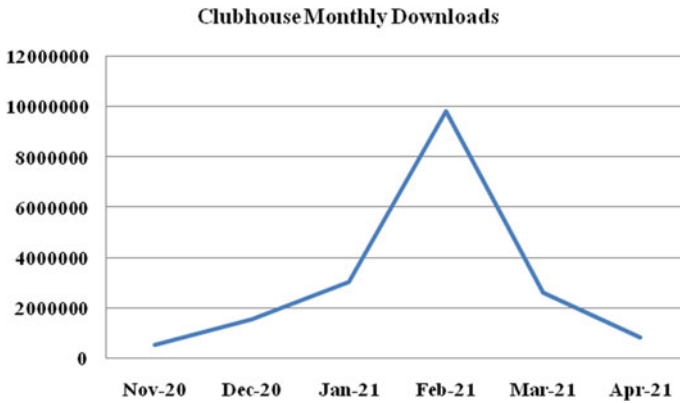
Fig. 3 Months on the *x-axis* and monthly app downloads on the *y-axis*. User's interest over time on Clubhouse (as per internet monthly downloads) [6]

4   Research and Methodology

A SWOT Analysis is being carried out by secondary research. Furthermore, a quantitative survey through a customized questionnaire is carried out to understand the collective opinions of the users. Also, a few direct interviews are carried out as a part of the qualitative survey user personas.

4.1   SWOT Analysis

The SWOT Analysis is carried out by secondary research to understand deeper insights about the sustainable growth of Clubhouse App [8, 9], by referring through various journals, websites, web blogs, reviews, etc.

Strengths. Clubhouse's major strength is to act as a learning platform. As per the research conducted by Whistle Wise in March 2021, 87% of the users consider Clubhouse as a learning platform where they are able to learn and also enable knowledge sharing on various topics like Tech, Business, and Sports, etc.

Weaknesses. As per the survey by Whistle Wise, only a mere 40% of users finds the app highly engaging; which is even lesser than the number of users listening to other podcasts daily. Hence, serious efforts to understand the problems in terms of User Experience need to be taken care of to improve User Engagement.

Opportunities. Brand endorsement and Ads are the major opportunities lying ahead of Clubhouse as 69% of the users are open to accommodating ads in the app, and 70% of the users want brands to join Clubhouse [8].

Table 1 SWOT analysis overview [8, 9]

Strengths	Weaknesses	Opportunities	Threats
• Learning platform • Knowledge sharing • Inclusivity	• Less user engagement • UX issues • Inability to hear finished room sessions • Lesser average than podcasts	• Brands entry to app • Ads • Promotions • Paid events	• Existing segment leaders like Facebook, Twitter etc. • Users finding competitors more engaging over long durations due to variety of content

Threats. Competitors like Facebook, Twitter, and Instagram, etc. post a major threat to Clubhouse as they are the segment leaders, and more than half a population of users of age between 18 and 34 years still finds the competitors more engaging and interactive due to the availability of more variety contents [8] (Table 1).

4.2 Dichotomous Survey Questionnaire

A modified Dichotomous Questionnaire [10] was created and shared through various social media platforms like WhatsApp, Gmail, etc. to get insights on how the user experience of the app was. The questionnaire was formulated in such a way that relevant insights on the UX side of the app were availed from the survey.

5 Results

5.1 Demographic Characteristics

Of the 33 clubhouse users that participated in the online survey, 66.7% of the users were male, and 33.3% of the users were female (Table 2).

Table 2 Demographic characteristics

Parameters	Categories	N (%)
Gender	Male	22 (66.7%)
	Female	11 (33.3%)

Table 3 Dichotomous survey results with conditions on the *left*, number of inputs and percentage on the *right*

Dichotomous survey	
Conditions	*N* (%)
Felt anxious while on-boarding	21 (63.6)
Hesitant to enter room discussions	22 (66.7)
Found it hard to understand room discussions	24 (72.7)
Observed unwanted notifications	20 (60.6)
Missed desired room discussions	19 (57.6)
Use clubhouse regularly like other social media apps	6 (18.2)
Wish to have a better user experience	28 (84.8)

5.2   Dichotomous Survey

From the 33 Clubhouse users who took part in the online Google survey, 63.6% of participants stated that they felt anxious during the initial onboarding process. 66.7% of participants found it hesitant to enter the 'room' discussions initially. 72.7% of participants found it confusing to understand the functioning of the room discussions. 60.7% reported that unwanted notifications which were not related to their following or interests were observed after the onboarding process. 57.6% stated they had missed discussions that they wished to be a part of. A majority of 81.8% admitted that they do not use Clubhouse as regularly as they use other social media apps like Facebook, Instagram, etc. More importantly, 84.8% suggested a better user experience of the app would help them in using the app more often (Table 3).

6   Discussion

From the survey done among 33 Clubhouse users, it is quite evident that more focus should be given to the User Experience to increase User Retention for the platform. As per the reports, the Clubhouse app download numbers have been showing a decline post the month of February 2021 [6]. Several reasons for the decline can be observed from the secondary data research. As per the reports by 'mint', Clubhouse was launched during the time of a lockdown and isolation period. During such a period, it gave a new communication platform to the users which was a new experience for everyone. But over time when the restrictions were reduced, people got much easier ways to have direct communications and discussions possible. Hence, the novelty of Clubhouse slowly got reduced [11]. More than 50% of users are of the 18–34 age group and around 40% are of the 35–54 age group [3]. A large user base of the app is taken over by the Generation Z (Gen Z, a common term for the generation born between 1997 and 2012 [12]) category. As per the studies, the Gen Z population is a population that is more prone to the technological era and hence their brains perceive

visual content more effectively than other types, whereas Clubhouse was inherently an audio-based social media platform [3].

From the online survey carried out, the respondents clearly show difficulties they faced while using the Clubhouse app which in turn makes the users reluctant to use the app regularly. This shows light on the drawbacks the current UX of the app is having. A good User Experience is an unavoidable factor in the success of any product, whether digital or tangible [12]. The usability of a platform determines its long-term success [12]. For a worldwide product like Clubhouse, a large demographic user base has to be taken into account to make the experience of the user better and hence trustworthy. To build a platform that offers a great User Experience, usability heuristics should be taken into account [12, 13]. The usability heuristics allow troubleshooting the problems in digital problems and help in resolving them. This enables to make the experience better for the user.

In Fig. 4, a design suggestion is being shown in comparison with the existing design. Unlike the current design, in the landing screen after onboarding, the user is greeted with a pop-up that directs the user to the rooms at the same time assuring the user that they will be on mute by default when they enter. This follows the initial usability heuristics principle of 'Visibility of System Status' [12]. It assures the users upfront that they are on mute and can confidently navigate across the room. This allows the user to predict the next steps, which will build trust in the platform. This increases the usability factor and urges the user to explore more through the app [12].

In Fig. 5, the existing design of the room section is compared with the design recommendation. In the redesigned layout, the users can access a 'highlights' section, which would have the necessary highlight recordings of that discussion. The users will be able to access those recordings and get an idea about the discussion, and then speak if interested or move to the other room if needed.

Such UX-related changes can be incorporated to make the UX better for the Clubhouse App. This would help the stakeholders achieve the desired business impact [12] by increasing User Engagement and User Retention in the platform. The research gives initial insights on the fact that even though Clubhouse is an audio social platform that is very different from other social media apps of the Gen Z category [3], a regular and structured UX enhancement would increase the user footprint for the app.

7 Conclusion

The above-discussed screens are a few preliminary low fidelity UI recommendations to improve the UX for the two scenarios of screens in the app only based on the survey results. The research was conducted among 33 participants due to various limitations. If the research topic addressed can be conducted on a broader scale, much more relevant insights on improving the User Experience of the Clubhouse platform can be availed. And hence, a broader UX redesign strategy can be derived. This derived strategy would assist in creating a better experience for the user, and
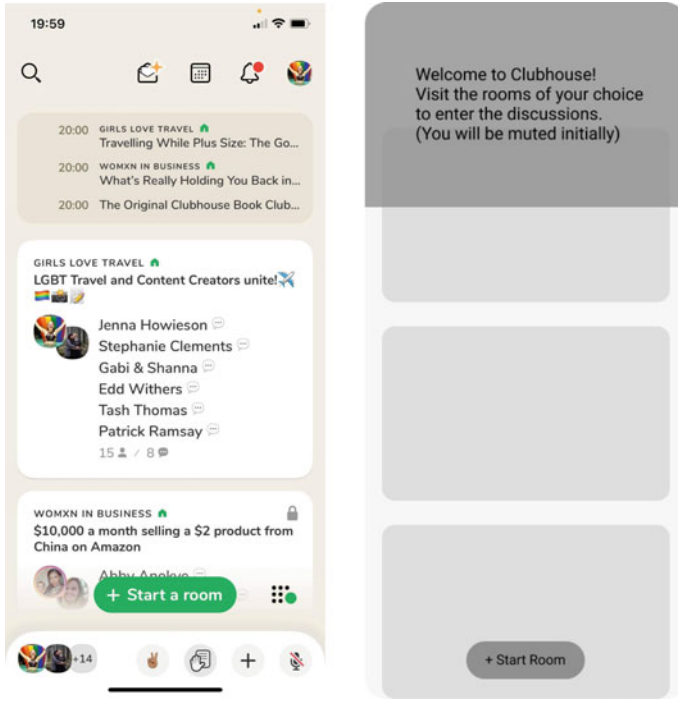
Fig. 4 Current landing screen layout versus redesigned low fidelity landing screen recommendation
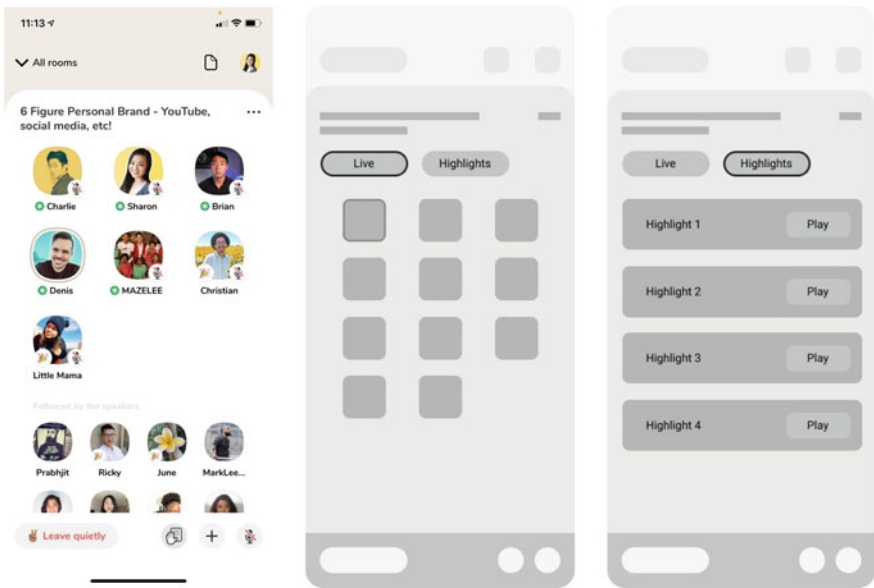
Fig. 5 Current room screen layout versus redesigned low fidelity room layout recommendation

hence, increase user retention, in turn assisting the stakeholders to achieve or move closer to the targeted business goal of the company.

References

1. Zhu, B.: Clubhouse: a popular audio social application. In: 2021 International Conference on Public Relations and Social Sciences (ICPRSS 2021), pp. 575–579. Atlantis Press (2021)
2. Strielkowski, W.: The Clubhouse phenomenon: do we need another social network? Preprints 2021030503 (2021). https://doi.org/10.20944/preprints202103.0503.v1
3. Chen, N.: Behind Clubhouse's trajectory and phenom. Preprints 2021060103 (2021). https://doi.org/10.20944/preprints202106.0103.v1
4. Adler, J.M., Skalina, L.M., McAdams, D.P.: The narrative reconstruction of psychotherapy and psychological health. Psychother. Res. **18**(6), 719–734 (2008)
5. Gkritsi, E.: Clubhouse invites for sale on Alibaba's used goods app (2021)
6. https://www.businessofapps.com/data/clubhouse-statistics/. Accessed 12 Nov 2021
7. https://www.mfmpod.com/162-why-clubhouse-will-fail/. Accessed 12 Nov 2021
8. https://teamwhistle.com/insights/2021/03/clubhouse-swot-analysis/. Accessed 12 Nov 2021
9. Humphrey, A.S.: SWOT analysis. Long Range Plan. **30**(1), 46–52 (2005)
10. McClendon, M.J.: Response-order effects for dichotomous questions. Soc. Sci. Q. **67**(1), 205 (1986)
11. https://www.livemint.com/. Accessed 12 Nov 2021
12. https://www.insiderintelligence.com/insights/generation-z-facts/#:~:text=Generation%20Z%20(aka%20Gen%20Z,2020%20and%20entering%20the%20workforce/. Accessed 29 Nov 2021
13. Jokela, T.: The early phases of UX: why they are important (more than evaluation), and what they are? In: International Workshop on the Interplay Between User Experience (UX) Evaluation and System Development (I-UxSED 2012), p. 49 (2012)

Effect of Learning Environment to Create Empathy and Learning Outcomes Among Design Students

Vikram Mathur and Anirban Chowdhury

1 Introduction

The age group of 18–25 year olds ordinarily find themselves in rather confusing scenarios for themselves. On one hand they get congratulated and hailed as the youngest adult set of society but then as soon as they begin to exercise their rights in their new found status, they are often snubbed and criticized by the older lot for speaking their mind. They are kept from taking decisions and often the behavioral patterns of their elders continue to nag and bully them. These scenarios leads to frustration and a sense of rebellion within this group. They mostly tend to retaliate by silently avoiding any kind of involvement, engagement or discussion as they feel they will be belittled and again bullied into doing as per the wishes of their elders [1]. Thanks to technological advancements, this group finds its escape through the various avenues of social networks, search engines and derive enormous pleasure by indulging into the different sections of the virtual world and seeking out opportunities which they cannot access in their physical world. Such interludes with the virtual world provide for learnings and exposure to opportunities and information [2].

The world is getting smaller for the young adult learners as they dapple with technology and come aware of so much that is on offer. Pursuing their ambitions, they develop high expectations of achieving their aspirations in the most meaningful manner. They crave qualitative support, advice and resources to do this [3]. Unfortunately, many of them face so much pressure, criticism and opposition from their family, friends and teachers (see Fig. 1) that they withdraw into their cocoons and leave their future to fate.

V. Mathur (✉) · A. Chowdhury
School of Design, University of Petroleum and Energy Studies, Bidholi, Dehradun 248007, India
e-mail: vikrammathur@ddn.upes.ac.in

A. Chowdhury
e-mail: anirban.chowdhury@ddn.upes.ac.in
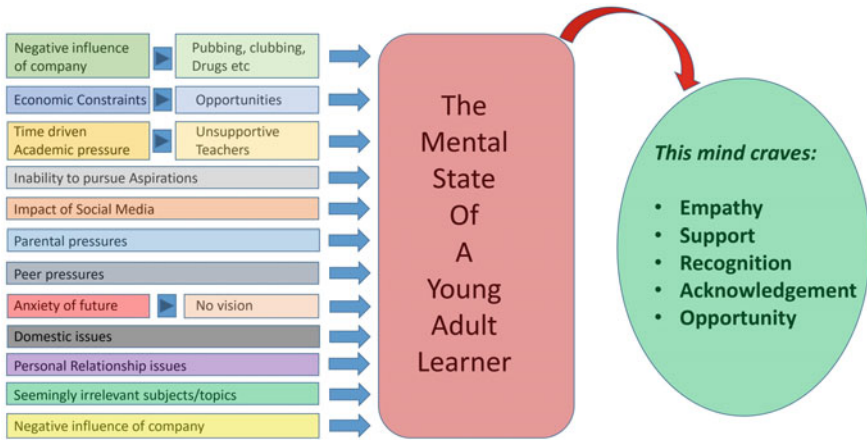
Fig. 1 The mental state of a young adult learner [4]

The education system up to secondary school completion, is meant to provide a basic level of awareness, learning and understanding of the various facets of life. It provides for an overall understanding under the umbrellas of subjects such as Science, Social Studies, Language and Mathematics. Unfortunately, with time the syllabi for each of these subjects has grown though the learning period remains the same. This has resulted in an acute pressure build-up on the learner as well as the teacher [5]. The syllabus being vast, the teacher is forever fighting to complete the course on time and therefore is mostly challenged to match-up with the grasping pace and capacity of his learner. Thus the pressure now passes onto the learner. Alongside, the parents of the learner who remain anxious for the future of their ward, want their ward to score high to remain ahead of the competition. They panic and unwittingly pass-on their anxiety to their ward. Finding himself cornered, this young learner resorts to shallow learning methods like rote. Continual practice of rote makes him habituated to this unhealthy method of progressing through school [6]. By the time he completes secondary school and enters higher secondary school, rote is a way of life. This technique rewards him with a high score and helps him secure admission to university.

Again, family, friends and teachers at school become the deciders of which field of study, choice of program and institute will be best [7]. The non-assertive and placid ones among these young adults land up in study programs which are not aligned with their personal goals. They have only one way to get through the undesirable situation they now face, the rote method.

Unfortunately, a study program in design education does not facilitate progression by rote. It is an intense process of experiential learning which calls for reasoning, interpretation and analysis and then application of the assimilated learnings to find/devise solutions for the realized problem [8]. The process being extremely derivative in nature does not necessarily lead to the same solution each time. So,

learners who have not selected the design program after due diligence, find the going excruciatingly challenging.

An effective education in design can only be achieved by training the mind to sensitively identify, relate and respond to the need. In order to develop the sensitivity capacities of the learner, intensive sessions of discussions, brainstorming and honest exchange of opinions and ideas become very necessary.

Nature is impartial and creates equally. Circumstances, situations and life experiences create variants within us apart from culture, race, traditions, beliefs, etc. But aptitude is defined by nature. Aptitude is the only aspect design schools can examine when aspirants seek admission [8]. Once the aspect of aptitude is found present, building the correct attitude becomes necessary. All fields need their own attitudinal build-up; for example, the defense forces build for discipline as they need their team members thinking and executing their work in the least amount of time and to perfection. Even the slightest lapse could cause total failure. This aspect of training falls under the theory of Behaviorism Instructional Design. As instructors of design, we need to achieve this in our own way.

1.1 Comparison of Teaching in Face to Face, Online and HBO Modes

The learning process comprises two phases—teaching and self-learning. These are also referred to as contact (synchronous) and non-contact (asynchronous) learning [9]. The 'teaching' or 'contact' phase of learning includes all the learning that happens when the learner receives direct instruction from the instructor or teacher. The self-learning/non-contact/asynchronous learning provides for the learner to spend time in research and effectively forming his/her learning outcomes through recollection, assimilation and reflection [9].

The contact learning phase is thus critical and needs to be delivered with care. At this point in time, with advancements in technology, teaching can be facilitated in many more modes other than the customary old school method of 'blackboard and chalk'. There are of course the physical classrooms where face to face instruction is administered, but then there is the online mode, wherein technology provides for remote instruction between teacher and his learner(s) using the virtual classroom. Then there is the Hybrid Online (HBO) mode which comprises both the face to face as well as the online modes. In this mode, the learner receives instruction in the face to face (physical classroom) mode as well as the online (virtual classroom) mode [10].

The HBO mode seems to produce best results as it facilitates some learning to the learner that s/he can learn at a personally suitable pace. It also facilitates some physical interaction between the learner and the teacher which helps in the learning process. Online lessons can be recorded and played/re-played to suit the learning pace of the learner [11].

For design instruction, the HBO mode works best as it helps to provide for teacher-learner physical and virtual interaction as well as allows the teacher to provide for well-directed asynchronous activities/self-learning exercises for the learner [12].

1.2   Why Empathy-Based Teaching Pedagogy?

Today's design learner is a young adult (see Fig. 1), who has just finished school and expects to receive the requisite learnings to make the transition into the field of design thought and processes. Each learner comes saddled with mental baggage of the past comprising his/her own peculiar experiences, thoughts and interpretations [13]. Their minds are so busy with these that in many cases, there is no room for new thought or fresh interpretations. The teacher needs to leave behind the old school methods of knowledge transfer that assumes that the student will capture the teaching and interpret the same as his/her learnings. Improvising on his methods, the teacher needs to ensure the creation of enough opportunity and space in the learning minds, for new interpretations [14].

An understanding of where the learner is positioned and beginning the instruction from there has been found to yield better learning outcomes as the learners begin to add their new learnings to their existing knowledge structures [15].

2   Aim and Objectives

This paper aims to examine the effectiveness of empathy-based mentoring pedagogy in creating better learning outcomes by observing differences in two available modes of instruction: Online mode versus Hybrid Online mode.

3   Methods

Two student cohorts Cohort 2019–23 (10 students) and Cohort 20–24 (13 students), enrolled at the program of Interior Design, University of Petroleum and Energy Studies, Dehradun, pursuing the course of Domestic Interiors were considered for the research purpose of this paper. For the sake of convenience, this paper will now refer to Cohort 2019–23 as 'Batch 1' and Cohort 2020–24 will be referred to as 'Batch 2'. Batch 1 was administered the course in online mode, in September 2020 when the COVID-19 pandemic had forced everything into lockdown, whereas Batch 2 was taught the course in September 2021 when the classes were being conducted in the Hybrid mode.

3.1 Development of Empathy-Based Pedagogy for Teaching Design Students

Empathy can be categorized into three types—Cognitive, Emotional and Compassionate. Cognitive empathy deals with understanding how our students feel and what they think. This can help us communicating with them. Emotional empathy (or affective empathy) deals with the ability of sharing the other person's feelings. It helps in building an emotional connection with them. Compassionate empathy (or empathic concern) is about taking action and helping out in any manner [16].

Design being a subject that deals with understanding and converting intangible aspects into tangible values, requires it is learners to be conditioned and prepared to delve into matters with a five sensing approach. The educators need to ensure that their learners are available in this frame of mind.

Talking to students from the very start and engaging with them on topics of their interest creates a rapport. Once the ice is broken, formalities and hierarchies take a backseat and conversations begin to happen. These conversations should be directed at identifying career and life goals. Encouraging students to share their visions and constraints can open the doors to forming strategies to subject matter deliveries and meaningful discussions. The teacher can thus step up his game by being the mentor instead of just being the knowledge provider.

Cognitive empathy helps in building the rapport and affective empathy helps to innovate on effective learning styles that will bring creativity into the learning outcomes. A learner yearns to share ideas and is excited by the thought of receiving feedback on his effort. This feedback provides stimulation for betterment and the will to excel.

3.2 Conditions of Empathy Treatment (Online vs. HBO)

The Online platform facilitates visual and voice communication in the digital medium. The HBO platform facilitates the Online mode and face to face interaction. Learnings would happen on both platforms but perhaps the empathy factor would be more contributive in case of HBO.

There were mixed feelings about how the course would proceed. Students had been confined to their homes for 6 months and were attending classes on their laptop screens. Online mode does curtail interaction in certain ways. Though the internet would facilitate an audio-visual communication, the Internet signal playing truant, would break the mental connections the teacher and his students would be trying to establish. Visual connection being limited the strength of body language would not be utilized optimally. Also, the slightest disruption at their homes would completely distract the students making the teacher's job all the more challenging. In addition to all this, this course is the first interior design project experience for the student at the program.

4   Results and Discussion

Batch 1 submitted their summative assessment work on time and their work had all the deliverables as per the stipulations mentioned in the Assessment Brief provided at the start of the course. The learning outcomes are shown in Fig. 2. Student feedback was great and honestly provided. They were very enthusiastic as this was their first design project course at the design program.

Batch 2 also submitted their summative assessment work on time containing all the deliverables (as mentioned in the Assessment Brief) but also supplemented their work with many more supporting documents like free-hand sketches, physical models and detailed drawings. The learning outcomes are shown in Fig. 3. The student feedback was far beyond great and their honest joy was wholesomely communicated through their work and dedication to prove their worth to themselves and their teachers. 50% students were attending classes in face to face mode whereas the rest continued to attend online mainly due to travel issues.

4.1   Teacher–Student Interaction (Attendance and Participation)

Being pandemic lockdown times, both cohorts (particularly Batch 1) were a frustrated lot due to their confinement at home and so the learning set spent the first few sessions with their teacher talking about their lives at home. There was a barrage of rants and exclamations of self-pity. The teacher was patient and empathetic to their issues even though they were communicating online. Gradually steering the conversation away and into their individual domestic areas, they began discussing how different areas in
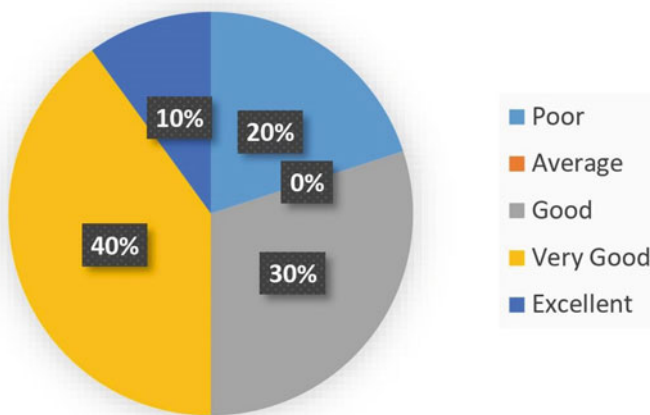
Fig. 2 Learning outcomes in the online mode of instruction
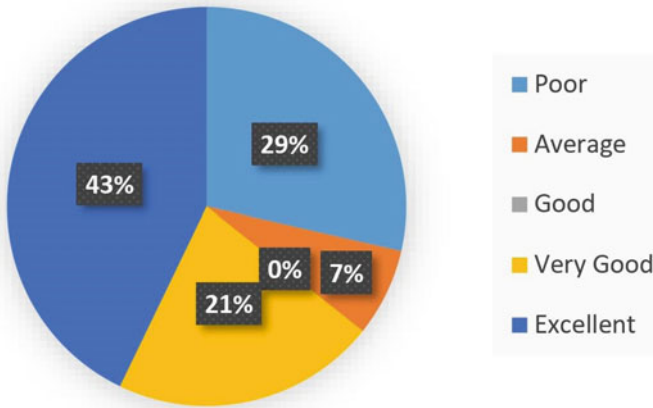
Fig. 3 Learning outcomes in the HBO mode of instruction

their homes serviced their needs. The teacher was gradually succeeding in growing their interest in what had to be taught to them. Showing empathy had worked well and there was good attendance in the class (Fig. 4.). Engagement grew at every session as the teacher continued the practice of empathy in personal as well as class related work.

In the case of Batch 2, empathy worked much better in terms of engagement and learning outcomes. As the lockdown had ended and students were returning to the university during that time, the attendance record (Fig. 5) could not remain too accurate. However, maximum students attended physical class.

Fig. 4 Student attendance in the online mode of instruction
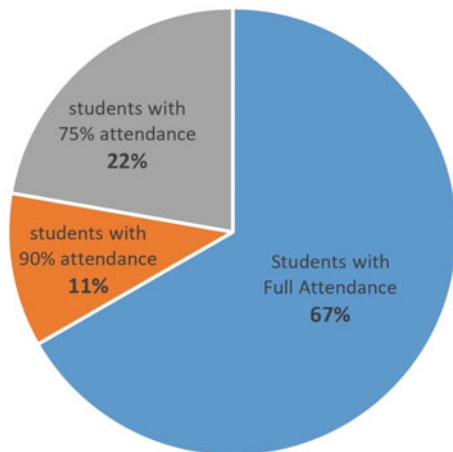
Fig. 5 Student Attendance
in the HBO mode of
instruction
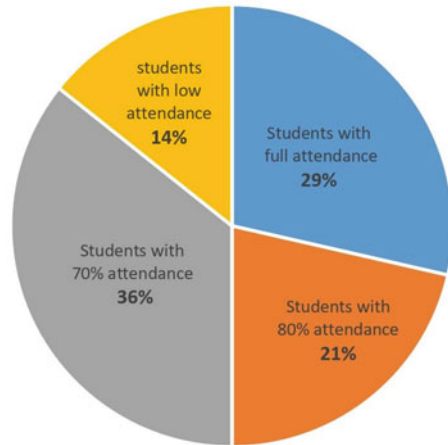
4.2 Student Satisfaction

In both batches, students have engaged very well and given very positive feedback
for the instruction and support they received. They felt that they enjoyed the course
and felt very confident about doing more such interior design project work in the
future. They were specific to mention that their first time experience of working on
an interior design project had been very reassuring and enlightening. The faculty
conducting the course for both batches has had these students come for advice and
guidance even after the completion of the course on other courses and issues.

The scores show that Batch 1 scored much lower than Batch 2 even though the
content, teacher, instruction, empathetic support remained the same. Though there is
one case of a high score (75marks) in Batch 1, the average score across the cohort is
65 marks. Batch 2 on the other hand, the scores are all above 70 marks barring one
case. The cohort that was taught in the hybrid mode seems to have performed much
better and secured 9% higher (on an average) as compared to their senior cohort.

4.3 What Kind of Empathy Is Involved?

Cognitive and emotional empathy were used to develop strong relationships for long
term learning and open discussion. The learner feels supported when the teacher
begins the instruction after locating the learners understanding level. This measure
reassures even the slowest learner in the learner set.

The teacher felt that the connection with the students physically in class was
way stronger than with the ones online. The online sessions are always recorded and
available to students for reference. Beyond the class sessions, the online students only
referred to the recordings whereas the ones attending physically, would also reach

out to their teacher in person or call for doubt clarifications on many occasions. The empathy approach worked out much stronger in the 'face to face' mode. Student engagement, involvement and learning outcomes were very much better than the 'online' mode, though the modus operandi remained constant.

Other faculty members at the department have reported that students of these cohorts have been actively engaging with them in meaningful discussion and seem to find their self-motivation to indulge more holistically in their academic pursuits.

5   Conclusions

In today's time and age, the distractions are enormous in scale as well as number. As their teachers in design, the teacher needs to catch their attention (and arrest it) by creating the ideal learning environment to generate empathy and learning outcomes among our students.

Since design as a subject has hardly any text books, most of the learning is meant to happen through interaction, immersion in self-thought and self-interpretation. Of these, the self-thought and self-interpretation needs to be done personally, whereas interactions need to happen with the rest of the world around. Interaction should be interpreted as a dialog that the learner has with just any and everything s/he can find access to. The teacher/guide/mentor in design is only meant to give direction and ensure free flow of thoughts for the learning mind. As a designer, one needs to interact, familiarize and form intimate bonds with any and everything. In short, s/he needs to five sense the world. The deeper these understandings, the better s/he will prove as a designer. Appreciating the kind of sensitive person, the 'future designer' needs to be, the teacher's role becomes very clear too. This 'learning' mind needs to be conditioned to become a mature sensing mechanism capable of sensing, interpreting, analyzing, concluding and storing information in a systematic manner for effective recall and precise application. As stated earlier (and illustrated in Fig. 1), these young learners arrive at the program with so much pre-loaded mental baggage that there is hardly any mental space for what we want to achieve with them. It therefore becomes necessary for design educators to develop an ideal learning environment to create empathy and learning outcomes among the design students.

References

1. Fuller, R. W., Gerloff, P.: Dignity for All: How to Create a World Without Rankism, 1st edn. Berrett-Koehler Publishers, Oakland (2008)
2. Valkenburg, P.M., Piotrowski, J.T.: Plugged in: How Media Attract and Affect Youth, 1st edn. Yale University Press, London (2017)
3. Appleby, D.C.: The soft skills college students need to succeed now and in the future. Psychol. Stud. Network (2017)

4. Mathur, V.: Empathy, vulnerability and learning theories in higher education. In: HWWE 2021 (2021)
5. Jain, G., Singhai, M.: Academic stress amongst students: a review of literature. Prestige e-J. Manag. Res. **4**(2), 58–60 (2017)
6. Johnson, B.: When Rote Learning Makes Sense. [Online] (2010)
7. OECD: Equity and Quality in Education: Supporting Disadvantaged Students and Schools. OECD Publishing (2012)
8. McLeod, S.A.: Kolb—learning styles. Simply Psychol. (2017)
9. Hrastinski, S.: Asynchronous and synchronous E-learning. EDUCAUSE Quart. **31**(4) (2008)
10. Lederman, D.: Will shift to remote teaching be boon or bane for online learning? insidehighered.com (2020)
11. Dhawan, S.: Online learning: a panacea in the time of COVID-19 crisis. J. Educ. Technol. Syst. **49**(1), 5–22 (2020)
12. Fabriz, S., Mendzheritskaya, J., Stehle, S.: Impact of Synchronous and asynchronous settings of online teaching and learning in higher education on students' learning experience during COVID-19. Front. Psychol. **12**, 733554 (2021)
13. Nguyen, H.T.: Teaching and teacher education. Sci. Direct **25**(5), 655–662 (2009)
14. Holdhus, K. et al.: Improvisation in teaching and education—roots and applications. Cogent Educ. **3**(1) (2016)
15. National Research Council: How People Learn: Brain, Mind, Experience, and School: Expanded Edition. The National Academies Press, Washington, DC (2000)
16. Bariso, J.: EQ applied: The Real-World Guide to Emotional Intelligence: How to Make Emotions Work for You, Instead of Against You. Borough Hall (2018)

Strategizing Total User Experience Design for Better Business Outcome

Anirban Chowdhury

1 Introduction

A designer generally considers principles of human factors engineering to provide different design solutions as a good ergonomics leads to good design. For example, if the dimension of a backpack to carry a laptop does not fitting with human body dimensions (anthropometric parameters), does not have proper cushioning on the belt and back support, this backpack might not be comfortable and usable as there is a probability of back and shoulder pain if carrying laptops in such backpack and thus user dissatisfaction. Hence, usability and comfort factors are important for product design and ultimately for the better user experience. From this example, it can be argued that human factors have direct influence on user satisfaction about a product use. Therefore, is now acceptable fact that "Good Design means Good Ergonomics" [1–3]. As a science of interaction, application of ergonomics/Human Factors Engineering (HFE) is not only limited to the product user experience but also service experience, brand experience and the experience at organizational level because the key focus of HFE is human well-being.

On the contrary economics is the subject which is also focused on human well-being through channelizing the money flow, tangible and intangible assets in a systematic way. Tangible assets might be a product (e.g., a car); whereas, intangible assets are human skills in form of a service. The HFE is important for management of experiential aspects of both of these tangible and intangible assets. Hence, Ergonomics/HFE is related to the economics. In addition, it is evident that people love to purchase and use products which are ergonomically designed. Therefore, it is now established that "Good Ergonomics means Good Economics".

A. Chowdhury (✉)
School of Design (SoD), University of Petroleum and Energy Studies (UPES), Dehradun, Uttarakhand 248007, India
e-mail: chowdhuryanirban14@gmail.com

Schema Activation => Construction => Application

Fig. 1 Steps in schema construction method (SCM)

It is observed that current job entry level UX designers are unable to relate UX strategies with the business strategies, in India. Often, they only focus on usability and esthetics (beautification) of a user interface. They also ignore the service part of a product or a software. Another, crucial facts about Indian startups and newly established UX consultancy providers are—UX awareness at Organizational level and UX maturity level is comparatively lower (hostility stage according to UX maturity model [4]). Often, these firms also ignore service system aspect for their UX design solution. Long back, H. Daly (1974) argued that ultimate effectiveness/stability of a business or economy is depending on the ration between the service and throughput. Throughput stands for the inevitable cost of maintaining the stocks of people and artifacts. The throughput should be minimized subject to the maintenance of a chosen level of stocks. Goal of all services is satisfaction. Services are yielded by the stocks of artifacts (product/software) and people. Therefore, aim of this paper is to develop a framework which will help to young designers to correlated Business, UX design, and underlying human factors to achieve a better business outcome.

2 Methodology

This paper covers literatures and secondary data collected from online resources such as Google Scholar, Science Direct, JSTOR. A systematic literature review has been conducted to filter out to important resources and data as per objectives of this study. Then, all the data were presented in the form of literature and a Schema Construction Method (SCM) (see Fig. 1) [5] has been applied to derive a framework which allows young designers (Indian) to related their design to UX strategies and Business Outcomes with examples from current business cases.

3 Concept of Total User Experience (TUX)

According to Xu [6] (Intel Corporation, USA), UX ecosystem is important rather than the UX at individual level (either product or service or organizational level). He has highlighted about different touchpoints in product or software UX lifecycle. These are—marketing information, order process, app/product entry point, installation information, workflow, functionality (backend/frontend), system performance, UI and Usability, Online help, content service, content delivery process, user manual, user training, user support, upgrade process and end of life process [6]. Hence, the Total User Experience (TUX) is an end-to-end process for proving design solutions.

Fig. 2 The TUX and UX lifecycle
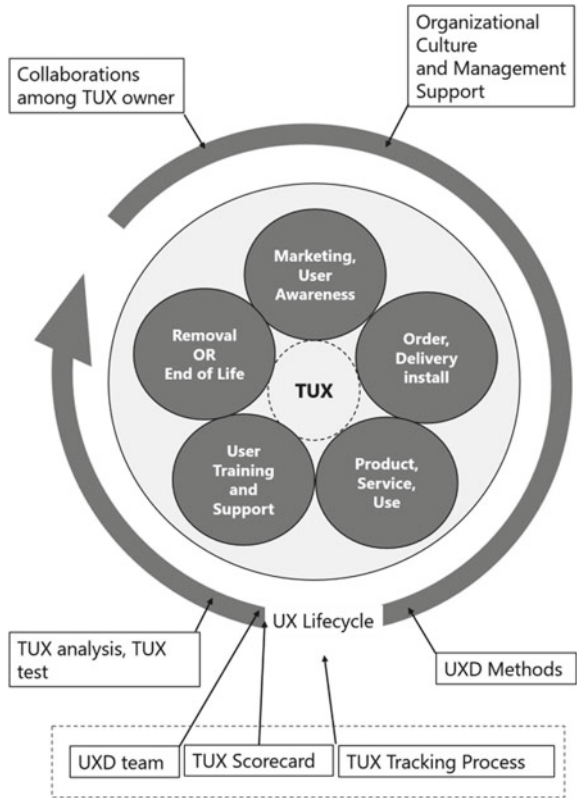
The consumer journey mapping approach helps in identification of these above-mentioned touchpoints and reinforcing the TUX practices [6]. However, in current practice, all firms are not focusing on TUX approach (Fig. 2).

The TUX process has six distinct steps.

Build a UXD team (should be inter disciplinary to handle all the touch points and members should have ability to communicate UXD to non-designers).

1. Conduct TUX gap and needs analysis (based on competitive analysis of existing products or services but not only usability and user interface; and organizational requirements)
2. Define a UXD scorecard and a tracking process (scorecard is required benchmarking of business success across all the TUX touch points)
3. Execute and collaborate on UXD (interdisciplinary team work together and take necessary actions)
4. Conduct an integrated end-to-end TUX test (checking whether all the TUX touch points in a simulated environment are represented like the real UX ecosystem)
5. Improve TUX and make end users ready for release (the project team needs to make it a high priority to fix identified issues and ensure end user readiness).

There is a novelty of idea of TUX lies on 3 steps in TUX process. The Conduct TUX gap and needs analysis are important as it helps to identify gaps in current use of products or services not only just not just in UI and usability. The Execute and collaborate on UXD and Conduct an integrated end-to-end TUX test are the stages very crucial as a UX designer needs to collaborate with business analyst, operation personnel, software architect, service designers, back-end tech-support providers, communication and marketing experts in addition to all other touch points of UX lifecycle. Therefore, to execute and follow the TUX process following aspects are very important: 1. Collaboration among TUX owner; and, Organizational Culture and Management Support.

4 UX Strategies and Human Factors

At the initial stage of UX practice, one school of experts thought that usability is the most factor that ensures user satisfaction and thus the good user experience [3, 4]. Sanders [7] talked about the role of esthetics in user experience. Jordan [8, 9], Desmet [10] and Norman [11] strongly agreed and established the role of hedonic needs, attitudes and emotions for in contribution to the user experience. In this context, usability standard ISO 1941 (1998) is important where there was emphasis given on effectiveness, effort and satisfaction of the users, to provide the basis of usability testing and technology acceptance [6].

The most of the UX strategies are depending on five key values related to the product choice such as functional, social, conditional (love, personality, etc.), epistemic (usability: safety + trust + utility + ease of use + comfort) and emotional (pleasure and any other affective state) [12]. Among these personality, usability and emotion (e.g., the reward points redemption causes happiness/to customers at Pantaloon or Big-bazaar) are directly related to Psychological Human Factors. The socio-economic values (e.g., discounts in massage services in massage parlor or saloons in India or any other cost-effective solutions to target bigger marker) are related to social human factors. On the other side, functionality (e.g., back-end server fault causes data acquisition error and thus dissatisfaction to end users of a software) is indirectly related the human factors via usability (as system error is a usability factor in this example).

5 Good UX Strategy Means Good Business

Balance between UX strategies and business process/requirements is very crucial for implementation of UX strategies. A good UX designer should have understanding of market, value propositions, business model and revenue streams; they should have a clear idea on the impact of application of a UX strategy in the business outcome context. Therefore, the UX strategies should ensure value addition to the

product/service/software, a good brand experience, helps to improve business model, improve money flow and returns on investments but not only improves/ensures the esthetics and usability of an interface. If the UX strategies aiding the business in this manner the it could be argued that "Good UX Strategy means Good Business".

UX strategies—A good UX designer should have understanding of market, value propositions, business model and revenue streams; they should have a clear idea on the impact of application of a UX strategy in the business outcome context. Therefore, the UX strategies should ensure value addition to the product/service/software, a good brand experience, helps to improve business model, improve money flow and returns on investments but not only improves/ensures the esthetics and usability of an interface. If the UX strategies aiding the business in this manner the it could be argued that "Good UX Strategy means Good Business".

6 UX Strategy-Based Business (UXSBB) Framework

According to UXSBB framework (see Fig. 3.), identification of HF related needs is important at different levels/touchpoints of UX lifecycle. Considerations of HF
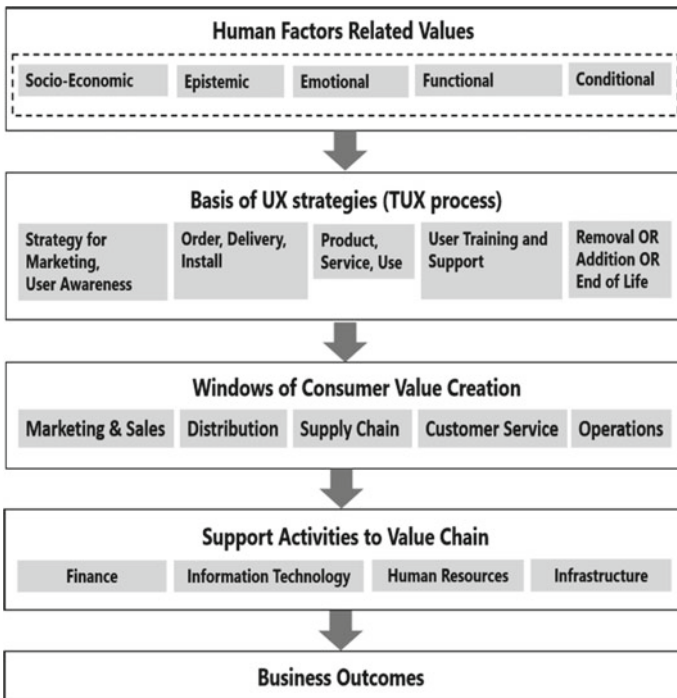
Fig. 3 UXSBB framework: propagation of HF to Business Outcomes using UX strategies

leads to a better UX strategies and thus it helps in consumer value creation in various ways such as values related to the marketing and sales, distribution, supply chain, consumer service and operations. Table 1 represents the case studies on UX strategies that were useful for better business outcomes considering HF. Support for value chain activities (in the contexts of finance, information technology/other technology, human resource, and infrastructure) are required to implement consumer values in terms of product/service. In addition, campaigning and communication to UX team members and other cross functional team members are important to ensure all the practices related to TUX process. The UX campaigning is also helpful for building of UX awareness and UX culture development at organizational level.

Table 1 Examples of propagation of HF to UX strategies to business outcomes

Human factor(s)	UX strategy	Business case
Motivation and persuasion	Continuous sale of apparel using discount coupons	Treands, Pantaloon, etc.
Emotion	Making Happy to Customers Scratch Cards for Lottery	Honda Bikes
Personality and social status	Matching cars with user's personality through providing the car customization at high cost	BMW
Esthetics and visual pleasure	Appeal of the Bose Speakers	Bose India
Functionality, usability and ambitiousness	3 AI Cameras for HQ photographs with improvement of depth perception and 3D capture	Apple iPhone 11
Socio-economic	Dual AI camera phone with HQ images and depth perception in low price	MI 7 mobile phone
Emotion/pleasure	Good quality boarding and after boarding services along with timely departures and beforetime arrivals	IndiGo Airline
Trust and satisfaction	Authentic user reviews for online purchase of products, logistic services (timely delivery and home door product return) and secure transactions (money back in case of product damage)	Amazon
Safety	Regaining customer base using free of cost product damage/insurance service)	Airtel

(continued)

Table 1 (continued)

Human factor(s)	UX strategy	Business case
Empathy	Adaptive AI-based voice user interface solution	Amazon Alexa
Excitement	Birthday cake, surprise photograph in photo frame and birthday songs when dine in a restaurant	Barbeque Nation
Love (intimacy)	Word of mouth behavior of friends often influence purchase of gadgets for VR games, e.g., InMind VR	VR box, Google Cardboard etc
Ethnocentrism	Non-Indian brand of shoe created a brand image of Indian corporate	Bata
Emotion and trust	Fear of death secures afterlife responsibilities and thus satisfaction and trust to the customer	Life Insurance Company
Emotion	Disease/disorder awareness campaign generates fear to people without have medical knowledge and thus goes for medical check ups	Fortis Hospital

7 Conclusions

The fact of the matter is designers should consider the human factors to opt better user experience strategies in all kinds of design deliverables; and, sensibly relate and apply UX strategies with business outcomes using the proposed UXSBB framework. Proposed framework also enables knowledge on application of different UX strategies for different business context.

References

1. Hedge, A., Dorsey, J.A.: Green buildings need good ergonomics. Ergonomics 56(3), 492–506 (2013)
2. Demirbilek, O., Sener, B.: Product design, semantics and emotional response. Ergonomics **46**(13–14), 1346–1360 (2003)
3. Chowdhury, A., et al.: Usability is more valuable predictor than product personality for product choice in human-product physical interaction. Int. J. Ind. Ergon. **44**(5), 697–705 (2014)
4. Nielsen, J.: Corporate UX maturity (2006). Available: https://www.nngroup.com/articles/ux-maturity-stages-1-4/. Accessed on 20 Oct 2019
5. Alvarez, M.C.: Knowledge Activation and Schema Construction (1990)

6. Xu, W.: User experience design: beyond user interface design and usability. In: Ergonomics—A Systems Approachs. InTech (2011)
7. Sanders, E.B.-N., Dandavate, U.: Design for experiencing: new tools. In: First International Conference on Design and Emotion, TU Delft (1999)
8. Jordan, P.W.: Putting the pleasure into products. IEE Rev. **43**(6), 249–252 (1997)
9. Jordan, P.W.: Designing Pleasurable Products: An Introduction to the New Human factors. CRC Press, Boca Raton (2002)
10. Desmet, P.: Designing Emotions (2002)
11. Norman, D.A.: Emotional Design: Why We Love (or Hate) Everyday Things. Basic Civitas Books (2004)
12. Sheth, J.N., Newman, B.I., Gross, B.L.: Why we buy what we buy: a theory of consumption values. J. Bus. Res. **22**(2), 159–170 (1991)

Predictive and Behavioral Analytics for Big Data Architecture

N. Sudhakar Yadav, N. Ravikanth Motupalli, K. Jamal, and Y. Usha Rani

1 Introduction

Big data analysis has come to the top of the list of issues of interest to both professionals and academia in recent years. The rapid expansion of digital devices, internet usage, tablet, and smartphone use, and other types of data generation generate massive amounts of data all the time. Big data, in contrast to conventional data, is derived from a range of sources and presented in a variety of ways [4]. The volume, diversity, and speed with which this data is generated provide significant difficulties for data center managers. Computer, storage, and analytical capabilities, on the other hand, have addressed these issues. Large datasets may now be stored in a simple and cost-effective manner.

Given the peculiarities of Big Data, particular consideration must be given to it throughout the data extraction and ingestion process from a variety of sources. Any framework should be capable of efficiently processing massive amounts of data, as well as assimilating and processing organized, semi-structured, and unstructured data. Batch and real-time processing should be supported by the software.

N. Sudhakar Yadav · Y. Usha Rani
Department of IT, VNR Vignana Jyothi Institute of Engineeing and Technology, Hyderabad, India

N. Ravikanth Motupalli (✉)
Department of CSE, VNR Vignana Jyothi Institute of Engineeing and Technology, Hyderabad, India
e-mail: ravikanth_m@vnrvjiet.in

K. Jamal
Department of ECE, GRIET, Hyderabad, India

© The Author(s), under exclusive license to Springer Nature Singapore Pte Ltd. 2023
B. B. V. L. Deepak et al. (eds.), *Recent Trends in Product Design and Intelligent Manufacturing Systems*, Lecture Notes in Mechanical Engineering, https://doi.org/10.1007/978-981-19-4606-6_55

2 Literature Survey

Research method recommends that a comprehensive A literature review should be conducted to aid in the identification of the research environment and issues. That is how we are able to comprehend the solution that has been previously provided by other academics. Extensive study of the literature and consideration of possible research avenues are required to fully comprehend the flaws in the approach provided [2]. We will look at the many different dimensions of bigger ones that exist. Science and information technology (ICT). This research also looks at how experts and the ability to upgrade big data processing systems may help. Increasing the effectiveness of the decision-making process. This is a goal that is often taken into consideration. Each industry's decision-making process must be transformed as a result. The big data study we provide is extensive, encompassing some of the different huge data frameworks that may be used to cope with future data analysis and decision-making situations. Large-scale use and effect of Big Data Analytics have been proven in a variety of sectors. In this part, we looked at the literature on big data tools, approaches, and methods, among other things. In addition to this, ZigBee, NFC, and Bluetooth were widely used for intra-communication [3]. The upsides and downsides based on application needs are briefly discussed [1, 21].

Academics and information technology experts are united in their belief that big data is increasing. The majority of data analysis and decision-making processes have been in place for just a few years during the past few years. Keep in mind that there is a lot of information and its structures. Available in a number of locations help us better grasp the direction and direction of the research across various disciplines in the future. In this particular area, we are discussing literature. A thorough analysis of the current and upcoming technologies in the area of big data educational domain is discussed [5]. Zwolińska et al. [22] proposes a manufacturing execution systems system that connects the world machines and business systems while taking into account the specific approaches of production systems, as well as the personalization of software for such production system automation.

Investigate several tools and methods for large-scale data analysis to see which ones work best. Specific to a domain are the difficulties [4]. Doug Laney, in the 2011 Gartner Data Management Report, highlighted the importance of three characteristics: volume, variety, and speed. It was determined if Hadoop and MapReduce were suitable for various distributed applications created by Fernández et al. [5]. The advantages and disadvantages of the MapReduce model were evaluated, and the results were compared to the results of the existing traditional versions of this new model. Additionally, a few alternative frameworks for addressing the disadvantages of MapReduce programming are suggested. Enhanced software engineering schematic design techniques to aid in the design and implementation of software-based applications with a focus on data management [7]. In the food and beverage industry, a method for automation based on the integration of MES with other manufacturing systems is presented, which simplifies design and implementation [13]. A study conducted by paper [8] in Big Data Analytics is looking at the use of Semantic

Web technology. They examined the importance of large-scale data analysis in the field of life sciences.

Paper [9] performed extensive research and analysis of the big data environment. Big data improvements are being driven by advances in hardware, software, techniques, and frameworks. It investigated the effect of two growing areas, cloud computing, and big data, on one another and on one another's impact. They introduced the fundamental concept of big data. Paper [10] investigation of the instruments, techniques, and approaches used in the big data ecosystem is another excellent source of knowledge. Big data analysis was used by Wang and Krishnan in clinical data [11]. Kevin Ashton originated the term Internet of Things (IoT) in 1999 in the context of supply chain management [16]. The breakthroughs, as well as creative applications, are extremely encouraging and point to a bright future for IoT on the one hand, but various hurdles on the other. Security, big data analytics, scalability, Quality of Service (QoS), and energy management are just a few of the problems [15]. This study extends on and completes a preliminary proposal to address these issues, focusing on the design of an architecture for industry 4.0 that accompanies better software engineering architectural design procedures to expedite the design and implementation of software-based solutions with an emphasis on digital management [18]. Architectural design requirements were gathered using an attribute-driven design (ADD) technique based on smart production scheduling, manufacturing process management, and active inspection and maintenance, repair, and overhaul (MRO) eventualities [17]. A generic approach based on machine learning methods is provided in [19] for strongly correlating errors observed in historical process log data with the upcoming log file, according to a prediction limit. They offered a detailed overview of machine learning algorithms for big data analysis in the healthcare sector in their paper [20].

They presented a small number of algorithms and techniques that are often utilized in clinical analysis of large amounts of data. The drawbacks of these techniques have been investigated in detail. The study also looks at hypothesis testing and statistical techniques, as well as the software tools that are used to put these approaches into action. Chen et al. [13] conducted a study of the data analysis space.

For Big Data Analytics, the performance and accuracy of different data mining techniques are compared. They concentrated on identifying extra value in data mining issues via the utilization of large amounts of data. Several researchers, including paper [14], have addressed the problem of data variety and heterogeneity in the context of big data. Many difficulties have been discovered, including concerns with data intake, data management, intrusion detection, and data privacy, all of which have been addressed [12]. With regard to a variety of industries. These MapReduce-based data processing frameworks were put through their paces. He suggested a model in which declarative programming would serve as an interface to data [16]. Reduce the processing foundation on which decisions are made.

3   Proposed Work

Big data were characterized in many ways. Big data [17] define datasets as those that are too big for conventional data processing methods and thus need the management of new technologies to be effective. The term "big data" is defined as applications that need sophisticated and one-of-a-kind storage, administration, analysis, and visualization technologies in order to deal with such large and complicated data sets and analytics technology. Big data is not only defined by its amount, but also by its rapid speed, diversity, breadth, and connection with other things in the natural world. In a nutshell, big data refers to large amounts of data.

Data generated in a matter of hours with terabytes and petabytes of storage. Traditional database management systems can't keep up with the needs of storing, analyzing, and administering vast amounts of data from a wide range of sources. Figure 1 shows the simplified architecture of big data and analytics and shows how enormous volumes of data are generated from many sources, as well as how insights may be used to help in decision-making.
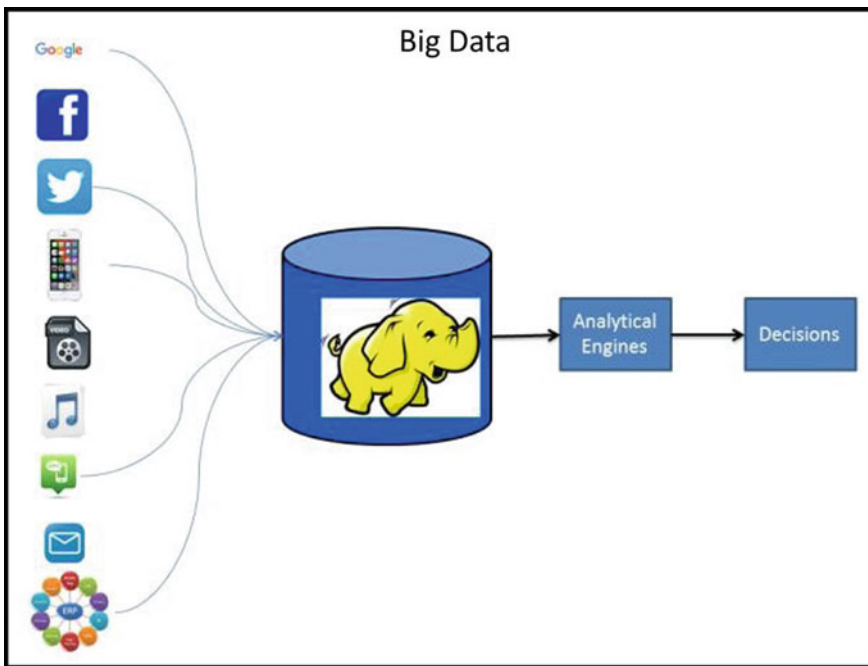
Fig. 1 Architecture of big data analytics

3.1 Different Types Data

All different kinds of data are generated by different sources, and these data types may be generally categorized as structured, unstructured, and semi-structured data. Information that is structured: Information that has been categorized Retail outlets, batch processing, Enterprise systems, and extended business systems like supply chain and customer relationship management systems are all examples of structured sources of data [21, 22]. In a relational database, the data is organized into well-defined table structures that are easy to navigate. ETL tools and procedures are used by traditional relational database management systems to retrieve, convert, and store data into a warehouse.

3.2 Characteristics of Big Data

Big Data, for example, in terms of volume, pace, and variety, may be mainly described by the three Vs. Terabytes or petabytes of data are gathered over several hours in commercial or social media systems, indicating that big data is very enormous in volume. Every 40 months, the amount of data is doubled (Davenport 2014) [14]. Increases in the number of mobile devices are occurring at an unprecedented pace. More than 40 billion wireless gadgets are expected to connect to the internet during the next five years, according to John Chambers of Cisco. Apple's John Sculley, a well-known CEO, and business leader, wants to usher in the digital age of the next generation by using four high-speed technologies: cloud computing, the internet, data, and mobile. The confluence of these four major technologies will result in increased data speed at an exponential pace in the near future.

3.3 Traditional Data in Their Entity

Traditionally, corporate data is stored in a database management system that has been well-defined. In recent decades, several major corporations have adopted enterprise resource planning (ERP) systems to improve operational efficiency and reduce costs [10]. These enterprise resource planning systems (ERP systems) or individual applications gather huge quantities of transaction data around the clock. There have been circumstances when massive volumes of data were obtained, such as the government's official statistics collected every decade. Furthermore, because these incidents were rare, there has been no pressing need to analyze the real-time data. This massive data set has been gradually transferred to the data warehouse in order to be processed further. The data landscape has altered substantially on a variety of fronts since the internet entrenched itself as the backbone of communication and information:

1. The advent of the internet has expedited the process of globalization and development of multinational corporations, owing to the fact that communication is now fast, inexpensive, and easy throughout the globe.
2. A variety of new kinds of semi-structured data have developed, including websites, and emails, among others. The inclusion of information on social media platforms has resulted in an exponential rise in the volume, speed, and variety of data.

There is a constant flow of information from a variety of sources when it occurs in large data. In the absence of a dependable data source or organization, Every hour, Facebook receives hundreds of posts, as well as millions of picture uploads, which are collected in a database.

4   Big Data Analytics

Big Data Technology is based on previous data analysis methods and employs statistical methodology such as regression, principal component analysis, and other similar techniques. It provides real-time analysis by combining high-speed data retrieval with sensor information. The subjects of information science, data science, statistics, and mathematical models are all multidisciplinary fields that may be studied together or separately. Statistical methods such as regression, multivariate statistical, and multidimensional statistical, as well as mathematical knowledge and experience, are used to construct equations.

The test on bog data revealed that increased technology has resulted in a massive amount of big data and that academics are in the process of finding new paths of evaluating this data in order to extract valuable information. Investigators and users are no longer interested in learning what occurred and why it occurred (descriptive analytics), but rather in learning the answers to questions like what is occurring now and what is anticipated to occur in the future (predictive analysis). As a result, business analysis can be separated into three areas, as indicated in Fig. 2: descriptive, prediction, and prescriptive insights. In the next section, we will build predictive analysis, taking into consideration the significance of this technique for many stakeholders in society and business.

4.1   Analytics for Prediction

Predictive analytics uses data mining, pattern identification, statistics, deep learning, machine intelligence, and information gathering to find relevant patterns in data [1]. It also refers to the straightforward application of data analysis tools to solve issues or answer questions. Cutting-edge analytical approaches are used. Business intelligence (BI) and big data, when integrated with statistical methodologies, are
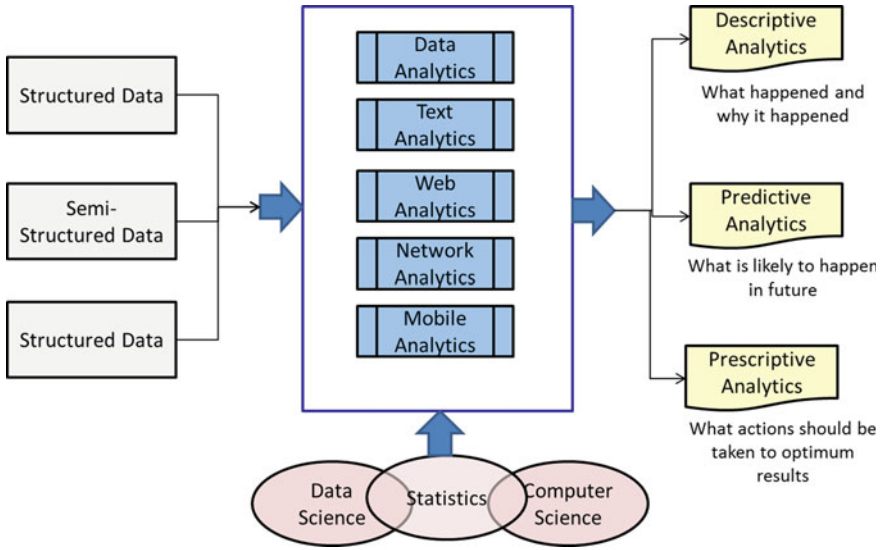
Fig. 2 An existing study of Predictive analytics

making tremendous progress. Business intelligence methods aid in the study of data from multiple sources, allowing managers to make well-informed decisions. Experts in the field of research design the questions and variables, however in predictive analysis, the model and association decisions are made based on the data [1]. It's a method of systematic analysis in which a computer program searches for patterns and inherent relationships among variables of the study in a dataset. It is proposed to select the optimal connection regression coefficients for each link in order to reduce model errors. The technique makes considerable use of complicated information systems and requires numerous iterative cycles for best results.

4.2 Social Analytical Media (Social Media Analytics)

Text messages, music, pictures, and videos, among other things, make up the bulk of social media data. Text, videos, pictures, music, and other forms of communication are used to share information. The typical process that consumers undertake while purchasing items is shown in the following figure. They also share their thoughts and social media posts on the product both before and after it has been bought. Companies may use technology to help them achieve their business objectives and make tactical decisions in support of those objectives. The processing ability based on predictive study is depicted in Fig. 3. Next that, we will discuss various ways in which social media analysis may be beneficial to businesses in the following part.

Fig. 3 Processing based on predictive study

5 Opportunities and Difficulties in Big Data Analytics

Our goal is to establish an open source Big Data enabling technology solution architecture, and the following are the primary principles for developing a strong Big Data Analytics platform. Data Archiving: A centralized solution for analytic archiving that allows data to be kept online for analytics rather than being moved offline, as well as seamless data lifecycle management and cataloging of information assets.

5.1 Efficacy in Relation to Time

Individuals who are able to extract value from a particular data source in real-time may benefit from data from organized or unstructured sources. There are many examples of real-time data being used to address problems. Natural disasters may disrupt vital supply networks. In nations like India, where the logistics system is fragmented, the infrastructure is weak, and many large and small companies are engaged, the impact is larger [8]. There is a need to proactively monitor supply chain risks in real-time in order to avoid, react and prevent future disruptions and occurrences.

5.2 Difficulties with Huge Amount of Data

Because of its enormous scale and scope, big data presents some particularly difficult problems. The vast majority of companies are overwhelmed by the amount of data being generated at such a fast pace. The toughest challenges are measurement inaccuracies, as well as size and quality issues. The tremendous volume of data collected and stored every day at lower costs drives big data. It is an efficient statistical method.

Noise, heterogeneity, correlation, and inefficiency are all issues associated with big data that must be addressed.

5.2.1 Data Size and Quality

Due to the expansion of the data, handling large amounts of it is problematic. Traditional databases can be managed with Excel or even other ETL software, but big data necessitates the use of a specialized technology framework such as Hadoop.

5.2.2 Bigger Space

With so many variables, it's easy to create a misleading correlation, allowing some variables to mislead you about their relationship to the model outcome. Nonessential variables are likely included in the model. Large sample sizes result in high processing costs and algorithmic instability.

5.2.3 System Reliability

Data dependability is another element to consider. Unstructured data is notoriously untrustworthy, prone to errors and data loss. The information is gathered through social media, smartphones, emails, and text messages [12]. Data is gathered from a variety of sources, including computer systems and industrial sensors (Le and Pang 2013). To extract tiny amounts of valuable information, data mining takes a long time and requires a lot of unlinked data. As a result, it's really taxing. Hunting for a needle in the haystack could be difficult.

5.2.4 Data Precision and Adequacy

Although the dataset is vast and multidimensional, it does not reflect the entire population. When using social media as a source of huge, unstructured data, only those who connect or participate in the online conversation are included in the data.

Similarly, platforms such as Twitter restrict access to restricted data sets based on pre-defined requirements. Any biases in data interpretation should be controlled for by researchers.

5.2.5 Analytics Setup

Like any other IT project, Big Data Analytics has its own set of problems that must be handled inside an organization. With analytics comes increased starting expenses, changing business trends, and providing qualified information specialists.

Implementing Big Data Analytics may be difficult due to many factors like data quantity and completeness issues, a lack of business support, insufficient personnel and knowledge, and technological issues in the database, to name a few. There are a variety of additional problems associated with big data, including data cycle management, data redundancy, analysis, data secrecy, energy management, collaboration, and data confidentiality. A memory statistics structure enables you to do the following search operations on triples in a single memory: Return the set $(s, o)|s, p, o$ Di that contains the members of the input set p, given the input p. (s, o). Please enter the set $o | s, p, o$ Di for both the s and the p parameters, as well as the set $o|s, p, o$ Di for the o parameter. For each of the three values of o and p, the set $s|s, p, o$ Di must be returned as a result. The fact that all of the aforementioned inquiries need a predicate that is well-known results in a threefold increase in the number of workers who use the predicate in question. It is necessary to calculate a predicate-base based on the resulting predicate index (abbreviated P-index).

6 Conclusion

Big Data's provenance delivers a different mixture of challenges and opportunities. As previously stated, a systematic approach may be used to collect, store, and analyze large amounts of data. The interdisciplinary field of analytics requires years of experience and skill in order to extract meaningful insights from a sea of data. Data quantity and completeness, a lack of corporate support, a shortage of people and expertise, as well as database software problems, are just a few of the challenges that must be overcome in order for Big Data Analytics to be successfully implemented and used. Big data brings with it a slew of new issues, including data life cycle management, data redundancy, analysis, data confidentiality, energy management, collaboration, and data secrecy, to name a few examples.

References

1. Abbott, D.: Applied Predictive Analytics: Principles and Techniques for the Professional Data Analyst. Wiley, New York (2014)
2. Adomavicius, G., Tuzhilin, A.: Toward the next generation of recommender systems: a survey of the state-of-the-art and possible extensions. IEEE Trans. Knowl. Data Eng. **17**(6), 734–749 (2005)
3. Al-Garadi, M.A., Mohamed, A., Khalid Al-Ali, A., Du, X., Ali, I., Guizani, M.: A survey of machine and deep learning methods for internet of things (IoT) security. IEEE Commun. Surv. Tutorials **22**(3), 1646–1685 (2020)
4. Alstete, J.W., Cannarozzi, E.G.M.: Big data in managerial decision-making: concerns and concepts to reduce risk. Int. J. Bus. Continuity Risk Manage. **5**(1), 57–71 (2014)
5. Ang, K.L.-M., Ge, F.L., Seng, K.P.: Big educational data & analytics: survey, architecture and challenges. IEEE Access **8**, 116392–116414 (2020)

6. Assunção, M.D., Calheiros, R.N., Bianchi, S., Netto, M.A.S., Buyya, R.: Big data computing and clouds: trends and future directions. J. Parallel Distrib. Comput. **79**, 3–15 (2015)
7. Atat, R., Liu, L., Wu, J., Li, G., Ye, C., Yang, Y.: Big data meet cyber-physical systems: a panoramic survey. IEEE Access **6**, 73603–73636 (2018)
8. Bag, S., Anand, N.: Modelling barriers of sustainable supply chain network design using interpretive structural modelling: an insight from food processing sector in India. Int. J. Autom. Logistics **1**(3), 234–255 (2015)
9. Batra, S.: Big data analytics and its reflections on DIKW hierarchy. Rev. Manage. **4**(1/2), 5 (2014)
10. Bharathi, S.V., Mandal, T.: Prioritising and ranking critical factors for sustainable cloud ERP adoption in SMEs. Int. J. Autom. Logistics **1**(3), 294–316 (2015)
11. Borra, E., Rieder, B.: Programmed method: developing a toolset for capturing and analyzing tweets. Aslib J. Inform. Manage. (2014)
12. Boyd, D., Crawford, K.: Critical questions for big data: provocations for a cultural, technological, and scholarly phenomenon. Inf. Commun. Soc. **15**(5), 662–679 (2012)
13. Chen, X., Nophut, C., Voigt, T.: Manufacturing execution systems for the food and beverage industry: a model-driven approach. Electronics **9**(12), 2040 (2020)
14. Coursaris, C.K., van Osch, W., Balogh, B.A.: Informing brand messaging strategies via social media analytics. Online Inform. Rev. (2016)
15. Dehkordi, S.A., Farajzadeh, K., Rezazadeh, J., Farahbakhsh, R., Sandrasegaran, K., Dehkordi, M.A.: A survey on data aggregation techniques in IoT sensor networks. Wirel. Networks **26**(2), 1243–1263 (2020)
16. Evtodieva, T.E., Chernova, D.V., Ivanova, N.V., Wirth, J.: The internet of things: possibilities of application in intelligent supply chain management. In: Digital Transformation of the Economy: Challenges, Trends and New Opportunities, pp. 395–403 (2020)
17. Hinojosa-Palafox, E.A., Rodríguez-Elías, O.M., Hoyo-Montaño, J.A., Pacheco-Ramírez, J.H., Nieto-Jalil, J.M.: An analytics environment architecture for industrial cyber-physical systems big data solutions. Sensors **21**(13), 4282 (2021)
18. Hinojosa-Palafox, E.A., Rodríguez-Elías, O.M., Hoyo-Montaño, J.A., Pacheco-Ramírez, J.H.: Towards an architectural design framework for data management in Industry 4.0. In: 2019 7th International Conference in Software Engineering Research and Innovation (CONISOFT), pp. 191–200. IEEE (2019)
19. Kolokas, N., Vafeiadis, T., Ioannidis, D., Tzovaras, D.: A generic fault prognostics algorithm for manufacturing industries using unsupervised machine learning classifiers. Simul. Model. Pract. Theory **103**, 102109 (2020)
20. Li, W., Chai, Y., Khan, F., Jan, S.R.U., Verma, S., Menon, V.G., Li, X.: A comprehensive survey on machine learning-based big data analytics for IoT-enabled smart healthcare system. Mob. Networks Appl. 1–19 (2021)
21. Shah, J.L., Bhat, H.F.: CloudIoT for smart healthcare: architecture, issues, and challenges. In: Internet of Things Use Cases for the Healthcare Industry, pp. 87–126 (2020)
22. Zwolińska, B., Tubis, A.A., Chamier-Gliszczyński, N., Kostrzewski, M.: Personalization of the MES system to the needs of highly variable production. *Sensors* 20(22), 6484 (2020)

IoT and Machine Learning for Traffic Monitoring, Headlight Automation, and Self-parking: Application of AI in Transportation

Anurag Sinha, Abhishek Singh, Prince Shubham, Vivek Raj, and Md. Ramish

1 Introduction

Governments give significant attention to road infrastructure in emerging and industrialized nations. You think that the road infrastructure will improve your economy in numerous ways. The car industry has also improved its vehicles, notably in vehicle speed, in many respects. The road accidents have significantly high-detrimental impacts compared to older times because of modern high-speed cars. Many studies worldwide have shown that the percentage of accidents is high at night compared [1]. It is no less typical for accidents to be high during the day and in the worst weather conditions like different weather condition. It has many components assuming significant part during these mishaps, however, the top most justification behind these mishaps are helpless deceivability of the drivers. The light emanates from automobiles that blind the drivers for a few seconds in the other direction. Only after a few seconds of normal light can the motorist see things well again. There are also many blind spots in the roadways that are not straight and with many curves, which cause crashes in mountainous areas or on roads with multiple turns. The government of nations is more focusing on road infrastructure as well as road safety. The automobile

A. Sinha (✉)
Department of Information Technology, Amity University Jharkhand, Ranchi, India
e-mail: anuragsinha257@gmail.com

A. Singh
Department of Computer Science and Engineering, JIS College of Engineering, Kalyani, West Bengal, India

P. Shubham · V. Raj
Department of Computer Science and Engineering, Amity University, Ranchi, Jharkhand, India

Md. Ramish
Department of Electronics and Communication Engineering, Amity University, Ranchi, Jharkhand, India

industry is also putting their effort to improve vehicles in numerous characteristic, mainly in safety of the vehicles and the speed of the vehicles. One of the most popular branches of AI is machine learning. There are other classes of AI which include probabilistic models, deep learning, game theory, and artificial neural network systems. They are applied in wide range of sectors. In recent, it has been the leading research area in transportation engineering, especially in traffic monitoring, automatic smart head light system, and self-parking in cars. One of the major issues of developing countries is traffic congestion, which harms the economic and social development as well as daily lives of people. Today, the major challenges of traffic congestion are estimation of traffic and monitoring. As the development in transportation sector by collecting traffic information, authorities are putting more effort on traffic congestion monitoring. For the smooth journey of travelers, traffic monitoring provides with the required time to plan in the distribution of resources [2]. Traffic monitoring discussed in this paper can be define as a valuation of factors related to traffic congestion into the short-term future by applying different machine learning methodologies.

As the technology is developing so much, we have reached at a point where we can control our car without touching it or sitting in it, in past and present, we have this technology but in RC cars. In today's era, we are running the vehicles as we used to run our RC cars in childhood. There are automation features in existing cars which are insufficient to allow cars to drive itself. But with the self-driving car, we can make the presence of cars on the road constantly. Today, self-driving is no longer a high-tech dream, but it is becoming a reality. Autonomous car can be dangerous to some but also has its advantages. Drivers give a lot of consideration in changing the high shaft to low radiate as well as the other way around, which makes part of the issue to the drivers who are in the inverse direction. Barely, any extravagance vehicles have programmed brilliant headlights framework that changes high bar to low radiate at whatever point required, however, the economy vehicle is not given this innovation. This paper attempts to plan a solitary programmed savvy front lamp framework which can satisfy all the requirements for the front light and the tail light of the vehicle [3].

Problem Statement and Paper Organization

The major concern of the transportation during nighttime is path clearance in highways during rainy and foggy days. So, automation in daylight may counter the specific problem during nighttime by automating the headlight controlling system using IoT and machine learning. This chapter is organized in mainly four sections. The first section of the chapter discusses about the identification with relevant literature study and the rest part of the paper contains methodical survey of the technology used.

2 Related Work and Research Gap Identification

In this chapter, we have analyzed several techniques for headlight beam automation by taking reference from several paper from regulated journals like Wiley, Hindawi,

Table 1 Paper used for comparative study and survey

Reference number	Survey
[4]	Management system to avoid accidents due headlight glaration
[7]	Proposed vehicle detection method for nighttime
[8]	Nighttime vehicle detection by image and sensor-based approach
[9]	AdaBoost and SVM Blob Learning-based approaches
[10]	Sensor-based approaches to headlight controlling and obstacles alerting system

IEEE, Conference papers out of which we have selected few paper for comparative study and research gap identification. Same is mentioned below in Table 1. In paper [4], author has introduced technique to tackle accidents due to glare lighting on highway, however, the concept is good but more precise IoT technology should have been introduced. In paper [5], authors have provided technique for vehicle detection during nighttime using computer vision but the more precise technology should have been introduced using deep learning for object identification during nighttime. In paper [6], authors have shown significant amount of work to detect vehicle by sensor base technology, however, vehicle to vehicle node technology can be developed for better enhancement of algorithm. In paper [4], authors have shown several ML algorithms for classification of objects and headlight control system. But some more innovative system can be developed using deep learning. In paper [7], authors have shown sensor-based approaches to headlight controlling and obstacles alerting system, however, objects detection system can be developed using computer vision for detecting minute obstacle on road. In paper [4], it is shown "approaches based by IoT, Arduino, and sensor on smart headlight to avoid accidents", however, more sensor can be used to detect proximity.

Problem Identification

Problem recognition-driving at night with main beam of headlight on this is one of the normal shortfalls of our drivers in evening driving, extraordinarily on dim or gravely lit streets that we by and large have in rustic regions and furthermore along a significant number of the streets in our urban communities and towns. Driving civility forces a unique obligation on the driver that the approaching driver is not impeded by the stun of headlights. Driving Vision and Glare: The natural eye, one of the most intricate organs and the best endowment of nature, is outfitted with an assortment of transformation capacities. Nonetheless, it is weakened by glare. The natural eye's powerlessness to deny glare sources in the typical visual field during the long development interaction may be on the grounds that nature was unconscious of man's capability to make incapacitating sources-the most genuine of which is vehicle front lamp glare.

Fog Light Dazzle—The amaze impact is one of the serious issues looked by a driver in evening driving. So one needs to stop the extreme focus light from the eyes of the approaching driver or street clients to forestall the astonish impact. Programmed

Fig. 1 Glare in highway

dipper is one such component, which is utilized for wellbeing late evening driving without the extraordinary astonishing impacts. Current problem faced by motorists are dealing with an immense issue because of this high-light emission falls straightforwardly onto their eyes during driving. There are numerous clinical statistical data points which support their issues of late evening driving.

Troxler Effect—Troxler effect is a phenomenon where the optical in means is affecting the vision site of a person's at a particular point of time, and it creates the illuminations when something's arrives in front of your eye side and the unchanging stimulus of the reflections is taken away from the fixation point, will meet things disappear. In highways, the Troxler effect comes in a blurring way where the eyes introduced with the impressive light which is coming in the 10,000 lemons which experiences via glare on highways. The multiple vehicles lighting on the highways open the over repetitiveness of the bars and the lights which is coming at later effect, it makes the reflection more complex in the clear side during high-beam environment in night [11] (Fig. 1).

Mishaps Because of Troxler Effect—As talked about before, there are numerous mishaps caused because of Troxler impact. Numerous mishap cases are seen where a huge vehicle, cinfronting a sluggish more modest vehicle while the last is attempting to go beyond. However, in comprehensive and conventional vehicle lighting system, the automation is not done but in upcoming self-driving cars and vehicle are coming with embedded automated (i.e. computer vision based) lighting system to overcome this problem statement. The nearby object detection in computer vision and Internet of vehicle things (IoVT) is being proven as cutting edge technology in new of vehicle system. Because of inordinate splendor, the driver of the huge vehicle is dazed (Fig. 2).
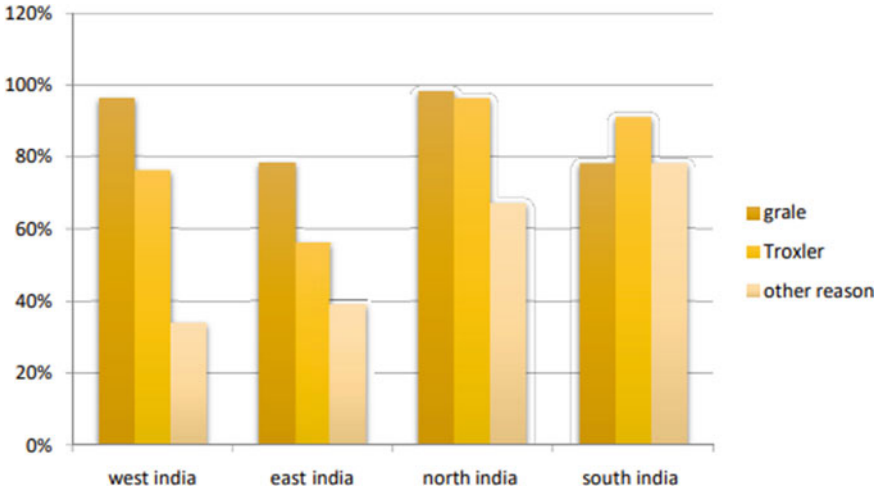
Fig. 2 Statistics of accident on highway

3 Application of AI in Smart Parking and Traffic Monitoring

3.1 Artificial in Traffic Monitoring

The most well-known strategy which we ran over during our exploration is LoRa long range wide area network. It is the innovation utilized for low-power wide area network (LPWAN). Savvy sensors are utilized to gather information, then it is moved to the LoRa cloud stand, then, at that point, the stand goes through an information investigation process, which is utilized as a contribution for intelligent transport management system (ITMS). ITMS incorporates traffic expectation through LoRa, the executives of stopping, and so on. The most extreme issue nowadays is traffic, practically every one of them of all shapes and sizes urban communities are dealing with the issue of traffic. There is two major issues behind the blockage of traffic are dynamic traffic stream and static traffic light. Consequently, for tackling this issue, this paper centers on traffic checking utilizing LoRa (long range wide area network technology). LoRa is an innovation that is associated with low-power wide area networks (LPWANs), which is a remote media transmission-wide region organization. This innovation gives solid traffic checking to the savvy urban communities just as creating urban communities. Figure 3 shows the working of the proposed framework. The information which is gathered from the sensors is moved to the proposed LoRa cloud stand. Then, at that point, the stand runs AI and information investigation calculation, which are utilized as a contribution of ITMS. Here, the ITMS work includes controlling the progression of traffic through LoRa introduced signals, designating leaving to the vehicles, providing clinical benefits, and ensuring
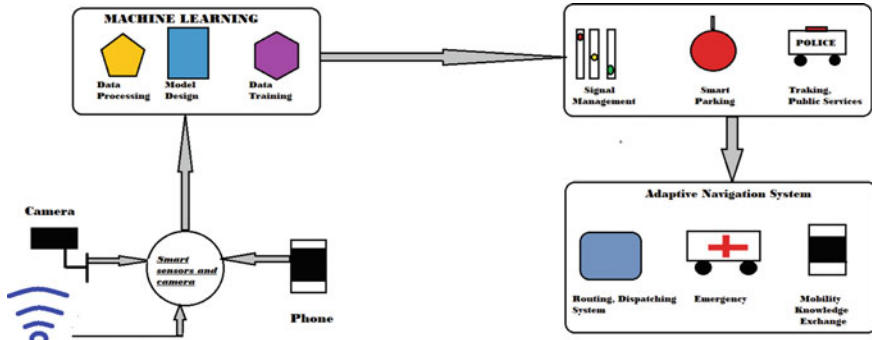
Fig. 3 System overview of LoRa-based intelligent traffic management system the below points proposed how the mechanism run above the method

the urban areas. Subsequently, it is important to gather information, and the legitimate observing of information is done as such ITMS ought to be in touch with the LoRa cloud stand [11]. The two introduced traffic lights on each roadside will move the information to the cloud server, then, at that point, the information is shipped off the AI calculation, and the further, forecast is made that whether or not the street is blocked. According to the review done before this strategic relapse calculation depends on that main, this code made our framework safer. It is one of the most controlled and oversaw machine learning calculations. The calculation predicts the genuine and esteemed result dependent on the two significant sources of info that is thickness and voyaging time. With this proposed arrangement of traffic observing, there will be a decrease in contamination and fuel utilizations. It can likewise give most brief way to the driver in a crisis.

3.2 Machine Learning in Self-Parking System in Cars

Components used in proposed system:-

I. **Arduino UNO Board**: It consists the microcontroller for the program to read the steering action.
II. **Ultrasonic Sensors**: Sensor identifying the object or vehicles near by the car.
III. **Raspberry Pi**: It is used to collect data from Pi camera and ultrasonic sensors.
IV. **Pi Camera**: It is portable camera that supports Raspberry Pi, for collecting the image.
V. **Acceleration Detectors**: It is a sensor for measuring the steering rotation and speed.
VI. **Buzzer** [4]: It is audio device which is used to beep sound.

In Fig. 4, it is aim to develop automatic parking system by lane detection and object detection. The system consists of three unit, first is input unit containing a Pi

camera and ultrasonic sensors, the second is processing unit or server, and the third is Arduino.

Firstly, in the input unit, the Raspberry Pi board is connected with the Pi camera and ultrasonic sensors to stream input data. And a program will be running in the Raspberry Pi to stream images collected by the Pi camera and to send sensor data through a Wi-Fi connection [8]. Then, the processing part will take place in which the data will be collected from the Raspberry Pi, and steering prediction, object detection, distance measurement using monocular vision and signal detection, and then, all these command will be send to Arduino. A multithread TCP server program will run on the Raspberry Pi to receive image frames and sensor data. The neural network will be trained to make steering prediction based on object detection. For safety, a buzzer will be also used in the car if by chance the prediction gone wrong, the buzzer will start beeping loudly, and the driver will be allowed to stop the car manually by applying the brakes as shown in Fig. 5a
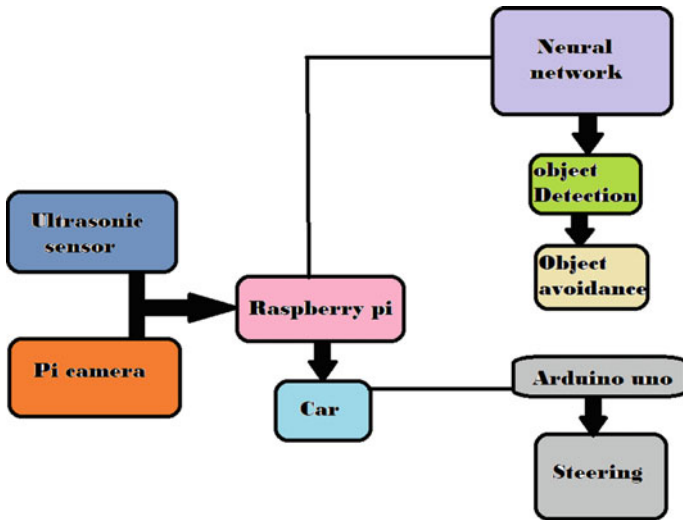
Fig. 4 Block diagram of proposed system
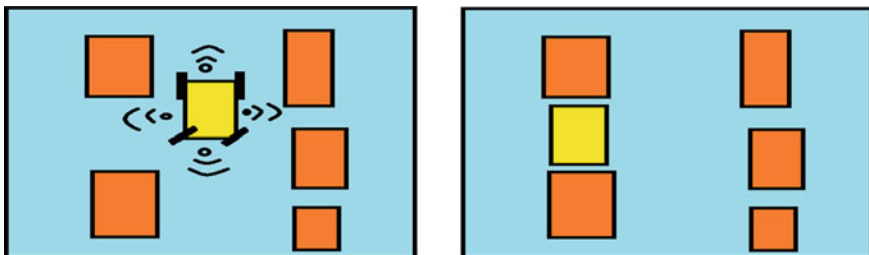
Fig. 5 a Flowchart for object detection, **b** making use of sensors for parking

In Fig. 5b, the project work is done on automatic parking system in cars. Further, it can be simulated on hardware equipmnts and be implemented on prototype.

4 Proposed Conceptual Model for Machine Learning and IoT in Automatic Smart Headlight System

Components used in Proposed System

  i. **Arduino UNO Board**: This kind of sensors comprises as they are regulated programmable chip-based system which use for the contribution of the intact piece of lighting in the film.
 ii. **Light Detecting Sensors**: This kind of sensors use for state estimating the ray of light in a constant plane.
iii. **Radar Sensor**: This kind of sensors is used for estimating precipitation level. **Fog Sensors**: Sensor for estimating mist and precipice specification of the fog.
 iv. **Video Imagining Sensors**: Kind of sensors is used for identifying the right in front of vehicles, and left and right side of the vehicle passing through.
  v. **Speed Increase Detectors**: Kind of sensors is used to identify the total distance of the contrast vehicle coming from opposite side.
 vi. **Loop Detectors**: Kind of sensors is used for differentiating between the diverse of the street planes.

This section of the paper is intended to propose the architectural model for self-parking system, where we are using different kind of senses in which the preliminary stage of the model shows that Adriano board is placed in between the electronically free chess small controller which are connected with it and to identify the level of light into outer of the vehicle during the nighttime. The light detecting senses are being used where the outer drove lights will be turned on when it is turned turnout to be darker, and the architectural board shows that the low light will be on during the distance measuring sensor signifies that there is no vehicles coming backside of the vehicles in front of the column and thus it will be **on** and the other lights will be **off**.

To make this system useful to the sensors on the most noteworthy mark of the vehicle observe whether the vehicle is in the open space or inside a construction, if it is in a design, then the high-column lights will not be ON regardless, when there are no vehicles the converse way [12]. The side light will get enacted when there is a vehicle recognized by the sensors, the lights will rely upon the specific point of controlling development. This movement will consequently turn as an afterthought marker dependent on the revolution heading, assuming it is not actuated by the driver. At the equivalent in more tasteful vehicles, the camera of that side will be initiated, and the data will be shown on the screen of the car. The side lights will likewise get turned ON and OFF consistently with a blaring sound assuming the vehicle goes near the track lines, and for the driver data, it will be shown on the screen of the vehicle as shown in Fig. 7 (Fig. 6).
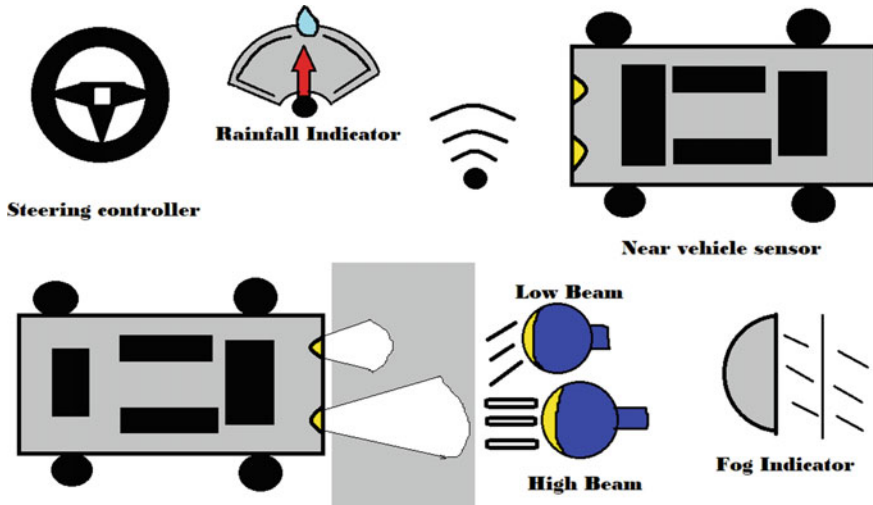
Fig. 6 Automated controls needed for vehicles
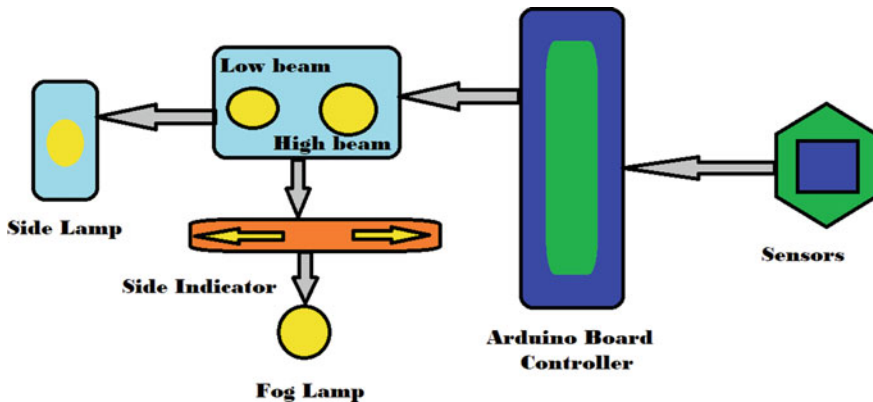
Fig. 7 Circuit diagram

The main front light of the vehicle is connected with 2 of the bulbs, which is used in the system and one shows the high and other shows low when it comes to the commonplace. In India, the need of the frontline, it is one of the significant thing. After the evening time and this is generally comes when the vehicles are traveling on the highways. IoT smart lighting uses wireless switches, eliminating the need to wire light switches directly to fixtures. The shocking mode of the system is used, where the light of a city to hell when the driving for the long distance is totally independent on this lights when you are traveling during the nighttime. To come across with one city to another city in the red in swift mood is a bit typical, so the low are the less of the segment is incredible in terms of its segmentations off the light, so it is utilized

under the normal night conditions where this first segment is positive day slow at the street. And the high segment has more expended vision of the lies on the highways where this shows the beam of 128 100 lumens, which is categorized on the basis of the 2 balls which is defected and depicted in the Fig. 8. And here, we have utilized the upper fiber of the light for the scoop segment where. The front light is connected with the vision and required Asian silly in the evening time, and it connects with the both of the launch of the system and this upper segment of the scope bar is utilizing the manual switching which is available in the vehicles [9].

Similarly, when the power is on on the specific timing, it shows the total connection between the. Radar system of the high-level beam and the lower level be of the same system and it total invoke the vehicle in the closeness of the other vehicles based on this distance measurement sense and this SDR sensors assets the total age level in the position of the vehicle is observed and this will send a senses West conductions to the switch, and it connects in like a manner that no context is opposed with the flow of the Barbie games get turns on and positive as it exchanged with the terminal of the dialled conditions of the vehicle. There for the low light invokes LED with turned on regularly, shown by the different LED bulbs and the left half of the elimination of the. Senses are to copy the presence of progressing vehicle is displayed in Fig. 9.
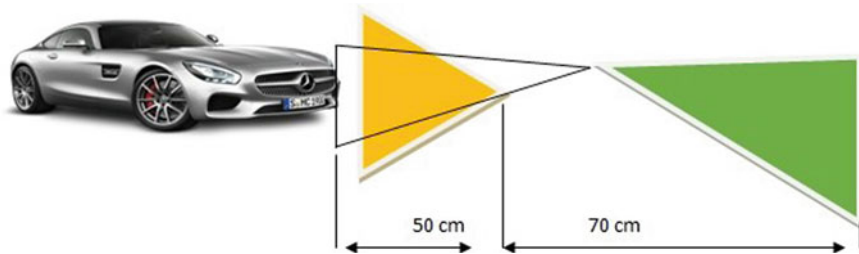
Fig. 8 Assortment of dipper beam (**a**) and higher beam (**b**) of a vehicle
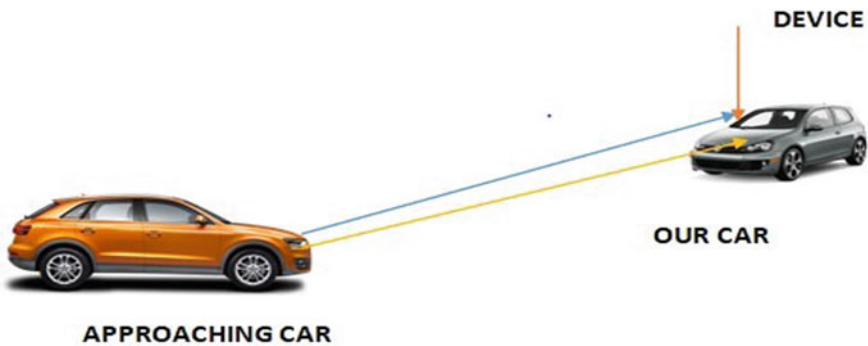
Fig. 9 Positioning of the gadget

The discovery rate, bogus positive per picture, and midrate for the recommended approach are significant execution boundaries. Discovery rate is determined as a proportion of vehicles appropriately recognized to the all-out number of realities on the ground. Nonetheless, bogus up-sides per picture are processed as the proportion of all-out bogus up-sides got to the all-out number of tests in assessment dataset. The missed rate is determined as a proportion between the absolute number of missed identification and the quantity of information tests. The consequences of the trial examination are introduced in [13]. Nonetheless, 94.84% of bogus up-sides in each picture is 0.156 and 0.617 is missed [10, 14].

5   Results and Discussion

5.1   Classifier Performance

For each feature extracted, classifier training was carried out. 450 photos with positive and negative content were presented for each classificatory in order to find classification accuracy where SVM gives 98% of accuracy, AdaBoost 76%, edge hog-1 87%, neural network 90.8%, respectively [13]. Weights for each feature shall be computed to be used during the testing phase, depending on the accuracy of each feature. Detection performance is as follows for each classifier. In Fig. 10, the total accuracy of classification accuracy is given, and in Fig. 11, total testing samples used in testing validation are given in which out of 450 samples, 230 is used for ground truth sample detection, and 70 is for true and false positive [15, 16].
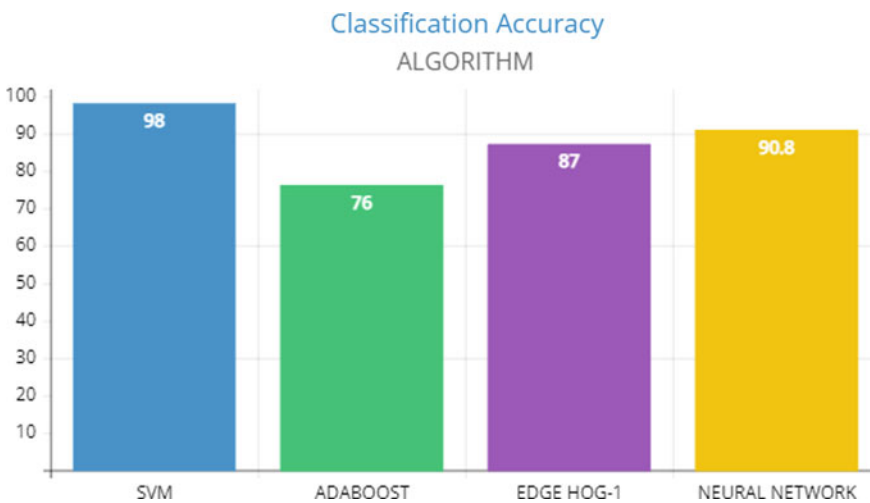
Fig. 10 Classification accuracy
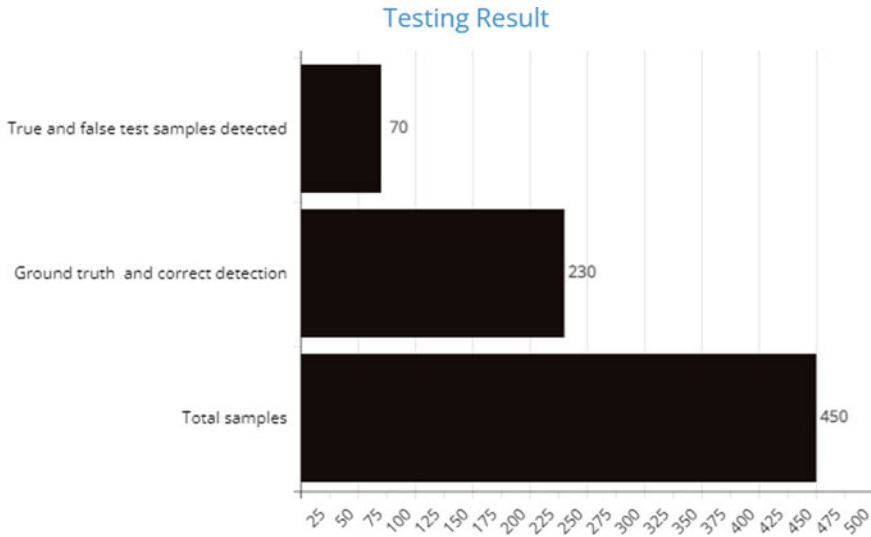
Fig. 11 Number of samples used in testing and validation

6   Conclusions and Future Scope

In this proposed research paper, we have introduced that how Internet of things and artificial intelligence can be a prominent application area for the transportation where we can monitor the traffic based on the GPS using machine learning and tracking system. Also based on the object detection and self-parking system can be made where the self-parking cars can automatically detect the lodge and parking area on the basis of these latest technologies. Indeed, we have proposed the headlight automation based on the object detection using deep learning and Internet of things where the headlight can be automated to reduce the beam and to reduce the accident during the nighttime on the highways. For which we have used the four different classifiers, support vector machine, AdaBoost, Edge horse, and neural networks, which has been compared with the different accuracy based on the training and testing validation samples. As per the future scope for this particular research, the simulation of the headlight automation can be done using different kind of senses such as Arduino and LoRa sensor. Moreover, the simulation can be tested using the IoT simulation framework and based on the machine learning algorithm, it can be tested by computer vision technology for the object detection in the vehicles. Indeed, the self-parking and traffic monitoring system can be simulated using the surveillance camera and Internet of things framework based on the requirement of the types of vehicle and traffic system.

References

1. Amato, G., Carrara, F., Falchi, F., Gennaro, C., Meghini, C., Vairo, C.: Deep learning for decentralized parking lot occupancy detection. Expert Syst. Appl. **72**, 327–334 (2017). https://doi.org/10.1016/j.eswa.2016.10.055

2. Aqib, M., Mehmood, R., Albeshri, A., Alzahrani, A.: Disaster management in smart cities by forecasting traffic plan using deep learning and GPUs. In: Mehmood R, Bhaduri B, Katib I, Chlamtac I (eds.) Smart Societies, Infrastructure, Technologies and Applications, vol. 224, pp. 139–154. Springer, Berlin. https://doi.org/10.1007/978-3-319-94180-6_15

3. Arifuzzaman, M., Aniq Gul, M., Khan, K., Hossain, S.M.Z.: Application of artificial intelligence (AI) for sustainable highway and road system. Symmetry **13**(1), 60 (2020). https://doi.org/10.3390/sym13010060

4. Fang, Y.-C., Tzeng, Y.-F., Wen, C.-C., Chen, C.-H., Lee, H.-Y., Chang, S.-H., Su, Y.-L.: a study of high-efficiency laser headlight design using gradient-index lens and liquid lens. Appl. Sci. **10**(20), 7331 (2020). https://doi.org/10.3390/app10207331

5. Bae, J.J., Suda, T.: Survey of traffic control schemes and protocols in ATM networks. Proc. IEEE **79**(2), 170–189 (1991). https://doi.org/10.1109/5.64405

6. Bhattarai, D., Aguilar, L., Park, C., Kim, C.: A review on properties of natural and synthetic based electrospun fibrous materials for bone tissue engineering. Membranes **8**(3), 62 (2018). https://doi.org/10.3390/membranes8030062

7. Hu, Y., Gao, S., Lunga, D., Li, W., Newsam, S., Bhaduri, B.: GeoAI at ACM SIGSPATIAL: Progress, challenges, and future directions. SIGSPATIAL Special **11**(2), 5–15 (2019). https://doi.org/10.1145/3377000.3377002

8. Kim, H., Kwon, S., Kim, S.: Hyperspectral image-based night-time vehicle light detection using spectral normalization and distance mapper for intelligent headlight control. Sensors **16**(7), 1058 (2016). https://doi.org/10.3390/s16071058

9. Liao, Q., Zhu, M., Wu, L., Pan, X., Tang, X., Wang, Z.: Deep learning for air quality forecasts: a review. Current Pollution Reports **6**(4), 399–409 (2020). https://doi.org/10.1007/s40726-020-00159-z

10. Mumtaz, Z., Ullah, S., Ilyas, Z., Aslam, N., Iqbal, S., Liu, S., Meo, J., Madni, H.: An automation system for controlling streetlights and monitoring objects using Arduino. Sensors **18**(10), 3178 (2018). https://doi.org/10.3390/s18103178

11. Karpenko, A., Kinnunen, T., Madhikermi, M., Robert, J., Främling, K., Dave, B., Nurminen, A.: Data exchange interoperability in IoT ecosystem for smart parking and EV charging. Sensors **18**(12), 4404 (2018). https://doi.org/10.3390/s18124404

12. Kuyer, L., Whiteson, S., Bakker, B., Vlassis, N.: Multiagent reinforcement learning for urban traffic control using coordination graphs. In W. Daelemans, B. Goethals, K. Morik (eds.) Machine Learning and Knowledge Discovery in Databases, vol. 5211, pp. 656–671. Springer, Berlin (2008). https://doi.org/10.1007/978-3-540-87479-9_61

13. Park, K., Shin, C., Song, Y.-S., Lee, H.-J., Shin, C., Kim, Y.: Recyclable and mendable cellulose-reinforced composites crosslinked with Diels-Alder adducts. Polymers **11**(1), 117 (2019). https://doi.org/10.3390/polym11010117

14. Lu, X., Ai, Y., Tian, B.: Real-time mine road boundary detection and tracking for autonomous truck. Sensors **20**(4), 1121 (2020). https://doi.org/10.3390/s20041121

15. Pham, T.-A., Yoo, M.: Nighttime vehicle detection and tracking with occlusion handling by pairing headlights and taillights. Appl. Sci. **10**(11), 3986 (2020). https://doi.org/10.3390/app10113986

16. Qin, Z. (Tony), Tang, J., Ye, J.: Deep reinforcement learning with applications in transportation. In: Proceedings of the 25th ACM SIGKDD International Conference on Knowledge Discovery & Data Mining, pp. 3201–3202 (2019). https://doi.org/10.1145/3292500.3332299

Intelligent Manufacturing Systems: Advanced Manufacturing Processes

Speckle Image-Based Surface Roughness Parameter Characterization of Milled Surfaces

J. Mahashar Ali, H. Siddhi Jailani, and M. Murugan

1 Introduction

The machined parts surface finish is one of the important quality metric of any machining operation. Conventionally, a contact stylus type instrument is used. A stylus instrument has a sharp stylus traversing over the surface being measured along a line. The vertical motion of the stylus is magnified electronically and the surface profile along the line of measurement is recorded. The required parameters are then computed by suitable signal processing technique. The main limitation of the stylus measurement of surface roughness is twofold (i) It is an offline process and (ii) The tip radius of the 'sharp' stylus intrudes the measurement. Besides the stylus measurement, a range of other non-contact methods [1] has evolved for measuring the surface texture with varying accuracies. These methods include white light interferometric (WLI) microscopy, confocal microscopy speckle interferometry, laser speckle contrast, speckle correlation, profiling and optical interferometry [2]. The comparison of the optical and the stylus method of surface roughness measurement is also reviewed. Jiang and Whitehouse [3] documented various challenges in their review, posed by surface metrology in the past decade. In recent years, surface roughness and its defects has been evaluated using the following methods like ANNs, through sub pixel edge detection, through the colour distribution statistical matrix [4, 5]. Though there are many works that were carried out in this direction of surface roughness

J. Mahashar Ali (✉) · H. Siddhi Jailani
Department of Mechanical Engineering, B S Abdur Rahman Crescent Institute of Science and Technology, Chennai 600048, India
e-mail: mahashar@crescent.education

M. Murugan
School of Mechanical Engineering, Vellore Institute of Technology, VIT, Vellore Campus, Vellore 632014, India

measurement the reliability and accuracy requirements remain far from the industrial requirement. But the developments of image processing technology in remote sensing and biometrics have established the possibility of obtaining a simple, fast, economical and reliable online/on-site image-based surface roughness measuring system [6, 7].

1.1 Image-Based Surface Roughness Measurement

The unaided human estimation of surface roughness is either by running ones figure over the surface or by visually examining it. While the stylus instruments mimic the human figure 'having a feel' of the surface, many attempts were made in the past to determine the surface roughness using a vision system handling images of the surfaces. Cuka et al. [8] prepared specimens with different roughness and their surface images were obtained using a special fixture and a microscopic camera. Using the captured images of the surfaces, the distribution of the distance between the tool marks was also computed and used for determining the nature of the tool condition. Mahashar and Murugan [9] used the white light image distribution parameters of turned surfaces to predict the surface roughness. Tian et al. [10] in their review on surface roughness measurement using active vision and light scattering present a comprehensive review of various methods to capture and use the light scatterings for surface roughness characterization. The review also predicts the possibility of, an active vision system with a laser source throwing a pre-set pattern on the workpiece and capturing the image, measuring online, surface characteristics like roughness, waviness and form error through suitable image processing.

1.2 Speckle Image Based Surface Roughness Measurement

When surfaces are illuminated by a coherent, monochromatic light source, the unevenness of the surface leads to constructive and destructive interference of the reflected light. This, in turn, leads to speckle image formation. Hence speckle image-based surface roughness evaluation has been an active line of research. Hamed et al. [11] used an arbitrary threshold to convert the grayscale speckle image into a binary black and white image. The degree of agglomeration was quantified from the binary images and the same correlates well with the roughness measured using a stylus instrument. Pearsson [12] captured two different speckle images using a video camera, one by a laser beam and the other by changing the incident angle to $0.5°$. From the two images the correlation was carried out. This characterization approach is suitable for R_a, lesser than 1 μm. Mahashar et al. [13] compared the milled specimens roughness through the monochromatic laser are illuminated speckle images and white light images. They found that the correlation are better with the speckle images.

1.3 Wavelet Transform and Surface Texture

In wavelet analysis, a signal is decomposed to many levels, which are then rescaled and translated to form the original signal. 1-D continuous wavelets are written [14] thus:

$$\Psi_{a,b}(x) = \frac{1}{\sqrt{a}} \Psi \left(\frac{x - b}{a} \right) \tag{1}$$

where $\Psi(x)$ is indeed the wavelet operator, 'a' denotes the scale variable, and 'b' denotes the translation variable. Wavelet analysis of a surface profile involves decomposing the signal into a family of wavelets. Pour [15] used time-series Fourier transform and wavelets to estimate surface roughness. Wavelet transform facilitated the extraction of variations on the surface profile at various frequencies, so that undesired frequencies, which contribute for the noise, can be eliminated.

Roughness measurement using vision-based methodology has also received larger attention in the manufacturing industry, as this opens up the possibility of automating the inspection process also. It had become a standard industrial practice to have 100% dimensional inspection of critical parts using vision-based systems. In our investigation, the primary objective is to develop a speckle image-based surface roughness parameter that is reliable and economical for characterizing the surface roughness of milled surfaces.

2 Specimen Preparation and Surface Roughness Measurement

In this work, it is proposed to (i) Measure the various roughness parameters using a conventional stylus-based instrument and (ii) Capture the speckle images of surfaces and evolve various image-based metrics. The correlation between conventional roughness parameters and image-based parameters is being studied with the objective of evolving a robust image-based metric. A 50 mm square flat medium carbon steel of 10 mm thickness were prepared by using the end milling operation. A 50 mm diameter end milling cutter with single carbide insert was used to perform the milling. By varying the feed, different specimens with different roughness were obtained. The other cutting parameters like depth of cut (0.1 mm) and cutting speed (190 m/min) were kept constant. The feed rates used are between 0.211 and 2.223 mm/tooth. Figure 1 shows the photograph of milled specimens.

Surface profile of all the nine specimens was taken using Taylor Hobson Talysurf surface roughness tester as shown in Fig. 2. Each profile along a straight line in the middle region of the specimen was taken for a 6 mm measuring length with a stylus tip radius of 2 μm.

Fig. 1 Milled specimens

Fig. 1 Milled specimens
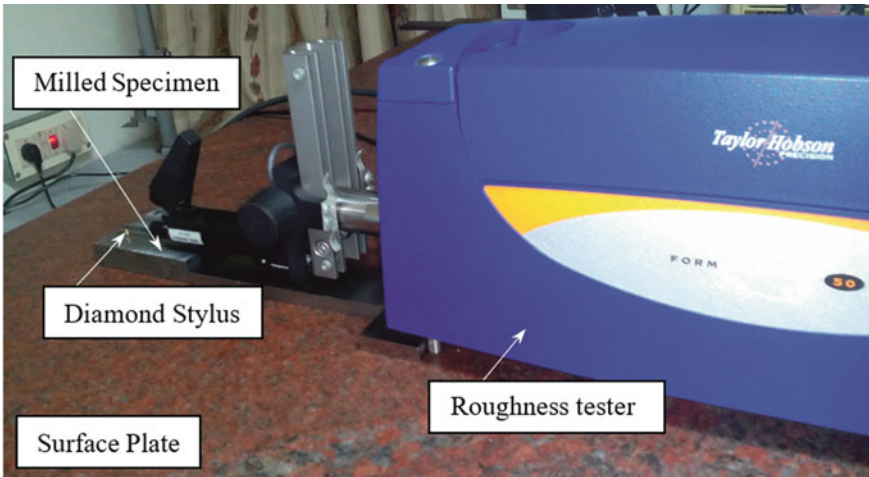
Fig. 2 The Talysurf—surface roughness tester

For processing the roughness parameters a 0.08 cm cut-off length was used. Roughness parameters R_a, R_{da} and R_{dq} were computed and tabulated in the Table 1.

Table 1 Roughness values of the specimen at various levels of roughness

Specimen No.	Stylus parameters		
	R_a (µm)	R_{da}	R_{dq}
1	1.8	9.2	12.7
2	2.1	10.7	14.2
3	2.4	11.5	15.2
4	5.7	10.2	13.8
5	7.5	12.8	17.0
6	9.5	14.2	21.4
7	10.6	9.4	12.8
8	12.8	12.0	16.9
9	13.4	13.5	18.6

3 Image Acquisition and Analysis

The speckle images of these specimens illuminated by a line laser source were captured and processed. A separate camera stand designed used for holding the work piece and light source. Figure 3 shows the setup for experimentation.

Fig. 3 The experimental setup of image acquisition
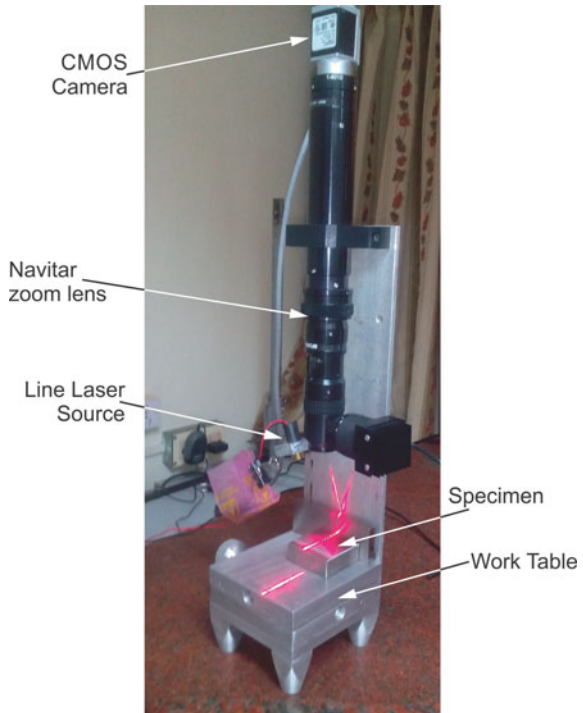
Table 2 The CMOS camera specifications

Description	Specification
Type of sensor	Aptina MT9PO31 rolling shutter CMOS
Sensor size (optical)	1 / 2.5"
Resolution (H × V pixels)	2592 × 1944
Data output format	(8, 12, 12 Packed)
Maximum frame rate	14 frames per second
Containment of exposure	The camera API allows for programming
Synchronisation	Using an external trigger or an Ethernet connection
Power requirement	2.5 W/2.2 W
Camera size	42 × 29 × 29 mm
Weight of the camera	Approximately <90 g

The laser source utilized was the 'Quarton Laser Module VLM-635–27 LPT-10 Redline'. Basler high end CMOS camera with zoom 45× was used to capture the image. The specification of camera is given in Table 2. Surface line speckle images with image resolution of 2592 × 1944 pixels was captured by keeping the camera normal to the milled surface. Figure 4 shows the sample of a captured speckle image.

Image normalization to eliminate the lighting variations was done by the following expression [16].

$$a(p, q) = \left(\frac{b(p, q) - \min(b)}{\max(b) - \min(b)} \right) \times 255 \tag{2}$$

Fig. 4 Image of a specimen taken by Line laser source
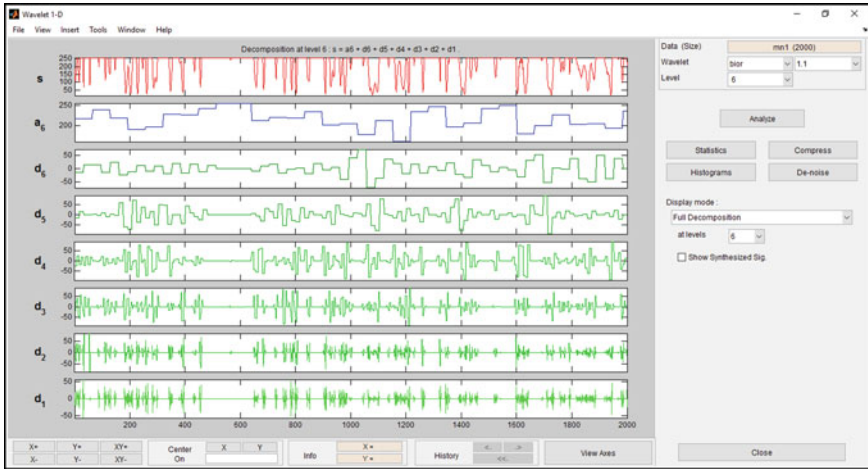
Fig. 5 Wavelet transformed signal vectors [MATLAB]

$a(p, q)$ is the image matrix's standardized pixel intensity, whereas $b(p, q)$ is the intensity of each pixel in the image matrix, and $\min(b)$ and $\max(b)$ are the minimum and highest values of the image matrix's pixel intensity, respectively. From each normalized speckle image, a one-dimensional three-pixel row band image signal is considered in the middle region. The one-dimensional image vector is generated by averaging the pixel intensity values in the respective columns of the three-pixel row. The choice of averaging three-pixel values was to align the width of a band to that of the stylus radius of the stylus instrument. This alignment is to facilitate subsequent correlation with the roughness values obtained using a stylus instrument. MATLAB programme modules were developed to generate the one-dimensional signal vector for each of the nine images.

In the literature, bi-orthogonal wavelets (bior 1.1) were employed to quantify surface roughness [14, 17]. Figure 5 depicts a signal vector that has been wavelet processed.

The surface roughness details are contained in the 4th and 5th order detail coefficients [17, 18]. This is due to the matching wavelengths syncing with the stylus instrument's cut-off values. The 4th and 5th level detailed coefficients would be further analyzed, as well as the distribution characteristics of these detail coefficients, such as RMS and variance, are calculated and tabulated. The obtained image parameters are shown in Table 3.

4 Results and Discussion

The correlation between the image parameters as well as the numerous stylus-based roughness parameters are being investigated. The trends in Fig. 6a, b show that the

Table 3 The specimen image parameters

Specimen No.	Image parameters			
	4th order detailed coefficients		5th order Detailed Coefficients	
	RMS	VAR	RMS	VAR
1	11.2510	126.6449	14.4783	209.7229
2	10.7675	115.9956	8.7225	76.1181
3	09.5210	90.6927	9.3754	87.9413
4	16.8795	285.0514	19.1856	368.2663
5	20.3880	415.8726	26.1126	682.1991
6	19.0277	362.2277	26.4843	701.7582
7	23.5327	560.1188	21.6281	468.0037
8	20.9392	438.6336	24.0098	576.7510
9	21.5431	464.3209	24.1713	584.5360

RMS and Variance of the image signal intensity vector's 4th level detail coefficient values are extremely well associated with the roughness parameter R_a, with high R^2 values of 0.8442 for RMS and 0.8355 for variance.

The following words can be used to explain how the RMS and Variance values increase as the surface roughness increases. A higher R_a value implies a rough surface, which generates more light scattering when lit with a line laser source, resulting in a speckle image with more variance in image intensity values. When these images are analyzed through the wavelet transform and when the analysis is focused on wavelengths pertaining to the roughness values of the surfaces, this variation in intensities are further magnified leading to higher values of RMS and variance. There is also a linear link between the two, with R^2 values of 0.6976 for RMS and 0.6804 for variance on 5th order detail coefficients.

$$y = 1.0634x + 9.3216$$
$$R^2 = 0.8442$$

(a)

$$y = 34.499x + 65.562$$
$$R^2 = 0.8355$$
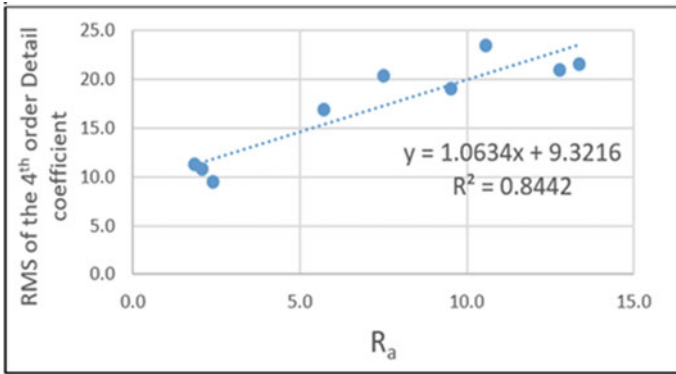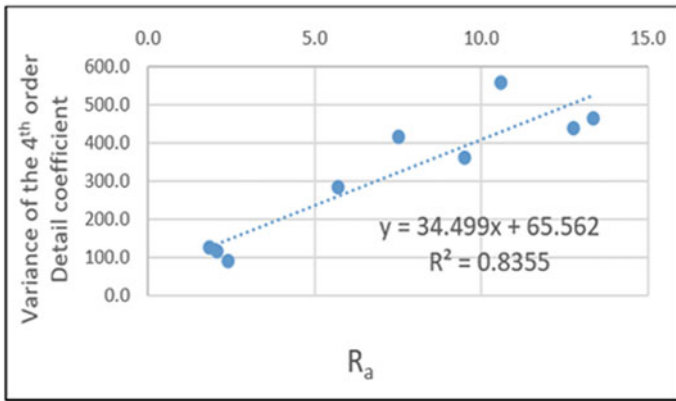
(b)

Fig. 6 **a**, **b** RMS and Variance of the 4th level detail coefficient versus R_a

5 Conclusion

The author presents a non-contact and in-situ evaluation of surface roughness based on images. When the material was irradiated with a line laser source, the speckle picture was captured. The 4th and 5th level detail coefficents were retrieved after wavelet transformation of the speckle image. The stylus parameter was calculated to confirm the hypothesis. As picture parameters, the RMS and Variance of the 4th level detail coefficient vector were determined. The following is the conclusion:

- The image parameters RMS and Variance correspond strongly with the stylus parameter, as can be seen from the trends of R_a.
- Especially, the correlation graphs of 4th level detail coefficient shows a strong linear relationship with R^2 values of 0.8442 for RMS and the R^2 value of 0.8355 for the variance.

- The primary reason for the strong correlation between speckle based image parameter 4th level detail coefficient and stylus parameter is the cut-off values of the stylus instrument are aligned with the wavelength of the 4th level detail coefficient vectors.

References

1. Vorburger, T.V., Rhee, H.-G., Renegar, T.B., Song, J.-F., Zheng, A.: Comparison of optical and stylus methods for measurement of surface texture. Int. J. Adv. Manuf. Technol. **33**(1–2), 110–118 (2007)
2. Wang, Y., Xie, F., Ma, S., Dong, L.: Review of surface profile measurement techniques based on optical interferometry. Opt. Lasers Eng. **93**, 164–170 (2017)
3. Jiang, X.J., Whitehouse, D.J.: Technological shifts in surface metrology. CIRP Ann. Manuf. Technol. **61**(2), 815–836 (2012)
4. Samtaş, G.: Measurement and evaluation of surface roughness based on optic system using image processing and artificial neural network. Int. J. Adv. Manuf. Technol. **73**(1–4), 353–364 (2014)
5. Martínez, S.S., Vázquez, C.O., García, J.G., Ortega, J.G.: Quality inspection of machined metal parts using an image fusion technique. Measurement **111**, 374–383 (2017)
6. Tangjitsitcharoen, S., Boranintr, V.: Integration of in-process monitoring and statistical process control of surface roughness on CNC turning process. Int. J. Comput. Integr. Manuf. **26**(3), 227–236 (2013)
7. Quintana, G., Bustillo, A., Ciurana, J.: Prediction, monitoring and control of surface roughness in high-torque milling machine operations. Int. J. Comput. Integr. Manuf. **25**(12), 1129–1138 (2012)
8. Cuka, B., Cho, M., Kim, D.-W.: Vision-based surface roughness evaluation system for end milling. Int. J. Comput. Integr. Manuf. **31**(8), 727–738 (2018)
9. Ali, J.M.: Murugan M : Surface roughness characterisation of turned surfaces using image processing. Int. J. Mach. Mach. Mater. **19**(4), 394–406 (2017)
10. Tian, G.Y., Lu, R.S., Gledhill, D.: Surface measurement using active vision and light scattering. Opt. Lasers Eng. **45**(1), 131–139 (2007)
11. Hamed, A., El-Ghandoor, H., El-Diasty, F., Saudy, M.: Analysis of speckle images to assess surface roughness. Opt. Laser Technol. **36**(3), 249–253 (2004)
12. Persson, U.: Surface roughness measurement on machined surfaces using angular speckle correlation. J. Mater. Process. Technol. **180**(1–3), 233–238 (2006)
13. Ali, J.M., Jailani, H.S., Murugan. M.: Surface roughness evaluation of milled surfaces by image processing of speckle and white-light images. In: Advances in Manufacturing Processes, pp. 141–151. Springer, Berlin (2019)
14. Jiang, X., Scott, P., Whitehouse, D.: Wavelets and their applications for surface metrology. CIRP Ann. Manuf. Technol. **57**(1), 555–558 (2008)
15. Pour, M.: Simultaneous application of time series analysis and wavelet transform for determining surface roughness of the ground workpieces. Int. J. Adv. Manuf. Technol. **85**(5–8), 1793–1805 (2016)
16. Gonzalez, R.C., Woods, R.E.: Digital Image Processing. Prentice Hall, Upper Saddle River (2002)
17. Ali, J.M., Jailani, H.S., Murugan, M.: Surface roughness evaluation of electrical discharge machined surfaces using wavelet transform of speckle line images. Measurement **149**, 107029 (2020)
18. Chen, X., Raja, J., Simanapalli, S.: Multi-scale analysis of engineering surfaces. Int. J. Mach. Tools Manuf **35**(2), 231–238 (1995)

Influence of Mechanical Vibrations on Impact Strength of 1018 Mild Steel Butt-Weld-Joints

Bade Venkata Suresh, Y. Shireesha, and P. Srinivasa Rao

1 Introduction

Welded joints can be lightweight and durable than bolted or riveted joints. Welding variables in the weld zone affect the quality of the finished product as well as the existence of the weld joint. Weld bead reliability is greatly influenced by parameters such as electrode size, weld-current, arc length, travel speed and weld-voltage. Aside from being popular and effective joints, almost any fabrication process has advantages and disadvantages. Welding does have a substantial heat affected zone because of the accumulation of a large amount of heat generated during the welding process over a small region; there is a possibility of residual stresses being generated throughout the weld. Even more research is being done because residual stresses are a major issue throughout welding. One of most frequently used stress-relieving strategies are heat-treated and mechanical refining. However, both are costly and time-consuming, as well as requiring a significant amount of effort. The vibrational stress relief process, which would be adapted after welding, with resonance frequency and non-echoing dynamic loading behaviours of limited steel alloy, is being considered to enhance mechanical characteristics such as strength and toughness, but there is still a decrement in the fatigue-strength performance of test samples with non-echoing dynamic loading weld with the pulsation aided joining [1]. "VSR" has been

B. Venkata Suresh (✉) · Y. Shireesha
Department of Mechanical Engineering, GMR Institute of Technology, Rajam, Andhra Pradesh 532127, India
e-mail: suresh.bv@gmrit.edu.in

Y. Shireesha
e-mail: y.shireesha@gmrit.edu.in

P. Srinivasa Rao
Department of Mechanical Engineering, Centurion University of Technology and Management, Paralakhemundi, Odisha 761211, India

used for SS-weld samples with an overall mass of more than 34 tonnes that are tested for cyclic stress–strain. The plate was treated for around 15 min at a resonance frequency of 47.83 Hz. The number of cycles and the magnitude of dynamic stress are used to assess the effectiveness of VSR. The Differences are around 11% reduction in the longitudinal residual-stresses [2]. The "Vibratory Stress Relief" approach is explained and compared to heat treatment in order to determine the vibration energy impact on stress concentration in heat affected and weld zone. The results of this study's X-ray diffraction show that vibratory stress relief can be employed to lessen residual strains generated during the welding process [3].

Throughout the VSR technique the result of residual stresses on surface stress scattering were examined. The "VSR" technique is most commonly used to diminish residual defects in manufacturing method, and their differences in the microstructures were clearly visible where mechanical characteristics are enhanced, and also this technique is useful for high end applications for suitable results [4]. In nuclear-reactor the SS-plate specimens were considered for VSR technique. The outcomes are exposed that there is reduction in residual stress about 56% of the hoist-machine and around 31% for SS-plate after execution with the VSR technique [5]. Simulation of the VSR technique was performed on SS-304-L weld samples by the analysis process to observe the repeated strain–stress. The dynamic strain possesses cyclic creep characteristics, according to the experimental data. Creep and its speed were influenced by cyclic loading. The greater the loading, the greater the creep and its speed, and the longer the strain took to stabilize. After a variety of cyclic stress amplitudes, the residual stresses at the weld zone were determined using the X-ray diffraction method. The cyclic creep mechanism during VSR processing was depicted as a reduced residual stress, according to the experimental data [6]. The stresses in the direction of transverse and longitudinal were decrease and increase with any trend at low frequency. Residual stresses remained constant at high frequencies. As a result, the rigid body motion effect at above frequencies is originated to be unproductive in terms of residual stress reduction [7]. Shafts of different shapes were considered to assess the variation in residual stresses produced during welding. The results of this study show that torsional shear-stresses can moderately diminish residual stresses in shafts that shear stress aids in the transformation of retained austenite to subsequent phases, and that this influences residual stresses caused by interphase effects [8]. Whilst the specimens were cooling, the influence of vibration on residual stresses caused by the welding process was investigated. Vibration was imparted to them throughout a temperature range that was specified. There are three batches under investigation, each with a different temperature range. Residual stresses were observed to be improved all three batches, with no discernible movement. The results of the actions appear to be undesirable, and it is concluded that vibration at 400 and 320 °C did not significantly alter the ultimate state of residual stresses, as these are not significantly changed with the vibration curve [9].

The effect of vibratory stress on microstructure of the weld and stress-distribution was investigated. The residual stress perpendiculars to weld line were measured. The results of the stress levels reveal that they are diminished around 60–75 MPa at very initial stage that is at initial 5 s of excitations. During post-weld vibratory

treatment, the escalation of excitations does not result in the further reduction in stress intensities, and optical microscopy reveals no differences in crystal-structure. The crystals grow in a predetermined direction during welding due to vibratory treatment. The weldment's hardness improved by 25% as a result of the grain refining. The orientation of the crystals is linked to this rise [10].

2 Experimental Structure

2.1 Methodology

Welding is a metal or non-metal joining procedure that can be done with or without the use of heat, pressure, or filler material. Welded joints are lighter than bolted or riveted joints. The superiority of weld and lifetime of joint are determined by welding parameters in the process. Weld bead quality is heavily influenced by variables such as electrode size, weld-current, arc length, travel speed and weld-voltage. Aside from being commonly used and effective joints, every fabrication process has advantages and disadvantages. Welding has a significant heat affected zone because the huge quantity of heat created during the welding process is concentrated over a small region; there is a risk of residual strains forming in the joints. Due to the fact that residual stresses are a key issue during welding, a lot of study is being done. The most prevalent stress-relieving treatments are heat treatment and mechanical processing. However, these are both costly and time intensive, as well as requiring a great deal of effort. Offering of mechanical excitations throughout welding process, increases mechanical and metallurgical characteristics of any material.

2.2 Chemical Composition

Weld joints were prepared with and without inducing vibrations by using a consumable electrode. The Filler material ER4111 is chosen for welding process. Composition of ER4111 filler metal is in terms of weight % is Carbon (C)—0.12 (max.), Manganese (Mn) 0.30–0.60 (max.), Silicon (Si)—0.40 (max), Phosphorus (P)—0.04 (max), Sulphur (S)—0.04 (max.) and Ferrous (Fe) is the base material shown in Table 1.

2.3 Vibratory Welding Equipment Setup

In this experimentation, new vibratory-setup is developed for inducing vibrations during the weld process. The vibrations are transferred mainly through table and

Table 1 Chemical composition of Mild Steel [11]

Chemical composition	
Element	Composition
Iron	98.81–99.26%
Carbon	0.18%
Manganese	0.6–0.9%
Phosphorous	0.04% max
Sulphur	0.05% max

electrode with "vibration-motor & D.C-motor", respectively. The main parts include in this setup which are producing vibrations is "Vibration-motor & D.C-Motor". The line diagram of the vibration setup is shown in Fig. 1. The vibrating table consists of a 10 mm thickness flat surface plate of cast iron which is supported with four springs at each corner. These springs are placed in a solid rod connected rigidly to the plate and legs of the table. These springs are used to observe the deflections produced due to un-even vibrations caused by vibration-motor to avoid damage to the system. Along with the specimen vibrations, the electrode is also vibrated with different D.C-Motor. This D.C-Motor rotor is physically in contact with the electrode by fixing the motor to an electrode holder with a clamp. The Speed of the D.C-Motor rotor is controlled by a pulse width modulation device [11]. The power supply altered from AC to DC with an adapter.
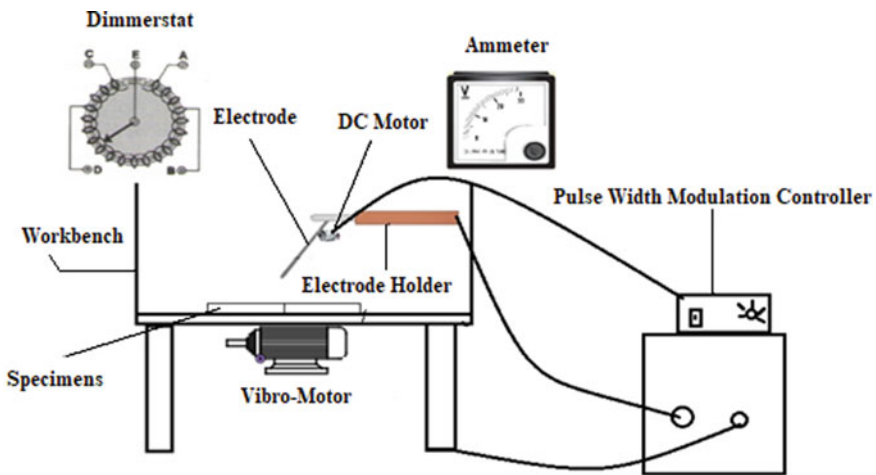
Fig. 1 Experimental setup of vibratory welding
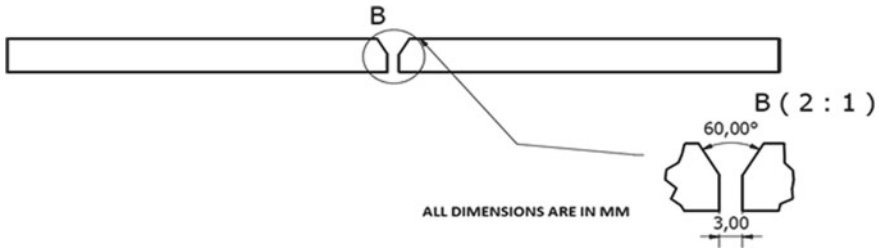
Fig. 2 Specimen preparation of mild steel 1018

2.4 Preparation of Weld Joint Specimens

In this experimentation, the shielded metal arc welding-(SMAW) process is considered to prepare weld joints and for analysis 1018 mild steel material is considered. Single 'V' butt joints are considered for preparing weld joints. Mild steel plates with dimensions of $200 \times 100 \times 5$ mm are connected rigidly over the vibration platform with fixtures shown in Fig. 2.

2.5 Vibratory Welding Parameters

In this type of welding technique, various parameters will affect the weld joint strength. Those parameters are current, speed, voltage, spark, and size of the electrode which are stationary at 100A, 0.35 mm/s, 23 V, 3 mm, and 3.15 mm diameter respectively. The current work consists of vibration parameters that are the voltage of "vibration-motor, D.C-Motor and constant vibration time" is chosen for investigation.

Vibration time denotes the vibrating time of specimens during welding. Here vibration time-limited to 100 s at a voltage of "vibration-motor and voltage of D.C-Motor", because for mild steel 25,000 °C is fusion temperature during arc welding and at 5400 °C it crystallizes according to the mild steel phase diagram. Dropping temperatures are observed with the "Digital Infrared Thermometer" from 25,000 to 5400 °C. The average period is 100 s for attaining 5400C to 25000C. Therefore, 100 s constant vibration time is taken at each voltage of "vibration-motor and voltage of D.C-Motor" for observation of welded joint mechanical properties. The mechanical properties improvements in welded joints were negligible after crystallization so, 100 s vibrations time is restricted. And considered the vibration-motor maximum voltage is 230 V and D.C-Motor's maximum voltage is 20 V. Whenever the vibration-motor crosses 230 V, the amplitude exceeds 0.5 mm the arc gap will increase. In such a typical situation welding process is impossible. Therefore the voltage higher bound is restricted at 230 V and 20 V of "Vibration-motor and D.C-Motor" respectively.

And the lower bound is taken for the Vibration-motor and D.C-Motor does not work at a voltage which is less than 50 V and 12 V, respectively [12].

2.6 Impact Test

The impact is carried out for welded specimens on the Charpy impact testing machine. Figure 3 shows the specimen inserted in the testing machine. As per ASTM (E23) the specimens were prepared and the dimensions are shown in Fig. 4 [13]. A specimen with notch is inserted in machine and the heavyweight pendulum is permitted to strike the workpiece from a stationary height. The specimens after impact test are shown in Fig. 5.

Fig. 3 Specimen on Charpy impact testing machine
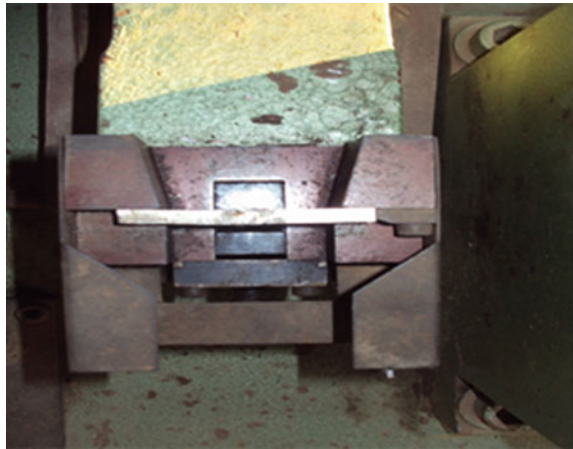
Fig. 4 Dimensions of impact test specimen
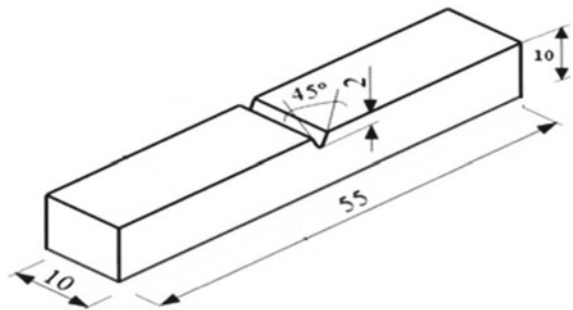
Fig. 5 Specimens after impact failure

3   Results and Discussion

The impact strength is conducted for all the samples at vibration-motor voltage range from 50 to 230 V at an interval of 20 V, D.C-Motor voltage from 12 to 20 V at an interval of 2 V, and 100 s of specimen vibration. The test is executed on Charpy Testing Machine to measure the impact strength of the vibratory welded specimens. Totally 50 experiments for all combinations of different levels of the parameters are conducted and the amount of energy observed by the specimens is noted and compared with each other.

It can be observed that the change of vibration parameters has a significant effect on impact strength. By observing the graphs below it is identified that the difference in impact strength at different vibration input variables on the weld joint.

The change of Impact strength with the chosen variables is shown in Fig. 6a–f exhibits a comparison which indicates that the voltage of vibration-motor and D.C-Motor with a constant time of vibration has more influence on impact strength and the max values were observed at 190 V of vibration-motor and 18 V of D.C-Motor. And also, the impact strength of the non-vibratory welded joint is 45 J and it is less compared to weld joints made with 190 V of vibration-motor, 18 V of D.C-Motor, and 100 s of the time of vibration. So, it concludes that a 17% improvement in impact strength obtained when it is compared with joints made without vibration.

4   Microstructure Analysis of Mild Steel 1018 Specimens

Figure 7 depicts the microstructure analysis performed on weldments made at various frequencies. By looking at the microstructure, we can see that the 0 Hz frequency weldments, which are free of vibration, have massive dendrites and a larger grain size, as seen in the Fig. 7a. Whenever the range of vibrational frequency is significantly expanded, the grain structure improvement is recognized; the grain structure enhancement occurs because dendritic diameters are shrinking as frequency increases. The continual improvement is evident as the frequency of welding increases. Figure 7c
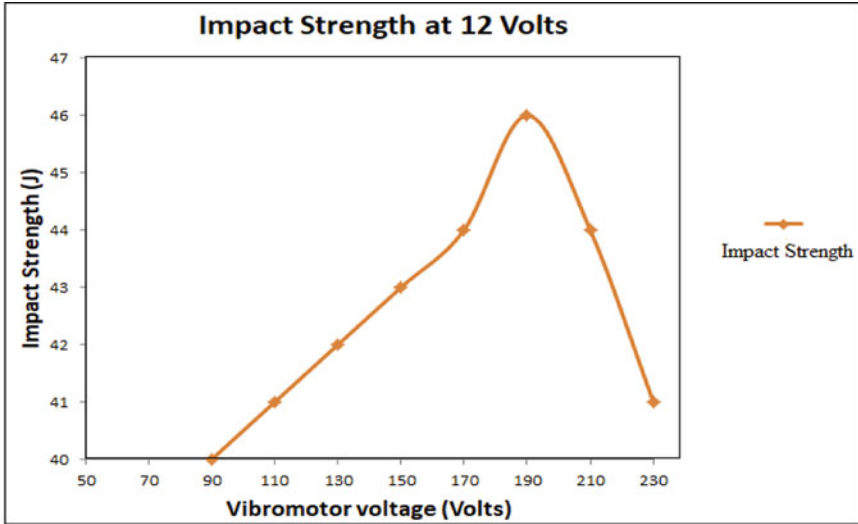
a. Impact strength of specimen at 190V, 12V, and 100 secs.
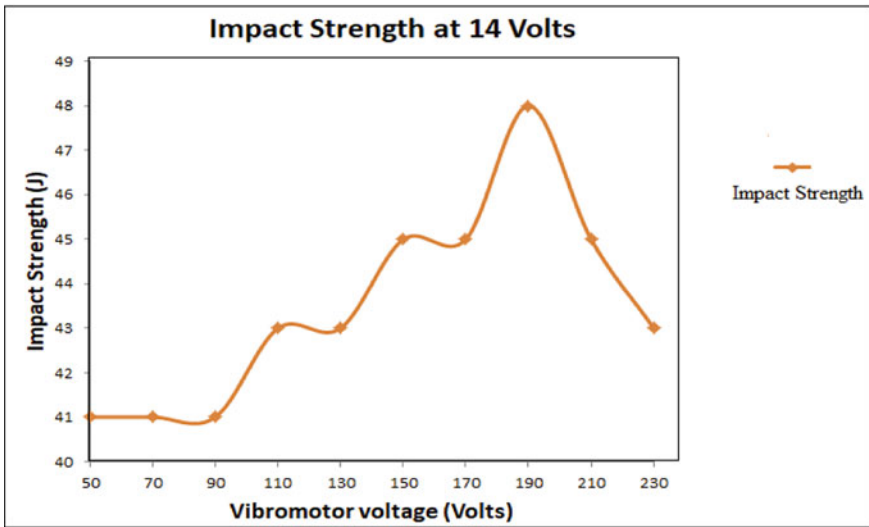
b. Impact strength of specimen at 190V, 14V, and 100 secs.

Fig. 6 Impact strength at different vibration input parameters

shows a fine grain structure due to fine filler material distribution at 190 V of vibration-motor and also 18 V of the D.C-motor. Due to the fine dissemination of filler material the fine grain-refinement occurring, this result is due to molten pool refining.
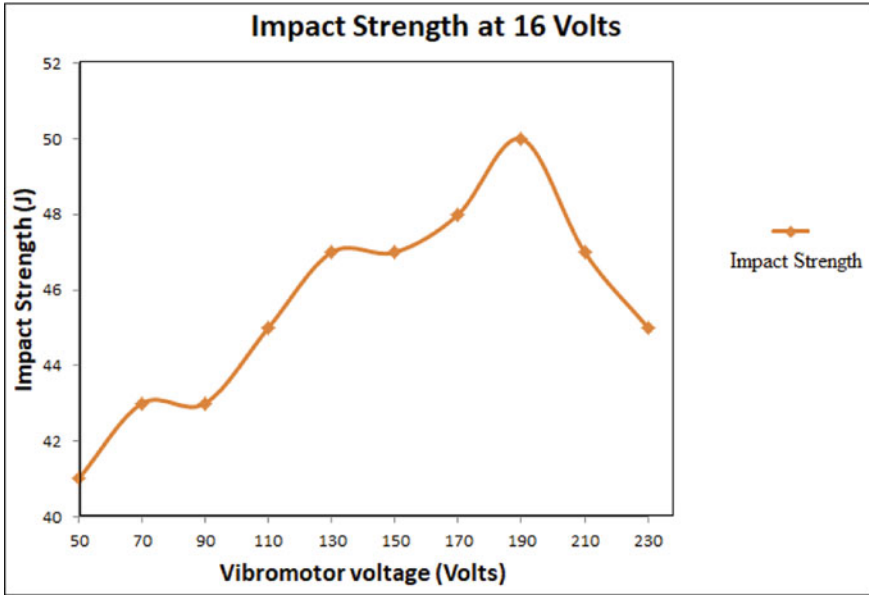
c. Impact strength of specimen at 190V, 16V, and 100 secs
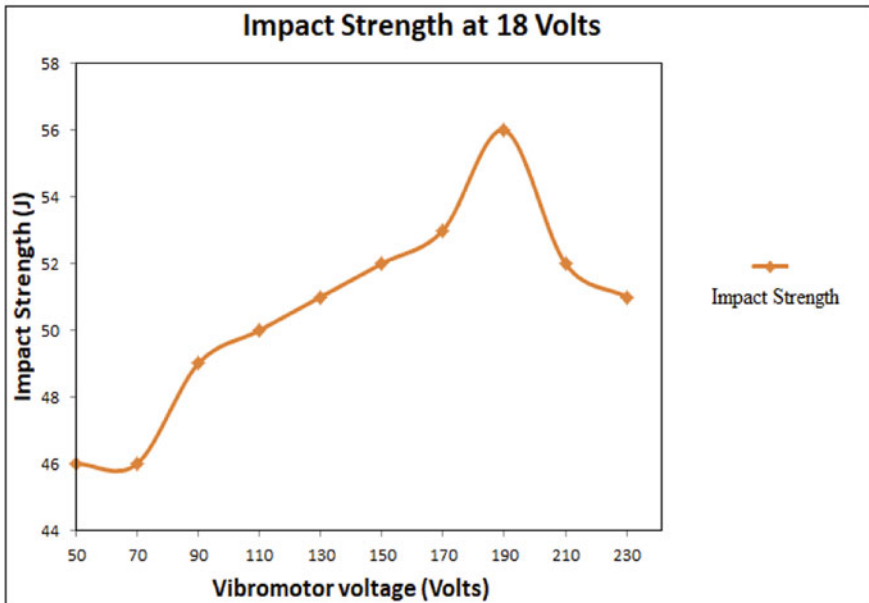
d. Impact strength of specimen at 190V, 18V, and 100 secs.

Fig. 6 (continued)
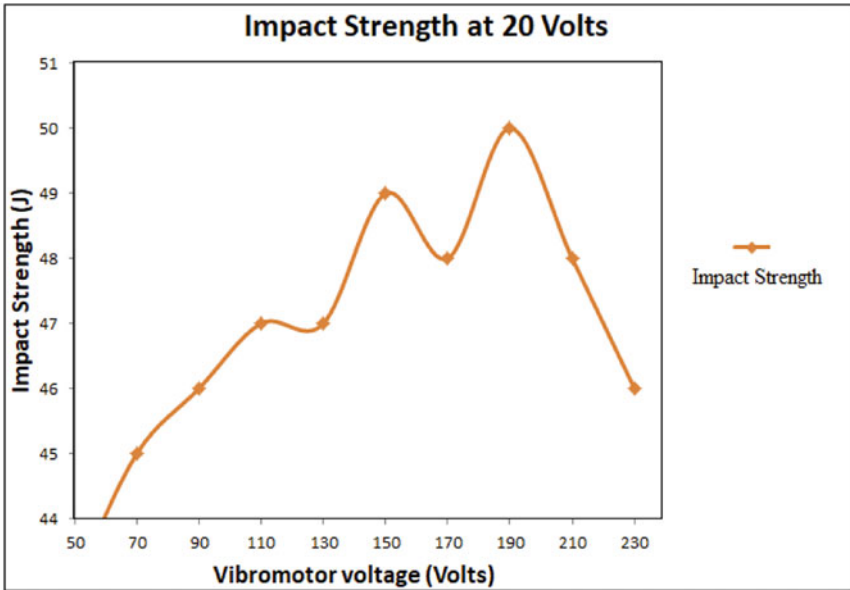
e. Impact strength of specimen at 190V, 20V, and 100 secs.
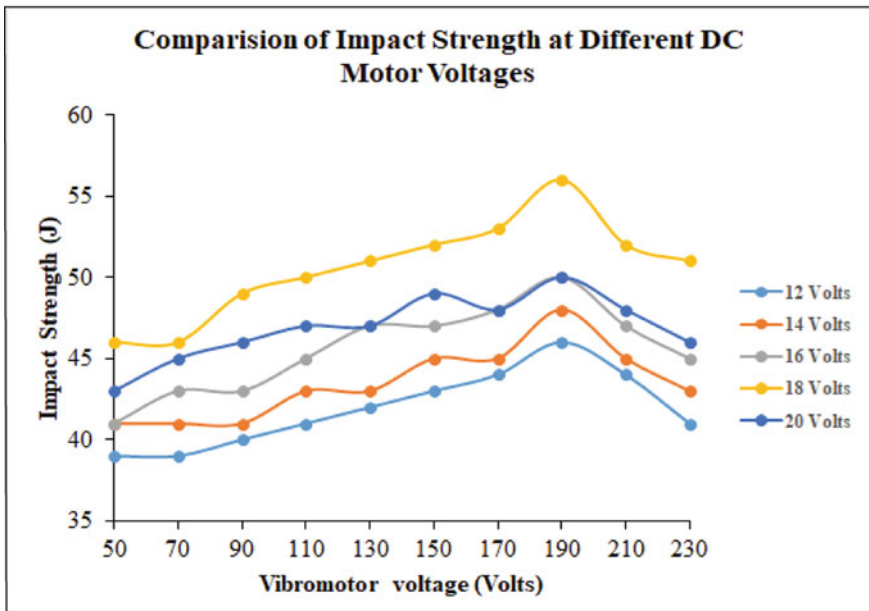
f. Comparison of Impact strength with Voltages.

Fig. 6 (continued)

(a)Without vibrations

(b) At 190V and 12V

(c) At 190V and 16V

(d) At 190V and 18V
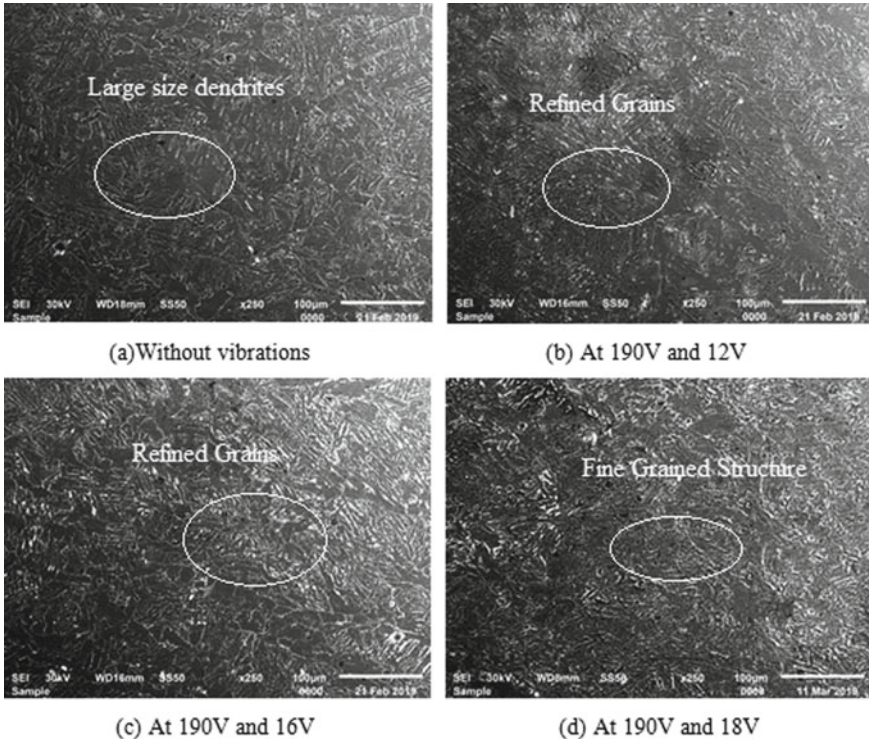
Fig. 7 Microstructures of the Mild steel weldments with and without

Increases in vibrations, more than 190 V for vibration-motors and 18 V for D.C-Motors results in an increase in dendritic size. This is because the arc gap widens as the frequency rises.

5 Conclusion

Mechanical-vibrations throughout the welding confirm an influence on 1018 Mild Steel material impact strength. The weld-specimens impact strength with mechanical excitations has significantly increased, when compared conventional welding process. The test-specimens devoid of mechanical excitations were originated to record low impact strength, when it is related with specimens prepared with mechanical excitations. Mechanical vibration has more influence on impact strength and the best results are observed at 190 V of vibration-motor and 18 V of D.C-Motor. And also, impact strength of the normal weld joint is 45 J and it is less compared to weld joints made with mechanical vibration. With this it is concludes that a 17% improvement in impact strength obtained when it is compared with joints made without

vibration. The microstructure examination exposes the reason for enhancing impact strength. The fine refinement of grain arrangement is the main reason to enhance impact strength and refines molten pool before solidification. Due to refinement in molten state some of the weld-defects get minimized. Conventional weld process contains large size dendrites, leads to weld-defects, which are minimized by breaking down to small dendrites size with the insistence of vibrations.

References

1. Walker, C.A., Waddell, A.J., Johnston, D.J.: Vibratory stress relief—an investigation of the underlying processes. Proc. Inst. Mech. Eng. Part E J. Process Mech. Eng. **209**(1), 51–58 (1995)
2. Tewari, S.P.: Effects of transverse oscillation on tensile properties of mild steel weldments. ISIJ Int. **39**(6), 570–574 (1999)
3. Munsi, A.S.M.Y., Waddell, A.J., Walker, C.A.: Vibratory weld conditioning—the effect of rigid body motion vibration during welding. Strain **35**(4), 139–143 (1999)
4. Musin, A.S.M.Y., Waddell, A.J., Walker, C.A.: The influence of vibratory treatment on the fatigue life of welds: a comparison with thermal stress relief. Strain 37(4)
5. Munsi, A.S.M.Y., Waddell, A.J., Walker, C.A.: Vibratory stress relief—an investigation of the torsional stress effect in welded shafts. J. Strain Anal. Eng. Design **36**(5), 453–464 (2001)
6. Sakthivel, P., Sivakumar, P.: Effect of vibration in Tig and arc welding using AISI 316 stainless steel. Int. J. Eng. Res. Sci. Technol. **3**(4), 116–130 (2014)
7. Pučko, B., Gliha, V.: Charpy toughness of vibrated microstructures. Metalurgija **44**(2), 103–106 (2005)
8. Rao, D.L., et al.: Reduce the residual stress of welded structures by post-weld vibration. Mater. Sci. Forum. **490** (2005)
9. Zhu, Z.Q., Chen, L.G., Rao, D.L.: Relieving welding residual stress by applying vibratory weld conditioning. Mater. Sci. Forum **490** (2005)
10. Joseph, A., et al.: Evaluation of residual stresses in dissimilar weld joints. Int. J. Press. Vessels Pip. **82**(9), 700–705 (2005)
11. Bade, V.S., Srinivasa Rao, P., Govinda Rao, P.: The effect of vibratory conditioning on tensile strength and microstructure of 1018 mild steel. World J. Eng. **17**(6), 837–844 (2020). https://doi.org/10.1108/WJE-07-2020-0296
12. Bade, V.S., Srinivasa Rao, P., Govinda Rao, P.: Experimental investigation on influence of electrode vibrations on hardness and microstructure of 1018 mild steel weldments. World J. Eng. **17**(4), 509–517 (2020)
13. Suresh, B.V., Shireesha, Y., Srinivasa Rao, P.: Effect of electrode vibration welding on impact and tensile strength of 1018 mild steel weld joints. In: Dave, H.K., Dixit, U.S., Nedelcu, D. (eds.) Recent Advances in Manufacturing Processes and Systems. Lecture Notes in Mechanical Engineering. Springer, Singapore (2022). https://doi.org/10.1007/978-981-16-7787-8_26

DEMATEL Approach to Prioritizing the Critical Factors of PAT Affecting Manufacturing System

Vikram Singh and Somesh Kumar Sharma

1 Introduction

In the present era, the manufacturing sector is facing competition to satisfy the consumer's desire. All this requires a flexible manufacturing system to be emerged. Therefore, research is going on in full swing in the manufacturing sector to meet the requirements of production system. The focus of every manufacturing organization is to rapidly increase its efficiency, performance, production and wealth. To achieve all this, the manufacturing system is adopting digital production which is driven by agent based technology.

Agent technology is very modern, on which every scientist and researcher is keeping eyes and its role in the manufacturing system is commendable. The agent makes the system fast, flexible and secure by exchanging data across the manufacturing system. The agent system works from production to maintain whole life of products. Maintenance is very important in the manufacturing system which remains a challenge for the entire manufacturing sector as industrialists are spending more than 50% of their income on it. It is playing its role in improving the productivity, performance, safety, security and economy [1–5] of the organizations. Rapid research into maintenance systems is leading to the emergence of modern terms such as e-maintenance [6] which provide information through online and offline modes as well as scheduled maintenance, monitoring, fault identification Prognosis and diagnosis. In maintenance, the term prognosis means to predict the life of product [7–10] and collect right information at the right time [11].

The merging of prognosis and agent technology works effectively in manufacturing system to reduce investment on maintenance and improve overall performance

V. Singh (✉) · S. K. Sharma
Mechanical Engineering Department, National Institute of Technology, Himachal Pradesh, Hamirpur 177005, India
e-mail: vikram_phdme@nith.ac.in

and efficiency of manufacturing organizations. PAT is the latest recognized term in manufacturing and research on the application of PAT has been little explored so far. Keeping this in mind, we have made a small effort to work in this area. The aim of this work is defined below.

1.1 Objective of the Research

The objective of our study is to enumerate the key factors for the initiation and execution of PAT on scheduling, operation, and maintenance to enhance the overall performance of manufacturing organizations. In order to achieve the defined objective, first of all, variables associated with PAT have been identified from the literature and based on the knowledge of experts. Secondly, the identified variables of PAT are grouped as principal variables and governing variables. Then, current research utilized the DEMATEL approach to prioritize the key variables of PAT influencing manufacturing organizations' performance. In this research, we are talking about the system that is generated in nature and that complies with multiple manufacturing organizations in the country of different industrial backgrounds.

The remaining articles in our paper are organized as follows: In Sect. 2, a literature review was performed, identifying, reorganizing, and categorizing variables of PAT and in Sect. 3, methodology, which has the design of rating Performa, the introduction of DEMATEL. In Sect. 4, Analysis and Discussion and at last, Sect. 5 completes the paper with conclusion, limitations and future scope.

2 Literature Review

As PAT has gained fame in the manufacturing sector, scientists and researchers are consistently striving to innovate in this field. But research in this field is going very slowly due to the wide range of agent technology. Along with the development of agent technology, some other technologies are also developing, such as cloud computing and information technology. These are used for internet based maintenance. Therefore, cloud computing is used interchangeably with a model in a production system [12]. Keeping in mind the role of PAT in manufacturing systems and our research objectives, we have studied the literature in various fields as listed in Table 1.

Going through this literature and on the basis of data collected from the experts, we have identified five major variables and 21 governing variables [38] of PAT and they are grouped as shown in Table 2.

Table 1 Literature reviewed

S. No.	Domain	Reviewed papers	References
1	Manufacturing	14	[2, 3, 14, 17–19, 26, 27, 33–38]
2	Maintenance	12	[1, 6, 8, 11, 13, 21–24, 28, 29, 31]
3	Prognosis	4	[8–10, 38]
4	Planning and scheduling	3	[15, 16, 30]
5	Other	5	[4, 5, 12, 25, 32]

Table 2 Hypothetical Domain of PAT

S. No.	Principle variables	Governing variables of PAT	References
1	Manufacturing process (F_1)	• Production planning (A_1)	[14, 34]
		• Production scheduling (A_2)	[16]
		• Manufacturing disturbances (A_3)	[17]
		• Virtual manufacturing (A_4)	[35]
		• Decision support tool (A_5)	[13, 19, 20]
		• Distributed digital manufacturing (A_6)	[3, 21]
2	Fault identification (F_2)	• Integration of monitoring, diagnosis, and prognosis (A_7)	[21]
		• Internet-enabled predictive maintenance (A_8)	[22, 23]
		• Diagnosis (A_9)	[7, 21]
		• Prognosis (A_{10})	[38]
		• Proactive maintenance (A_{11})	[14, 24]
3	Integration of Manufacturing system with maintenance (F_3)	• Integration of manufacturing system (A_{12})	[5, 27, 35, 38]
		• Machine down time (A_{13})	[28]
		• Inventory expenses (A_{14})	[29]
		• Setup time (A_{15})	[30]
4	Organizational productivity (F_4)	• Cycle time (A_{16})	[31]
		• Organizational input (A_{17})	[32]
		• Organizational output (A_{18})	[33]
5	Organizational control (F_5)	• Control system architecture (A_{19})	[21, 34–36]
		• Networking between agents (A_{20})	[3, 28]
		• Just in time (A_{21})	[37]

Table 3 List of experts

S. No.	List of companies	Numbers	Position of experts
1	Academicians	1	Professor
2	metal industry	1	Shift Manager
3	Hygiene, health and nutrition	1	Executive Engineer
4	Home care and beauty and personal care	1	Electrical and Instrumentation Executive
5	Stainless steel industry	1	Manager
6	Oil and gas industry	1	Associate Manager

3 Research Methodology

3.1 Questionnaire Design

In the previous section, we identified five major variables and twenty-one governing variables of PAT, grouped in Table 2. A performance questionnaire was designed to collect information from the experts. While designing the questionnaire, we have assured the presence of each selected variable [38] as per the requirements of the DEMATEL approach. The designed Performa is prepared in MS Office Word and sent to the experts listed in Table 3. Experts were requested to give responses to variables of PAT which help to increase organizational overall performance. Therefore, the performa was prepared accordingly.

3.2 DEMATEL Approach

The Battle Memorial Institute for Science and Human Relations Program in Geneva developed an approach in 1972–1976 to study complex group problems [39]. It helps in analyzing the key variables and drives the interrelation among these variables. The study of the DEMATEL approach also shows that it is used to build the digraphs to present causal and effect relationships and classify interdependence between the variables. In view of this, we have applied the DEMATEL approach in this research. Stepwise implementation of the DEMATEL approach is shown in Fig. 1 and discussed below:

3.2.1 Collection of Data

Data is collected on the designed performa and the detail of respondent is given in Table 3.
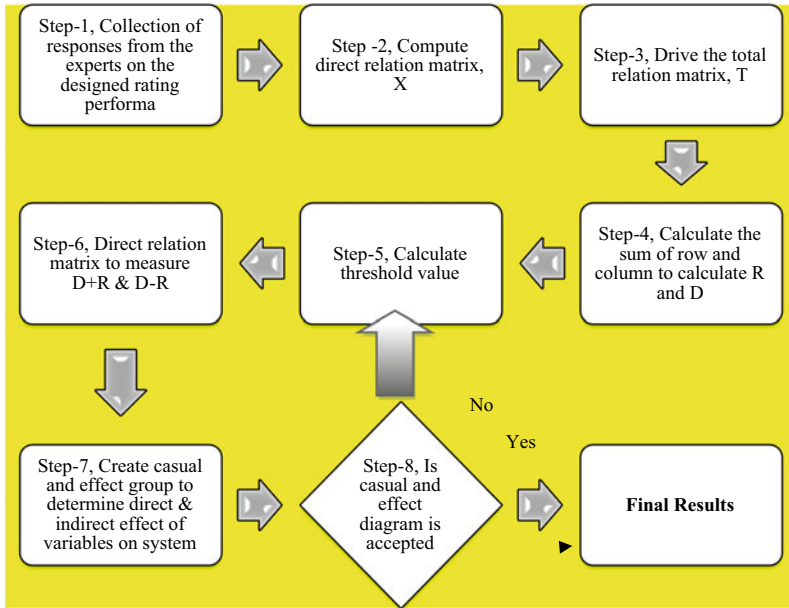
Fig. 1 Research flow chart

3.2.2 Construction of Direct Relation Matrix Using Comparison Scale

After the collection of data from experts, they analyze the effect of one and all rows on the column elements present in the matrix. The direct effect of one on other variables is rated as 0, 1, 2, and 3, which define zero influence, less influence, intermediate influence, and great influence, respectively. The direct relationship matrix was derived from responses collected from the experts. Then the average of these responses was calculated to a generate direct relation matrix and is shown in Table 4.

Table 4 Direct relation matrix

		F_1	F_2	F_3	F_4	F_5
D	F_1	0	2.5	2.17	2	2.5
	F_2	2.33	0	3	2	1.5
	F_3	2.83	2.83	0	2.83	2.67
	F_4	2	2.33	1.83	0	1.83
	F_5	1.5	0.33	1.17	2.17	0

Table 5 Normalized matrix

		F_1	F_2	F_3	F_4	F_5
X	F_1	0	0.24	0.18	0.17	0.23
	F_2	0.23	0	0.27	0.15	0.15
	F_3	0.24	0.27	0	0.26	0.23
	F_4	0.17	0.21	0.20	0	0.18
	F_5	0.14	0.05	0.11	0.18	0

Table 6 Total relation matrix

		F_1	F_2	F_3	F_4	F_5	D
T	F_1	0.56	0.75	0.71	0.69	0.76	3.47
	F_2	0.76	0.58	0.78	0.70	0.72	3.54
	F_3	0.87	0.89	0.66	0.86	0.87	4.14
	F_4	0.68	0.71	0.69	0.52	0.70	3.30
	F_5	0.46	0.40	0.43	0.50	0.35	2.14
	R	3.33	3.32	3.27	3.27	3.38	

3.2.3 Measure the Normalized Matrix, X.

The normalized matrix is determined by dividing every element of the direct relation matrix by the highest value computed after computing the sum, row wise and column wise. The normalized matrix 'X' is as follows in Table 5.

3.2.4 Total Relation Matrix, T

'T' matrix is computed from the normalized matrix by subtracting 'X' with identity matrix 'I', calculating the inverse of this result as '$(I - X)^{-1}$', and multipling $(I - X)^{-1}$ with the 'X' matrix. Calculate the sums of matrix T's rows and columns. The sum of rows and columns in the total relation matrix 'T' is expressed by the term D and R respectively, as in Table 6.

3.2.5 Calculation of Row and Column Sum

The row and column sum are calculated in Table 6 to measure Term R and D.

Table 7 Matrix based on threshold value

	F_1	F_2	F_3	F_4	F_5
F_1	0	0.75	0.71	0.69	0.76
F_2	0.76	0	0.78	0.70	0.72
F_3	0.87	0.89	0	0.86	0.87
F_4	0.68	0.71	0.69	0	0.70
F_5	0	0	0	0	0

Table 8 Final relation matrix

	D	R	$D + R$	$D - R$
F_1	3.47	3.33	6.79	0.14
F_2	3.54	3.32	6.86	0.22
F_3	4.14	3.27	7.41	0.87
F_4	3.29	3.27	6.57	0.02
F_5	2.14	3.38	5.53	−1.25

3.2.6 CalculateThreshold Value

This is determined by calculating the average of 'T' matrix and our research calculated threshold value of 0.664. It helps to determine the internal relationship matrix. The elements of 'T' matrix are compared with the threshold value. Number above threshold value remains as it is in the matrix and lower number is marked 'zero' as shown in Table 7.

3.2.7 Final Relation Matrix

It is calculated by adding and subtracting D and R to determine '$D + R$' & 'D-R'. The terms '$D + R$' and 'D - R' the degree of importance and net effect caused by the variables of PAT on the system, and the final relation matrix is shown in Table 8.

3.2.8 Diagram for Cause and Effect Relationship.

Figure 2 presents the casual and effective as well as interrelated relationship between primary variables of PAT.
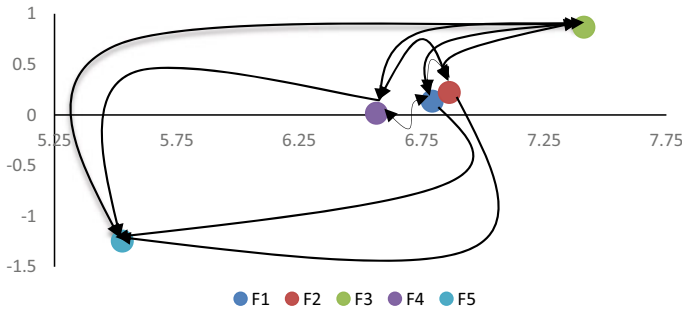
Fig. 2 Causal and effect with Interrelations between primary variables

4 Analysis and Discussion

The DEMATEL approach is used to measure the degree of importance, interrelationship, as well as direct and indirect effects of the variables. Each is represented in the final relation matrix Table 9 in which the term '$D + R$' represents the degree of importance and the '$D - R$' effect generated by variables on production.

Table 9, In the F_1 group, we can see that A_1 and A_4 are the important variables due to obtaining the larger '$D + R$' values, i.e., 11.36 and 10.73, and the least importance goes to A_5 by obtaining a 9.88 minimum value of '$D + R$'. If we talk about the Casual and Effect groups, then after achieving the positive value of '$D - R$' A_1, A_2 and A_5 come in the Casual group and due to the negative value of '$D - R$', A_3, A_4 and A_6 come in the effect group. Based on Fig. 3, A_1, is the most important variable and has a direct effect on the remaining five variables. Nevertheless, A_2 and A_5 also have effects on A_3, A_4 and A_6, and all six variables are related to one another.

Table 9, In the F_2 group, we can see that A_7 and A_9 are the important variables due to obtaining the larger '$D + R$' values, i.e., 8.185 and 7.99, and the least importance goes to A_{11} by obtaining a 7.093 minimum value of '$D + R$'. For the Casual and Effect groups, variables A_7, A_9, and A_{11} after achieving a positive value of '$D - R$' come in the Casual group and due to the negative value of '$D - R$', A_8 and A_{10} come in the Effect group. Based on the Fig. 4, A_7 is the most important variable and has a direct effect on the remaining four variables. Nevertheless, A_9 and A_{11} also have effects on A_8 and A_{10} and all five variables are related to each other.

Table 9, In the F_3 group, we can see that A_{13} and A_{14} are the important variables due to obtaining the larger '$D + R$' values, i.e., 11.224 and 10.619, and the least importance goes to A_{12} by obtaining a 7.465 minimum value of '$D + R$'. For the Casual and Effect groups, variables A_{12}, A_{13}, and A_{14} after achieving a positive value of '$D - R$' come in the Casual group and due to a negative value of '$D - R$', A_{15} comes in the Effect group. Based on the Fig. 5, A_{13} is the most important variable and has a direct effect on the remaining three variables. Nevertheless, A_{12} and A_{14} also have effects on A_{15}, and all four variables are related to each other.

Table 9 Impact of governing variable on principal variables

Principal variable	PAT governing variable	$D - R$	$D + R$
F_1	A_1	0.81	11.36
	A_2	0.96	10.9
	A_3	−0.39	10.24
	A_4	−0.56	10.73
	A_5	0.23	9.88
	A_6	−1.03	10.37
F_2	A_7	0.597	8.185
	A_8	−0.898	7.597
	A_9	−0.301	7.999
	A_{10}	1.44	7.913
	A_{11}	−1.44	7.093
F_3	A_{12}	0.71	7.465
	A_{13}	0.381	11.224
	A_{14}	0.594	10.619
	A_{15}	−1.685	10.238
F_4	A_{16}	1.639	7.009
	A_{17}	0.369	7.784
	A_{18}	−2.007	7.505
F_5	A_{19}	1.677	5.603
	A_{20}	−0.39	6.261
	A_{21}	−1.286	5.129
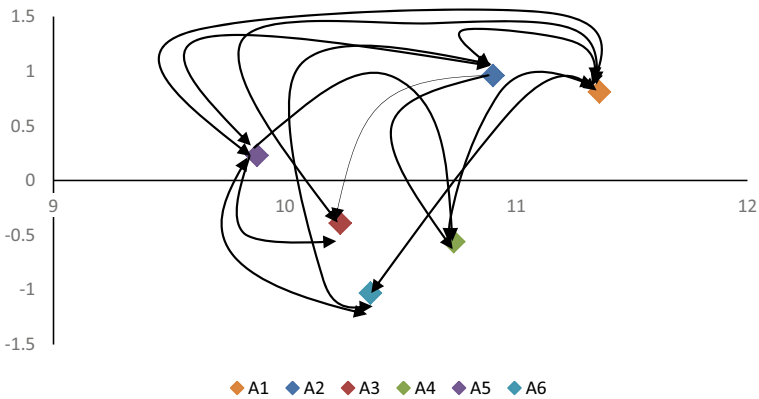
Fig. 3 Causal and effect with Interrelations between variables of F_1
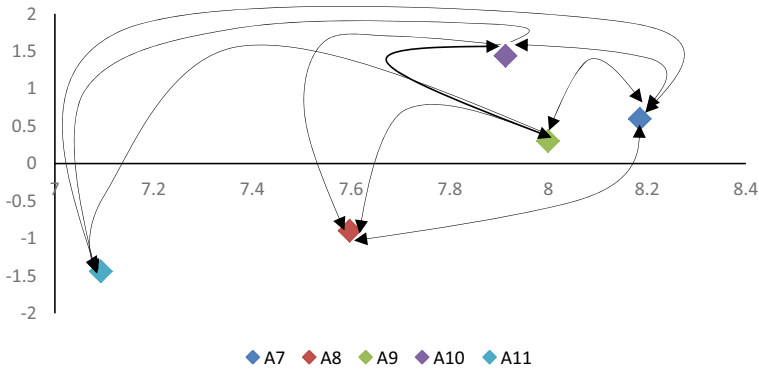
Fig. 4 Causal and effect with Interrelations between variables of F_2
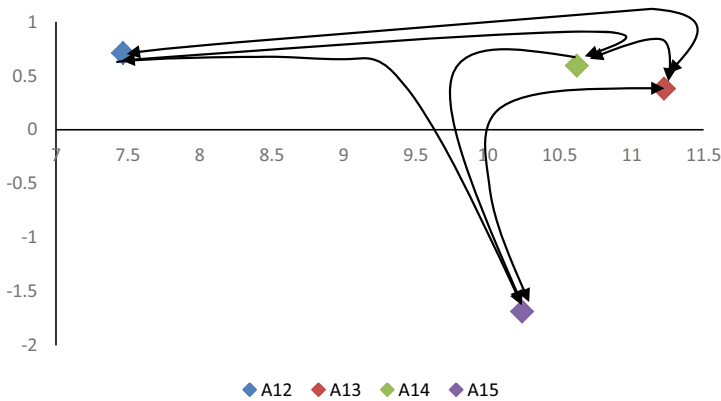
Fig. 5 Causal and effect with Interrelations between variables of F_3

Table 9, In the F_4 group, we can see that A_{17} and A_{18} are the important variables due to obtaining the larger '$D + R$' values, i.e., 7.784 and 7.505, and the least importance goes to A_{16} by obtaining a 7.009 minimum value of '$D + R$'. For the Casual and Effect groups, variables A_{16} and A_{17}, after achieving a positive value of '$D - R$', come in the Casual group, and due to the negative value of '$D - R$', A_{18} comes in the Effect group. Based on the Fig. 6, A_{17} is the most important variable and has a direct effect on the remaining two variables. Nevertheless, A_{16} also has an effect on A_{18}, and all three variables are related to each other.

Table 9, In the F_5 group, we can see that A_{20} and A_{19} are the important variables due to obtaining the larger '$D + R$' values, i.e., 6.261 and 5.603, and the least importance goes to A_{21} by obtaining a 5.129 minimum value of '$D + R$'. For the Casual and Effect groups, variable A_{19}, after achieving a positive value of '$D - R$', comes in the Casual group and due to negative value of '$D - R$', variables A_{19} and A_{21} come in the Effect group. Based on the Fig. 7, A_{20} is the most important variable and has
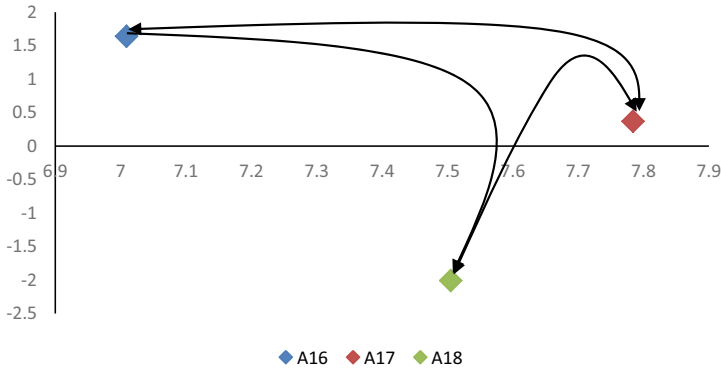
Fig. 6 Causal and effect with Interrelations between variables of F_4
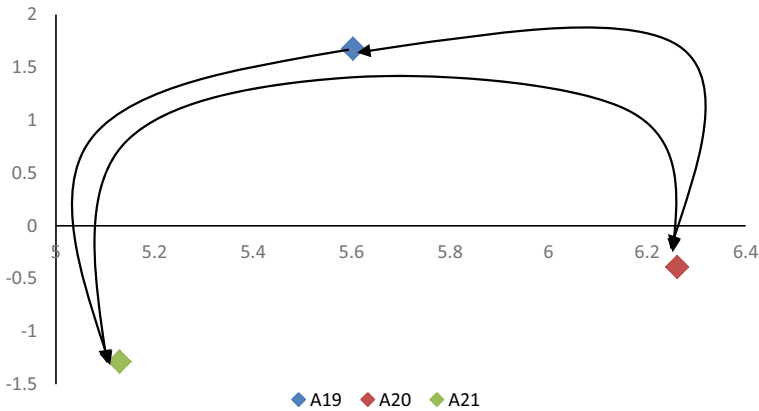
Fig. 7 Causal and effect with Interrelations between variables of F_5

a direct effect on the remaining two variables. Nevertheless, A_{19} also has effects on A_{18} and A_{21}, and all three variables are related to each other.

5 Conclusions, Limitations and Future Scopes

As per the current scenario, demand for hybrid products is increasing day by day. To achieve this desire, manufacturing organizations are enhancing production process configuration by replacing the hardware with software systems. Due to technological advancement, organizations are facing a lot of challenges, which reduce the performance of manufacturing organizations. This research tries to introduce PAT in the manufacturing sector to increase its overall performance. In which, after a detailed study of literature and resonances collected from the experts, twenty six

total variables of PAT are selected. A DEMATEL approach has been applied to prioritize the importance and determine the interrelation between the variables of PAT. This approach also helps to analyse the variables of PAT through casual and effect diagrams.

Results show that, the integration of manufacturing system with maintenance has great importance, as it obtains the higher value of '$D + R$' calculated in final relation matrix Table 9, followed by manufacturing process, fault identification, organization productivity, and organization control. This study also shows that not only the principal variables influence the manufacturing system, but the governing variables have a similar impact on the system. This paper advises industrial organizations to focus more on the prioritized variables which have evolved in our research. Apart from this, the industrial organizations will also have to focus on the other selected variables, as each variable has its own importance. Today industrialists, claim they spend more than 50% of their profit on maintenance. This can be reduced by integration of manufacturing with maintenance, as suggested in this research. This will monitor the functioning of manufacturing activities as well as perform the maintenance simultaneously, reducing the risk of shutdown, production delay and equipment life. This will ultimately not only help to increase the performance but also reduce the maintenance time and cost. This research has its own limitations as its results are based on human knowledge, some of which is incorrect due to misjudgement. Future studies could use other multi-criteria decision-making approaches to validate the results, and the number of responses would be enhanced by connecting more experts from different domains.

References

1. Sharma, S.K.: Maintenance reengineering framework: a case study. J. Qual. Maint. Eng. **19**(2), 96–113 (2013)
2. Chan, F.T.S., Swarnkar, R., Tiwari, M.K.: Infrastructure for coordination of multi-agents in a network-based manufacturing system. Int. J. Adv. Manuf. Technol. **31**, 1028–1033 (2007)
3. Mahesh, M., Ong, S.K., Nee, A.Y.C.: A web-based multi-agent system for distributed digital manufacturing. Int. J. Comp. Integr. Manuf. **20**(1), 11–27 (2007)
4. Schrader, P.G., Lawless, K.A.: The knowledge, attitude, & behavior approach: how to evaluate performance and learning in complex environments. Perform. Improve. **43**(9), 8–15 (2004)
5. Jiao, J., Zhang, W., Zhao, Z., Cha, J.: An integrated intelligent approach to process diagnosis in process industries. Int. J. Prod. Res. **37**(11), 2565–2583 (1999)
6. YuR, I.B., Panetto, H.: A multi-agents based e-maintenance system with case-based reasoning decision support. Eng. Appl. Artif. Intell. **16**, 321–333 (2003)
7. Zhenyou, Z., YiW, K.W.: Intelligent fault diagnosis and prognosis approach for rotating machinery integrating wavelet transform, principal component analysis and artificial networks. Int. J. Adv. Manuf. Technol. **1**(68), 763–773 (2013)
8. Sikorska, J.Z., Hodkiewicz, M., Ma, L.: Prognostic modeling options for remaining useful life estimation by industry. Mech. Syst. Signal Process. **25**, 1803–1836 (2011)
9. Linxia, L., Jay, L.: Design of a reconfigurable prognostics platform for machine tools. Expert Syst. Appl. **37**, 240–252 (2010)
10. Eyandro, L.S.T., Benny, T., et al.: A novel framework to link prognostics and health management and product-service systems using online simulation. Comput. Ind. **63**, 669–679 (2012)

11. Mirabedini, S.N., Hossein, I.: A scheduling model for serial jobs on parallel machines with different preventive maintenance. Int. J. Adv. Manuf. Technol. **70**, 1579–1589 (2014)
12. Zhang, Q., Cheng, L., Boutaba, R.: Cloud computing: state-of the-art and research challenges. J. Inter. Serve Applicant. **1**, 7–18 (2010)
13. Yam, R.C.M., Tse, P.W., Li, L., Tu, P.: Intelligent predictive decision support system for condition-based maintenance. Int. J. Adv. Manuf. Technol. **17**(5), 383–391 (2001)
14. Shaw, C.F., keith, A.S., Kevin, K.J.: Manufacturing planning and predictive process model integration using software agents. Adv. Eng. Inform. **19**, 135–142 (2005)
15. LiX, C.Z., Liang, G., Weidong, L., Xinyu, S.: An agent based approach for integrated process planning and scheduling. Expert Syst. Appl. **37**, 1256–1264 (2010)
16. Cowling, P.I., Ouelhadj, D., Petrovic, S.: A multi agent architecture for dynamic scheduling of steel hot rolling. J. Intell. Manuf. **14**, 457–470 (2003)
17. Brennan, R.W., William, O.: Performance analysis of a mullti-agent scheduling and control system under manufacturing disturbances. Prob. Plan. Cont: Manag. Operat. **15**(2), 225–235 (2004)
18. Xu, Z., Zhao, Z., Baines, R.W.: Constructing virtual environments for manufacturing simulation. Int. J. Prod. Res. **38**(17), 4171–4191 (2000)
19. Shaw, M.J.: Dynamic scheduling in cellular manufacturing systems: a framework for networked decision making. J. Manuf. Syst. **7**(2), 83–94 (2004)
20. Pechoucek, M., Vokrinek, J., Becvar, P.: A multi-agent support for manufacturing decision making. IEEE Intell. Syst. **20**(1), 67–74 (2005)
21. Wörn, H., Längle, T., Albert, M., Kazi, A., Brighenti, A., Seijo, S.R., Christopher Senior Bobi, M.A.S., Collado, J.V.: DIAMOND: distributed multi-agent architechcture for monitoring and diagnosis. Prod. Plan Count. Manag. Operat. **15**(2), 189–200 (2004)
22. Jaime, C.V.: Development in the application of ICT in condition monitoring and maintenance. Comput. Ind. **60**, 1–20 (2009)
23. Muller, A., Crespo Marquez, A., Iung, B.: On the concept of e maintenance: review and current research. Reliab. Eng. Syst. Saf. **93**, 1165–1187 (2008)
24. Weerahandi, S., Kurien, T.V., Sadrian, A.: Estimating and optimizing the efficacy of predictive systems in proactive maintenance. Telecom. Syst. **6**(1), 315–327 (1996)
25. Lin, G.Y.-J., Solberg, J.J.: Integrated shop floor control using autonomous agents. IIE Trans. **24**(3), 57–71 (1992)
26. Santiago, A., Rosa, M.S.: An information system for computer integrated manufacturing systems. Rob. Comp. Integr. Manuf. **13**(3), 217–228 (1997)
27. Ercan, O., Esra, K.T.: A general framework of a reference Model for integrated manufacturing system (REMIMS). Eng. Appl. Artif. Intell. **22**, 855–864 (2009)
28. Xinhua, L., Xiaolong, C., Guomin, S., Bihong, X.: Development of a virtual maintenance system with virtual hand. Int. J. Adv. Manuf. Technol. **70**, 2241–2247 (2014)
29. Huiskonen, J.: Maintenance spare parts logistics: special characteristics and strategic choices. Int. J. Prod. Econ. **71**(1), 125–133 (2001)
30. Yunfei, C., Fengqi, Y., John, M.W.: Hybrid method integrating agent-based modeling and heuristic tree search for scheduling of complex batch processes. Comp. Chem. Eng. **60**, 277–296 (2014)
31. Miltenburg, J., Sparling, D.: Managing and reducing total cycle time: models and analysis. Int. J. Prod. Econ. **46**, 89–108 (1996)
32. Lin, H.F., Lee, G.G.: Impact of organizational learning and knowledge management factors on e-business adoption. Manag. Decis. **43**(2), 171–188 (2005)
33. Maurice, B., Mohamad, Y.J.: Developing an input-output activity matrix (IOAM) for environmental and economic analysis of manufacturing system and logistics chains. Int. J. Prod. Econ. **143**, 589–597 (2013)
34. Changqing, L., Yingguang, L., Weiming, S.: Integrated manufacturing process planning and control based on intelligent agents and multi-dimensional features. Int. J. Adv. Manuf. Technol. **75**, 1457–1471 (2014)

35. Ottaway, T.A., Burns, J.R.: An adaptive production control system utilizing agent technology. Int. J. Prod. Res. **38**(4), 721–737 (2000)
36. Cheeseman, M.J., Swann, P., Hesketh, G.B., Barnes, S.: Adaptive manufacturing scheduling: a flexible and configurable agent-based prototype. Prod. Cont.: Manag. Operat. **16**(5), 479–487 (2005)
37. Yang, J., Deane, R.H.: A lot size reduction model for just-in-time manufacturing systems. Integr. Manuf. Syst. **13**(7), 471–488 (2002)
38. Sharma, S.K., Vishwakarma, S., Nishant, J.: Prognosis agent technology: influence on manufacturing organization. Int. J. Adv. Manuf. Technol. **92**, 135–446 (2017)
39. Chung-Wei, L., Gwo-Hashiung, T.: Identification of a threshold value for the DEMATEL method: using the maximum mean de-entropy algorithm. In: MCDM 2009, CCIS 35, pp. 789–796 (2009)

Deep-Drilling of SS-316L on Orbital EDM with Copper Electrode Tube

Anoop Aggarwal, Gurdyal Singh, Prabhjot Singh, Gaurav Jain, and Sunil Kumar

1 Introduction

With the continuing downsizing of component components in contemporary industries, a strong tendency has emerged to develop efficient techniques for producing high-quality products featuring the drilling of small holes. It creates a cylindrical hole in the substance being drilled. It is a complicated machining method in which a hole is created by spinning a tool against a solid material. Deep drilling means to drill a hole ten times deeper than the hole diameter. In industries that use electronics or computers, such as aerospace, medical, automotive, and micro-fabrication, a process for making small holes is required [1]. Deep-hole drilling is regarded as a difficult operation due to the restricted cutting space, poor cutting conditions, difficult chip-breaking, and chip-removal [2, 3].

Pharmaceuticals, medical implants, marine, biomedical, food processing, aerospace, and the automotive sectors are among the industries that employ SS-316L. These materials have been carefully chosen for biomedical implants such as orthopedic, dental, and joint replacements [4, 5]. The SS-316L material was selected due to its suitability for a range of applications as shown in Fig. 1.

Deep-drilling is traditionally accomplished with a ram-type EDM. However, drilling holes is challenging due to the electrode tube's smaller diameter and length, as well as the wide distance between the workpiece and electrode holder [6, 7]. As a result of this challenge, the experiment was moved to orbital EDM. It's a machining process that allows to drill burr-free holes in a variety of materials, regardless of hardness, as long as they're electrically conductive. In orbital EDM, the electrode-tube rotates about its axis, as well as moves on an orbital trajectory. This creates a large

A. Aggarwal (✉) · G. Singh · P. Singh · G. Jain · S. Kumar
Chitkara University Institute of Engineering and Technology, Chitkara University, Rajpura, Punjab, India
e-mail: anoopagg123@gmail.com

659
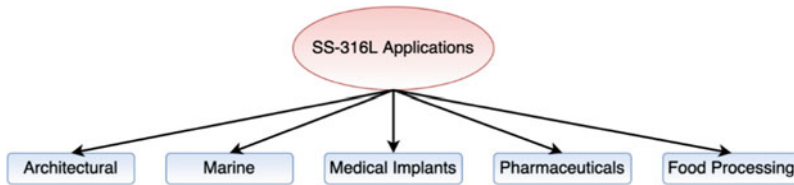
Fig. 1 Applications of SS-316L material

gap between the workpiece and electrode tool that helps in promoting debris flushing from the machining area. This increased flushing aids in reducing tool wear, improves the surface finish, and increases the metal removal rate especially during drilling of deep-holes [8]. Wong et al. [9] investigated the consequences of flushing rates on surface finish and discovered an optimal flow rate for minimizing surface roughness. Singh et al. [10] investigated the graphite powder mixed dielectric medium on the surface properties of super Co-605 by using EDM with graphite tool electrode and found that surface characteristic were significantly affected by machining polarity, peak current, and pulse-on-time. In another study, Aggarwal et al. [11] used the brass electrode on EDM to machine stainless Steel-316L and analyze the effects of process parameters on MRR and EWR.

This work uses Orbital-EDM to deep-drill SS-316L material with a copper electrode-tube. The effect of various governing parameters was discussed to determine their optimum level to achieve maximum MRR along with minimum EWR. As Brass and copper are good conductor of electricity. The experiments on brass electrode-tube had already been conducted by researchers. So, in the present work, copper electrode-tube has been selected for experimentation.

2 Experimentation

The experimental procedure adopted in the present study involved different steps as shown in Fig. 2. The detailed procedure followed has been discussed in the sub-sections.

2.1 Selection and Purchasing of Materials

The material substrate in the form of a circular cross-section with a diameter of 11 mm was procured. The certified list of chemical composition, physical and mechanical properties for the SS-316L as provided by the manufacturer has been listed in Table 1. Optimum parameters are selected through Taguchi L-28 orthogonal array.

Fig. 2 Steps of the experiment
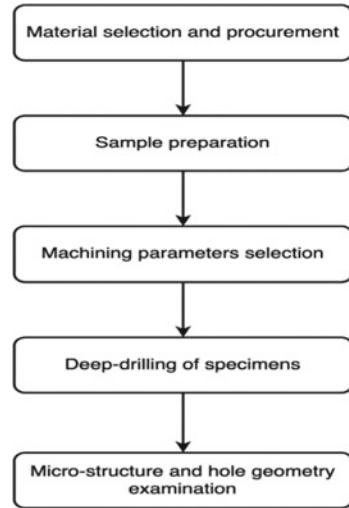
Table 1 Physical, chemical, and mechanical characteristics of the substrate material as received

Composition of chemicals		Mechanical properties	
Chemicals	*%*	*Properties*	*Value*
C	0.08	Tensile strength (MPa)	485
Mg	2	Brinell hardness (HB) max	214
Si	0.75	0.2% proof (MPa) minimum yield strength	172
Cr	16.00–18.00	Rockwell hardness B (HR B) max	93
Ni	10.00–14.00	Minimum elongation (percentage in 50 mm)	41
Mo	2.00–3.00	Tensile strength (MPa)	485
P	0.045		
S	0.03	**Physical properties**	
N	0.1	*Properties*	*Value*
Fe	Balance	Melting Range	1390–1440 °C
		Specific heat 0–100 °C	500 J/kg K
		Density	8.027 g/cm^3

2.2 Sample Preparation

The sample was produced in accordance with ASTM metallographic guidelines. The test specimens were cut from SS-316L substrate and then faced on a lathe machine on both sides to create a smooth surface. Figure 3 shows the final produced sample, which has a diameter of 11 mm and a thickness of 5 mm. Figure 4 depicts the microstructure of SS-316L as photographed by them.

Fig. 3 SS-316L sample
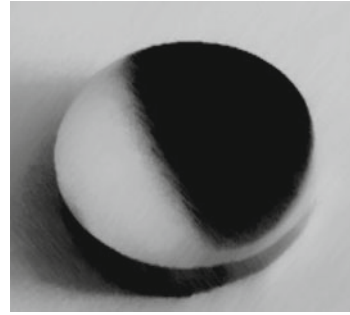
Fig. 4 Microstructure of
SS-316L (500X)
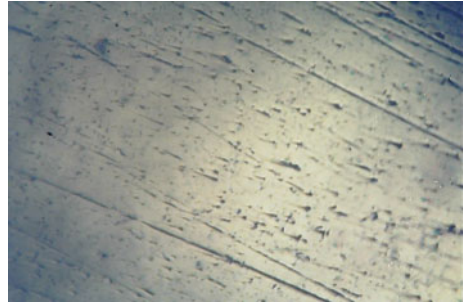
2.3 Machining Parameters Selection

Copper electrode-tube was used as the tool and water was as di-electric fluid during machining. Straight polarity was set with the workpiece as an anode (+ve) and a cathode (-ve) tool. Power supply voltage, pulse duration, peak current are electrical parameters, while the rotational speed of the electrode and dielectric fluid flushing pressure are non-electrical parameters. During deep-drilling of SS-316L material, the effect of pulse duration, supply voltage, fluid flushing pressure and peak current on the output parameters Material Removal Rate (MRR) and Electrode Wear Rate (EWR) was investigated.

MRR is the material removed from the workpiece during the machining process within a specified time interval [12]. It is defined as the ratio of the volume of metal removed volume with respect to time and expressed as mm^3/min (Eq. 1).

$$\text{MRR} = \frac{\text{Volume of metal removed from specimen}}{\text{drilling time}} \tag{1}$$

EWR is the material removed from the electrode-tube during the machining process within a specified time interval [12]. The EWR was calculated in mm^3/min as per the relation given in Eq. (2).

Table 2 Factors that should be considered, along with their significance

S. No.	Parameters of machining	Level		
		1	2	3
1	Peak current, I_p (A)	3	4	5
2	Pulse-on-time, t-on(μs)	3	4	5
3	Duty factor, t	50	60	75
4	Pressure of flushing (kg/cm^2)	0.1	0.3	0.5

$$\text{EWR} = \frac{\text{Initial volume of electrode} - \text{tube material removed during machining}}{\text{drilling time}}$$

$$(2)$$

The polarity or peak current had a greater effect on MRR and EWR as compared to non-electrical parameters. After a thorough examination of the literature, the machining parameters and their corresponding levels were chosen. Wang et al. used seven independent variables classified as electrical or non-electrical [13]. Table 2 shows the machining levels and their parameters finalized for present study.

2.4 Microstructure and Hole Geometry Examination

2.4.1 Microstructure Examination

The samples' microstructure was analyzed to determine if it matched the characteristics mentioned in different standard manuals (ASTM) and published articles. The substrate's microstructure was evaluated in between cutting the specimen after the variables and their levels for experimentation were chosen. Everything was carried out under the supervision of a metallurgical microscope.

2.4.2 Examination of the Drilled hole's Circularity

After conducting the experimentation on orbital EDM, the circularity, overcut, and ovalness of the drilled hole were examined with the tool-maker microscope's (Metzer optical instruments Pvt. Ltd., Mathura, India) various testing of the drilled hole was examined. Dimensions of the holes were measured by using Dewinter Microcam 4.0 software.

3 Discussion and Conclusions

The results of the experimentation work were analyzed, and graphs between various parameters were created in order to get the optimum MRR and EWR. The goal of the research was to figure out what the average values were for various parameters and electrode-tube materials.

3.1 *Process Parameters Effect on EWR.*

Figure 5 depicts the average effect on EWR decreases from 20.845 to 7.913 units as peak current increased from 03 to 05 A. According to the findings, the results at 05 amperes peak current was lesser for EWR. In EWR, lesser will be better, so concluded that the results at 05 A were best.

Figure 6 shows that the average effect on EWR increased from 12.360 to 16.720 units as pulse-on-time increased from 03 to 04 μs. From 04 to 05 μs pulse-on-time, there was a decrease from 16.720 to 16.253 units. According to the data, the outcomes at 03 μs were observed to be less for EWR. Less is better in EWR, therefore the findings at 03 μs were the best.

Figure 7 depicts the average effect on EWR increased from 16.364 to 17.166 units as the duty factor increased from 50 to 60%. From 60 to 75% duty factor, there was a decrease from 17.166 to 12.134 units. According to the findings, the results at 75% duty factor were seen to be lesser for EWR. In EWR, lesser will be better, so the results at 75% duty factor were best.

Figure 8 depicts the average effect on EWR increased from 14.565 to 15.163 units as flushing pressure increased from 0.1 to 0.3 kg/cm^2. From 0.3 to 0.5 kg/cm^2

Fig. 5 Peak current's average effect on EWR
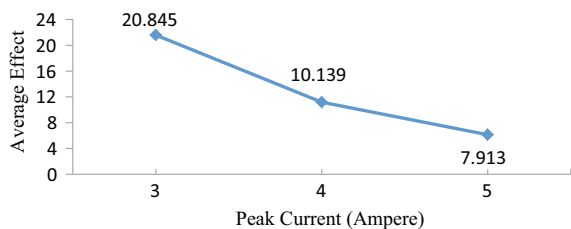
Fig. 6 EWR's average effect of pulse-on-time
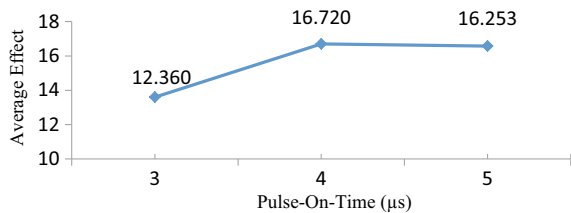
Fig. 7 The average effect of the duty factor on EWR (percentage)
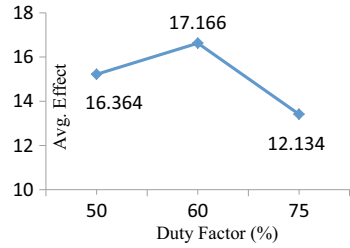
Fig. 8 The influence of flushing pressure on EWR
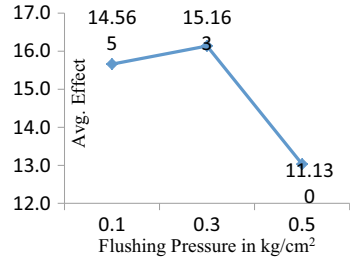
flushing pressure, there was a decrease from 16.163 to 11.130 units. According to the findings, the results at 0.5 kg/cm^2 flushing pressure were determined to be lesser for EWR. Because less is better in EWR, the results at 0.5 kg/cm^2 flushing pressure were the best.

3.2   Process Parameters Effect on MRR.

Figure 9 shows that the average effect on MRR increased from 52.687 to 52.761 units as peak current increased from 3 to 4 A. From 4 A peak current to 5 A peak current, there was a decrease in average impact. At 5 A, the average effect was 50.831 units. The results at 4 A peak current were determined to be greater for MRR, according to the findings. The results at 4 A peak current were best.

Figure 10 shows that the average effect on MRR increased from 52.119 to 54.286 units as the pulse-on-time increased from 3 to 4 μs. From 4 to 5 μs pulse-on-time,

Fig. 9 The average effect of peak current on MRR
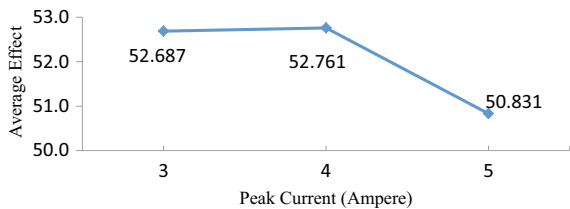
Fig. 10 The influence of
pulse-on time on MRR
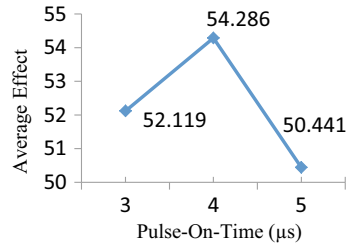
there was a decrease in average impact. At 5 μs, the average impact was 50.441 units. The results at 4 μs were found to be high, according to the findings. As a result, the outcomes are the best at this stage.

As shown in Fig. 11, the average effect on MRR increased from 52.655 units to 54.489 units at 50–60%. From a duty factor of 60–75%, there was a decrease in average impact. The average effect at 75% was observed as 49.167 units. It has been concluded that the average effect value at 60% was high comparatively for MRR. As a result, the outcomes are the best at this stage.

The average effect on MRR was increasing from 52.038 to 53.796 units at 0.1–0.3 kg/cm², as shown in Fig. 12. Decrease in average effect was observed from 0.3 to 0.5 kg/cm² flushing pressure. The average effect at 0.5 kg/cm² was observed as 51.094 units. It has been concluded that for MRR, the average effect value at 0.3 kg/cm² was high. As a result, the findings are the best at this point.

Fig. 11 MRR's average
duty factor effect
(percentage)
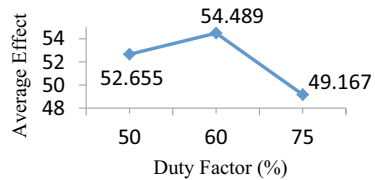
Fig. 12 Flushing pressure's
average effect on MRR
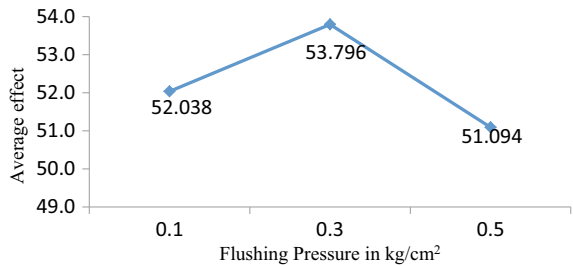
4   Conclusions

At 3-A peak current, the SS-316L workpiece was micro drilled using copper electrode tube material. With 3-A peak current at 50% duty factor, the EWR of SS-316L and copper electrode tubes was greater than 75%, but the MRR of SS-316L and copper electrode tubes was lower. For milling SS-316L workpieces and copper electrode tubes, a 3-A peak current at a duty factor of 75% was found to be optimum. Experiments at cryogenic temperatures using a dielectric other than water will be possible in the future.

References

1. Endo, H., Murahashi, T., Marui, E.: Accuracy estimation of drilled holes with small diameter and influence of drill parameter on the machining accuracy when drilling in mild steel sheet. Int. J. Mach. Tools Manuf **47**, 175–181 (2007)
2. Biermann, D., Bleicher, F., Heisel, U., Klocke, F., Möhring, H.C., Shih, A.: Deep hole drilling. CIRP Ann. **67**, 673–694 (2018)
3. Wang, Z.M., Ezugwu, E.O., Su, D.: Advances in the precision machining of small deep holes. J. Mater. Process. Technol. **68**, 257–261 (1997)
4. Morsiya, C.: A review on parameters affecting properties of biomaterial SS 316L, Australian Journal of Mechanical Engineering (2020) 1–11
5. Lodhi, M.J.K., Deen, K.M., Greenlee-Wacker, M.C., Haider, W.: Additively manufactured 316L stainless steel with improved corrosion resistance and biological response for biomedical applications. Addit. Manuf. **27**, 8–19 (2019)
6. Govindan, P., Joshi, S.S.: Experimental characterization of material removal in dry electrical discharge drilling. Int. J. Mach. Tools Manuf **50**, 431–443 (2010)
7. Han, F., Jiang, J., Yu, D.: Influence of discharge current on machined surfaces by thermo-analysis in finish cut of WEDM. Int. J. Mach. Tools Manuf **47**, 1187–1196 (2007)
8. Bamberg, E., Heamawatanachai, S.: Orbital electrode actuation to improve efficiency of drilling micro-holes by micro-EDM. J. Mater. Process. Technol. **209**, 1826–1834 (2009)
9. Wong, Y.S., Lim, L.C., Lee, L.C.: Effects of flushing on electro-discharge machined surfaces. J. Mater. Process. Technol. **48**, 299–305 (1995)
10. Singh, A.K., Kumar, S., Singh, V.P.: Effect of the addition of conductive powder in dielectric on the surface properties of superalloy Super Co 605 by EDM process. Int. J. Adv. Manuf. Technol. **77**, 99–106 (2015)
11. Aggarwal, A., Singh, P., Singh, G., Kumar, S., Jain, G.: Deep drilling of stainless steel-316L with brass electrode on orbital EDM. In: Advances in Mechanical Engineering, Lecture Notes in Mechanical Engineering, p. 2021. Springer, Singapore (2021)
12. Cyril Pilligrin, J., Asokan, P., Jerald, J., Kanagaraj, G., Mukund Nilakantan, J., Nielsen, I.: Tool speed and polarity effects in micro-EDM drilling of 316L stainless steel. Prod. Manuf. Res. **5**, 99–117 (2017)
13. Wang, C.C., Yan, B.H.: Blind-hole drilling of Al_2O_3/6061Al composite using rotary electro discharge machining. J. Mater. Process. Technol. **102**, 90–102 (2000)

Parametric Optimization of Nanopowder Blended Electrical Spark Machining AISI D3 DIE Steel Employing Grey Relational Analysis

K. Santarao [ID], **C. L. V. R. S. V. Prasad** [ID], **and G. Swaminaidu** [ID]

1 Introduction

In the last few years, amongst available unconventional machining techniques, Electric Spark Machining (ESM) has gained prominence due to its effectiveness in machining precise, complex shapes with special micro-features on difficult-to-cut tools, die and mould materials irrespective of their hardness [1–4]. This process relies on the restrained thermal erosive effect on the stock surface, wrapped up by a dielectric, due to inveterate sparks struck in the inter-electrode gap [5]. This approach is now widely implemented by tool as well as dies, motor, aerospace and surgical equipment manufacturers [6]. Despite astounding process capacities, low volumetric material extraction rates, as well as poor surface quality, are some of the limitations linked to conventional electrical discharge machining. To address these issues, researchers worldwide have implemented three methods. In the foremost approach, termed Powder Blended Electric Spark Machining (PBESM), fine powder either in micro or nano size is suspended in the dielectric, which enhances homogeneous sparking amongst powder particles, forming shallow craters on the workpiece's surface. Also, the ploughing action of conductive material in dielectric fluid enhances the material extraction rate [7]. In the second method, the tool is rotated, which flushes debris accumulated within the discharge gap, thereby improving the material withdrawal rate [8]. The third method is to vibrate the workpiece, which reduces the machining time [9]. The first method, out of the three, provides a higher quality machined surface and adds functional features to the machined surface [10].

K. Santarao (✉) · C. L. V. R. S. V. Prasad

Department of Mechanical Engineering, GMR Institute of Technology, Rajam, India

e-mail: santarao.k@gmrit.edu.in

G. Swaminaidu

Department of Metallurgical Engineering, JNTU-GV College Of Engineering, Vizianagaram, India

Unlike traditional Electric Spark Machining, Powder Blended Electric Spark Machining has a different machining technique [11]. Upon applying 80–320 V voltage in the gap of 25–50 μ present between the electrode and the workpiece, an electric voltage in the range of 105–107 V/m is generated. Due to this, the powder particles not only gain energy but also assemble themselves in a crisscross series fashion, forming an interlock among them [12]. This series configuration promotes linking the discharge gap. Also, the developed electric field accelerates the charged particles to behave like conductors, which not only props up the breakdown but also increases the spark gap. Owing to the linking effect, a diminution in dielectric insulating strength is observed. A premature explosion occurs in the gap due to a developed 'short circuit'. In turn, the applied fine-grained powder changes (expands and broadens) the plasma channel. Thus, the sparks are consistently dispersed among the powdered particles, diminishing the spark's electric density. As a result, craters up to a small depth are produced on the workpiece's exterior surface. This enriches the surface finish [7].

Early in 1980 Erden and Bilgin [1] stated that intentionally added artificial impurities to dielectric has a significant effect on EDM performance. Since then, several researchers focused on investigating the influence of artificial additives in dielectric when machining materials through electric spark machining. Baljinder Singh [2] deliberated the effect of 325 μm aluminium powder in the dielectric fluid along with other electrical parameters on H11 steel surface roughness employing L18 array and reported that polarity, suspended powder play a major role in the response. Abhishek Abrol [3] mixed 45–55 μm chromium powder in kerosene to examine the simultaneous influence of powder along with pulse on time, peak current and pulse off time when machining AISI D2 die steel and found that current is the momentous factor for MRR and TWR. Mohd. Junaid Mir [4] presented the discharge current, pulse time and aluminium powder (46 μm) concentration optimized levels for surface roughness study on H11 steel and published that concentration and peak current are major influencing parameters targeting surface roughness. Suspending 37, 44 and 74 μm sized aluminium powder of quantities 0–12 g/L in EDM oil supplied by the manufacturer Anil Kumar et al. [5] fabricated circular holes on Inconel 718 using copper electrode. It is stated that powder concentration and size influenced EDM efficiency. It was also mentioned that highest Material Removal Rate (MRR) is obtained for 44 μm powder at 6 g/L concentration. Kansal et al. [6] utilized 0–6 g/L quantity of 20–30 μm aluminium powder into kerosene available commercially to machine Al-10%SiCp material for 40 min time. MRR was reported to be increased by the addition of aluminium powder up to a particular concentration (3 g/L). Also, it was stated that most influential parameters on the performance of EDM are peak current and concentration of added powder.

In another attempt by Kansal et al. [7] to optimize process parameters utilizing Taguchi design, 25 mm diameter blind holes were drilled on AISI D2 Die steel when dipped in kerosene doped with 0–4 g/L 30 μm silicon powder. It was highlighted that effect of nozzle flushing at inter-electrodes gap on machining efficiency is negligible. For SKD-11, Tzeng Yih-Fong et al. [8] claimed 70–80 nm powder blended Hercules ED 320H had better surface finish. MP Jahan et al. [9] machined cemented tungsten

carbide with 55 nm Gr blended ELF EDM3 oil. GS Prihandana et al. [10] used ultrasonicated 55 nm Gr blended kerosene on silver-tungsten and reported improved surface quality. 40–47 nm SiC and 45–55 nm Al2O3 blended Idemistu Daphene cut oil on stainless mould steel reduced the average surface roughness, according to PC Tan et al. [11]. Houriyeh Marashi et al. [12] accomplished that 40 to 60 nm Ti powder mixed hydrocarbon oil led to an MRR improvement of D2 steels.

An examination into literature accessible on PBESM, it is pragmatic that only elementary research exertion has been conceded in improving machining efficiency of PBESM. Hence, current research exertion concentrates on multi-characteristic optimization whilst machining AISI D3 steel by means of copper tool with and without ceramic nanopowder suspended in commercially available EDM oil using Taguchi Method coupled with Grey Relation Analysis.

2 Experiment Set-Up and Method

2.1 Machine

The experiments were carried out on the Electric Discharge Machine S-50 ZNC of ELECTRONICA MACHINE TOOLS (Pvt. Ltd). In this machine, several input variables can be varied. This machine has a machining tank that holds 140 L of EDM oil. A new experiment set-up for Nano Powder Blended ESM (NPBESM) is developed to lessen the quantity of dielectric utilized and to avoid filtering system damage owing to nanopowder clogging in filters. For a detailed description of the same, the readers are encouraged to refer article published by the author [13].

2.2 Workpiece, Electrode and Powder Material

AISI D3 die-Steel block of 45 mm × 32.5 mm × 12 mm is used as workpiece. Copper of dimensions 150 mm × ϕ9.5 mm is considered as tool in this experimentation. SiC (Conductive) of 50 nm size was obtained from SRL Pvt. Ltd., India for this study.

2.3 Parameters and Experiment Plan

Four quantitative process variables, each with three levels as listed in Table 1 are considered for experimentation. It could require a whole of eighty-one (3^4) sets of experiments to optimize the variables if a full factorial design is carried out [14] which remains a significant challenge.

Table 1 Process variables and levels

Process variable, technical form, (Units)	Code	Levels		
		L1	L2	L3
Powder concentration, PC, (g/L)	N	0	0.5	1
Gap voltage, Vg, (V)	M	50	60	70
Pulse on time, T_{ON}, (μs)	X	50	100	150
Peak current, Ip, (A)	K	5	6	7

Table 2 Actual values in L9 orthogonal array

Experiment trail	Ip (A)	Ton (μs)	Vg (V)	PC (g/L)	Decision matrix [D]		
					MSR (mm^3/min)	EWR (mm^3/min)	SR (μm)
1	5	50	50	0	0.45	0.074	6.575
2	5	100	60	0.5	1.31	0.187	4.550
3	5	150	70	1	0.77	0.374	5.105
4	6	50	60	1	1.17	0.374	4.630
5	6	100	70	0	0.70	0.299	4.555
6	6	150	50	0.5	1.41	0.224	4.720
7	7	50	70	0.5	1.60	0.112	4.975
8	7	100	50	1	0.45	0.074	6.575
9	7	150	60	0	1.31	0.187	4.550

To overcome this issue, the Taguchi approach employs orthogonal arrays that are meant to consider the whole parameter space and its impact on response with a small number of tests [15, 16]. As suggested by Datta et al. [17] and Harmesh Kumar et al. [18] an L9 orthogonal array was used in this study. Throughout the experiments, positive polarity, 30 min machining time, 10% duty factor are fixed. The levels of the process variables are fixed after conducting pilot experiments. L9 orthogonal array with actual values is presented in Table 2. Each machining case was repeated three times to minimize the error.

3 Machining Performance Assessment

Material Subtraction Rate (MSR), Surface Roughness (SR) and Electrode Wear Rate (EWR) are selected as responses. The difference in weights of workpiece and tool, before and after experimentation are measured on SHIMADZU (AUX 200) analytical balance, respectively. Numerical values are then substituted in Eqs. (1) and (2) [19] to calculate MSR and EWR

Fig. 1 AISI D3 die-steel
workpieces after machining

$$\mathrm{MSR} = \frac{[(W_{\mathrm{bm}} - W_{\mathrm{am}}) \times 1000]}{(D_w \times t)} \tag{1}$$

$$\mathrm{EWR} = \frac{[(E_{\mathrm{bm}} - E_{\mathrm{am}}) \times 1000]}{(D_e \times t)} \tag{2}$$

where MSR, EWR is in mm^3/min, W_{bm}—workpiece weight prior to machining (g), W_{am}—workpiece weight subsequent to machining (g), D_w—density of the workpiece (7.7 g/cm^3), E_{bm}—weight of electrode/tool ahead of machining (g), E_{am}—weight of electrode/tool past machining (g), D_e—density of the electrode/tool (8.9 g/cm^3), t—machining time (minutes).

Surface Roughness (SR) is formulated as SR $= \frac{1}{S} \int_0^S |h(z)dz|$ where $h(z)$ is the value of roughness profile, and S is evaluation length. It is measured along horizontal, vertical diameters on the face of blind holes by means of Mitutoyo make (SJ-201) surface roughness tester and the average value is considered for analysis. Experimental findings are shown in Table 2. Workpieces after machining with all sets of experiments are presented in Fig. 1.

4 Results and Discussion

4.1 Grey Relational Technique

Grey Relation Technique (GRT) is an important technique that simplifies a complex multi-response optimization to optimization of Single Response Grey Relational Grade (SRGRG). This approach was initially established by Deng [20] and then has been efficiently employed in several disciplines of machining processes.

B Satyanarayana [21] applied Taguchi procedure together with grey relational technique to find out effective levels of feed, depth of cut and speed when performing

simultaneous minimization of cutting force, surface roughness and tool flank wear. Tamrin [22] employed grey relational technique to establish optimum levels of power consumed, stand-off distance and welding speed for multi-performance (mean weld width, mean kerf width, weld tensile strength) analysis in Carbon Dioxide laser unification of disparate materials.

In an attempt to perform multi-response optimization of wear characteristics of a hybrid composite, Saravanakumar [23] used grey relational analysis. In another effort to model and optimize multi-response milling characteristics Murat Sarıkaya [24] implemented Taguchi coupled with Grey Relational Analysis.

As a result, GRT was discovered to be used in a variety of machining applications. On the other hand, literature on multicriteria optimization of NPBEDM variables implementing GRT is still in developing stage. In the current experimental exploration, the grey relation method is employed to determine the most favourable process input variables that give high MRR with superior surface finish in NPBEDM of tool steel. Determining GRG (Grey Relational Grade) is the key point of GRT. Four steps involved to find out GRG for a multi-objective optimization are stated in Fig. 2 followed by a brief explanation of each step.

4.2 Decision Matrix Formation

In this stage, an $m \times n$ decision matrix [D] is constructed where m and n represent a number of experiment trails and performance response values, respectively. Here $m = 9$ and $n = 3$ (MSR, EWR and SR). [D] is shown in Table 2.

4.3 Data Pre-processing

Each numeral (y_{ij}) in Decision matrix [D] is normalized to scale down between 0 and 1 incorporating strategies (3) and (4).

$$\text{Higher-the-better } x_{ij} = \frac{\left(y_{ij} - \min\left(y_{ij}\right)\right)}{\left(\max\left(y_{ij}\right) - \min\left(y_{ij}\right)\right)} \tag{3}$$

Table 3 Normalized values and grey relational coefficients of responses

Experiment trail	Normalized values			Grey relational coefficients		
	MSR	EWR	SR	MSR	EWR	SR
1	0.000	1.000	0.007	0.333	1.000	0.335
2	0.748	0.623	1.000	0.665	0.570	1.000
3	0.278	0.000	0.728	0.409	0.333	0.648
4	0.626	0.000	0.961	0.572	0.333	0.927
5	0.217	0.250	0.998	0.390	0.400	0.995
6	0.835	0.500	0.917	0.752	0.500	0.857
7	1.000	0.873	0.792	1.000	0.798	0.706
8	0.870	0.373	0.794	0.793	0.444	0.708
9	0.652	0.980	0.000	0.590	0.962	0.333

$$\text{Smaller-the-better } x_{ij} = \frac{\left(\max(y_{ij}) - y_{ij}\right)}{\left(\max(y_{ij}) - \min(y_{ij})\right)} \tag{4}$$

where $y_{ij} = j$th performance response for ith trail, $\max(y_{ij})$ and $\min(y_{ij}) = $ maximum and minimum values of all jth performance responses. $x_{ij} = $ normalized numeral. Table 3 depicts normalized values for the EWR, MSR and SR.

4.4 Grey Relational Coefficient Calculation

Using normalized SNR values found in the preceding stage, the Grey Relational Coefficients (GRCs) of performance responses are calculated after substituting in the Eq. (5) [25].

$$\gamma\left(x_{0j}, x_{ij}\right) = \frac{\Delta_{\min} + \xi \Delta_{\max}}{\Delta_{ij} + \xi \Delta_{\max}} \text{for } i = 1, 2, \ldots, m \text{ and } j = 1, 2, \ldots .n \tag{5}$$

where $x_{0j} = $ reference value of jth response ($x_{0j} = 1$), $\Delta_{ij} = |x_{0j} - x_{ij}|$, $\Delta\max = \max\{\Delta_{ij}, i = 1, 2, \ldots, m; j = 1, 2, \ldots n\}$, $\Delta\min = \min\{\Delta_{ij}, i = 1, 2, \ldots, m; j = 1, 2, \ldots n\}$ and $\xi = $ distinguishing coefficient, $\xi \in (0, 1]$. In common $\xi = 0.5$ is applied when calculating GRCs [19, 25]. Table 3 depicts GRC values for the EWR, MSR and SR.

4.5 Grey Relational Grade Calculation

Grey Relational Grade is the approach used to quantify grey relational interstice. A Grey Relational Grade, often known as a degree, is a partisan sum of Grey Relational Coefficients that is frequently computed using Eq. (6) [25].

$$\varsigma_i = \left(\frac{1}{n}\right) \sum_{k=1}^{n} \gamma(k) \tag{6}$$

where ς_i is Grey Relational Grade for ith experiment, k is experimental trial. Table 4 depicts GRGs evaluated employing (6).

A careful observation of Fig. 3 reveals that GRG for the 7th experiment is highest which equals to 0.835 indicating that the related experiment outcome is near to the best-normalized value and has the preeminent multi-performance characteristics amongst nine experiments.

The mean of the grey relation grade for a unique level of machining criteria is computed using MINITAB 17 software and listed in Table 5. Whilst the values in end row of Table 5 are collated, it is spotted that the variation amid the highest and least value of GRG for N is bigger than other factors. This stipulates that SiC nanopowder blending has a compelling effect on multi-performance characteristics. From Table 5, it is also observed that $K_3X_1M_2N_2$ is the condition for higher GRG, i.e. optimal setting for higher MSR, lower Electrode Wear Rate and Surface Roughness (Table 5).

Table 4 Grey relational grades of responses

Experiment trail	Grey relational grade	Rank
1	0.556	8
2	0.745	2
3	0.463	9
4	0.611	6
5	0.595	7
6	0.703	3
7	0.835	1
8	0.648	4
9	0.628	5

Fig. 3 Variation in GRG for all nine trails
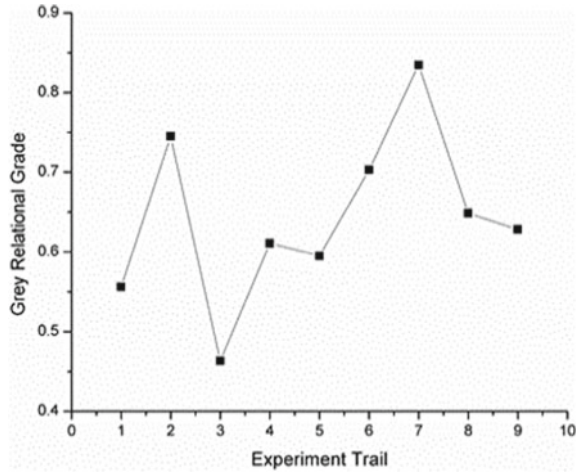
Table 5 Average GRG by parameter Level

	Machining parameters	K	X	M	N
Average GRG by parameter level	L1	0.5882	**0.6672**	0.6358	0.5931
	L2	0.6363	0.6628	**0.6614**	**0.7608**
	L3	**0.7037**	0.5982	0.6310	0.5742
	High-Low	0.1156	0.0690	0.0304	0.1866

Higher GRG corresponding to a unique level for each parameter are highlited in bold

Table 6 GRG results substituting initial and best favourable machining criteria

	Preliminary machining criteria	Optimal machining criteria	
	$K_1X_1M_1N_1$	Predicted $K_3X_1M_2N_2$	Experimental $K_3X_1M_2N_2$
Grey relational score	0.556	0.865	0.866

4.6 Affirmation Test

As the most favourable machining criteria levels are identified, the concluding step includes verifying the enhancement in performance characteristics. The Grey Relational Grade involving best possible levels of the machining criteria can be estimated using Eq. (7) [23].

$$\hat{\alpha} = \alpha_m + \sum_{i=1}^{q}(\overline{\alpha}_i - \alpha_m) \tag{7}$$

Table 6 presents verification experiment results using optimal conditions. It is evident from Table 6 that multitude performance assessors in NPBESM process significantly enhanced employing Grey Relation Procedure.

5 Conclusions

The Grey Relational Analysis procedure is employed to attain optimized governing factors levels of NPBESM involving multifarious-performance assessors namely Material Subtraction Rate, Surface Roughness and Electrode Wear Rate. Taguchi L9 orthogonal arrangement was incorporated for the experiment work. Observations from the present work are as follows:

The optimum levels of process parameters are peak current 7 Amp, Pulse On Time 50 µs, Gap Voltage 50 V in addition to powder concentration 0.5 g/L. These are typically the endorsed levels of parameters for acquiring increased material amputation, a lesser wear on electrode and in addition, reduced surface roughness.

It is instituted that nano powder blending has more substantial influence on performance assessors when compared with other considered parameters.

Experiments executed with above stated optimal levels affirmed an appreciable enhancement not only in machining effectiveness but also on grey relation grade.

The above study comprehends that the optimization of complex multi-functional properties can be simplified by Taguchi procedure coupled with Grey Analysis.

References

1. Erden, A., Selahattin, B.: Role of impurities in electric discharge machining. In: Proceedings of the Twenty-First International Machine Tool Design and Research Conference (pp. 345–350). 8th-12th Sept, Swansea (1980). https://doi.org/10.1007/978-1-349-05861-7
2. Sing, B., Singh, P., Tejpal, G., Singh, G.: An experimental study of surface roughness of H11 Steel in EDM process using copper tool electrode. Int. J. Adv. Eng. Technol. **3**, 130–133 (2012)
3. Abrol, A., Sharma, S.: Effect of chromium powder mixed dielectric on performance characteristic of AISI D2 Die steel USING EDM. Int. J. Res. Eng. Technol. **4**, 232–246 (2015)
4. Mir, M.J., Sheikh, K., Singh, B., Malhotra, N.: Modeling and analysis of machining parameters for surface roughness in powder mixed EDM using RSM approach. Int. J. Eng. Sci. Technol. **4**, 45–52 (2012)
5. Kumar, A., Maheshwari, S., Sharma, C., Beri, N.: Analysis of machining characteristics in additive mixed electric discharge machining of nickel-based super alloy inconel 718. Mater. Manuf. Process. **26**, 1011–1018 (2011). https://doi.org/10.1080/10426914.2010.527415

6. Kansal, H.K., Singh, S., Kumar, P.: An experimental study of the machining parameters in powder mixed electric discharge machining of Al 10%SiCP metal matrix composites. Int. J. Mach. Mach. Mater. **1**, 396–411 (2006). https://doi.org/10.1504/IJMMM.2006.012349

7. Kansal, H.K., Singh, S., Kumar, P.: Effect of silicon powder mixed EDM on machining rate of AISI D2 die steel. J. Manuf. Process. **9**, 13–22 (2007). https://doi.org/10.1016/S1526-6125(07)70104-4

8. Yih-Fong, T., Fu-Chen, C.: Investigation into some surface characteristics of electrical discharge machined SKD-11 using powder-suspension dielectric oil. J. Mater. Process. Technol. **170**, 385–391 (2005). https://doi.org/10.1016/j.jmatprotec.2005.06.006

9. Jahan, M.P., Rahman, M., Wong, Y.S.: Study on the nano-powder-mixed sinking and milling micro-EDM of WC-Co. Int. J. Adv. Manuf. Technol. **53**, 167–180 (2011). https://doi.org/10.1007/s00170-010-2826-9

10. Prihandana, G.S., Mahardika, M., Hamdi, M., Wong, Y.S., Mitsui, K.: Accuracy improvement in nanographite powder-suspended dielectric fluid for micro-electrical discharge machining processes. Int. J. Adv. Manuf. Technol. **56**, 143–149 (2011). https://doi.org/10.1007/s00170-011-3152-6

11. Tan, P.C., Yeo, S.H., Tan, Y.V.: Effects of nanopowder additives in microelectrical discharge machining. Int. J. Precis. Eng. Manuf. **9**, 22–26 (2008)

12. Marashi, H., Sarhan, A.A.D., Hamdi, M.: Employing Ti nano-powder dielectric to enhance surface characteristics in electrical discharge machining of AISI D2 steel. Appl. Surf. Sci. **357**, 892–907 (2015). https://doi.org/10.1016/j.apsusc.2015.09.105

13. Santarao, K., Prasad, C.L.V.R.S., Swaminaidu, G.: Influence of dominant variables and their optimization for nano powder blended EDM process. Indian J. Eng. Mater. Sci. (2019)

14. Thiagarajan, C., Sivaramakrishnan, R., Somasundaram, S.: Modeling and optimization of cylindrical grinding of Al/SiC composites using genetic algorithms. J. Brazilian Soc. Mech. Sci. **34**, 32–40 (2012)

15. Ranjit, K.R.: A Primer on the Taguchi Method. Society of Manufacturing Engineers (2010)

16. Phillip J, R.: Taguchi Tecgniques for Quality Engineering. McGraw-Hill (2005)

17. Datta, S., Bandyopadhyay, A., Pal, P.K.: Application of Taguchi philosophy for parametric optimization of bead geometry and HAZ width in submerged arc welding using a mixture of fresh flux and fused flux. Int. J. Adv. Manuf. Technol. **36**, 689–698 (2008). https://doi.org/10.1007/s00170-006-0894-7

18. Kumar, H., Davim, J.P.: Role of powder in the machining of Al-10%Sicp metal matrix composites by powder mixed electric discharge machining. J. Compos. Mater. **45**, 133–151 (2011). https://doi.org/10.1177/0021998310371543

19. Talla, G., Gangopadhyay, S., Biswas, C.K.: Multi response optimization of powder mixed electric discharge machining of aluminum/alumina metal matrix composite using grey relation analysis. Procedia Mater. Sci. **5**, 1633–1639 (2014). https://doi.org/10.1016/j.mspro.2014.07.351

20. Julong, D.: Introduction to grey system theory. J. Grey Syst. **1**, 1–24 (1989)

21. Satyanarayana, B., Janardhana, G.R., Rao, D.H.: Optimized high speed turning on Inconel 718 using Taguchi method based Grey relational analysis. Indian J. Eng. Mater. Sci. **20**, 269–275 (2013)

22. Tamrin, K.F., Nukman, Y., Sheikh, N.A., Harizam, M.Z.: Determination of optimum parameters using grey relational analysis for multi-performance characteristics in CO_2 laser joining of dissimilar materials. Opt. Lasers Eng. **57**, 40–47 (2014)

23. Saravanakumar, A., Sasikumar, P., Harisagar, P.T., Balachandar, N., Kavin, M.: Multi response optimization of wear properties of hybrid composite using grey relational analysis. Int. J. Appl. Eng. Res. **10**, 5840–5848 (2015)

24. Sarıkaya, M., Yılmaz, V., Dilipak, H.: Modeling and multi-response optimization of milling characteristics based on Taguchi and gray relational analysis. Proc. Inst. Mech. Eng. Part B J. Eng. Manuf. **230**, 1049–1065 (2016)

25. Marichamy, S., Saravanan, M., Ravichandran, M., Veerappan, G.: Parametric optimization of electrical discharge machining process on α–β brass using grey relational analysis. J. Mater. Res. **31**, 2531–2537 (2016). https://doi.org/10.1557/jmr.2016.213

Study the Influences of Various Input Variables on Material Removal Rate During μEDM Machining of Super Alloy Material

Sudhansu Ranjan Das and Anshuman Das

1 Introduction

In various industrial sectors, such as biomedical, defense, aerospace, space, automotive, transportation and other production industries, micro-products are playing the vital role nowadays. There are mainly two reasons which are available for which the demand of micro-product in different industries are increasing day by day. One is industrial safety and other is pollution. As less energy is required in the production of micro-holes. So there is a chance of less pollution and more safety can be obtained. Various manufacturing processes are involved to produce the micro-products, micro-EDM is one of them. The range of size involved in micro-products is varying from 1 to 999 microns. There are basically two types of micro-machining processes, one is tool based and other is mask based. Surface roughness below 0.1 μ can be achieved with micro-EDM. Thermal energy which is generated through electrical energy is mainly responsible. The major restriction involved in micro-EDM process is only conductive material can be machined through micro-EDM process. It is a non-contact type machining process, there is a spark gap which is present between electrode and work piece. Hard to cut and difficult to machine materials are normally preferred to be machined through this process. Steels, graphite and conductive materials are normally preferred. The major difference between the EDM and micro-EDM is the radius of plasma channel which is developed at the time of spark. The intensity of peak energy during the spark is limited for the material removal. Small electrodes and wire used in this process. The efficiency, precision and spark energy depend upon the use. The dimensions considered for the test specimen, i.e. 30 * 30 * 2.6 mm

S. R. Das
Veer Surendra Sai University of Technology, Burla, Odisha 768018, India

A. Das (✉)
DIT University, Dehradun, Uttarakhand 248009, India
e-mail: anshuman.das2009@gmail.com

are unique. The range of parameters selected is unique. After conducting the experiments, electrode was ground to remove the taper part. By which with a minimum number of electrodes, we have cover up many experiments. By which tool cost was minimized.

2 Literature Review

The following literatures have been considered in the current experimental investigations for the analysis of experimental outcomes. Sakpal [1] conducted the micro-EDM machining operation on Titanium alloy using a Cu-W electrode. From the results, it was found that voltage, capacitance and rotation of electrode played a key role in MRR enhancement. Capacitance and pulse on time are found to be dominant for taper ratio. Moreover, capacitance and pulse on time are found to be dominant for side gap. Bhosle et al. [2] analyzed the taper angle during micro-electro discharge machining-assisted drilling of Inconel 600. Capacitance was found to be the most dominating parameter rather than voltage and feed rate. Saxena et al. [3] examined the impact of three machining variables on several responses such as material removal rate (MRR), radial over cut (ROC) tool wear ratio (TWR), residual stress and surface roughness. All the input parameters are found to be significant on the responses. Dong et al. [4] examined the aspect ratio of micro-holes which was machined on C17200 Beryllium Copper. Machining was performed using two dielectric fluids. And machining was conducted with different current levels. Various responses are examined like machining speed, electrode wear, dia and taper angle. Results delineated that deionized water-based machining was more effective than kerosene based. Various machining characteristics like MRR, quality of micro-holes, electrode wear and machining time were studied by Plaza et al. [5] when Titanium alloy was machined. From the experiments, it was found that electrode at a helix angle of $45°$ and flute length of $50\ \mu$, the machining time was reduced by 37% and hole of $800\ \mu$ dia was achieved. On Nitinol Titanium-based shape memory alloy, micro-EDM machining operation was conducted by Vijay Abu et al. [6]. The experimental outcomes showed that MRR was greatly affected by capacitance, tool material and voltage. Satyanarayana et al. [7] studied the effect of various machining parameters on different machining attributes while machining metal matrix composites. From the experimental results, some interesting outcomes are observed like MRR increased with current. When electrode was rotating at higher speed, responses like, MRR, TWR and surface finish increased. Polarity and tool materials are the insignificant parameters on MRR. The micro-structure of the machined surface was studied by Kim et al. [8] from the graphical analysis, it was confirmed that feed and depth of cut were inversely proportional to each other regarding the machined micro-morphology. Dillip et al. [9] predicted the material removal through a numerical technique during micro-EDM of Inconel-718. Both numerical and experimental results are compared, and it was found both results are compatible to each other with a minimum error. Sivaprakasam et al. [10] experimentally investigated the

nano-powder-assisted micro-wire EDM process on Inconel-718. Kerf width, material removal rate and surface roughness are considered as responses. Voltage, capacitance and powder concentration are the input parameters. With the presence of graphite nano-powder, better results are obtained.

2.1 Research Gap

The following three research gap was found:

- Very few μ-EDM machining was observed on Inconel-718.
- Response surface methodology (RSM) methodology has not been employed by the researchers in a large scale.
- Cu-W (Copper and Tungsten)-based electrode has not been used in a large scale by the researchers particularly in micro-EDM.

3 Experimental Details

3.1 Selection of Work Piece Material

In the current experimental work, Inconel-718, in the form of plates is considered. Because its application is quiet vital in the aerospace industries. This type of super alloy has adequate properties like thermal, mechanical and physical. That's why it is used to manufacture various parts of a turbo jet or air craft. The dimension of the plate was 30 * 30 * 2.6 mm. The figure of the work piece before and after machining is shown in Fig. 1.

(a) Before machining   **(b)** After machining
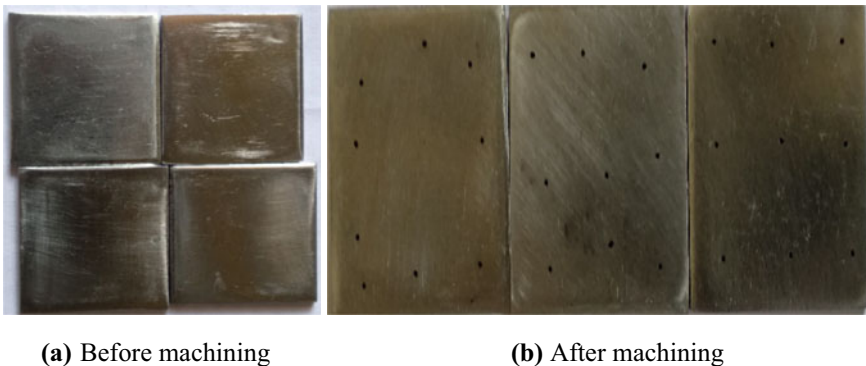
Fig. 1 Work piece before and after machining
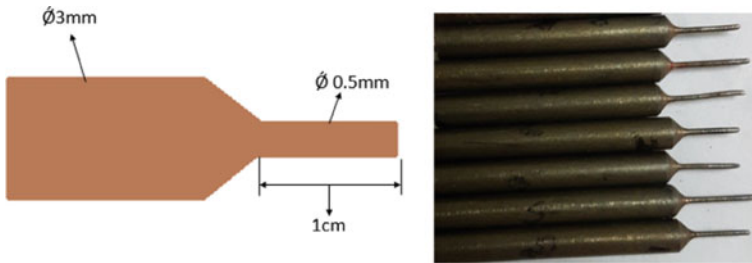
Fig. 2 Electrode design and shape of electrode after machining

3.2 Selection of Tool Material

A Copper-Tungsten (Cu-W)-based electrode material was selected in this work, 30% Copper and 70% Tungsten utilized. In nonconventional machining, the selection of electrode material is quiet important. The cutting tool is shown in Fig. 2.

After machining, particularly in micro-EDM, the tapering will be there in the electrode. So without changing the electrode, it is very difficult to conduct the second run. Maximum authors have changed the tools after each experimental run. And as we know tool cost significantly influences the total cost of machining. In the current experiment, after each run, the tool was removed by cutting and then ground. By which with the minimum numbers of electrodes, we are able to conduct 27 experiments resulting minimizing the tool cost which is important in present scenario.

3.3 RSM-Based Experimental Planning

The experimental layout was framed according to response surface morphology (Box–Behnken design) using Minitab 17 statistical software. Four types of input variables are selected like "current, pulse on time, pulse off time and spark gap". Each variable was differed at three levels like low (−1), medium (0) and high (1) given in Table 1 Das et al. [11]. Total 27 no. of experiments is conducted. The EDM machined used in the current experimental work shown in Fig. 3.

Table 1 Machining parameters with their levels

S. No.	Process parameter	Low level (−1)	Medium level (0)	High level (1)
1	Current	2	4	6
2	Pulse on time	10	15	20
3	Pulse off time	5	10	15
4	Spark Gap	40	50	60
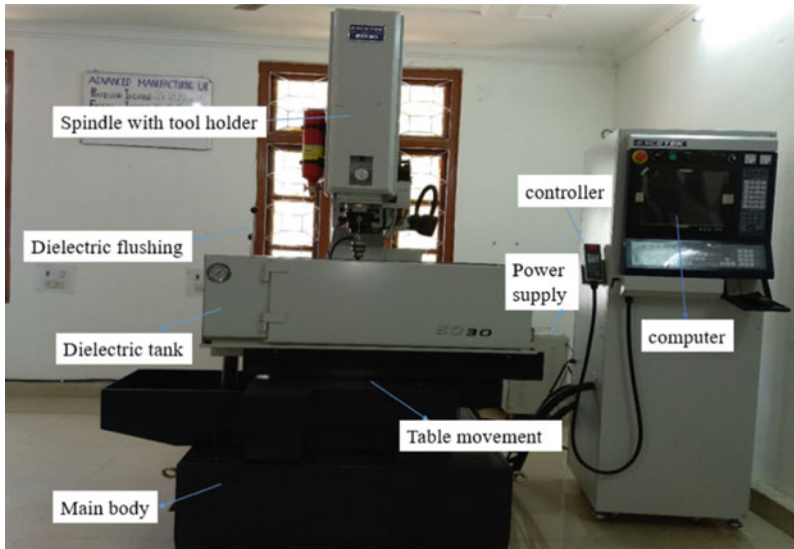
Fig. 3 Experimental setup

4 Results and Discussion

4.1 Measurement of Material Removal Rate (MRR)

On the basis of mass, i.e. (gm/min), the MRR was estimated with the help of weight measuring machine as shown in Fig. 4. The least count of the machine was 0.001 gm. Material removal rate was defined as the quantity of material removed from the surface of the specimen in a unit time under the given condition of machining. The MRR was tabulated in Table 2. The MRR was measured in the given formula shown in Eq. 1.

Before machining weight in gm $= W_1$

After machining weight in gm $= W_2$

Time required for machining, t (min)

Material removal rate is given by gm/min.

$$\text{MRR} = \frac{W_1 - W_2}{t} \tag{1}$$

A second-order mathematical model was developed using both input and output variables to set a correlation between them which is shown in Eq. 2. The output parameter was taken as MRR and four machining variables are considered like
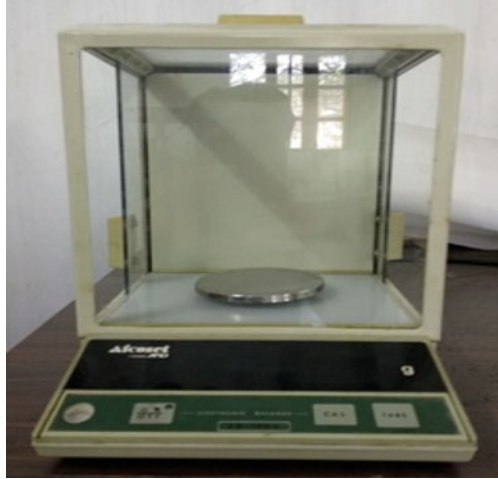
current, pulse on time, pulse off time and spark gap. The coefficient of determination was found as $R^2 = 96.12$ for experimented and for adjusted, it were found as 91.59%. Regression analysis is done from the experimental data to obtain the quadratic model. The equation is given below for MRR.

$$
\begin{aligned}
1.\text{MRR} \times 10^{-4} = {} & 19.1 + 3.42 * \text{Current} - 2.472 * \text{Pulse on time} \\
& - 0.420 * \text{Pulse off time} + 0.081 * \text{Spark gap} \\
& - 0.406 * \text{Curent}^2 - 0.0428 * \text{Pulse on time}^2 \\
& - 0.0223 * \text{Pulse off time}^2 - 0.00788 * \text{Spark gap}^2 \\
& + 0.2432 * \text{Current} * \text{Pulse on time} \\
& - 0.2453 * \text{Current} * \text{Pulse off time} \\
& + 0.0104 * \text{Current} * \text{ Spark gap} \\
& + 0.0565 * \text{Pulse on time} * \text{Pulse off time} \\
& + 0.0465 * \text{Pulse on time} * \text{ Spark gap} \\
& + 0.0134 * \text{Pulse off time} * \text{Spark gap}
\end{aligned} \tag{2}
$$

4.2 Analysis Variance (ANOVA)

To check the variables affecting the output responses significantly ANOVA analysis was conducted, which is tabulated in Table 3.

Summary of the above model

Table 2 Observation table

S. No.	Current (Amp)	Pulse on time (μs)	Pulse off time (μs)	Spark gap (μmm)	MRR × 10⁻⁴ (gm/m)
1	4	15	15	40	8.04
2	2	15	10	40	6.161
3	2	20	10	50	6.19
4	4	20	5	50	12.42
5	4	20	10	60	16.19
6	2	15	10	60	10.22
7	6	10	10	50	12.35
8	4	15	10	50	14.83
9	6	15	5	50	20.04
10	4	10	15	50	10.517
11	6	20	10	50	18.55
12	4	15	15	60	12.71
13	4	10	5	50	14.28
14	2	15	15	50	9
15	2	15	5	50	7.7769
16	6	15	10	40	13.56
17	4	20	15	50	14.31
18	4	20	10	40	9.409
19	4	15	10	50	14.33
20	6	15	15	50	11.45
21	4	10	10	60	10.73
22	4	15	5	40	14.73
23	4	15	5	60	16.73
24	4	10	10	40	13.24
25	2	10	10	50	9.72
26	4	15	10	50	14
27	6	15	10	60	18.451

S	R-sq	(Adjusted R-sq (Predicted)	R-sq
1.06331	96.12%	91.59%	77.99%

Table 3 ANOVA analysis table (material removal rate)

Source	Degrees of freedom	Adjusted sum of square	Adjusted mean square	F-value	P-value	Remarks
Model	14	335.877	23.991	21.22	0.000	Significant
Linear	4	240.632	60.158	53.21	0.000	Significant
Current	1	171.257	171.257	151.47	0.000	Significant
Pulse on time	1	3.236	3.236	2.86	0.116	
Pulse off time	1	33.167	33.167	29.33	0.000	Significant
Spark Gap	1	32.971	32.971	29.16	0.000	Significant
Square	4	15.978	3.994	3.53	0.040	Significant
Current * Current	1	14.089	14.089	12.46	0.004	Significant
Pulse on time * pulse on time	1	6.114	6.114	5.41	0.038	Significant
Pulse off time * pulse off time	1	1.663	1.663	1.47	0.248	
Spark Gap * spark gap	1	3.308	3.308	2.93	0.113	
2-way interaction	6	79.268	13.211	11.68	0.000	Significant
Current * pulse on time	1	23.668	23.668	20.93	0.001	Significant
Current * pulse off time	1	24.074	24.074	21.26	0.001	Significant
Current * spark gap	1	0.173	0.173	0.15	0.702	
Pulse on time * pulse off time	1	7.989	7.989	7.07	0.021	Significant
Pulse on time * spark gap	1	21.581	21.581	19.09	0.001	Significant
Pulse off time * spark gap	1	1.782	1.782	1.58	0.233	
Error	12	13.568	1.131			
Lack of fit	10	13.218	1.322	7.57	0.122	Not significant
Pure error	2	0.349	0.175			
Total	26	349.44				

Fig. 5 Material removal rate versus current and pulse on time
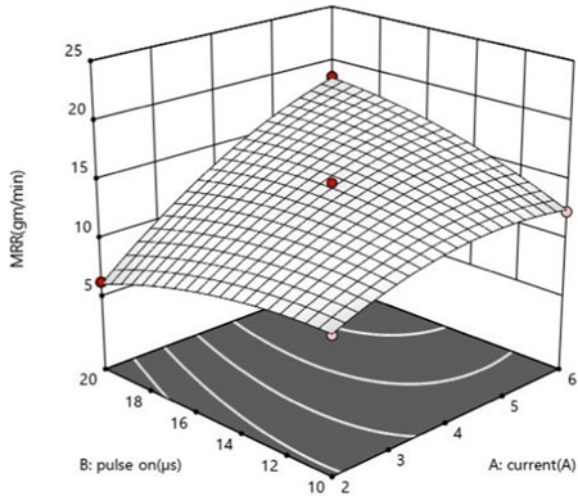
4.3 Effect of Input Variables on Material Removal Rate

With the increment in both current and pulse on time, MRR increased which is shown in Fig. 5. Low MRR was observed, when pulse on time was at high level and current was at low level. But current was observed to be the dominating parameter for MRR as shown in the surface plot. The thermal loading is mainly depends upon the current, which influences the material removal rate. Higher the current, more temperature will be generated and from both the terminals, material removal rate will be increased. Spark generated between the electrode and work piece and the intensity of the spark mainly influenced by the carbon deposition. Inappropriate sparks mainly depend upon the carbon deposition. If pulse off time will be more, the carbon deposition will be less resulting more MRR.

The material removal rate was enhanced with the increment of current and with decrement of pulse off time which is shown in Fig. 6. MRR was high when current was high and pulse off time was low. When current was low and pulse off time was low, low MRR was obtained. Because when current will be low, the flow of current will be also lower between the two electrodes resulting less thermal energy. Current was observed to be the most significant parameter for material removal rate from the graph.

Ehen current was increased and spark gap was increased, MRR was increased which shown in Fig. 7. When gap was at highest level and current was at highest level, maximum MRR was found. And with low current and low gap, low MRR was observed. Current and spark gap are two influential factors for the MRR increment. Because the flow of dielectric fluid mainly depends upon the spark gap. If spark gap will be proper, the flow will be proper and adequate thermal energy can be obtained between the two terminals.

Fig. 6 Material removal rate versus current and pulse off time
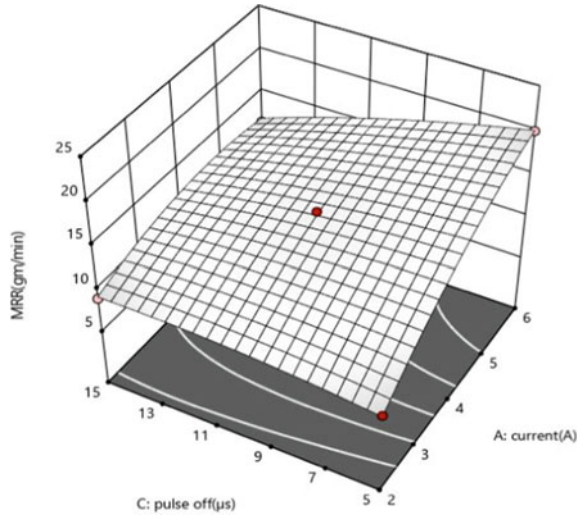
Fig. 7 Material removal rate versus current and spark gap
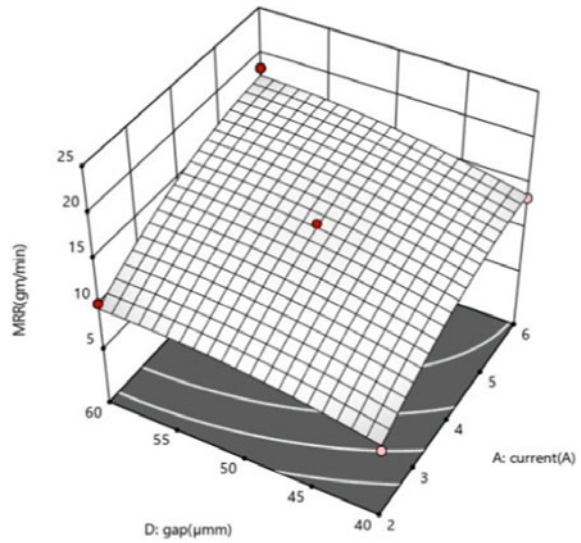
One interesting phenomena was observed regarding the pulse on and pulse off time. The MRR was found to be highest with the lowest value of both pulse on and pulse off time. However, minimum MRR was observed at lowest pulse on and highest pulse off time shown in Fig. 8. Regarding the MRR, both the pulse on and pulse off time were found to be the insignificant parameters.

Fig. 8 Material removal rate versus pulse on time and pulse off time
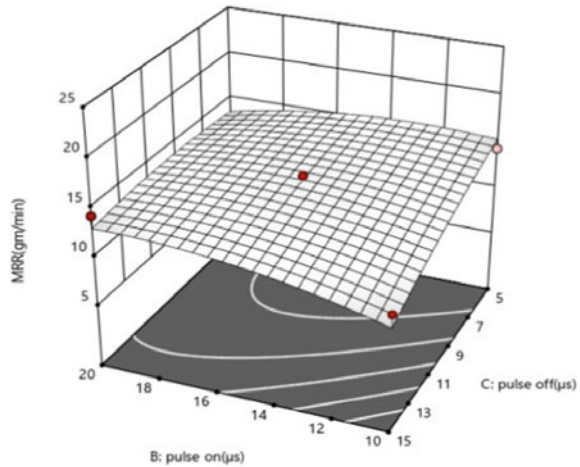
5   Conclusions

In the current experimental work, the prime motive is to analyze the impact of four various types of machining variables on the material removal rate. Depending on the experimental results, the conclusions are given below:-

MRR increased with increment in current. Both pulse off time and gap influenced the MRR. Highest MRR was achieved with 6Amp current. More roughness was there with high MRR. However, heat-affected zone was less with highest MRR.

References

1. Sakpal, U., S., Jagtap, S., P.: Optimization of micro EDM drilling process parameters for titanium alloy by rotating electrode. Procedia Manuf. **20**(1), 119–126 (2018)
2. Bhosle, B., R., Sharma, B., S.: Multi objective optimization of micro EDM drilling process of Inconel 600 alloy. Mater. Today Proc. **4**(2), 1988–1997 (2017)
3. Saxena, K.K., Agarwal, S., Khare, K.S.: Surface characterization, material removal mechanism and material migration study of Micro EDM process on conductive SiC. Procedia CIRP. **42**(1), 179–184 (2016)
4. Dong, S., Wang, Z., Wang, Y., Liu, H.: An experimental investigation on enhancement of surface quality of micro holes for be-cu alloys using micro EDM with multi diameter electrodes and different dielectrics. Procedia CIRP. **42**(1), 257–262 (2016)
5. Plaza, S., Sanchez, A.J., Perez, E., Gil, R., Izquierdo, B., Ortega, N., Pombo, L.: Experimental study on Micro EDM drilling of TiAl4V using helical electrode. Precision Eng. **38**(4), 821–827 (2014)
6. Babu, V.T., Ravishankar, D.V., Koorapati, D.E.P.: Investigation of process parameters in micro EDM machining. Int. J. Innov. Res. Sci. Eng. Technol. **3**(10), 1–14 (2014)
7. Satyanarayana, K.G., Rajadurai, A., Mohan, B.: Effect of SiC and rotation of electrode on electric discharge machining of Al-SiC composites. J. Mater. Process. Technol. **124**(3), 297–304 (2002)

8. Lim, H., S., Wong, Y., S., Rahman, M., Lee, M., E.: A study on the machining of high aspect ratio micro structures using micro EDM. Microsyst. Technol. **8**(6), 395–401 (2002)
9. Dillip, D.G., John, G., Panda, S., Mathew, J.: Finite-volume-based conservative numerical scheme in cylindrical coordinate system to predict material removal during micro-EDM on Inconel 718. **42**(90), 1–18 (2020)
10. Sivaprakasam, P., Hariharan, P., Gowri, S.: Experimental investigations on nano powder mixed micro wire EDM process of inconel-718 alloy. **1**, 1–26 (2019)
11. Das, A., Pradhan, S., Das, R, S., Analysis on hole overcut during micro-EDM of Inconel 718. 1–7 (2022)

Artificial Neural Network Model for the Evaluation of Tensile Strength of Vibratory-Assisted TIG Welded Aluminium Weldments

M. Vykunta Rao, Kothakota Purushotham, and M. V. A. Raju Bahubalendruni

1 Introduction

Magnesium and aluminium alloys are joined using tungsten inert gas welding process. Weld pool is protected from the atmospheric contaminants by the inert gas. Manual metal arc welding is completely replaced by TIG welding for the joining of aluminium and magnesium alloys. The generation of residual stresses during the welding process is a regular occurrence. This is because of different temperatures maintained on the specimen. Residual stresses cause the material to deform, resulting in fatigue failure. By using vibration-assisted welding, residual stresses can be reduced. The specimens to be welded are vibrated in dual modes during vibration-assisted welding. The first is to vibrate the specimen during welding at its normal frequency and the second is vibrating the specimen other than the natural frequency. P. G. Rao et al., created a prediction model using a generalized regression computational model to build a relationship with vibration parameters like input vibromotor voltage, vibration duration and vibratory weldment impact resistance and bending strength. A comparison is made with experimental data to validate the practicality of the created prediction tool [1, 2]. Soft computing techniques gained more attention in recent times. Compressive strength of fused deposition models has been estimated using two approaches one is general regression neural network (GRNN) and the other is multi-gene genetic algorithm by taking raster angle, thickness of layer and orientation as an input parameter [3]. GRNN-based estimation model was created

M. Vykunta Rao (✉) · K. Purushotham
Department of Mechanical Engineering, GMR Institute of Technology, Rajam, Andhra Pradesh, India
e-mail: vykuntarao.m@gmrit.edu.in

M. V. A. Raju Bahubalendruni
Department of Mechanical Engineering, National Institute of Technology Puducherry, Karaikal, India
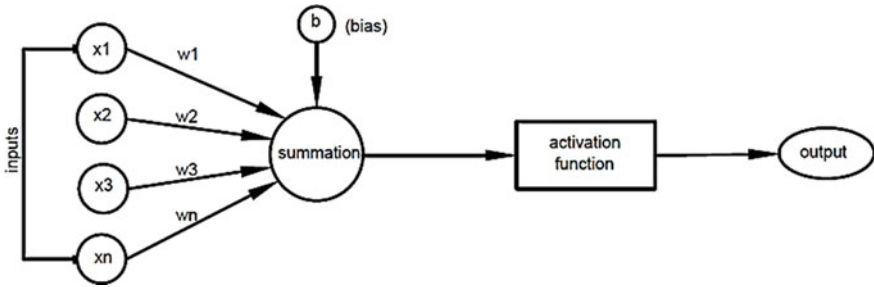
Fig. 1 Outlook of neuron [7]

to evaluate the tensile strength of aluminium 5052-H32 aluminium alloy weldments for the given vibromotor voltage input and the specimen vibration time [4].

Humans will have little effort in recognizing various objects from a vast amount of visual information in their surroundings. Pattern recognition is made possible through human intelligence. Computing systems will get benefitted if this human intelligence is transferred. The term 'artificial neural network' refers to computer systems whose fundamental concept is inspired by biological neural networks [5]. McCulloch and Walter Pitts (1943) proposed artificial neural network computation systems. Figure 1 shows the outlook of neuron. Computing networks in ANN are parallel that share some basic properties with biological neural systems. Similar to our biological neurons, multiple input signals are given to neurons. Each input has a certain relative weight that influences the output. Similar to the biological neuron systems, some inputs are more important than other inputs so these are combined to form an impulse. The intensity of the input signal is determined by weights, which are adjustable coefficients inside the network. The summation block, which approximately corresponds to the actual cell body, produces the neuron's output signal by adding all of the weighted inputs algebraically [6]. ANN has several applications, i.e. recognition of patterns, the prediction of parameters, optimization, associative memory and controls.

ANN model was used to evaluate the safety of shiwalik slopes in the region of the Himalayan [8]. Slope stability analysis has greater importance in designing infrastructure projects in residual soil. Authors designed an ANN model for slope stability and observed the reliability of the model by considering several performance indicators such as co-efficient of determination, root mean square error (RMSE) [8]. In India, pedestrian fatal crash frequency is more. ANN model developed to predict the pedestrian fatal crash frequency at the junctions. Three different learning algorithms were used to develop ANN model. by the trial and error method, number of neurons was varied. Finally, sensitivity analysis conducted and found that motorized vehicle speed has the most significant impact on fatal pedestrian collisions [9]. Researchers extended their work to estimate the wind power output, speed of the wind and direction of wind using multilayer feed-forward technique, support vector regression and adaptive neuro-fuzzy interference for a given pressure, temperatures,

Fig. 2 TIG welding of aluminium welded joints [13]

relative humidity and local time [10]. ANN was used as an intelligent system to review the performance and prediction levels of solar energy systems [11]. Previous studies reveal that artificial neural networks are thus helpful in building the relationship between several input parameters and the output parameters with less cost. An attempt is made to develop an artificial neural network model for the prediction of the tensile strength of 5052 H32 aluminium alloy weldments for a given voltage of the vibromotor and time at which the specimen is vibrated.

2 Experimentation

For the experiment, Aluminium 5052 H32 alloy specimens are considered for vibration welding. Vibratory welding setup has a platform that is vibrated and unbalanced eccentric circulating vibromotor. Figs. 2 and 3 show the tungsten inert gas welding of aluminium welded joints. Vibrations are applied to the specimen via an unbalanced vibromotor, a surface plate and the springs that support the vibration platform. The voltage of the vibromotor is controlled to vibrate the specimens at varying frequencies and amplitudes. Vibrating the specimen causes the molten weld pool to oscillate, resulting in the production of reduced dendritic structure. Rao et al., discussed the complete experimentation in detail [12, 13]. The focus of this study is to create an ANN model to predict ultimate tensile strength (i.e. output) for a particular vibromotor voltage and the specimen vibration time.

3 Artificial Neural Network

The ANN Learning algorithm is made up of three layers: input, hidden and output. In the input layers, there will be input nodes, which provide information to the network. Input layers pass the information to the hidden nodes. Other than passing the data to the hidden layer, computations are not performed on the input nodes. Every node in the following adjacent layer to another node and each connection has a given
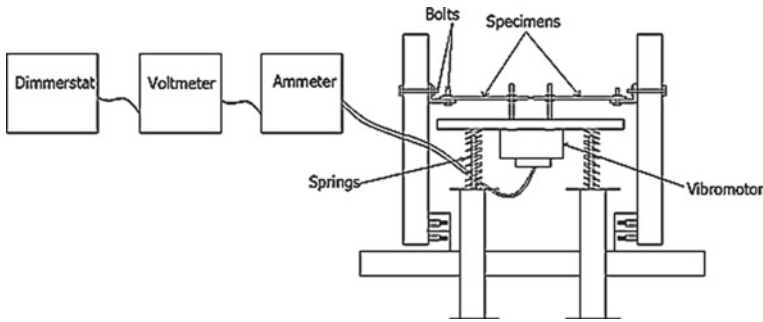
Fig. 3 Vibratory welding setup [12]

weight. A neuron's weight was calculated by how essential it is in contrast to other impulses. Layers that are hidden between input and output are known as hidden layer. Hidden nodes achieve computations and transfer information to the output nodes. If the number of hidden layers increases, the longer time it takes to produce output so that complex problems can be solved. Output illustrates the response of input layer with respect to the hidden layer.

3.1 ANN Training Process

In this, ANN has been modelled to obtain the connection among the voltage input to the vibromotor and time of vibration to the ultimate tensile strength of aluminium alloy weldments. The time of vibration and voltages to the vibromotor are the input parameters and UTM is the output parameter for the ANN. ANN requires three sets of data sets, i.e. training, validation and testing data sets. With the 57 experimental data sets, 47 random data sets are considered for training and validation and the remaining 10 sets are for testing.

Feed-forward back propagation algorithm used for ANN model is shown in Fig. 4. In the feed-forward network, the signals only travel in one direction, i.e. toward the output. Backpropagation is the method in which the weights are fine-tuned based on the rate of error in the previous iteration so that reliability of the model will enhance. Levenberg-Marquardt method (L-M method) selected as a learning algorithm. Trainlm is a network training function that updates weight and bias values based on L-M method [14]. Any network may be trained using the Trainlm function as long as its weight, net input and transfer functions include derivative functions. Tansig is a function of transfer. Transfer functions compute the output of a layer based on its net input.

The feed-forward is the most often used approach for neural network training is backpropagation algorithm. It is a best method for prediction. In this, the difference between the desired and actual output is propagated back to the layers, i.e. from the

input layer   hidden layers   output layer

if the ouput is deviated more than required
than it will throw back error which will
change weights and bias to fit data
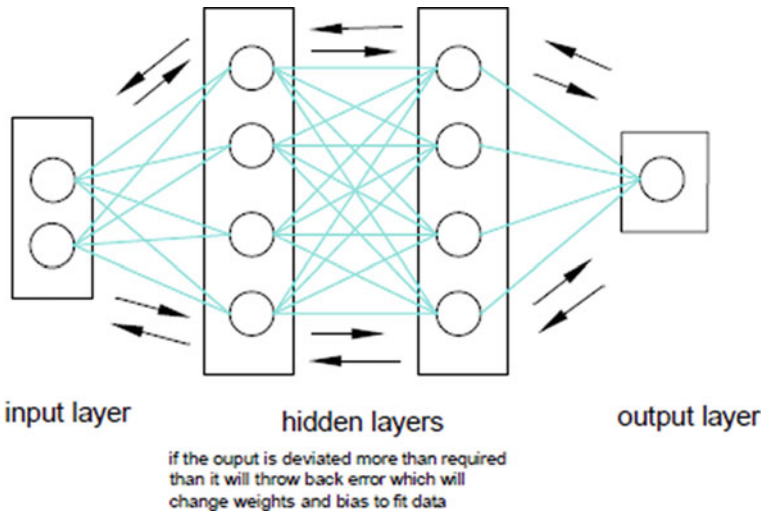
Fig. 4 Feed-forward back propagation algorithm [9]

output layers to hidden and hidden layers to input and the corresponding weights are changed. An epoch is a cycle that progresses from input to output and from output to input. Network model is trained by giving known input and output data. The network continues through several epochs like this until the error is within a given tolerance. This training procedure provides weights to all of the neurons in all of the layers. As a result, the weights produced from a trained network are utilized to calculate the network's output to unknown data.

Bias function (b_q) is added to the product of weight (W_{pq}) between the neuron 'p' to the hidden layers neuron 'q' and input layers each input to obtain the net input (I_q) is given in eq. (1).

$$I_q = \sum_{p=1}^{n} x_p W_{pq} + b_q \tag{1}$$

Tansig activation function (eq.(2)) passes net input to hidden layer to create output y_q in Eq. (3). From the hidden layer, the output signal y_q is sent to all 'r' neurons in the output layer O_r and calculates the input to the r neurons of the output layer is O'_r in Eq. (4). Weight w'_{qr} is the connection between the 'q' neuron in the hidden layer to the 'r' neuron of the output layer and the bias is b'_r. It calculates the output layer signals using Eq. (5) [7].

$$f(I) = \frac{2}{1 + e^{-2I}} - 1 \tag{2}$$

$$y_q = f(I_q) \tag{3}$$

Fig. 5 Training data set
percentage deviation
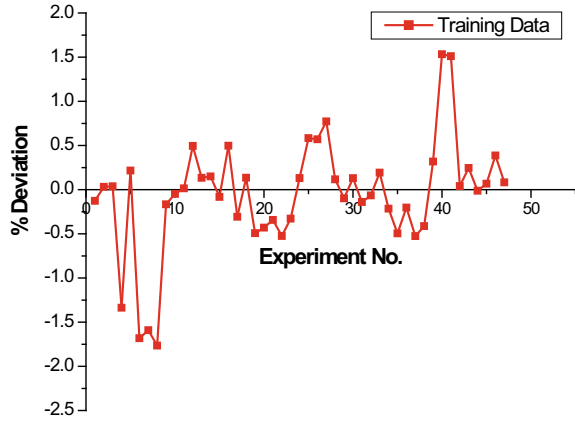
$$O'_r = \sum_{q=1}^{h} y_q w'_{qr} + b'_r \tag{4}$$

$$O_r = f(O'_r) \tag{5}$$

4 Results and Discussions

The ANN estimate model for estimating the tensile strength (UTS) of weld joints has been built in the training. From the literature the experimental data is considered as input for the ANN model. Training data percentage deviations are shown in Fig. 5. 47 number of experimental used as training data. The prepared ANN model shows the maximum percentage deviation as -1.765, i.e. prepared model is 98.23% accurate for training data. Figure 6 shows the testing data set percentage deviation. From Fig. 6 the maximum percentage deviation in the testing data is 2.22%. As a result, the created model can estimate ultimate tensile strength with 97.77% accuracy for an unknown voltage input to the vibromotor and vibration period.

5 Conclusions

ANN model developed to understand the relationship between tensile strength (UTS) of vibratory-assisted aluminium weldments to vibromotor voltage input and vibration time during welding. ANN model was created among vibratory aided gas tungsten arc welding (TIG) parameters and tensile strength (UTS) of 5052 H32 aluminium

Fig. 6 Percentage deviation of testing data set
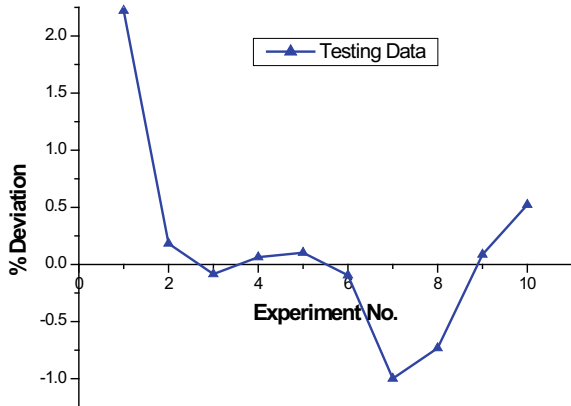
alloy weldments. The created ANN model is tested using results of the experiment. This trained ANN model can also predict the aluminium alloy weld joint ultimate tensile strength with an accuracy of 97.77%.

References

1. Rao, P.G., Rao, P.S., Gopala Krishna, A.: A smart prediction tool for estimating the impact strength of welded joints prepared by vibratory welding process. Proc. Inst. Mech. Eng., Part E: J. Process Mech. Eng. **231**(2), 343–346 (2017)
2. Rao, P.G., Rao, P.S., Krishna, A.G.: Evaluation of bending strength of the vibratory welded joint using regression technique. Int. J. Offshore Polar Eng. **25**(03), 227–230 (2015)
3. Panda, B.N., Bahubalendruni, M.R., Biswal, B.B.: A general regression neural network approach for the evaluation of compressive strength of FDM prototypes. Neural Comput. Appl. **26**(5), 1129–1136 (2015)
4. Vykunta Rao, M., Raju Bahubalendruni, M.V.A., Chintada, V.B.: General regression neural network-based frame work for the evaluation of ultimate tensile strength of vibratory-assisted welded joints. In: Recent Advances in Manufacturing, Automation, Design and Energy Technologies (pp. 173–180). Springer, Singapore
5. Dongare, A.D., Kharde, R.R., Kachare, A.D.: Introduction to artificial neural network. Int. J. Eng. Innovative Technol. (IJEIT) **2**(1), 189–194 (2012)
6. Park, Y.S., Lek, S.: Artificial neural networks: multilayer perceptron for ecological modeling. In: Developments in Environmental Modelling (Vol. 28, pp. 123-140). Elsevier, (2016)
7. Mohamed, Z.E.: Using the artificial neural networks for prediction and validating solar radiation. J. Egypt. Math. Soc. **27**(1), 1–13 (2019)
8. Ray, A., Kumar, V., Kumar, A., Rai, R., Khandelwal, M., Singh, T.N.: Stability prediction of Himalayan residual soil slope using artificial neural network. Nat. Hazards **103**(3), 3523–3540 (2020)
9. Chakraborty, A., Mukherjee, D., Mitra, S.: Development of pedestrian crash prediction model for a developing country using artificial neural network. Int. J. Inj. Control Saf. Promot. **26**(3), 283–293 (2019)
10. Khosravi, A., Koury, R.N.N., Machado, L., Pabon, J.J.G.: Prediction of wind speed and wind direction using artificial neural network, support vector regression and adaptive neuro-fuzzy inference system. Sustain. Energy Technol. Assessments **25**, 146–160 (2018)

11. Elsheikh, A.H., Sharshir, S.W., Abd Elaziz, M., Kabeel, A.E., Guilan, W., Haiou, Z.: Modeling of solar energy systems using artificial neural network: a comprehensive review. Solar Energy **180**, 622–639 (2019)
12. Vykunta Rao, M., Srinivasa Rao, P., Surendra Babu, B.: Vibratory weld conditioning during gas tungsten arc welding of al 5052 alloy on the mechanical and micro-structural behavior. World J. Eng. **17**(6), 831–836 (2020)
13. Rao, M.V., Rao, P.S., Babu, B.S.: Effect of vibratory tungsten inert gas welding on tensile strength of aluminum 5052–H32 alloy weldments. Mater. Focus **6**(3), 325–330 (2017)
14. Fu, X., et al.: Training recurrent neural networks with the Levenberg–Marquardt algorithm for optimal control of a grid-connected converter. **26**(9), 1900-1912 (2014)

Process Parameters Optimization in Drilling Using Taguchi Method

Bikash Banerjee [ID]**, Anish Kumar Dhar, Soumyadeep Bhattacharjee, and Nischay Kumar Mahato**

1 Introduction

To create or enlarge a hole into or through a workpiece material drilling process is used. One of the most important processes in manufacturing industry is drilling. Drilling covers around 28% of all machining processes. Burr is unwanted materials remain after machining process. Burr is produced by all traditional machining processes. During machining operation, plastic deformation is the main cause of formation of burr. The presence of burr on drilling workpiece creates a problem in both assembly line and handling. Dey et el. [1] studied an experiment using artificial neural network (ANN). Obtained result from this experiment stated that minimum burr height and burr thickness are produced at maximum drill diameter, higher point angle and minimum spindle speed. ANN model gives a very close matching to the experiment results but a small deviation. Kundu et al. [2] investigated that unwanted burr is present in the workpiece during drilling. To optimize burr height with backup assist is developed by controlling different process parameters. The obtained result shows that for better drilling processes backup support is more important. Hashimura et al. [3] investigate that to minimize burr in drilling process, process parameters play a vital role. In this paper a fundamental structure is presented depends on various work materials to minimize burr. Formation of burr is analyzed by finite element analysis. The result showed that by controlling process parameters like feed rate and cutting angle, burr formation is minimized. Sathiyamurthy and Ramamoorthy [4] developed a 3D model to optimize burr by finite element method. Burr is occurs in most of the drilling process. Additional cost is needed to remove the burr, which is cost-effective in manufacturing industry. Patil et el. [5] studied on deburring process

B. Banerjee (✉) · A. K. Dhar · S. Bhattacharjee · N. K. Mahato
Department of Mechanical Engineering, Abacus Institute of Engineering and Management, Hooghly, India
e-mail: bikashbanerjee25@gmail.com

to remove the burr completely. The result showed that burr size decreases with the increase of feed rate. At 39º burr point, angle burr height is minimum. Takazawa [6] and Glilliespie [7] investigated a deburring process for burr formation. Liu et al. [8] investigated on burr formation for composite material in drilling process. Chang and Bone [9] studied on burr formation optimization using ultrasonic drilling operation. Banerjee et al. [10] designed a new horn and analysis using ANSYS for ultrasonic machining. Banerjee et al. [11] investigated parametric optimization of AL/SiC metal matrix composites during ultrasonic machining process.

The aim of this work is to measure the burr height and burr thickness under different machining parameters. Different parameters are point angle, spindle speed and drill bit diameter. Also to find out the minimal burr height and thickness produced in this drilling process.

2 Experimental Details

Total experiment is carried out under cooling conditions in a drill machine. Three different twist drill diameters were selected. The diameters are 8.62 mm, 9.42 mm and 11.35 mm. High-speed steel (HSS) cutting tool is used to drill aluminium bar workpiece of dimensions 152 mm * 40 mm * 15 mm. Burr height and burr thickness is found out, which is most important to characterize burr seize.

3 Experimental Procedure

The aluminium block was fixed in the vice. With the help of tachometer spindle speed was measured. To obtain correct spindle speed this process was used. Initially, bar was marked for making hole at a separate distance. A trial process was done before the final drilling process. First of all twist drill angles of three different diameters, 8.62 mm, 9.42 mm and 11.35 mm had same point angle 115° was measured. Then total of nine experiments was done for each of twist angle (3) and corresponding three spindle speeds. Secondly, at drill bit angle 102° next set of experiment was done. For the final experiment drill point angle was set to 84°. Total 27 numbers of experiments were conducted. In every machining process cutting fluid was used. To measure the burr height digital vernier caliper was used. Four side burr height was measured and then average burr height was taken. Same steps were done for measuring burr thickness. Different parameters for conducting experiment are shown in Table 1.

Table 1 Different parameters for conduction experiment

Parameters	Level 1	Level 2	Level 3
Drill diameter in mm	8.62	9.42	11.35
Point angle in degree	84	102	115
Spindle speed in rpm	628	1265	2217

4 Result Investigation and ANOVA Analysis

Experiments result in drilling process by using Taguchi's L27 orthogonal array has shown in Table 2. To determinate the output parameters like burr height and burr thickness, the input parameters like spindle speed, point angle and drill bit diameter were given in drilling process.

ANOVA has been used to determine the importance of machining parameters on burr formation. Some parameter of machining is more important than others' process parameters. Percentage contribution has been done to establish the importance of machining parameters with the help of ANOVA. Minitab 18 software has been used to determine 3-away ANOVA. ANOVA results for burr height are shown in Table 3.

If F-test values are greater than F-table values, then process parameters would be significant. Table 1 in this paper shows drill point angle is most significant and gives 94% confidence level. Burr height contribution is 33.42%. Drill bit dia. and spindle speed have 20.97% contribution level whereas point angle and spindle speed has 18% contribution level. From this, it is stated that point angle plays a significant role during drilling process and gives maximum burr height.

Table 4 shows the ANOVA result of burr thickness. It is clear that point angle acts a vital role during drilling process and which gives 94% confidence level. F-Test vale is 9.20 is greater than F-table value (2.8) = 4.56. Point angle gives burr thickness about 44.90%, where RPM and drill bit dia. gives 12.71% contribution level and point angle and drill bit dia. give 10.21% contribution level to burr thickness.

From Figs. 1 and 2 it is observed that by controlling process parameters like spindle speed, drill bit dia. and point angle, average burr height is shown. It is observed that average burr height shows when drill bit diameter is 9.42 mm.

Also, drill bit dia. at 8.65 mm and 11.45 mm average burr height shown. Average burr height is shown when point angle is 102°. If point angle is increased then burr height also increased. At 628 rpm in case of spindle speed, average burr height is shown. Spindle speed also varies from 626 to 1262 rpm to obtain average burr height (Table 5).

Figures 3 and 4 shows the mean effect plot and interaction plot for burr thickness, respectively. It was observed that value of burr thickness low at low-level drill bit diameter, i.e. 8.62 mm. Burr thickness will be increased up to intermediate value of drill bit dia. then it is decreased. Burr thickness is decreased with the increased of point angle. In case of spindle speed, bur thickness is increased with the increased of spindle speed (Table 6).

Table 2 Obtained results of Burr height and Burr thickness

S. No	Drill bit diameter (mm)	Spindle speed (r.p.m)	Point angle (°)	Height of Burr (mm)	Thickness of burr (mm)
1	8.62	628	84	5.66	0.782
2	8.62	1265	84	3.41	0.486
3	8.62	2217	84	6.62	0.653
4	8.62	628	102	4.79	0.370
5	8.62	1265	102	3.92	0.670
6	8.62	2217	102	4.42	0.540
7	8.62	628	115	2.89	0.420
8	8.62	1265	115	4.56	0.380
9	8.62	2217	115	4.29	0.510
10	9.42	628	84	6.64	0.760
11	9.42	1265	84	6.83	0.940
12	9.42	2217	84	4.62	0.844
13	9.42	628	102	4.61	0.402
14	9.42	1265	102	3.35	0.443
15	9.42	2217	102	3.66	0.750
16	9.42	628	115	3.51	0.355
17	9.42	1265	115	6.12	0.444
18	9.42	2217	115	5.21	0.594
19	11.35	628	84	5.76	0.834
20	11.35	1265	84	6.99	0.680
21	11.35	2217	84	4.70	0.784
22	11.35	628	102	2.66	0.560
23	11.35	1265	102	4.44	0.484
24	11.35	2217	102	3.60	0.410
25	11.35	628	115	2.45	0.408
26	11.35	1265	115	6.35	0.702
27	11.35	2217	115	3.25	0.289

5   Conclusion

Burr is unwanted materials remain in the workpiece after machining. This experimental work has been done to established burr optimization strategy. From this work, it has been concluded that,

- Point angle is most important parameter which gives 94% contribution level and burr height is 33.42%.
- Drill bit dia. and spindle speed has 20.97% contribution level whereas point angle and spindle speed have 18% contribution level.

Table 3 ANOVA results of burr height

Source	DOF	Adj. SS	Adj. MS	F-Value	P-Value	Percentage
Drill bit dia. (D)	2	1.30	0.643	0.91	0.436	2.78
Point angle (P)	2	15.762	7.880	11.07*	0.002	33.40
RPM (R)	2	3.005	1.5030	2.10	0.181	6.42
D * P	4	2.561	0.640	0.91	0.503	5.52
D*R	4	9.890	2.4749	3.45	0.061	20.97
P * R	4	8.965	2.2411	3.13	0.075	18.89
Error	8	5.688	0.7101			12.02
Total	26	47.171				

*Significant. F-value (2.8) = 4.56, F-value (4.8) = 3.81 at 95 at 94% confidence level

Table 4 ANOVA results for burr thickness

Source	DOF	Adj. SS	Adj. MS	F- value	P-value	Percentage
Drill bit dia. (D)	2	0.0120	0.006106	0.26	0.700	1.31
Point angle (P)	2	0.4150	0.207441	9.20	0.007	44.90
RPM (R)	2	0.0310	0.015594	0.68	0.526	3.40
D * P	4	0.0945	0.023602	1.07	0.400	10.20
D * R	4	0.1180	0.029541	1.32	0.342	12.77
P * R	4	0.0730	0.018300	8.80	0.551	7.90
Error	8	0.1798	0.022480			19.50
Total	26	0.9235				100

*Significant. F-value (2.8) = 4.56, F-value (4.8) = 3.81 at 95 at 94% confidence level
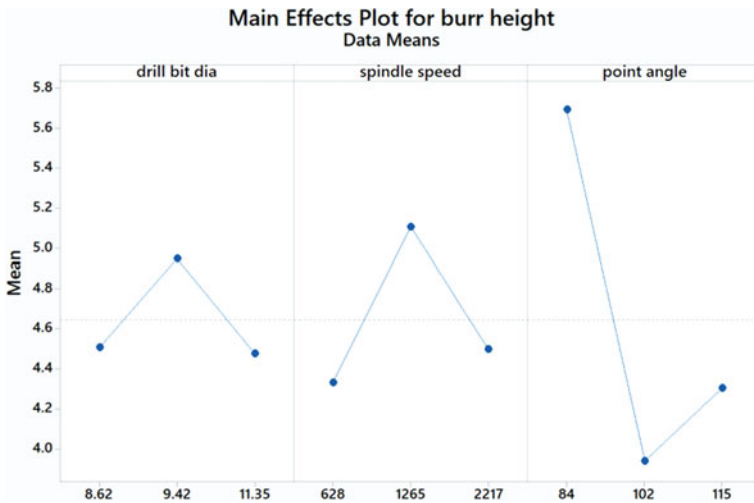
Fig. 1 Mean effect plot for burr height
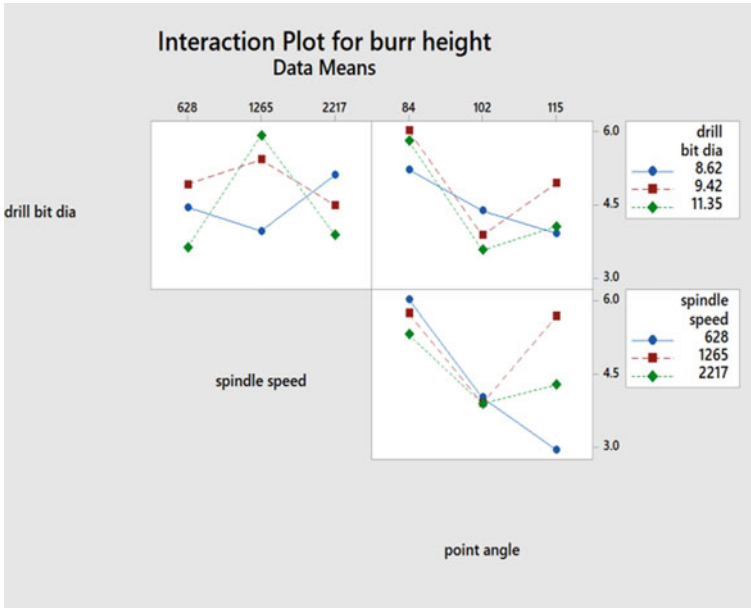
Fig. 2 Interaction plot for burr height

Table 5 Optimum level process parameters for burr height

Process parameters	Drill bit diameter	Point angle	Spindle speed
Optimum levels	11.35 mm	102°	628 rpm

- Feed also plays a vital role during machining. It is clear that alternation of spindle speed and point angle gives positive effect on burr formation.
- The best machining value of different process parameters for burr height are spindle speed of 628 rpm, drill bit diameter of 11.35 mm and point angle of 102°.
- The best machining value of different process parameters for burr thickness are spindle speed of 628 rpm, drill bit diameter of 11.35 mm and point angle of 115°.
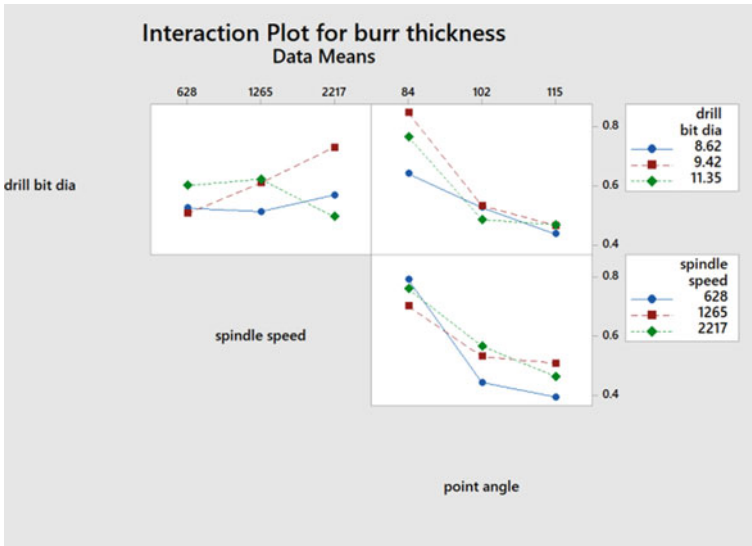
Fig. 3 Mean effect plot for burr thickness
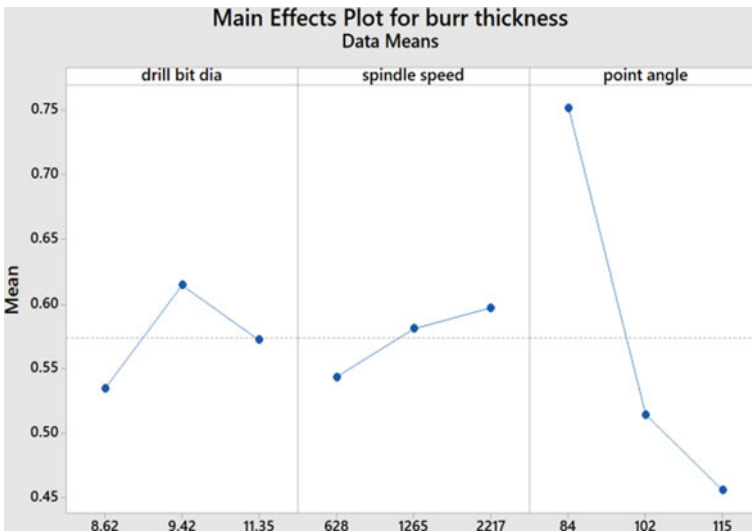
Fig. 4 Interaction plot for burr thickness

Table 6 Optimum level process parameters for burr thickness

Process parameters	Drill bit diameter	Point angle	Spindle speed
Optimum levels	8.62 mm	115°	628 rpm

References

1. Dey, B., Mondal, N., Mondal, S.: Experimental study to minimize the burr formation in drilling process with artificial neural networks (ANN) analysis. In: IOP Conference series: Materials science and Engineering, vol. 377, pp. 2–6. (2018)
2. Kundu, S., Das, S., Saha, P.P.: Optimization of drilling parameters to minimize burr by providing back-up support on aluminium alloy. Procedia Eng. **97**, 230–240 (2014)
3. Hashimura, M., Chang, Y.P.: Analysis of burr formation mechanism in orthogonal cutting. J. Manuf. Sci. Eng. **121**(1), 1–7 (1999)
4. Sathiyamurthy, S., Ramamoorthy, M.: Dynamic analysis of drilling burr formation process. Int. J. Latest Technol. Eng. Manage. Appl. Sci. **5**(2), 74–76 (2016)
5. Patil, R., Shinde, S., Joshi, S.S., Marla, D.: Experimental analysis of burr formation in drilling of Ti-6AL-4V alloy. Int. J. Mechatron. Manuf. Syst. **9**(3), 237 (2016)
6. Takazawa, K.: The challenge of burr technology and its worldwide trends. Bull. Jpn Soc. Precis. Eng. **22**(3), 165–170 (1988)
7. Gilliespie, L.K..: Deburring technology for improved manufacturing. Soc. Manuf. Eng. (1981)
8. Liu, D., Tang, Y., Cong, W.L.: A review of mechanical drilling for composite laminates. Compos. Struct. **94**(4), 1265–1279 (2012)
9. Chang, S.S.F., Bone, G.M.: Burr size reduction in drilling by ultrasonic assistance. Rob. Comput. Integr. Manuf. **21**, 442–450 (2005)
10. Banerjee, B., Pradhan, S., Das, S., Chakraborty, A., Dhupal, D.: Horn design and analysis in ultrasonic machining using ANSYS. Adv. Mater. Process. Technol. **7**, (2021)
11. Banerjee, B., Chakraborty, A., Das, S., Dhupal, D.: Process parameters optimization of AL/SiC metal matrix composites during ultrasonic machining process. In: E3S Web of Conferences, vol. 309, p. 01156. (2021)

Modeling of Inkjet-Based Micro-additive Manufacturing Process Performance Using Deep Learning Algorithms

Tiasa Das, Adrija Biswas, and Shibendu Shekhar Roy

1 Introduction

The recent twenty-first century has brought forward an ample amount of changes in the manufacturing world. The most predominant among them was the introduction of additive manufacturing in the industrial sector. It is a revolutionary approach which focuses on formation of different components with layer by layer deposition. Basically, it obtains data from any computer software (usually CAD or 3D scanners) and instructs the hardware to produce an object by adding layers subsequently. With the establishment of Industry 4.0, more and more industries have started relying on the several advantages of the additive manufacturing processes. This method promises an accurate and precise product in less time. The entire process is quite eco-friendly as compared to its other competitors.

There are a varied range of microproducts available nowadays that have a complicated 3D microstructure with high aspect ratios [1]. 3D micro-additive modeling techniques have made it easier to build up highly accurate and precise microproducts. The ability of this process to fabricate products with an extreme high level of geometric exactness has intrigued many brilliant minds of the industry. It has opened up a whole new demographic for people to invest in the manufacturing world. Due to its numerous advantages, micro-additive manufacturing has proved to be a better alternative to other fabrication processes like lithography based or micro-machining processes. Inkjet printing is a type of 3D micro-additive manufacturing process [2].

Printed electronics is a very recent and developing field which is overcoming the complexities and difficulties faced by people worldwide. It is basically a set of printing methods used for printing several electrical components on certain substrates. It brings down the cost of fabrication, time taken for manufacturing,

T. Das (✉) · A. Biswas · S. S. Roy
Department of Mechanical Engineering, National Institute of Technology, Durgapur, India
e-mail: tiasadas2013@hotmail.com

and several other factors [3]. Material handling has become very easy. For the preparation of printed electronics, nearly, all industrial printing methods are employed. In printed electronics, layer by layer deposition of ink approach is followed much like that of the traditional printing methods. Development of adequate printing materials and ink material is the major focus in this field. The inks used are commonly made from organic materials [4]. Inkjet printing can be of two types—piezo electric and drop on demand.

Electrohydrodynamic (EHD) printing works on the 'drop on demand' mode of inkjet printing [5]. Nozzle clogging and inconsistency of the droplet frequency is one of the major drawbacks of inkjet printing [6]. This drawback can be overcome by the EHD printing technique as it easily produces nano-level droplet with a high resolution. At the time of printing, the droplet meniscus changes according to the shape of a cone, known as Taylor's cone [7]. This cone allows a steady and continuous deposition of droplets which in turn stops clogging [8]. Advances in EHD printing technology have made possible some major breakthroughs in this field. In recent years, this technology has spread out in the printed electronics field and has been rampant ever since.

Chen et al. [9] experimented and successfully printed droplets with less diameter than nozzle which can result in high resolution printing by conventional method. Kim et al. [10] investigated for the right selection of process parameters to get the desired droplet formation, droplet size, and frequency. Barton et al. [11] used e-jet frequency as response to design some control system for EHD inkjet printing. An. and associates [12] investigated the influence of ink material on e-jet droplet frequency. Li et al. [13] investigated the applied voltage effect on mode of droplet formation. Park et al. [14] used different nozzles to investigate the droplet diameter variation. Wang et al. [15] and other researchers [16] also had investigated the effect of process parameter on Taylor cone formation, droplet diameter, etc.

It is extremely important that the droplet diameter and the droplet frequency are set at its maximum accuracy to get products with high level of precision. So in this study, both the parameters that is, droplet diameter and droplet frequency, are considered. These are modeled through different neural network systems which forms the backbone of deep learning algorithms and compared with each other to obtain the most accurate parameter. Such types of algorithms can be used as a tool for establishing smart manufacturing systems in several industries. The high level of accuracy and precision of this neural network system provides an optimistic solution for several 3D printing industries.

2 Experimental Setup

The experimental setup of electrohydrodynamic inkjet printing-based micro-additive manufacturing process was developed during this work which is shown in Fig. 1. This micro-additive manufacturing system contains following major subsystems; the substrate positioning system, ink delivery device, electrical/electronic control

system, and droplet visualization mechanism. The ink used in the present study is PEDOT: PSS as a functional material during experimentation. It is a conducting polymer solution with water-soluble characteristics. This ink material can be used in a flexible and stretchable substrate like polyethylene terephthalate (PET). This combination of the ink and the substrate can be employed for manufacturing micro-electrodes in the applications of flexible printed applications. The ink contains 1–5% ethanol, 5–10% diethylene glycol, (Sigma Aldrich 2019). Some other properties of the ink are density: 0.985 gm per milliliter, viscosity: 7–12 centipoise. The ink material was delivered to the metallic nozzle with the help of a syringe pump [17]. This pump executes two purposes concurrently; it acts as the reservoir of material of ink and as a supply system for applying pressure by which the material was transferred to the nozzle. Among the substrate targeted and the nozzle, a function generator applied a high voltage. The analog pulse signal was generated by the function generator with a specific duty cycle and frequency. The created pulse width modulated signal has been provided to the amplified, and the voltage signal was amplified around 1000 times. In order to deposit the magnified voltage, it has to be supplied to the metallic zone. The electronic XY stage fitted the flexible polyethylene terephthalate (PET) substrate. Having a resolution of 0.1 μm and a velocity of 205 mm/s, the positioning was done. A motion controller controlled the position and speed of the stage. In case of Z-axis, the supported column was used to mount the print head which allowed the single linear axis movement of the stage. A command which is user defined is given along with a definite acceleration and velocity according to which the movement of the scanning stage happens in order to make an user-specified pattern. The needle made of stainless steel which has the length as 51 mm and internal diameter as 0.836 mm was utilized as an ejection nozzle. The optical microscope was used to visualize the droplets which were deposited. The microscope which has the capability of magnification around 100 times captured the image. The features which were printed on the substrate were uniform. The processing software which was embedded within the microscope determined the deposited drop diameter and consecutive drop pitch. The experiments were carried out using different process parameter setting and ranges as mentioned in Table 1. In this study, three parameters are considered as input process parameters, which include the stand-off height, voltage, rate of flow. The responses were the droplet diameter and droplet frequency. Table 1 illustrates all the process parameters taken and their estimated value range.

3 Proposed Methodology

For this study, two response parameters—droplet diameter and droplet frequency have been considered. This is mainly because these two parameters are key determining factors for the accuracy and precision of the products obtained from EHD printing. In order to develop a relationship between chosen input process parameters and output responses, statistical modeling and deep learning algorithms based on soft computing or computational intelligence techniques are taken into account.
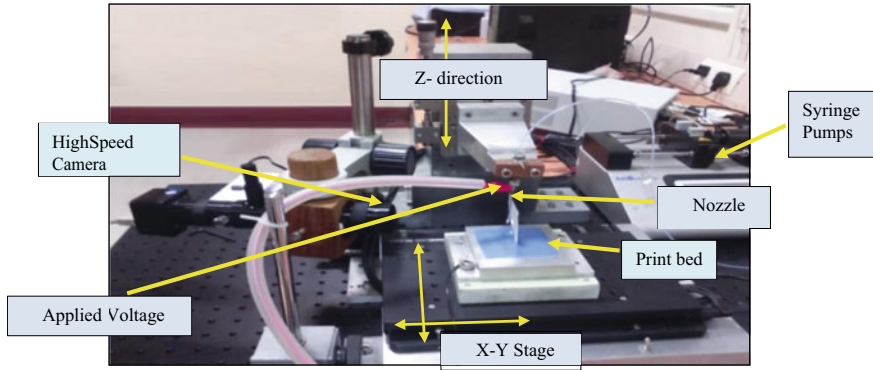
Fig. 1 Experimental setup

Table 1 Process parameters and their working ranges

Process parameters	Unit	Working range		
		Low	Medium	High
Stand-off height (A)	mm	4.50	5.00	5.50
Voltage (B)	kV	3.80	4.40	5.00
Rate of flow (C)	μl/s	10.00	25.00	40.00

3.1 Second-Order Regression Analysis

To attain a certain relationship between input and output parameters, regression analysis is done. According to the proposed DOE, levels of each input parameter are chosen. Some test cases are done to validate the correct percentage contribution of each input parameter over the chosen output parameter which are again obtained through some selective tests. In this paper, the following nonlinear second-order regression equation is used to get the approximate accurate relationship between the input and output factors [18]:

$$y = \beta_0 + \sum_{j=1}^{k} \beta_j X_j + \sum_{j=1}^{k} \beta_{jj} X_j^2 + \sum \sum_{j<i} \beta_{ji} X_j X_i + \varepsilon \quad (1)$$

where the process response is given by y; the process control parameter is denoted by X; the regression coefficient is denoted by β; the experimental error by ε and the investigated process control parameters by j and i.

As depicted in Eq. 1, the linear effect of i, j (process parameters) is captured by Xj, while its nonlinear effect is represented by X_j^2, and the parametric interaction is exhibited by $X_i X_j$. Equation 1 can be expressed with one response variable and three control parameters as shown below in Eq. 2:

$$y = \beta_0 + \beta_1 X_1 + \beta_2 X_2 + \beta_3 X_3 + \beta_{11} X_1^2 + \beta_{22} X_2^2$$
$$+ \beta_{33} X_3^2 + \beta_{12} X_1 X_2 + \beta_{13} X_1 X_3 + \beta_{23} X_2 X_3 \tag{2}$$

β factors are can be determined by least square method by solving some normal set of equations.

Here, forward mapping is done for droplet diameter and frequency with the help of three types of neural networks, namely back propagation neural network (BPNN), radial basis function network (RBFN), and recurrent neural network (RNN). The outcomes of all the three types are found out and compared to obtain the most accurate method.

3.1.1 Back Propagation Neural Network (BPNN)

Back propagation neural network is a form of an artificial feed forward neural network where multiple layers have been divided into an input layer, a hidden layer, and an output layer. It learns with training. According to the differences between the training and the output data, the initial weights are fixed arbitrarily and are modified later. The backward and forward methods are repeated until the differences between the output data and training data become accurate. A gradient descent algorithm has been used in case of the standard BPNN. Along the performance function gradient, the weights of the network are adjusted inversely. Thus, the real value and predicted value gets closer.

3.1.2 Radial Basis Function Network (RBFN)

A radial basis function network is a form of an artificial neural network which represents its own input patterns with the help of a layer in between, which is already given with a definite number of units. An activation function is used to characterize each and every unit of the intermediate layer which are defined intentionally. This is a three-layer forward network.

3.1.3 Recurrent Neural Network (RNN)

The recurrent neural network is a network having a memory function which can be used further for processing information sequentially. The RNN is having a memory which collects data about the calculations going on in the present state. The neurons of the hidden layers are linked through a chain. Along with the current input, the current output also depends upon the past network status.

All the above three neural network systems are unique in its own ways. The BPNN is known for its speed and ease of programming. It does not need any prior knowledge. For RBFN, all the hidden units are responsible for performing computations. It

provides a huge advantage as here the first set of parameters can be derived independently from the second set. The plus factor for the RNN system is its eidetic memory in which it can remember all its previous input data. This helps in expanding the datasets available for training. All these three neural networks boasts of extremely high accuracy which is why they are considered for our study.

4 Simulation Result and Discussion

In this study, the main concern is to model the response parameters, i.e., droplet diameter and frequency (Hz) of EHD printing in terms of its input parameters like nozzle substrate gap (mm), applied potential difference (kV), and ink flow rate (μl/s).

The full-factorial DOE founded data have been utilized to accomplish the statistical regression analysis [18]. Response surface methodology (RSM) was used to analyze the inter-relationship among three input process variables and responses. The quadratic regression equations for the width and height of the deposited layer were developed as follows.

$$
\begin{aligned}
\text{Droplet diameter} = {}& 3208.26 - 1310.25 \times \text{G} + 140 \times \text{V} \\
& + 31.01 \times \text{F} + 120.59 \times \text{G}^2 - 56.05 \\
& \times \text{V}^2 - 0.0785 \times \text{F}^2 + 54.47 \times \text{G} \times \text{V} \\
& - 2.83 \times \text{G} \times \text{F} - 0.40 \times \text{V} \times \text{F}
\end{aligned}
$$

$$
\begin{aligned}
\text{Droplet frequency} = {}& -15.3 + 8.64 \times \text{G} + 4.7 \times \text{V} - 0.0615 \\
& \times \text{F} - 0.862\text{G} \times \text{G} - 0.418 \times \text{V} \times \text{V} \\
& - 0.000032\text{F} \times \text{F} - 0.097\text{G} \times \text{V} \\
& + 0.01244\text{V} \times \text{F} - 0.00093\text{F} \times \text{G}
\end{aligned}
$$

where G is the nozzle substrate gap, V is the voltage applied, and F is the ink flow rate.

Different parameters of neural networks (like the rate of learning, the amount of hidden layer neurons, the coefficient of the momentum factor and transfer function) have been examined parametrically. Attaining an optimum network giving the minimum deviations while predicting by using the learning in an incremental mode is the aim of the above investigation. In case of hidden layer neurons, the tan-sigmoid transfer function has been used. The input and output values are normalized before training the network. The following equation is used to normalize the input and output factors,

$$
z_i = (\Delta^U - \Delta^L) \frac{x_i - x_i^{\min}}{x_i^{\max} - x_i^{\min}} + \Delta^L \tag{3}
$$
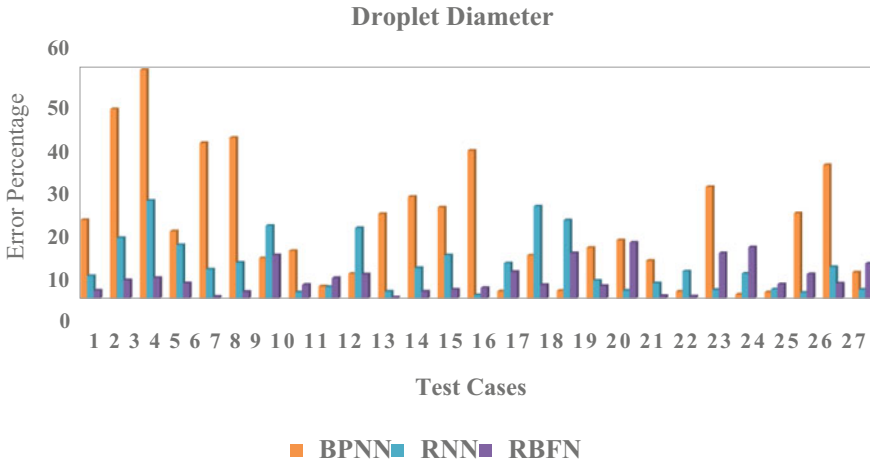
Fig. 2 Absolute error percentage in prediction of droplet diameter

where x_i is first normalized to z_i and the range is set in $[\Delta^U, \Delta^L]$. The maximum and minimum values of x_i is x_i^{max} and x_i^{min}, respectively.

After training, the experimental inputs are also normalized and sent to the networks to predict the droplet frequency and diameter. The predicted outputs are then denormalized. For testing purpose, 27 datasets have been considered in this study which in turn generates 503 datasets that were used to train the neural network systems. Experimental outputs and predicted outputs of three different networks, back propagation neural network, recurrent neural network, and radial basis neural network have been compared graphically as shown in Figs. 2 and 3. When it comes to droplet diameter prediction, the error percentage obtained from back propagation network was 18.55%; from recurrent network, it was 8.4%, and from radial basis network, it was 5.05%. When it comes to droplet frequency prediction, error percentage from back propagation network was 2.09%; from recurrent network, it was 2.14%, and from radial basis network, it was 0.79%.

The RBFN system has universal approximation and regularization capabilities. Moreover, it has a simpler structure, higher robustness, and a much faster training process. That is why it can undoubtedly be considered as the best prediction tool.

5 Conclusion

Droplet diameter is a widely used index of deposit characteristics which is significant in case of the overall performance of the electrohydrodynamic micro-additive fabrication method. To measure the efficiency of EHD inkjet printing in terms of printing resolution, droplet frequencies are very significant. Both the parameters are required to be modeled properly to get desired performance. To compare the accuracy in their
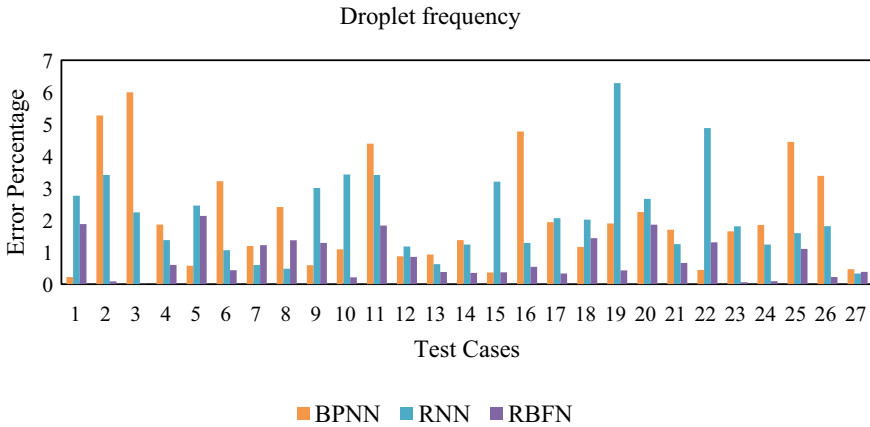
Fig. 3 Absolute error percentage in prediction of droplet frequency

predictions, three different networks have been chosen, namely back propagation neural network, recurrent neural networks, and radial basis neural network. From the comparison, it can be inferred that, in both the cases of droplet frequency and diameter, radial basis function network tends to outperform the other two in terms of modeling accuracy.

References

1. Mohammed, V., Herman, S., Shoufeng, Y.: A review of 3D micro-additive manufacturing technologies. Int. J. Adv. Manuf. Technol. **67**(5–8), (2012)
2. Das, R., Ball, A.K., Roy, S.S.: Modelling of EHD inkjet printing performance using soft computing—based approaches. J Braz. Soc. Mech. Sci. Eng. **40**, 454 (2018)
3. Diana, G.S.: Intelligent packaging. Nanomaterials for food packging. (2018)
4. Maria, P., Jacob, H.: Printed Films: Material Science and Application in Sensors, Electronics and Photonics, 2nd edn. Woodhead Publishing (2012)
5. Kim, J., Oh, H., Kim, S.S.: Electrohydrodynamic drop-on-demand patterning in pulsed cone jet mode at various frequencies. J. Aerosol. Sci. **39**, 819–825 (2008)
6. Onses, M.S., Sutanto, E., Fereira, P.M.: Mechanisms, capabilities and applications of high resolution electrohydrodynamic jet printing. Small **11**, 4237–4266 (2015)
7. Feihuang, F., Saja, A., Shervanthi, H.V., Manish, KT.: High resolution 3D printing for healthcare underpinned by small scale fluidics. In: 3D Printing in Medicine, pp. 167–206 (2017)
8. Yu, M., Ahn, K.H., Lee, S.J.: Design optimization of ink in electrohydrodynamic jet printing: effect of viscoelasticity on the formation of Taylor cone jet. Mater. Des. **89**, 109–115 (2016)
9. Chen, C.-H., Saville, D.A., Aksay, I.A.: Electrohydrodynamic "drop-and-place" particle deployment. Appl. Phys. Lett. **88**, 154104 (2006)
10. Kim, J., Oh, H., Kim, S.S.: Electrohydrodynamic drop-on-demand patterning in pulsed cone-jet mode at various frequencies. J. Aerosol. Sci. **39**, 819–825 (2008)
11. Barton, K., Mishra, S., Alex Shorter, K., Alleyne, A., Ferreira, P., Rogers, J.: A desktop electrohydrodynamic jet printing system. Mechatronics **20**, 611–616 (2010)

12. An, S., Lee, M.W., Kim, N.Y.: Effect of viscosity, electrical conductivity, and surface tension on direct-current-pulsed drop-on-demand electrohydrodynamic printing frequency. Appl. Phys. Lett. **105**, 214102 (2014)
13. Li, J.L.: On the meniscus deformation when the pulsed voltage is applied. J Electrostat **64**, 44–52 (2006)
14. Park, J., Park, J.W., Nasrabadi, A.M., Hwang, J.: Methodology to set up nozzle-to-substrate gap for high resolution electrohydrodynamic jet printing. Appl. Phys. Lett. **109** (2016)
15. Wang, X., Xu, L., Zheng, G., Cheng, W., Sun, D.: Pulsed electrohydrodynamic printing of conductive silver patterns on demand. Sci. China Technol. Sci. **55**, 1603–1607 (2012)
16. Lee, M.W., Kang, D.K., Kim, N.Y., Kim, H.Y., James, S.C., Yoon, S.S.: A study of ejection modes for pulsed-DC electrohydrodynamic inkjet printing. J. Aerosol. Sci. **46**, 1–6 (2012)
17. Ball, A.K., Das, R., Das, D., Roy, S.S., Murmu, N.C.: Design, development and experimental investigation of E-jet based additive manufacturing process. Mater. Today Proc. **5**, 7355–7362 (2018)
18. Shucai, Y., Chunsheng, H., Minli, Z.: A prediction model for titanium alloy surface roughness when milling with micro-textured ball-end cutters at different workpiece inclination angles. Int. J. Adv. Manuf. Technol. (2018)

Additive Manufacturing Techniques in Fabrication of Soft Robotic Sensors and Actuators: A Review

Baibhav Kumar, Vijay Kumar Dalla, and Aditya Haldar

1 Introduction

Additive manufacturing (AM), also known as 3D printing, combine materials with building items from 3D designs, generally formed layer by layer method. In contrast to subtractive production processes, which include machining. With technological advancements, 3D printing is becoming more widely used to manufacture end-use parts [1]. The additional design freedom afforded by AM might be used to improve the functioning of end-use items manufactured with AM. However, not all materials are printed, limiting their use in construction because several AM elements are not robust or resilient enough. As a result, the latest research emphasis in the AM industry has shifted to novel materials and methods developed to facilitate the printing of widely used industrial materials, including composites [2], ceramics [3], and elastomers. Soft robots may now be designed more complexly and manufactured more quickly thanks to advances in fabricating soft materials. Soft robotics, which takes its influence from the environment, is a fast-expanding new field of robotics. Robots are essentially soft and elastically adjustable, allowing them to alter their shape to environmental restrictions and impediments [4] depicted in Fig. 1. Conventional robotic systems are primarily composed of stiff mechanical parts like links and joints, allowing them to execute highly quick, accurate, efficient, and repeated motion control functions. On the other hand, robotic systems must be less stiff and more flexible to conduct more adaptable and flexible engagements with complicated unexpected situations and become more realistic and suitable with interpersonal interactions. Automated agriculture sector robots for handling raw food [5], medical equipment for surgery, wearable soft robots for rehabilitation, and robotic bin picking are a few instances of applicability.

B. Kumar · V. K. Dalla (✉) · A. Haldar
National Institute of Technology Jamshedpur, Jamshedpur, Jharkhand, India
e-mail: vijaydalla.me@nitjsr.ac.in
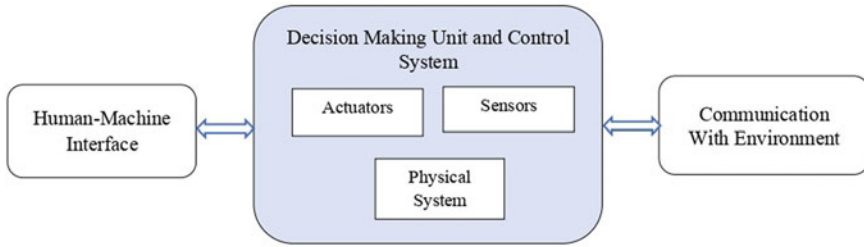
Fig. 1 A schematic diagram for the working principle of soft robotics [6–8]

Soft robotics necessitates the utilization of flexible and soft substances such as polymers, elastomers that can be used to create highly flexible frameworks and to attain stiffness other substances are also required to attain desired modification, movement patterns, and/or positional control [6]. Nevertheless, achieving fully soft robotic systems is difficult. It needs collaboration among researchers and technologists to integrate soft and flexible transducers, detectors, controls, circuitry, and power supply into a single independent soft unit. In contrast, designing automated systems for modeling and manufacturing flexible structures poses certain hurdles to the soft robotics sector. Figure 2 illustrates the research scope related to the manufacturing process and application area for designing parts of soft robots. At different sizes, there are several current initiatives to fabricate soft robots. Some research works have reviewed 3D printing techniques and raw material for soft robotics in terms of material optimization, printer characteristic optimization, design of soft sensors and actuators using different printing materials [7] and their in-vitro and in-vivo applications.
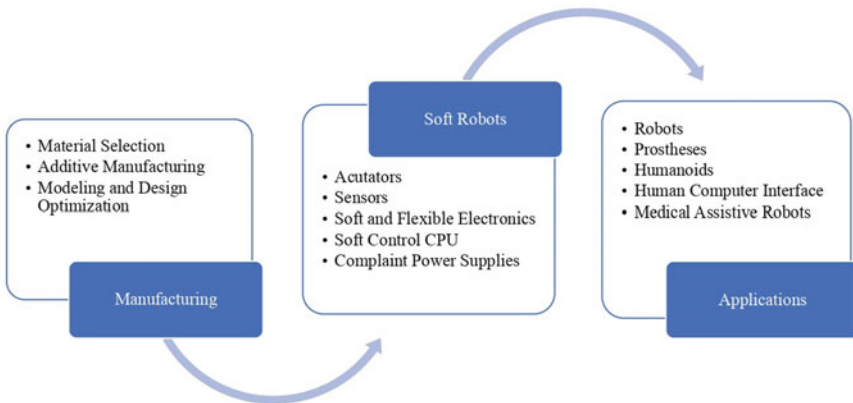
Fig. 2 A schematic diagram for manufacturing of soft robots for specific applications

This paper explores a brief overview of soft sensors and actuators. This paper also focused major contribution of researchers to enlighten the appropriate additive manufacturing or 3D printing process for designing soft sensors and soft actuators along with their limitations. Then in further sections, this paper presented the discussion about the qualities of soft robotic materials and suitable AM processes.

The remaining section of this paper is illustrated as follows: Sect. 2 gives an overview of soft actuators and sensors. Section 3 provides a brief discussion about the significant contribution of AM for manufacturing actuators and sensors in soft robotics. Section 4 gives discussions and limitations of different research. Finally, in Sect. 5 conclusion and future research scope of this paper are presented.

2 Soft Actuators and Sensors

Soft actuator/sensor was a more crucial part of a soft robotic manipulator [9–14]. The soft actuator should be bendable, fast, highly functioning in two directions, possessing the capacity to be compressed, extend, contract, and twist at relative precision while producing sufficient output strengths. Moreover, the soft robotic model involves highly sensitive, highly reliable, repeatable, bendable, as well as highly elastic soft sensors which withstand but also recognize various types of deforms such as deformation, state of being compressed, curving, and having to turn to complete as well as stabilize the operation of the soft actuators [15–20].

2.1 Soft Actuators

The technological criteria for fabricating soft actuator are to design model using AM technologies. These technologies show the advantages over conventional manufacturing procedures. Specialized resources capable of achieving the desired attributes of the finalized output should be specifically chosen. The present soft actuators by 3D printing are divided into two categories: First "semi 3D printed soft actuators", second "3D printed soft actuators". Having the capacity to operate even without additional assembly, this categorization illustrates the benefits of 3D printed soft actuators over partly 3D printed soft actuators. The main benefits of 3D printed soft actuators are that they will be created in a one-step, making them more cost-effective and accessible for customized requirements than partially 3D printed competitors, which need the expert operator and post-processing installation. Some common soft actuator are described as below:

Shape memory polymer (SMP) soft actuators: These are similar as human muscular system, responding to such a variety of stimuli, including light, electricity, electromagnetic field, thermal, pH, and dampness fluctuations. The shape memory factor influences how SMP responds to external stimulation like temperature, dampness, electric inputs, lighting, or magnetic forces (SME). Little physical

weight, excellent strain recoveries, tissue compatibility, and good biodegradability are among the benefits of Shape memory polymer [14].

Photopolymer/light-activated polymers (LAP) soft actuators: These are another form of SMP triggered by light stimuli. The LAP actuators may be usually operated with speedy reaction and no physical touch using simply light frequency and intensity variations. The fundamental disadvantage of these is that they need preloading that works in tandem with exposed for radiation to generate shape change or surface deviates [21].

Hydraulics and pneumatics soft actuators: As a consequence of their inherent compliance and capacity to induce muscular tension, Pneumatic soft actuators have motivated researchers to create softer, not-so-heavy, and tissue compatibility soft actuators for soft robots. A soft skin gripper was designed and built using a 3D printing machine to create most soft skin components [22].

Electroactive polymer soft actuators: Dielectric elastomers (DE), synthetic composite nanomaterials like ion-exchange polymer metal composites IPMC, ion-exchange electroactive polymer, polyelectrolyte (PE) gels, as well as gel-metal nanoparticles composites are typical polymers used to create a three-dimensional layered structures that may be tuned to serve like soft actuator [23].

Magnetic soft actuators: Polymagnet actuator is among the most modern 3D printed soft actuators. The functionality saves fuel in specific engineering settings by replacing conventional mechanic springs with more efficient and precise [24].

Printed active composite soft actuators: To create soft actuators, the 3D printed, unique class metamaterial composite 3D printing process has created an opportunity to put multiple stages of a material into a composite construction. An advanced thermo-mechanical actuator produced by 3D printing was also designed using laminate layers, then lamina constructed of glass active composite materials [25].

2.2 Sensors

In soft robotics, generally, soft sensors are used. These sensors usually measure strain and measure the robot's position or stiffness. These sensors are integrated with actuators so that the measurements can be fed into the actuators and respond accordingly [26]. For better performance of soft robots sensing should be tactical and proprioceptive. There are a variety of sensors, but here, a brief classification based on the type of transducer used for sensing is presented below:

Resistive Sensors and Piezoresistive Sensors: Resistive sensors and Piezoresistive Sensors work on change in resistivity due to strain produced in a conductive material. For making soft resistive sensors, conductive liquids like low-melting point metals and metal alloys and all kinds of ionic liquids are embedded in elastomers or conductive polymers (CP), and conductive polymer hydrogels (CPH) of good stretchability is used. The conductive liquid sensors (CLS) problems are their high density, temperature restriction in conductivity, and high resistance in an ionic solution. Also, their fabrication is difficult as there are chances of leakage, despite being some advantages

of CPs and CPHs over CLSs, their biodegradability, large hysteresis and nonlinearity, slow responses, long recovery time, sensitivity, and stretchability trade-off [26].

Capacitive Sensors: These sensors measure the capacitance change caused by geometry changes when an elastic body is strained. These sensors are made up of highly stretchy, conductive materials as their electrodes. Its drawbacks are that it is sensitive to dust, oil, water vapor, etc., shows proximity effect in conducting parts, and is sensitive to pressure and strain simultaneously.

Optical Sensors: Optical sensors sense variations in components of light due to mechanical variation in the transmission medium. Its drawbacks are such as complex and expensive fabrication, less flexibility.

Magnetic Sensors: These sensors work on the Hall effect. When a material's relative position and orientation change accordingly to the permanent magnet, the output voltage changes; magnetic sensors are economical, compact, easily integrated into the system, and highly sensitive. The problem with magnetic sensors is that it is affected by environmental magnetic field variations and interact with ferromagnetic materials [27].

Inductive Sensors: These sensors work on inductance change by transducer mechanisms, such as Mutual inductance, Magnetic reluctance [28–30].

But these sensor shows restricted use due to complex signal conditioning electronics and requires certain characteristics.

3 Major Contribution of AM for Manufacturing Actuators and Sensors in Soft Robotics

The primary and most critical stage in the development of a soft robot is the selection and design of the soft actuation concept. Some of additive manufacturing techniques used for designing soft robotic actuators and sensors are briefly described in this section.

A shape memory polymer (SMP) was manufactured by using modified fused-deposition modeling (FDM) using optimum operating conditions Yang et al. [31]. However, the process has a speed limit and extruder temperature as at higher speed and temperature the surface roughness was increased. After conducting a calibration test on the sensors, it was found that there was a uniform change in the wavelength with respect to load change. A new technique for directly printing a readily available soft bellows-type actuator of complex geometry and a high degree of freedom (DOF) using the fluid deposition method (FDM) was discussed in Yap et al. [33]. The paper also puts light on pros and cons of three categories of techniques for fabricating and the lost wax technique proposed by Marchese et al. [34]. There is a huge scope of research in this field due to a lack of study for the relationship between printing material hardness and printer parameters like temperature. A detailed study of graphene-based gas sensors was printed using direct ink writing (DIW) technology using pneumatic driven robotic deposition technique was presented in Loh

et al. [35]. The behavior of the sensor limits its application to low voltage. Development of a light-responsive underwater actuator by using a modified untethered liquid crystalline (LC) ink was presented in Pozo et al. [36]. The major limitation in the experiment was the printing speed as the response of the actuator depends upon the molecular alignment of the material. Development of a photosensitive polypyrrole formulation for printing a 3D conjugated polymer, an electroactive material, by using light-based additive manufacturing was presented in Cullen et al. [37] because conventional methods are limited to fabrication of transducers having which are restricted to only simply linear and bending modes operation. It was seen that the developed sensor possesses a small electromechanical behavior and piezoresistive properties. Also, it was seen that by the use of 3D printing technology, micro-scale conjugated polymer structures can be continuously developed with complex 3D geometries. Kamat et al. [38] have presented the fabrication and characterization of a polydimethylsiloxane (PDMS) cantilever flow sensor embedded with serpentine graphene nanoparticles (GPN) on the cantilever base as a piezo resistor strain gauge using high-resolution 3D printing, soft lithography, and drop-casting. However, the testing was limited to only compressive loading thus, there is a lack of data for the response of the sensor in tensile loading. Jabari et al. [39] demonstrated the development and characterization of a graphene silicone highly conductive structure printed by using piezoelectric pneumatic material jetting (PPMJ) system. This method is fabricated ten times faster than currently used extrusion-based methods as it prints using ink drops. This method used beads as a building unit of a 3D structure. Carrico and Leang [40] presented a novel method of printing ionic polymer metal composites (IPMC) which can be used in soft robots as actuators or sensors, especially in an underwater robotic system. The paper also discusses the drawbacks of printing IPMC with conventional 3D printing devices and changes made in the printing device to eliminate the issue. Valentine et al. [41] presented a novel hybrid 3D printing method for producing soft functional and pressure sensors. The hybrid printer integrates the direct ink writing (DIW) technique with the automated pick-and-place(P-P) technique to directly produce an electronic component of the dielectric elastomeric material of specific layouts with different surface mounts. But this limited the number of integrated surface-mount elements. Lin et al. [42] presented a novel method to develop a human skin-compatible wireless charging electrocardiogram (ECG) device for using it in both sitting and standing positions by hybrid 3D printing technique using bottom-up process by a pressure-driven direct ink writing (DIW) with automated pick-and-place process (APP) controlled by software written by Qt. A complex circuit can be developed using this technique with high accuracy. The need for soldering was also eliminated as printable pads were used to connect electrodes at the desired point. Carranza et al. [43] presented a method to fully develop the world's first three-dimensional (3D) electric circuit modeled in 3D modeling software using a hybrid 3D printing process. The hybrid 3D printing consisted of fused-deposition modeling 3D printer and micro-dispensing (μD) technology.

According to the above study, key findings of researchers are presented in Table 1 for manufacturing actuators and sensors in soft robotics.

Table 1 Key findings of soft components manufactured by AM

Technique used	Material	Application	Speed (in mm/s)	Quality	Drawbacks	References
FDM	SMP	Robotic grippers	90 with extrusion and 150 without extrusion	Good	Limited speed and extruder temperature	[31]
FDM	PLA	Fiber Bragg Grating-based pressure sensor	–	Good	Lack of test data	[32]
FDM	Thermoplastic elastomer NinjaFlex	Gripper, Hand Exo skeleton	30	Better than other soft actuators	Lack of study of the relationship between material hardness and the extruder temperature	[33]
DIW	Graphene	Gas sensing	25–125 depending on extruder temperature	Good but costly	Heating of sensors limits the operation to low voltage	[35]
Vat	3D conjugated photopolymer	Piezo resistor	3 per inch^2	Good	Small response of sensor and actuators	[36]
PBF	Stainless steel	Air flow sensor	800	Excellent	No data for tensile loading and the sensor was not waterproof	[38]
Hybrid material jetting Printer	Graphene-based nano composites	Highly conductive sensor	–	Excellent	The strength of the silicone used in ink	[39]
FDM	Nafion membarane for making IPMC	Actuators and Sensors	500	Excellent and ready to use	Hydrolyzation is carried outside the printer	[40]
Hybrid DIW Printer	TPU, AgTPU	Wearable electronic system	–	Good	The pressure sensor works up to a certain pressure range and the number of hard components was restricted due to strength concern	[41]
Hybrid DIW printer	Ecoflex and PDMS	Wireless chargeable ECG	–	Excellent	Hydrolyzation of the elastomers is required before printing for proper adhesion	[42]
Hybrid FDM Printer	ABS and DuPont CB028 silver paste	3D LED blinker circuit	50	Excellent	Repeated homogenization of the metallic paste, cleaning of metallic printer for 15–30 min, not fully automated	[43]

4 Discussion

From the above literature reviews, it may be concluded that for printing a soft component using 3D printing technologies, the selection of proper material is a must. The material chosen must be cheap and can be easily modified according to needs. For example, in [32], the FBG sensor was fabricated by the most commonly used soft material PLA, which is easily printable. Similarly, in [33], the material used is a thermoplastic elastomer. Thus, it can be seen that in the FDM process, the raw materials used as a filament were soft, and hence its application is limited to print components composed only from soft materials. Whereas the DIW technique use inks, which can be metal or nonmetal depending on need. For example, in [35], the gas sensor was developed with a metallic ink which was prepared in-house. Therefore, from here, it was observed that for the preparation of ink, the material chosen was so that it can be chemically treated, and the desired property was achieved. In [36], the whole sensor material was made separately and then printed. Hence, whichever method is used to print, the material must be chosen accordingly.

Next, the printer should be chosen according to the component to be produced. For instance, if there is a need to print a pressor sensor that should be embedded with a bed [32], then the FBD method is best as suitable material is available which can be readily printed at the desired location. Again, in [37], there is a need for a specific purpose sensor that cannot be readily printed using FBD as no such material is available. Hence, it is essential to develop a material that can be printed. Therefore, here DIW technology is suitable. Again, in this competitive era, there is a need for fast and highly accurate products. So, the printer should also be chosen in such a way that it can print is as fast as possible with high accuracy. However, the accuracy is of less concern today as there are different design software that can be integrated with the printers so that they can directly print the whole component on a single platform. But this is not applicable to speed as different printing techniques have different printing speeds of printing a product at its level best. Further, it is very interesting to observe that these printers can be integrated, and there is a scope of integrating these printers with conventional subtractive manufacturing technologies. This advantage of coupling different manufacturing technologies is revolutionizing the manufacturing processes and bringing a revolution in soft robotics as these hybrid techniques can manufacture soft and hard components together on a single substrate. This hybrid manufacturing technique is now able to print to date impossible 3D circuits [43].

According to the above discussions presented, Fig. 3 represents the most trending AM techniques for designing and manufacturing soft robotics materials to achieve quality aspects such as surface finish, materials, design, printing speed, strength. Figures 4 and 5 show the timeline in advancements of 3D techniques for soft robotics fabrication in terms of accuracy and cost, respectively. Accuracy and cost are the most promising parameters that have been considered in past research [36–44].

At last, in every technique there are some drawbacks. Some of them are illustrated below [40–43]:

- A wide range of materials is not available commercially for printing purposes.
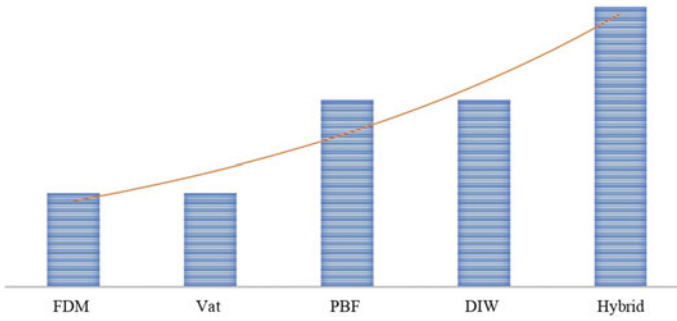
Fig. 3 Trending AM techniques for soft robotics materials
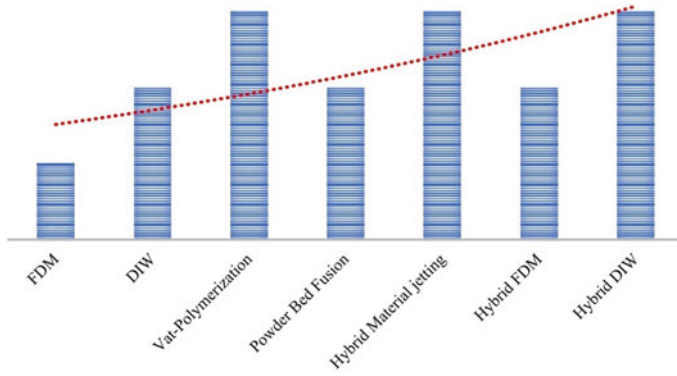
Fig. 4 Accuracy characterization of AM techniques soft robotics materials
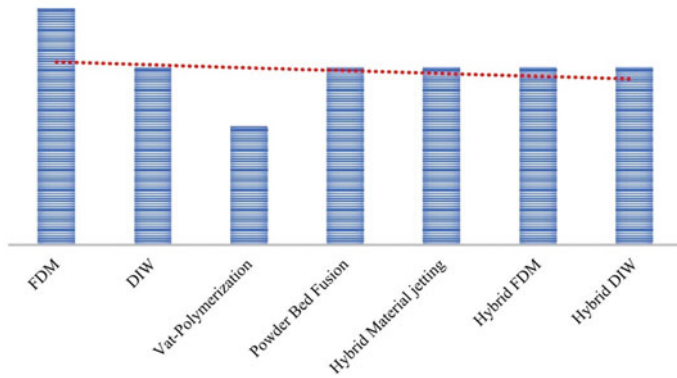
Fig. 5 Cost effectiveness of AM techniques for soft robotics materials

- Only a few technologies like FDM and some hybrid printers are being commercially used to print soft robots.
- Characterization of very few materials has been done yet.
- Chemical Treatment of some materials is done outside the printer.
- Proper cleaning and additional arrangement for pre-treating are needed where metallic ink is used because of their non-homogeneity.
- Limited integration of hard components with soft components due to strength issues.
- Optimization of the printer.

5   Conclusion

Nowadays, soft robots have emerged as a solution for the restricted application of hard robots due to their rigid components. This paper presents a short briefing of soft robots along with different types of soft actuators and sensors. Different 3D printing technologies have also been studied. It was observed that incorporating minor addition of components in the printer has eliminated various issues, such as an air-cooling arrangement that can be integrated into the printer to get a uniform temperature of nozzle during printing. This shows the modification has improved the printing quality. Similarly, the replacement of a conventionally used extruder with a plunger-based extruder controlled by a stepper motor has resolved the issue of a continuous supply of raw material to maintain the backpressure in the production process. The chemical treatment of IPMC raw material made it possible to directly print a soft actuator. The modification in the filament extruder gear eliminated the issue of slipping of the filament. To print ready to use sensors and actuators at a fast rate and with high accuracy, hybrid printers are used. However, and it was found that there is a wide range of research scope in the future for characterization and optimization of printing parameters for different materials used in soft robotics.

References

1. Goh, G.D., Agarwala, S., Goh, G.L., Dikshit, V., Sing, S.L., Yeong, W.Y.: Additive manufacturing in unmanned aerial vehicles (UAVs): challenges and potential. Aerosp. Sci. Technol. **63**, 140–151 (2017)
2. Goh, G.D., Dikshit, V., Nagalingam, A.P., Goh, G.L., Agarwala, S., Sing, S.L., Wei, J., Yeong, W.Y.: Characterization of mechanical properties and fracture mode of additively manufactured carbon fiber and glass fiber reinforced thermoplastics. Mater. Des. **137**, 79–89 (2018)
3. Sing, S.L., Yeong, W.Y., Wiria, F.E., Tay, B.Y., Zhao, Z., Zhao, L., Tian, Z., Yang, S.: Direct selective laser sintering and melting of ceramics: a review. Rapid Prototyp. J. **23**, 611–623 (2017)
4. Kim, S., Laschi, C., Trimmer, B.: Soft robotics: a bioinspired evolution in robotics. Trends Biotechnol. **31**, 287–294 (2013)
5. Chowdhary, G., Gazzola, M., Krishnan, G., Soman, C., Lovell, S.: Soft robotics as an enabling technology for agroforestry practice and research. Sustainability **11**, 6751 (2019)

6. Calisti, M., Giorelli, M., Levy, G., Mazzolai, B., Hochner, B., Laschi, C., Dario, P.: An octopus-bioinspired solution to movement and manipulation for soft robots. Bioinspir. Biomim. 6 (2011)

7. Wallin, T.J., Pikul, J., Shepherd, R.F.: 3D printing of soft robotic systems. Nat. Rev. Mater. **36**(3), 84–100 (2018)

8. Alici, G.: Softer is harder: what differentiates soft robotics from hard softer is harder: what differentiates soft robotics from hard robotics? Robotics?

9. Zolfagharian, A., Kouzani, A.Z., Khoo, S.Y., Moghadam, A.A.A., Gibson, I., Kaynak, A.: Evolution of 3D printed soft actuators. Sens. Actuators A Phys. **250**, 258–272 (2016)

10. Mu, X., Sowan, N., Tumbic, J.A., Bowman, C.N., Mather, P.T., Qi, H.J.: Photo-induced bending in a light-activated polymer laminated composite. Soft Matter **11**, 2673–2682 (2015)

11. Wang, Y., Pham, D.T., Ji, C.: Self-healing composites: a review. Cogent Eng. **2**(1), 1075686 (2015)

12. Ozbolat, I.T., Hospodiuk, M.: Current advances and future perspectives in extrusion-based bioprinting. Biomaterials **76**, 321–343 (2016)

13. Wang, S., Lee, J.M., Yeong, W.Y.: Smart hydrogels for 3D bioprinting. Int. J. Bioprinting. **1**, 3–14 (2015)

14. Mao, Y., Ding, Z., Yuan, C., Ai, S., Isakov, M., Wu, J., Wang, T., Dunn, M.L., Qi, H.J.: 3D printed reversible shape changing components with stimuli responsive materials. Sci. Reports **61**, 1–13 (2016)

15. Dang, W., Hosseini, E.S., Dahiya, R.: Soft robotic finger with integrated stretchable strain sensor. In: Proceedings of IEEE Sensors (2018)

16. Garrad, M., Feeney, I., Conn, A.T., Rossiter, J., Nemitz, M.P., Hauser, H.: An all soft, electro-pneumatic controller for soft robots. In: IEEE 4th International Conference on Soft Robotics RoboSoft, pp. 547–550. (2021)

17. Carrico, J.D., Hermans, T., Kim, K.J., Leang, K.K.: 3D-Printing and machine learning control of soft ionic polymer-metal composite actuators. Sci. Rep. **9**, 17482 (2019)

18. Adam Bilodeau, R., White, E.L., Kramer, R.K.: Monolithic fabrication of sensors and actuators in a soft robotic gripper. In: IEEE International Conference on Intelligent Robots and Systems, pp. 2324–2329. (2015)

19. Sachyani Keneth, E., Kamyshny, A., Totaro, M., Beccai, L., Magdassi, S.: 3D Printing materials for soft robotics. Adv. Mater. **33**, 2003387 (2021)

20. Miriyev, A., Stack, K., Lipson, H.: Soft material for soft actuators. Nat. Commun. **81**, 1–8 (2017)

21. Ivanova, O., Elliott, A., Campbell, T., Williams, C.B.: Unclonable security features for additive manufacturing. Addit. Manuf. 24–31 (2014)

22. Morin, S.A., Kwok, S.W., Lessing, J., Ting, J., Shepherd, R.F., Stokes, A.A., Whitesides, G.M.: Elastomeric tiles for the fabrication of inflatable structures. Adv. Func. Mater. 24 (2014)

23. Zarek, M., Layani, M., Cooperstein, I., Sachyani, E., Cohn, D., Magdassi, S.: 3D Printing of shape memory polymers for flexible electronic devices. Adv. Mater. **28**, 4449–4454 (2016)

24. Magnetic shear force transfer device. (2012)

25. Maute, K., Tkachuk, A., Wu, J., Jerry Qi, H., Ding, Z., Dunn, M.L.: Level set topology optimization of printed active composites. J. Mech. Des. 137 (2015)

26. Yap, Y.L., Sing, S.L., Yeong, W.Y.: A review of 3D printing processes and materials for soft robotics. Rapid Prototyp. J. **26**, 1345–1361 (2020)

27. Lazarus, N., Bedair, S.S.: Bubble inductors: Pneumatic tuning of a stretchable inductor. AIP Adv. **8**, 056601 (2017)

28. Wang, H., Totaro, M., Beccai, L.: Toward perceptive soft robots: progress and challenges. Adv. Sci. **5** (2018)

29. Shih, B., Christianson, C., Gillespie, K., Lee, S., Mayeda, J., Huo, Z., Tolley, M.T.: Design considerations for 3D printed, soft, multimaterial resistive sensors for soft robotics. Front. Robot. AI. **30** (2019)

30. Ozioko, O., Karipoth, P., Hersh, M., Dahiya, R.: Wearable assistive tactile communication interface based on integrated touch sensors and actuators. IEEE Trans. Neural Syst. Rehabil. Eng. **28**, 1344–1352 (2020)

31. Yang, Y., Chen, Y., Wei, Y., Li, Y.: 3D printing of shape memory polymer for functional part fabrication. Int. J. Adv. Manuf. Technol. **849**, 2079–2095 (2015)
32. Abro, Z.A., Hong, C., Zhang, Y., Siddiqui, M.Q., Rehan Abbasi, A.M., Abro, Z., Bin Tariq, S.Q.: Development of FBG pressure sensors using FDM technique for monitoring sleeping postures. Sens. Actuators A Phys. **331**, 112921 (2021)
33. Kai, Y., Yong, N.: YeowChen-Hua: high-force soft printable pneumatics for soft robotic applications. Soft Robot. **3**, 144–158 (2016)
34. D., M., D., O., RusDaniela: autonomous soft robotic fish capable of escape maneuvers using fluidic elastomer actuators. Soft Robot. **1**, 75–87 (2014)
35. Loh, H.A., Graves, A.R., Stinespring, C.D., Sierros, K.A.: Direct ink writing of graphene-based solutions for gas sensing. ACS Appl. Nano Mater. **2**, 4104–4112 (2019)
36. del Pozo, M., Liu, L., da Cunha, M.P., Broer, D.J., Schenning, A.P.H.J.: Direct ink writing of a light-responsive underwater liquid crystal actuator with atypical temperature-dependent shape changes. Adv. Funct. Mater. **30** (2020)
37. Cullen, A.T., Price, A.D.: Fabrication of 3D conjugated polymer structures via vat polymerization additive manufacturing. Smart Mater. Struct. **28**, 104007 (2019)
38. Kamat, A.M., Jayawardhana, B., Kottapalli, A.G.P.: PDMS flow sensors with graphene piezoresistors using 3D-Printing and soft lithography. Proc. IEEE Sens. (2020)
39. Jabari, E., Liravi, F., Davoodi, E., Lin, L., Toyserkani, E.: High speed 3D material-jetting additive manufacturing of viscous graphene-based ink with high electrical conductivity. Addit. Manuf. **35** (2020)
40. Carrico, J.D., Leang, K.K.: Fused filament 3D printing of ionic polymer-metal composites for soft robotics. Smt Matr. Struc. 70–82 (2017)
41. Valentine, A.D., Busbee, T.A., Boley, J.W., Raney, J.R., Chortos, A., Kotikian, A., Berrigan, J.D., Durstock, M.F., Lewis, J.A.: Hybrid 3D printing of soft electronics. Adv. Mater. **29** (2017)
42. Lin, R., Li, Y., Mao, X., Zhou, W., Liu, R.: Hybrid 3D printing all-in-one heterogenous rigidity assemblies for soft electronics. Adv. Mater. Technol. **4** (2019)
43. Carranza, G.T., Robles, U., Valle, C.L., Gutierrez, J.J., Rumpf, R.C.: Design and hybrid additive manufacturing of 3-D/volumetric electrical circuits. IEEE Trans. Compon. Packag. Manuf. Technol. **9**, 1176–1183 (2019)
44. Frank, J.R., Grant, G.T.: 3D Printing in Medicine. Springer, Cham (2017)

Fabricating Micro-Holes Through Micro-EDM Process and Their Circularity Testing

Abhinav Kumar ⓘ**, Deepak Kumar** ⓘ**, and Nirmal Kumar Singh** ⓘ

1 Introduction

Micro-EDM is useful for making microstructures, and devices for many applications in industry, robotics, and nowadays in the medical field like bio-implant [1]. The significant difference between macro and micro-EDM lies in the flow of discharge energy, tool dimension, and frequency of the pulse power generator [2]. The functioning mechanism of micro-EDM is similar to that of traditional EDM in which a sequence of electrical discharge takes place between two electrodes i.e., tool electrode and workpiece under some voltage potential. This applied voltage potential breaks the insulating strength of the dielectric at optimum confined gap and spark occurs with high heat, this high heat melts and evaporates both electrodes [3]. The main benefit of this type of machining process is that it can machine materials of any hardness without any mechanical stress, chatter, vibration. The only limitation is material should have minimum electrical conductivity [4]. Micro-EDM machines can generate any intricate shape and design that is a replica of the tool, by the application of orbiting, the thread can be also generated on the workpiece [5]. In micro-EDM, controlling the servo gap of less than 10 μm is a challenging task. Generally, the servo mechanism is used to maintain the constant spark gap. The well-defined servo control mechanism avoids bad signals like arching and short-circuiting during discharge. Singh et al. [6] fabricated the microholes on titanium alloy (Ti-6Al-4V) through energy synchronization in the interelectrode gap in the die sink EDM process. They investigated the impact of energy synchronization on tool, workpiece, and dielectric under varying gap current and discharge on time. They achieved a high aspect ratio (17.4) of microholes. Xu et al. [7] fabricated the micro-holes on copper foil layer-based printed circuit board (PCB) through the micro-EDM

A. Kumar · D. Kumar (✉) · N. K. Singh
Indian Institute of Technology (Indian School of Mines), Dhanbad, Jharkhand 826004, India
e-mail: deepakme521@gmail.com; deepak.17dr000452@mech.ism.ac.in

principle. They achieved the microholes without any burr formation near the edge at a rotational speed of the tool electrode (10,000 rpm). Maity et al. [8] fabricated the high aspect ratio microholes through the micro-EDM process and optimized the process variable for circularity, recast layer, and machining time using the Taguchi method. Similarly, Kumar et al. [9] made up the microhole of high aspect ratio (10.9) on carbon fiber reinforced plastics (CFRP) via the micro-EDM principle. They optimized the process parameters for minimum tool erosion rate (TER) and maximum material erosion rate (MER) through the Taguchi method.

In the current work, a micro-EDM system is used for fabricating the microholes on a thin nickel sheet. It was found that the microholes are well defined in shape and size. The morphology and elemental characterization of the microholes were examined by high-definition FESEM images and EDX spectroscopy technique respectively. The circularity tolerance of the fabricated microholes was found 62 μm, 98 μm, 124 μm for 650 μm diameter tool corresponding to set peak current 300 mA, 350 mA, 400 mA respectively.

2 Materials and Methods

2.1 Mechanism of Micro-EDM

Micro-EDM is the thermoelectric machining process in which material is removed due to the thermal impact of electrical discharge. These discharges were created in the interelectrode gap by breaking the dielectric strength of the dielectric by applying some voltage potential. The voltage at which the dielectric strength breaks is called the breakdown voltage. The breakdown of dielectric creates a plasma channel which poses the minimum resistance to make the flow of current. The flow of current appears as electrical discharge. Moreover, this flow of current finally generates a large amount of heat and the material is removed in form of micro-scale debris due to the melting and evaporation of both electrodes. The removal of the micro debris particle forms the micro confined cavity which is called a micro crater. The schematic of the micro-EDM setup with their peripheral components is exposed in Fig. 1.

2.2 Materials and Machining Environment

The workpiece was made of a nickel sheet with a thickness of 0.1 mm (Supplier: Sachin metals, Mumbai). Due to high corrosion/wear resistance at elevated temperatures, the material is preferred in gas turbines blades, aircraft engines, and combustion chambers. The combustor elements are invariably subjected to significant thermal stress as well as a highly corrosive environment. As a result, in such a harsh environment, the material must be able to retain appropriate mechanical and chemical
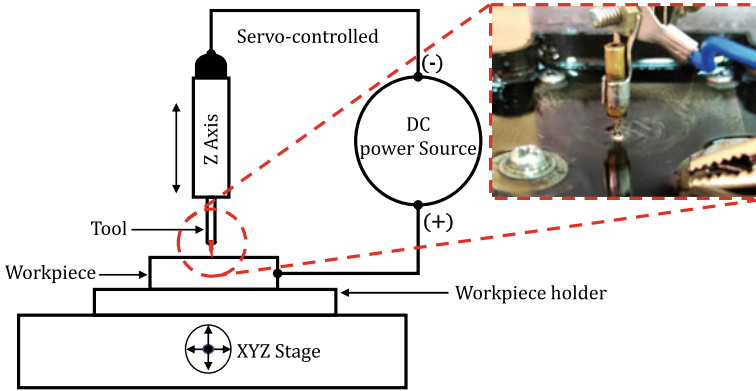
Fig. 1 Schematic diagram of micro-EDM setup with their peripheral components

properties [10]. The created microhole on the treated nickel sheet is shown in Fig. 2a.
The tool electrode material was chosen to be a circular tungsten rod having a diametral
length of 0.65 mm (Supplier: Special metal, Bangalore) as demonstrated in Fig. 2b.
Table 1 reveals the thermo-physical properties of the work material while Table 2
indicates the machining condition applied for fabricating the microholes.
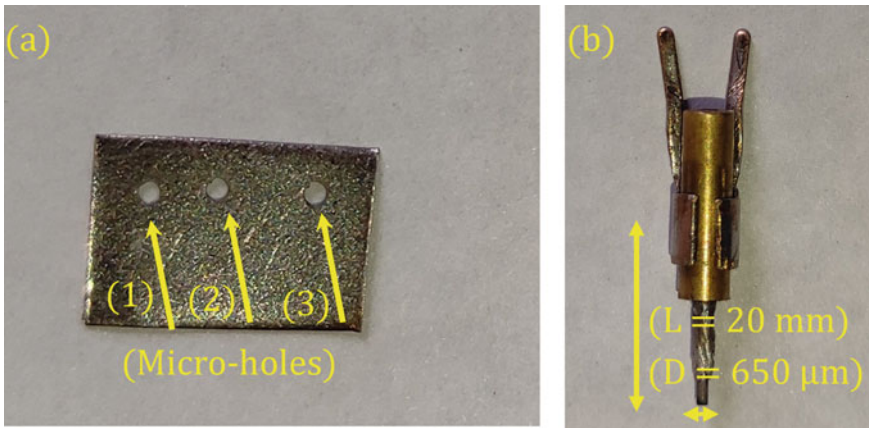
Fig. 2 **a** Nickel sheet with fabricated microholes and **b** tungsten micro rod

Table 1 Thermo-physical properties of nickel sheet

Thermo-physical properties	Value
Composition	99.9% Ni
Density	8.902 g/cm^3
Melting point	1455 °C
Hardness	638 VH
Electrical resistivity	69.3 nΩ·m

Table 2 Specifications of materials and machining conditions

a. Material selected			
Workpiece	Nickel thin sheet (100 μm thickness)		
Tool	Tungsten (ø 650 μm)		
Dielectric media	EDM oil		
Polarity	Straight		
b. Machining conditions	Hole-1	Hole-2	Hole-3
Open circuit voltage	24 V	24 V	24 V
Set peak current	300 mA	350 mA	400 mA
Discharge voltage	13.5 V	14 V	14.5 V
Discharge current	245 mA	250 mA	255 mA
Machining time	8 min	6 min	5 min

3 Results and Discussions

3.1 Morphological Characterization Through FESEM

The morphological characterization of the fabricated microholes was carried out by high-resolution field emission scanning electron microscopy (FESEM, Supra-55, Zeiss). The surface morphology of the fabricated microholes at varying peak current settings (300 mA, 350 mA, 400 mA) is represented in Fig. 3a–c. The figures denote that as the current intensity increases the amount of flow of discharge energy increases. The enhancement in the discharge energy deteriorated the circularity of the fabricated microholes. Moreover, it was noted that the formation of the recast layer increases near the edge interface region of the microhole surface and it is varying between 6.5–7.5 μm. The formation of the recast layer was due to the insufficient flushing pressure or due to the non-uniform splashing of molten material during the discharge time. Additionally, the edged unevenness can be easily detected when investigating the created micro-hole edges. Uneven edges are caused by irregular tool erosion and a lack of appropriate spark gap between the tool and the workpiece. Later on, the fabricated micro-holes circularity was measured by image processing software called Image J. It was found that lateral tool erosion contributes more

toward circularity inaccuracy. The circularity of the microholes was defined in terms of the radial distance between the two concentric circles. The change between the outer diameter of the circumscribed microholes and inscribing circle denotes the circularity. Table 3 indicates the measurement of circularity and circularity tolerance. It was observed that the circularity tolerance varied between 62 and 124 µm for the actual hole diameter of 650 µm. Figure 3d shows the calculation of circularity for microhole-1, and other holes' circularity is calculated similarly.
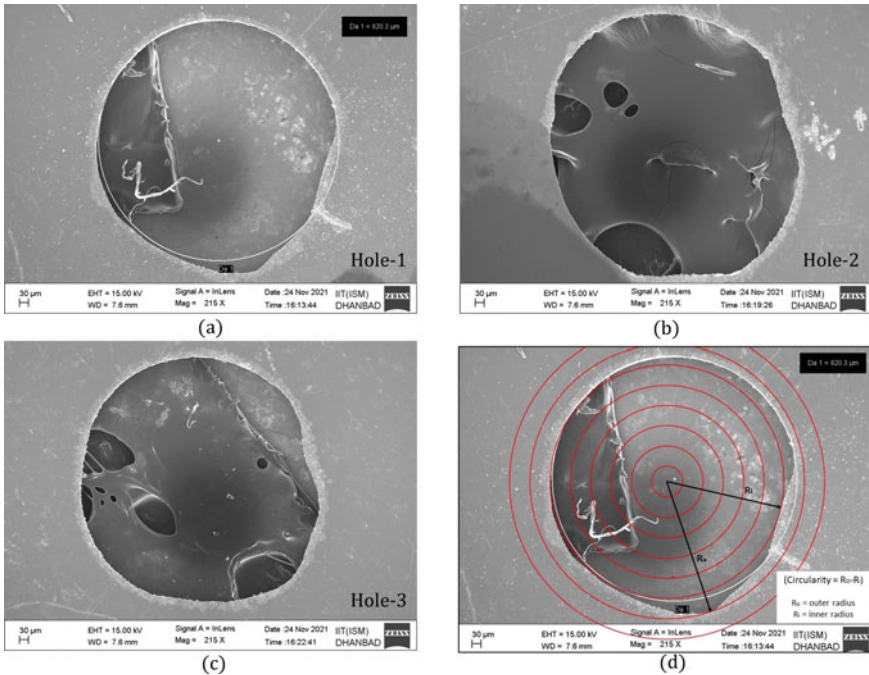
Fig. 3 **a**, **b**, **c** Morphological characterization of the fabricated microholes **d** circularity calculation

Table 3 Dimension of tool and microholes and circulation tolerance

	Hole-1 (µm)	Hole-2 (µm)	Hole-3 (µm)
Tool diameter	650	650	650
Average hole diameter	748	759	800
Circularity	62	98	124
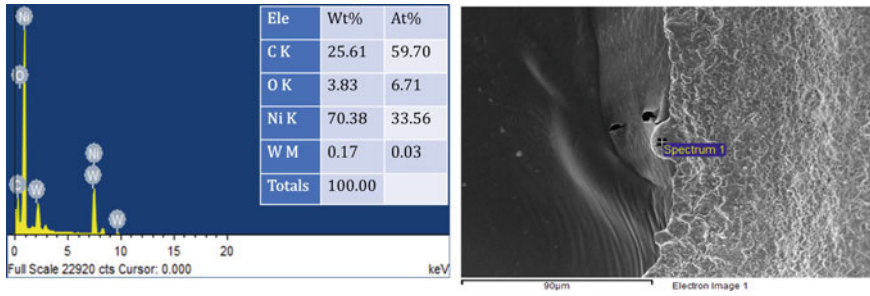
Fig. 4 EDX spectrum of the interface region of the microholes

3.2 EDX Analysis of Fabricated Microholes

The elemental characterization of the microholes was investigated using energy-dispersive X-ray spectroscopy (EDX). The presence of nickel in the EDX spectrum indicates that nickel is coming from its compositional part. Moreover, the availability of the tungsten on the machined surface indicates that there is a material migration and diffusion phenomenon happens. The EDX spectrum near the interface region of microholes with their compositional elements is shown in Fig. 4.

4 Conclusions

The followings are the conclusion from the above experimental investigation:

1. The microholes of diameter 748 µm, 759 µm, and 800 µm have been successfully fabricated from a tungsten micro tool of diameter 650 µm.
2. The circularity tolerance was found 62 µm, 98 µm, 124 µm for 650 µm tool diameter.
3. FSESEM image indicates that the microholes are a little bit deviated from the actual dimension due to side spark.
4. The presence of tungsten on the micro-hole interface region indicates the material transfer phenomenon that happens within the gap.

References

1. Jain, S., Parashar, V.: Critical review on the impact of EDM process on biomedical materials. Mater. Manuf Process (2021). https://doi.org/10.1080/10426914.2021.1942907
2. Zahiruddin, M., Kunieda, M.: Comparison of energy and removal efficiencies between micro and macro EDM. CIRP Ann. Manuf. Technol. **61**, 187–190 (2012). https://doi.org/10.1016/j.cirp.2012.03.006

3. Kumar, D., Singh, N.K., Bajpai, V.: Recent trends, opportunities and other aspects of micro-EDM for advanced manufacturing: a comprehensive review. J. Brazilian Soc. Mech. Sci. Eng. (2020). https://doi.org/10.1007/s40430-020-02296-4

4. Mohd Abbas, N., Solomon, D.G., Fuad, B.M.: A review on current research trends in electrical discharge machining (EDM). Int. J. Mach. Tools. Manuf. **47**, 1214–1228 (2007). https://doi.org/10.1016/j.ijmachtools.2006.08.026

5. Kumar, S., Dave, H.K., Desai, K.P.: A parametric study of radial tool actuation in orbital EDM. Adv. Mater. Process. Technol. **1**, 394–403 (2015). https://doi.org/10.1080/2374068X.2015.1133769

6. Singh, R., Dvivedi, A., Kumar, P.: EDM of high aspect ratio micro-holes on Ti-6Al-4V alloy by synchronizing energy interactions. Mater. Manuf. Process. (2020). https://doi.org/10.1080/10426914.2020.1762207

7. Xu. B., Feng, X.K., Wu, X.Y., Luo, F., Fu, L.Y., Zhai, X.T., et al.: Micro-EDM-assisted machining micro-holes in printed circuit board. Int. J. Adv. Manuf. Technol. 2021. https://doi.org/10.1007/s00170-021-06709-z

8. Maity, K.P., Singh, R.K.: An optimisation of micro-EDM operation for fabrication of micro-hole. Int. J. Adv. Manuf. Technol. (2012). https://doi.org/10.1007/s00170-012-4098-z

9. Kumar, R., Agrawal, P.K., Singh, I.: Fabrication of micro holes in CFRP laminates using EDM. J. Manuf. Process. (2018). https://doi.org/10.1016/j.jmapro.2018.01.011

10. Kang, S.H., Kim, D.E.: Investigation of EDM characteristics of nickel-based heat resistant alloy. KSME Int. J. **17**, 1475–1484 (2003). https://doi.org/10.1007/BF02982327

An Adaptive Neuro-fuzzy-Based Methodology for Prediction of Surface Roughness in Wire Arc Additive Manufacturing

Arshia Biswas and Shibendu Shekhar Roy

1 Introduction

In this era of Industry 4.0, additive manufacturing (AM) is believed to have the potential of bringing about a revolution in the manufacturing arena for its numerous benefits like design liberty, reduced inventory costs, mass customization, increased material proficiency, the ability to build object with complicated geometric in a short period, as well as fast prototyping [1]. Out of seven different AM processes, robotic wire arc additive manufacturing (WAAM) has gained more importance. Wire arc additive manufacturing is an advanced metal 3D printing technology that has one of the most increasing interests in aerospace, automobile, and other engineering applications. This technique is also beneficial for its properties like higher material usage efficiency, maintainability, cost-effectivity, a greater rate of deposition, and energy efficiency [2]. In recent years, WAAM is also becoming most popular in the defense field because of its ability to build large metals [3]. The quality of the surface of the WAAM manufactured parts plays a very important role in their performances, as a better quality surface significantly improves corrosion resistance, fatigue strength, etc. [4]. Therefore, the desired deposition characteristics can only be obtained by the right selection of input parameters. In the present work, the input variables are welding speed, wire feed speed, and overlap ratio. But on the other hand, the deposition mechanism is dependent on numerous uncontrollable factors which makes the process almost impossible to get a proper right solution. Therefore, modeling and prediction of deposition characteristics, namely surface roughness, are a very important parameter to define the WAAM process as WAAM has a vital role in advanced manufacturing since it is one of the promising additive manufacturing methods.

A. Biswas · S. S. Roy (✉)

Department of Mechanical Engineering, National Institute of Technology Durgapur, Durgapur, India

e-mail: shibendu.roy@me.nitdgp.ac.in

However, this can contend that the deposited feature depends on controllable inputs such as voltage, current, standoff distance together with wire material properties, weld speed, and inert gas flow. But the exact contribution of each of the process variables on the response is difficult to evaluate. Therefore, the desired deposition characteristics can only be obtained by the right selection of input parameters, and to map these input–output parameters, a very thorough study has been done regarding multi-pass welding by Cao et al. [5]; by Fang et al. [6] and by Somlo et al. [7]. Prominent contributions have been made by different authors for the past few years on such different deposition parameters. Van et al. [8] studied various process parameters that influence the geometrical, metallurgical, and mechanical consistency of the weld. Wu et al. [9] studied the influence of voltage, travel speed, and welding on the geometry of single weld beads in the wire arc additive manufacturing of stainless steel components. Using the Taguchi method, Bharat et al. [10] studied the effects of welding parameters on the additively deposited layer width. Rai et al. [11] and Aykut et al. [12] have employed multilayer perceptron (MLP) or artificial neural network (ANN) approaches to anticipate various weld bead characteristics based on the input process parameter. Different machine learning models have been comprehensively evaluated by researchers all over the world to predict the surface roughness of deposited layers by WAAM, in order to enhance the surface integrity of deposited layers by WAAM. With the passage of time, more precise models incorporating various optimizers were produced. Yaseer et al. [3] used mainly two machine learning (ML) models, such as random forest and ANN, to predict surface roughness, with the random forest model being reported to be a comparably superior one. 2nd order regression models were also utilized to sketch the input and output connection of the WAAM process in a research report by Ma et al. [13]. Other researchers like Liang et al. [14], Martina et al. [15] have mentioned the use of 3rd order regression models to carry out the same task. Different ML models like ANFIS and SVR were analyzed by Xia et al. [16] to predict the surface roughness of the weld bead.

This study proposes an application of adaptive neuro-fuzzy-based methodology for modeling and predicting the surface roughness of the depositing layer for three controllable process variables (welding speed, wire feed speed, and overlap ratio). The proposed method uses a hybrid learning method for supervised learning of the first-order Takagi–Sugeno-type fuzzy system. Several membership functions are present in the fuzzy interference system, among them three different MFs, namely trapezoidal, bell, and Gaussian, were used to compare the predicted response and experimental outputs.

2 Proposed Adaptive Neuro-fuzzy-Based Methodology

In this study, an adaptive neuro-fuzzy-based methodology is proposed to model surface roughness in the WAAM process.

2.1 Fuzzy and Adaptive Neuro-fuzzy System

A fuzzy inference system is operated based on some decision-making rule base systems like the 'if-then' rule. Without applying precise quantitative evaluation, a fuzzy system can model the reasoning process of the human being in qualitative form. This type of fuzzy modeling was explained by Takagi and Sugeno [17]. Fuzzification of the input parameters takes place before entering into the architecture, and defuzzification is done to the system outputs to convert it in a crisp set from a fuzzy set. The proper design of the number of fuzzy sets of input parameters, the type of membership functions, and the type and number of rules are very important to achieve the desired system. Though, it often uses trial and error procedures to work. The entry of fuzzy logic into the neural network systems makes it better for getting a significant response from the network.

The Takagi–Sugeno fuzzy model is used to create the suggested neural-fuzzy system. It takes advantage of adaptive system design to make learning and adaptation simpler. With two fuzzy rules, Fig. 1 depicts the adaptive neural-fuzzy system architecture [17].

1. If (p is P_1) and (v is V_1) then $g_1 = r_1 p + r_1 v + t_1$
2. If (p is P_2) and (v is V_2) then $g_2 = r_2 p + r_2 v + t_2$

where P_i and V_i represent the input fuzzy sets, g_i represents the outputs, r_i, s_i, and t_i are the decision parameters that will be estimated during the supervised learning. The architecture of the proposed method consists of five layers of neurons.

1st Layer-Fuzzy Layer: There is chance of adoption in every node of this layer. The nodes are defined as

$$O_{1,i} = \mu_{P_i}(p) \quad \text{where} \ i = 1, 2 \tag{1}$$
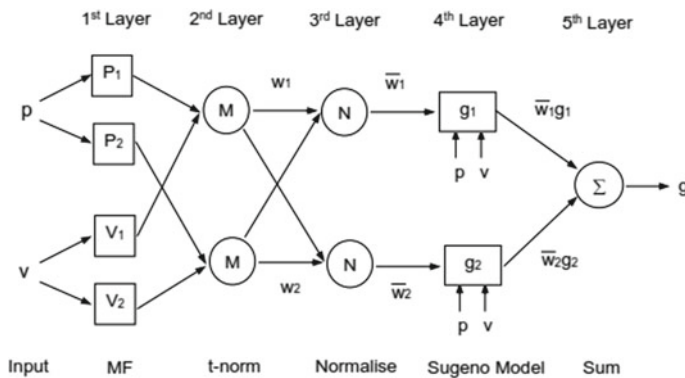
Fig. 1 Basic adaptive neuro-fuzzy architecture

$$O_{1,i} = \mu_{V_i}(v) \quad i = 3, 4 \tag{2}$$

where $\mu_{P_i}(p)$ and $\mu_{V_i}(v)$ are membership value for different fuzzy membership function (MF).

For the trapezoidal MF, $\mu_{V_i}(v)$ is given by

$$\mu_{V_i}(v) = \max\left(\min\left(\frac{v - a_i}{b_i - a_i}, 1, \frac{d_i - v}{d_i - c_i}\right), 0\right)$$

For Gaussian membership function, $\mu_{V_i}(v)$ is given by

$$\mu_{V_i}(v) = e^{\frac{-(v-c_i)^2}{2\sigma^2}} \tag{3}$$

where and $\{a_i, b_i, c_{i,}, d_i\}$ and $\{\sigma, c_i\}$ represent the premise parameters.

2nd Layer-Product Layer: Each node in the product layer is a fixed type node without any modification of the parameters. The output of the nodes of this layer is given as

$$O_{2,i} = w_i = \mu_{P_i}(p) \times \mu_{V_i}(v) \quad i = 1, 2 \tag{4}$$

w_i signifies the rule firing strengths.

3rd Layer-Normalized Layer: No adoption takes place in this layer. The fixed parameter values can be normalized by the following relations:

$$O_{3,i} = \overline{w}_i = \frac{w_i}{w_1 + w_2} \tag{5}$$

4th Layer-De-fuzzy Layer: In every node of this layer, the parameters will be adopted with node function as

$$O_{4,i} = \overline{w}_i g_i = \overline{w}_i (r_i p + s_i v + t_i) \tag{6}$$

where r_i, s_i, and t_i are consequent parameters.

5th Layer-Total Output Layer: This layer's output may be written as

$$O_{5,i} = \sum_{i=1}^{2} \overline{w}_i g_i \tag{7}$$

2.2 Supervised Learning of the Proposed System

In the proposed adaptive neuro-fuzzy architecture, the first and fourth layer are adaptive layers. In the 1st layer, the premise parameters are related to the input MFs and can be modified by proper adoption. The consequent parameters in the 4th layer represent the first-order polynomial. The purpose of the learning method is to modify both premise and consequent parameters to obtain the optimal adaptive neural-fuzzy system. The supervised learning methodology is based on hybridization of the least squares and gradient descent method for tuning premise and consequent parameters. Once the premise parameters evaluated, the least square approach is used to optimize the subsequent parameters. The gradient descent method is used to determine the ideal value of the premise parameters after acquiring the optimum values of consequent parameters.

3 Simulation Results and Discussions

Firstly, the suggested neuro-fuzzy system for modeling the surface roughness of the deposited layer under various operating circumstances must be constructed. To do so, a link must be formed between various training process characteristics and process performance. Xia et al. [16] used a robotic wire arc additive manufacturing system and 1.2 mm diameter mild carbon steel (ER 70S-6) filler wire in their trials. To investigate the impact of welding speed (S), wire feed speed (V), and overlap ratio (F) on surface roughness, the input process variables of welding speed (S), wire feed speed (V), and overlap ratio (F) were used.

The setting of welding speed (S) includes 4, 5.5, and 7 m/min; those of wire feed speed (V) include 5, 7, and 8.3 m/min; the overlap ratio (F) is set at 10, 20, and 25%. RSM was used to analyze the inter-relationship among three input process variables and responses. The quadratic regression equations for the surface roughness of the deposited layer were developed as follows.

Surface roughness (Ra) $= 0.635 - 0.198S + 0.137V + 1.01F + 0.007S^2 + 0.00061V^2 - 8.92F^2 - 0.00315SV + 0.399SF - 0.341VF$.

In this study, welding speed (S), wire feed speed (V), and overlap ratio (F) are inputs, whereas the surface roughness of the deposited layer is the output. After careful study, a 300 training data set is used from the above regression equations in adaptive neural-fuzzy system for modeling surface roughness. The membership function used for the input variables is trapezoidal, bell, and Gaussian shape. The fuzzy expressions for the welding speed are low speed (LoS); medium speed (MeS); high speed (HiS), for wire feed speed are slow velocity (SlV); medium velocity (MeV); high velocity (HiV), and for overlap ratio are low ratio (LoR); medium ratio (MeR); high ratio (HiR).

The number fuzzy rules are fixed by the nos. of levels of input parameters which are divided. This each level of input parameters is called the fuzzy set of input

parameters. In this study, three inputs such as welding speed, wire feed speed, and overlap ratio are subdivided further into 3 nos. fuzzy sets. Therefore, twenty seven rules can be exhibited in this proposed architecture. The ith rule for 1st-order Sugeno fuzzy system will follow:

IF welding speed (S_i) is high (HiS) AND wire feed speed (V_i) is high (HiV) AND overlap ratio (f_i) is low (LoR) THEN width of the layer is ($q_i S_i + r_i V_i + s_i f_i + t_i$), where q_i, r_i, s_i, and t_i are the consequent parameters. The flowchart for modeling the process performance using adaptive neuro-fuzzy system has been shown in Fig. 2.

The adaptive neuro-fuzzy system's first 6000 learning cycles have been completed. The suggested system is then created using hybrid learning. The surface roughness of the deposited layer is compared in Table 1 between expected values and true experimental output [16]. Figure 3 shows the absolute average error percentage of predicted surface roughness for test cases using ANFIS with three different membership functions. The absolute average error percentage of predicted surface roughness has been seen to be equal to 9.86%, 3.51%, 2.25%, and 2.21% for a regression model, trapezoidal MF, Gaussian MF, and bell-shaped MF, respectively. In almost all the cases, the bell and Gaussian membership function show slightly more accurate value than

Fig. 2 Flowchart of proposed adaptive neuro-fuzzy system
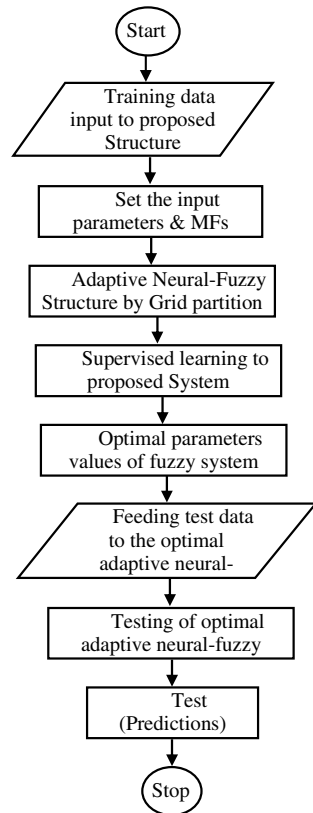
trapezoidal MF. This is because of the non-linear behavior of the response parameter concerning process parameters.

Table 1 Predicted surface roughness for trapezoidal MF, Gaussian MF, and bell MF

Welding speed	Wire feed speed	Overlap ratio	Surface roughness	Predicted surface roughness (mm)			
				Regression	Trapezoidal	Gaussian	Bell
7.0	8.3	0.25	0.312	0.2737	0.3117	0.2933	0.2889
7.0	8.3	0.2	0.406	0.4258	0.4056	0.3809	0.3783
7.0	8.3	0.1	0.611	0.5961	0.6104	0.5853	0.5815
7.0	7.0	0.25	0.185	0.2230	0.1841	0.1725	0.1724
7.0	7.0	0.2	0.259	0.3529	0.2577	0.2423	0.2439
7.0	7.0	0.1	0.504	0.4789	0.5015	0.4868	0.4879
7.0	5.0	0.25	0.201	0.149	0.1963	0.1985	0.1984
7.0	5.0	0.2	0.24	0.2448	0.2342	0.2366	0.2369
7.0	5.0	0.1	0.318	0.3026	0.3104	0.3145	0.3147
5.5	8.3	0.25	0.311	0.3291	0.3096	0.2988	0.2982
5.5	8.3	0.2	0.603	0.5111	0.6002	0.5866	0.5877
5.5	8.3	0.1	0.719	0.7412	0.7157	0.7022	0.7027
5.5	7.0	0.25	0.291	0.2722	0.286	0.2832	0.2844
5.5	7.0	0.2	0.419	0.4320	0.4116	0.4086	0.4111
5.5	7.0	0.1	0.612	0.6179	0.6013	0.6013	0.6036
5.5	5.0	0.25	0.213	0.1887	0.1985	0.2116	0.2118
5.5	5.0	0.2	0.25	0.3144	0.2326	0.2481	0.2485
5.5	5.0	0.1	0.416	0.4321	0.3874	0.414	0.4144
4.0	8.3	0.25	0.36	0.4159	0.3557	0.3547	0.3549
4.0	8.3	0.2	0.662	0.6278	0.6538	0.6549	0.6559
4.0	8.3	0.1	0.852	0.9179	0.8416	0.8447	0.8456
4.0	7.0	0.25	0.312	0.3529	0.2997	0.3088	0.3095
4.0	7.0	0.2	0.64	0.5426	0.6139	0.6358	0.6371
4.0	7.0	0.1	0.834	0.7883	0.8003	0.8297	0.8309
4.0	5.0	0.25	0.271	0.26	0.2326	0.2705	0.2706
4.0	5.0	0.2	0.382	0.4156	0.3268	0.3813	0.3815
4.0	5.0	0.1	0.601	0.5931	0.5147	0.6003	0.6005

Fig. 3 Percentage error in prediction of surface roughness in three MF
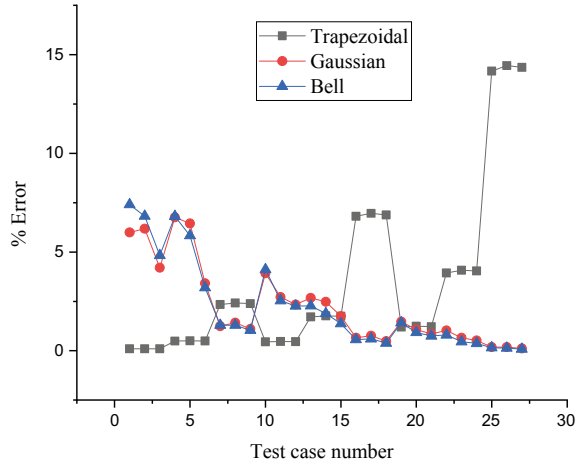
4 Concluding Remarks

To characterize and forecast surface roughness of deposition, the WAAM technique employs an adaptive neuro-fuzzy structure based on a first-order Takagi–Sugeno fuzzy system. Hybridization of least squares and gradient descent method is used. An adaptive neuro-fuzzy-based methodology has been effectively generated optimal trapezoidal, bell, and Gaussian-shaped membership functions distribution and fuzzy rules. The predicted response of the proposed architecture is compared with real experimental response values. The adopted bell-shaped MF in the adaptive neuro-fuzzy system has shown the most accurate output than the trapezoidal membership function.

References

1. Praveen, B.A., Lokesh, N., Buradi, A., Santhosh, N.: A comprehensive review of emerging additive manufacturing (3D printing technology): methods, materials, applications, challenges, trends and future potential. Mater. Today Proc. (2021)
2. Karunakaran, K.P., Suryakumar, S., Pushpa, V., Akula, S.: Low cost integration of additive and subtractive processes for hybrid layered manufacturing. Robot. Comput. Integr. Manuf. (2010)
3. Ahmed, Y., Heping, C.: Machine learning-based layer roughness modeling in robotic additive manufacturing. J. Manuf. Process. 543–552 (2021)
4. Ding, D., Pan, Z., Cuiuri, D., Li, H.: A multi-bead overlapping model for robotic wire and arc additive manufacturing (WAAM). Robot. Comput. Integr. Manuf. 101–110 (2015)
5. Cao, Y., Zhu, S., Liang, X., Wang, W.: Overlapping model of beads and curve fitting of bead section for rapid manufacturing by robotic MAG welding process. Robot. Comput. Integr. Manuf. 641–645 (2011)
6. Fang, H.C., Ong, S.K., Nee, A.Y.C.: Adaptive pass planning and optimization for robotic welding of complex joints. Adv. Manuf. 93–104 (2017)

7. Somlo, K., Sziebig, G.: Aspects of Multi-pass GTAW of Low Alloyed Steels. IFAC Papers OnLine 101–107 (2019)
8. Van, T., Dinh, S., Tat, K., Henri, P.: Wire and arc additive manufacturing of 308L stainless steel components: optimization of processing parameters and material properties. Int. J. Eng. Sci. Technol. 1015–1026 (2021)
9. Wu, W., Xue, J., Zhang, Z., Yao, P.: Comparative study of 316L depositions by two welding current processes. Int. J. Manuf. Process. 1502–1508 (2019)
10. Bharat, K., Anandakrishnan, V.: Experimental investigations on the effect of wire arc additive manufacturing process parameters on the layer geometry of Inconel 825. Mater. Today Proc. (2019)
11. Rai, R., Shettigar, A., Rao, S.S., Shriram: Development of a surface roughness prediction system for machining of hot chromium steel (AISI H11) based on artificial neural network. J. Eng. Appl. Sci. (2010)
12. Aykut, S.: Surface roughness prediction in machining castamide material using ANN. Acta Polytech. Hung. (2011)
13. Ma, G., Zhao, G., Li, Z., Yang, M., Xiao, W.: Optimization strategies for robotic additive and subtractive manufacturing of large and high thin-walled aluminum structures. Int. J. Adv. Manuf. Technol. (2019)
14. Liang, Z.: Characteristics of metal droplet transfer in wire-arc additive manufacturing of aluminum alloy. Int. J. Adv. Manuf. Technol. (2018)
15. Martina, F., Mehnen, J., Williams, SW., Colegrove, P., Wang, F.: Investigation of the benefits of plasma deposition for the additive layer manufacture of Ti–6Al–4V. J. Mater. Process. Technol. (2012)
16. Xia, C., Pan, Z., Polden, J., Li, H., Xu, Y., Chen, S.: Modelling and prediction of surface roughness in wire arc additive manufacturing using machine learning. J. Intell. Manuf. (2021)
17. Takagi, T., Sugeno, M., Fuzzy identification of systems and its applications to modeling and control. IEEE Trans. Syst. Man Cybern. **SMC-15**(1), 116–132 (1985)

Analysis of Productivity and Surface Characteristics of A356-TiB₂ Nanocomposites in EDM

Shailesh Dewangan, Santosh Kumar Sharma, Amit Kumar Vishvakarma, and Chitrakant Tiger

1 Introduction

In recent times, the need of micro-components is increasing vigorously, particularly in aerospace, automobile, medicine, and biotechnology. Electric discharge machining (EDM) emerges as the most powerful non-traditional machining methods. It is successful and widely accepted processes for production of complicated shapes, brittle, and hard materials. EDM is an erosion technique through which rapid recurring sparks are produced between the workpiece and tip of the tool in order to remove the later materials [1, 2]. Furthermore, EDM processes are effectively being used to machine composite materials into desired complex shapes. In EDM, conductive materials are suitable as the work piece. The sparks generated between tool and workpiece inside a dielectric fluid cause material removal. The principle behind the material degradation in EDM is anticipated by fusion and vaporization at localized region of the workpiece [3]. Recently, EDM has wide applications especially for high-strength alloys and composites [4]. The present era indicates that micromachining is quiet a challenging task for advanced materials such as superalloys and composites [5].

EDM is generally analyzed with multiple responses. Thus, parametric optimization is one of the major research areas in EDM [6, 7]. Dewangan et al. [8] analyzed the optimization of μEDM of Ti–6Al–4 V alloy and suggested that it is capacitance a significant parameter for MRR. In recent decades, composites have emerged, as a potential material for engineering applications [9]. Recently, in-situ aluminum metal matrix composites (AMMCs) have emerged as the most promising materials

S. Dewangan (✉) · A. K. Vishvakarma · C. Tiger
Department of Mechanical Engineering, Chouksey Engineering College, Bilaspur, Chhattisgarh, India
e-mail: shaileshdewangan123@gmail.com

S. K. Sharma
Department of Mechanical Engineering, CSIT, Durg, Chhattisgarh, India

749

to eliminate the inherent defects of conventional composites. The key advantages these composites provide are their superior mechanical properties, hardness, wear, and rigidity. AMMCs, owing to their low density and low cost, have evolved prominently. Machining these materials, however, becomes a challenging task primarily because of high abrasive properties of reinforcements. Matrixes, such as aluminum, magnesium, and steel, are preferred materials. The common reinforcements used are SiC, B_4C, Al_2O_3, TiC, and TiB_2 [10]. However, in-situ-formed $Al-TiB_2$ composites have extraordinary properties which make them a promising for aero applications [11].

In last few years, domination of studies on conventional machining of MMCs over modern machining methods is witnessed. Thus, it is clear that an in-depth understanding is further required on non-traditional processes of MMCs [12]. Therefore, the current work is an effort to investigate machining of non-traditional process methods; the main purpose of this research is to deliver the innovative trends in modern machining aspects of metallic composites. The machining of EDM for making composite equipment overcomes the barriers and meets the aerospace industry's needs. This article presents EDM characteristics $A356-TiB_2$ nanocomposites and their potential applications in the industry. Thus, the aim of the current research is to investigate the effectiveness of non-conventional EDM as applied to $A356-TiB_2$ nanocomposites.

2 Experimentation

The EDM experiments have been performed on Elektra CNC EDM with Model Company Electronica. The experiment setup of EDM is shown in Fig. 1. The dielectric fluid used was common grade oil and a side pressure of 0.3 kgf/cm^2. The workpieces of square shaped $60 \times 18 \times 5$ mm were machined from $A356-TiB_2$ composites for performing the EDM experiments. Further details of composite synthesis are described in earlier reports [13]. A copper electrode tool of diameter (10 mm) was used. Table 1 presents the levels of parameters with their designation.

2.1 Electric Discharge Machining of Composites

The responses considered was MRR and SR on composite material [14]. Response surface methodology was adopted to examine the responses over the entire factors and to locate interested regions where the responses reach optimum values. A total of 30 experiments was accomplished and to investigate the various impact on machining parameter like I_p, T_{on}, T_{au}, and V on SR and MRR. Calculated MRR and SR values with different experimental settings are shown in Table 2. The weight loss method is used to measure the material removal rate. And this is the weight loss method.
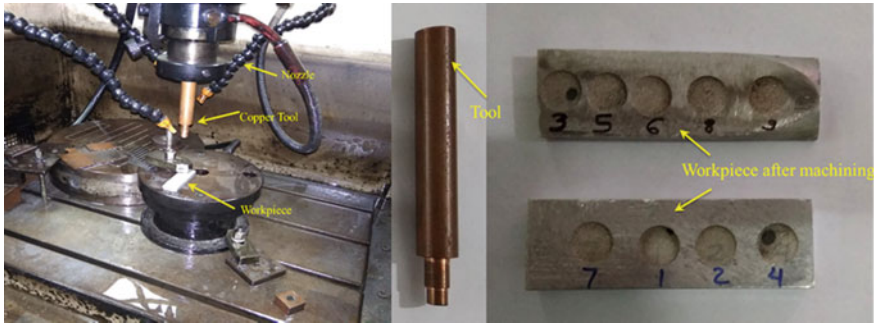
Fig. 1 Experimental setup of EDM machine

Table 1 Levels of EDM machining parameters

Factor designation	Name of the factor	Units	Level		
			Low (−1)	Center (0)	High (+1)
A	Pulse current (Ip)	A	5	100	15
B	Pulse-on time (T_{on})	μs	50	100	150
C	Duty cycle (T_{au})	%	80	85	90
D	Voltage (V)	V	40	45	50

And this is the ratio of the weight before and after machining of the workpiece to time with the density of the workpiece. This formula is demonstrated in Eq. 1. The surface roughness (Ra) was measured using portable style-type profilometer, and it is expressed in microns. The analysis was conducted using 'Design Expert 11' software, and the regression equations were obtained [15].

$$\text{MRR} = \frac{W_b - W_a}{t \rho_w} \tag{1}$$

where W_b = Before experiment weight of workpiece and W_a = After experiment weight of workpiece. t denotes the machining time, and ρ_w symbolizes density of workpiece.

3 Result and Discussions

3.1 Material Removal Rate

The 3D plots for MRR connection to the input factors are demonstrated in Fig. 2. Referring to the 3D surface plots of MRR, it is noted that when the current and

Table 2 Design model of experiments and results

Run	Pulse current (I_p)	Pulse-on time (T_{on})	Duty cycle (T_{au})	Voltage (V)	MRR (mm^3/min)	SR (μm)
	A	B	C	D		
1	15	150	90	40	15.876	6.67
2	5	50	80	50	3.786	2.56
3	10	100	85	45	8.897	4.01
4	10	100	85	45	9.876	3.98
5	15	150	80	50	16.812	6.65
6	15	50	90	50	18.987	7.98
7	5	50	90	40	4.012	3.45
8	15	50	80	40	19.786	8.76
9	5	150	80	40	2.123	0.98
10	5	150	90	50	2.001	0.87
11	5	50	90	50	4.987	2.51
12	15	50	90	40	19.876	7.23
13	5	150	80	50	3.001	0.87
14	10	100	85	45	8.675	3.87
15	15	150	90	50	17.897	5.97
16	10	100	85	45	8.987	3.67
17	15	50	80	50	19.876	7.98
18	5	50	80	40	4.789	2.87
19	15	150	80	40	17.234	5.98
20	5	150	90	40	2.562	0.76
21	10	100	85	35	9.876	4.98
22	10	100	85	55	9.765	4.89
23	10	100	85	45	9.543	4.65
24	10	50	85	45	12.897	5.98
25	15	100	85	45	15.987	6.76
26	10	100	85	45	10.879	5.14
27	5	100	85	45	0.345	1.32
28	10	100	75	45	11.987	5.89
29	10	150	85	45	9.998	4.01
30	10	100	95	45	10.001	5.56

voltage increase, the MRR increases drastically. Thus, pulse-on time and off time are identified as the critical parameters for MRR. This is anticipated due to an increase in discharge current produces a powerful spark of high temperature; as a result, the material melts and erodes away from the work piece. [16].
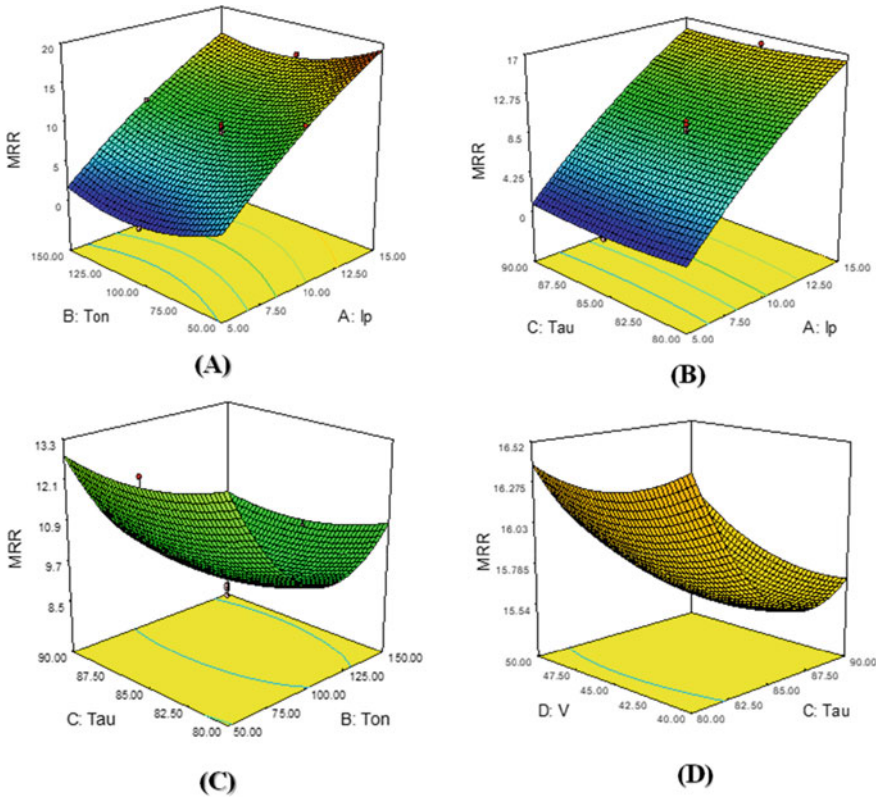
Fig. 2 Surface plots for MRR **a** MRR versus I_P and T_{on}, **b** MRR versus I_p T_{au} and T_{au}, **c** MRR versus T_{au} and T_{on}, **d** MRR versus V and T_{au}

Referring to Table 3, F-value of 241.57 implies that model for MRR is significant. The predicted R^2 and adjusted R^2 are 97.9% and 99.22%, respectively. The mathematical models developed for output responses were evaluated using ANOVA and F test [17]. This shows that the regression model has a good link between the independent variables, MRR confirming the model to be statistically significant. The empirical models developed for output responses MRR are presented in Eq. 2.

$$\begin{aligned} MRR = {} & +9.20 + 7.48A - 1.19B - 0.22C + 0.036D \\ & - .018AB - 0.058AC + 0.032AD - 0.029BC \\ & + 0.17BD + 0.13CD - 1.07A^2 + 2.21B^2 \\ & + 0.43C^2 + 0.13D^2 \end{aligned} \tag{2}$$

Table 3 ANOVA results for MRR

Source	SS	DOF	MS	F	P
Model	1059.58	14	75.68	241.57	<0.0001
A-I_p	1008.38	1	1008.38	3218.54	<0.0001
B-T_{on}	25.66	1	25.66	81.91	<0.0001
C-T_{au}	1.12	1	1.12	3.57	0.0813
D-V	0.031	1	0.031	0.100	0.7569
AB	0.50	1	0.50	1.59	0.2301
AC	0.055	1	0.055	0.17	0.6830
AD	0.016	1	0.016	0.052	0.8230
BC	0.013	1	0.013	0.042	0.8407
BD	0.47	1	0.47	1.50	0.2423
CD	0.25	1	0.25	0.80	0.3873
A^2	3.59	1	3.59	11.47	0.0049
B^2	15.29	1	15.29	48.80	<0.0001
C^2	5.00	1	5.00	15.96	0.0015
D^2	0.48	1	0.48	1.54	0.2363
Residual	4.07	13	0.31		
Lack of fit	3.54	10	0.35	1.99	0.3111
Pure error	0.53	3	0.18		
Cor total	1067.09	29			
SD = 0.56				$R^2 = 0.9962$	
Mean = 10.33				R^2 adjusted = 0.9920	
Coefficient of variation = 5.42				Predicted $R^2 = 0.9790$	
Predicted residual error of SS (PRESS) = 22.36				Adequate precision = 45.678	

3.2 Analysis of Surface Roughness

The depth of the craters created during sparking determines the roughness of the surface in machining. The high discharge between workpiece and tool creates crater wear. In Fig. 3, surface plots indicate that pulse current has most influences as compared to other factor because higher pulse current cause more energy released for melting, so later, cracks are formed resulting a poor surface finish [18]. So, it is essential to identify the optimum parameters to control the SR. Surface roughness value is directly effective on factors like pulse current and pulse-on time. Optimal setting of input parameters is thus crucial arrive at optimal responses of SR.

Similarly, referring to Table 4, F-value of 162.56 indicates that model for SR is significant. The experimental models developed for output responses SR are shown in Eq. 3.

$$\text{SR} = +4.15 + 2.69A - 0.96B - 0.051C - 0.089D + 0.036AB - 0.074AC$$
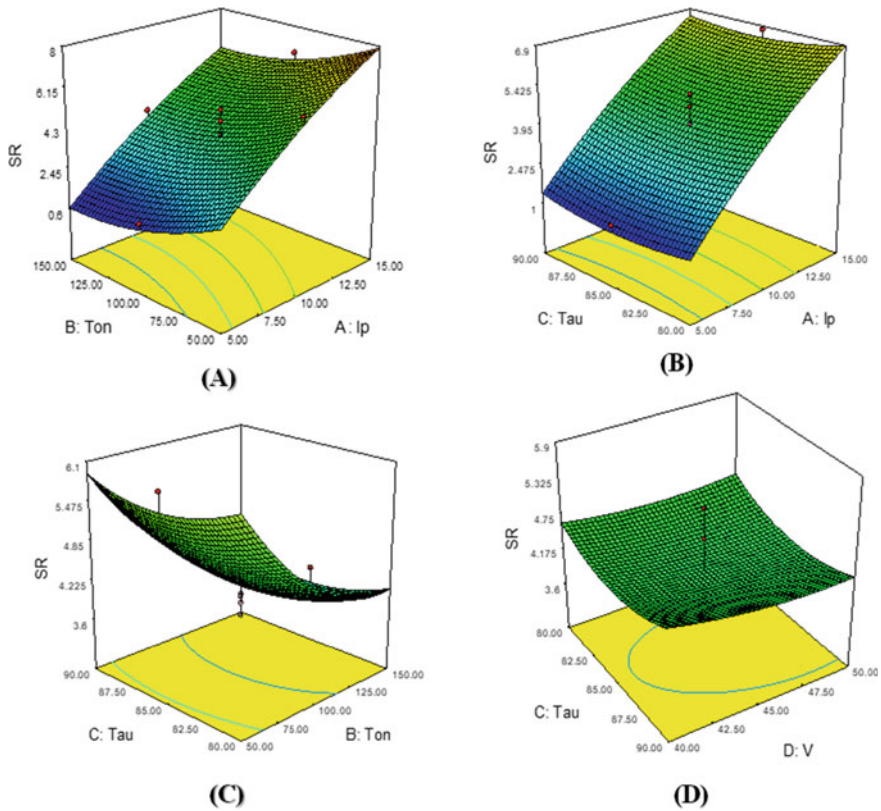
Fig. 3 Surface plots for SR **a** SR versus I_P and T_{on}, **b** SR versus T_{au} and I_p, **c** SR versus T_{au} and T_{on}, **b** SR versus T_{au} and **b** SR versus T_{au} and V

$$+ 0.034AD + 0.0087BC + 0.12BD - 0.056CD$$
$$- 0.39A^2 + 0.57B^2 + 0.3C^2 + 0.1D^2 \tag{3}$$

3.3 Surface Morphology of A356-TiB$_2$ Nanocomposite Material

The top surface morphology of EDMed surface was studied using optical micrographs of A356-TiB$_2$ nanocomposites. These optical images of different experimental setting are shown in Fig. 4. When during the machining of EDM, the very high discharge energy established in single-point sparking zone, so the metal is melting and vaporized. Further, the surface of nanocomposite is re-solidified and destruct in the dampen state and not removed by flushing, so this layer is formed

Table 4 Results of ANOVA for SR

Source	SS	DOF	MS	f	P
Model	151.42	14	10.82	162.56	<0.0001
A-I_p	130.36	1	130.36	1959.32	<0.0001
B-T_{on}	16.45	1	16.45	247.32	<0.0001
C-T_{au}	0.062	1	0.062	0.93	0.3519
D-V	0.19	1	0.19	2.87	0.1142
AB	0.021	1	0.021	0.32	0.5836
AC	0.087	1	0.087	1.31	0.2734
AD	0.018	1	0.018	0.27	0.6095
BC	1.225E−003	1	1.225E−003	0.018	0.8941
BD	0.23	1	0.23	3.39	0.0885
CD	0.051	1	0.051	0.76	0.3989
A^2	0.47	1	0.47	7.08	0.0196
B^2	1.01	1	1.01	15.13	0.0019
C^2	2.47	1	2.47	37.14	<0.0001
D^2	0.29	1	0.29	4.29	0.0587
Residual	0.86	13	0.067		
Lack of fit	0.72	10	0.072	1.55	0.3973
Pure error	0.14	3	0.047		
Cor total	154.61	29			
SD = 0.26 Mean = 4.58 Coefficient of variation = 5.63 PRESS = 4.69			$R^2 = 0.9943$ R^2 adjusted = 0.9882 Predicted $R^2 = 0.9692$ Adequate precision = 40.585		

micro-crack and pores [19]. The microcracks and micro-holes are evident in same figure.

4   Conclusions

In this work, a brief review on modern machining aspects of A356-TiB$_2$ nanocomposite with influence of machining parameter. The following conclusions may be drawn from the current study.

- According to the analysis material, removal rate is greatly influenced by pulse current and pulse-on time, and another factor does not affect as compare to pulse current.
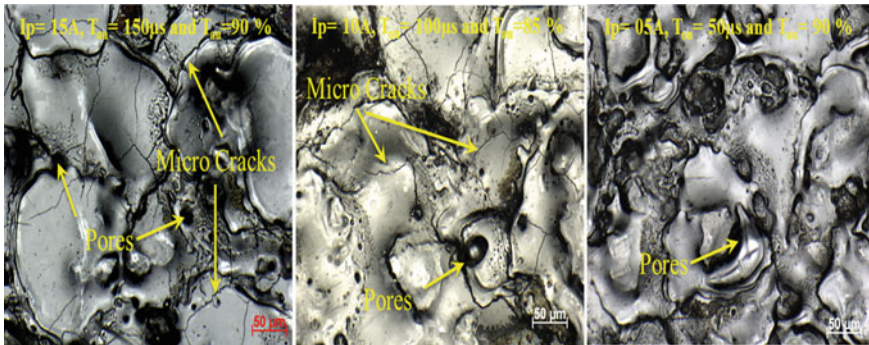
Fig. 4 Surface profiles of EDM-processed composites

- Analysis of surface roughness, when compared to other factors, pulse current has the greatest impact because greater pulse current causes more energy to be released for melting, resulting in later cracks, and a poor surface finish.
- In today's world, EDM provides supreme prospects for design and production of functional parts. Thus, surface morphology is very accurate in machining of EDM in A356-TiB$_2$ nanocomposites.

References

1. Kumar, P., Dewangan, S., Pandey, C.: Analysis of surface integrity and dimensional accuracy in EDM of P91 steels. Mater. Today Proc. **33**, 5378–5383 (2020)
2. Das, S., Paul, S., Doloi, B.: Feasibility assessment of some alternative dielectric mediums for sustainable electrical discharge machining: a review work. J. Brazilian Soc. Mech. Sci. Eng. **42**(4), 1–21 (2020)
3. Jadam, T., Sahu, S.K., Datta, S., Masanta, M.: Powder-mixed electro-discharge machining performance of Inconel 718: effect of concentration of multi-walled carbon nanotube added to the dielectric media. Sādhanā **45**(1), 135 (2020)
4. Bhattacharyya, B., Gangopadhyay, S., Sarkar, B.R.: Modelling and analysis of EDMED job surface integrity. J. Mater. Process. Technol. **189**(1–3), 169–177 (2007)
5. Gao, S., Huang, H.: Recent advances in micro- and nano-machining technologies. Front. Mech. Eng. **12**(1), 18–32 (2017)
6. Jebarose, J.S., Udaya, P.J., Divya, S.A., Sarala, R.C.: Multi-objective optimization of process parameters of wire EDM for machining of AMCs (LM$_5$/ZrO$_2$) using grey relational analysis. Mater. Today Proc. (2021)
7. Srinivasan, V.P., Palani, P.K., Balamurugan, S.: Experimental investigation on EDM of Si$_3$N$_4$–TiN using grey relational analysis coupled with teaching-learning-based optimization algorithm. Ceram. Int. **47**(13), 19153–19168 (2021)

8. Dewangan, S., Deepak Kumar, D., Jha, S.K., Biswas, C.K.: Optimization of micro-EDM drilling parameters of Ti–6Al–4V alloy. Mater. Today Proc. **33**, 5481–5485 (2020)
9. Gururaja, S., Ramulu, M., Pedersen, W.: Machining of MMCs: a review. Mach. Sci. Technol. **17**(1), 41–73 (2013)
10. Bains, P.S., Sidhu, S.S., Payal, H.S.: Fabrication and machining of metal matrix composites: a review. Mater. Manuf. Process. **31**(5), 553–573 (2016)
11. Jiang, R., Chen, X., Ge, R., Wang, W., Song, G.: Influence of TiB_2 particles on machinability and machining parameter optimization of TiB_2/Al MMCs. Chin. J. Aeronaut. **31**(1), 187–196 (2018)
12. Shyha, I., Rudd, M.: Electro-discharge machining of metal matrix composite materials. Adv. Mater. Process. Technol. **2**(2), 235–244 (2016)
13. Deepak kumar, S., Jha, S.K., Karthik, D., Mandal, A.: Fatigue analysis of A356-TiB2 (5 wt%) in-situ nano composites. Mater. Today Proc. **18**, 774–779 (2019)
14. Prabhu, M., Shanmughasundaram, P.: Material characterization and parametric optimization of unconventional machining of tin and tac reinforced stir casted vitallium metal matrix composite. Mater. Res. **23**(3) (2020)
15. Soundhar, A., Zubar, H.A., Sultan, M.T.B.H.H., Kandasamy, J.: Dataset on optimization of EDM machining parameters by using central composite design. Data Br. **23**, 103671 (2019)
16. Jithin, S., Joshi, S.S.: Surface topography generation and simulation in electrical discharge texturing: A review. J. Mater. Process. Technol. 298 (2021)
17. Das, S., Acharya, U.S., Rao, V.V.N.S., Paul, S., Roy, B.S.: Assessment of the surface characteristics of aerospace grade AA6092/17.5 SiCp-T6 composite processed through EDM. CIRP J. Manuf. Sci. Technol. **33**, 123–132 (2021)
18. Dewangan, S., Jha, S. K., Kumar, S. D.: Analysis of discharge characteristics during EDM Process. Lect. Notes Mech. Eng. 521–527 (2020).
19. Suresh Kumar, S., Uthayakumar, M., Thirumalai Kumaran, S., Varol, T., Canakci, A.: Investigating the surface integrity of aluminium based composites machined by EDM. Def. Technol. **15**(3), 338–343 (2019)

Interlaminar Shear Strength of 3D Printed PLA Material

Chagam Manohar Reddy, B. Sharath Chandra, G. Sumithra, K. Raja Narendar Reddy, Shakuntala Ojha, Dheeraj Kumar, and G. Raghavendra

1 Introduction

Three-dimensional (3D) printing is renowned as an emerging technology for the customized manufacturing. By increasing in functional of 3D printed parts and 3D printing techniques had been broadly used in various applications like in cultural creativity, concrete technology, construction projects, drug delivery, bio sensors, aerospace engineering, biomedicine, automotive electronics, cloud manufacturing, manufacturing complex components, etc.

The research on application of 3D printing were also discussed in various studies. Gargi Jani investigated on 3D printing technology in the forensic-science which is an advanced technology in the India and explained present current need by developing and incorporating 3D printing technology in the Indian-forensics [1]. Jian Hui Lim discussed about stress-cognizant for a 3D printing of free form concreting type structures and observed printing technique plan convincing improvement with mechanical attributes [2]. Jianzhuang Xiao investigated on huge scale 3D printing concreting type technology and its present status and coming opportunities and it showed that some guidance for the upcoming work were facilitated for the use of huge scale 3D printing concreting type technology in practise of constructing particular one [3]. Larissa A Melnyk investigated on combination of three-dimensional

C. Manohar Reddy · B. Sharath Chandra · G. Sumithra (✉) · K. Raja Narendar Reddy · S. Ojha
Department of Mechanical Engineering, Kakatiya Institute of Technology and Science, Warangal,
Telangana 506015, India
e-mail: gst.me@kitsw.ac.in

C. Manohar Reddy
e-mail: chagammanoharreddy74@gmail.com

G. Sumithra · D. Kumar · G. Raghavendra
Department of Mechanical Engineering, National Institute of Technology, Warangal,
Telangana 506004, India

Table 1 History of 3D printing technology

1984–86	Charles Hull invents 3D printing and coins the term "Stereo Lithography"
1992	First 3D printer built by 3D systems
1999	First application of 3D printing in the medical field–creating the human bladder
2000	Miniature human kidney created through 3D Printing
2006	The selective Laser sintering machine–printing multiple materials & fields
2009	First usable prosthetic leg–this opens the door for customized products using 3D printing
2011	3D printers start offering 14 K gold as printable material

printed type technology in pharmaceutical compounding and its progress, prospects and challenges and found that power of 3D printing of remedy as a power planning by achieving personalized precision type curing [4]. Jiangping Yuan investigated on the precision and arithmetic and reviewing of colour reproducing in complete colour 3D printing and showed future related viewpoint of the universal colour reproducing framework for precision complete colour 3D printing were explained, which will be prevented by the constraints of the printed type materials and together with its arithmetic boundary conditions [5].

The history of 3D printing gives the evolution of additive manufacturing with various technologies and equipment to produce efficient and effective products and it is clearly explained in Table. 1.

There are three main methods that are used for developing a product Subtractive manufacturing, Injection moulding and Additive manufacturing. The subtractive manufacturing is a type of developing process of a product that mainly focus on continuous cutting away the raw-material from the solid block like as the metal producing process. It is done manually, or by using Computer Numeric Controlled (CNC) machinery process. The injection moulding is a type of product developing process which is mainly used and focussed for producing products in very large volumes. Since the name itself indicates, product parts were produced or manufactured to inject heating material into the mould.

The additive manufacturing which is also known as 3D printing, 3D is an emerging technology which will be used to manufacture in a sequentially layering of materials to create three-dimensional objects with the help of computers. Since 35 years, Charies W. Hull framed a thought towards building components by 3D printing technology [6]. Additive manufacturing is currently being used in product design and manufacturing, consumer electronics, dental and medical applications, food and finally, construction on Earth.

Many researches were done on 3D printing to study the characteristics of printed object. Tianyun Yao et al. investigated on the supreme tensile strength of 3D printing polylactic acid (PLA) materials by using various printing orientations from the surface of printing bed and showed that the highest tensile strength will be reduced when the print angle will become lower or if the layer will become thick [6]. Veronica Geraldine Zaragoza investigated on the manufacturing process of 3D printed plastic
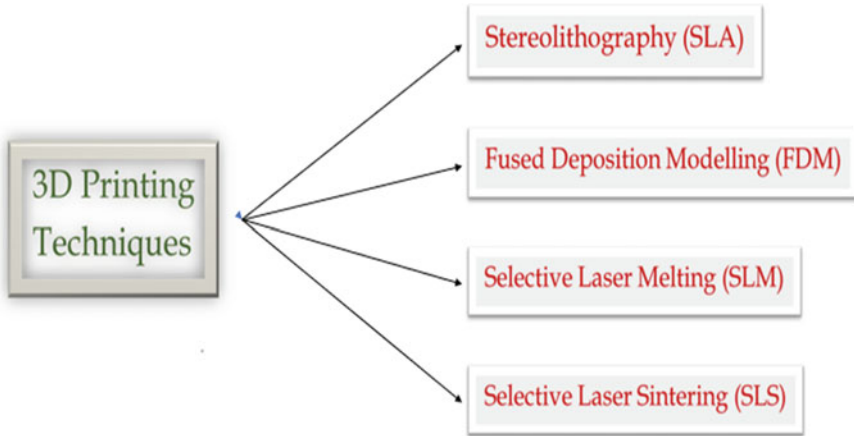
Fig. 1 Various 3D printing techniques

tools for air bend applicable things and its performance and found that polymeric material printing-parameters will affect the production of the polymeric type tools and also PLA dies by printing by using a printing pattern of 45-90-45° will exhibit the best performance [7].

Products that are developed by using 3D printing follows four different types of 3D printing type techniques are shown in Fig. 1.

The stereo lithography (SLA) is a type of 3D printing technique, which will be known as optical-fabrication, stereo lithography apparatus, resin type printing or photo solidification. This technique is used to create models, patterns, prototypes, and the producing objects in a manner of layer-by-layer fashion by considering the photo-chemical processes by which the light causes oligomers and the chemical-monomers by cross linking together for the formation of polymers.

The selective laser melting (SLM) is also considered as a type of metal additive manufacturing technique, which was considered the bed of powder by using the source of heat by creating metal parts. The selective laser sintering (SLS) is type of 3D printing type producing technique, which will be used the laser to manufacture products as the source of power to sinter the powder material and to aim the lasering automatically at the points in space by defining the 3D model and bind the material jointly by creating a solid type structure.

The fused deposition modelling (FDM) is the extensively preferred and flexible 3D printing technique used for developing products by fusing the material which is in solid form layer-by-layer deposition to get a final. This technique had been utilized in the automobile industry, lightweight tools to final functional components and ranging from testing models. It decreases the time it takes to create manufacturing tools by up to 85%. So many types of materials will be used with FDM techniques which includes the most common thermoplastics, pastes, chocolate, and even exotic materials like metal or wood infused thermoplastic. It is very cheap and fairly efficient.

The various studies on FDM explained the effect of 3D printing products that were manufactured by FDM are, Mohammed Hikmat investigated on tensile property basis of PLA parts which were fabricated by fused deposition modelling 3D printing technology and found that strength of part which was influenced by selecting processing parameters, where the only one of three like building orientation, diameter of nozzle and density of infill analytically were important and greatly effect the outcome observed [8]. Tianyun Yao investigated on failure of tensile strength and division angle of FDM 3D printing PLA material and found the failure of tensile strength which will be high with the increasing in the print angle or by lowering of layer thickness [9].

In this work the specimens were printed as per standard dimensions by using PLA material. The specimens were printed by varying infill densities like 10, 20, 30, 40, and 100%. Later these specimens were tested for shear strength.

2 Materials and Experiment

2.1 Printing Material

The printing material used for this study is Polylactic Acid (PLA), which is a thermoplastic material used as a filament to print the products in the 3D printing machine. PLA is comparatively easy to work with, usually requiring minimal effort to produce quality parts, especially on an FDM 3D printer. PLA material is also available in various colours as shown in Fig. 2. As it is created from natural or recycled materials, PLA is also embraced for its eco-friendliness, biodegradability, and many other characteristics.

The purpose of using PLA in 3D printing is because of its versatile advantages like it is easy to print, inexpensive, wide range of colour and options, biodegradable and eco-friendly, non-toxic and less fumes whilst it is burning. PLA is not only used in 3D printing but also used in food-packing, medical, prototyping, structural applications, textiles, cosmetics. Material properties of PLA are strength, flexibility, temperature

Fig. 2 Different colour filaments of PLA material

Table 2 Properties of PLA filament

Property	Unit	Value
Density	g/cm^3	1.25
Melting point	°C	195–215
Tensile strength	Mpa	50
Tensile modulus	Mpa	3600
Flexural strength	Mpa	83
Flexural modulus	Mpa	3800
Yield strength	Mpa	60
Impact strength IZOD	J/m	9.61

resistance, UV resistance, chemical resistance and strong mechanical properties and tribological properties as shown in Table 2.

The performance of PLA material is primarily used for 3D printing, unlike other plastics such as ABS or polycarbonate that are predominantly used in other ways. Overall, PLA has a great printing performance, due to a few factors. First, PLA does not require a heated bed, enclosure, or direct drive extruder, so the equipment needed to print this material is not expensive, sometimes costing under $100. Materials like ABS, PETG, and TPU all require at least one of these things to create quality prints. Second, PLA is widely accessible, and the consumer 3D printing industry has grown enough that PLA filament is readily available online. It is also pretty cheap, starting from around $20 kg. Other filaments, like PETG, costs a few extra dollars per kilogramme, and there are fewer options. Third, PLA is quite tolerant of varying print settings (within reason), so achieving a good print is pretty easy without a lengthy testing process to perfect slicer settings. Most default slicer profiles will leave you with a satisfactory model right off the bat, and just a little bit of adjustment can improve your prints even more. In contrast, ABS, PETG, and TPU are all sensitive to slicer settings, so your slicer profiles for these materials need to be delicately tuned to produce good prints. Last, PLA can be printed more quickly than most other materials, and due to the desire for rapid prototyping, PLA is popular for quickly developing prototypes. No one wants to wait around for days until their first prototype is produced because, by then, they may have moved on to the next prototype. The effect of internal structure of a specimen printed by using PLA material was studied by Can Tang on effecting the process characteristics which will affect the mechanical properties of 3D printed of a PLA lattice structures and showed that plastic platform stress of lattice structures and yield strength showed a lower trend and densification strain showed the increasing trend [10].

Fig. 3 Flash forge dreamer 3D printing machine
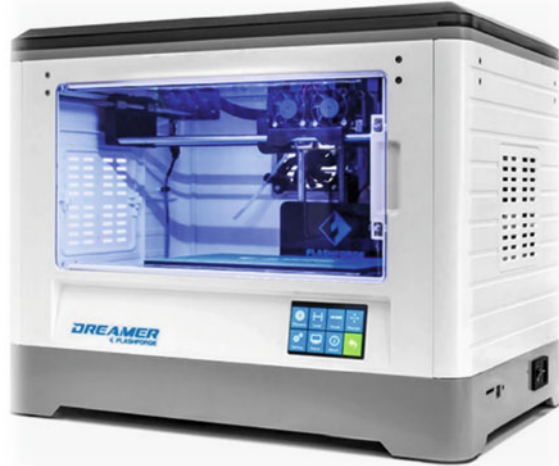
2.2 3D Printing Machine

3D printing specimens that are used for testing in this research were printed by Flash Forge Dreamer 3D printer with filament of 1.75 mm diameter as shown in Fig. 3. The flash forge dreamer is a compatible 3D printer, which has ability to produce high quality prints constantly of resolutions as same as 100 μ and it also featured a versatility type printing chamber of different filament printing. The building plate of 3D printer is made of 6.5 mm thickness alloy of type aluminium the same type of grade used in the aerospace industry and the excellent heat distribution and never deformed. The printing process parameters were controlled and specified by flash print 3D printing slicing software. The materials of Flash Forge Dreamer is compatible to PLA, ABS, PETG, and TPU95A filaments and thickness of printing layer of range from 0.05 mm to 0.4 mm, nozzle diameter of 0.4 mm. The print speed range of (30–100) mm/s and maximum extruder temperature of 240 °C.

2.3 Dimensions of Specimen

To determine flexural strength of 3D printed PLA material, specimens were produced by taking standard dimensions which are compatible to the testing machine. As our objective is to obtain how much load it can withstand and various stresses produced to cause failure. So, rectangle shape specimen of $(100 \times 20 \times 4)$ mm was considered for the testing, as it is shown Fig. 4.
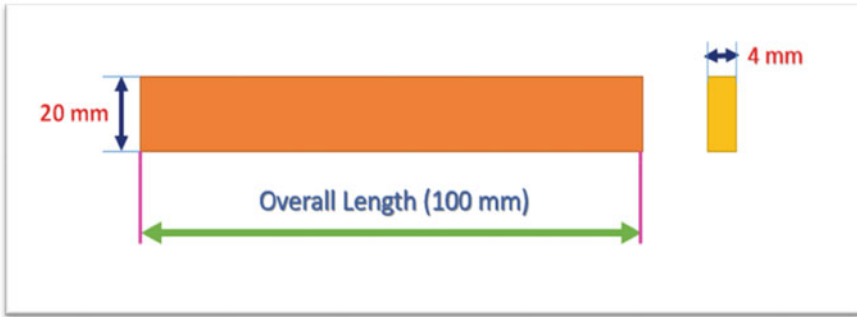
Fig. 4 Specimen dimensions for flexural test

2.4 Design and Printing of Specimens

The process flow of 3D printing involves three segments Designing, Setting and Printing of a three-dimensional specimen or object as shown in Fig. 5. The 3D specimen was prepared by using CATIA software by taking standard dimensions. Then after the 3D model was saved in stereo lithography (STL) file format which is to be understandable from 3D printing software as shown in Fig. 6 which joint that slices the 3D model by selecting process parameters like layer height, infill density, speed, shape, supports and temperature of the filament. The 3D printing software used in this study is Flash Print which is especially applicable to Flash Forge Dreamer 3D Printing Machine and software used for setting the process parameters is different for different 3D printing machines. Finally, the sliced model is exported as a G code which is readable by the 3D printer for creating the 3D shape.

2.5 Printing Types of Specimens

There were 5 different printing specimens. These were obtained by changing the infill densities 10, 20, 30, 40, and 100% in Flash Print printing software. Sample specimens of infill density 100% as shown in Fig. 7. The objects (specimens) were printed in a layer-by-layer fashion throughout the FDM type of 3D printing process. To study the flexural strength of PLA material, specimens of different infill densities were printed in this study.

2.6 Testing of Specimens

The printed specimens of various infill density percentages of 10, 20, 30, 40, and 100 were taken to find out the flexural strength of PLA material under Universal
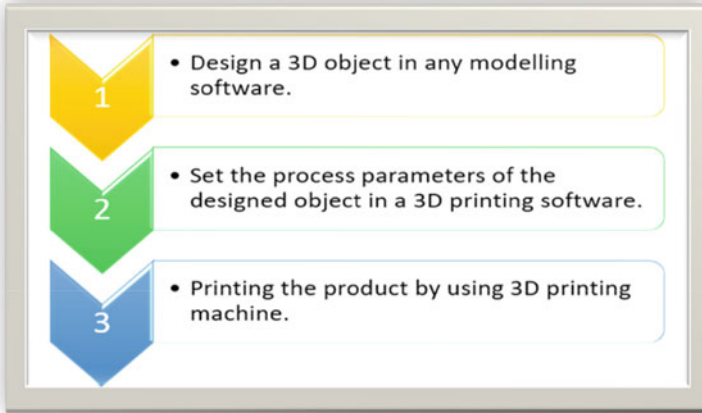
Fig. 5 Process flow of 3D printing
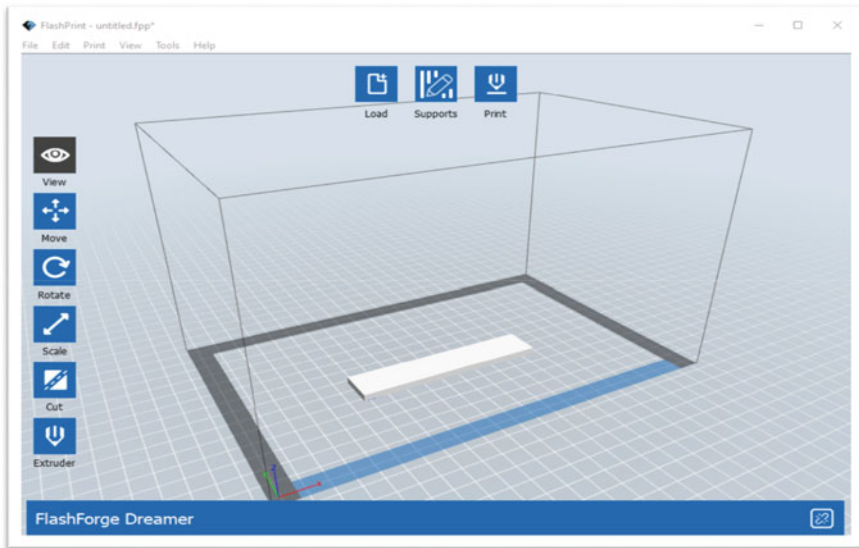
Fig. 6 3D printed specimen in flash print software for setting the process parameters

Testing Machine of capacity 30 KN as shown in Fig. 8. Marking the specimens with a straight line at the centre (50 mm from any end), 25 mm away left and right from the centre was done to place the specimen in the correct position on the testing machine as shown in Fig. 9.

Fig. 7 3D printed specimens of infill density 100%
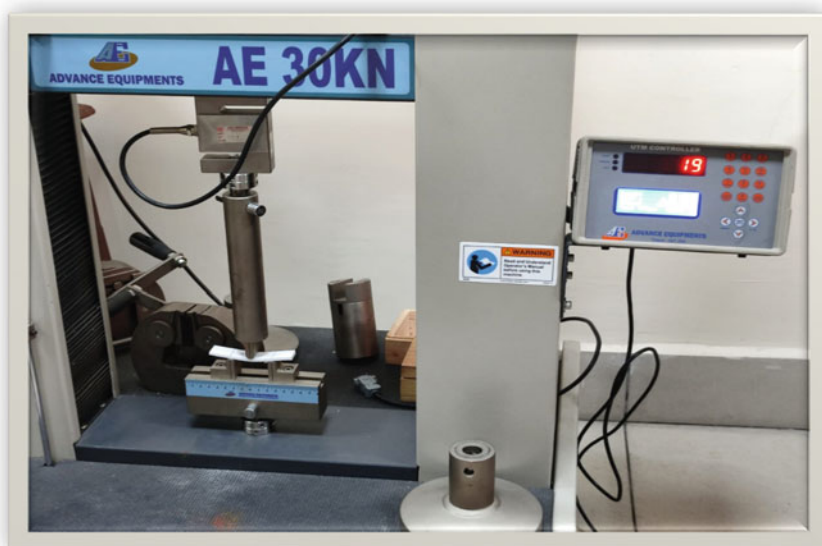
Fig. 8 Specimen under flexural testing by using universal testing machine

Fig. 9 Specimen removal after failure occurs in flexural testing

3   Results and Discussion

The flexural strength of 3D printed PLA material proceeded by the FDM method were studied and the failure (cracking) of specimens of different infill densities observed after testing as shown in Fig. 10. The peak load of different specimens of infill density 10, 20, 30, 40, and 100 are 19 kg, 22 kg, 26 kg, 28 kg, and 55 kg, respectively. The relation between load and displacement was observed in the graph shown in Figs. 11, 12, 13, 14 and 15 for different specimens. Area of failure and flexural strength was also observed.

From the above graphs, it is observed that maximum load was applied for 100% infill density specimen and the specimen is having higher strength compared to other specimens.

4   Conclusion

3D printing is an advanced and trending manufacturing technology to produce complex shapes and it has a vast applications. 3D printing is a multi-disciplinary technology, which involves in all types of things in the world like in medicine, construction, robotics, product development, aerospace, aeronautics, automobiles, etc., The PLA material, which is a thermoplastic and biodegradable used in this study gave better outcomes by testing 3D printed PLA specimens. Results showed that the increase in the infill density of 3D printed specimen increase the flexural strength.
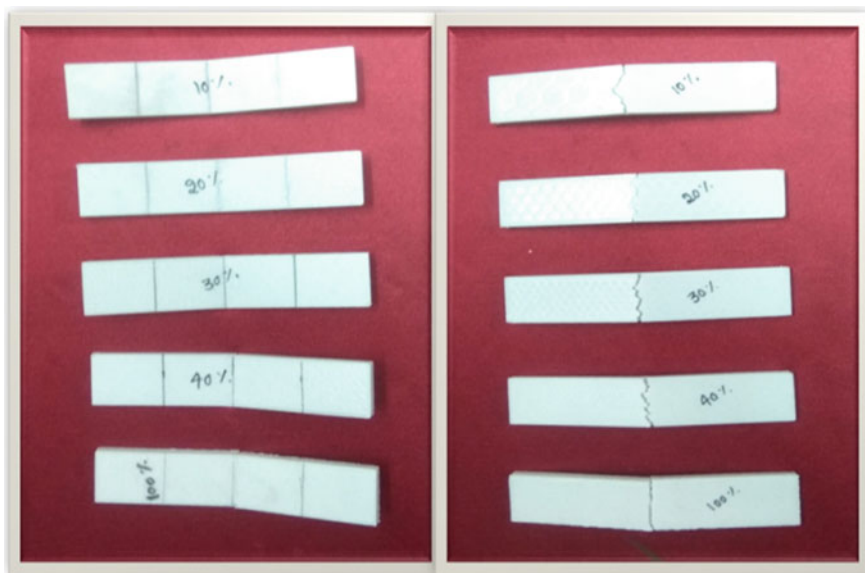
Fig. 10 Failure of 3D printed specimens of different infill densities, top view and bottom view
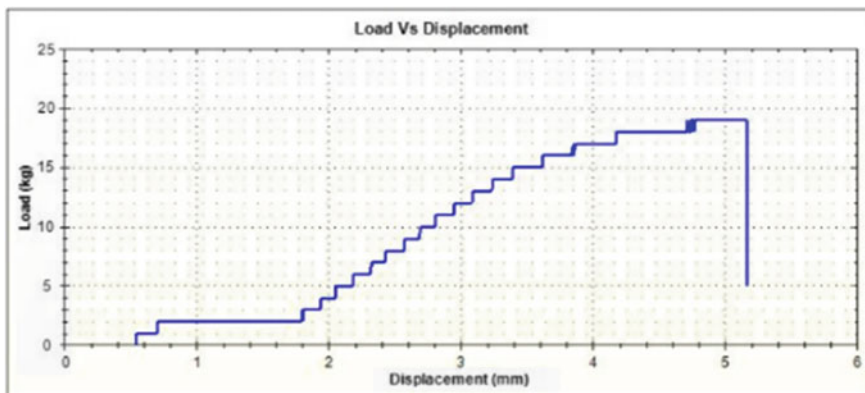
Fig. 11 3D printed specimen of infill density 10% under flexural test
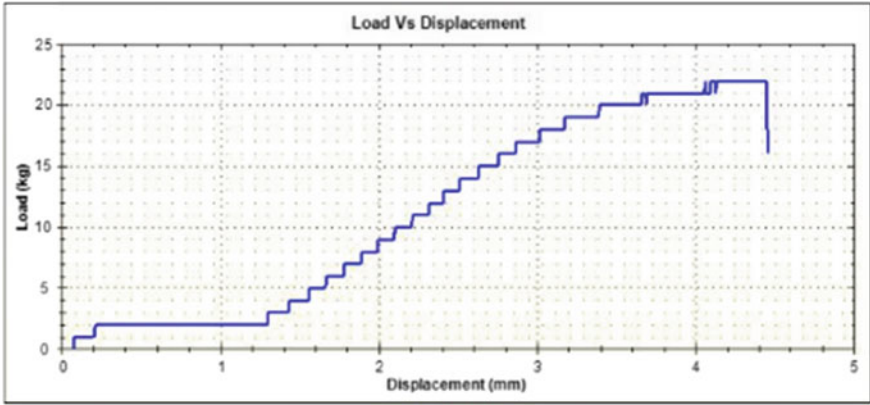
Fig. 12 3D printed specimen of infill density 20% under flexural test
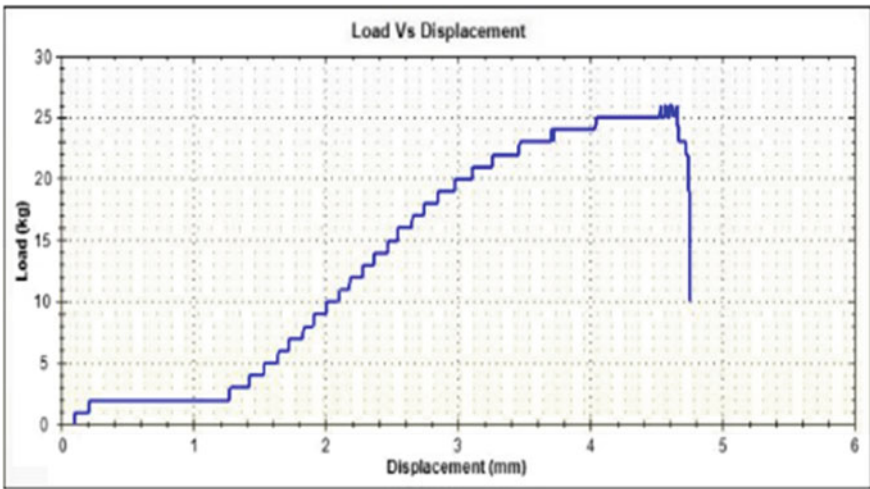
Fig. 13 3D printed specimen of infill density 30% under flexural test
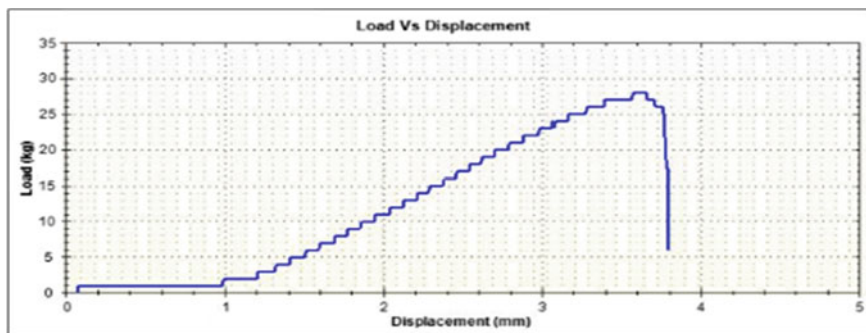
Fig. 14 3D printed specimen of infill density 40% under flexural test
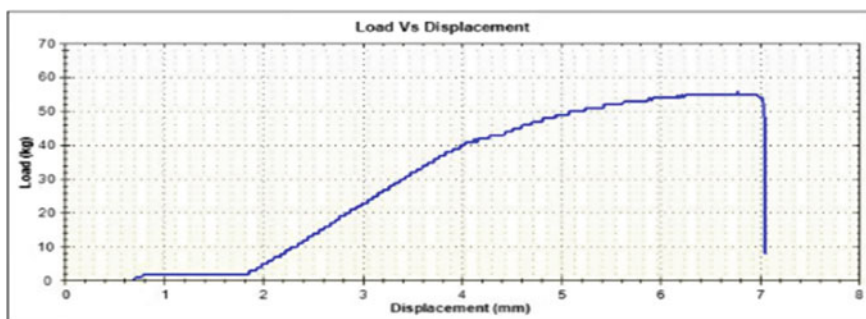
Fig. 15 3D printed specimen of infill density 100% under flexural test

References

1. Jani, G., et al.: Three-Dimensional (3D) printing in forensic science—an emerging technology in India. Ann. 3D Printed Med. 100006 (2021)
2. Lim, J.H., et al.: Stress-cognizant 3D printing of free-form concrete structures. J. Build. Eng. **39**, 102221 (2021)
3. Xiao, J., et al.: Large-scale 3D printing concrete technology: current status and future opportunities. Cem. Concr. Compos. 104115 (2021)
4. Melnyk, L.A., Oyewumi, M.O.: Integration of 3D printing technology in pharmaceutical compounding: progress, prospects, and challenges. Ann. 3D Printed Med. 100035 (2021)
5. Yuan, J., et al.: Accurate and computational: a review of color reproduction in Full-color 3D printing. Mater. Des. **209**, 109943 (2021)
6. Yao, T., et al.: A method to predict the ultimate tensile strength of 3D printing polylactic acid (PLA) materials with different printing orientations. Compos. Part B: Eng. **163**, 393–402 (2019)
7. Zaragoza, V.G., et al.: Manufacturing and performance of 3D printed plastic tools for air bending applications. J. Manuf. Process. **66**, 460–469 (2021)
8. Hikmat, M., Rostam, S., Ahmed, Y.M.: Investigation of tensile property-based Taguchi method of PLA parts fabricated by FDM 3D printing technology. Results Eng. **11**, 100264 (2021)

9. Yao, T., et al.: Tensile failure strength and separation angle of FDM 3D printing PLA material: Experimental and theoretical analyses. Compos. Part B: Eng. **188**, 107894 (2020)
10. Tang, C., et al.: Effect of process parameters on mechanical properties of 3D printed PLA lattice structures. Compos. Part C: Open Access **3**, 100076 (2020)

Intelligent Manufacturing Systems: Optimization of Process parameters

Firefly Algorithm Established Economic Load Dispatch with Loss Coefficients

O. Satya, Gummadi Srinivasa Rao, and B. Venkateswararao

1 Introduction

The chief objective of the electrical utility corporation is to offer continuous electrical supply to the customer without intermission. In such progression, economic operation of the system and entire demand fulfilment is essential to attain such that whole demand need be equally pooled among the units. Sharing the load among generating units reduces the load of generation. By doing this, fuel cost can be reduced. The reduction in the fuel cost further reduces the transmission losses. Foremost thoughts of fulfilling the objective function are loss minimization and fuel cost reduction. It can be obtained by economic load dispatch (ELD). It is established based on actual valued organization. In contemporary policy, only the cost function is assessed, and a global min. solution is figured self-sufficiently of the cost function [1]. It has also shared the generation among the different generating units, in this, less operating cost generating units utilized more effectively compared to the highest operating cost generating units. It is a constrained problem, and many methods have been established to solve these problems. For example, mathematical approaches are used in solving the economic load dispatch problems such as Newton–Raphson scheme, and estimated Newton–Raphson way is well-organized method. Though mathematical approaches are used in solving the economic load dispatch problems, these methods slowly started falling back because of difficulty in calculations and large solving time. Thus, use of optimization techniques into this field of power system became necessary [2]. And many deterministic optimization approaches also used to solve

O. Satya · G. S. Rao · B. Venkateswararao (✉)
Department of EEE, V. R. Siddhartha Engineering College, Vijayawada, Andhra Pradesh 520007, India
e-mail: bvrao.eee@gmail.com

G. S. Rao
e-mail: vasu1in@vrsiddhartha.ac.in

ELD problem like lambda iteration method, linear programming, gradient method, dynamic programming, nonlinear programming and quadratic programming. The mathematical computation becomes easier with the introduction of these optimization techniques. On the other hand, these approaches require enormous determinations in terms of computation. Due to difficulties of computing, hence, developing well-organized algorithm to catch optimal solution becomes vital. Thus, advanced optimization techniques started evolution. Cracking economic load dispatch, viz. genetic algorithm, particle swarm optimization, artificial bee colony optimization, bacterial foraging and also their alternatives came into picture [3].

Optimization procedure genetic algorithms (GA) are used for cracking ED problems in the last decade [4]. Tabu search is the other optimization techniques that is used in resolving ELD problem [5]. In reference [6], details analysis of system constraints of economic load dispatch were explained. In detail explanation of metaheuristic, optimization techniques were explained in [7]. In reference [8], need of economic load dispatch was given thoroughly. In this reference, economic load dispatch and generating operating cost were explained thoroughly [9]. Importance of optimization techniques in power systems was discussed in detail in this reference [10]. The recent fast metaheuristic algorithms have revealed the efficacy in allocating best values for finding the optimal solution. In this paper, newly introduced bioinspired established optimization technique firefly algorithm (FA) is well-known on the blinking behavior of fireflies. It was accompanying that the FA is further healthy and effective.

2 ELD Problem Structure

Statistically, the ELD is denoted in Eq. 1 with:

$$\text{Min} : O(x, u) \tag{1}$$

Focus to: $I(x, u) \leq 0$.
$E(x, u) = 0$.
$O(x, u)$: ELD objective function, $I(x, u)$: set of disparity restrictions, $E(x, u)$: set of likeness restrictions.

2.1 Cost Minimization

The goal of this is to reduce the cost. The total fuel cost function (F_1) for a quantity of thermal generating units can be illustrated by the following Eq. 2:

$$F_1 = \left(\sum_{i=1}^{NTG} \alpha_i + \beta_i P_{TGi} + \gamma_i P_{TGi}^2 \right) \$/h \qquad (2)$$

2.2 Constraints

Equality OPF constraints are present in Eqs. 3 and 4

$$P_{Gi} - P_{Di} - P_l = 0 \qquad (3)$$

$$Q_{Gi} - Q_{Di} - Q_l = 0 \qquad (4)$$

Dissimilarity constraints
The OPF inequality restrictions are

(a) Generator restrictions given in Eqs. 5, 6 and 7:

$$V_{Gi}^{\min} \leq V_{Gi} \leq V_{Gi}^{\max}; i \in N_g \qquad (5)$$

$$P_{Gi}^{\min} \leq P_{Gi} \leq P_{Gi}^{\max}; i \in N_g \qquad (6)$$

$$Q_{Gi}^{\min} \leq Q_{Gi} \leq Q_{Gi}^{\max}; i \in N_g \qquad (7)$$

(b) Transformer restrictions given in Eq. 8

$$T_i^{\min} \leq T_m \leq T_i^{\max}; i \in N_c \qquad (8)$$

(c) Shunt compensator restrictions provided in Eq. 9:

$$Q_{ci}^{\min} \leq Q_{ci} \leq Q_{ci}^{\max}; i \in N_c \qquad (9)$$

2.3 Test System

The data for six-unit system for an IEEE-30 system is as follows:

- The data is on 100 MVA base.
- For the analysis of this system, $V_{Pi\ \min}$, $V_{Pi\ \max}$, $\delta_{Pi\ \min}$, $\delta_{Pi\ \max}$ for i bus is 0.9 p. u., 1.1 p. u., $-45°$ and $+45°$, respectively. Here, $V_{Pi\ \min}$, $V_{Pi\ \max}$ are minimum and maximum voltage for ith bus considered in per unit. Similarly, $\delta_{Pi\ \min}$, $\delta_{Pi\ \max}$

are minimum and maximum degree of randomness considered according to the firefly algorithm for ith bus measured in degrees.

- The total cost rate of the system for six thermal units is given as:

$$F_T = F_1 + F_2 + F_3 + F_4 + F_5 + F_6 \tag{10}$$

- Thus, the six thermal generating units deliberated are having dissimilar characteristics, those are

$$F_1 = 0.00375 P_{G1}^2 + 2.00 P_{G1} + 0\$/h \tag{11}$$

$$F_2 = 0.01750 P_{G2}^2 + 1.75 P_{G2} + 0\$/h \tag{12}$$

$$F_3 = 0.06250 P_{G3}^2 + 1.00 P_{G3} + 0\$/h \tag{13}$$

$$F_4 = 0.00834 P_{G4}^2 + 3.25 P_{G4} + 0\$/h \tag{14}$$

$$F_5 = 0.02500 P_{G5}^2 + 3.00 P_{G5} + 0\$/h \tag{15}$$

$$F_6 = 0.02500 P_{G6}^2 + 3.00 P_{G6} + 0\$/h \tag{16}$$

- Active and reactive power constraints are considered which are given below:

$$50 \text{ MW} \leq P_{G1} \leq 200 \text{ MW} \tag{17}$$

$$20 \text{ MW} \leq P_{G2} \leq 80 \text{ MW} \tag{18}$$

$$15 \text{ MW} \leq P_{G3} \leq 50 \text{ MW} \tag{19}$$

$$10 \text{ MW} \leq P_{G4} \leq 35 \text{ MW} \tag{20}$$

$$10 \text{ MW} \leq P_{G5} \leq 30 \text{ MW} \tag{21}$$

$$12 \text{ MW} \leq P_{G6} \leq 40 \text{ MW} \tag{22}$$

$$-20 \text{ MVAR} \leq Q_{G2} \leq 100 \text{ MVAR} \tag{23}$$

$$-15 \text{ MVAR} \leq Q_{G3} \leq 80 \text{ MVAR} \tag{24}$$

$$-15 \text{ MVAR} \leq Q_{G4} \leq 60 \text{ MVAR} \tag{25}$$

$$-10 \text{ MVAR} \leq Q_{G5} \leq 50 \text{ MVAR} \tag{26}$$

$$-15 \text{ MVAR} \leq Q_{G6} \leq 60 \text{ MVAR} \tag{27}$$

- Also, the B-loss coefficient matrix of six-unit system is given below.

$$B = \begin{bmatrix} 0.0017 & 0.0002 & 0.1522 & -0.0001 & -0.0005 & -0.0002 \\ 0.0012 & 0.0014 & 0.0009 & 0.0001 & -0.0006 & -0.0001 \\ 0.0007 & 0.0009 & 0.0031 & 0 & -0.0010 & -0.0006 \\ -0.0001 & 0.0001 & 0 & 00.0024 & -0.0006 & -0.0008 \\ -0.0005 & -0.0006 & -0.0010 & -0.0006 & 0.0129 & -0.0002 \\ -0.0002 & -0.0001 & -0.0006 & -0.0008 & -0.0002 & 0.0150 \end{bmatrix} \tag{28}$$

3 Firefly Optimization Algorithm

Firefly algorithm is one of the swarm based, developed by Xin-She Yang, gained attractiveness because of less computation time, easy to implement and understand. FA is based on flashing behavior of lightning bugs [11]. It has several similarities with other algorithms like PSO, artificial bee colony optimization (ABC) and bacterial foraging (BFA) algorithms. The blinking lights obey certain physical rules, light concentration with the growth of distance. In general, the fireflies are a type of insects, having wings, living in tropical environment, producing cold light chemically, mostly yellow, green, pale-red lights are produced and their larvae are called glow-worm. Attraction of fireflies is shown in Fig. 1. The main crafty of firefly algorithm can be well-defined on 2 issues, those are variation of light intensity and formulation of attractiveness. Firefly algorithm can be employed on the distinct objective function [12]. In this ELD problem, generation bounds are stopping criterion of algorithm. Ease of implementation is its main advantage.

4 Simulation Results

The metaheuristic, nature-inspired, optimization algorithm, i.e., firefly algorithm is applied to six-unit system for minimizing fuel cost function. The data of generator cost coefficients, generation restrictions and B-coefficient matrix of 6-unit system is considered from standard IEEE-30 bus system. The two test cases discussed those are:
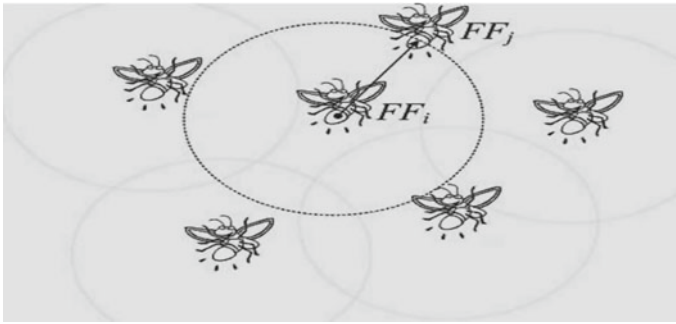
Fig. 1 Attraction of fireflies

(1). Economic load dispatch with 6 thermal unit system by neglecting losses.
(2). Economic load dispatch with 6 thermal unit system by considering losses.

4.1 Case Study-1: Six Thermal Unit System by Neglecting Losses

In this process, the preliminary clarification is generated arbitrarily within achievable range. The factors of the firefly algorithm recycled in the delinquent are prearranged in Table 1. The consequences for best megawatt generation of six generators are given in Table 2, and the results for best cost calculation are given in Table 3. The convergence characteristic plot is shown in Fig. 2. From Table 2, it can be observed that best possible output is generated for each generator within the specified limits as provided above. From Fig. 2, it can be observed that the firefly algorithm converges in 10–20 iterations. Also, from Table 3, it can be observed that the best possible cost (i.e., optimum cost) is achieved.

Table 1 Bounds recycled in firefly algorithm

S. No.	Stricture	Bound value
1	Overall no. of fireflies	20
2	Extreme no. of iterations	100
3	Randomness factor (α)	0.2
4	Attractiveness bound at $r = 0$, (β_0)	2
5	Absorption quantity (γ)	1

Table 2 Results for ELD by neglecting losses using firefly algorithm

Generator No.	Power generation (MW)
1	185.40
2	46.87
5	19.12
8	10.00
11	10.00
13	12.00

Table 3 Result for fuel cost and elapsed time using FA

Description	Using FA
Fuel cost ($/h)	767.6021
Elapsed time (s)	1.286669
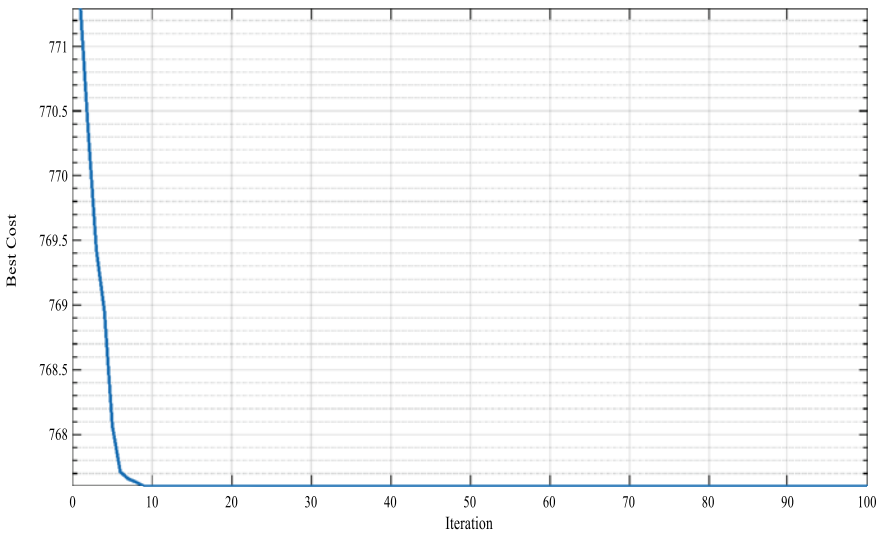
Fig. 2 Convergence characteristics plot of FA without losses

4.2 Case Study-2: Six Thermal Unit System by Considering Losses

In this way, the initial elucidation is made erratically within possible range. The constraints of the firefly algorithm charity in the delinquent are set in Table 4. The outcomes for best megawatt generation of generators are given in Table 5, and the results for best cost calculation and total losses are given in Table 6. The convergence characteristic plot is shown in Fig. 3. From Table 5, it can be observed that best possible output is generated for each generator within the specified limits as provided

Table 4 Constraints recycled in firefly algorithm

S. No.	Factor	Bound value
1	Entire number of fireflies	30
2	Extreme no. of iterations	50
3	Randomness bound (α)	0.2
4	Attractiveness factor at r = 0,(β_0)	2
5	Absorption coefficient (γ)	1

Table 5 Results for ELD by considering losses using firefly algorithm

Generator No.	Power generation (MW)
1	186.40
2	46.83
5	19.72
8	10.00
11	10.00
13	12.00

Table 6 Result for fuel cost, total losses and elapsed time using FA

Description	Using FA
Fuel cost ($/hr)	779.6898
Total losses (MW)	1.56
Elapsed time (s)	0.0357

above. From Fig. 3, it can be observed that the firefly algorithm converges in 5–10 iterations. Also, from Table 6, it can be observed that the best possible cost (i.e., optimum cost) is achieved with minimum losses.

4.3 Comparison of Fuel Cost for Dissimilar Methods for IEEE-30 Bus System by ignoring Losses

From Table 7, it can be observed that the fuel cost is calculated for six-generator units for IEEE-30 system by using different methods by neglecting losses in the system. From this, it can be inferred that the fuel cost calculated by firefly algorithm is the best fuel cost.
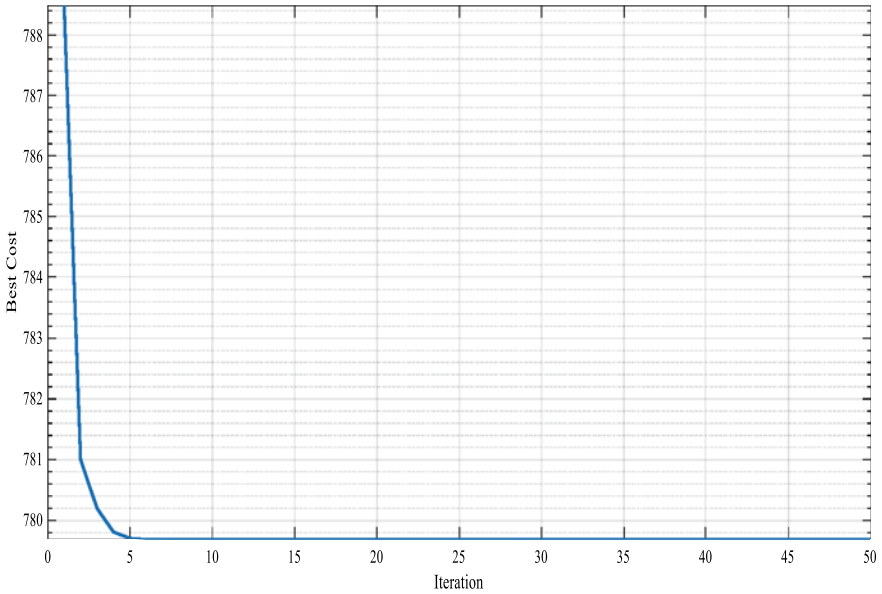
Fig. 3 Convergence characteristics plot of FA with losses

Table 7 Assessment of fuel cost for IEEE-30 bus system by ignoring losses

Process	Fuel cost ($/h)	Elapsed time (s)
Lambda iteration method	785	2.00271
Nonlinear programming	777.6026	0.72594
Quadratic programming	777.6026	0.168912
Genetic algorithm	777.6024	1.374535
Firefly algorithm	767.6021	1.286669

4.4 Comparison of Fuel Cost for Diverse Methods for IEEE-30 Bus System by Considering Losses

From Table 8, it can be observed that the fuel cost is calculated for six-generator units for IEEE-30 system by using different methods by considering losses. From this, it can inferred that the fuel cost calculated by firefly algorithm is the best fuel cost. Hereafter, the firefly algorithm is additional convergent and give optimal solution. As explained in the paper, every method has their way of solving and the results obtained from the firefly algorithm can explain that using the firefly algorithm provide the better optimization result, that is the best solution.

Table 8 Relationship of fuel cost for IEEE-30 bus system by seeing losses

Technique	Fuel cost ($/h)	Elapsed time (s)
Lambda iteration method	783.27	2.105946
Nonlinear programming	783.59	0.347736
Quadratic programming	788.37	0.190577
Genetic algorithm	784.28	1.87542
Firefly algorithm	779.6898	0.0357

5 Conclusion

In this paper, ELD problem solved with firefly algorithm by considering two different cases those are without and with losses for achieving best generation. It was observed that without considering the losses to meet the load demand of 283.4 MW, the cost required with FA is 767.6021 $/h, in the second case, with considering the losses to meet the same demand, it is required to generate more power that was 284.95 MW, it indicates that losses were 1.56 MW and generation cost was also increased to 779.6898 $/h. From the obtained results, it was observed that FA produces the better results compared to other methods like lambda iteration, NLP, QP and GA techniques.

References

1. Chaitanya, S.N.V.S.K., Ashok Bakkiyaraj, R., Venkateswara Rao, B.: Optimal Reactive Power Dispatch of Interconnected Power System Using Firefly Algorithm. In: Komanapalli V.L.N., Sivakumaran N., Hampannavar S. (eds.) Advances in Automation, Signal Processing, Instrumentation, and Control. Lecture Notes in Electrical Engineering, vol. 700. Springer, Singapore (2021). https://doi.org/10.1007/978-981-15-8221-9_22
2. P. Ramkee, Chaitanya, S.N.V.S.K., Rao, B.V., Ashok Bakkiyaraj, R.: Optimal reactive power dispatch under load uncertainty incorporating solar power using firefly algorithm. In: Advances in Energy Technology 2021. Lecture Notes in Electrical Engineering, vol. 766. Springer Nature Singapore Pte Ltd. (2021). https://doi.org/10.1007/978-981-16-1476-7_39
3. Rao, G.S., Obulesh, Y.P., Rao, B.V.: Enrichment of distribution system stability through artificial bee colony algorithm and artificial neural network. In. Handbook of Research on Smart Power System Operation and Control (pp. 35–55). IGI Global (2019).https://doi.org/10.4018/978-1-5225-8030-0.ch002
4. Nadakuditi G., Mohan Rao U., Bathina V., Pandi S. Economic load dispatch in microgrids using real-coded genetic algorithm. In: Soft Computing in Data Analytics Advances in Intelligent Systems and Computing book series, (vol. 758, pp. 377–386). Springer, Singapore, (2018). https://doi.org/10.1007/978-981-13-0514-6_38
5. Srinivasa Rao, G.: Voltage profile improvement of distribution system using distributed generating units. Int. J. Electr. Comput. Eng. **3**(3), 337–343 (2013)
6. Ahn, S.J., Moon, S.I.: Economic scheduling of distributed generators in a microgrid considering various constraints. In: IEEE Power and Energy Society General Meeting, Calgary, AB (2009). Kaur, A., Singh, H.P., Bharadwaj, A.: Analysis of economic load dispatch using genetic algorithm. Int. J. Appl. Innov. Eng. Manag. **3**, 240–246 (2014)
7. Oukennou, A., Sandali, A.: Novel voltage stability index for electric power system monitoring. Int. J. Electr. Comput. Eng. Syst. **10**, 1–9 (2019)

8. Yang, X.S.: Bat Algorithm for multi objective optimization. Int. J. Bio-inspired Comput. **3**(5), 267–274 (2011). https://doi.org/10.1504/IJBIC.2011.042259

9. Lakshmi, P., Rao, B.V., Devarapalli, R., Rai, P.: Optimal power flow with bat algorithm for a power system to reduce transmission line losses using SVC. In: 2020 ICEFEET, (pp. 1–5). (2020). https://doi.org/10.1109/ICEFEET49149.2020.9186964

10. Lakshmi, P., Rao, B.V., Devarapalli, R., Prasad, U.: BAT algorithm based optimal power flow for power system consisting of wind power plants and static VAR compensator. In: Michael Faraday IET International Summit 2020 (MFIIS 2020), held on 3–4 Oct 2020, Organized by IET Kolkata Network, The Institution of Engineering and Technology

11. Yang, X.S.: Firefly algorithm, levy flights and global optimization. In: Research and Development in Intelligent Systems XXVI, (pp. 209–218). Springer, London, UK (2010). https://doi.org/10.1007/978-1-84882-983-1_15

12. Yang, X.-S.: Firefly algorithms for multimodal optimization. Stochast. Algorithms Found. Appl. SAGA **5792**, 169–178 (2009). https://doi.org/10.1007/978-3-642-04944-6_14

The Application of TOPSIS Method for Optimization of Machining Parameters During Hard Turning of H13 Tool Steel

K. Anoop and Kalyan Chakraborty

1 Introduction

The machining process is one of the important production routes to manufacture mechanical components. But for better machining performance, sometimes, it becomes essential to optimize the process parameters. The hard turning is beneficial in comparison with the grinding. The production rate and the economic production improve due to hard turning. The selection of proper process parameters is an important requirement with the manufacturing shop floor. This is for higher machining performance. The response parameters, namely surface roughness, chip reduction coefficient (considered as a measure of cutting force), chip type, etc., can be considered to assess the quality of the manufactured component.

Studies were performed on sustainable machining techniques. Sustainable machining techniques and parameters were identified on which sustainability of a process is evaluated. The fuzzy TOPSIS decoupled method was utilized to evaluate sustainable machining techniques. The cryogenic machining, dry machining, minimum quantity lubrication (MQL) machining, and high-pressure jet machining were selected for the study. The linguistic variables represented by fuzzy numbers are transformed in to crips numbers. Cryogenic machining was identified as the best alternative sustainable technique [1]. The effectiveness of the Taguchi-based simple additive weighting and Taguchi-based TOPSIS methodologies was analyzed. The AlMg3 (AA 5754) alloy was machined in the computer numerical control (CNC) lathe using the carbide tool. The metal removal rate and surface roughness were considered as process responses. Similar parametric conditions were identified in respect of speed, feed, and depth of cut by both the methodologies. In addition to this finding, both the methodologies indicated the DOC as the most significant and feed

K. Anoop · K. Chakraborty (✉)
National Institute of Technology, Silchar, Assam 788010, India
e-mail: chakrabortykalyan623@gmail.com

as the least significant parameters. Obtained percentage contributions by the DOC using T-SAW and T-TOPSIS methodologies were 65.22% and 65.35%, respectively. The T-SAW methodology was identified as the very simple effective method to identify proper parametric setting with reference to the other multi-criteria decision-making approaches [2]. The fuzzy–TOPSIS decoupled methodology was used for the optimization. The machining was for twenty-seven different experimental conditions. According to ANOVA, depth of cut was the most significant factor for cutting force and tool wear. The optimality condition was thereafter attained [3]. The poor productivity, higher manufacturing cost, and the problem with the cooling method have been reported for machining of 17–4 precipitated hardened stainless steel. The Taguchi gray relational and the Taguchi TOPSIS optimization method were applied to optimize the multi-responses during the turning of this steel. The Taguchi gray relational method optimized the machining conditions. The effects of the process parameters and the interaction on the machining performance have been studied [4]. Optimal parameter setting was obtained by applying multi-attribute decision-making methods (MADMs). Ti-6Al-4 V alloy was turned following Taguchi's L27 DOE methodology under MQL conditions using Jatropha-carcass oil (JCO) bio-based lubricant. The textured carbide tool was used for the machining. The analytic hierarchy process, TOPSIS, and simple additive weighting methods were used to optimize machining parameters. The response parameters were surface roughness, flank wear, force, and temperature. Optimal parameter setting was obtained at $v = 80$ m/min, $f = 0.05$ mm/rev., doc $= 0.10$ mm. Finally, results of TOPSIS and SAW were compared [5]. The effect of DOC, cutting length, speed, and feed on surface roughness, flank wear, power consumption, and MRR was analyzed for high-speed machining of Ti-6Al-4 V alloy. BPNN along with TOPSIS fuzzy decoupled approach was used to optimize the machining performance. The predicted machining responses were in agreement with the experimental results at the optimal condition [6]. The metal matrix composite (90% magnesium and SiC%) was produced by stir casting. Turning was performed the following central composite design. The input parameters (three levels) and output responses (surface roughness, surface hardness, and out of roundness) were considered for the analysis. The weightage of the TOPSIS method was evaluated by using the entropy method. The multi-attributes were optimized using the TOPSIS method. The literature review shows the inadequate studies on the application of the TOPSIS method in hard turning process parameter optimization. Optimal condition was obtained at the speed of 500 rpm, feed of 0.2 mm/rev., and doc of 0.2 mm [7]. The aim of the present study is to (I) optimize the hard turning parameters (H13 tool steel) using the TOPSIS method, (ii) analyze the significance and interaction of the hard turning parameters using the ANOVA and Taguchi methodology, and (iii) explain an approach to validate the optimization result.

Fig. 1 Turned H13 tool steel
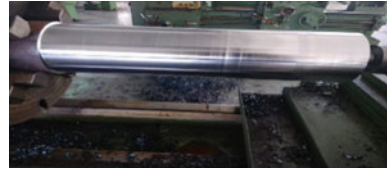
Table 1 Machining parameters and levels

Parameters/levels	−1(1)	0(2)	1(3)
Speed, v, (m/min)	64	80	100
Feed, f, (mm/rev.)	0.07	0.10	0.14
DOC (mm)	0.67	1.0	1.5

2 Experimental Procedures

H13 tool steel was procured in the form of a cylindrical bar. The workpiece was turned in the lathe using Tungaloy made tool insert (Fig. 1). 27 experiments were performed. The experiments were performed according to 3^3 factorial designs. Machining parameter levels and corresponding values are shown in Table 1. The experimental sequence is 1(−1 −1 −1), 2(−1 −1 0), 3(−1 −1 1), 4(−1 0 −1), 5(−1 0 0), 6(−1 0 1), 7(−1 1 −1), 8(−1 1 0), 9(−1 1 1), 10(0 −1 −1), 11(0 −1 0), 12(0 −1 1), 13(0 0 1), 14(0 0 0), 15(0 0 1), 16(0 1 −1), 17(0 1 0), 18(0 1 1), 19(1 −1 −1), 20(1 −1 0), 21(1 −1 1), 22(1 0 −1), 23(1 0 0), 24(1 0 1), 25(1 1 −1), 26(1 1 0), 27(1, 1, 1).

The surface roughness values were measured by using the 3D optical surface profilometer. The chip reduction coefficients were determined by using the Eq. (1)

$$CRC = \frac{t2}{t1} \tag{1}$$

where $t2 =$ formed chip thickness (mm) and $t1 =$ uncut chip thickness (mm). Finally, chip surfaces were examined by the scanning electron microscope.

3 The TOPSIS Methodology

The multi-objective optimization of hard turning parameters was done by TOPSIS method. In this study, the surface roughness and the CRC were the objectives for optimization. The composite index was obtained by using the TOPSIS method. Usual steps of TOPSIS method were selected to convert the multiple responses to a single response [8, 9].

4   Results and Discussion

4.1   Topsis

Respective values of Ra and CRC are 1(1.9880, 6.9613), 2(1.5900, 10.3480), 3(1.5000, 11.5083), 4(1.1870, 9.8023), 5(1.2769, 11.0930), 6(1.2080, 10.9843), 7(1.0720, 7.5994), 8(1.4640, 12.3784), 9(1.3630, 10.6629), 10(2.6770, 11.0055), 11(1.6480, 8.8342), 12(1.6040, 9.8508), 13(1.4780, 9.0969), 14(1.7930, 7.5348), 15(1.5600, 9.1007), 16(1.6880, 7.2569), 17(1.6030, 9.1878), 18(1.2020, 4.0386), 19(1.8290, 2.2596), 20(2.2880, 9.2431), 21(1.2060, 9.2928), 22(1.6750, 7.4418), 23(0.8720, 8.1318), 24(1.6800, 4.8139), 25(1.3520, 6.1713), 26(1.1090, 8.0469), 27(1.5580, 8.3536). Respective normalized values are 1(0.2421, 0.1512), 2(0.1936, 0.2248), 3(0.1827, 0.2500), 4(0.1445, 0.2130), 5(0.1554, 0.2410), 6(0.1471, 0.2386), 7(0.1305, 0.1651), 8(0.1783, 0.2689), 9(0.1660, 0.2317), 10(0.3260, 0.2391), 11(0.2007, 0.1919), 12(0.1953, 0.2140), 13(0.1800, 0.1976), 14(0.2183, 0.1637), 15(0.1900, 0.1977), 16(0.2056, 0.1577), 17(0.1952, 0.1996), 18(0.1464, 0.0877), 19(0.2227, 0.0491), 20(0.2786, 0.2008), 21(0.1469, 0.2019), 22(0.2040, 0.1617), 23(0.1062, 0.1767), 24(0.2046, 0.1046), 25(0.1646, 0.1341), 26(0.1350, 0.1748), 27(0.1897, 0.1815). Respective weighted normalized values are 1((0.1210, 0.0756), 2(0.0968, 0.1124), 3(0.0913, 0.1250), 4(0.0723, 0.1065), 5(0.0777, 0.1205), 6(0.0735, 0.1193), 7(0.0653, 0.0826), 8(0.0891, 0.1345), 9(0.0830, 0.1158), 10(0.1630, 0.1196), 11(0.1003, 0.0960), 12(0.0977, 0.1070), 13(0.0900, 0.0988), 14(0.1092, 0.0818), 15(0.0950, 0.0989), 16(0.1028, 0.0788), 17(0.0976, 0.0998), 18(0.0732, 0.0439), 19(0.1114, 0.0245), 20(0.1393, 0.1004), 21(0.0734, 0.1009), 22(0.1020, 0.0808), 23(0.0531, 0.0883), 24(0.1023, 0.0523), 25(0.0823, 0.0670), 26(0.0675, 0.0874), 27(0.0949, 0.0907). The closeness coefficients were obtained (after separation measures) as 1(0.4595), 2(0.4155), 3(0.4021), 4(0.5301), 5(0.4660), 6(0.4834), 7(0.6512), 8(0.3897), 9(0.4610), 10(0.0931), 11(0.4620), 12(0.4305), 13(0.4948), 14(0.4842), 15(0.4737), 16(0.5270), 17(0.4584), 18(0.8207), 19(0.6758), 20(0.2654), 21(0.5474), 22(0.5214), 23(0.6514), 24(0.6440), 25(0.6709), 26(0.6227), 27(0.5084). Subsequently, first rank was obtained by expt. no. 18, second rank was obtained by expt. no. 19, and third rank was obtained by expt. no. 25. The optimum process parameters were identified at experiment number 18 (Rank 1), i.e., at (011) using the TOPSIS method.

4.2   The ANOVA and Interaction

The results of the ANOVA for Ra and CRC are shown in Tables 2 and 3. It is seen that the feed is the most influential parameter (since F ratio $= 4.11 > 3.4928$) for surface roughness response (Table 2). From ANOVA Table 3, it is seen that speed is the most significant parameter for the CRC response (since F ratio $= 3.58 > 3.4928$).

Table 2 The ANOVA for Ra

Source for Ra	F ratio	% cont.
v	2.14	12.16
f	4.41*	25.11
d	1.02	5.81
Total		
error		56.92

*Significant AT 95% Confidence level, $F_{2, 20, 0.95} = 3.4928$ (tabulated F ratio in statistical table), $F_{2, 20, 0.95} = 4.41$ (obtained for surface roughness), $F_{2, 20, 0.95} = 3.58$ (obtained for CRC)

Table 3 The ANOVA for CRC

Source for CRC	F ratio	%cont
v*	3.58*	23.04
f	0.08	
d	1.88	0.54
Total		
error		64.35

*Significant AT 95% Confidence level, $F_{2, 20, 0.95} = 3.4928$ (tabulated F ratio in statistical table), $F_{2, 20, 0.95} = 4.41$ (obtained for surface roughness), $F_{2, 20, 0.95} = 3.58$ (obtained for CRC)

4.2.1 Average Surface Roughness Response

At $f = -1$ and $d = -1$, Ra increases and thereafter decreases with increase of speed (Fig. 2a). At $f = 0$ and $d = 0$, the Ra increases and thereafter decreases with the increase of speed (Fig. 2a). At $f = 1$ and $d = 1$, the Ra decreases and thereafter increases with the increase of speed (Fig. 2a). At $v = -1$ and $f = -1$, Ra decreases with increase of DOC (Fig. 2b). At $v = 0$ and $f = 0$, the Ra increases and thereafter decreases with the increase of DOC (Fig. 2b). At $v = 1$ and $f = 1$, the Ra decreases and thereafter increases (Fig. 2b). At $v = -1$ and $d = -1$, the Ra reduces for the higher feed (Fig. 2c). At $v = 0$ and d $= 0$, the Ra increases and thereafter reduces for the higher feed (Fig. 2c). At $v = 1$ and $d = 1$, the Ra increases and thereafter decreases with the feed (Fig. 2c). Overall study indicates that feed is the most influential parameter for the surface roughness response as seen in Fig. 2c ($v = -1$ and $d = -1$). This is in agreement with the ANOVA result (Table 2).

4.2.2 Average CRC Response

At $f = -1$ and $d = -1$, the CRC increases and thereafter decreases with the increase of speed (Fig. 2d). At $f = 0$ and $d = 0$, the CRC decreases and thereafter increases with the increase of speed (Fig. 2d). At $f = 1$ and $d = 1$, the CRC decreases and
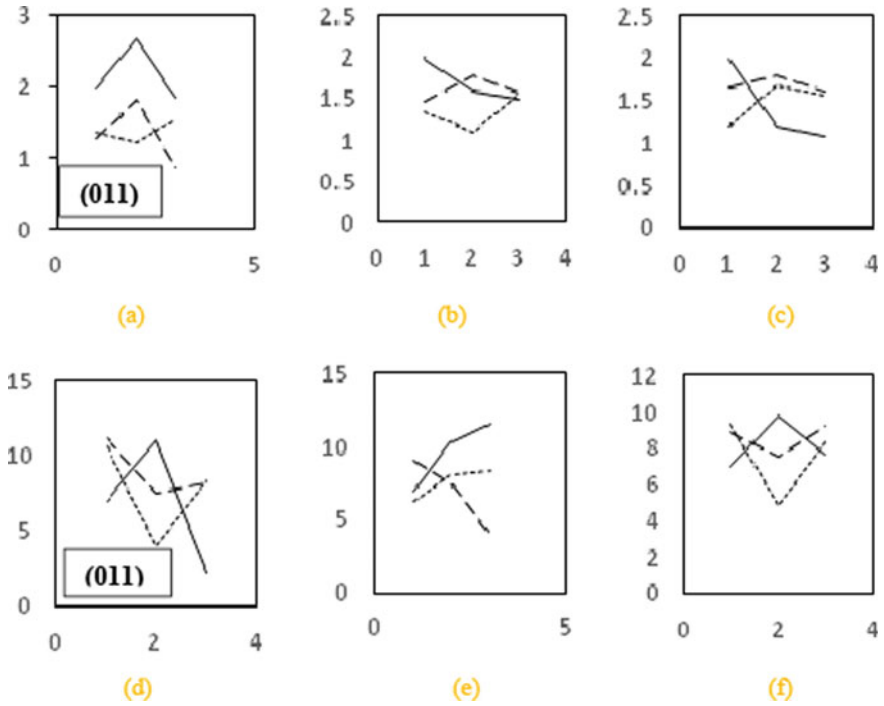
Fig. 2 Variations of Ra and CRC with reference to speed, DOC, and feed **a** X (v), Y (R$_a$), **b** X (DOC), Y (R$_a$), **c** X (f), Y (R$_a$), **d** X (v), Y (CRC), **e** X (DOC), Y (CRC), **f** X (f), Y (CRC). *Legend* solid line (−1 −1), dashed line (0 0), dotted line (1 1)

thereafter increases with the increase of speed (Fig. 2d). At $v = −1$ and $f = −1$, the CRC increases with the increase of DOC (Fig. 2e). At $v = 0$ and $f = 0$, the CRC reduces for the higher DOC (Fig. 2e). At $v = 1$ and $f = 1$, the CRC raises for the higher DOC (Fig. 2e). At $v = −1$ and $d = −1$, the CRC increases and thereafter reduces for the higher feed (Fig. 2f). At $v = 0$ and $d = 0$, the CRC decreases and thereafter raises for the higher feed (see Fig. 2f). At $v = 1$ and $d = 1$, the CRC decreases and thereafter raises for the higher feed (Fig. 2f). Overall study indicates that speed is the most influential parameter for the CRC response as seen in Fig. 2d ($v = −1$ and $d = −1$). This is in agreement with the ANOVA result (Table 3). From Fig. 2a–f, it is found that an effect of the interaction is always operating.

4.3 The Validation Study

Figure 3a–c show the results of surface roughness values from the 3D surface roughness profilometer at (011), (−111), and (111). The best result is obtained at (011) (Fig. 3a) which is again in agreement with the results from the TOPSIS method.

a) (011) (b) (-111) (c) (111)
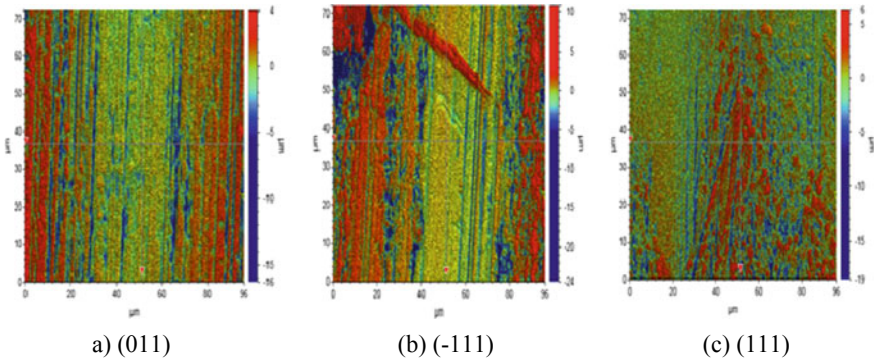
Fig. 3 Surface roughness images by the 3D optical surface roughness profilometer

Figure 4a–c show the photo macrographs of obtained chips at (011), (−111), and (111) conditions. The collected chips at (011) (Fig. 4a) show that the chips are of tubular semicontinuous type (preferable). The chips at (−111) (Fig. 4b) are of smaller discontinuous type (not preferable). Figure 4c shows long ribbon type continuous chips at (111). Long continuous chip type is also not preferable because of the problem of chip disposability. This chip study also indicates that the best possible chip formation mode can be at (011) which is again in agreement with the result from the TOPSIS method. Thus, the optimization result by the TOPSIS method has been validated. The experimental chips were examined under the scanning electron microscope. The chip formation mode was found to be favorable only at (011) condition. The chip top surface (see Fig. 5a) indicated that the chip formation process occurred by the successive lamellar shear sliding mechanism. The surface (under) of the chip also showed the favorable chip formation mode. The chip (under) surface (Fig. 5b) showed the absence of material sticking action, absence of material side flow, absence of any crack, etc. Thus, an ideal chip formation mechanism is revealed at this machining condition. The chip at (011) showed the most favorable chip formation mode among all the experimental chips at various machining conditions. This finding is also in agreement with the result from the TOPSIS method. Thus, the results indicate that the TOPSIS method is appropriate for solving multi-criteria optimization of process parameters.

(a) (011) (b) (-111) (c) (111)
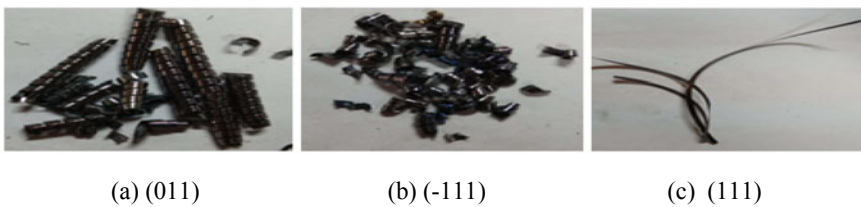
Fig. 4 Chip types at different levels
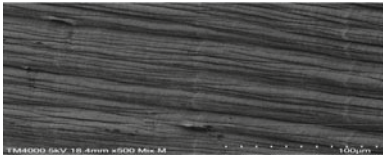
(a) Chip (top) surface (011) X1000
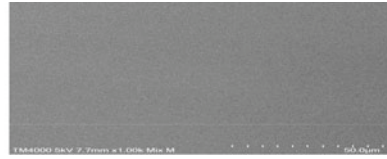
(b) Chip (under) surface (011) X500

Fig. 5 SEM images of chip surfaces at (011)

5 Conclusions

The TOPSIS method can be applied to optimize the process parameters. The optimality condition was obtained at (011), i.e., at the speed of 80 m/min, feed of 0.14 mm/rev, and DOC of 1.5 mm. The results on the average responses using the Taguchi methodology are in agreement with results from the ANOVA. The effect of interaction on the process responses is always operating. The optimization results using the TOPSIS method can be validated by the qualitative assessment.

References

1. Digalwar, A.K.: Application of fuzzy topsis for evaluating machining techniques using sustainable metrics. In: 2018 IOP Conference Series: Materials Science and Engineering (vol. 346, p. 012039). (2018)
2. Sahu, A.K., Sahu, N.K., Sahu, A.K., Rajput, M.S., Narang, H.K.: T-SAW methodology for parametric evaluation of surface integrity aspects in AlMg3 (AA5754) alloy: comparison with T-TOPSIS methodology. Measurement **132**, 309–323 (2019)
3. Khan, A., Maity, K.: Application potential of combined fuzzy-TOPSIS approach in minimization of surface roughness, cutting force and tool wear during machining of CP-Ti grade II: Soft Comput. **23**, 6667–6678 (2019)
4. Sivaiah, P., Chakradhar, D.: Performance improvement of cryogenic turning process during machining of 17–4 PH stainless steel using multi objective optimization techniques. Measurement **136**, 326–336 (2019)
5. Singh, R., Dureja J.S., Dogra, M., Randhawa, J.S.: Optimization of machining parameters under MQL turning of Ti-6Al-4V alloy with textured tool Using multi-attribute decision-making methods. World J. Eng. **16**(5), 648–659 (2019)
6. Abbas, A.T., Sharma, N., Anwar, S., Luqman, M., Tomaz, I., Hegab, H.: Multi-response optimization in high-speed machining of Ti-6Al-4V using TOPSIS-fuzzy integrated approach. Materials **13**, 1104 (2020)
7. Prasad, K.R.A, Nair, V.P., Jaishwin, S.K.J., Arvind Narayanan, V.K.A., Naren, A., John, M.R.S.: Optimization of turning parameters for magnesium silicon carbide using TOPSIS method. In: 3rd International Conference on Advances in Mechanical Engineering (ICAME 2020). IOP (2020)

8. Balasubramanian, S., Selvaraj, T.: Application of integrated Taguchi and TOPSIS method for optimization of process parameters for dimensional accuracy in turning of EN25 steel. J. Chin. Inst. Eng. **40**(4), 267–274 (2017)
9. Sen, B., Hussain, S.A.I., Mia, M., Mandal, U.K., Mondal, S.P.: Selection of an ideal MQL-assisted milling condition: an NSGA-II-coupled TOPSIS approach for improving machinability of Inconel 690. Int. J. Adv. Manuf. Technol. **103**, 1811–1829 (2019)

Optimization of Process Parameters for Tribological Behaviour of AA7075+WC Metal Matrix Composite Using ANOVA

Y. Phaneendra, B. N. Dhanunjaya Rao, R. Bammidi, Bh. Nagesh, and I. N. Niranjan Kumar

1   Introduction

Aluminium Metal Matrix Composites (MMCs) and their alloys are widely used in high-strength structural applications since they are part of family of high-performance lightweight materials, highly conductive and ductile [1]. In the aerospace and automobile industries, Many structural applications are well-suited to aluminium-based alloys [2]. Aluminium is currently one of the most preferred matrix materials for metal matrix composites. In order to fulfil the global need for environmentally friendly, low-weight, high-performance, corrosion and wear-resistant materials, research has transitioned from the materials of monolithic to composite materials during the previous two decades [3, 4]. The prepared specimen was subjected to a tribology test with a pin-on-disc apparatus. Due to their advantageous properties that may be adjusted by adding certain reinforcements, MMCs are gradually becoming fascinating materials for advanced aeronautical applications [5]. Over the years, a number of composite materials have been used in a variety of functional applications [6], structural applications and non-structural applications in a variety of engineering fields [7]. In Aluminium MMCs, reinforcement can take the shape of particles, whiskers, continuous/discontinuous fibres in various volume/weight fractions [8]. Aluminium MMCs can be customised to meet the needs

Y. Phaneendra (✉) · B. N. Dhanunjaya Rao
Department of Mechanical Engineering, Vignan's Institute of Information Technology (A), Visakhaptnam, India
e-mail: phaneendraauce@gmail.com

R. Bammidi
Department of Mechanical Engineering, Aditya Institute of Technology and Management (A), Tekkali, India

Y. Phaneendra · Bh. Nagesh · I. N. Niranjan Kumar
Department of Marine Engineering, Andhra University, Visakhaptnam, India

of various industries [9]. The properties of Aluminium MMCs can be tailored to the needs of diverse industrial applications by combining the suitable matrix, reinforcement and fabrication process [10]. MMCs are ideal for various applications that require a combination of mechanical strength properties, thermal properties and damping capabilities in a low-density material [11]. MMCs are more useful in aerospace and automotive applications related to the tribological behaviour of material along with strength properties [12, 13]. Because of its superior corrosion and wear resistance, MMCs are used in the automotive industry for pistons, brake drums and cylinder blocks [14]. The weight of the reinforcements ranged between 1 and 2%. Concentration, mechanical characteristics and dry sliding wear were all evaluated on the composite [15]. Based on literature collected, many researchers are focused on findings on wear behaviour of MMCs but lacking in predicting the influencing factors by optimisation process. Here, the work is aimed at investigating the influencing parameters on its wear behaviour of nanoparticle reinforced MMCs composite. Aluminium is considered as metal matrix and WC is considered as nano reinforcement to fabricate MMCs through stir-casting metallurgy technique. It was discovered that the type of reinforcement and its volume percentage had a substantial relationship. The findings indicated that the particle reinforcement is the most effective way to improve MMC wear resistance.

2 Experimental Procedure

2.1 Materials Required

Because of its better characteristics the Al-7075 alloy is chosen as matrix and the percentage of chemical composition is as follows, that is Si (0.45), Fe (0.50), Cu (1.8–2.0), Mn (0.2), Mg (2.0–2.8), Cr (0.18–0.25), Zn (4.8–5.9), Ti (0.20) and others (0.05), respectively. The reinforcement chosen is 150 to 160 microns average-sized WC. Because of its high hardness and thermal conductivity, WC improves the wear resistance of the Al/WC metal matrix composite after being incorporated into a soft ductile aluminium base matrix.

2.2 Metal Matrix Composite Preparation

Significant interfacial adhesion (wetting) between the dispersion medium and the matrix is required to obtain good mechanical characteristics in the composite. Many researchers have used the stir-casting process to produce metal matrix composites because it is easy and inexpensive [13].

The Al 7075 alloy is first melted to a temperature of 800 °C in an electrical furnace, as illustrated in Fig. 1. As illustrated in Fig. 3, to make cylindrical samples,

Fig. 1 Al 7075 alloy
Melting in electrical furnace
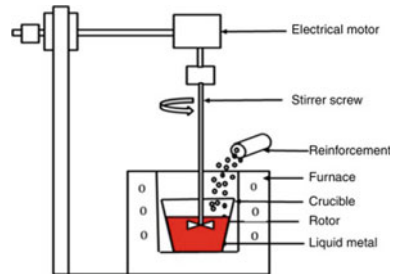
the liquified metal mixture is injected into a split piece die and then the desired components are prepared by machining for 10 mm diameter (Fig. 2).

Fig. 2 As-Cast Al 7075 alloy
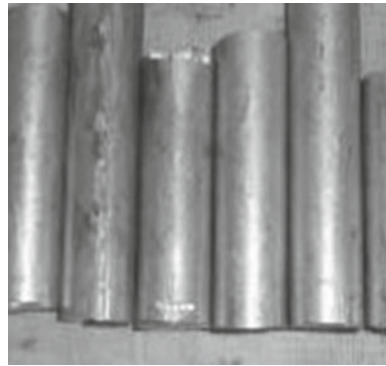
Fig. 3 Machined Al 7075/WC composite sample

Table 1 Process parameters and their levels

Factors	Levels		
	1	2	3
Load (N)	10	20	30
Sliding Speed (m/s)	400	600	800
Sliding Distance (m)	1000	1500	2000

2.3 Wear Behaviour

The exploratory approach aims to identify the critical elements and combinations of parameters that influence the wear process in order to reduce the wear rate and COF as much as possible. The studies were meant to determine the connection between the influencing parameters such as sliding speed, applied load and sliding distance using an orthogonal array. The sliding wear properties were evaluated for composite using the pin-on-disc apparatus as discussed before. The cast samples were machined to diameter of 10 mm and 25 mm lengths, after which the pieces were tested (Table 1).

2.4 Design of Experiments

The number of components and their relations, the number of levels for the relations and the desired experimental precision or economic constraints all impact the choice of orthogonal array. The Taguchi model's run sequence was used to conduct a total of nine trials. The signal-to-noise relationship (S/N), which condenses multiple data points throughout a test, is influenced by the type of feature to be analysed [16]. The properties of the S/N ratio may be classified into three groups: 'the nominal is better,' 'the bigger the better' and 'the smaller the better.' Smaller the better' features are used to assess the dry wear resistance. The 'smaller is better' characteristic of Taguchi is utilised for calculating the S/N wear ratio and the friction coefficient.

3 Result and Discussion

In order to get the lowest wear rate (WR) and friction coefficient feasible, the experimental method seeks to uncover essential elements and combinations of factors that impact our wear mechanism. These experiments were conceived using an orthogonal array to determine if the sliding speed, weight and sliding distance are related. Taguchi proposes a conceptual technique of analysing S / N ratios that involves diagramming effects and illustrating the essential components graphically.

3.1 Results of Experiment Statistical Analysis

The results were achieved by utilising an orthogonal array to conduct the experiment for different combinations of factors. MINITAB 20 tool, was used to analyse the measured data, which is designed for design of experiments (Tables 2 and 3).

Figures 4, 5, 6 and 7 show a visual impact of 1% on wear rate and COF of process parameters whereas Figs. 8, 9, 10 and 11 show a 2% influence on rate of wear and friction coefficient of the process parameters in graphically.

Tables 4 and 5 demonstrate that the applied friction coefficient is most influenced by the load. Therefore, the load applied is an essential control element that has to be considered during the friction coefficient with a respective sliding speed and sliding distance.

Table 2 Results for Al-7075/ 1% WC of L9 Orthogonal array

	Experimental values		S/N ratios	
Experiments	COF WC 1%	SWR WC 1%	COF WC 1%	SWR WC 1%
R1	0.180	0.000471	14.8945	66.5396
R2	0.270	0.0003297	11.3727	69.6376
R3	0.300	0.000262975	10.4576	71.6017
R4	0.345	0.000191017	9.2436	74.3786
R5	0.360	0.000153075	8.8739	76.3019
R6	0.335	0.000302225	9.4991	70.3934
R7	0.263	0.000154383	11.5899	76.2280
R8	0.287	0.000277367	10.8525	71.1389
R9	0.257	0.000230267	11.8126	72.7554

Table 3 Results for Al-7075/ 2% WC of L9 Orthogonal array

	Experimental values		S/N ratios	
Experiments	COF WC 2%	SWR WC 2%	COF WC 2%	SWR WC 2%
R1	0.410	0.0005181	7.7443	65.7117
R2	0.520	0.0003506	5.6799	69.1029
R3	0.320	0.0002747	9.8970	71.2212
R4	0.325	0.0001962	9.7623	74.1438
R5	0.355	0.0001629	8.9954	75.7622
R6	0.340	0.0002630	9.3704	71.6017
R7	0.297	0.0001099	10.5546	79.1800
R8	0.343	0.0001622	9.2857	75.7972
R9	0.313	0.0001308	10.0799	77.6656

Fig. 4 Main effect plots for S/N ratio—COF (1%WC)

Fig. 5 Main effect plots for means—COF (1%WC)

Fig. 6 Main effect plots for S/N ratio—WR (1%WC)
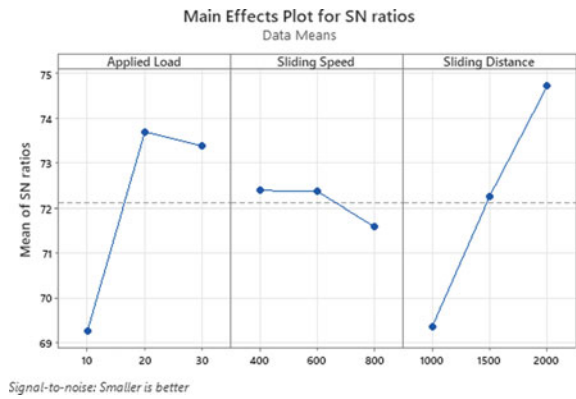
Fig. 7 Main effect plots for means—WR (1%WC)

Fig. 8 Main effect plots for S/N ratio—COF (2%WC)
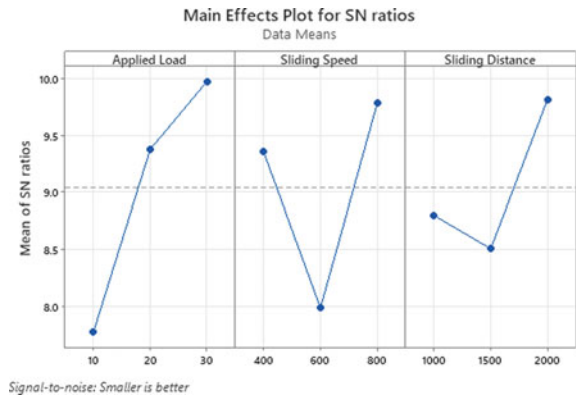
Fig. 9 Main effect plots for means—COF (2%WC)
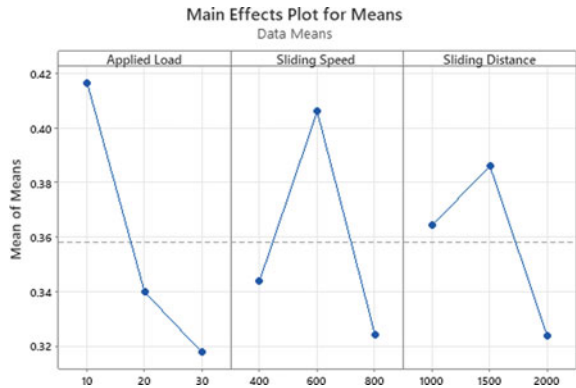
Fig. 10 Main effect plots for S/N ratio—WR (2%WC)

Fig. 11 Main effect plots for means—WR (2%WC)

Table 4 Analysis of variance for means (specific wear rate) (1%WC)

Source	DF	Seq SS	Adj SS	Adj MS	F	P	% Contribution
Load	2	0.000015	0.000015	0.000008	120.93	0.008	51.7
Speed	2	0.000001	0.000001	0.000000	7.84	0.113	3.5
Distance	2	0.000013	0.000013	0.000006	101.20	0.010	44.8
Residual error	2	0.000000	0.000000	0.000000			
Total	8	0.000029					

Table 5 Analysis of variance for means (specific wear rate) (2%WC)

Source	DF	Seq SS	Adj SS	Adj MS	F	P	% Contribution
Load	2	0.0000015	0.0000015	0.000000	1.50	0.400	15.32
Speed	2	0.0000023	0.0000023	0.000000	0.87	0.535	23.46
Distance	2	0.000006	0.000006	0.000003	53.55	0.018	61.22
Residual error	2	0.000000	0.000000	0.000000			
Total	8	0.0000098					

3.2 Analysis of Variance (ANOVA) for Wear Test

Analysis of Variance (ANOVA) was performed to analyse the effect of the wearing factors, namely load application, speed of sliding and distance of sliding that impact performance measurements considerably. From the analysis of variance of Al-7075/ 1% WC reinforced composites, Highest impact on the specific rate of wear is 51.7% applied load, preceded by 44.8% sliding distance and applied load of 3.5% and for COF the applied load has highest influence of 64.6%, sliding speed of 12.7% and sliding distance of 10.2%.

For Al-7075/ 2% WC metal matrix composites, the sliding distance has major impact of 61.22% on specific rate of wear, preceded by sliding speed of 23.46% and applied load of 15.32% and for coefficient friction the applied load is shown highest influence of 42.74%, sliding speed of 28.91% and sliding distance of 15.84%.

3.3 Conformation Test

The confirmation experiments are conducted with the arbitrary levels for the specified factors and the results (i.e. specific wear rate and COF) are compared with the predicted results from the developed regression equation for Al-7075/ 1 and 2% WC MMCs. Three experiments are conducted for each confirmation test of wt% of WC among which highest accuracy for 1 wt% WC is 95.83% for SWR and 97.9% for COF followed by the 2 wt% composite with 97.02% for SWR and 95.16% for COF.

4 Conclusions

Tribological behaviour of Al-7075 aluminium alloy enhanced by stir-casting method with tungsten carbide particles (1% to 2% weight to WC). Using a pin-on-disc wear test, wear & frictional characteristics of the reinforced AA7075+WC metal matrix composites were investigated.

1. For Al-7075/ 1% WC metal matrix composites, the applied load has the major impact of 51.7% on specific wear rate, preceded by sliding distance of 44.8% and applied load of 3.5% and for coefficient friction the applied load has highest influence of 64.6%, sliding speed of 12.7% and sliding distance of 10.2%.
2. The sliding distance has a maximum effect of 61.22% in the case of Al-7075/ 2% WC metal matrix composites on the specific rate of wear, accompanied by 23.46% of sliding speed and a 15.32% of applied load, with a maximum influence of 42.74% on the applied load and a sliding speed of 28.91% and a sliding distance of 15.84%.

We predicted from the preceding findings that the applied load & sliding distance in both wt% of AA7075+WC composites had the largest effect in the specific wear

rate. In the same way, the load used in both composites is essential parameter, which has a substantial effect on COF. The trials were therefore effectively designed using Taguchi to forecast the tribological performance of composites.

References

1. Cheung, C.F., Chan, K.C., Lee, W.B.: Surface characterization in ultra-precision machining of Al/SiC metal matrix composites using data dependent systems analysis. J. Mater. Proces. Technol. **140**(1–3), 141–146 (2003). https://doi.org/10.1016/S0924-0136(03)00698-8
2. Raju, P.R.M., Rajesh, S., Raju, K.S.R., Ramachandra Raju, V.: Effect of reinforcement of Nano Al_2O_3 on mechanical properties of Al2024 NMMCs. Mater. Today Proc. **2**(4–5), 3712–3717 (2015). https://doi.org/10.1016/j.matpr.2015.07.152
3. Phaneendra, Y., Niranjan Kumar, I.N., Kumar, V.V.R.: Thermo-Mechanical treated high strength AA-7xxx aluminium alloy by cold and cryo-rolling study their mechanical properties corrosion and microstructure correlation. (2019). (Online). Available: www.scientific.net
4. Bhowmik, A., Dey, S., Dey, D., et al.: Dry sliding wear performance of Al7075/SiC composites by applying grey-fuzzy approach. SILICON **13**, 3665–3680 (2021). https://doi.org/10.1007/s12633-020-00930-3
5. Hwu, B.-K., Lin, S.-J., Jahn, M.-T.: Haterums science & Emglmeerlwg effects of process parameters on the properties of squeeze-cast Sic,-606 1 Al metal-matrix composite. (1996)
6. Dhanunjayarao BN, Sanivada UK, Swamy Naidu NV, Fangueiro R (2022) Effect of graphite particulate on mechanical characterization of hybrid polymer composites. J Ind Text 51(2_suppl):2594S–2615S. https://doi.org/10.1177/15280837211010670
7. Dhanunjayarao, B.N., et al.: 3D Printing of fiber reinforced polymer nanocomposites: additive manufacturing. In: Handbook of Nanomaterials and Nanocomposites for Energy and Environmental Applications. Springer International Publishing, Cham (2020). https://doi.org/10.1007/978-3-030-11155-7_166-1
8. Baskaran, S., et al. Taguchi grey relational analysis of dry sliding wear behaviour of annealed AA7075-TiC metal matrix composites. Appl. Mech. Mater. 541–54 (2014). Trans Tech Publications, Ltd., pp. 258–262 (2014). Crossref. https://doi.org/10.4028/www.scientific.net/amm.541-542.258
9. Singla, M., Deepak Dwivedi, D., Singh, L., Chawla, V.: Development of aluminium based silicon carbide particulate metal matrix composite. (2009)
10. Kumar, A., Patnaik, A., Bhat, I.K.: Optimization of sliding wear performance of Ti metal powder reinforced Al 7075 alloy composite using Taguchi method. In: Chandrasekhar, U., Yang, LJ., Gowthaman, S. (eds.) Innovative Design, Analysis and Development Practices in Aerospace and Automotive Engineering (I-DAD 2018). Lecture Notes in Mechanical Engineering. Springer, Singapore (2019). https://doi.org/10.1007/978-981-13-2718-6_47
11. Rana, R.S., Purohit, R., Sharma, A.K., Rana, S.: Optimization of wear performance of Aa 5083/10 Wt% Sic p composites using taguchi method. Procedia Mater. Sci. **6**, 503–511 (2014). https://doi.org/10.1016/j.mspro.2014.07.064
12. Dwivedi, D.K.: Adhesive wear behaviour of cast aluminium-silicon alloys: overview. Mater. Des. **31**(5), 2517–2531 (2010). https://doi.org/10.1016/j.matdes.2009.11.038
13. Madhavarao, S., Raju, C.R., Madhukiran, J., Varma, S., Varma, R.: A study of tribological behaviour of aluminum-7075/SiC metal matrix composite. (2018). (Online). Available: www.sciencedirect.comwww.materialstoday.com/proceedings
14. Karaaslan, A., Kısasöz, A., Atapek, Ş.H., Güler, K.A.: Dry sliding wear behavior of cast A7075 and A7075/SAF 2205 composite material. High Temp. Mater. Proces. **35**, no. 5, 2016, pp. 487–492. https://doi.org/10.1515/htmp-2015-0004
15. Veeresh Kumar, G.B., Rao, C.S.P., Selvaraj, N.: Mechanical and tribological behavior of particulate reinforced aluminum metal matrix composites—a review. (2011)

16. Dhanunjayarao BN, Neigapula VSN (2022) Parametric optimization for dimensional correctness of 3D printed part using masked stereolithography: Taguchi method. Rapid Prototyping J. https://doi.org/10.1108/RPJ-03-2022-0080

Experimentation for a Better Magnetic Force Microscopy Probe

P. H. J. Venkatesh, Asit Kumar Meher, P. Sreenivasulu, Sumansekhar Takri, M. Tarun, and R. Rudrabhi Ramu

1 Introduction

The atomic force microscope lens (AFM) is a mechanical profilometer that recognizes powers with the assistance of a cantilever. The significant motivation behind this magnifying instrument is to evaluate powers or associations between a sharp examining tip and an example surface, which made the way for the formation of extra filtering probe microscopes (SPMs) including the magnetic force microscope (MFM). This breakthrough enables AFM to characterize the surface properties of thin conducting and non-conducting films without exposing them to electron beam radiation [1]. At the molecular level, organic materials such as fragile thin sheets were photographed. Organic macromolecules, polymers, pottery, and glasses would all be able to be considered with AFM. The instrument is constantly being enhanced, in addition to being applicable to a wide range of materials [2–5].

Present Address:
P. H. J. Venkatesh (✉) · A. K. Meher · R. Rudrabhi Ramu
Department of Mechanical Engineering, Vignan's Institute of Information Technology (A), Visakhapatnam, Andhra Pradesh, India
e-mail: venky61788@gmail.com

P. Sreenivasulu
Department of Mechanical Engineering, JB Institute of Engineering and Technology (A), Hyderabad, Telangana, India

M. Tarun
Department of Mechanical Engineering, Gayatri Vidya Parishad College of Engineering (A), Madhurawada, Visakhapatnam, India

Present Address:
S. Takri
Department of Cryogenic Engineering, Indian Institute of Technology Kharagpur, Kharagpur, West Bengal, India
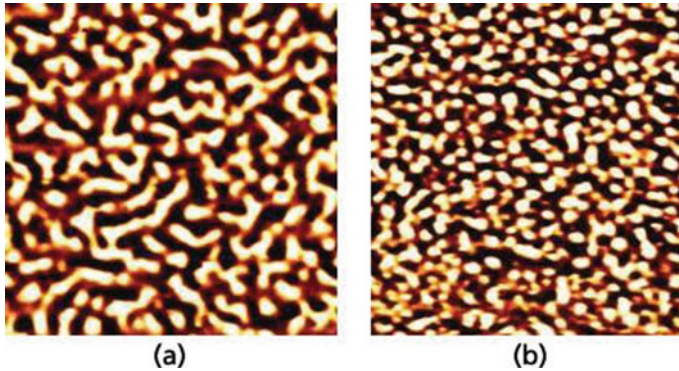
Fig. 1 MFM image of CoCr film

An AFM utilizes a cantilever with an extremely sharp tip to examine an example surface. The tip moves toward the surface because of the short proximity, alluring power between the surface and the tip [6].

Magnetic force microscopy (MFM) is an atomic force microscopy (AFM) technique in which a magnetic-coated AFM tip is used to probe local magnetic fields with the standard AFM spatial resolution, allowing images representing the local magnetic characteristics of nanoscale objects to be recorded [1, 4, 7].

1.1 Different Modes of AFM

The most imagnetic force imaging method involves scanning the sample two times. Figure 1 depicts MFM and AFM scans of a CoCr thin film (Courtesy–Park AFM Systems). Figure 2 depicts the SPM system that was used [8, 9].

1.2 Working Principle

The sample (with magnetic properties) is mounted on a stage that moves along the Z-axis for this technique. The magnetic force between the tip/probe and the sample causes the cantilever to bend and the oscillations to be recorded, while the specimen is resting under the cantilever's tip. In addition to the magnetic forces between the sample surface and the tip, van der Waals forces are at work in this setup [7, 10–12]. These are weaker forces that exist between the atoms of the tip and those of the sample surface (van der Waal forces). They are, nonetheless, more fragile than attractive powers relying upon the distance between the two. The cantilever sways as the tip goes (all over) across the example surface, causing changes in the rakish avoidances of the light bar reflecting off the cantilever's surface.

Fig. 2 SPM setup in the cryogenic engineering center

1.3 Sputtering

Faltering is an actual peculiarity that happens when tiny particles of a strong material are catapulted from its surface subsequent to being barraged by lively plasma particles. It happens normally on the external surface of the objective material and is removed. Its capacity to follow up on incredibly fine layers of material [11] (Figs. 3, 4 and 5).
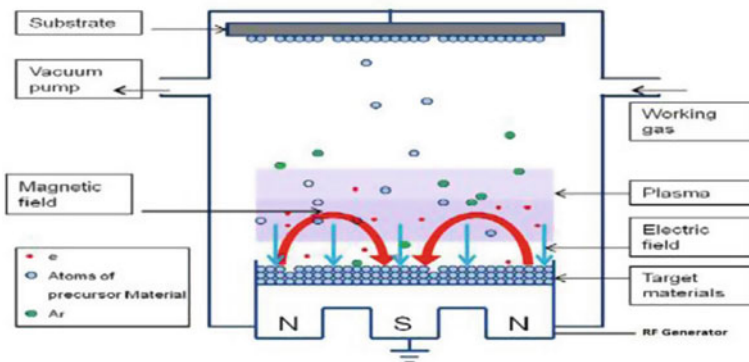
Fig. 3 Sputtering block diagram [11]
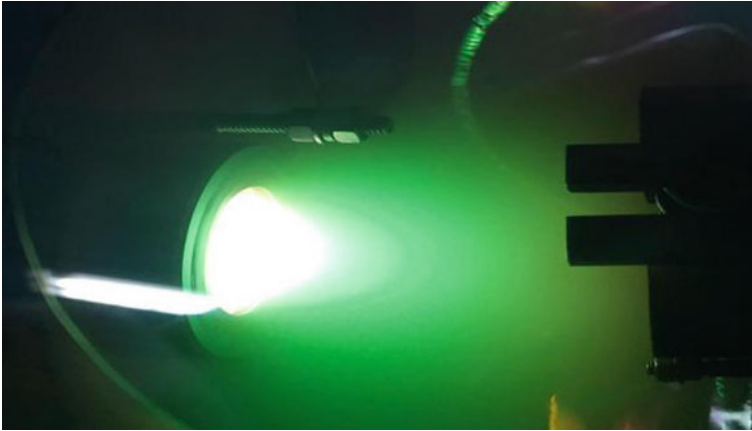
Fig. 4 Plasma generation during deposition
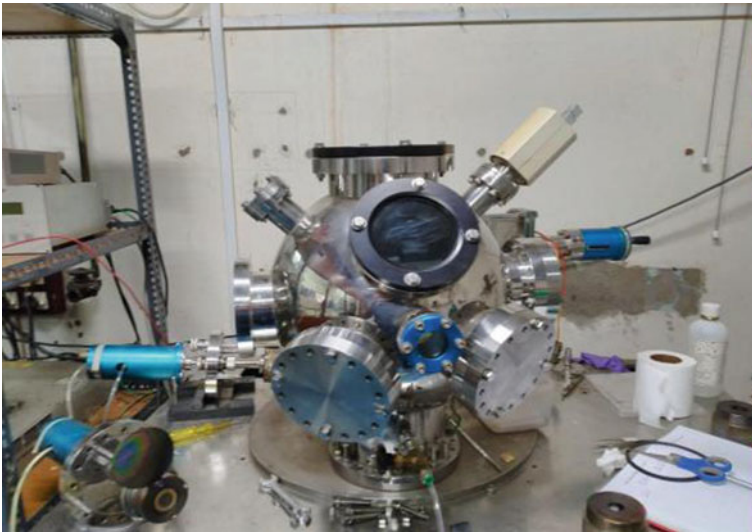
Fig. 5 Sputtering chamber in cryogenic engineering center

2 Methodology

The main objective of the experiment to investigate an optimum deposition condition which will result the film having Hc < 100Oe and Ms < 300emu/cc and to coat Silicon based AFM cantilever tips with magnetic material using the optimum deposition condition. Characterize the coated tip surface and magnetic properties and to
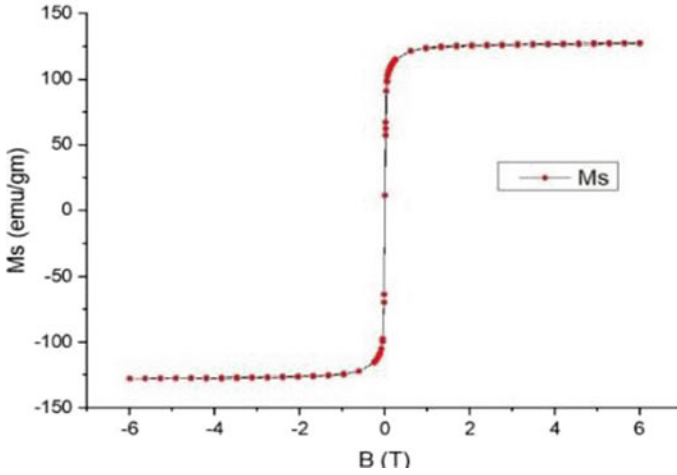
Fig. 6 M-H plots of the Kanthal sample [11]

magnetize the coated tip along the tip direction and to perform MFM scan with the developed tip and study its performance [2, 3, 6].

2.1 Selection of Material

The main objective of this work was to coat the existing silicon-based AFM tip with a magnetic material having low coercivity (Hc $\sim$ 50Oe) and saturation magnetization (Ms $\sim$ 300emu/cc). Main motive of selecting FeGa as a magnetic coating material is that it has high saturation magnetostriction and has many applications in sensors, actuators, and energy harvesting devices.

Amount of 7 mg kanthal and scanned it by using SQUID under 3 condition:

6-T magnetic field at a temperature of 300° K
6-T magnetic field at a temperature of 100° K
0.1-T magnetic field at a temperature of 300° K.

By taking the data points, we have plotted the curve of the magnetic field and saturation magnetization in origin (Fig. 6).

2.2 Thin Film Deposition

To obtain a thin film coating over the AFM probe, it was necessary to obtain an optimum deposition condition which will yield with a good surface adhesion to

silicon, uniform grain structure, and desired magnetic properties. To obtain the optimized condition, several trials were required with varying the parameters and check the deposition results to finalize a condition which will be suitable [6, 8, 13]. From the literature, it has been observed that substrate temperature while deposition plays an important role in controlling the surface and magnetic properties. In thin work after several trials, it was observed that while the RF power is kept at 100 W, with Argon flow rate 20 cc/min the plasma was stable and the target was not overheating. So, keeping these two parameters fixed, the substrate temperature was varied to find an optimum value. A sample area of $2.5 \times 2.5 \, \mu m^2$ was chosen for filtering. Figures 10 show the outer layer of the stored films. As it tends to be seen that each of the saved movies show uniform growth. The grain size was found to increment with expanding substrate temperature, with a base grain size of 2.60 nm at room temperature and a maximum grain size of 10 nm at 3500 °C. Further annealing the sample at 3500 C caused an increase in grain size [10, 11, 14] (Table 1; Figs. 7, 8 and 9).

Magnetic measurement

Table 1 Surface roughness and grain size against deposition temperature

Sample	Deposition temp (°C)	Annealing (min)	Ra (nm)	Grain size (nm)
1	RT	–	1.86	2.60
2	150	–	2.16	4.85
3	250	–	2.40	7.5
4	350	–	2.57	10
5	350	60 min	2.84	13.96
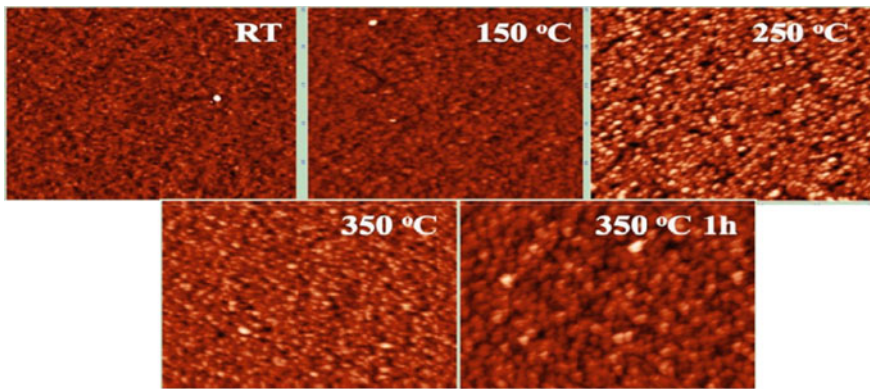
Fig. 7 AFM image of FeGa deposited film at the various conditions
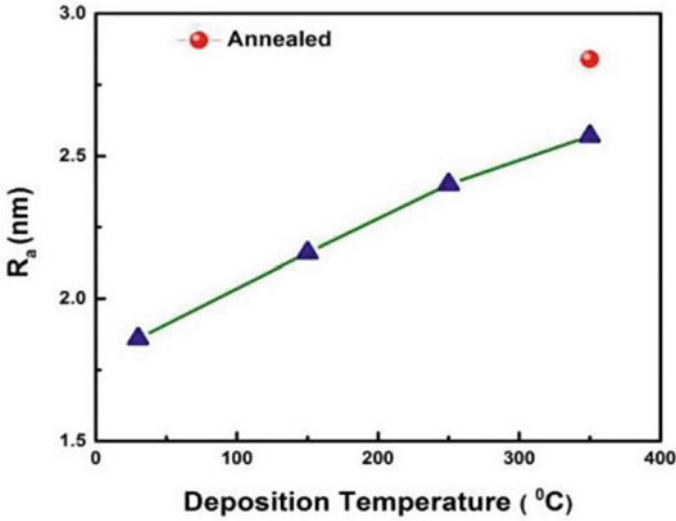
Fig. 8 Deposition temperature versus surface roughness
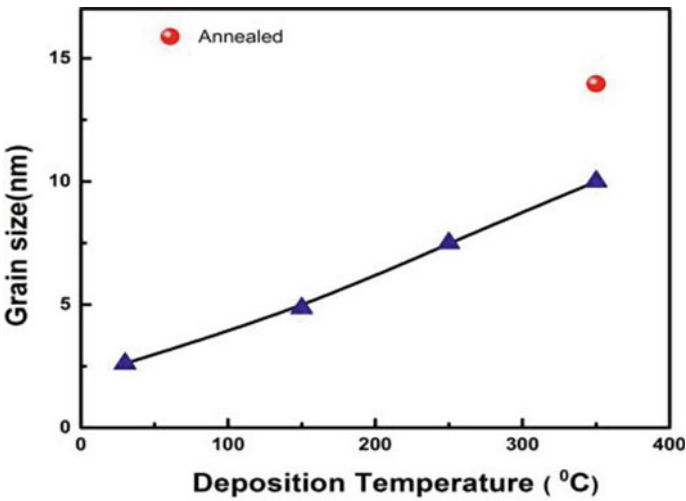
Fig. 9 Deposition temperature versus grain size

2.3 Coating of AFM Tip

Commercial AFM tips (NT-MDT spectrum instruments) were used as a base tip for the preparation of MFM probes. The tips have a chip size of 3.6 × 1.6 × 0.45 resonant frequency around 135–145 kHz. The tip cantilever length was 124 ± 5 μm, and the spring constant was 3.5 ± 0.2 N/m [8–10] (Figs. 11 and 12).
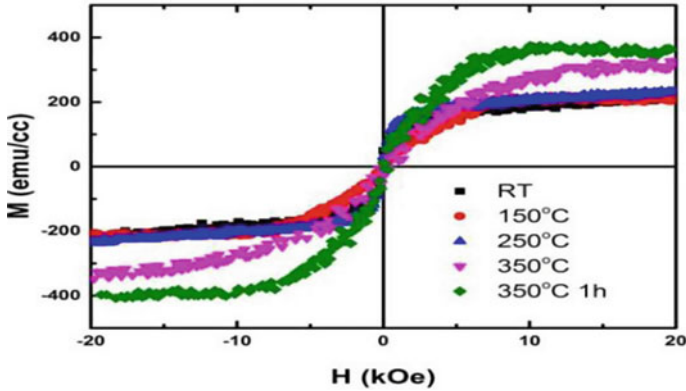
Fig. 10 Variation of saturation magnetization with the applied field at the various condition [6, 7]
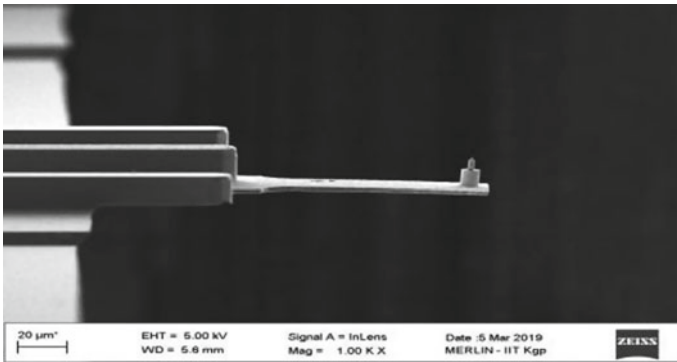
Fig. 11 SEM image of coated AFM tip

3 Results

The tip was coated and characterized, and comparative scans have been carried out using standard tips and the sputter coated tip. A 500 nm nickel film is used as a sample on which AFM scan is performed with both coated and uncoated AFM tip. The AFM scan was carried out in non-contact mode extracting the height signal to image surface topography of the nickel film, commercially available uncoated AFM tips have a resonant frequency of around 150 kHz, but after mounting the coated tip, it was observed that the resonant frequency was increased to around 157 kHz. In present work for the same tip, the value of other terms was kept constant. As it can be seen that the linear frequency is then directly proportional to the moment of inertia. So, an increase in the linear frequency can be attributed to a change in the moment of inertia which is a clear sign of an increase in the tip thickness due to uniform deposition. The nickel film was scanned by both coated and uncoated tip
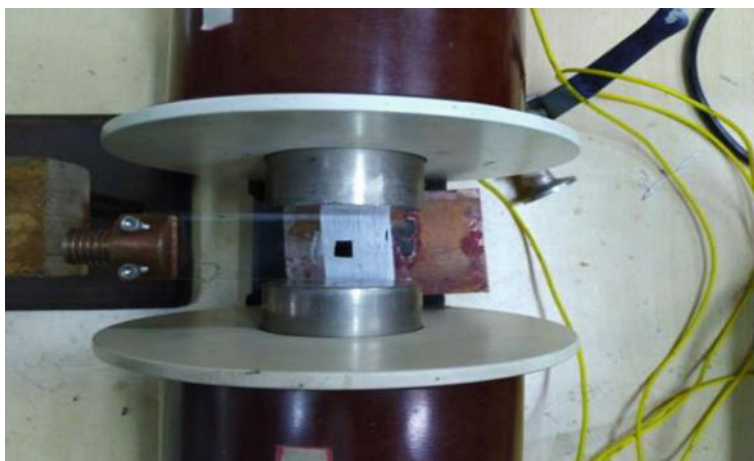
Fig. 12 Magnetizing the coated tip

for comparative analysis. The scanned area of 2.5 × 2.5 μm was selected, linear scanned was performed at a line rate of 1 Hz. Both the coated and uncoated tip were kept at a constant height, and the input magnitude at both cases was kept the same by adjusting the photo diode and laser intensity. Figure 13 (right) and Fig. 13 (left) depict the compared scan using the coated and uncoated tip. It can be observed from the image that despite coating the standard AFM tip with FeGa alloy we get an image which is almost similar to what we get by scanning with an uncoated standard tip (Fig. 13 and 14; Table 2).
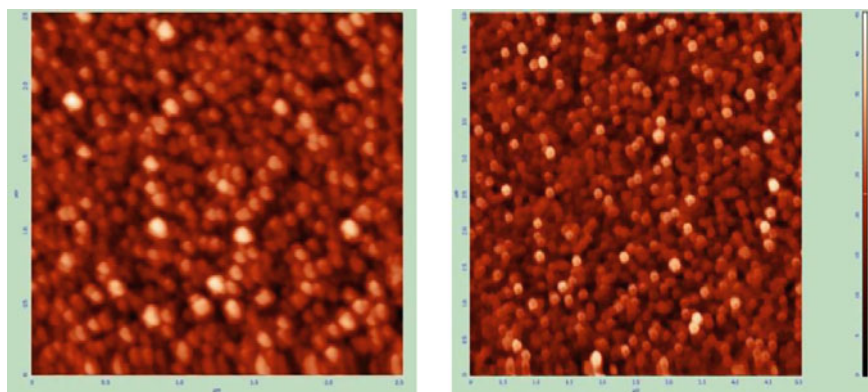
Fig. 13 AFM image scanned by coated tip (right) and standard tip (left)
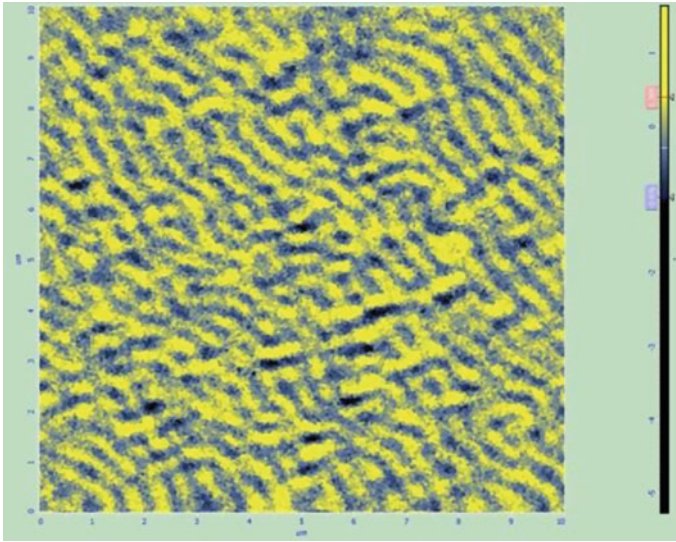
Fig. 14 Magnetic domain of nickel film

Table 2 Roughness and grain size comparison

S. No.	Tip	Roughness Average Value (nm)	R.M.S s(nm)	Grain Size(nm)
1	Standard AFM	4.56	5.79	22.4
2	Coated AFM tip	4.57	5.86	22.54

3.1 Comparison of Scan Done by MFM

A smaller area is selected for the comparative scan. Figure 18 shows the comparison between the images obtained by the standard commercial MFM tip and the magnetically coated AFM tip. As it can be seen from the figure that in the same area the larger domains are captured by the commercially available standard tip, in fact the coated tip also detects the magnetic domain, but it is smaller in size. As the interaction between the domain and tip was very less for the coated tip when compared to the standard one, the force signal is low, so the contrast is less. Before scanning the standard nickel film was magnetized along the parallel direction. Formation of domains was observed, while scanning with a standard MFM tip and the same area was again scanned by the coated tip. In both cases, two pass technique was used and in these condpass, the tip was lifted to a height of 100 nm to eliminate the effect of VanDer Waals forces so that only magnetic dipole interactions are made to be dominant. The scanned area of 2.5 × 2.5 μm was selected, and linear scanned was performed at a line rate of 0.6 Hz (Fig. 15).
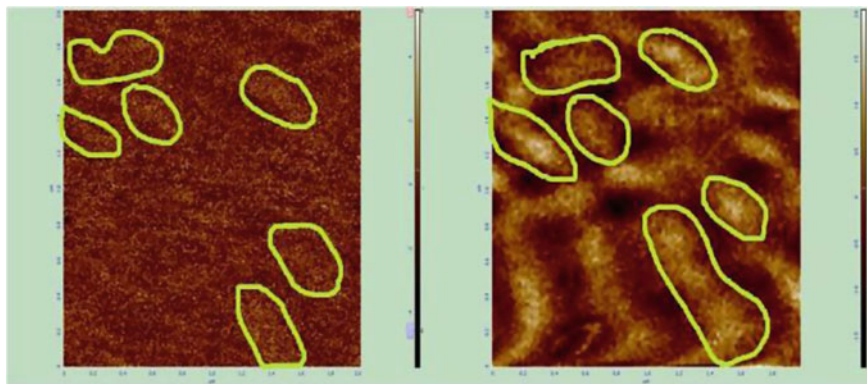
Fig. 15 Comparison of MFM image by the coated and uncoated tip

4   Conclusion

The experiment and analysis, the commercial AFM tip can be converted to MFM tip by using a sputtering deposition process, we can further enhance the resolution of the image that we get from MFM by assisting the deposition with a rotating substrate holder and focused ion milling to increase the sharpness which ultimately increases the contrast of the image.

References

1. Loper, S., Elings, V., Dugas, M.: Optimization of thin-film tips for magnetic force microscopy. IEEE Trans. Magn. **30**(6), 4503–4505 (1994). https://doi.org/10.1109/20.334130
2. Rugar, D., Mamin, H.J., Guethner, P., Lambert, S.E., Stern, J.E., McFadyen, I., Yogi, T.: Magnetic force microscopy: general principles and application to longitudinal recording media. J. Appl. Phys. **68**(3), 1169–1183 (1990). https://doi.org/10.1063/1.346713
3. Sueoka, K., Inagami, K., Imamura, T., Tatebe, K., Mukasa, K.: Magnetic force microscope (MFM) imaging with electrodeposited tips. 1419–1422 (2002). https://doi.org/10.1109/imtc.1994.352162
4. Huang, H.S., Lin, M.W., Sun, Y.C., Lin, L.J.: Improving the spatial resolution of a magnetic force microscope tip via focused ion beam modification and magnetic film coating. Scr. Mater. **56**(5), 365–368 (2007)
5. Hsu, Y.N., Jeong, S., Laughlin, D.E., Lambeth, D.N.: Effects of Ag underlayers on the microstructure and magnetic properties of epitaxial FePt thin films. J. Appl. Phys. **89**(11 II), 7068–7070 (2001). https://doi.org/10.1063/1.1360683
6. Martin, Y., Wickramasinghe, H.K.: Magnetic imaging by "force microscopy" with 1000 Å resolution. Appl. Phys. Lett. **50**(20), 1455–1457 (1987). https://doi.org/10.1063/1.97800
7. Moler, K.A.: Ferromagnet-coated carbon nanotube tips for high-resolution magnetic force microscopy. In: INTERMAG 2006—IEEE International Magnetics Conference, vol. 2, p. 389 (2006). https://doi.org/10.1109/INTMAG.2006.376113
8. Borrego, J.M., Blázquez, J.S., Conde, C.F., Conde, A., Roth, S.: Structural ordering and magnetic properties of arc-melted FeGa alloys. Intermetallics **15**(2), 193–200 (2007)

9. Jen, S.U., Yao, Y.D., Chen, Y.T., Wu, J.M., Lee, C.C., Tsai, T.L., Chang, Y.C.: Magnetic and electrical properties of amorphous CoFeB films. 053701 (2006)

10. Li, J., Chen, N., Wei, D., Futamoto, M.: Micromagnetic studies of ultrahigh resolution magnetic force microscope tip coated by soft magnetic materials. IEEE Trans. Magn. **51**(1) (2015). https://doi.org/10.1109/TMAG.2014.2337835

11. Adolphi, B., McCord, J., Bertram, M., Oertel, C.G., Merkel, U., Marschner, U., Schäfer, R., Wenzel, C., Fischer, W.J.: Improvement of sputtered Galfenol thin films for sensor applications. Smart Materials and Structures, **19**(5), (2010)

12. Zhang, X., Zhan, Q., Dai, G., Liu, Y., Zuo, Z., Yang, H., Li, R.W.: Effect of buffer layer and external stress on magnetic properties of flexible FeGa films. J. Appl. Phys. **113**(17), 2013–2016 (2013). https://doi.org/10.1063/1.4793602

13. CR-06 A multilayer magnetic force microscopy tip and comparison of its imaging performance with conventional tips. **1748**(2003), 2003 (2006)

14. Liu, C., Jen, S., Shieh, J., Juang, J., Chang, Y., Chian, H., Chang, H.: Magnetic properties of Fe 55 Pd 45 films deposited on Si (100) nano-meter wide pillars. nanomedicine & nanotechnology. 5–7 (2014). https://doi.org/10.4172/2157-7439.S5-006

15. Varghese, B., Piramanayagam, S.N., Yang, Y., Kai Wong, S., Khume Tan, H., Kiat Lee, W., Okamoto, I.: Equiatomic CoPt thin films with extremely high coercivity. J. Appl. Phys. **115**(17), 17B707 (2014). https://doi.org/10.1063/1.4861213

Multi-objective Design Optimization of EV Battery Tray

Anand Amrit, Mohit Bahl, and Suhant Ranga

1 Introduction

Electric vehicle (EV) battery tray is the most vital element of a battery system that provides structural integrity to the battery pack while providing protection against fluid ingress from the environment [1]. The major conflicting objectives of an EV battery tray are rigidity, weight, and cost. A rigid battery tray can survive severe vehicle accidents, preventing damage to the battery, while its weight can significantly impact the range of the electric vehicle. These objectives can be analyzed early in the design phase using physics-based simulations like Finite Element Analysis (FEA). However, with the complexity of the engineering problem, these simulations can be computationally expensive making it impossible to carry out design optimization which utilizes thousands of design evaluations. Hence an efficient multi-objective optimization technique is necessary that uses such high-fidelity physics-based simulations to provide optimal solutions cheaply.

Multi-objective design strategies have been developed that utilize a combination of design space reduction, multi-fidelity and data-driven models to accelerate the optimization procedure [2–4]. A fast design exploration technique exists that utilizes sequential domain patching and multi-fidelity models to obtain an approximated Pareto front quickly [5]. Sometimes it is not necessary for the designer to obtain all the Pareto optimal solutions due to time and cost constraints. Hence a point-by-point Pareto set identification technique is available that provides optimal solutions at the

A. Amrit (✉) · S. Ranga
Rivian Automotive, LLC, Irvine, California, USA
e-mail: amrit38@gmail.com

M. Bahl
DURA Automotive Services (I) Pvt Ltd., Hyderabad, India
e-mail: Bahl.M@duraauto.com

vicinity of a target solution [6, 7]. Further, there are other accelerated optimization techniques [8] that can quickly generate the entire Pareto front.

There have been several efforts in the past to optimize the battery tray for electric vehicles. A composite design optimization method is used to obtain trade-offs between mass, amount of deflection, and natural frequency [9]. A cold spraying additive manufacturing technique is utilized to obtain an efficient battery tray with minimum deformation during vibration and higher natural frequency [10]. In the present market condition, customers look for products that are low-cost but of high quality and reliability. Original Equipment Manufacturer (OEMs) demand their suppliers to be cost competitive while meeting all functional requirements. While innovative technology can be used to develop a smart expensive product that performs job efficiently, low-cost products that can do satisfactory job will always be preferable as it gives profit (in dollars). This paper utilizes the methods described above [2–8] to develop a multi-objective optimization framework for design exploration on an EV battery tray. At the end, a design is obtained that beats market in price while satisfying most of the design constraints.

2 Methodology

This section describes an innovative multi-objective optimization process flow that has been specifically developed to generate a battery tray design that meets functional requirements and is manufacturable. Since the battery trays are made up of sheet metals by stamping and extrusion processes, it is important to arrive at an optimized design that is defined by gauge thicknesses.

2.1 Pareto Front

Multi-objective design exploration is important to solve problems pertaining to most engineering systems. Designers need to make design decisions based on multiple conflicting objectives. Applying optimization techniques on one objective/criteria can lead to a design with poor performances on other objectives. In such cases, no single solution exists that simultaneously optimizes all the objectives. Hence it is necessary to obtain non-dominated or Pareto optimal solutions that are a compromise between several conflicting objectives. The set of all the Pareto optimal solutions is known as the Pareto front in which none of the objective functions can be improved in value without degrading some of the other objective values [8].

2.2 *Multi-objective Optimization Algorithm*

The multi-objective optimization (MOO) algorithm is formulated in terms of two scalar design objectives, F_1 and F_2. The MOO algorithm produces a sequence of designs $\mathbf{x}^{(k)}$, $k = 1, 2, …, N$, when the below algorithm is executed:

Step 1: Design space reduction. We initially search for two extreme points of the Pareto (a set of optimal solutions of the trade-off). The two extreme points can be obtained by:

$$x^{(1)} = \arg \min_x F_1(f(x)) \tag{1}$$

$$x^{(2)} = \arg \min_x F_2(f(x)) \tag{2}$$

where F_1 and F_2 are the two conflicting objectives. 'x' is the design vector and 'f' is the expensive FEA model. '$x^{(1)}$' and '$x^{(2)}$' are obtained by hands-on design exploration using parameter sweeps guided by engineering experience or by performing single objective optimizations using a computer code. The designs of these two extreme points are used as the lower and upper bounds of the design space (reduced design space) where the multi-objective optimization process is executed as shown below:

$$\text{Lower bounds} = \min(x^{(1)}, x^{(2)}) \tag{3}$$

$$\text{Upper bounds} = \max(x^{(1)}, x^{(2)}) \tag{4}$$

Step 2: Training data. By a rule of thumb $2n + 1$ (n is the total number of design variables) designs of the battery tray are evaluated on high-fidelity FEA models to obtain the objective values.

Step 3: Prediction Model. Using the information from the model evaluations in step 2, a fast statistical model known as kriging interpolation model is constructed. The details of the kriging interpolant and its construction is described in Amrit et al. [8]. The kriging model is very fast and takes few seconds to predict the objective values for any design compared to FEA which takes several hours.

Step 4: Optimization. The fast Kriging model constructed in step 3 is utilized in a multi-objective optimization algorithm to find a trade-off between the conflicting objectives. Genetic Algorithm (GA from Matlab), a population-based metaheuristic method is the multi-objective optimization engine used here [8]. It uses the kriging model to evaluate thousands of designs in the reduced design space within a few minutes.

Step 5: Results. Step 4 produces the Pareto front containing the optimal solutions. The designer needs to select the best design from this solution set and tune it to gauge thickness. The tuned design is then evaluated on FEA to obtain accurate performance.

Step 6: Decision. If the designer is satisfied then terminate the process. Otherwise, the design is included in the training data in step 2 to construct a refined kriging model and the cycle continues.

3 Results

The multi-objective optimization process shown in Fig. 1 is applied on the battery tray design problem. This section describes the Pareto front generation, final solution selection, and comparison with baseline design.

3.1 Problem

A parametric 3D CAD model of baseline design for the EV battery tray is generated in CATIA as shown in Fig. 2a. The conflicting objectives of interest are: (1) weight (kgs), (2) intrusion due to side impact load (mm), (3) cost (dollars), (4) bending

Fig. 1 Multi-objective optimization process flow diagram

(a)   (b)
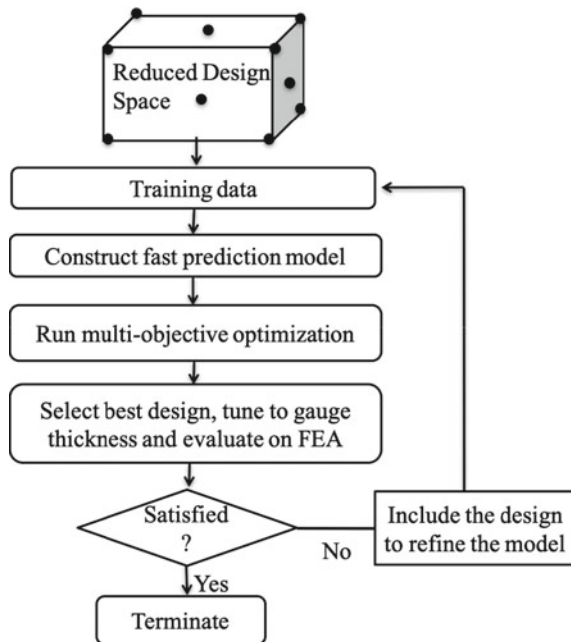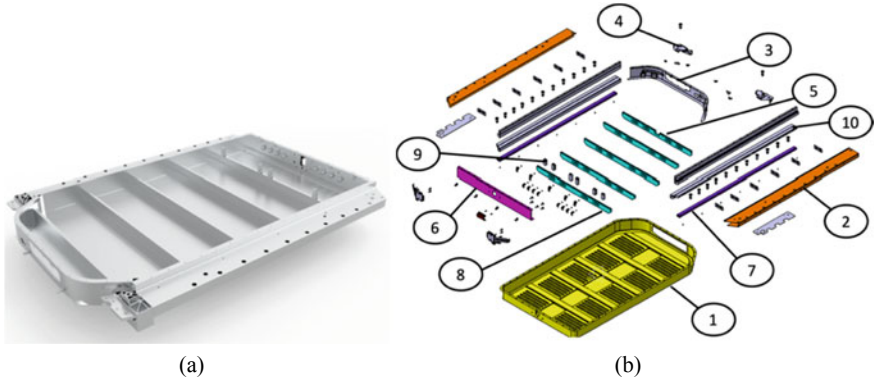
Fig. 2 a Baseline battery tray design, **b** child parts with part number

displacement (mm) and (5) torsional displacement (mm). All the load cases involve applying a load of a specific amount (as shown in Fig. 3) to analyze the amount of resistance provided by the battery tray. This is quantified by the amount the battery tray deflects in the direction of load application. The battery tray is constrained (DOF = 0) in all 4 corners during the load analysis. The multi-objective optimization problem formulation is shown below:

$$\min_{l \le x \le u} \text{Weight}, \quad \min_{l \le x \le u} \text{Intrusion} \tag{5}$$

subject to

$$\text{Cost} \le \$1000, \tag{6}$$

$$\text{Bending displacement} \le 0.27 \text{ mm}, \tag{7}$$

$$\text{Torsional displacement} \le 8.16 \text{ mm}. \tag{8}$$

The battery tray consists of several child parts (see Fig. 2b) made from sheet metal of various gauge thicknesses. Since the shape of the parts cannot be altered due to manufacturing and design constraints, only the thicknesses of these child parts (parts numbered in Fig. 2b) are used as the design variable for the multi-objective optimization problem. The details of the ten design variables shown in Fig. 2b is given in Table 1. Further, steel and aluminum are also considered as design variables where in the child parts can be of either material (Table 1).

Table 1 Comparison of baseline and optimized child parts

Part. No.	Description (baseline thickness)	Baseline weight (kg)	Optimized thickness (mm)	Optimized weight (kg)
1	Tray tub (1.2 mm)	13.86	1.52	29.5
2	Side rail (1.2 mm)	16.44	1.37	18.19
3	Front rail (1.2 mm)	3.04	1.06	2.10
4	Rear closeout (1.2 mm)	0.17	1.37	0.30
5	Cross member front (1.2 mm)	1.84	1.06	1.1
6	Rear rail (1.2 mm)	3.89	1.06	2.51
7	Striker (1.2 mm)	1.36	1.37	2.13
8	Cross member (1.2 mm)	2.20	1.06	1.77
9	Tie down (1.2 mm)	0.29	1.37	0.55
10	Side rail (1.2 mm)	3.5	1.37	5.5
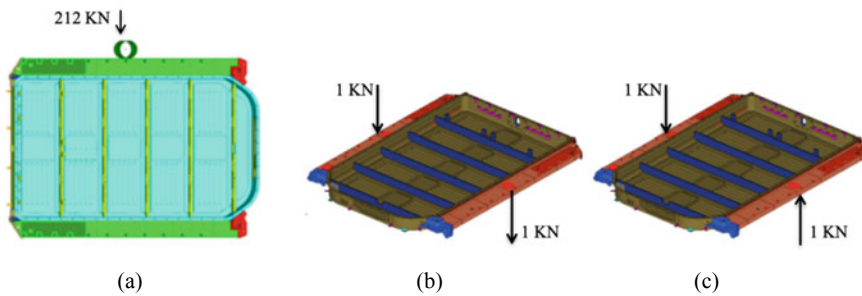
Fig. 3 **a** Side impact load, **b** bending load, **c** torsional load

3.2 Pareto Front Exploration

The two extreme points of the reduced design space are obtained by minimizing each of the conflicting objectives separately (i.e., weight and intrusion) which later form the bounds of the reduced design space. The number of design variables utilized in the multi-objective design optimization of the battery tray is $n = 12$ (child parts shown in Table 1 + type of materials). Hence, $2n + 1$, i.e., 25 designs are selected randomly within the reduced design space. Each of those designs is evaluated on an FEA model constructed in Abaqus (commercial software) and boundary conditions are applied to analyze the side impact load, bending load, torsional load, and weight. A training data set consisting of all design points and corresponding performance values is generated and the optimization algorithm is executed as discussed in Sect. 2.2.

The multi-objective optimization did not provide any feasible solution using all the objectives (as shown in eqs. 5–8). Hence it is decided to perform two different optimizations: (1) minimize weight, minimize intrusion and (2) minimize cost, minimize weight. All other constraints except the cost are involved in both optimizations. The compromise between the various conflicting objectives containing optimum solutions and the selected solution (made entirely of steel) are indicated in Fig. 4. The baseline design made entirely of aluminum is able to satisfy all the constraints except cost. Figure 4a indicates that the baseline aluminum design is far away from the Pareto front (optimal solutions shown in red dots). It means there are no solutions that can match the performance of the baseline aluminum design without increasing the cost. Similarly in Fig. 4b, it is found that the cost of the battery tray cannot be reduced without increasing the weight. This is evident as steel is 3 times cheaper than aluminum but at the same time, the former is 2.5 times denser than the latter. Hence, a solution is selected (shown in Fig. 4) that meets the intrusion performance and is very cheap. Table 1 indicates the effect of optimization on the thickness and weight of each child part. All the conflicting objectives of interest for baseline and optimized design are summarized in Table 2. It indicates the optimized design meets the side impact intrusion and torsional displacement constraints. The bending displacement constraints of the battery tray are off by 0.1 mm only which is acceptable. Although the weight of the optimized design is heavier than the baseline design (by 20 kgs), but is 7 times cheaper than the baseline design. The main reason behind selecting the steel battery tray design is its cost which beats the market competitors. Further, a steel battery tray is easier to manufacture than that of aluminum. Figure 4a shows the selected design is not from the Pareto front but slightly above it. This is because the solutions at the Pareto front have sheet metal thicknesses other than the gauge thicknesses. Hence a nearby solution is selected that had thicknesses as per the sheet metal gauge.

(a)   (b)
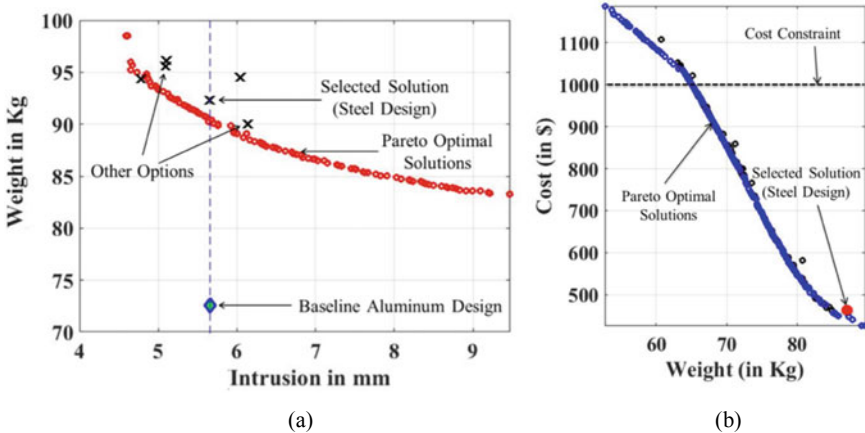
Fig. 4 Pareto optimal solutions for **a** weight and intrusion **b** cost and weight

Table 2 Comparison of baseline and optimized EV battery tray

	Baseline design (aluminum design)	Optimized design (steel design)
Weight (kg)	72.7	92.3
Side impact intrusion (mm)	5.63	5.65
Torsion displacement (mm)	8.16	7.76
Bending displacement (mm)	0.27	0.37
Cost ($)	3000	400

4   Conclusion

An efficient multi-objective optimization method is developed to solve the EV battery tray design problem. Two different multi-objective optimization are executed for weight, side impact intrusion and cost with bending, and torsional displacement constraints. The design variables consist of thicknesses of all child parts and types of material (steel and aluminum). The target is to develop an inexpensive design that is able to beat the competitors in the market and is easy to manufacture. The Pareto front representing the optimum trade-offs solutions between multiple conflicting objectives has been explored and an innovative steel battery tray design is selected as the best design. The selected design is almost 7 times cheaper than the baseline aluminum design with some negative effects on the weight. Future work will deal with the generalization of the proposed optimization algorithm that can handle large number of conflicting objectives and many design variables. Further research is needed on the weight reduction of the battery tray while meeting other functional objectives.

References

1. Coronado, K., Lyons, J., Curtis, R., Wang, T.: High voltage hybrid battery tray design optimization. SAE Technical Paper 2011–01–067 (2011). https://doi.org/10.4271/2011-01-0671
2. Amrit, A., Leifsson, L.: Applications of surrogate-assisted and multi-fidelity multi-objective optimization algorithms to simulation-based aerodynamic design. Eng. Comput. **37**(2), 430–457 (2019). https://doi.org/10.1108/EC-12-2018-0553
3. Amrit, A., Leifsson, L.T., Koziel, S., Tesfahunegn, Y.A.: Efficient multiobjective aerodynamic optimization by design space dimension reduction and cokriging. In: 17th AIAA/ISSMO Multidisciplinary Analysis and Optimization Conference, AIAA AVIATION Forum, (AIAA, p. 3515). (2016)
4. Leifsson, L.T., Koziel, S., Amrit, A.: Design optimization by manifold mapping response correction and low-fidelity model preconditioning. In: 55th AIAA Aerospace Sciences Meeting, AIAA SciTech Forum, (AIAA 2017–0705)

5. Amrit, A., Leifsson, L.: Fast multi-objective aerodynamic optimization using sequential domain patching and multi-fidelity models. J. Aircr. **57**(3), 388–398 (2020). https://doi.org/10.2514/1.C035500

6. Amrit, A., Leifsson, L., Koziel, S.: Aerodynamic design exploration through point-by-point pareto set identification using local surrogate models. In: AIAA/ASCE/AHS/ASC Structures, Structural Dynamics, and Materials Conference. Kissimmee, Florida (2018)

7. Amrit, A., Leifsson, L., Koziel, S.: Multi-fidelity aerodynamic design trade-off exploration using point-by-point pareto set identification. Aerosp. Sci. Technol. **79**, 399–412 (2018). https://doi.org/10.1016/j.ast.2018.05.023

8. Amrit, A., Leifsson, L., Koziel, S.: Design strategies for multi-objective optimization of aerodynamic surfaces. Eng. Comput. **34**(5), 1724–1753 (2017). https://doi.org/10.1108/EC-07-2016-0239

9. Bao, N., Zhao, R..: Design optimization of battery holder for electric vehicle. In: 2018 6th International Conference on Mechanical, Automotive and Materials Engineering (CMAME), pp. 79–84. (2018). https://doi.org/10.1109/CMAME.2018.8592441

10. Pal, S.K., Singh, S., Singh, H., Phung, Le., Yooyen, S., Sleesongsom, S.: Intelligent design optimization of battery pack enclosure for electric vehicle by considering cold-spraying as an additive manufacturing technology. Energy Storage **2**(3), (2020). https://doi.org/10.1002/est2.148

Optimization of Cathodic Protection Design for Oil and Gas System

Noel Martin and Aezeden Mohamed

1 Introduction

Corrosion is one of the major problems faced throughout Papua New Guinea and across the globe which profoundly contributes towards major losses in company's income. It has been so far widely concerning for especially oil and gas industries that operate and extract such minerals from both onshore and offshore rigs where there is a continuous trend of corrosion from established structures from time to time which exert an enormous pressure on the extraction, distribution and ultimately profit margins [1].

Papua New Guinea faces similar problems which sometimes drastically hinder the progress of abstracting and processing natural oil and gas due to high concentrations of water vapour and dissolved chloride including other corrosive chemical compositions such as oxygen, carbon dioxide and hydroxides.

There are few other ways of mitigating and reducing the rate of corrosion that can save companies time and money which has been considered to be important mechanisms that can successfully control corrosion acceleration. The cathodic protection method of protecting steel structures is used to date and combat corrosion on oil and gas pipeline industries [2]. Corrosion protection engineers have vastly studied wide area in relation to cathodic protection notion, however only two methods of cathodic protection used today known as impressed current cathodic protection and sacrificial anodes or galvanic anodes protection system. Both play same role in protecting

N. Martin
Department of Civil Engineering, Papua New Guinea University of Technology, Lae, Papua New Guinea

A. Mohamed (✉)
Department of Mechanical Engineering, Papua New Guinea University of Technology, Lae, Papua New Guinea
e-mail: aezeden.mohamed@pnguot.ac.pg

structure from corrosion with slight improvement or changes in methods in which they apply to protect the structure. Alotau is one of the provinces in the country where Puma Energy facilities are established and used sacrificial anodes method of protecting steel facilities [3].

2 Electrolytic Process

The electrolytic process is the chemical composition in which the electrons (electricity) gain or loses depending on their potential. This involves anode, cathode, electrolyte and therefore ultimately referred to as electrochemistry. The same principle is practiced in cathodic protection of structures from corrosion. Alotau terminal Puma Energy site is not different.

2.1 Cathode

Cathode is the electrode where it gains electrons or is protected from reducing in size. This is where reduction occurs, which the gain of hydrogen ions and releasing of oxygen electrons which then reacts with anodes metals to form metal oxides [4]. This is where the electrons are passed chemically and do not attract corrosive electrons and instead gain hydrogen ions to remain protected from reducing in size or corrosion.

2.2 Electrolyte

Electrolyte is the medium or place where transferring and gaining of electrons from cathode and anode occurs. It's the place where ions flow. Thus, electrolyte is any area which in contact with anode and cathode to allow for transfer of electrons or electrons migrate where the chemical reaction is allowed to happened as designated in Fig. 1.

In order for the corrosion to occur, entire components of electrochemistry must be present for the reaction to provide chemical reaction as shown in Fig. 1. The absence of either of the members would mean that there will be no chemical reaction. The corrosion reaction occurs in the presence of cathode and anode in an electrolyte. The element proposed to be corroded is known as anode and the protected electrode is the cathode.
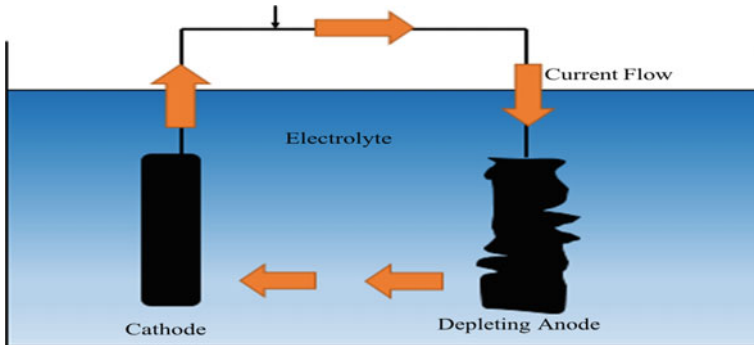
Fig. 1 The metallic path for the electrolysis process which the same notion or principal is applied in cathodic protection [5]

2.3 Anodes

In electrochemistry, anode is described as electrode which reduces in size during chemical reaction and ultimately has high potential (negatively charged ions). At anode, the negatively charged high potential ions are discharged and driven or forced towards less active elements known as cathode [6]. The oxidation reaction is imminent at anode while reduction occurs at cathode. Ultimately, it is where exchange of electrons (electricity) in the cycle of electrolysis.

Therefore, the most obvious part of the corrosion cell is the anode where it loses its electrons to combine with other elements where the resulting component for metals is normally iron oxide.

2.4 Metallic Path

Metallic path is another important component of the electrochemical circuits that completes the reaction to occur [7]. This path allows the electrons to flow through and importantly connects both anode and the cathode in an electrolyte.

The electrochemical shell consists of components mentioned however, absence of either one of the members will mean that no corrosion reaction.

$$\text{Zn} \rightarrow \text{Zn}^{2+} + 2e^- \qquad \text{Cu}^{2+} + 2e^{2+} \rightarrow \text{Cu}\,(s) \qquad (1)$$
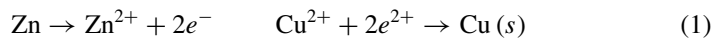
2.5 Anode/Cathode Relationship

As noted, an electrode becomes anode or cathode depending on the naturally electrical potential it acquires in electrochemical corrosion cells in comparison with other electrodes. The potential (voltage) difference between anode and the cathode is known as the electromotive force of the cell. The electrode which is more electrically active or more negative in potential undergoes degrading and corrosion is normally the anodes. This is where the naturally existing potential compared to others will be subject to immediate reaction by attracting electrons from cathode and as such, corrodes which happened to be normally anodes as specified in Fig. 2.

The electrode which is more electrically inactive or Nobel is referred to as the cathode. By definition is cathode and does not corrode. This is where the electrical potentials are less and thus attracted by the anodes which give up its electrons and as a result, anodes corrode.

3 Alotau CP Site

Table 1 and graph explained are from Alotau Province cathodic protection (CP) site in PNG and reference electrodes used were copper/copper sulfate (Cu/CuSO$_4$) and Silver/Silver Chloride (Ag/AgCl), respectively. Graphs are evaluated, analyzed and described separately depending on the portable reference electrodes used to collect raw data and results.

The table showing data collected using copper sulfate electrode in Alotau terminal. The results are as discussed and plotted, respectively. Note that all data collected are for sacrificial anodes only and not impressed current cathodic protection system.
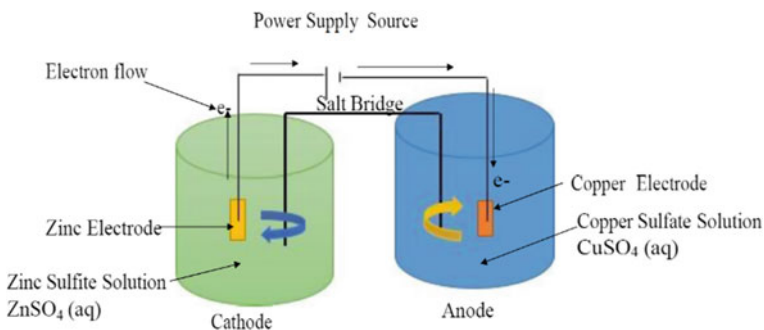
Fig. 2 The combination of the electrochemical reactions is summarized by this diagram

Table 1 Results of potential difference using copper/copper sulfate (Cu/CuSO$_4$) as reference electrode (RE) for both protected (P) unprotected in millivolts (mV)

Location	RE	P (mV)	UP (mV)
Alotau site	Cu/CuSO$_4$	−1080	NA
	Cu/CuSO$_4$	−0906	−0500
	Cu/CuSO$_4$	−0920	−0528
	Cu/CuSO$_4$	−1032	NA
	Cu/CuSO$_4$	−0916	−0450
	Cu/CuSO$_4$	−0916	−0460
	Cu/CuSO$_4$	−0996	NA
	Cu/CuSO$_4$	−0916	−0480
	Cu/CuSO$_4$	−0900	−0490
	Cu/CuSO$_4$	−1032	NA
	Cu/CuSO$_4$	−0916	−0450
	Cu/CuSO$_4$	−0916	−0460
	Cu/CuSO$_4$	−1055	−1062
	Cu/CuSO$_4$	−1035	−0427
	Cu/CuSO$_4$	−0916	−0460
	Cu/CuSO$_4$	−1021	−0522
	Cu/CuSO$_4$	−1215	−0530
	Cu/CuSO$_4$	−1109	−0535
	Cu/CuSO$_4$	−1318	−1062
	Cu/CuSO$_4$	−1270	−0427
	Cu/CuSO$_4$	−1270	−0460
	Cu/CuSO$_4$	−1318	−1062

3.1 Reference Electrode Used Copper–Copper Sulfate (Cu/CuSO$_4$)

Protected Structure: Figure 3 represents the data sent from Alotau as designated in detail on Table 1 which was recorded using copper/copper sulfate reference electrode (Cu/CuSO$_4$). The graph denotes that the potential protection has been rendered to the structure on sacrificial anodes protection areas. It has been observed that there are fluctuations on protective structure possibly due to formation of calcareous invisible materials being formed. The blue line has seen not steady because of the protective current sometimes becomes stray current in which it does not follow intended path and instead follow metal paths. The optimum protective voltage readings against reference electrodes is considered to be −0.85 V or −850 to −880 mV as per AS2832.1.2015.

For the section of structures established in Alotau, it has been noted that portion of the structures protected by cathodic means has been protected significantly. However, some values went far greater than −1.2 V which is normally the values expected
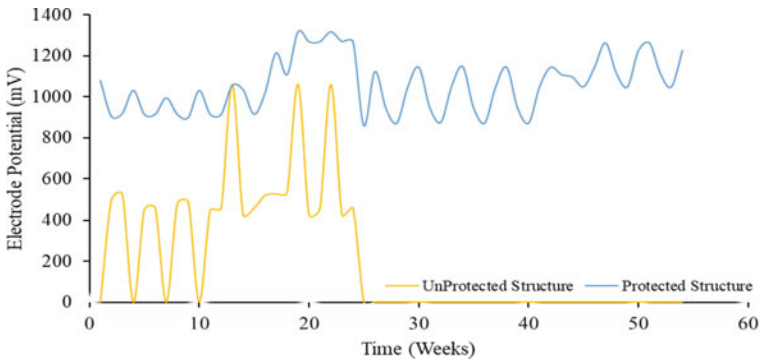
Fig. 3 Graph showing voltage discharge and data recorded from underground structures in Alotau terminal, PNG

from the impressed current protective method. As such, it is expected that according to Australian Standard AS2832.1.2015, the anodes used were believed to be zinc because it is economically viable and simple for instillation and is abundant in nature but the magnitude of protection is shallow compared to magnesium.

Unprotected Structure: For the unprotected sections of the structure, there is an inconsistency in corrosion where portion of the structure is partly protected while some parts were poor and corrosion has already attacked the metal structure. This is because as far as the level of protection is concerned and amount of voltage and current discharged throughout the system, sacrificial anodes do not adequately protect the structure because of the weak supply of potential from anodes without external voltage reinforcement supply preferably from power supply source. This greatly weakens the system and some parts of the structure have been on consistent attack by corrosion. As per unprotected line (orange line) from Fig. 3, 95% of the line graph falls below −880 mV which denotes the adequate protection level [8]. This does not mean the pipe or steel tank is leaking but it is vulnerable to failure and damage soon.

The Bunker Lines and wharf end ships have not been performing in accordance to standards and specifications. This is because the sacrificial anodes have been in short supply of energy to drive the protective current through or possibly due to stray current. This is vividly explained in Fig. 4.

For some days, the level of protection required was complete nil and zero as designated (Fig. 3). The corrosion has consumed much of the structure when the size of protection needed was nil and fell in zero lines. It was also concluded that the structure does not meet −850 mV standard for corrosion protection and is not in compliance with the international corrosion protection standards and Australian standards of cathodic protection. As such was not cathodic protection on the intended corrosive section and thus considered fail and deficiency or declining.

Some possible notions from the orange lines are as follows but not limited to: No Cathodic protection on the structure; Adequate number of days/weeks/months
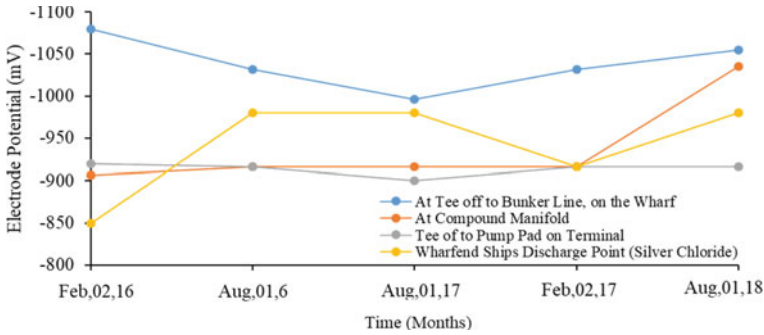
Fig. 4 Six (6) monthly CP results of different terminals in Alotau

the metal has been exposed to corrosion; Vulnerable to failure; Level of protection rendered by sacrificial anodes system is considered inadequate and weak; Anodes maybe exceptionally short and inadequate and thus requires reinforcement; Polarization currently do not reach the structure.

From Fig. 4, the different CP results have been obtained from (2016 to 2018) on designated structure locations named. Only Compound Milford and Pump pad have been protected by the sacrificial anodes system in accordance with Australian standards and specifications AS2832.1.2015 which denotes that the CP values within −850 mV or nearest and are considered to be protected.

It is obvious that the amount of protective current has been hindered due to impedance on the metal's paths and circuits. As such, the values signify significant increase in its protective potential which resembles that of impressed current method though protected by sacrificial anodes system.

There was no passivity or no barrier in which the corrosion had been halted and stopped. The deterioration has actively consumed the metals and as a result, the possibility of oxygen dissolved is at its peak [9].

This is also in conjunction with the type of backfill materials used. The elective backfill materials used result to better transfer of protective current within the electrolytic system.

This is because the performance of all corrosion prevention systems is vastly determined by the type of backfill material used. Higher the electrolytic materials will mean the flow of current is less or clogged. In this case, there were no selective materials used because the values are way above standards specification manual as designated in Fig. 4. The performance of sacrificial anodes systems is not in compliance with standards and thus requires corrosion engineers to check the system immediately.
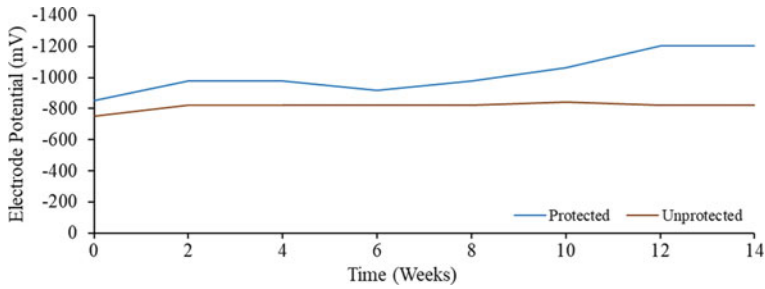
Fig. 5 Potential recorded from submerged structure in Alotau terminal

3.2 Reference Electrodes Used, Silver Chloride (Ag/AgCl)

Protected Sections: According to Fig. 5, the level of protection given to the cathodic protection has been adequate and polarization effect seemed effective from the duration of sacrificial anode protection system installed. The protected graph maintained and emits its level of current discharge through natural potential difference preferably from buried zinc anodes. The stray current was considered minor because the line indicated is within the allowable range of protection and is in accordance with the standards and regulations specified. It is also noted that impedance did not bother because the potential supplied by installed electrodes effectively drove impressive current through electrolyte regardless of any magnitude of resistance encountered throughout the cathodic protection period.

The polarization effect has ambient cover on entire targeted cathodes/structures substrate and thus performed its assigned duty to protect the structure without possible impedance. This has shown on the graph in which the values fall between -850 and -1000 mV which is also the effective cathodic protection in accordance with Australian standards and specification guidelines AS2832.1.2015. The protected structure has effectively been protected in sections of sacrificial anodic protection substrate/surface areas.

It is also vivid that there is a possibility of stray current occurred because the protected graph has gone passed 1100 mV and further went up to 1200 mV. This clearly indicated that there are calcareous materials formed which defended and defiance cathodic protection.

Unprotected Sections: For the unprotected portion of sacrificial anodic protection, the values were concurrently fall above -750 mV but below -850 mV as indicated on graph denoted by gray bars. As per Australian standards and specifications, it does not meet the regulation standards and is thus considered noncompliance and declining CP. However, this does not mean the protective current not reached the structure substrate but the level, magnitude and strength of potential emitted by the anodes do not effectively drive the current in full. There was loss of current along the

Table 2 The silver/silver chloride (Ag/AgCl) reference electrodes (RE) potentials (mV) for protected (P) and unprotected (UP) structures

Location	RE	P (mV)	UP (mV)
Alotau (PNG) Different locations as discussed in materials and methods sections	Ag/AgCl	−0850	−750
	Ag/AgCl	−0980	−820
	Ag/AgCl	−0980	−820
	Ag/AgCl	−0916	−820
	Ag/AgCl	−0980	−820
	Ag/AgCl	−1065	−841
	Ag/AgCl	−1206	−820
	Ag/AgCl	−1206	−820

way due to friction or electrolytic resistance and possible impedance while travelling via electrolyte.

Few sections may be affected by joins and junctions which the hazards or obstacles are passed from instillation works. For cathodic protection to occur on both sides of the joins, there are certain criteria used to wield the structures together. This was what exactly happened when the joints have become obstacles and cathodic prevention to flow through entire structure (Table 2).

Also noted from the two distinct graphs (Figs. 3 and 4) which have different portable reference electrodes and observed major differences in comparison and silver chloride has shown better results compared to copper sulfate. With respect to the standard hydrogen electrode, silver chloride electrode is +0.25 voltage in seawater [10]. Thus, it is possible that Fig. 5 indicated the measurement of cathodic protection data at submerged pipelines in seawater. The portable or permanent silver chloride electrode is useful in seawater where there's a lot of chloride content.

The copper sulfate portable electrodes have been used in underground with its electrode potential of 0.316 V at 25 °C with respect to standard hydrogen electrodes. Graph 4 designates the CP reading taken from underground structures and that's the difference known.

The CP system in Alotau terminal of submerged structures seemed to behave exceptionally and maintained the standards of cathodic system specifications in accordance with Australian standards as per both protected and unprotected structures indicated (Fig. 5).

Protected line falls on the optimum margins which designate effective CP protection in compliance to regulations and guidelines AS2832.1.2015. However, for unprotected structure, it still maintained good position and lies between −700 and − 800 mV denoted as designated (Fig. 5). The CP protection on submerged pipelines is considered well protected compared to buried pipelines.

4 Conclusion

According to the data, it has been concluded that the magnitude of cathodic protection rendered to the steel structures in Alotau Puma Energy CP site is inadequate and thus considered decline in CP protection. Sacrificial anodes potential to transmit protective current have been exhausted and minimized due to lot of quantiles of steel being fed on certain few installed anodes for protection. As such, it is vigorously recommended that possible replacement option has to be open for immediate construction.

The impressed current (ICCP) method of cathodic protection was prepared and is remain possible target for replacement as current sacrificial anodes no longer function and perform as anticipated. Impressed current cathodic protection is the best method of steel facilities from corrosion prevention because it has an external power supply that drives the impressive current from anode to cathode and in this way, it is more reliable and best than sacrificial anodes which only uses potential difference from anodes and cathodes.

References

1. Bashi, S.M., Mailah, N.F., Radzi, M.M.: Cathodic protection system. In: Proceedings of National Power Engineering Conference, PECon 2003, vol. 7, no. July 2015, pp. 366–370 (2003)
2. Mohamed, A.: Intergranular corrosion fatigue fracture surface analysis of nickel alloy. In: 1st International Conference on Structural Integrity, vol. 114, no. 09, pp. 754–759 (2015)
3. Little, D., Sears, L.: Introduction to corrosion your friendly TSC corrosion staff. Int. J. Corros. **2**(6), 5 (2013)
4. Mohamed, A., Cahoon, J.R., Caley, W.F.: Anodic polarization behaviour of nickel-based alloys in neutral and very acidic solutions. J. Corros. Sci. Eng. **15**(09), 1–30 (2012)
5. Guyer, J.P., Asce, F., Aei, F.: An introduction to cathodic protection principles. J. Chem. Eng. Inf. **877**(5) (2014)
6. Shaw, B.A., Kelly, R.G.: What is corrosion? Corros. Steel Ceram. **1**(4), 24–26 (2006)
7. Ashworth, V.: 18 Principles of cathodic protection. Int. Conf. CP Des. **2**(May), 3–10 (2010)
8. Kisan, M., Sangathan, S., Nehru, J., Pitroda, S.G.: Cathodic protection of buried pipeline/structure for transportation of natural gas, oil and liquids—code of practice. J. Anodes Impressed Curr. CP Syst. **12**(5), 23 (2006)
9. ISO, S.: International standard petroleum, petrochemical and natural of pipeline systems. J. Anodes Impressed Curr. CP Syst. **20**(9), 36 (2015)
10. Choi, B., Lee, S., Kim, J., Oh, J.: Cathodic protection of onshore buried pipelines considering economic feasibility and maintenance. J. Adv. Res. Ocean Eng. **2**(4), 158–168 (2016)

Selection of Optimal Process Parameters for Electric Discharge Machining of 13/8 PH Steel Using Genetic Algorithm

V. Sindhuja, J. Laxman, K. Eswaraiah, and M. D. Sameer

1 Introduction

Electric discharge machining (EDM) consists of high maneuverability and precision which make its usage an ideal way to machine complex geometries with high accuracy. This machining process is also known as spark erosion, since electrically conductive materials are machined by controlled sparks between electrode and work piece. The optimal parameters help in improving dimensional quality, reducing production time and cost [1]. Due to its high-thermal resistance and shear resistance, 13/8 precipitation-hardening (PH) steel is used in the aerospace industry extensively [2]. The aim of the current research is to provide a comprehensive and detailed report on its machinability in a die sinking EDM. Optimization is performed for high MRR with optimal values of input parameters. Because of rapid industrialization, various materials are machined using EDM process. Many researchers had performed machining on various materials considering electrical and non-electrical parameters for optimization [3–5]. Laxman and Guru Raj [6] had performed experiment of EDM process parameters effect on titanium super alloy using Taguchi L27 array considering MRR, TWR, and SR as response parameters. Their research proved that the single objective technique Taguchi is more effective than performing all experiments. In 2017, Chandramouli and Eshwaraiah [7] performed optimization of 17-4 PH steel using Taguchi considering surface roughness and material removal rate as output response parameters in Minitab, using copper tungsten electrode. Rajmohan et al. [8] had performed optimization of machining parameters in EDM of 304 stainless steel. They used Taguchi for optimization on die sinking EDM machine. Rajesh and Anand [9] used response surface methodology and genetic algorithms for machining

V. Sindhuja · J. Laxman · K. Eswaraiah · M. D. Sameer (✉)
Department of Mechanical Engineering, Kakatiya Institute of Technology and Science, Warangal 506015, India
e-mail: mds.me@kitsw.ac.in

Al alloy HE9 grade. They have used different parameters such as current flow rate, pulse-ON, pulse-OFF, and gap to find the metal removal rate and tool wear rate. Ozkavak et al. [10] experimented on Inconel 718 using gene expressing programing (GEP) and artificial neural networks (ANN). They found that ANN was more accurate in predicting the surface roughness when compared with GEP. From the literature survey, it is evident that lot of work was done on optimization of process parameters on different hardened steels using various techniques. In this study, the authors have aimed to improve the MRR of 13/8 PH steels by employing Taguchi and genetic algorithm, at same time, the best possible MRR for to find the optimal process parameter combination.

2 Experimental Details

The experiments were performed on die sinking EDM of Askar microns model V3525 with servo head mechanism that has constant gap voltage of positive polarity. Commercial 30 grade EDM oil is used as dielectric liquid. Three phase AC supply of 230 V power is supplied to machine. Manual side flushing is performed during machining. The electrode tool used was 10 mm diameter copper tungsten with composition of 70% copper and 30% tungsten. Copper tungsten electrodes have high-thermal conductivity, electrical conductivity, low-thermal expansion that results less tool wear rate. The work piece material is 13–8 PH steel with dimensions 50 mm × 50 mm × 25 mm. Its mechanical properties are high strength, great corrosion resistance, and superior toughness. It is used in aerospace industries, injection molding equipment, petrochemical industries, nuclear industries, etc. Its relatively high strength compared to other variants of steel make it an extremely difficult machine material but in turn makes it a suitable test piece for an EDM machine that is perfectly adequate in such a scenario. Chemical composition of 13–8 PH steel is presented in Table 1.

Selection of Parameters: The effect of four parameters input current (IP), pulse-on time (TON), pulse-off time (TOFF), tool lift time (TLT) was investigated for 5 min of machining time with each experiment setup is given in Table 2. Manual flushing is performed for removal of debris from machining zone. Parameters are selected according to the experiment requirements. Initially, pilot experiments are conducted to know the trend of each input parameter with response parameters, then Taguchi orthogonal array was generated in Minitab, those experiments were performed.

Taguchi Method: Dr. Genichi Taguchi developed this method to evaluate mean and variance of the experimental data to determine the process effectiveness [12]. This method organizes input data of various levels in an orthogonal array of various sizes which include L9, L18, L27, L36, L54, etc. The orthogonal arrays have all levels of factors equally. The usage of these arrays depending upon the need of the user results to reduction time, resources and improve quality of experimentation. The quality of parameters in Taguchi method is determined by S/N ratio. For MRR, larger is better

Table 1 Chemical composition of work piece [11]

Element	Composition
Carbon (C)	0.05%
Manganese (Mn)	0.10%
Silicon (Si)	0.10%
Phosphorous (P)	0.010%
Nickel (N)	0.10%
Sulfur (S)	0.008%
Chromium (Cr)	12.25–13%
Nickel (Ni)	7.5–8%
Molybdenum (Mo)	2–2.5%
Aluminum (Al)	0.90–1.35%
Iron (Fe)	Balance

Table 2 Levels of controlling factors

Factor notation	Factor	Level 1	Level 2	Level 3
IP	Peak current	3	6	9
TON	Pulse on time	20	50	100
TOFF	Pulse off time	10	20	50
TLT	Tool lift time	3	4.5	6

characteristic is considered as more MRR is desirable property of experimentation. Using Minitab-19, L27 orthogonal array was developed using 4 factors and 3 levels by Taguchi method. S/N ratio is a logarithmic function of desired output that serves as an objective function for optimization in Taguchi method. According to this method, optimization signifies best levels of control factors.

MRR is calculated from initial and final weights during experimentation on digital weighing balance of type AY220 with 0.001gm precision. The work piece is machined for 5 min with each set of combination in experimentation table (L27). The machined workpiece is shown in Fig. 1. MRR can be calculated using Eq. (1)

$$MRR = \frac{(W1 - W2)}{T} \tag{1}$$

where $W1$ is weight before machining, $W2$ is weight after machining and T is machining time.

Analysis of Variance (ANOVA): Contribution of each input parameter determines the output response. So ANOVA is performed to predict percentage contribution of each parameter on output response. ANOVA provides statistical data of sum of squares (SS), mean square (MS), Fisher ratio (*F*-value), *P*-value. The sum of squares determines deviation of experimental data from mean of data. *F*-value is the ratio of
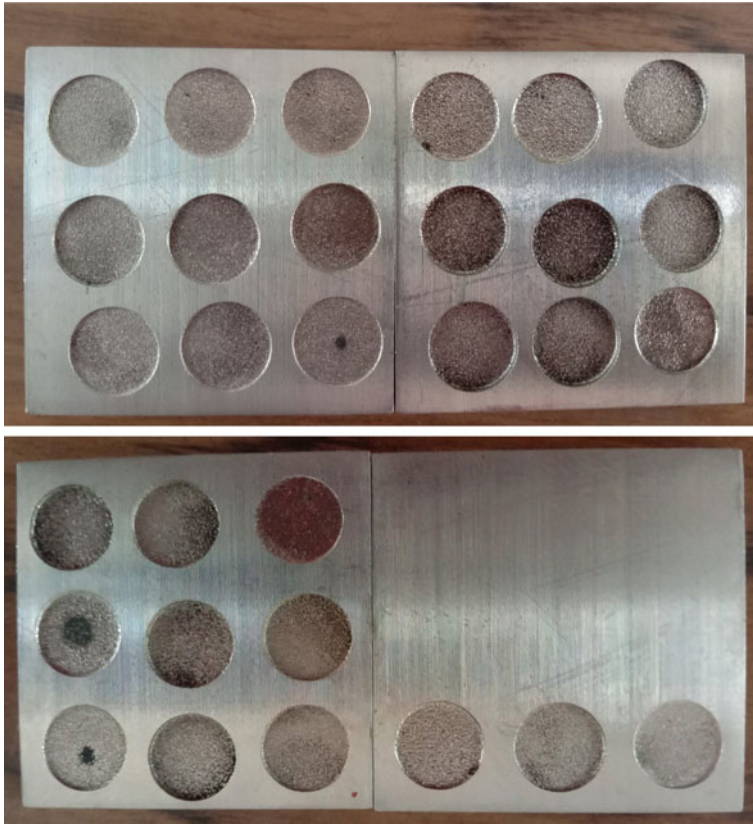
Fig. 1 Work pieces after machining

mean square of the term to mean square of error of a term. The term with more *F*-value effects the output response with small changes only. *P*-value is the probability to get result as least as actual observed values.

Genetic Algorithm: Genetic algorithm is an implicitly triggered evolutionary algorithm that is based on the idea of an evolution tree in a living being with specific inclusions of words like genes, chromosomes, mutations, crossovers, genetic tree, population, and population growth [13]. It is used to create a solid foundation for a search strategy that envelops a vast area to include as many generations and as many mutations as possible in order to reach a viable solution to a problem that requires a lot of manpower and human effort. Initially, a pre-defined set of population values are considered to start the basis of the RNG growth. This population is in itself being implicitly developed by the algorithm when it is executed to maintain a high level of automation and self-reliance. The population generated has its range of values taken from the user with the process parameters as the input values. Once the initial population is generated, the algorithm takes the crossover percentage as well as the

number of iterations to be performed, which is the number of times the generations formed should be crossed over. This ensures the creation of the fittest generation that can be achieved from the original population. Only the fittest values generated are the useful result parameters, and the others can be ignored. As the number of iterations increase, a drastic change can be observed, where the fittest values start becoming increasingly prominent, while the unfit values diminish. With the formation each new unique descendants, the strongest and fittest pairs are mated, to ensure the continuation of their hierarchy. In optimization toolbox of MATLAB, genetic algorithm is performed by increasing number of generations, change of fitness value becomes negligible, and the program terminates. Generally, optimization tool box is used for minimization. For maximization, we used objective function as by suitable transformations.

3 Results and Discussion

The out response, i.e., MRR for all the experiments using different process parameters in the current study is presented in Table 3. From response table of signal to noise ratio, i.e., Table 4, the most contributing factor to determine output response from their rank can be predicted. So IP, TON, TLT, and TOFF effect MRR in the respective decreasing order. IP effects MRR the most, and TOFF effects MRR the least. Regression equation is developed in Minitab for MRR. Regression analysis is used to estimate values of dependent variables from independent variables. This regression equation is used in genetic algorithm as a fitness function.

$$\begin{aligned} MRR = &- 30.3 - 16.83IP + 0.844TON - 0.109TOFF + 26.7TLT \\ &+ 2.184(IP)^2 - 0.00345(TON)^2 + 0.0040(TOFF)^2 \\ &- 3.20(TLT)^2 - 0.0241(IP)(TON) - 0.0386(IP)(TOFF) \\ &+ 0.108(IP)(TLT) - 0.00124(TON)(TOFF) \\ &- 0.0240(TON)(TLT) + 0.0275(TOFF)(TLT) \end{aligned}$$

The main effect plot for SN ratio is shown Fig. 2. It can be observed that increase in IP increases MRR. This phenomenon can be attributed to increase in discharge current leads to more melting and vaporization of work piece [14]. It can also be noted that from the mean effect plot increase in TON improves MRR as spark energy increase leading to more machining of workpiece. Similarly, as the TOFF increases, spark time decreases leading to reduced MRR. Furthermore, it also observed that as the tool lift time (TLT) increases, MRR increases initially then decreases. This phenomenon can be because initially oxygen causes more sparks in machining zone and then further increase in TLT leads to decrease in metal removal rate.

Fitness functions for MRR in MATLAB R2020:

function f = MRR_OPT(r)

Table 3 L27 input parameters and output result MRR

S. No.	IP (A)	TON (μs)	TOFF (μs)	TLT (μs)	MRR (g/min)
1	3	20	10	3	5.54
2	3	20	20	4.5	6.48
3	3	20	50	6	2.28
4	3	50	10	4.5	9.86
5	3	50	20	6	5.92
6	3	50	50	3	11.72
7	3	100	10	6	18.72
8	3	100	20	3	23.66
9	3	100	50	4.5	32.62
10	6	20	10	4.5	17.58
11	6	20	20	6	7.88
12	6	20	50	3	12.12
13	6	50	10	6	9.78
14	6	50	20	3	25.80
15	6	50	50	4.5	22.26
16	6	100	10	3	20.26
17	6	100	20	4.5	19.90
18	6	100	50	6	5.92
19	9	20	10	6	48.67
20	9	20	20	3	44.82
21	9	20	50	4.5	51.02
22	9	50	10	3	66.56
23	9	50	20	4.5	69.20
24	9	50	50	6	59.79
25	9	100	10	4.5	69.78
26	9	100	20	6	50.16
27	9	100	50	3	56.02

Table 4 Response table for signal to noise ratios

Level	IP	TON	TOFF	TLT
1	19.80	22.63	26.50	27.14
2	23.01	26.74	26.14	28.06
3	35.12	28.55	25.28	22.72
Delta	15.32	5.92	1.22	5.33
Rank	1	2	4	3
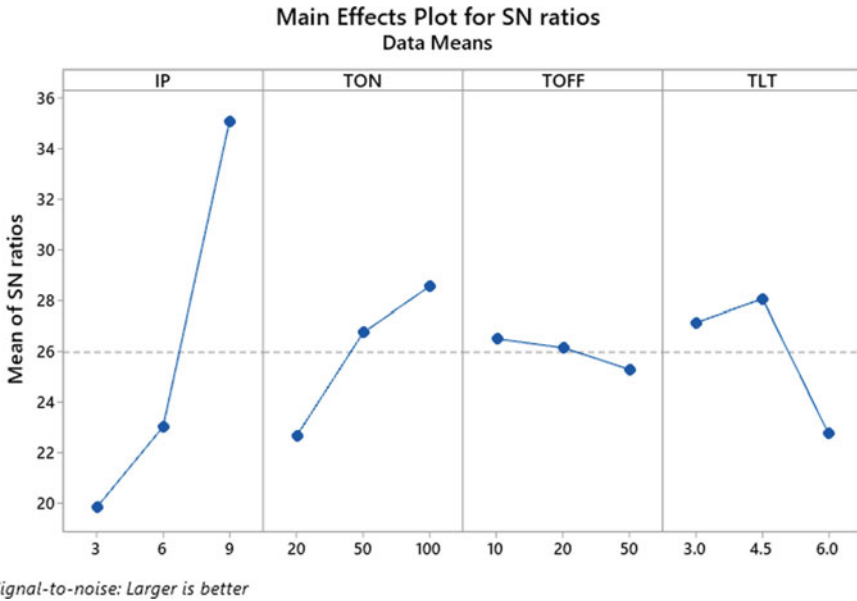
Fig. 2 Main effect plots for SN ratio

$$
\begin{aligned}
f = {} & -(-30.3 - 16.83r_1 + 0.844r_2 - 0.109r_3 + 26.7r_4 \\
& + 2.184r_1^2 - 0.00345r_2^2 + 0.0040r_3^2 - 3.20r_4^2 \\
& - 0.0241r_1r_2 - 0.0386r_1r_3 + 0.108r_1r_4 - 0.00124r_2r_3 \\
& - 0.0240r_2r_4 + 0.0275r_3r_4)
\end{aligned}
$$

The following commands are entered in optimization toolbox as shown in Fig. 3.
Solver: genetic algorithm (GA),
Number of variables: 4.
Variation of factors in the fitness function is as follows:

$$
3 < r_1 < 9
$$
$$
20 < r_2 < 100
$$
$$
10 < r_3 < 50
$$
$$
3 < r_4 < 6.
$$

Setting of optimal parameters causes efficient machining. Genetic algorithm provides more accurate to obtain result of objective function, i.e., MRR. Taguchi provides accurate parameter values of IP, TON, TOFF, and TLT to optimize MRR. Comparison of Taguchi and genetic algorithm optimization is given in Table 5. Genetic algorithm uses a wide range of parameter combinations. Taguchi is single optimized, and it is robust optimization technique. Optimization assists to know the
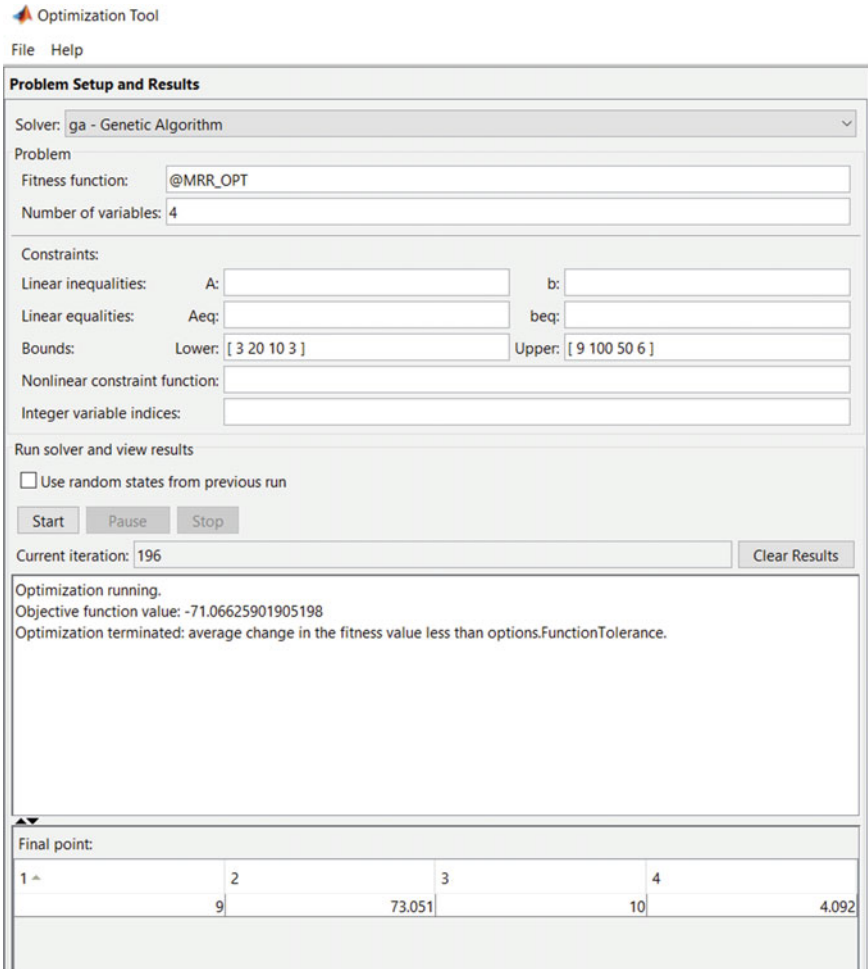
Fig. 3 Genetic algorithm toolbox in MATLAB

best values without manual experimentations that save time and cost of production. Further study of various other parameters of this material, i.e., 13-8 PH steel can be carried out to know other response parameters.

Table 5 Comparison of Taguchi and genetic algorithm optimization

Parameter	Taguchi method	Genetic algorithm
Levels (IP, TON, TOFF, TLT)	9, 100, 10, 4.5	9, 73.051, 10, 4.092
MRR (g/min)	69.78	71.066

4 Conclusions

Electric discharge machining of 13/8 PH steel was successfully carried out, and enhanced MRR was achieved with genetic algorithm. The following conclusions were drawn from the present study.

- Peak current is the most significant parameter affecting the MRR, and TOFF is least significant parameter affecting the MRR.
- As input parameters such as peak current, TON, and TLT were increased, the MRR was also increased.
- Metal removal rate was reduced with increase in TOFF.
- The highest MRR of 71.066 g/min was achieved when genetic algorithm optimization technique was used, and 69.2433 g/min MRR was achieved when Taguchi technique was used.
- The optimal process combination of parameters for Taguchi technique was found to be 9 IP, 100 TON, 10 TOFF, 4.5 TLT whereas for genetic algorithm was 9 IP, 73.051 TON, 10 TOFF, and 4.092 TLT.

References

1. Kumar, S., Varol, T., Canakci, A., Kumaran, T., Uthayakumar, M.: A review on the performance of the materials by surface modification through EDM. Int. J. Lightweight Mater. Manuf. **4**(1), 127–144 (2021). https://doi.org/10.1016/j.ijlmm.2020.08.002
2. Guo, Z., Sha, W., Vaumousse, D.: Microstructural evolution in a PH13-8 stainless steel after ageing. Acta Mater. **51**(1), 101–116 (2003). https://doi.org/10.1016/s1359-6454(02)00353-1
3. Kao, J., Tsao, C., Wang, S., Hsu, C.: Optimization of the EDM parameters on machining Ti–6Al–4V with multiple quality characteristics. Int. J. Adv. Manuf. Technol. **47**(1–4), 395–402 (2009). https://doi.org/10.1007/s00170-009-2208-3
4. Straka, Ľ., Hašová, S.: Optimization of material removal rate and tool wear rate of Cu electrode in die-sinking EDM of tool steel. Int. J. Adv. Manuf. Technol. **97**(5–8), 2647–2654 (2018). https://doi.org/10.1007/s00170-018-2150-3
5. Senthil Kumar, R., Suresh, P.: Experimental study on electrical discharge machining of Inconel using RSM and NSGA optimization technique. J. Braz. Soc. Mech. Sci. Eng. **41**(1) (2018). https://doi.org/10.1007/s40430-018-1526-5
6. Laxman, J., Guru Raj, K.: Mathematical modeling and analysis of EDM process parameters based on Taguchi design of experiments. J. Phys.: Conf. Ser. **662**(1), 012025 (2015)
7. Chandramouli, S., Eswaraiah, K.: Experimental investigation of EDM process parameters in machining of 17-4 PH Steel using Taguchi method. Mater. Today: Proc. **5**(2), 5058–5067 (2018)
8. Rajmohan, T., Prabhu, R., Subba Rao, R., Palanikumar, K.: Optimization of machining parameters in electrical discharge machining (EDM) of 304 stainless steel. Procedia Eng. **3**(1), 1030–1036 (2012)
9. Rajesh, R., Anand, M.: The optimization of the electro-discharge machining process using response surface methodology and genetic algorithms. Procedia Eng. **38**(1), 3941–3950 (2012). https://doi.org/10.1016/j.proeng.2012.06.451
10. Varol Ozkavak, H., Sofu, M., Duman, B., Bacak, S.: Estimating surface roughness for different EDM processing parameters on Inconel 718 using GEP and ANN. CIRP J. Manuf. Sci. Technol. **33**(1) 306–314 (2021). https://doi.org/10.1016/j.cirpj.2021.04.007

11. https://www.twmetals.com/products/bars/stainless-steel/13-8-ph.html
12. Taguchi, G.: Quality engineering (Taguchi methods) for the development of electronic circuit technology. IEEE Trans. Reliab. **44**(2), 225–229 (1995). https://doi.org/10.1109/24.387375
13. Chatterjee, S., Laudato, M., Lynch, L.: Genetic algorithms and their statistical applications: an introduction. Comput. Stat. Data Anal. **22**(6), 633–651 (1996). https://doi.org/10.1016/0167-9473(96)00011-4
14. Arooj, S., Shah, M., Sadiq, S., Jaffery, S., Khushnood, S.: Effect of current in the EDM machining of aluminum 6061 T6 and its effect on the surface morphology. Arab. J. Sci. Eng. **39**(5), 4187–4199 (2014). https://doi.org/10.1007/s13369-014-1020-z

A Review of Routing Algorithms for Intelligent Route Planning and Path Optimization in Road Navigation

Noopur Tyagi, Jaiteg Singh, and Saravjeet Singh

1 Introduction

In the area of road navigation, finding a least-cost (time and length) path is an essential research topic. We prefer to use a navigation system even if we know the path. Digital navigation has revolutionized the way of path planning. GPS system is used to make it possible for outdoor navigation, but satellite signals are too weak to get inside constructions. Indoor routing needs a mobile base station and Wi-Fi. Signal breakups due to the high concentration of users could be responsible for the failure of these approaches. Due to technical issues like attenuation, signal loss, electronic equipment, navigation system requires more effort in indoor path planning [1]. The bio-inspired algorithm works fine for dynamically changing environments. These algorithms help to find out the effective and efficient path. The purpose of this study is to discover an efficient path having the least cost, time, and length. We have reviewed the best bio-inspired algorithms for the shortest pathfinding.

This systematic review paper provides insight into the route planning algorithms that have been developed in the last few years (2015–2021) as described in Fig. 1. The review began with 146 potentially eligible papers, eventually resulting in the full inclusion of 35 papers. A total of 35 studies were considered in this review, and most of the cited papers are of recent years. To the best of our knowledge, this is the only paper that discussed recently used bio-inspired algorithms for path routing and

N. Tyagi (✉) · J. Singh · S. Singh
Chitkara University Institute of Engineering and Technology, Chitkara University, Punjab, India
e-mail: noopur.tyagi@chitkara.edu.in

J. Singh
e-mail: jaiteg.singh@chitkara.edu.in

S. Singh
e-mail: saravjeet.singh@chitkara.edu.in
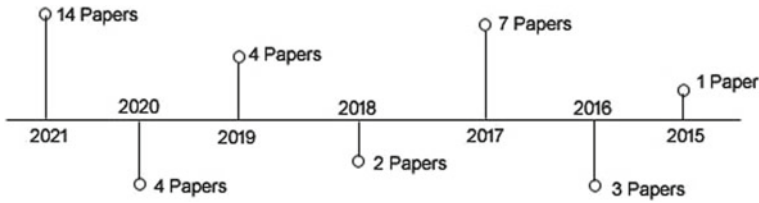
Fig. 1 Year-wise citation including in this manuscript

path optimization in road navigation. This study also highlighted the technologies and purpose of using the algorithms in both environments (indoor and outdoor).

Few scholars have deeply researched the field and produced shortest path problem (SPP) algorithms. There are various algorithms used for finding optimal path such as Dijkstra, A*, hybrid algorithms, ant colony algorithm, and particle swarm optimization. The first contribution in this paper is about the various algorithms for intelligent route planning. After the introduction, Sect. 2 highlights the area of related work. Section 3 covers the bio-inspired routing algorithms with case studies, and Sect. 4 gives the concluding remark of this paper.

1.1 Classification of Path Planning

Path Planning: It is one of the crucial parts of the field of navigation. By proposing correct path planning, problems in various fields have been solved. It can be applied widely in unknown environments by applying the proper algorithm. Every decision in the path planning algorithm is selected according to the information available. To reach a particular objective from a simple trajectory to guide in an unknown environment, path planning has been applied in various fields. Based on the environment, algorithms, completeness, path planning can be classified as shown in Fig. 2.

Optimal algorithms guarantee to provide the optimal solution through exploration of a complete set of available solutions, whereas heuristic algorithms explore the available solutions and provide the approximately best solution that is close to the optimal solution. Hybrid approach-based algorithms combine the positive points of both approaches.

2 Related Studies

Over the years, researchers have suggested several types of routing algorithms for path planning. To simplify the problems associated with path planning, this article includes the recent work done in this area. The basic objective of this section is to look at the research activities in the field of road navigation for path optimization.
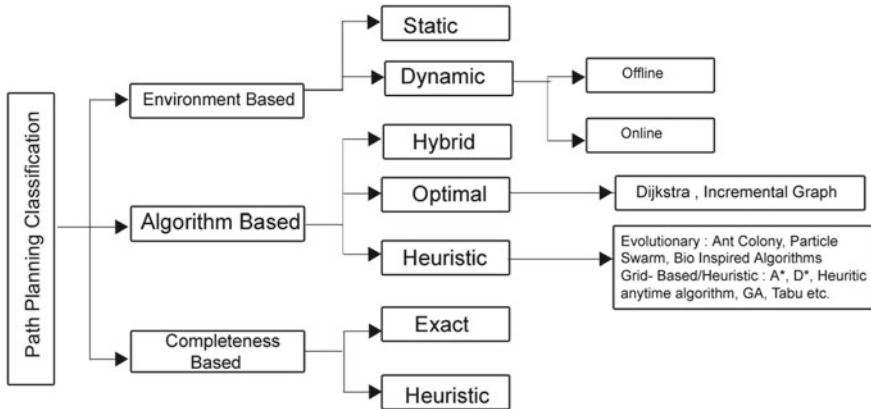
Fig. 2 Classification of path planning

Liang et al. proposed an enriched ant colony optimization algorithm (ACOCA) for tourism route planning based on a context-aware mechanism [2]. It was observed that ACOCA has better optimization and convergence time as compared to the ant colony algorithm (ACO). ACO is a kind of swarm intelligent algorithm. Similarly, Miao et al. proposed an enhancement in adaptive ant colony optimization (IAACO) to overcome the limitations of ant colony algorithm (ACO) in indoor path planning for mobile robots [3]. IAACO also has better convergence speed and a stronger ability to find the optimization solution for path planning. Likewise, Wu et al. proposed a hybrid ant colony (HACO) algorithm to reduce the transportation distance and cost and solve the vehicle routing problem with a time window [4].

Yan et al. presented indoor traveling sales problem (ITSPs) path planning [5]. Dijkstra and branch and bound algorithm were used as general solutions to ISTP path and found that this algorithm can compute the shortest path. Asaduzzaman et al. [6] proposed an effective algorithm for multi-destination shortest path problem (EAMDSP). It was implemented in indoor applications and found more efficient for multi-destination search.

Gao and Lu [7] presented an improved particle swarm optimization (PSO) algorithm to improve the convergence speed and optimization speed. It reduced the complexity by adjusting the inertia weight in the iterative process of PSO. Equally, Jiang et al. proposed a hybrid ant colony particle swarm optimization by integrating particle swarm optimization into the ant colony algorithm to establish multi-objective vehicle logistics path optimization [8]. Krell et al. [9] presented particle swarm optimization (PSO) to develop autonomous robot navigation (ARN) that can navigate in an unfamiliar surroundings. Table 1 describes the literature we have studied.

Table 1 Tabular form of literature studied

Author	Year	Environment	Proposed algorithm	Major ground	References
Liang et al.	2021	Outdoor	ACOCA	Route planning	[2]
Miao et al.	2021	Indoor	IAACO	Mobile robot path planning	[3]
Wu et al.	2021	Outdoor	HACO	Vehicle routing problem with time window	[4]
Yan et al.	2021	Indoor	Dijkstra and Branch and bound	To solve ISTP path planning	[5]
Asaduzzaman et al.	2021	Indoor	EAMDSP	Multi-destination search	[6]
Gao and Lu	2021	Outdoor	Improved PSO	Logistic route optimization	[7]
Jiang et al.	2021	Outdoor	Hybrid any colony particle swarm optimization	Multi-objective vehicle logistics path optimization	[8]
Krell et al.	2019	Unknown	PSO	ARN	[9]

2.1 Challenges and Research Gap

From the above literature studies, we have provided the vision on how to improve the efficiency in road navigation in this section. Several challenges and gaps are mentioned below:

- Firstly, incorporate the input information such as road information, destination information, and mobile information (fuel, vehicle related conditions, etc.) to decide the algorithm.
- Data availability and completeness of data.
- Lack of GPS signals.
- Vulnerability to GPS signal and spoofing attacks.
- Exact address matching for both indoor and outdoor environment is a challenge.
- Deployment of nodes is still a challenge to find initial point in route discovery. It may lead to inaccurate routing.
- Designing a protocol is a challenge because it is assumed that sensors with GOS and other techniques are already given.

3 Bio-inspired Algorithm for Shortest Path

A number of algorithms are utilized in generating the shortest path; among these, particle swarm optimization (PSO), ant colony optimization algorithm (ACO), genetic algorithm (GA), A*, and Dijkstra are discussed below:

Table 2 Fusion of PSO with different algorithms for indoor positioning

Author (year)	Year	Algorithms	Technology	Purpose	References
Wang et al.	2016	Artificial neural network + PSO algorithm	RFID	Indoor positioning	[15]
Cai et al.	2017	Simulated annealing + PSO	Visible light communication (LED)	Indoor high-precision 3D positioning system	[16]
Chen and Zou	2017	Kalman filter + PSO algorithm	Wi-Fi	Indoor positioning	[14]
Guo et al.	2019	KNN algorithm + PSO algorithm	Zigbee	Indoor positioning	[13]

Particle Swarm Optimization (PSO): Particle swarm optimization is an evolutionary metaheuristic algorithm proposed by Kennedy and Eberhart in 1995 [10]. To solve the intelligent vehicle navigation problem, PSO is the best solution as it is easy to describe and has a fast converging speed [11]. It has been widely used in various areas such as neural network training, dynamic environment optimizations, and many applications. PSO is based on an intelligent swarm algorithm that simulates the activities of organisms by using particle movement in the swarm [12]. To start the optimization, firstly, a random particle is initialized and then determines the optimum solution on the basis of the fitness function. Guo et al. proposed a PSO algorithm to attain more accurate model parameter estimation in indoor positioning systems because it is difficult to estimate the parameters of the path loss model by ordinary methods [13]. Similarly, Chen and Zou used the PSO algorithm with Kalman filter to get better results of indoor positioning based on Wi-Fi and reduce positioning error [14]. Integration of particle swarm optimization with algorithms for indoor positioning system is described in Table 2. Depicts the fusion of PSO with different algorithms for indoor positioning.

Ant Colony (ACO) Algorithm: It is one of the evolutionary methods inspired by the behavior of "simulated ants" to solve the path planning problems [17]. It is similar to fingerprint matching, as fingerprint matching compares the geomagnetic attributes with the database to obtain an optimal solution similarly ant colony algorithm finds that the current attribute belongs to a certain position or not with the help of pheromones (a substance left by ants). It doesn't need any memory to store the nodes. ACO algorithm achieves a better path very quickly in an indoor environment. Wang et al. proposed a 3D high-precision indoor positioning based on visible light communication using an ant colony algorithm to solve optimization problems [18]. Moreover, Yang et al. improve the result for optimal spatial allocation by using multiple ant colony optimization algorithm (MACO) [19]. The fusion of ACO with various algorithms for indoor positioning systems is described in Table 3 represents the variation of the ACO algorithm for various purposes.

Table 3 Variation of ACO algorithm for different purposes

Author (year)	Year	Algorithms	Purpose	References
Alani et al.	2020	ACO + A*	Single-source shortest path	[20]
Gao et al.	2020	Enhanced heuristic ant colony optimization	Mobile robot path planning	[21]
Husain et al.	2018	Inverted ant colony optimization	For search and rescue	[22]

Genetic Algorithm (GA): It is an evolutionary algorithm that is based on the natural selection of populations, repeating the evolutionary process, and finding the optimal solution [23]. To find a better solution for single point-based magnetic positioning (SBMP), Sun at el. used deep learning (DL), extreme learning machine (ELM). Along this, GA is used for initial parameters to address the robustness problem [24]. Similarly, for Wi-Fi and cellular network, a hybrid indoor positioning algorithm was addressed by Guo et al. [25]. It consists of principal component analysis and interpolation method for fingerprint database construction in offline mode. Adaptive genetic algorithm (AGA) to optimize backpropagation (BP) neural network positioning algorithm Gozuacik et al. planned a route to prevent loss of time and determine the location by using visible light communication (VLC). To find the most suitable route, GA was used in a closed area [26]. Table 4 shows the purpose and algorithm fused with GA for the indoor positioning system.

Dijkstra: It is a classic algorithm to find out the shortest path between two points. Due to its optimization capabilities, it is mainly used for path routing. AbuSalim et al. compared the Dijkstra with the Bellman–Ford algorithm on the basis of complexity and performance to discover the shortest path in various applications [27]. Ginting et al. solve the travel salesperson problem by using the Dijkstra algorithm, and clustering value is applied in priority values [28]. Asaduzzaman et al. modified the algorithm to multi-destination of Dijkstra algorithm for an indoor environment. Compared

Table 4 Fusion of GA with various routing algorithms

Author	Year	Algorithms	Proposed method	Purpose	References
Sun et al.	2021	GA + DL + ELM	SBMP	Sequence-based geomagnetic positioning technique	[24]
Guo et al.	2021	BP neural network + AGA	Hybrid indoor positioning	To reduce the cost time and for indoor positioning	[25]
Gozuacik et al.	2021	VLC + GA		Route planning and location determination	[26]

Table 5 Hybridization of Dijkstra algorithm with several routing algorithms

Author	Year	Algorithm	Purpose	Results	References
Kasantikul et al.	2015	Dijkstra + k-nearest neigbor (KNN) + particle filter	Route the destination	Increase the accuracy and robustness	[29]
Teh et al.	2021	Extended Dijkstra algorithm	Vision-based patrol robot-surveillance purpose	Capable to complete multiple cycles of testing with positive results	[30]
Zheng looi et al.	2021	A*,Dijkstra, dynamic window approach, time elastic band algorithms	Robot simulation and real environment	Achieve the required performance for the application and avoid the dynamic obstacles	[31]

the single-source destination to multi-mode destinations of Dijkstra algorithm and found the increase in efficiency by using multi-mode destination [6]. Table 5 describes the hybridization of the Dijkstra algorithm with several routing algorithms for various purposes.

A*: A* algorithm is a global planner and a variant of Dijkstra. It calculates the estimation distance by adding a heuristic function. As A* is fast, so it reduces the computational time. Alani et al. proposed a technique of hybrid A* and ant colony algorithm (ACO) to generate the shortest path [20]. Mujtaba and Singh introduced a new method of safe and shortest navigation by using a modified A* algorithm. This method reduced the probability of collisions with robots and obstacles [32]. Similarly, Guruji et al. proposed an A* algorithm with modifications for reducing the processing time. For this, he considered several cases and exhibit a 95% maximum [33]. Table 6 shows that different technologies can be used to search the shortest path by using the A* algorithm.

4 Performance and Analyzing of Path Planning

When deciding the algorithm for deciding the path, the selection of path parameter is the prime task. A few parameters are as follows:

No. of Nodes and Area: Understandably a "one size fits all" technique, algorithm, the method is a problematic decision because there is diversification in environments as shown in Fig. 3. Two different paths reach the destination node.

Table 6 A* algorithm for shortest path in different environments

Author	Year	Algorithms	Purpose	Technology	References
Guruji et al.	2016	Modified A* algorithm	To calculate the path length and processing time of robot movement	MATLAB simulation	[33]
Niu et al.	2021	Improved A* algorithm	Path planning for intelligent driving	Dynamic simulation environment	
Rachmawati and Gustin	2020	Dijkstra and A* algorithm	Shortest path/routing	Pycharm	[34]

Fig. 3 Graphical representation of parameter variations

Angel of Arrival (AOA): Principle of measuring angular direction from a locator placed at an unknown location.

Time of Arrival (TOA): It is a ranging technique based on knowing the exact time of the signal transmission and the arrival of the signal. By knowing these two points and the speed of light, distance from the reference point can be calculated.

Accuracy: It is one of the important parameters of navigation. Estimated position and actual position differences can decide the accuracy level.

5   Conclusion and Future Scope

In this article, various routing algorithms for intelligent path routing to find out the optimized path have been reviewed. The most significant bio-inspired algorithms for the shortest path have been studied. The use of the A* algorithm and the Dijkstra algorithm both give the same output in a regional scale map, but on a large scale, A*

will provide a faster solution than Dijkstra. Similarly, for the distance optimization problems, ACO provides a better result than PSO. Although PSO and GA both are evolutionary algorithms, still they do have disadvantages in that the usages are limited to a few problems. To overcome these problems, we believe that fusion algorithms and revised routing algorithms will improve the overall performance. Hybrid algorithms play a significant role in road navigation. In the future, on the basis of the research in this article, we will try to extend the research with a fusion of algorithms to get an optimized path. Precision and accuracy can be improved by the integration of algorithms.

References

1. Brena, R.F., García-Vázquez, J.P., Galván-Tejada, C.E., Muñoz-Rodriguez, D., VargasRosales, C., Fangmeyer, J.: Evolution of indoor positioning technologies: a survey. J. Sens. **2017** (2017)
2. Liang, S., Jiao, T., Du, W., Qu, S.: An improved ant colony optimization algorithm based on context for tourism route planning. PLoS One **16**(9) (2021)
3. Miao, C., Chen, G., Yan, C., Wu, Y.: Path planning optimization of indoor mobile robot based on adaptive ant colony algorithm. Comput. Ind. Eng. **156**, 107230 (2021)
4. Wu, H., Gao, Y., Wang, W., Zhang, Z.: A hybrid ant colony algorithm based on multiple strategies for the vehicle routing problem with time windows. Complex Intell. Syst. **2021**, 1–18 (2021)
5. Yan, J., et al.: Indoor traveling salesman problem (ITSP) path planning. ISPRS Int. J. Geo-Information **10**(9), 616 (2021)
6. Asaduzzaman, M., et al.: An efficient shortest path algorithm: multi-destinations in an indoor environment. Symmetry **13**(3), 421 (2021). https://doi.org/10.3390/sym13030421
7. Gao, Z., Lu, H.: Logistics route optimization based on improved particle swarm optimization. J. Phys. Conf. Ser. **1995**(1), 012044 (2021)
8. Jiang, J., Yu, N., Ye, J., Bai, W.: Vehicle logistics path optimization based on ant colony and particle hybrid algorithm. J. Phys. Conf. Ser. **1865**(4), 042086 (2021)
9. Krell, E., Sheta, A., Prassanth, A., Balasubramanian, R., King, S.A.: Collision-free autonomous robot navigation in unknown environments utilizing PSO for path planning. JAISCR **9**(4), 267 (2019)
10. Kennedy, J., Eberhart, R., bls gov: Particle Swarm Optimization
11. Han, G., Fu, W., Wang, W.: The study of intelligent vehicle navigation path based on behavior coordination of particle swarm. Comput. Intell. Neurosci. **2016** (2016)
12. Marinakis, Y., Migdalas, A., Sifaleras, A.: A hybrid Particle Swarm Optimization—variable neighborhood search algorithm for constrained shortest path problems. Eur. J. Oper. Res. **261**(3), 819–834 (2017)
13. Guo, H., Li, H., Xiong, J., Yu, M.: Indoor positioning system based on particle swarm optimization algorithm. Measurement **134**, 908–913 (2019)
14. Chen, X., Zou, S.: Improved Wi-Fi indoor positioning based on particle swarm optimization. IEEE Sens. J. **17**(21), 7143–7148 (2017)
15. Wang, Z., Shi, Wu, F., Zhang, J.: An RFID indoor positioning system by using Particle Swarm Optimization-based Artificial Neural Network. In: ICALIP 2016—2016 Int. Conf. Audio, Lang. Image Process.—Proc., pp. 738–742 (2017)
16. Cai, Y., Guan, W., Wu, Y., Xie, C., Chen, Y., Fang, L.: Indoor high precision three-dimensional positioning system based on visible light communication using particle swarm optimization. IEEE Photonics J. **9**(6) (2017)
17. Guo, Y.: Application of improved ant colony algorithm in indoor location. In: 2019 IEEE 5th Int. Conf. Comput. Commun. ICCC 2019, pp. 1935–1939 (2019)

18. Wang, P.F., Guan, W.P., Wen, S.S., Sun, M., Peng, Q., Wu, Y.X.: A 3-D high-precision indoor positioning strategy using the ant colony optimization algorithm based on visible light communication. Front. Res. Innov. Optoelectron. Technol. Ind. 361–370 (2018)
19. Yang, L., et al.: A multiple ant colony optimization algorithm for indoor room optimal spatial allocation. ISPRS Int. J. Geo-Information **6**(6), 161 (2017)
20. Alani, S., Hamdi, M.M., Baseel, A., Rashid, S.A.: A hybrid technique for single-source shortest path-based on A* algorithm and ant colony optimization conditional privacy-preserving authentication scheme in VANET View project UWB antenna for early breast cancer detection View project. IAES Int. J. Artif. Intell. **9**(2), 256–263 (2020)
21. Gao, W., Tang, Q., Ye, B., Yang, Y., Yao, J.: An enhanced heuristic ant colony optimization for mobile robot path planning. Soft Comput. **24**(8), 6139–6150 (2020)
22. Husain, Z., Ruta, D., Sare, F., Al-Hammadi, Y., Isakovic, A.F.: Inverted ant colony optimization for search and rescue in an unknown maze-like indoor environment. In: GECCO 2018 Companion—Proc. 2018 Genet. Evol. Comput. Conf. Companion, pp. 89–90 (2018)
23. Katoch, S., Chauhan, S.S., Kumar, V.: A review on genetic algorithm: past, present, and future. Multimed. Tools Appl. **80**(5) (2021)
24. Sun, M., Wang, Y., Xu, S., Yang, H., Zhang, K.: Indoor geomagnetic positioning using the enhanced genetic algorithm-based extreme learning machine. IEEE Trans. Instrum. Meas. **70** (2021)
25. Guo, T., Chai, M., Xiao, J., Li, C.: A hybrid indoor positioning algorithm for cellular and Wi-Fi networks. Arab. J. Sci. Eng. **2021**, 1–15 (2021)
26. Makalesi, A., Gözüaçık, E., Altıok, M., Gökrem, L.: Indoor navigation with visible light communication using genetic algorithm. Eur. J. Sci. Technol. **26**(26), 185–190 (2021)
27. Abusalim, S.W.G., Ibrahim, R., Saringat, M.Z., Jamel, S.: Comparative Analysis between Dijkstra and Bellman-Ford Algorithms in Shortest Path Optimization, vol. 917, pp. 1–12 (2020)
28. Ginting, H.N., Osmond, A.B., Aditsania, A.: Item Delivery Simulation Using Dijkstra Algorithm for Solving Traveling Salesman Problem, vol. 1201, pp. 1–10. Icera (2019)
29. Kasantikul, K., Xiu, C., Yang, D., Yang, M.: An enhanced technique for indoor navigation system based on WIFI-RSSI. In: International Conference on Ubiquitous Future Networks, ICUFN, Aug 2015, pp. 513–518 (2015)
30. Teh, C.K., Kit Wong, W., Min, T.S.: Extended Dijkstra algorithm in path planning for vision based patrol robot. In: Proceedings of the 8th International Conference on Computer and Communication Engineering, ICCCE 2021, Jun 2021, pp. 184–189 (2021)
31. Looi, C.Z., Ng, D.W.K.: A study on the effect of parameters for ROS motion planer and navigation system for indoor robot. Int. J. Electr. Comput. Eng. Res. **1**(1), 29–36 (2021)
32. Mujtaba, H., Singh, G.: Safe navigation of mobile robot using A* algorithm. Int. J. Appl. Eng. Res. (2021). ripublication.com. Accessed Aug 28
33. Guruji, A., Agarwal, H.: Time-efficient A* algorithm for robot path planning. Procedia Technol. (2021). Accessed Aug 28
34. Rachmawati, D., Gustin, L.: Analysis of Dijkstra's algorithm and A∗ algorithm in shortest path problem. J. Phys. Conf. Ser. **1566**(1) (2020)
35. Niu, C., Li, A., Huang, X., Li, W., Xu, C.: Research on global dynamic path planning method based on improved A∗ algorithm. Math. Probl. Eng. **2021** (2021)

Crack Detection in a Cantilever Composite Beam Using Fuzzy Logic System with Regression Analysis

Monalisa Das, Sasmita Sahu, and Dayal R. Parhi

1 Introduction

From the past several years, advanced composite material has gained an active research area in various applications such as sports, automobile, marine, aerospace, and military sector. These materials are dominating other renowned conventional materials used prier for these above-mentioned applications because of their superior properties. Excellent strength-to-wait ratio at a reasonable cost makes the composites a big replacement for conventional metallic materials. Other distinctive properties of composite materials such as corrosion resistance, enhanced fatigue resilience, excellent surface profile, and tailored performance caused hasty increase in the applications of composite materials [1].

Nowadays, applications of hybrid composites in different sectors are steadily increasing. Hybrid composites are formed by combine mixing of two or more-reinforced fibers having different properties in a resin. These composites due to hybridization are owning combined advantages of the individual components and concurrently justifying their less desirable qualities [2, 3]. Synthetic fibers such as aramid fibers and carbon fibers have played a primary role in the production of high-performance composites for a large variety of structural applications. Aramid fibers used for making composites which are taken as material for making sports accessories, helicopter blades, naval vessels, and especially ballistic applications such as helmets, combat shields, and armored vehicles [4]. From many researches, it has been

M. Das · S. Sahu (✉)
School of Mechanical Engineering, KIIT, Deemed to Be University, Bhubaneswar, Odisha 751024, India
e-mail: sasmita.sahufme@kiit.ac.in

D. R. Parhi
Department of Mechanical Engineering, NIT Rourkela, Rourkela, Odisha 769008, India

observed that aramid fiber-reinforced polymer composites exhibit amazing mechanical characteristics, including high-strength-to-weight ratio, superb abrasion resistance, excellent impact resistance, and high-energy absorption capacity. For above reasons, these composites have been greatly preferred for structures or machine parts work in high-impact loading environments [5]. Carbon fiber can have a quality to arrest crack propagation in composite structures. They have excellent tensile properties, large thermal and chemical stabilities, excellent creep resistance, and thermal and electrical conductivities. Carbon fiber-reinforced in polymer (CFRP) composites is mostly favored for structural applications as they are capable of bearing heavy loads and more durable [6]. In recent years, due to these reasons, CFRP composites are gaining demand in various industries including aerospace, medical, military, sporting goods, lightweight cylinders and pressure vessels, automotive parts, turbine blades, civil structures etc., [7–9]. From the above, it is found that hybrid composites with aramid fiber or carbon fiber are mostly suitable for structural parts of aerospace, marine, and automobiles. The hybrid composite formed by combination reinforcement of carbon fiber and aramid fiber with polymer provides superior performance that the composites reinforced with either carbon fiber or aramid fiber (Kevlar). Hybridization of brittle carbon fibers with ductile Kevlar fiber remarkably promoted impact strength, energy absorption property, shear strength, and damage tolerance of carbon-Kevlar epoxy composite in compared to the corresponding CFRP and KFRP composites [10]. In this work for the damage analysis, a cracked carbon/Kevlar-reinforced epoxy hybrid composite has been considered.

Although having large advantages, composites are prone to significant damage in their service life. Presence of damage leads alteration in dynamic properties of composite. When such damage in structure touches a perceptible level, a serious accident will be happened. Damage in many forms presents in a composite such as matrix cracking and delamination. Among those damages, crack type damage is the most important damage for composite structural elements. To avoid catastrophic failure, it is required to identify the incipient damage at very early stage and continuous monitoring of its growth in composite parts and structures. For that automatic damage inspections are made to identify the damage of in-service structures. Therefore, now, structural health monitoring is a great challenge both structural and aerospace industries [11, 12]. For structural damage detection, there are so many unconventional methods are available. But these methods are not more efficient because they are expensive and time consuming. Nowadays, artificial intelligence and soft computing methods are efficiently replacing unconventional methods in various industries. In recent years, vibration analysis method is mostly preferred for damage detection in machine components and structures [13–15]. It has been noticed that even if a very small hairline crack can make a catastrophic failure. The presence of minute damage in composite structures used for aerospace leads to hazardous human causality. So, the crack identification and localization in aerospace are being a vital subject for aerospace is being a vital subject for aerospace researcher. For those above reasons, regular and immediate health monitoring of materials for aerospace applications is necessary [16, 17].

In this current research work, a novel structural health monitoring technique for fault identification has been suggested. A fuzzy logic system (FLS) has been constructed here. In big civil structures like bridges, buildings and in aircraft, spacecraft structures exact damage location identification, and prediction of its intensity is really difficult [18–20]. But existence of a minute hairline crack in these structures may cause a very serious failure, which could be harmful to human being. As so many research works have been done on FLS for crack identification, through the inclusive literature review, it has been noticed that FLS has some loopholes to be applied. Though most of the data from the field are given by a person where there is a chance that the data mining process may not be proper. It is known to all that due to the data mining process, there may be some un-clarified data, which may create problem to get a proper solution. To minimize the error data, one data mining method like regression analysis (RA) has been integrated to reduce the percentage of error [21–23].

In this work, to detect crack location and size of a cantilever composite beam, a distinctive NDT method is developed. This technique is based on fuzzy logic system with regression analysis. At the starting of the process, first, finite element analysis (FEA) has been conducted. Data are collected from this FEA. As it is shown that, initiation of crack in materials leads to alteration in its physical properties such as stiffness. Alteration in stiffness of material leads to change in dynamic properties such as the natural frequencies and the mode shapes. Here to keep this suggested methodology simple, only the natural frequencies of the first three mode shapes are taken as input variables, and the damage depth and damage location are taken as the output variables to this system. Collecting data from the FEA a data pool is generated. After that the values of all the input and output parameters are being normalized by dividing with the respective values of the undamaged composite beam.

2 Finite Element Analysis of Composite Cantilever Beam With an Edge Crack

In this work, finite element analysis (FEA) is applied for the vibration analysis of a composite cantilever cracked beam. In vibration analysis of this beam, natural frequency of considered damaged composite beam has been extracted. For this analysis, a carbon/Kevlar-reinforced hybrid composite cantilever beam element with an edge crack has considered. This cantilever beam is subjected to generalized loading condition as shown in Fig. 1a and its cross-sectional view is in Fig. 1b.

The dimensions of crack composite beam considered for this present work are mentioned as below.

Length of composite beam $(L) = 800$ mm.
Width of composite beam $(W) = 40$ mm.
Height of composite beam $(H) = 6$ mm.
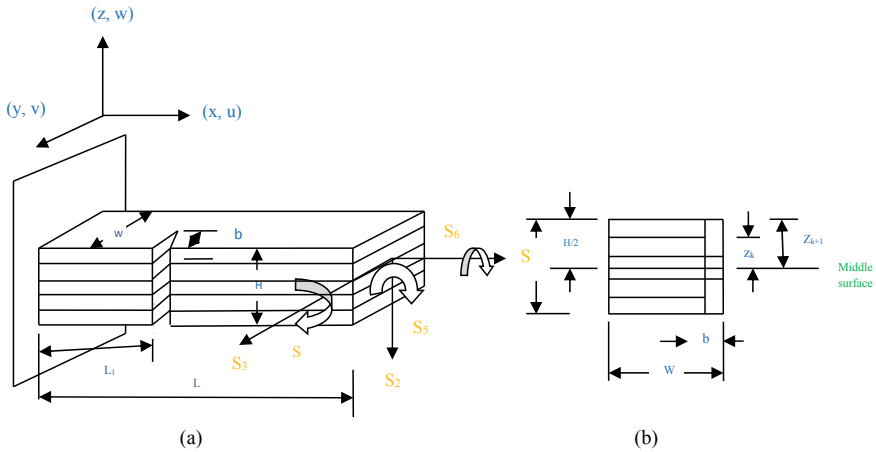
Fig.1 **a** Representation of force loading system on a composite cantilever beam with an edge crack, **b** cross-sectional view of beam

When a crack is developed in beam like elastic elements, their stiffness decreases lead to degradation of structure. It introduces local flexibility in the structure, whose effect is alteration in vibration characteristics such as natural frequency and mode shape. Damage detection and its severity calculation in a structural element will be done by finding its stiffness. By finding the stiffness of the damaged (like crack) beam, its natural frequency and mode shape will be calculated. To find stiffness matrix for cracked composite beam, first flexibility matrix is extracted. Then, inverse of flexibility matrix is taken. The process for finding out stiffness matrix and natural frequency for beam is expressed below.

The additional elastic strain energy of the beam due to existence of crack is expressed as

$$U_c^e = \int_A E(a)\,dA \tag{1}$$

In the above equation, '$E(a)$' represents function of strain energy release rate, and 'A' represents cross-sectional area of rectangular cracked composite beam.

The function of strain energy release rate for laminated composite beam with a crack, i.e., $E(a)$ can be expressed as

$$E(a) = D_1 \left\{ \sum_{q=1}^{6} K_{Iq} \right\}^2 + D_2 \left\{ \sum_{q=2}^{6} K_{IIq} \right\}^2$$

$$+ D_3 \left\{ \sum_{q=2}^{6} K_{IIIq} \right\}^2 + D_{12} \left\{ \sum_{q=1}^{6} K_{Iq} \right\} \left\{ \sum_{q=2}^{6} K_{IIq} \right\} \tag{2}$$

where K_{Iq}, K_{IIq}, and K_{IIIq} are the stress intensity factor of the three fracture modes I, II, and III, respectively, corresponding to generalized loading S_q. $D_1, D_2, D_3,$ and D_{12} are the coefficients which are constants and their value depending on the material parameters [24].

$$D_1 = -0.5B_{22}\text{Im}\left(\frac{x_1+x_2}{x_1x_2}\right), D_2 = -0.5A_{11}\text{Im}(x_1+x_2),$$
$$D_3 = -0.5(\sqrt{y_{44}y_{55}}), D_{12} = B_{11}\text{Im}(x_1x_2) \tag{3}$$

where x_1 and x_2 are constants.

Generally, the flexibility coefficients are the function of the crack shape and stress intensity factor.

Now, the flexibility coefficients are expressed as below by referring [25].

$$C_{ij} = \frac{\partial u_i}{\partial S_i} = \frac{\partial^2 U_c}{\partial S_i \partial S_j} = \frac{\partial^2}{\partial S_i \partial S_j} \int_A E(a)\mathrm{d}A \quad (i, j = 1, 2, \ldots 6) \tag{4}$$

where u_i represents the displacement of beam in i direction due to the application of load S_i.

Substituting the value of $E(a)$ in Eq. (4), we get

$$C_{ij} = \frac{\partial^2}{\partial S_i \partial S_j} \int_{-H/2}^{H/2} \int_0^a [D_1(K_{I1} + K_{I4} + K_{I5})^2$$
$$+ D_2 K_{II3}^2 + D_3(K_{III2} + K_{III6})^2 + D_{12}(K_{I1} + K_{I4} + K_{I5})K_{II3}]\mathrm{da}\,\mathrm{dz} \tag{5}$$

For the investigation of composite beam, there are three independent variables exist which need to be considered when calculating its flexibility coefficient. These variables are named as axial displacement, vertical displacement, and rotational displacement. In this situation, flexibility coefficient can be expressed as

$$C_{ij} = \frac{\partial^2}{\partial S_i \partial S_j} \int_{-H/2}^{H/2} \int_0^a [D_1(K_{I1} + K_{I4})^2 + D_3 K_{III2}^2]\mathrm{da}\,\mathrm{dz}$$

$$= \frac{\partial^2}{\partial S_i \partial S_j} \int_{-H/2}^{H/2} \int_0^a [D_1(K_{I1}^2 + 2K_{I1}K_{I4} + K_{I4}^2) + D_3 K_{III2}^2]\mathrm{da}\,\mathrm{dz} \tag{6}$$

The stiffness coefficient of the cracked laminated composite cantilever beam is expressed as

$$k_c = C_{ij}^{-1} \tag{7}$$

After calculating the stiffness of the cracked laminated composite cantilever beam, the natural frequencies of damaged cantilever beam can be calculated The natural frequency (f_n) of cracked composite cantilever beam is calculated by using the below expression.

$$f_n = \frac{k_c}{2\pi} \sqrt{\frac{EIg}{wL^4}} \tag{8}$$

where 'E' represents the modulus of elasticity, 'I' represents the area moment of inertia, 'g' represents the gravitational acceleration, 'w' represents the uniform load per unit length.

3 Fuzzy Mechanism for Fault Detection

This suggested method is in general a process of data mining. Data mining is the method of revealing patterns and other precious information from huge data sets. For the extraction and discovery of hidden patterns from a large data set, data mining uses machine learning and statistical models. There is an alternate name for data mining which is called as knowledge discovery in data (KDD) [26]. In this data mining process, numerous natural frequencies of a cracked composite cantilever beam structure for various crack depth and crack locations are found by using finite element analysis (FEA). In case of conventional logic, a solution or result may be considered as either 'true' or 'false'. But every system has some imprecision involved in it. Conventional logic cannot able to clear these vagueness or uncertainty associated with the considered system. Also there are certain amounts of haziness involved in structural damage identification. To watch out this problem, here, fuzzy logic has been recommended for damage detection. This unconventional logic is a step forward of conventional logic. In actual, fuzzy logic can accurately control the mathematical model of any real-life problem. FLS has an ability of taking human like decisions, but this strength of FLS sometimes acts as one of its weaknesses.

A fuzzy controller with number of input parameters 3 and number of output parameters 2 has been developed. The usual linguistic representations for the inputs are expressed below.

Normalized first fundamental frequency = 'nfff'.
Normalized second fundamental frequency = 'nsff'.
Normalized third fundamental frequency = 'ntff'.
Likewise, the usual linguistic terms used to express the outputs are
Normalized crack depth = 'ncd'.
Normalized crack length = 'ncl'.

Based on above fuzzy subset, different fuzzy rules are outlined and defined in a generalized way. The general way of the fuzzy rules is expressed as follows:

$$\text{If } \left(\text{nfff is nfff}_i \text{ and nsff is nsff}_j \text{ and ntff is ntff}_k\right) \text{ then } \left(\text{ncd is ncd}_{ijk} \text{ and ncl is ncl}_{ijk}\right)$$
$$(9)$$

where $i = 1\text{--}12, j = 1\text{--}12, k = 1\text{--}12$.

Because 'nfff', 'nsff', and 'ntff' each have assigned by 12 membership functions.

From the Eq. (1), two set of rules can be derived. Those set of rules are expressed as follows.

$$\left.\begin{array}{l} \text{If } \left(\text{fff is fff}_i \text{ and sff is sff}_j \text{ and tff is tff}_k\right) \text{ then cd is cd}_{ijk} \\ \text{If } \left(\text{fff is fff}_i \text{ and sff is sff}_j \text{ and tff is tff}_k\right) \text{ then cl is cl}_{ijk} \end{array}\right\}$$
$$(10)$$

According to the standard fuzzy logic control method [24], for the fuzzy rule, a factor W_{ijk} is defined as follows:

$$w_{ijk} = \mu_{\text{fff}_i}(\text{freq}_i) \wedge \mu_{\text{sff}_j}(\text{freq}_j) \wedge \mu_{\text{tff}_k}(\text{freq}_k)$$

where freq_i, freq_j, and freq_k are represent the 1st, 2nd, and 3rd relative natural frequencies of the cantilever composite beam with crack, respectively.

Now, implementing the composition rule of interference. Then, values of the membership functions of relative crack location $(\text{location})_{\text{ncl}}$ and relative crack depth $(\text{depth})_{\text{ncd}}$ have been illustrated below [27].

$$\left.\begin{array}{l} \mu_{\text{rcl}_{ijk}}(\text{loc}) = w_{ijk} \wedge \mu_{\text{rcl}_{ijk}}(\text{loc}) \quad \forall_{\text{length}} \in \text{rcl} \\ \mu_{\text{rcd}_{ijk}}(\text{dep}) = w_{ijk} \wedge \mu_{\text{rcd}_{ijk}}(\text{dep}) \quad \forall_{\text{depth}} \in \text{rcd} \end{array}\right\}$$
$$(11)$$

Then, the final outcome coming out after combining outputs of all the fuzzy rules can be written as follows:

$$\left.\begin{array}{l} \mu_{\text{rcl}}(\text{loc}) = \mu_{\text{rcl}_{1\,1\,1}}(\text{loc}) \vee \ldots \vee \mu_{\text{rcl}_{ijk}}(\text{loc}) \vee \ldots \vee \mu_{\text{rcl}_{12\,12\,12}}(\text{loc}) \\ \mu_{\text{rcd}}(\text{dep}) = \mu_{\text{rcd}_{1\,1\,1}}(\text{dep}) \vee \ldots \vee \mu_{\text{rcd}_{ijk}}(\text{dep}) \vee \ldots \vee \mu_{\text{rcd}_{12\,12\,12}}(\text{dep}) \end{array}\right\}$$
$$(12)$$

Using the center of gravity method, the numerical results of normalized crack location and normalized crack depth are calculated [27] as

$$\left.\begin{array}{l} \text{Normalized crack location} = \text{ncl} = \frac{\int \text{loc}.\mu_{\text{ncl}}(\text{loc}).d(\text{loc})}{\int \mu_{\text{ncl}}(\text{loc}).d(\text{loc})} \\ \text{Normalized crack depth} = \text{ncd} = \frac{\int \text{dep}.\mu_{\text{ncd}}(\text{dep}).d(\text{dep})}{\int \mu_{\text{ncd}}(\text{dep}).d(\text{dep})} \end{array}\right\}$$
$$(13)$$

4 Application of Regression Analysis to Construct Mamdani FLS Adaptive

In the earlier section, already, it has been specified that there is some uncertainty lies in collection of data. This is happening because of involvement of human expertise in framing fuzzy rules according to the relationship within the independent and dependent variables of the real-life problems. For minimization of these uncertainty involved in the data collection, regression analysis is applied in FLS. Regression analysis is a technique of data mining which is applied to fit an equation to a data set. In this current paper, regression analysis plays a role as supervised learning. It creates a model between the independent and dependent variables using the statistical and mathematical modeling. This statistical modeling will develop the relationship in between input and output variables.

The initial equation for the regression analysis is given below

$$Q = a + bP + c \tag{14}$$

where Q = Effect,

P = Cause,

a = Constant,

b = Slope of the regression line,

c = Error expression/residual factor.

For this present analysis, Q = nfff, nsff, ntff, and P = ncd, ncl.

This work is primarily associated with the dynamic responses given by the structural element with presence of damage. The schematic illustration provided in Fig. 2 explained the use of regression analysis (RA) for the growth of adaptiveness of fuzzy logic system (FLS).

5 Result and Discussions

Below two tables, i.e., Tables 1 and 2 represent a complete comparison of the results coming out from fuzzy logic system (FLS) without data training and fuzzy logic system (FLS) with data training using regression analysis (RA). For generation of data, the natural frequencies obtained from first three natural frequencies (FEA) as mentioned in introduction section are normalized. The first five columns offer the normalized or dimensionless values of the dependent and independent variables. After that the value of error percentage is estimated using the equation given below.

$$\text{Percentage of Error} = \{(\text{data from FEA} - \text{data from the proposed technique})/(\text{data from FEA})\}$$
$$\times 100 \tag{15}$$
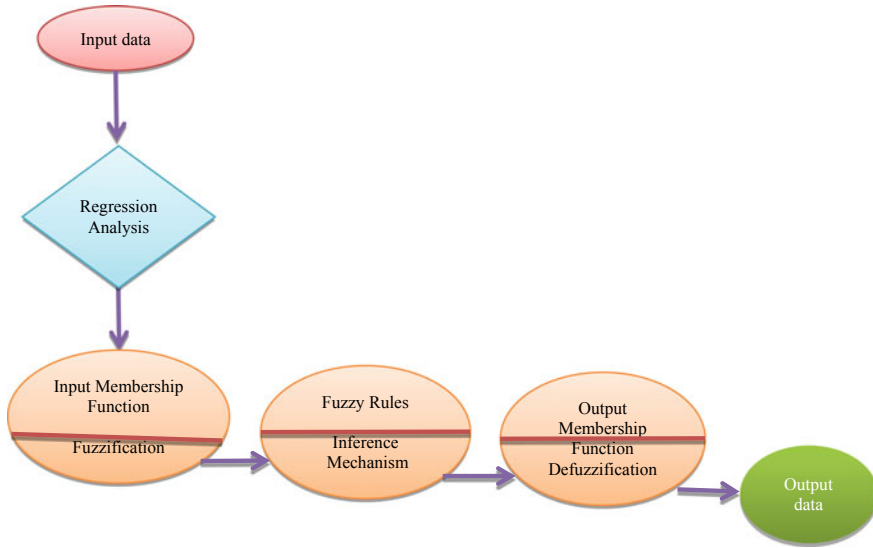
Fig. 2 Schematic representation of the proposed method

6 Conclusion

Health monitoring of structures is being extremely important to prevent dangerous premature structural failure, by that maintaining sustainability and conserving the working life of structures. Many researchers have been investigated on it. As a result, various damage identification methods and significant techniques have been developed. Vibration signature-based NDT methods for the purpose of structural fault identification, localization, and quantification are more familiar among these. In this particular research work, a unique NDT technique has been suggested for crack identification and determination of crack size and location. Fuzzy logic system (FLS) and regression analysis (RA) both are associated in this proposed NDT method. In fuzzy control, during the data generation and rules framing in FLS, human errors are involved. To eliminate those errors, regression analysis (RA) is applied. It has been observed that use of RA in FLS, eliminate the errors in generation of data. Basing on the outcomes, it has been concluded that the constructed technique predicts the exact fracture (crack) site in form of normalized crack location (ncl) and finds its size in form of normalized crack depth (ncd) at a high accuracy. This adaptive fuzzy logic system gives superior result than the fuzzy logic system and also helps in reduction in significant quantity of computational time.

Table 1 Results from FLS

S. No.	ntff	nsff	ntff	ncd	ncl	ncd by the FLS technique	ncl by the FLS technique	% of error in ncd	% of error in ncl
1	0.9924	0.9914	0.9968	0.322	0.2186	0.3078	0.2087	4.41	4.53
2	0.9933	0.9929	0.9979	0.3	0.207	0.2867	0.1968	4.43	4.92
3	0.9948	0.9943	0.9975	0.2873	0.232	0.2743	0.2207	4.52	4.87
4	0.9961	0.99774	0.998	0.122	0.2187	0.1167	0.2087	4.34	4.53
5	0.9977	0.9978	0.9967	0.275	0.3624	0.2619	0.347	4.76	4.25

Table 2 Results from adaptive FLS

S.No.	nfff	nsff	ntff	ncd	ncl	ncd by the FLS technique	ncl by the FLS technique	% of error in ncd	% of error in ncl
1	0.9924	0.9913	0.9967	0.321	0.2186	0.3121	0.2119	2.77	3.06
2	0.9932	0.9927	0.9979	0.3	0.207	0.293	0.1999	2.33	3.43
3	0.9947	0.9941	0.9973	0.2873	0.233	0.2786	0.225	3.03	3.43
4	0.9961	0.99773	0.998	0.124	0.2186	0.1198	0.213	3.39	2.56
5	0.9976	0.9978	0.9967	0.275	0.3621	0.2659	0.3515	2.51	2.93

References

1. Gay, D., Hoa, S.V.: Composite Materials: Design and Applications. CRC press (2007)
2. Gururaja, M.N., Rao, A.H.: A review on recent applications and future prospectus of hybrid composites. Int. J. Soft Comput. Eng. **1**(6), 352–355 (2012)
3. Swolfs, Y., Verpoest, I., Gorbatikh, L.: Recent advances in fibre-hybrid composites: materials selection, opportunities and applications. Int. Mater. Rev. **64**(4), 181–215 (2019)
4. Singh, T.J., Samanta, S.: Characterization of Kevlar fiber and its composites: a review. Mater. Today Proc. Elsevier Ltd 1381–1387 (2015)
5. Steinke, K., Groo, L., Sodano, H.A.: Laser induced graphene for in-situ ballistic impact damage and delamination detection in aramid fiber reinforced composites. Compos. Sci. Technol. **202**, 108551 (2021)
6. Huang, X.: Fabrication and properties of carbon fibers. Materials **2**(4), 2369–2403 (2009)
7. Soutis, C.: Carbon fiber reinforced plastics in aircraft construction. Mater. Sci. Eng. A **412**(1–2), 171–176 (2005)
8. Wang, D.C., Liu, Q.Z., Ke, F.: Application of carbon fiber reinforced composites in automobiles. Automobile Technol. Mater. **4**, 33–36 (2005)
9. Roberts, T.: The Carbon Fiber Industry: Global Strategic Market Evaluation 2006–2010, pp. 93–177. Materials Technology Publications, Watford, UK (2006)
10. Wan, Y.Z., Lian, J.J., Huang, Y., He, F., Wang, Y.L., Jiang, H.J., Xin, J.Y.: Preparation and characterization of three-dimensional braided carbon/Kevlar/epoxy hybrid composites. J. Mater. Sci. **42**(4), 1343–1350 (2007)
11. Feng, D., Feng, M.Q.: Output-only damage detection using vehicle-induced displacement response and mode shape curvature index. Struct. Control Health Monit. (2016)
12. Dziedziech, K., Pieczonka, L., Kijanka, P., Staszewski, W.J.: Enhanced nonlinear crack-wave interactions for structural damage detection based on guided ultrasonic waves. Struct. Control Health Monit. (2016)
13. Ranjbaran, A., Ranjbaran, M.: New finite-element formulation for buckling analysis of cracked structures. J. Eng. Mech. (2014)
14. Carden, E.P., Fanning, P.: Vibration based condition monitoring: a review. Struct. Health Monit. **3**(4), 355–377 (2004)
15. Sun, Z., Nagayama, T., Su, D., Fujino, Y.: A damage detection algorithm utilizing dynamic displacement of bridge under moving vehicle. Shock Vib. (2016)
16. Baviskar, P.R., Tungikar, V.B.: Multiple cracks assessment using natural frequency measurement and prediction of crack properties by artificial neural network. Int. J. Adv. Sci. Technol. **54**, 23–37 (2013)
17. Quila, M., Sarkar, S.C.S.: Free vibration analysis of an un-cracked and cracked fixed beam. J. Mech. Civ. Eng. **11**(3), 76–83 (2014)
18. Hui, N.B., Mahendar, V., Pratihar, D.K.: Time-optimal, collision-free navigation of a car-like mobile robot using neuro-fuzzy approaches. Fuzzy Sets Syst. **157**(16), 2171–2204 (2006)
19. Hakim, S.J.S., Razak, H.A.: Damage identification using experimental modal analysis and adaptive neuro-fuzzy interface system (ANFIS). In: Topics in Modal Analysis I, vol. 5, pp. 399–405. Springer, New York, NY (2012)
20. Eftekhari, M., Eftekhari, M., Majidi, M.: Securing interpretability of fuzzy models for modeling nonlinear MIMO systems using a hybrid of evolutionary algorithms. Iran. J. Fuzzy Syst. **9**(1), 61–77 (2012)
21. Golnaz, S.S., Nigro, M.B., Pakzad, S.N., Pan, Y.: Structural damage detection and localisation using multivariate regression models and two-sample control statistics. Struct. Infrastruct. Eng. ahead-of-print 1–17 (2014)
22. Kumar, P.G., Devaraj, D.: Fuzzy classifier design using modified genetic algorithm. Int. J. Comput. Intell. Syst. **3**(3), 334–342 (2010)
23. Worden, D.N.K., Cross, E.J.: On robust regression analysis as a means of exploring environmental and operational conditions for SHM data. J. Sound Vib. **347**, 279–296 (2015)

24. Krawczuk, M., Ostachowicz, W., Zak, A.: Modal analysis of cracked, unidirectional composite beam. Compos. B Eng. **28**(5–6), 641–650 (1997)
25. Nikpur, K., Dimarogonas, A.: Local compliance of composite cracked bodies. Compos. Sci. Technol. **32**(3), 209–223 (1988)
26. Weiss, S.M., Indurkhya, N.: Predictive Data Mining: A Practical Guide. Morgan Kaufmann (1998)
27. Parhi, D.R.: Navigation of mobile robot using a fuzzy logic controller. J. Intell. Robot. Syst. Theory Appl. **42**(3), 253–273 (2005)

Intelligent Manufacturing Systems: Robotics and Automation

A Literature Review on Application of Lean Manufacturing Techniques

Sushil S. Mishra and Ravi Terker

1 Introduction

Lean manufacturing concept was first invented in Japan, and Toyota firms were some earliest firms that used lean practices. Lean manufacturing assists in up-gradation of production processes and also raises employees moral and job satisfaction [1]. Generally, lean means manufacturing of products without generation of excess [2].

There is difference among lean manufacturing and conventional manufacturing. In traditional manufacturing systems, main focus is on inventory of the system whereas, As far as lean manufacturing is considered it opposes the same. According to lean ideology, inventory is measured as waste in firm. Exploring the dissimilarity between conventional manufacturing and lean manufacturing is very indispensable for firms if they want to apply lean practices [3].

As complexity in the market is increasing day by day, so awareness about perception of market dynamics is necessary if firms want to implement better manufacturing systems [4]. Basically, lean manufacturing is of the opinion that customers will always pay for the quality of services which he gets rather than the mistakes, for which he will not pay anything [5]. Majority of the elements that were considered for application of lean techniques included Value stream mapping which requires to convert natural resources into finished goods by mapping of process and flow of information specific to production line [6], push and pull system is one where pull system depends upon customer requirements and push system depends upon

S. S. Mishra
Department of Mechanical Engineering, Viva Institute of Technology, Mumbai, Maharashtra 401305, India
e-mail: sushilmishra@viva-technology.org

R. Terker (✉)
Department of Mechanical Engineering, NMIMS University, Mumbai, Maharashtra 51, India
e-mail: Ravi.Terker@nmims.edu

fixed schedule [7], KANBAN which is workflow management method for defining, managing and improving services [8].

Introduction of lean manufacturing practices in any particular type of firm has direct impact on its manufacturing process. In present world, customers have distinct outlook on manufacturing process. They acknowledge that product value is defined by opinion of customer and not from manufacturing process used. Main aim of lean manufacturing is to reduce or rather dispose of wastes from the firms. Moreover, a waste in firms can be something that shall not enhance value of the product. Lean techniques when used along with SWOT analysis assist in removal of wastes from the organization [9]. Lean manufacturing techniques when applied successfully help firms to increase their production and reduces the inventory [9]. The conclusive aim of lean manufacturing system is to eliminate all waste within the firm. The fundamental aim of lean manufacturing system is to manufacture product of best quality and at lowest possible cost in less time by removing wastes [10]. Application of lean manufacturing techniques gives positive results by reducing waste through continuous and systematic improvements [11]. However, it is the internal desire from organizations to implement lean techniques that become inspiration for them [12].

1.1 Different Stages for Application of Lean Techniques

1. **Removal of wastes**: One of the basic purposes of lean manufacturing is removal of waste; typically one can use value stream analysis to identifying waste full activities occurring at the plant.
2. **Reduce unnecessary inventory**: Overstocking can be essentially problematic if some inventory becomes obsolete, Moreover cost of maintaining inventory exceeds the actual benefit which firm can get.
3. **Shorting product cycle**: Presently the goods which used to take weeks for manufacturing can be manufactured within hours by using enhanced production capabilities. Followers of lean manufacturing always support production in small batches.
4. **Speed up response time**: Traditionally manufacturers depend upon forecast for market requirements, but this is not the best approach for fast-changing customer demand, Eventually, it will be preferable to develop system that can act swiftly.
5. **Seek customer feedback**: After designing the features for core product a methodical method for customer feedback should be developed. The system should be supple enough to adapt to changes, Following this step can enable one to satisfy customer needs within firms basic framework.
6. **Stretch out to suppliers**: This also helps strengthen existing relationships vital to your manufacturing operation.

Most of the industries in undeveloped countries are using old and obsolete techniques of manufacturing. According to Mahapatra and Mohanty [13], Companies in India use labor only physically and not intellectually. There was no customer

opinion and proposal system whatsoever. According to study conducted by Singh et al. [1] in Indian automobile and manufacturing industries, they concluded that if any firms need to implement lean then main focus should be on management and market issues. Sharma et al. [14] established that for accurate application of lean manufacturing principles, supply issues are very crucial. Many big firms like M&M, TCS, and CUMMINS have effectively implemented lean manufacturing philosophies. Further companies, like ATLAS COPCO, Bajaj, L&T, and Boyce, have become more globally competitive.

2   Methodology Used for Analysis

Presently most economic method to do any research is either by using internet or database. But nowadays there is such a large propagation of information is there, whether effective or non-effective, authenticated or non-authenticated and mainly they are either useful or non-useful. Therefore, Scopus journals stood first to start the research for quality research papers, so initially "lean management", "lean principles" "lean manufacturing", and "Toyota production system" were used as search keywords. During starting some books were also helpful and leading conference proceedings were also used for research. As an outcome of which a group of findings was recognized from the review. This paper will help in demonstrating better perception of lean manufacturing techniques and challenges faced by company during application of lean manufacturing. Initially, there appeared at least 5000 research papers related with the topic lean. This list was then reduced by using different keywords, by using different combinations of the words the list was reduced to about 200 papers for lean application and about 100 papers for lean manufacturing and about 50 papers for lean application challenges. Generally, articles referred for this review are mostly which are published after 2005 however some important articles and papers which are published before 2005 were also concerned. Though, there were many deficiencies in methodology which was adapted. First was accessibility of the papers. Primary database included Emerald, Taylor & Francis, Elsevier, IEEE, and Springer publishing groups. Moreover, one thing what author wants to clear that all the papers that were reviewed may not contain this keyword and all the papers having these keywords might not have been reviewed.

3   Literature Review

Lean techniques are defined into several steps, they include firstly how to define customer values, second is about value streaming, and lastly seeking for excellence [15]. As stated by Wong et al. [16], the key characteristic of lean manufacturing could be defined by some sets of collective factors and areas, which are eventually indispensable for application of lean manufacturing techniques. However, there are

a no. of techniques that are used while implementing lean manufacturing. According to Bayou and Korvin [17], manufacturing leanness is a technique where generally inputs are less and outputs are better. Singh et al. [18] concluded that lean deployment techniques, for example, lean tools, value stream mapping, kanban, etc. have benefited the industry. According to Bhasin and Burcher [19] lean is more like an attitude fairly than the strategy, if any firm or organization need to get rewards from lean application than supplier along with customer requirement are must. Moreover, lean manufacturing techniques are rather those which aim at unceasing improvement in order to get better results. According to Bhuiyan and Baghel [20] who studied the continuous improvement process from past to present, he stated that in continuous improvement there are few diverse techniques that are used to get better results such as six sigma, lean six-sigma, etc. Moreover, according to Hopp and Spearman [21] with respect to attain better levels of production, continuous improvement techniques are very important through removing variableness in the system and hence lowering the defects in any firm (Fig. 1).

However, when we talk about lean manufacturing techniques the term waste becomes very important hence so as to study lean it is vital to distinguish between different types of waste one is evident and other one is non-evident. Evident waste are those waste that piles up due to excess production, more waiting time, more inventory, lethargic transportation, etc. and non-evident waste generally arises due to variability. Dhamija et al. [22] presented in their study that basically lean technique
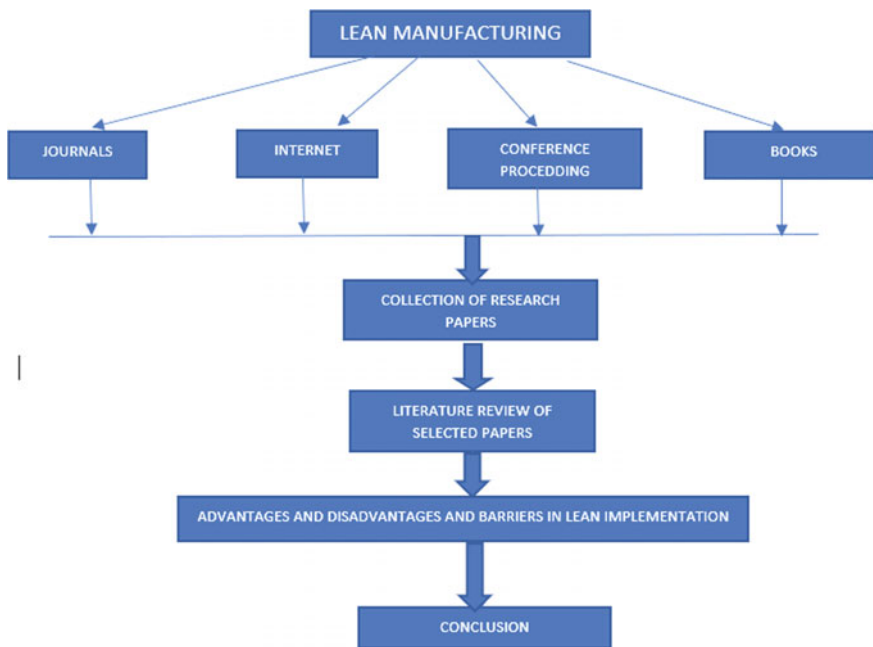

Fig. 1 Lean manufacturing flowchart for literature review

implementing firms are those which uses fewer material for product manufacturing, minimum workforce for production, reduced time for design and development, and less resources as well energy. Lean firms are basically are those which focus on customer demand and hence produce goods that are of high quality in more efficient way. Rose et al. [23] in his study presented some lean techniques which are more practical and applicable to micro and medium-scale firms. They advocated that so as to get entire benefit of lean practices, firms should implement them regularly, or else inconsistency may not allow firm to achieve full success.

According to study done by Yan-jiang et al. [24] he found that there are few distinguish factors that are indispensable for application of continuous improvement activities. Malik et al. [25] in his study compared continuous improvement techniques between two countries. Where he stated that though continuous improvement activities gave better results in both the cases, however, proportional impact was different. Mahapatra and Mohanty [13], also studied about adoption of lean manufacturing activities in micro and medium-sized firms which also showed good results. Kuo et al. [26] in his work showed the link among doing manufacturing using lean principles and performance of manufacturing where he stated that some issues such as relationships with customer, involvement with suppliers, and supply chain management have better effect on performance.

Ferdousi and Ahmed [27], in their research with respect to garment industries in Bangladesh found there is certain improvement in performance through applying lean manufacturing techniques. Wong et al. [28] during his study stated that education about waste management and continuous improvement techniques with respect to lean manufacturing are some methodologies that are easily understood by firms owners and organizations, he also found out that techniques such as 5S and kaizen remain few other significant lean tools which are additionally helpful for companies, he also concluded that application of lean practices on small along with large organizations and found that large firms have better application performance. Lyonnet et al. [29], developed certain methodologies and determined their penetration level regarding lean manufacturing technique and its application. He found that few methodologies for example value stream mapping, pull system are rarely used. Nordin et al. [30], in his study in Malaysian automobile industries, found that two lean techniques that is 5s and Kaizen are mostly used for getting better results from lean manufacturing techniques application. According to Eroglu and Hofer [31], where he studied the effect of inventory on the organization, his results concluded that almost more than 30% of companies showed no notable effect of inventory leanness in performance of firms.

Santosh Kumar et al. [32] applied lean technique and reduced the cycle time in a lorry body assembly line and hence improved the efficiency of that product line. Also, according to him lean manufacturing is more like a business strategy that continuously improves the process involved in manufacturing. Also, Ratneshwar Singh et al. [33] who studied TPM application in machine shop found there is reduction in break down time and it improved overall efficiency. According to him tpm application depends upon various parameters such a 5s, planned maintenance, kaizen, etc. which can be applied one by one and which result in increase in overall efficiency.

There is large no. of different techniques which are used in lean manufacturing. Various tools like value stream mapping (VSM) Kaizen, Kanban, 5S, TPM, etc. are used to remove numerous wastes that occurred during the manufacturing of the product. Many authors used different techniques to demonstrate the state of lean application technique. Bayou and Korvin [17] in their work proved that the manufacturing leanness is a smart technique accustomed to attain goals in fewer input to additional output. The measurement of leanness was considered by several features: relative, dynamic, long-term fuzzy logical, objective, integrative and inclusive. Singh et al. [18] showed a relationship between lean application and paybacks in industry with the aid of lean tools and value stream mapping (VSM). Paper presented to states of industry: current and future state.

Generally, a technique that is applied for findings and eliminating various waste are recognized as lean manufacturing techniques, Now in this part, several case studies with respect to lean manufacturing are presented, however as we discussed already here are numerous tools which are used in organization for removal of waste, some of these tools are just in time, kaizen, mrp, Kanban, 5s, and VSM, etc.

4   Case Studies

Lean manufacturing is the name given to a team-based systematic approach for discovering and eliminating different kinds of waste [9]. This section is composed of various cases of lean manufacturing. There are numerous tools that are effectively used for removal of wastes from any manufacturing firm. These tools include just in time, value stream mapping (VSM), kaizen, material requirement planning, kanban, 5s, etc. (Table 1).

4.1   Just in Time

Just in time is considered as core of the lean manufacturing. It is linked with lean techniques. Just in time production gives correct part at the correct place at correct time. Karlsson and Ahlstrom [34] in their work showed that every event and process must be processed in accurate form and according to accurate necessity to produce goods at the appropriate time, final aim is to provide each event with one part at one point and at the matching time when it is required, it is this principle on which Jit works. According to the author, decreasing lead time, lot sizes, and decreasing buffer sizes are significant features of jit. Plant size, plant age, and unions are some important factors that are discussed by Shah and Ward [35]. According to them, Jit has positive effect on efficiency however TQM has less impact. Gunasekaran and Lyu [36] studied the application of jit in Taiwan in micro-scale industry, initially, training was arranged for workers, and eventually, after application of 5s tools Seiri, Seito, Seize, Seiketsu, and Shitsuke were carried out for the betterment of the quality

Table 1 Some lean tools and their functions

S. No.	Lean tools	Functions and benefits
1	5s	1. Cost reduction by eliminating unnecessary tools or machine 2. Simplify work and increase productivity by reducing search 3. Prevention of breakdowns by inspecting tools or machines during cleaning
2	Continuous flow	Lower stock levels and shorter production cycle time
3	Jit	1. Reduction in the number of products and parts outstanding 2. Jit also contributes to elimination of losses 3. Simplification and smoothing of production
4	Kaizen	Achieve visible and faster results than with the more traditional continuous improvement
5	Kanban	A visual method for planning an entire workshop without the need of expensive MRP software or planning staff
6	VSM	1. In particular it makes it possible to visualize the total cycle time and to understand that it is share of production time in relation to the interoperation time 2. It is an ideal basis for identifying areas to be investigated in more details to understand malfunction
7	Waste elimination	The identification and systematic reduction of waste is a major lever for simplifying processes and reducing their variability

of products and the manufacturing of the company. Workers were given training in preventive maintenance with respect to equipment on which they use and on machine on which they operate. Initially, the forecast system which was adopted was push system which was replaced by pull system so that goods can be manufactured at the appropriate time with right quantity. Gupta et al. [37] analyzed barriers faced by small-scale and mid-sized companies while implementing jit, according to him bigger problem with smes while implementing jit was absence of negotiating authority of smes with outside world.

4.2 Kaizen

Generally, in kaizen meaning of kai is change and Zen indicates betterment. So meaning of kaizen is to change unceasingly for improvement which involves each and every employee of the company [38]. Its main focus is on complete improvement of the product and satisfaction of the customer. Detecting, targeting, and eradicating waste (muda) in machine operations, and different approaches used to control labor and production refer to kaizen in manufacturing companies. Rawabdeh [5], stated that housekeeping, standardization, and removal of waste are the three factors on which the kaizen approach depends. Chandrasekaran et al. [39] used kaizen philosophy to find answer to the problem of part mismatching in assembly line of an automobile company, gradually kaizen approach was used to remove problems with the assistance

Table 2 5s details

First "s"	Seiri or tidiness	Sort	Sorting out of the unnecessary parts
Second "s"	Seiton or orderliness	Set	All the parts should be arranged at proper place
Third "s"	Seiso or cleanliness	Shine	All working areas should be clean
Fourth "s"	Seiketsu	Standardize	Standardization means writing down what is being done, where and by whom
Fifth "s"	Shitshuke	Sustain	Maintain discipline

of data and eventually finding and selecting one best solution from various other available. Some of the benefits which were achieved after implementing kaizen are complete removal of surplus and substantial savings in expenditure.

4.3   5s

5S is a methodology that is adopted from letters of Japanese words: Seiri, Seiton, Seiso, Seiketsu, and Shitsuke. This methodology is generally used to shape the workplace and hence increasing the efficiency. In actual scenario, 5s was initially intended for manufacturing organizations only, however same methodology could be used in office or administrative environments for getting better results. Gunasekaran and Lyu [40] studied execution of 5s in Taiwan Company which were manufacturer of automobile lamps. Moreover Simmons et al. [41] while their study in medium-scale companies found that more lead times, bad quality, and lower efficiency to be the big problem. Basically, 5S as a tool is used by firms for standardization of their work and hence increasing the efficiency. Normally, 5S indicates clean housekeeping, standardizing and maintaining them effectively [42] (Table 2).

4.4   *Value Stream Mapping (VSM)*

Value stream mapping as name suggests is nothing but mapping of all the current production activities. In which generally key areas are identified, where upgrading is desired and to find unnecessary events as same could be discontinued as they don't contribute in manufacturing of goods [43]. VSM is an excellent diagrammatical or a paper pencil tool that aids to find and analyses the workflow to differentiate the value added and non-value-added activities. Lean concepts and techniques are used collectively in VSM. In Value stream mapping generally, two maps are created where initial map shows present state of assembly and another one makes a futuristic path for the improvement of the operations [44]. Rother and Shook [45] have talked about VSM in which existing state of product is analyzed and after doing proper analysis of

all the parameters a new map with improved futuristic stage of product is developed where main aim is to reduce waste, reduce lead times and improvement in material flow. VSM particularly shows the inventory, process time, Lead time, waiting time, etc. According to Pattanaik and Sharma [46], all the production processes must be studied thoroughly to reduce activities that are unessential and which will contribute in decreasing lead time, cycle time, moving time, and other wastes. Goriwondo et al. [47] studied execution of VSM in bread making manufacturing firm and found certain advantages, i.e., after application of VSM defects were reduced by almost 23% excessive inventory reduced by 15% and unessential activities reduced by 30%. Singh et al. [1] implemented VSM technique in a manufacturing firm and found certain benefits after application, firm achieved reduction in process inventory almost by 80%, inventory of final goods was reduced to about 18%, lead time was condensed to about 80% and workers output was improved up to 17%. Rajenthira Kumar et al. [48] implemented VSM technique in a production line of a paint shop in manufacturing firm, throughout the study they found various processes which were adding to unnecessary activities of paint shop. Actual mapping showed almost 70% of unproductive activities were present. Paranitharan et al. [49] in their study analyzed and redesigned assembly line in automobile company, Inspection of layout displayed that there is separate location for assembly and cylinder greasing operation and after doing proper analysis the layout was redesigned and trolley was arranged to overcome this problem Fawaz et al. [50] stated that simulation methodology can be applied to assess performance parameters before application of lean techniques, as prediction of levels throughout the assembly line is not feasible because in static modeling one cannot predict levels of inventory as scenarios can be different, so simulation technique is indispensable for accuracy of inventory levels [51]. Value stream mapping as name suggests is nothing but mapping of all the current production activities where generally key areas are identified and where enhancement is required and to find unproductive activities so that they can be discontinued as they don't contribute in production system values [52].

4.5 Kanban

Kanban is a type of lean manufacturing system in which movements of materials in assembly line is carried through cards it was formed to manage inventory levels the overall production and components supply, In Kanban system generally, a supplier must supply parts to production lines only when required as a result there will no excessive storage near production facilities.

Junior et al. [53] said that the implementer of Kanban can easily classify and analysis the variation in Kanban system with the knowledge which he acquired during application of diverse Kanban systems. According to Sipper et al. [54] Kanban system can be characterized by card system which is used for signaling production and transportation activities. Alvarez et al. [55] used VSM technique along with kanban system for application of lean manufacturing on assembly line, present state was

studied about the production line, cycle time, lead time and all other activities were noted, and it was concluded that conventional push system was used for production lines, which created difficulty in assembly lines. And eventually, a Kanban system was proposed so that traditional push system can be replaced by pull system. Abdulmalek and Rajgopal [56] made a simulation to demonstrate the condition earlier and afterward application of Kanban system. Excessive inventories, a no. of non-essential activities, are few of the shortcomings which were analyzed, and eventually Kanban system proved to be beneficial for better production flow.

4.6 *Waste Elimination*

A view from the study of various articles indicates that about 70% of unwanted waste in manufacturing systems generates due to inventories. The inventories might be categorized as raw material inventory, assembly line inventory, and final goods inventory. Inventories have a vital role in any organization's turnover, A detailed literature from manufacturing companies indicated that about 30% of firms attempt to rise their inventory turnover [57]. Moreover, target of lean manufacturing firms is comprehensive removal of waste, as we already discussed with respect to customer view anything that doesn't enhance quality of the product is termed as waste. As stated by Sakakibara et al. [58] excessive raw material inventory is due to poor production plans, in appropriate raw material availability, and needless transportation between different work stations. Waste from inventories can be reduced by reducing rejection rates, Lead time, quality levels, and delivery rates. However, this waste can be identified by using proper tools and lean techniques. Upadhye et al. [9] in their work claim to have perfectly executed lean philosophy in a company. Initially, lean philosophy approach was considered only for large and medium firms. Various lean manufacturing tools such as kaizen, jit, vsm, takt time, Kanban, etc. proved to be successful in sorting and removing unwanted waste from the firm's production facilities.

5 Barriers to Lean Application

Unfortunately, many micro and medium firms didn't show any interest in adopting LM [59]. Roslin et al. [60] stated that it is very simple to tell those lean practices can be implemented easily however practically it is not that simple. Just visualize how come organizations will be willing to overhaul their complete setup for implementing lean techniques as nobody wants to change their setup until it is extremely needed. Introduction of lean manufacturing methodologies in any firm will force them to change their work culture, now such things become barrier to lean application. Hence to let these changes in organization extra work should be done [61, 62]. As workers see some changes in work environment then it becomes difficult for them to responds

to these changes. However, this barrier would be controlled by embracing a culture of effective conveying and training for everybody in the firm.

Empowerment of workforce and their participation can be encouraged in lean manufacturing applications by assigning them a certain responsibilities [63]. Level of understanding would be increased if suitable education and communication will be provided and will help to develop motivating culture in any organization. Puvanas-varan et al. [64], James [65], and Crute et al. [66] in their work recognized some barriers while implementing lean techniques. Some of them are lack of interest from seniors and middle management, improper management of lean methodologies, and attitude of labors and employees who are resistant to change. According to Achanga, Shehab, Roy, and Nelder [67] and Salaheldin [68] it is not possible to implement lean techniques if adequate support from top management is not provided. Achanga et al. [69] also said that un-adequate financial resources also act as barrier for execution of lean techniques in minor industries. Abdul-Nour, Lambert, and Drolet [70] and Salaheldin et al. [68] in their work concluded that absence of skilled workers and resources also acts as hindrance for lean application. Chong et al. [71] also stated that time management also works like a barrier in the application process. The premier aim is to preserve industry and machineries in good running conditions without any hindrance but it becomes difficult for both owners along with workers. According to Stanleigh [72], every small change will be judged whether good or bad. Although there are large no. of studies that shows various advantages associated with execution of lean techniques, some companies are also present which show failures in adoption of lean methodologies. As we know lean application has become important virtually for each and every firm but not all the organization have ability to implement lean this is because there is absence of proper framework for application of lean tech-niques [42]. According to a particular study that was carried out in United States, it was found that only about 25% of organization were successful in lean application techniques and got benefited [73]. One of the reasons for the failure of application is that framework for lean adaptation is not available or mainly it is available only for large-scale firms [74]. But in spite of some effective execution of lean manufacturing in large industries smes still face the heat in application of lean methodologies [75]. But there are large no. of small-scale manufacturing firms rather than big organiza-tion. However, till now very less no. of company owners have shown interest in lean application [76]. As execution of lean methodologies involves a proper road map and well-defined processes, Anvari et al. [77], which is absent for small-scale companies. Although it is well-proven fact that application of lean techniques is fruitful for any organization but still there are large no. of firms present which were unable to adopt lean techniques and are considered failure in lean adoption [78].

6 Paybacks of Lean Manufacturing

Forza [79] stated that lean manufacturing is superior to traditional system. According to numerous writers for instance [80–86] application of lean techniques also helps

firms to increase their competitiveness. Sohal and Eggleston [87], specified in their findings that almost two third of the industries are of the opinion that application of lean manufacturing techniques improves their strategical competitiveness by further improving customer relationships. For maintaining a productive customer feedback arrangement, effective and courteous, and obliging responses to customer queries will assist firms to avoid complication in future and helps in maintaining customer trust [52]. These activities can aid firms to increase their sustainability and profits. According to Lathin [88] conventional mass producers can get up to 80% a reduction in inventory, 92% in quality cost, 90% in lead time, and a 50% increase in labor productivity if lean technique are applied properly. Claudius Consulting [89] also said that lean technique application can aid companies to reduce costs by 18 and 65%, lowers waste by 46%, increase productivity up to 40%, and reduce floor area and inventory requirements by 64%. Nystuen [81] also conducted a study that showed that travel time can be reduced by 80%, inventory up to 80%, and product lead time by 13% by applying lean manufacturing methodologies in the firm. Bicheno e al. [90], Hines [91], Liker [92], and Womack and Jones [93] in their studies found that lean manufacturing practices are well-liked and used in the automotive sector as compared to other sectors (Table 3).

Application of lean manufacturing practices always leads to positive enhancement in any firm. Besides having direct benefits of lean manufacturing some indirect benefits are also there that play important role in any industry's success. Some of the benefits are:

Development in quality and safety.
Reduction of time for traceability.
Positive variations in work culture.
Decrease of fatigue and stress.

Table 3 Considerable dissimilarity among lean manufacturing and conventional manufacturing approaches

S. No.	Activity	Lean manufacturing	Traditional manufacturing
1	Production	Driven by customer demand (pull)	Driven by sales forecast (push)
2	Inventory levels	Inventory are reduced	High inventory level
3	Cycle time	Short cycle time	Long cycle time
4	Flexibility	Good	Bad
5	Management layers	Fewer layers of management	Many layers of management
6	Lead time	Short	Long
7	Focus	Value stream processes	Products and cost
8	Batch size	Small	Bigger
9	Financial benefits	More	Less

7 Conclusion

There is large amount of literature is available concerned with lean manufacturing which shows us different kinds of research and practices which are followed throughout the world, but as we all know lean technique is very broadly implemented in manufacturing firms hence still further research is required in lean manufacturing. Firms where positive execution of lean technique happened show that lean application requires collective efforts right from the workers to middle management to top management. Moreover, if workforces of the organizations are aware about lean philosophy, various methodologies associated with lean and implementing strategies' in various situations then it turns like an added advantage and plays an important role while implementing lean manufacturing. Various lean tools and techniques which are demonstrated here through various case studies exhibited that there are lot of advantages some of them such as decrease in inventory level, shorting of lead time, reduction of waste generation, financial benefits which are visible but some invisible benefits are also there such as lowering of stress and fatigue, positive change in work culture of organization, and reduction in time which was used for tracing any problem. Various surveys were also taken to find the level of understanding of lean manufacturing tools within the organization. Nevertheless, despite of the circumstances that lean application has various advantages associated with them, but there are few barriers also which are becoming hindrance for proper application of lean techniques. Some of the barriers are financial problems, not ready to change, which is likely a psychological problem, lack of sense of responsibility, and finally lack of awareness regarding lean application, but it has been proved without any dilemma that if any firm or organization needed to increase their competitive edge then adoption of lean attitude becomes almost indispensable in present scenario almost every industry has to leave conservative attitude and align their work practice which is more toward lean. In the similar way workers and employees also requires to change their attitude and embrace new changes for the sake of company and ultimately for themselves also.

References

1. Singh, B., Garg, S.K., Sharma, S.K., Grewal, C.: Lean implementation and its benefits to production industry. Int. J. Lean Six Sigma **1**, 157–168 (2010)
2. Vamsi Krishna Jasti, N., Kudale, R.: A literature review of empirical research methodology in lean manufacturing. Int. J. Oper. Prod. Manag. **34**(8), 1080–1122 (2014)
3. Andrew, L.M.: A lean route to manufacturing survival. Assem. Autom. **26**, 265–272 (2006)
4. Gadalla, M.A.: A conceptual framework to excogitate agile from lean transformation. Int. J. Rapid Manuf. **1**, 308–322 (2010)
5. Rawabdeh, I.A.: A model for the assessment of waste in job shop environments. Int. J. Oper. Prod. Manag. **25**, 800–822 (2005)
6. Rother, M., Shook, J.: Learning to See: Value Stream Mapping to Add Value and Eliminate Muda. The Lean Enterprise Institute, Inc., Brookline, MA (1999)

7. Dengiz, B., Akbay, K.S.: Computer simulation of a PCB production line: metamodeling approach. Int. J. Prod. Econ. **63**, 195–205 (2000)
8. Graves, R., Konopka, J.M., Milne, R.J.: Literature review of material flow control mechanisms. Prod. Plan. Control **6**(5), 395–403 (1995)
9. Upadhye, N., Deshmukh, S.G., Garg, S.: Lean manufacturing system for medium size manufacturing enterprises: an Indian case. Int. J. Manag. Sci. Eng. Manag. **5**, 362–375 (2010)
10. Dennis, P.: Lean Production Simplified. Productivity Press, New York (2007)
11. Narayanamurthy, G., Gurumurthy, A.: Leanness assessment: a literature review. Int. J. Oper. Prod. Manag. **36**(10), 1115–1160 (2016)
12. Bamford, D., Forrester, P., Dehe, B., Leese, R.G.: Partial and iterative lean implementation: two case studies. Int. J. Oper. Prod. Manag. **35**(5), 702–727 (2015)
13. Mahapatra, S.S., Mohanty, S.R.: Lean manufacturing in continuous process industry: an empirical study. J. Sci. Ind. Res. **66**, 19–27 (2007)
14. Sharma, S.K., Gupta, R.D., Kumar, A., Singh, B.: Supplier issues for lean application. Int. J. Eng. Sci. Technol. **3**, 3900–3905 (2011)
15. Womack, J.P., Jones, D.T.: Lean Thinking. Banish Waste and Create Wealth in Your Corporation. Simon & Schuster, New York (1996)
16. Wong, Y.C., Wong, K.Y., Ali, A.: Key practice areas of lean manufacturing. In: International Association of Computer Science and Information Technology, Spring Conference, pp. 267–271 (2009). ISBN: 978-0-76
17. Bayou, M.E., de Korvin, A.: Measuring the leanness of manufacturing systems—a case study of Ford Motor Company and General Motors. J. Eng. Technol. Manag. (2008)
18. Singh, B., Garg, S.K., Sharma, S.K.: Development of index for measuring leanness: study of an Indian auto component industry. Meas. Bus. Excell. **14**(2), 46–53 (2010)
19. Bhasin, S., Burcher, P.: Lean viewed as a philosophy. J. Manuf. Technol. Manag. **17**, 56–72 (2006)
20. Bhuiyan, N., Baghel, A.: An overview of the continuous improvement: from the past to the present. Manag. Decis. **43**, 761–771 (2005)
21. Hopp, W., Spearman, M.: To pull or not to pull: what is the question? Manuf. Serv. Oper. Manag. **6**, 133–148 (2004)
22. Dhamija, S., Srivastava, P., Khanduja, D., Agarwal, V.P.: Value stream mapping: a tool to achieve leanness. In: National Conference on Present Scenario and Advanced Technology in Mechanical Engineering, JMIT, Radaur, District Yamunanagar, Haryana, India, 14–15 Dec 2011, pp. 28–34 (2011)
23. Rose, A.M.N., Deros, B.M., Rahman, M.N.A., Nordin, N.: Lean manufacturing best practices in SMEs. In: Proceedings of the 2nd International Conference on Industrial Engineering and Operations Management (IEOM 2011), Kuala Lumpur, Malaysia, 22–24 Jan 2011, pp. 872–877. IEOM Research Solutions Pty Ltd (2011). ISBN: 978-0-9808251-0-7
24. Yan-jiang, C., Dan, W., Lang, X.: Influencing factors of continuous improvement and tendency to change. In: IEEE International Conference on Management of Innovation and Technology, Singapore, vol. 1, pp. 181–185 (2006)
25. Malik, S.A., Lu, L.-b., Tian, Y.-z., Sun, X.-l.: Continuous improvement practices in Asian developing countries: a comparative analysis between Chinese and Pakistani manufacturing industry. In: Proceedings of the 14th International Conference on Management Science and Engineering (ICMSE), Harbin, PR China, 20–22 Aug 2007, pp. 692–697. Institute of Electrical and Electronics Engineers (2007). ISBN: 978-7-5603-2278-0
26. Kuo, T., Shen, J., Chen, Y.: A study on the relationship between lean production practices and manufacturing performance. In: Proceedings of the International Symposium of Quality Management, Kaohsiung, Taiwan, 8–9 Nov 2008, pp. 1–8 (2008)
27. Ferdousi, F., Ahmed, A.: An investigation of manufacturing performance improvement through lean production: a study on Bangladeshi garment firms. Int. J. Bus. Manag. **4**, 106–116 (2009)
28. Wong, Y.C., Wong, K.Y., Ali, A.: Key practice areas of lean manufacturing. In: International Association of Computer Science and Information Technology, Spring Conference, pp. 267–271 (2009). ISBN: 978-0-7695-3653

29. Lyonnet, B., Pillet, M., Pralus, M.: Lean manufacturing in the screw cutting sector: assessment of maturity level. Int. J. Rapid Manuf. **1**, 256–277 (2010)
30. Nordin, N., Deros, B.M., Wahab, D.A.: A survey on lean manufacturing application in Malaysian automotive industry. Int. J. Innov. Manag. Technol. **1**, 374–380 (2010)
31. Eroglu, C., Hofer, C.: Lean, leaner, too lean? The inventory-performance link revisited. J. Oper. Manag. **29**, 356–369 (2011)
32. Santosh Kumar, S., Pradeep Kumar, M.: Procedia Mater. Sci. **5**, 1853–1862 (2014). International Conference on Advance Materials and Engineering AMME 2014
33. Singh, R., Gohil, A.M., Shah, D.B., Desai, S.: Procedia Eng. **51**, 592–599 (2013)
34. Karlsson, C., Ahlstrom, P.: Assessing changes towards lean production. International. Journal of Operations & Production Management **16**, 24–41 (1996)
35. Shah, R., Ward, P.T.: Lean manufacturing: context, practice bundles, and performance. J. Oper. Manag. **21**, 129–149 (2003)
36. Gunasekaran, A., Lyu, J.: Application of just-in time in a small company: a case study. Prod. Plan. Control **8**, 406–412 (1997)
37. Gupta, R., Garg, D., Gupta, H.: Difficulties of implementing JIT in SMEs. Int. J. Appl. Eng. Res. **6**, 3246–3250 (2011)
38. Singh, J., Singh, H.: Kaizen philosophy: a review of literature. J. Oper. Manag. **8**, 51–72 (2009)
39. Chandrasekaran, M., Kannan, S., Pandiaraj, P.: Quality improvement in automobile assembly production line by using Kaizen. Manuf. Technol. Today **7**, 33–38 (2008)
40. Gunasekaran, A., Lyu, J.: Application of just-intime in a small company: a case study. Prod. Plan. Control **8**, 406–412 (1997)
41. Simmons, L., Holt, R., Dennis, G., Walden, C.: Lean application in a low volume manufacturing environment: a case study. In: Proceedings of the 2010 Industrial Engineering Research Conference. Mississippi State University, Center for Advanced Vehicular Systems Extension Canton, MS, USA. IIE (2010)
42. Jadhav, J.R., Mantha, S., Rane, S.B.: Exploring barriers in lean implementation. Int. J. Lean Six Sigma **5**, 122–148 (2014). https://doi.org/10.1108/IJLSS-12-2012-0014
43. Mangla, S.K., Sharma, Y.K., Patil, P.P., Yadav, G., Xu, J.: (2019) Logistics and distribution challenges to managing operations for corporate sustainability: study on leading Indian diary organizations. J. Clean. Prod. **238**, 117620. https://doi.org/10.1016/j.jclepro.2019.117620
44. Angelis, J., Fernandes, B.: Int. J. Lean Six Sigma **3**(1), 74–84 (2012). https://doi.org/10.1108/20401461211223740
45. Rother, M., Shook, J.: Learning to See: Value Stream Mapping to Add Value and Eliminate MUDA, 2nd edn. The Lean Enterprise Institute, Brookline, MA (1999)
46. Pattanaik, L.N., Sharma, B.P.: Implementing lean manufacturing with cellular layout: a case study. Int. J. Adv. Manuf. Technol. **42**, 772–779 (2009)
47. Goriwondo, W.M., Mhlanga, S., Marecha, A.: Use of value stream mapping tool for waste reduction in manufacturing. Case study for bread manufacturing in Zimbabwe. In: Proceedings of the 2011 International Conference on Industrial Engineering and Operations Management Kuala Lumpur, Malaysia, pp. 236–241. IEOM Research Solutions Pty Ltd (2011). ISBN: 978-0-9808251-0-7
48. Rajenthirakumar, D., Mohanram, P.V., Harikaarthik, S.G.: Process cycle efficiency improvement through lean: a case study. Int. J. Lean Think. **2**, 46–58 (2011)
49. Paranitharan, K.P., Begam, M.S., Abuthakeer, S.S., Subha, M.V.: Redesigning an automotive assembly line through lean strategy. Int. J. Lean Think. **2**, 1–14 (2011)
50. Abdulmalek, F.A., Rajgopal, J.: Analyzing the benefits of lean manufacturing and value stream mapping via simulation: a process sector case study. Int. J. Prod. Econ. **107**, 223–236 (2007)
51. McDonald, T., Van Aken, E.M., Rentes, A.F.: Utilizing simulation to enhance value stream mapping: a manufacturing, case application. Int. J. Logist. Res. Appl. **5**(2), 213–232 (2002)
52. Luthra, S., Mangla, S.K., Yadav, G.: An analysis of causal relationships among challenges impeding redistributed manufacturing in emerging economies. J. Clean. Prod. **225**, 949–962 (2019). https://doi.org/10.1016/j.jclepro.2019.04.011

53. Junior, M.L., Filho, M.G.: Variations of the Kanban system: literature review and classification. Int. J. Prod. Econ. **125**, 13–21 (2010)
54. Sipper, D., Bulfin, Jr., R.L.: Production: Planning, Control, and Integration, McGraw-Hill, New York (1997)
55. Alvarez, R., Calvo, R., Pena, M.M., Domingo, R.: Redesigning an assembly Line through lean manufacturing tools. Int. J. Adv. Manuf. Technol. **43**, 949–958 (2009)
56. Abdulmalek, A., Rajgopal, J.: Analyzing the benefits of lean manufacturing and value stream mapping via simulation: a process sector case study. Int. J. Prod. Econ. **107**, 223–236 (2007)
57. Demete, K., Matyusz, Z.: The impact of lean practices on inventory turnover. Int. J. Prod. Econ. **133**(1), 154–163 (2011)
58. Sakakibara, S., Flynn, B.B., Schroeder, R.G., Morris, W.T.: The impact of just-in-time manufacturing and its infrastructure on manufacturing performance. Manag. Sci. **43**(9), 1246–1257 (1997)
59. Bhamu, J., Singh Sangwan, K.: Lean manufacturing: literature review and research issues. Int. J. Oper. Prod. Manag. **34**(7), 876–940 (2014)
60. Roslin, E.N., Shamsuddin, A., Dawal, S.Z.M.: Discovering barriers of lean manufacturing system application in Malaysian automotive industry. In: Advanced Materials Research, vol. 845, pp. 687–691. Trans Tech Publications (2014)
61. Stanleigh, M.: Effecting successful change management initiatives. Ind. Commer. Train. **40**, 34–37 (2008)
62. Barker, B.: The identification of factors affecting change towards best practice in manufacturing organizations. Manag. Decis. **36**, 549–556 (1998)
63. Yadav, G., Seth, D., Desai, T.N.: Application of hybrid framework to facilitate lean six sigma application: a manufacturing company case experience. Prod. Plan. Control **29**, 185–201 (2018). https://doi.org/10.1080/09537287.2017.1402134
64. Puvanasvaran, P., Megat, H., Hong, T.S., Muhamad, M.R.: The roles of communication process for an effective lean manufacturing application. J. Ind. Eng. Manag. **2**, 128–152 (2009)
65. James, T.: Wholeness as well as leanness. Manuf. Eng. **85**, 14–17 (2006)
66. Crute, V., Ward, Y., Brown, S., Graves, A.: Implementing lean in aerospace—challenging the assumptions and understanding the challenges. Technovation **23**, 917–928 (2003)
67. Achanga, P., Shehab, E., Roy, R., Nelder, G.: Critical success factors for lean application within SMEs. J. Manuf. Technol. Manag. **17**, 460–471 (2006)
68. Salaheldin, S.I.: JIT application in Egyptian manufacturing firms: some empirical evidence. Int. J. Oper. Prod. Manag. **25**, 354–370 (2005)
69. Achanga, P., Shehab, E., Roy, R., Nelder, G.: Critical success factors for lean application within SMEs. J Manuf. Technol. Manag. **17**(4), 460–471 (2006). https://doi.org/10.1108/17410380610662889
70. Abdul-Nour, G., Lambert, S., Drolet, J.: Adaptation of JIT philosophy and technique to small-sized manufacturing firms: a project management approach. Comput. Ind. Eng. **35**, 419–422 (1998)
71. Chong, S.: Business process management for SMEs: an exploratory study of application factors for the Australian wine industry. J. Inf. Syst. Small Bus. **1**, 41–58 (2007)
72. Stanleigh, M.: Effecting successful change management initiatives. Ind. Commer. Train. **40**, 34–37 (2008). Taylor, D., Brunt, D. (eds.): Manufacturing Operations. Thompson, London (2001)
73. Gandhi, N.S., Thanki, S.J., Thakkar, J.J.: Ranking of drivers for integrated lean green manufacturing for Indian manufacturing SMES. J. Clean. Prod. **171**, 675–689 (2018)
74. Alhuraish, I., Robledo, C., Kobi, A.: A comparative exploration of lean manufacturing and six sigma in terms of their critical success factors. J. Clean. Prod. **164**, 325–337 (2017)
75. Panwar, A., Jain, R., Rathore, A.P.S.: Lean application in Indian process industries—some empirical evidence. J. Manuf. Technol. Manag. **26**(1), 131–160 (2015)
76. Helleno, A.L., Moraes, A.J.I.d., Simon, A.T.: Integrating sustainability indicators and lean manufacturing to asses manufacturing processes: application case studies in Brazilian industry. J. Clean. Prod. **153**, 405–416 (2017)

77. Anvari, A., Zulkifli, N., Sorooshian, S., Boyerhassani, O.: An integrated design methodology based on the use of group AHP-DEA approach for measuring lean tools efficiency with undesirable output. Int. J. Adv. Manuf. Technol. **70**, 2169–2186 (2014). https://doi.org/10.1007/s00170-013-5369-z

78. Henao, R., Sarache, W., Gomez, I.: Lean manufacturing and sustainable performance: trends and future challenges. J. Clean. Prod. **208**, 99–116 (2019)

79. Forza, C.: Work organization in lean production and traditional plants: what are the differences? Int. J. Oper. Prod. Manag. **16**(2), 42–62 (1996)

80. Billesbach, T.: Applying lean production principles to a process facility. Prod. Invent. Manag. J. **35**, 3–14 (1994)

81. Nystuen, T.: Big results with less. Qual. Prog. **35**(10), 51–55 (2002)

82. Oliver, N.: Lean production practices. Br. J. Manag. **7**, 1–10 (1996)

83. Parker, V.: Burt's Bee's application of production processes. Tribune Bus. News **1–3**, 2–4 (2003)

84. Siekman, P.: Cessna tackles lean manufacturing. Fortune **141**, 222–231 (2000)

85. Taylor, D., Brunt, D. (eds.): Manufacturing Operations. Thompson, London (2001)

86. Vasilash, G.: Lean: a silver lining. Automotive Design and Production (2001)

87. Sohal, A., Eggleston, A.: Lean production: experience amongst Australian organizations. Int. J. Oper. Prod. Manag. **14**, 1–17 (1994)

88. Jasti, N.V.K., Sharma, A.: Lean manufacturing application using value stream mapping as a tool: a case study from auto components industry. Int. J. Lean Six Sigma **5**, 89–116 (2014). https://doi.org/10.1108/IJLSS-04-2012-0002

89. Claudius Consulting: Lean Manufacturing. Claudius Consulting, York, UK (2004). Retrieved from: www.claudiusconsulting.co.uk

90. Bicheno, J.: The New Lean Tool Box. Picsie, London (1999)

91. Hines, P.: Value stream mapping. Addison Wesley, London (1999)

92. Liker: The Toyota Way model: an alternative framework for lean construction. Total Qual. Manag. Bus. Excell. (2004).https://doi.org/10.1080/14783363.2013.820022

93. Womack, J., Jones, D.: Lean Thinking. Simon & Schuster, London (2003); **25**(4), 287–304 (2008)

Simulation of an Industrial Robot Using RobotStudio and RoKiSim

Amit Talli and **Arunkumar Giriyapur**

1 Introduction

Industrial robots are responsible for transforming the landscape of manufacturing industries into smart and intelligent manufacturing. Researchers have clearly expressed the role of autonomous robots in smart factories [1]. In [2], the authors highlighted the growing interest in automation and robotics. The All India Council for Technical Education (AICTE) has identified robotics as one of the thrust areas for the Faculty Development Programme (FDP). These FDPs are intended to gain knowledge, skills and provide future directions to academicians, practitioners, and researchers [3].

Industrial robots have many roles in industries, health care, education, space, underwater, etc. Human–Robot Collaboration (HRC) is one of the emerging research areas in robotics [4]. However, the mathematical concepts of serial manipulators are crucial and challenging. Techniques to solve problems such as kinematics and dynamics are computationally demanding, time-consuming, and impractical [5]. Several studies, for instance [6–8], have reported the problem in visualization and understanding the kinematics of serial manipulators. One primary problem with robot kinematics is that the analytical technique is tedious and time-consuming. This poses some problems when developing equations for different robots due to calculation errors. One way to overcome this problem is to derive equations using the symbolic math toolbox and verify with a simulation tool.

Several experts have developed software tools for simulation, such as RoboAnalyzer, RoKiSim, and Robotics Toolbox, to name a few simulation tools [9, 10]. These

A. Talli (✉) · A. Giriyapur
Department of Automation and Robotics, KLE Technological University, Hubballi 580031, India
e-mail: amit@kletech.ac.in

A. Giriyapur
e-mail: aaron@kletech.ac.in

895

software tools can be implemented to solve the kinematics of industrial manipulators. The aim of the paper is to formulate the kinematic equations for a 6R (six revolute joints) industrial robot using the symbolic math toolbox. Then, simulation is carried out in RoKiSim and RobotStudio. This approach is intended to create awareness and generate interest among the students and teachers. A similar strategy can be implemented with other industrial robots regardless of any software tool intended for industrial robots. This method is viable due to the simulation tool without any hardware requirement. The overall structure of the paper is organized into six distinct sections. The methodology is described in Sect. 2. Section 3 describes the kinematics of the IRB 1600. Section 4 describes the kinematic of the IRB 1600 robot. Section 5 highlights the results, followed by a conclusion in Sect. 6.

2 Methodology

The methodology section discusses the strategy adopted for a 6R industrial robot simulation. An industrial robot from ABB company is selected. In this study, we opted for IRB 1600, a six degrees of freedom (6-DoF) industrial robot for the simulation. The method is essentially the same as reported in the previous papers [5, 11, 12]. The current method adopted RoKiSim and RobotStudio to simulate and validate developed equations. We used a commercially available software package from ABB known as RobotStudio [13]. This software validates the kinematic solutions obtained from RoKiSim and analytical results. A free software package downloaded from www.parallemic.org/RoKiSim.html, known as RokiSim 1.7, was adopted for the simulation [14]. Figure 1 depicts the methodology.
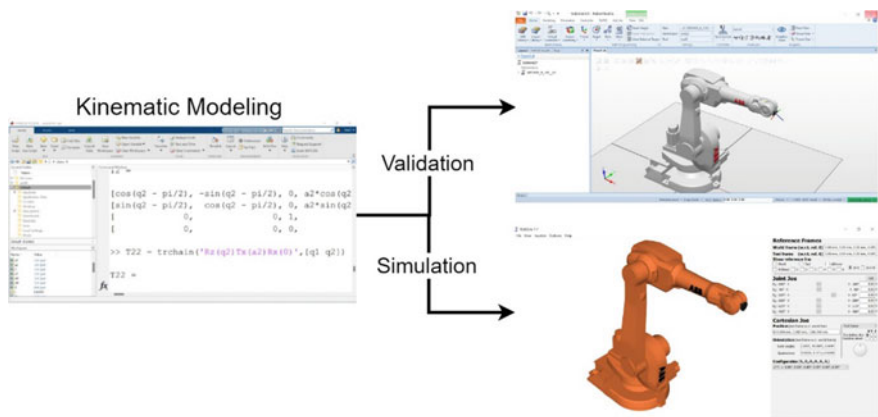

Fig. 1 Methodology

Developing the kinematic equations analytically for 6R serial manipulators is tedious and computationally demanding. The equations were formulated using the symbolic math toolbox available in MATLAB.

3 Description of IRB 1600

Figure 2 presents the IRB 1600 industrial robot from ABB company used to simulate the robot using RoKiSim and RobotStudio. It consists of six degrees of freedom or six revolute joints used for industrial applications such as arc welding, material handling, cleaning, dispensing, and packing. The robot has seven links, excluding base and a payload of 6 kg. The Denavit–Hartenberg (DH) parameters describing the robot's structure are presented in Table 1.
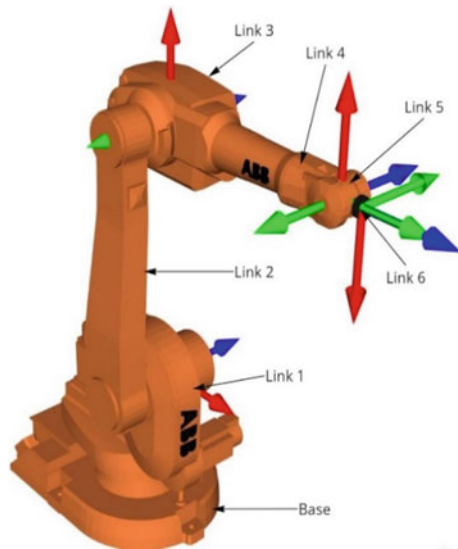
Fig. 2 IRB 1600

Table 1 DH parameters of IRB 1600 industrial robot [15]

Joint/link	θ_i	d_i (mm)	a_i (mm)	α_i (°)	Joint limit (°)
Link 1	θ_1	486.5	150	−90	180 to −180
Link 2	$\theta_2 - 90°$	0	700	0	90 to −90
Link 3	θ_3	0	0	−90	65 to −245
Link 4	θ_4	600	0	90	200 to −200
Link 5	θ_5	0	0	90	115 to −115
Link 6	$\theta_6 + 180°$	65	0	0	400 to −400

Table 1 illustrates the DH parameters consisting of the structural details of joints and links.

The DH table has four parameters describing the mathematical representation of serial chain manipulators.

4 Kinematics

The present section describes the forward kinematics equations for IRB 1600.

$$
{}^{base}_{1}T = \begin{pmatrix} \cos(q_1) & 0 & \cos(q_1) & 0.15*\cos(q_1) \\ \cos(q_1) & 0 & \cos(q_1) & 0.15*\sin(q_1) \\ 0 & -1 & 0 & 0.4865 \\ 0 & 0 & 0 & 1 \end{pmatrix} \tag{1}
$$

$$
{}^{1}_{2}T = \begin{pmatrix} \cos(q_2 - pi/2) & -\sin(q_2 - pi/2) & 0 & 0.7*\cos(q_2 - pi/2) \\ \sin(q_2 - pi/2) & \cos(q_2 - pi/2) & 0 & 0.7*\sin(q_2 - pi/2) \\ 0 & 0 & 1 & 0 \\ 0 & 0 & 0 & 1 \end{pmatrix} \tag{2}
$$

$$
{}^{2}_{3}T = \begin{pmatrix} \cos(q_3) & 0 & -\sin(q_3) & 0 \\ \sin(q_3) & 0 & \cos(q_3) & 0 \\ 0 & -1 & 0 & 0 \\ 0 & 0 & 0 & 1 \end{pmatrix} \tag{3}
$$

$$
{}^{3}_{4}T = \begin{pmatrix} \cos(q_4) & 0 & \sin(q_4) & 0 \\ \sin(q_4) & 0 & -\cos(q_4) & 0 \\ 0 & 1 & 0 & 0.6 \\ 0 & 0 & 0 & 1 \end{pmatrix} \tag{4}
$$

$$
{}^{4}_{5}T = \begin{pmatrix} \cos(q_5) & 0 & -\sin(q_5) & 0 \\ \sin(q_5) & 0 & \cos(q_5) & 0 \\ 0 & -1 & 0 & 0 \\ 0 & 0 & 0 & 1 \end{pmatrix} \tag{5}
$$

$$
{}^{5}_{6}T = \begin{pmatrix} -\cos(q_6) & \sin(q_6) & 0 & 0 \\ -\sin(q_6) & -\cos(q_6) & 0 & 0 \\ 0 & 0 & 1 & 0.065 \\ 0 & 0 & 0 & 1 \end{pmatrix} \tag{6}
$$

The forward or direct kinematics technique uses the homogeneous matrices with the help of DH parameters from Table 1. The simplification of transformation matrix is performed using symbolic math toolbox to arrive at the homogeneous matrices

shown in Eq. (7). The solution to forward or direct kinematics is expressed as

$$
{}^{\text{Base}}_{6}T = \begin{bmatrix} & & & P_x \\ & \text{Orientation} & & P_y \\ & & & P_z \\ 0 & 0 & 0 & 1 \end{bmatrix} \tag{7}
$$

where $[P_x, P_y, P_z]^T$ denote the position of link-6 with reference to base link. Equation (1) is obtained by matrix multiplication from base to link-6 [16]. The other contents of the matrix represent the orientation of link-6.

5 Simulation

Figure 3 shows the home position of IRB 1600 in RobotStudio. The home position refers to the initial configuration of the robot. In this case, the joint angles for the initial configuration are $[0° \ 0° \ 0° \ 0° \ 30° \ 0°]^T$. Equations (8)–(10) are stored in the matrix form shown in Eq. (7). Substituting the joint angles in Eqs. (8)–(10) computes the position of link 6 as $P_x = 806.29$ mm, $P_y = 0$, and $P_z = 1154$ mm. The simulation tools reported similar values, as shown in Figs. 3 and 4.

$$
\begin{aligned}
P_x = {} & 0.15 * \cos(0) - 0.065 * (\sin(\text{pi}/6) * (\sin(0) * \sin(0) \\
& + \cos(0) * (\cos(0) * \cos(-\text{pi}/2) * \cos(0) \\
& - \cos(0) * \sin(-\text{pi}/2) * \sin(0))) + \cdots \\
& + 0.7 * \cos(0) * \cos(-\text{pi}/2)
\end{aligned} \tag{8}
$$

$$
\begin{aligned}
P_y = {} & 0.150 * \sin(0)0.6 * (\cos(\text{pi}/2) * \sin(0) * \sin(0) \\
& + \cos(0) * \sin(0) * \sin(\text{pi}/2)) + 0.065 * (\sin(\text{pi}/6) \\
& * (\cos(0) * \sin(0) + \cdots + \cos(0) * \sin(0) * \sin(-\text{pi}/2))) \\
& + 0.7 * \cos(-\text{pi}/2) * \sin(0)
\end{aligned} \tag{9}
$$

$$
\begin{aligned}
P_Z = {} & 0.4865 - 0.6 * (\cos(-\text{pi}/2) * \cos(0) \sin(\text{pi}/2) \\
& * \sin(0))0.065 * (\cos(\text{pi}/6) * (\cos(\text{pi}/2) * \cos(0) \\
& - \cdots + \cos(0) * \sin(-\text{pi}/2))) - 0.7 * \sin(-\text{pi}/2)
\end{aligned} \tag{10}
$$

RobotStudio database contains various industrial robots. The RobotWare and IRC5 controller should be installed to enable the virtual controller. The RobotStudio is also equipped with RAPID programming and virtual flex pendant functionality, which is helpful to train before working on the actual ABB industrial robot. Figure 3 shows the home position of the IRB 1600 robot and the status of joint values using the
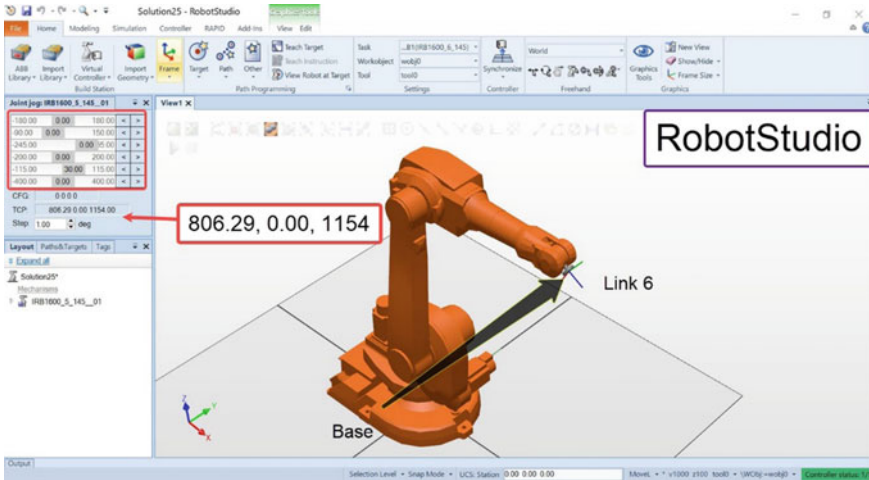
Fig. 3 Home position of IRB 1600 in RobotStudio
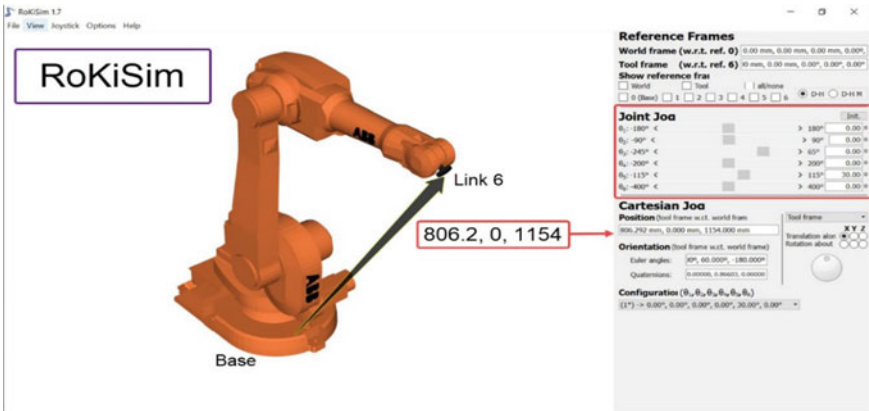

Fig. 4 Home position of IRB 1600 in RoKiSim

joint jog option. The RobotStudio tool is used to validate and correlate the kinematic equations and the pose of IRB 1600.

Figure 4 shows the interface of RoKiSim software. RoKisim is freely available to download from the Web site directly [14]. The software consists of some popular industrial robots from various manufacturers. Figure 4 shows the home position of the ABB IRB 1600, and the position values correlate well with the RobotStudio presented in Fig. 3.

Figures 5 and 6 show the similar pose of IRB 1600 and the position values in the software tools. Furthermore, the simulation is carried out for different joint angles.

Figure 5 shows the position values in virtual flex pendant for joint values [28° −11° −19° 0° 30° 0°]^T.

Similarly, the joint values [28° −11° −19° 0° 30 0°]^T are entered in RoKiSim to cross-check the values obtained in both the softwares. The position of IRB 1600 in RoKiSim is illustrated in Fig. 6. The pose of IRB 1600 is consistent in RoKiSim and RobotStudio.
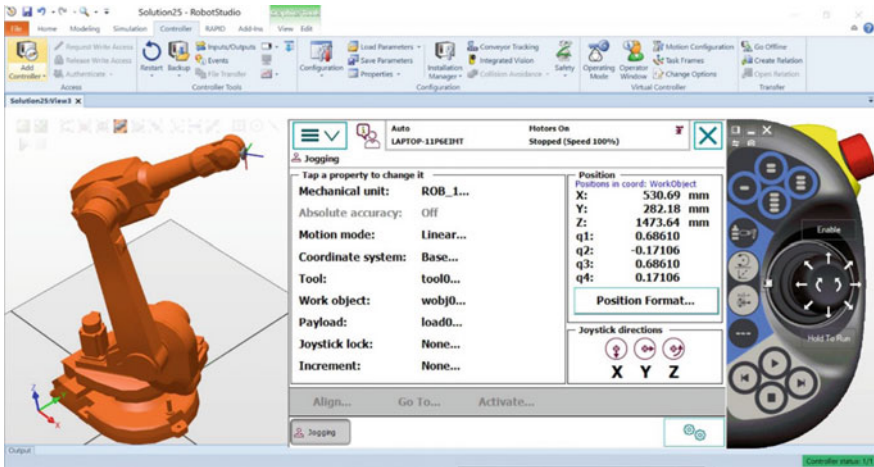

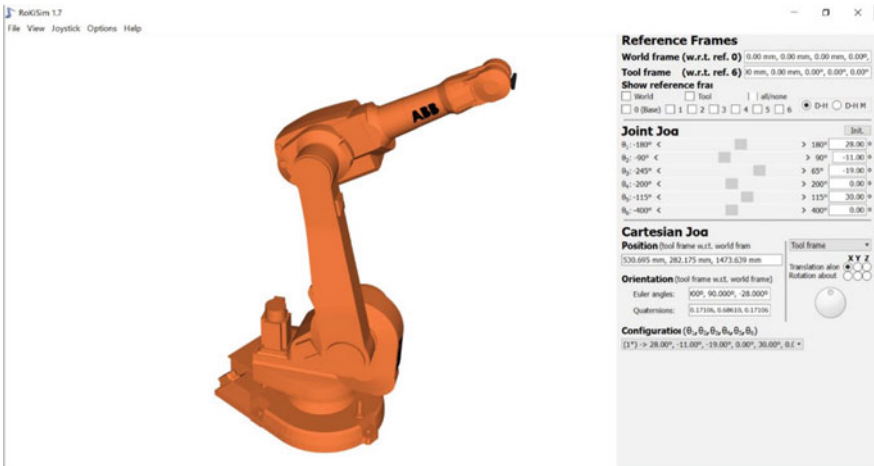**Fig. 5** Position values in flex pendant
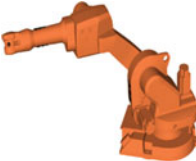
Fig. 6 Position of IRB 1600 in RoKiSim for [28° −11° −19° 0° 30° 0°]^T

Table 2 Position of IRB1600

Joint value	RobotStudio	RoKiSim	Pose
$[0° \ 0° \ 0° \ 0° \ 30° \ 0°]^T$	805.29, 0.0, 1154	806.29, 0.0, 1154	
$[28° \ -11° \ -19° \ 0° \ 30° \ 0°]^T$	530.69, 282.18, 1473.64	530.69, 282.17, 1473.63	
$[-146° \ 46.53° \ -48° \ -68° \ 115° \ -137°]^T$	$-1055.59, -635.55,$ 960.85	$-1054.02, -634.04,$ 960.70	

6　Results and Discussions

This section presents the data obtained from the RobotStudio and RokiSim of the IRB 1600 robot. Table 2 shows the position values and pose for three sets of joint angle vectors carried in RobotStudio and RoKiSim. These values correlate well in both softwares.

7　Conclusion

To sum up, our work shows the simulation process of the industrial robot using the commercially available software known as "RobotStudio" and the free software available directly known as "RoKiSim". The kinematic equations are deduced using MATLAB. Furthermore, the simulations are performed using RoKiSim. Then, simulation data obtained from RoKiSim is validated through RobotStudio. This approach

will be helpful in expanding the growing body of literature in the simulation of industrial robots and enhance our understanding of robot kinematics. The present study has only derived forward or direct kinematic expressions. Further work needs to be carried out to validate the values experimentally.

References

1. Alcácer, V., Cruz-Machado, V.: Scanning the industry 4.0: a literature review on technologies for manufacturing systems. Eng. Sci. Technol. Int. J. **22**, 899–919 (2019). https://doi.org/10.1016/j.jestch.2019.01.006
2. Goel, R., Gupta, P.: Robotics and industry 4.0. Presented at the (2020). https://doi.org/10.1007/978-3-030-14544-6_9
3. Areas, T.: Areas of AICTE Training and Learning (ATAL) Academy FDP's, pp. 2–3
4. Inkulu, A.K., Bahubalendruni, M.V.A.R., Dara, A., SankaranarayanaSamy, K.: Challenges and opportunities in human robot collaboration context of industry 4.0—a state of the art review. Ind. Robot. (2021). https://doi.org/10.1108/IR-04-2021-0077
5. Sabnis, C., Anjana, N., Talli, A., Giriyapur, A.C.: Modelling and simulation of industrial robot using solidworks. In: Rao, Y.V.D., Amarnath, C., Regalla, S.P., Javed, A., Singh, K.K. (eds.) Advances in Industrial Machines and Mechanisms, pp. 173–182. Springer, Singapore (2021)
6. Sadanand, R., Prakash Joshi, R., Chittawadigi, R.G., Saha, S.K., Joshi, R.P., Chittawadigi, R.G., Saha, S.K.: Virtual experiments for integrated teaching and learning of robot mechanics using roboanalyzer. Lect. Notes Mech. Eng. 59–68 (2016). https://doi.org/10.1007/978-81-322-2740-3_7
7. Patwardhan, A., Prakash, A., Chittawadigi, R.G.: Kinematic analysis and development of simulation software for Nex Dexter robotic manipulator. Procedia Comput. Sci. **133**, 660–667 (2018). https://doi.org/10.1016/j.procs.2018.07.101
8. Gupta, V., Chittawadigi, R.G., Saha, S.K.: Robo analyzer: robot visualization software for robot technicians. In: ACM International Conference on Proceeding Series Part F1320, pp. 1–5 (2017). https://doi.org/10.1145/3132446.3134890
9. Othayoth, R.S., Chittawadigi, R.G., Joshi, R.P., Saha, S.K.: Robot kinematics made easy using RoboAnalyzer software. Comput. Appl. Eng. Educ. **25**, 669–680 (2017). https://doi.org/10.1002/cae.21828
10. Corke, P.: MATLAB toolboxes: robotics and vision for students and teachers. IEEE Robot. Autom. Mag. **14**, 16–17 (2007). https://doi.org/10.1109/M-RA.2007.912004
11. Talli, A., Marebal, D.: End-effector position analysis of SCARA robot by using MATLAB. In: Santhosh, K.V., Rao, K.G. (eds.) Smart Sensors Measurements and Instrumentation, pp. 25–33. Springer, Singapore (2021)
12. Talli, A., Marebal, D.: Kinematic analysis and simulation of robotic manipulator based on roboanalyzer. In: Santhosh, K.V., Rao, K.G. (eds.) Smart Sensors Measurements and Instrumentation, pp. 59–69. Springer, Singapore (2021)
13. RobotStudio | ABB Robotics. https://new.abb.com/products/robotics/robotstudio. Accessed 10 Oct 2021.
14. RoKiSim-Robot Kinematics Simulator 1.7. https://www.parallemic.org/RoKiSim.html. Accessed 26 May 2021
15. IRB 1600 | ABB Robotics-Industrial Robots | ABB Robotics. https://new.abb.com/products/robotics/industrial-robots/irb-1600. Accessed 10 Oct 2021
16. Krishnan, M.G., Ashok, S.: Kinematic analysis and validation of an industrial robot manipulator. In: IEEE Region 10 Annual International Conference Proceedings/TENCON 1393–1399 (2019). https://doi.org/10.1109/TENCON.2019.8929712

Mobile Robot Path Planning Using Neuro-Sugeno-Fuzzy Gravitational Technique in a Cluttered Environment

S. Mohanty, Vikas, S. S. Dash, A. K. Behera, D. R. Parhi, and S. K. Pradhan

1 Introduction

Planning of optimum path is a major task for robotic engineers worldwide. Pandey and Parhi [1] in their work used fuzzy wind driven method for path navigation of the robot in both the static and dynamic environment. Parhi et al. [2, 3] used different hybrid techniques towards the path planning objective. They also introduced the different navigational technique for the path planning purpose. The results and experiments were carried in both simulation and experimental platform. Ma et al. [4] used multiple robots for the path navigation in different environments. The work was found to give acceptable results. Deepak et al. [5, 6] use the inverse kinematics for the mobile manipulator. The work gave promising results. Several similar works were done towards the path navigation objectives. Kumar et al. [7, 8] used the sine cosine technique for the path-based navigation in a cluttered environment. Aouf et al. [9] used wheeled-based navigation using the fuzzy algorithm to prevent collision in its path. Lamini et al. [10] used fuzzy-based reinforcement learning leaping algorithm for the navigation of robot. Mohanta et al. [11] used petri-GA algorithm for the path navigation of the mobile robot. Bailey [12] used different extensive techniques for outdoor arena. Murray and Little [13] used stereo-based vision technique for the path navigation of the mobile robots. Bhattacharjee et al. [14] used a similar approach where they used the ABC optimization technique for the navigation. Lidoris et al. [15] used the ACE-based explorer for a highly populated arena. Pandey et al. [16] used

S. Mohanty (✉) · Vikas · S. S. Dash · A. K. Behera · D. R. Parhi
Robotic Laboratory, Mechanical Engineering Department, NIT Rourkela, Rourkela, Odisha 769008, India
e-mail: 1975suranjan@gmail.com

S. K. Pradhan
Robotic Laboratory, Mechanical Engineering Department, CET-Bhubaneshwar, Bhubaneshwar, Odisha 751003, India

different AI technique for navigation of robots. Mataric [17] used a distributed-based model towards the navigational approach. Li et al. [18] used Mecanum-based wheeled robot for the path-based navigation of the robot in different workspace. Leonard and Durrant-Whyte [19] used sonar-based sensing techniques for navigation. Toufan and Niknafs [20] used different approach for the path-based navigation of the robot. The work was done on both the environments. Oriolo et al. [21] used perception-based mobile robot navigation for the navigation purpose. Das et al. [22] used NFSMC-based technique for the robotic navigation. Tiwari et al. [23] used autonomous robot in a dynamic environment towards the path navigation objective. Jeddisaravi et al. [24] used different approach for the path navigation objectives. Nasr et al. [25] used a similar approach towards navigation. Fox et al. [26] used the dynamic window approach for the collision prevention. Chen et al. [27] used a similar approach. Savkin et al. [28] used the safe navigation technique for the locomotion. Chiang et al. [29] used a path guided technique for path optimization. Marques et al. [30] used different sensors for the path navigation in a complex environment. The novelty of this work is that it uses a hybrid method which consists of three algorithms neural, Sugeno-fuzzy, gravitational algorithm for path planning of robot.

2 Fire Bird-V Robot

The fire bird robot is used for the above experiment. It is a mobile robot. The top view and font view are given in Fig. 1. It has two wheels. Its top is circular in shape. In experiment, seven positions of robots are taken. It has 4 DOF robotic arm. The diameter of wheel is 51 mm. Its speed will not exceed 24 cm/s. It can carry 2 kg of load.
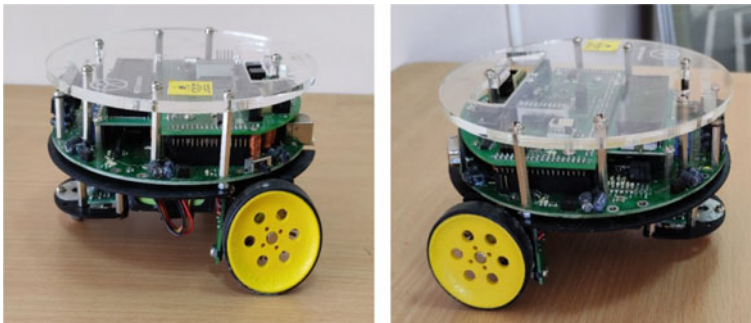

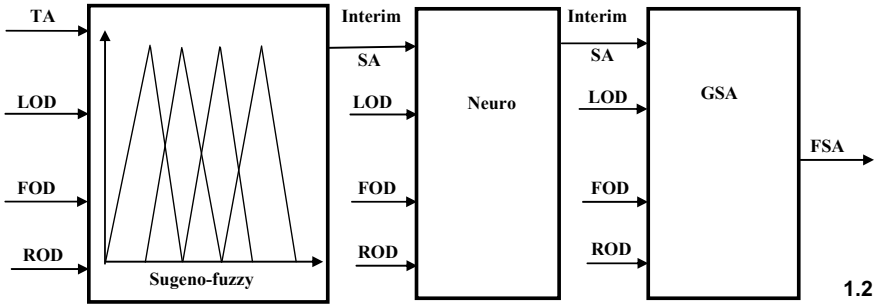**Fig. 1** View of fire bird-V robot

Fig. 2 Neuro-Sugeno-fuzzy gravitational search algorithm

3　Neuro-Sugeno-Fuzzy Gravitational Search Algorithms

Here, neuro-Sugeno-fuzzy-gravitational search method is implemented and analyzed. Various inputs are supplied to Sugeno-fuzzy controller, and accordingly, the output is obtained. There are two interim steering angle outputs from Sugeno-fuzzy section and neuro section. During the analysis essence of Sugeno-fuzzy, neural network and gravitational search algorithm are combined to get the final steering angle from the corresponding input parameters such as FOD, LOD, ROD, and TA. In the Sugeno-fuzzy section, triangular membership functions are used. In the neural section, backpropagation algorithm is used. In gravitational algorithm, the corresponding algorithms are used (Fig. 2).

4　Results and Discussion

The mobile robot used for experiment is fire bird-V robot. Seven experiments have been done using Fire bird-V robot in seven different positions. Seven simulation figures have been drawn showing the exact position of robot in experiment. It has been calculated that the average deviation is within 5.5% between simulation and experimental data. In both the tables, 26 number of exercises have been given (Figs. 3 and 4).

S. No.	Simulation Path (m)	Experimental Path (m)	% deviation	Simulation Time (ms)	Experimental Time (ms)	% error	Simulation Time (ms)
1	3.34	3.52	5.38	40,510	41,583	2.64	40,510
2	3.59	3.87	7.79	43,630	45,854	5.09	43,630
3	9.07	9.65	6.39	112,130	117,567	4.84	112,130
4	5.11	5.36	4.89	62,635	64,367	2.76	62,635
5	4.25	4.52	6.35	51,887	54,013	4.09	51,887

(continued)

(continued)

S. No.	Simulation Path (m)	Experimental Path (m)	% deviation	Simulation Time (ms)	Experimental Time (ms)	% error	Simulation Time (ms)
6	8.07	8.40	4.08	99,630	107,238	7.63	99,630
7	3.09	3.33	7.76	37,387	40,849	9.25	37,387
8	6.21	6.73	8.37	76,385	83,829	9.74	76,385
9	7.27	7.68	5.63	89,635	93,477	4.28	89,635
10	3.23	3.34	4.02	39,135	41,091	4.99	39,135
11	6.48	6.67	2.93	79,780	86,143	7.97	79,780
12	2.16	2.33	7.87	25,780	29,301	1.36	25,780
13	7.78	7.96	2.31	96,010	100,925	5.11	96,010
14	4.88	5.10	4.50	59,760	62,918	5.28	59,760
15	6.28	6.54	4.14	38,135	39,154	2.62	38,135
16	6.48	6.69	3.24	79,780	83,092	4.15	79,780
17	9.37	9.63	2.77	115,889	123,795	6.82	115,889
18	3.48	3.65	4.88	42,260	44,400	5.06	42,260
19	5.20	5.35	2.88	63,780	68,449	7.32	63,780
20	4.79	5.16	7.72	58,635	60,894	3.85	58,635
21	4.24	4.37	3.06	51,780	53,979	4.24	51,780
22	6.83	6.98	2.19	84,135	86,827	3.19	84,135
23	8.32	8.69	4.44	102,780	108,580	5.64	102,780
24	9.26	9.63	3.99	102,760	108,585	5.66	102,760
25	9.31	9.68	3.97	58,630	60,899	3.87	58,630
26	9.36	9.73	3.95	84,130	86,232	2.49	84,130

The given paper represents the path navigation experiment of fire bird-V robot. In this experiment, path length and time taken have been calculated by simulation as well as actual experiment. There is an average deviation about 5.5% between the simulation result and experimental result. This deviation occurred due to two reasons. First reason is that some assumptions have been taken during simulation which are not taken during experiment. The second one is slippage occurs between robot wheels and floor whilst moving.

5 Conclusion

The present work makes use of the neuro-Sugeno-fuzzy-gravitational search method for the path-based navigation. In the present work, the controlling strategy of fire bird-V robot in a crowded environment has been discussed. Here, the different controlling parameters like the front obstacle distance (FOD), left obstacle distance (LOD), and right obstacle distance (ROD) were used as the input parameters, whilst turning angle
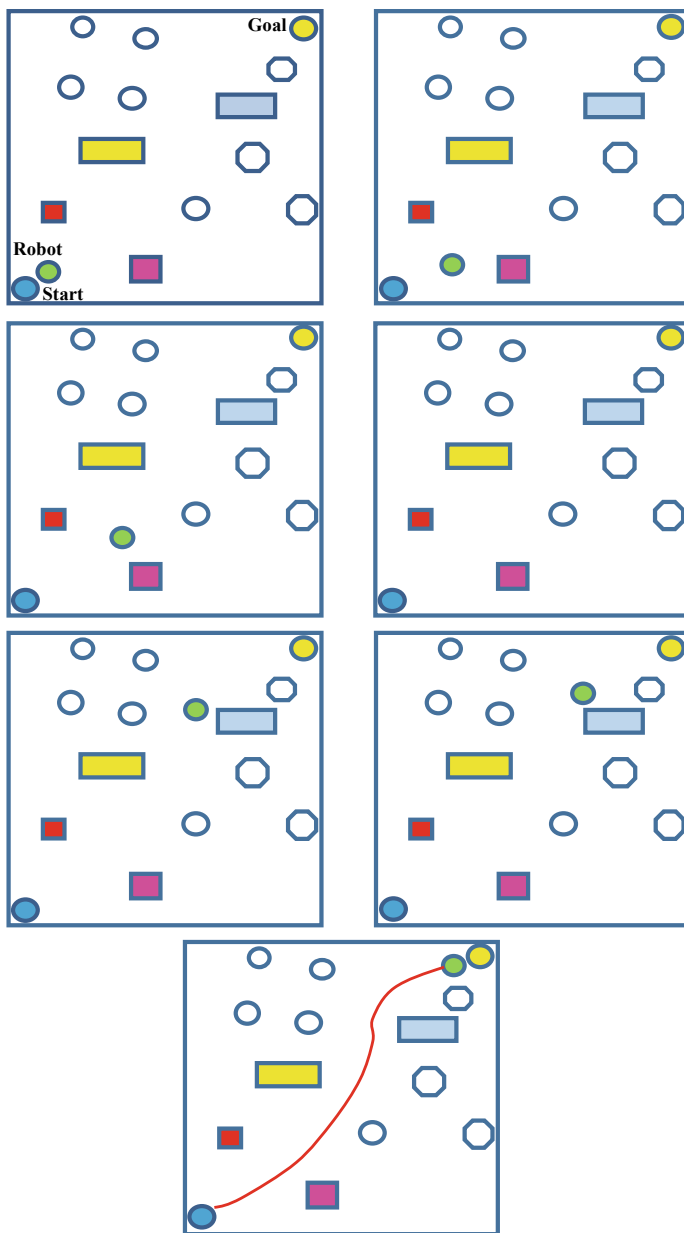
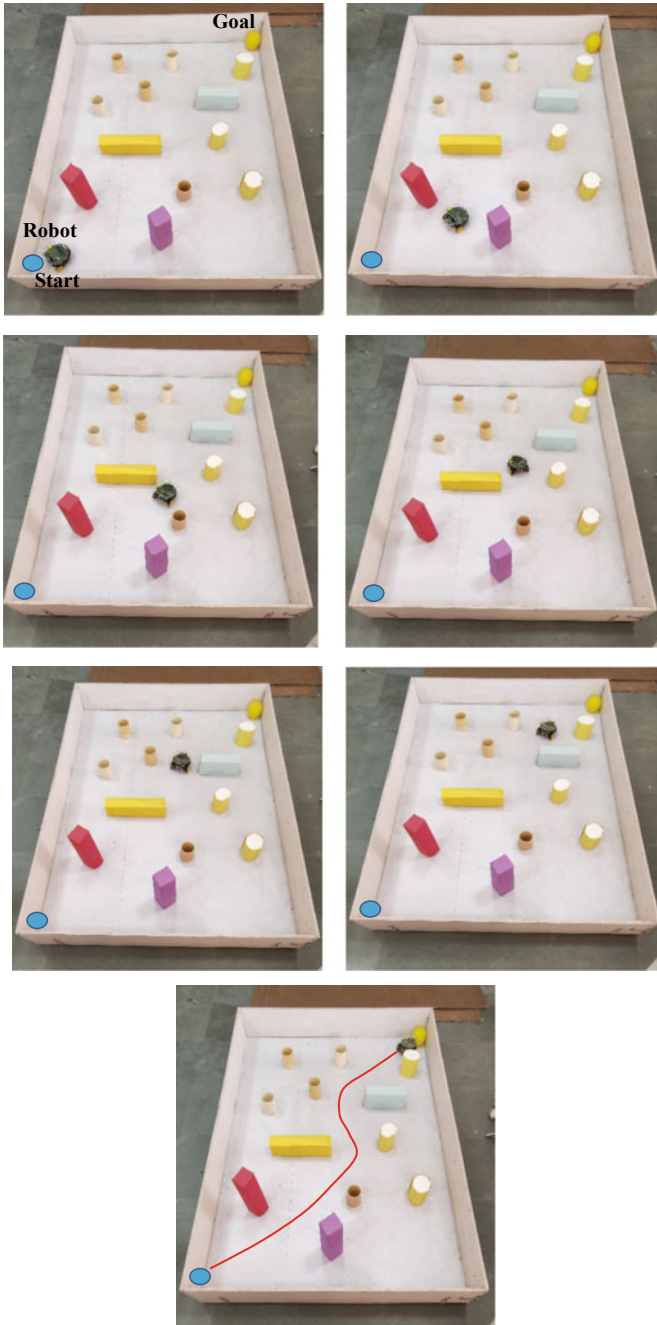**Fig. 3** Simulation-based results

Fig. 4 Experimental-based results

(TA) is the output parameter. Using the above data, final steering angle is obtained. During comparison, the gap between simulation and experimental data is found to be within 5.5%. From above analysis, it is found that developed technique can be used effectively on robot navigation. This technique can be modified in the future for getting more robust navigational techniques.

References

1. Pandey, A., Parhi, D.R.: Optimum path planning of mobile robot in unknown static and dynamic environments using Fuzzy-Wind Driven Optimization algorithm. Defence Technol. **13**(1), 47–58 (2017)
2. Parhi, D.R.K., Kumar, D.A.: Analysis of methodologies applied for diagnosis of fault in vibrating structures. Int. J. Veh. Noise Vib. **5**(4), 271–286 (2009)
3. Parhi, D.R., Singh, M.K.: Navigational strategies of mobile robots: a review. Int. J. Autom. Control **3**(2–3), 114–134 (2009)
4. Ma, J., Liu, Y., Zang, S., Wang, L.: Robot path planning based on genetic algorithm fused with continuous Bezier optimization. Comput. Intell. Neurosci. **2020** (2020)
5. Deepak, B.B.V.L., Parhi, D.R., Amrit, A.: Inverse kinematic models for mobile manipulators. Casp. J. Appl. Sci. Res. **1**(13), 322 (2012)
6. Deepak, B.B.V.L., Parhi, D.R.: Kinematic analysis of wheeled mobile robot. Autom. Syst. Eng. **5**(2), 96–111 (2011)
7. Kumar, S., Parhi, D.R., Kashyap, A.K., Muni, M.K., Dhal, P.R.: Navigational control and path optimization of mobile robot using updated sine–cosine algorithm in obscure environment. In: Current Advances in Mechanical Engineering, pp. 989–996. Springer, Singapore (2021)
8. Kumar, S., Parhi, D.R., Pandey, K.K., Muni, M.K.: Hybrid IWD-GA: an approach for path optimization and control of multiple mobile robot in obscure static and dynamic environments. Robotica **39**, 2033–2060 (2021)
9. Aouf, A., Boussaid, L., Sakly, A.: Same fuzzy logic controller for two-wheeled mobile robot navigation in strange environments. J. Robot. **2019** (2019)
10. Lamini, S.B.C., Fathi, Y., Behlima, S.: A fuzzy path planning system based on a collaborative reinforcement learning. Int. Rev. Autom. Control **10**(2) (2017)
11. Mohanta, J.C., Parhi, D.R., Patel, S.K.: Path planning strategy for autonomous mobile robot navigation using Petri-GA optimisation. Comput. Electr. Eng. **37**(6), 1058–1070 (2011)
12. Bailey, T.: Mobile Robot Localisation and Mapping in Extensive Outdoor Environments. Australian Centre for Field Robotics, Department of Aerospace, Mechanical and Mechatronic Engineering, University of Sydney, Sydney, Australia (2002)
13. Murray, D., Little, J.J.: Using real-time stereo vision for mobile robot navigation. Auton. Robot. **8**(2), 161–171 (2000)
14. Bhattacharjee, P., Rakshit, P., Goswami, I., Konar, A., Nagar, A.K.: Multi-robot path-planning using artificial bee colony optimization algorithm. In: 2011 Third World Congress on Nature and Biologically Inspired Computing (NaBIC), pp. 219–224. IEEE (2011)
15. Lidoris, G., Rohrmuller, F., Wollherr, D., Buss, M.: The Autonomous City Explorer (ACE) project—mobile robot navigation in highly populated urban environments. In: 2009 IEEE International Conference on Robotics and Automation, pp. 1416–1422. IEEE (2009)
16. Pandey, K.K., Pol, M.S., Parhi, D.R.: Using an AI Technique Navigation and Path Planning for Mobile Robot on Webots Platform (2014)
17. Mataric, M.J.: A distributed model for mobile robot environment-learning and navigation (1990)
18. Li, Y., Dai, S., Shi, Y., Zhao, L., Ding, M.: Navigation simulation of a Mecanum wheel mobile robot based on an improved A* algorithm in Unity3D. Sensors **19**(13), 2976 (2019)

19. Leonard, J.J., Durrant-Whyte, H.F.: Directed Sonar Sensing for Mobile Robot Navigation, vol. 175. Springer (2012)
20. Toufan, N., Niknafs, A.: Robot path planning based on laser range finder and novel objective functions in grey wolf optimizer. SN Appl. Sci. **2**(8), 1–19 (2020)
21. Oriolo, G., Ulivi, G., Vendittelli, M.: Fuzzy maps: a new tool for mobile robot perception and planning. J. Robot. Syst. **14**(3), 179–197 (1997)
22. Das, M.S., Samanta, A., Sanyal, S., Mandal, S.: Support value-based NFSMC for wheeled mobile robot path tracking in unknown environments. Wirel. Pers. Commun. **119**, 2991–3011 (2021)
23. Tiwari, A.K., Guha, A., Pandey, A.: Dynamic motion planning for autonomous wheeled robot using minimum fuzzy rule-based controller with avoidance of moving obstacles. Int. J. Innov. Technol. Expl. Eng. **9**(1), 4192–4198 (2019)
24. Jeddisaravi, K., Alitappeh, R.J., Guimarães, F.G.: Multi-objective mobile robot path planning based on A* search. In: 2016 6th International Conference on Computer and Knowledge Engineering (ICCKE), pp. 7–12. IEEE (2016)
25. Nasr, S., Mekki, H., Bouallegue, K.: A multi-scroll chaotic system for a higher coverage path planning of a mobile robot using flatness controller. Chaos Solitons Fractals **118**, 366–375 (2019)
26. Fox, D., Burgard, W., Thrun, S.: The dynamic window approach to collision avoidance. IEEE Robot. Autom. Mag. **4**(1), 23–33 (1997)
27. Chen, W., Wang, N., Liu, X., Yang, C.: VFH* based local path planning for mobile robot. In: 2019 2nd China Symposium on Cognitive Computing and Hybrid Intelligence (CCHI), pp. 18–23. IEEE (2019)
28. Savkin, A.V., Matveev, A.S., Hoy, M., Wang, C.: Safe robot Navigation Among Moving and Steady Obstacles. Butterworth-Heinemann (2015)
29. Chiang, H.T., Malone, N., Lesser, K., Oishi, M., Tapia, L.: Path-guided artificial potential fields with stochastic reachable sets for motion planning in highly dynamic environments. In: 2015 IEEE International Conference on Robotics and Automation (ICRA), pp. 2347–2354. IEEE (2015)
30. Marques, C., Lima, P.: Avoiding obstacles-multisensor navigation for nonholonomic robots in cluttered environments. IEEE Robot. Autom. Mag. **11**(3), 70–82 (2004)

Gravity Search Algorithm-Based Path Planning of Single Humanoid Based on the Study of Different Artificial Intelligence Techniques

Vikas, Dayal R. Parhi, Abhishek K. Kashyap, and B. B. V. L. Deepak

1 Introduction

With the advances towards robotic navigation, path optimization has emerged as a major requirement in the different areas ranging from industries to the medical field and has gained huge popularity worldwide. It has been a topic of research with greater improvement towards optimization for path optimization of the robots. Different artificial intelligent techniques have paved a way for a more optimum path planning navigation of the humanoids. The present work discusses the different classical and reactive approaches used by the different researchers towards the path planning of robots. The tabular representation shows the effectiveness of the different path planning approaches and how they can be used as per the different environmental scenarios. The tabular representation shows the effectiveness of the different path planning approaches and how they can be used as per the different environmental scenarios (Fig. 1).

Kumar et al. [1] in their work used the reactive path planning approach, i.e. linear regression model and merged it with the classical approach (AACO) to obtain the optimum path planning results. Huang et al. [2] have been carried out where the distance of the obstacle from the front (called FOD), from left (called LOD) and from the right (called ROD) are considered as the inputs and based on these input parameters, the output (turning angle (TA)) is obtained. Kashyap et al. [3] used different hybrid techniques towards humanoid navigation in a cluttered space. They found that the use of hybridized methods provides more accurate results as far as the optimum path planning is concerned. Parhi et al. [4] and Mohanty and Parhi [5] have used the hybrid controller for humanoid navigation in complex unknown terrain. Guo

Vikas (✉) · D. R. Parhi · A. K. Kashyap · B. B. V. L. Deepak
Robotics Laboratory, Mechanical Engineering Department, NIT Rourkela, Rourkela, Odisha 769008, India
e-mail: vikaspce2k8@gmail.com

Fig. 1 Different path planning approaches [1]
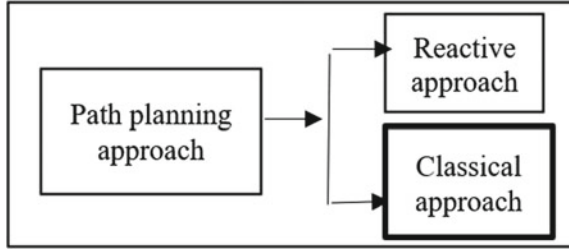
et al. [6] used a neural network along with the deep learning technique to design an intelligent controller for the path optimization of different terrains. The simulation and experimental results were then compared and were within the acceptance limit. Several similar works [7, 8] were carried out towards the path planning of humanoids in a different environment.

2 Different Navigational Techniques for Humanoid Navigation

2.1 Classical Approach

Linear Regression Model

The method is a widely known forecasting method. Linear regression [9] is a statistical attempt to model the independent variable in terms of the dependent variables using linear fitting. The independent variable is often called the explanatory variable and does not directly depend upon the dependent variables. The general equation for the simple regression technique follows as:

$$y_j = \alpha + \beta x_j + e, \tag{1}$$

where, $j = 1,2,3\ldots$

The controller based on the above approach is designed using the input parameters to obtain the output for the humanoid. A set of training patterns is set for the humanoids depending upon the environment and accordingly, the turning angle is found. The higher the training patterns, the higher will be the convergence. As soon as the humanoid senses an obstacle within its threshold distance, the RA-based controller gets activated and based upon the training pattern calculates the turning angle. Zhang et al. [10] used the regression-based model in their work. Zhao et al. [11] used a similar approach for a mobile robot.

Fig. 2 Steps for PSO [15]
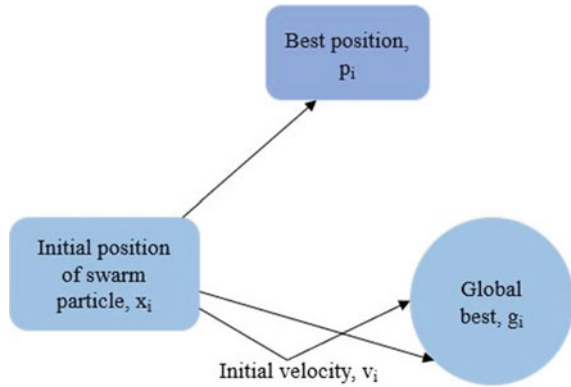
2.2 Reactive Approach

Particle Swarm Optimization

The technique was introduced by Kennedy and Eberhart [12] in 1995. The swarm intelligent technique is an outcome of the collective behaviour of social insect colonies and other animal colonies. Here, the particle in the population occupies a position and velocity within the space, which they adjust to attain the goal. The particles of the swarm memorize the best location identified by it and communicate the information regarding the same (Fig. 2).

The method is used extensively towards the path planning of the humanoid. Deepak et al. [13, 14] in their paper worked towards the navigation of mobile robots using the PSO approach. They used it to improve upon the fitness function by focusing more on the shortest distance approach for robotic navigation. Similar hybrid-based work was done. Sahu et al. [15] in their work used the above controller for intelligent path navigation. The work was carried out on both the platform and used the distance from the obstacle as the governing input parameter to calculate the output. Rossides et al. [16] used the above technique for dynamic stability. The work was more focused on stability during the path planning. Ajeil et al. [17] used a multi-hybrid technique where different techniques were merged towards path optimization of mobile robots in difficult terrain.

Genetic Algorithm

The GA [18] is a heuristic approach inspired by Charles Darwin's theory of natural evaluation. Being a natural selection approach, the fittest among the individuals are identified to help the decision-making. Here, the offspring inherits the characteristics of the parents depending upon the fitness of the parent, the offspring will be more fit with a larger chance of survival. The process iterates continuously till the best optimal result is achieved. Batle et al. [19] in their paper applied GA for the path navigation of the mobile robot in complex terrain. They used the matrix-based genetic algorithm in both platforms to test for the best optimum path of travel. Tsai et al. [20] used

the genetic approach towards the path navigation of robots. Davies and Jnifene [21] used a similar approach. Rath et al. [22, 23] also used a similar approach.

3 Implementation of Gravitational Search Algorithm (GSA) Towards Path Planning

The method [24] is a heuristic technique that shares a resemblance with the swarm intelligent technique. Li et al. [25] used the above method for path navigation. Das et al. [26, 27] used a similar approach towards path navigation objectives. GSA being a gravity-based optimization technique is based upon the law of gravity with performance evaluated based on the masses. The GSA-based optimization technique makes use of the movement of the agent in population size. The mass of any jth particle of the population is represented as:

$$m_j(t) = \frac{\mathrm{fit}_j(t) - \mathrm{worst}(t)}{\mathrm{best}(t) - \mathrm{worst}(t)} \tag{2}$$

$$M_j(t) = \frac{m_j(t)}{\sum_{j=1}^{N} m_j(t)}, \tag{3}$$

where N is the population size, $\mathrm{fit}_j(t)$ represents the fitness at a particular time instant, worst (t) represents the worst fitness function and best (t) is the best fitness function. The objective is to minimize the distance of humanoid from the source to the destination, so the objective is a minimization problem:

$$\mathrm{worst}(t) = \mathrm{maxfit}_j(t), \ \mathrm{best}(t) = \mathrm{minfit}_j(t) \tag{4}$$

The agent's position from a set of the population can be described as:
$X_j(t) = \left(X_j^1(t), ..., X_j^e(t), ..., X_j^m(t) \right)$, where $X_j^m(t)$ represents the position of the jth agent in m-dimensional space.

The velocity of the agent is:

$$v_j^e(t) = r.v_j^e(t-1) + a_j^e(t-1), \tag{5}$$

where r is the random variable in intervals 0 to 1 and a_j^e is the acceleration of the jth particle in e-dimensional space.

The force acting by the agent in the population is given as:

$$F_j^e(t) = \sum_{i=1, j \neq i}^{N} r.F_{j,i}^e(t) = G(t) \cdot \frac{M_{\mathrm{p},j}(t) M_{\mathrm{a},i}(t)}{E_{j,i}(t) + c_1} \left[X_j^e(t) - X_i^e(t) \right] \tag{6}$$

where, $C1$ is a constant, $G(t)$ is gravitational constant, $M_{a,i}(t)$ and $M_{p,j}(t)$ is the active and passive gravitational mass. The Euclidean distance between any two agents:

$$E_{j,i}(t) = \sqrt{\sum_{e=1}^{q}\left[X_j^e(t) - X_i^e(t)\right]} \tag{7}$$

The position and velocity are further updated as: $X_j^e(t) = X_j^e(t-1) + v_j^e(t)$
The steps for GSA are mentioned below:

Step 1: Initialize the population.
Step 2: Evaluate the fitness of the agent.
Step 3: Update the global best and worst population.
Step 4: Calculate the mass and acceleration of the agent.
Step 5: Update the velocity and acceleration.
Step 6: Iterate from step 2.
Step 7: End.

The robot used for our research is a humanoid Nao v4.0 robot, which can mimic the human-like behaviour for smooth locomotion. Developed by the Aldebaran group, France, the humanoid is an autonomous programmable medium-sized robot. Nao has 25 degrees of freedom (DOF) and various sensors fitted for obstacle avoidance. The work took 3–4 months to obtain the results (Fig. 3).

The controller is designed using the GSA algorithm and path optimization is carried out in the unknown environment. As soon as the humanoid senses an obstacle, the controller gets activated. The threshold distance for the humanoid is set as 30 cm. During the entire navigation, the robot targets the goal and the controller is designed to keep the distance to be minimum and hence achieve the shortest path of travel. The arena was chosen as 200×250 cm^2 and obstacles were located at different locations. The red ball indicates the source and the green ball indicates the goal for the navigation of the humanoid (Fig. 4).

In comparison with the different methods discussed earlier, it was found from the literature survey [1, 28] that the classical approach in itself needs a large training to achieve a good result. Moreover, the designed controller is advantageous over the PSO-based algorithm [24] as it is capable of avoiding local traps. The work can be further extended towards the use of different hybrid techniques with simultaneous focus on stability (Table 1).

4 Conclusion

Based on the different path planning approaches carried out for humanoid navigation, the following conclusions are obtained.

(a)   (b)

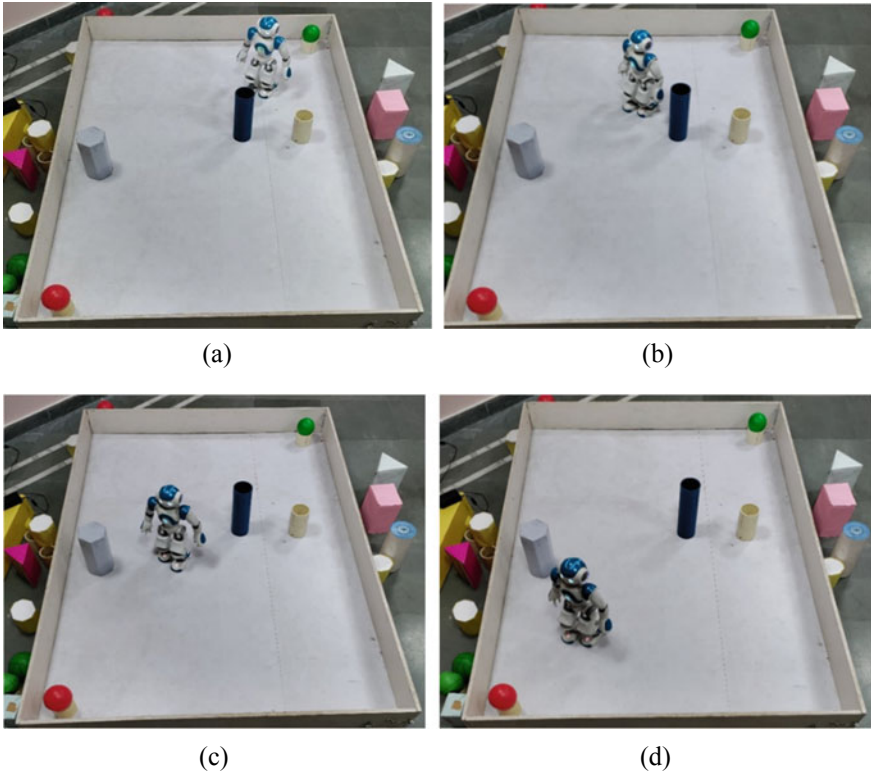(c)   (d)

Fig.3 Humanoid navigation in a real-time environment

1. The majority of researches are carried out using reactive optimization techniques, as they are not environmental specific and decisions can be made using the controllers themselves without any specific training pattern.
2. The designed controller was implemented for a single humanoid and the experimental and simulation results were found very close to one another.
3. The percentage error in both the simulation and experimental platforms was very less (less than 5%) and is within the acceptable limits.
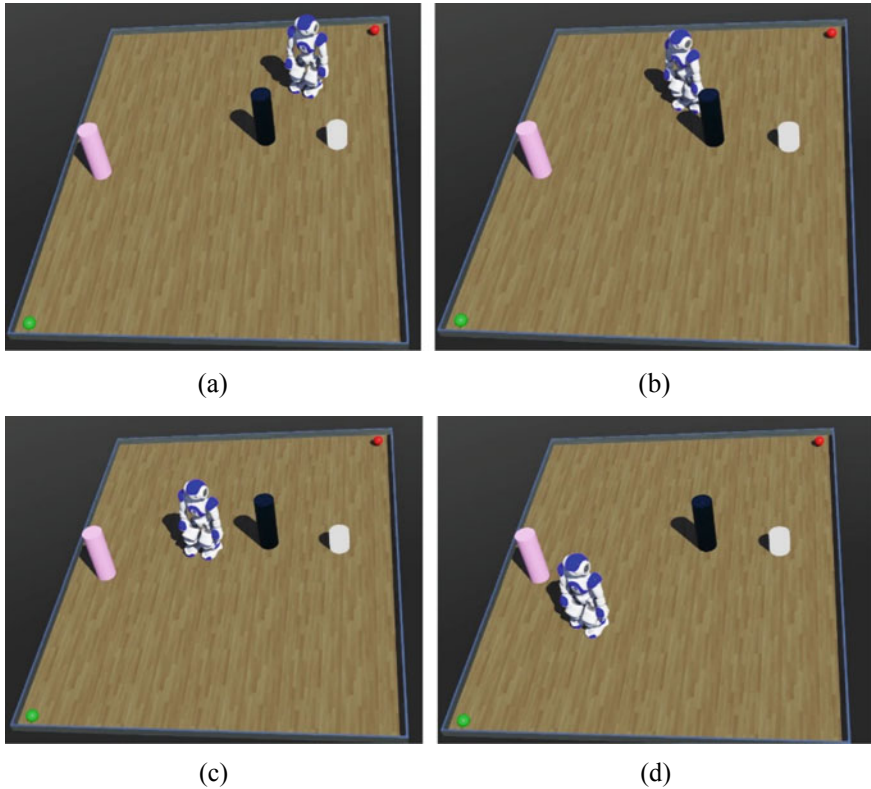
(a)

(b)

(c)

(d)

Fig. 4 Humanoid navigation in WEBOT simulation environment

Table 1 Experimental and simulation results for single humanoid navigation

Number of runs	Experimental		Simulation		% Error in path length	% Error in time
	Length of path (cm)	Time taken (s)	Length of path (cm)	Time taken (s)		
1	306.1	38.1	292.1	36.1	4.57	5.25
2	307.2	38	291.2	35.8	5.20	5.79
3	304.2	36.90	288.9	35.3	5.03	4.33
4	306.1	38.21	290.2	36.2	5.19	5.26
5	306.4	36.8	289.3	34.36	5.58	6.63

References

1. Kumar, P.B., Sahu, C., Parhi, D.R.: A hybridized regression-adaptive ant colony optimization approach for navigation of humanoids in a cluttered environment. Appl. Soft Comput. **68**, 565–585 (2018). https://doi.org/10.1016/j.asoc.2018.04.023

2. Huang, H.C., Tsai, C.C.: Global path planning for autonomous robot navigation using hybrid metaheuristic GA-PSO algorithm. In: SICE Annual Conference 2011, pp. 1338–1343. IEEE (2011)

3. Kashyap, A.K., Parhi, D.R., Kumar, S., Pandey, A., Muni, M.K., Ranjan Dhal, P.: Safe navigation of humanoid robot in cluttered terrain using ant lion optimizer tuned RA approach. In: Current Advances in Mechanical Engineering, pp. 997–1006. Springer, Singapore (2021). https://doi.org/10.1007/978-981-33-4795-3_92

4. Parhi, D.R., Sahu, C., Kumar, P.B.: Navigation of multiple humanoid robots using hybrid adaptive swarm-adaptive ant colony optimization technique. Comput. Animation Virtual Worlds **29**(2), e1802 (2018). https://doi.org/10.1002/cav.1802

5. Mohanty, P.K., Parhi, D.R.: Navigation of autonomous mobile robot using adaptive network based fuzzy inference system. J. Mech. Sci. Technol. **28**(7), 2861–2868 (2014). https://doi.org/10.1007/978-81-322-1665-0_50

6. Guo, N., Li, C., Gao, T., Liu, G., Li, Y., Wang, D.: A fusion method of local path planning for mobile robots based on LSTM neural network and reinforcement learning. Math. Probl. Eng. (2021)

7. Yang, S.X., Luo, C.: A neural network approach to complete coverage path planning. IEEE Trans. Syst. Man Cybern. Part B (Cybernetics) **34**(1), 718–724 (2004). https://doi.org/10.1109/TSMCB.2003.811769

8. Lingelbach, F.: Path planning using probabilistic cell decomposition. In: IEEE International Conference on Robotics and Automation, 2004. Proceedings. ICRA'04, vol. 1, pp. 467–472. IEEE (2004). https://doi.org/10.1109/ROBOT.2004.1307193

9. Aalen, O.O.: A linear regression model for the analysis of life times. Stat. Med. **8**(8), 907–925 (1989)

10. Zhang, J., Li, J., Yang, H., Feng, X., Sun, G.: Complex environment path planning for unmanned aerial vehicles. Sensors **21**(15), 5250 (2021)

11. Zhao, L., Putman, J., Wang, W., Balkcom, D.: PLRC*: a piecewise linear regression complex for approximating optimal robot motion. In: 2020 IEEE/RSJ International Conference on Intelligent Robots and Systems (IROS), pp. 6681–6688. IEEE (2020)

12. Kennedy, J., Eberhart, R.: Particle swarm optimization. In: Proceedings of ICNN'95—International Conference on Neural Networks, vol. 4, pp. 1942–1948. IEEE (1995)

13. Deepak, B.B.V.L., Parhi, D.R., Raju, B.M.V.A.: Advance particle swarm optimization-based navigational controller for mobile robot. Arab. J. Sci. Eng. **39**(8), 6477–6487 (2014). https://doi.org/10.1007/s13369-014-1154-z

14. Deepak, B.B.V.L., Parhi, D.R., Kundu, S.: Innate immune based path planner of an autonomous mobile robot. Procedia Eng. **38**, 2663–2671 (2012)

15. Sahu, C., Kumar, P.B., Parhi, D.R.: An intelligent path planning approach for humanoid robots using adaptive particle swarm optimization. Int. J. Artif. Intell. Tools **27**(05), 1850015 (2018). https://doi.org/10.1142/S021821301850015X

16. Rossides, G., Metcalfe, B., Hunter, A.: Particle swarm optimization—an adaptation for the control of robotic swarms. Robotics **10**(2), 58 (2021)

17. Ajeil, F.H., Ibraheem, I.K., Sahib, M.A., Humaidi, A.J.: Multi-objective path planning of an autonomous mobile robot using hybrid PSO-MFB optimization algorithm. Appl. Soft Comput. **89**, 106076 (2020)

18. Goldberg, D.E., Samtani, M.P.: Engineering optimization via genetic algorithm. In: Electronic Computation, pp. 471–482. ASCE (1986)

19. Patle, B.K., Parhi, D.R.K., Jagadeesh, A., Kashyap, S.K.: Matrix-binary codes based genetic algorithm for path planning of mobile robot. Comput. Electr. Eng. **67**, 708–728 (2018). https://doi.org/10.1016/j.compeleceng.2017.12.011

20. Tsai, C.-C., Huang, H.-C., Chan, C.-K.: Parallel elite genetic algorithm and its application to global path planning for autonomous robot navigation. IEEE Trans. Industr. Electron. **58**(10), 4813–4821 (2011). https://doi.org/10.1109/TIE.2011.2109332

21. Davies, T., Jnifene, A.: Multiple waypoint path planning for a mobile robot using genetic algorithms. In: IEEE International Conference on Computational Intelligence for Measurement Systems and Applications, pp. 21–26 (2006). https://doi.org/10.1109/CIMSA.2006.250741

22. Rath, A.K., Parhi, D.R., Das, H.C., Kumar, P.B., Muni, M.K., Salony, K.: Path optimization for navigation of a humanoid robot using hybridized fuzzy-genetic algorithm. Int. J. Intell. Unmanned Syst. (2019). https://doi.org/10.1108/IJIUS-11-2018-0032
23. Rath, A.K., Parhi, D.R., Das, H.C., Kumar, P.B., Mahto, M.K.: Design of a hybrid controller using genetic algorithm and neural network for path planning of a humanoid robot. Int. J. Intell. Unmanned Syst. (2020). https://doi.org/10.1108/IJIUS-10-2019-0059
24. Rashedi, E., Nezamabadi-Pour, H., Saryazdi, S.: GSA: a gravitational search algorithm. Inf. Sci. **179**(13), 2232–2248 (2009)
25. Li, P., Duan, H.: Path planning of unmanned aerial vehicle based on improved gravitational search algorithm. Sci. China Technol. Sci. **55**(10), 2712–2719 (2012)
26. Das, P.K., Behera, H.S., Jena, P.K., Panigrahi, B.K.: Multi-robot path planning in a dynamic environment using improved gravitational search algorithm. J. Electr. Syst. Inf. Technol. **3**(2), 295–313 (2016)
27. Das, P.K., Behera, H.S., Panigrahi, B.K.: A hybridization of an improved particle swarm optimization and gravitational search algorithm for multi-robot path planning. Swarm Evol. Comput. **28**, 14–28 (2016)
28. Kumar, A., Kumar, P.B., Parhi, D.R.: Intelligent navigation of humanoids in cluttered environments using regression analysis and genetic algorithm. Arab. J. Sci. Eng. (Springer Science & Business Media BV) **43**(12) (2018)

Inverse Kinematic Solution for 6-R Industrial Robot Manipulator Using Convolution Neural Network

Hare Shankar Kumhar [ID] **and Vikas Kukshal** [ID]

1 Introduction

A robot manipulator, also known as an industrial robot, is a continuous system made up of several joints driven by actuators. Forward kinematic equations with trigonometric terms can be used in robotics to define the location of the end effector in Cartesian space [1]. Whereas the inverse kinematics deals with the end effector positions connected to joint locations, as well as its many configurations [2]. The inverse kinematics solution is a transformation between position, orientation, and joint variables used in robot motion analysis, off-line programming, trajectory planning, and other applications [3]. Furthermore, inverse kinematics solutions for a redundant robot are infinite. Redundant manipulators (RMs) are widely employed in various industries, including industrial and agricultural production, equipment manufacture, and surgical operations [4]. As a result, various artificial optimization techniques like CNN, particle swarm optimization (PSO), artificial bee colony technique, and firefly technique [5] are the best fit for the problem. The solution to forward and backward kinematic problem is required every time when a robot's manipulator is employed in industries for a specific purpose (modeling, simulation, control, etc.). The tolerances provided while manufacturing or assembly of a robot manipulator are rectified through calibration. For a particular robot geometry, calibration is always unique and operates similar to a system identification procedure. It entails either fixed well-known references in the robot's workspace or a precise measurement system that provides information about the end–effector's pose [6].

A robotic arm with more than two links will need complex trigonometric equations for the calculation. Hence, the geometric techniques are best suited for finding

H. S. Kumhar (✉) · V. Kukshal
Department of Mechanical Engineering, National Institute of Technology Uttarakhand, Srinagar, (Garhwal) 246174, India
e-mail: mt20mec001@nituk.ac.in

solutions related to robotic arms with fewer degrees of freedom. Numerical and geometrical methods are used in iterative techniques in a repeated manner until the model achieves the desired output level. These techniques have several advantages, including the ability of converging into a single solution which is independent of the starting location and the ease with which a high-DOF robotic arm model may be implemented [7]. For example, the inverse kinematics problem of planar serial revolute manipulators was solved using workspace density derived from Fourier transforms and convolution theorems [8].

A CNN can be said as a computer programming system that replicates the neurological structure and function of a human. It commonly utilizes machine learning and artificial intelligence. In the current scenario, the neural network is the most widely utilized machine learning tool. Its technique trains a neural network to find the intrinsic patterns present in the data which is under inquiry by simulating the working of a human brain. The operating idea of a neural network involves learning from prior data sets, such as the input training data set, and then utilize provided testing data set to determine if the system is effective or not [9]. The inverse kinematics problem of a robotic manipulator is very complex and cannot be simulated in most mathematical models. So, the neural network seems to be a promising alternative because of its accuracy and adaptability of changes [10].

Many studies are reported related to inverse kinematics problems using CNN because of its capacity to learn non-linear algebraic as well as complex trigonometric equations. The manipulator is given random joint angles as input within a preset range for each joint. The manipulator goes to a location based on the joint space co-ordinate when a random joint angle is supplied. The data set is created using this information (joint angle and corresponding location). When the training of the network is done with the data set, then for any position and orientation of end effector, the required angles of joint may be calculated by solving the inverse kinematics equations [11].

There is not any research work done in the past literature about inverse kinematic solution for PUMA 700 series industrial robot manipulator. Using CNN for inverse kinematic solution of this robot makes this research work novel in its kind. This present research work is organized in a manner that it contains the analysis for inverse kinematics of 6-R robot manipulator. Further, it provides CNN model-based inverse kinematics solution and the data set generation. The result obtained is analyzed to determine the overall regression values.

2 Inverse Kinematics Analysis

The inverse kinematics deals with the situation where the position and orientation of the end effector are known, and the corresponding joint angles are required to reach that position. For this analysis, Denavit—Hartenberg (D–H) parameters are very important. The D–H parameters generally describe various joint variables and link parameters. In order to find the D–H parameters, the Eq. (1) needed to be solved for required conditions.

Table 1 The D–H parameters of PUMA 700 series robot manipulator

Link	Link length a_i [m]	Angle of link twist (α_i) [deg]	Offset of link (d_i) [m]	Joint angles (ξ_i) [deg]	Joint angle range [deg]
1	0	−90	0	90	−160 to 160
2	650	0	0.19	0	−110 to 110
3	85	+90	0	90	−135 to 135
4	0	−90	0.6	0	−266 to 266
5	0	+90	0	0	−100 to 100
6	0	0	0.125	0	−300 to 300

$$
\begin{aligned}
{}^{i-1}_{i}T &= T(d_i)T_z(\xi_i)T_x(a_i)T_x(\alpha_i) \\
&= \begin{bmatrix}
\cos\xi_i & -\sin\xi_i & 0 & a_{i-1} \\
\sin\xi_i\cos\alpha_{i-1} & \cos\alpha_{i-1}\cos\xi_i & -\sin\alpha_{i-1} & -d_i\sin\alpha_{i-1} \\
\sin\xi_i\sin\alpha_{i-1} & \cos\xi_i\sin\alpha_{i-1} & \cos\alpha_{i-1} & d_i\cos\alpha_{i-1} \\
0 & 0 & 0 & 1
\end{bmatrix}
\end{aligned} \tag{1}
$$

where ${}^{i-1}_{i}T$ represents the homogenous transformation matrix, α_{i-1} are the angles of rotation and a_{i-1} are the translation from x_{i-1} axis, d_i are the translation and ξ_{i-1} are the rotation about Z_{i-1} axis. The following equation expresses the forward kinematics of the robot manipulator:

$$
{}^{0}_{1}T(\xi_1){}^{1}_{2}T(\xi_2){}^{2}_{3}T(\xi_3){}^{3}_{4}T(\xi_4){}^{4}_{5}T(\xi_5){}^{5}_{6}T(\xi_6) = T_{\text{end}} \tag{2}
$$

where T_{end} is the configuration of end effector relative to the base frame.

In the case of inverse kinematic problem, T_{end} is known, and there is the need to calculate the joint angles (ξ_i) [12]. The D–H parameters for the PUMA 700 series robot manipulator are mentioned in Table 1. Using these parameters, various joint angles can be found for a desired end effector's position.

Now using Eq. (1) and the D–H parameters, ${}^{i-1}_{i}T$ can be calculated as follows:

$$
T_{01} = \begin{bmatrix}
\cos(\xi_1) & -\sin(\xi_1) & 0 & 0 \\
\sin(\xi_1) & \cos(\xi_1) & 0 & 0 \\
0 & 0 & 1 & 0 \\
0 & 0 & 0 & 1
\end{bmatrix} \tag{3}
$$

$$
T_{12} = \begin{bmatrix}
\cos(\xi_2) & -\sin(\xi_2) & 0 & 0 \\
0 & 0 & -1 & -0.19 \\
\sin(\xi_2) & \cos(\xi_2) & 0 & 0 \\
0 & 0 & 0 & 1
\end{bmatrix} \tag{4}
$$

$$T_{23} = \begin{bmatrix} \cos(\xi_3) & -\sin(\xi_3) & 0 & 0.65 \\ 0 & 0 & 1 & 0.6 \\ -\sin(\xi_3) & -\cos(\xi_3) & 0 & 0 \\ 0 & 0 & 0 & 1 \end{bmatrix} \tag{5}$$

$$T_{34} = \begin{bmatrix} \cos(\xi_4) & -\sin(\xi_4) & 0 & 0.085 \\ \sin(\xi_4) & \cos(\xi_4) & 0 & 0 \\ 0 & 0 & 1 & 0 \\ 0 & 0 & 0 & 1 \end{bmatrix} \tag{6}$$

$$T_{45} = \begin{bmatrix} \cos(\xi_5) & -\sin(\xi_5) & 0 & 0 \\ \sin(\xi_5) & \cos(\xi_5) & 0 & 0 \\ 0 & 0 & 1 & 0 \\ 0 & 0 & 0 & 1 \end{bmatrix} \tag{7}$$

$$T_{56} = \begin{bmatrix} \cos(\xi_6) & -\sin(\xi_6) & 0 & 0 \\ 0 & 0 & 1 & 0.125 \\ -\sin(\xi_6) & -\cos(\xi_6) & 0 & 0 \\ 0 & 0 & 0 & 1 \end{bmatrix} \tag{8}$$

The configuration of the end effector for a 6-DOF manipulator with respect to the base is given by

$$^0_6T = \begin{bmatrix} r_{11} & r_{12} & r_{13} & p_x \\ r_{21} & r_{22} & r_{23} & p_y \\ r_{31} & r_{32} & r_{33} & p_z \\ 0 & 0 & 0 & 1 \end{bmatrix} \tag{9}$$

where r_{ij} are the different directional rotational elements and p_x, p_y, and p_z are the position vector elements.

3   Data Set Generation and CNN Model

The robot manipulator's starting position was set to origin of the co-ordinate system, i.e., all joint angles are zero. Then, different values of all parameters $[r_{11}, r_{12}, r_{13}, r_{21}, r_{22}, r_{23}, r_{31}, r_{32}, r_{33}, p_x, p_y, p_z]$ were calculated using forward kinematics Eq. (9) for various joint angles. Using these forward kinematics equations, the required data set is generated. These data were utilized for training, validating, and testing the neural network.

After the data set generation, a CNN model is required for the analysis of inverse kinematics. CNN is composed of various convolutional layers, pooling layers, and hidden layers. It acts like a human brain's network in terms of processing various
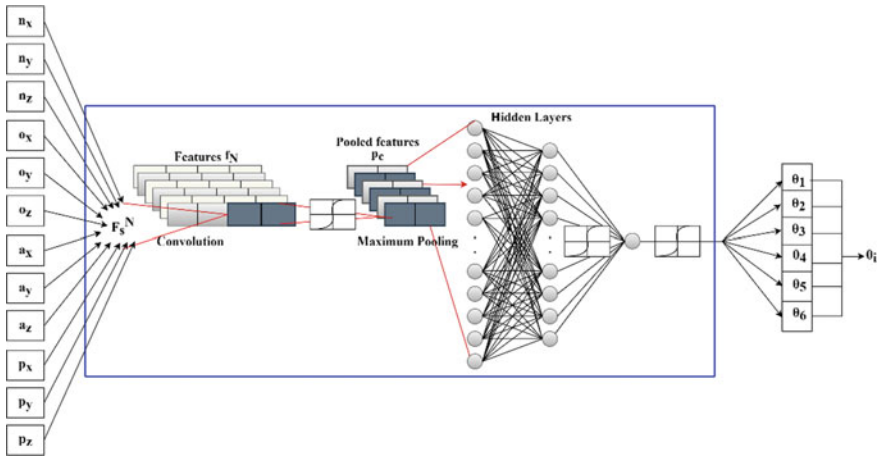
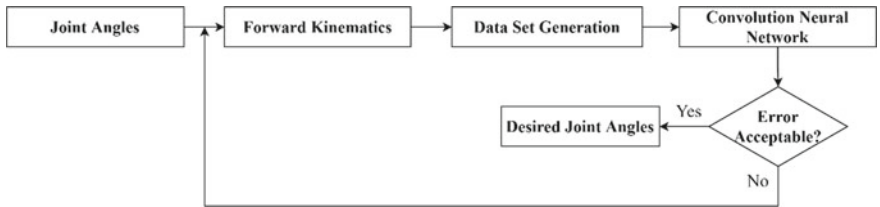**Fig. 1** Structural representation of convolution neural network

Fig. 2 Workflow diagram for the process of the neural network

information, establishment of model, etc. The network consists of a huge number of joints called the nodes in connection with each other. A particular output function is represented by each node. This function is called the activation function. A weighted value of the passing signals through the connection is represented by each connection between the nodes. This can be compared as the memory of the network [13]. Figure 1 is a structural representation of a CNN for the solution of inverse kinematics model. The neural network is designed with 12 input and 6 output nodes containing 10 hidden layers in between them.

This process is iterative in nature which contains various steps. The workflow of this study is shown in Fig. 2.

4 Results and Discussion

In this study, the training of the CNN is done using input data set, and after validation and testing, various regression plots are analyzed. While verifying the neural network,

the total error, E, is calculated using the Eq. (10) and minimized for better regression value.

$$E = \sqrt{(\xi_1^* - \xi_1)^2 + (\xi_2^* - \xi_2)^2 + (\xi_3^* - \xi_3)^2 + (\xi_4^* - \xi_4)^2 + (\xi_5^* - \xi_5)^2 + (\xi_6^* - \xi_6)^2} \quad (10)$$

where ξ_i^* are target values and ξ_i are output values. After the training, validation, and testing of the network, the following results for the joint angles $\xi_1, \xi_2, \xi_3, \xi_4, \xi_5$, and ξ_6 are obtained as presented in Figs. 3 and 4.

The majority of mathematical models are incapable of simulating the difficult inverse kinematics problem. Convolution neural network (CNN), on the other hand,
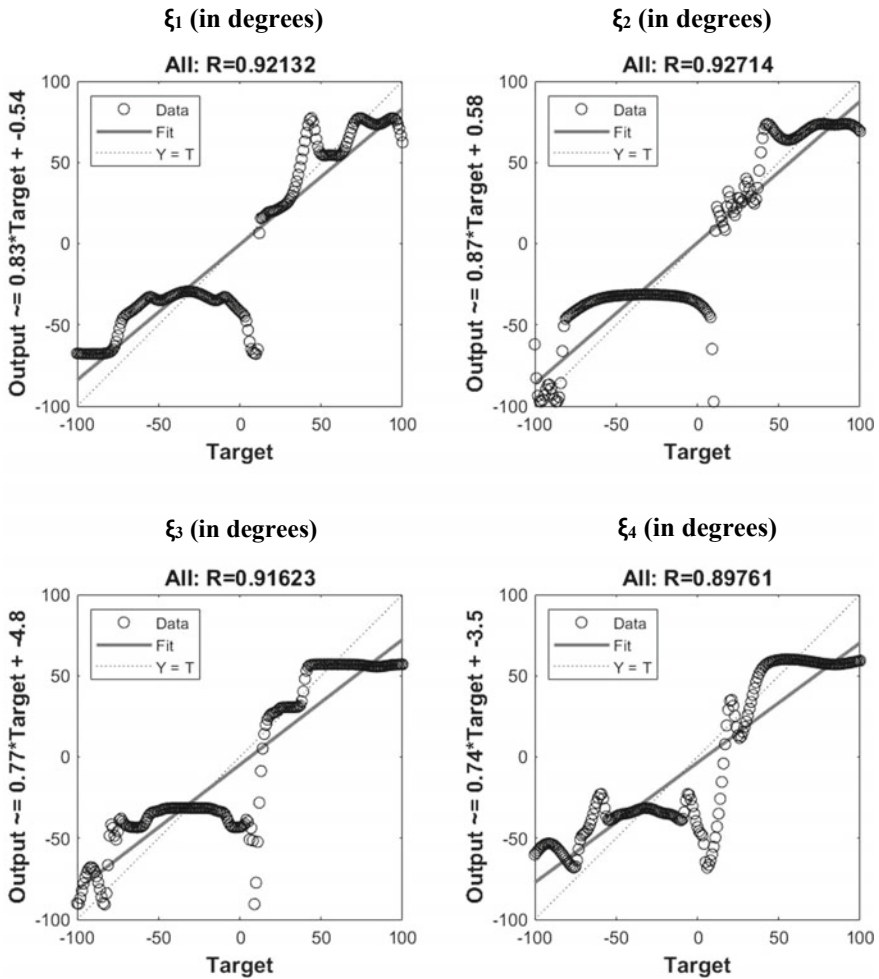

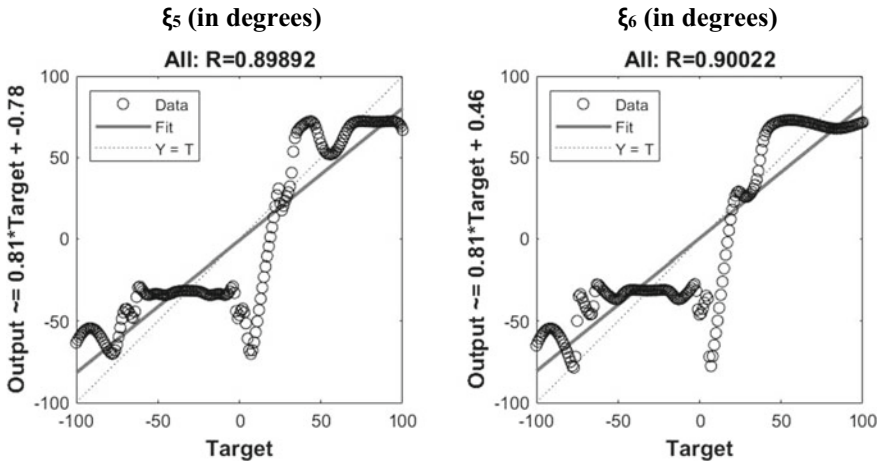**Fig. 3** Regression plots for $\xi_1, \xi_2, \xi_3,$ and ξ_4

Fig. 4 Regression plots for ξ_5 and ξ_6

uses pairings of input–output data sets to calculate various model parameters. It can always be updated to improve the result and enhance accuracy [14].

It is observed that during training, the regression values for joint angles ξ_1, ξ_2, ξ_3, ξ_4, ξ_5, and ξ_6 are 0.92205, 0.93699, 0.93988, 0.91486, 0.89538, and 0.89277, respectively. While during testing, the regression values reduced to 0.89014, 0.8809, 0.8289, 0.82957, 0.89592, 0.91118, respectively. But when the network is further trained with more data, the overall regression values for joint angles reach to 0.92132, 0.92714, 0.91623, 0.89761, 0.89892, 0.90022, respectively. In the work done by Peng et al. similar methodology has been used but the neural network used was ANN for ABB IRB 7600-500 robot, and the regression values obtained in that study were in the range of 0.85–0.88 [2]. Here, all the regression values are around 0.9 or more, which are better than the previous results and are within the acceptable limits. Hence, this work is novel for using PUMA 700 series robot model, and its results are improved than the previous works.

5 Conclusion

The 6-DOF robot manipulator with revolute joints and link length similar to the PUMA 700 series industrial robot manipulator is modeled using MATLAB software. Because the inverse kinematics equation for this robot manipulator is complex, it cannot be simulated using most mathematical models. Therefore, in this paper, convolution neural network method is proposed to solve the inverse kinematics model of a 6-R industrial robot manipulator. Results of the proposed method are analyzed, and the overall regression values are around or more than 0.9, so its accuracy was found within the acceptable range, and the computational time is also significantly

less. This CNN-based inverse kinematics solution model can be a useful tool for production engineers to analyze and estimate the robot manipulator's motion accurately and achieving the goals of Industry 4.0. The future scopes of this work include using other neural networks and comparing their results to the proposed method.

References

1. Srisuk, P., Sento, A., Kitjaidure, Y.: Forward kinematic-like neural network for solving the 3D reaching inverse kinematics problems. In: 2017 14th International Conference on Electrical Engineering/Electronics, Computer, Telecommunications and Information Technology (ECTI-CON), pp. 214–217. IEEE (2017)
2. Peng, Y., Peng, Z., Lan, T.: Neural network based inverse kinematics solution for 6-R robot implement using R package neuralnet. In: 2021 5th International Conference on Robotics and Automation Sciences (ICRAS), pp. 65–69. IEEE (2021)
3. He, D., Shi, F., Tan, S., Deng, Q.: Research on inverse kinematics algorithm of 6-DOF industrial robot based on RBF-PID. In: Journal of Physics: Conference Series, vol. 1624, no. 4, p. 042017. IOP Publishing (2020)
4. Dong, H., Li, C., Wu, W., Yao, L., Sun, H.: A novel algorithm by combining nonlinear workspace partition with neural networks for solving the inverse kinematics problem of redundant manipulators. Mech. Sci. **12**(1), 259–267 (2021)
5. Dereli, S., Köker, R.: IW-PSO approach to the inverse kinematics problem solution of a 7-DOF serial robot manipulator. Sigma J. Eng. Nat. Sci. **36**(1), 77–85 (2018)
6. Csiszar, A., Eilers, J., Verl, A.: On solving the inverse kinematics problem using neural networks. In: 2017 24th International Conference on Mechatronics and Machine Vision in Practice (M2VIP), pp. 1–6. IEEE (2017)
7. Aravinddhakshan, S., Apte, S., Akash, S.M.: Neural network based inverse kinematic solution of a 5 DOF manipulator for industrial application. In: Journal of Physics: Conference Series, vol. 1969, no. 1, p. 012010. IOP Publishing (2021)
8. Athulya, P.S., George, N.: A computer vision approach for the inverse kinematics of 2 DOF manipulators using neural network. In: 2020 IEEE Recent Advances in Intelligent Computational Systems (RAICS), pp. 80–85. IEEE (2020)
9. Kumhar, H.S., Sarita, K., Kumar, S.: Dynamic-balance monitoring scheme for industrial fans using neural-network based machine learning approach. In: Interdisciplinary Research in Technology and Management, pp. 612–618. CRC Press (2021)
10. Singh, R., Kukshal, V., Yadav, V.S.: A review on forward and inverse kinematics of classical serial manipulators. In: Advances in Engineering Design, pp. 417–428. Springer, Singapore (2021)
11. Almanza, C., Baquero, J.M., Jiménez-Moreno, R.: Robotic hex-nut sorting system with deep learning. Int. J. Electr. Comput. Eng. (IJECE) **11**(4), 3575–3583 (2021)
12. Singh, R., Kukshal, V., Yadav, V.S.: Mathematical modelling, design and simulation of a bipedal walker. In: Modeling, Simulation and Optimization, pp. 531–544. Springer, Singapore (2021)
13. Toquica, J.S., Oliveira, P.S., Souza, W.S., Motta, J.M.S., Borges, D.L.: An analytical and a deep learning model for solving the inverse kinematic problem of an industrial parallel robot. Comput. Ind. Eng. **151**, 106682 (2021)
14. Dash, K.K., Choudhury, B.B., Khuntia, A.K., Biswal, B.B.: A neural network based inverse kinematic problem. In: 2011 IEEE Recent Advances in Intelligent Computational Systems, pp. 471–476. IEEE (2011)

A Hybrid Algorithm Based Static Obstacle Avoidance for a Wheeled Base

Shifa Sulaiman and A. P. Sudheer

1 Introduction

Static obstacle avoidance algorithm helps to move the wheelbase from start location to goal location following an optimum path without collision. Conventional path planning algorithms consume more time to calculate optimum paths compared to hybrid path planning algorithms. Different types of path planning algorithms such as bio-inspired algorithms, multifusion-based algorithms, etc. for generating optimized paths from start to end location are explained [1]. The path planning algorithm using A star algorithm is introduced in [2]. The different variants of A star algorithms such as theta star, Lazy theta star, Any angle propagation A star are demonstrated in [3–5]. Path planning algorithm using updated version of A star algorithm is carried out [6]. The Simultaneous localization and Mapping (SLAM) is also employed for localization purposes. A star algorithm employed to determine an optimal path for a vehicle parking purpose is explained [7]. A modification of A star algorithm considering large curves for the mobile robot path planning process for navigation in industrial floors is carried out [8]. Relaxed version of Dijkstra algorithm and A star algorithm is used for determining the optimal path in [9]. The proposed approach is compared with the traditional method for proving the advantages of proposed algorithm. Dynamic version of A star known as D star algorithm used in 3D environment is introduced [10] for planning the path. The D star lite algorithm based on node selection strategy to avoid the generation of path close to obstacles are discussed [11]. The heuristic function and evaluation function are optimized to reduce the computational time. A combined method of D star algorithm and the Particle Swarm Optimization (PSO)

S. Sulaiman (✉) · A. P. Sudheer
Mechatronics Laboratory, Mechanical Engineering Department, NIT Calicut, Calicut, India
e-mail: shifa_p170114me@nitc.ac.in

A. P. Sudheer
e-mail: apsudheer@nitc.ac.in

technique is used to generate an optimized path in [12]. D star lite algorithm employed for avoiding static obstacles is introduced [13]. An improved variant of D star lite algorithm used for obstacle avoidance in a configuration space with multiple robots are demonstrated [14]. Each robot is assumed as an obstacle for every other robot in this method. Field D star algorithm is explained [15] for a mobile robot to determine the optimum path in a grid-based environment. The obstacle avoidance algorithm for a non-holonomic mobile platform with manipulators are given [16]. A polynomial-based approach is employed for creating smooth and continuous path. The final path is short and consumes less computational time as compared to conventional grid path planning 3D algorithms. Cubic spline-based obstacle avoidance is explained in [17]. A cubic spline function is introduced [18] for smoothening the determined path avoiding obstacles from start to goal location. A collision avoidance strategy for high-speed mobile robots considering the motion dynamic equations are given [19]. An objective function is also introduced for calculating the motion towards goal location, the velocity of robot and distance to the obstacle in the planned trajectory. Path planning in a multi-robot environment in real-time is demonstrated [20–22].

PRM [23] is a sampling method used for creating nodes and local paths in the configuration space. PRM is employed along with active algorithms for generating final paths. The three Dimensional PRM algorithm is described in [24]. The creation of nodes in PRM environment is described in [25]. A technique for decreasing the number of checks to avoid collision during planning is introduced [26]. The method reduces the computational time during planning process. An edgeless PRM technique known as Grid Road Map (GRM) is introduced in [27]. The technique is employed for planning path in configuration spaces with obstacles. A method for reducing the path length generated using PRM algorithm along with an active algorithm is illustrated in [28].

In this paper, the static obstacle avoidance of a mobile robot for carrying an upper body humanoid robot is carried out. Lazy PRM technique along with LPA star algorithm are used for generating the path. Lazy PRM creates the nodes whereas the LPA star algorithm generates the path through these nodes. An experimental evaluation of the proposed approach is also done using the mobile platform.

Section 2 introduces the different path planning algorithms and the proposed hybrid algorithm. The results and discussions regarding the proposed algorithm along with the experimental validation is given in Sect. 3. Section 4 depicts the conclusion and future works.

2   Hybrid Path Planning for Avoiding Static Obstacle

A combination of Lazy PRM and LPA star algorithm is used for finalizing the optimized path. Lazy PRM is an improvised version of PRM algorithm for reducing the computational effort while planning the optimized path. LPA star algorithm generates the final path by connecting the local paths already created using Lazy PRM approach.

2.1 PRM and Lazy PRM Algorithms

PRM [23] is a type of passive path planning algorithm and is always combined with other active algorithms for generating optimum paths. PRM algorithm can be employed for generating nodes in the configuration space. The path connecting nodes are known as local paths/edges. The PRM algorithm is faster in generating nodes and local paths. These local paths or edges can be connected later to form the optimum path using LPA star algorithm. The nodes and local paths are created in free space only. The obstacle spaces are avoided for generating nodes and local paths. If the generated nodes and local paths cannot result in a feasible path, the nodes are updated by changing the density to form a new set of local paths. The number of nodes and the distance between connected nodes can be varied. K-S PRM strategy is adopted in this paper for connecting 'K' number of nodes within 'S' radius for creating local paths.

In Lazy PRM [26] technique, the starting and ending nodes are examined initially and move towards the centre of the path for collision checks. The nodes present in the collision areas are removed and replaced to reduce the number of collision checks. At first, all the edges are checked with a coarse resolution and later stepwise checking is done. The data related to checked nodes and local edges are stored for avoiding repeated checking, thereby reducing the computational time.

2.2 LPA Star Algorithm

The cost function of LPA star algorithm [29] with heuristic function is given in Eq. (1)

$$F'_{\text{LPA}}(s) = G'_{\text{LPA}}(s) + H'_{\text{LPA}}(s) \tag{1}$$

$G'_{\text{LPA}}(s)$ is defined as the minimum distance from start node, s_{start} to current node, s. The minimum value of $G'_{\text{LPA}}(s)$ or Rhs (s) is selected as the final cost. Rhs (s) in LPA star algorithm is calculated based on the Eq. (2)

$$\text{Rhs}\,(s) = \begin{cases} 0, & \text{if } s = s_{\text{start}} \\ \min_{s\,\in\,\text{Pred}\,(s)} \left(G'_{\text{LPA}}(s') + C'_{\text{LPA}}(s', s)\right), & \text{otherwise} \end{cases} \tag{2}$$

where $C'_{\text{LPA}}(s', s)$ denotes the cost of moving the robot from s to another node s'. If values are same for all nodes with respect to their starting distances, then the nodes are locally consistent as given in Eq. (3)

$$G'_{\text{LPA}}(s) = \text{Rhs}(s) \tag{3}$$

However, all nodes are not always locally consistent and use $H'_{\text{LPA}}(s)$ value for determining the shortest cost. LPA star consists of a priority queue, which consists of

locally inconsistent nodes. These nodes are updated later to locally consistent nodes. The priority of the node in LPA star algorithm is determined based on a key value. A 2D key value is used for the order of expansion. $K_1'(s)$ and $K_2'(s)$ are the two corresponding key values as given in Eqs. (4) and (5).

$$K_1'(s) = \min \left(G_{\text{LPA}}'(s) \, \text{Rhs}(s) + H_{\text{LPA}}'(s) \big(s, s_{\text{goal}} \big) \right) \tag{4}$$

$$K_2'(s) = \min \left(G_{\text{LPA}}'(s), \, \text{Rhs}(s) \right) \tag{5}$$

The nodes with smallest key values are expanded one by one for determining the optimized path from start node to end node.

2.3 Hybrid Algorithm for Avoiding Static Obstacles

In this paper, sampling-based and node-based algorithms are combined together to form a hybrid algorithm for generating path between start and goal locations by avoiding static obstacles. The nodes are formed in the configuration space using Lazy PRM strategy. A hybrid algorithm combining Lazy PRM and LPA star algorithm are illustrated for avoiding static obstacles. The steps adopted for avoiding the static obstacles are shown in Fig. 1.

The nodes are created in the free space based on Lazy PRM technique. The local paths are created by connecting the nodes. LPA star algorithm then finds out the optimized path based on cost by avoiding collision with static obstacles. If the algorithm detects any collision then the nodes are updated by changing the node density.

3 Results and Discussions

3.1 Path Planning Using Hybrid Algorithm

The hybrid algorithm developed in this paper is used to plan an optimum path between start and goal nodes. The proposed algorithm can be employed for avoiding static obstacles. A safety zone of fixed radius is considered around the obstacles and the hybrid algorithm is applied. In this section, the experimental validation of the proposed hybrid algorithm for avoiding static obstacles using a non-holonomic mobile platform is also presented. An environment is created as shown in Fig. 2 for simulating the mobile platform using the hybrid algorithm. The obstacles are represented as black regions whereas the free space is given in white colour.

The nodes in the free space is created using Lazy PRM algorithm as explained in Sect. 2. The path connecting the start node and end node is created using LPA

Fig. 1 Steps involved in hybrid algorithm
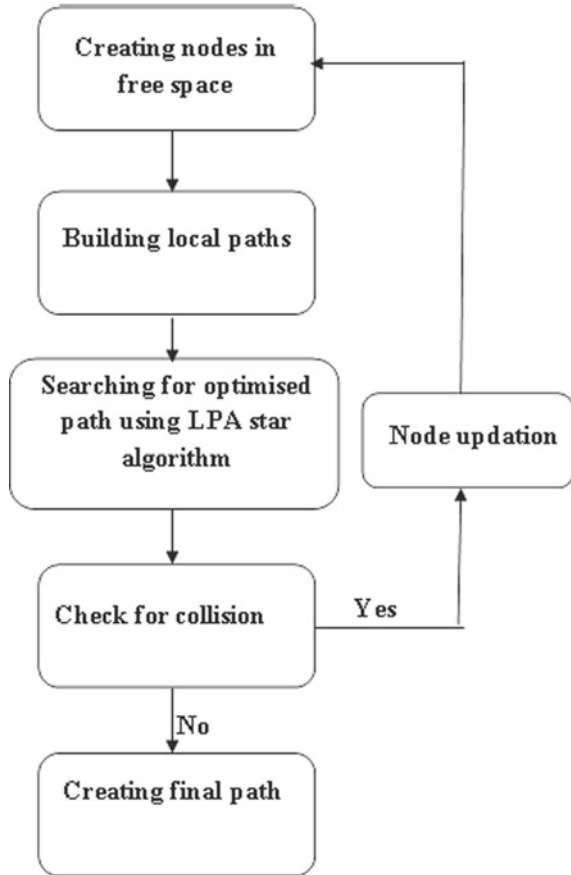
star algorithm. The final path created for avoiding static obstacles in the given environment is shown in Fig. 3.

The path created is of discrete nature due the discrete local paths and can be avoided by applying smoothening step post planning as shown in Fig. 4. A fourth-degree polynomial can be used for fitting the waypoints.

The parameters and properties of environment considered for creating path between start and end node is given in Table 1.

The proposed algorithm is able to generate path with less amount of time as compared to algorithm using conventional LPA star algorithm as shown in Fig. 5. The time also increases with the number of nodes. The number of nodes are fixed as 5000. The increase in nodes above 5000 increases the computational time as shown in Fig. 5.

The time taken for generating the final path is obtained as 0.261 s with 5000 nodes. The length of path determined between the start and end node is calculated as 5760 mm.
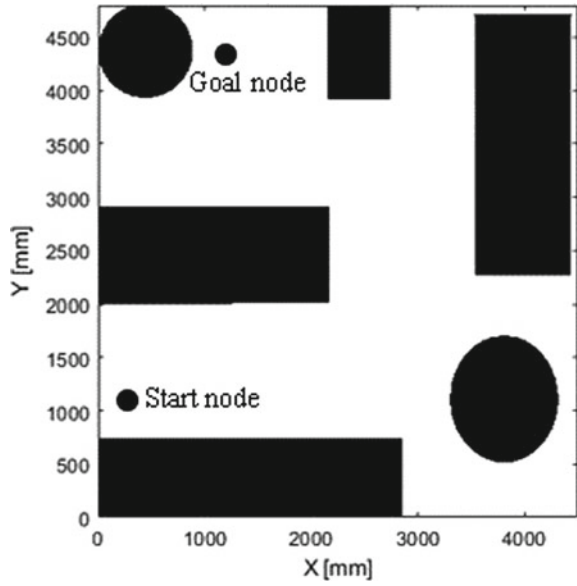
Fig. 2 Obstacle map

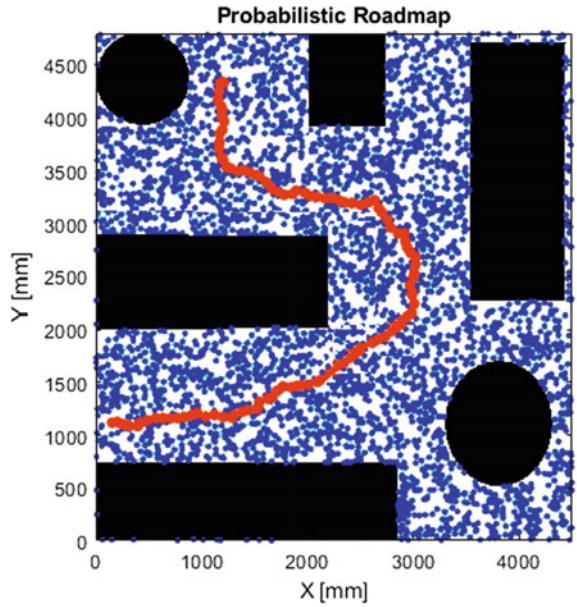**Fig. 3** Path generated avoiding static obstacles
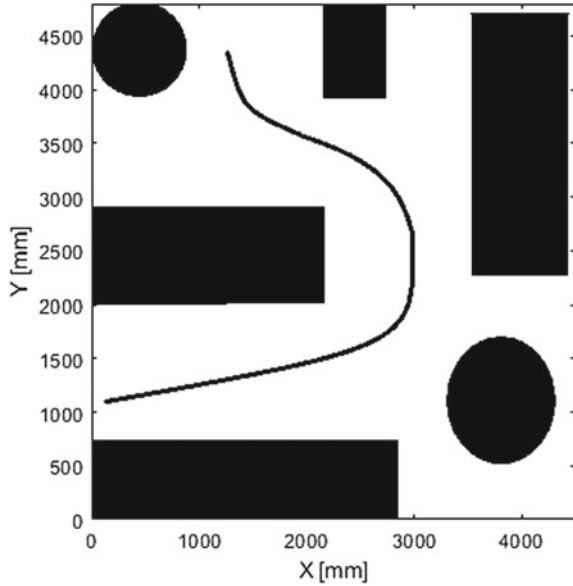
Fig. 4 Path smoothened using polynomial function

Table 1 Parameters used for simulation

Sl. No	Parameters	Value	Unit
1	Dimension of environment map	4.500 × 5000	m
2	Number of nodes	5000	Nos
3	Velocity of mobile robot	0.15	m/s
4	K-parameter	50	Nos
5	Connection distance	0.02	m

3.2 Experimental Validation of Path Planning Algorithm for Avoiding Static Obstacles

The proposed hybrid algorithm approach simulated in Sect. 3.1 is experimentally validated using the same environment. The environment for validating the hybrid algorithm is shown in Fig. 6. The obstacles and free space is also shown. The mobile platform starts from the initial location and moves towards the goal location avoiding the static obstacles in the generated path. The waypoints are already generated in simulation using the proposed algorithm.

The mobile platform moves through the pre-known environment. ArUCO markers [30] are used for recording the positions of mobile platforms while motion. The movement of the mobile platform is tracked using an ArUCO marker as shown in Fig. 7.

The variations of positions of mobile platforms are due to slight variations in joint motor actuation and jerk motions of mobile platform wheels.
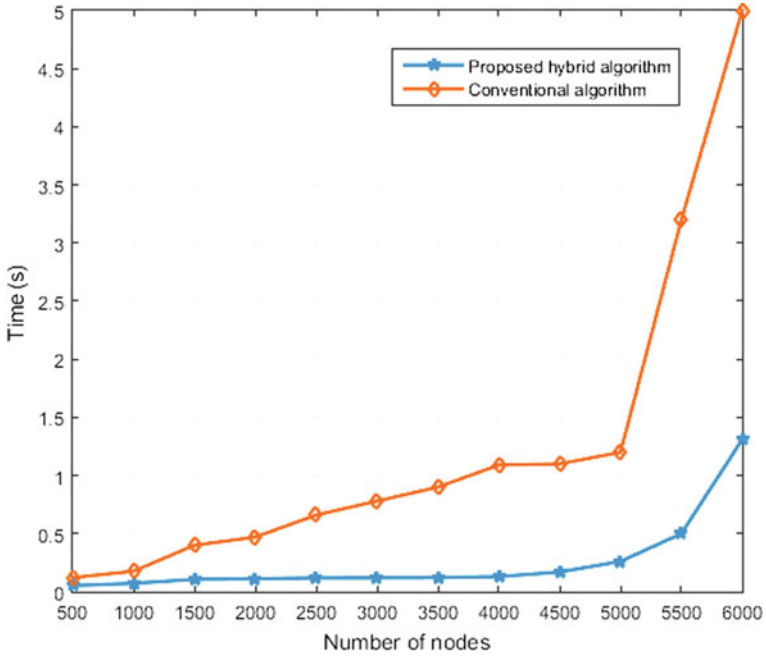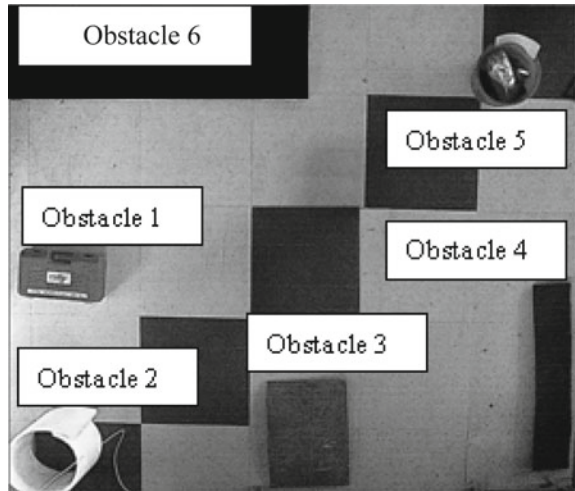
Fig. 5 Comparison of proposed algorithm with conventional algorithm

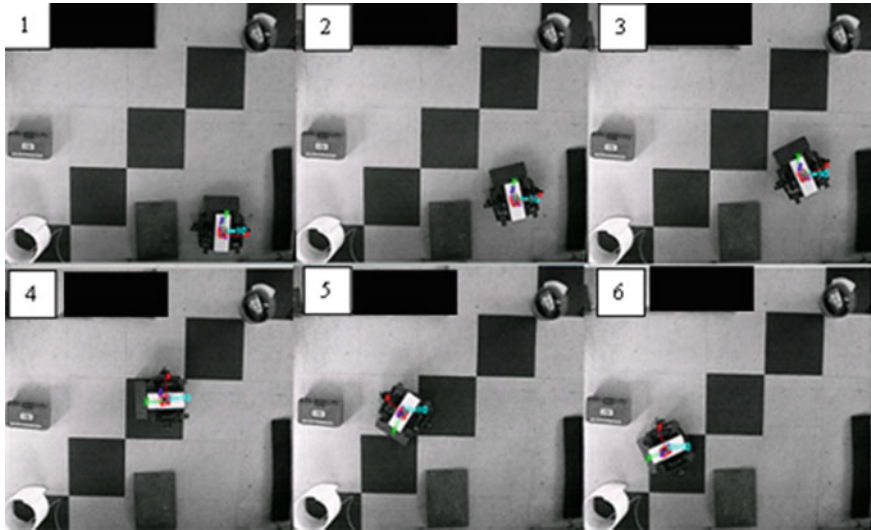**Fig. 6** Position of static obstacles in the configuration space

Fig. 7 Motion of mobile platform in the free space avoiding obstacles

4 Conclusion and Future Scope

Lazy PRM, as well as LPA star algorithm, are combined together to generate an optimized path from start node to end node. The hybrid algorithm reduces the complexity to a lower degree of computations. The Lazy PRM approach is adopted for reducing the computation time for creating nodes and local paths. The Lazy PRM algorithm decreases the time for collision checking through the generation of local paths. The creation of nodes and interconnection of nodes to form edges using PRM algorithm takes very less memory and computational time than using other algorithms. The mobile platform is considered as a point mass in this paper. The dimensions can be included in future works for avoiding collision with static obstacles. The hybrid path planning algorithms are not considering dynamic obstacles in this paper, which can also be included in future works. A controller can be designed for the obstacle avoidance algorithms in future works. A stable and intelligent controller will also be designed and implemented for various applications.

References

1. Yang, L., Qi, J., Song, D., Xiao, J., Han, J., Xia, Y.: Survey of robot 3D path planning algorithms. J. Control Sci. Eng. **2016** (2016)
2. Hart, P.E., Nilsson, N.J., Raphael, B.: A formal basis for the heuristic determination of minimum cost paths. IEEE Trans. Syst. Sci. Cybern. **4**(2), 100–107 (1968)
3. De Filippis, L., Guglieri, G., Quagliotti, F.: Path planning strategies for UAVS in 3D

environments. J. Intell. Rob. Syst. **65**(1–4), 247–264 (2012)

4. Nash, A., Koenig, S., Tovey, C.: Lazy theta star: any-angle path planning and path length analysis in 3D. In: Proceedings of the Third Annual Symposium on Combinatorial Search, vol. 2, pp. 153–154. Atlanta, Ga, USA (2010)

5. Nash, A., Daniel, K., Koenig, S., Felner, A.: Theta^*: any-angle path planning on grids. In: AAAI, vol. 7, pp. 1177–1183 (2007)

6. Duchon, F., et al.: Path planning with modified A star algorithm for a mobile robot. Procedia Eng. **96**, 59–69 (2014)

7. Cheng, L., Liu, C., Yan, B.: Improved hierarchical A-star algorithm for optimal parking path planning of the large parking lot. In: 2014 IEEE International Conference on Information and Automation (ICIA) 2014, pp. 695–698 (2014). https://doi.org/10.1109/ICInfA.2014.6932742

8. Kang, N.K., Son, H.J., Lee, S.H.: Modified A-star algorithm for modular plant land transportation. J. Mech. Sci. Technol. **32**, 5563–5571 (2018)

9. Ammar, A., Bennaceur, H., Châari, I., Koubâa, A., Alajlan, M.: Relaxed Dijkstra and A* with linear complexity for robot path planning problems in large-scale grid environments. Soft Comput. **20**, 4149–4171 (2016)

10. Carsten, J., Ferguson, D., Stentz, A.: 3D field D*: improved path planning and replanning in three dimensions. In: IEEE International Conference on Intelligent Robots and Systems, pp. 3381–3386 (2006). https://doi.org/10.1109/IROS.2006.282516

11. Xie, K., Qiang, J., Yang, H.: Research and optimization of D-start lite algorithm in track planning. IEEE Access **8**, 161920–161928 (2020)

12. Raheem, F.A., Ibrahim, U.: Path planning algorithm using D* heuristic method based on PSO in dynamic environment. Am. Sci. Res. J. Eng. Technol. Sci. **49**, 257–271 (2018)

13. Kumar Das, P., Patro, S.N., Panda, C.N., Balabantaray, B.: D* lite algorithm based path planning of mobile robot in static environment. Int. J. Comput. Commun. Technol. **3**, 286–290 (2012)

14. Al-Mutib, K., Alsulaiman, M., Emaduddin, M., Ramdane, H., Mattar, E.: D* lite based real-time multi-agent path planning in dynamic environments. In: Proceedings of the CIMSim 2011 3rd International Conference on Computational Intelligence, Modelling and Simulation, pp. 170–174 (2011). https://doi.org/10.1109/CIMSim.2011.38

15. Ferguson, D., Stentz, A.: Field D*: an interpolation-based path planner and replanner. In: Springer Tracts in Advanced Robotics, vol. 28. Springer, Berlin, Heidelberg (2007)

16. Papadopoulos, E., Poulakakis, I., Papadimitriou, I.: On path planning and obstacle avoidance for nonholonomic platforms with manipulators: a polynomial approach. Int. J. Rob. Res. **21**, 367–383 (2002)

17. Connors, J., Elkaim, G.: Analysis of a spline based, obstacle avoiding path planning algorithm. In: IEEE Vehicular Technology Conference, pp. 2565–2569 (2007). https://doi.org/10.1109/VETECS.2007.528

18. Lian, J., Yu, W., Xiao, K., Liu, W.: Cubic spline interpolation-based robot path planning using a chaotic adaptive particle swarm optimization algorithm. Math. Probl. Eng. **2020** (2020)

19. Fox, D., Burgard, W., Thrun, S.: The dynamic window approach to collision avoidance. IEEE Robot. Autom. Mag. **4**, 23–33 (1997)

20. Bruce, J.R.: Real-time motion planning and safe navigation in dynamic multi-robot environments. ProQuest Diss. Theses **3248503** 204 (2006)

21. Muthiah, M., Saad, A.: Multi robot path planning and path coordination using genetic algorithms. In: Proceedings of the SouthEast Conference ACMSE 2017, pp. 112–119 (2017). https://doi.org/10.1145/3077286.3077327

22. Hassani, I., Maalej, I., Rekik, C.: Robot path planning with avoiding obstacles in known environment using free segments and turning points algorithm. Math. Probl. Eng. **2018** (2018)

23. Kavraki, L.E., Svestka, P., Latombe, J.C., Overmars, M.H.: Probabilistic roadmaps for path planning in high dimensional configuration spaces. IEEE Trans. Robot. Autom. **12**(4), 566–580 (1996)

24. Hsu, D., Kindel, R., Latombe, J.-C., Rock, S.: Randomized kinodynamic motion planning with moving obstacles. Int. J. Robot. Res. **21**(3), 233–255 (2002)

25. Bohlin, R., Kavraki, L.E.: Path planning using lazy PRM. In: Proceedings 2000 ICRA. Millennium Conference. IEEE International Conference on Robotics and Automation. Symposia Proceedings (Cat. No. 00CH37065), vol. 1, pp. 521–528. IEEE (2000)
26. Bahar, M.R.B., Bahar, H.B., Hashemzadeh, F.: Grid roadmap based real time path planning. In: Proceedings of the 2011 17th International Conference on Automation and Computing ICAC 2011, pp. 75–79 (2011)
27. Chen, J., Zhou, Y., Gong, J., Deng, Y.: An improved probabilistic roadmap algorithm with potential field function for path planning of quadrotor. In: Chinese Control Conference (CCC) 2019-July, pp. 3248–3253 (2019)
28. Gang, L., Wang, J.: PRM path planning optimization algorithm research. WSEAS Trans. Syst. Control **10**, 148–153 (2015)
29. Koenig, S., Likhachev, M.: D^* lite. Aaai/iaai **15** (2002)
30. Avola, D., Cinque, L., Foresti, G.L., Mercuri, C., Pannone, D.: A practical framework for the development of augmented reality applications by using ArUco markers. In: International Conference on Pattern Recognition Applications and Methods 2016 Feb 24, vol. 2, pp. 645–654. SCITEPRESS (2016)

Automated Vision Application in Industrial Defect Identification

Peter Oyekola and Aezeden Mohamed

1 Introduction

Structural failures is a major cause of loss of life and the second principal cause of asset failures in industries, [1, 2]. And the Study of this failures is a necessary step in mitigating incidence and possibility of future failures. This process requires acquiring knowledge on the failure mechanisms of structures and its breakdown.

Lots of financial investment goes into study of techniques of managing corrosion to control its impact on resources. Major materials used in storage facilities for fluids are made of Carbon steel which is highly susceptible to corrosion hence these facilities requires effective corrosion management [3] to reduce the rate of occurrence. As seen in Yunovich et al. [4] on the direct costs implications of corrosion in the industry, it becomes clear that although corrosion cannot be completely avoided, we can however reduce the impact of structural failures by being proactive in industrial maintenance culture. Studies also shows that the major reasons why this failure occur are due to inadequate awareness or attention to the causative factors of corrosion, inadequate risk analysis at design stage or before any component change, lack of information [5].

Steel is an industrially important material that is widely implemented in most industrial structures and construction materials due to its inherent properties and characteristics. It is the backbone of most structures used in industries such as transport industry (trains, ship's hull, etc.), oil and gas industry (pipelines, storage tanks,

P. Oyekola
Department of Mechanical Engineering, Tennessee Technological University, Cookeville, TN 38501, USA

A. Mohamed (✉)
Department of Mechanical Engineering, Papua New Guinea University of Technology, Lae 411, Papua New Guinea
e-mail: aezeden.mohamed@pnguot.ac.pg

pressure vessels, etc.), energy generation (wind turbine, hydrokinetic turbines, etc.), silos and storage [6, 7].

Despite its huge variety of industrial application, its greatest nemesis is the most certain issue of oxidation which initiates the start of corrosive degradation over time as well as defects such as cracks, fatigue [8]. For this reason, periodic inspections are usually carried out in other to detect the initiation and presence of defects which could potentially become fatal if not properly controlled or addressed.

The vulnerability of material to corrosion is determined partially by forecasts based on water chemistry and temperature environment of operation. This makes marine structure vulnerable to failure as they are constantly exposed to fluid all through their life span [9].

The current design aims to leverage the use of an open sources object detection technique developed by Google Inc. which is known as Tensor Flow. This algorithm has seen recent development and adaptation in self-driving cars, obstacle avoidance, automation logic, etc. [10]. Similarly, a model of object detection can be applied in identification of surface cracks, corrosion as well as other pre-trained defect generally found in practical applications.

2   Problem Statement

Metallic structures constitute a large part of industrial materials due to its huge range of applications. Inspection of this facilities can be tedious and extremely cost intensive in terms of time loss, effort, equipment, etc. Furthermore, human limitations like stress, work rate, accessibility issues, and hazardous environment can severely affect quality inspection of critical equipment and some proper pipe inspection cannot be done.

Additionally, most company's policy on safety is 'Zero Accidents or Incidents', however, it is relatively easy to ignore the consequence of failure due to crack and corrosion which can be catastrophic and may leads to loss of man hours, stoppage of production and even death for severe cases. This therefore necessitates the need for a mobile advanced system that can be easily deployed for use in a more efficient and accurate inspection of failures in structural members while minimizing downtime for inspections, risk and increasing efficiency at the same time.

3   Literature Review

The failure of any equipment or loaded structural member relates to behaviors the like of which renders the structure unsuitable in performing its intended design purpose. Failure may be initiated by the occurrence of static loads as well as dynamic loading conditions such as impacts, fatigue of material as well as wear and tear. Generally, ductile materials are more susceptible to failure while the brittle counterpart are

usually more inclined toward fracture. On some rare scenarios, failure might be both ductile and brittle given that some underlying conditions are met such as in low temperature application [11].

Common failure modes experienced are therefore not limited to fracture due to imposed static load and exposure to high temperature application [12]. The propagation of fracture failure usually begins with the initiation of a crack followed by the propagation of that crack due to imposed stress on the material. Brittle cracks tend to propagate quite rapidly as compared with the ductile cracks which are relatively more stable.

Fatigue failure is also subjected to fluctuation of stresses which occurs in moving equipment such as shafts, machine components, most often, the stress leading to this failure are well below the yield point stress associated with the material static load. This failure generated over a period of time due to stress and strain cycling [13]. Almost all material save glass are susceptible to this kind of failure.

Corrosion is a common destructive and non-reversable occurrence. It manifests as an attack on metallic structures which originates at the surface of the metal. Most forms of metallic corrosion are usually electrochemical in nature given that it involves the transfer of electrons from one point to another in form of oxidation [12]. Known factors which cause or activate the initiation of corrosion include temperature, material composition as well as velocity of fluid. The various forms of corrosion are galvanic, pitting, crevice corrosion, selective leaching, erosion, stress corrosion and intergranular corrosion [14].

Inspection personnel are trained to recognize specific signs of decline which signifies a loss of structural integrity with potential of leading to structural failure. Sometimes this may be visually obvious like corrosion or crack along the exterior of structures (surface cracks). Other times, defect such as internal cracks, deck delamination, can only be detected using specialized equipment [15].

Visual Inspection is the most basic non-destructive testing method owing to the high cost of advanced inspection techniques. However, the downsides of this method are the dependency one the training of the inspector, visual perception, and state-of-mind. External factors which also contributes the accuracy of this technique are intensity of light, complexity of structure, and accessibility [16].

Ultrasonic inspection and Ground Penetrating Radar (GPR) however are used for subsurface flaw detection where the former involves the application of high frequency acoustic wave [17] while the later works by transmitting high frequency electromagnetic pulses from a radar antenna onto the structure [18]. Practical use of GPR techniques have successfully been applied in the oil and gas industry for inspection and localisation of subsea pipes [19], detection of buried hazards in mining sites [20], as well as recent application in civil and construction sectors as predominant requirement for non-destructive inspection is in high demand [18, 21].

More recently, the adaptation of Artificial Intelligence (AI) in inspections as well as other robotic applications have seen tremendous applications such as in self-driving cars. This defines a system which is capable of performing tasks which typically require some level of human intelligence as seen in visual perception, pattern recognition, etc. It is a broad umbrella which covers areas such as machine
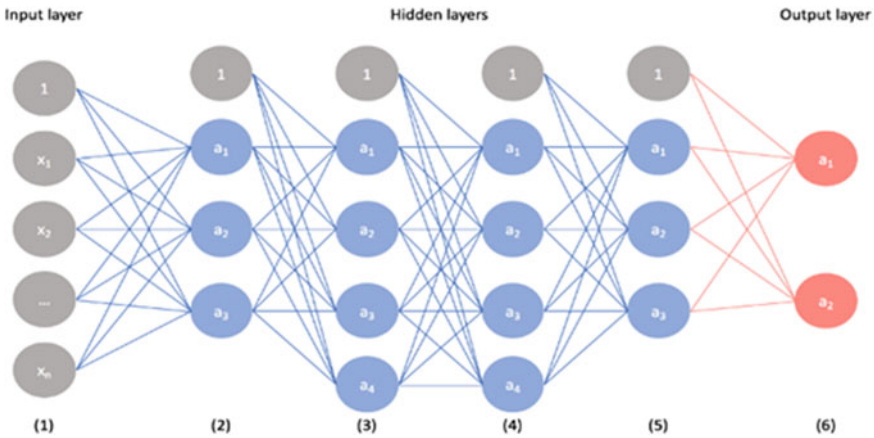
Fig. 1 Visualization of neural network architecture [24]

learning and deep learning which is a subset of machine learning which in this case refers to hidden layers in a neural network [22].

Convolutional Neural Network (CNNs) is a special classification of deep learning in neural networks which is based on the application of two-dimensional structure of visual imaging or other signals which can be generalized for application with other datasets which contains a defined grid-like topology. The success of CNNs in its application to image processing are the local connections, pooling, and usage of multiple layers as well as the image weights [23]. CDNNs makes use of convolutional layers, fully connected layers, and max pooling layers with less connections and parameters thereby making it easier in processing and training images with insubstantial loss in performance. This has encouraged its application in image processing as well as other complex problems as seen in Yun et al. [24]. For this project the You Only Look Once version 4 (YOLOv4) neural network was applied in the detection of cracks and corrosion (Fig. 1).

4   Research Methodology

In the inspection of structures, there is a similar configuration across all setup which involves the illumination of the target through either natural lights or other means, this illuminated scene is then captured by the camera to generate a digital image governed by the incorporated camera lens which introduces a field of view of the areas to capture. This digital image is then sent for processing to generate a final description of the inspected surface. It can therefore be seen that the vision systems are usually made of two major subsystems which are the real time capturing and the processing subsystems [25]. The former is majorly hardware-based and consist of the

digital camera, source of illumination, etc. while the latter is majorly software-based to analyze and gives an indication of surface conditions.

The software system is based on a machine learning algorithm which is equipped on an unmanned robot. This form of inspection can be used in assessing surfaces which will be difficult to assess by human operators such as high pressure or radiation environments and other areas where a direct unobstructed view of the inspection plane cannot be obtained without the use of optical instruments or device such as microscopes, telescope, and the more use of digital cameras more recently. The robot provides real time analysis of sections to be inspected. The image feedback is then analyzed to build up an automated defect classification system based on extracted features of the surface captured, training image set as well as the application of statistical inference algorithms.

4.1 Image Classification and Object Detection

Classification of images is a common application of CNNs as applied in computer vision. It is based on the principle of the recognition of some dominant or outstanding object in an image several image. With the increase in complexity of classification problems, systems with greater performance requirements are continually needed. Over time, it is discovered that in other to develop a system with improve accuracy, there is a need for deeper and more complicated networks which generally leads to an increase in the time required for model training as well as computational cost.

Building up on the successful implementation of the image classification using CNNs, the goal of the detection of objects in an input dataset is to localize as well as classify objects in the image. This is made possible by labeling each of the objects to be detected using a bounding box to define its exact location as well as the class of the object such that the confidence score reflects a true indication of its existence.

The YOLO model which have recently come to limelight is capable of directly prediction the specific locations of the bounding boxes as well as class probabilities in a single evaluation. This method is the preferred methodology implemented in the detection of cracks and corrosion in this study (Fig. 2).
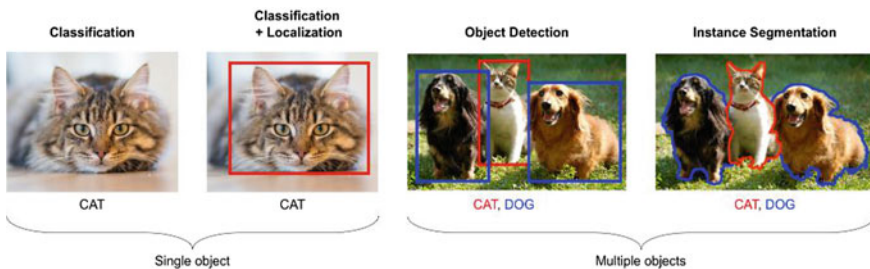

Fig. 2 Image classification and object detection

4.2 YOLOv4

YOLOv4 is a CNN-based methodology applied in detection of objects via camera systems. While this method has seen improved accuracy over time, they have now been used in standalone processing management systems which aids in reducing human input into a system. However, the accuracy of this model as well as speed of detection is heavily dependent on the usage of a Graphics Processing Unit (GPU). Most accurate detections systems require a large amount of GPU in training datasets of large batch size. However, YOLOv4 is capable of functioning with just one conventional GPU.

In other to develop the model to detect the presence of surface defects such as cracks and corrosion on surfaces of industrial structures, the process was initiated by gathering detailed images of defects on different surfaces such as tanks, columns, vessel hulls, some of these images were sourced from open source models online while others were gotten from site visit to industrial environments such as ports and mining companies. Subsequently, all the images were annotated while defining the base classes which were 'cracks', 'corrosion'. The key steps in successful implementation are;

- Set Google Colab as a Cloud VM with Free GPU
- Installing the required system dependencies for GPU (Cuda 10.1, Cudnn, tensorflow-gp==2.3.0rc0, opencv-python==4.1.1.26, lxml, tqdm, absl-py, matplotlib, easydict, pillow)
- Cloning and building Darknet by adjusting GPU and OPENCV settings
- Downloading and converting YOLOv4 weights (Previously trained weights)
- Gather custom training and validation datasets for cracks and corrosion (1500 dataset)
- Configuring custom YOLOv4 Cloud Training
- Train custom YOLOv4 Object Detector
- Validate custom Model with mAP
- Test run YOLOv4 with TensorFlow on images, video and webcam
- Convert TensorFlow model into a TensorFlow Lite tflite model
- Run YOLOv4 with TensorFlow Lite on the robot.

A total of one thousand five hundred images were gathered for each of the classes. These images were used as the training dataset which were resized and properly renamed to allow for faster processing. Additionally, the images for cracks and corrosion were sequentially arranged such that it alternated between each other (Figs. 3, 4 and 5).

In order to create custom datasets, for YOLOv4, the files needed are

- Cracks and corrosion datasets
- Custom configuration file (.cfg)
- obj.data and obj.names files (these contains the details of the intended classes to be detected which in this case are just cracks and corrosion, i.e., two classes)
- train.txt files which will enable the evaluation of the trained weights.

Fig. 3 Sample crack dataset

The bounding box information are contained in a text file generated using a data annotation tools LabelImg among other options. By using this tool, the object to be detected in the input image is bounded by a box as well as the corresponding classes which are present in the image. This annotation process was done for all the training dataset one at a time. For custom detection purpose, there are platforms where already annotated models could be gotten such as open Images v6. However, due to the nature of this project, the annotation has to be done manually as shown in Fig. 6.

The information containing the coordinate of the bounding boxes from the annotation process above is stored in a.txt file. The file contains the number of classes as well as XMin, XMax, YMin, YMax: coordinates of the box, in normalized image coordinates. XMin is in [0, 1], where 0 is the leftmost pixel, and 1 is the rightmost pixel in the image. Y coordinates go from the top pixel (0) to the bottom pixel (1). However, in order to accommodate a more intuitive representation and give the maximum flexibility, every.txt annotation is made in the form of 'name_of_the_class left top right bottom', where each coordinate is denormalized. So, the four different values correspond to the actual number of pixels of the related image.
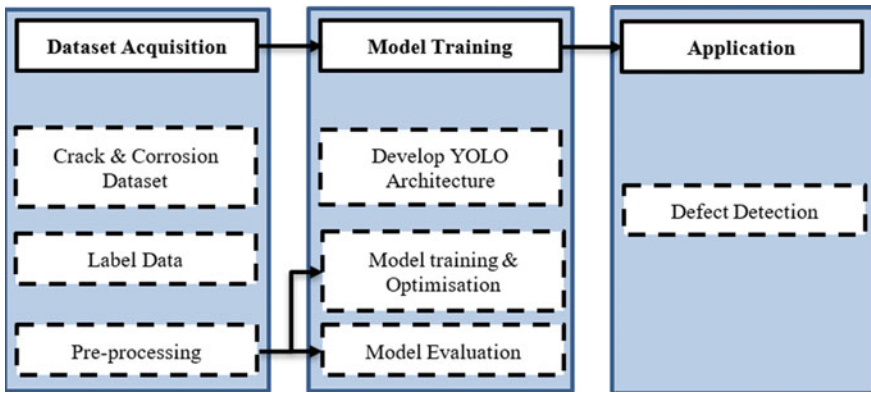
Fig. 4 Sample corrosion dataset

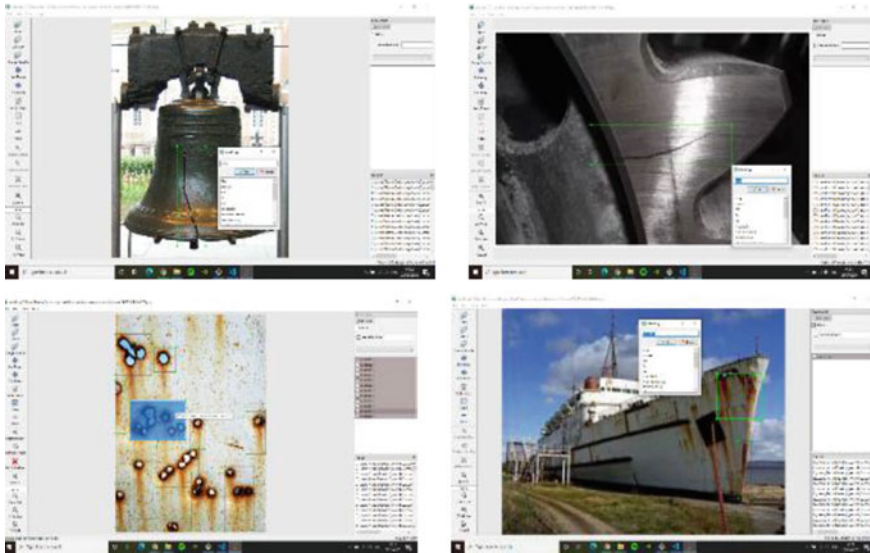**Fig. 5** Implemented YOLOv4-Lite algorithm

Fig. 6 LabelImg interface for annotation of input images

4.3 Model Training and Testing

In training the detection model, the Single Shot Detection (SSD) model was adopted. It is an open source variety of the COCO-weighted models and it conveniently balances speed and performance which will come in handy during real time inspection.

Additionally, Google Colab which is also an open source platform offering free GPU computing was implemented in training the model. This offered a 16 GB of RAM as well as NIVIDIA GPU for model training. In other to further improve the system performance, certain parameters to adjust includes the steps, batch size, number of iterations, etc. this was edited from the original configuration file using the following settings;

$$\text{batch} = 64$$
$$\text{subdivisions} = 16$$
$$\text{Classes} = 2(\text{cracks, corrosion})$$

The value of the max_batches must not be lower than 6000 this means for classes between one and three, the set value will be 6000. However, for a class of 5, this will then be 10,000.

$$\text{max\_batches} = (\text{numberofclasses}) \times 2000 = 6000$$
$$\text{steps} = 4800, 5400, \text{ i.e.,}$$

steps $=$ (80% ofmax _batches), (90% ofmax_batches)

filters $=$ (numberofclasses $+ 5) \times 3 = 21$

width $= 416$

height $= 416$

The average loss during the initial training process was roughly about 2000 but this slowly decreases with increasing number of iterations until it stabilizes as a loss of under 0.5 after about 3000 iterations. Also, after every 1000 iterations, the Mean Average Precision (MAPs) values are plotted. This showed that between 3000 and 4000 iterations, the training can be stopped since there is no significant increase in accuracy and decrease in loss.

4.4 Camera Requirements

The choice of selecting suitable camera for and inspection model requires detailed attention to the inspection requirements. Generally, the first requirement is the use of a high-quality camera of which due to advancement in technology, cameras which meets this specification are now compact enough to be mounted on unmanned systems. Also, the robot might be applied in areas with limited or no light access hence, this would require a night vision system to enable adequate inspection without compromising model effectiveness.

While there are a variety of cameras to choose from, one of the desirable features in selecting a good vision system is the resolution offered by the camera. This determines the quality of images as well as allows for better precision. Therefore, the camera resolution, pixel size, and sensor size are combined factors which can be exploited in the requirement for high quality images. In situations whereby the system intends to identify defects depicted with limited pixel numbers, the extraction of its geometrical properties such as dimensions or orientation might become difficult [26].

Additionally, the cameras field of view (fov) is another factor which affects the resolution. The minimum camera resolution in each direction which is required in this instance can be estimated from the relation below,

$$\text{Minimum resolution} = \frac{\text{Smallest defect pixels number} \times \text{fov}}{\text{Smallest defect size}}$$

Going by this analysis, the use of any 4 or 5 MP camera which comes with a resolution of 2046×2046 pixels will offer good resolution with a great picture quality which is sufficient enough for the intended application even if future upgrades are required.

The focal length offered by the lens was the determining factor in selecting the lens used in the inspection robot. When a lens has its focal length equal to the diagonal dimension of the sensor, the perspective generated is usually normal when viewed.
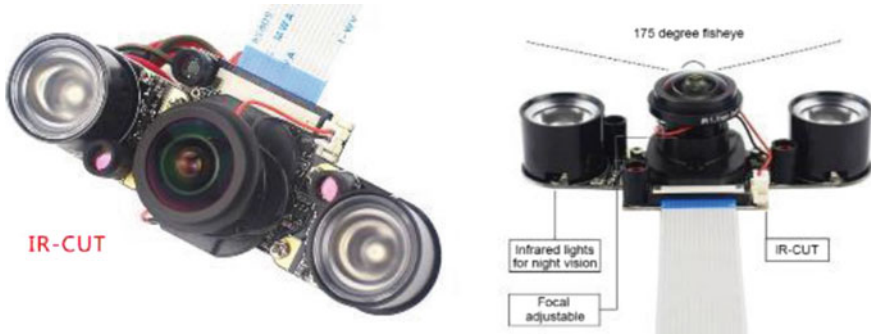
Fig.7 IR-CUT night vision focal adjustable 5MP fish eye camera

On the other hand, if the length is shorter than the sensor diagonal length (normal focal length), this are referred to a wide-angle lens given that there are capable of capturing a wider field of view which can come in handy when trying to inspect objects within working distance which represents how far the object to be inspected is from the lens. The equation for estimating the required focal length of the lens is given as,

$$\text{Focal Length} = \frac{\text{working dist} \times \text{sensor size}}{\text{fov}}$$

Given that the camera module will be installed on a moving robot, the wide-angle lens with fisheye view of 1750 was selected. In practical inspection, since there is no fixed working distance between object and the camera, the estimation of the focal length required was based on minimum and maximum values of inspection conditions. This yielded a focal length of 12 and 156 mm assuming working distance of 550 and 650 mm, respectively. The implementation of the fisheye lens provides aerial image within the region of interest (Fig. 7).

4.5 System Installation

The final implementation design was entirely based on the requirements imposed by the robot's application. The elements comprising the vision system are the camera, lens, on-board computer, waterproof enclosure as well as the pan and tilt mount.

The camera sits inside the clear waterproof containment box which rests on the pan and tilt mount providing a wide range of view about the horizontal and vertical axis. As a result, the camera is capable of rotating about a workspace angle of 1450 about the vertical axis while the range of movement on the horizontal axis is 1800.

The camera is connected to the raspberry pi 4B board through the use of flex cables which offers flexibility of movement with a limitation of affordable distance between the camera and the computer.

For proper optimized detection, the confidence threshold of the model was set at 25% which means that for a detection bounding box to be displayed, the model must be at least 25% confident. This can be varied based on the detection expectation.

5 Result and Discussion

In validating the defect identification system, the robot was tested using images which were not using in the training process as well as live field testing. The training algorithm was set to perform 10,000 iteration of the complete dataset which is equivalent to 1000 iterations for one epoch.

The resulting accuracy of the model reached 91% average precision which is much better when compared to the previous versions trained in the preceding versions of YOLO. This makes detecting object which are relatively small improved for crack identification. On the other hand, the detection system was more accurate in identifying corrosion which do not cover up an entire surface (Fig. 8).

From the figure above, the mean average precision of the model increases with corresponding increase in the size of the input image. More so, for detecting defects on images of varying sizes, the difference in accuracy of the system is small given that the multi-scaled training method implemented ensured that the system could handle and predicting with a high precision inputted samples of varying sizes. Furthermore, the use of a fisheyes lens of good resolution offers a wide-angle view of 1750 which increases the chances of picking out defects on different kinds of surface (Fig. 9).

As seen in the detected samples above, the regions where defects are identified are effectively indicated using a bounding box where a confidence score which indicates the certainty at which the model effectively identifies the object. The confidence score represents a value between 0 and 1 where zero indicates a zero percent recognition hence no bounding box is drawn, while a confidence score of 1 is a hundred percent certainty which is hardly achievable due to various factors such as the condition of light in the inspection region, blurry and partially covered objects, camera resolution, reflection of lights.

For this model, the minimum certainty before a bounding box can be displayed was set to 25%. Effectively, for any value below 0.25, a positive identification will not be displayed irrespective of whether the object actually exist or not. For future reference, this value could be increased or reduced based on the level of precision desired.

The major source of errors encountered was due to improper data annotation and arrangements for training. Although there is no defined rule for image annotations, a more precise model will require that the annotated objects on the images captured the exact item to be identified with little or no interference from other background images and noise (Figs. 10 and 11).
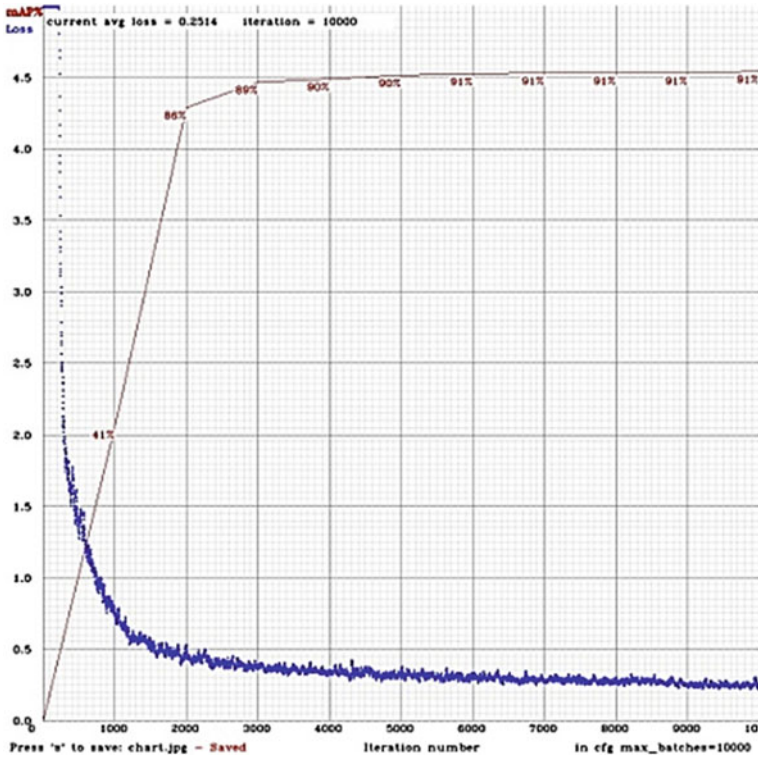
Fig. 8 Training iterations and precision

Some of the errors encountered might be caused by the imbalance in training data as well as arrangements as earlier mentioned. Given that the model was being trained to recognize two classes (crack and corrosion), this meant that training data for both classes were collected. The total training data for cracks were 700 while 500 images were used to represent the corrosion dataset. By having a balanced class representation, there will be room for better class comparison as well as a better obtained value for the mean average precision.

6   Conclusion

The defect identification system employed in this paper involved the use of machine learning algorithm in classifying common defects found in industrial environment. This is achieved using an installed adjustable focus wide-angle fish eye lens camera mounted in front of the robot and controlled on a mounted pan a and tilt mount. The camera receives live video streams of its inspection plane which is sent to the on-board computer for processing to identify the possible defects in real time.
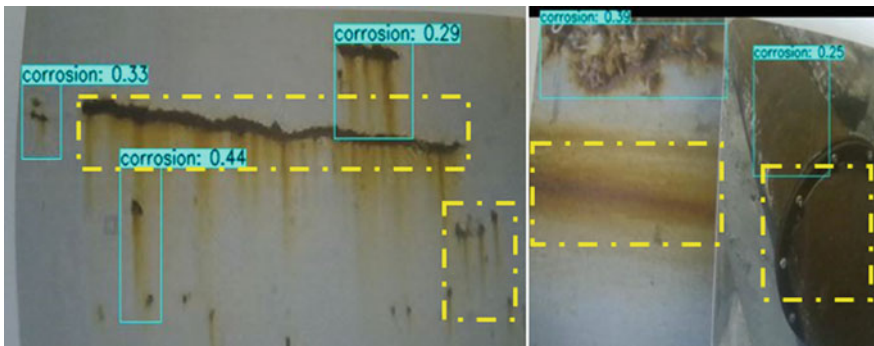
Fig. 9 Sample detection results

Fig. 10 Missed details (yellow)

The video feedback is then analyzed to build up an automated defect classification system based on extracted features of the surface captured, training image set as well as the application of statistical inference algorithms. This is further enhanced using Graphical Processing Unit on the computer for a faster processing rate. The trained model is based on open sourced images of defects available online as well as from site visits and the confidence threshold of the model was set at 25% for optimized detection.
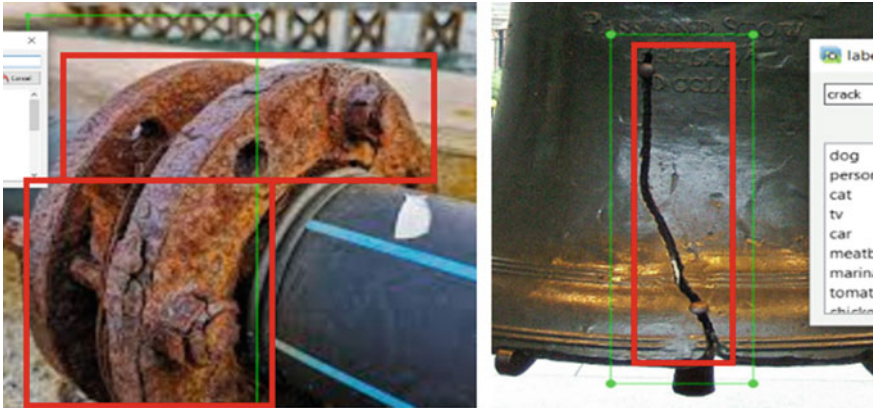
Fig. 11 Annotation error (red box is the ideal bounding box)

References

1. Speight, J.G.: Oil and Gas Corrosion Prevention: From Surface Facilities to Refineries (2014)
2. Ratnayake, R.M.C.: Modelling of asset integrity management process: a case study for computing operational integrity preference weights. Int. J. Comput. Syst. Eng. (2012)
3. Koch, G.H., Brongers, M.P.H., Thompson, N.G., Virmani, Y.P., Payer, J.H.: Corrosion Costs and Preventive Strategies Publication No. FHWA-RD-01-156. Corrosion (2001)
4. Yunovich, L., Thompson, M., Balvanyos, N.G., Lave, T.: Corrosion Costs and Preventative Strategies in the United States (FHWA-RD-01-156) (2001)
5. Elsevier's R&D Solutions for Oil and Gas, Don't let corrosion put holes in your net gains (2018)
6. Mazínová, I., Florian, P.: Materials selection in mechanical design. In: Lecture Notes in Mechanical Engineering (2014)
7. Peter, O., Mohamed, A., Emmanuel, V., Tochukwu, N.: Corrosion effects on low carbon steel marine heat exchanger. Int. J. Adv. Sci. Technol. **29**(7), 10066–10072 (2020)
8. Groysman, A.: Corrosion problems and solutions in oil, gas, refining and petrochemical industry. Koroze a Ochr. Mater. **61**(3), 100–117 (2017)
9. Mohamed, A., Oyekola, P.: Carbon dioxide corrosion in oil and gas industry. Int. J. Adv. Sci. Technol. **29**(7), 10053–10065 (2020)
10. Oyekola, P., Mohamed, A., Pumwa, J.: Robotic model for unmanned crack and corrosion inspection. Int. J. Innov. Technol. Explor. Eng. **9**(1), 862–867 (2019)
11. Reeves, T., Mendat, C., Shaver, E.: Root cause analysis. In: Applied Human Factors in Medical Device Design (2019)
12. Clayton, C.R.: Materials science and engineering: an introduction. Mater. Sci. Eng. (1987)
13. Raut, S.P., Raut, L.P.: A review of various methodologies used for shaft failure analysis. Int. J. Eng. Res. Gen. Sci. (2014)
14. Bharatiya, U., Gal, P., Agrawal, A., Shah, M., Sircar, A.: Effect of corrosion on crude oil and natural gas pipeline with emphasis on prevention by ecofriendly corrosion inhibitors: a comprehensive review. J. Bio Tribo Corros. (2019)
15. Boopathy, G., Surendar, G., Nema, A., Anand, T.P.P.: Review on non-destructive testing of composite materials in aircraft applications. Int. J. Mech. Eng. Technol. (2017)
16. FHWA, Pavement Performance Measures and Forecasting and the Effects of Maintenance and Rehabilitation Strategy on Treatment Effectiveness (Revised) (2017)

17. Cerniglia, D., Scafidi, M., Pantano, A., Rudlin, J.: Inspection of additive-manufactured layered components. Ultrasonics (2015)
18. Liu, R.C., Ren, W., Wang, H., Guo, C.: Ground-penetrating radar. In: Principles of Modern Radar: vol. III: Radar Applications (2014)
19. Pasolli, E., Melgani, F., Donelli, M.: Automatic analysis of GPR images: a pattern-recognition approach. IEEE Trans. Geosci. Remote Sens. (2009)
20. Francke, J.: A review of selected ground penetrating radar applications to mineral resource evaluations. J. Appl. Geophys. (2012)
21. Asadi, P., Gindy, M., Alvarez, M.: A machine learning based approach for automatic rebar detection and quantification of deterioration in concrete bridge deck ground penetrating radar B-scan images. KSCE J. Civ. Eng. (2019)
22. Seeja, G., Arockia Selvakumar, A., Berlin Hency, V.: A survey on swarm robotic modeling, analysis and hardware architecture. Procedia Comput. Sci. (2018)
23. Milosevic, N.: Introduction to Convolutional Neural Networks (2020)
24. Lu, Y., et al.: Identification of metastatic lymph nodes in MR imaging with faster region-based convolutional neural networks. Cancer Res. (2018)
25. Czimmermann, T., et al.: Visual-based defect detection and classification approaches for industrial applications—a survey. Sensors (Switzerland) (2020)
26. Chitradevi, B., Srimanthi, P.: An overview on image processing techniques. ISRN Signal Process. (2014)

Space Robotics: A Comprehensive Study of Major Challenges and Proposed Solutions

Abhishek Shrivastava and Vijay Kumar Dalla

1 Introduction

Outer space has a harsh environment, high temperature, and radiation so human access is very difficult. To assist human research activity in space for developing a space module and planetary surface research, robots are contributing to the research of solar system [1]. Space servicing is an important task to be performed in the area of space science. Many countries have started research in the vast area of space science [2]. Ideas to do research in the field of space robotics started in 1980. The design of robot structure was started initially; this report was first published in NASA in 1983. It was thought earlier to construct space station using autonomous free-flying robots, but at last this task was completed by human extravehicular activities (EVA) with the utility of shuttle remote manipulator system (SRMS) and Canadarm-2 [3]. The main achievement in space robotics was the development of orbital free-flying space robot for performing the important task of repairing, refueling propellants, orbiting and rescuing the satellite [4]. However, servicing unmanned non-cooperative space satellite in space orbit such as tumbling satellite with unidentified properties by redundant robots is facing many scientific issues. Moreover, autonomous control of non-cooperative satellite is uphill task for future research work. Space robotics is enhancing its applications in the field of lunar research to mitigate space debris hazard concerned for an astronaut in ISS. Space debris can be mitigated by re-orbiting the robot by removing the satellite from the orbit before the damage. Sanguino [5] studied that the first space robot traveled on the extraterrestrial body was Lunokhod (1970), which was remotely operated from earth surface and traveled approximately 10.5 km on the surface of the moon. Furthermore, Woffinden and Geller [6] studied

A. Shrivastava (✉) · V. K. Dalla

National Institute of Technology Jamshedpur, Jamshedpur 831014, India

e-mail: abhishekujyan@gmail.com

that rendezvous docking is necessary for space missions performed through navigation. In the past, docking operation was performed by manned spacecraft but later on, National Space Development Agency of Japan (NASDA) and European Space Agency (ESA) started working on unmanned spacecraft to supply materials to International Space Station (ISS). Space robots perform docking, refueling, rescuing operations in space. The maintenance of the space station is also performed by a robot. Later, the National Aeronautics and Space Administration (NASA) realized the importance of space robotics in on-orbit servicing after 1980 [7]. Mainly, the on-orbit space manipulator is equipped with group of three key components, the operation satellite, an (*n*-DOF) space robot fixed to the operation satellite, and the objective space manipulator to be serviced through on-orbit servicing by space robot. Jung et al. [8] suggested that impedance control strategy is required for force and position control of space manipulator. Mainly, the impedance control strategy is implemented by electric driven robots based on the torque control system of the hydraulic actuator [9]. However, it is difficult to perform obstacle avoidance through hydraulic drive unit so second order dynamic compliance system is suggested by Zhao et al. [10] for hydraulic drive unit with better impedance control of walking legged robot. Later, Uyama and Narumi [11] proposed that the hybrid impedance control scheme can be utilized to detumble a non-cooperative satellite. Many researchers studied that space debris removal and on-orbit servicing require a high level of autonomy so obstacle avoidance is the main criterion to be studied to support on-orbit servicing in the near future. In advance, a collision-free trajectory planning of space manipulators is required for obstacle avoidance. Qian et al. [12] also suggested that obstacle avoidance can also be performed by the technique of the trajectory planning method. In the trajectory planning method collision path avoidance algorithm is utilized to provide low-level control to a robot path avoiding any collision within the workspace of a space robot [13].

2 Background of Existing Space Robotic Manipulators

On 1981, the shuttle remote manipulator system (SRMS) was tried on the second mission of the space. SRMS also known as (Canadarm-2) which has served for more than 15 years. It is an automated arm which consists of shoulder, elbow, and wrist joints having six degrees of freedom. SRMS had the drawback of not having fault-tolerant joint control system which lacked redundancy in joint, but later on differentially gear train mechanism consisting of non-linear power equation reduced joint control system equation into linear state equation [14]. Figure 1 shows the manipulator arm performing space station construction STS-61B on a space mission.

On April 26, 1993, the spacelab mission D-2 [15] was successfully tested on shuttle Columbia. This experiment was successful in the field of earth observation and telecommunication etc. Moreover, the European Retrievable Carrier (EURECA) was landed successfully on July 1st 1993 at space center named Kennedy in Florida to perform advanced orbital research and to enhance flight operation chances for
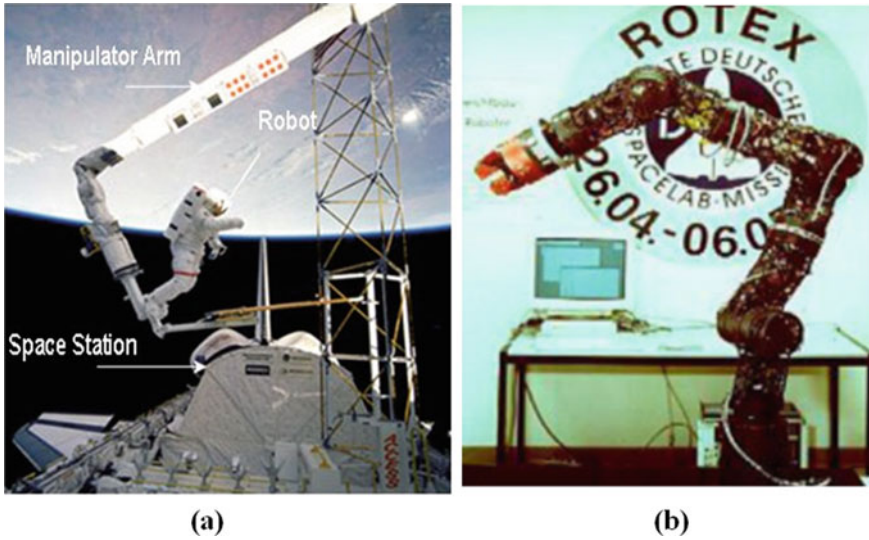
Fig. 1 **a** Demonstration of space station construction STS-61B on a space mission. **b** ROTEX of DLR [14]

ESA astronaut. Later on, the engineering test satellite (ETS-7) was developed by NASDA in view to experiment rendezvous docking (RVD) operation in orbit of space to give logical support to the space station [16, 17]. Table 1 shows technical details of engineering test satellite developed since recent past. It is highlighted that Canadarm-2 is also utilized for collision avoidance in space robot. JEMRS have more mass (7000 kg) compared to other engineering satellites shown in Table 1 (Fig. 2).

Table 1 Technical details of engineering test satellites

S. No.	Satellite name	Length (m)	Mass (kg)	Wrist joint	Elbow joint	Shoulder joint
1	CANADARM [15]	15.2	410	Pitch/yaw/roll	Pitch	Pitch/yaw
2	CANADARM-2 [3]	17.6	1641	Pitch/yaw/roll	Pitch	Pitch/yaw/roll
3	ERA [16]	11.3	630	Pitch/yaw/roll	Pitch	Pitch/yaw
4	JEMRMS [17]	9.9	7000	Pitch/yaw/roll	Pitch	Pitch/yaw

Fig. 2 Variation of joint angle with time for joint position trajectory [18]
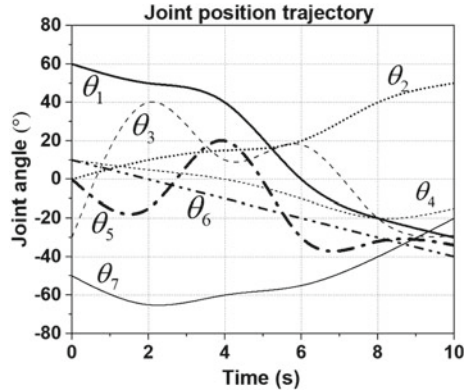
3   Major Challenges and Proposed Solutions

3.1   On-Orbit Servicing

During on-orbit servicing, space manipulator needs to perform docking, refueling, rescuing operations in space. The maintenance of the space station is performed by a robot. Many researchers are exploring influential ways to motivate the development of advanced on-orbit servicing technology for capturing the target satellite. The capturing process during on-orbit servicing requires 4 phases: (1) The first phase is observation and planning in which analysis of motion and physical properties of target satellite is performed. (2) The second phase is controlling robotic arm motion to move toward the grasping object. (3) The third phase is real capturing phase or physical interception phase, in which manipulator capture the target satellite with required force control. (4) The fourth phase is post capturing phase in which target satellite is stabilized along with on-orbit servicing system.

In space missions, manipulator berthing and autonomous docking is performed with a flexible and cooperative target. However, in practical issue, an unestablished or non-cooperative targets need to be managed that requires high level of advance technology. Shan et al. [18] suggested to hold the uncooperative target fixture by fixing the nozzle cone of GEO satellites. However, for handling tumbling motion, the chaser arm must be in straight line motion against moving target. For this, residual relative velocities need to be diminished. This needs automatic control to allocate angular momentum of the fixed target after a successful capture in space orbit [19]. After successful on-orbit servicing operation performed by space satellite, a multiple servicing satellites were proposed for the visual inspection and active debris removal in space station. For this, Garg and Sharma [20] solved multiple objective optimization problem by using particle swarm optimization technique. However, heat transfer problems arise during on-orbit servicing due to heat dissipation in component of spacecraft. To fix this problem, Guo et al. [21] modeled flexible thermal control system (F-TCS) with a heat collection bus, heat dissipation bus, inter-platform

service interfaces, and connection brunches. In F-TCS heat generated by a spacecraft is transferred to cold plates though 3-way valve having PID controller, which automatically adjusts fluid flow rate passing the radiator bus to form appropriate cooling temperature for the heat collection bus.

During on-orbit servicing task, the servicing satellites need to follow desired trajectory while approaching the target satellite. While performing on-orbit servicing operation, the system's linear and angular momentum should be conserved in absence of external force. However, angular momentum equations are not represented in integrated form, which states that they are non-holonomic. Later, researchers developed solutions for robot path planning by using non-holonomic property in space manipulator [22–24]. Moreover, Zhengcang et al. [25] proposed fixed-attitude-restricted (FAR) motion controller to allow manipulator arm motion without any reaction moments to its base of spacecraft. Zhan et al. [26] proposed novel control scheme for space robot to detumble a non-cooperative target with collision avoidance in dynamic or static situation. Joints acceleration control limits and dynamic unreliability of space robot and cooperative target is considered with use of trajectory tracing control scheme. However, full inertial parameters were lacking in this control scheme, which caused dynamic disturbances in robot. Meng et al. [27] utilized eddy current for contactless detumbling a non-cooperative target satellite. To verify efficacy of this control scheme, finite element simulations are carried out to calculate the effect of electromagnetic force on a non-cooperative target. For capturing tumbling target, combined system, i.e., static and dynamic system must be stabilized to provide safety during on-orbit servicing. To solve this issue, Luo et al. [28] proposed detumbling and stabilization strategy based on angular momentum transfer by considering joint velocity limits.

3.2 Impedance Control

Impedance control is a technique for dynamic control relating force and pose of space manipulator. The proportional integral derivative (PID) controller [29] controls the end-effectors tip position of space robot. Mostly, the impedance control strategy was performed by electric driven robots based on the torque control system of the hydraulic actuator. On the other hand, hydraulic drive unit was proposed to control legged robot motion during walking of space robot. Servo valve is electrically operated valve which controls the hydraulic fluid transmitted to actuator. Force sensor controls both forces/torques applied to base of robot, whereas position sensor controls the position of joints. Accumulators are used to hold multiple objects.

DLR developed a gripper by using the concept of "artificial muscle" which leads to powerful, and high dynamic actuators [30, 31]. This is more superior to those pneumatic and hydraulic technologies and further it is developed in the form of completely programmable spring with desirable impedance control. Uyama and Narumi [32] proposed hybrid impedance control scheme for detumbling single serial link manipulator. Pathak et al. [33] suggested that impedance control at the end-effector of

robot can be achieved by passive degree of freedom in the controller. For multiple co-operative space manipulator Dalla and Pathak [34] developed impedance control scheme by pulling flexible wire. However, during such capturing operation some internal torques and forces are originated in the object.

3.3 Obstacle Avoidance

Space debris removal and on-orbit servicing require a high level of autonomy so obstacle avoidance is the main criterion to be studied to support on-orbit servicing in the near future. In advance, a collision-free trajectory planning of space manipulators is required for obstacle avoidance. Moreover, obstacle avoidance can also be performed by the technique of the trajectory planning method. In the trajectory planning method collision path avoidance algorithm was used to provide low-level control to a robot path avoiding any collision within the workspace of a space robot. Later, Zhao et al. [10] studied obstacle avoidance of hexapod robot for detecting tasks.

Alternatively, Zong et al. [35] proposed mixed integer predictive control (MIPC) technique having joint angle torques, joint angle ranges, and joint velocity to avoid obstacle avoidance. Later, Bao and Zelinka [36] suggested obstacle avoidance also can be performed by migrating algorithm with sensors attached to it, in which trajectory intermediate points are used to find target position of any required task. Space robots working in a dynamic environment requires collision-free trajectory planning, so dynamic control algorithm (DW4DO) was proposed to avoid obstacle avoidance [37, 38]. Wang et al. [39] studied the use of nonlinear prediction model (NMPC) for redundant space robot to approach detumbling target in intricate space environment. In case of low-speed autonomous vehicle (AV), Chen et al. [40] suggested control algorithm using barrier function to provide safety to the spacecraft. Many researchers suggested that hyper redundant snake like serial manipulator has high utilization in medical robotics, and rescue operation is space. However, due to large redundant joints motion planning is challenging. For providing mobility in task planning, Menon et al. [41] proposed an algorithm derived from calculus of variation for motion planning of hyper redundant robot. In this control scheme, motion at each joint is calculated in such way that all links deviates any obstacle present in the space environment. During obstacle avoidance, it is recommended that spacecraft should follow optimal path and should not stuck in local minimum. However, by using artificial potential field algorithm spacecraft cannot avoid obstacle in the vicinity of target due to high velocity constraints in local minimum. To solve this issue, Roshtami et al. [42] developed improved artificial potential field algorithm to solve local minimum problem during obstacle avoidance. In that case obstacle is both static and dynamic, Q learning and artificial neural network is the scheme to provide autonomous control of spacecraft. Later, Kim and Khosla [43] improved artificial potential field algorithm by using harmonic potential function to reduce the significance of local minima in cluttered environment. In this scheme, arbitrary shaped obstacle can be represented

Table 2 List of collision-free trajectory planning techniques for space manipulator placed on outsized orbital structure

S. No.	References	Trajectory control method
1	Kamegawa et al. [44]	Reflexive control of space robot through proximity sensors
2	Parra et al. [45]	Based on configuration control approach
3	Fan and Liu [46]	Based on two-stage iterative algorithm

Table 3 List of collision-free trajectory planning techniques for space manipulator placed on undersized orbital structure

S. No.	References	Trajectory control method
1	Yao et al. [47]	Based on artificial potential field method
2	Rosmann et al. [48]	Based on nonlinear optimization technique
3	Rybus [49]	Based on rapidly-exploring random trees technique
4	Khadem et al. [50]	Based on nonlinear model predictive control

having potential over the surface. However, computational cost was more due to involvement of each joint in collision avoidance. For this, researchers suggested to use ring around obstacle, so that wrist of robot is inside the ring instead of its all joints.

However, trajectory control method shown in Table 2 proved to have high computational cost, to compensate this drawback later, collision-free trajectory planning techniques for space robot placed on undersized satellites are proposed as shown in Table 3.

Robotic assistance to astronauts will have vital role in space activities. Project work having human–robot collaboration requires an instinctive design between user and machine interface [51–54]. This kind of man–machine collaboration will improve the safety of such system. Since 1980s major work took place in automation for helping the human decision-making using pilot assistant and reducing the workload.

4 Conclusion and Discussion

It has been shown that planetary robotic system, on-orbit servicing, impedance control, and obstacle avoidance are of increasing interest in the field of space robotics. As a result, many enabling techniques for space robotics have been developed by the researchers across the world in the past four decades. These development works reported in 55 publications have been reviewed with an emphasis on the key areas of engineering test satellites, obstacle avoidance, on-orbit servicing, impedance control, and space exploration mission. In addition, obstacle avoidance (i) collision-free trajectory planning technique for space manipulator placed on outsized orbital structure, (ii) collision-free trajectory planning technique for space manipulator placed

on undersized orbital structure. From the literature survey, technical details of engineering test satellites are discussed. The most challenging aspect of a space mission is performing servicing of non-cooperative satellites with completely autonomous control, detumbling of non-cooperative satellites via impedance control, and dynamic control of autonomous moving targets with lowest rendezvous attitude. This paper provides a comprehensive study of the key challenges and projected solutions for obstacle avoidance, on-orbit servicing, and impedance control for fully autonomous space missions in the near future in order to inspire and assist in the advancement of research development in space technology. At last, after reviewing 55 research articles future research trends in space robotics are found which is listed below:

(i) In near future servicing of non-cooperative satellite with fully autonomous control is required to be explored.
(ii) Further work is required to be done in detumbling non-cooperative satellites through impedance control in near future.
(iii) Research scope in space astronomy and solar system planets.

References

1. Ahmed, S., Dalla, V.K., Prasad, N.: Motion planning control of cooperative two redundant space robots. In: 5th International Conference on Advances in Robotics, June 30–July 4 2021, IIT Kanpur, ACM, New York, NY, USA, 6 pp.
2. Catlin, D., Blamires, M.: Designing robots for special needs education. Technol. Knowl. Learn. **24**(2), 291–313 (2019)
3. Fong, T., Rochlis Zumbado, J., Currie, N., Mishkin, A., Akin, D.L.: Space telerobotics: unique challenges to human–robot collaboration in space. Rev. Hum. Factors Ergon. **9**(1), 6–56 (2013)
4. Yoshida, K.: Achievements in space robotics. IEEE Robot. Autom. Mag. **16**(4), 20–28 (2009)
5. Sanguino, T.D.: 50 years of rovers for planetary exploration: a retrospective review for future directions. Robot. Auton. Syst. **1**(94), 172–185 (2017)
6. Woffinden, D.C., Geller, D.K.: Navigating the road to autonomous orbital rendezvous. J. Spacecr. Rocket. **44**(4), 898–909 (2007)
7. Hirzinger, G., Landzettel, K., Brunner, B., Fischer, M., Preusche, C., Reintsema, D., Albu-Schäffer, A., Schreiber, G., Steinmetz, B.M.: DLR's robotics technologies for on-orbit servicing. Adv. Robot. **18**(2), 139–174 (2004)
8. Jung, S., Hsia, T.C., Bonitz, R.G.: Force tracking impedance control of robot manipulators under unknown environment. IEEE Trans. Control Syst. Technol. **12**(3), 474–483 (2004)
9. Yoo, S., Lee, J., Choi, J., Chung, G., Chung, W.K.: Development of rotary hydro-elastic actuator with robust internal-loop-compensator-based torque control and cross-parallel connection spring. Mechatronics **1**(43), 112–123 (2017)
10. Zhao, Y., Chai, X., Gao, F., Qi, C.: Obstacle avoidance and motion planning scheme for a hexapod robot Octopus-III. Robot. Auton. Syst. **1**(103), 199–212 (2018)
11. Uyama, N., Narumi, T.: Hybrid impedance/position control of a free-flying space robot for detumbling a noncooperative satellite. IFAC-Papers On Line **49**(17), 230–235 (2016)
12. Qian, X., Altché, F., Bender, P., Stiller, C., de La Fortelle, A.: Optimal trajectory planning for autonomous driving integrating logical constraints: an MIQP perspective. In: 2016 IEEE 19th International Conference on Intelligent Transportation Systems (ITSC) 1 Nov 2016, pp. 205–210. IEEE (2016)

13. Dalla, V.K., Pathak, P.M.: Reconfiguration of joint locked hyper-redundant space manipulator. In: Proceedings of the 2015 Conference on Advances in Robotics 2 Jul 2015, pp. 1–6 (2015)
14. Hörmann, A., Meier, W., Schloen, J.: A control architecture for an advanced fault-tolerant robot system. Robot. Auton. Syst. **7**(2–3), 211–225 (1991)
15. Rahmann, H., Hilbig, R., Flemming, J., Slenzka, K.: Influence of long-term altered gravity on the swimming performance of developing cichlid fish: including results from the 2nd German Spacelab Mission D-2. Adv. Space Res. **17**(6–7), 121–124 (1996)
16. Oda, M.: ETS-VII: achievements, troubles and future. In: Proceedings of the 6th International Symposium on Artificial Intelligence and Robotics & Automation in Space: ISAIRAS 2001, Jun 2001
17. Oda, M.: Experiences and lessons learned from the ETS-VII robot satellite. In: Proceedings 2000 ICRA. Millennium Conference. IEEE International Conference on Robotics and Automation. Symposia Proceedings (Cat. No. 00CH37065) 24 Apr 2000, vol. 1, pp. 914–919). IEEE (2000)
18. Shan, M., Guo, J., Gill, E.: Review and comparison of active space debris capturing and removal methods. Prog. Aerosp. Sci. **1**(80), 18–32 (2016)
19. Dalla, V.K., Pathak, P.M.: Trajectory tracking control of a group of cooperative planar space robot systems. Proc. Inst. Mech. Eng. Part I: J. Syst. Control Eng. **229**(10), 885–901 (2015)
20. Garg, H., Sharma, S.P.: Multi-objective reliability-redundancy allocation problem using particle swarm optimization. Comput. Ind. Eng. **64**(1), 247–255 (2013)
21. Guo, W., Li, Y., Li, Y.Z., Wang, S.N., Zhong, M.L., Wang, J.X., Zhang, J.X.: Construction and experimental verification of a novel flexible thermal control system configuration for the autonomous on-orbit services of space missions. Energy Convers. Manag. **15**(138), 273–285 (2017)
22. Dalla, V.K., Pathak, P.M.: Curve-constrained collision-free trajectory control of hyper-redundant planar space robot. Proc. Inst. Mech. Eng. Part I: J. Syst. Control Eng. **231**(4), 282–298 (2017)
23. Shrivastava, A., Dalla, V.K.: Failure control and energy optimization of multi-axes space manipulator through genetic algorithm approach. J. Braz. Soc. Mech. Sci. Eng. **43**(10), 1–7 (2021)
24. Dalla, V.K., Pathak, P.M.: Docking operation by multiple space robots for minimum attitude disturbance. Int. J. Model. Simul. **38**(1), 38–49 (2018)
25. Zhengcang, C., Yuquan, L., Luo, H.: Analysis of dynamics of a floating-base N-DOF space manipulator system. In: 2016 2nd International Conference on Control, Automation and Robotics (ICCAR), 28 Apr 2016, pp. 233–237. IEEE (2016)
26. Zhan, B., Jin, M., Yang, G., Zhang, C.: A novel strategy for space manipulator detumbling a non-cooperative target with collision avoidance. Adv. Space Res. **66**(4), 785–799 (2020)
27. Meng, Q., Zhao, C., Ji, H., Liang, J.: Identify the full inertial parameters of a non-cooperative target with eddy current detumbling. Adv. Space Res. **66**(7), 1792–1802 (2020)
28. Luo, J., Xu, R., Wang, M.: Detumbling and stabilization of a tumbling target using a space manipulator with joint-velocity limits. Adv. Space Res. **66**(7), 1689–1699 (2020)
29. Han, D., Huang, P., Liu, X., Yang, Y.: Combined spacecraft stabilization control after multiple impacts during the capture of a tumbling target by a space robot. Acta Astron. (2020)
30. Liu, Y.Q., Yu, Z.W., Liu, X.F., Cai, G.P.: Active detumbling technology for high dynamic non-cooperative space targets. Multibody Syst. Dyn. **47**(1), 21–41 (2019)
31. Bennett, S.: Development of the PID controller. IEEE Control Syst. Mag. **13**(6), 58–62 (1993)
32. Uyama, N., Narumi, T.: Hybrid impedance/position control of a free-flying space robot for detumbling a non-cooperative satellite. IFAC-PapersOnLine **49**(17), 230–235 (2016)
33. Pathak, P.M., Mukherjee, A., Dasgupta, A.: Impedance control of space robots using passive degrees of freedom in controller domain
34. Dalla, V.K., Pathak, P.M.: Impedance control in multiple cooperative space robots pulling a flexible wire. Proc. Inst. Mech. Eng. C J. Mech. Eng. Sci. **233**(6), 2190–2205 (2019)
35. Zong, L., Luo, J., Wang, M., Yuan, J.: Obstacle avoidance handling and mixed integer predictive control for space robots. Adv. Space Res. **61**(8), 1997–2009 (2018)

36. Bao, D.Q., Zelinka, I.: Obstacle avoidance for swarm robot based on self-organizing migrating algorithm. Procedia Comput. Sci. **1**(150), 425–432 (2019)
37. Llamazares, Á., Molinos, E., Ocaña, M., Ivan, V.: Improved dynamic obstacle mapping (iDOMap). Sensors **20**(19), 5520 (2020)
38. Dalla, V.K., Pathak, P.M.: Power-optimized motion planning of reconfigured redundant space robot. Proc. Inst. Mech. Eng. Part I: J. Syst. Control Eng. **233**(8), 1030–1044 (2019)
39. Wang, M., Luo, J., Walter, U.: A non-linear model predictive controller with obstacle avoidance for a space robot. Adv. Space Res. **57**(8), 1737–1746 (2016)
40. Chen, Y., Peng, H., Grizzle, J.: Obstacle avoidance for low-speed autonomous vehicles with barrier function. IEEE Trans. Control Syst. Technol. **26**(1), 194–206 (2017)
41. Menon, M.S., Ravi, V.C., Ghosal, A.: Trajectory planning and obstacle avoidance for hyper-redundant serial robots. J. Mech. Robot. **9**(4) (2017)
42. Rostami, S.M., Sangaiah, A.K., Wang, J., Liu, X.: Obstacle avoidance of mobile robots using modified artificial potential field algorithm. EURASIP J. Wirel. Commun. Netw. **2019**(1), 70 (2019)
43. Kim, J.O., Khosla, P.: Real-time obstacle avoidance using harmonic potential functions
44. Kamegawa, T., Akiyama, T., Suzuki, Y., Kishutani, T., Gofuku, A.: Three-dimensional reflexive behavior by a snake robot with full circumference pressure sensors. In: 2020 IEEE/SICE International Symposium on System Integration (SII), 12 Jan 2020, pp. 897–902. IEEE (2020)
45. Parra, P., Polo, Ó.R., Carrasco, A., da Silva, A., Martínez, A., Sánchez, S.: Model-driven environment for configuration control and deployment of on-board satellite software. Acta Astron. (2020)
46. Fan, Y., Liu, X.: Two-stage auxiliary model gradient-based iterative algorithm for the input nonlinear controlled autoregressive system with variable-gain nonlinearity. Int. J. Robust Nonlinear Control **30**(14), 5492–5509 (2020)
47. Yao, Q., Zheng, Z., Qi, L., Yuan, H., Guo, X., Zhao, M., Liu, Z., Yang, T.: Path planning method with improved artificial potential field—a reinforcement learning perspective. IEEE Access **22**(8), 135513–135523 (2020)
48. Rösmann, C., Makarow, A., Bertram, T.: Online motion planning based on nonlinear model predictive control with non-Euclidean rotation groups. arXiv preprint arXiv:2006.03534 (2020)
49. Rybus, T.: Point-to-point motion planning of a free-floating space manipulator using the rapidly-exploring random trees (RRT) method. Robotica **38**(6), 957–982 (2020)
50. Khadem, M., O'Neill. J., Mitros, Z., da Cruz, L., Bergeles, C.: Autonomous steering of concentric tube robots via nonlinear model predictive control. IEEE Trans. Robot. (2020)
51. Zhao, Y., Liu, H., Gao, K.: An evacuation simulation method based on an improved artificial bee colony algorithm and a social force model. Appl. Intell. **6**, 1–24 (2020)
52. Nourbakhsh, I.R., Sycara, K., Koes, M., Yong, M., Lewis, M., Burion, S.: Human-robot teaming for search and rescue. IEEE Pervasive Comput. **4**(1), 72–79 (2005)
53. De Visser, E., Parasuraman, R.: Adaptive aiding of human-robot teaming: effects of imperfect automation on performance, trust, and workload. J. Cogn. Eng. Decis. Mak. **5**(2), 209–231 (2011)
54. Dalla, V.K., Pathak, P.M.: Trajectory control of curve constrained hyper-redundant space manipulator. In: Proceedings of the 14th IFToMM World Congress, 4 Nov 2015, pp. 367–374.

國立臺灣大學機械系

Enhancement of Magnetic Flux Density Using a Novel Electromagnets Configurations in Belt-Type Magnetorheological Finishing Setup

Prince Oliver Horo, Prabhat Kumar, Saurabh Singh Rathore, and Dilshad Ahmad Khan

1 Introduction

With the growth of contemporary technologies, the goal in the modern era is to enhance the accuracy and precision of products at the nano-scale level in order to perform a certain desired function.

For the industries such as medical science, space science, automobile, defense, electronics, etc. surface finishing plays an essential function in extending the component's service life.

Because of their least controlled, labor-intensive, and time-consuming characteristics, final finishing operations in manufacturing are sometimes a matter of great concern [1]. Ultrafine finishing of complex geometry, internal grooves, and free-form surfaces with the aid of conventional process is a challenging task to implement. Despite the various applications of conventional processes like grinding, lapping, honing, and polishing, these are incapable of producing surfaces with close tolerances because of uncontrolled cutting forces and thermal stresses induced during the interaction of the workpiece and tool.

P. O. Horo (✉) · P. Kumar · S. S. Rathore · D. A. Khan
Department of Mechanical Engineering, National Institute of Technology, Hamirpur, Hamirpur, Himachal Pradesh 177005, India
e-mail: prince@nith.ac.in

P. Kumar
e-mail: 20mme208@nith.ac.in

S. S. Rathore
e-mail: 20mme213@nith.ac.in

D. A. Khan
e-mail: dilshad@nith.ac.in

To run over the problems associated with the conventional processes magnetic field-assisted finishing processes were developed by the Center for Optics Machining (COM), Rochester USA.

The Rochester (USA) based Center for Optics Machining (COM), developed magnetic field-assisted finishing process to overcome the issues associated with traditional processes [2].

Magnetorheological finishing (MRF) process relies on Magnetorheological (MR) fluid which consists of the abrasive particle along with carrier medium. The magnetic field causes the MR fluid particles to stiffen; in other words, the MRF process uses a flexible fluid whose bonding strength is determined by a magnetic field that can be regulated externally.

Kordonski and Golini [3] observed that removal rate is a well-defined function of fluid viscosity, finding that a viscosity change of 1% results in a change in material removal as roughly 1.5% in their experimental investigation.

In their other study, Kordonski and Golini [4] performed an experimental study on a wide range of optical surface shapes, including aspheres, and discovered that the MRF process can significantly reduce surface error with an 81% correction rate, meeting customer specification. Kim et al. [5] proposed a surface finishing method for a 3-dimensional silicon microchannel structure. Soek and Kim [6] presented an MR fluid-based machining process for shaping curved surfaces. Cheng et al. [7] developed a wheel-shaped tool having two-axis that supports a dual magnetic field for the surface finishing of optical aspheric components based on the MRF technique. Sidpara and Jain [8] studied the effect of process parameters on the forces acting on the workpiece surface during the MRF process. The magnetorheological fluid-based honing process, proposed by Singh et al. [9], is a newly developed design for the interior surface finishing of ferromagnetic cylindrical workpieces.

Grover and Singh [10] focused on improving the design of the Magnetorheological Fluid-based honing process by replacing the magnetic flat end surface tool with the curved permanent magnet tool. In this paper, a novel belt and pulley type MRF setup has been designed to overcome the complication of limited spot finishing by increasing the workspace, also a novel configuration of set of three electromagnets has been disclosed which can satisfactorily generate uniform magnetic flux density in the base plate as well is in the MR fluid.

2   Construction Details of a Belt-Type Magnetorheological Finishing Setup

Figure 1 depicts the schematic of the belt-type magnetorheological finishing setup. A single electromagnet having 3500 turns and 100 mm in length with an axially passing core of 25 mm diameter and 110 mm length is designed to generate the magnetic flux density. A ferromagnetic soft material (AISI 1010) is elected as the core material. An iron base plate, over which the belt is moved, rests on the top of
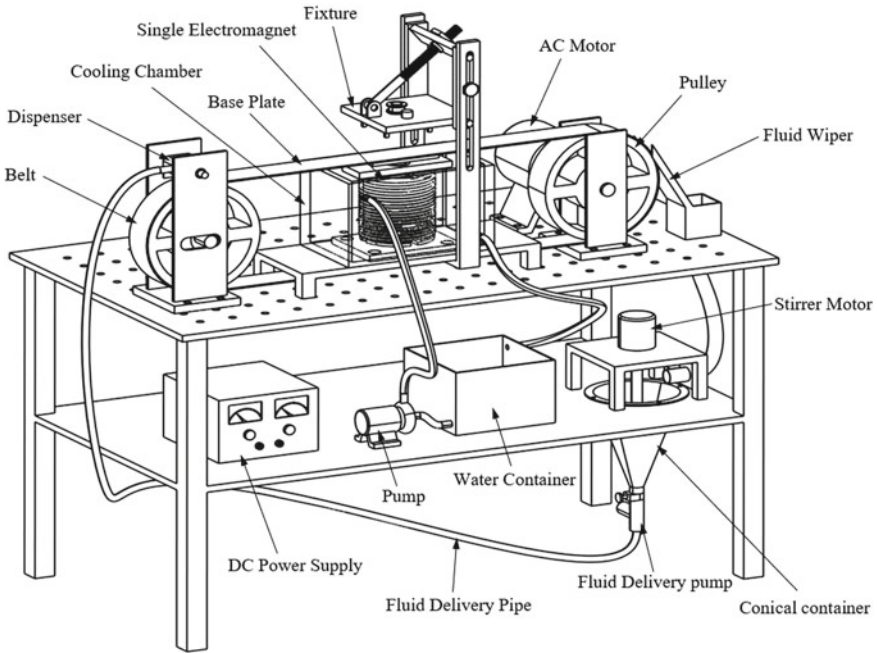
Fig. 1 Belt type finishing setup with single electromagnet

the core. A fixture is provided in the setup that can slide vertically and can also rotate on its own vertical axis.

The dispenser attached at one end of the pulley dispenses the MR fluid over the running belt. The MR fluid when comes in acquaintances with the applied magnetic field changes its rheological properties, later on losing the acquaintances with the magnetic field the MR fluid regains its original state. The MRP fluid is then transferred into a conical container where it is continuously stirred to avoid the sedimentation of CIPs and abrasives and it dispensed again with the help of a pump. The DC power supply is used to generate and control the magnetic field strength. Electromagnet is housed in housing to cool the electromagnet against the temperature rising.

3 Result and Discussion

In the first stage of simulation, a mild steel workpiece of 30 mm length, 50 mm width, and 10 mm thickness has been elected for the simulation. Simulation results of the magnetic flux distribution are shown in Fig. 2. The results show that the magnetic flux density is higher at the base plate around the central region and reduces as the distance increases from the center.
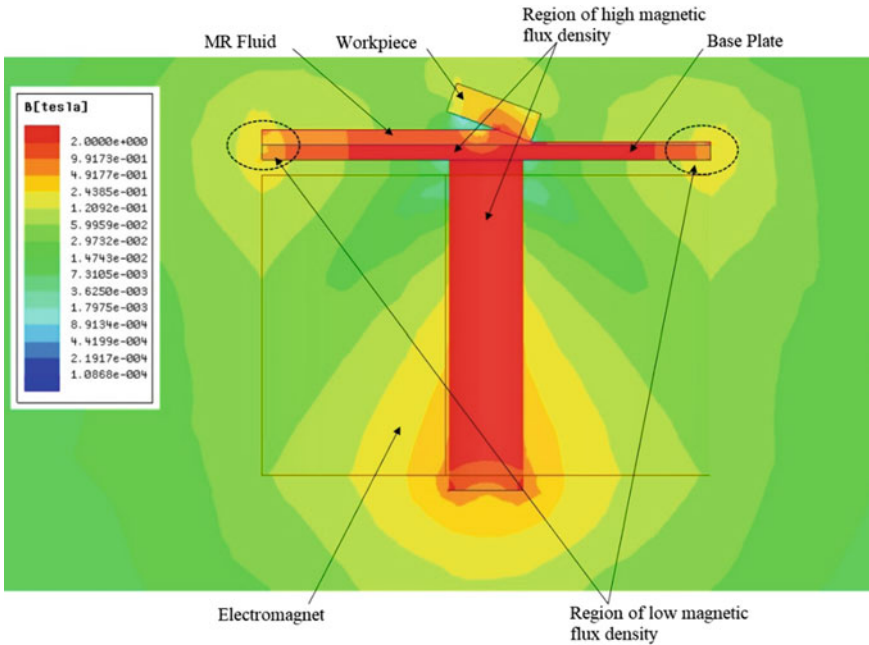
Fig. 2 Magnetic flux density distribution with single electromagnet

Although the magnetic flux density is good at the middle region of the base plate sufficient for the finishing but problem with this design is that the span of the finishing the workpiece is reduced. The objective is to increase the workspace of the setup so that a large area of the workpiece can be finished in a single run. These simulation results with single electromagnet show an assuring result but do not comply with the objective. Also, if the size of the electromagnet is increased, the number of turns of the electromagnet will also increase which will result in an enormous amount of heat generated inside the electromagnet.

In first stage of simulation, the setup has been designed with a single electro-magnet to achieve a uniform magnetic flux density at the whole base plate. Simula-tion results show that the higher magnetic flux density is in the middle of the plate only and decreases away from the middle region. Again, it is also associated with the problem of working space and its heftiness, as mentioned earlier. To overcome the above-mentioned problem, the whole setup is redesigned with a set of three vertical electromagnets. The basic idea is to increase the workspace and to reduce the size of the electromagnet to run over the issue of overheating.

To validate the new design of multiple electromagnets, in the second stage of simulation, magnetic simulation has been performed on the set of three vertical electromagnets. Each electromagnet has 2000 number of turns, 100 mm of length, and a core diameter of 25 mm. the electromagnets are placed close to each other at a center-to-center distance of 110 mm. The result of the magnetic simulation (Fig. 3)
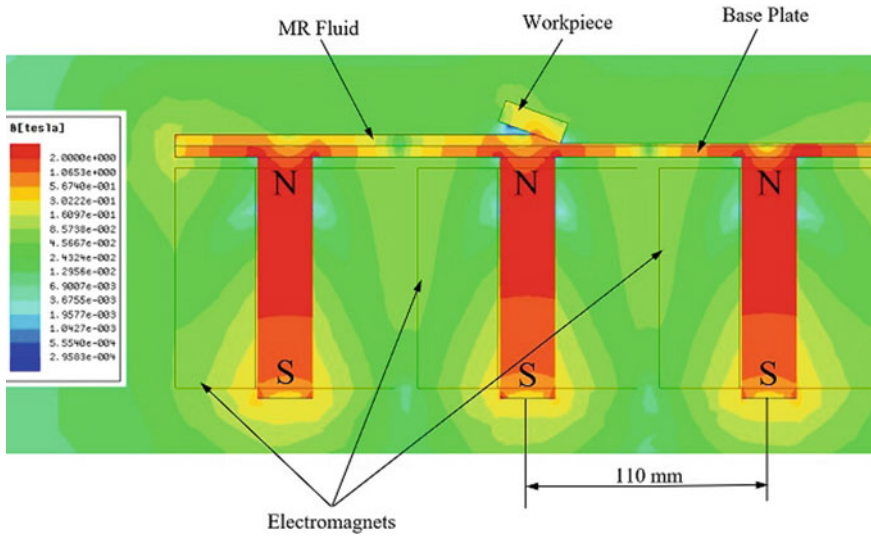
Fig. 3 Magnetic flux density distribution with three electromagnets

shows that the magnetic flux density in the base plate is higher around the outer surface of the core connected to it and decreases in radial direction. The same results are achieved when the electromagnets are placed close to each other in that case the magnetic flux lines emerging from one electromagnet conflict with the magnetic flux lines of the other electromagnet. Due to these interactions of the magnetic flux lines, the magnetic flux density decreases away from the central region (around the core). So, strength of the magnetic flux density varies along the length of the base plate.

To overcome the problems related with the above-mentioned stages, a new configuration of the electromagnet has been evaluated by performing the magnetic simulations. In this configuration of the electromagnets, instead of placing all the electromagnets vertically, the middle one among the three is placed horizontally.

Figure 4 depicts the magnetic simulation with one horizontally places electromagnet. The result shows an enhancement in the magnetic flux density of the core as well as of the base plate. Taking a reference from left-hand side to the right-hand side, the polarity of the two vertical electromagnets is opposite to each other and the magnetic polarity of middle electromagnet is shown in the figure (Fig. 4). The magnetic field line emerging from the north pole of the left-hand side magnet forms a loop with the south pole of the right-hand side electromagnet. Similarly, the magnetic field lines emerging from the north pole of the right-hand side electromagnet form a loop with the south pole of the left-hand side electromagnet, thus forming an aura of magnetic field lines which fully covers the set of electromagnets. However, the magnetic flux density in the MRP fluid is lower in the workpiece surface. The much better results of the magnetic simulations have been achieved if the polarity of the midst electromagnet is reversed from the previous case as shown in Fig. 5. The result reveals that an enhanced magnetic flux density is achieved in each of the core as

well as in the base plate. The magnetic flux density distribution in the base plate is sufficiently higher and uniform in greater span of the base plate. Also, the magnetic flux density distribution is higher and uniform throughout the MRP fluid layer.

Based on the result of above-shown simulation, a novel belt-type MRF setup will be fabricated with the set of three electromagnets, with one placed horizontally
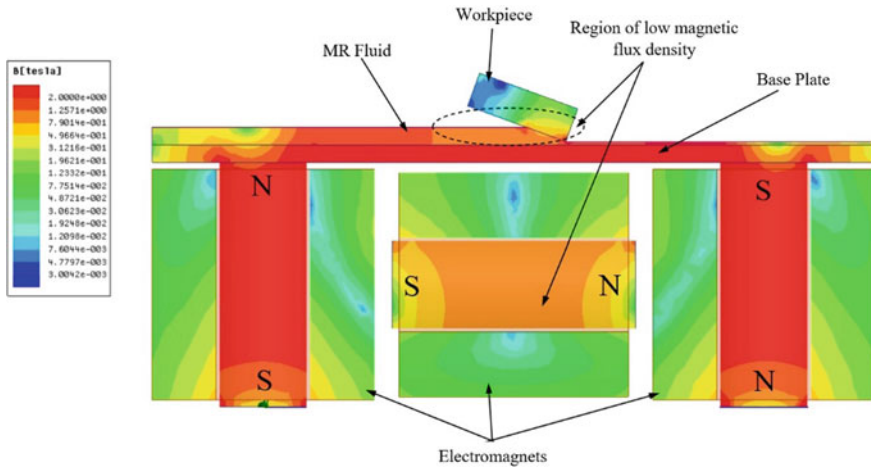

Fig. 4 Magnetic flux density distribution with middle electromagnet in horizontal position
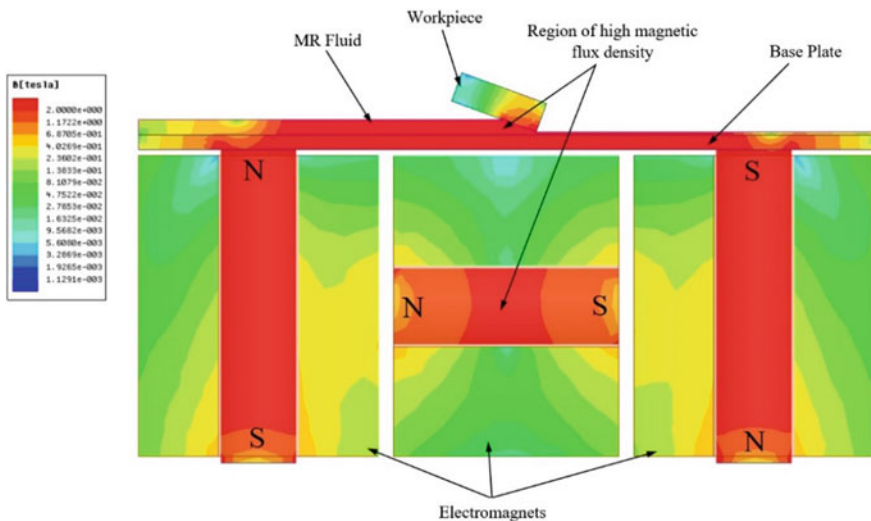
Fig. 5 Magnetic flux density distribution with middle electromagnet in horizontal position, a modified configuration of electromagnets

among them. Further, pilot experiment shall be performed to analyze the process capabilities of the proposed setup.

4 Conclusion

The series of magnetic simulations have been performed to analyze the performance of the different configurations of the electromagnets in the belt-type magnetorheological finishing setup. Simulation results show that a single electromagnet gives promising results but at the cost of increased size of the electromagnets which leads to the phenomenon of overheating. Set of three vertical electromagnets do not indicate a satisfactory result as each of the electromagnets perform individually and the magnetic flux lines of one electromagnet conflict with the magnetic flux lines of other electromagnets. The simulation results show that a higher magnetic flux density is achieved with a set of three electromagnets keeping one electromagnet in horizontal position in between two vertical electromagnets with the magnetic poles in opposite order. The horizontally placed electromagnet is kept in such a way that the magnetic poles of the horizontal electromagnet are of same nature as that of the top poles of the vertical electromagnets. The study based on the magnetic simulation has confirmed the use of a set of three electromagnets, with one electromagnet placed horizontally results in the increment of the magnetic flux density in the base plate which complies with the objective of the finishing large size flat and externally curved surfaces with enhanced and uniform magnetic flux density.

References

1. Sidpara, A., Jain, V.K.: Nano–level finishing of single-crystal silicon blank using magnetorheological finishing process. Tribol. Int. **1**(47), 159–166 (2012)
2. Kordonski, W.I., Jacobs, S.D.: Magnetorheological finishing. Int. J. Mod Phys. B **10**(23n24), 2837–2848 (1996)
3. Kordonski, W.I., Golini, D.: Fundamentals of magnetorheological fluid utilization in high precision finishing. J. Intell. Mater. Syst. Struct. **10**(9), 683–689 (1999)
4. Kordonski, W., Golini. D.: Progress update in magnetorheological finishing. Int. J. Mod. Phys. B **13**(14n16), 2205–2212 (1999)
5. Kim, W.B., Lee, S.H., Min, B.K.: Surface finishing and evaluation of three-dimensional silicon microchannel using magnetorheological fluid. J. Manuf. Sci. Eng. **126**(4), 772–778 (2004)
6. Seok, J., Kim, Y.J., Jang, K.I., Min, B.K., Lee, S.J.: A study on the fabrication of curved surfaces using magnetorheological fluid finishing. Int. J. Mach. Tools Manuf. **47**(14), 2077–2090 (2007)
7. Cheng, H.B., Yam, Y., Wang, Y.T.: Experimentation on MR fluid using a 2-axis wheel tool. J. Mater. Process. Technol. **209**(12–13), 5254–5261 (2009)
8. Sidpara, A., Jain, V.K.: Experimental investigations into forces during magnetorheological fluid based finishing process. Int. J. Mach. Tools Manuf. **51**(4), 358–362 (2011)
9. Paswan, S.K., Bedi, T.S., Singh, A.K.: Modeling and simulation of surface roughness in magnetorheological fluid based honing process. Wear **15**(376), 1207–1221 (2017)
10. Grover, V., Singh, A.K.: Improved magnetorheological honing process for nanofinishing of variable cylindrical internal surfaces. Mater. Manuf. Process. **33**(11), 1177–1187 (2018)

Experimental Investigation to Enhance the Performance of Freezer with Phase Change Material

Mummina Vinod, V. Mahesh Chakravarthi, Mangam Venu, and Duvvuri Vamsee Krishna
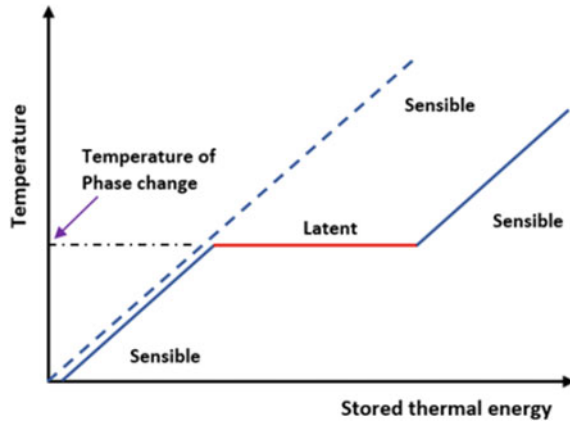
1 Introduction

Air conditioners, refrigerators and freezers are the most power consuming devices because of their continuous operation. In this condition, enhancing the efficiency of the refrigerator is a significant issue about energy saving and global warming. To increase the efficiency of the refrigerators a lot of techniques are introduced but out of all these latent heat storage using phase change material (PCM) is a novel method [1, 2]. PCM is an element which can discharge or store a huge amount of heat energy by transforming its phase and it is also known as latent heat thermal energy storage (LHTES) material [3], so by incorporation of PCM in freezer or refrigerator enhances device performance [4] and also reduce the power consumption by maintain constant temperature in the device during its compressor off mode position. LHTES system is best efficient technique to store thermal energy [5] and it is used in a variety of applications which includes metal processing, heating and cooling of space, storage and processing of food, thermal energy storage, spacecraft thermal systems, etc. The working principle of latent and sensible heat storage system [6] is shown in Fig. 1. Phase transformation temperature of the PCM place a key role to get the best results. Amongst the PCMs studied, Glycol solution is the potential substances for this purpose [7] because it is having high storage capacity of latent heat, non-corrosiveness, odourless, low-viscosity, low volatility and hygroscopic liquid. The solubility and reactivity of glycol solution provides the basis for many applications. Hence, we used ethylene glycol as PCM for this investigation. In conventional freezer or refrigerator, refrigerant absorbs the heat from the evaporator cabinet throughout compressor ON mode position. When the compressor is off, the cabinet temperature increases due to heat released by the food. If PCM is placed

M. Vinod (✉) · V. Mahesh Chakravarthi · M. Venu · D. V. Krishna
Vishnu Institute of Technology, Bhimavaram 534202, India
e-mail: vinodmummina@gmail.com

around the evaporator, it will absorb the majority of heat by transforming from solid phase to liquid phase during OFF mode of the compressor. Until the melting process completes, the temperature is steady. The heat stored during this process is named as latent heat and it is shown in Fig. 1 [6]. Because of this process, we can maintain the desired temperature in the cabin for a specific time interval during the compressor off mode. When this liquid phased PCM is physically contacted with the evaporator coil, the refrigerant inside the coil can extract stored heat from PCM by conduction heat transfer process during ON time of compressor. Figure 2 [8] shows the working of PCM in a freezer. In the present work we fabricated a commercial freezer and we used ethylene glycol as PCM to enhance the performance of the freezer. The experiment was done with and without PCM at different load conditions and these values are compared with each other. The performance of the freezer is enhanced up to 80% due to this method and power consumption is also decreased.

1.1 Material Required for the Fabrication of Freezer

The outer tank of the freezer is made up of stainless steel (SS) sheet of 24 gauge thickness. This sheet is made into five sheets of each having 480 mm × 480 mm of dimension. These sheets are joined together by tig welding to form an outer tank. The evaporator body is kept inside the master tank. The PCM is made contact with the evaporator coil and the master tank. The master tank is in square cross section made with galvanized iron (GI) with 360 mm × 360 mm dimension. The evaporator body contains copper tubes for refrigerant flow around the evaporator of 10 mm diameter. GI sheet is used to make an evaporator tank with side 305 mm × 360 mm dimension. Cover plates are provided for both master and outer tanks. The master tank cover plate is made with a GI sheet of area 400 mm × 400 mm. The outer tank cover plate is made with an SS sheet of area 480 mm × 480 mm. The refrigerant
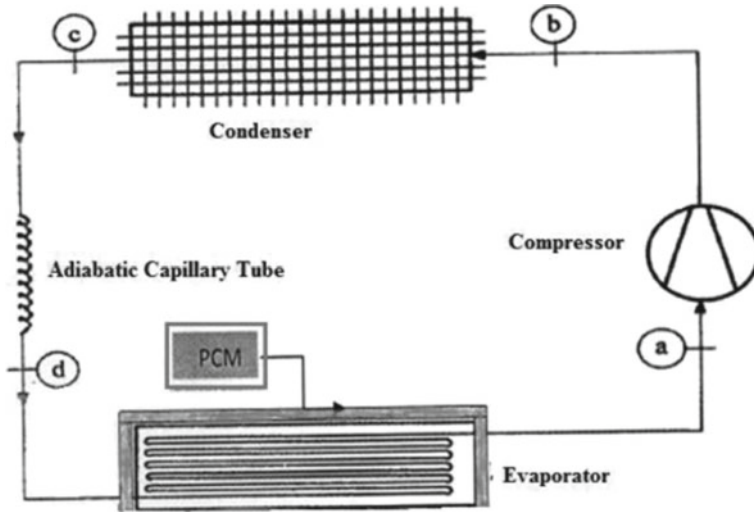
Fig. 2 Working of PCM in a freezer

used for this investigation is R-134a. Table 1 shows the technical specifications for the components of the freezer.

2 Experiment Setup

The commercial freezer was developed with required materials as shown in Fig. 3. Four thermocouples are arranged, to find the temperature of the refrigerant at the outlet and inlet of the condenser and compressor. These thermocouples are calibrated by the procedure defined in Merlone et al. [9]. A pressure gauge (500 psi) is coupled across the condenser outlet and capillary tube inlet to measure the condenser outlet pressure. Capillary tube outlet is connected to the inlet of the evaporator. Another pressure gauge of 250 psi connected across capillary tube outlet and evaporator inlet to measure pressure drop in expansion device also known as evaporator inlet measure. Finally, the phase change material (Glycol Solution) is arranged in the form of packets at four sides around the evaporator in contact with the evaporator coil as shown in Fig. 4. The leak tests are performed before pumping the refrigerant into the tubes.

Table 1 Technical specification of the freezer

Name of the components	Units
Evaporator	
Type of evaporator	Plate type evaporator
Cabinet volume	33 L
Length of cabinet	305 mm
Breadth of cabinet	305 mm
Height of cabinet	360 mm
Heat transfer mode	Free convection
Evaporator material	Galvanized sheet of 0.5 mm thickness
Evaporator coil material	Copper of 10 mm diameter
Condenser	
Type of condenser	Forced convection air cooled condenser
Length and height of condenser	204 mm × 204 mm
Material of the tube	Copper of 10 mm diameter
Material of the fin	Aluminium
Compressor	
Type of compressor and model	Hermetic reciprocating compressor, MA42LPJG Energy efficiency ratio, EER–3.8 Btu/Wh
Power rating	96 W
Expansion device	
Capillary tube	1.5 mm diameter
Pressure gauges	
Condenser outlet pressure gauge capacity	500 psi
Evaporator inlet pressure gauge capacity	250 psi

3 Result and Discussion

The freezer is switched ON and runs the freezer for one hour without inserting PCM packets and raising the thermal load inside the evaporator cabin. The values are noted at every 15 min interval as shown in Table 2. We can observe that at every interval the evaporator inlet and condenser outlet pressures are increased due to increase in thermal load. The outlet and inlet temperatures of compressor and condenser are raised with increase in pressure. Enthalpy values are shown in Table 3, which are taken from P-h chart of refrigerant R-134a.

The COP of the freezer can be calculated by using Eq. (1) [10] and the COP of the freezer at different load conditions with and without PCM are shown in Table 6.

$$\text{Coefficient of performance, COP} = \frac{\text{Refrigeration effect}}{\text{Workdone by compressor}} = \frac{h_1 - h_4}{h_2 - h_1} \quad (1)$$
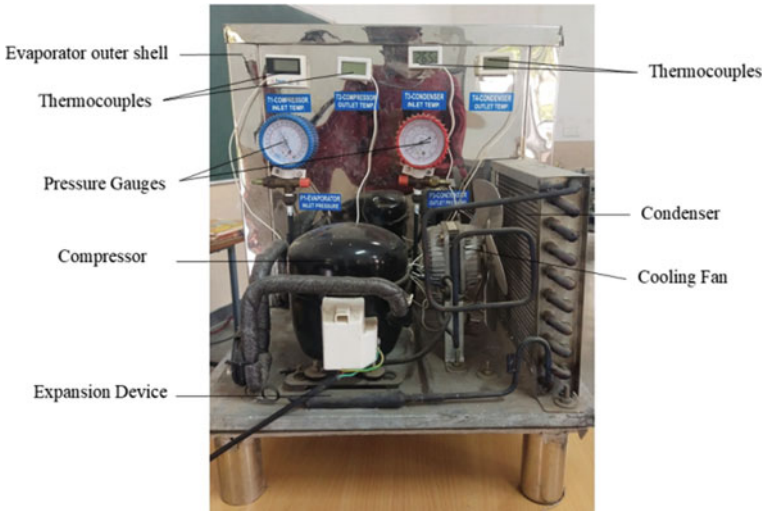
Fig. 3 Experimental setup of commercial freezer

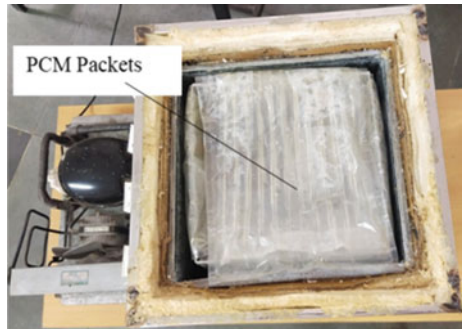**Fig. 4** Arrangement of
PCM around the evaporator

PCM Packets

Table 2 Experimental values without PCM

Time	Load	Inlet pressure of the evaporator	Outlet pressure of the condenser	Inlet temperature of the compressor	Outlet temperature of the compressor	Inlet temperature of the condenser	Outlet temperature of the condenser
Min	kg	P_1 bar	P_3 bar	T_1 °C	T_2 °C	T_3 °C	T_4 °C
0–15	1	0.29	8	22.4	68.5	58.4	31.7
15–30	2	0.29	8.5	27.7	70.8	60.8	33.5
30–45	3	0.49	9.2	23.2	74.5	63.1	36.8
45–60	4	0.58	10.9	24.4	78	68.7	36.9
60–75	5	0.58	14.8	17.8	79.6	69.6	35.7

Table 3 Enthalpy values without PCM

Compressor inlet enthalpy (h_1) kJ/kg	Compressor outlet enthalpy (h_2) kJ/kg	Condenser outlet enthalpy (h_4) kJ/kg
422	452	244
426	454	246
422	456	251
423	458	251
417	453	249

Again the experiment is conducted by inserting PCM packets around the evaporator and allows running for 2–3 h until the glycol solution (PCM) freezes. The values are noted at every 15 min interval as shown in Table 4. Enthalpy values are shown in Table 5, which are taken from P-h chart of refrigerant R-134a. The comparison of COP for two different conditions is shown in Table 6.

From the comparison graph as shown in Fig. 5 simply we can say that by using PCM in the cooling devices the COP increases and it is dependent on load conditions.

The Percentage of COP improved by using PCM

$$\frac{\text{COP}_{\text{with PCM}} - \text{COP}_{\text{without PCM}}}{\text{COP}_{\text{without PCM}}} \times 100\% \tag{2}$$

Table 4 Experimental values with phase change material

Time	Load	Inlet pressure of the evaporator	Outlet pressure of the condenser	Inlet temperature of the compressor	Outlet temperature of the compressor	Inlet temperature of the condenser	Outlet temperature of the condenser
Min	kg	P_1 bar	P_3 bar	T_1 °C	T_2 °C	T_3 °C	T_4 °C
0–15	1	0.3	10.3	26.5	65.1	56.5	10.3
15–30	2	0.4	12.7	28.9	70.5	61.8	12.7
30–45	3	0.6	12.5	29.6	73.6	63.6	12.5
45–60	4	0.8	14.7	29.6	75.3	66.4	14.7
60–75	5	0.9	16.7	31.1	79.2	70.2	16.7

Table 5 Enthalpy values with PCM

Compressor inlet enthalpy (h_1) kJ/kg	Compressor outlet enthalpy (h_2) kJ/kg	Condenser outlet enthalpy (h_4) kJ/kg
425	444	240
427	446	245
428	450	246
427	448	247
428	449	246

Load (kg)	COP without PCM	COP with PCM
1	5.9	9.74
2	6.63	9.58
3	5	8.07
4	4.97	8.56
5	4.7	8.71

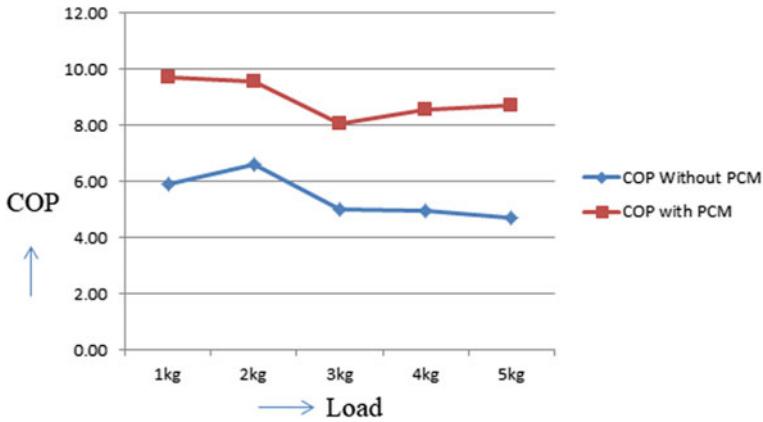**Table 6** COP comparison of freezer without PCM and with PCM

Fig. 5 COP Comparison of freezer without PCM and with PCM

By using Eq. (2) we can calculate the percentage of COP improved for PCM and there is 40–80% increase in COP with PCM around the evaporator, the COP value depends upon the thermal load in the evaporator.

4   Conclusion

Experimental investigation to enhance the performance of the commercial freezer with using ethylene glycol as a phase change material was done. In this experimental study, it has been observed that the COP of a freezer increases from 40 to 80% with PCM at various thermal load conditions. The COP of the freezer without PCM varies from 4 to 6, but the COP of the freezer with PCM varies from 8 to 10. By using PCM in the cooling devices we can reduce power consumption and increase the COP. The heat transfer rate also increases in the evaporator cabinet due to the use of PCM around the evaporator.

References

1. Pavithran, A., Sharma, M., Shukla, A.K.: Energy utilization reduction of domestic refrigerator using phase change materials. In: Sikarwar, B.S., Sundén, B., Wang, Q. (eds.) Advances in Fluid and Thermal Engineering. Lecture Notes in Mechanical Engineering. Springer, Singapore (2021)
2. Gupta, K.K., Ramachandran, M.: Effect of ethylene glycol as phase change material in a cold storage unit on retention of cooling. IOP Conf. Ser.: Mater. Sci. Eng. **377**, 012190 (2018)
3. Oni, T.O., Awopetu, J.B., Adeleye, S.A., Uguru-Okorie, D.C., Adeyanju, A.A., Olukayode, N.E.: Development of a latent heat thermal energy storage material-based refrigeration system. Int. J. Heat Technol. **39**(2), 469–476 (2021)
4. Khan, M.I.H.: Conventional refrigeration systems using phase change material: a review. Int. J. Air-Cond. Refrig. **24**(3), 1630007 (2016)
5. Oro, E., de Gracia, A., Castell, A., Farid, M.M., Cabeza, L.F.: Review on phase change materials (PCMs) for cold thermal energy storage applications. Appl. Energy **99**, 513–533 (2012)
6. Raj, V., Goswami, T.K.: Use of phase change material (PCM) for the improvement of thermal performance of cold storage. MOJCRR. **1**(2) (2018)
7. Zhang, J., Li, H., Tu, J., Shi, R., Luo, Z., Xiong, C., Jiang, M.: Shape stability of polyethylene glycol/acetylene black phase change composites for latent heat storage. Hindawi Adv. Mater. Sci. Eng. **9**, 3954163 (2018)
8. Patil, U.N., Thakur, M.P., Koli, T.A., Patil, V.H.: An investigation of performance improvement in refrigeration test rig by using phase change material (PCM): research. Int. J. Innov. Eng. Sci. **4**(10) (2019)
9. Merlone, A., Iacomini, L., Tiziani, A., Marcarino, P.: A liquid bath for accurate temperature measurements. Measurement **40**, 422–427 (2007)
10. Khan, M.I.H., Afroz, H.M.M.: Effect of phase change material on a performance of a household refrigerator. Asian J. Appl. Sci. **6**(2), 56–67 (2013)

Impact of IDMA Scheme on Power Line Communication

Raj Gaurang Tiwari, Pratibha, Sandeep Dubey, and Ambuj Kumar Agarwal

1 Introduction

Electronic communication is the reliable transmission of this currency over an unreliable physical medium. Digital data is to be transmitted through a high-volume, high-bit-rate channel. Several applications are in operation at high speed and a hard and fast affiliation is commonly most well-liked. If utilities can provide communication across power lines to customers, it might be a huge leap in communications. Each house would be connected at any time, with services available.

The use of the Internet has increased exponentially during the past several years. This category of network connectivity across the power line might turn utilities into communication service providers and open up a new, rapidly expanding sector. Network communications, in contrast to power-connected applications, need very high-bit-rates and, in rare situations, long reaction times (such as video and TV). While this makes designing a communication system more difficult, academics have focused on it relentlessly in recent years. Many commercially available devices employ bit rates between 10 and 100 kb/s for low-demand activities like meter reading, however, there are still others under testing that claim a bit rate of one Mb/s [1–19].

R. G. Tiwari (✉) · A. K. Agarwal
Chitkara University Institute of Engineering and Technology, Chitkara University, Punjab, India
e-mail: rajgaurang@chitkara.edu.in

A. K. Agarwal
e-mail: ambuj.agarwal@chitkara.edu.in

Pratibha · S. Dubey
Shri Ramswaroop Memorial Group of Professional Colleges, Lucknow, India
e-mail: pratibha.dubey@srmcem.ac.in

S. Dubey
e-mail: sandeep@srmcem.ac.in

Consequently, since the power line was firstly intended to be used for power distribution rather than communication, more complex communication methods are necessary. Power line communication has become a highly sought-after transmission medium because of its ease of installation and international accessibility. Multiple access strategies are facilitated by a variety of transmission line systems [2]. Increased bit rates are the key emphasis of today's research, which is necessary to handle high-speed network applications.

1.1 Historical Overview of Power Line Communication (PLC)

The history of power transmission cables in an electronic communication was discussed by Dostert [3]. Before the popularity of radio, broadcasting had a long history. 1864 was the first evidence of electrically induced action and response across long distances, described by medical practitioner M. Loomis in the US. In the 1880s, Hertz carried out experiments to support Maxwell's hypothesis [4]. Ripple carrier signaling (RCS) was used in the 1930s on medium and low voltage distribution lines (10–20 kV). According to Dostert, Siemens and AEG in Potsdam were the first to employ RCS systems in Germany [6]. H. Armstrong, the inventor of frequency modulation (FM) radio, patented the technology in 1933 [7]. FM reduces noise from electrical equipment and the surrounding environment in an RN audio transmission. To transmit radio programs through power lines, PLT was often utilized.

A "typical twenty-five-volt battery" powered the first portable transistor radio released by Regency in 1954 [8]. Sony's first transistor radio was debuted in 1960, and t was pocket-sized and ran on a little battery [9].

Internet-related ideas about using energy distribution systems and home networks for broadband communications began to emerge in the 1990s. Line channel features, modulation methods, and communication protocols have seen a substantial increase in investment over time [10–13].

In this paper, we have thrown the light on power line communication (PLC), so that we can communicate utilizing the presently existing power lines. This paper also describes an "Interleave-Division Multiple Access (IDMA)" system that can alleviate various difficulties caused by both frequency selective fading and impulsive noise.

The remaining part of this paper is organized as follows: Sect. 2 describes the interleave-division multiple access (IDMA). Section 3 portrays the use the use of IDMA technique with the PLC. Section 4 summarizes simulation results. Section 5 describes the performance of Power Line Communication with Different Interleavers. Section 6 wraps up the paper.

2 Interleave-Division Multiple Access (IDMA) Scheme

Mainly for prime spectral potency, enhanced performance and reduced receiver difficulties the interleaver mainly based multiple access strategy has been investigated. This technology uses interleaving to divide signals from different users and is termed interleave-division multiple access (IDMA) [14, 15].

2.1 Transmitter and Receiver for IDMA

Figure 1 demonstrates the transmitter system for various access ways with K concurrent users. d_k is the supplied data. The d_k of user-k is encoded supported by a low-rate code C, which results in a coded sequence termed $c_k \equiv [c_k(1), \ldots, c_k(j), \ldots, c_k(J)]^T$. The c_k components are coded bits. Associate interleaver k permutes this c_k to generate $x_k \equiv [x_k(1), \ldots, x_k(j), \ldots, x_k(J)]^T$. The CDMA forum refers to the components as "chips".

"Interleave-division multiple access (IDMA)" is named after the interleavers that identify these users (IDMA). The interleaver's k should change based on the user, according to IDMA.

$$e(x_k(j)) \equiv \log\left(\frac{p(y|x_k(j) = +1)}{p(y|x_k(j) = -1)}\right), \quad \forall k, j \tag{1}$$
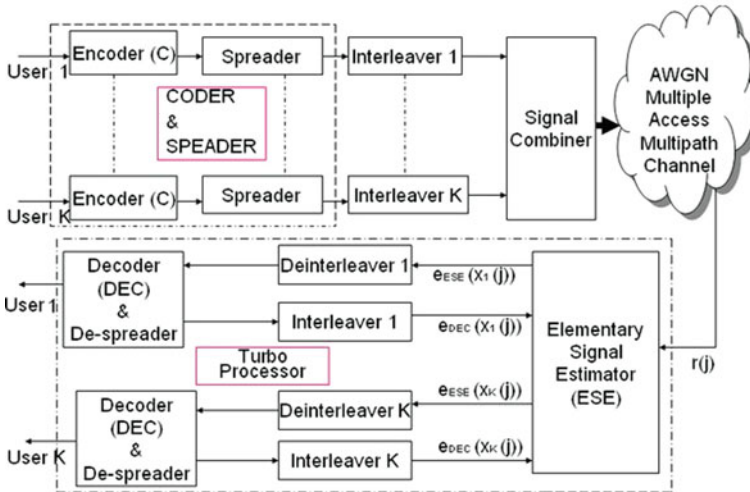

Fig. 1 IDMA transmitter and (iterative) receiver architectures with K concurrent users [19]

"LLRs are denoted by subscripts $e_{ESE(xk(j))}$ and $e_{DEC(xk(j)),}$, depending on whether they are formed by ESE or DECs. The ESE's received channel output is y in (1). For the DECs, y in (1) is the deinterleaved ESE outputs". To handle the LLRs generated by ESE and DECs [16, 17], a global turbo-type repeated approach is used.

2.2   The Basic ESE Function

With no memory and chip matching filtering, the received signal from K users is recorded as follows:

$$r(j) = \sum_{k=1}^{k} h_k x_k(j) + n(j), \quad j = 1, 2, \ldots, J \tag{2}$$

where

h_k: "channel coefficient for user-k"

$\{n(j)\}$: "Samples of an AWGN process having variance $\sigma^2 = N0/2$".

The receiver identifies the channel coefficients $\{h_k\}$ a priori. A single sample $r(j)$ will be applied at a time because to the usage of random interleavers $\{\pi_k\}$. Equation (2) can be written as

$$r(j) = h_k x_k(j) + \xi_k(j) \tag{3}$$

$$\xi_k(j) \equiv r(j) - h_k x_k(j) = \sum_{k' \neq k} h_{k'} x_{k'}(j) + n(j) \tag{4}$$

$\xi_k(j)$: "Distortion containing interference and noise in $r(j)$ with relation to user-k".

The central limit theorem identifies $\xi_k(j)$ as a Gaussian variable and $r(j)$ as a conditional Gaussian probability density function.

$$p(r(j)|x_k(j) = \pm 1) = \frac{1}{\sqrt{2\pi \operatorname{Var}\xi_k(j)}} \exp\left(\frac{(r(j) - (\pm h_k + E(\xi_k(j))))^2}{2\operatorname{Var}(\xi_k(j))} \right) \tag{5}$$

this $E(\cdot)$ and $\operatorname{Var}(\cdot)$ are mean and variance functions.

2.3 Algorithm for Chip-By-Chip Diagnosis in a Individual Path Channel

(a) *Evaluation of Interference Mean and Variance*

$$E(r(j)) = \sum_k h_k E(x_k(j)) \tag{6}$$

$$\text{Var}(r(j)) = \sum_k |h_k|^2 \text{Var}\big(x_k(j) + \sigma^2\big) \tag{7}$$

$$E(\xi_k(j)) = E(r(j) - h_k E(x_k))(j)) \tag{8}$$

$$\text{Var}(\xi_k(j)) = \text{Var}(r(j)) - |h_k|^2 \text{Var}(x_k(j)) \tag{9}$$

(b) *LLR Creation*

$$e_{\text{ESE}}(x_k(j)) = 2h_k \cdot \frac{r(j) - E(\xi_k(j))}{\text{Var}(\xi_k(j))} \tag{10}$$

3 IDMA with PLC

PLC is receiving a lot of attention currently days, therefore during this section a trial has been created to use IDMA technique with the PLC [18]. Owing to its inherent properties IDMA is potential candidate for transmission techniques. In this simulation, IDMA with PLC and an AWGN channel was compared against IDMA with an AWGN channel.

Random interleaver has been used in this situation. The IDMA scheme is also tested in each AWGN and Power Line channel scenario to see how it performs. At the receiver side, the information length is 512 bits, and the spreading length is sixteen (for 10 iterations). BPSK and QPSK modulation techniques were chosen since these modulation schemes are widely used in wireless channels at this time. A single cell environment and a single transmitter-one receiver configuration were assumed for all simulations in MATLAB-7.9. Also, all users are believed to have the same amount of storage space.

4 Simulation Results of PLC with IDMA Scheme

Plots 1, 2, 3 and 4 shows the performance of the IDMA scheme with power line channel yet as IDMA system in AWGN Channel atmosphere. Simulation is performed with power line channel and with AWGN atmosphere additionally with none forward error correction coding. Here 512 bits data length and therefore the spreading length for every user has been taken are sixteen, whereas for iterative decoding at the receiver, the opted iteration count is ten in all told the simulations delineated here. Purpose of using power line channel is to reduce Eb/No and BER $\leq 10^{-4}$.

In Plot 1 bit error rate performance of PLC with IDMA system has been shown, 512 bits data length is to be taken and therefore the value of EbNo is fifteen dB, the result has been found with a completely different range of users like 8, 16, 32, 64.

Moreover, to judge the performance of PLC with IDMA, it is been compared with ancient IDMA system in AWGN channel atmosphere as IDMA system has already been tested in AWGN channel atmosphere and comparing projected system therewith performance of line communication system with IDMA scheme will be analyzed. In Plot 2 EbNo has 2 completely different values like 5 and 10 dB. Here within the results performance of PLC with IDMA is incredibly near to the original IDMA scheme.
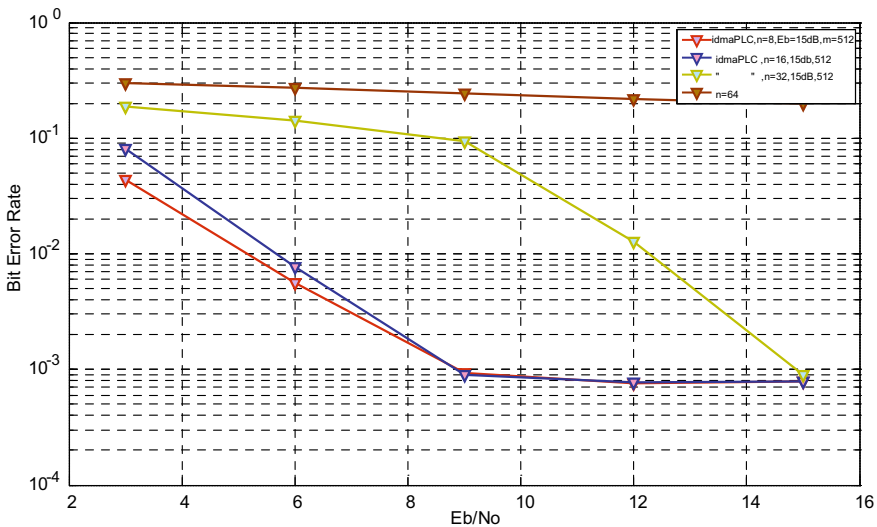
Plot 1 Results of PLC IDMA at different numbers of users in same environment conditions
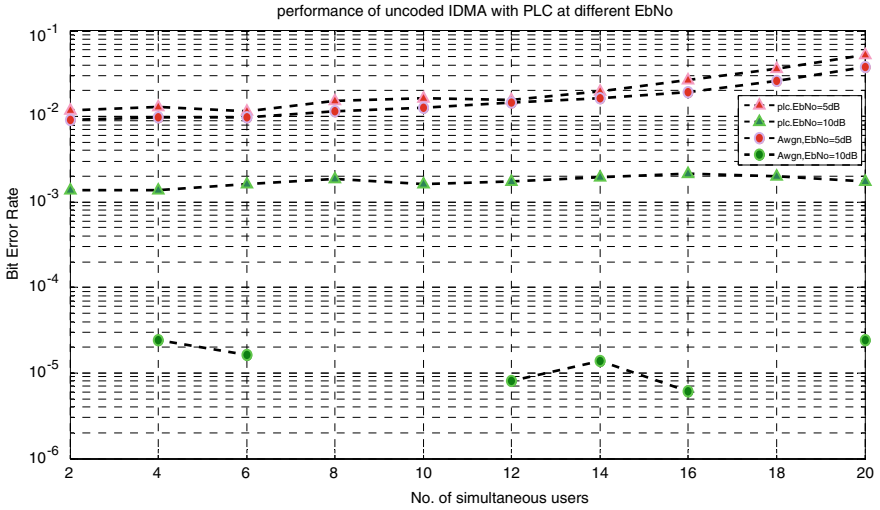
Plot 2 Comparison of PLC with AWGN at the different EbNo
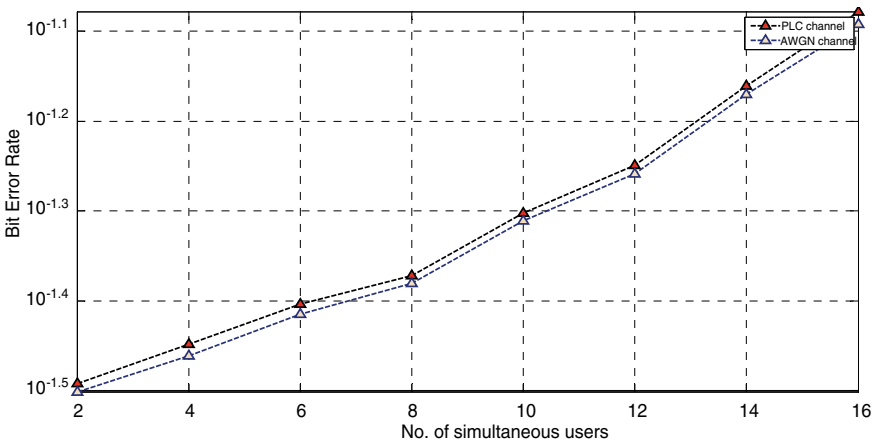
Plot 3 Performance of PLC with increased user count

In Plot 3, curve between a range of synchronic users and bit error rate has been drawn.

In Plot 4, ½ rate convolution coding is employed with IDMA scheme. Comparison has been created with uncoded IDMA with power line channel and AWGN atmosphere each, having twenty users.
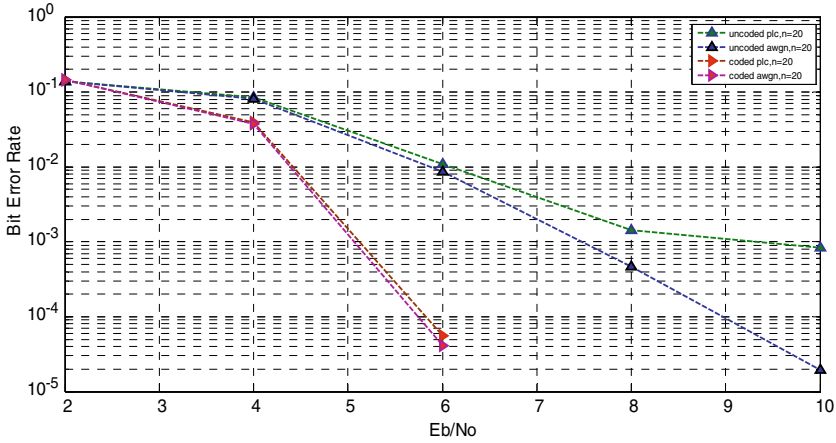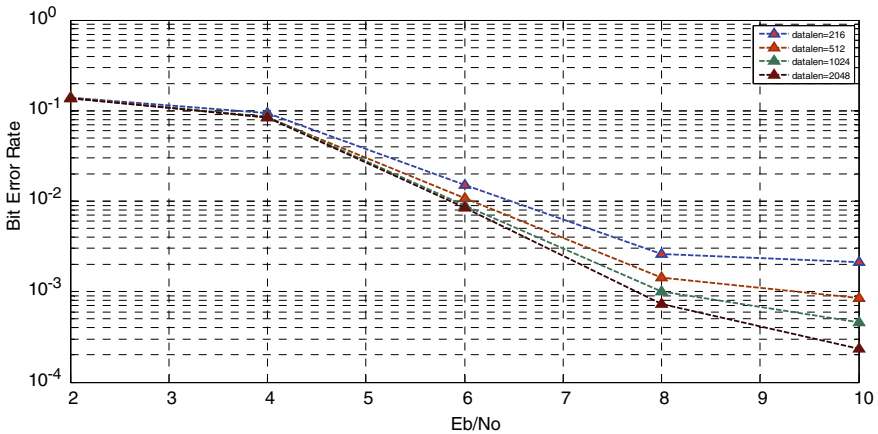
**Plot 4** Simulation of IDMA with PLC and simulation of IDMA (with AWGN with coding and without coding)

5 Performance of Power Line Communication with Different Interleavers

5.1 With Uncoded Random Interleaver

To achieve BER $< = 10.4$, the primary goal is to reduce the Eb/No ratio. The bit error rate of the PLC using the IDMA method is shown in Plot 5.

**Plot 5** Behavior of uncoded IDMA systems with 20 no of users
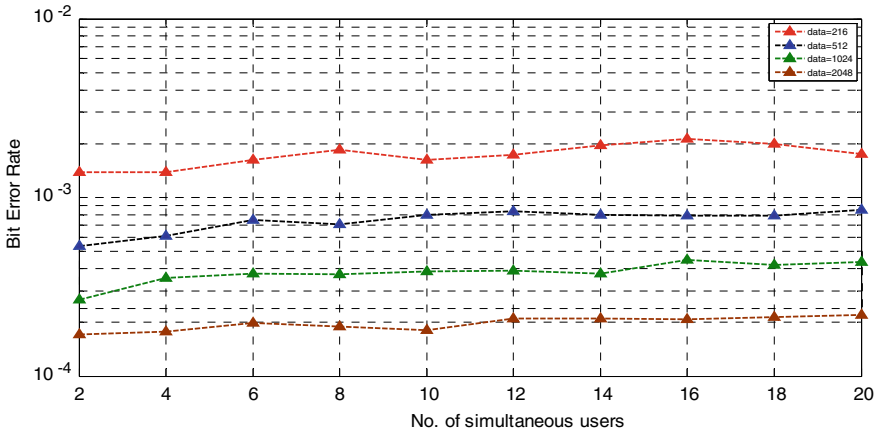
Plot 6 Plot of Number of users versus bit error rate having different data length

Plot 6 shows bit error rate performance estimated with regard to user count, information length has conjointly varied from 216 to 2048. Bit error rate is nearly constant even with the variation in user count. During this case data length used is 512 bits which is same for all users, variety of iterations chosen are ten. No coding is employed and information length for each user is equal that's 512 bits. Utilizing QPSK modulation BER performance of the system improved. Thus from the result it is clear that utilizing QPSK, taking little EbNo sensible results can be found.
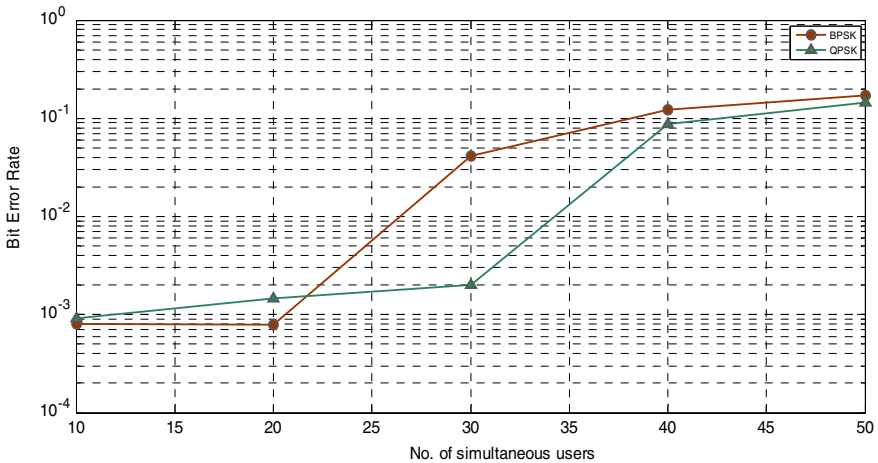
5.2 With Uncoded Tree-Based Interleaver

Plots 7 and 8 analyze the results of power line communication using an IDMA system using a tree-based interleaver.

In Plot 8 simulation results of PLC with IDMA system having tree-based interleaver here with totally different user count like $n = 8, 16, 32$ different information lengths like 256 bits, 512 bits, 1024 bits, and 2048 bits block size taken here is 20 and Eb/No is 10 dB. In Plot 8 performance of system delineated above has been analyzed using BPSK and QPSK modulation.
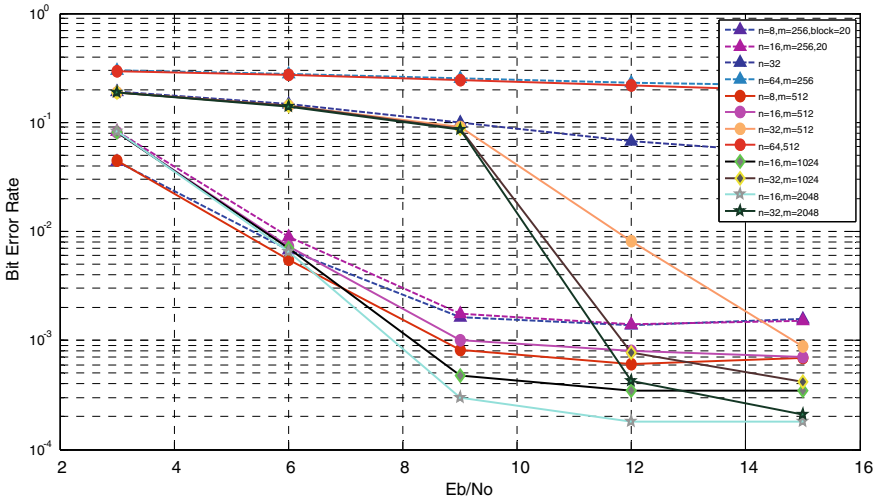
Plot 7 Simulation of PLC with uncoded IDMA with tree base interleaver

Plot 8 PLC IDMA with tree-based interleaver AT $m = 1024$

6 Conclusion

In this paper, we have discussed about power line communication (PLC), so that we can communicate utilizing the presently existing power lines. PLC can be integrated with coding and used with IDMA system using many modulation techniques and many interleavers to generate different communication strategies for PLC.

To understand the effect of utilizing IDMA in power line communication, IDMA system has been discussed with its transmitter and receiver. This system is simulated in MATLAB-7.8 and results had been studied how this impairment can affect the communication system. Performance is found to be extremely similar to the original IDMA. We have also thrown the light on different types of interleavers. Since interleavers like tree-based interleaver and prime number interleavers have many advantages, less computational complexity, band width and memory requirement, improve the system performance. Therefore an effort has been made to use efficient interleavers and evaluate Bit error rate performance of this system; results are very close to performance of IDMA system.

References

1. Hao, D., Yao, P., Hoeher, P.A.: Analysis and design of interleaver sets for interleave-division multiplexing and related techniques. In: Proceedings of the 5th International Symposium on Turbo Codes and Related Topics, pp. 432–437 (2008)
2. Lien, S.Y., Shieh, S.L., Huang, Y., Su, B., Hsu, Y.L., Wei, H.Y.: 5G new radio: waveform, frame structure, multiple access, and initial access. IEEE Commun. Mag. **55**(6), 64–71 (2017)
3. Dostert, K.: RF-models of the electrical power distribution grid. In: Proceedings of the 1998 International Symposium on Power-line Communications and its Applications, Tokyo, Japan (1998)
4. Mulligan, J.F.: Introduction to electric waves, being researches on the propagation of electric action with finite velocity through space by Heinrich Hertz 1. In: Heinrich Rudolf Hertz (1857–1894), pp. 163–192. Routledge (2019)
5. Corcoran, B., Tan, M., Xu, X., Boes, A., Wu, J., Nguyen, T.G., Chu, S.T., Little, B.E., Morandotti, R., Mitchell, A., Moss, D.J.: Ultra-dense optical data transmission over standard fibre with a single chip source. Nat. Commun. **11**(1), 1–7 (2020)
6. Ndjiongue, A.R., Ferreira, H.C.: Power line communications (PLC) technology: more than 20 years of intense research. Trans. Emerg. Telecommun. Technol. **30**(7), e3575 (2019)
7. Patil, V.L.: The entry of television. In: Chronological Developments of Wireless Radio Systems before World War II, pp. 131–146. Springer, Singapore (2021)
8. Guarnieri, M.: Seventy years of getting transistorized [historical]. IEEE Ind. Electron. Mag. **11**(4), 33–37 (2017)
9. Ayres, R.U.: The transistor transition: 1945–1969. In: The History and Future of Technology, pp. 425–466. Springer, Cham (2021)
10. Agarwal, H., Tiwari, P., Tiwari, R.G.: Exploiting sensor fusion for mobile robot localization. In: 2019 Third International Conference on I-SMAC (IoT in Social, Mobile, Analytics and Cloud) (I-SMAC), pp. 463–466. IEEE (2019)
11. Chhabra, R., Verma, S., Rama Krishna, C.: A survey on driver behavior detection techniques for intelligent transportation systems. In: 2017 7th International Conference on Cloud Computing, Data Science & Engineering-Confluence, pp. 36–41. IEEE (2017)
12. Tiwari, R.G., Husain, M., Srivastava, V., Singh, K.: A hypercube novelty model for comparing E-commerce and M-commerce. In: Proceedings of the 2011 International Conference on Communication, Computing & Security, pp. 616–619 (2011)
13. Agarwal, A.K., Rani, L., Tiwari, R.G., Sharma, T., Sarangi, P.K.: Honey encryption: fortification beyond the brute-force impediment. In: Advances in Mechanical Engineering, pp. 673–681. Springer, Singapore (2021)
14. Patel, A.: Interleave-division multiple access systems with invert tree based interleavers with unequal power sharing algorithm. In: 2020 International Conference on Inventive Computation Technologies (ICICT), pp. 700–704. IEEE (2020, February)

15. Sony, D., Keerthi, P., Aditya, O., Sravya, N.: Simulation and performance analysis of interleave division multiple access (IDMA) in comparision with code division multiple access (CDMA). Asian J. Appl. Sci. Technol. (AJAST) **5**(2), 90–94 (2021)
16. Zhang, J., Chen, Z., Zhang, S.E.: EXIT analysis of interleaver division multiple access system with LDPC code. In: IOP Conference Series: Earth and Environmental Science, vol. 693, No. 1, p. 012059. IOP Publishing (2021, March)
17. Chen, Y., Xiao, Y.: EP-based detection for uplink OFDM-IDMA with carrier frequency offsets. In: 2020 IEEE 91st Vehicular Technology Conference (VTC2020-Spring), pp. 1–5. IEEE (2020, May)
18. Agarwal, P., Shukla, M.: Effect of various interleavers on uncoded and coded OFDM-IDMA over PLC. In: 2020 5th International Conference on Communication and Electronics Systems (ICCES), pp. 275–279. IEEE (2020, June)
19. Gupta, K., Shukla, C.K., Tiwari, S., Shukla, M.: Performance evaluation of modulation techniques with iterative IDMA receivers using optimum tree based interleaver. In: 2011 International Conference on Communication Systems and Network Technologies, pp. 510–513. IEEE (2011)